QA: QA

MDL-NBS-HS-000011 REV 03

June 2007

Saturated Zone Site-Scale Flow Model

NOTICE OF OPEN CHANGE DOCUMENTS - THIS DOCUMENT IS IMPACTED BY THE LISTED CHANGE DOCUMENTS AND CANNOT BE USED WITHOUT THEM.

----

1) ACN-001, DATED 10/01/2007

Prepared for:
U.S. Department of Energy
Office of Civilian Radioactive Waste Management
Office of Repository Development
1551 Hillshire Drive
Las Vegas, Nevada 89134-6321

Prepared by:
Sandia National Laboratories
OCRWM Lead Laboratory for Repository Systems
1180 Town Center Drive
Las Vegas, Nevada 89144

Under Contract Number
DE-AC04-94AL85000

DISCLAIMER

This report was prepared as an account of work sponsored by an agency of the United States Government. Neither the United States Government nor any agency thereof, nor any of their employees, nor any of their contractors, subcontractors or their employees, makes any warranty, express or implied, or assumes any legal liability or responsibility for the accuracy, completeness, or any third party's use or the results of such use of any information, apparatus, product, or process disclosed, or represents that its use would not infringe privately owned rights. Reference herein to any specific commercial product, process, or service by trade name, trademark, manufacturer, or otherwise, does not necessarily constitute or imply its endorsement, recommendation, or favoring by the United States Government or any agency thereof or its contractors or subcontractors. The views and opinions of authors expressed herein do not necessarily state or reflect those of the United States Government or any agency thereof.

Saturated Zone Site-Scale Flow Model

MDL-NBS-HS-000011 REV 03

June 2007

ACKNOWLEDGEMENTS

This work relied on the expertise and hard work of dedicated scientists and support staff too numerous to list here. The primary contributors including their areas of responsibility are:

Scott James (SNL)	Lead author, project integrator, and team lead
Bill Arnold (SNL)	General scientific consultant and water-table rise analyst
Al-Aziz Eddebbarh (LANL)	Co-lead author
June Fabryka-Martin (LANL)	Geochemist largely responsible for Appendices A, B, and F
Terry Miller (LANL)	Generation of HFM input files for FEHM and Appendix G
Bob Roback (LANL)	Chief geochemist responsible for Appendices A and B
Dave Rudeen (RHYM)	Data qualification and model validation and Appendices C and D
Tim Vogt (ISSI)	HFM development and potentiometric surface in Appendix E

INTENTIONALLY LEFT BLANK

Model Signature Page/Change History

Complete only applicable items.

1. Total Pages: ~~636~~ 638 6/21/07

2. Type of Mathematical Model

☒ Process Model ☐ Abstraction Model ☐ System Model

Describe Intended Use of Model

The purpose of the saturated zone site-scale flow model is to describe the spatial distribution of groundwater as it moves from the water table below the repository, through the saturated zone, and to the point of uptake by the receptor of interest.

3. Title

Saturated Zone Site-Scale Flow Model

4. DI (including Revision No. and Addendum No.):

MDL-NBS-HS-000011 REV 03

	Printed Name	Signature	Date
5. Originator	S.C. James	Scott James	6/19/2007
6. Independent Technical Reviewer	M. Zhu	M Zhu	6/19/07
7. Checker	C.L. Axness	Carl Axness	6/19/07
8. QCS/Lead Lab QA Reviewer	R.E. Spencer	Robert Spencer	6/20/07
9. Responsible Manager/Lead	B.W. Arnold for	Kenneth Rehfeldt	6/20/07
10. Responsible Manager	S.P. Kuzio		6/20/07

11. Remarks

Change History

12. Revision No. and Addendum No.	13. Description of Change
REV 00	Initial Issue.
REV 00, ICN 01	Change bars were used in REV 00, ICN 01, to indicate corrections to the original document.
REV 01	Change bars are not used in REV 01 because there were extensive changes to the original document.
REV 01 ERRATA 1	Response to CR 2234.

REV 02	Description and presentation of alternative model. The alternate models are developed to evaluate the impact of new data and analyses on the saturated zone site-scale model predictions. The new data include a revised and reinterpreted hydrogeologic framework model conceptual model, boundary fluxes and recharge derived from the 2001 regional flow model and the 2004 UZ flow model, and the latest Nye County water-level data. The alternative models also include the incorporation of different conceptualization of site-scale features including the large hydraulic gradient, Solitario canyon fault, anisotropy etc. The revision also contains as Appendix A the analysis titled "Geochemical and Isotopic Constraints on Groundwater Flow." This report addresses CR-1873D resulting from BSC Surveillance No. BQA-SI-04-002: This report addresses comments from the Regulatory Integration Team. The entire model documentation was revised, because the changes were too extensive to indicate individual changes.
REV 03	Change bars were not used because this revision presents a completely new flow model. This major change updates the SZ flow model with the new hydrogeologic framework model, new Nye County Early Warning Drilling Program data through Phase IV and information from the recent USGS update to the Death Valley regional groundwater flow system model (Belcher 2004 [DIRS 173179]). The entire model documentation was revised. Changes were too extensive to show changes with change bars. The work scope of this report addresses actions related to (often through complete reformulation of the report) the following CRs: 4734, 6012, 6493, 6767, 6842, 7089, 7182, and 8337.

CONTENTS

Page

CONTENTS (Continued)

Page

CONTENTS (Continued)

Page

CONTENTS (Continued)

Page

FIGURES

Page

FIGURES (Continued)

Page

FIGURES (Continued)

Page

FIGURES (Continued)

Page

FIGURES (Continued)

Page

INTENTIONALLY LEFT BLANK

TABLES

Page

TABLES (Continued)

Page

TABLES (Continued)

Page

INTENTIONALLY LEFT BLANK

ACRONYMS AND ABBREVIATIONS

ACC	accession number
ACM	alternative conceptual model
AR	Amargosa River: group of boreholes located on the west side of Amargosa Desert
AR/FMW	Group of boreholes located near the confluence of the Amargosa River and Fortymile Wash drainages
ASCII	ASCII
ATC	Alluvial Testing Complex
BSC	Bechtel SAIC Company, LLC
CFR	code of federal regulations
CF-SW	Crater Flat Southwest
CMB	chloride mass balance
CR	condition report
CRWW	Coffer Ranch Windmill Well
CVFE	control-volume finite element
DFGP	Desert Farms Garlic Plot
DIC	Dissolved inorganic carbon
DIRS	document reference system
DOC	dissolved organic carbon
DOE	Department of Energy
DOS	disk operating system
DTN	data tracking number
DVRFS	Death Valley Regional (ground water) Flow System
ESF	Exploratory Studies Facility
EWDP	Early Warning Drilling Program
FEHM	finite-element heat and mass transfer numerical analysis computer code
FEPs	features, events, and processes
FMW-E	Fortymile Wash-East: group of boreholes in the Amargosa Desert east of Fortymile Wash
FMW-N	Fortymile Wash-North: group of boreholes east and northeast of Yucca Mountain
FMW-S	Fortymile Wash-South: group of boreholes along or near the main channel of Fortymile Wash in Amargosa Desert
FMW-W	Fortymile Wash-West: group of boreholes in the Amargosa Desert west of Fortymile Wash
GF	Gravity Fault: group of boreholes located on east side of the Amargosa Desert
GSIS	geoscientific information system
HFM	hydrogeologic framework model
HFM2006	revised hydrogeologic framework model

HGU	hydrogeologic unit
LA	license application
LANL	Los Alamos National Laboratory
LHG	large hydraulic gradient
LM	Levenberg-Marquardt (optimization algorithm for PEST)
LW	Amargosa Valley (formerly Lathrop Wells): group of boreholes located along U.S. Highway 95
MVA	middle volcanic aquifer
NAD-27	North American Datum of 1927
NAD-83	North American Datum of 1983
NC-EWDP	Nye County Early Warning Drilling Program
NSP	Nevada State Plane
NTS	Nevada Test Site
NWRPO	Nye County Waste Repository Program
OV/NWA	Oasis Valley/Northwest Amargosa Valley: group of boreholes located in that region
PC	personal computer
QAP	quality assurance plan
QARD	*Quality Assurance Requirements and Description*
RMSE	root-mean-square error
SCM	Software Configuration Management
SCW	Solitario Canyon Wash: western group of boreholes
SNL	Sandia National Laboratories
SSD	sum-of-squares difference
STN	software tracking number
SZ	saturated zone
TDOC	total dissolved organic carbon
TDS	total dissolved solids
TDMS	technical data management system
TIC	Technical Information Center
TM	Timber Mountain: group of boreholes north of Yucca Mountain
TSPA	total system performance assessment
TWP	technical work plan
UGTA	underground testing area
USGS	United States Geologic Survey
UTM	Universal Trans Mercator
UZ	unsaturated zone

YM-S	Yucca Mountain South
YMP	Yucca Mountain Project
YMRP	*Yucca Mountain Review Plan, Final Report*

HYDROGEOLOGIC UNITS AND CHEMICAL ELEMENTS

Tac	Calico Hills formation
Tcb	Bullfrog tuff of the Crater Flat Group
Tcp	Prow Pass tuff of the Crater Flat Group
Tct	Tram tuff of the Crater Flat Group
Tlr	Lithic Ridge tuffs

$\delta^{13}C$	delta carbon-13
δD	delta hydrogen-2, or delta deuterium
$\delta^{18}O$	delta oxygen-18
$\delta^{34}S$	delta sulfur-34
$\delta^{87}Sr$	delta strontium-87

INTENTIONALLY LEFT BLANK

1. PURPOSE

The purpose of this model report is to document revision of *Saturated Zone (SZ) Site-scale Flow Model* (BSC 2004 [DIRS 170037]) for Yucca Mountain, Nevada, in accordance with SCI-PRO-006, *Models*. This report provides validation and confidence in the flow model developed in support of the total system performance assessment (TSPA) for the license application (LA). The output from this report provides the flow model used in *Site-Scale Saturated Zone Transport Model*, (SNL 2007 [DIRS 177392]), which in turn provides output to the *SZ Flow and Transport Model Abstraction* (SNL 2007 [DIRS 177390]). In particular, the output from the SZ site-scale flow model is used by the SZ site-scale transport model to simulate the groundwater flow pathways and radionuclide transport to the accessible environment for use in *SZ Flow and Transport Model Abstraction* (SNL 2007 [DIRS 177390]), which feeds the TSPA calculations. Figure 1-1 shows the relationship of this report to other saturated zone reports that also pertain to SZ flow and transport. The figure also depicts the relationship between SZ models and analyses. It should be noted that Figure 1-1 does not contain a complete representation of the data and parameter inputs and outputs of all saturated zone reports, nor does it show inputs external to this suite of saturated zone reports.

Since the development, calibration, and validation of the SZ site-scale flow model (CRWMS M&O 2000 [DIRS 139582]), more data have been gathered and analyses have been completed. The data include new stratigraphic and water–level data from Nye County wells, single- and multiple-well hydraulic testing data (SNL 2007 [DIRS 177394]), and new hydrochemistry data (Appendix B). New analyses include the 2004 transient Death Valley Regional (ground water) Flow System (DVRFS) model (Belcher 2004 [DIRS 173179]), the creation of a new hydrogeologic framework model (HFM), called HFM2006 (SNL 2007 [DIRS 174109], DTN: MO0610MWDHFM06.002 [DIRS 179352]), and the 2003 unsaturated zone (UZ) flow model (BSC 2004 [DIRS 169861]). The new data and analyses were used to construct the SZ site-scale flow model presented in this report to support TSPA-LA. The intended use of this work is to provide a flow model that generates flow fields that are used to simulate radionuclide transport in saturated volcanic rock and alluvium under natural-gradient flow conditions. Simulations of water-table rise were also conducted for use in downstream transport and abstraction modeling. The SZ site-scale flow model simulations were completed using the three-dimensional, finite-element heat and mass transfer computer code, FEHM V2.24, STN: 10086-2.24-02 [DIRS 179539]. Concurrently, the process-level transport model and methodology for calculating radionuclide transport in the SZ at Yucca Mountain using FEHM are described in *Site-Scale Saturated Zone Transport* (SNL 2007 [DIRS 177392]). The velocity fields are calculated by the flow model, described herein, independent of the transport processes, and are then used as inputs to the transport model. Justification for this abstraction is presented in *Saturated Zone Flow and Transport Model Abstraction* (SNL 2007 [DIRS 177390]).

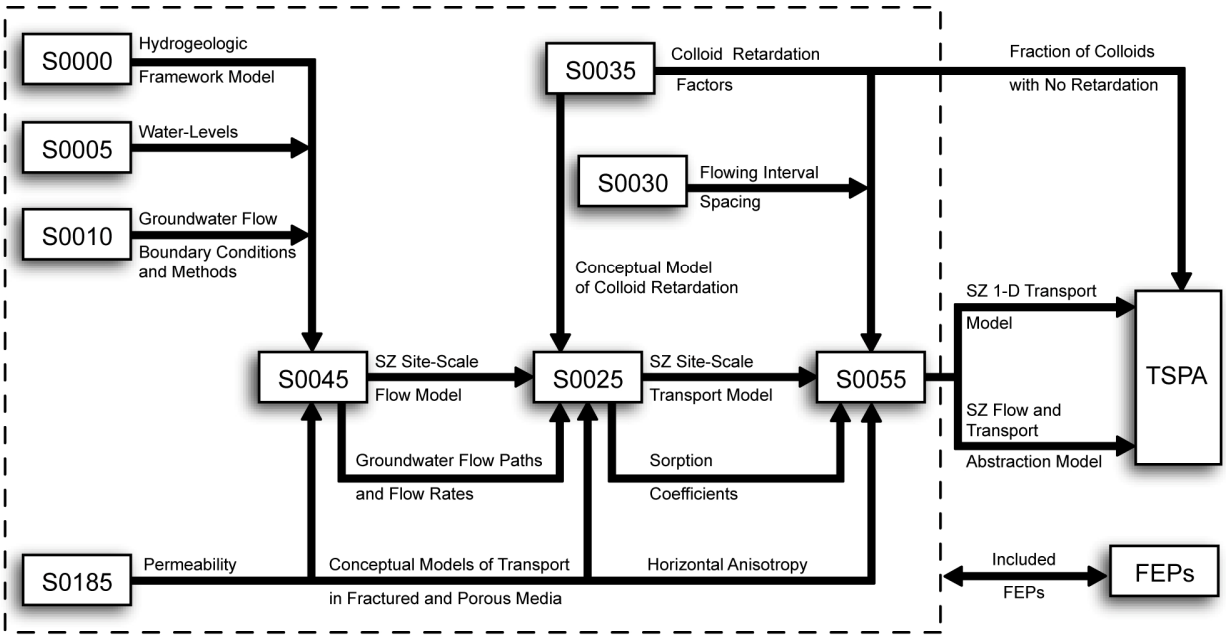

Legend

S0000 - Hydrogeologic Framework Model	MDL-NBS-HS-000024
S0005 - Water-Level Data Analysis	ANL-NBS-HS-000034
S0010 - Recharge and Lateral Groundwater Flow Boundary Conditions	ANL-NBS-MD-000010
S0025 - Site-Scale Saturated Zone Transport	MDL-NBS-HS-000010
S0030 - Probability Distribution for Flowing Interval Spacing	ANL-NBS-MD-000003
S0035 - Saturated Zone Colloid Transport	ANL-NBS-HS-000031
S0045 - Site-Scale Saturated Zone Flow Model	MDL-NBS-HS-000011
S0055 - Saturated Zone Flow and Transport Model Abstraction	MDL-NBS-HS-000021
FEPs - Features, Events, and Processes in SZ Flow and Transport	DTN: MO0508SEPFEPLA.002
S0185 - Saturated Zone In-Situ Testing	ANL-NBS-HS-000039

00438DC_001d.ai

NOTE: This figure is a simplified representation of the flow of information among SZ reports. See the most recent revision of each report for a complete listing of data and parameter inputs. This figure does not show inputs external to this suite of SZ reports.

FEPs = features, events, and processes; SZ = saturated zone; TSPA = total system performance assessment.

Figure 1-1. Generalized Flow of Information among Reports Pertaining to Flow and Transport in the SZ

This model report is governed by *Technical Work Plan: Saturated Zone Flow and Transport Modeling* (BSC 2006 [DIRS 177375]). All activities listed in the technical work plan (TWP) that are appropriate to the SZ site-scale flow model are documented in this report. The TWP (BSC 2006 [DIRS 177375]) cites procedures that were in effect at the time the work described in this report was planned and approved. Following the transition of the science work scope from Bechtel SAIC Company, LLC (BSC) to Sandia National Laboratories (SNL), new procedures have been issued since October 2, 2006.

Model-validation activities presented in this report lead to increased confidence that the model is a reasonable representation of groundwater flow likely to occur at Yucca Mountain near the repository site. Model confidence-building activities consist of the following comparisons between observed data and model simulations:

- Observed hydraulic heads and gradients not used for model development and calibration
- Hydraulic properties obtained from model calibrations and those obtained from field and laboratory testing
- Flowpaths obtained from the model and those inferred from analysis of field hydrochemistry and isotopic data.

Alternative conceptual models and the implications of these models for flow field, flowpaths, and transport times simulations are evaluated relative to the SZ site-scale flow model.

A number of relevant features, events, and processes (FEPs) are addressed in Section 6.2.

Uncertainty inherent to parameters, conceptualization, and modeling is discussed in Section 6 and propagated, as appropriate, in Section 8.

The SZ site-scale flow model is limited to steady state use (no transient conditions) for TSPA purposes. When using the SZ site-scale flow model for TSPA calculations, there are limitations that must be noted in regard to the following: changes to input parameter values, useable pathline distances, and overall model recharge fluxes. These are discussed more fully in Section 8.

Important technical issues addressed by this model report, and the sections in which they are discussed, include:

- Horizontal and vertical anisotropy, reasonable range for uncertainty (Sections 6.3.1.9, 6.4.3.11 and 6.7.1)
- Updated potentiometric data (Appendix E)
- Alternative conceptual flow models (Section 6.6)
- Validation of SZ site-scale flow model (Section 7)
- Comparison of volumetric and mass flow rates at the boundaries with those of the 2004 DVRFS model (Section 6.5.2.2).

Modeling objectives addressed in this model report are:

- Reflect the current understanding of the SZ flow

- Enhance model validation and uncertainty analyses
- Incorporate new data collected since the TSPA-SR (CRWMS M&O 2000 [DIRS 143665]).

This report is cited by *Features, Events, and Processes for Total System Performance Assessment* (SNL 2007 [DIRS 179476]).

This model report addresses the Condition Reports (CR) associated with previous versions as follow:

- CR 4734 identified an editorial error in a section callout in the previous revision of this report (BSC 2004 [DIRS 170037], p. 8-8). For this revision, cross-references have been checked and verified throughout the product development and review processes.
- CR 6012 identified two issues with the previous version (BSC 2004 [DIRS 170037)]: the need to establish traceability for boundary fluxes used as calibration targets in the base-case flow model, and the need to assess the impact of differences between the boundary fluxes documented in the flow model analysis and model report (AMR) and those in the boundary flux report (BSC 2004 [DIRS 170015]). Sections 6.3.1.6, 6.4.3.8, 6.5.2.2, and Appendix C establish the traceability of the boundary fluxes extracted from the 2004 DVRFS model and used as calibration targets in the SZ site-scale flow model.
- CR 6493 identified as an issue that hydraulic heads simulated by the SZ flow alternative conceptual models appear to be unreasonably high in part of the model domain. This CR is no longer applicable because there are no calibrated alternative conceptual models in this report. Nevertheless, the revised, calibrated SZ site-scale flow model (Section 6.5) shows no such high heads.
- CR 6767 raised a question about the possible need to incorporate new technical data produced by the USGS on ^{14}C and $^{234}U/^{238}U$ activity ratios into the delineation of groundwater flow paths using geochemical indicators. Appendix B incorporates geochemical and isotopic data (including ^{14}C and $^{234}U/^{238}U$ ratios) that were not available for use in earlier versions and evaluates the consistency delineation of groundwater flowpaths.
- CR 6842 identified an incorrect software name and reference numbers in Table 3-1 of the previous revision. This report lists the correct software names in Table 3-1 and in Section 9. To prevent recurrence, confirmation across the software baseline report, DIRS, and this model report was included during the checking process.
- CR 7089 identified editorial issues in the previous revision. Because this is a complete revision of the SZ site-scale flow model, these editorial issues are no longer applicable.

- CR 7182 questioned the use of head boundaries with no vertical head variation. Section 6.3.1.6 presents the rationale for not varying the head vertically.

- CR 8337 identified errors in the constant head boundary condition specified along the southern boundary of the alternate SZ flow models. Because this is a complete revision of the SZ site-scale flow model, and there are no calibrated alternative models presented in this report), this CR is no longer applicable. Despite the inapplicability of this CR, care was taken to ensure that the southern boundary was correctly specified as the heads extracted from the potentiometric surface (Appendix E).

INTENTIONALLY LEFT BLANK

2. QUALITY ASSURANCE

Development of this model report and the supporting modeling activities are subject to the Office of Civilian Radioactive Waste Management Quality Assurance Program as indicated in the TWP (BSC 2006 [DIRS 177375]) developed under LP-2.29Q-BSC, *Planning for Science Activities*. Approved quality assurance procedures identified in the TWP (BSC 2006 [DIRS 177375], Section 4) have been used to conduct and document the activities described in this model report. The TWP (BSC 2006 [DIRS 177375], Section 8) also identifies the methods used to control the electronic management of data.

Planning and preparation of this report was initiated under the BSC QA Program. Therefore, forms and associated documentation prepared prior to October 2, 2006, the date this work transitioned to the Lead Laboratory, were completed in accordance with BSC procedures. Forms and associated documentation completed on or after October 2, 2006 were prepared in accordance with Lead Laboratory procedures.

This model report provides calibrated values for hydrologic properties of the SZ portion of the lower natural barrier (i.e., SZ below and downgradient from the repository), which is important to the demonstration of compliance with the postclosure performance objectives defined at 10 CFR 63.113 [DIRS 176544]. Therefore, the lower natural barrier is classified in *Q-List* (BSC 2005 [DIRS 175539], Table A-1) as "SC" (Safety Category), reflecting its importance to waste isolation, as defined in LS-PRO-0203, *Q-List and Classification of Structures, Systems, and Components*. This report contributes to the analysis and modeling data used to support performance assessment; the conclusions do not directly impact engineered features important to safety, as defined in LS-PRO-0203.

INTENTIONALLY LEFT BLANK

3. USE OF SOFTWARE

3.1 SOFTWARE TRACKED BY CONFIGURATION MANAGEMENT

The computer codes used directly in the SZ site-scale flow model are summarized in Table 3-1. Table A3-1 lists additional software used in the hydrochemistry analysis to support an indirect corroboration activity for validation (see Appendix A). Section E2 discusses software used to develop the potentiometric surface. The qualification status of the software is indicated in the Software Configuration Management (SCM) database. All software was obtained from SCM and is appropriate for the application. Qualified codes were used only within the range of validation as required by IM-PRO-003, *Software Management*. All software baselined after October 2, 2006 was qualified per IT-PRO-0012, *Qualification of Software,* and validated per IM-PRO-005 *Software Independent Verification and Validation*. Computer codes listed in Table 3-1 were selected for use in the analysis report because they were appropriate for the intended use. Software used directly in modeling tasks also satisfy at least one of the following conditions (as documented in the table footnotes) in that they were:

- Developed specifically for the tasks considered in this report
- Best available codes for modeling conditions specific to the YMP.

The codes developed specifically for the tasks considered in this report and for the YMP were validated for the parameter ranges expected for Yucca Mountain. The range of use and the limitations on output of each code are specified in the Software Management Report of each code. As it can be concluded from these reports, the limitations on input and output should only be considered when these codes are used outside of the YMP. Otherwise, no special limitations on input and output exist. The codes that fall into one of the categories above are described in Sections 3.1.1 through 3.1.4.

Table 3-1. Computer Codes Used in the SZ Site-Scale Flow Model

Software Name and Version (V)	Software Tracking Number (STN)	Description	Computer Type, Platform, and Location	Date Base-lined
CORPSCON V.5.11.08 [DIRS 155082]	10547-5.11.08-00	Software package for conversion of coordinates	Windows NT 4.0	8/27/01
FEHM V2.24[a] [DIRS 179539]	10086-2.24-02	Solution to SZ flow	PC or Sun Ultra Sparc with Sun Solaris 5.7 or 5.8 operating system	12/1/06
LaGriT V1.1[a] [DIRS 173140]	10212-1.0-00	Software package for grid generation, analysis, and visualization	Sun Ultra Sparc with Sun OS 2.7 operating system at LANL	8/8/01
PEST V5.5 [DIRS 161564]	10289-5.5-00	Preconditioning and parameter optimization for FEHM [DIRS 179539] runs	Sun Ultra Sparc with Sun Solaris 5.7 or 5.8 operating system at LANL	12/3/02

Table 3-1. Computer Codes Used in the SZ Site-Scale Flow Model (Continued)

Software Name and Version (V)	Software Tracking Number (STN)	Description	Computer Type, Platform, and Location	Date Base-lined
EarthVision 5.1 [DIRS 167994]	10174-5.1-00	Commercial software for 3D model building and visualization used for contouring, plotting, and visualization of the data and for evaluation of results	Silicon Graphics Octane workstation running IRIX 6.5	09/18/00
Extract V1.0[b] [DIRS 163070]	10955-1.0-00	Pre/postprocessor used to extract lateral flow data from the USGS regional flow model	Sun UltraSPARC - SunOS 5.7 operating system at SNL	12/11/02
Extract V1.1[b] [DIRS 163071]	10955-1.1-00	Pre/postprocessor used to extract lateral flow data from the USGS 2001 regional flow model	Sun UltraSPARC - SunOS 5.7 operating system at SNL	12/11/02
EXT_RECH V1.0[b] [DIRS 163072]	10958-1.0-00	Pre/postprocessor used to extract recharge data from the USGS regional flow model	Sun UltraSPARC - SunOS 5.7 operating system at SNL	12/11/02
Mult_Rech V1.0[b] [DIRS 163073]	10959-1.0-00	Pre/postprocessor that scales recharge data from the USGS regional flow model and maps the data to a new grid	Sun UltraSPARC - SunOS 5.7, Solaris 2.7 operating system at SNL	12/18/02
Xread_Distr_Rech V1.0[b] [DIRS 163074]	10960-1.0-00	Pre/postprocessor used to extract recharge data from the USGS 1999 regional flow model	Sun UltraSPARC - SunOS 5.7 operating system at SNL	12/11/02
Xread_Distr_Rech_UZ V1.0[b] [DIRS 163075]	10961-1.0-00	Pre/postprocessor that maps recharge data onto a new grid excluding the UZ flow model region	Sun UltraSPARC - SunOS 5.7 operating system at SNL	12/11/02
Xread_Reaches V1.0[b] [DIRS 163076]	10962-1.0-00	Pre/postprocessor that maps local recharge from four stream channels onto a new grid	Sun UltraSPARC - SunOS 5.7 operating system at SNL	12/11/02
Xwrite_Flow_New V1.0-125[b] [DIRS 163077]	10963-1.0-125-00	Used both to map the combined UZ and SZ site-scale fluxes onto a 125-m grid and to create a flux file that is compatible with FEHM [DIRS 179539] flow macros	Sun UltraSPARC - SunOS 5.7 operating system at SNL	12/11/02

Table 3-1. Computer Codes Used in the SZ Site-Scale Flow Model (Continued)

Software Name and Version (V)	Software Tracking Number (STN)	Description	Computer Type, Platform, and Location	Date Base-lined
Zones V1.0 [b] [DIRS 163078]	10957-1.0-00	Used to extract zonal designation data from the USGS 2001 regional flow model	Sun UltraSPARC - SunOS 5.7 operating system at SNL	12/11/02

[a] Developed for the YMP.

[b] Developed specifically for the tasks considered in this report.

DOS = disk operating system; HFM = hydrogeologic framework model; LANL = Los Alamos National Laboratory; PC = personal computer; SNL = Sandia National Laboratories; SZ = saturated zone; USGS = U.S. Geological Survey; UZ = unsaturated zone.

3.1.1 Parameter Optimization

The parameter estimation code PEST V5.5 (STN: 10289-5.5-00; [DIRS 161564]) is used to perform the parameter optimization for the hydrogeologic and feature permeabilities. The PEST code is based on the Levenberg-Marquardt (LM) algorithm. This software was not used to generate flow model output. Rather, it is used to calibrate the flow model by minimizing the difference between observed and simulated head and boundary fluxes values.

3.1.2 Flow Modeling

FEHM V2.24 (STN: 10086-2.24-02; [DIRS 179539]) is used to solve for a steady-state flow solution and to provide model output. The range of validation for the FEHM code was developed with the YMP specific data. Consequently, the input and output parameters are within their validation ranges.

3.1.3 Particle Tracking

The FEHM code is used within its validated range to determine the steady-state flow solution (see Section 3.1.2). FEHM has two different particle-tracking routines and herein the *sptr* macro is used, but only insofar as to illustrate flowpaths. The particle-tracking portion of FEHM is discussed extensively in *Site-Scale Saturated Zone Transport* (SNL 2007 [DIRS 177392], Section 6.4.2).

3.1.4 Grid Generation

The grid generation software package LaGriT V1.0 (STN: 10212-1.1-00; [DIRS 173140]) is used within its validation limits for creation, analysis, and visualization of grids. LaGriT is a set of software macros that uses the HFM conceptual model data to create computational grids. The software macros translate the coordinate and attribute information into a form that is valid for finite-element heat and mass (FEHM) compilations.

3.2 EXEMPT SOFTWARE

Several additional, exempt (IM-PRO-003), commercially available software packages were used for data handling, formatting, and data visualization in the preparation of SZ site-sale flow

Model. These additional software packages are Microsoft Access (97 and 2000) and Microsoft Excel (97 and 2003 SP2). Each of these additional software packages was used on the Windows 2000 platform. No calculations were performed by these commercial software packages and the only output is in the form of visualizations, such as those found in Figures 6-14 through 6-17 and the appendices. Input files or sources are identified with each figure. Surfer was used for visualization and is therefore exempt per IM-PRO-003, Section 2.0, 5th paragraph, 2nd dash. Access and Excel were used for formatting data and were exempt per IM-PRO-003, Section 2.0, 5th paragraph, 1st dash. Each of these exempt software packages is controlled by YMP Software Configuration Management.

- *Excel* 97 or 2003-SP2 was used to preprocess data from the U.S. Geological Survey (USGS) traces for FEHM zone definitions as well as for other standard calculations and visualizations. The calculation of basic statistics was used with standard functions only.

- *Surfer* for Windows, v8.06.39 was used for plotting and visualization of analysis results in figures shown in this report. The results were visually checked for correctness.

- *Igor Pro*, v4.091 was used for plotting and visualization of analysis results in some figures shown in this report. The results were visually checked for correctness.

- *Microsoft Access* 1997 SR2, was used to identify model nodes that are located a specified distance from an *x*,*y* coordinate.

- *GMV* and *Adobe Illustrator*, v10 were used to visualize and illustrate the computational mesh, geochemical analyses, and related data.

- *AquaChem*, V3.7, was used to create trilinear diagrams showing proportions of major ions in groundwater and *x*-*y* scatter plots.

- *Adobe Illustrator*, v10 was used to create flow-path maps.

Outputs from *Excel*, *Surfer*, *Igor*, *Microsoft Access*, *GMV*, *Adobe Illustrator*, and *AquaChem* were visually checked for correctness. This output can be found in the Technical Data Management System (TDMS) within data packages that have been assigned data tracking number (DTN) numbers. The DTNs are identified in appropriate places throughout Section 6 to allow the independent reviewer to reproduce or verify results by visual inspection or hand calculation.

AutoCad 2002 and *EarthVision 7.5.2* were used for data visualization and are, therefore, exempt under of IM-PRO-003, Paragraph 1.4.2. *UltraEdit V11.10* was used for formatting data and was exempt under IM-PRO-003, Paragraph 1.4.1. Each of these exempt software packages is controlled by YMP Software Configuration Management.

3.3 PROTOTYPE SOFTWARE

PEST V11.1 (STN: 611582-11.1; [DIRS 179480]) was used as a prototype in advancing science analysis. This software was not used in quality-affecting work; rather, the earlier qualified

version *PEST V5.5* (STN: 10289-5.5-00; [DIRS 161564]) was used for quality-affecting work. *PEST V11.1* was used to analyze, in a prototype/scoping manner, the FEHM predictive uncertainty for specific discharge, which was calculated with *SPDIS.EXE* (STN: 611598-00-00; [DIRS 180546]).

INTENTIONALLY LEFT BLANK

4. INPUTS

4.1 DIRECT INPUT

Input information used in this model report comes from several sources, which, along with their DTNs, are summarized in Table 4-1. The data referenced in Table 4-1 contain information necessary to construct the numerical model, set boundary conditions, calibrate the model, and check the calibration. The data are fully appropriate for the SZ site-scale flow model. All data listed in Table 4-1 are qualified or will be qualified according to SCI-PRO-001, *Qualification of Unqualified Data*, upon finalization of this report. Per SCI-PRO-006 (Attachment 2), no data used as input and listed in Table 4-1 are used for model validation.

Table 4-1. Direct Input Data Sources

Data Description	Data Tracking Number	File Name
Hydraulic head data and well locations as described by BSC 2004 [DIRS 170009]	GS010908312332.002 [DIRS 163555][a]	*mean312411.xls*
Potentiometric surface	MO0409SEPPSMPC.000 [DIRS 179336]	*S00005_fig6-2.pdf*
Plot of temperature profiles in wells	MO0102DQRBTEMP.001 [DIRS 154733]	*All*
Fault locations	GS010608312332.001 [DIRS 155307]	*tert_flts.e00*
Fault locations (U.S. Highway 95)	GS010908314221.001 [DIRS 162874]	*All*
HFM for SZ site-scale flow and transport model, containing unit surfaces	MO0610MWDHFM06.002 [DIRS 179352]	*output.zip*
UZ flow model output	LB03023DSSCP9I.001 [DIRS 163044]	*Meshes.tar.gz* *preq_lA.tar.gz* *preq_mA.tar.gz* *preq_uA.tar.gz*
Fortymile Wash infiltration	MO0102DQRGWREC.001 [DIRS 155523]	*All*

[a] This DTN was used to establish well locations and water levels for model calibration. While this same DTN was used in validation (Appendix A), it was used solely to establish a common frame of reference (i.e., common well locations were used, but water levels were not used in the analysis in Appendix A).

HFM = hydrogeologic framework model; SZ = saturated zone.

The data listed in Table 4-1 are direct model inputs, after appropriate manipulation by the software listed in Table 3-1.

Table 4-2. Intermediary Direct Input Data Sources (see also Table 8-1)

Data Description	Data Tracking Number	File Name
Lateral mass flow targets and infiltration boundary conditions	SN0612T0510106.003[a]	*wt_250_04.dat* *east_bdy_2004* *north_bdy_2004* *south_bdy_2004* *west_bdy_2004* *Analysis.xls*
Nye County Early Warning Program well location, open interval, and water-level data	SN0702T0510106.007[b]	*All*

[a] See Appendix C for development and qualification of this DTN for intended use in this report.
[b] See Appendix D for development and qualification of this DTN for intended use in this report.

The data listed in Table 4-2 are direct model inputs that come from intermediary product output as developed and qualified in Appendices C and D.

4.2 CRITERIA

The general requirements to be satisfied by the TSPA are stated at 10 CFR Part 63 [DIRS 176544]. The acceptance criteria that will be used by the NRC to determine whether the technical requirements have been met are identified in *Yucca Mountain Review Plan*, *Final Report* (YMRP) (NRC 2003 [DIRS 163274]).

Acceptance Criteria from YMRP Section 2.2.1.3.8.3 (NRC 2003 [DIRS 163274]), Flow Paths in the Saturated Zone

The applicable acceptance criteria in the YMRP (NRC 2003 [DIRS 163274], Section 2.2.1.3.8.3) are given below. How they are addressed by this report is described in Section 8.4.

Acceptance Criterion 1: *System Description and Model Integration Are Adequate*.

(1) Total system performance assessment adequately incorporates important design features, physical phenomena, and couplings, and uses consistent and appropriate assumptions, throughout the flowpaths in the SZ abstraction process;

(2) The description of the aspects of hydrology, geology, geochemistry, design features, physical phenomena, and couplings, that may affect flowpaths in the SZ, is adequate. Conditions and assumptions in the abstraction of flowpaths in the SZ are readily identified, and consistent with the body of data presented in the description;

(4) Boundary and initial conditions used in the total system performance assessment abstraction of flowpaths in the SZ are propagated throughout its abstraction approaches. For example, abstractions are based on initial and boundary conditions consistent with site-scale modeling and regional models of the Death Valley regional groundwater flow system;

(5) Sufficient data and technical bases to assess the degree to which features, events, and processes have been included in this abstraction are provided;

(6) Flowpaths in the SZ are adequately delineated, considering natural site conditions;

(7) Long-term climate change, based on known patterns of climatic cycles during the Quaternary period, particularly the last 500,000 years, and other paleoclimate data, are adequately evaluated;

(8) Potential geothermal and seismic effects on the ambient SZ flow system are adequately described and accounted for;

(9) The impact of the expected water table rise on potentiometric heads and flow directions, and consequently on repository performance, is adequately considered; and

(10) Guidance in NUREG–1297 (Altman et al. 1988 [DIRS 103597] and NUREG–1298 (Altman et al. 1988 DIRS 103750]), or other acceptable approaches for peer review and data qualification is followed.

Acceptance Criterion 2: ***Data Are Sufficient for Model Justification.***

(1) Geological, hydrological, and geochemical values used in the license application to evaluate flowpaths in the SZ are adequately justified. Adequate descriptions of how the data were used, interpreted, and appropriately synthesized into the parameters are provided;

(2) Sufficient data have been collected on the natural system to establish initial and boundary conditions for the abstraction of flowpaths in the SZ;

(3) Data on the geology, hydrology, and geochemistry of the SZ used in the total system performance assessment abstraction are based on appropriate techniques. These techniques may include laboratory experiments, site-specific field measurements, natural analogue research, and process-level modeling studies. As appropriate, sensitivity or uncertainty analyses, used to support the U.S. Department of Energy total system performance assessment abstraction, are adequate to determine the possible need for additional data; and

(4) Sufficient information is provided to substantiate that the mathematical groundwater modeling approach and model(s) are calibrated and applicable to site conditions.

Acceptance Criterion 3: ***Data Uncertainty Is Characterized and Propagated Through the Model Abstraction.***

(1) Models use parameter values, assumed ranges, probability distributions, and bounding assumptions that are technically defensible, reasonably account for uncertainties and variabilities;

(2) Uncertainty is appropriately incorporated in model abstractions of hydrologic effects of climate change, based on a reasonably complete search of paleoclimate data;

(3) Uncertainty is adequately represented in parameter development for conceptual models, process-level models, and alternative conceptual models, considered in developing the abstraction of flowpaths in the SZ. This may be done either through sensitivity analyses or through use of conservative limits. For example, sensitivity analyses and/or similar

analyses are sufficient to identify SZ flow parameters that are expected to significantly affect the abstraction model outcome; and

(4) Where sufficient data do not exist, the definition of parameter values and conceptual models is based on appropriate use of expert elicitation, conducted in accordance with NUREG–1563 (Kotra et al. 1996 [DIRS 100909]). If other approaches are used, the U.S. Department of Energy adequately justifies their uses.

Acceptance Criterion 4: ***Model Uncertainty Is Characterized and Propagated Through the Model Abstraction.***

(1) Alternative modeling approaches of features, events, and processes are considered and are consistent with available data and current scientific understanding, and the results and limitations are appropriately considered in the abstraction;

(2) Conceptual model uncertainties are adequately defined and documented, and effects on conclusions regarding performance are properly assessed. For example, uncertainty in data interpretations is considered by analyzing reasonable conceptual flow models that are supported by site data, or by demonstrating through sensitivity studies that the uncertainties have little impact on repository performance;

(3) Consideration of conceptual model uncertainty is consistent with available site characterization data, laboratory experiments, field measurements, natural analogue information and process-level modeling studies; and

(4) Appropriate alternative modeling approaches are consistent with available data and current scientific knowledge, and appropriately consider their results and limitations, using tests and analyses that are sensitive to the processes modeled.

Acceptance Criteria from Section 2.2.1.1.3 (NRC 2003 [DIRS 163274]), System Description and Demonstration of Multiple Barriers

Acceptance Criterion 3: ***Technical Basis for Barrier Capability is Adequately Presented.***

The technical bases are consistent with the technical basis for the performance assessment. The technical basis for assertions of barrier capability is commensurate with the importance of each barrier's capability and associated uncertainties.

4.3 CODES, STANDARDS, AND REGULATIONS

No codes, standards, or regulations other than those identified in Section 4.1 were used in this model report.

5. ASSUMPTIONS

A list of the assumptions used in this model report is provided in Table 5-1. The rationale and confirmation status for each status assumption is also provided. The upstream assumptions associated with the rationale below do not impact the results of the model.

Table 5-1. Assumptions

No.	Assumption	Rationale	Location in this Report
1	Horizontal anisotropy in permeability, as it applies to the fractured and faulted volcanic units along the flowpaths, is adequately represented by a permeability tensor that is oriented in the north-south and east-west directions.	This assumption is introduced due to the difficulty to (1) establish with certainty the direction of horizontal anisotropy and to align the model axes along the principle axes or (2) build the model with a 9-component tensor. One analysis of the probable direction of horizontal anisotropy shows that the direction of maximum transmissivity is N 33°E (Winterle and La Femina 1999 [DIRS 129796], p. iii), indicating that the anisotropy applied on the SZ site-scale model grid is within approximately 30° of the inferred anisotropy.	Used throughout
2	The hydrogeologic properties, including permeabilities, for all units in the SZ site-scale flow model may be represented with homogeneous values. These properties are uniform within each stratigraphic unit.	This assumption is introduced due to the lack of information on the areal heterogeneity within the SZ. The flow model is designed to simulate the groundwater flow field at a scale of many kilometers. For simulating flow at that scale, effective flow parameters are generally acceptable. Thus, the use of homogeneous properties within a particular flow unit is acceptable. The calibration process provides “best fit” parameters for the SZ model. Where appropriate, additional zones or parameters are supplied to represent spatial differences in hydrogeology. These zones are justified in the sections in which they are used (see, for example, Sections 6.4.3.1 and 6.4.3.4).	Used throughout

DVRFS = Death Valley Regional Flow System; LA = license application; NTS = Nevada Test Site; SZ = saturated zone.

INTENTIONALLY LEFT BLANK

6. MODEL DISCUSSION

6.1 MODELING OBJECTIVES

The purpose of the SZ site-scale flow model is to describe the steady-state flow of groundwater as it moves from the water table below the repository, through the SZ, and to the accessible environment. The flow model estimates the SZ advective processes that control the movement of groundwater and dissolved radionuclides and colloidal particles that might be present.

The previous versions of the SZ site-scale flow model were developed in support of the TSPA-SR (CRWMS M&O 2000 [DIRS 153246]) and the TSPA-LA (BSC 2004 [DIRS 170037]). This model revision includes the following modifications to: (1) reflect the current understanding of SZ flow, (2) enhance model validation and uncertainty analyses, (3) improve locations and definitions of fault zones, (4) enhance grid resolution (500-m grid spacing to 250-m grid spacing), and (5) incorporate new data collected since the TSPA-SR:

- Implementation of the updated hydrogeologic framework model (HFM) that incorporates recent geologic data obtained from the Nye County Early Warning Drilling Program (DTN: MO0610MWDHFM06.002 [DIRS 179352]) and the 2004 DVRFS (Belcher 2004 [DIRS 173179])

- A potentiometric surface updated with water-level data from Phases III and IV of the NC-EWDP (Output DTN: MO0611SCALEFLW.000)

- Additional water-level calibration target data from Phases III and IV of the Nye County Early Warning Drilling Program (Output DTN: SN0702T0510106.007)

- Boundary volumetric/mass flow rates and recharge data from the 2004 DVRFS (Belcher 2004 [DIRS 173179]) and the 2003 UZ flow model (BSC 2004 [DIRS 169861])

- Use of field and laboratory tests (hydraulic and tracer data collected since TSPA-SR) to establish and confirm the conceptual model for flow, constrain model parameter calibration, and provide data for model validation and confidence building (SNL 2007 [DIRS 177394], Section 6).

This modeling analysis is a direct feed to *Site-Scale Saturated Zone Transport* (SNL 2007 [DIRS 177392]) because it provides the SZ flow fields for transport calculations.

6.2 FEATURES, EVENTS, AND PROCESSES CONSIDERED IN THE MODEL

As stipulated in *Technical Work Plan for: Saturated Zone Flow and Transport Modeling* (BSC 2006 [DIRS 177375]), this model report addresses the FEPs pertaining to SZ flow that are included (i.e., Included FEPs) for TSPA-LA listed in Table 6-1. SZ FEPs that were excluded (i.e., Excluded FEPs) for TSPA-LA are described in *Features, Events, and Processes for the Total System Performance Assessment* (SNL 2007 [DIRS 179476]). Table 6-1 provides a list of FEPs that are relevant to this model analysis in accordance with their assignment in the LA FEP list (DTN: MO0508SEPFEPLA.002 [DIRS 175064]). Specific reference to the various sections

within this document where issues related to each FEP are addressed is provided in Table 6-1. A detailed discussion of these FEPs as well as their implementation in TSPA-LA is documented in *Features, Events, and Processes for the Total System Performance Assessment* (SNL 2007 [DIRS 179476]).

Table 6-1. Features, Events, and Processes Included in TSPA-LA and Relevant to this Model Report

FEP No.	FEP Name	Sections Where Disposition is Described	Discussed in Supporting Documents
1.2.02.01.0A	Fractures	Sections 6.3.1.10, 6.4.3.7	Upstream Feeds[a] BSC 2004 [DIRS 170014] Corroborating[b] SNL 2007 [DIRS 177394]
1.2.02.02.0A	Faults	Sections 6.3.1.10, 6.4.3.7	Upstream Feeds[a] SNL 2007 [DIRS 174109] DTNs: GS010608312332.001 [DIRS 155307], GS010908314221.001 [DIRS 162874] Corroborating[b] BSC 2006 [DIRS 177394]
1.3.07.02.0A	Water table rise affects SZ	Section 6.6.4	Upstream Feeds[a] BSC 2006 [DIRS 177394]
2.2.03.01.0A	Stratigraphy	Sections 6.3.1.2, 6.4.3.1, 6.4.3.3, 6.4.3.10	Upstream Feeds[a] SNL 2007 [DIRS 174109]; Corroborating[b] BSC 2004 [DIRS 170014] BSC 2006 [DIRS 177394]
2.2.03.02.0A	Rock properties of host rock and other units	Sections 6.4.3.1, 6.4.3.3, 6.4.3.10	Upstream Feeds[a] SNL 2007 [DIRS 174109] Corroborating[b] BSC 2006 [DIRS 177394]
2.2.07.12.0A	Saturated groundwater flow in the geosphere	Sections 6.3.1.1, 6.4.1, 6.4.2; Figures 6-1; A-6.7.6, A-6.7.7, A-6.7.8, A-6.7.9, and A-6.7.11	Upstream Feeds[a] DTN: MO0507SPAINHFM.000 [DIRS 174523] Corroborating[b] BSC 2004 [DIRS 170014] BSC 2006 [DIRS 177394]
2.2.07.13.0A	Water-conducting features in the SZ	Sections 6.3.1.2, 6.4.3.7	Upstream Feeds[a] SNL 2007 [DIRS 174109] Corroborating[b] BSC 2004 [DIRS 170014] BSC 2006 DIRS 177394]
2.2.07.15.0A	Advection and dispersion in the SZ	Sections 6.4.1, 6.4.2	Upstream Feeds[a] DTN: MO0507SPAINHFM.000 [DIRS 174523] Corroborating[b] BSC 2006 [DIRS 177394]
2.2.10.03.0A	Natural geothermal effects on flow in the SZ	Sections 6.3.2 and 6.4.3.10	Upstream Feeds[a] SNL 2007 [DIRS 174109]
2.2.12.00.0B	Undetected features in the SZ	Section 6.3.2	Upstream Feeds[a] SNL 2007 [DIRS 174109]

[a] Aspects of the SZ FEPs screening position adopted in this report are a result of SZ analyses performed in a directly upstream SZ model or analyses. N/A indicates that there are no upstream feeds.

[b] Corroborating-SZ analysis or model report that indirectly supports the FEP topic.

FEP = features, events, and processes; SZ = saturated zone.

6.3 THE CONCEPTUAL MODEL

Yucca Mountain is located in the Great Basin about 150 km northwest of Las Vegas, Nevada. The mountain consists of a series of fault-bounded blocks of ash-flow and ash-fall tuffs and a smaller volume of lava deposited between 14 and 11 Ma (one million years (refers to age)) from a series of calderas located a few to several tens of kilometers to the north (Sawyer et al. 1994 [DIRS 100075]). Yucca Mountain itself extends southward from the Pinnacles Ridge toward the Amargosa Desert, where the tuffs thin and pinch out beneath the alluvium (Figure 6-1). The tuffs dip 5 to 10 degrees to the east over most of Yucca Mountain.

The Solitario Canyon Fault separates Yucca Mountain from Crater Flat, which is in the western portion of the model domain. Crater Flat is west of Yucca Mountain and separated from it by Solitario Canyon, which is the surface expression of the Solitario Canyon Fault—a steeply dipping scissors fault with down-to-the-west displacement of as much as 500 m in southern Yucca Mountain (Day et al. 1998 [DIRS 100027], pp. 6 to 7). Underlying Crater Flat are thick sequences of alluvia, lavas, and tuffs that have been locally cut by faults and volcanic dikes. East of Yucca Mountain, and separated from it by Fortymile Wash, is Jackass Flats, which is underlain by a thick sequence of alluvium and volcanic rocks. Timber Mountain, approximately 25 km to the north of the repository area, is a resurgent dome within the larger caldera complex when eruptions supplied the tuffs at Yucca Mountain.

The SZ site-scale flow model presented in this report describes our current state of knowledge of the saturated flow system. The boundaries of the numerical model for SZ flow and transport are indicated on Figure 6-1 in blue. The domain was selected to be: (1) coincident with grid cells of the DVRFS model (DTN: MO0602SPAMODAR.000 [DIRS 177371]) where site-scale model (FEHM) nodes correspond to regional model (MODFLOW-2000) cell corners in the horizontal plane; (2) sufficiently large to reduce the effects of boundary conditions on estimating permeabilities and calculated flow fields near Yucca Mountain; (3) sufficiently large to assess groundwater flow at distances beyond the 18-km compliance boundary from the repository area; (4) small enough to minimize the model size for computational efficiency and to include structural feature detail affecting flow; (5) thick enough to include part of the regional Paleozoic carbonate aquifer (the bottoms of the site- and regional-scale models are equal at −4,000 m below sea level); and (6) large enough to include borehole data from the Amargosa Desert at the southern end of the modeled area. The hydrogeologic setting of the SZ flow system in the vicinity of Yucca Mountain was summarized by Luckey et al. (1996 [DIRS 100465], p. 13). Yucca Mountain is part of the Alkali Flat-Furnace Creek sub-basin of the Death Valley groundwater basin (Waddell 1982 [DIRS 101062], pp. 15 to 16). Discharge within the sub-basin occurs at Alkali Flat (Franklin Lake Playa) and, possibly, Furnace Creek in Death Valley (Figure 6-1). Water inputs to the sub-basin include groundwater inflow/outflow along the northern, eastern, and western boundaries of the sub-basin, recharge from precipitation in high-elevation areas of the sub-basin, and recharge from surface runoff in Fortymile Canyon and Fortymile Wash. North and northeast of Yucca Mountain, recharge from precipitation also occurs at Timber Mountain, Pahute Mesa, Rainier Mesa, and Shoshone Mountain (Luckey et al. 1996 [DIRS 100465], p. 13).

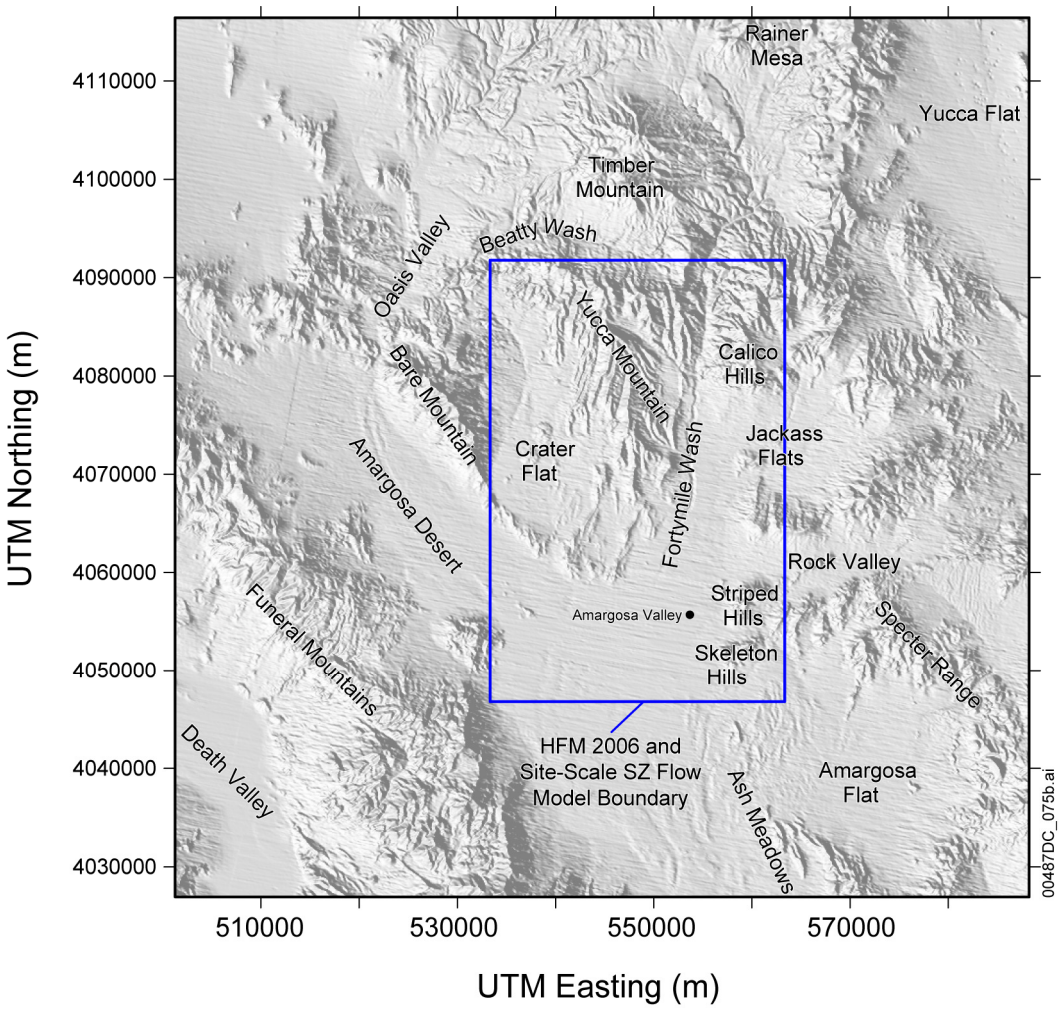

Source: DTN: GS010908314221.001 [DIRS 162874].

NOTE: The blue rectangle indicates the boundary of the SZ flow and transport models.

SZ = saturated zone; UTM = Universal Transverse Mercator.

Figure 6-1. Important Physiographic Features Near Yucca Mountain Including Some of Those Explicitly Included the SZ Site-Scale Flow Model

The general conceptual model of flow in the SZ site-scale flow model domain is that groundwater flows southerly from recharge areas of higher precipitation at higher elevations north of Yucca Mountain, through the Fortymile Wash and toward the Amargosa Desert (see Appendices A and B). Within the model domain, recharge occurs from infiltration of both precipitation and flood-flows through Fortymile Wash and its tributaries. In the southeastern part of the model area (within the Ash Meadows groundwater basin), considerable flows enter and exit the area through the lower carbonate aquifer system (BSC 2004 [DIRS 170015], Section 6.2). This aquifer system is believed to underlie much of the Alkali Flat-Furnace Creek groundwater basin based on inferences from Death Valley regional groundwater flow data (Belcher 2004 [DIRS 173179], Figure F-46). However, the flow patterns of groundwater in this area and their relationship to flow in the Ash Meadows groundwater basin system are poorly understood. Outflow from the SZ site-scale flow model area occurs primarily across the

southern boundary of the model. The constant head boundary condition applied to the southern boundary reflects head decreases from pumping by irrigation wells in the Amargosa Farms area. Although the irrigation wells are not explicitly modeled in the SZ site-scale model, the effects of this pumping are reflected in the lower heads of the southern boundary condition.

6.3.1 Key Features

Several important physiographic features are shown in Figure 6-2. Within the boundaries of the model domain, there are at least seven primary components that affect the local flow system and potential radionuclide transport:

- HFM and the faults
- Solitario Canyon Fault
- Recharge to SZ
- Crater Flat Tuff hydrogeologic units
- Shallow alluvial aquifer of Fortymile Wash
- Regional carbonate aquifer
- Large, moderate, and small hydraulic gradients.

The HFM (SNL 2007 [DIRS 174109]) is a conceptual model providing a three-dimensional interpretation of the hydrostratigraphic unit locations and the structure within the SZ site-scale flow and transport model domain. The HFM does not provide any hydraulic parameters; rather, it provides a conceptualization of hydrogeologic units that serves as the basis for calibrating hydraulic parameters. Faults are superimposed on the HFM as described in Sections 6.4.3.1 and 6.4.3.7.

The Solitario Canyon Fault is important because it could provide a vertical flowpath from the surface to the SZ. Depending on its conceptualization, it also acts as a barrier to flow that might otherwise travel from Crater Flat to Yucca Mountain.

Recharge to the SZ is important because it impacts transport time of radionuclides that could potentially escape from the repository. Flow through the lateral boundaries from the steady-state stress period of the 2004 DVRFS (Belcher 2004 [DIRS 173179]) supplies target boundary volumetric/mass flow rates for the site-scale model. Vertical recharge due to infiltration of rain and runoff at the land surface contributes to a small downward gradient below and around the repository.

The three Crater Flat tuffs are likely to be among the more permeable hydrogeologic units near the repository and, thus, are the most likely paths for potential radionuclide transport. Calibrated values of these three permeabilities will be representative of not only these units in the HFM, but also functions of the model formulation and contamination by cross correlations. A discussion of parameter and prediction uncertainties is presented in Section 6.7.

The shallow alluvial aquifer in Fortymile Wash is important because it bounds the likely flowpaths for fluid leaving the repository area and also has desirable retardation characteristics for many radionuclides.

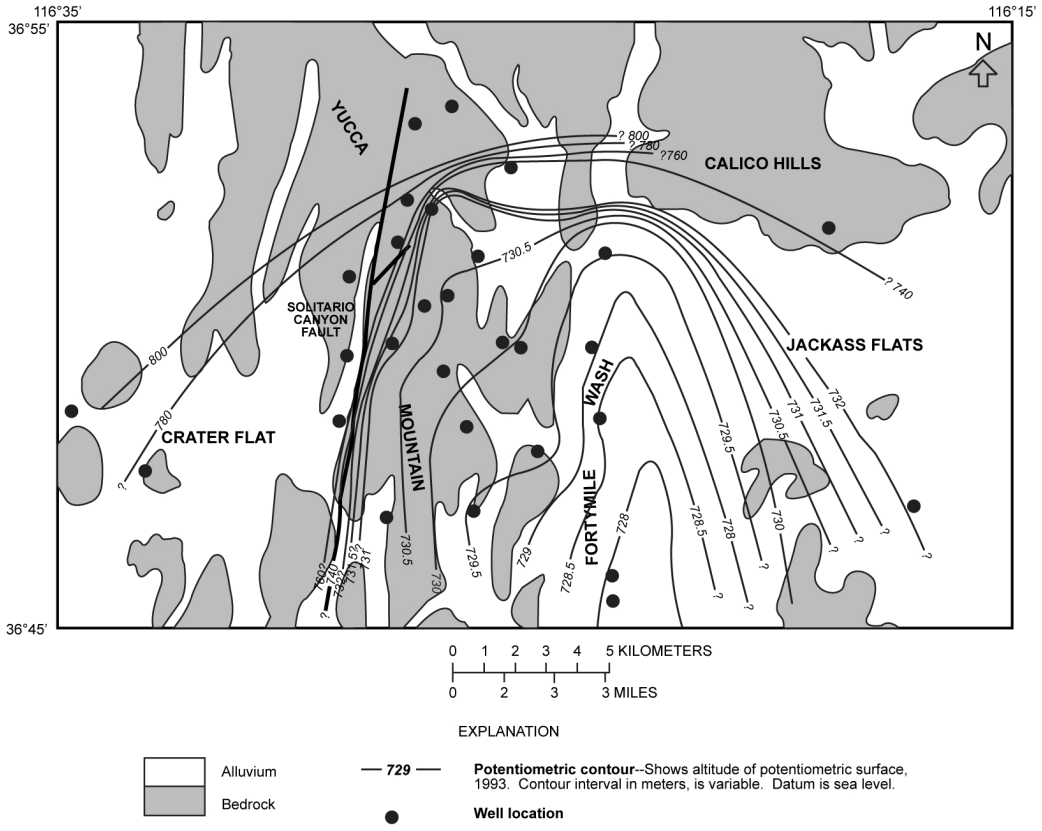

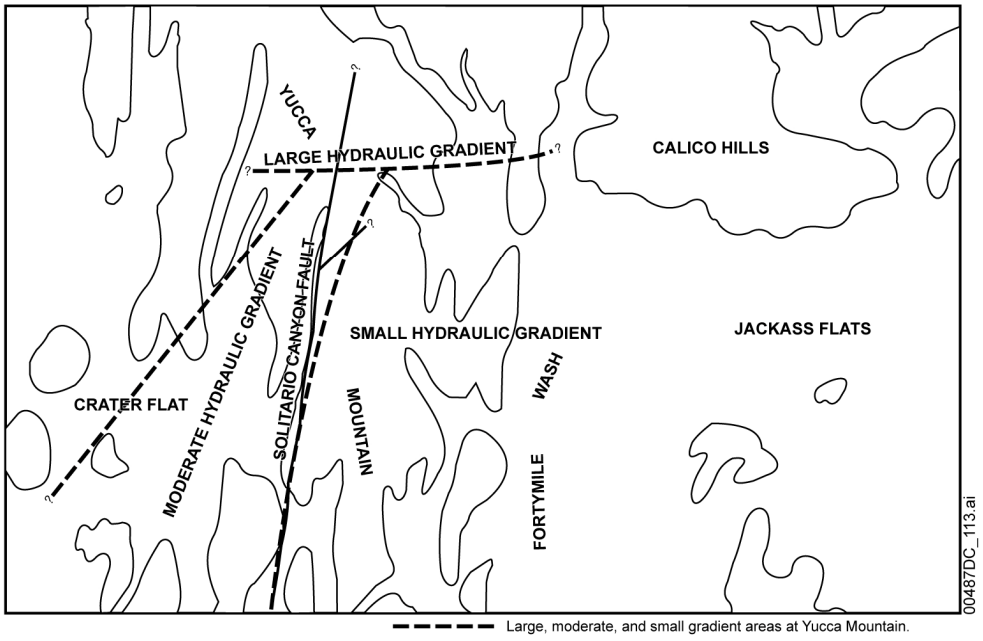

Source: Tucci and Burkhardt (1995 [DIRS 101060], Figures 2, 4, and 5).

NOTE: An updated potentiometric surface is developed in Appendix E.

Figure 6-2. Potentiometric Surface Map and Gradient Areas Developed Using Water-Level Data from 1993

The regional carbonate aquifer underlies the likely flowpaths for fluid leaving the repository area. This aquifer also provides an upward gradient that keeps the flowpaths shallow and effectively isolates the local Yucca Mountain system from the regional carbonate aquifer. Much of the flow through the model domain passes through the lower carbonate aquifer.

In Figure 6-2, the large, moderate, and small hydraulic gradients control the flow field below and downgradient from the repository. It is important to accurately represent these gradients to ensure consistency between model results and the inferred potentiometric surface.

Hydrochemical studies conducted at and near Yucca Mountain over the last 25 years are summarized in Appendices A and B. Appendix A summarizes data that were available up to approximately 2002, whereas Appendix B examines data that have come available since then. The appendices provide analyses of groundwater recharge rates, flow directions and velocities, and mixing proportions of water from different source areas based on geochemical and isotopic constraints. They also provide an evaluation of chemical reactions in the groundwater system, the evolution of groundwater as it moves along a flowpath, and groundwater-mixing relationships. The appendices also examine groundwater residence times based on ^{14}C ages. Appendix A evaluates water/rock interactions to provide a basis for ^{14}C age corrections. Appendix B presents a comparison of ^{14}C ages based on organic and inorganic carbon ages. The appendices provide a comparison of patterns of groundwater movement outlined by the SZ flow model with flow patterns inferred strictly from hydrochemical and isotopic data. In this way, the combined analyses documented in the appendices serve as an independent corroboration of the SZ site-scale flow model.

6.3.1.1 Groundwater Flow

As described by Luckey et al. (1996 [DIRS 100465], p. 17), the Tertiary volcanic section at Yucca Mountain consists of a series of ash flow and bedded ash fall tuffs that contain minor amounts of lava and flow breccia. Individual ash flow tuffs may be several hundred meters thick, whereas bedded ash fall tuffs generally are less than a few tens of meters thick. Ash flow tuffs range from nonwelded to densely welded, and the degree of welding varies both horizontally and vertically in a single flow unit. Nonwelded ash flow tuffs, when unaltered, have moderate to low matrix permeability but high porosity. Permeability is decreased by secondary alteration, and fractures are infrequent and often closed in the low-strength nonwelded tuffs. Consequently, these rocks generally constitute laterally extensive SZ confining units in the Yucca Mountain area. The properties of partly welded tuffs vary between those of fractured, welded tuffs and those of altered, nonwelded tuffs. The densely welded tuffs generally have minimal primary porosity and water-storage capacity, but they can be highly fractured. Where interconnected, fractures can easily transmit water, and highly fractured units function as aquifers. In general, the bedded ash fall tuffs have high primary porosity and can store large amounts of water. Their matrix permeability is moderate to low, depending on the degree of alteration. North of Yucca Mountain, the Claim Canyon caldera has altered the geologic units in the region yielding changes in their hydrogeologic properties. The bedded ash fall tuffs generally function as confining units, at least when compared to less porous but densely fractured ash flow tuffs. Lavas, flow breccias, and other minor rock types are neither thick nor widely distributed in the Yucca Mountain area. Their hydraulic properties probably are as variable as the properties of the ash flow tuffs, but the relatively limited spatial distribution of

these minor rock types makes them generally unimportant to the hydrogeology of Yucca Mountain.

Luckey et al. (1996 [DIRS 100465], p. 17) state that even fractured tuffs and lavas may not easily transmit water because lithostatic loading keeps the fractures closed. In addition, where volcanic glass has been partly replaced by zeolites and clays, particularly in the originally glassy nonwelded tuffs, these secondary minerals substantially decrease permeability and slow groundwater flow through the rock. The degree of alteration can affect the water-transmitting characteristics of the volcanic sequence. Alteration, particularly in the Calico Hills Formation, increases toward the north of Yucca Mountain and probably accounts for the apparent decrease in hydraulic conductivity to the north. Alteration also tends to increase with depth and is pervasive below the Calico Hills Formation.

Fractures vary in length, orientation, connectivity, aperture width, and amounts and types of coatings, all of which may affect flow. The physical parameters of fractures are characterized by outcrop mapping, borehole logging, and mapping in the Exploratory Studies Facility. In the UZ, water seeps were not observed during outcrop mapping or during mapping in the Exploratory Studies Facility.

Fractures at Yucca Mountain originated as a result of initial cooling of the volcanic deposits and later as a result of tectonic activity. For example, in the Tiva Canyon welded hydrologic unit, two sets of vertically-oriented cooling fractures were observed dipping nearly vertically and striking toward the northwest and northeast. A third set of tectonic joints commonly abuts the cooling joints, and these three sets of joints form an orthogonal, three-dimensional network. An extensive discussion of fractures in the Yucca Mountain area is presented in *Yucca Mountain Site Description* (BSC 2004 [DIRS 169734], Section 3.5).

Fracture aperture characteristics are poorly known from direct observation, and for modeling, reliance is placed on indirect effects such as changes in permeability. In general, the stress due to overburden loading across high-angle fractures will be less than across low-angle fractures, resulting in higher vertical than horizontal permeability. Stratification effects will also be present in many units. This will tend to have the opposite effect; that is, the horizontal permeability will be larger than the vertical permeability.

The volcanic rocks consist of alternating layers of welded and nonwelded ash flow and ash fall (bedded) tuff deposits. Each of the ash flow units is underlain by an associated bedded tuff layer. The ash flow units vary in degree of welding (or recrystallization). Maximum welding is generally found near the center of the ash flow, where heat was retained the longest, and the degree of welding decreases upward and downward toward the ash flow boundaries.

The welded units typically have low matrix porosities and high fracture densities, whereas the nonwelded and ash fall units have relatively higher matrix porosities and lower fracture densities. The fracture density correlates to the degree of welding of the volcanic rocks.

Where glassy tuff has been saturated for long periods (e.g., beneath the water table), the original glassy material generally has been altered to zeolite or clay minerals. Such alteration does not affect porosity greatly because pore spaces are not filled, but the permeability of the rocks is

greatly reduced by alteration of the connectivity between the pore spaces. Alteration of silica to zeolites or clay minerals is not an important factor in densely welded zones because cooling fractures dominate permeability.

The SZ flow system to the south of Yucca Mountain transitions from a fractured tuff aquifer to a valley-fill (alluvium) aquifer before reaching the approximately 18-km performance compliance boundary at the southern boundary of the Nevada Test Site (NTS). Underlying Crater Flat is a thick sequence of alluvium, lavas, and tuffs that have been locally cut by faults and volcanic dikes. East of Yucca Mountain, and separated from it by Fortymile Wash, is Jackass Flats, which is underlain by a thick sequence of alluvium and volcanic rocks. Characterization of the valley-fill system was conducted just outside the southwest corner of NTS at the Alluvial Testing Complex (ATC), which is the site of Nye County Early Warning Drilling Program (NC-EWDP) well NC-EWDP-19D, and at NC-EWDP-22S, which is about 4.5 km north–northeast of the ATC. Single- and cross-well tracer tests were conducted in these wells and tests indicated producing zones with permeabilities consistent with other alluvial systems (3 to 20×10^{-12} m^2) interbedded with lower permeability (0.1×10^{-12} m^2) clay-rich zones (SNL 2007 [DIRS 177394], Sections 6.4.5 and F7). In addition to flow in the volcanic rocks and alluvium in the SZ, a significant portion of the groundwater flows through the lower carbonate aquifer.

In general, it is believed that the matrix porosity of the ancient marine limestones and dolomites of the lower carbonate aquifer is negligible (Winograd and Thordarson 1975 [DIRS 101167], p. C14), and that the large discharge from that aquifer system at Ash Meadows is due to flow through solution-enlarged fractures and along faults (Dudley and Larson 1976 [DIRS 103415], pp. 5 and 9). Borehole UE-25 p#1 penetrates the lower carbonate aquifer near Yucca Mountain. Another deep well, NC-EWDP-2DB was completed in the carbonate aquifer as part of the NC-EWDP. These deep wells helped improve the understanding of hydrologic conditions in the aquifers, including the deep carbonate aquifer, and helped to confirm the direction and magnitude of groundwater flow in that aquifer. Significant upward gradients were observed in wells UE-25 p#1 and NC-EWDP-2DB (BSC 2004 [DIRS 170009], Table 6-4).

6.3.1.2 Hydrologic Features

HFM2006 represents the distribution of geologic units within the SZ site-scale flow model (SNL 2007 [DIRS 174109], Section 6.4). Faults and other hydrogeologic features (Figure 6-3) such as zones of alteration that affect SZ flow were also included. Locations of faults come from fault trace maps that are derived from data collected during borehole drilling as well as locations where the faults intersect the land surface. Faults in the model area dip at various angles, but most are high-angle faults. Faults believed important to flow near Yucca Mountain are modeled explicitly. Given the large uncertainties in their orientations, faults were simply treated as vertical features. Section 6.4.3.1 discusses how these features were constructed in the HFM. Figure 6-3 illustrates many observed faults in the Yucca Mountain region, but not all of these were explicitly included in the model.

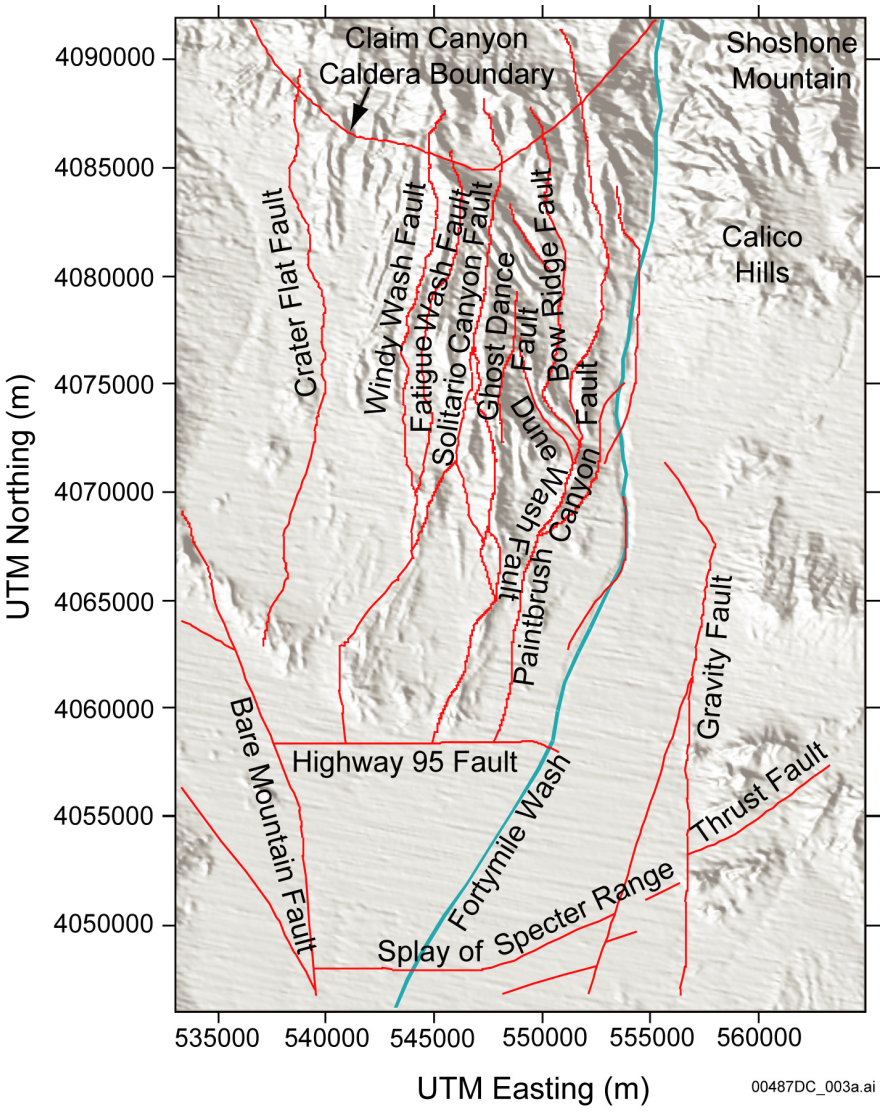

Source: DTN: GS010908314221.001 [DIRS 162874] (faults).

NOTE: The geographic coordinates of the different geologic features are the result of interpretation of the geologic map, including geologic cross sections, and lithostratigraphic and structural data from boreholes as described in *Hydrogeologic Framework Model for the Saturated Zone Site Scale Flow and Transport Model* (SNL 2007 [DIRS 174109]). The conversion of the geographic coordinates was done using standard Geographic System Information (GIS) functions. Here, the location of the U.S. Highway 95 Fault was modified based on a subsequent USGS interpretation (DTN: GS010908314221.001 [DIRS 162874]).

UTM = Universal Transverse Mercator.

Figure 6-3. Location of Faults in the Yucca Mountain Region

6.3.1.3 Flow Field

Using the potentiometric surface map (Figure 6-4 and Appendix E) the general direction of groundwater flow within the SZ site-scale flow and transport model domain for the horizontally isotropic case is from north to south. That is, the direction of flow is generally perpendicular to the water–level contours (anisotropic media may have flowpaths in directions non-orthogonal to the water-level contours). Based on the interpretation of the water–level data, the water table

exhibits a steep gradient throughout the northern part of the model area (north of the repository) and the contours curve southward to the west of Crater Flat (see Appendix E).

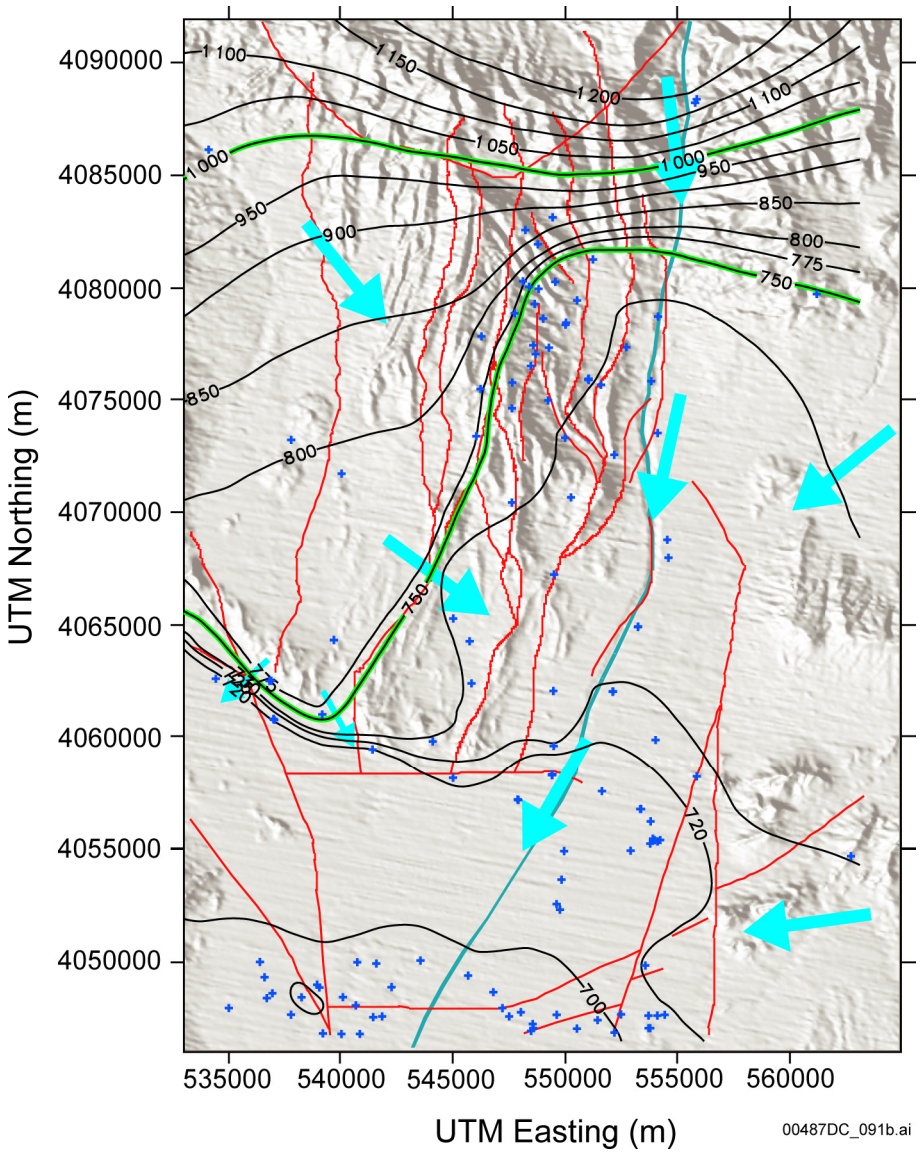

Source: DTN: GS010908314221.001 [DIRS 162874] (Faults)

Output DTN: MO0611SCALEFLW.000 (Water-level contours from Appendix E).

NOTE: The inferred groundwater flow directions are based on Assumption 1 in Appendix A (see Table A5-1). The red lines are selected faults; blue crosses indicated the location of hydraulic head measurements. The potentiometric surface is in black and inferred flow directions are indicated with blue arrows.

UTM = Universal Transverse Mercator.

Figure 6-4. Potentiometric Surface and Inferred Flow Directions

Several faults are interpreted as barriers to groundwater flow based on field data near the Solitario Canyon Fault, west of the repository, which demonstrates a differential of about 45 m (148 ft) in the potentiometric surface (Figure 6-4). In Crater Flat and on the southern part of

Yucca Mountain, flow is directed nearly easterly toward Fortymile Wash. A more-detailed water-level map of the immediate vicinity of Yucca Mountain (Figure 6-2) indicates that flows from the west and east converge at Fortymile Wash and turn southward toward the Amargosa Desert. The cause of the easterly gradient in Crater Flat and southern Yucca Mountain may be the U.S. Highway 95 Fault that acts as a groundwater barrier near the northern margin of the Amargosa Desert. Figure 6-2 is a water-level map using 1993 data, but newer data do not contradict any part of this discussion (see derivation of the potentiometric surface in Appendix E).

As discussed in Section 6.3.2.5, the potentiometric level in well UE-25 p#1, which penetrates the lower carbonate aquifer, is about 752 m (2,467 ft), 21 m (69 ft) higher than in nearby wells. This result indicates a potential for upward flow from the lower carbonate aquifer; however, other lines of evidence suggest that such flow is small. The direction of flow and hydraulic gradient cannot be determined from a single well; however, regional relationships suggest that the general direction of flow in the lower carbonate aquifer should be southerly to southeasterly in the SZ site-scale flow model domain (NRC 1998 [DIRS 107770], p. 109). South of the model domain, there is geochemical evidence for a westward component of flow in the carbonate aquifer (Appendix B, Figure B6-15).

Most monitoring wells in the Yucca Mountain area show little variation in water level over time (Luckey et al. 1996 [DIRS 100465], p. 29). In contrast, water levels in the heavily pumped Amargosa Farms area have declined substantially since intensive irrigation development began in the 1950s. Kilroy (1991 [DIRS 103010], p. 18) reported a water level decline of as much as 9 m (30 ft) by 1987, and La Camera and Locke (1997 [DIRS 103011], Figure 4) show an additional decline of about 3.4 m (11 ft) through 1996 at well AD-5, about 14 km (8.7 mi) southwest of the Amargosa Valley.

6.3.1.4 Large, Moderate, and Small Hydraulic Gradients

Three regions of distinct hydraulic gradients of the potentiometric surface at Yucca Mountain (Figure 6-4) are recognized: (1) a large hydraulic gradient (LHG) of 0.13 between water-level altitudes of 1,030 m (3,380 ft) and 750 m (2,460 ft) to the north of Yucca Mountain, (2) a moderate hydraulic gradient of 0.05 west of the crest of Yucca Mountain, and (3) a small hydraulic gradient of 0.0001 to 0.0003 extending from the Solitario Canyon Fault to Fortymile Wash. These gradients are evident on detailed potentiometric surface maps presented by Ervin et al. (1994 [DIRS 100633]), Tucci and Burkhardt (1995 [DIRS 101060]), as well as on the maps with large contour intervals compiled by D'Agnese et al. (1997 [DIRS 100131]). The large contour-interval maps do not portray the small or moderate gradients adequately because of limitations imposed by contour intervals; however, the large gradient is recognizable on all of these maps.

Luckey et al. (1996 [DIRS 100465]) present detailed descriptions of these gradient features and discuss interpretations of their causes. The LHG has been the subject of numerous theories and could be the result of the Claim Canyon caldera and its associated alteration of hydrogeologic properties. Permeability changes in similar environments have been studied by economic geologists (Norton and Knapp 1977 [DIRS 147379]). The LHG is discussed by Luckey et al. (1996 [DIRS 100465], pp. 21 to 25) and their theories regarding its genesis are summarized here:

- The gradient is the result of flow through the upper volcanic confining unit, which is nearly 298-m (984-ft) thick near the large gradient. This large thickness of low-permeability material creates a barrier to flow that causes water to back up behind it, increasing hydraulic head to the north, and leading to the large gradient.

- The gradient represents a semi-perched system where flow in the upper and lower aquifers is predominantly horizontal, while flow in the upper confining unit would be predominantly vertical. In this scenario, the large hydraulic gradient is a manifestation of water leaking out of the upper aquifer, through the confining unit, and into the lower aquifer. Farther south, water has drained out of the perched aquifer and now only the lower heads of the deeper aquifer are measured. The difference in heads between the northern-perched water levels and the southern deeper aquifer levels is manifested as a large gradient.

- The gradient represents a drain down a buried fault from the volcanic aquifers to the lower carbonate aquifer. In this case water levels drop quickly as the feature is approached from the north much in the same way water levels drop into the cone of depression caused by a pumping well. In this case, the feature is linear; the result is a region of steep hydraulic gradient rather than a cone of depression around a single well.

- The gradient represents a spillway in which a fault marks the effective northern limit of the lower volcanic aquifer. In this scenario, water flows more readily in the lower volcanic aquifer, which is located south of the LHG. This effectively "drains off" the high hydraulic heads and establishes a lower water level. North of this location, the lower permeabilities create a barrier to flow that maintains high water levels.

- The large gradient results from the presence at depth of the Eleana formation, a part of the Paleozoic upper confining unit, which overlies the lower carbonate aquifer in much of the Death Valley region. The Eleana formation is absent at borehole UE-25 p#1 at Yucca Mountain, which penetrated the lower carbonate aquifer directly beneath the lower volcanic confining unit.

It is important to accurately represent the LHG in the numerical model and to understand how it affects estimates of groundwater specific discharge and flowpaths from below the repository. To model the LHG, the concept of a hydrogeologically altered portion of the model domain representing the Claim Canyon caldera complex is introduced (see Section 6.3.1.11). It is explicitly included in the SZ site-scale model construction as a zone of altered (decreased) permeability. Because the LHG occurs north of Yucca Mountain, changes in the model's simulated pathlines from the repository due to the LHG conceptualization (so long as it is represented in some form) are minimal as long as the gradients downstream of Yucca Mountain are modeled accurately.

The cause of the moderate hydraulic gradient is better understood than that of the LHG, and Luckey et al. (1996 [DIRS 100465], p. 25) suggest that the Solitario Canyon Fault and its splays function as a barrier to flow from west to east due to the presence of low-permeability fault gouge or to the juxtaposition of more permeable units against less permeable units.

The small hydraulic gradient occupies most of the repository area and the downgradient area eastward to Fortymile Wash. Over a distance of 6 km (3.7 mi) between the crest of Yucca Mountain and Fortymile Wash, the hydraulic head declines only about 2.5 m (8.2 ft). The small gradient could indicate highly transmissive rocks, little groundwater flow in this area, or a combination of both (Luckey et al. 1996 [DIRS 100465], p. 27).

The potentiometric map (Appendix E), which includes head data from the recently drilled NC-EWDP boreholes, indicates that the small hydraulic gradient extends southward to U.S. Highway 95.

6.3.1.5 Vertical Gradients

Information on vertical hydraulic gradients in the SZ is available from NC-EWDP wells (BSC 2004 [DIRS 170009]) and from *Ground-Water Conditions in Amargosa Desert, Nevada-California, 1952-87* (Kilroy 1991 [DIRS 103010]) for wells in the Amargosa Desert. The following discussion of vertical gradients is based on the work by Luckey et al. (1996 [DIRS 100465], pp. 27 to 29) and *Water-Level Data Analysis for the Saturated Zone Site-Scale Flow and Transport Model* (BSC 2004 [DIRS 170009], Sections 6.3.2 and 7.1.1).

Water-Level Data Analysis for the Saturated Zone Site-Scale Flow and Transport Model (BSC 2004 [DIRS 170009], Section 6.3.2) reports on potentiometric level measurements in multiple depth intervals in 17 boreholes at Yucca Mountain. Differences in potentiometric levels at different depth intervals in the same borehole ranged from as little as 0.10 m (0.33 ft) in borehole USW H-4 to as much as 54.7 m (179.5 ft) in USW H-1 (BSC 2004 [DIRS 170009], Table 6-4). Downward gradients were also observed with a maximum head difference of −38 m (125 ft) at NC-EWDP-1DX. Aside from well NC-EWDP-1DX located along U.S. Highway 95 south of Crater Flat, the largest head differences were between the lower carbonate aquifer or the adjoining lowermost lower volcanic confining unit and the overlying lower volcanic aquifer. Between the upper part of the lower volcanic confining unit and the lower volcanic aquifer the differences in potentiometric levels generally were 1 m (3 ft) or less.

Some potentiometric levels were higher in the lower intervals of the volcanic rocks than in the upper intervals, indicating a potential for upward groundwater movement. Of 17 wells with the ability to measure a vertical gradient, six showed a significant (> 5 m [16.4 ft]) upward gradient (USW H-1, USW H-3, UE-25 p#1, NC-EWDP-2D/-2DB, NC-EWDP-4PA/-4PB, and NC-EWDP-19P/-19D), six showed essentially no (< 2 m [6.6 ft]) head differences between uppermost and lowermost monitored intervals (USW H-4, USW H-5, USW H-6, UE-25 c#3, NC-EWDP-9SX, and NC-EWDP-12PA/-12PB/-12PC), and five showed a downward gradient (UE-25 b#1, USW G-4, UE-25 J-13, NC-EWDP-1DX, NC-EWDP-3S/3D). Overall, it appears that there is a notable upward vertical gradient between the lower and upper volcanic aquifer at locations nearest Yucca Mountain (USW H-1, USW H-3, and UE-25 p#1). Away from Yucca Mountain the direction of the vertical hydraulic gradient varies from location to location. For example, at locations UE-25 J-13, NC-EWDP-1DX, and NC-EWDP-3S, there is a downward gradient in the upper portion of the volcanic units. For wells in the lower Fortymile Wash, such as NC-EWDP-2D/2DB, NC-EWDP-4PA/-4PB, NC-EWDP-9SX (probes 1 and 2), NC-EWDP-12PA/-12PB, and NC-EWDP-19P/-19D, the gradients are slightly to moderately upward.

Potentiometric levels in the Paleozoic carbonate aquifer in borehole UE-25 p#1 are about 752 m (2,467 ft), or about 21.4 m (70.2 ft) higher than levels in the overlying lower volcanic aquifer. The potentiometric levels in the Paleozoic carbonate aquifer in borehole NC-EWDP-2DB is about 7.2 m (23.6 ft) higher than the overlying volcanic unit at NC-EWDP-2D. These data indicate a potential for upward groundwater movement from the Paleozoic rocks to the volcanic rocks. Because of the large difference in potentiometric levels in these two aquifers, they seem to be hydraulically separated (Luckey et al. 1996 [DIRS 100465], p. 28). Testing at the C-wells complex in 1984 suggested a hydraulic connection between the lower volcanic aquifer and the carbonate aquifer; however, testing in 1995 and 1996, using more-reliable water-level measurement equipment did not confirm the hydraulic connection (Luckey et al. 1996 [DIRS 100465], p. 28).

In borehole UE-25 p#1, the lowermost 70 m (230 ft) of the older tuffs (lower volcanic confining unit) had potentiometric levels similar to those in the carbonate aquifer, indicating a hydraulic connection between the lowermost part of the lower volcanic confining unit and the carbonate aquifer. Such a connection could be expected in the hanging-wall rocks adjacent to a fault; and, this type of connection is supported by calcification of the basal tuffs in the borehole. The remaining 237 m (778 ft) of the lower volcanic confining unit had a potentiometric level similar to that of the lower volcanic aquifer (Luckey et al. 1996 [DIRS 100465], p. 28). The upward hydraulic gradient observed in wells NC-EWDP-2D/-2DB supports the conceptual model that water levels in the carbonate aquifer are higher than in the overlying volcanic units in portions of the SZ site-scale flow model domain (BSC 2004 [DIRS 170009], Section 7.1.1).

No obvious spatial patterns in the distribution of vertical hydraulic gradients around Yucca Mountain are apparent; however, some generalizations can be made as to the distribution of potentiometric levels in the lower sections of the volcanic rocks. Potentiometric levels in the lower volcanic confining unit are relatively high (altitude greater than 750 m [2,477 ft]) in the western and northern parts of Yucca Mountain and are relatively low (altitude about 730 m [2,411 ft]) in the eastern part of Yucca Mountain. Based on potentiometric levels that were measured in borehole UE-25 p#1 and NC-EWDP-2D/-2DB, the potentiometric levels in the lower volcanic confining unit in boreholes USW H-1, USW H-3, USW H-5 and USW H-6 may reflect the potentiometric level in the carbonate aquifer. Boreholes UE-25 b#1 and USW G-4 do not seem to fit the pattern established by the other boreholes. These two boreholes penetrated only 31 m (102 ft) and 64 m (210 ft), respectively, into the lower volcanic confining unit and had potentiometric levels (about 730 m [2,395 ft]) that were similar to potentiometric levels in the lower volcanic aquifer. Penetration of the other four boreholes into the lower volcanic confining unit ranged from 123 m (403 ft) in borehole USW H-3 to 726 m (2,382 ft) in borehole USW H-1. In boreholes USW H-1, USW H-3, USW H-5, and USW H-6, the potentiometric levels in the lower volcanic confining unit are influenced by the potentiometric level in the carbonate aquifer (Luckey et al. 1996 [DIRS 100465], p. 29). *Water-Level Data Analysis for the Saturated Zone Site-Scale Flow and Transport Model* (BSC 2004 [DIRS 170009], Section 6.3.2) notes that the water levels measured in USW UZ-14 and USW H-5 are somewhat anomalous and are likely due to features or processes not included in this flow model. Such interpretations are bases for limiting the impact of these data on model results by reducing their importance during calibration (see Section 6.5.1.2).

At several wells, including USW H-1 and USW H-6, small hydraulic gradient reversals at several depths are observed (BSC 2004 [DIRS 170009], Table 6-4). These small reversals may be explained by small-scale heterogeneities in the hydrostratigraphic units or measurement errors (BSC 2004 [DIRS 170009], Section 6.3.2). The confidence in the vertical hydraulic head differences is greatest for the locations with the largest hydraulic head differences.

Vertical hydraulic gradients could have an important impact on the analysis of the effectiveness of the SZ as a barrier to radionuclide transport in that they keep the flowpath from the repository in the shallow groundwater. Based on available data, a spatially extensive upward gradient can be inferred between the carbonate aquifer and the volcanic aquifers, which indicates that, at least for the immediate Yucca Mountain area, radionuclide transport would be restricted to the volcanic system (BSC 2004 [DIRS 170009], Section 7.1.1). Insufficient data are available to specify an upward gradient in the constant-head boundaries.

Kilroy (1991 [DIRS 103010], pp. 11 to 16, Table 3) presents vertical gradient data for 21 nested piezometers, one well cluster, and one river and well pair in the Amargosa Desert area. However, none of these locations is within the area of the SZ site-scale model domain. Upward gradients generally were associated with freshwater limestones, carbonate rock outcrops, and structural features (Kilroy 1991 [DIRS 103010], p. 16). The association with carbonate rocks is attributed to a hydraulic connection with the carbonate aquifer regional flow system and, especially, to the Spotted Range-Mine Mountain fault zone, which is a conduit for flow from the carbonate aquifer to the basin fill.

6.3.1.6 Lateral Boundary Conditions

The constant head boundary conditions used in the SZ site-scale flow model are derived from hydraulic heads extracted from the potentiometric surface (Appendix E). The data are used to form fixed-head boundary conditions on the lateral sides of the model that may vary horizontally along the boundaries, but not in the vertical direction. Constant vertical head yields no vertical flows at the boundaries. These boundary conditions contrast with the observed upward gradient in the area near well UE-25 p#1, which is near the center of the model domain. Nevertheless, upward gradients can be obtained away from the boundaries despite the applied boundary conditions. This is because permeability differences between the hydrogeologic units propagate the high head in the north of the model through the higher permeability carbonate rocks farther into the model interior than the lower permeability volcanic confining unit overlaying the carbonate rocks. Furthermore, conceptually, the high heads in the northern thermally altered region may propagate increased pressures through the regional lower carbonate aquifer that subsequently provides an upward gradient in the southern, low-head portion of the model domain overlain by confining volcanic units. Overall, there are insufficient data (see Section 6.3.2.5) to specify a vertical gradient in constant head boundary conditions (only six of the 17 wells with vertical gradient measurements showed a significant upward gradient).

Of special note is the southern boundary of the model, which is near a large number of wells in the Amargosa Valley. Near the southern boundary, numerous measurements have been taken over the last 100 years. Some of the earlier measurements represent predevelopment states, while later measurements reflect changes in water levels due to pumping. The boundary conditions represent water levels affected by pumping and are described by *Recharge and*

Lateral Groundwater Flow Boundary Conditions for the Saturated Zone Site-Scale Flow and Transport Model (BSC 2004 [DIRS 170015], Sections 6.5 and 6.7).

Most of the inflows to, and outflows from, the SZ site-scale flow model occur as groundwater flows across the lateral boundaries. The best estimates of flow rates are the cell-by-cell fluxes calculated by the 2004 DVRFS (Belcher 2004 [DIRS 173179]; see also Appendix C). Fluxes from the steady-state stress period were used during the calibration of the SZ site-scale flow model as targets. These fluxes provide some consistency with the regional-scale flow model, which is based on a regional mass balance and calibrated to spring flow data. There are differences between the regional- and site-scale flow models due to notable differences in their conceptual models including the use of different grid resolutions and methods to simulate flow. Thus, it was necessary to average the fluxes over many grid blocks on each side of the model. Output from the regional flow model is linked to the SZ site-scale flow model during calibration. Volumetric/mass flow rates derived from the regional flow model are provided as calibration targets during SZ site-scale flow model calibration in much the same way that water levels are used for targets. Data from the regional model are qualified for use in this report (Appendix C). Because of the differences in the two models, only general agreement on volumetric/mass flow rates between the two models is expected, and obtained.

Consistent with the regional flow model, the bottom boundary condition of the SZ site-scale flow model has zero-flux specified. Direct evapotranspiration from the water table is not considered in this analysis because depth to water is too great for this process to be important. The top boundary condition was a specified flux recharge map described in Section 6.3.1.7, portions of which are derived from the regional model, the UZ model, and streamflow studies along Fortymile Wash. Because the flow model is a steady-state model, there are no boundary condition temporal variation requirements.

6.3.1.7 Recharge

The recharge to the flow model was derived from three sources: regional-scale SZ model (Belcher 2004 [DIRS 173179]), the 2003 UZ flow model (BSC 2004 [DIRS 169861]), and Fortymile Wash data (Savard 1998 [DIRS 102213]), see Section 6.4.3.9. Recharge from the UZ site-scale model (percolation flux) was taken as the flow through the base of that model, the domain of which includes approximately 40 km^2 (19.3 mi^2) that defines the footprint of Yucca Mountain, but is only a small fraction of the SZ model domain. The UZ flow model uses dual permeability, and accordingly, the output includes volumetric/mass flow rates for fracture and matrix flow. These data are combined into a total volumetric flow rate and an average percolation flux (BSC 2004 [DIRS 170015], Table 6-4 and Figure 6-4).

The technique for estimating recharge from all three sources is detailed in *Recharge and Lateral Groundwater Flow Boundary Conditions for the Saturated Zone Site-Scale Flow and Transport Model* (BSC 2004 [DIRS 170015], Figure 6-8 and Section 6.2.4), but is summarized here:

- The distributed vertical recharge, primarily in the northernmost portion of the SZ site-scale flow model domain, was extracted from the 2004 SZ regional-scale flow model (DTN: MO0602SPAMODAR.000 [DIRS 177371]). No recharge within the UZ

flow model area was included from the regional flow model because this was accounted for separately as percolation through the unsaturated zone by the UZ model (see below).

- The recharge through each node of the UZ flow model is extracted and the corresponding recharge to the SZ site-scale flow model node was calculated (the UZ flow model grid is finer than the SZ site-scale grid).

- Estimates of recharge from the infiltration of surface flows in Fortymile Wash are given by linear reaches (discrete segments) along the wash. Recharge estimates were interpolated to at least a 500-m (1,640-ft) -wide recharge zone for most of the wash and a broader area of distributary channels in the Amargosa Desert (BSC 2004 [DIRS 170015], Table 6-3, Figure 6-6).

6.3.1.8 Discharge

There is no measurable natural discharge (i.e., springs or evapotranspiration within the SZ site-scale flow model domain); therefore, natural discharge to the surface is not considered.

6.3.1.9 Heterogeneity

Physical and chemical heterogeneity of the rocks and water in the SZ can affect groundwater flow and the transport of contaminants in the SZ. The principal forms of heterogeneity in the SZ site-scale model domain are physical and may be primary (i.e., related to the formation of the rocks) or secondary (i.e., related to events subsequent to their formation).

The most obvious form of primary heterogeneity is the mode of origin (i.e., volcanic rocks, clastic rocks, carbonate rocks, and alluvial deposits), which is the primary basis for subdividing the rocks into hydrogeologic units. Within each major category, further subdivisions are possible. Probably the major form of primary heterogeneity affecting groundwater flow in the SZ site-scale model domain results from the origin of the volcanic rocks (i.e., ash flow or air fall pyroclastic deposits, lava flows, and volcanic breccias). The pyroclastic rocks (termed tuffs) are primarily nonwelded to densely welded, vitric to devitrified ash flow deposits separated by nonwelded vitric air fall deposits. Thus, primary physical heterogeneity relates to whether the deposits resulted from massive eruptions of hot volcanic ash from volcanic centers that moved downslope, or whether they resulted from explosive eruptions that injected volcanic fragments into the air to fall out as bedded ash fall tuffs.

The thicker flow deposits, up to several hundred meters thick, were very hot, resulting in welding of the fragments into a dense mass. Thinner flows retained heat less effectively, resulting in partly welded to nonwelded ash flow tuffs. Ash fall tuffs, generally less than tens of meters thick, are cooled in the atmosphere and characteristically glassy (vitric) (Luckey et al. 1996 [DIRS 100465], p. 17).

The mode of origin controls the porosity and permeability of the volcanic rocks. The densely welded tuffs generally have minimal primary porosity and water-storage capacity, but commonly are highly fractured and function as aquifers (Luckey et al. 1996 [DIRS 100465], p. 17). Nonwelded ash flow tuffs, when unaltered, have moderate to low matrix permeability but high

porosity, and commonly constitute confining units. Ash fall tuffs have high primary porosity and moderate to low permeability, and they generally act as confining units.

As the tuff deposits cooled, they were subjected to secondary processes, including formation of cooling fractures, recrystallization or devitrification, and alteration of the initial glassy fragments to zeolite minerals and clay minerals, all of which affect the hydrologic properties of the rocks. Beginning with deposition and throughout their subsequent history, the rocks have been subjected to tectonic forces resulting in further fracturing and faulting. They also have been subject to changes in the position of the water table, which greatly affects the degree of alteration of the initially glassy deposits.

The forms of secondary heterogeneity most affecting the SZ are fracturing, faulting, and alteration of glassy materials to zeolites and clay minerals. Fractures, where interconnected, transmit water readily and account for the permeable character of the welded tuffs. Cooling fractures, which are pervasive in welded tuffs, tend to be strata-bound and confined to welded portions of flows, whereas tectonic fractures tend to cut through stratigraphic units, as do faults.

Nonwelded deposits are less subject to fracturing and more subject to alteration of the initial glassy deposits to zeolites and clay minerals, both of which reduce permeability. The presence of perched-water bodies in the UZ is attributed to the ubiquitous presence of a smectite-zeolite interval at the base of the Topopah Spring tuff, which, in the absence of through-going fractures, essentially stops the vertical movement of water (Luckey et al. 1996 [DIRS 100465], p. 46).

The heterogeneity in permeability of different types of deposits led to the subdivision of the Yucca Mountain geologic section into five basic SZ hydrologic units: upper volcanic aquifer, upper volcanic confining unit, lower volcanic aquifer, lower volcanic confining unit, and lower carbonate aquifer. To accommodate the more extensive area of the SZ flow model, HFM2006 (SNL 2007 [DIRS 174109], Table 6-5) includes 22 additional units above and below these basic five units. Near Yucca Mountain, volcanic deposits generally form laterally extensive stratigraphic units; however, due to physical heterogeneity, porosity and permeability are highly variable both laterally and vertically.

In the southern part of the SZ site-scale flow model domain, the volcanic deposits thin and inter-finger with valley fill deposits. The latter are heterogeneous (sand and gravel) because of their mode of deposition (Walker and Eakin 1963 [DIRS 103022], p. 14), but are not subject to the fracturing, faulting, and alteration types of heterogeneity that affect the volcanic rocks.

Within the SZ site-scale model area, little specific information is available on the lower carbonate aquifer. However, information from nearby areas (D'Agnese et al. 1997 [DIRS 100131], p. 90, Figures 46 and 47) suggests that the lower carbonate aquifer is minimally heterogeneous with reasonably high permeability attributed to pervasive solution-enlarged fractures.

Heterogeneity in material properties is a common characteristic of hydrogeologic units at the Yucca Mountain site and it exists at scales ranging from pore scale to regional scale. The larger-scale heterogeneity, at scales of kilometers to tens of kilometers, is effectively addressed via the different units within HFM2006, incorporation of specific hydrogeologic features

(e.g., faults and structural zones), and anisotropy. The pore scale heterogeneities are averaged via the concept of macroscopic parameters defined on the basis of a representative elementary volume (Freeze and Cherry 1979 [DIRS 101173], pp. 69 to 70). Groundwater flow equations use parameters defined on the basis of the representative elementary volume. For predominantly porous units such as bedded tuffs and alluvia, the size of the representative elementary volume may be on the order of a few cubic centimeters (de Marsily 1986 [DIRS 100439], p. 15). For fractured rocks (volcanics and carbonates), the size of the representative elementary volume is less well defined, but is typically related to the density of fracturing and is generally much larger than for granular material (Freeze and Cherry 1979 [DIRS 101173], p. 73). The 250-m grid spacing used for the flow model is sufficiently large to allow the use of representative-elementary-volume-defined parameters for groundwater flow. In fact, the grid spacing is large enough that subgrid scale heterogeneity needs to be considered with regard to radionuclide transport. Subgrid heterogeneity leads to enhanced dispersion with increasing scales of transport (de Marsily 1986 [DIRS 100439], pp. 247 to 248). Additionally, the uncertainty in the density of fracturing at the subgrid scale leads to uncertainty in the groundwater velocity and matrix diffusion. Flow modeling accounts for subgrid heterogeneity by defining scaled dispersivities and flowing interval spacing (BSC 2004 [DIRS 170014]) in the transport abstraction modeling (SNL 2007 [DIRS 177390], Section 6.5.2) as random variables characterized by probability density functions.

Heterogeneity at intermediate scales between the grid size of 250 m and the large-scale features of the HFM are addressed using uncertainty in the anisotropy of hydraulic conductivity. A primary concern related to intermediate scale heterogeneity is the possibility of a fast pathway (Freifeld et al. 2006 [DIRS 178611], Table 4) along a relatively continuous path. In the fractured volcanic aquifers beneath Yucca Mountain, the fast path, if it exists, is likely to be related to a fracture or structural feature. The hydraulic testing at the C-wells complex (SNL 2007 [DIRS 177394], Section 6.2) suggest that at a large scale (about 1 km^2), hydraulic conductivity can be characterized as homogeneous, but anisotropic. The direction of anisotropy is primarily related to the dominant direction of fractures and faulting. The impact of possible fast paths at an intermediate scale of heterogeneity is incorporated in the transport simulations through probability distributions of specific discharge, horizontal anisotropy in permeability, and flowing interval spacing (SNL 2007 [DIRS 177390], Section 6.5.2). The aggregate uncertainty in these and other parameters related to radionuclide transport yield simulated SZ transport times for nonsorbing species on the order of 100 years in some Latin Hypercube Sampled realizations of the SZ system (SNL 2007 [DIRS 177390], Figure 6-28).

As noted previously, the properties of each hydrogeologic unit in the model are assumed uniform, but uncertain, with the value assigned during the calibration process. Nevertheless, heterogeneity of material properties at a variety of scales is included in the model via several different mechanisms. First, large-scale heterogeneity is defined by the distribution of units in HFM2006 and the discrete hydrogeologic features incorporated in the SZ site-scale flow model (Table 6-7). Subgrid heterogeneity is included in the transport simulations through the probability distributions for flowing interval spacing and dispersivity. Finally, intermediate scale heterogeneity, which is most likely to be reflected in possible fast paths at scales up to several kilometers, is included as uncertainty in anisotropy. Uncertainty in the HFM is discussed in Section 6.4.3.1.

6.3.1.10 Role of Faults

Faults and fault zones are hydrogeologic features that require special treatment in the SZ site-scale flow and transport models. Faulting and fracturing are pervasive at Yucca Mountain and they affect groundwater flow patterns because they may act as preferred conduits or barriers to groundwater flow. The role that faults play in facilitating or inhibiting groundwater flow depends on the nature of the fault (i.e., whether the faults are in tension, compression, or shear) and other factors such as the juxtaposition of varying geologic units along the fault plane, the rock types involved, fault zone materials, secondary mineralization, and depth below land surface.

Faunt (1997 [DIRS 100146]) investigated the effect of faulting on groundwater movement in the Death Valley region and developed a map of fault traces (Faunt 1997 [DIRS 100146], Figure 10) including diagrams (Faunt 1997 [DIRS 100146], Figure 11) showing the orientation of faults within the principal structural provinces of the region. Faunt (1997 [DIRS 100146], p. 38) grouped the faults into three categories depending on their orientations relative to the present-day stress field (i.e., those in relative tension, compression, or shear).

Faults in relative tension are more likely to be preferential conduits for groundwater, and faults in shear or compression are more likely to impede groundwater movements. Faults modeled to have the most evident effects on groundwater movement, such as effects on potentiometric contours, include the Solitario Canyon, U.S. Highway 95, Crater Flat, and Bare Mountain Faults (see Figure 6-4), all of which appear to act as barriers to groundwater flow. The following features are afforded special consideration in the SZ site-scale flow model: the Crater Flat Fault, the Solitario Canyon (with Windy Wash and Stage Coach splays), the U.S. Highway 95, the Bare Mountain, and Sever Wash Faults. In addition, zones are developed for the Fortymile Wash Structure and Lower Fortymile Wash alluvial regions that appear to act as conduits that focus flow. Other that the Fortymile Wash faults, these features are assigned anisotropic permeabilities that are 10 times more permeable in both directions parallel to the fault (*x*-*z* or *y*-*z* directions).

6.3.1.11 Altered Northern Region

The Claim Canyon caldera is an area of extensive alteration that seems to have resulted in a generalized reduction in permeability in many of the hydrogeologic units in this area (this area is hereinafter referred to as the altered northern region). The concept of the altered northern region allows different permeabilities to be assigned to the same geologic unit depending on whether or not a unit resides within the altered northern region (see Section 6.4.3.7). Deeper units (including the intrusive, crystalline, and lower clastic confining units and the lower carbonate aquifer) are excluded from this alteration because the caldera complex was not present during their genesis. Conceptually, this facilitates modeling of the LHG and it also makes intuitive sense because it is unlikely that permeabilities even within the same geologic unit would have identical values when they are separated by many kilometers (across the model domain from north to south). In the SZ site-scale model formulation, faults that fall within the altered northern region may have diminished impact on the model and could reasonably be removed from consideration here. A notable exception is Sever Wash Fault that retains a distinct permeability

from the underlying geologic units despite residing within the altered northern region. Sever Wash appears to be important in facilitating southeasterly flow near the repository area.

6.3.2 Groundwater Flow Processes

Simplifications used in modeling the groundwater flow process include those inherent to the SZ regional- and site-scale flow models (modeling assumptions), and those made in estimating parameters that are used as input to these models. The effective-continuum representation of fracture permeability is used because on the scale represented by the SZ site-scale flow model, the site is well represented by a continuum flow model. Aquifer hydraulic tests show evidence of fracture flow near Yucca Mountain (Geldon et al. 1997 [DIRS 100397]). Numerical modeling of fracture properties is done in one of three ways: discrete-fracture models, effective-continuum models, or dual-continuum models. Dual-continuum models are not needed because transient simulations are not performed. For steady-state SZ flow calculations, dual-continuum formulations are equivalent to single-continuum formulations. Discrete-fracture models represent each fracture as a distinct object within the modeling domain. Although a discrete-fracture model might reproduce the flow system more accurately, flow modeling is adequately conducted using a continuum model because:

- At Yucca Mountain, studies of the density and spacing of flowing intervals generally indicate that flow occurs through fracture zones (BSC 2004 [DIRS 170014], Figure 6-2). The fractures or fracture zones are located in various geological units, and in most cases, no single zone dominates groundwater flow. Geochemical studies (see Figure A6-62) independently confirm a south-southeasterly trace of the particle flowpath. For the limited set of wells examined by Luckey et al. (1996 [DIRS 100465], Figure 11), flow appears to be carried through fracture zones separated by a few tens of meters rather than through a few individual fractures.

- Significant portions of the geology comprise alluvial units through which flow and transport are appropriately modeled using a continuum model.

- The drawdown response to pumping at wells surrounding the C-wells complex in multi-well pump tests indicates a well-connected fracture network in the Miocene tuffaceous rocks in this area (Geldon et al. 1998 [DIRS 129721], p. 31).

The following assumptions also apply to the continuum modeling approach used in the SZ site-scale flow model:

- Estimates of discharge from the volcanic aquifer, developed from the SZ Expert Elicitation Panel (CRWMS M&O 1998 [DIRS 100353], p. 3-8) are applicable to the flowpath from below the repository to a distance of approximately 5-km down gradient in the volcanic units and were primarily based on data from hydraulic testing in wells in volcanic units and the hydraulic gradient inferred from water-level measurements. The relative values of groundwater flux in the volcanic aquifer and along the flowpath farther to the south are constrained by the calibration of the SZ site-scale flow model (reasonable extrema bound the calibration process).

- Horizontal anisotropy in permeability is adequately represented by a permeability tensor that is oriented in the north-south and east-west directions. In support of the TSPA-LA, horizontal anisotropy is considered for radionuclide transport in the SZ (SNL 2007 [DIRS 177394], Section 6.2.6). The numerical grid of the SZ site-scale flow model is aligned north-south and east-west, and values of permeability are specified in directions parallel to the grid. One analysis of the probable direction of horizontal anisotropy shows that the direction of maximum transmissivity is N 33°E (Winterle and La Femina 1999 [DIRS 129796], p. iii), indicating that the anisotropy applied on the SZ site-scale model grid is within approximately 30° of the inferred anisotropy. A detailed description of the horizontal anisotropy calculations is found in *Saturated Zone In-Situ Testing* (BSC 2006 [DIRS 177394], Appendix C6). Sensitivity analyses were performed to assess the impact of uncertainty in the anisotropy and are presented in *Saturated Zone Flow and Transport Model Abstraction* (SNL 2007 [DIRS 177390], Section 6.5.2.10).

- Horizontal anisotropy in permeability may apply to the fractured and faulted volcanic units of the SZ system along the groundwater flowpaths that run from the repository to points south and east of Yucca Mountain. The inferred flowpath from beneath the repository extends to the south and east. This is the area in which potential anisotropy could have an impact on radionuclide transport in the SZ. Given the conceptual basis for the anisotropy model, it is appropriate to apply anisotropy only to those hydrogeologic units that are dominated by groundwater flow in fractures. A more detailed discussion of anisotropy is provided in Section 6.4.3.11.

- Changes in the water-table elevation (due to future climate changes) will have negligible effect on the direction of the groundwater flow near Yucca Mountain although the magnitude of the groundwater flux will change. This supposition has been studied at regional (D'Agnese et al. 1999 [DIRS 120425]; Winterle 2003 [DIRS 178404]; Winterle 2005 [DIRS 178405]) and subregional scales (Czarnecki 1984 [DIRS 101043]). These studies found that the flow direction did not change significantly under increased recharge scenarios. The studies were based on confined aquifer models that did not take into account the free surface boundary at the water table or the saturation of geological units that currently are in the UZ overlying the present-day SZ. These UZ tuffs generally have a lower permeability than those in the SZ, and as such, UZ units that become saturated are not likely to yield faster fluxes in the SZ (BSC 2004 [DIRS 169861], Appendix A).

- Future water supply wells that might be drilled near Yucca Mountain (including outside the regulatory boundary) will have a negligible effect on the hydraulic gradient. Water levels at the southern boundary of the SZ site-scale flow and transport models (in the Amargosa Valley) currently reflect the effect of well pumpage (Luckey et al. 1996 [DIRS 100465], p. 41).

- In the analysis presented in this report, temperature is modeled to be proportional to the depth below the ground surface. Modeling a uniform temperature gradient with depth is equivalent to a model of uniform geothermal heat flux through a medium of homogeneous thermal conductivity. In addition, the temperature at the ground surface is held constant. Data indicate that the temperature gradients generally become more

linear with increasing depth below the water table. The goal of assigning temperature variations with depth in the SZ site-scale flow model is to account for resulting variations in fluid viscosity at different depths in the SZ.

- A confined-aquifer solution is used in the SZ site-scale flow model. The approach treats the upper boundary as if there is no UZ and, therefore, solves a simplified and more computationally efficient numerical model. In the numerical model, the top surface has boundary conditions of recharge flux (infiltration). The confined aquifer solution is enforced by assigning negative porosity to all nodes above the water table. This forces FEHM to model the system as fully saturated. If this procedure were not adopted, small variations in head around the water table would result in FEHM testing for an air phase, thus decreasing efficiency. The drawback of this approach is that the top surface of the numerical model corresponds to the measured water table and may be inconsistent with the model-derived water table. This discrepancy could affect flux through the model domain, but errors would be minimal because changes in the water-table elevation would be small in comparison to the saturated thickness of the model. Care was taken during the calibration process to model the small-head gradient area to the south and east of Yucca Mountain accurately. Specified-head boundary conditions on the lateral boundaries were set with no vertical gradient; however, it should be noted that the model allows for vertical flows that arise from recharge and heterogeneity. The numerical approach used is similar to the classical Dupuit-Forcheimer method (Bear 1979 [DIRS 105038]).

6.4 FORMULATION OF THE CONCEPTUAL MODEL

6.4.1 Mathematical Description of the Conceptual Model

An effective continuum approach is adopted for simulating groundwater flow through the fractured rock and alluvial materials within the domain of the SZ site-scale flow model. Based on this conceptualization, the equations governing groundwater flow can be derived by combining the equations describing the conservation of fluid mass and Darcy's Law. The equation for conservation of fluid mass (Bear 1972 [DIRS 156269], Equation 4.3.7]) expressed in the notation given by (Tseng and Zyvoloski 2000 [DIRS 179068]) is:

$$\frac{\partial A_{mass}}{\partial t} + \overline{\nabla} \cdot \overline{f}_{mass} + q_{mass} = 0, \qquad \text{(Eq. 6-1)}$$

where $\overline{\nabla}$ is gradient operator, A_{mass} is the fluid mass per unit volume (kg/m^3) given by:

$$A_{mass} = \phi \rho_l, \qquad \text{(Eq. 6-2)}$$

$\overline{f}_{mass}$ is the fluid mass flux vector (kg/m^2/s) given by:

$$\overline{f}_{mass} = \rho_l \overline{v}, \qquad \text{(Eq. 6-3)}$$

ϕ is the porosity in the system (dimensionless), ρ_l is the fluid density (kg/m^3), $\overline{v}$ is the fluid velocity vector (m/s) (or, more specifically, areal flux or specific discharge (volume fluid/unit area/s), pore velocity is $\overline{v}/\phi$), and q_{mass} is the fluid mass source (kg/m^3/s).

The velocity of the fluid can be expressed by the generalized Darcy's Law for an anisotropic medium (Bear 1972 [DIRS 156269], Equations 5.2.6 and 5.6.1]) as:

$$\overline{v} = \frac{\underline{k}}{\mu} \cdot \left(\overline{\nabla} P - \rho_l g \hat{z} \right), \qquad \text{(Eq. 6-4)}$$

where μ is the dynamic viscosity of the fluid (kg/m/s), P is the fluid pressure (Pa), $\underline{k}$ is the permeability tensor (m^2), g is the acceleration due to gravity (m/s^2), and $\hat{z}$ is the unit vector in the direction of gravity (downward). In the case where flow is aligned in the direction of the principal axes of permeability (Bear 1972 [DIRS 156269], Equation 5.6.1), $\underline{k}$ may be expressed as $\underline{k} = \begin{bmatrix} k_1 & 0 & 0 \\ 0 & k_2 & 0 \\ 0 & 0 & k_3 \end{bmatrix}$.

Equations 6-1 and 6-4 can be combined to yield the fundamental equation describing groundwater flow (see Tseng and Zyvoloski 2000 [DIRS 179068], Equation 1 for isotropic case):

$$\frac{\partial A_{mass}}{\partial t} - \overline{\nabla} \cdot \left(\underline{D}_{mass} \overline{\nabla} P \right) + \frac{\partial (k_3 \rho_l^2 g / \mu)}{\partial z} + q_{mass} = 0 \qquad \text{(Eq. 6-5)}$$

where $\underline{D}_{mass}$ is the hydraulic conductivity (m/s) tensor calculated as:

$$\underline{D}_{mass} = \frac{\rho_l}{\mu} \underline{k}. \qquad \text{(Eq. 6-6)}$$

Groundwater flow is simulated in the SZ site-scale flow model by obtaining a numerical solution to this equation. Solution of this equation for pressure requires the specification of the pressure at the boundaries of the solution domain. For steady-state calculations, solution of this equation does not require specification of initial conditions (initial pressure distribution throughout the solution domain), because Equation 6-5 (at very large times for constant boundary conditions) represents steady-state flow, which is independent of initial conditions. Fluxes are determined using Equation 6-4 with pressure gradients obtained through "post-processing" of the pressure solution to Equation 6-5.

It is assumed that a steady-state model is sufficient to be used during calibration and also sufficient for the intended use of the SZ site-scale flow model. There are two potential causes of transient flow that are relevant to this assumption: (1) changes in climate over the past 15,000 years, and (2) pumping from wells within and south of the model domain during approximately the last 50 years. Use of the steady-state assumption requires that the modern-day flow system has had sufficient time to equilibrate to both of these perturbations to the natural system. It is noted that transient tests (C-wells and Alluvial Testing Complex) were performed

and that permeability values derived from those tests were considered in the validation of the numerical model. It is not expected that the model can reproduce the transient tests, largely due to the 250-m-gridblock sizes. Because transient pumping is not used in any Yucca Mountain radionuclide migration simulations and steady-state gradients are modeled accurately with the model, this does not invalidate the steady-state assumption. Climate change and other transient impacts are incorporated in the SZ flow and transport abstractions (SNL 2007 [DIRS 177390], Section 6.5). Furthermore, the effects of water table rise on flowpaths are investigated here in Section 6.6.4.

The conceptual model of the long-term groundwater flow in this region includes the hypothesis that recharge rates and, consequently, the elevation of the water table and groundwater flow rates, were larger during the last glacial pluvial period. The time required for the flow system to equilibrate to a more arid climate depends primarily on the hydraulic conductivity of the rocks and the amount of water that must be drained from storage to lower the water table.

It is likely that equilibration to the drier climate has occurred given: (1) the long time (thousands of years) since the climate change was completed, (2) the relatively small amount of water stored (small specific yield) in fractured volcanic rocks that make up much of the model domain near the water table, and (3) the relatively large hydraulic conductivity of the fractured volcanic rocks.

The time required for the flow field to arrive at steady-state with respect to pumping from wells is much shorter than the time required for equilibration to climate change. It depends primarily upon the time required for changes in water level to be transmitted through the SZ. Fast transmittal is expected in fractured volcanic rock because of their relatively large hydraulic conductivity and small specific storage. The fact that the modern-day flow system on the scale of this model domain has equilibrated to pumping is supported by the lack of consistent, large-magnitude variations in water levels observed in wells near Yucca Mountain (Luckey et al. 1996 [DIRS 100465], pp. 29 to 32). A transient response to pumping would be expected, instead, to result in a continued decrease in water levels. Overall, pumping rates are typically negligible compared to the total mass of fluid in the system, which is on the order of 10^{16} kg.

6.4.2 Computational Model

The FEHM V2.24 (STN: 10086-2.24-02; [DIRS 179539]) software code is used for SZ site-scale modeling to obtain a numerical solution to the mathematical equation describing groundwater flow, Equation (6-5). FEHM is a nonisothermal, multiphase flow and transport code that simulates the flow of water and air and the transport of heat and solutes in two- and three-dimensional saturated or partially saturated heterogeneous porous media. The code includes comprehensive reactive geochemistry and transport modules and a particle-tracking capability. Fractured media can be simulated using equivalent-continuum, discrete-fracture, dual-porosity, or dual-permeability approaches. A subset of the FEHM code capabilities was used in the SZ site-scale flow model because only a single-phase, isothermal flow model is solved.

Particle tracking is a numerical technique that simulates the transport of fluid "particles." Particle-tracking techniques have a long history of use in similar applications (e.g., Pollock 1988

[DIRS 101466]; Tompson and Gelhar 1990 [DIRS 101490]; Wen and Gomez-Hernandez 1996 [DIRS 130510]). Particle tracks can be used to represent and estimate flowpaths.

The control-volume finite element (CVFE) method is used in FEHM to obtain a numerical solution to the groundwater flow equation over the model domain. Finite-element methods are based on the assumption that a continuum may be modeled as a series of discrete elements. For each element, equations based on a discretized form of the groundwater flow equation are written that describe the interaction of that element with its neighbors. These equations describe the hydrologic behavior of the elements. This discretization leads to a set of equations that must be solved numerically to estimate groundwater pressure at each node throughout the model domain.

The CVFE method has been used extensively in petroleum-reservoir engineering (Forsyth 1989 [DIRS 144110]). The CVFE method solves for the potentials using a finite-element technique while the control-volume aspect establishes local mass conservation and upstream weighting (Verma and Aziz 1997 [DIRS 143606]). Quadrilaterals and triangles in two dimensions and hexahedra and tetrahedra in three dimensions are divided into volumes associated with gridblocks and areas associated with interblock distances. Gridblock volumes are the Voronoi volumes (Forsyth 1989 [DIRS 144110]) associated with each gridblock. Voronoi volumes are also called perpendicular bisector volumes. A Voronoi volume is formed by boundaries that are orthogonal to the lines joining adjacent gridblocks and that intersect the midpoints of the lines (Verma and Aziz 1997 [DIRS 143606]). Any point within a Voronoi volume is closer to its associated gridblock than to any other node in the grid. Implementing the CVFE method on simple elements with constant properties is equivalent to the traditional finite-element method.

The stiffness coefficients (e.g., elements of the stiffness matrix) of the traditional finite-element method can be interpreted as linear functions of the area through which the fluid passes while traveling from one node to its neighbor. A stiffness coefficient uses the area of the boundary of the Voronoi volume that intersects the line joining adjacent nodes. LaGriT V1.0 (STN: 10212-1.1-00; [DIRS 173140]) produced this CVFE grid. These coefficients are used to form control-volume difference equations for the conservation equations. This method is not traditional because equation parameters are defined by node, not element, but this method leads to an intuitive understanding of the numerical method.

In FEHM, the nodal definition of equation parameters leads naturally to a separation of the nonlinear and purely geometric parts. This separation is detailed by Zyvoloski (1983 [DIRS 101171]) and is valid over lower-order elements. The nonlinear part uses average inverse kinematic viscosity, which is ρ/μ., between two nodes, although the average is usually taken to be the upstream nodal value. The result is a much more stable code for solving nonlinear problems that retains much of the geometric flexibility of finite elements. This method has been used in FEHM since 1983 (Zyvoloski 1983 [DIRS 101171]) and has been extensively verified. Harmonic weighting of the intrinsic permeability is used. It is noted that the SZ site-scale flow model has a spatially varying viscosity term (due to spatially varying temperature) and interblock fluid fluxes are modeled by upwinding the viscosity terms. Newton-Raphson iteration is applied to the system of equations, which is solved with a multidegree of freedom and preconditioned, conjugate gradient method using either the

generalized minimum residual method or the biconjugate gradient-squared acceleration technique.

6.4.3 SZ Site-Scale Flow Model Inputs

The development of the SZ site-scale flow model involves the input of data from a number of sources, including water-level and head distributions, definitions of the hydrogeologic units, distributions of recharge flux and lateral fluxes into the model domain, feature and fault distributions, temperature profiles in wells, and boundary conditions. The data sources for these inputs are identified in Table 4-1.

Incorporation of these inputs into the SZ site-scale flow model first requires the generation of a hydrogeologic framework conceptualization and a computational grid. The HFM conceptualization and known features of the site were used to design a geologically-zoned grid for flow modeling. Once a computational grid is formulated, HFM data inputs were used to assign hydrogeologic units and features, recharge fluxes, hydrogeologic properties, and boundary conditions at nodes throughout the model domain.

6.4.3.1 Hydrogeologic Framework Model (HFM) Overview

The HFM (SNL 2007 [DIRS 174109]) is a conceptual model providing a three-dimensional interpretation of the hydrostratigraphic unit locations and structure within the SZ site-scale flow and transport model domain. It was developed using standard geologic methods and software based on all appropriate data from the Yucca Mountain area. The geometry of geologic units is defined with EARTHVISION V5.1 (STN: 10174-5.1-00; [DIRS 167994]) framework files, hereafter referred to as HFM2006 (DTN: MO0610MWDHFM06.002 [DIRS 179352]), which characterize a three-dimensional geocellular model of the base HFM for the SZ. HFM2006 extends from the land surface to the base of the 2004 regional groundwater flow model at −4,000 m elevation (Belcher 2004 [DIRS 173179], Figure B-2) and has a top surface coincident with the topographic surface. Horizontally, the HFM2006 is constructed with boundaries coincident with finite difference cells in DVRFS (Belcher 2004 [DIRS 173179]). HFM2006 is constructed by combining a set of structural contour maps representing the tops of hydrogeologic units using EARTHVISION and it includes data from geologic maps and sections, borehole data, geophysical data, and existing geologic models. This representation enables the computational grid to be populated with an initial set of hydrologic properties for the calibration of the SZ site-scale flow model. HFM2006 and its development are documented in *Hydrogeologic Framework Model for the Saturated-Zone Site-Scale Flow and Transport Model* (SNL 2007 [DIRS 174109]). The updated HFM (DTN: MO0610MWDHFM06.002 [DIRS 179352]) is a three-dimensional representation of the hydrogeologic units surrounding the location of the Yucca Mountain geologic repository and is developed specifically for use in the SZ site-scale flow model. HFM2006 is updated with information collected since development of the recent update to the DVRFS (Belcher 2004 [DIRS 173179]) and with the new NC-EWDP data through Phase IV. These boreholes provide new stratigraphic information south of Yucca Mountain and mostly north of U.S. Highway 95. The hydrogeologic layers of the HFM2006 form a series of alternating aquifers and confining units and alluvium above the regional carbonate aquifer that comprise one or more contiguous geologically defined stratigraphic units that can be grouped according to measured or inferred common hydrologic properties. These

units (Table 6-2) provide a geometric representation of hydrogeology and structure and are used as a basis for assigning hydrologic properties within the SZ site-scale flow model domain.

The DVRFS HFM consists of 28 surfaces representing the top elevation of each of the 27 hydrogeologic units plus the base at −4,000-m elevation, and a horizontal grid consisting of a rectangular array of nodes with 125-m spacing (SNL 2007 [DIRS 174109], Section 6). HFM2006 consists of 24 surfaces because unit IDs 10, 13, 22, and 25 are not present in its model area (SNL 2007 [DIRS 174109], Tables 6-2 and 6-3). An important goal of the HFM2006 was to match geologic units with the regional DVRFS HFM. This match allows more direct comparisons with the regional conditions and parameters, without a transition at the site-scale model boundary, and facilitates use of boundary volumetric/mass flow rates extracted from the regional-scale model for use as target boundary conditions during site-scale model calibration. Permeabilities (hydraulic conductivities for the regional model) may not match across model boundaries because these parameters are calibrated independently. The HFM2006 surface grids exactly reproduce the DVRFS Model grid nodes except where more detailed data are available, primarily within the domain of the Geologic Framework Model (GFM) (DTN: MO0012MWDGFM02.002 [DIRS 153777]) and near NC-EWDP boreholes area. These more detailed areas are important considerations in understanding the SZ flow system and they help define the boundaries of the fractured tuff aquifers immediately beneath and down gradient from Yucca Mountain, and the alluvial aquifer from which groundwater discharges in the Amargosa Valley. Data from the NC-EWDP investigations better constrain the location of the tuff-alluvium contact at the water table and better characterize the thickness and lateral extent of the alluvial aquifer north of U.S. Highway 95 (SNL 2007 [DIRS 177390], Section 6.5.2.2).

Recent NC-EWDP drilling revealed a larger formation of alluvial material (Unit 26) in HFM2006 replacing volcanic and sedimentary unit previously thought to be present. It also revealed more of Unit 20 (Timber Mountain Volcanics) to the south of the GFM area than was previously indicated.

This report describes SZ flow modeling using HFM2006, which incorporates the newer DVRFS HFM (Belcher 2004 [DIRS 173179]), GFM2000 (DTN: MO0012MWDGFM02.002 [DIRS 153777]), and all NC-EWDP data through Phase IV.

Table 6-2. Hydrogeologic Units for the Hydrogeologic Framework Model

Hydrogeologic Units in HFM2006				
Unit ID	**Abbreviation**	**Unit Name**	**Description**	**Stacking Order**
28	YAA	Younger alluvial aquifer	Pliocene to Holocene coarse-grained basin-fill deposits	27
27	YACU	Younger alluvial confining unit	Pliocene to Holocene playa and fine-grained basin-fill deposits	26
26	OAA	Older alluvial aquifer	Pliocene to Holocene coarse-grained basin-fill deposits	25
25	OACU	Older alluvial confining unit	Pliocene to Holocene playa and fine-grained basin-fill deposits (not in HFM2006 domain)	24
24	LA	Limestone aquifer	Cenozoic limestone, undivided	23

Table 6-2. Hydrogeologic Units for Hydrogeologic Framework Model (Continued)

Hydrogeologic Units in HFM2006				
Unit ID	**Abbreviation**	**Name**	**Description**	**Stacking Order**
23	LFU	Lava-flow unit	Cenozoic basalt cones and flows and surface outcrops of rhyolite-lava flows	22
22	YVU	Younger volcanic-rock unit	Cenozoic volcanic rocks that overlie the Thirsty Canyon Group (not in HFM2006 domain)	21
21	Upper VSU	Volcanic- and sedimentary-rock unit	Cenozoic volcanic and sedimentary rocks, undivided, that overlie volcanic rocks of SWNVF	20
20	TMVA	Thirsty Canyon-Timber Mountain volcanic-rock aquifer	Miocene Thirsty Canyon and Timber Mountain Groups, plus Stonewall Mountain Tuff, undivided	19
19	PVA	Paintbrush volcanic-rock aquifer	Miocene Paintbrush Group	18
18	CHVU	Calico Hills volcanic-rock unit	Miocene Calico Hills Formation	17
17	WVU	Wahmonie volcanic-rock unit	Miocene Wahmonie and Salyer Formations	16
16	CFPPA	Crater Flat-Prow Pass aquifer	Miocene Crater Flat Group, Prow Pass Tuff	15
15	CFBCU	Crater Flat-Bullfrog confining unit	Miocene Crater Flat Group, Bullfrog Tuff	14
14	CFTA	Crater Flat-Tram aquifer	Miocene Crater Flat Group, Tram Tuff	13
13	BRU	Belted Range unit	Miocene Belted Range Group (not in HFM2006 domain)	12
12	OVU	Older volcanic-rock unit	Oligocene to Miocene; near the NTS consists of all volcanic rocks older than the Belted Range Group. Elsewhere, consists of all tuffs that originated outside of the SWNVF	11
11	Lower VSU	Volcanic- and sedimentary-rock unit	Cenozoic volcanic and sedimentary rocks, undivided; where named Cenozoic volcanic rocks exist, lower VSU underlies them	10
10	SCU	Sedimentary-rock confining unit	Paleozoic and Mesozoic sedimentary and volcanic rocks (not in HFM2006 domain)	9
7	UCA	Upper carbonate-rock aquifer	Paleozoic carbonate rocks (UCA only used where UCCU exists, otherwise UCA is lumped with LCA)	8
6	UCCU	Upper clastic-rock confining unit	Upper Devonian to Mississippian Eleana Formation and Chainman Shale	7
9	LCA_T1	Lower carbonate-rock aquifer (thrusted)	Cambrian through Devonian predominantly carbonate rocks – thrusted	6
8	LCCU_T1	Lower clastic-rock confining unit (thrusted)	Late Proterozoic through Lower Cambrian primarily siliciclastic rocks (including the Pahrump Group and Noonday dolomite) – thrusted	5
5	LCA	Lower carbonate-rock aquifer	Cambrian through Devonian predominantly carbonate rocks	4
4	LCCU	Lower clastic-rock confining unit	Late Proterozoic through Lower Cambrian primarily siliciclastic rocks (including the Pahrump Group and Noonday dolomite)	3

Table 6-2. Hydrogeologic Units for Hydrogeologic Framework Model (Continued)

Hydrogeologic Units in HFM2006				
Unit ID	Abbreviation	Name	Description	Stacking Order
3	XCU	Crystalline-rock confining unit	Middle Proterozoic metamorphic and igneous rocks	2
2	ICU	Intrusive-rock confining unit	All intrusive rocks, regardless of age	1

Source: HFM2006 (SNL 2007 [DIRS 174109], Table 6-2) and from Belcher (2004 [DIRS 173179], Table E-1).

NOTE: The hydrogeologic names, descriptions, and stacking order are from Belcher (2004 [DIRS 173179]) and are used for the HFM2006 and SZ computational grid to maintain consistency across models.

HFM2006 was constructed to represent faults and other hydrogeologic features (such as zones of alteration) that affect SZ flow. Fault trace maps show faults on cross sections and the locations where faults intersect the land surface. Faults in the model area dip at multiple angles, but most are high-angle faults. Given fault dip uncertainty and grid resolution constraints, these features were simplified and implemented as vertical features. Faults deemed important to flow near Yucca Mountain were explicitly considered in the model and are identified separately and discussed in Section 6.4.3.7. These features are included in the SZ numerical model as distinct permeability zones in FEHM.

Important thrust faults were represented by repeating hydrogeologic units in HFM2006. When geologic, structural, or stratigraphic surfaces are stored as arrays, they cannot have multiple *z*-values at one location. This limitation means that thrust faults and mushroom-shaped intrusions cannot be represented by an array. To deal with these problems, simplifying techniques were used. Where units were repeated by thrust faults, two different grids were created for the same hydrogeologic unit. A unit boundary map was then added to define an outline for the perimeter of the thrust sheet. Within this boundary, hydrogeologic structural altitude values were treated as defining unique additional hydrogeologic unit(s). Where units were continuous across this boundary, altitudes of surfaces are the same on each side of the boundary, making the boundary "invisible." Because of significant uncertainty in orientation, extent, and hydrogeologic properties for many of the faults in the SZ site-scale model domain, only those faults and other features of hydrologic importance were constructed in HFM2006 (SNL 2007 [DIRS 174109], Figures 6-2 and 6-3).

The top of HFM2006 is truncated by the 2006 potentiometric surface as described in Appendix E. The surface contour map was constructed using potentiometric data from various borehole locations (BSC 2004 [DIRS 170009], Figure 6-2) supplemented with new data from NC-EWDP. Data from the uppermost-completed borehole intervals were used and elevations were derived from USGS 3-arc-second 1-by-1 degree digital elevation model files.

6.4.3.2 Grid Generation

The computational grid for the SZ site-scale flow model was developed using LaGriT V1.1 (STN: 10212-1.1-00; [DIRS 173140]), which is a software tool for generating, editing, and optimizing multi-material unstructured finite element grids (triangles and tetrahedra). LaGriT maintains the geometric integrity of complex input volumes, surfaces, and geologic data and produces an optimal grid (Delaunay, Voronoi) elements. The computational grid figures in the

following sections are created with General Mesh Viewer (GMV), a grid-visualization software product that enables accurate and detailed analyses of LaGriT grid properties. GMV is distributed through the LANL web site at: http://laws.lanl.gov/XCM/gmv/GMVHome.html.

The grid was designed so that in the horizontal, its nodes are coincident with the grid cell corners of the 2004 DVRFS (Belcher 2004 [DIRS 173179]), with even multiples of 125 m in the UTM coordinate system. The grid for the flow model extends upward along the vertical coordinate to the ground surface, although those nodes located above the water table are computationally inactive. A confined aquifer solution using the water-table elevation to define the top of the flow system is implemented and described in Section 6.4.1. The extension of the grid to the ground surface allows, if desired, the simulation of a dynamic water table. The depth of the flow-model grid drops to 4,000 m (9,020 ft) below sea level to match the depth of HFM2006 and it includes more of the regional carbonate aquifer than previous model versions. The extent of the computational grid is shown in Table 6-3 and Figure 6-5.

Table 6-3. Coordinates of the Base-Case SZ Site-Scale Model Domain

Location	HFM Surfaces (m)	Grid Extents (m)	Grid Total Distance (m)
UTM Easting, meters	530,750 to 565,250	533,000 to 563,000	30,000
UTM Northing, meters	4,044,250 to 4,093,750	4,046,500 to 4,091,500	45,000
Bottom to ground surface	−4,000 to 2,018.5	−4,000 to 2,200	5,950 at highest point

Sources: DTN: MO0610MWDHFM06.002 [DIRS 179352] (HFM2006).

Output DTN: SN0612T0510106.004 (SZ site-scale flow model).

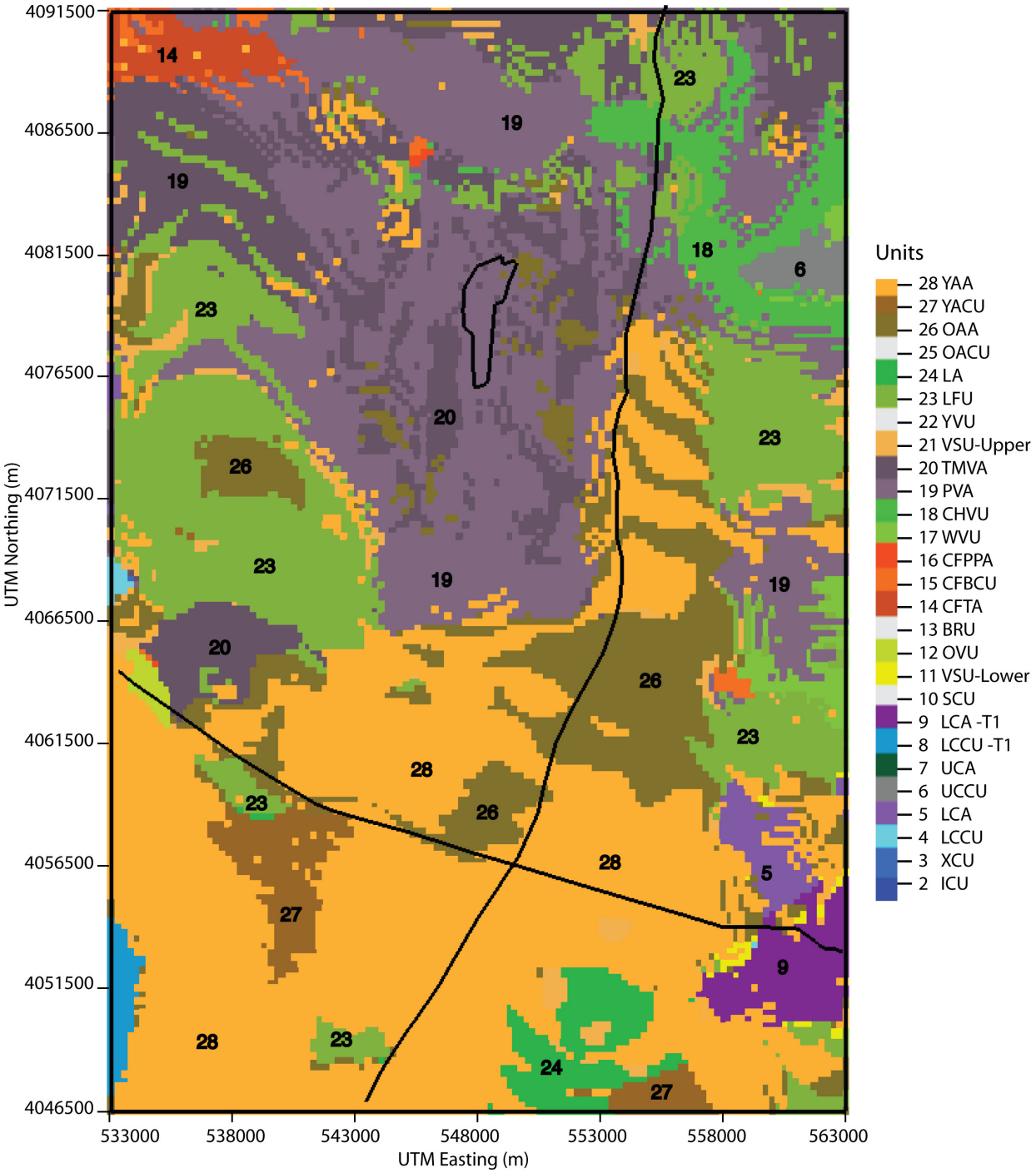

Source: DTN: MO0610MWDHFM06.002 [DIRS 179352].

NOTES: Source for the repository outline, which is for Illustration purposes only is from SNL 2007 [DIRS 179466]. This view shows the top of the 250-m computational grid, which is coincident with the domain topology. The different colors in the figure indicate the material units as defined by hydrogeologic surfaces described in Table 6-2. Black lines show the repository outline, U.S. Highway 95, and a line tracing north-south along Fortymile Wash.

UTM = Universal Transverse Mercator.

Figure 6-5. Top of the 250-m SZ Site-Scale Computational Grid

A structural grid using orthogonal hexahedral elements comprises the SZ site-scale flow model. Previous models of Yucca Mountain SZ flow and transport (Czarnecki et al. 1997 [DIRS 100377]) have used both unstructured (finite-element) meshes and structured orthogonal grids. However, the principal reason structured grids are used for this work is to facilitate the use of streamline particle-tracking capabilities in FEHM. Although structured meshes are not as flexible as unstructured meshes in fitting complex geometry, tests have shown that they provide accurate solutions so long as there is adequate resolution to represent the geometry of the different materials in each hydrogeologic layer. Moreover, there must be enough resolution to account for any large gradients. The sufficiency of grid resolution is usually investigated by running a flow model using various grids of differing resolutions. If little difference is found among model results using grids of increasing resolution, those resolutions at which the model differences become minimal can be used to identify suitable grid resolutions. A study of the accuracy of both the flow and transport solution was performed on 10 grids with horizontal resolutions ranging from 500 to 10,000 m to determine the appropriate horizontal grid resolution for the SZ site-scale flow model (Bower et al. 2000 [DIRS 149161]). Though 500-m spacing is sufficient for these models, higher resolution can better capture the interface between materials. But as resolution increases, so do the number of grid nodes. For FEHM simulations, the final grid must stay under 2 million nodes, additional restrictions due to operating system and LaGriT QA controls, further constrain the grid to under 1 million nodes. The 250-m grid spacing used for this model provides improved accuracy over older 500-m spacing, improving the representation of the material interfaces.

More important than the horizontal spacing, high grid resolution in the vertical dimension is needed for capturing material units that are thin, or that pinch out into other materials. Each grid layer in the structured grid is horizontal, but the layers of the physical hydrogeologic units are gently sloping with approximately 7% dip to the east. Therefore, a finer and nonuniform grid resolution is used in the vertical dimension to capture the geometry of the sloping hydrogeologic units. The vertical grid spacing is selected to provide sufficient resolution to accurately represent flow along critical flow and transport pathways in the SZ. A finer resolution is used near the water table in the vicinity of the repository (~700 m) and progressively coarser resolution is used for the deeper portions of the aquifer. The vertical grid spacing ranges from 10 m (33 ft) near the water table to 600 m (1,969 ft) at the bottom of the model domain. The vertical dimension of the model domain is divided into 12 zones, and constant vertical grid spacing is adopted in each of these zones. The computational grid starts as a rectangular shape with 121 nodes along the x-axis and 181 nodes along y-axis and 67 along z-axis. Grid nodes above the ground surface are identified and removed resulting in a variable total number of nodes along the z-axis for any given x, y location. In total, 67 layers are included in the vertical dimension that extends from +2,200 m (7,218 ft) to –4,000 m (−13,1230 ft) elevation. The structure of the vertical layering used in the SZ site-scale flow and transport model grid is summarized in Table 6-4 and are shown in the three-dimensional views in Figures 6-6 and 6-7. The material properties were assigned to the intersections of the grid layers. At the locations where the grid is coarse, some of the HFM layers were not represented. However, in the areas of greatest interest, the grid is sufficiently fine and the resolution of the HFM is on the same level as the resolution of the grid.

The top surface of the mesh is an irregular stair stepped surface created by removing any element above a digital elevation model (DEM). Because the top surface will not exactly match the DEM, a decision is made to use the following criteria. If the centroid (average value of the eight corner nodes of a hexahedral element) is above the DEM the element is removed. The final truncated grid has a stair stepped top surface with some associated grid nodes above the DEM. Figure 6-7 is an image of the full computational grid showing the top surface to illustrate how topography is represented. The inset shows a close-up at the top of the grid showing the vertical changes in grid resolution. The image is a view of the northwest corner where water table surface is located about 150 m below the ground surface. These figures show how grid resolution approximates the units defined by the HFM2006 surfaces.

Table 6-4. Vertical Grid Spacing Used in the SZ Site-Scale Flow Model

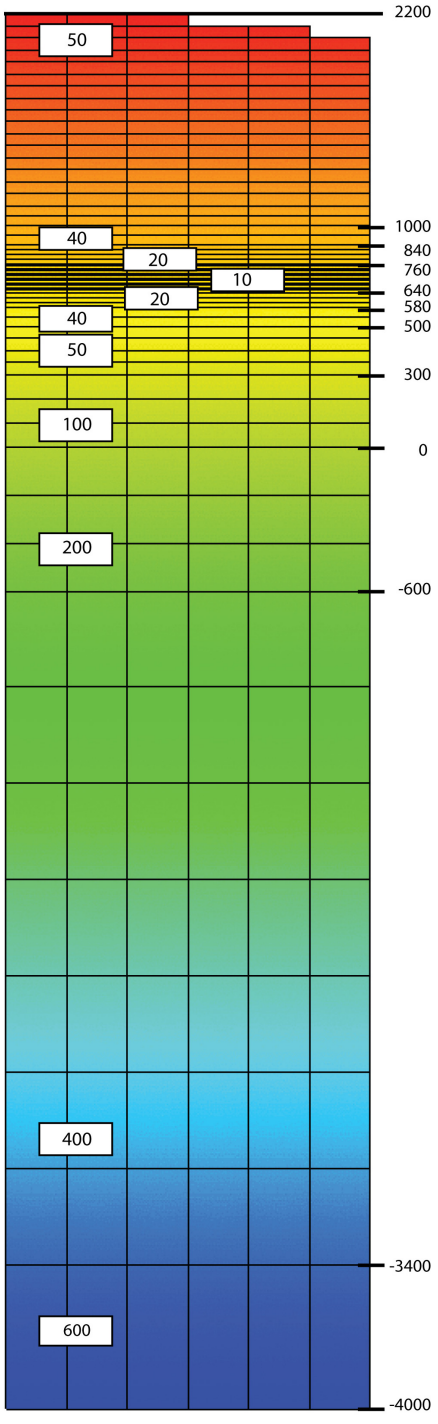

Spacing Boundaries Elevation (m)	Layer Thickness (m)	Number of Grid Layers	Vertical Length (m)
2,200	The top is variable and based on truncation by topology		
1,000	50	24	1,200
840	40	4	160
760	20	4	80
640	10	12	120
580	20	3	60
500	40	2	80
300	50	4	200
0	100	3	300
−600	200	3	600
−3,400	400	7	2,800
−4,000	600	1	600

Source: Output DTN: LA0612TM831231.002.

NOTE: The image shows the vertical distribution of the grid layers. Boxed numbers are the layer thicknesses and numbers along image right are elevation (MASL) where layer thicknesses change. The top of this grid is truncated by the ground surface resulting in a variable top elevation.

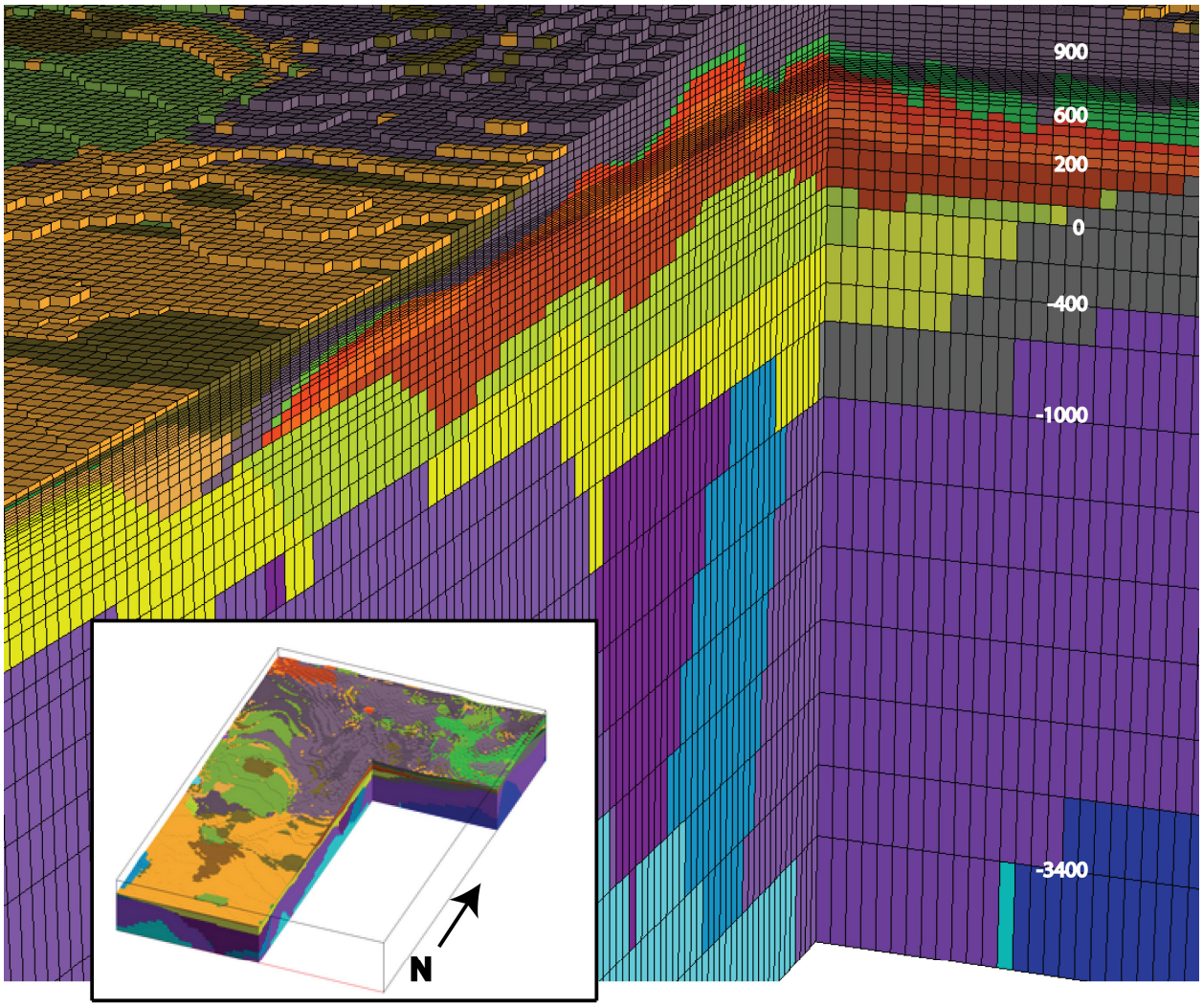

Source: Output DTN: LA0612TM831231.002.

NOTES: For illustration purposes only, view shows a cut away of the computational grid with 3× vertical exaggeration. Grid spacing at the bottom of the grid is at 600 m, then 400, 200, 100, 50, 40, 20, with 10 m near an elevation of 700 m. Spacing then increases with elevation from 10 to 20 and 40 m, with 50-m spacing near the higher elevations in the north. The inset at the bottom of the image shows the location of the cut out in relation to the full grid. The grid points are colored with the values of the hydrogeologic Units 2 through 28 as described in Table 6-2.

UTM = Universal Transverse Mercator.

Figure 6-6. Close-Up View of Computational Grid (3× Vertical Exaggeration) Showing Cut Away at UTM Easting = 549,000 m and UTM Northing = 4,078,000 m Through the Yucca Mountain Repository

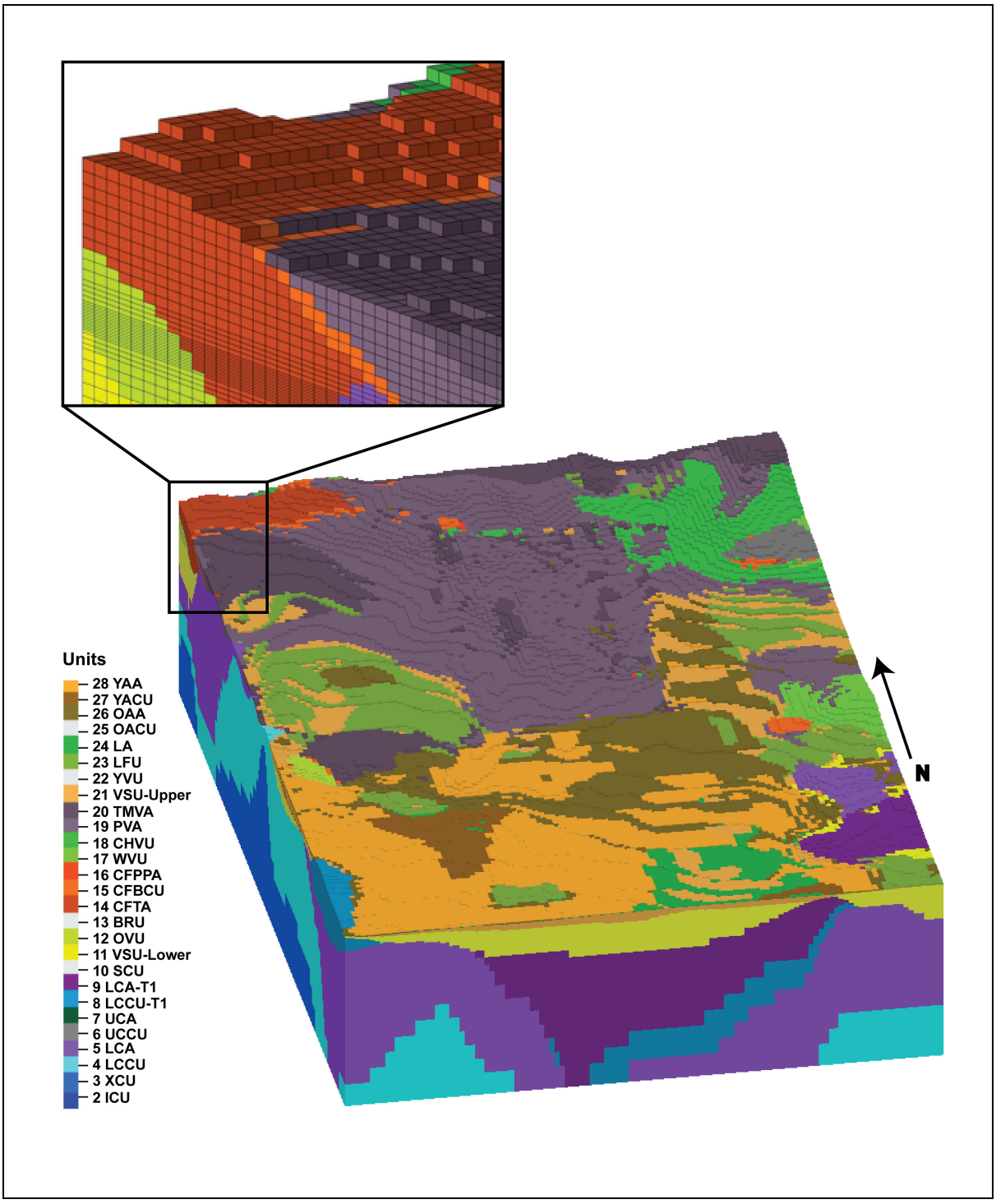

Source: Output DTN: LA0612TM831231.001.

NOTE: The grid extends 533,000 to 563,000 m from west to east, and 4,046,500 to 4,091,500 m south to north (Coordinates UTM North American Datum 27). Detail shows the grid blocks and ground surface at the northwest top corner of the grid.

UTM = Universal Transverse Mercator.

Figure 6-7. View of the 250-m Computational Grid (2× Vertical Exaggeration) Showing Node Points Colored by Hydrogeologic Units Values from HFM2006

6.4.3.3 Hydrogeologic Properties

HFM2006 provides the hydrogeologically-defined geometry for SZ flow and transport process models and is used to assign geologic properties to the nodes of the computational grid. The physical hydrogeologic unit present at each node in the computational grid was established during the computational grid construction. The HFM2006 surface files represent the top surface of each hydrogeologic layer in the model framework and were imported into LaGriT to identify the hydrogeologic layer designation for each node and cell of the computational grid. Cells above the ground surface were identified using the HFM2006 surfaces, then they were removed from the grid. Quality checks were performed to ensure that the final grid is correct. These include histograms of element volume and element aspect ratio as described by Bower et al. (2000 [DIRS 149161]). Once the grid geometry was evaluated and the material units conform as needed to the input HFM, FEHM modeling input files are generated. These files include the mesh geometry, lists of nodes on external boundaries, and node lists sorted by material property.

All nodes were automatically and visually checked to ensure that they were assigned the correct material identification corresponding to the input HFM. Lists of the number of nodes associated with each material were compared to the volume of each material in the EARTHVISION framework to confirm that the hydrogeologic units are identified correctly.

When evaluating the computational grid for SZ flow and transport, the hydrogeologic properties of the grid are compared to the hydrogeologic framework used as input. It is expected that the grid units will differ slightly from the HFM due to differences in grid spacing (i.e., 250 versus 125 m). The grid units should still resemble the input HFM and areas of importance should be replicated accurately. The flow pathways are expected to leave the repository and travel in a south-southeasterly direction towards Fortymile Wash and the 18-km compliance boundary. From the 18-km boundary to the end of the model, the flowpaths should trend to the south-southwest and generally follow Fortymile Wash. Outlines of the repository, Fortymile Wash, and U.S. Highway 95 are included on Figure 6-5 as reference to these areas.

6.4.3.4 Evaluation of Hydrogeology represented in the SZ Computational Grid

All nodes were automatically and visually checked to ensure that they were assigned the correct material. The number of nodes assigned to each hydrogeologic unit and their associated element volumes are presented in Table 6-5. Lists of the number of nodes associated with each material were compared to the volume of each material in the HFM2006 to confirm that the hydrogeologic units are identified correctly. To check that hydrogeologic properties are being assigned in accord with the HFM2006, relative unit volumes are compared. Differences will occur between the HFM and grid units due to variations in grid element sizes in the computational grid. Volumes represented by the HFM2006 surfaces are included for comparison. Large grid elements less accurately capture thin layers as shown when comparing unit volumes. Figures showing the grid units are supplied in Appendix G to confirm that differences are reasonable and acceptable.

Table 6-5. SZ Computational Grid and HFM2006 Volume Comparisons by Unit

Unit	Names	SZ Computational Grid			HFM2006 Surfaces	
		Tetrahedral Elements Number	Volume of Elements per Unit (m)	% Fractional Volume	Volume between surfaces (m)	% Fractional Volume
28	YAA	32,106	4.75×10^{9}	0.07	1.15×10^{10}	0.17
27	YACU	7,788	8.11×10^{8}	0.01	9.89×10^{8}	0.01
26	OAA	137,772	2.09×10^{10}	0.31	2.35×10^{10}	0.34
24	LA	18,834	2.08×10^{9}	0.03	2.18×10^{9}	0.03
23	LFU	38,208	8.56×10^{9}	0.13	1.48×10^{10}	0.22
21	Upper VSU	316,716	5.53×10^{10}	0.81	5.58×10^{10}	0.82
20	TMVA	152,586	3.77×10^{10}	0.56	4.38×10^{10}	0.64
19	PVA	838,668	2.35×10^{11}	3.47	2.45×10^{11}	3.59
18	CHVU	280,368	9.29×10^{10}	1.37	9.45×10^{10}	1.38
17	WVU	122,802	2.52×10^{10}	0.37	2.57×10^{10}	0.38
16	CFPPA	140,064	3.38×10^{10}	0.56	3.78×10^{10}	0.55
15	CFBCU	439,698	1.35×10^{11}	1.98	1.35×10^{11}	1.98
14	CFTA	584,232	2.85×10^{11}	4.20	2.85×10^{11}	4.17
12	OVU	158,982	1.68×10^{11}	2.47	1.69×10^{11}	2.48
11	Lower VSU	461,478	5.97×10^{11}	8.78	5.96×10^{11}	8.72
9	LCA_T1	185,736	3.00×10^{11}	4.42	3.00×10^{11}	4.39
8	LCCU_T1	101,550	2.63×10^{11}	3.87	2.64×10^{11}	3.86
7	UCA	24,900	8.33×10^{9}	0.12	8.83×10^{9}	0.12
6	UCCU	238,248	2.18×10^{11}	3.21	2.21×10^{11}	3.24
5	LCA	793,620	2.55×10^{12}	37.59	2.54×10^{12}	37.13
4	LCCU	275,532	1.07×10^{12}	15.77	1.08×10^{12}	15.79
3	XCU	47,490	2.23×10^{11}	3.28	2.26×10^{11}	3.30
2	ICU	106,974	4.50×10^{11}	6.62	4.55×10^{11}	6.67
Totals		5,504,352	Element Volume 6.79×10^{12}		Sum Volume 6.83×10^{12}	

Source: Output DTN: LA0612TM831231.001.

NOTES: HFM2006 volumes represent the best achievable volumes when matching surface resolutions. The computational grid lengths are 250 m in the horizontal and depths range from 10 to 600 m in the vertical. Units 10, 13, 22, and 25 are not found within the domain of the SZ site-scale flow model.

Figures 6-8 through 6-10 represent sections cut through the computational grid and can be compared to matching sections cut through HFM2006 (SNL 2007 [DIRS 174109], Figures 6-5 and 6-6). The first figure is a north-to-south vertical section cut at an easting of 552,500 m. This section was selected because it is located approximately along the flowpath from Yucca Mountain to the south. The second figure is a west-to-east vertical section cut at a northing of 4,064,000 m and it is located within the area of the newest NC-EWDP well data used in HFM2006. This section cuts across most of the faulting in the area and demonstrates where the faulting is represented in the more widely spaced data of the regional model, which served as the basis for HFM2006. As can be seen in this figure, some of the offsets on the faults are preserved through changes in altitude of a given hydrogeologic unit. Given the depth to which the model extends and the lack of information in most of the modeled volume, this seems to be a rational simplification (SNL 2007 [DIRS 174109], Section 6).

Figure 6-10 is a 5× vertical exaggeration detail of the west-east cross section. The spacing is shown with the grid lines and the accuracy imposed by grid resolution is apparent. Units at the lower levels and with large 200- to 600-m edge lengths capture only a coarse representation of the deeper units. Vertical spacing of 10 to 20 m in the shallower units do a much better job of capturing the hydrogeologic unit shapes where increased accuracy is needed.

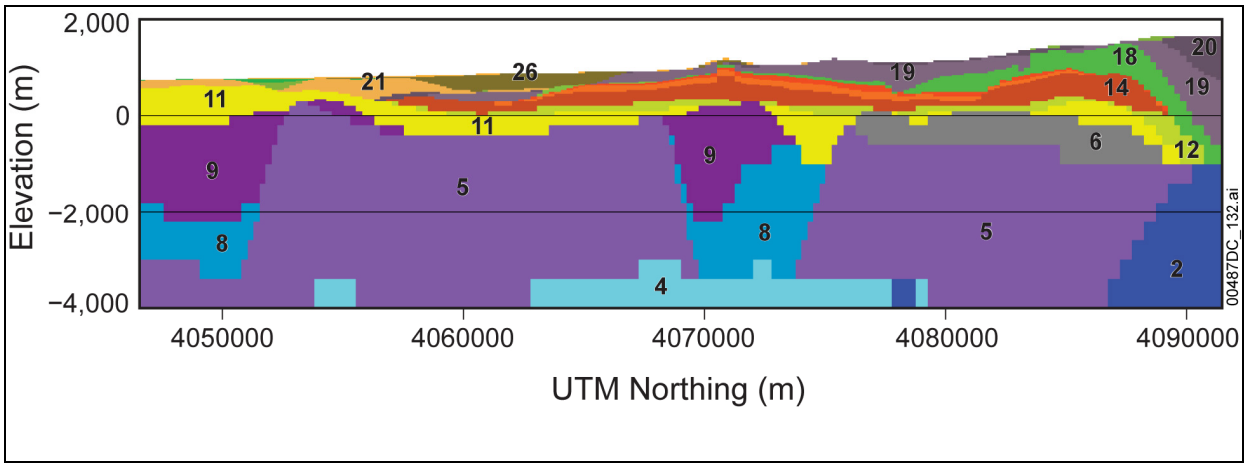

Source: Output DTN: LA0612TM831231.001.

NOTE: Coordinates in UTM, Zone 11, NAD27 meters, 2× vertical exaggeration. Unit numbers are the hydrogeologic numbers defined by HFM2006 in Table 6-2. The colors correspond to those in the legend for Figure 6-7.

UTM = Universal Transverse Mercator.

Figure 6-8. Hydrogeologic Units Present at North-South Cross Section in the SZ Computational Grid at UTM Easting = 552,500 m

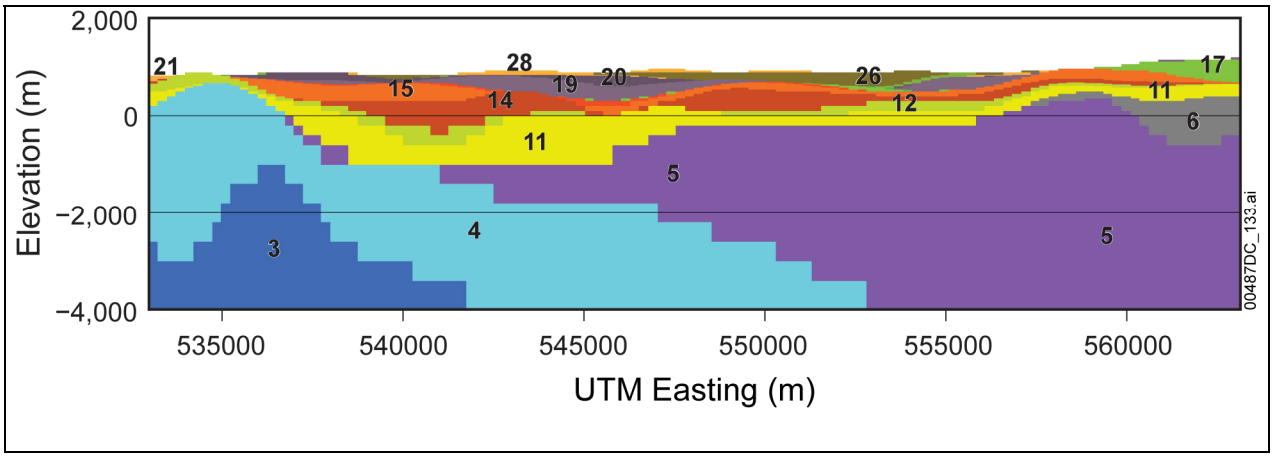

Source: Output DTN: LA0612TM831231.001.

NOTE: Coordinates in UTM, Zone 11, NAD27 meters, 2× vertical exaggeration. Unit numbers are the hydrogeologic numbers defined by HFM2006 in Table 6-2. The colors correspond to those in the legend for Figure 6-7.

UTM = Universal Transverse Mercator.

Figure 6-9. Hydrogeologic Units Present at West-East Cross Section in the SZ Computational Grid at UTM Northing = 4,064,000 m

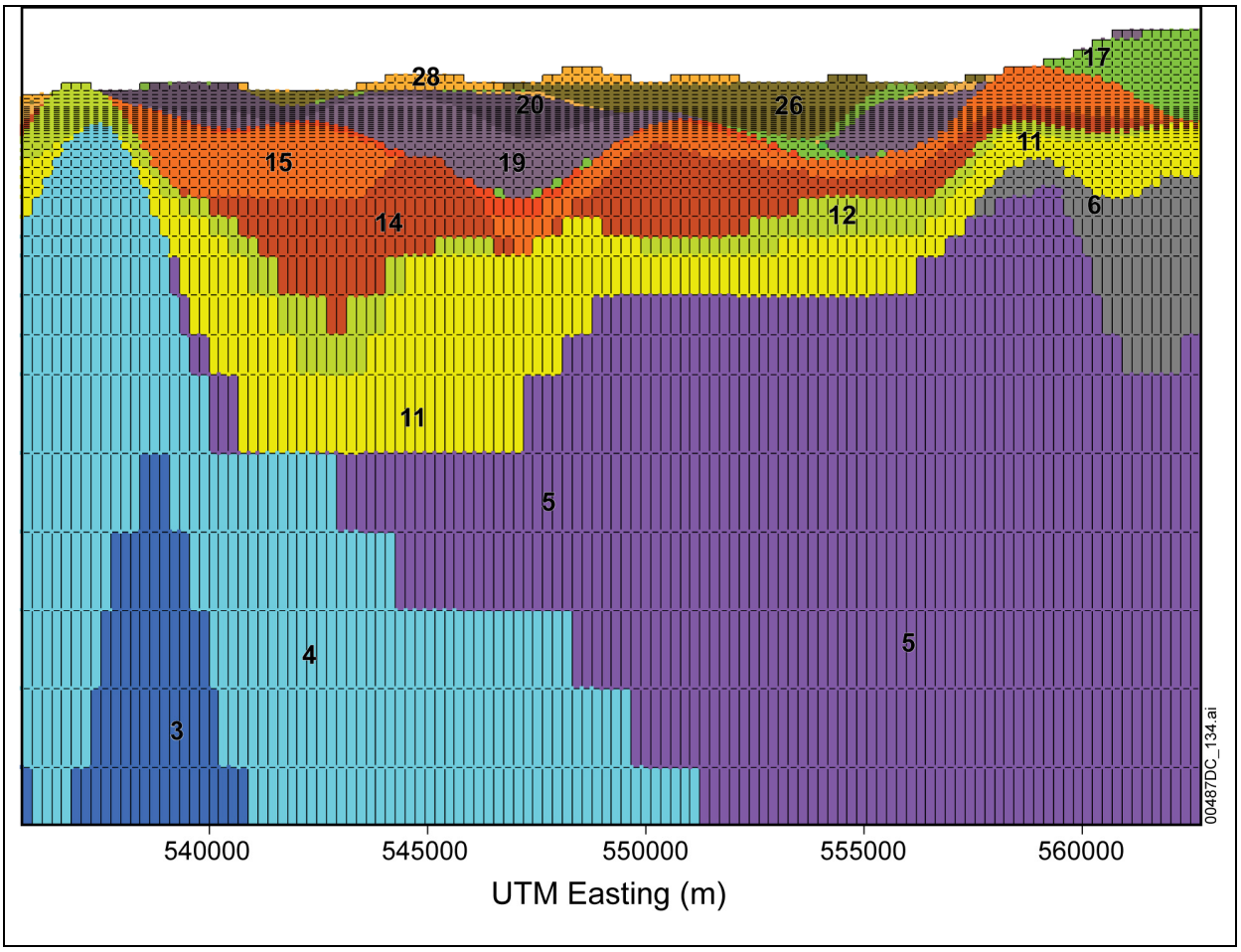

Source: Output DTN: LA0612TM831231.001.

NOTE: Coordinates in UTM, Zone 11, NAD27 meters, 5× vertical exaggeration. Unit numbers are the hydrogeologic numbers defined by HFM2006 in Table 6-2. This image shows the spacing of the grid in the vertical direction. The grid nodes used in FEHM flow modeling are shown here at the vertices of each grid block. Grid nodes and volumes are colored according to HFM2006 hydrogeology. The colors correspond to those in the legend for Figure 6-7.

UTM = Universal Transverse Mercator.

Figure 6-10. Hydrogeologic Grid Nodes and Spacing at West-East Cross Section in the SZ Computational Grid at UTM Northing = 4,064,000 m

6.4.3.5 Hydrogeology at the Water Table

A new water-table surface is used in conjunction with HFM2006 and is discussed in Appendix E. The water-table surface defines which grid nodes are below and above the water table, those that are above the water table are inactivated in the FEHM flow model. This results in node elevations at the top of the flow model that range from ~1,200 m in the north to ~700 m in the south. The hydrogeologic units at the water table top are shown in Figure 6-11, which compares well with HFM2006 view at the water table (SNL 2007 [DIRS 174109], Figure 6-7c).

Table 6-6. SZ Computational Grid Nodes by Unit

Unit	Abbreviation	Nodes per Unit Under Top Surface	Nodes per Unit Under Water Table Surface
28	YAA	9,965	197
27	YACU	1,580	247
26	OAA	24,148	10,637
24	LA	3,289	1,387
23	LFU	8,608	2,751
21	Upper VSU	53,911	42717
20	TMVA	27,940	18,131
19	PVA	143,658	94,149
18	CHVU	47,905	29,189
17	WVU	21,116	14,576
16	CFPPA	23,461	20,242
15	CFBCU	73,939	67,436
14	CFTA	98,162	93,327
12	OVU	27,152	26,691
11	Lower VSU	78,182	76,856
9	LCA_T1	31,608	28,588
8	LCCU_T1	17,848	17,053
7	UCA	4,228	4,201
6	UCCU	40,842	33,533
5	LCA	135,186	131,312
4	LCCU	52,891	52,745
3	XCU	10,018	10,015
2	ICU	20,708	20,708
	Totals	956,345	774,177

Source: Output DTN: LA0612TM831231.001.

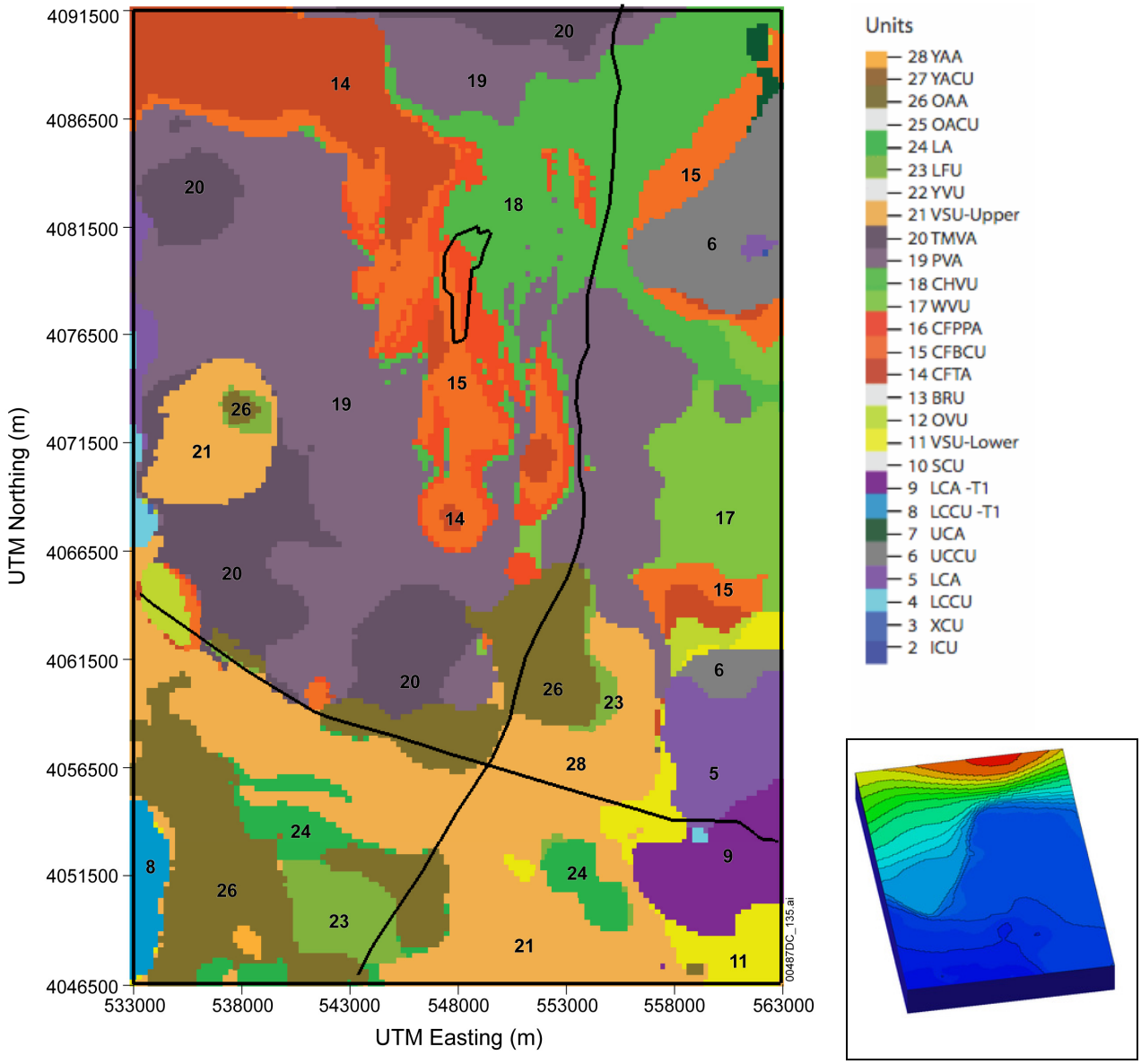

Source: Output DTN: LA0612TM831231.001.

NOTE: For illustration purposes only. The figure depicts grid points at the water-table surface. The black lines are used for reference and are the repository outline (SNL 2007 [DIRS 179466]), U.S. Highway 95, and Fortymile Wash. The inset shows the computational grid colored by the water table elevations ranging from 680 m in the south to 1,230 m in the north.

UTM = Universal Transverse Mercator.

Figure 6-11. Hydrogeologic Units Present at the Water-Table Surface in the SZ Computational Grid

The resolution of the computational grid was designed to have the smallest vertical spacing in the vicinity of the water-table below the repositorysurface and below. Therefore, the computational grid honors the hydrogeology of the HFM2006 as can be seen in these figures. Updates to the HFM2006 show differences most evident in the southern part of the model where the volcanic and sedimentary unit replaces the valley-fill aquifer as the most pervasive unit. Updates to the HFM2006 also include increased abundance of the Crater Flat group to the west

of Yucca Mountain and the occurrence of Lava Flow unit to the east of Fortymile Wash and to the north of U.S. Highway 95. These changes may have influence on the calibration and specific discharge simulations of the flow model.

Further comparisons can be made across each unit by comparing HFM2006 layer thickness and distribution maps (SNL 2007 [DIRS 174109], Appendix C) to the distribution of grid nodes for each hydrogeologic unit (SNL 2007 [DIRS 174109], Appendix A) and are presented in Appendix G. Figures for each grid unit include the distribution of each unit for the full model domain, and a second figure showing the grid units truncated by the water table surface. The truncated grid units show the active grid nodes for the FEHM modeling domain. Both sets of images are views looking directly down at the top, with south toward the page bottom and showing the horizontal distribution for each unit 1 through 28. The shapes of the HFM2006 maps (SNL 2007 [DIRS 174109], Appendix C) and the grid units (SNL 2007 [DIRS 174109], Appendix A) compare reasonably given that the grid resolution is 250 m and the HFM2006 is 125 m and that vertical grid resolution varies from 10 to 600 m.

6.4.3.6 Uncertainty

Uncertainty in the SZ computational grid is a function of HFM2006 and the resolution of the grid in relation to the flowpaths. Large grid spacing and associated loss of hydrogeologic unit shape accuracy are chosen to correspond with areas deep in the model and beyond the flowpath regions. Areas of highest resolution were chosen in the shallow units and in the area of the water table below the repository. Uncertainties in the HFM2006 relate most importantly to the quantity and location of available qualified data, and secondly to the interpretation of surfaces and the representation of important faults and structures. Uncertainties due to the definition of the hydrogeologic units are propagated through the flow and transport model abstraction (SNL 2007 [DIRS 177390]).

Model uncertainties in the HFM2006 can be attributed to interpretations and simplifications driven largely by the distribution and availability of data. The data distribution over the SZ area is uneven, much of the volume is unsampled, and many of the inputs are interpretations. As a result, the expected error in the HFM2006 varies significantly over the model area. Some of the surfaces, such as that of the upper volcanic aquifer in the area of the repository, are relatively well defined by more than one data set (derived from the surface hydrogeologic unit map and borehole lithologic logs). Others, especially the units that crop out less commonly, are less well defined and are extrapolated from sparse data. In the area of the repository, the unit locations are relatively well known. Even in this area, however, only one borehole penetrates the Paleozoic rocks. Data uncertainty increases with depth and distance from the repository as data become sparse and the effects of faults deeper in the system become unknown. As a result, the model contains an inherent level of uncertainty that is a function of data distribution and geologic complexity. Additional limitations include data-poor regions in the deeper Paleozoic carbonate region (SNL 2007 [DIRS 174109], Section 6.4.3).

HFM2006 is constructed with a horizontal grid spacing of 125 m, but most of the model domain does not contain sufficient geologic detail to support this resolution. This results in smoothly interpreted or interpolated surfaces at a resolution finer than justified by the geologic data. This finer resolution does not add any additional error. Specific borehole data and other measured

data were incorporated where available. The site-scale flow model indicates that as long as the horizontal spatial ambiguity in the location of hydrogeologic contacts is less than 250 m (the horizontal grid cell size), there is insignificant impact on model specific discharge or flux calculations (Section 6.7.3) Because flow leaving the repository area is confined to a few of the most permeable units, the vertical dimension of the computational flow grid deserves special consideration (vertical resolution is variable with the smallest spacing of 10 m located between 640 and 760 m). The vertical uncertainty of the input data is variable with borehole contacts at approximately plus or minus 3 m (10 ft). Uncertainty in relatively less complex areas of the GFM with some geologic constraints has been described as plus or minus 23.8 m (78 ft) at a distance of about 1,000 m from a known data point (BSC 2004 [DIRS 170029], Section 6.6.3). The depth from the top of the upper layer of the HFM2006 model to the water table (Output DTN: MO0611SCALEFLW.000) is less than 1,000 m and averages 255 m over the model area. This distance constraint provides confidence that the uncertainty is less than that described for some of the GFM (SNL 2007 [DIRS 174109], Section 6.4.3).

As with HFM2006, the upper portion of the grid, less than 1,000 m deep and close to the surface provides less uncertainty than the deeper portions of the model.

6.4.3.7 Features

To represent discrete features and regions having distinct hydrological properties within the model domain, a set of ten hydrogeologic features were identified and incorporated into the flow model. The hydrogeologic features included in the SZ site-scale flow model primarily represent faults, areas of mineralogical alteration, and areas of alluvial deposition. The features described here are typically defined as vertical in nature (faults) although some are defined areally (zones of altered permeability). Features are distinct from the subhorizontal geological formations, which form zones with distinct geometry and material properties and are described in Section 6.3.1.10. Each of the features described in this report comprises multiple geologic formations and represents a zone of altered (enhanced, reduced, and/or anisotropic) permeability within the individual formations. Each feature has an impact on the SZ site-scale flow model. The geometric definition, description, nature of permeability alteration, and impact on the model for each of these features are described in Table 6-7. In the table, the numbers in the parentheses refer to zone numbers in the input file for FEHM. The features are shown in Figure 6-12, which is based on the Yucca Mountain area geologic map (DTN: GS010908314221.001 [DIRS 162874]) and shows feature representation in the SZ site-scale flow model. The permeability values associated with the features described in Table 6-7 are presented and discussed in Section 6.5.1.3.

The Lower Fortymile Wash alluvial zone was added because of the distinct character of the Fortymile Wash in the southern part of the model. Field observations indicate possible channelization with attendant textural contrasts with surrounding alluvial material (Oatfield and Czarnecki 1989 [DIRS 149438]). This zone of increased permeability was constrained by a quadrilateral with vertices listed in Table 6-7 and included only members of alluvial units (surfaces 24 and 26 to 28 in Table 6-2).

A zone was defined near Yucca Mountain with a quadrilateral whose vertices are listed in Table 6-7. This zone serves two purposes: to define the extent of the anisotropic region in the

volcanic units (Units 12, 14, 15, 16, 17, 18, 19, 20, and 25), and to provide boundaries for a zone of enhanced permeabilitiy in the Crater Flat tuffs to better approximate the small haydraulic gradient in the region. The zone was defined based on responses of USW H-4, UE-25 C#1, UE-25 WT#14, and UE-25 WT#3 to pumping at the C-holes from May 1996 to November 1997. Furthermore, this zone did not include wells USW H-5, G-1, and UZ-14 because, although these wells are located east of the Solitario Canyon Fault, they showed anomlaous heads closer to those observed in wells located west of Solitario Canyon Fault (USW H-6, WT-7, and WT-14). This indicates that some non-characterized feature or process is impacting the water levels just to the east of Solitario Canyon Fault and the newly defined zone allows the model to better represent these data The quadrilateral is defined to encompass the small-gradient area southeast of the repository between Solitario Canyon and Fortymile Wash Faults without including wells USW H-5, G-1, and UZ-14, but including wells USW H-4, UE-25 C#1, UE-25 WT#14, and UE-25 WT#3.

Most hydrogeologic units (the 19 units with areal extents that reach into the north of the model including all units except the lower clastic confining unit thrust, lower carbonate aquifer thrust, Wahmonie volcanic unit, limestone aquifer, and the young alluvial confining unit) have been divided into northern and southern zones near the Claim Canyon caldera boundary to represent the altered northern zone (see Section 6.3.1.11). This zone of decreased permeability with geometry described in Table 6-7 facilitates model representation of the LHG north of Yucca Mountain. Except for Sever Wash Fault, fault nodes do not reside in this region. The altered northern region is defined with an arc that intersects the model domain and it is defined by a circle with center 546,500; 4,102,400 (UTM easting and northing) and radius 21,100 m. This designation was selected such that the defining circle roughly corresponds to the center of the caldera complex and the radial extent includes wells: GEXA Well #4, UE-29 a#2, UE-29 UNZ#91, UE-25 WT#6, USW G-2, and USW WT-24. Breaking the hydrogeologic units into independent northern and southern zones yields 19 additional calibration parameters. Figure 6-13 illustrates the radial extent of the altered northern region.

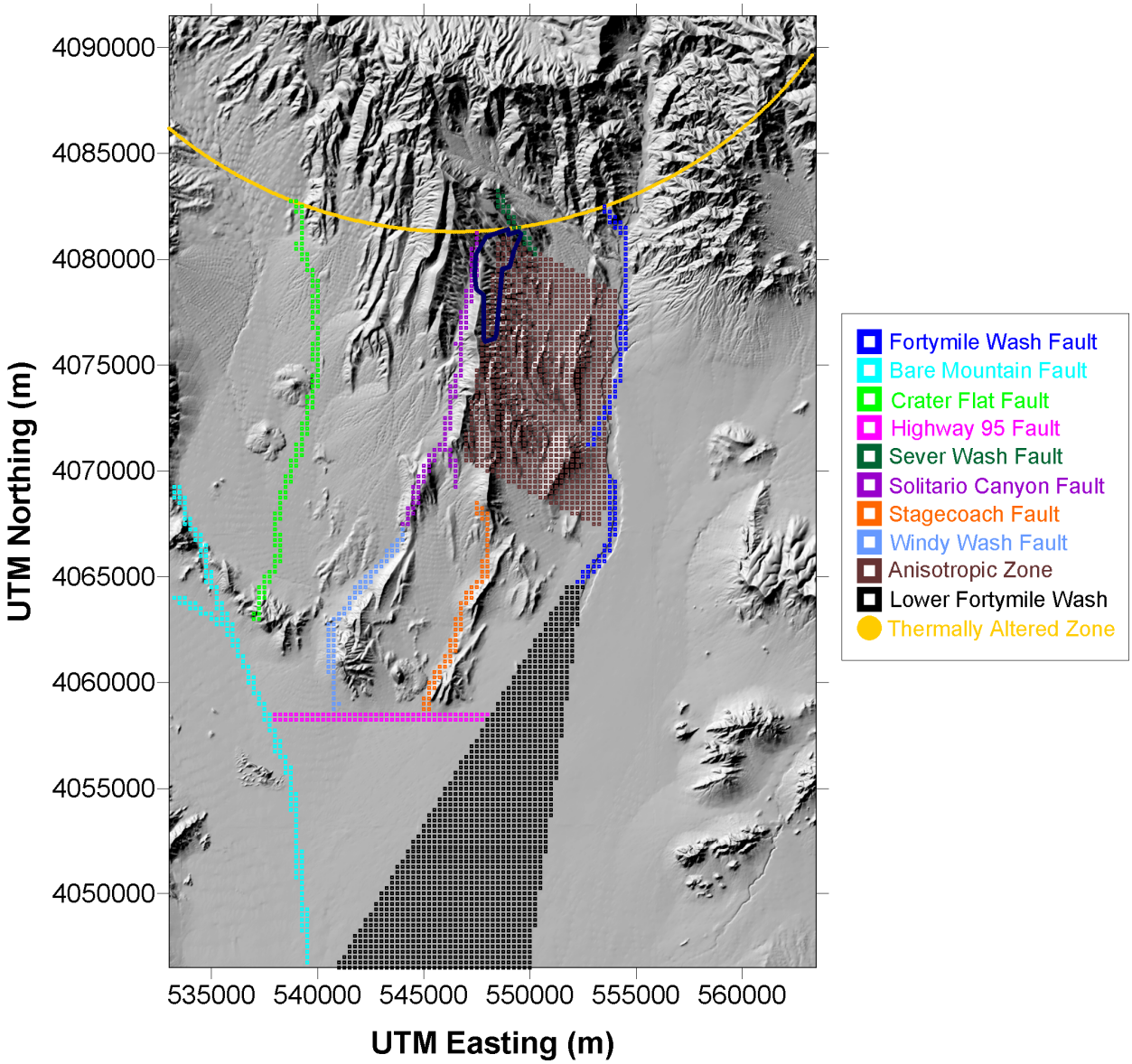

Source: Output DTN: SN0612T0510106.004, *feature_set.zonn* and *aniso.zonn*).

NOTE: Source for repository outline: SNL 2007 [DIRS 179466]. Fault traces are labeled in the legend. FEHM zone number correspond to the following regions: 39 – Anisotropic zone; 40 – Fortymile Wash Fault; 41 – Bare Mountain Fault; 42 – Crater Flat Fault; 43 – U.S. Highway 95 Fault; 44 – the Solitario Canyon Fault; 45 – Sever Wash Fault; 46 – Stagecoach Fault; 47 – Windy Wash Fault; 50 – Lower Fortymile Wash.

UTM = Universal Transverse Mercator.

Figure 6-12. Geologic Features Included in the SZ Site-Scale Flow Model

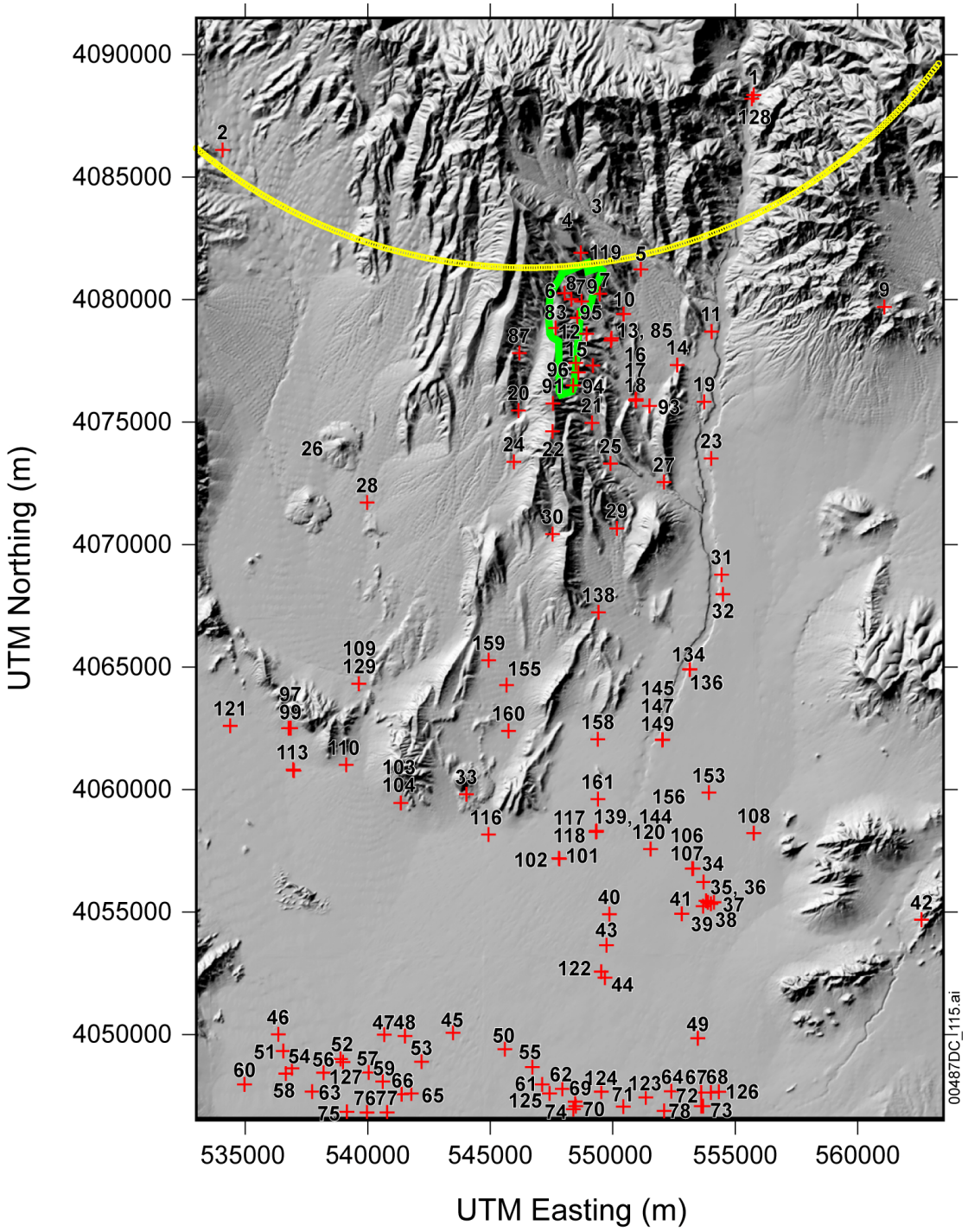

Source: Output DTN: SN0612T0510106.004, *north_zones.zonn*.

NOTE: Source for repository outline: SNL (2007 [DIRS 179466]). The altered northern region is dilineated by the yellow arc. Calibration wells are shown on the plot with numbers corresponding to Table 6-8.

UTM = Universal Transverse Mercator.

Figure 6-13. The Altered Northern Region and Well Locations

Table 6-7. Hydrological Features in the SZ Site-Scale Flow Model

Feature Name and Description	Number of Nodes	Hydrogeological Characteristics	Impact on Model
1. Fortymile Wash Fault (#401 and #402) This is a north-south trending feature east of Yucca Mountain. Vertically, it extends from top to bottom of the model.	3,317 and 2,028	Possible control of fluid pathways near Yucca Mountain. Because this fault is likely a conducting feature, it is defined isotropically.	The fault is a possible preferential flow path
2. Bare Mountain Fault (#41) – This is a northwest- to southeast-trending feature in the southwestern corner of the model. Vertically, it extends from top to bottom of the model.	7,939	This fault has a vertical permeability anisotropy factor of 10.	The fault directs flow from Crater Flat to the Amargosa Desert
3. Crater Flat Fault (#42) – This is a north-south trending feature in the western half of the model, starting south of the Claim Canyon and terminating near U.S. Highway 95, almost halfway between the western boundary of the model and the Solitario Canyon Fault. Vertically, it extends from top to bottom of the model.	7,095	This fault has plane parallel permeability anisotropy factor of 10.	The fault generates a higher head in the western half of the model thereby limiting the influx from the western boundary (it restricts the flow to the east)
4. U.S. Highway 95 Fault (#43) – This is an east-west trending feature in the lower half of the western portion of the model. Vertically, it extends from top to bottom of the model, but it does not continue through the alluvial units defining the Lower Fortymile Wash zone.	3,633	This fault has plane parallel permeability anisotropy factor of 10.	This fault restricts flow in the north-south direction and supports high heads to its north
5. Sever Wash Fault (#46) – This is a northwest-southeast trending feature. Vertically, it extends from top to bottom of the model.	2,437	This fault has a vertical permeability anisotropy factor of 10.	This fault may serve to divert southerly flow around the repository to the east thereby facilitating southeast flowpaths from the repository
6. Solitario Canyon Fault (#44) – This is a north-south trending feature just to the west of Yucca Mountain. Vertically, it extends from top to bottom of the model.	7,041	This fault has plane parallel permeability anisotropy factor of 10.	This fault generates a higher head to the west of Yucca Mountain and impedes flow from Crater Flat to Yucca Mountain
7. Stage Coach Fault (#45) – This fault forms the eastern splay starting at the southerly end of the Solitario Canyon Fault. Vertically, it extends from top to bottom of the model.	1,182	This fault has plane parallel permeability anisotropy factor of 10.	This fault generates a higher head to the west and impedes flow from the east
8. Windy Wash Fault (#47) – This fault forms the eastern splay starting at the southerly end of the Solitario Canyon Fault. Vertically, it extends from top to bottom of the model. Only that portion of the fault south of its connection to the Solitario Canyon Fault is used in the model.	2,437	This fault has plane parallel permeability anisotropy factor of 10.	This fault generates a higher head to the west and impedes flow from the east

Table 6 7. Hydrological Features in the SZ Site-Scale Flow Model (Continued)

Feature Name and Description	Number of Nodes	Hydrogeological Characteristics	Impact on Model
9. Lower Fortymile Wash Alluvial Zone (#50)[a] – This is a region to the south of Yucca Mountain in the southern half of the model that connects to the southern end of Fortymile Wash Fault. Vertically, it extends from top to bottom of the model, but it only comprises alluvial units.	a	This zone represents the possible increased permeability due to Fortymile Wash	This zone influences the SZ site-scale flow model and it is expected to be important to TSPA due to its effect on solute transport
10. Anisotropic/Crater Flat Zone (#39/#60)[b] – This is a region east of the Solitario Canyon Fault and west of Fortymile Wash Fault. It is included in the model to facilitate representation of the small-gradient area southeast of the repository and also to allow the model to better represent the heads in wells USW H-5, G-1, and UZ-14. Vertically, it extends from top to bottom of the model, but it comprises only Crater Flat tuffs. This zone also defines the horizontally anisotropic region, but in this instance, it includes all volcanic units within this quadrilateral (Units 12, 14, 15, 16, 17, 18, 19, 20, and 25).	b	This zone represents a possible permeability increase in the Yucca Mountain region for the Crater Flat units. Also, this zone defines the horizontally anisotropic volcanic units.	This zone may affect the gradient near the repository and also the specific discharge

Source: DTN: GS010908314221.001 [DIRS 162874].

Output DTN: SN0612T0510106.004.

NOTES: Faults are defined as nodes that fall within 180 m of the coordinates defining the fault as listed in DTN: GS010608312332.001 [DIRS 155307] with the location of the U.S. Highway 95 fault updated in DTN: GS010908314421.001 [DIRS 162874]. Linear interpolation was used to specify fault location coordinates to ensure that spacing between data points defining the fault was never more than 125 m from its neighbors. This guarantees that the fault will be defined with a stair-stepping appearance when viewed from above (each fault node is connected to at least two other fault nodes in the horizontal. Fortymile Wash fault was defined as all nodes within 250 m of the specified fault coordinates.

[a]This zone is defined by a bounding quadrilateral (UTM): (x_1,y_1) = 540,000; 4,046,500; (x_2,y_2) = 550,000; 4,046,500; (x_3,y_3) = 552,100; 4,062,400; (x_4,y_4) = 550,840; 4,062,400.
[b]This zone defined by a bounding quadrilateral (UTM): (x_1,y_1) = 548,500; 4,081,288; (x_1,y_1) = 554,100; 4,078,462; (x_1,y_1) = 553,445; 4,067,200; (x_1,y_1) = 546,800; 4,070,549.
Anisotropy in the horizontal hydraulic conductivity was based on responses of USW H-4, UE-25 C#1, UE-25 WT#14, and UE-25 WT#3 to pumping at the C-holes from May 1996 to November 1997. The range of anisotropies and their directions were calculated by SNL (2007 [DIRS 177394], Appendix C6.2). The calculated directions of anisotropy from this effort (derived from the shape of the cone of depression from the C-wells test) support the principally north-south anisotropy direction between the C-holes and USW H-4 along Antler Wash. The zone must be large enough to include wells USW H-4 on the west, UE-25 WT#14 on the east, and UE-25 WT#3 in the south. Overall, the zone of anisotropy is defined to include all volcanics (Units 12, 14, 16, 17, 18, 19, 20, and 25) that fall within a generalized region east of the Solitario Canyon Fault and west of Fortymile Wash Fault.

SZ = saturated zone; TSPA = total system performance assessment; UTM = Universal Transverse Mercator.

6.4.3.8 Boundary and Initial Conditions

The lateral boundary conditions are described in Section 6.3.1.6. Historically, groundwater has been extracted from wells in the Amargosa Valley south of Yucca Mountain. Drawdown from the wells is represented in the potentiometric surface map that was used to establish southern boundary head conditions derived from the potentiometric surface. Consequently, the effect of pumping on flow within the model domain is accounted for by the head values specified along the southern boundary and the truncation by the water table. A small amount of pumping also has occurred from within the southern portion of the site-scale model domain, but ignoring this pumping is assumed to have little effect on the calculated flowpaths and flow times to compliance boundaries. No explicit representation of pumping is included in this model.

The initial conditions (initial pressure or head distribution) are not relevant because the SZ site-scale flow model is formulated for steady-state flow.

6.4.3.9 Recharge

Nodes above the water table were inactivated by specifying a negative porosity. Recharge (infiltration) was applied to the top surface of the active computational grid (at the water table) as a flux boundary condition by distributing an infiltration map onto the computational mesh (Figure 6-14). The process used to specify the recharge for the SZ site-scale flow model is outlined in *Recharge and Lateral Groundwater Flow Boundary Conditions for the Saturated Zone Site-Scale Flow and Transport Model* (BSC 2004 [DIRS 170015], Section 6.2). The recharge data were developed with some correlation to the landscape and geology at ground surface based on data from the 2004 DVRFS (Belcher 2004 [DIRS 173179], Figure C-8), the 2003 UZ flow model (BSC 2004 [DIRS 169861]), and data from Savard (1998 [DIRS 102213]) for the Fortymile Wash Fault and the Lower Fortymile Wash alluvial zone. Although redistribution of infiltration in the UZ is likely to change the pattern of recharge, these data are considered sufficient for the flow model. The data used from the 2004 DVRFS are qualified for one time use in this report in Appendix C. It is worth noting that the data reported by Savard (1998 [DIRS 102213]) for infiltration along the Fortymile Wash Fault actually indicate less infiltration than the surrounding nodes as interpreted from the 2004 DVRFS (Belcher 2004 [DIRS 173179]) (see Figure 6-14).

Total recharge was about 61.3 kg/s (1.93×10^6 m^3/yr or 1,570 acre-ft/yr). Of this total, about 5.6 kg/s (1.76×10^5 m^3/yr or 143 acre-ft/yr) was attributed to flux from the UZ flow model area and about 2.0 kg/s (6.20×10^4 m^3/yr (50 acre-ft/yr) was attributed to infiltration along Fortymile Wash, leaving a remainder of about 53.7 kg/s (1.707×10^6 m^3/yr or 1,375 acre-ft/yr) from distributed recharge. The recharge in each node of the regional model was extracted and the corresponding recharge to the SZ site-scale model node was calculated (the regional model grid has a resolution of 1,500 m, which is six times coarser than the site-scale model grid resolution).

Target groundwater inflows approximately along the eastern, northern, and western boundaries of the SZ site-scale flow model total 337.8 kg/s (10.7×10^6 m^3/yr or 8,650 acre-ft/yr), 158.9 kg/s (5.0×10^6 m^3/yr or 4,065 acre-ft/yr), and 120.3 kg/s (3.8×10^6 m^3/yr or 3,080 acre-ft/yr), respectively (Appendix D). These inflows, totaling 617.2 kg/s (19.5×10^6 m^3/yr or 15,790 acre-ft/yr), represent 10 times the estimated recharge applied at the water table due to

infiltration. Of the total inflow across the eastern boundary, 273.1 kg/s (8.6×10^6 m^3/yr or 6,970 acre-ft/yr), or 81%, occurs across the southern 6 km, nearest the Amargosa Desert, and nearly all of that occurs in bottom layers of the regional-scale flow model and represents flows in the lower carbonate aquifer (D'Agnese et al. 1997 [DIRS 100131], p. 90, Figures 46 and 47; Belcher 2004 [DIRS 173179]). Much of the inflow to the SZ site-scale flow model from the 2004 DVRFS (Belcher 2004 [DIRS 173179]) is through the bottom layer of that model, which largely comprises the lower carbonate aquifer and may be up to 3-km thick. However, because the 2004 DRFS (Belcher 2004 [DIRS 173179]) uses the HUF package, it cannot be assumed that model layers correspond to hydrogeologic unit contacts (as is the case for the SZ site-scale flow model). Thus, it is difficult to estimate how large a fraction of the total flow through the volcanics can be attributed to infiltration. Across all 16 layers of the 2004 DVRFS (Belcher 2004 [DIRS 173179]), 61.3 kg/s represents about 10% of the total inflow while across the top 15 layers, it represents approximately 19% of the total inflow. A recent update to infiltration estimates in the region immediately surrounding Yucca Mountain (SNL 2007 [DIRS 174294]) was used to supply new percolation fluxes to the UZ flow model, which yielded a weighted flow through its footprint of 8.4 kg/s under present-day climatic conditions (SNL 2007 [DIRS 175177], Table 6.2-7). While this is a 49% increase over the previous net infiltration through the UZ footprint (5.6 kg/s), it remains a small portion of the infiltration budget, 13%, and a correspondingly smaller portion of the entire flow budget through the lateral boundaries, equal to about 1%.

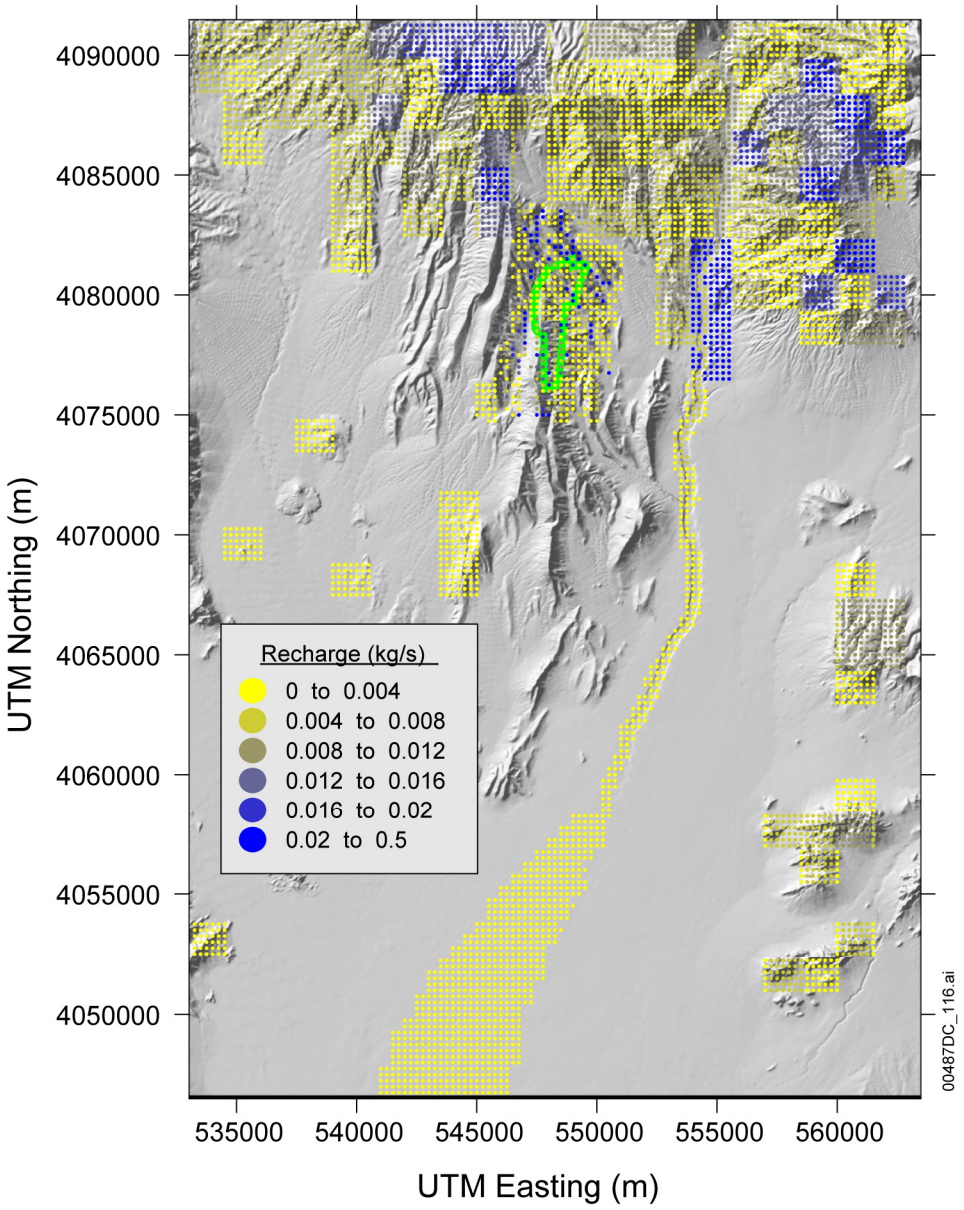

Source: Repository outline (green curve) (SNL 2007 [DIRS 179466])
Infiltration data: Output DTN: SN0612T0510106.003 (*wt_250_04.dat*).

NOTE: Recharge map combines the components of recharge from the 2004 DVRFS , recharge below the UZ site-scale model domain and focused recharge along Fortymile Wash using a 250-m grid resolution.

UTM = Universal Transverse Mercator.

Figure 6-14. Recharge Applied to the SZ Site-Scale Flow Model

6.4.3.10 Nodal Hydrogeologic Properties

Hydrogeologic properties must be specified for each node in the computational grid. Using the grouping definitions generated during the grid-building process, permeabilities are assigned to each node. Temperatures (hence viscosities) are also applied and porosities can be defined for transport simulations if desired.

The parameter values for viscosity depend on the temperature at each node and a uniform vertical temperature gradient is assumed. The assumption of a uniform temperature gradient with depth is equivalent to assuming uniform geothermal heat flux through a medium of homogeneous thermal conductivity. In addition, the temperature at the ground surface is assumed constant. The data on temperature in boreholes presented by Sass et al. (1988 [DIRS 100644]; DTN: MO0102DQRBTEMP.001 [DIRS 154733], Figures 4, 5, 6, 7, 8, and 10) indicate that there is significant variability in the temperature gradient at different locations and within individual wells, presumably from advective redistribution of heat from infiltration and vertical groundwater flow. The data were used to estimate an approximate average temperature gradient and representative surface temperature for the site. As noted by Sass et al. (1988 [DIRS 100644], p. 2), there is considerable variability in the temperature gradients among the wells from about 15°C/km to nearly 60°C/km. The approximate average value of the temperature gradient in the wells is 25°C/km, and the average surface temperature is about 19°C (yielding maximum temperatures of 167.75°C at the bottom of the model domain). However, these data also indicate that the temperature gradients become increasingly linear with depth below the water table. It is important to note that the goal of assigning temperature variations with depth in the SZ site-scale flow model is to account for resulting variations in fluid viscosity at different depths in the SZ. The linear approximation of the temperature gradient is adequate to capture the general effects of variations in groundwater viscosity with depth in the SZ site-scale flow model.

The density also varies with temperature, but the effect is much smaller than that of viscosity, and therefore density is treated as a constant. Using a variable viscosity allows the calibration of intrinsic permeability to be made instead of hydraulic conductivity. The former is a rock property, whereas the latter is both a rock and fluid property. This approach, in turn, allows for more accurate flux calculations at the boundaries of the model.

The approach taken to incorporate groundwater temperature in the SZ site-scale model was to assign the average temperature gradient (25°C/km) multiplied by depth below surface plus the average surface temperature (19°C) to all nodes in the model domain. All temperatures remain fixed, and the heat-transport equations are not solved in the simulation. Thus, the specified values of temperatures were used to calculate the local groundwater viscosity, but temperature variations do not yield variable-density flow processes because density was treated as a constant in all calculations.

6.4.3.11 Vertical Anisotropy

A fractured or porous media exhibits anisotropy when hydraulic properties are not uniform in all directions. For Yucca Mountain, anisotropic permeability potentially affects the specific discharge, the flowpaths, and the flowpath lengths in the volcanic tuffs and alluvium. During calibration of the SZ site-scale flow model, anisotropy ratios were held constant. The SZ site-scale flow model includes a horizontal to vertical anisotropy ratio of 10:1, a typical value, in most alluvial units, particularly younger units (CRWMS M&O 1998 [DIRS 100353], Table 3-2). Non-alluvial units (i.e., the intrusive confining unit, crystalline confining unit, lower clastic confining unit, lower carbonate aquifer, upper clastic confining unit, upper carbonate aquifer, lower clastic confining unit thrust, and lower carbonate aquifer thrust) were modeled with isotropic permeability because the geology indicates this is a reasonable assumption. Faults may be modeled with anisotropic permeability; often with permeabilities in plane of the fault (strike

and vertical) multiplied by 10 (e.g., Solitario Canyon fault permeabilities in the *y*- and *z*-directions are 10 times that in the cross-fault direction). The permeabilities of major faults are used as calibration parameters; however, the anisotropy ratios were constant during the calibration process. A 10:1 horizontal to vertical anisotropy was also assigned in the Lower Fortymile Wash Alluvial Zone.

6.5 SZ SITE-SCALE FLOW MODEL RESULTS

6.5.1 Model Calibration

Calibration is the process by which values of important model parameters are estimated and optimized to produce the best fit between model output and observed data. Calibration is generally accomplished by adjusting model input parameters (e.g., permeabilities) to minimize the difference between observed and simulated conditions (in this case, comparing simulated and observed head values and lateral boundary volumetric/mass flow rates). Model calibration may be performed manually or through automated optimization procedures. Automated optimization procedures generally employ a carefully prescribed mathematical process that selects the optimal set of parameters based on minimizing an objective function describing the difference between observed and simulated conditions. These procedures typically provide the most structured and thorough means of calibrating a model, and, frequently, they provide useful additional information regarding model sensitivity to parameters and other useful statistical measures. Consequently, an automated optimization procedure is used to calibrate the SZ site-scale flow model. However, manual adjustments to the calibration are also performed to ensure accurate representation of the small hydraulic gradient region southeast of the repository by ensuring that simulated particle pathlines do not contradict flow directions inferred from the potentiometric map.

A description of the calibration technique includes discussions of: optimization procedures; model outputs, whose differences between observed values (calibration targets) were minimized; and parameters that were varied during calibration.

6.5.1.1 Calibration Criteria

Proper calibration of the SZ site-scale flow model requires consideration of the full range of available data, which include field data for water levels and hydraulic heads, permeability data from field and laboratory tests, locations of known faults and other geologic data, and hydrochemical data. Opinions expressed by the Expert Elicitation Panel (CRWMS M&O 1998 [DIRS 100353]) must also be considered. The goal during development of the SZ site-scale flow model was to deliver to performance assessment a model that, given data sparseness, is as realistic as possible.

6.5.1.2 Parameter Optimization Procedure

The SZ site-scale flow model was calibrated with the commercial parameter estimation code, PEST (Watermark Computing 2002 [DIRS 161564]). PEST is a Levenberg-Marquardt (LM)-based optimization algorithm. The LM package is a well-established algorithm (Press et al. 1992 [DIRS 103316], pp. 678 to 683), it is robust, and widely applicable. It will search for the minima of a multidimensional function. In this case, the "function" is a weighted

sum-of-squares difference (SSD) between a set of observations (the heads in 161 wells in the Yucca Mountain region plus lateral boundary volumetric/mass flow rates from the regional flow model) and the solution to the partial differential equation that describes saturated flow. PEST computes the derivatives of the SSD function with respect to the various parameters. As discussed, those parameters optimized during calibration are the intrinsic permeability or permeability multiplier of each of the various hydrogeologic units, faults, and features. To estimate optimized permeabilities:

1. An initial estimate or guess for each unknown parameter is specified at the beginning of the fitting process

2. FEHM computes the resulting heads for the initial estimate of parameters

3. The results are returned to the PEST code

4. Through a series of FEHM simulations with perturbations in the parameters, the PEST LM package computes the derivative of the SSD function with respect to each of the parameters

5. The LM package then determines the amount to change each parameter's current value to improve the fit to the data through a mathematical process that combines gradient information and second derivative (approximated) information

6. This process is repeated until the fit to data is within a prescribed tolerance or until no further improvement is possible.

This coupling between PEST and FEHM allows any variable in FEHM to be used as a fitting parameter, regardless of whether it is a flow- or transport-related parameter. PEST simply finds the local minima of the target function. To enable PEST to search for the global minimum, a procedure is attached to the code that carries out a simulated annealing process, which specifies how PEST moves from one local minimum to another, better local minimum. This process is repeated until no further improvement occurs. The simulated annealing process (Press et al. 1992 [DIRS 103316], pp. 436 to 448) is simple in principle: the approach is to reject an improved solution occasionally, move to a new location in parameter space, and continue the search. Theory indicates that this technique will eventually find the global or a near-global minimum. In the flow model, the procedure includes resetting the value of the LM step-size parameter after each local minimum is found.

The SZ site-scale flow model was calibrated to achieve a minimum difference between observed water levels and simulated water levels, and also between volumetric/mass flow rates along specific boundary segments simulated by the SZ regional- and site-scale models. For calibration targets, 161 water level and head measurements were used. This was the complete set of wells available at the time of calibration. Measurements (DTN: GS010908314221.001 [DIRS 162874]; BSC 2004 [DIRS 170009], Table A-1; this report, Appendix E) represent either water levels or deeper head measurements. The deeper measurements represent average values over "open" or "packed-off" intervals, and the coordinates of the observations represent midpoints of the open interval, midpoint of the bottom of the open interval and the average water level, or the depth of the node at the water table, whichever is smallest. The calibration targets

represent steady-state values and where pumping is taking place, as in the Amargosa Valley, current water levels are used. When comparing simulated water levels to target water levels, the model represents water levels at the target locations by assigning the target head value to the nearest FEHM node. Refer to Appendix E of *Water-Level Data Analysis for the Saturated Zone Site-scale Flow and Transport Model* (BSC 2004 [DIRS 170009]) for a complete description of many water levels, well locations, and measurement depths. Nye County data used in the calibration are qualified for intended use in Appendix D and presented in Output DTN: SN0702T0510106.007.

Well NC-EWDP-19-IM2 was completed with five well screens, although no packers were installed. Hence, water level measurements were assumed to be taken at the weighted midpoint of the five intervals yielding a weighted measurement location of 599.2 m (the midpoint between the bottom of the bottom interval and the top of the top interval is 612.0 m and the water level is 813.24 m).

It should be noted that two probes from Nye County wells were not used in the calibration process: NC-EWDP-3S probe 1 and NC-EWDP-9SX probe 3. Originally well NC-EWDP-3S had a Westbay casing installation that included three zones. Nye County geologists encountered some undisclosed problems with the well and had to reinstall the Westbay casing. On March 31, 2001, the reinstallation was completed, but it eliminated probe 1, leaving just probes 2 and 3 (Gilmore 2006 [DIRS 179104]). Only a single data point was ever taken from probe 1 and hence this datum was not used in calibrating the model. Regarding NC-EWDP-9SX probe 3, Tucci (2001 [DIRS 155410], pp. 21, 24, 27, and 48 of 80) states that the data from this probe were not reliable because of potential probe or packer malfunction.

During the calibration process, emphasis was placed on minimizing the difference between observed and simulated water levels at selected target locations based on probable flow pathways. This was accomplished by multiplying the squared differences at that location by a weighting factor. A weighting factor of 1 (i.e., standard importance) was applied to most calibration targets. However, a preferential weighting factor ($\Sigma = 20$) was applied to 22 calibration targets in the small-gradient region to the south and east of Yucca Mountain. These calibration targets were given high weighting because they are in the likely groundwater pathway leaving the repository site and because small changes in head in this area often yield a large effect on the flow direction. Six calibration targets are north of Yucca Mountain in the high head region. These are either assigned a low weighting (0.1, which implies little importance) if they were thought to represent perched conditions, or a weight of 10 to help ensure that no unphysical "mounding" of water occurs. Four additional water levels that are assumed to represent perched conditions are assigned weights of 0.1. Three wells in the moderately high head area just west of the Solitario Canyon Fault are assigned weights of 20 because their accuracy ensures proper representation of this fault as a hydraulic barrier. Because Crater Flat tuffs are important to estimated flowpaths, those wells completed in these units (and not already assigned a high weight for being in the flowpath), are given a weight of 5. Two wells, USW UZ-14 and USW H-5, were deweighted because of anomalously high heads. The high potentiometric heads in these two boreholes is attributed to the presence of a splay of the Solitario Canyon Fault penetrated by the boreholes (Ervin et al. 1994 [DIRS 100633], pp. 9 to 10). This splay is believed to be an extension of the hydrologic barrier to west-to-east groundwater flow from Crater Flat (related to the Solitario Canyon Fault). The high heads in USW H-5 (about 775 m)

are related to heads in Crater Flat (ranging from 775 to 780 m), and this borehole defines part of the moderate hydraulic gradient along the western edge of Yucca Mountain. Borehole USW UZ-14 is in a transition zone between the large and moderate hydraulic areas, and the high potentiometric level (about 779 m) is related to either of these areas. Rousseau et al. (1999 [DIRS 102097], p. 172) hypothesized that perched water in USW UZ-14 could be caused by a nearby projected growth fault that impedes percolation of water from the surface. The high heads in USW UZ-14 also could be caused by the low permeability rocks in the upper part of the SZ at that borehole. These hypotheses, in combination with the lack of a corresponding feature or process in the qualified DTN used to specify faults, supports the deweighting of USW UZ-14 and USW H-5 (essentially, without an explicit feature, the model should not be asked to match anomalous heads). Wells showing an upward gradient are assigned a weight of 10 because it is important to reproduce this phenomenon. If multiple calibration targets (head measurements) are available from a single well, the sum of weights from each well sum to the specified value (e.g., four measurements from USW H-1 each have weights of 7, 1, 1, and 1). Well names including a complete listing of all target water-level values, target locations, and the weighting applied to each target are provided in Table 6-8. In addition to water levels, volumetric/mass flow rates through three of the four lateral boundary segments were used as calibration targets (west, north, and east). Each of the three lateral boundaries was supplied with a cumulative weight of 5 (see Table 6-11).

Table 6-8. Comparison of Observed Hydraulic Heads from the SZ Site-Scale Flow Model and Model Computed Head Data

Site Name	Fig. 6-16	Node Number	*x* (UTM) (m)	*y* (UTM) (m)	*z* (elevation) (m)	Measured Water Level (Head Data)[a] (m)	Modeled Head	Weight
UE-29 a #2	1	897244	555753	4088351	990.8	1,187.7	1,150.46	10
GEXA Well 4	2	847393	534069	4086110	859.2	1,009.0	1,006.01	10
UE-25 WT#6	3	846002	549352	4083103	840[b]	1,034.6	870.93	0.1
USW G-2	4	845756	548143	4082542	840[b]	1,020.2	880.16	0.1
UE-25 WT #16	5	673914	551146	4081234	714.1	738.3	734.93	1
USW UZ-14	6	695253	548032	4080260	725.0[c]	779.0	734.71	0.1
UE-25 WT #18	7	695259	549468	4080238	722.1	730.8	734.60	20
USW G-1	8	279088	548306	4080016	125.7	754.2	745.78	1
UE-25 a #3	9	607533	561084	4079697	681.4	748.3	773.84	20
UE-25 WT #4	10	673064	550439	4079412	709.0	730.8	734.56	20
UE-25 WT #15	11	650823	554034	4078694	698.7	729.2	735.80	20
USW G-4	12	431672	548933	4078602	542.2	730.6	734.58	20
UE-25 a #1	13	453456	549925	4078330	584.0	731.0	734.54	20
UE-25 WT #14	14	650092	552630	4077330	703.6	729.7	734.36	20
USW WT-2	15	649954	548595	4077028	702.0	730.6	734.57	20

Table 6 8. Comparison of Observed Hydraulic Heads from the SZ Site Scale Flow Model and Model Computed Head Data (Continued)

Site Name	Fig. 6-16	Node Number	*x* (UTM) (m)	*y* (UTM) (m)	*z* (elevation) (m)	Measured Water Level (Head Data)[a] (m)	Modeled Head	Weight
UE-25 c #3	17	386668	550930	4075902	474.3	730.2	734.44	20
UE-25 c #2	18	430349	550955	4075871	553.2	730.2	734.43	20
UE-25 WT #13	19	649370	553730	4075827	703.8	729.1	734.28	20
USW WT-7	20	735215	546151	4075474	740.9	775.8	783.67	20
USW WT-1	21	670881	549152	4074967	708.4	730.4	734.50	20
USW G-3	22	320225	547543	4074619	318.1	730.5	735.52	1
UE-25 J-13	23	341668	554017	4073517	354.8	728.4	734.24	20
USW WT-10	24	713413	545964	4073378	734.2	776.0	781.34	20
UE-25 WT #17	25	670037	549905	4073307	705.4	729.7	734.41	1
USW VH-2	26	319581	537738	4073214	282.8	810.4	915.89	1
UE-25 WT #3	27	669682	552090	4072550	705.8	729.6	734.24	20
USW VH-1	28	406468	539976	4071714	490.5	779.4	779.16	1
UE-25 WT #12	29	646936	550168	4070659	702.6	729.5	734.31	1
USW WT-11	30	624903	547542	4070428	691.9	730.7	734.55	1
UE-25 J-12	31	558381	554444	4068774	659.6	727.9	733.52	20
UE-25 JF #3	32	558018	554498	4067974	662.7	727.8	733.33	20
Cind-R-Lite Well	33	663479	544027	4059809	710.2	729.8	737.29	1
Ben Bossingham	34	639932	553704	4056228	697.4	718.4	718.57	1
Fred Cobb	35	595767	553808	4055459	675.6	702.8	717.89	1
Bob Whellock	36	595768	553883	4055398	682.0	704.1	718.08	1
Louise Pereidra	37	639571	554131	4055399	698.0	705.6	718.30	1
Joe Richards	38	595647	554008	4055337	679.3	701.6	717.80	1
NDOT Well	39	595646	553685	4055242	682.1	705.4	717.61	1
James H. Shaw	40	551707	549863	4054911	664.3	706.7	716.24	1
Airport Well	41	507917	552818	4054929	636.5	705.3	716.85	1
TW-5	42	617340	562604	4054686	688.7	725.1	724.32	1
Richard Washburn	43	573003	549746	4053647	669.9	707.7	713.55	1
Richard Washburn	44	594178	549679	4052322	675.3	704.4	703.36	1
Nye County Develop. Co.	45	505460	543481	4050069	638.6	694.3	698.58	1
Fred Wooldridge	46	571134	536350	4050006	673.8	691.9	696.21	1
Fred J. Keefe	47	593053	540673	4049994	676.7	694.3	702.57	1
Leslie Nickels	48	527353	541518	4049937	654.7	694.3	701.66	1
L. Mason	49	636785	553471	4049848	699.2	722.1	709.95	1
Unknown	50	570929	545596	4049403	667.6	697.8	694.28	1
Davidson Well	51	570772	536552	4049329	672.0	690.1	694.41	1

Table 6 8. Comparison of Observed Hydraulic Heads from the SZ Site Scale Flow Model and Model Computed Head Data (Continued)

Site Name	Fig. 6-16	Node Number	*x* (UTM) (m)	*y* (UTM) (m)	*z* (elevation) (m)	Measured Water Level (Head Data)[a] (m)	Modeled Head	Weight
Eugene J. Mankinen	52	592562	538889	4049000	678.6	707.4	694.95	1
Donald O. Heath	53	526872	542194	4048892	651.6	694.1	693.54	1
Elvis Kelley	54	614213	536903	4048621	685.1	691.0	692.66	1
Manuel Rodela	55	614373	546718	4048669	686.7	693.6	693.32	1
Charles C. DeFir Jr.	56	614218	538196	4048442	685.7	706.9	693.77	1
William R. Monroe	57	570423	540035	4048450	669.5	693.7	699.29	1
DeFir Well	58	570410	536655	4048405	671.1	690.2	692.51	1
Edwin H. Mankinen	59	548282	540608	4048083	662.8	695.2	696.00	1
Bill Strickland	60	592062	534967	4047966	677.0	689.2	690.31	1
M. Meese	61	548308	547120	4047963	664.6	686.4	692.57	1
Theo E. Selbach	62	570092	547941	4047782	673.3	696.2	693.08	1
C.L. Caldwell	63	526249	537727	4047670	654.5	691.4	691.66	1
Leonard Siegel	64	570110	552390	4047685	667.2	709.0	705.40	1
James K. Pierce	65	548045	541778	4047596	664.0	690.4	690.90	1
James K. Pierce	66	591846	541381	4047563	677.1	705.6	691.02	1
Cooks West Well	67	613916	553609	4047631	690.2	720.1	709.67	1
Cooks East Well	68	613918	554006	4047633	693.4	718.9	711.52	1
Nye County Land Co.	69	591753	548466	4047261	680.0[c]	690.1	693.27	1
Amargosa Town Complex	70	569731	548492	4047077	668.3	688.8	693.45	1
Nye County Develop. Co.	71	482135	550431	4047057	615.4	691.2	692.53	1
Lewis C. Cook	72	635454	553612	4047076	702.5	717.4	709.89	1
Lewis C. Cook	73	613554	553687	4047077	688.7	714.8	711.25	1
Amargosa Valley Water	74	569731	548393	4046953	673.9	701.3	693.45	1
Earl N. Selbach	75	569573	539147	4046844	672.1	696.5	693.59	1
Lewis N. Dansby	76	547675	539968	4046817	664.7	694.2	693.52	1
Edwin H. Mankinen	77	613381	540788	4046821	686.2	694.0	692.81	1
Willard Johns	78	591646	552097	4046882	678.9	699.5	699.93	1
USW H-1 tube 1	79	213387	548727	4079926	–495.5	785.5	756.57	7

Table 6 8. Comparison of Observed Hydraulic Heads from the SZ Site Scale Flow Model and Model Computed Head Data (Continued)

Site Name	Fig. 6-16	Node Number	*x* (UTM) (m)	*y* (UTM) (m)	*z* (elevation) (m)	Measured Water Level (Head Data)[a] (m)	Modeled Head	Weight
USW H-1 tube 2	80	300991	548727	4079926	193.0	736.0	734.60	1
USW H-1 tube 3	81	454298	548727	4079926	562.5	730.6	734.61	1
USW H-1 tube 4	82	607605	548727	4079926	680.5	730.8	734.61	1
USW H-5 upper	83	650798	547668	4078841	704.2	775.5	734.91	0.1
USW H-5 lower	84	387986	547668	4078841	446.4	775.6	734.72	0.1
UE-25 b #1 lower	85	256468	549949	4078423	–8.8	729.7	734.58	10
UE-25 b #1 upper	86	344072	549949	4078423	366.2	730.6	734.54	10
USW H-6 upper	87	562704	546188	4077816	662.9	776.0	786.21	10
USW H-6 lower	88	321793	546188	4077816	315.8	775.9	781.82	10
USW H-4 upper	89	365365	549188	4077309	395.5	730.4	734.55	10
USW H-4 lower	90	255860	549188	4077309	45.0	730.5	739.48	10
USW H-3 upper	91	452236	547562	4075759	576.9	731.5	734.60	5
USW H-3 lower	92	342731	547562	4075759	343.2	755.9	736.09	5
UE-25 p #1 (Lwr Intrvl)	93	211341	551501	4075659	–410.3	752.4	740.54	20
USW SD-7	94	518306	548384	4076499	637.7	727.6	734.56	20
USW SD-9	95	607241	548550	4079256	678.3	731.1	734.61	20
USW SD-12	96	650196	548492	4077415	696.7	730.0	734.58	20
NC-EWDP-1DX, shallow	97	768353	536848	4062509	784.1[b]	787.2	782.97	1
NC-EWDP-1DX, deep	98	270572	536848	4062509	133.1	749.1.8	772.59	1
NC-EWDP-1S probe 1	99	749061	536851	4062504	751.8	787.4	782.95	1
NC-EWDP-1S probe 2	100	708052	536851	4062504	730.8	787.5	782.83	1
NC-EWDP-2D[d]	101	399481	547823	4057170	507.1	706.1	716.64	1
NC-EWDP-2DB	102	246174	547800	4057196	–77.0	712.6	717.93	1
NC-EWDP-3D	103	334841	541352	4059450	337.8	719.2	736.39	5
NC-EWDP-3S probe 2	104	597653	541349	4059450	682.8	719.9	737.17	2.5

Table 6 8. Comparison of Observed Hydraulic Heads from the SZ Site Scale Flow Model and Model Computed Head Data (Continued)

Site Name	Fig. 6-16	Node Number	*x* (UTM) (m)	*y* (UTM) (m)	*z* (elevation) (m)	Measured Water Level (Head Data)[a] (m)	Modeled Head	Weight
NC-EWDP-3S probe 3	105	510049	541349	4059450	642.3	719.9	737.17	2.5
NC-EWDP-4PA	106	618271	553246	4056772	687.0	718.0	718.65	1
NC-EWDP-4PB	107	443063	553281	4056774	582.5	723.5	718.66	1
NC-EWDP-5SB	108	662800	555756	4058222	707.8	723.6	720.97	1
NC-EWDP-7S	109	769212	539638	4064323	760[b]	830.3	767.21	0.1
NC-EWDP-9SX probe 1	110	767636	539118	4061010	765.3	766.4	757.59	1
NC-EWDP-9SX probe 2	111	748344	539118	4061010	751.3	767.2	757.56	1
NC-EWDP-9SX probe 4	112	620271	539118	4061010	694.8	767.3	757.45	1
NC-EWDP-12PA	113	576340	536985	4060772	666.7	722.9	755.86	1
NC-EWDP-12PB	114	576340	536952	4060799	666.7	723.0	755.86	1
NC-EWDP-12PC	115	663935	536951	4060814	713.7	720.8	755.67	1
NC-EWDP-15P	116	684593	544927	4058163	716.9	722.4	720.59	1
NC-EWDP-19P	117	618981	549329	4058292	694.7	707.3	717.66	1
NC-EWDP-19D	118	421872	549317	4058271	549.7	711.8	717.65	1
USW WT-24	119	717538	548697	4081909	734.8	840.1	836.46	10
NC-Washburn-1X	120	618627	551544	4057569	687.0	714.4	718.00	1
BGMW-11	121	577177	534386	4062600	673.4	715.9	711.17	1
Richard Washburn	122	638100	549529	4052567	739.9[b]	703.9	703.74	1
L. Cook	123	613786	551348	4047432	690.0[b]	713.2	698.36	1
Unknown	124	591999	549532	4047668	680.0[b]	689.5	693.04	1
Amargosa Water	125	613771	547420	4047594	690.3[b]	690.4	692.58	1
Lewis C. Cook	126	635820	554329	4047666	700.0[b]	715.7	712.36	1
Unknown	127	614463	538989	4048877	690.7[b]	690.8	694.95	1
USW UZ-N91	128	921140	555680	4088196	1,150.0[b]	1,186.7	1,184.03	10
NC-EWDP-7SC	129	687476	539632	4064317	724.1[c]	828.5	767.18	0.1
NC-EWDP-7SC-Z1	130	769212	539632	4064317	760.0[b]	830.3	767.21	0.1
NC-EWDP-7SC-Z2	131	769212	539632	4064317	760.0[b]	830.4	767.21	0.1

Table 6 8. Comparison of Observed Hydraulic Heads from the SZ Site Scale Flow Model and Model Computed Head Data (Continued)

Site Name	Fig. 6-16	Node Number	*x* (UTM) (m)	*y* (UTM) (m)	*z* (elevation) (m)	Measured Water Level (Head Data)[a] (m)	Modeled Head	Weight
NC-EWDP-7SC-Z3	132	729744	539632	4064317	741.0	821.7	767.20	1
NC-EWDP-7SC-Z4	133	643748	539632	4064316	704.5	792.5	767.16	0.1
NC-EWDP-10P Deep	134	534660	553149	4064916	650.4	726.9	730.55	1
NC-EWDP-10P Shallow	135	644165	553149	4064916	696.4	726.9	730.54	1
NC-EWDP-10S-Z1	136	644165	553140	4064899	696.0	727.0	730.54	1
NC-EWDP-10S-Z2	137	534660	553140	4064899	650.3	727.5	730.55	1
NC-EWDP-18P	138	645239	549416	4067233	702.3	711.2	732.66	1
NC-EWDP-19IM1-Z1	139	618981	549317	4058291	691.1	711.9	717.66	0.1
NC-EWDP-19IM1-Z2	140	553278	549317	4058291	659.1	712.1	717.65	0.1
NC_EWDP-19IM1-Z3	141	487575	549317	4058291	628.6	712.5	717.64	0.1
NC_EWDP-19IM1-Z4	142	443773	549317	4058291	589.0	713.3	717.64	0.1
NC_EWDP-19IM1-Z5	143	421872	549317	4058291	545.0	711.8	717.65	0.1
NC_EWDP-19IM2	144	465674	549337	4058291	599.2	723.3	717.64	1
NC_EWDP-22PA Deep	145	533203	552020	4062038	652.0	724.8	724.55	1
NC_EWDP-22PA Shallow	146	642708	552020	4062038	700.9	724.8	724.54	1
NC_EWDP-22PB Deep	147	401797	552038	4062037	514.9	724.8	724.71	1
NC_EWDP-22PB Shallow	148	445599	552038	4062037	584.9	724.8	724.55	1
NC_EWDP-22S-Z1	149	642708	552019	4062020	700.3	724.9	724.54	1
NC_EWDP-22S-Z2	150	533203	552019	4062020	651.7	724.9	724.55	1
NC_EWDP-22S-Z3	151	445599	552019	4062020	584.9	724.9	724.55	1
NC_EWDP-22S-Z4	152	401797	552019	4062020	514.8	724.9	724.71	1
NC_EWDP-23P Deep	153	532122	553923	4059875	649.2	724.3	721.93	1
NC_EWDP-23P Shallow	154	641627	553923	4059875	704.0	724.2	721.93	1
NC_EWDP-16P	155	687500	545665	4064263	722.3	729.4	739.27	1
NC_EWDP-19PB Deep	156	553278	549337	4058316	659.5	707.9	717.65	1
NC_EWDP-19PB Shallow	157	640882	549337	4058316	702.1	707.4	717.66	1
NC_EWDP-24P	158	686426	549386	4062055	786.4	727.1	725.30	1

Table 6 8. Comparison of Observed Hydraulic Heads from the SZ Site Scale Flow Model and Model Computed Head Data (Continued)

Site Name	Fig. 6-16	Node Number	*x* (UTM) (m)	*y* (UTM) (m)	*z* (elevation) (m)	Measured Water Level (Head Data)[a] (m)	Modeled Head	Weight
NC_EWDP-27P	159	687981	544935	4065276	728.2	728.6	739.53	1
NC_EWDP-28P	160	686653	545746	4062393	718.7	729.3	738.82	1
NC_EWDP-29P	161	663380	549396	4059606	719.2[b]	724.8	719.12	1

Source: DTN: GS010908312332.002 [DIRS 163555].

Output DTN: SN0612T0510106.004, *sz06.pest*.

[a]Head data refer to the observed mean hydraulic head (m).

[b]Screen midpoint is above the potentiometric surface, therefore the modeled hydraulic head for this well is taken to be the uppermost active cell immediately below the potentiometric surface.

[c]Average of lower interval and water level was calculated to specify the measurement location (ensures that measurement falls in an active cell).

[d]Well location in DTN: GS010908312332.002 [DIRS 163555] is incorrectly stated as *x* = 547744, *y* = 4057164.

UTM = Universal Transverse Mercator.

NOTES: The "Fig. 6-16" label in the second column of the table refers to the well numbers given in Figure 6-16.

The information on well name, UTM coordinates easting and northing, and measured heads is from DTN: GS010908312332.002 [DIRS 163555] and Output DTN: SN0702T0510106.007. The measured heads in Table 6-8 correspond to the average hydraulic head or water-table altitude data. Mean hydrostatic heads were calculated as time averages over the period of available measurements and were rounded to the nearest tenth of a meter.

Appendix D qualifies Nye County data from Phases III and IV for use in this report. Note that well locations of NC-EWDP Phases III and IV wells have been recalculated with CORPSCON V5.11.08.00 (STN: 10547-5.11.08, [DIRS 155082]) and may differ from those found elsewhere (e.g., BSC 2004 [DIRS 170009], Table A-1) (see Appendix F).

The *z* elevation shown in Table 6-8 is from Output DTN: SN0612T0510106.004. These data are stored in file *well_locations.macro*. This file provides well UTM coordinates and measurement depths.

The model heads shown in Table 6-8 are from Output DTN: SN0612T0510106.004. The modeled heads are stored in file *sz06.pest*. This file provides initial, intermediate, and final values of calibrated heads. The final heads are located at the end of this file and correspond to the simulation time equal to 3.6525×10^{10} days. Each well is represented by its nearest node. The relationship between the wells and the nodes is provided in Table 6-8. There are 161 water levels in the output file.

6.5.1.3 Calibration Parameters

The model formulation and the FEHM code require a specified permeability at each node. Sets of nodes are grouped into specific permeability zones based on similar permeability characteristics as identified in HFM2006 (SNL 2007 [DIRS 174109]). A single permeability value is assigned to each zone, and these zonal permeabilities are the parameters optimized during model calibration. Permeability zones correspond to hydrogeologic units identified in the HFM2006 conceptual model or to specific hydrogeologic features (see Table 6-7). All of the nodes within a specific hydrogeologic unit were assigned a calibrated permeability unless this node was included in one of the permeability zones established for specific hydrogeologic

features or faults. The zone sizes were fixed based on data from HFM2006. Uncertainty associated with geologic contacts is discussed in Section 6.7.3.

Recall that vertical anisotropy is assigned a value of 10:1 (horizontal to vertical) in the volcanic and valley-fill units (above Unit 9). Lower permeability in the vertical direction than in the horizontal direction typically occurs in stratified media, and the ratio of 10:1 is in the generally accepted range (CRWMS M&O 1998 [DIRS 100353], Table 3-2). For a site-specific example, the relatively high vertical gradient observed in well UE-25 p#1 suggests that vertical permeability is lower than horizontal permeability (minimal hydraulic connectivity). Nine wells (see Section 6.3.1.5) exhibited vertical gradients (BSC 2004 [DIRS 170009], Table 6-4). The uncertainty associated with the vertical anisotropy is discussed in Section 6.7.2.

Specific hydrogeologic features thought to potentially impact groundwater flow are classified as distinct permeability zones. The permeability variable or permeability multiplication factor used for a specific feature was assigned to all of the nodes within that feature. The hydrogeologic features for which special permeability zones were established are primarily faults, fault zones, and areas of hydrogeologic alteration (Section 6.5.2). As previously discussed, these features are distinct from the subhorizontal hydrogeologic units identified in HFM2006. Each of the identified hydrogeologic features includes multiple geologic formations and represents a zone of altered permeability within individual formations.

Twenty-three permeability zones were established based on the geologic units within the SZ site-scale model domain from HFM2006 for model calibration. Additional (usually low) permeability zones reflecting altered northern region were added to the model to help establish known system characteristics (like the LHG). These were established by dividing existing (base) geologic units into altered northern regions with permeabilities defined by multipliers. These permeability multipliers are calibration parameters that modify the permeability values assigned to geologic units in the altered northern regions. Eight additional zone representing faults and the Lower Fortymile Wash alluvium were established because they were identified as important structural features (e.g., the Solitario Canyon Fault) or were necessary for some conceptual feature, such as the LHG north of Yucca Mountain (which is partially established in the model domain with help from the altered northern region).

As required by PEST, upper and lower bounds were placed on each permeability variable during parameter optimization with limits chosen to reflect maximum and minimum field values (permeability) or a realistic range of values (permeability multipliers). A list identifying permeability zones, its calibrated permeability parameter, and the upper and lower bounds specified for the parameter is provided in Table 6-9.

Table 6-9. Calibration Parameters Used in the SZ Site-Scale Flow Model

Parameter Name (zone number)	Geologic Unit or Feature	Calibrated Value (m^2)	Minimum Value (m^2)	Maximum Value (m^2)
ICU (2)	Intrusive Confining Unit (granite)	9.9×10^{-17}	1.0×10^{-19}	1.0×10^{-10}
XCU (3)	Crystalline Confining Unit (granite)	1.0×10^{-16}	1.0×10^{-19}	1.0×10^{-10}
LCCU (4)	Lower Clastic Confining Unit	9.7×10^{-17}	1.0×10^{-19}	1.0×10^{-10}
LCA (5)	Lower Carbonate Aquifer	9.7×10^{-15}	2.0×10^{-15}	1.0×10^{-10}

Table 6-9. Calibration Parameters Used in the SZ Site-Scale Flow Model (Continued)

Parameter Name (zone number)	Geologic Unit or Feature	Calibrated Value (m^2)	Minimum Value (m^2)	Maximum Value (m^2)
UCCU (6)	Upper Clastic Confining Unit	9.8×10^{-16}	1.0×10^{-19}	1.0×10^{-10}
UCA (7)	Upper Carbonate Aquifer	1.1×10^{-12}	1.0×10^{-19}	1.0×10^{-10}
LCCUT1 (8)	Lower Clastic Confining Unit Thrust	9.8×10^{-19}	1.0×10^{-19}	1.0×10^{-10}
LCAT1 (9)	Lower Carbonate Aquifer Thrust	5.6×10^{-12}	1.0×10^{-19}	1.0×10^{-10}
VSUL (11)	Volcanic and Sedimentary Units (lower)	1.1×10^{-14}	1.0×10^{-19}	1.0×10^{-10}
OVU (12)	Older Volcanic Unit	9.8×10^{-16}	1.0×10^{-19}	1.0×10^{-10}
CFTA (14)	Crater Flat-Tram Aquifer	9.4×10^{-13}	1.0×10^{-19}	1.0×10^{-10}
CFBCU (15)	Crater Flat-Bullfrog Confining Unit	5.2×10^{-14}	1.0×10^{-19}	1.0×10^{-10}
CFPPA (16)	Crater Flat-Prow Pass Aquifer	3.1×10^{-12}	1.0×10^{-19}	1.0×10^{-10}
WVU (17)	Wahmonie Volcanic Unit	9.8×10^{-14}	1.0×10^{-14}	1.0×10^{-10}
CHVU (18)	Calico Hills Volcanic Unit	2.4×10^{-13}	1.0×10^{-19}	1.0×10^{-10}
PVA (19)	Paintbrush Volcanic Aquifer	6.5×10^{-14}	1.0×10^{-19}	1.0×10^{-10}
TMVA (20)	Timber Mountain Volcanic Aquifer	9.5×10^{-14}	1.0×10^{-19}	1.0×10^{-10}
VSU (21)	Volcanic and Sedimentary Units (upper)	8.7×10^{-13}	1.0×10^{-19}	1.0×10^{-10}
LFU (23)	Lava Flow Unit	8.9×10^{-14}	1.0×10^{-19}	1.0×10^{-10}
LA (24)	Limestone Aquifer	9.8×10^{-14}	1.0×10^{-19}	1.0×10^{-10}
OAA (26)	Older Alluvial Aquifer	1.5×10^{-13}	1.0×10^{-19}	1.0×10^{-10}
YACU (27)	Young Alluvial Confining Unit	9.9×10^{-15}	1.0×10^{-19}	1.0×10^{-10}
YAA (28)	Young Alluvial Aquifer	9.8×10^{-13}	1.0×10^{-19}	1.0×10^{-10}
ICUm (102)	ICU multiplier	0.3	1.0×10^{-6}	1.0
XCUm (103)	XCU multiplier	0.2	1.0×10^{-6}	1.0
LCCUm (104)	LCCU multiplier	0.2	1.0×10^{-6}	1.0
LCAm (105)	LCA multiplier	0.2	1.0×10^{-6}	1.0
UCCUm (106)	UCCU multiplier	9.7×10^{-3}	1.0×10^{-6}	1.0
UCAm (107)	UCA multiplier	2.0×10^{-2}	1.0×10^{-6}	1.0
LCCUT1m (108)	LCCUT1 multiplier	9.8×10^{-3}	1.0×10^{-6}	1.0
VSULm (111)	VSUL multiplier	1.0×10^{-2}	1.0×10^{-6}	1.0
OVUm (112)	OVU multiplier	9.9×10^{-3}	1.0×10^{-6}	1.0
CFTAm (114)	CFTA multiplier	1.0×10^{-2}	1.0×10^{-3}	1.0
CFBCUm (115)	CFBCU multiplier	9.1×10^{-3}	1.0×10^{-6}	1.0
CFPPAm (116)	CFPPA multiplier	1.4×10^{-3}	1.0×10^{-6}	1.0
CHVUm (118)	CHVU multiplier	2.3×10^{-3}	1.0×10^{-6}	1.0
PVAm (119)	PVA multiplier	9.6×10^{-3}	1.0×10^{-3}	1.0
TMVAm (120)	TMVA multiplier	9.8×10^{-3}	1.0×10^{-6}	1.0
VSUm (121)	VSU multiplier	1.0×10^{-2}	1.0×10^{-6}	1.0
LFUm (123)	LFU multiplier	1.0×10^{-2}	1.0×10^{-6}	1.0
OAAm (126)	OAA multiplier	1.0×10^{-2}	1.0×10^{-6}	1.0
YAAm (128)	YAA multiplier	1.0×10^{-2}	1.0×10^{-6}	1.0
YMZm (39)	Yucca Mountain zone multiplier	8.9	1.0	1.0×10^{3}
4wfz (40)	Fortymile Wash Fault Zone	1.4×10^{-10}	1.0×10^{-19}	1.0×10^{-10}
bmfz (41)	Bare Mountain Zone	9.9×10^{-16}	1.0×10^{-19}	1.0×10^{-10}
cffz (42)	Crater Flat Fault Zone	9.7×10^{-17}	1.0×10^{-19}	1.0×10^{-10}
h95z (43)	Highway 95 Fault Zone	1.0×10^{-14}	1.0×10^{-19}	1.0×10^{-10}
swfz (45)	Sever Wash Fault Zone	9.8×10^{-18}	1.0×10^{-19}	1.0×10^{-10}
scfz (44)	Solitario Canyon Fault Zone	5.0×10^{-16}	1.0×10^{-19}	1.0×10^{-10}
stfz (46)	Stage Coach Fault Zone	4.7×10^{-16}	1.0×10^{-19}	1.0×10^{-10}

Table 6-9. Calibration Parameters Used in the SZ Site-Scale Flow Model (Continued)

Parameter Name (zone number)	Geologic Unit or Feature	Calibrated Value (m^2)	Minimum Value (m^2)	Maximum Value (m^2)
wwfz (47)	Windy Wash Fault Zone	4.8×10^{-16}	1.0×10^{-19}	1.0×10^{-10}
wash (50)	Lower Fortymile Wash	2.0×10^{-11}	1.0×10^{-19}	1.0×10^{-10}

Output DTN: SN0612T0510106.004, *sz_site_2006.pst*.

In addition to the PEST optimization described above, several manual adjustments were made to improve the model in ways that were not possible during the PEST run. Specifically, during calibration, only water levels (and lateral volumetric/mass flows) were considered in the objective function and hence head gradients or important head differences between wells were not explicitly considered. Manual adjustments were made to ensure that the flow direction southeast of the repository (in the small-gradient, anisotropic region) matched the direction inferred from the range and distribution of head values in this area. These adjustments modified the direction of particle paths emanating from the repository (to match the direction inferred from differences in the measured water levels) while maintaining good calibration (low objective function and low weighted RMSE for heads). The specific discharge was adjusted by changing the permeability of several units as listed in Table 6-10. Specific discharges were manipulated without adversely affecting the heads or gradient in the small hydraulic gradient area near Yucca Mountain. Table 6-8 shows the units that were adjusted during hand calibration, their PEST optimized permeability values, and their hand calibrated values. It should be noted that an additional zone corresponding to the Bullfrog Tuff within the quadrilateral defined by the Yucca Mountain zone was added during hand calibration with a permeability of 5×10^{-13} m^2 to ensure that the small hydraulic gradient region observed southeast of the repository is honored by the model and the flow paths from below the repository did not terminate aolng the eastern model boundary.

Table 6-10. Hand Calibration Results used in the SZ Site-Scale Flow Model

Parameter Name (unit/zone number)	Geologic Unit or Feature	Hand-Calibrated Value (m^2)	PEST-Calibrated Value (m^2)
LCAT1 (9)	Lower Carbonate Aquifer	5.6×10^{-12}	5.6×10^{-14}
CFBCU (15)	Bullfrog Tuff	$5.2. \times 10^{-14}$	5.2×10^{-14}
CFPPA (16)	Prow Pass Tuff	3.1×10^{-12}	1.1×10^{-13}
PVA (19)	Paintbrush Volcanic Aquifer	6.5×10^{-14}	2.5×10^{-13}
VSU (21)	Volcanic and Sedimentary Unit	8.7×10^{-13}	8.7×10^{-16}
OAA (26)	Older Alluvial Aquifer	1.5×10^{-13}	8.8×10^{-13}
CFPPAm (116)	Prow Pass Tuff Multiplier	1.4×10^{-3}	9.4×10^{-3}
CHVUm (117)	Crater Hills Volcanic Unit Multiplier	2.3×10^{-3}	2.3×10^{-3}
4wfz (40)	Fortymile Wash Fault Zone	1.4×10^{-10}	6.4×10^{-11}
wash (50)	Lower Fortymile Wash Alluvial Zone	2.0×10^{-11}	5.2×10^{-13}

Output DTN: SN0612T0510106.004, *sz_site_2006_calibrated.pst*.

6.5.2 Calibration Results

A model of this complexity proved challenging to calibrate. One issue is that for broad ranges of parameter values the response surface of the objective function was quite flat; however, for certain parameter vectors, the objective function could quickly become sensitive. For example, when the permeability of a fault was higher than that of the surrounding unit, the fault would have no impact on flowpaths, but once its permeability drops below that of surrounding units, the fault significantly changed the flow field. Another issue related to an inability to include soft data in the calibration process due to software quality assurance constraints (hence the hand calibration measures). Some trade-off between minimum objective function had to be made to match soft data for flowpath direction particularly in the small hydraulic gradient region.

6.5.2.1 Water Levels

The water levels simulated by the calibrated SZ site-scale flow model are compared to the observed water level at each of the calibration target locations in Table 6-8. The location of each target observation well is shown in Figure 6-13. The calibration targets (water levels) are taken from *Water-Level Data Analysis for the Saturated Zone Site-Scale Flow and Transport Model* (BSC 2004 [DIRS 170009], Attachment I; DTN: GS010908312332.002 [DIRS 163555]) and NC-EWDP (Appendix D and also Output DTN: SN0702T0510106.007). The updated potentiometric surface (Appendix E) was used to truncate the top of the flow model grid and to provide the boundary conditions around the perimeter of the model. Of the 161 water-level calibration targets presented in Table 6-8, 105 values were obtained from *Water-Level Data Analysis for the Saturated Zone Site-Scale Flow and Transport Model* (BSC 2004 [DIRS 170009], Attachment I), ten values were obtained from DTN: GS010908312332.002 [DIRS 163555], and the rest can be found in Output DTN: SN0702T0510106.007. The distribution of residuals (the differences between measured and modeled heads), along with the potentiometric (left) and simulated water-level (right) surfaces, is provided in Figure 6-15. The actual water levels (not the interpolated potentiometric surface) in each well are used for comparison.

The weighting scheme (Table 6-8) used with PEST focused the calibration in high-confidence areas (i.e., the small-gradient area) or areas important to TSPA calculations (i.e., along the flow path). A low-weight target value instructs PEST to essentially ignore the value while a high value forces PEST to respect the target value at the expense of other observations. Alternate weighting schemes were investigated (e.g., uniform weighting or weights inversely proportional to the variance in observation data) but were discarded when they yielded physically inconsistent flowpaths (.e.g., pathlines that terminate along the eastern model boundary).

The calibrated SZ site-scale flow model has a weighted (see Table 6-8) root-mean-square error (RMSE) of 0.82 m when considering only differences between observed and modeled heads (lateral flux calibration targets were not included). The modeled head at the node nearest to the well location was used for the comparison (no interpolation was needed because of the 250-m grid size). Without weighting, the RMSE is 24.39 m. Compared to the overall head drop of approximately 500 m in the model domain, the 24.39-m average residual corresponds to a 5% error. As shown in Figure 6-16, a comparison between measured water-level data and the potentiometric surface yielded an RMSE of 20.7 m (weighted RMSE of 8.8 m). Thus, the

RMSE for calibrated model is only 18% worse than the best-fit potentiometric surface (24.39 m compared to 20.70 m). Moreover, the weighted RMSE of the calibrated model is an order of magnitude better than the best-fit potentiometric surface and this indicates excellent model agreement in high weight areas of the model domain—areas felt to be the most important to get accurate model simulations (i.e., downgradient from the repository). Because of the 10-m minimum layer thickness, head differences of less than this magnitude are within the uncertainty range of the model.

As can be seen in Figure 6-15, the largest head residuals (~100 m) are in the northern part of the model in the altered northern region and in the vicinity of the moderate hydraulic gradient. These residuals are largely the result of the low weighting factor of (0.1) and the possibility that they reflect perched conditions (see Section 6.5.2.1 for a description and Section 6.7.7 for a discussion of perched water effects). In the figure, a negative residual means that the calibrated value was lower than the target data (note that the PEST record file shows opposite signs; a negative residual means that the calibrated value was higher than observed). The next highest head residuals border the Crater Flat and Solitario Canyon Faults. These residuals (~25 m) are most likely the result of 250-m grid blocks not being able to resolve the 780-m to 730-m drop in head in the short distance just east of the above-mentioned features. There may be additional complicating factors such as varied hydrologic characteristics in the Solitario Canyon Fault along its north-south transect. In the model, the fault acts as a barrier, but is defined with only one calibration parameter. This may not be adequate to represent the local behavior of such a long feature. For example, well USW G-1, about 1,000 m from the Solitario Canyon fault, shows an 8-m difference between measured and simulated heads. The measured head for this well (754 m), located on the east side of the fault, is closer to measured head values on the west side of the fault. Because the majority of wells on the east side have heads of approximately 745 m, the simulated head for USW G-1 has a calibrated result close to that value. Overall results indicate that the model adequately represents the water table near Yucca Mountain. In the vicinity of the 18-km compliance boundary and south, the modeled potentiometric surface is typically on the order of 5 m higher than the observed water levels although the estimated gradients match well (see Section 7.2.1).

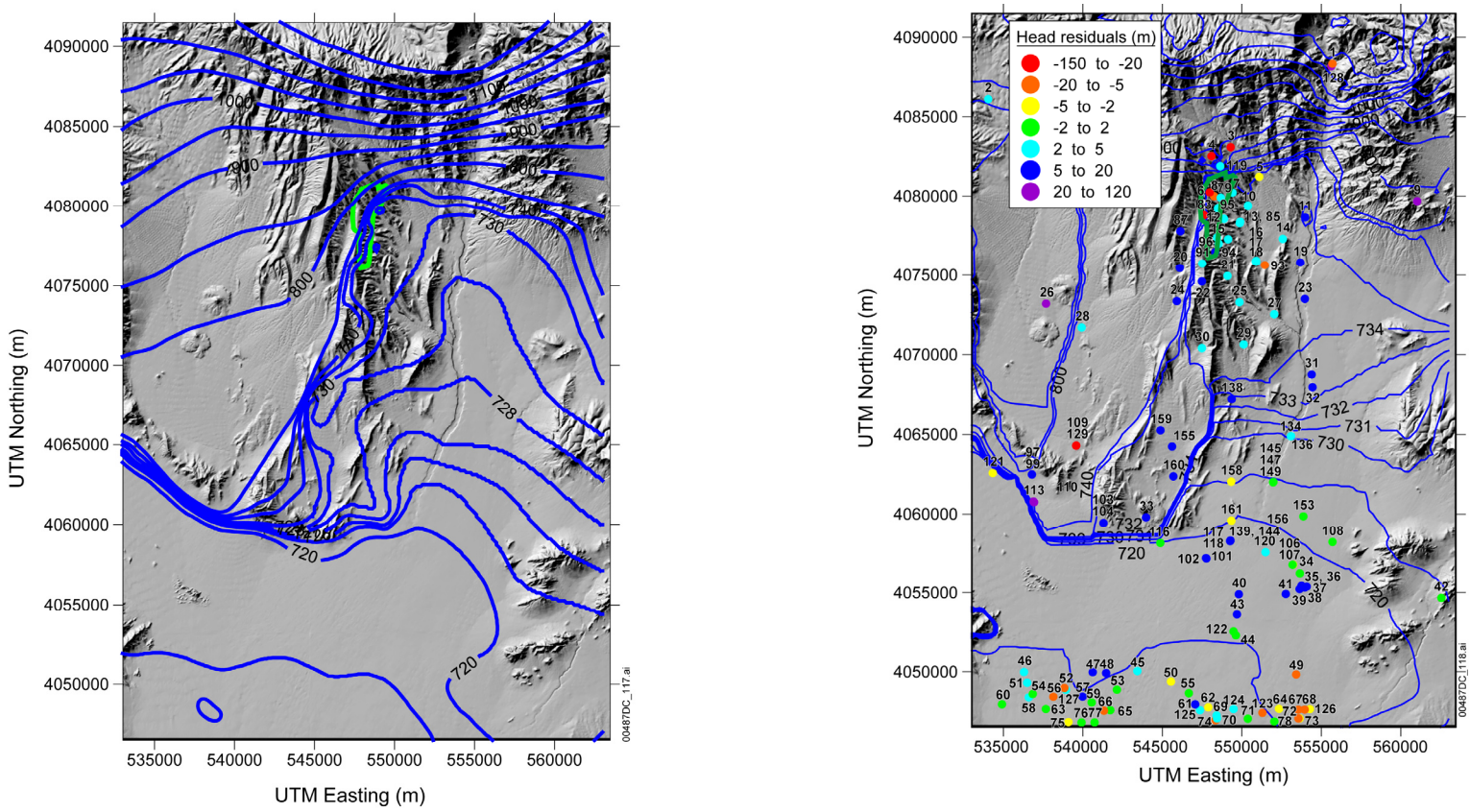

Sources: SNL 2007 [DIRS 179466] (repository outline); DTN: GS010908312332.002 [DIRS 163555] (well locations and water levels).

Output DTNs: SN0610T0510106.001, and SN0702T0510106.007 (well locations and water levels); MO0611SCALEFLW.000 (potentiometric surface), left panel; SN0612T0510106.004 (model potentiometric surface), right panel.

NOTES: Symbols in right panel represent well locations. Head residual is the simulated value minus the observed value. The wells are numbered to correspond to the second column of Table 6-8 (multiple-depth wells only show the heads corresponding to the highest screened interval altitude).

UTM = Universal Transverse Mercator.

Figure 6-15. Contour Plot of Potentiometric Surface (Left Panel) and Simulated Water-Level Data with Residual Heads (Right Panel)

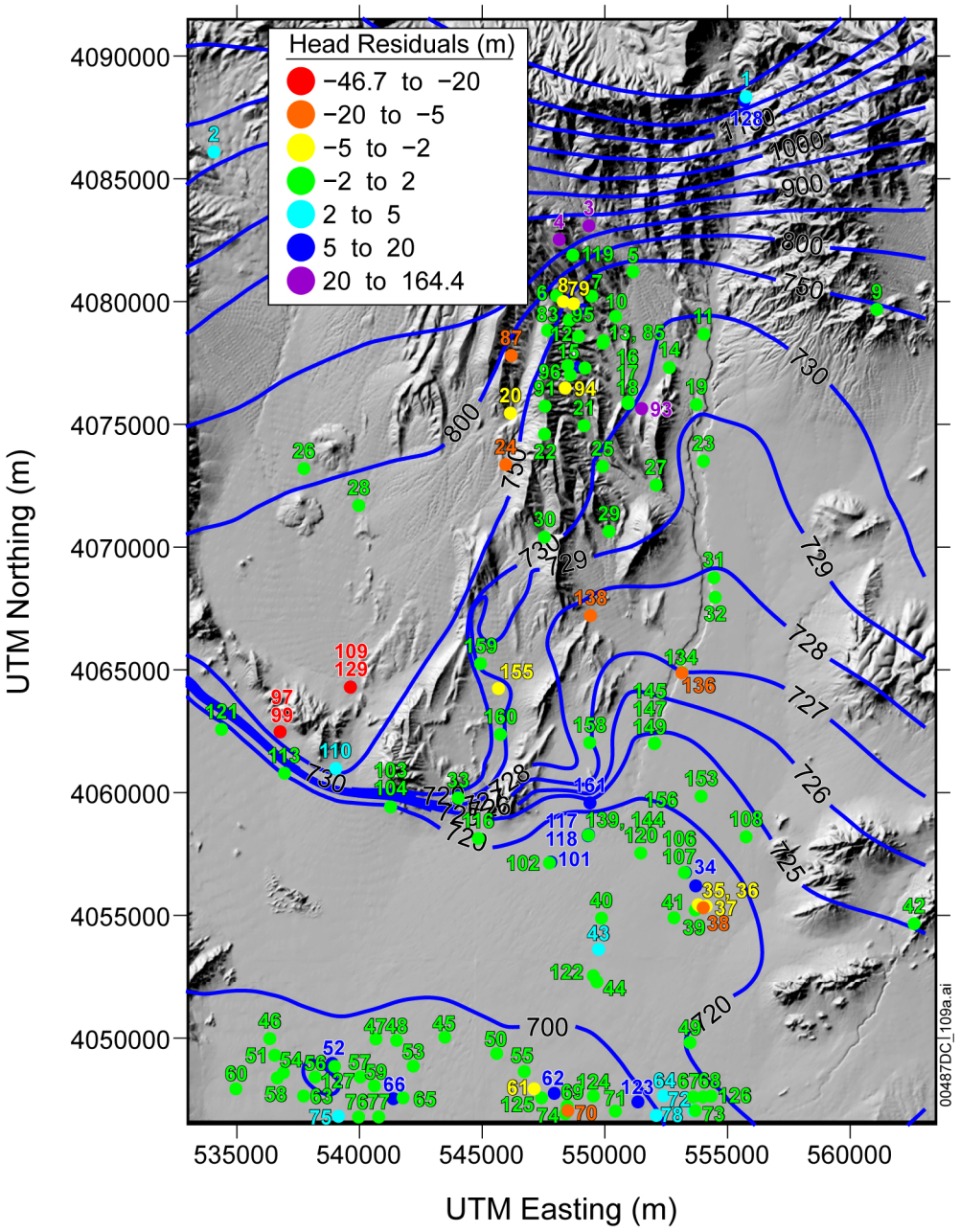

Source: DTN: GS010908312332.002 [DIRS 163555]

Output DTNs: MO0611SCALEFLW.000 (potentiometric surface); SN0610T0510106.001, and SN0702T0510106.006 (well locations and water levels).

NOTE: The wells are numbered to correspond to the second column of Table 6-8 (multiple-depth wells only show the number corresponding to the highest screened interval altitude). Color of the symbol indicates the head residual which is the simulated value minus the observed value. The contours represent the potentiometric surface.

UTM = Universal Transverse Mercator.

Figure 6-16. Well Locations and Head Residuals between Measured Water-Level Data and the Potentiometric Surface Used to Construct Model Boundary Conditions

6.5.2.2 Comparing Volumetric/Mass Flow Rates from the Regional-Scale Model with Volumetric/Mass Flow Rates from the Calibrated Site-Scale Model

The SZ site-scale flow model corresponds to only a small part of the DVRFS, which is used to supply target lateral volumetric/mass flow rates. A comparison between the two models was suggested by the Expert Elicitation Panel (CRWMS M&O 1998 [DIRS 100353]). The regional flow model simulates a closed system and uses data from spring discharges to calibrate the water flux through the system (Belcher 2004 [DIRS 173179]). Thus, this model provides a rough estimate of volumetric/mass flow rates expected through the SZ site-scale model domain.

The regional model HFM is described by Belcher (2004 [DIRS 173179], Chapter E). The SZ site-scale flow model uses an equivalent HFM, which is described in *Hydrogeologic Framework Model for the Saturated Zone Site-Scale Flow and Transport Model* (SNL 2007 [DIRS 174109]).

In Section 6.3.1.6, the methodology for applying fixed-head lateral boundary conditions to the SZ site-scale flow model was described. With fixed-head boundary conditions, the flux through a boundary is a function of the permeabilities on that boundary. Flux targets were derived from the values simulated by the 2004 regional model (Appendix C). A comparison of the calibration target volumetric/mass flow rates and volumetric/mass flow rates derived from the calibrated SZ site-scale flow model is made in Table 6-11. The western boundary, for instance, has a total flux of 120.3 kg/s (3.8×10^6 m^3/yr) across it for the target flux values and 101.0 kg/s (3.2×10^6 m^3/yr) across it in the calibrated model. The difference in southern volumetric/mass flow rates, which is simply a sum of the other boundary volumetric/mass flow rates plus the recharge (528.1 kg/s), is a decrease of about 23%. The weighted RMSE for boundary volumetric/mass flow rates is 35.3 kg/s. It should be noted that in Table 6-11, the sum of all target boundary volumetric/mass flow rates (64.7 kg/s) is not equal to the sum of all volumetric/mass flow rates through the calibrated flow model (64.1 kg/s) because different infiltration boundary conditions were applied to each model (see Section 6.4.3.9 and Figure 6-14).

Factors that affect the flux match between the regional- and site-scale models include the horizontal and vertical resolution and the permeability distribution. The horizontal resolution of the site-scale flow model is 36 times finer than the regional model (250-m versus 1,500-m grid block size). The vertical resolution of the SZ site-scale flow model is about four times finer than the regional model (67 versus 16 layers). The increased resolution at the site scale means that, compared to the regional-scale model, volumetric/mass flow rates calculated by the SZ site-scale flow model may depend more strongly on a few units. Flux distribution in the regional model is also impacted by the use of permeability classes. In the regional model, permeabilities (actually hydraulic conductivities) associated with specific units are not defined. Rather, the permeabilities are grouped into classes, which are assigned to a particular grid block based on the percentages of the rock types contained in the grid block. Thus, although the regional-scale model was based on the same complex HFM used for the site-scale model, the regional model used only four permeability classes. Because of these fundamental differences, it is not possible to reproduce the distribution of volumetric/mass flow rates corresponding to the sides of the SZ site-scale flow model, when examined on a unit-by-unit basis. Nevertheless, the difference in the total flux across the southern boundary between the SZ site-scale flow model and the

regional model is within the range considered acceptable by the Expert Elicitation Panel (CRWMS M&O 1998 [DIRS 100353]).

Table 6-11. Comparison of Target and Site-Scale Volumetric/Mass Flow Rates

Boundary Zone (Range in m)	Target Mass/Volume Flows		Site-Scale Mass/Volume Flows		Calibration Weight
	Flow (kg/s)	Flow (m^3/yr)	Flow (kg/s)[a]	Flow (m^3/yr)[a]	
North (533,000–563,000)	–158.9	-5.0×10^6	–57.1	-1.8×10^6	5
West (4,046,500–4,091,500)	–120.3	-3.8×10^6	–101.0	-3.2×10^6	5
$East_1$ (4,046,500–4,052,500)	–273.1	-8.6×10^6	–232.1	-7.3×10^6	1
$East_2$ (4,052,501–4,058,500)	33.3	1.0×10^6	–97.4	-3.1×10^6	1
$East_3$ (4,058,501–4,069,000)	–127.8	-4.0×10^6	260.9	8.2×10^6	1
$East_4$ (4,069,001–4,079,500)	30.2	9.5×10^5	–206.6	6.5×10^6	1
$East_5$ (4,079,501–4,091,500)	–0.4	-1.2×10^4	–30.7	-9.7×10^5	1
South (533,000–563,000)	681.9	2.2×10^7	528.1	1.7×10^7	NA

Source: Appendix D (qualified for one time use).

Output DTN: SN0612T0510106.004, *sz06.pest*.

NOTES: Negative values indicate flow into the model. South boundary volumetric/mass flow rates were not used as targets for the calibration of the SZ site-scale flow model; rather, they were calculated from the balance of infiltration and the volumetric/mass flow rates across north, west, and east boundaries.

[a] Mass flows are approximate because of the technique FEHM uses in the *flxz* macro to sum and print boundary flows.

Conversion factor: $m^3/yr = \frac{m^3}{1,000\,kg} \cdot \frac{86,400\,s}{day} \cdot \frac{365.25\,day}{yr} \cdot \frac{kg}{s}$

6.5.2.3 Simulated Flow Paths

The particle-tracking capability of FEHM illustrates flow paths simulated by the calibrated SZ site-scale flow model. One hundred particles were distributed randomly over the area of the repository and allowed to migrate subject to advection only (non-dispersive) until they reached the model boundary (Figure 6-17). The pathways generally leave the repository and travel in a south-southeasterly direction to the 18-km compliance boundary. From the 18-km boundary to the end of the model, the flowpaths trend to the south-southwest and generally follow Fortymile Wash. Some of the pathways follow fault zones along Fortymile Wash (Zone 40 of Figure 6-12). The hydrogeologic units through which the flow below the repository passes consist of the Crater Flat group (Bullfrog, Tram, and Prow Pass) with most of the flow in the Bullfrog unit, the upper volcanic aquifer, the upper volcanic confining unit, the valley fill unit, and the undifferentiated valley-fill unit. Figure 6-17 includes a vertical cross section of the path lines. Evident in the figure is the shallow depth of the path lines along most of the pathways south of UTM Northing 4,065,000 m, which is consistent with data supporting an upward head gradient. In Section 7, the fluid pathways are compared with those inferred from geochemical data.

6.5.2.4 Specific Discharge

Using the calibrated SZ site-scale flow model, specific discharge was estimated as the average over 100 particles. These particles were randomly distributed below the repository and tracked until they traveled across UTM Northing 4,037,361 m (5 km south of the southern tip of the repository). Pathlength divided by travel time yields the specific discharge for a particle and the average across 100 particles was 0.36 m/yr (1.08 ft/yr) for the calibrated model. End members of the 100-particle plume had specific discharges of 0.11 and 0.66 m/yr. The Expert Elicitation Panel (CRWMS M&O 1998 [DIRS 100353], Figure 3-2e) estimated a median specific discharge of 0.6 m/yr (2.0 ft/yr) for the 5-km (3-mile) distance. Thus, reasonable agreement is found between the specific discharge simulated by the calibrated SZ site-scale flow model and that estimated by the Expert Elicitation Panel (CRWMS M&O 1998 [DIRS 100353]). Mass balance error for all runs was essentially zero.

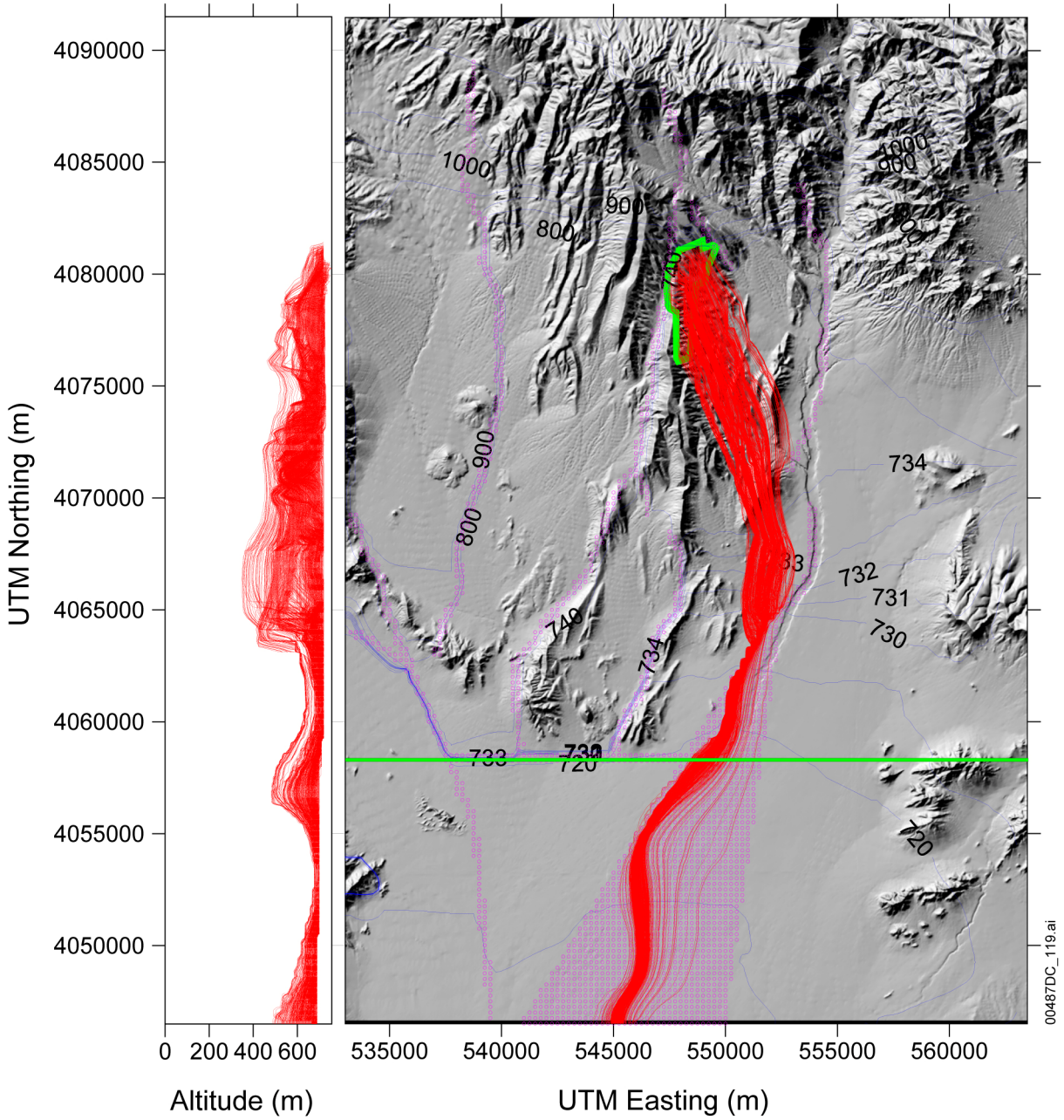

Source: SNL 2007 [DIRS 179466] (Repository outline).

Output DTNs: SN0612T0510106.004 (water levels) and SN0704T0510106.008 (particle tracks).

NOTE: The contours represent the modeled potentiometric surface. Altitude is in meters above mean sea level. The green line across the model at UTM Northing equal to 4,058,256 m represents the 18-km compliance boundary. Pink represents special geologic features (see Table 6-7 and Figure 6-12). 1,000 particles are simulated to improve flowpath clarity.

UTM = Universal Transverse Mercator.

Figure 6-17. Flow Paths for Particles Released (uniformly but randomly distributed) below the Repository Area

6.6 CONSIDERATION OF ALTERNATIVE CONCEPTUAL MODELS

The SZ site-scale flow model propagates information through the SZ flow and transport model abstraction (SNL 2007 [DIRS 177390]) to the performance assessment calculations, which are used to evaluate potential risks to groundwater users downgradient from the repository area. The results of these performance assessment calculations depend upon the specific discharge of groundwater leaving the repository area as well as on the flow paths and the distribution of flow among the various hydrostratigraphic units that carry, deflect, or otherwise affect the flow. For this report only, the specific discharge was evaluated with SPDIS.EXE (STN: 611598-00-00 [DIRS 180546]), which calculates the average travel distance divided by corresponding travel time to reach a specified northing location (e.g., 5 km downgradient) across 100 particles. It is important to note that SPDIS.EXE yields a convenient metric to compare specific discharges, which represents surrogates for flow fields generated from the model. The alternative conceptual models (ACMs) presented here were investigated because they represented a hydrologic concern such as water table rise due to climate change or were related to a model feature (anisotropy) that had a possibility of affecting the specific discharge calculations. This section presents analyses of the ACMs, their representation in the numerical model, and a discussion about possible impacts on the model outputs. ACMs affecting model outputs are discussed here, although this uncertainty is not directly propagated to the radionuclide breakthrough curves in the TSPA calculations. Specifically, it should be noted that the SZ flow and transport abstraction model does not use the SZ site-scale flow model as a source of direct input to the assessment of uncertainty in groundwater specific discharge. The two direct inputs used to establish the groundwater specific discharge multiplier are DTNs: MO0003SZFWTEEP.000 [DIRS 148744] and LA0303PR831231.002 [DIRS 163561] (SNL 2007 [DIRS 177390], Table 4-1 and Section 6.5.2.1).

The calibrated SZ site-scale flow model described in detail in Section 6.5 also provides the basis for the ACMs discussed here. That is, the same numerical grid and HFM were used throughout this section. Various parameterization schemes were used to define the ACMs (e.g., change in potentiometric surface). The following ACMs were evaluated:

- Removal of vertical anisotropy: This ACM relates to removal of vertical anisotropy in permeability
- Removal of horizontal anisotropy: This ACM relates to removal of horizontal anisotropy in the volcanic units downgradient from Yucca Mountain
- Removal of the altered northern region: This ACM relates to removal of the permeability multipliers that reduce the permeability in the northern region, which help the model honor the observed high head
- Increase in permeability in the *z*-direction for the Solitario Canyon Fault
- Water table rise: This ACM relates to future water table rise.

6.6.1 Removal of Vertical Anisotropy

Anisotropy occurs when hydraulic properties have different values in the three principal directions: vertical, horizontal along the direction of maximum permeability, and horizontal along the direction of minimum permeability. The ratio of horizontal to vertical permeability, 10:1, is in the generally accepted range provided by the Expert Elicitation Panel (CRWMS M&O 1998 [DIRS 100353], Table 3-2). The results upon removal of vertical anisotropy (i.e., 1:1) are shown in Figure 6-18. Specific discharge across the 5-km boundary increases by 28% from 0.36 to 0.46 m/yr. Weighted RMSE increase significantly (89%) from 0.82 to 1.55 m and non-weighted RMSE increase 20% from 24.39 to 29.21 m. Differences in fluxes through the boundary zones defined in Table 6-11 changed by no more than 8% (decreases from –101 to –107 kg/s and –57 to –62 kg/s on the west and north boundaries, respectively). Not surprisingly, without vertical anisotropy, particles travel deeper in the system (from 353 m for the anisotropic case to –175 m without vertical anisotropy). Overall, 10:1 vertical anisotropy yields better flow calibration because removal of vertical anisotropy degrades the accuracy and representativeness of the model results.

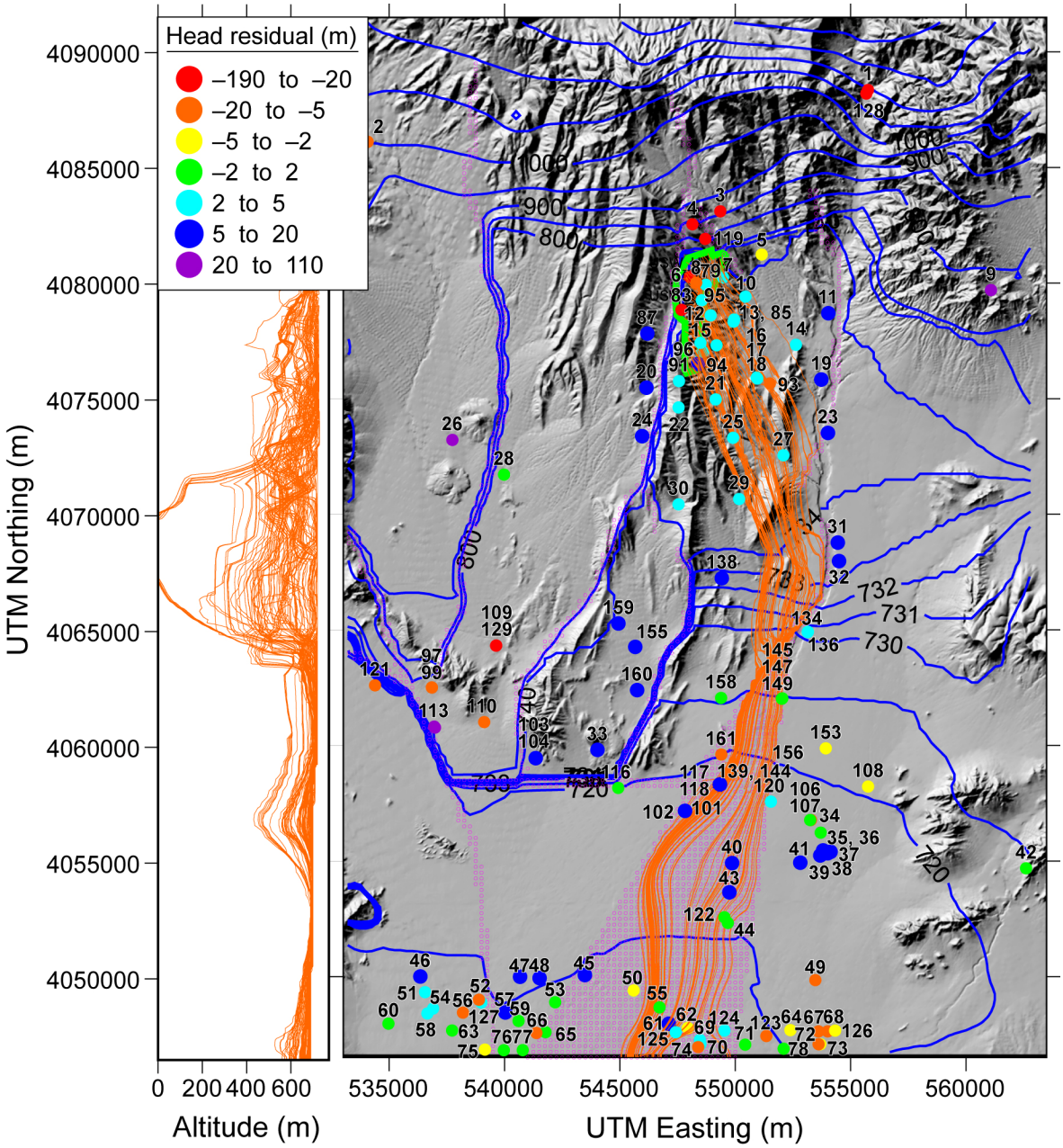

Source: SNL 2007 [DIRS 179466] (for repository outline).

NOTE: For illustration purposes only. Altitude is in meters above mean sea level. Legend represents the water level difference in meters (simulated value minus measured value). The wells are numbered to correspond to the second column of Table 6-8 (multiple-depth wells only show the number corresponding to the highest screened interval altitude).

UTM = Universal Transverse Mercator.

Figure 6-18. Particle Tracks for a Model without Vertical Anisotropy

6.6.2 Removal of Horizontal Anisotropy

Anisotropy in the volcanic units near Yucca Mountain was investigated using an ACM with variable horizontal anisotropy ratios (north–south to east–west permeability changes). The area to which the anisotropy ratio was applied is bounded by the quadrilateral shown in Figure 6-12. This effect was investigated by rerunning the calibrated model with a 1:1 horizontal permeability ratio in this region and checking the sensitivity of the modeled water levels and flow paths. A detailed description of the development of the horizontal anisotropy distribution used in this model is found in *Saturated Zone In-Situ Testing* (SNL 2007 [DIRS 177394], Section 6.2.6 and Appendix C6). This alternate conceptual model is carried through to TSPA where flow fields are generated using the distribution defined in *Saturated Zone In-Situ Testing* (SNL 2007 [DIRS 177394], Section 6.2.6 and Appendix C6). Modeling the Yucca Mountain volcanic zones as isotropic yielded insignificant changes to the weighted RMSE for head residuals (0.82 m). Specific discharge across the 5-km boundary decreases by 31% from 0.36 to 0.25 m/yr and associated pathlines are shown in Figure 6-19. The pathlines, as expected, have a more easterly trend immediately downstream from the repository as compared to the calibrated model (Figure 6-17). Also, pathlines go somewhat deeper to 319 from 353 m for the horizontally isotropic case. Because horizontal anisotropy impacts specific discharge results, this parameter has been included in the TSPA analysis and, is therefore fully accounted for in terms of effect on repository performance.

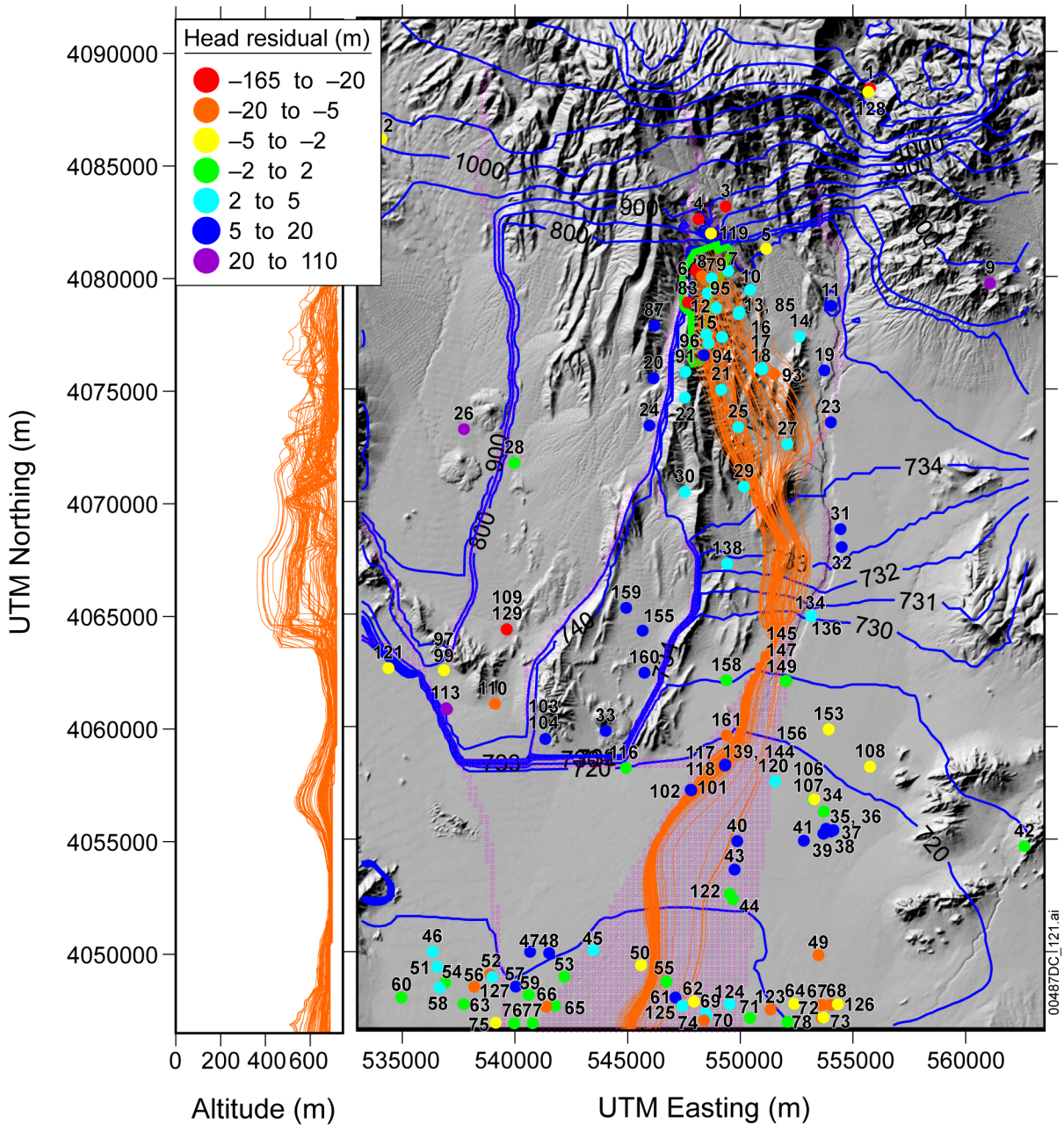

Source: SNL 2007 [DIRS 179466] (for repository outline).

NOTE: For illustration purposes only. Altitude is in meters above mean sea level. Legend represents the water level residual (m) (simulated value minus the observed value). The wells are numbered to correspond to the second column of Table 6-8 (multiple-depth wells only show the number corresponding to the highest screened interval altitude).

UTM = Universal Transverse Mercator.

Figure 6-19. Particle Tracks for Isotropic Yucca Mountain Volcanic Units

6.6.3 Removal of LHG and Change to the Solitario Canyon Fault Anisotropy

A LHG just north of Yucca Mountain has been inferred from hydraulic head measurements. Previous revisions of the AMR assumed an artificial low-permeability east-west feature included in the model simply to obtain an acceptable representation of the LHG. This model implements the LHG with a more defensible conceptual model—the altered northern region (see Sections 6.3.1.11 and 6.4.3.7 where alteration due to the Claim Canyon Caldera north of Yucca Mountain divides hydrogeologic units into distinct northern and southern zones). Although the genesis of the LHG has yet to be fully explained, logic dictates that so long as the LHG in this region is faithfully represented (regardless of its conceptualization), effects on flowpaths are minimal because the region is upgradient from the zone of interest (and away from zones that are weighted heavily during calibration). However, removal of the LHG from the conceptual model yielded an increase in specific discharge across the 5-km boundary to 4.79 m/yr (an increase by nearly a factor of 15) because the zone of reduced permeability was eliminated from the altered northern region (permeability multipliers set to one, but no recalibration performed) and the overall flux of water through the northern model boundary was significantly increased. The weighted RMSE was increased by nearly a factor of 8 to 6.20 m. Clearly, removal of the LHG from the conceptual model yields a model that does not match observations, hence its existence (not its conceptualization) is critical to an accurate model.

Changing the vertical anisotropy in the Solitario Canyon Fault from a factor of 10 to 1,000 its across-the-fault permeability yielded a 3% increase in specific discharge across the 5-km boundary to 0.37 m/yr. Weighted head residuals, however, actually decreased by 2 % to 0.80 m (non-weighted residuals increased by 1% to 24.67 m). This indicates that different conceptualizations for anisotropy of the Solitario Canyon Fault do not impact water levels, but can impact specific discharge to some degree.

6.6.4 Water Table Rise

6.6.4.1 Water Table Rise below Repository

In addition to modeling SZ flow under contemporary conditions, it is also necessary to consider conditions as the climate changes in the future. A higher water table is expected in the Yucca Mountain region for future wetter climatic conditions. A rise in the water table could impact radionuclide transport in the SZ, but it is handled in a simplified manner. A higher water table has clear impacts on radionuclide transport in the UZ by shortening the transport distance between the repository and the water table. SZ modeling analyses considered in this report indicate that a rise in the water table will cause some of the flow paths from below the repository to the accessible environment to be in units with lower values of permeability than the ones saturated by the present-day water-table conditions.

Several independent lines of evidence are available for estimating the magnitude of rise in the water table below the repository at Yucca Mountain under previous glacial-transition climatic conditions (Forester et al. 1999 [DIRS 109425], pp. 56 and 57). Mineralogic alteration (zeolitization and tridymite distribution) in the UZ at Yucca Mountain shows no evidence that the water table has risen more than 60 m (200 ft) above its present position in the geologic past (Levy 1991 [DIRS 100053], p. 477). Analyses of $^{87}Sr/^{86}Sr$ ratios in calcite veins of the

unsaturated and saturated zones at Yucca Mountain indicated previous water-table elevations of 85 m (279 ft) higher than present (Marshall et al. 1993 [DIRS 101142], p. 1,948). Recently completed wells at paleospring discharge locations near the southern end of Crater Flat, which are inactive sites of Pleistocene spring discharge, revealed shallower-than-expected groundwater with depths of only 17 to 30 m (56 to 100 ft) to the water table (Paces and Whelan 2001 [DIRS 154724]; BSC 2004 [DIRS 168473], Table I-1). These findings indicate that the water-table rise during the Pleistocene at these paleospring locations could not have been more than about 30 m (100 feet) due to formation of discharge locations. The results of the mineralogical and geochemical studies showing a maximum water-table rise of up to 85 m reflect evolution of past climates for the last 1 million years, which included the effects of glacial climates. The maximum water-table rise under monsoon and glacial-transition climates is, therefore, expected to be less than 85 m because the monsoon and glacial-transition climates are warmer and dryer than the glacial climate (Sharpe 2003 [DIRS 161591]).

Interpretation of the water levels in wells at the southern end of Crater Flat, in relation to water-table rise, is complicated by several factors. The paleospring discharge locations at the southern end of Crater Flat are not along the flow path from Yucca Mountain. Also, a higher groundwater flow rate (increased hydraulic gradient) is expected under future wetter climatic conditions. However, the principles of hydrogeology specify that a uniform rise in the water table could only occur if the increased saturated thickness (and its effect on transmissivity) accommodates the additional groundwater flow through the aquifer. For the geology within the model domain, an increase in gradient to accommodate the increase in flow will results in a nonuniform water-table rise with higher increases upgradient of flow. A higher groundwater flow rate implies a higher hydraulic gradient, a larger transmissivity, or both along any given flow line. Thus, the water table at upgradient locations would be expected to rise more than the water table at downgradient locations, resulting in a nonuniform rise in the water table across the flow system.

Two-dimensional groundwater flow modeling of the response to doubling mean annual precipitation indicated a maximum water table rise of 130 m (430 ft) in the vicinity of Yucca Mountain (Czarnecki 1985 [DIRS 160149]). This result is potentially overestimated because the analysis by Czarnecki (1985 [DIRS 160149]) was limited to two dimensions. In addition, average precipitation under monsoon and glacial-transition climates is less than twice the present-day value in the Yucca Mountain area, and the percolation flux resulting from the precipitation increase was also conservatively modeled (Czarnecki 1985 [DIRS 160149]). More recent groundwater flow modeling of the regional flow system under paleoclimate conditions (the DVRFS) simulated water levels of 60 to 150 m (200 to 490 ft) higher than present below Yucca Mountain (D'Agnese et al. 1999 [DIRS 120425], p. 2). Coarse resolution of the numerical grid in this model is believed to have resulted in potential overestimation of water table rise (150 m).

The uncertainty in water-table rise has been evaluated by considering these multiple lines of evidence and new geochemical data using a multidisciplinary workshop approach, as documented by *Total System Performance Assessment Model/Analysis for the License Application* (SNL 2007 [DIRS 178871]). Given that these various sources of information on water-table rise result in significant variations in the estimate and that none of the sources is clearly definitive, a subjective approach to quantifying uncertainty was used and a consensus

uncertainty distribution was derived. The median value from the uncertainty distribution for the average water-table rise beneath the repository from that assessment is 50 m (SNL 2007 [DIRS 178871]). This 50-m increase in the water table elevation at the repository is consequently used in the adaptation of the SZ site-scale flow model described below.

6.6.4.2 Incorporation of Water-Table Rise into the SZ Flow and Transport Models

The effects of climate change on radionuclide transport simulations in the SZ are incorporated into the TSPA analyses by scaling the simulated SZ breakthrough curves by a factor representative of the alternative climate state (SNL 2007 [DIRS 178871]). The scaling factor used in this approach is the ratio of average SZ groundwater flux under the future climatic conditions to the flux under present conditions. This approach approximates the impacts of future, wetter climatic conditions in which the SZ groundwater flux will be greater. However, this approach implicitly models the same flow path for radionuclide transport through the SZ under wetter climatic conditions of the future. In reality, significant rise in the water table due to climatic changes would result in different flow paths through the SZ system, including the potential for encountering different hydrogeologic units by radionuclides during transport.

The objective of this modeling task is to adapt the SZ site-scale flow model to include the effects of estimated water-table rise. The SZ site-scale transport model is used in a separate report to compare the results of particle-tracking simulations using this adapted model to the simple flux scaling approach used in TSPA analyses. Flow modeling for this task is presented in this report and the transport simulations are presented in *Site-Scale Saturated Zone Transport* (SNL 2007 [DIRS 177392], Appendix E). The flux-scaling approach to simulation of climate change results in more rapid radionuclide transport in the SZ, relative to the more realistic situation in which water-table rise is included in the modeling (SNL 2007 [DIRS 178871]). The purpose of this section is to provide an adapted version of the SZ site-scale flow model for incorporation in the SZ site-scale transport model.

6.6.4.2.1 Estimating Water Table Rise from Climate Change

Rise in the water table during wetter glacial transition conditions at Yucca Mountain is a complex function of greater recharge to the SZ and changes to the amount and spatial distribution of lateral fluxes from the regional SZ system. Although the analyses discussed in this report are for glacial-transition climatic conditions, they are a reasonable approximation of changes to the SZ for time periods beyond 10,000 years in the future. The conclusions are thus applicable to TSPA analyses that extend to peak simulated dose. Simulations of groundwater flow under wetter climatic conditions with the SZ regional-scale flow model (D'Agnese et al. 1999 [DIRS 120425]) indicate that groundwater flow paths from below Yucca Mountain do not significantly change under glacial climatic conditions. These simulations also show that groundwater surface discharge from the SZ for the wetter glacial climatic conditions would not occur along the flow path from Yucca Mountain at any location closer than the regulatory boundary of the accessible environment, approximately 18 km south of the repository.

The estimated elevation of the water table under wetter, glacial-transition conditions within the domain of the SZ site-scale flow model was calculated in an Excel spreadsheet by assuming linear increases in the elevation of the water table. This estimated increase in water level was

calculated by assuming a 20-m rise at locations with a present-day water table elevation of 700 m, a 50-m rise at locations with a present-day water table elevation of 740 m, and a 100-m rise at locations with a present-day water table elevation of 1,000 m. The estimated higher water table for glacial-transition climatic conditions at other locations was calculated by linear interpolation or extrapolation. In addition, the rise in the water table was limited by the topographic surface.

This approach results in a water-table rise of approximately 50 m in the area beneath the proposed repository, which is the median value from the uncertainty distribution derived for this parameter (SNL 2007 [DIRS 178871]). The approach also approximately preserves the direction of the horizontal hydraulic gradient at the water table, which is consistent with the results of the SZ regional-scale flow model with regard to the simulated flow paths from beneath the repository under wetter climatic conditions (D'Agnese et al. 1999 [DIRS 120425]).

The estimated elevation of the water table under wetter, glacial-transition climatic conditions, as calculated with the approach described above, is shown in Figure 6-20. Note that the pattern of the contours for the water table is generally similar to the present water table (see Figure 6-4), with the exception of the area in Fortymile Canyon in the northern part of the model domain. The deflection of the water table contour in Fortymile Canyon corresponds to an area in which the water table rise has been limited by the topographic surface. There is little information upon which to base estimates of the water table configuration under future climatic conditions in the area to the north of Yucca Mountain in the SZ site-scale flow model domain. Regardless, the approach used to estimate water-table rise to the north of the repository has little impact on the simulated flow system down gradient of Yucca Mountain in the SZ site-scale flow model.

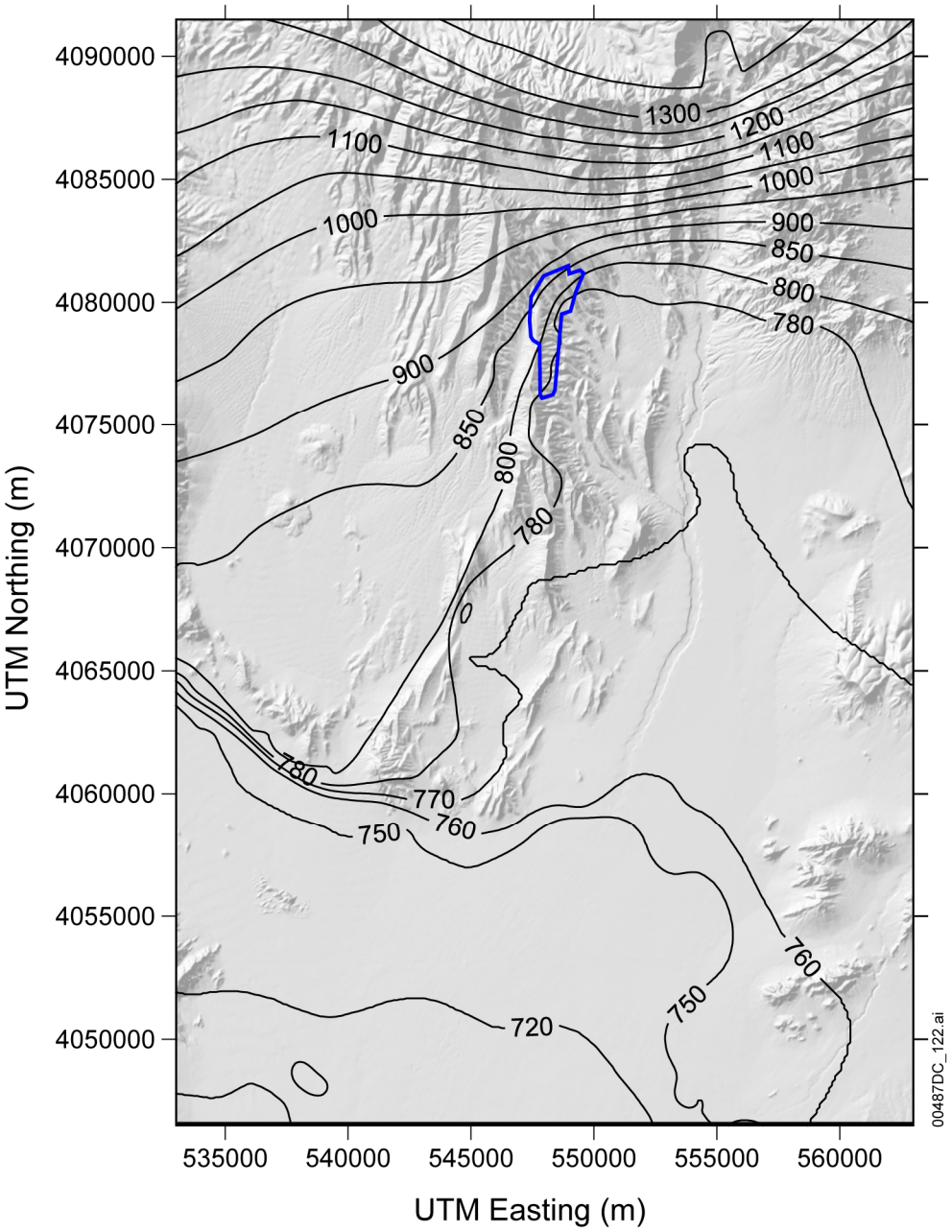

Sources: SNL 2007 [DIRS 179466] (repository outline); Output DTN: SN0702T0510106.006 (water table rise).

NOTE: Repository outline shown with a bold blue curve. For illustration purposes only.

UTM = Universal Transverse Mercator.

Figure 6-20. Estimated Water Table Elevations for Future Glacial-Transition Climatic Conditions

Figure 6-21 shows the estimated depth to the water table under wetter, glacial-transition climate conditions, as calculated by the approach described above. The areas in which the estimated water table is within 5 m of the topographic surface are shaded blue. The larger of these areas in the southwestern part of the domain contains three distinct paleospring deposits located along U.S. Highway 95 and at the southern end of the Crater Flat. This shows consistency between the

estimated higher water table and the geologic features associated with Pleistocene spring discharge. The specific paleospring locations are probably controlled by structural features too small to be resolved with this model. Another site of shallow estimated groundwater shown in Figure 6-21 is Fortymile Canyon. Paleospring deposits are not observed in Fortymile Canyon, but it is reasonable to postulate that such deposits would not be preserved in this geomorphic location. It is also reasonable that the water table would rise to the extent that upper Fortymile Wash would become a perennial gaining stream in Fortymile Canyon under wetter climatic conditions. The areas of predicted shallow groundwater near and on the southern boundary of the model domain do not correspond to specifically identified paleodischarge locations, but paleospring deposits could have been buried by aggradation of alluvium in these locations.

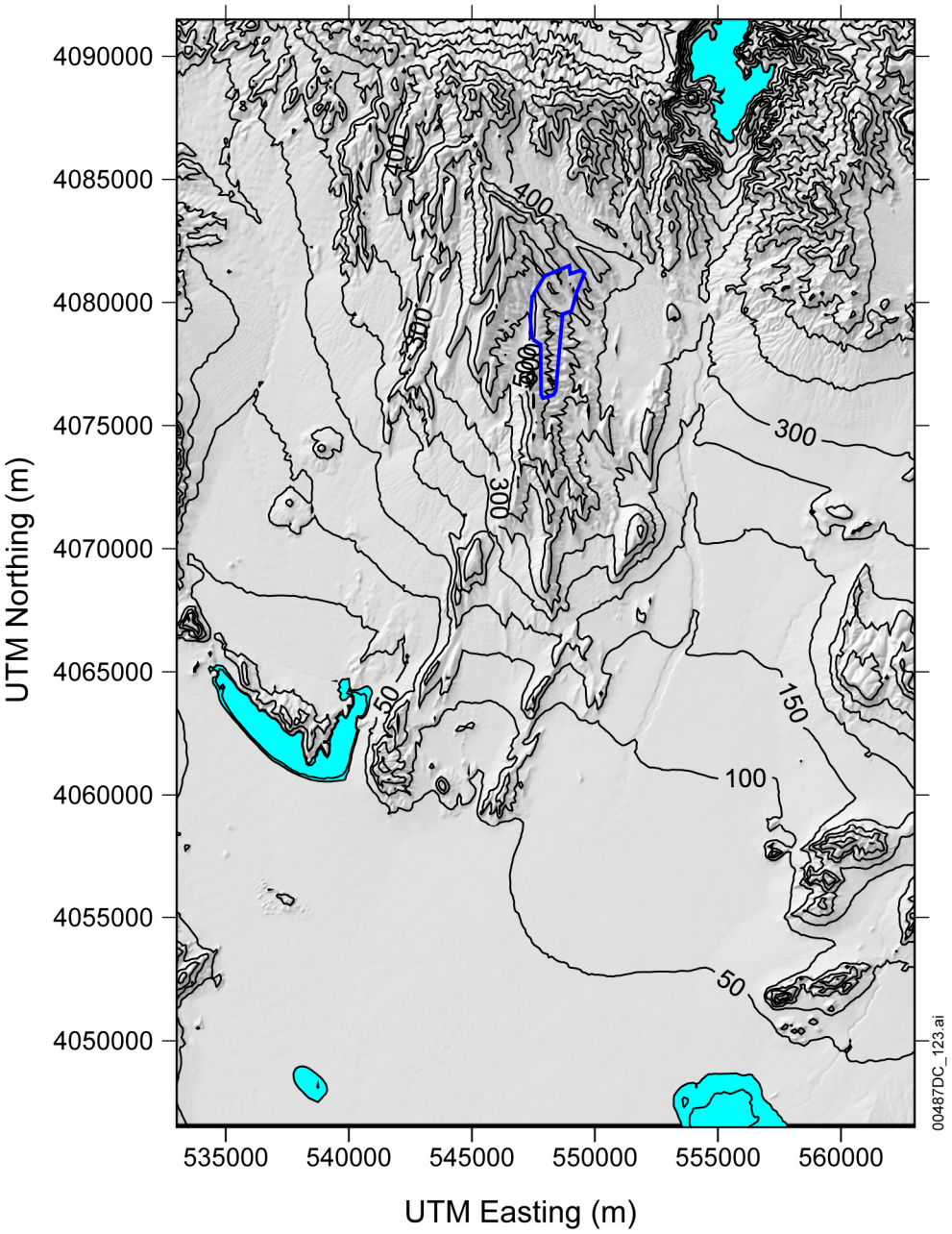

Sources: SNL 2007 [DIRS 179466] (repository outline); Output DTN: SN0702T0510106.006 (depth to water).

NOTE: Repository outline shown with a bold blue line. Areas with estimated depth to the water table of less than 5 m are shaded blue. For illustration purposes only.

UTM = Universal Transverse Mercator.

Figure 6-21. Estimated Depth to the Water Table for Future Glacial-Transition Climatic Conditions

Analyses of the impacts of climate change and water table rise on groundwater flow in the area near Yucca Mountain have been conducted using an independently developed site-scale flow model by Winterle (2003 [DIRS 178404], 2005 [DIRS 178405]). These modeling studies included increased values of specified head at the flow model boundaries, increased recharge,

and potential discharge of groundwater from springs activated by the higher water table. Winterle (2003 [DIRS 178404], 2005 [DIRS 178405]) concluded that neither the increase in the water-table elevation nor the discharge of groundwater from springs significantly affected the flow paths from beneath Yucca Mountain. Comparison of the predicted locations of shallow groundwater under glacial-transition climatic conditions (Figure 6-21) with the simulated locations of potential discharge locations (Winterle 2005 [DIRS 178405], Figure 3) indicates similar results. Both approaches indicate similar patterns of potential discharge at the southern end of Crater Flat and in two areas near the southern boundary of the SZ site-scale flow model domain. However, this report's analysis results predict potential discharge in Fortymile Canyon, wheras the Winterle (2005 [DIRS 178405], Figure 3) results apparently do not.

In summary, a reasonable estimate of the water table elevation under wetter, glacial-transition conditions is developed for the SZ site-scale flow model domain. The estimated rise in the water table is consistent with the conclusion that the general direction of flow paths from beneath the proposed repository would not change for wetter climatic conditions, although differences in hydrogeologic units occurring at the water table below the repository would have an impact on local flowpaths. In addition, the pattern of the estimated rise in the water table is generally consistent with the locations of paleospring deposits within the domain.

6.6.4.2.2 Water Table Rise in the SZ Site-Scale Flow Model

The SZ site-scale flow model is adapted to the higher estimated water table for glacial-transition climatic conditions by creating a new grid with an upper surface corresponding to the higher water table. The lateral and bottom boundary locations remain the same in this adaptation of the model. The spatial distributions of hydrogeologic units at the water table in the flow model under present-day conditions and in the adapted model with the higher estimated water table are shown in Figures 6-22 and 6-23, respectively.

Comparison of Figures 6-22 and 6-23 indicates potentially significant differences in the hydrogeologic units present in the SZ below the repository and along the inferred flow path to the south and east of the repository at depths corresponding to the position of the water table at the different climatic conditions. The upper volcanic confining unit is more widely distributed at the water table below the repository under estimated future glacial-transition climatic conditions than it is under present-day conditions, particularly under the northern and eastern parts of the repository. Under estimated future conditions, to the south of the repository, the alluvium unit is present at the water table over a somewhat broader area compared to present-day conditions.

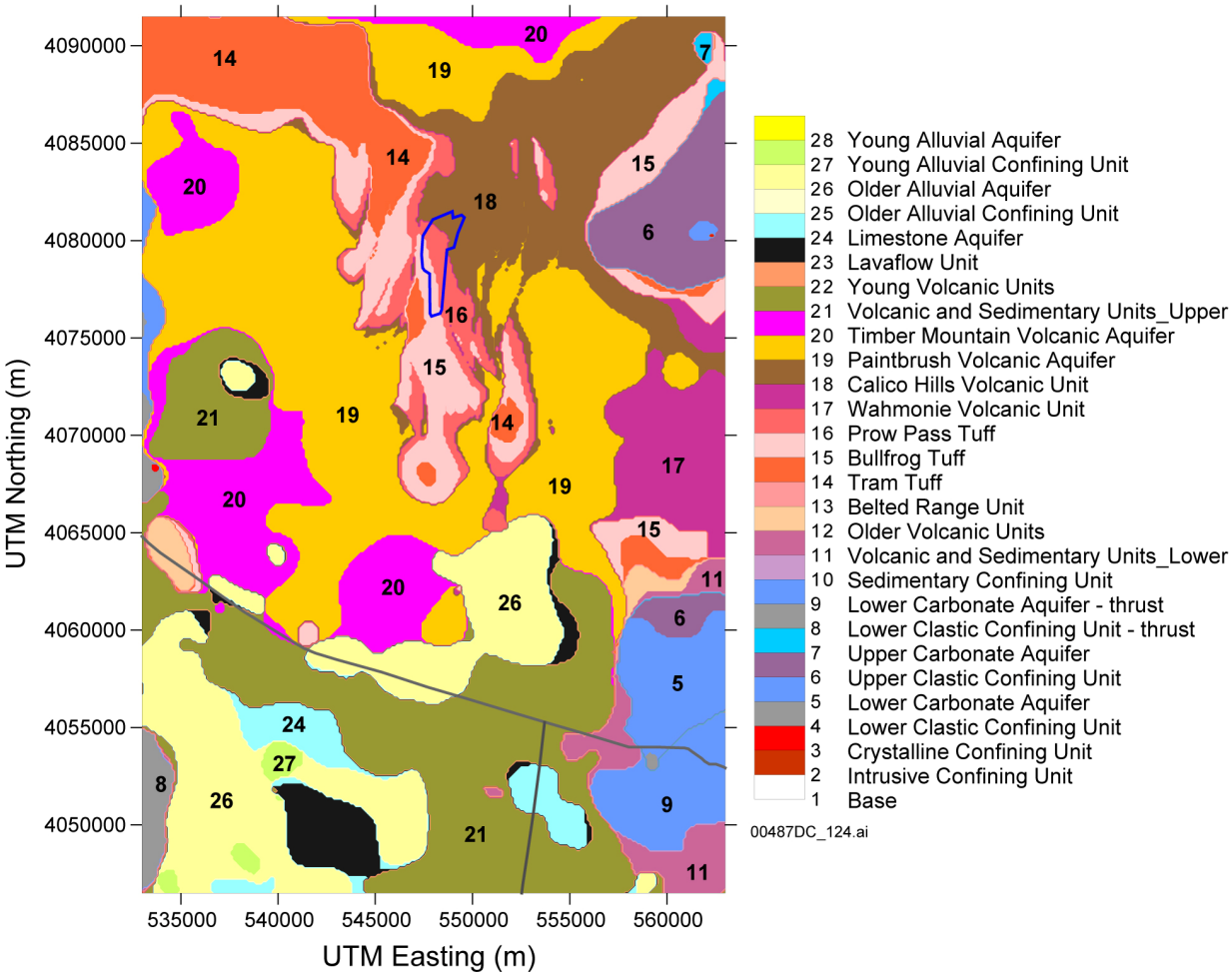

Source: SNL 2007 [DIRS 179466] (repository outline).

NOTE: Repository outline shown with a bold blue curve. For illustration purposes only.

UTM = Universal Transverse Mercator.

Figure 6-22. Hydrogeologic Framework Model Units at the Water Table for Present-Day Conditions

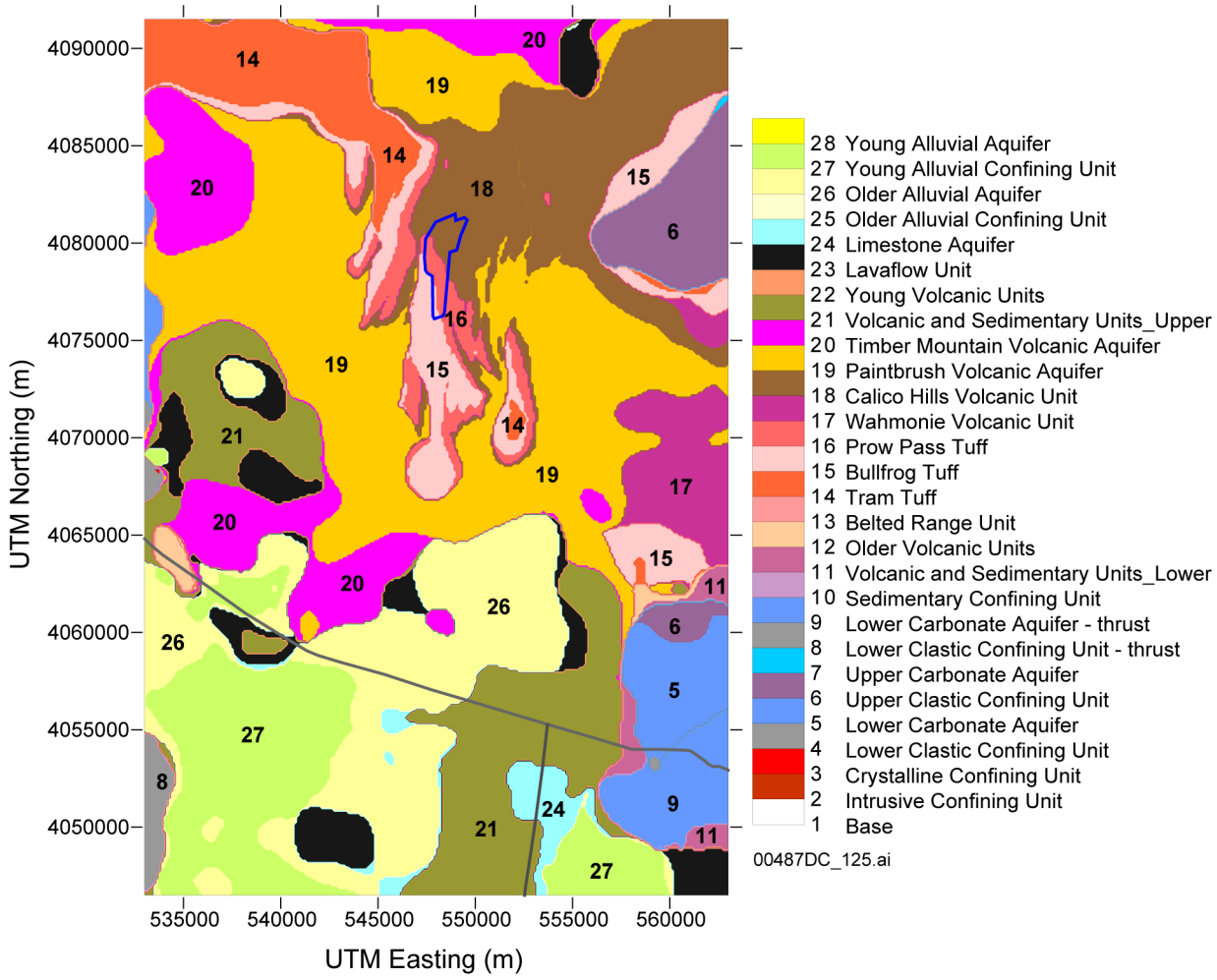

Source: SNL 2007 [DIRS 179466] (repository outline).

NOTE: Repository outline shown with a bold blue curve. For illustration purposes only.

UTM = Universal Transverse Mercator.

Figure 6-23. Hydrogeologic Framework Model Units at the Water Table for Estimated Future Glacial-Transition Climatic Conditions

Figure 6-24 illustrates the modeled potentiometric surface for the flow model using calibrated effective permeabilities subject to water-table rise. The specific discharge across the 5-km boundary was 1.26 m/yr after the water-table rise. The SZ site-scale transport simulations with the higher water table are considered in *Site-Scale Saturated Zone Transport* (SNL 2007 [DIRS 177392], Appendix E).

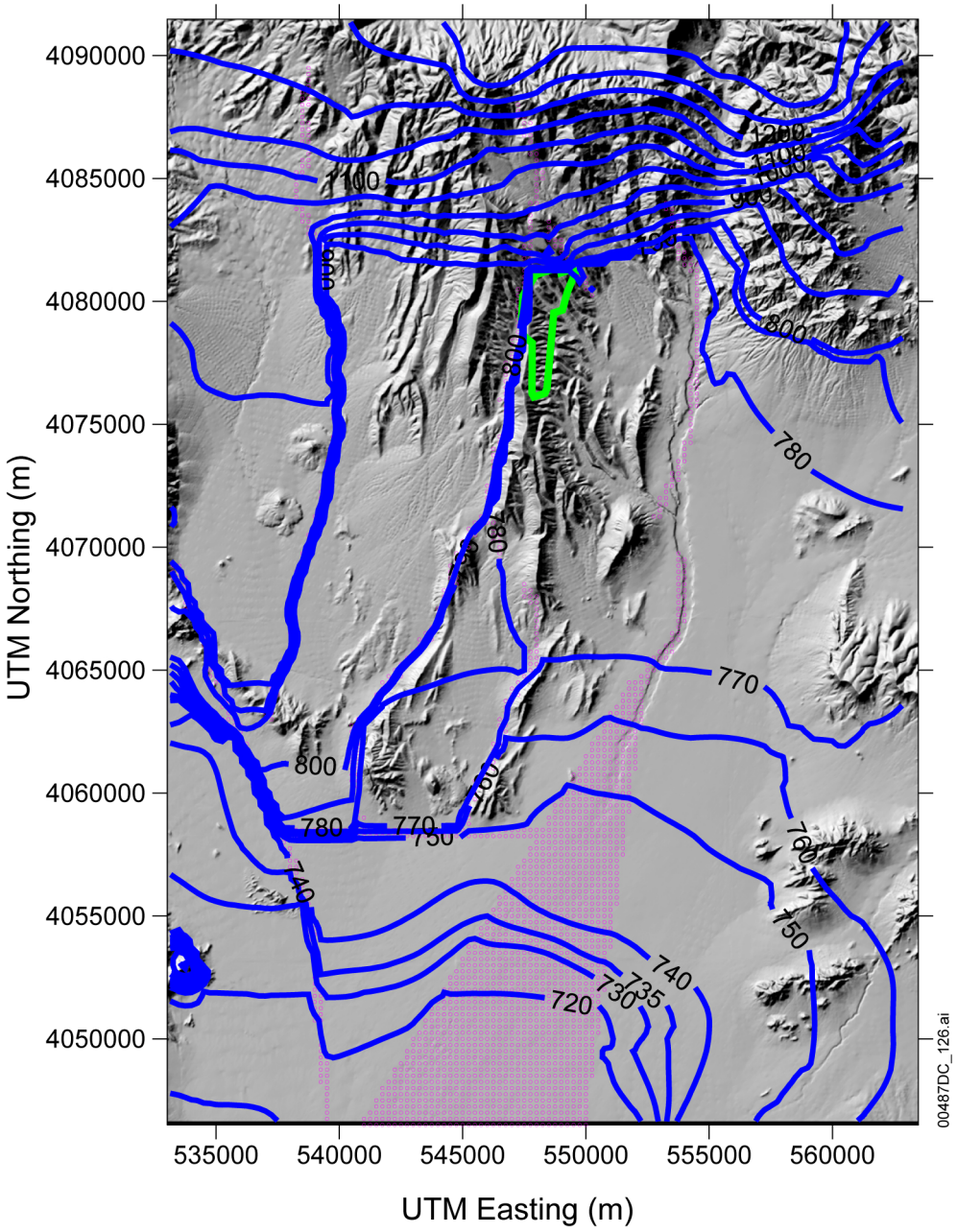

Source: SNL 2007 [DIRS 179466] (repository outline).

Output DTN: SN0702T0510106.006 (FEHM model of water-table rise).

NOTE: For illustration purposes only. The contours represent the modeled potentiometric surface. Altitude is in meters above mean sea level. Pink represents special geologic features (see Table 6-7 and Figure 6-12).

UTM = Universal Transverse Mercator.

Figure 6-24. Simulated Potentiometric Surface After a Rise in the Water-Table

6.7 UNCERTAINTY

Characterizing and understanding the flow through the saturated zone is important for assessing the overall containment strategy for safely sequestering radioactive materials at the Yucca Mountain repository. Uncertainty in flow modeling arises from a number of sources including, but not limited to, the conceptual model of the processes affecting groundwater flow, water–level measurements and simplifications of the model geometry, boundary conditions, hydrogeologic unit extent and depth, and the values of permeability assigned to hydrogeologic units. This section discusses and attempts to quantify uncertainties in the SZ site-scale flow model because all uncertainty contributes to inaccuracy in system representation and response (uncertainty in model predictions). Such uncertainty is an inescapable aspect of geologic modeling. In addition to the discussion in this section, parameter uncertainty is addressed in the model abstraction document (SNL 2007 [DIRS 177390], Section 6.5) and a thorough discussion of uncertainty analysis is given in Appendices H and I. *Saturated Zone Flow and Transport Model Abstraction* (SNL 2007 [DIRS 177390], Sections 6.5.2.1 and 6.5.2.10) includes additional quantitative analysis on horizontal anisotropy in permeability and groundwater specific discharge. *Saturated Zone In-Situ Testing* (SNL 2007 [DIRS 177394]) addresses the uncertainty related to the spatial distribution of the observation wells. Overall, it is understood that model predictions are always uncertain, thus it is important to minimize and quantify this uncertainty. It should be noted that the uses of PEST V11.1 (STN: 611582-11.1-00; [DIRS 179480]) and SPDIS (STN: 611598-00-00; [DIRS 180546]) are non-quality affecting analyses of the qualified results produced by PEST V5.5 (STN: 10289-5.5-00; [DIRS 161564]) and that they in no way change the conclusions of this report. Instead, this analysis sheds light on some of the details going on behind the scenes during the calibration process (e.g., differentiating null from solution space errors and evaluating data worth and parameter importance).

Estimating uncertainty in a modeled process is a wide ranging field of active research spanning many disciplines including hydrologic modeling, surface water flow and transport, medical imaging, geophysics, etc. A fundamental aspect of geologic modeling is the calibration phase where model parameters (in this case permeabilities) are adjusted until the model's replication of historical field measurements is judged to be "reasonably good." It is then assumed that this constitutes sufficient justification to use the model to make predictions to be used in site management. For the SZ site-scale flow model developed here, PEST ([DIRS 161564], 2006 [DIRS 178612]) was used to minimize the objective function comprising a weighted sum of squares of water-level measurements and fluxes across the lateral model boundaries (minimize the differences between measured and modeled data). Additional information was also used to hand calibrate the model, namely gradients that indicate that flowpaths emanating from below the repository should travel in a southeasterly direction. Future efforts could explicitly include soft data (e.g., local specific discharge estimates from well tests or elicitation) in the PEST calibration process.

When performing an uncertainty assessment on model results, which are solely dependent upon the parameter values supplied to the model, it is important to recognize two fundamental types of uncertainty in a model: null space and solution space uncertainties (see Appendix H). Null space uncertainty is that which arises in a calibrated model prediction due to the necessary simplifications made during model development (e.g., using a predefined HFM, applying constant BCs, representing heterogeneity with a homogenized geologic unit, single porosity

model of a dual porosity medium, etc.). It represents the differences between real world predictions and their simulated equivalents arising from the inability of model parameters to represent the innate complexity of the real world. Solution space uncertainty is contained in a model parameter that arises from the fact that its estimation through calibration is based on noisy data (including that induced by the simplification process required when constructing a hydrologic model).

Regularization theory shows how parameters employed by a calibrated model must, of necessity, be "smoothed" or "blurred" versions of real-world hydraulic properties (Appendix H). Figure 6-25 is a conceptualization of how estimated modeled parameters are "contaminated" during the modeling process. The figure reflects how model (effective) parameters are the transformation of real world parameters through the current conceptual model of the system. This transformation yields estimates for the simplified parameter field, which is required for solution of the inverse problem (model calibration). This indicates that it should not be presumed that estimated parameters always match real world parameters except in an average sense over large areas (and possibly with an averaging kernel that crosses parameter boundaries). The "resolution matrix" presented conceptually in Figure 6-25 encapsulates the details of the conceptual model development (averaging process during parameterization). The more diagonally dominant the resolution matrix, the closer the model parameters approximate the real world hydraulic properties throughout the model domain. Off-diagonal elements indicate spatial averaging or "contamination" of model parameters induced by necessary simplification and homogenization required for calibration of the model.

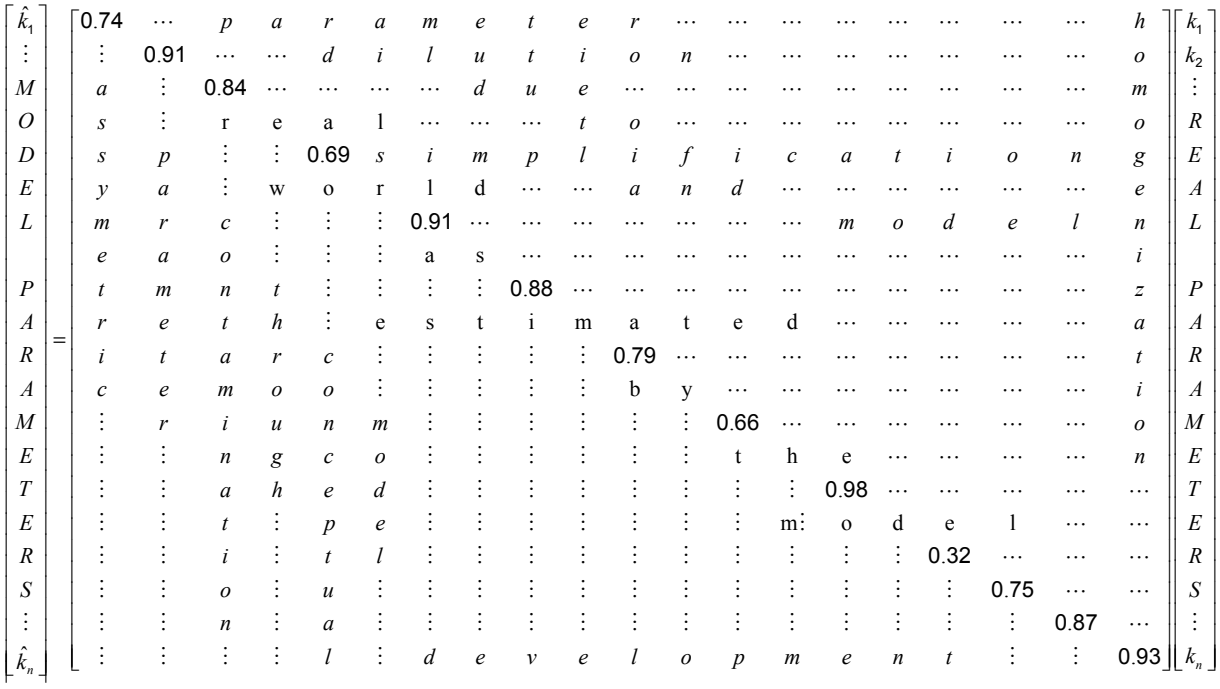

NOTES: Specifically, real-world parameters are averaged during the parameter estimation process required for model calibration. A better resolution matrix will have smaller off-diagonal elements (increased diagonal dominance) yielding model parameters that are closer approximations to the real parameters. Unfortunately, this can only occur where real-world heterogeneity is small and calibration data are ubiquitous and noise-free.

Figure 6-25. Conceptual Representation of the Resolution Matrix Illustrating How Estimated Model Parameters Are "Contaminated" During the Modeling Process

The following description distinguishes null space uncertainty from solution space uncertainty with regard to its impact on model predictions of specific discharge 5 km from the proposed repository. Despite the fact that specific discharge 5 km from the repository is only a surrogate for the flow fields passed on to TSPA, it was selected as the predictive metric for this analysis because it reflects changes in the flow field . Solution space uncertainty is a product of a noisy data set (uncertainty in calibration data) plus model imperfections (structural noise introduced through the use of effective parameters). Solution space uncertainty may be reduced through the calibration process, but null space error is irreducible given an established conceptual model and calibrating data set. Null space uncertainty can only be reduced by collecting additional data that contain information relevant to the currently inestimable combination of parameters (null space). Null space exists because we acknowledge that the model complexity (due to, for example, the constraints of HFM2006 that assign uniform permeability to an individual hydrogeologic unit) falls short of what can be uniquely estimated given the current calibration data set. That is, it is a direct consequence of the limited descriptive capacity for a data set to reproduce modeled hydraulic properties (i.e., parameters, including spatial variability) upon which a prediction depends. This is especially apparent in our inability to represent hydraulic property detail. If the model prediction depends upon this detail, this prediction is prone to increased uncertainty. Null space is the space spanning parameter set combinations that can be added to the calibrated parameter set without affecting calibration (a null space matrix is orthogonal to parameter space and thus there exist certain combinations of parameters that yield an equally calibrated model but

significantly different predicted model metrics, like specific discharge). Thus, null space uncertainty is the uncertainty in the prediction from a calibrated model due to the inability of the calibrating data set to inform those parameters that contribute to the model output metric (in this case, prediction of specific discharge). Recent advances in uncertainty assessment facilitate quantification of the null space error despite the inability to reduce it (given a specified, calibrated model and data set).

6.7.1 Uncertainty in Specific Discharge

In previous flow and transport and abstraction models of the SZ, the specific discharge was varied from one-tenth of its nominal value to ten times its nominal value in performance assessment calculations (BSC 2001 [DIRS 157132], Section 6.2.5). Based on recent calibration experience and the evaluation of permeability data from Yucca Mountain and other sites, the range was reduced to 1/8.93 times its nominal value to 8.93 times the nominal value (SNL 2007 [DIRS 177390], Section 6.5). The nominal value is obtained from a predictive run of the calibrated SZ site-scale flow model (Section 6.5). It should be noted that because the numerical model is linear, the calibration of the model can be preserved by scaling the fluxes, recharge, and permeabilities by exactly the same ratio. A new uncertainty analysis procedure is available in recent releases of the PEST software. Although PEST V11.1 is not qualified, it is still extremely useful in analyzing and describing the results from qualified codes. A general introduction and discussion of the latest techniques in uncertainty and sensitivity analyses is presented in Appendices H and I.

The PEST V11.1 (STN: 611582-11.1-00; [DIRS 179480]) PREDVAR suite of codes (Watermark Computing 2006 [DIRS 178613]) was used to analyze FEHM's predictive uncertainty for specific discharge. First, null space and solution space uncertainties are quantified. This analysis, if done a priori, can help to determine if calibrating the conceptual model to the existing dataset will significantly reduce uncertainty in the selected predictive model metric. The effect of calibrating each model parameter (or each set of parameters when considering the permeability multipliers for the altered northern region, which were lumped) in reducing uncertainty in specific discharge 5 km from the repository is presented in Figure 6-26. Red bars are normalized contributions to uncertainty (they have unit sum) in specific discharge from uncalibrated parameters and blue bars are the same contribution from calibrated parameters. This figure can be interpreted as the answer to the following question: Assuming perfect knowledge of a parameter, how do the rest contribute to reduction in uncertainty of a prediction? Specifically, the contribution of calibrating each parameter with respect to reducing uncertainty in specific discharge is illustrated. There is seemingly little value gained in reducing uncertainty in specific discharge across the 5-km boundary through the calibration process. The uncertainty for specific discharge decreased 56% after calibration. It is not surprising to see such a small reduction in predictive uncertainty for specific discharge because calibration data did not include an estimate for specific discharge. If a specific discharge measurement was explicitly included in the automatic calibration process, a greater reduction in uncertainty would be expected. In these figures, a parameter's "contribution" to uncertainty is assessed through repeating the predictive uncertainty analysis under an assumption of perfect knowledge of that parameter type and measuring the decrease in predictive error thereby incurred. That is, each parameter is sequentially assigned it calibrated value with zero error bars and the resulting impact on decreased uncertainty in a prediction is assessed. In some circumstances,

post-calibration contribution to predictive uncertainty for a parameter type can exceed its pre-calibration contribution (significant examples include CFTA, CHVU, H95Z, and WASH). This is a reflection of the fact that perfect knowledge of one parameter (zero error bars applied to an estimated parameter) may allow better estimates to be made of another parameter to which it is highly correlated. Thus, to the extent that the prediction depends on the second parameter type, the advantages of assumed perfect knowledge of the first parameter are thereby amplified. Without a detailed analysis beyond the scope of this report, it is difficult to ascertain how hand calibrations contribute to a reduction in predictive uncertainty in specific discharge. Not surprisingly, fault permeabilities dominate specific discharge uncertainty because they have first-order impacts on flow magnitudes and directions.

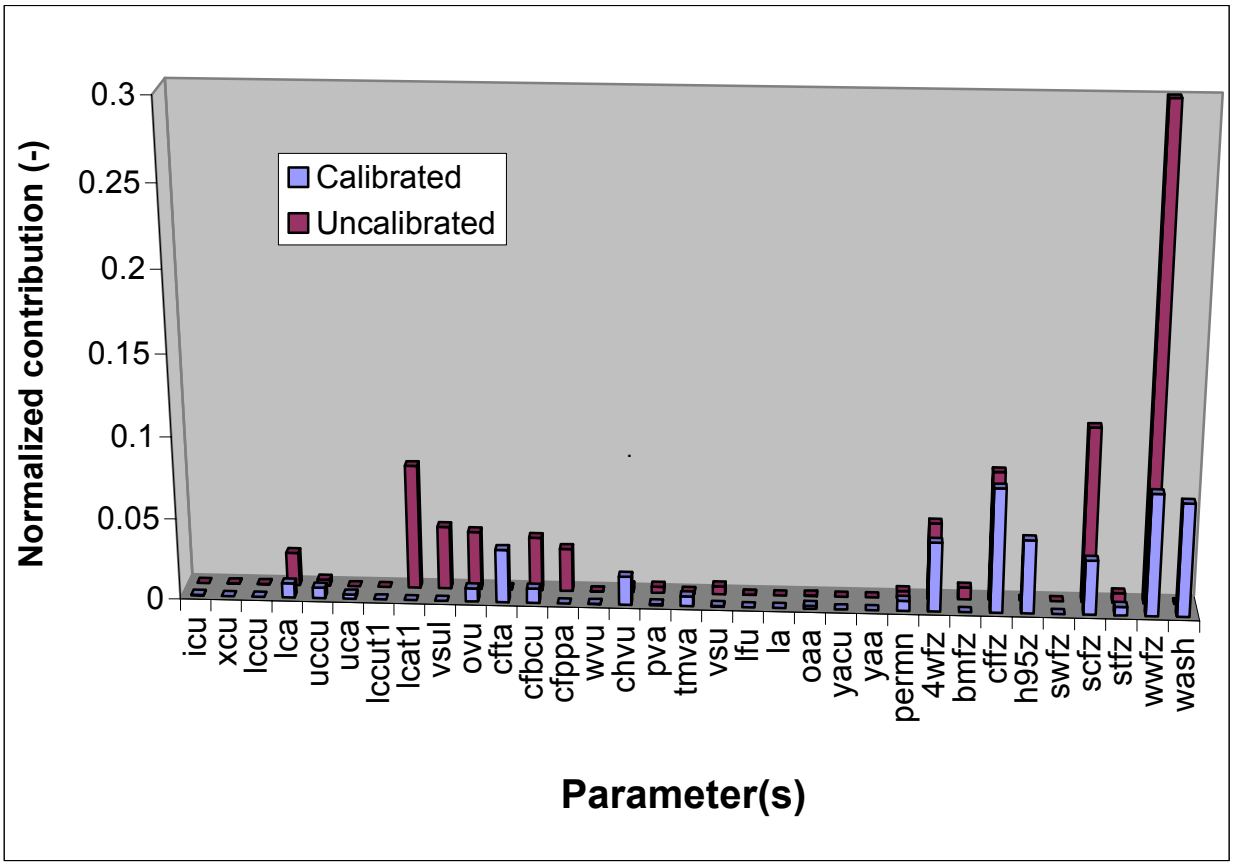

Source: Output DTN: SN0705T0510106.009.

NOTE: Parameter names are listed and defined in Table 6-9, “permn” comprises all permeability multipliers for the altered northern region and the Crater Flat zone.

Figure 6-26. Uncalibrated and Calibrated Model Parameter Impact on Normalized Uncertainty in Specific Discharge

The second sort of analysis that can be performed with PREDVAR is an analysis of the worth of existing observations or groups of observations as related to reducing model predictive uncertainty for specific discharge. This information can also be used to assess the worth of acquiring additional data, something truly valuable to site characterization decision making. In this analysis, the inclusion of a hypothetical observation of specific discharge (SPD) allowed an

analysis of its potential worth to the calibration process. Figure 6-27 shows the relative worth of groups of observations for reducing specific discharge uncertainty. Not surprisingly, observation groups NYE COUNTY, CRATER FLAT, and FLUX are important observations for reducing predictive uncertainty in specific discharge. FLUX is important because it directly impacts overall flows through the model and should therefore be important to specific discharges throughout the model domain. Head observations in the altered northern region (HIGH HEAD), along the inferred flow path (PATH), and those considered perched (PERCHED) are of lesser importance in reducing uncertainty is specific discharge.

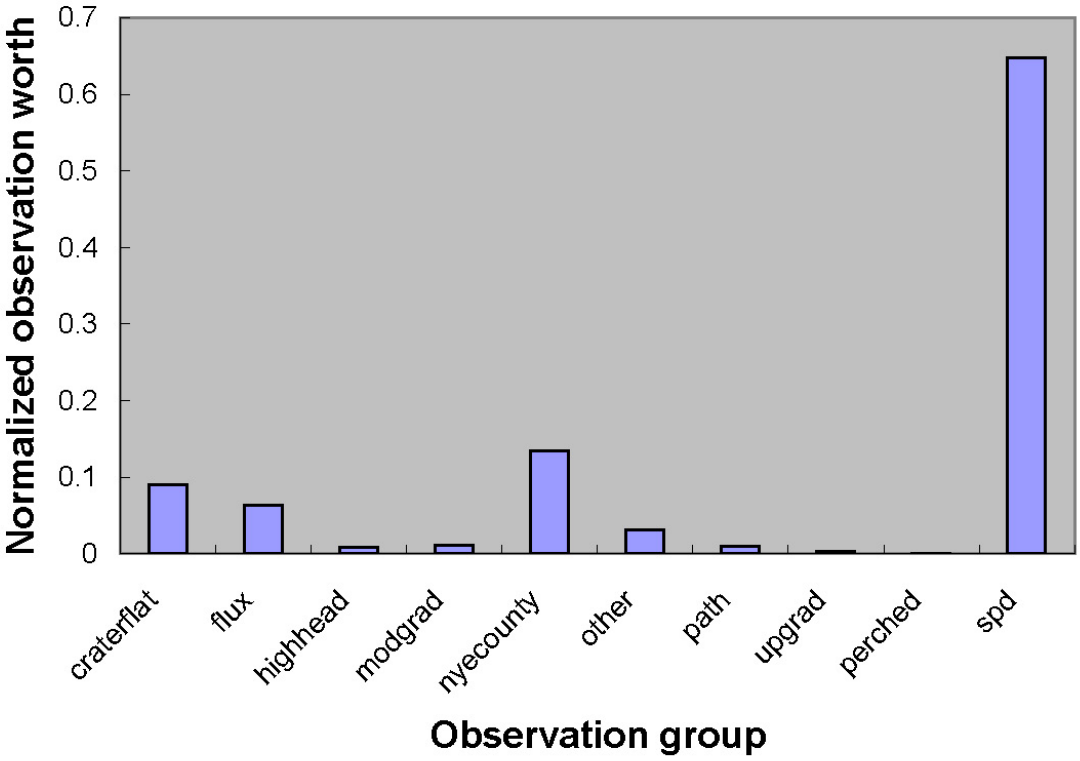

Source: Output DTN: SN0705T0510106.009.

NOTE: Observation groups are listed and defined in Table 6-9, "flux" are the boundary flux target observations and "spd" Is a hypothetical specific discharge observation that could be used in calibration.

Figure 6-27. Value of Observation Group to Reducing Uncertainty in Specific Discharge

6.7.2 Nonlinear Analysis

A methodology for nonlinear analysis of predictive error was applied to the Yucca Mountain model. Its theoretical basis is described in Appendix I. Applying the nonlinear analysis to the specific discharge prediction made by the SZ flow model yielded a maximum of 1.60 m/yr across the 5-km boundary (less than a factor of three times the maximum value of 0.66 m/yr). The nonlinear analysis is undertaken such that model calibration is maintained and only the null space is modified. By changing combinations of parameters that make no impact on the calibration objective function (weighted RMSE between modeled and measured head data and

boundary fluxes), the specific discharge was maximized to a value of 1.60 m/yr (Output DTN: SN0705T0510106.009). This indicates that even a model maintaining calibration can have significant "wiggle room" in its predictions. Note also that this maximization process was undertaken with the specific intent of seeing just how high the specific discharge could go for a nominally calibrated model. The chances for the exact combination of (null space) parameters required to make this happen in real life is low and this maximized specific discharge therefore represents a reasonable upper bound for this calibrated model. Furthermore, visualization of the flow field arising from this combination of permeabilities yielded an unrealistic scenario where flow exited the eastern boundary of the model.

6.7.3 Discussion of the Effect of Hydrogeologic Contact Uncertainty on Specific Discharge

The HFM conceptual model for the SZ site-scale flow model was created from a variety of field data and exists in electronic form as Earthvision surfaces (SNL 2007 [DIRS 174109]). There is uncertainty in the spatial positions of these surfaces primarily due to lack of data. These surfaces were used to generate the finite-element mesh such that each element is assigned those hydrogeologic properties found at the center of the element as discussed in Section 6.4.3.1. There is interest in how uncertainties in the representation of hydrogeologic-unit horizontal locations affect flux or specific discharge calculations. Due to the coarseness of the finite-element mesh, some horizontal uncertainty in the HFM can be entertained. As long as the horizontal spatial ambiguity in the location of hydrogeologic contacts is less than 125 m (one-half the grid block dimension), there is essentially zero impact on model specific discharge or flux calculations.

Because flow leaving the repository area is confined to a few of the most permeable units, the vertical dimension deserves special consideration. From the SZ site-scale flow model, it is known that the fluid leaves the repository area through the Crater Flat Tuffs and migrates to alluvial units. The flow paths in areal and vertical views are reproduced in Figure 6-17. Note that the vertical thickness of the flowing zone varies between 25 and 400 m, and the elevation changes from 400 to 700 m above sea level. From Table 6-4, the spacing in this part of the finite element mesh varies from 10 to 50 m. Consider, for example, that the uncertainty in the vertical location of a geologic contact 50 m in the portion of the model where the flow path is 400 m thick. Changing a single element's hydrogeologic designation, either to or from one unit to another could not result in a change to the average local specific discharge by more than a factor of 50/400 (13%). This is well within the overall specific discharge uncertainty range (Section 6.7.1). The vertically thin flow path south of UTM Northing coordinates 4,065,000 m (Figure 6-17) results in a greater impact from geologic uncertainty. Here the fluid flow is vertically constrained to about 25 m. If the bottom contact of the local hydrogeologic unit were to change by 10 m (the thickness of a single layer), this could result in a change to the average specific discharge in that area of up to 40%. Integrated specific discharge calculations will be affected to a lesser degree. A study of the impacts of hydrogeologic contact location uncertainty reveals:

- Sensitivity to uncertainty in the hydrogeologic contact surfaces in the horizontal directions is much less than in the vertical direction due to the averaging effect of 250-m grid block spacing

- The change in specific discharge due to the 50-m uncertainty in the vertical hydrogeologic surface can produce up to a 13% change in the local specific discharge near the repository and in the alluvial flow regions

- 10-m uncertainty in the vertical hydrogeologic surface can produce up to a 40% change in the local specific discharge in the transitional zone (south of UTM Northing 4,065,000 m).

Because of the averaging effect across elements in the integrated specific-discharge calculations (0 to 18 km), a 50% regional change in a relatively small portion of the 0- to 18-km compliance boundary affects model results only moderately. The range of uncertainty considered for specific discharge in the SZ flow and transport abstractions model is significantly greater than the uncertainty in the HFM (SNL 2007 [DIRS 174109], Section 6.4.3).

6.7.4 Site Data

In the 18-km compliance region (green line on Figure 6-17), performance assessment calculations are also strongly influenced by travel of fluid in the alluvial aquifer. Estimates of groundwater specific discharge in the SZ have been obtained from field-testing at the ATC (SNL 2007 [DIRS 177394], Section 6.4.5). The ATC is approximately located at the boundary of the accessible environment, as specified in regulations for the Yucca Mountain Project, 10 CFR 63.302 [DIRS 176544]. The location of the ATC is approximately 18 km from Yucca Mountain, and testing was performed in the alluvium aquifer. Estimates of groundwater specific discharge at the ATC range from 0.47 to 5.4 m/yr (DTN: LA0303PR831231.002 [DIRS 163561]; SNL 2007 [DIRS 177394], Table 6.5-6). From the calibrated SZ site-scale flow model, the specific discharge to the 18-km compliance boundary is 0.55 m/yr. This calculation integrates transport through all volcanic and alluvial units from introduction below the repository to the 18-km compliance boundary and its relatively low value can partially be attributed to slow flows through the volcanic units.

In addition to the information from the Expert Elicitation Panel (CRWMS M&O 1998 [DIRS 100353]) (related to specific discharge in the volcanics), other data are available for specific discharge in the alluvium (SNL 2007 [DIRS 177394], Tables 6.5-5 and 6.5-6). The measured specific discharge at the ATC spans a factor of 7.8 (i.e., 1.2 to 9.4 m/yr) while at NC-EWDP-22S the range was 11.5 (0.47 to 5.4 m/yr). There are no site data available for specific discharge in volcanic units, but the Expert Elicitation Panel (CRWMS M&O 1998 [DIRS 100353], p. 3-43) typically suggested larger ranges (approximately two orders of magnitude or more). A factor of 1/8.93 to 8.93 times the nominal value that combines volcanic and alluvial uncertainties with Bayesian updating is used as a multiplier for the specific discharge throughout the model domain in the latest performance assessment calculations (SNL 2007 [DIRS 177390], Section 6.5.2). It is worth noting that the specific discharge is variable along any given flowpath and that it can either increase or decrease locally due to flow focusing, hence significant variability and uncertainty is expected locally, but these fluctuations are smoothed when averaged over kilometer-scale portions of the model domain. For example, across the 100 flow paths in the calibrated model, the range of specific discharges spans approximately an order of magnitude across both the 5- and 18-km boundaries. Nevertheless, the overarching criterion that the range in uncertainty of specific discharge encapsulate

uncertainty within the domain (with minimal overestimation) is met by TSPA. Historical details, including figures, of the specific discharge distribution and associated sampling techniques are contained in *Saturated Zone Flow and Transport Model Abstraction* (SNL 2007 [DIRS 177390], Section 6.5.2.1) and no differentiation is made between specific discharge in the volcanics or alluvium.

6.7.5 Remaining Uncertainties in Specific Discharge Estimates

The analyses and corresponding assignment of an uncertainty range for the groundwater specific discharge assume that the porous continuum approach is appropriate for the fractured volcanic tuffs. A remaining uncertainty is whether or not the continuum approach can be employed at the scale of the model. An alternative conceptual model not yet explicitly examined is one in which most of the flow from Yucca Mountain moves through faults rather than through the unfaulted rock. To test this alternative model, the known faults need to be included explicitly in the numerical grid of the SZ site-scale flow and transport models. Although the grid-generation and flow-calculation capabilities exist to do this, the need to calibrate the model efficiently and perform particle-tracking transport simulations has taken priority and led to the adoption of structured grids that make explicit inclusion of faults difficult. Important faults are included in the model to capture their impact on flow and transport. Furthermore, the adoption of a range that includes larger specific discharge values and smaller effective porosities introduces realizations that replicate the behavior of a fault-dominated flow and transport system. Therefore, the suite of performance assessment transport simulations currently used likely encompasses the range of behavior that would be obtained with a fault-based flow and transport model.

Finally, it is noted that model linearity assures that a global, constant-multiplier increase in permeability and corresponding increase in infiltration will yield an equal increase in specific discharge throughout the model domain without impacting the head RMSE. Although the net infiltration was defined by specified data sets (Belcher 2004 [DIRS 173179]; BSC 2004 [DIRS 169861]; Savard 1998 [DIRS 102213]), model permeabilities could be globally adjusted such that flux through the southern boundary increased to match that of the regional model (discussed in Section 6.5.2.2). The resulting 23% increase in specific discharge throughout the model domain is still within the uncertainty range of the entire SZ site-scale flow model and well within the specific discharge multiplier used in TSPA (SNL 2007 [DIRS 177390]); also see Sections 6.7.1, 6.7.4, 7.2.3, and 8.3.1 of this document).

6.7.6 Effect of Perched Water on Flow Paths and Specific Discharge

Perched water was not explicitly modeled in the SZ site-scale flow model because the weights applied to these observations were insignificant (0.1). It is noted that the conceptualization of the LHG through introduction of the altered northern region yielded water levels in wells UE-25 WT#6 and USW G-2 (suspected to be perched) that were much lower than the reported water levels. From Table 6-8, it can be seen that some modeled water levels are about 150 m lower than the data in this area to the north of Yucca Mountain; but this is consistent with the perched water-level interpretation in that area (BSC 2004 [DIRS 170009], Section 5). The area of suspected perched water is near the steepest hydraulic gradient in the model and these hydraulic gradients occur over only a few model elements. Thus, if there is some specific reason

to closely model this portion of the model domain, additional discretization may be needed to quantify possible effects on local flow direction and specific discharge. Fortunately, the LHG is upgradient of the repository and as long as it is honored by the model, it only minimally affects particle flow paths and transport times. Therefore, uncertainty due to perched water on flow paths and specific discharge is not propagated forward into the saturated zone flow and transport abstraction model.

6.7.7 Representing Faults with Reduced Permeability Grid Blocks

Computational limitations (i.e., insufficient memory and/or processor speed) preclude the implementation of a finite-element model of the SZ model domain that explicitly models individual fractures and faults on a one-to-one scale. For example, if the exact location, orientation, and dimensions were known for each fracture/fault in the system, the number of elements (and computation time) required to model the system would increase by several orders of magnitude. Therefore, major faults are conceptualized in the SZ site-scale flow model as zones of enhanced/reduced permeability that simulate inhibited/preferential flow in faults with grid blocks that are nominally 250×250 m^2 in the horizontal directions. Fault properties are necessarily volume-averaged throughout an element. On the one hand, representing faults with 250×250 m^2 elements certainly accounts for the uncertainties in their geographic location. Discussion of the observed relationship between the aquifer test and faults is provided in *Saturated Zone In-Situ Testing* (SNL 2007 [DIRS 177394], Section 6.2.4 and Appendix C7). On the other hand, the hydrogeologic properties are "smeared" across a relatively large area, precluding the use of some fault-specific site data in the calibration targets.

Volume-averaged representations of faults are commonly used in numerical modeling. Furthermore, because element permeability values are calibrated to field observations that are several grid blocks away from faults, it is believed that the large-grid-block representation is adequate for the purpose of flow modeling "away" from the fault. While the precise flow regime within the fault may not be representative, overall flow through the system, particularly at the model boundaries, is not significantly affected by the volume-averaged approach because fault volumes are such small fractions of the model volume (average of ~0.4% each).

6.7.8 Scaling Issues

Scaling issues are some of the most complex hydrology modeling problems to overcome, and it is an active field of contemporary research in geohydrology (Neuman 1990 [DIRS 101464]; Harter and Hopmans 2004 [DIRS 178488]). Although there are many approaches that address the effects of scaling on model results, none has been widely accepted as the best method. Transport models are particularly sensitive to scaling issues in both space and time. For example, distribution coefficients measured on the order of hours to months in the laboratory for a performance assessment model are dubiously applied to contaminant transport over millennia. However, flow modeling is much less sensitive to scaling issues in both space and time. First, time scales are relatively unimportant because hydrogeologic properties change little over the course of millennia. While water-level data and infiltration rates may change over such long time periods, any flow model can easily account for these changes given appropriate boundary conditions. Second, while hydrogeologic properties measured through borehole pumping tests may not be appropriate to apply at distances far from the sample site (distance scaling), the SZ

site-scale flow model described here does not use these measured properties directly. Instead, they are used to aid and validate calibration. Therefore, although it may be inappropriate to assign geologic properties based on distant measurements, the calibration techniques used in this SZ site-scale flow model moderate the negative impact of such scaling issues.

6.7.9 Flowpath Uncertainty

There are several metrics that could be used to evaluate uncertainty in specific discharge, but to be consistent with specific discharge calculations, the flowpath lengths from release below the repository to the 5- and 18-km boundaries are examined. It should be noted that the random distribution of intial particle positions below the repository can significantly impact particle length, if for no other reason than particles are distributed over a 5-km distance in the north-south direction. Flowpaths are notably affected by the N−S:E−W horizontal anisotropy applied to the volcanic units in the anisotropic zone (Figure 6-12). Average flowpath length across the 5-km boundary for 5:1 N−S:E−W horizontal anisotropy is 6.0 km (range of 3.1 to 8.6 km). The flowpath length across the 18-km boundary ranges from 19.4 to 25.4 km, with an average of 22.9 km. Average pathlengths across the 5-km boundary for 20:1 and 0.05:1 N−S:E−W anisotropies are 9.6 and 6.2 km, respectively. Correspondingly, they are 29.7 and 22.8 km across the 18-km boundary. For the isotropic case, average flowpath lengths are 6.0 and 23.2 km across the 5- and 18-km boundaries, respectively.

6.8 DESCRIPTION OF BARRIER CAPABILITY

This model report is a compilation of information and processes affecting flow in the SZ around Yucca Mountain. As such, it provides a description of the SZ barrier flow component. The two main features of the barrier described here are: (1) the specific discharge, which affects the transport time of the radionuclides that may be released at the water table below the repository horizon and travel to the accessible environment; and (2) the flow paths that will affect the travel length and, therefore, transport times.

The result for specific discharge ranges from 0.1 to 0.66 m/yr across the 5-km boundary. The average particle flow path starting at the repository footprint at the water table is likely to remain near the water table, traveling southeast as it leaves the repository area and follow Fortymile Wash, where it traverses primarily alluvial material. Transport times are expected in the range of a few thousands of years (SNL 2007 [DIRS 177392], Section 6.5).

Uncertainty affects permeability ranges and flow paths. These parameters, in conjunction with the head gradient, comprise the components of the specific discharge calculations. The flowpaths proved to be fairly insensitive to changes to the conceptual model provided the moderate and small gradient observations were adequately represented. No single change in permeability caused a corresponding (linear) change in specific discharge because of the constraints imposed by neighboring units.

The SZ flow model is used in the site-scale SZ transport model report (SNL 2007 [DIRS 177392]) to generate both concentrations-versus-time and concentrations-versus-distance curves that are needed to demonstrate the capabilities of the saturated zone as a transport barrier.

INTENTIONALLY LEFT BLANK

7. VALIDATION

Model validation is the process of testing the appropriateness of the conceptual, mathematical, and numeric representation of the system being modeled. The SZ site-scale flow model is designed to provide an analysis tool that facilitates understanding of flow in the aquifer beneath and downgradient from the repository. The flow model is also a computational tool to provide the flow fields for performing radionuclide migration predictions in the saturated zone. For these predictions to be credible, the SZ site-scale flow model must be validated for its intended use. This statement means that there is established confidence that a mathematical model and its underlying conceptual model adequately represents with sufficient accuracy the phenomenon, process, or system in question. Based on the material presented in these sections, this requirement is considered satisfied.

The validation criteria and confidence building activities during development are discussed in Section 7.1; the validation results are discussed in Section 7.2; and the summary of the validation effort is presented in Section 7.3.

The data used in validation activities are discussed in the following sections and are summarized below:

- Observed hydraulic heads and gradients not used for model development and calibration. This includes NC-EWDP Phase V potentiometric data not available when model calibration was conducted (DTN: MO0612NYE07122.370 [DIRS 179337]).
- Hydraulic parameters derived from hydraulic testing at the C-wells, Alluvial Testing Complex, and single-well testing at other wells (SNL 2007 [DIRS 177394]).
- Flowpaths derived from hydrochemistry and isotope analyses (Appendices A and B).

7.1 VALIDATION CRITERIA

The model validation approach for the SZ site-scale flow model is presented in *Technical Work Plan for Saturated Zone Flow and Transport Modeling* (BSC 2006 [DIRS 177375], Section 2.2.2), which states that the SZ site-scale flow model requires Level II validation. The validation plan was developed under the BSC procedures in effect at the time. The BSC Level II validation is equivalent to Level I validation as described in SCI-PRO-002. Nevertheless, the site-scale SZ flow model was validated to Level II requirements. The Level II validation includes the six steps of confidence building during model development as described in SCI-PRO-002 and at least two post-development activities as described in SCI-PRO-006, Section 6.3.2. To satisfy the model validation requirements, the following four post-development validation activities (BSC 2006 [DIRS 177375], Section 2.2.2.1) were performed (comparisons of site data to):

- Predicted hydraulic heads and the observed potentiometric map. New water-level data are compared to modeled water-level data. Validation will be considered acceptable if the absolute value of the difference between simulated and observed hydraulic heads are within 10 m (the minimum model layer thickness).

- Predicted flow paths and those derived from the hydrochemistry and isotope analysis. This method involves the model simulation of flow paths. Validation is considered acceptable if the flow paths simulated by the model are bounded by those inferred from hydrochemical and isotope analyses.

- Calibrated hydraulic parameters and those derived from hydraulic testing at the C-wells, the ATC, the NC-EWDP-22 site, and single-well testing at other wells. If this comparison is used, validation will be considered acceptable if the absolute value of the difference between calibrated permeabilities and those derived from hydraulic testing and laboratory measurement is less than or equal to 50% of the field and laboratory derived hydraulic conductivity (permeability) from material along the flow path from the water table directly beneath the repository to the compliance boundary. For the implementation of this work activity, it should be clarified that the acceptance criterion used herein is model-calibrated permeabilities must be within a factor of 2 (i.e., between 1/2 and 2) of the 95% confidence interval on the field-test-derived mean permeabilities. This method is also relevant to model simulation of specific discharge because specific discharge is directly proportional to hydraulic conductivity (permeability).

- Predicted specific discharge and the conclusions of the Expert Elicitation Panel (CRWMS M&O 1998 [DIRS 100353]). Model validation is acceptable if the modeled output of specific discharge is within the range provided by expert elicitation.

These validation activities and acceptance criteria reflect the essential functions of the SZ system with regard to the transport time and radionuclide mass delivery to the accessible environment. The results of these post-development validations are discussed in Section 7.2.

7.1.1 Confidence Building During Model Development to Establish Scientific Basis and Accuracy for Intended Use

For Level II validation, the development of the model should be documented in accordance with the requirements of Section 6.3.1 (C and D) of SCI-PRO-006. The development of the SZ site-scale flow model was conducted according to the following criteria (italicized). The paragraphs following each criterion describe how it was satisfied.

1. *Evaluate and select input parameters and/or data that are adequate for the model's intended use to be consistent with* SCI-PRO-002 [Attachment 3 Level I (1)].

   The inputs to the SZ site-scale flow model have all been obtained from controlled sources (see Table 4-1). The input parameter and data used to develop and calibrate the SZ site-scale flow model are adequate for the intended use of providing TSPA with flow fields necessary to predict radionuclide transport in the saturated zone below the repository to the accessible environment.

2. *Formulate defensible assumptions and simplifications that are adequate for the model's intended use to be consistent with* SCI-PRO-002 [Attachment 3 Level I (2)].

Discussion of assumptions and simplifications are provided in Sections 5 and 6.3. The conceptual model of flow in the saturated zone and the components of the model are discussed in Section 6.3. As discussed in detail in Section 7, further confidence building in sub-model components of the SZ site-scale flow model was conducted through comparison of the conceptual model of SZ flow with the results of field tests conducted at the C-wells complex and at the ATC. The following observations were made from testing at both the C-wells and the ATC regarding the two assumptions:

- Testing at the ATC indicated that a homogeneous, confined-aquifer analytical solution provided a good match to drawdown data; and,

- Testing at the C-wells indicated that the volcanic tuffs are a fracture-dominated system (SNL 2007 [DIRS 177394], Section 6.5).

Long-term testing at the C-wells yielded responses that could be fitted with effective-continuum physical equations and homogeneous hydrologic properties. These tests support the concept that the saturated zone can be modeled as an effective continuum with homogeneous properties. Thus, this criterion is considered satisfied.

3. *Ensure consistency with physical principles, such as conservation of mass, energy, and momentum, to an appropriate degree commensurate with the model's intended use to be consistent with* SCI-PRO-002 [Attachment 3, Level I (3)].

   Consistency with physical principles is demonstrated by the conceptual and mathematical formulations in Sections 6.3 and 6.5 through selection and use of the flow and transport simulator, FEHM (STN: 10086-2.24-02 [DIRS 179539]) in Section 3. The governing equations for non-isothermal flow implemented in FEHM are based on conservation of mass and energy and Darcy's law. As discussed in detail in Section 7.2, further confidence building in the SZ site-scale flow model was conducted through comparisons to field tests conducted at the C-wells complex and the ATC (SNL 2007 [DIRS 177394], Section 6.5).

4. *Represent important future state (aleatoric), parameter (epistemic), and alternative model uncertainties to an appropriate degree commensurate with the model's intended use to be consistent with* SCI-PRO-002 [Attachment 3, Level I (4)].

   The SZ site-scale flow model is a steady-state model that does not require temporal conditions (initial and future conditions). The model incorporates parameter and alternative models uncertainties. The range of uncertainties is used in the modeling abstraction feeding the TSPA predictions.

5. *Ensure simulation conditions have been designed to span the range of intended use and avoid inconsistent outputs or that those inconsistencies can be adequately explained and demonstrated to have little impact on results to be consistent with* SCI-PRO-002 [Attachment 3, Level I (5)].

The SZ site-scale flow model uses the water-level potentiometric surface (Appendix E) to derive constant-head boundary conditions. The model was calibrated to 161 hydraulic head measurements. Recharge and lateral boundary flux targets were developed from the DVRFS flow model (Belcher 2004 [DIRS 173179]), the UZ flow model (BSC 2004 [DIRS 169861]), and infiltration data through Fortymile Wash (Savard 1998 [DIRS 102213], Section 6.3) Initial conditions were not required for the steady state model. Sections 6.6 and 6.7 provide detailed discussion of various model results.

6. *Ensure that model predictions (performance parameters) adequately represent the range of possible outcomes, consistent with important uncertainties and modeling assumptions, conceptualizations, and implementation. to be consistent with* SCI-PRO-002 [Attachment 3 Level I (6)].

   A discussion of model uncertainties is provided in Section 8.3. Sensitivity of the output to some of the uncertain input parameters is discussed in Sections 8.3.1 through 8.3.2.

7.1.2 Hydraulic Gradient Comparison to Build Model Confidence During Development

To build confidence in the SZ site-scale flow model, a comparison between field data and the model simulations of the hydraulic gradients along the flowpaths from the repository has been performed using water-level data employed as calibration targets. The water-level data from a series of seven wells (Figure 7-1a) extending from the immediate area of the repository (USW H-6) to NC-EWDP-32P are presented in Figure 7-1b. The wells used in gradient calculations were selected because they were on or close to the simulated flowpath and they traverse the Solitario Canyon Fault. The simulated and observed hydraulic gradients for non-validation wells are presented in Table 7-1. The differences in observed and simulated water levels between wells USW H-6 and USW-25 WT-2 are due to the manner in which the model accounts for the effect of the splay of the Solitario Canyon Fault, which lies in the general area of these wells. However, while the model does not accurately simulate the precise location for the drop in head across the fault, largely because of the 250-m grid blocks, the overall hydraulic gradient simulated between USW H-6 and USW-25 WT-2 agrees reasonably well with the measured value (within 14%). For the segments between USW-25 WT-2 and NC-EWDP-22PC/24PB, where the simulated hydraulic gradients differs from the observed gradients by 50 to 152% , however, in absolute terms the differences between the observed and simulated hydraulic gradients is quite close to zero. Consider that the water table is extremely flat in that area and the accuracy of land surface altitude is 0.1 m (BSC 2004 [DIRS 170009]). The relatively large error (58%) for the segment between the new wells NC-EWDP-22PC/24PB to NC-EWDP-19P/2D is again due to the rapid water-level change near U.S. Highway 95 fault, which is not precisely reproduced in the model. Nevertheless, measured and modeled gradients are sufficiently close to lend credibility to and build confidence in the model results.

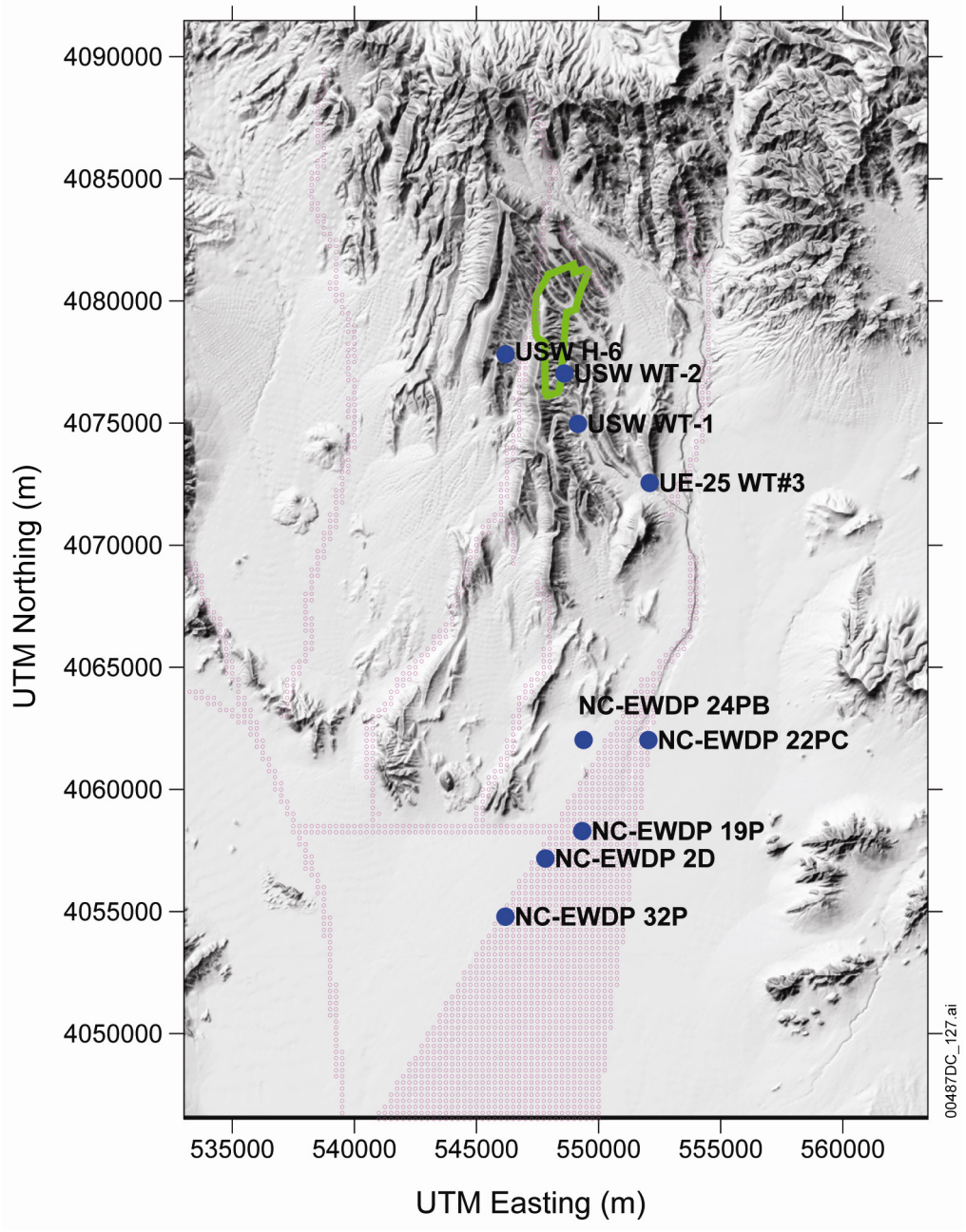

NOTE: Pink represents special geologic features (see Table 6-7 and Figure 6-12).

Figure 7-1a. Location of wells for Measured and Simulated Head Along Flowpath

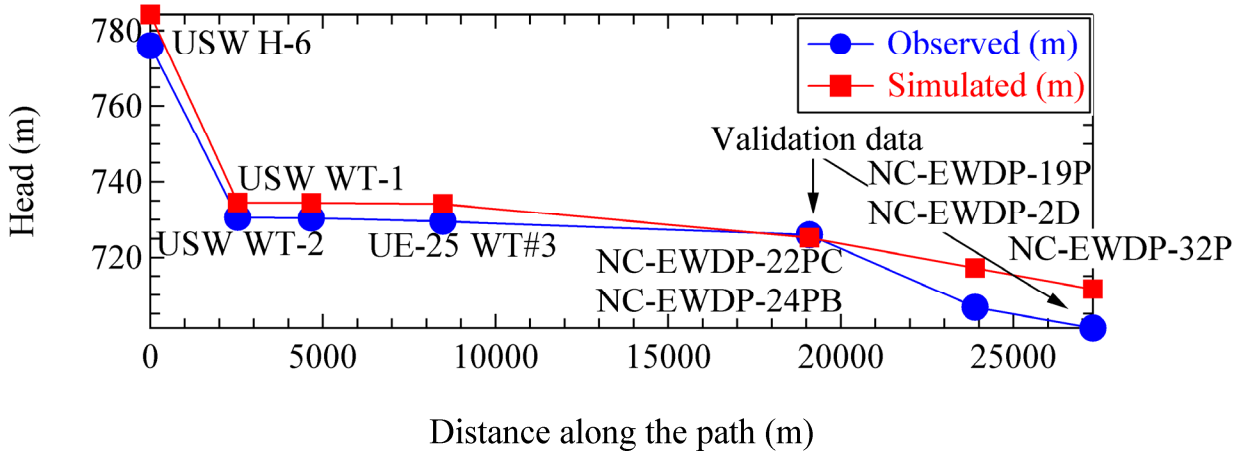

Sources: DTN: GS010908312332.002 [DIRS 163555] (non-NC-EWDP wells); SNL 2007 [DIRS 179466] (repository outline).

Output DTNs: SN0612T0510106.004 (modeled heads); SN0702T0510106.007 (NC-EWDP aggregated Phase III, IV, and V well data).

NOTE: Calculations are from data in Table 7-2. For illustration purposes only.

UTM = Universal Transverse Mercator.

Figure 7-1b. Measured and Simulated Head Along Flowpath

Table 7-1. Predicted and Observed Hydraulic Gradient for Identified Wells Used for Confidence Building During Development

Flow Segment	$\Delta H/\Delta L$ (Measured)	$\Delta H/\Delta L$ (Simulated)	Relative Error
USW H-6 to USW-25 WT-2	1.79×10^{-2}	2.04×10^{-2}	0.14
USW-25 WT-2 to USW-25 WT-1	9.37×10^{-5}	4.68×10^{-5}	−0.50
USW-25 WT-1 to UE-25 WT#3	2.10×10^{-4}	7.89×10^{-5}	−0.63
UE-25 WT#3 to NC-EWDP-22PC/24PB	3.37×10^{-4}	8.48×10^{-4}	1.52
NC-EWDP-22PC/24PB to NC-EWDP-19P/2D	4.03×10^{-3}	1.69×10^{-3}	−0.58
NC-EWDP-19P/2D to NC-EWDP-32P	1.59×10^{-3}	1.62×10^{-3}	0.02

Source: DTN: GS010908312332.002 [DIRS 163555] (non-NC-EWDP wells).

Output DTNs: SN0612T0510106.004 (modeled heads); SN0702T0510106.007 (NC-EWDP aggregated Phase III, IV, and V well data).

NOTES: Calculations are from data in Table 7-2.
NC-EWDP-22PC/24PB uses the average location and head values for wells NC-EWDP-22PC and NC-EWDP-24PB.
NC-EWDP-19P/2D uses the average location and head values for wells NC-EWDP-19P and NC-EWDP-2D.

7.1.3 Confidence Building After Model Development to Support the Scientific Basis of the Model

Model validation requires that mathematical models be validated by one or more of several methods given in Section 6.3.2 (1st and 9th bullets) of SCI-PRO-006. Validation of the SZ site-scale flow model as related to the procedural requirements mandates the following:

1. SCI-PRO-006, Section 6.3.2 (1st bullet): Corroboration of model results with the laboratory, field experiments, analog studies, or other relevant observations, not previously used to develop or calibrate the model.

   The SZ site-scale flow model was validated by comparing results from this model with the laboratory and field experiment and other observations. The validation criteria, testing, and results are described in detail in Section 7.2 of this report. Based on material presented in these sections, this criterion is considered satisfied.

2. SCI-PRO-006, Section 6.3.2 (9th bullet): Technical review through publication in a refereed professional journal. Although this is not required by the TWP, this post-development model validation activity adds to the confidence in the SZ site-scale flow model.

   A previous version of the SZ site-scale flow model and its results are described in the referenced professional publications by Eddebbarh et al. (2003 [DIRS 163577]) and Zyvoloski et al. (2003 [DIRS 163341]). These publications demonstrate additional confidence in the model, when taken in conjunction with the model validation activity described in Item 1 above because the same modeling techniques were used in this report. Moreover, this revision is based on an improved and updated HFM with more accurate fault locations, has more that four times as many grid nodes, and calibration yielded a lower residual (weighted RMSE).

7.2 VALIDATION RESULTS

The validation activities for the SZ site-scale flow model are carried out according to *Technical Work Plan for Saturated Zone Flow and Transport Modeling* (SNL 2007 [DIRS 177375], Section 2.2), which requires Level II model validation of the SZ site-scale flow model based on its relative importance to the performance assessment for the repository. The TWP states that the validation will include confidence building activities implemented during model development. In addition, it states that post-development model validation will consist of a comparison of simulated flowpaths to those derived from hydrochemistry and isotope analyses, plus two or more other comparisons as indicated in the technical work plan.

Water levels and gradients. For purposes of postdevelopment model validation, a comparison of simulated and observed water levels for all new water-level data is presented in Section 7.2.1. This comparison focuses on the NC-EWDP Phase V water-level data (DTN: MO0612NYE07122.370 [DIRS 179337]). A comparison of simulated and observed gradients along the flowpath from the repository is also presented to evaluate the impact of the difference between observed and simulated water levels on the estimates of specific discharge. Specific discharge is directly proportional to the hydraulic gradient. As previously established in

the TWP (BSC 2006 [DIRS 177375], Section 2.2.2), validation is considered acceptable if the differences between simulated and observed hydraulic gradients are not greater than 50% along the flowpath from the water table directly beneath the repository to the compliance boundary (differences may be greater than 50% away from this flowpath).

Specific discharges and permeabilities. The comparison of specific discharges based on calibrated hydraulic parameters (permeabilities) and those derived from hydraulic testing is presented in Section 7.2.2. This section summarizes data from Yucca Mountain and nearby areas available for determining the permeabilities of the hydrogeologic units represented in the SZ site-scale flow model and provides 95% confidences on the means. As discussed in Section 6.7.2 and Appendices H and I, calibrated values of the effective parameters should not be expected to be equivalent to real-world parameters because of the model's inability to represent the innate complexity of the system (heterogeneity). Therefore, the 50% difference between observed and calibrated permeabilities is applied to the range spanned by 95% confidence interval on the mean observed permeability. A factor of 3 (and ⅓) times the specific discharge is allowed between the highest and lowest limits of the range provided by site data and the Expert Elicitation Panel.

New permeability measurements are available from the ATC (SNL 2007 [DIRS 177394], Section 6.4) and are suitable for postdevelopment model validation. The measurements were taken along the flowpath from the repository. Section 7.2.2 compares these measurements with calibrated permeabilities. In addition, because new water-level data and permeability measurements are available at the ATC, simulated and observed values of hydraulic gradient and permeability at this location are used to calculate specific discharge. These calculated values are compared to the model-simulated specific discharge for the test location for purposes of post-development model validation. Furthermore, the ATC tracer tests also independently provide estimates of specific discharge from groundwater flow velocity for a range of flowing porosities (DTN: LA0303PR831231.002 [DIRS 163561]; SNL 2007 [DIRS 177394], Section 6.4); a comparison also was made between these estimates and model results. As established in the TWP (BSC 2006 [DIRS 177375], Section 2.2), validation is considered acceptable if the differences between measured specific discharge values are within the factor of 3 of those from the model.

Flowpaths. The comparison of the simulated flow pathways with those derived from the hydrochemistry and isotope analyses is presented in Section 7.2.4. The hydrochemistry and isotope analyses were not used during model development and calibration and, consequently, are suitable for post-development model validation. The flow-path comparison is considered acceptable if the flowpaths simulated by the model are bounded by those flowpaths inferred from hydrochemical and isotope analyses (Appendices A and B).

7.2.1 Comparison of Observed and Predicted Nye County Water Levels

Because well USW SD-6 received special consideration in *Water-Level Data Analysis for the Saturated Zone Site-Scale Flow and Transport Model* (BSC 2004 [DIRS 170009], Section 6.3.3) and was not used as a calibration target or in the construction of the potentiometric surface (Appendix E), it was selected for use in validation. Moreover, a qualified source of the well's

open interval was not available. *Water-Level Data Analysis for the Saturated Zone Site-Scale Flow and Transport Model* (BSC 2004 [DIRS 170009]) describes the use of this well as follows:

> The water-level information for Borehole USW SD-6 is provided in two DTNs: GS000808312312.007 [DIRS 155270] and GS001208312312.009 [DIRS 171433]. The three water-level elevations in those two DTNs range from 731.10 to 731.70 m. A water level of 731.2 m was used as part of model validation in the calibration of the SZ site-scale flow model (BSC 2001 [DIRS 155974], pp. 48 to 51). This is a more direct use of Borehole USW SD-6 water-level data than is the incorporation of this information into the potentiometric-surface map (Figure 6-1). An argument presented by Williams (2003 [DIRS 170977]) is that the SD-6 data would not have changed the potentiometric-surface map. This can be seen by observing the location of USW SD-6 on Figure 1-2 and noting that the contours on Figure 6-1 would not have changed with the addition of the new wells. The exclusion of Borehole USW SD-6 is justified on the basis of no impact.

Output from the SZ site-scale flow model, 734.8 m, over-predicts (by less than 4 m) the measured value of 731.2 m. USW SD-6 was located at UTM coordinates (547,577 m; 4,077,546 m) from DTN: GS010208312322.001 [DIRS 162908].

Since the calibration of the SZ site-scale model, water-level data for five additional wells have been posted as part of the NC-EWDP. These additions include wells installed at new locations and wells completed near existing locations. Comparison of the water levels observed in the new NC-EWDP wells with water levels simulated by the SZ site-scale flow model at these new locations provides an opportunity to validate the model. In addition, these new NC-EWDP wells can be used when comparing the measured and simulated hydraulic gradients along the flowpath from the repository. This comparison can be used to validate the SZ site-scale model quantitatively.

The SZ site-scale model was calibrated using 161 water-level and head measurements from 132 wells within the model domain, as described in Sections 6.5.1.2 and 6.5.1.3. Fifty-six of these measurements were from wells drilled and completed as part of the NC-EWDP. Measured and simulated heads for the five new Phase V wells to be used in the validation, along with their coordinates, are shown in Table 7-2.

Examination of the residuals reported in Table 7-2 indicates that the errors in simulated water levels depend on their location within the model domain. Figure 7-2 shows that NC-EWDP-32P, with the largest residual of 9.9 m, is located in an area of rapid water-level changes, along the U.S. Highway 95 fault, and the model is not able to fully replicate the steep head gradients observed in this area. Wells NC-EWDP-22PC and -24PB located north of U.S. Highway 95 near Fortymile Wash show small residuals of −0.4 and −1.3 m, respectively. Similar residual errors were observed using the water-level data available during model calibration. NC-EWDP-33P located just south of U.S. Highway 95 and west of Fortymile Wash shows good agreement with a residual of −4.8 m. Finally, NC-EWDP-13P located on the eastern edge of Crater Flats near Windy Wash fault in a region of high water levels also shows a low residual of −4.4 m. Overall, the observed residuals tend to improve for wells located further to the north and east in the

vicinity of Fortymile Wash where wells are in the simulated flowpath from the repository. Thus, these additional water-level data confirm the SZ site-scale model's capability to simulate water levels accurately in this portion of the flowpath from the repository.

Table 7-2. Wells Used in Validation of the Saturated Zone Site-Scale Flow Model with Observed and Predicted Water Levels

Well ID	Easting (UTM) (m)	Northing (UTM) (m)	*z* (elevation) (m)	Observed Head (m)	Modeled Head (m)	Residual Error (m)
NC-EWDP Phase V wells used for validation						
NC-EWDP-13P	543471	4066433	758.9	764.4	760.0	–4.4
NC-EWDP-22PC upper	552036	4062019	702.3	724.9	724.5	–0.4
NC-EWDP-24PB	549387	4062025	621.6	727.2	725.9	−1.3
NC-EWDP-32P upper	546183	4054789	696.4	701.7	711.6	9.9
NC-EWDP-33P upper	545117	4057146	713.1	720.8	716.1	–4.8
Non-NC-EWDP wells used in gradient calculations						
USW H-6 upper	546188	4077816	662.9	776.0	786.2	10.6
USW WT-2	548595	4077028	702.0	730.6	734.6	4.0
USW WT-1	549152	4074967	708.4	730.4	734.5	4.1
UE-25 WT#3	552090	4072550	705.8	729.6	734.2	4.6
NC-EWDP calibration wells used in gradient calculations						
NC-EWDP-19P	549329	4058292	694.7	707.3	717.7	10.4
NC-EWDP-2D	547823	4057170	507.1	706.1	716.6	10.5

Source: DTN: GS010908312332.002 [DIRS 163555] (non-NC-EWDP wells).

Output DTNs: SN0612T0510106.004 (modeled heads); SN0702T0510106.007 (NC-EWDP aggregated Phase III, IV, and V well data).

NOTE: Datum is mean sea level. *z* (elevation) is at the center of the screened interval.

UTM = Universal Transverse Mercator.

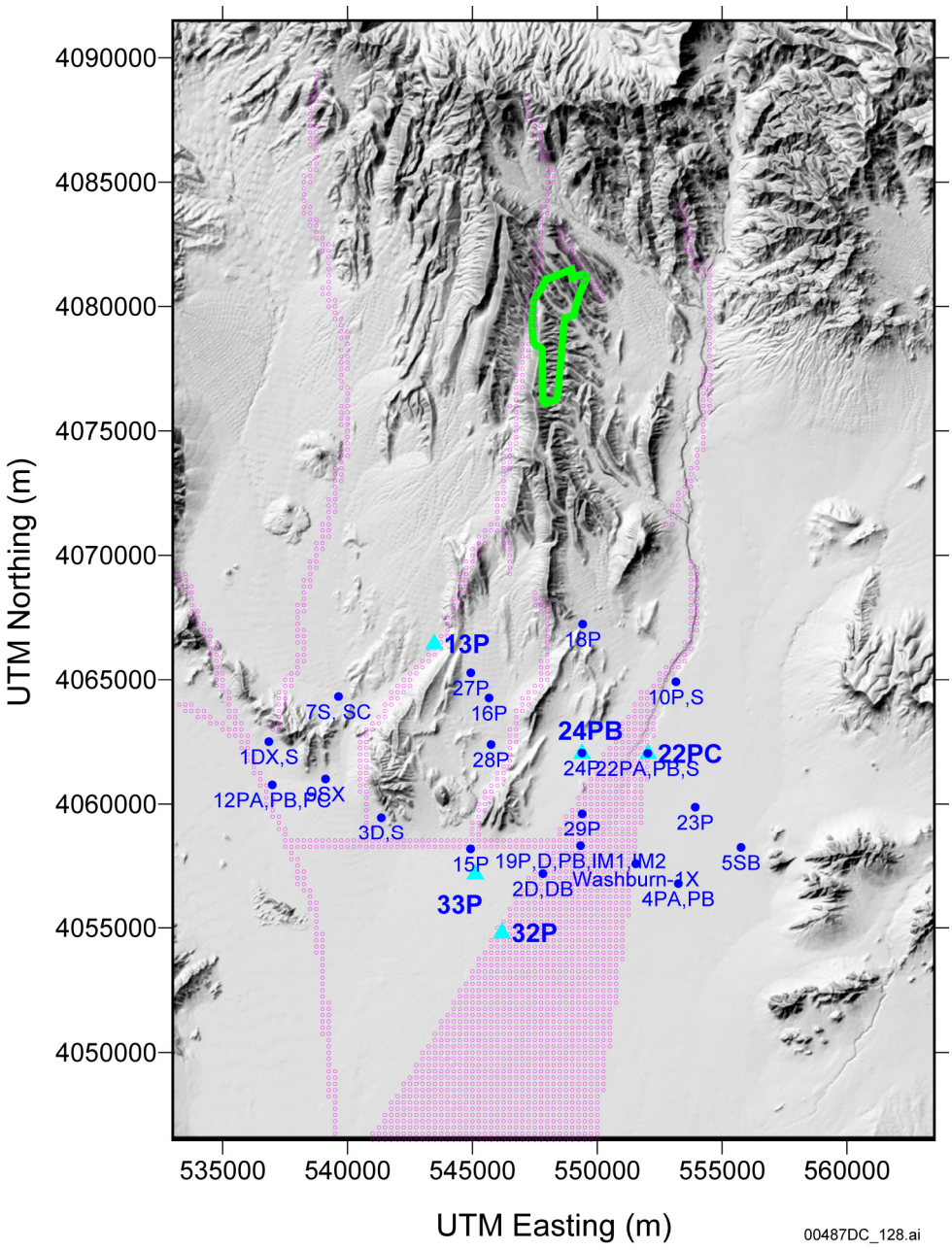

Sources: DTN: GS010908312332.002 [DIRS 163555] (non-NC-EWDP wells); SNL 2007 [DIRS 179466] (repository outline).

Output DTNs: SN0612T0510106.004 (modeled heads); SN0702T0510106.007 (NC-EWDP aggregated Phase III, IV, and V well data).

NOTE: For illustration purposes only. Well coordinates are listed in Table 7-2. Blue dots are NC-EWDP wells used in calibration. Light blue triangles with larger text are Phase V wells used in validation.

UTM = Universal Transverse Mercator.

Figure 7-2. Locations of NC-EWDP Wells

To further validate the SZ site-scale flow model, a comparison was made of the hydraulic gradients along the flowpath using water-level data from two wells that were not used during calibration (NC-EWDP-22PC and -32P). Table 7-3 presents gradients calculated for postdevelopment model validation. Predicted gradients are about a factor of two lower than observed because to the model does not capture the rapid water level change near U.S. Highway 95 fault. However, this region is south of the region of primary interest and, as discussed in Section 7.1.3, the model reproduces observed gradients over the relevant portion of the flowpath from the repository through Fortymile Wash to U.S. Highway 95 quite well. The validation is considered successful because the simulated hydraulic gradient agrees to within 50% with gradient calculations from data.

Table 7-3. Predicted and Observed Hydraulic Gradients for Post-Development Validation

Flow Segment	$\Delta H/\Delta L$ (Measured)	$\Delta H/\Delta L$ (Simulated)	Relative Error
NC-EWDP-24PB to NC-EWDP-32P	3.22×10^{-3}	1.81×10^{-3}	−0.44
NC-EWDP-22PC to NC-EWDP-32P	2.49×10^{-3}	1.39×10^{-3}	−0.44

Sources: DTNs: GS010908312332.002 [DIRS 163555] (non-NC-EWDP wells); SN0612T0510106.004 (modeled heads).

Output DTN: SN0702T0510106.007 (NC-EWDP aggregated Phase III, IV, and V well data).

NOTE: Calculations are from data in Table 7-2.

7.2.2 Comparison of Calibrated Effective Permeabilities to Field Test Results

The numerical model was calibrated by adjusting permeability values for individual hydrogeologic units in the model until the sum of the weighted residuals squared (the objective function) was minimized. The residuals include the differences between the measured and simulated hydraulic heads and the differences between the groundwater fluxes simulated with the SZ regional- and the site-scale models. Permeabilities estimated from hydraulic tests were neither formally included in the calibration nor considered in the calculation of the objective function. The field-derived permeabilities were instead used to check on the reasonableness of the final permeability estimates produced by the calibration.

Discussions of the permeability data from the Yucca Mountain area and nearby NTS as well as the Apache Leap site in Arizona are presented in the following subsections. A discussion of the general inferences about permeability that can be drawn from regional observations is also presented. Following these discussions, a comparison of calibrated effective permeabilities with the 95% confidence interval on the mean of measured permeability values is presented, including the analysis of the potential impact of calibrated permeability values on groundwater specific discharge.

7.2.2.1 General Permeability Data

Many factors affect the permeability of volcanic rocks at Yucca Mountain including: (1) the tendency of the rock either to fracture or to deform plastically in response to stress; (2) the ability of the rock to maintain open fractures, which is a function of the strength of the rock and overburden stress; (3) proximity to major zones of deformation, such as fault zones; and, (4) the degree of mineralization or alteration that would tend to seal fractures and faults. Other factors

being equal, rocks that tend to fracture are at shallow depth, have high compressive strength, are located in a fault zone, or are unmineralized and would be expected to have high permeabilities compared to rocks that do not possess these attributes. In addition to actual variations in permeability, the scale of measurement may also influence the permeability estimated by a test. This effect is most often observed when results of permeability tests conducted on cores that do not contain fractures are compared to the results of tests conducted in boreholes that contain fractured intervals. At Yucca Mountain, the relatively high permeabilities estimated from cross-hole tests compared to single-hole tests in the same rock unit have been attributed to the effects of scale (Geldon et al. 1998 [DIRS 129721]). In this case, the cause of the permeability increase in the cross-hole tests is attributed to the greater likelihood of including relatively rare but highly transmissive and continuous features in the larger rock volume sampled by the cross-hole tests. This assumption is reevaluated below based on recent analyses of air-injection tests conducted at the Apache Leap test site near Globe, Arizona. Permeability data from single- and multiple-borehole hydraulic tests at Yucca Mountain and single-borehole tests elsewhere at the NTS have been compiled and compared to permeabilities estimated during calibration of the SZ site-scale flow model.

7.2.2.1.1 Calico Hills

First, the geometric-mean permeability estimated for the Calico Hills Formation from single-hole tests ($k = 0.078 \times 10^{-12}$ m^2) is less than that estimated from cross-hole tests ($k = 0.17 \times 10^{-12}$ m^2). This observation indicates that factors other than the test method and the scale of the test are influencing results. One such factor may be proximity to faults. Several of the single-hole tests conducted in the Calico Hills Formation were performed in the highly faulted area near borehole UE-25 b#1, whereas faults were present only at deeper stratigraphic horizons at the C-wells where the cross-hole tests were done (Geldon et al. 1998 [DIRS 129721], Figure 3). Nonetheless, geologic contacts with open partings may also have enhanced permeability in the Calico Hills Formation at the C-wells (Geldon et al. 1998 [DIRS 129721], Figure 5). Second, both estimates of the mean Calico Hills Formation permeability are either larger than the mean permeability estimated for the carbonate aquifer from Yucca Mountain data ($k = 0.072 \times 10^{-12}$ m^2) or comparable to mean permeabilities estimated for the carbonate aquifer from data elsewhere at the NTS ($k = 0.6 \times 10^{-12}$ m^2). Although the permeability of the Calico Hills Formation may be locally higher than the mean permeability of the carbonate aquifer, it is unlikely that this relative difference between the two formation permeabilities can exist in general. The carbonate aquifer, along with the alluvial aquifers, is widely viewed as a major water-supply source in Southern Nevada (Dettinger 1989 [DIRS 154690]). In contrast, the Calico Hills Formation has properties similar to those of rocks deemed suitable for nuclear weapons tests below the water table at Pahute Mesa. The rocks at Pahute Mesa had properties (low intrinsic permeability due to zeolitization and sparse, poorly connected fractures) that were predicted, and later observed, to result in only small amounts of seepage into open test chambers during their construction (Blankennagel and Weir 1973 [DIRS 101233], pp. B30 to B31). Similar rocks in the unsaturated zone at Rainier Mesa produced perched water from isolated fault zones during construction of tunnels into the mesa; however, because the fault zones drained quickly and fault zones intersected later during tunneling also initially produced water, the fault zones were inferred to be relatively isolated both horizontally and vertically (Thordarson 1965 [DIRS 106585], pp. 42 to 43). At Yucca Mountain, the apparently widespread presence of perched water on top of the zeolitic Calico Hills Formation in northern Yucca Mountain

(Patterson 1999 [DIRS 158824]) indicates that the formation generally has low permeability compared to the rate of water percolation through the unsaturated zone, which has been estimated to average between 1 and 10 mm/yr in the vicinity of the repository under the present climate (Flint 1998 [DIRS 100033]). Water flowing under a unit gradient at a rate of 10 mm/yr (3.17×10^{-10} m/s) would seep through a rock having a permeability of $0.0000323 \times 10^{-12}$ m^2 (assuming a viscosity of 0.001 N-s/m^2 and a water density of 1,000 kg/m^3); so the field-scale vertical permeability of the Calico Hills Formation, which includes the effects of fracturing, presumably has permeabilities less than this value. Based on core measurements, the geometric-mean hydraulic conductivity for the zeolitic Calico Hills Formation is 4.5×10^{-11} m/s (Flint 1998 [DIRS 100033], Table 7), which is significantly higher than the low permeability ($0.0000323 \times 10^{-12}$ m^2) thought necessary for perched water. The calibrated effective permeability for the Calico Hills Volcanic unit was 0.46×10^{-12} m^2, which is on par with results from cross-hole testing.

7.2.2.1.2 Alluvial Testing Complex

From July through November 2000, pumping tests were conducted in well NC-EWDP-19D. The first test involved production from the entire saturated thickness of 136 m. The results indicated a transmissivity of about 21 m^2/day and an average hydraulic conductivity of 0.15 m/day, approximately equivalent to a permeability of 0.2×10^{-12} m^2 (SNL 2007 [DIRS 177394], Section 6.4.5 and Appendix F7). Subsequently, four screened intervals having a combined thickness of 84 m were tested individually. The combined transmissivities of these intervals totaled about 145 m^2/day, greatly exceeding the transmissivity determined for the initial open-hole test. There are at least two likely causes for the discrepancy. First, pumping apparently resulted in further well development, as fine materials were drawn into the well and discharged with the water. Second, the screened intervals are probably interconnected hydraulically, consistent with the complexity of fluvial-alluvial depositional environments, so that actual thicknesses of the producing zones were significantly greater than the screened intervals. The average permeability of the section is probably greater than the initial permeability determined from the open-hole test (0.2×10^{-12} m^2) but less than those calculated for the two deeper screened intervals, 1.5×10^{-12} and 3.3×10^{-12} m^2. Although thin, discontinuous zones may locally have higher permeabilities, these results indicate that significantly thick (greater than 10 m) and areally extensive zones at NC-EWDP-19D probably have average permeabilities between 0.1×10^{-12} and 1×10^{-12} m^2 (SNL 2007 [DIRS 177394], Sections 6.4.5 and Appendix F7).

7.2.2.1.3 Apache Leap

Fractured welded tuffs and relatively unfractured nonwelded tuffs occur both above and below the water table. Permeabilities measured in the unsaturated zone at Yucca Mountain using air may, therefore, have some relevance to the permeability values of similar rocks located below the water table. In the unsaturated zone, air-injection tests have been conducted from surface-based boreholes in both welded and nonwelded tuffs (LeCain 1997 [DIRS 100153]) and from test alcoves in and adjacent to the Ghost Dance Fault zone in the densely welded Topopah Spring tuff (LeCain et al. 2000 [DIRS 144612]). At Yucca Mountain, no water-injection tests were done in these same intervals to directly compare to the results of the air-injection tests. However, some understanding of the probable relation between permeabilities estimated from

air- and water-injection tests at Yucca Mountain can be made on the basis of tests in nonwelded to partially welded tuff at the Apache Leap experimental site in Arizona, where borehole air- and water-injection tests were made at ambient moisture conditions in the same depth intervals (Rasmussen et al. 1993 [DIRS 154688]). The Apache Leap data (Rasmussen et al. 1993 [DIRS 154688], Figure 5b) reveal a complex relation between permeabilities calculated from the two types of tests. Air-injection tests yielded lower permeabilities than water-injection tests in borehole intervals for which permeabilities calculated using both fluids indicated that fractures were sparse or absent. In these intervals, matrix pore water probably obstructed air movement. However, in test intervals for which air and water permeabilities were both relatively high, the air-injection tests resulted in permeabilities comparable to or higher than permeabilities from the water-injection tests. In these intervals, both fluids probably moved into drained fractures. Additionally, because gravitational influences on air are not as pronounced as for water in the unsaturated zone, air had more possible pathways for movement than water, so air permeabilities were often higher than water permeabilities. Overall, the correlation between air and water permeabilities from the borehole injection tests at Apache Leap was $r = 0.876$ (Rasmussen et al. 1993 [DIRS 154688], Figure 5b).

The test data from Apache Leap indicate that permeabilities calculated from air-injection test data in the unsaturated zone at Yucca Mountain probably provide good approximations to the water permeabilities, particularly in the densely welded intervals where drained fractures dominate the overall air permeability. The surface-based tests in four boreholes at Yucca Mountain showed that the highest air permeabilities (up to 54.0×10^{-12} m^2) were present at depths less than 50 m in the Tiva Canyon tuff, presumably because low lithostatic stresses at these depths allowed fractures to open (LeCain 1997 [DIRS 100153], Figures 7 to 10). However, permeabilities in the Tiva Canyon tuff typically decreased rapidly with depth, so that the permeabilities at depths greater than 50 m were less than 10^{-11} m^2. The geometric-mean permeabilities of the Tiva Canyon tuff in the four boreholes varied between 3.4×10^{-12} and 8.4×10^{-12} m^2 (LeCain 1997 [DIRS 100153], Table 1), with an overall geometric-mean permeability of 4.7×10^{-12} m^2 based on a total of 23 tests. Geometric-mean permeabilities of the Topopah Spring tuff at the four boreholes varied between 0.3×10^{-12} and 1.7×10^{-12} m^2 (LeCain 1997 [DIRS 100153], Table 5) with an overall geometric-mean permeability of 0.75×10^{-12} m^2 based on the results of 153 tests.

Work by Vesselinov et al. (2001 [DIRS 154706]) at the Apache Leap site has demonstrated that permeabilities determined from multiple single-well air-injection tests and simultaneous numerical inversion of multiple cross-hole air-injection tests provided comparable estimates of the mean permeability of the test volume. However, when the cross-hole tests were analyzed individually with an approach equivalent to type-curve analysis, which requires the assumption of a uniform permeability field and a particular flow geometry (spherical), the resulting mean permeability estimated for the test volume was several orders of magnitude higher than the mean permeability estimated from the single-hole analyses or the more detailed simultaneous numerical inversion of the cross-hole tests. The simultaneous numerical inversion of the cross-hole tests resulted in larger calculated variance in permeabilities than was estimated from the multiple single-hole tests, a result that may have been caused by round-off error associated with the numerical inversion. The conclusions of this work relevant to the present analysis are that the mean permeabilities would not have been a function of test methodology (single-hole or cross-hole analyses) except for the inability of standard cross-hole type-curve methods to

account for heterogeneity and departures of the actual flow field from the assumed flow geometry.

7.2.2.1.4 Tuffaceous Formations

The Prow Pass, Bullfrog, and Tram tuffs of the Crater Flat group contain both nonwelded to partially welded margins and partially to densely welded interiors (Bish and Chipera 1989 [DIRS 101195]; Loeven 1993 [DIRS 101258]). The initially vitric nonwelded to partially welded margins of these units have been largely altered to zeolites during hydrothermal events as a result of their thermodynamically unstable glass composition and their initially high permeabilities (Broxton et al. 1987 [DIRS 102004]). The partially to densely welded parts of these units have devitrified to mostly quartz and feldspar and have higher matrix permeabilities than the nonwelded to partially welded zeolitized margins (Loeven 1993 [DIRS 101258]; Flint 1998 [DIRS 100033]). Additionally, because the welded parts of the tuffs have a greater tendency to fracture, the densely welded parts of these units generally have higher secondary permeability. Thus, unless faults are locally present, the densely welded parts of the Prow Pass, Bullfrog, and Tram tuffs are expected to have substantially higher permeability than the nonwelded margins.

The densely welded parts of the Prow Pass, Bullfrog, and Tram tuffs are likely to have mean permeabilities that are less than the mean air permeabilities of the Tiva Canyon ($k = 4.7 \times 10^{-12}$ m^2) or Topopah Spring ($k = 0.75 \times 10^{-12}$ m^2) tuffs estimated from air-permeability tests (see Section 7.2.2.1.3). This likelihood is because greater lithostatic stresses at depth tend to close fractures and successive hydrothermal events have caused increasing degrees of alteration with depth (Broxton et al. 1987 [DIRS 102004]). Figure 7-3 shows the geometric-mean permeabilities from the single-hole air-permeability tests for the Tiva Canyon and Topopah Spring tuffs and the geometric-mean single-hole water permeabilities calculated for the Calico Hills Formation and the Prow Pass, Bullfrog, Tram, and Lithic Ridge tuffs. The single-hole permeabilities show the expected trends of decreasing permeability with depth. Conversely, the trends in the cross-hole permeability data from the C-wells (see Section 7.2.2.3.2 and Section 7.2.2.6, Figure 7-4) are exactly opposite those expected based on geologic reasoning; these trends could, however, reflect the proximity of each hydrogeologic unit to the Midway Valley fault, which intersects the C-wells in the upper part of the Tram tuff (Geldon et al. 1998 [DIRS 129721], Figure 3). Thus, it appears that permeability trends with depth at the C-wells are controlled by local conditions and do not reflect general trends in permeability established by the single-hole tests and expected from geologic reasoning.

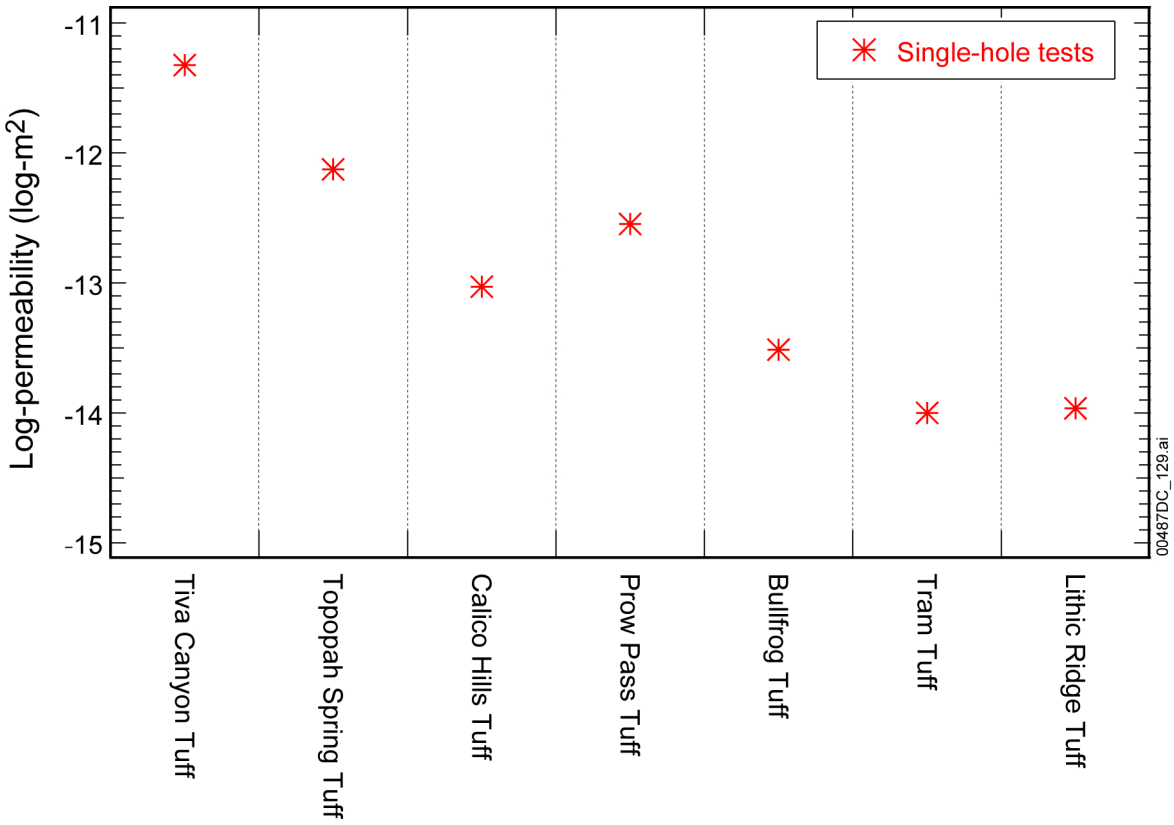

Source: DTNs: GS960908312232.012 [DIRS 114124] (Tiva and Topopah units); SNT05082597001.003 [DIRS 129714] (all other units). Used for corroboration only.

NOTE: All data are the geometric mean. Air permeability tests were conducted in the Tiva Canyon and Topopah Spring Tuffs. Water permeability tests were conducted in the other units.

Figure 7-3. Comparison of Single-Hole Air and Water Permeabilities

7.2.2.2 Implications of Permeability Data

The depth-dependent trends in mean hydrogeologic-unit permeabilities indicated by the combined air-permeability data from the unsaturated zone and the water-permeability data from the SZ (Section 7.2.2.3.2 and Section 7.2.2.6, Figure 7-4) are generally consistent with the trends expected as higher lithostatic stresses and more intense hydrothermal alterations close fractures at increasing depths. Conversely, permeabilities measured from cross-hole tests at the C-wells (Section 7.2.2.3.2 and Section 7.2.2.6, Figure 7-4) indicate trends that reflect proximity to the Midway Valley fault. Recent studies at the Apache Leap site in Arizona have indicated that single-hole and cross-hole tests should yield the same mean permeabilities once heterogeneity and departures from idealized flow geometries are properly taken into account. Therefore, except for the Calico Hills Formation, the single-hole permeabilities better reflect the true permeabilities of the hydrogeologic units in unfaulted areas and can be used to represent the hydrogeologic-unit permeabilities in specific-discharge calculations or in numerical models, provided any effects of faults are accurately taken into account. The geometric-mean permeability estimated for the Calico Hills Formation was probably unduly biased toward that of faulted locations by data from boreholes UE-25 b#1 and UE-25 J-13. In unfaulted areas, the Calico Hills Formation permeability is probably several orders of magnitude less than the

geometric-mean permeability calculated from the single-hole tests. The similarity of geometric-mean permeability values from cross-hole air-permeability testing in the Ghost Dance fault ($k = 14.6 \times 10^{-12}$ m^2) and the maximum permeabilities from cross-hole testing at the C-wells (54.0×10^{-12} m^2) indicate that values of 10.0×10^{-12} to 50.0×10^{-12} m^2 may be appropriate for fault-zone properties in numerical models so long as the modeled width reflects the true width of the fault; otherwise, the permeabilities in the model should be adjusted to preserve the overall transmissivity of the faults (SNL 2007 [DIRS 177394], Section 6.2.4 and Appendix C7). Anisotropy also needs to be considered because a fault that acts as a barrier to perpendicular flow may simultaneously provide a conduit to planar flow. The maximum permeability values that have been calculated for faulted locations at the C-wells and alcoves in the Ghost Dance Fault provide upper bounds on the permeabilities that would be representative of the tuffs at unfaulted locations ($k = 50.0 \times 10^{-12}$ m^2). The expected values of the tuffs are provided by the geometric means calculated from the single-hole tests and are one to several orders of magnitude less than this likely upper bound.

7.2.2.3 Permeability Data from the Yucca Mountain Area

Permeability data from single-hole and cross-hole tests were collected in the Yucca Mountain area from the early 1980s. Test results published up to 1997 were compiled in DTN: SNT05082597001.003 [DIRS 129714]. A statistical analysis of this data set is presented in this section. In addition to permeability data previously available during the development of the SZ site-scale model, additional permeability measurements are now available from the ATC.

7.2.2.3.1 Single-Hole Tests

The statistical analysis required that the test results be grouped by first compiling the permeability estimates for individual hydrogeologic units, where possible, and by considering progressively more general groupings for those cases in which the test interval spanned several hydrogeologic units. For instance, when the test interval was in the Prow Pass tuff, with or without some portion of the adjacent ash fall, the test results were grouped with other permeability estimates for the Prow Pass tuff. If other units within the middle volcanic aquifer (MVA), as defined by Luckey et al. (1996 [DIRS 100465], Figure 7), were also present in the test interval along with the Prow Pass tuff, the test results were considered to represent the MVA. If hydrogeologic units other than those in the MVA were present in the test interval along with the Prow Pass tuff, the permeability estimate for the test was grouped with the most general category, which is mixed tuffs. The mixed-tuff category includes data for all tests that would not fit into a more restrictive category. All tuffs older than the Lithic Ridge tuff are listed as Pre-Lithic Ridge tuffs (“older tuffs”). The other categories were named for the hydrogeologic unit to which they pertain.

There were several instances where several kinds of hydraulic tests (injection, drawdown, or recovery) were conducted in the same depth interval in the same borehole. The results of these tests could have been treated in several different ways. For example, (1) the data for a particular depth interval could have been averaged and primarily the single, average value considered in the statistical summary, in which case the statistical uncertainty could be interpreted as reflecting only the effects of spatial variability; or (2) all of the permeabilities that resulted from testing of the interval could have been used to calculate the summary statistics (this technique was used in this report). By considering multiple measurements from the same test interval, this statistical analysis attempts to reflect the effects of measurement uncertainty as well as the effects of spatial variability.

The base-10 logarithms of the permeabilities were calculated (Section 6.8) and a statistical analysis was performed on the log-transformed values for each category (CRWMS M&O 2000 [DIRS 139582]). The antilogarithms of the statistical parameters for each category were calculated and are listed in Table 6-24. The analysis indicates that the deepest tuffs, which are the Pre-Lithic Ridge tuffs (Pre-Tlr), and the mixed tuff group have the lowest permeabilities, and the Topopah Spring and Prow Pass tuffs have the largest permeabilities. Where they could be calculated, the 95% confidence limits indicate that the mean permeability values are constrained within relatively narrow limits, except for the Pre-Lithic Ridge tuffs.

The results also indicate that the Calico Hills Formation, which is a zeolitized tuff that functions as the upper volcanic confining unit (Luckey et al. 1996 [DIRS 100465], Figure 7), has a higher permeability than both the Bullfrog tuff and the carbonate aquifer. This paradoxical result may reflect the fact that, because it is unsaturated in the western half of Yucca Mountain, the Calico Hills Formation could be hydraulically tested only in the highly faulted eastern half of Yucca Mountain, whereas the other units were also tested in less intensely faulted areas to the west. Fortunately, calibrated effective permeabilities agree that the Calico Hills Volcanic unit has a higher permeability than both the carbonate aquifer and the Bullfrog tuff.

Single-well hydraulic testing of the saturated alluvium in well NC-EWDP-19D of the ATC was conducted between July and November 2000 (SNL 2007 [DIRS 177394], Appendix G). During this testing, a single-well test of the alluvium aquifer to a depth of 247.5 m below land surface was initiated to determine the transmissivity and hydraulic conductivity of the entire alluvium system at the NC-EWDP-19D location. In addition, each of the four intervals in the alluvium in NC-EWDP-19D were isolated and hydraulically tested to obtain transmissivity and associated hydraulic conductivity. This interval-testing program was initiated in an effort to evaluate heterogeneity in hydraulic properties over the thickness of the alluvium at NC-EWDP-19D to help determine the conceptual model of flow in the saturated alluvium south of Yucca Mountain. The results of this testing are presented in Table 7-4.

Table 7-4. Transmissivities, Hydraulic Conductivities, and Permeabilities Determined in the Single-Well Hydraulic Tests Conducted in the Alluvium in NC-EWDP-19D Between July and November 2000

Test Interval (ft below land surface)[a]	*Apparent* Transmissivity of Interval[b] (ft^2/day)	*Apparent* Transmissivity of Total Saturated Alluvium[c] (ft^2/day)	Hydraulic Conductivity Based on Sand Pack Thickness[d] (ft/day)	Hydraulic Conductivity Based on Distance from Water Table[e] (ft/day)	Permeability[f] (m^2)
Combined-Interval Test					
Four combined intervals	223	223	0.5	0.5	0.27×10^{-12}
Isolated-Interval Tests					
#1: 412–437	66	335	2.6	0.77	0.271×10^{-12}
#2: 490–519	7.5	N/A	0.26	0.045	0.0144×10^{-12}
#3: 568–691	223	306	1.89	0.78	0.235×10^{-12}
#4. 717–795	300	300	3.84	0.67	0.242×10^{-12}

Source: SNL 2007 [DIRS 177394], Appendix F.

[a] Depths correspond to upper and lower extent of sand packs.

[b] Transmissivity of the saturated alluvium from the water table to the bottom of the screen being tested was obtained by applying the Neuman (1975 [DIRS 150321]) solution to the drawdown in the interval tested. Ignoring screen #2, which is affected by a local clay layer, these transmissivities increase monotonically as the depth of the screen being tested increases.

[c] Transmissivity from interval tests for the screens #1, #3, and #4 for the entire saturated alluvium thickness tested are calculated by multiplying the transmissivity value in the second column, which is for the interval from the water table to the bottom of the screen being tested, by the ratio of 446 feet (the total saturated alluvium thickness tested) over the depth from the water table to the bottom of the screen being tested. Thus, for screen #1, $66 \times (446/88) = 334.5 \approx 335$ ft^2/day. For screen #3, $223 \times (446/342) = 290.8 \approx 291$ ft^2/day. No corrections are needed for the combined-interval test or for the test on screen #4.

[d] Assumes that interval thickness is the thickness of the interval sand pack. Sand pack (or gravel pack) is the term used for the coarse-grained material that fills the annulus between the slotted pipe (wellscreen) and the borehole wall in well completions. The sand pack generally extends a bit below the bottom and above the top of the slotted pipe to allow for any anomalies in the completion, so it is typically used as the "interval thickness" as opposed to the slotted pipe length. There is generally a bentonite grout plug placed above and below the sand pack to seal the annulus.

[e] Assumes that interval thickness is the distance from the water table to the bottom of the screened interval being pumped. Furthermore, the water table at the ATC is assumed to be 351 ft below land surface, which is the open-hole static water level in NC-EWDP-19D. However, there is a strong upward gradient from the volcanics to the alluvium at this location, and when individual zones in the alluvium are isolated, the static water level drops considerably (for instance, 368 ft below land surface in zone #1, and also in NC-EWDP-19P, which has a piezometer completed only in zone #1).

[f] Multiply the hydraulic conductivity (ft/day) in the fifth column by the factor 3.61×10^{-13} to convert to permeability in m^2.

7.2.2.3.2 Cross-Hole Tests

Permeability data from cross-hole tests were compiled, grouped, and analyzed in a manner similar to the permeability data for the single-hole tests (see Table 6-24). The cross-hole data originate from tests conducted at the C-wells complex. While the permeabilities of the Calico Hills formation are similar for both the single- and cross-hole tests, the permeabilities of the Prow Pass, Bullfrog, Tram tuffs of the Crater Flat group, and the MVA calculated from the cross-hole tests are one to several orders of magnitude greater than the mean permeabilities calculated from the single-hole tests. The differences in the mean permeability values between the single- and cross-hole tests generally have been attributed to the larger volume of rock

affected by the cross-hole tests (Geldon et al. 1997 [DIRS 100397]) that allows a larger number of possible flowpaths, including relatively rare, high-transmissivity flowpaths, to be sampled during the test. Furthermore, combinations of well losses, wellbore formation damage, and scale effects might also serve to increase estimated cross-hole permeabilities. However, some of the increase in permeability attributed to the effects of scale may also be due to the presence of a breccia zone associated with the Midway Valley fault in the Bullfrog and Tram tuffs at boreholes UE-25 c#2 and UE-25 c#3 (Geldon et al. 1997 [DIRS 100397], Figure 3). Thus, some of the difference in the mean permeabilities calculated for the single- and cross-hole tests may be due both to local conditions in the vicinity of the C-wells and to scale.

Another cross-hole hydraulic test was conducted at the ATC in January 2002. During this test, borehole NC-EWDP-19D was pumped in the open-alluvium section, while NC-EWDP-19IM1 and NC-EWDP-19IM2 were used as monitoring wells. NC-EWDP-19IM1 was packed off, isolating each of four intervals in the alluvium section, while NC-EWDP-19IM2 had only one packer inflated, isolating the alluvium section from the intervals below it. Analysis of the drawdown data from NC-EWDP-19IM2 indicated an estimated transmissivity of 307 m^2/day. The transmissivity estimate is approximately an order of magnitude higher than the 27.8-m^2/day value obtained from single-hole testing in NC-EWDP-19D. The differences between single- and cross-hole tests are likely the result of large head losses in the single-hole testing due to the well efficiency of NC-EWDP-19D. The tested interval in NC-EWDP-IM2, from the water table to the bottom of screen #4 is 133.5 m. Therefore, the intrinsic permeability measured in this test is 2.7×10^{-12} m^2.

Cross-hole tests were also conducted in NC-EWDP-22S from December 2004 to January 2005 (SNL 2007 [DIRS 177394], Appendix F). During this test, NC-EWDP-22S was pumped in the open alluvium section while NC-EWDP-22PA and -22PB were monitored. NC-EWDP-22S was screened in four intervals while -22PA and -22PB each had two packed off sections. Analyses of drawdown data yielded transmissivities ranging from 130 to 600 m^2/day. This corresponds to permeabilities between 0.059×10^{-12} and 5.8×10^{-12} m^2.

7.2.2.4 Permeability Data from the Nevada Test Site

Data from the NTS were examined to help constrain permeability estimates for hydrogeologic units that were either not tested or that underwent minimal testing at Yucca Mountain. These permeability data, as well as more qualitative observations concerning the permeability of some of the hydrogeologic units in the site-scale model area, are summarized in the following sections. Additionally, these reports, including those by Blankennagel and Weir (1973 [DIRS 101233]), Winograd and Thordarson (1975 [DIRS 101167]), and Laczniak et al. (1996 [DIRS 103012]), describe the hydrogeologic controls on groundwater movement at the NTS, thereby providing a regional perspective for groundwater flow at Yucca Mountain. Assessments of permeability data from the NTS for the lower carbonate aquifer, the valley fill aquifer, the welded tuff aquifer, and the lava flow aquifer are presented.

7.2.2.4.1 Lower Carbonate Aquifer (Unit 5)

The results of hydraulic tests in the lower carbonate aquifer were reported for eight boreholes by Winograd and Thordarson (1975 [DIRS 101167], Table 3). For two of the boreholes, only transmissivity estimates based on specific capacity were made. Where permeability estimates based on drawdown curves were also available, these permeability estimates are based on specific capacity and were much lower than the estimates based on the drawdown curves. At five boreholes where both drawdown and recovery tests were conducted, the permeabilities estimated from recovery tests were several times higher than those estimated from drawdown tests. Both the drawdown and recovery data exhibited complex responses to pumping that were attributed to test conditions as well as to aquifer properties. These responses were manifested on log-linear plots of time versus drawdown as straight-line segments with distinct breaks in slope. Because they were unable to explain the differences in the results from the drawdown and recovery tests, Winograd and Thordarson (1975 [DIRS 101167], p. C25) advised against the use of the transmissivities estimated from the recovery tests. The transmissivities estimated from drawdown tests in the lower carbonate aquifer are listed for six boreholes in Table 7-5 along with thicknesses of the test intervals and the calculated permeabilities. The permeabilities were calculated from hydraulic conductivity values using a viscosity of 0.001 Pa-s, a density of 1,000 kg/m^3, and a gravitation acceleration of 9.81 m/s^2. These viscosity and density values are appropriate for test temperatures of about 25°C. The actual test temperatures were not reported by Winograd and Thordarson (1975 [DIRS 101167]) although they may have been substantially higher (greater than 50°C) than the temperatures assumed in this calculation, in which case the calculated permeabilities may overestimate the true permeabilities measured by the tests by a factor of 2 to 3. A statistical analysis of the base-10 logarithms of the permeabilities listed in Table 7-5 resulted in an estimated mean permeability for the carbonate aquifer of 0.60×10^{-13} m^2. The 95% lower and upper confidence limits for the mean permeability were 0.139×10^{-12} m^2 and 2.58×10^{-12} m^2, respectively.

Table 7-5. Permeabilities Calculated for the Lower Carbonate Aquifer

Well	Thickness (ft)	Transmissivity[a] (gpd/ft)[b]	Hydraulic Conductivity (gpd/ft^2)	Permeability (m^2)
67-73	281	20,000	71.2	3.44×10^{-12}
67-68	996	39,000	39.2	1.89×10^{-12}
66-75	753	11,000	14.6	0.705×10^{-12}
88-66	872	1,300	1.49	0.0719×10^{-12}
75-73	750	3,800	5.07	0.245×10^{-12}
84-68	205	2,400	11.7	0.565×10^{-12}

Source: Winograd and Thordarson 1975 [DIRS 101167], Table 3.

NOTE: Statistics for the logarithm of permeability (log *k*) are:
Mean = –12.223.
Standard deviation = 0.605.
Median = –12.200.
Lower 95% confidence level for mean = –11.740.
Upper 95% confidence level for mean = –12.708.

[a]These transmissivities were estimated by Winograd and Thordarson (1975 [DIRS 101167], Table 3) from drawdown curves.
[b]gpd is gallons per day.

In addition to providing quantitative estimates of the permeability, Winograd and Thordarson (1975 [DIRS 101167]) made several qualitative observations regarding the distribution of permeability within the carbonate aquifers.

The permeability data for the carbonate aquifer showed no systematic decrease either with depth beneath the top of the aquifer or beneath the land surface (Winograd and Thordarson 1975 [DIRS 101167], p. C20). The inference that groundwater may circulate freely within the entire thickness of the lower carbonate aquifer is not negated by chemical data that indicate no significant increase in the dissolved-solids content to depths of several thousand feet (Winograd and Thordarson (1975 [DIRS 101167], p. C103).

No major caverns were detected during drilling in the lower carbonate aquifer, despite the fact that approximately 4,900 m of the lower carbonate aquifer was penetrated in 26 holes drilled in 10 widely separated areas, including over 1,500 m at 13 holes beneath the Tertiary/pre-Tertiary unconformity, where caverns might be expected to exist (Winograd and Thordarson 1975 [DIRS 101167], p. C19). Drill-stem tests in three holes in the Rock Valley and Yucca Flat indicated negligible to moderate permeability immediately below the unconformity (Winograd and Thordarson 1975 [DIRS 101167], p. C20). Outcrop evidence indicates that klippen, which are the upper plates of low-angle thrust faults and gravity slump faults, have a higher intensity of fracturing and brecciation than rock below the fault planes and may have above-average porosity and permeability (Winograd and Thordarson 1975 [DIRS 101167], pp. C19 to C20). Specific capacity data for five wells penetrating the upper plates of low-angle faults in southern Yucca Flat and the northwestern Amargosa Desert indicated relatively high transmissivities for these plates (Winograd and Thordarson 1975 [DIRS 101167], p. C28).

The presence of hydraulic barriers within the lower carbonate aquifer is indicated in the hydraulic response in two-thirds of the wells pumped, indicating that zones of above-average transmissivity may often not be connected to each other (Winograd and Thordarson 1975 [DIRS 101167], p. C116). However, this observation needs to be reconciled with hydraulic and chemical evidence supporting the existence of a "mega channel" extending over 64 km between southern Frenchman Flat and the discharge area at Ash Meadows (Winograd and Pearson 1976 [DIRS 108882]).

7.2.2.4.2 Valley Fill Aquifer (Units 11, 26, 27, and 28)

The valley fill aquifer, as defined by Winograd and Thordarson (1975 [DIRS 101167], Table 1, p. C37) is composed of alluvial fan, fluvial, fanglomerate, lakebed, and mudflow deposits in depressions created by post-Pliocene block faulting. As defined, the valley fill aquifer of Winograd and Thordarson (1975 [DIRS 101167]) probably includes the Volcanic and Sedimentary Unit – Lower (Unit 11), the Older Alluvial Aquifer (Unit 26), the Young Alluvial Confining Unit (Unit 27), and the Young Alluvial Aquifer (Unit 28).

Transmissivity estimates for the valley-fill aquifer were made at six boreholes in Emigrant Valley, Yucca Flat, and Frenchmen Flat (Winograd and Thordarson 1975 [DIRS 101167], Table 3). For two of the boreholes, only transmissivity estimates based on specific capacity data were available. However, these estimates are considered unreliable because of the lack of agreement with transmissivity estimates based on drawdown or recovery curves at boreholes in

which both types of estimates were made. The transmissivity estimates made from drawdown and recovery curves were consistent at wells where both types of tests were conducted, in which case the transmissivity values from the drawdown and recovery curves were averaged to produce the transmissivity estimates listed in Table 7-6. Values used for the viscosity, density, and gravity terms in the expression for permeability are the same as those used for the lower carbonate aquifer. Based on a statistical analysis of the logarithm of the permeabilities listed in Table 7-5, the mean permeability of the valley fill is 1.57×10^{-12} m^2, and the 95% lower and upper confidence limits for the mean permeability are 0.095×10^{-12} and 26.0×10^{-11} m^2, respectively. The relatively high mean permeability calculated for the valley fill is probably more reflective of the permeability of the Young Alluvial Aquifer (Unit 20) and, possibly, the Volcanic and Sedimentary Unit – Lower (Unit 11) than of the Young Alluvial Confining Unit (Unit 27). Calibrated effective permeabilities for these units ranged from 0.0091 to 0.91×10^{-11} m^2.

Table 7-6. Permeability Estimates for the Valley Fill Aquifer

Well	Thickness (ft)	Transmissivity (gpd/ft)	Hydraulic Conductivity (gpd/ft^2)	Permeability (m^2)
74-70 [b]	511	2,200 [a]	4.31	0.208×10^{-12}
74-70 [a]	217	9,350 [b]	43.1	2.08×10^{-12}
83-68	264	12,700 [b]	48.1	2.32×10^{-12}
91-74	264	33,500 [c]	126.9	6.12×10^{-12}

Source: Winograd and Thordarson 1975 [DIRS 101167], Table 3.

NOTE: Permeability estimates based on transmissivity data from Winograd and Thordarson 1975 [DIRS 101167], Table 3.
Statistics for the logarithm of permeability (log *k*) are:
Mean = –11.803.
Standard deviation = 0.623.
Median = –11.658.
Lower 95% confidence level for mean = –12.413.
Upper 95% confidence level for mean = –11.193.

[a] Average is the arithmetic sum of the results of one drawdown and two recovery tests.
[b] Average is the arithmetic sum of the results of one drawdown and one recovery test.
[c] Representative Value is the result of one recovery test.
gpd = gallons per day.

In addition to providing the quantitative estimates of the permeability of the valley fill, Winograd and Thordarson (1975 [DIRS 101167]) also made numerous observations regarding the permeability of the valley fill at particular locations in the area of the NTS. Of special interest to this report are those observations made for the valley fill in the Amargosa Desert. Winograd and Thordarson (1975 [DIRS 101167], pp. C84 to C85) noted that hydraulic head contours south of Amargosa Valley (formerly called Lathrop Wells) probably reflect the effects of upward leakage from the lower carbonate aquifer into poorly permeable valley fill along the Gravity Fault and associated faults and of the drainage of this water to more permeable sediments farther west. Immediately west of the Gravity fault, gravity data indicate that downward displacement of the pre-Tertiary rocks west of the fault is 152.4 to 457.2 m at a location one mile east of Amargosa Valley and 365.8 to 670.6 m at a point 1.6 km southeast of the inferred intersection of the Specter Range Thrust fault and the Gravity fault. The low permeability of the valley fill immediately west of the Gravity fault was indicated by drillers' logs that showed valley fill in this area to be mainly clay. Winograd and Thordarson (1975 [DIRS 101167], p. C85) argued

that the discharge across the Gravity fault near Amargosa Valley was probably small because only the lower-most part of the lower carbonate aquifer is present in the area and the lower clastic aquitard, which underlies the carbonate aquifer at shallow depths, would probably not transmit much water.

7.2.2.4.3 Welded Tuff Aquifer (Units 19 and 20)

The welded tuff aquifer corresponds to the Timber Mountain and Paintbrush Volcanic Aquifer units (Units 19 and 20) of Table 6-2. Results of hydraulic tests conducted in the welded tuff aquifer were reported by Winograd and Thordarson (1975 [DIRS 101167], Table 3) for four wells, but only two wells, both in Jackass Flats, had transmissivity estimates based on drawdown curves. Well 74-57 tested the Topopah Spring tuff and well 74-61 tested both the Topopah Spring tuff and the Basalt of Kiwi Mesa. Permeabilities calculated from the drawdown curves at these wells are listed in Table 7-7. The geometric-mean permeability, based on the estimated permeabilities in Table 7-7, is 5.3×10^{-12} m^2. Calibrated effective permeabilities for these units are 0.065 and 0.076×10^{-11} m^2 for the Paintbrush and Timber Mountain Volcanic Aquifers, respectively.

Table 7-7. Permeability Estimates for the Welded Tuff Aquifer

Well	Thickness (ft)	Transmissivity (gpd/ft)	Hydraulic Conductivity (gpd/ft^2)	Permeability (m^2)
74-61	290	28,000	96.6	4.7×10^{-12}
74-57	547	68,000	124.3	6.0×10^{-12}

Source: Winograd and Thordarson 1975 [DIRS 101167], Table 3.

NOTE: Permeability estimates based on transmissivities determined from drawdown curves (Winograd and Thordarson 1975 [DIRS 101167], Table 3). Statistics: The geometric-mean permeability is 5.3×10^{-12} m^2.

gpd = gallons per day.

7.2.2.4.4 Lava Flow Aquifer (Unit 23)

Rhyolitic lavas and welded and nonwelded tuffs fill the Silent Canyon caldera complex, which now lies buried beneath Pahute Mesa by younger tuffs, erupted from the Timber Mountain caldera complex to the south (Blankennagel and Weir 1973 [DIRS 101233], p. 6; Laczniak et al. 1996 [DIRS 103012], p. 36). The permeabilities of the lava flows beneath Pahute Mesa are assumed to be an appropriate analogue for the Lava Flow Aquifer (Unit 23) near Yucca Mountain.

A qualitative comparison of the water-producing attributes of the lavas and tuffs based on the concept of specific capacity (in gal/min/ft of drawdown) indicated that despite considerable overlap in their water-yield potential, the lavas generally were the most transmissive rocks tested, followed by the welded tuffs and, finally, the zeolitized nonwelded tuffs (Blankennagel and Weir 1973 [DIRS 101233], Figure 4). Pumping tests were conducted in 16 boreholes at Pahute Mesa, including 14 where the major water production came from the rhyolitic lava flows (Blankennagel and Weir 1973 [DIRS 101233], Table 3). The borehole names, uncased saturated thickness, measured transmissivities, and calculated hydraulic conductivities and permeabilities associated with these 14 tests are provided in Table 7-8. The geometric-mean permeability of the rhyolitic lava is estimated to be 0.314×10^{-12} m^2, with 95% lower and upper confidence

limits of 0.119×10^{-12} m^2 and 0.825×10^{-12} m^2, respectively. However, these estimates should be viewed as approximate lower bounds because other less permeable rocks (welded and nonwelded tuffs) are present in the test interval, and these less permeable rocks would cause the transmissivity to be lower than the transmissivity that would be expected if only lava had been present. Resistivity logs indicated that nonwelded tuffs could constitute as much as 73% of the upper 2,000 ft of saturated rock at the boreholes listed by Blankennagel and Weir (1973 [DIRS 101233], Table 2). Because most of the water pumped from the lava enters the wells from zones that constitute only 3% to 10% of the total saturated thickness (Blankennagel and Weir 1973 [DIRS 101233], p. 11), permeabilities in the lava may be locally much higher than the calculated mean value. Calibrated effective permeability for the Lava Flow Unit is 0.088×10^{-11} m^2.

Table 7-8. Permeabilities of the Lava Flow Aquifer

Well	Uncased, Saturated Thickness (ft)[a]	Transmissivity (gpd/ft)[b]	Hydraulic Conductivity (gpd/ft^2)[b]	Permeability (m^2)
UE-18r	3,375	23,000	6.82	0.328×10^{-12}
TW-8	4,422	185,000	41.8	2.01×10^{-12}
UE19b-1	2,310	56,000	24.2	1.17×10^{-12}
UE19c	2,099	12,000	5.72	0.275×10^{-12}
UE-19d	5,129	20,000	3.90	0.188×10^{-12}
UE-19fs	2,214	11,000	4.97	0.239×10^{-12}
UE-19gs	1,858	30,000	16.1	0.777×10^{-12}
UE-19h	1,383	140,000	101.0	4.87×10^{-12}
UE-19l	5,104	1,400	0.274	0.0132×10^{-12}
U-20a-2	2,434	18,000	7.40	3.56×10^{-13}
UE-20d	2,047	44,000	21.5	1.03×10^{-12}
UE-20e-1	4,573	8,300	1.82	0.873×10^{-12}
UE-20f	9,230	1,000	0.108	0.00521×10^{-12}
UE-20h	4,701	11,000	2.34	0.113×10^{-12}

Source: Blankennagel and Weir 1973 [DIRS 101233], Table 3.

NOTE: Statistics for the logarithm of permeability (log *k*) are:
Mean = –12.503
Standard deviation = 0.801
Median = –12.466
Lower 95% confidence level for mean = –12.923
Upper 95% confidence level for mean = –12.084

[a] Uncased, saturated thickness was calculated as the depth of the well minus the depth to water or casing, whichever was greater. The depth to water was used for TW-8, where the casing was perforated.
[b] gpd = gallons per day.

7.2.2.5 Inferences About Permeability from Regional Observations

In addition to the permeability values from the NTS summarized in the previous section, Winograd and Thordarson (1975 [DIRS 101167]) made numerous qualitative evaluations of the relative magnitude of permeability for different hydrogeologic units. These evaluations were based on examination of cores containing fractures and mineral infilling, the geologic setting and the magnitude of discharge of springs in the region, and the correspondence between changes in hydraulic gradients and the underlying hydrogeologic unit. Sections 7.2.2.5.1 through 7.2.2.5.3 focus on qualitative assessments of hydrogeologic units that have little actual test data and for which the qualitative evaluations, thus, assume relatively more importance.

7.2.2.5.1 Lower Clastic Aquitard (Units 3 and 4)

The Lower Clastic Aquitard of Winograd and Thordarson (1975 [DIRS 101167], Table 1) corresponds to the Crystalline and Lower Clastic Confining Units unit (Units 3 and 4) of Table 6-2. According to Winograd and Thordarson (1975 [DIRS 101167], p. C43), the large-scale transmissivity of the lower clastic aquitard is probably controlled by its interstitial permeability, which, based on the hydraulic conductivity of 18 cores (Winograd and Thordarson 1975 [DIRS 101167], Table 4), ranges from $0.000000034 \times 10^{-12}$ m^2 to $0.0000048 \times 10^{-12}$ m^2 and has a median value of $0.000000097 \times 10^{-12}$ m^2. Although the lower clastic aquitard is highly fractured, Winograd and Thordarson (1975 [DIRS 101167], p. C43) argued that fractures probably do not augment the interstitial permeability of the unit on a regional scale to the same degree as in the lower carbonate aquifer because:

- The argillaceous formations within the unit have a tendency to deform plastically, that is, by folding, rather than by fracturing. Thus, fracture continuity across the lower clastic aquitard is disrupted by the argillaceous layers

- Micaceous partings and argillaceous laminae tend to seal the fractures in the brittle quartzite parts of the unit, reducing or eliminating the ability of the fractures to transmit water

- The clastic rocks that constitute the unit have a low solubility; therefore, solution channels, which can further enhance permeability along fractures in carbonate rocks, are not likely to be present in this unit.

The low permeability of the lower clastic aquitard compared to the carbonate rocks also was indicated by the observation that, in the Spring Mountains, the total discharge issuing from the lower clastic aquitard is only a small fraction of the total discharge of the springs in the lower carbonate aquifer (Winograd and Thordarson 1975 [DIRS 101167], pp. C42 to C43, C53). The comparatively low permeability of the clastic aquitard also is indicated by a head drop across the lower clastic aquitard of 610 m over a distance of less than 12.8 km (an apparent hydraulic gradient of 0.0476 m/m) in the hills northeast of Yucca Flat (Winograd and Thordarson 1975 [DIRS 101167], Plate 1). In contrast, the hydraulic gradient in the carbonate aquifer ranges from 0.00112 m/m or less along the axis of the potentiometric trough in Yucca Flat to 0.0038 m/m) along the flanks of the trough (Winograd and Thordarson 1975 [DIRS 101167], p. C71). The calibrated effective permeability of these units are the second and third lowest of all calibrated

values at 0.000060×10^{-11} and 0.000066×10^{-11} m^2 for the Crystalline and Lower Clastic Confining Units, respectively.

7.2.2.5.2 Upper Clastic Aquitard (Unit 6)

The upper clastic aquitard is equivalent to the Upper Clastic Confining Unit (Unit 6) of Table 6-2. The upper clastic aquitard corresponds to the Eleana formation, which consists of argillite, quartzite, conglomerate, and limestone (Winograd and Thordarson 1975 [DIRS 101167], Table 1). The upper two-thirds of the unit consists mainly of argillite, whereas the lower one-third of the unit is principally quartzite (Winograd and Thordarson 1975 [DIRS 101167], p. C118). Winograd and Thordarson (1975 [DIRS 101167], p. C43) argued that fractures were unlikely to remain open in the rock at depth because of the plastic deformation behavior of the rock, which is evidenced by tight folds, and the fact that the formation serves as a glide plane for several thrust faults at the NTS. No core-scale permeability measurements exist, but based on analogy with the lower clastic aquitard, its interstitial permeability probably is less than 0.000048×10^{-12} m^2 (Winograd and Thordarson 1975 [DIRS 101167], p. C43). In the hills northwest of Yucca Flat, an approximately 610-m drop in hydraulic head in the pre-Tertiary rocks over a distance of less than 16 km (an apparent hydraulic gradient of 0.038 m/m) suggests a comparatively low regional permeability for the upper clastic aquitard. However, because land-surface elevation changes abruptly over this same distance and because water table elevations often mimic ground-surface elevations, it is not possible to isolate the effects of permeability from the effects of topography on the head gradient in this area. The calibrated effective permeability for the Upper Clastic Confining Unit is 0.00018×10^{-12} m^2.

7.2.2.5.3 Faults

A summary of the possible effects of faults on groundwater movement in the Death Valley region is presented by Faunt (1997 [DIRS 100146], p. 30). The transmissivity of faults was described to be a function of:

- The orientation of the fault relative to the minimum horizontal stress in the region
- The amount and type of fill material in the fault
- The relative transmissivities of hydrogeologic units juxtaposed by offset across the fault
- The solubility and deformation behavior of the rock adjacent to the fault
- Recent seismic history.

7.2.2.5.3.1 Orientation of Faults Relative to the Minimum Horizontal Stress in the Region

In the vicinity of Yucca Mountain, the mean azimuth of the minimum horizontal stress is 306 ± 11 degrees (Faunt 1997 [DIRS 100146], Table 4-4), so that faults with traces oriented north-northeast are expected to be more open and permeable than faults with traces oriented in directions that place them in either a shear or a compressive state. Faults oriented northwest, or perpendicular to the maximum horizontal stress direction, would be expected to be least transmissive, all other factors being equal. One example cited by Faunt (1997 [DIRS 100146], pp. 34 to 35) to illustrate the northeast-southwest trending structures that may have relatively high transmissivity is the "mega channel" formed in the Spotted Range-Mine Mountain shear zone between Frenchman Flat and Ash Meadows. The presence of a highly transmissive zone in the carbonate aquifer was indicated by a potentiometric trough in this area and relatively young

^{14}C ages of groundwater discharging from springs at the distal end of the trough (Winograd and Pearson 1976 [DIRS 108882]).

7.2.2.5.3.2 Amount and Type of Infilling Material in the Fault

Fine-grained gouge or clayey infilling material can cause faults to become poorly transmissive, even if their orientation relative to the stress field indicates they have the potential to be highly transmissive. The effects of deformation behavior, solubility, and infilling material in the clastic aquitards and carbonate aquifer were discussed in Sections 7.2.2.5.1 and 7.2.2.5.2. Solution channels along faults in the carbonate rock have the potential to further enhance the transmissivity of faults in this unit.

7.2.2.5.3.3 Relative Transmissivities of Hydrogeologic Units Juxtaposed by Offset Across the Fault

Where faults juxtapose hydrogeologic units with contrasting permeabilities, the hydrologic effects caused by juxtaposition may be difficult to isolate from the effects of the fault properties themselves. As indicated by Faunt (1997 [DIRS 100146], Figure 16), an increase in the local head gradient compared to the regional gradient can occur across a fault if:

- The fault is closed, thereby blocking flow
- The fault is open, thereby redirecting flow
- The permeability of the material downgradient of the fault is low compared to the upgradient material, so that flow across the fault is blocked
- The permeability of the material downgradient of the fault is high compared to the upgradient material, so that flow can drain away from the fault faster than it can be delivered by the upgradient material.

Evidence that springs in Ash Meadows are caused by the juxtaposition of poorly permeable sediments and rocks downgradient of the carbonate aquifer across the Gravity fault was presented by Winograd and Thordarson (1975 [DIRS 101167], p. C82). Hydraulic data in southern Indian Springs Valley were interpreted by Winograd and Thordarson (1975 [DIRS 101167], pp. C67 to C68) to indicate the presence of two hydraulic barriers related to the Las Vegas shear zone: (1) a northern barrier caused by the juxtaposition of the lower clastic aquitard and lower carbonate aquifer; and (2) a southern barrier, which was attributed to the presence of gouge along a major fault zone.

7.2.2.5.3.4 Recent Seismic History

The seismic history of the faults may indicate which faults have undergone recent movement. Recent movement on a fault may serve to break calcite or silica cement or other material that may have closed the fault. A map showing which faults or fault segments near Yucca Mountain have undergone recent movement was developed by Simonds et al. (1995 [DIRS 101929]). Of the faults that have been mapped near the repository area, only the Solitario Canyon fault and short segments of the Bow Ridge Fault near Exile Hill show evidence of late Quaternary (or more recent) movement.

7.2.2.6 Comparing Permeability Data to Calibrated Permeability Values

To check if the calibrated effective permeabilities are reasonable, the logarithms of permeabilities estimated during calibration of the model are compared to the logarithms of permeability estimated from pump-test data near Yucca Mountain and elsewhere at the NTS in Figure 7-4. Where they could be estimated, the 95% confidence limits for the mean logarithm of the permeability data error bars also are shown. For the Calico Hills Volcanic Unit, the Prow Pass, Bullfrog, and Tram tuffs, and the MVA permeabilities are shown for both the single- and cross-hole tests at the C-wells complex. As shown in Figure 7-4, most of the calibrated permeabilities fall within the 95% confidence interval on the mean measured permeability for single- and cross-hole tests or are within a factor of two of these ranges (within 50%). Therefore, with the exception of the lower clastic aquitard and the welded tuff, which are far from the flowpaths, the validation criterion for permeability is satisfied.

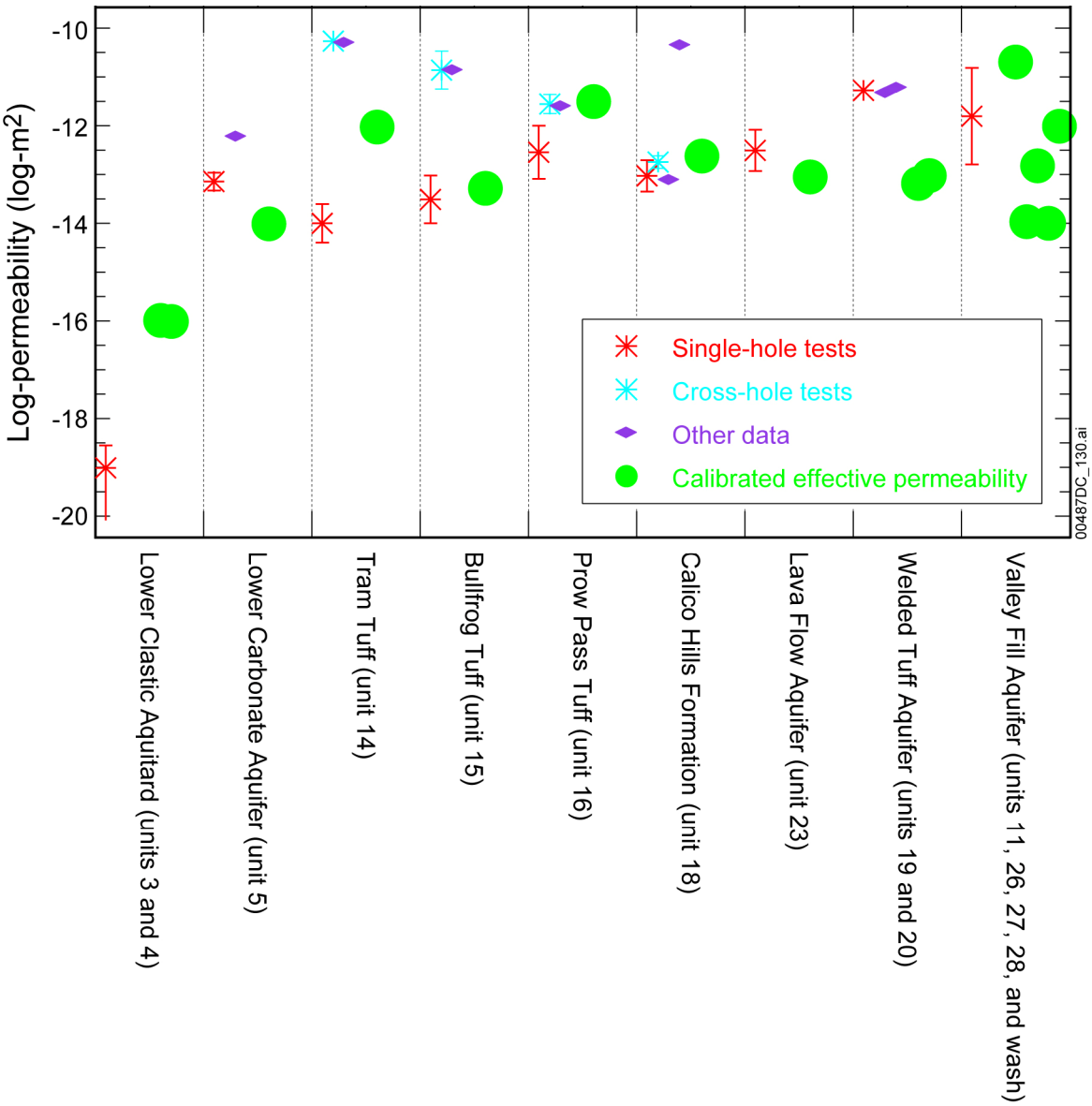

Source: DTN: SNT05082597001.003 [DIRS 129714].

NOTE: Bars on single- and cross-holes tests represents the 95% confidence interval on the mean.

Figure 7-4. Logarithms of Effective Permeabilities Estimated During Model Calibration Compared to Logarithms of Permeability Determined from Pump-Test Data

Calibrated effective permeabilities for the lower clastic aquitard are higher than those discussed in Section 7.2.2.5.1; however, the calibrated values are among the lowest in the model and consistent with the current understanding of the geology. Considering its depth below the surface and associated depth decay, it is perhaps surprising that the Lower Carbonate Aquifer (Section 7.2.2.4.1) permeabilities based on transmissivity measurements are among the highest in the model domain. The calibrated effective permeability for the Lower Carbonate Aquifer was nevertheless within the 95% uncertainty interval. Despite this lower calibrated effective

permeability, the Lower Carbonate Aquifer remained the primary water bearing unit in the model.

Overall, the calibrated effective permeabilities show trends consistent with permeability data from Yucca Mountain and elsewhere at the NTS. The calibrated effective permeability of the three Crater Flat tuffs and Calico Hills formation are all within the values measured in the field. The relatively high permeability estimated for the Tram tuff from the cross-hole tests may be at least partially attributable to local conditions at the site of these tests. A breccia zone is present in the Tram tuff at boreholes UE-25 c#2 and UE-25 c#3 (Geldon et al. 1997 [DIRS 100397], Figure 3) that may have contributed to a local enhancement in the permeability of the Tram tuff.

Calibrated effective permeabilities for units corresponding to the Lava Flow Aquifer and the valley fill aquifer are within the range of measured permeabilities. The calibrated effective permeabilities of units corresponding to the Welded Tuff Aquifer are more than an order of magnitude lower than field estimates, but no confidence intervals are available and calibrated values would probably fall within these limits if they were available.

7.2.3 Specific Discharge

Although the calibrated permeabilities of any geologic unit or feature in the SZ site-scale flow model indirectly influence the simulated specific discharge, those geologic units along the flowpath from the repository to the compliance boundary directly determine the simulated specific discharge. Particle tracking using the SZ site-scale model (see Section 6.5.2.4) indicates that fluid particles migrating from the repository generally enter the SZ in the Crater Flat units (see Figure 6-22). Because of the high permeabilities of these units and the small hydraulic gradient, the particles remain in those units until reaching their southern ends. At this point, flow generally enters the alluvial portion of the flow system after briefly transitioning through the Paintbrush Volcanic Aquifer. The flowpath through the alluvial deposits is represented in the SZ site-scale model by the Lower Fortymile Wash alluvium. Thus, those calibrated permeabilities that most directly control the simulation of specific discharge by the SZ site-scale model are those for the Crater Flat units and the Lower Fortymile Wash alluvia.

The 18-km compliance boundary shown on Figure 6-17 and discussed throughout other documents (SNL 2007 [DIRS 177392]) are strongly influenced by groundwater flow in alluvium. Estimates of specific discharge in the SZ were recently obtained from field-testing at the ATC (SNL 2007 [DIRS 177394], Section 6.5.5). The ATC is located approximately 18 km from Yucca Mountain at the boundary of the accessible environment as specified at 10 CFR 63.302 [DIRS 176544]. The specific discharge from the repository to the 18-km compliance boundary was 0.55 m/yr (average across all flowpath lengths divided by travel times), although much of the time along this flowpath is spent in the slower flowing volcanic units indicating that the specific discharge in the alluvial material is higher than in the volcanics. The technique used to estimate specific discharge at locations within the SZ site-scale flow model corresponding to the locations where measurements are available (UE-25 c#3, NC-EWDP-22S, and NC-EWDP-19P) was to isolate a cubic volume within 1,000 m of the well location extended to 10 m above and below the entire open interval and to calculate the average specific discharge across all flowing nodes. The ATC testing was performed in the alluvium aquifer and estimates of groundwater specific discharge at the ATC range from 0.5 to 12 m/yr.

For a discussion of flow porosity in alluvium see *Saturated Zone In-Situ Testing* (SNL 2007 [DIRS 177394], Section 6.4).At the NC-EWDP-22S location the testing specific discharge was estimated with three methods. Based on analyses using the peak arrival analysis the testing estimated values range between 0.5 and 1.2 m/yr. Based on the high-recovery analysis, the testing estimated values range between 2.2 and 5.4 m/yr). Based on the analysis of hydraulic head/conductivity data the testing estimated values range between 3 and 12 m/yr). The testing estimate is about 7.3 m/yr at NC-EWDP-19D. Model-simulated specific discharge at NC-EWDP-22S and -19P are 21.0 and 11.7 m/yr, respectively. These relatively high values correspond to the high effective permeability assigned to the Lower Fortymile Wash Alluvium model unit, but it is still within the factor of 3 specified in the TWP (see Section 7.2). Although there were no specific discharge measurements from the C-wells tests, the average modeled specific discharge at nodes surrounding the C-wells was 1.75 m/yr.

The model-simulated specific discharge at the NC-EWDP-22S location is higher than the test-derived values. At NC-EWDP-19D, the model-simulated value is slightly higher than the testing values. Several points could be made to explain this:

- Testing estimates come from a methodology that involves several assumptions that have never been "validated" in a situation where the actual specific discharge or seepage velocity is known. Thus, there may be unknown biases associated with the method that result in low estimates (alternatively, it could be argued that these biases might be in the other direction, yielding high estimates).

- Testing estimates are obtained over an extremely small scale relative to the flow-model scale. The discrepancies could easily be due to the fact that the few cubic meters interrogated in the tracer tests happen to be in a zone of lower specific discharge (due to slightly lower permeability) than the surrounding alluvium. Also, the measurements were made over only a 30-m (100-ft) interval of a 200-m (650-ft) -thick section of saturated alluvium, whereas the flow model integrates specific discharge over a significantly larger flow area. A somewhat more permeable layer above or below the test interval could easily account for the discrepancy. If one has a conceptual model that flow in the alluvium is focused into ancestral Fortymile Wash channels (as is commonly observed in this type of environment), then it is unlikely that the test interval would have intersected such a channel.

- The fact that the head and hydraulic conductivity estimates are closer to the modeled specific discharge is not surprising given that the hydraulic conductivity estimates were obtained from hydraulic tests that effectively interrogate a larger volume than the tracer tests. Also, they are partly based on heads along Fortymile Wash to which the flow model is calibrated.

- Finally, the zone of enhanced permeability along Fortymile Wash in the model may be partly responsible for an elevated estimate of specific discharge in the model. Flow will naturally channel into such a zone and the specific discharge can be expected to be higher in such a zone than in surrounding media. This again gets at the scale issue: if there is in fact such a zone, is it relatively homogeneous, or does it have significant heterogeneity within it that could account for the discrepancies?

The simulated average specific discharge across the 5-km boundary ranges from 0.35 to 0.38 m/yr for differing values of horizontal anisotropy in permeability ranging from 20 to 0.05 (0.36 m/yr for the expected horizontal anisotropy values of 5:1 N-S to E-W with end members of the 100-particle distribution of 0.11 to 0.66 m/yr). This compares to the 0.6 m/yr derived by the Expert Elicitation Panel (CRWMS M&O 1998 [DIRS 100353], Section 3.2) and is also within their range, which actually spans nearly five orders of magnitude. The data from ATC field testing yielded specific discharge estimates ranging from 1.2 to 9.4 m/yr while testing at NC-EWDP-22S ranged from 0.47 to 5.4 m/yr. A distribution of specific discharge multipliers was developed (SNL 2007 [DIRS 177390], Section 6.5.2.1) that ranged from 1/30th to 10 times the nominal value. Recently, that range was reduced to 1/8.93 and 8.93 times nominal specific discharge (SNL 2007 [DIRS 177390], Section 6.5.2). In addition to a distribution in specific discharge, uncertainty in effective porosity (variable effective porosity in conjunction with specific discharge can result in highly variable flow velocities through the SZ) is implemented through the use of a truncated normal distribution in the SZ transport abstraction model (SNL 2007 [DIRS 177390], Section 6.5.2.3). The details of the uncertainty distributions of specific discharge multiplier and effective porosity in the alluvium and their associated sampling techniques are contained in the SZ flow and transport abstraction model (SNL 2007 [DIRS 177390], Sections 6.5.2.1 and 6.5.2.3).

7.2.4 Comparison of Hydrochemical Data Trends with Calculated Particle Pathways

Groundwater flowpaths and mixing zones were identified in Appendices A and B in the analyses of the areal distributions of measured and calculated geochemical and isotopic parameters, scatter plots, and inverse mixing and reaction models Flowpaths of tracer particles were calculated with the SZ site-scale flow model. The particles were started below the repository footprint and allowed to transport downstream to the model boundary. These flow pathways are compared to flowpaths deduced from hydrochemical data shown in Figure 7-5. These flowpaths must be evaluated in the context of the hydraulic gradient while considering the possibility that flowpaths can be oblique to the potentiometric gradient because of anisotropy in permeability. Theses flowpaths were drawn by first using chemical and isotopic constituents generally considered to behave conservatively in groundwater such as chloride (Cl^-) and sulfate (SO_4^{2-}) ions. However, because no single chemical or isotopic species varies sufficiently to determine flowpaths everywhere in the study area, multiple lines of evidence were used to construct the flowpaths. This evidence includes the areal distribution of chemical and isotopic species, sources of recharge, groundwater ages and evaluation of mixing/groundwater evolution through scatter plots, and inverse mixing and reaction models as presented in Appendices A and B. The derivation of flow pathways from hydrochemical data is developed in detail in Appendices A and B and summarized in Sections B6.6 and B7.

Of particular interest are the Flow Paths 2 and 7 from this analysis. As shown in Figure 7-5, Flow Path 7 originates in the vicinity of the repository footprint and overlaps the model-calculated flowpaths. Flow Path 2 is also of interest, although it originates northeast of the repository, because it closely bounds Flow Path 7 to the east. Although flow pathways derived from hydrochemical data do not originate in the same location as particle tracks derived from the site-scale model, the paths converge east and south of the repository.

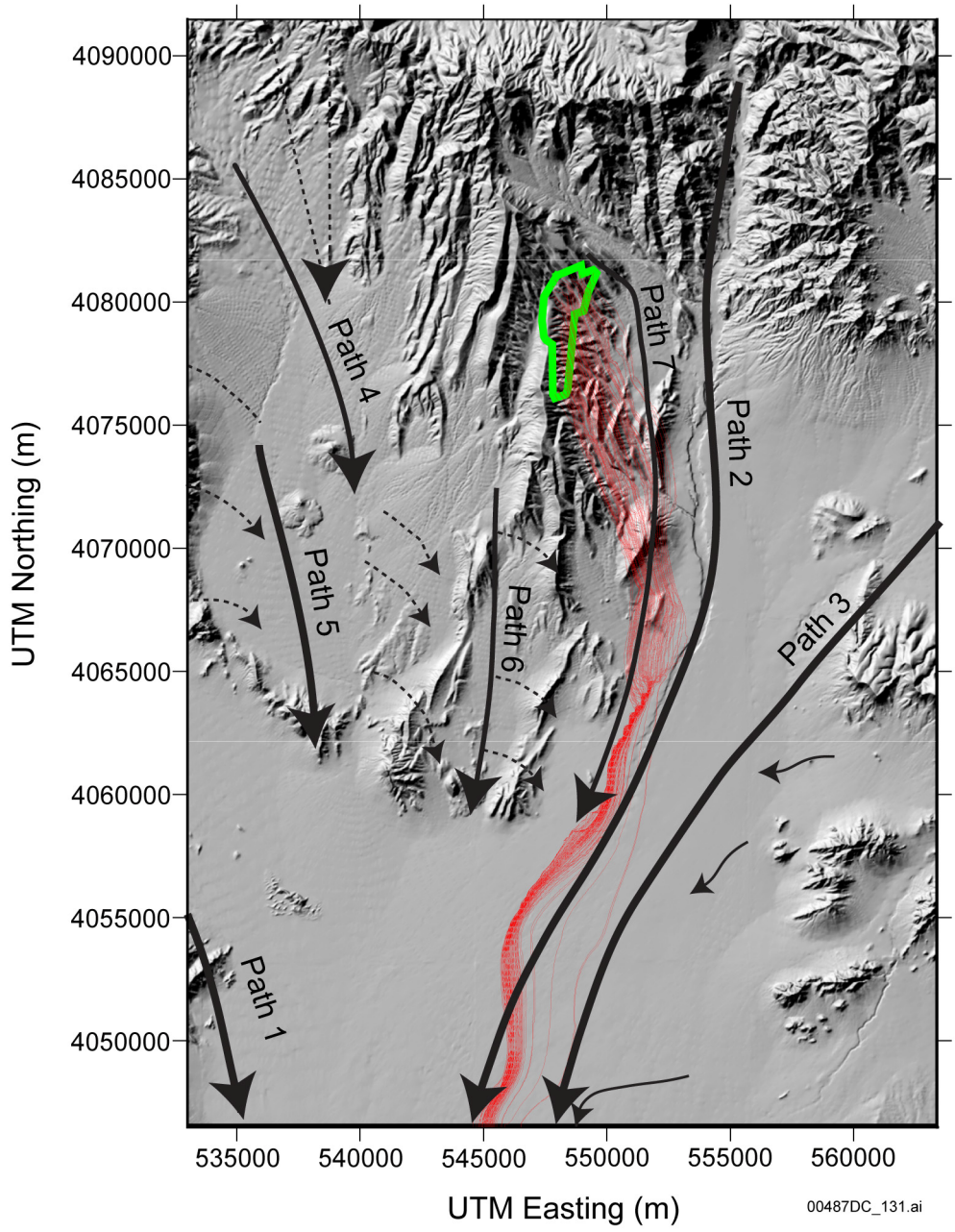

Source: Appendix B, Figure B6-15.

NOTE: Solid lines indicate a relatively high degree of confidence in the interpretations; dashed flow paths indicate relatively less confidence. Thin solid lines represent Path 8. Flowpaths inferred from hydrochemistry data are in black and flowpaths calculated for tracer particles starting at the inferred repository footprint are in red.

UTM = Universal Transverse Mercator.

Figure 7-5. Transport Pathways Deduced from Hydrochemistry Data Compared to Particle Pathways Calculated for the SZ Site-Scale Transport Model

7.3 VALIDATION SUMMARY

The SZ site-scale flow model has met the established validation criteria. A comparison of the simulated and observed water levels from the newly installed NC-EWDP Phase V wells demonstrates that the SZ site-scale flow model can reliably simulate the water levels and gradients along the flowpath from the repository. An analysis of the impact of the differences between observed and simulated hydraulic gradients on the flowpaths from the repository has identified only a minimal impact on the specific discharge that meets the validation criteria established for this comparison.

A comparison of the permeability measurements from the ATC with the calibrated effective permeability values for the valley fill aquifer has similarly indicated agreement between calibrated and measured values. An analysis of the impact of differences between calibrated and measured permeability on the flowpaths from the repository has demonstrated only a minimal impact on the specific discharge, which easily meets the validation criteria established for this comparison.

The comparison between the flowpaths simulated by the SZ site-scale flow model and those indicated by hydrochemical analyses has demonstrated close agreement between these flowpaths, with the flowpaths derived from hydrochemical analysis generally enveloping those simulated by the SZ site-scale flow model.

The SZ site-scale flow model has been validated by applying acceptance criteria based on an evaluation of the model's relative importance to the potential performance of the repository system. Activities for confidence building during model development have been satisfied (Sections 7.1.1 and 7.1.2). Also, all post-development model validation requirements defined in the TWP (BSC 2006 [DIRS 177375], Section 2.2) have been fulfilled (with justification for any changes in the validation criteria), including corroboration of model results with hydrochemical and water-level data that were not used in the model development (Sections 7.2.1, 7.2.3, and 7.2.4). The model development activities and the post-development model validation activities describe the scientific basis for the SZ site-scale flow model. No future activities are needed for model validation. The model validation activities establish that the SZ site-scale flow model is adequate and sufficiently accurate for the stated and intended purpose.

8. CONCLUSIONS

The SZ site-scale flow model is the culmination of enormous efforts incorporating volumes of geologic, hydrologic-testing, and geochemical data into a coherent representation of flow through the SZ near Yucca Mountain. This model is based upon a three-dimensional finite-element mesh with 250×250 m^2 horizontal elements that grid convergence studies have shown to represent the hydrogeologic framework adequately without introducing significant numerical error. Additionally, the model's vertical resolution varies from 10 to 600 m with finest resolution near the water table in the area under Yucca Mountain. This model is calibrated to and reproduces two important data sets: the observed potentiometric surface (water-level data) and boundary fluxes obtained from the SZ regional-scale flow model. In addition, the SZ site-scale flow model matches other data quantitatively and qualitatively. These data include permeability values derived from single- and multiple-well tests, hydrochemical data, and those specific discharges estimated from the Expert Elicitation Panel (CRWMS M&O 1998 [DIRS 100353], Section 3.2) and derived through field testing.

The SZ site-scale flow model matches much of the existing SZ-related data, particularly with respect to the inferred fluid pathways below the repository area. The hydrochemical data were used as a quality check for flowpath direction. The SZ model produced flowpaths from the repository area that agree with those inferred from geochemical information. However, there was a bias in the calibration, notably in the small-gradient area where the calibrated heads were consistently 2 to 5 m higher than the observations. More importantly, however, the gradient was accurately represented despite the bias.

When using the SZ site-scale flow model for TSPA calculations, three limitations must be noted:

- Changes to calibration parameter values. Some calibration parameters can be varied over a moderate range, and the overall calibration is not adversely affected. For example, calibration was performed assuming a single set of anisotropic horizontal permeabilities, while the performance assessment model runs incorporate a range of anisotropic permeabilities. Incorporating anisotropy resulted in a better calibration than isotropic conditions, but model runs using the limits to the distribution (0.05 and 20) yielded weighted RMSEs of 0.82 and 0.83 m, which also certainly maintain calibration. If anisotropies outside this range are used, an assessment on calibration should be made.

- Usable flowpath distances. The continuum approach used for the SZ site-scale flow model requires large grid blocks that effectively average fracture and rock matrix properties. To produce meaningful results, the flowpath should be long compared to the grid block size.

- Overall model recharge fluxes. Because the SZ site-scale flow model is linear, recharge fluxes may be changed to reflect uncertainty in specific discharge, so long as the boundary fluxes and permeabilities are changed proportionally.

8.1 SUMMARY OF MODELING ACTIVITIES

The SZ site-scale flow model was developed in several stages. First, the hydrogeology of a region around Yucca Mountain was numerically characterized by the DVRFS model (Section 6.3). Second, a detailed conceptual model of flow processes was developed for a smaller region (i.e., the site-scale) appropriate for TSPA calculations (Section 6.4). Third, a numerical model of groundwater flow was developed and calibrated (i.e., the SZ site-scale flow model, Section 6.4.2). Fourth, a series of validation activities was completed to provide confidence in the SZ site-scale flow model and its output (Section 7). Finally, results of this model were presented (Section 6.5.2) and the associated uncertainties were discussed (Section 6.7).

8.1.1 Saturated Zone Flow Characterization

Much information is available about the regional-scale hydrogeology at Yucca Mountain, both from site characterization activities as well as from numerous hydrogeologic studies that have been conducted at the NTS. Specifically, sufficient data are available to describe the stratigraphy, structure, and hydraulic properties of component media, recharge and discharge regions, and groundwater flowpaths.

The climate in the Yucca Mountain area is arid and the water table varies from hundreds of meters below ground surface in the northern part of the model to tens of meters below ground surface in the southern part of the model. Natural recharge to the saturated zone is from precipitation percolating through the unsaturated zone. Recharge occurs primarily in mountainous areas where there is more snow and rainfall (i.e., Yucca Mountain, including regions of higher elevation to the north and northeast, and the Spring Mountains 50 km southeast of Yucca Mountain). Estimates of recharge rates at the regional scale are based on empirical relationships and the SZ regional-scale model ensures equal SZ recharge and discharge. Flowpaths in the saturated zone are well characterized at the regional scale because numerous water-level measurements are available.

The fluxes from the SZ regional-scale flow model were used as targets because this model represents a calibrated water balance of the Death Valley hydrologic system with fluxes constrained by data from spring flows and infiltration rates. Boundary fluxes can help link the SZ site-scale flow model to other global-water-balance data, if necessary. The SZ site-scale flow model reasonably matched net flux data from the SZ regional-scale flow model.

In the area near Yucca Mountain, water-level measurements, hydraulic testing in wells, and geochemical analyses provide additional information about groundwater flow in the SZ. Water-level measurements indicate considerable differences in the magnitude of the hydraulic gradient between areas to the north (large hydraulic gradient), to the west (moderate hydraulic gradient), and to the southeast (small hydraulic gradient) of Yucca Mountain. The hydraulic gradient drives flow from the repository to the south and southeast. A vertical, upward hydraulic gradient from the underlying carbonate aquifer and the deeper volcanic units is also observed in some wells immediately downgradient of Yucca Mountain. Data on groundwater chemistry indicate significant spatial variability in geochemical and isotopic composition that results from differences in flowpaths, recharge locations, and groundwater age.

Because the performance of the Yucca Mountain repository is evaluated over thousands of years, the possible impacts of a future wetter climate must be considered. The general locations of areas of recharge and discharge depend primarily on the topography of the land surface. Modeling studies suggest that increased recharge would result in a higher water table and steeper hydraulic gradients. Field mapping of zeolite and paleospring deposits has confirmed that a higher water table existed during past, wetter climates and supports numerical simulations of the possible impacts of climate change. Consequently, wetter climates in the future are expected to result in faster groundwater flow rates along present-day flowpaths. The impacts of an elevated water table are discussed in the SZ transport model report (SNL 2007 [DIRS 177392], Section 6.6 and Appendix E1).

As groundwater in the Death Valley system moves from recharge to discharge areas, flow rates and paths depend largely on the hydraulic properties of the media along the flowpaths. Geologic studies have identified the important rock types and their spatial distribution. The rock types that play the largest role in regional hydrogeology are Paleozoic carbonates, Quaternary-Tertiary volcanic rocks, and Quaternary-Tertiary sediments and volcanic tuffs that fill structural depressions (referred to as valley-fill material in portions of this report). Relatively shallow flow occurs in the volcanic rocks and valley fill (primarily alluvium), and deeper flow occurs in the regionally extensive carbonate aquifer. Along the inferred shallow flowpath, groundwater flowpaths originate in volcanic rocks near the repository site and continue into younger valley-fill deposits at greater distances.

The permeabilities of the volcanic rocks near Yucca Mountain are increased by the presence of fractures. An extensive suite of field observations, interpretations of borehole logs, boreholes hydrologic tests, lab-scale tests, and field tracer tests (C-wells complex) confirms that fractures dominate groundwater flow in the volcanic rocks. However, flow in the alluvium occurs through the primary porosity of these sediments.

8.1.2 Conceptual Model of SZ Site-Scale Flow

The SZ site-scale conceptual model is a synthesis of what is known about flow processes at the scale required for TSPA calculations. This knowledge builds upon, and is consistent with, information collected across the regional scale, but it is more detailed because a higher density of data is available at the site-scale.

Information from geologic maps and cross sections, borehole data, fault-trace maps, and geophysical data were used to construct the HFM, a three-dimensional interpretation of the hydrostratigraphy and geologic structure of the SZ site-scale flow model. Rock stratigraphies within the framework model are grouped into 27 hydrogeologic units that are classified as having either relatively large permeability (aquifers) or relatively small permeability (confining units). The framework model specifies the position and geometry of these hydrogeologic units. In addition, the framework model identifies major faults that affect groundwater flow.

The source of most of the groundwater flow in the SZ site-scale flow model is lateral flow through the western, northern, and eastern boundaries. A small portion (approximately 10%) of the total flux through the SZ site-scale flow model is from precipitation and surface runoff infiltrating along Fortymile Wash. Outflow from the site-scale region is chiefly through the

southern boundary although there is some local outward flow on the eastern boundary. A small amount of water is removed by pumping wells located in the Amargosa Valley near the southern boundary of the model domain. As groundwater moves away from the repository, it first flows through a series of welded and nonwelded volcanic tuffs with relatively low specific discharge. These flowpaths eventually pass into alluvium where the specific discharge is greatest.

8.1.3 Mathematical Model and Numerical Approach

The mathematical basis (Section 6.4.1) and associated numerical approaches of the SZ site-scale flow model is designed to assist in quantifying the uncertainty in the rate and mass transport of radionuclides. In so doing, parameters such as effective permeability of rocks in the geologic framework model must be represented accurately. An automated parameter estimation approach is used to obtain the distribution of rock permeabilities yielding hydraulic heads that best matched measured values, as well as lateral-flow rates across model boundaries that are compatible with results from the SZ regional-scale flow model.

Calculations of groundwater flow (the flow field) are made under steady-state assumptions. The approach of not explicitly representing fractures in the volcanic rocks is reasonable at the scale required for the TSPA (tens of kilometers), but is less accurate at length scales shorter than the dimensions of model grid blocks (less than 250 m).

8.1.4 Model Validation and Confidence Building

Model development activities have been performed with confidence building criteria to ensure the scientific basis for the model (Section 7.1.1 and 7.1.2). Additional confidence in the results of the SZ site-scale flow model was built by comparing: (1) calculated to observed hydraulic heads and associated hydraulic gradients (Section 7.2.1); and (2) calibrated to measured permeabilities and therefore specific discharge (Section 7.2.2). In addition, it was confirmed that the flowpaths leaving the region of the repository are consistent with those inferred from independent water-chemistry data.

8.2 OUTPUTS

The primary technical output from this model (Section 6.5) comprises the SZ site-scale flow model and associated input and output files for current and future wetter climatic conditions. Output from the SZ site-scale flow model is used directly in SZ transport and abstractions models that yield radionuclide breakthrough curves. Specifically, the output from the SZ site-scale flow model can be used to simulate flowpaths from the water table beneath the repository horizon to the accessible environment and to estimate corresponding specific discharges. The computer files associated with the SZ site-scale flow model are archived in Output DTN: SN0612T0510106.004.

Additional technical outputs from this model report are listed in Table 8-1, but are considered intermediate outputs insofar as they were developed in this report to support the development, calibration, or validation of the primary technical output.

Table 8-1. Output Data

DTN	Intermediary?	Description
LA0612RR150304.001	Yes	NC-EWDP UTM coordinates
LA0612RR150304.002	Yes	Underground Testing Area geochemical data
LA0612RR150304.003	Yes	NC-EWDP geochemical data
LA0612RR150304.004	Yes	Hydrochemical flowpaths
LA0612RR150304.005	Yes	Uranium activity ratios for groundwaters
LA0612TM831231.001	No	LaGriT HFM2006 surfaces
MO0611SCALEFLW.000	No	Potentiometric surface
SN0610T0510106.001	Yes	NC-EWDP well location and water-level data
SN0612T0510106.003	Yes	Infiltration data
SN0612T0510106.004	No	SZ site-scale flow model output
SN0702T0510106.006	No	FEHM model of water table rise
SN0702T0510106.007	Yes	NC-EWDP well data used for SZ flow model potentiometric surface, calibration and validation
SN0704T0510106.008	No	Water-level and particle-track output from the calibrated model
SN0705T0510106.009	Yes	PEST v11.1 analyses

8.3 OUTPUT UNCERTAINTY

This section describes remaining uncertainties associated with the nominal flow field. Specifically, the section recommends how the uncertainty in metrics associated with model outputs (specific discharge and flowpaths) should be considered.

8.3.1 Specific Discharge Uncertainty Range

Because uncertainty in permeability translates into uncertainty in specific discharge (given a constant head gradient), insight gained when investigating permeability values during calibration has relevance to specific discharge estimates. Also, recall that for linear models such as this, calibration to hydraulic heads is preserved when scaling the fluxes, recharge, and permeabilities proportionally. The 95% confidence interval for calibrated permeabilities (Output DTN: SN0612T0510106.004, *sz_site_2006.rec*) typically spans 3 or more orders of magnitude. While this range could yield major changes in specific discharge in a homogeneous system, no single change in permeability by up to an order of magnitude yielded even a factor of 2 change in specific discharge because surrounding permeability values strongly impact the flow into/out of the altered unit. It can be concluded that even if calibrated permeabilities are in error by more than an order of magnitude for any given unit, the specific discharge output from the model will remain within the uncertainty limits developed elsewhere for use in TSPA (e.g., 1/8.93 to 8.93 times nominal value (SNL 2007 [DIRS 177390], Section 6.5.2.1)). Experience with the calibrated SZ site-scale flow model indicates that the range of specific discharges used for TSPA is large enough to encapsulate all the uncertainties assumed during the development and calibration of this model.

The specific discharge from the repository to the 18-km compliance boundary is 0.55 m/yr, although much of the distance along this flowpath is in the slower flowing volcanic units indicating that the specific discharge in the alluvial material is higher than in the volcanics. The technique used to estimate specific discharge at locations within the SZ site-scale flow model alluvial material corresponding to the locations where measurements are available (NC-EWDP-22S, and NC-EWDP-19P) was to isolate a cubic volume within 1,000 m of the well location extending 10 m above and below the entire open interval and to calculate the average specific discharge across all flowing nodes. Measured groundwater specific discharges from alluvial pump tests range from 0.47 to 9.4 m/yr (SNL 2007 [DIRS 177394], Tables 6.5-5 and 6.5-6). For the expected flow porosity in the alluvium of 0.18 (SNL 2007 [DIRS 177394], Section 6.4), the field-test-derived specific discharges ranged from 0.89 m/yr at NC-EWDP-22S to 7.3 m/yr at NC-EWDP-19P. Model-simulated specific discharges at NC-EWDP-22S and -19P are 20.97 and 11.75 m/yr, respectively. These relatively high modeled values correspond to the high effective permeability assigned to the model unit for the Lower Fortymile Wash alluvium, but they are still within the factor of 3 of the upper end of test-derived expected value (7.3 m/yr) and therefore meet the validation criterion established by the TWP (BSC 2006 [DIRS 177375, Section 2.2.2.1). Comparatively little sensitivity was seen to horizontal anisotropy in the volcanics; the modeled average specific discharge across the 5-km boundary ranges from 0.35 to 0.38 m/yr for values of N-S to E-W horizontal anisotropy in permeability of 0.05 to 20, respectively (SNL 2007 [DIRS 177394], Section 6.2.6). Although there were no specific discharge measurements from the C-wells tests, the modeled value was estimated at 1.75 m/yr within 1,000 m of the C-wells. Finally, the nonlinear maximum calibrated specific discharge estimated across the 5-km boundary downgradient from the repository is 1.60 m/yr (Section 6.7.2 and Appendix I), which is just less than 3 times the maximum value of 0.66 m/yr. This combination of permeabilities was specifically selected to maximize specific discharge, which is still well within the range established by the specific discharge multiplier used in SZ abstraction models (SNL 2007 [DIRS 177390], Section 6.5.2.1). That is, an uncertainty distribution in specific discharge is constructed where the nominal specific discharge is multiplied by 1/8.93 and 8.93 (BSC 2007 [DIRS 177390], Section 6.5.2). The details of the uncertainty distributions of specific discharge and effective porosity in the alluvium and their associated sampling techniques are outlined in the SZ abstraction model (SNL 2007 [DIRS 177390], Section 6.5.2.1 and 6.5.2.3).

8.3.2 Flowpaths Uncertainty

The flowpaths from the water table beneath the repository to the accessible environment directly affect breakthrough curves and associated radionuclide transport times (recall that flowpath length is used to calculate specific discharge). Because the flowpaths are close to the water table and transition from the volcanic tuffs to the alluvium, flowpath uncertainty directly affects the length of flow in the volcanic tuffs and in the alluvium.

Uncertainty in flowpaths is affected by anisotropy in hydraulic properties of the volcanic tuffs. Large-scale anisotropy and heterogeneity were implemented in the SZ site-scale flow model through direct incorporation of known hydraulic features, faults, and fractures (see Section 6.7.10). Horizontal anisotropy in the volcanic units was derived from analysis of hydraulic testing at the C-wells (SNL 2007 [DIRS 177394], Section 6.2.6 and Appendix C6). This scientific analysis report also recommends an uncertainty range in anisotropy that should be

used in the SZ site-scale flow model to account for uncertainty in the flowpaths and this parameter was carried forward through to SZ abstraction modeling (SNL 2007 [DIRS 177390], Section 6.5.2.10). For isotropic permeability, average flowpath length to the 18-km compliance boundary is approximately 22.9 km. For anisotropy ratios of 20:1 and 0.05:1 (N-S:E-W), average flowpath lengths are 29.7 and 22.8 km, respectively. This is an acceptable range of variability in model results in light of the bounds established by geochemical analyses (Figure 7-5). Also, recall that 5 km of this difference can be attributed solely to the random initial distribution of particles below the repository.

The model is adequate for its intended use of providing flow-field simulations as input to the SZ site-scale transport model necessary to generate radionuclide breakthrough curves.

8.4 HOW THE APPLICABLE ACCEPTANCE CRITERIA ARE ADDRESSED

This section describes how the acceptance criteria in the YMRP (NRC 2003 [DIRS 163274], Section 2.2.1.3.8.3), *Flowpaths in the Saturated Zone*, are addressed by this report.

Acceptance Criteria from Section 2.2.1.3.8.3, *Flowpaths in the Saturated Zone*

Acceptance Criterion 1: *System Description and Model Integration Are Adequate.*

Subcriterion (1): Section 1 explains that this model generates SZ velocity fields which are used as inputs for the model of transport in the SZ and are abstracted in the TSPA. The important physical phenomena are adequately incorporated in the SZ abstraction process as described in the following subsections: hydraulic gradients (Section 6.3.1.4); vertical gradients (Section 6.3.1.5); lateral boundary conditions (Section 6.3.1.6); Recharge (Section 6.3.1.7); Discharge (Section 6.3.1.8); heterogeneity (Section 6.3.1.9); faults (Section 6.3.1.10); and groundwater flow processes (Section 6.3.2.). The discussion of groundwater table rise in Section 6.6.4 uses consistent and appropriate assumptions about climate change.

Subcriterion (2): Aspects of hydrology, geology and geochemistry that may affect flowpaths in the SZ are described adequately in Section 6.3 and Appendices A and B.

Subcriterion (4): Section 6.3.1.7 states that the recharge to the flow model was derived from three sources: regional-scale SZ model (Belcher 2004 [DIRS 173179]), 2003 UZ flow model (BSC 2004 [DIRS 169861]), and Fortymile Wash data (Savard 1998 [DIRS 102213]). Recharge from the UZ site-scale model (percolation flux) was taken as the flow through the base of that model, the domain of which includes approximately 40 km^2 (19.3 mi^2) that encompasses an area only slightly larger than the footprint of Yucca Mountain, a small fraction of the SZ model domain. The SZ site-scale flow model uses appropriate recharge values from flow in the unsaturated zone.

Subcriterion (5): Section 6.2 provides a road map to sections and FEPs document where sufficient data and technical bases to assess the degree to which FEPs have been included in the flowpaths.

Subcriterion (6): Flowpaths in the SZ are adequately delineated, considering site conditions, as described in Section 6.5.2.3 and Appendices A and B. Section 6.5 shows how the flow model that was developed generates flow fields that simulate radionuclide transport in saturated porous rock and alluvium.

Subcriterion (7): The effects of climate on specific discharge flowpaths are evaluated in Section 6.6.4. Saturated zone modeling analyses considered in this report indicate that a rise in the water table will cause some of the flow paths from below the repository to the accessible environment to be in units with lower values of permeability than the ones saturated by the present-day water-table conditions. Furthermore, the approach used to estimate water-table rise to the north of the repository has little impact on the simulated flow system down gradient of Yucca Mountain in the SZ site-scale flow model. Results are presented in a data package (DTN: SN0702T0510106.006) for use by downstream users.

Subcriterion (8): Section 6.4.3.10 explains how the linear approximation of the temperature gradient captures the effect of geothermal heat flux on groundwater viscosity.

Subcriterion (9): The impact of the expected water table rise on potentiometric heads and flow directions, and consequently on repository performance, is adequately considered in Section 6.6.4.

Subcriterion (10): This report was prepared in accordance with the *Quality Assurance Requirements and Description* (QARD) (DOE 2006 [DIRS 177092], DOE/RW-0333P, Rev. 18), which commits to U.S. Nuclear Regulatory Commission guidance. Compliance with the QARD was determined through multiple reviews.

Acceptance Criterion 2: *Data Are Sufficient for Model Justification.*

Subcriterion (1): Sections 6.3, 6.4, and Appendices A and B identify the geological, hydrological, and geochemical information used in this model to evaluate flowpaths in the SZ and adequately justifies those values by identifying their reliable sources. Section 6.4.3 adequately describes how the data were used, interpreted, and appropriately synthesized into parameters by explaining how water level and head distributions, definitions of the hydrogeologic units, the distribution of recharge flux and lateral fluxes into the model domain, feature and fault distribution, temperature profiles in wells, and boundary conditions were incorporated into the SZ site-scale flow model. Section 6.4.3.1 describes the development of the hydrogeologic framework, which, with the known features of the site is used to design a grid for flow modeling. Section 6.4.3.2 describes the generation of the grid, which enables the data to be assigned to hydrogeologic units and features, recharge fluxes, hydrogeologic properties, and boundary conditions at node points. Section 6.4.3.3 describes the use of hydrogeologic properties, Section 6.4.3.7 describes the representation of features, Section 6.4.3.8 describes the use of the boundary conditions described in Section 6.3.1.6, Section 6.4.3.9 describes recharge, and Section 6.4.3.10 describes how the hydrogeologic properties are specified for each node in the computational grid. Section 7.2.2.4 describes the permeability data obtained at the NTS, including the lower carbonate aquifer (Section 7.2.2.4.1), the valley fill aquifer (Section 7.2.2.4.2), the welded tuff aquifer (Section 7.2.2.4.3), and the lava flow aquifer (Section 7.2.4.4).

Subcriterion (2): The sufficiency of the data collected on the natural system to establish boundary conditions on flowpaths in the SZ is demonstrated in Section 6.3.1. Section 6.3.1 describes the hydrogeologic setting of the SZ flow system near Yucca Mountain. Section 6.3.1.1 relates the geologic features to flow in the SZ. Section 6.3.1.2 describes the HFM that includes faults, zones of hydrothermal alteration, and other features that affect flow in the SZ. Section 6.3.1.3 uses the potentiometric surface map to determine the general direction of groundwater flow. Section 6.3.1.4 describes the hydraulic gradients and Section 6.3.1.5 describes the vertical gradients. Section 6.3.1.6 explains how the boundary conditions are derived from regional water level and head data form fixed-head boundary conditions on the lateral sides of the model. Section 6.3.1.7 describes the three components of recharge and Section 6.3.1.8 reports that no natural discharge is observed. Section 6.3.1.9 describes the observed physical and chemical heterogeneity of the rocks and water in the SZ. Section 6.3.1.10 describes the role of faults. Initial conditions are not included in the model because it is a steady-state model.

Subcriterion (3): The appropriateness of the techniques used to obtain the SZ geologic, hydrologic, and geochemical data used in this model is established in the reliable sources of the data listed in Section 4.1. Section 7.2.2.3 describes the acquisition of data on permeability from single-hole tests (Section 7.2.2.3.1) and cross-hole tests (Section 7.2.2.3.2). The HFM report discusses the acquisition of data related to hydrogeology (SNL 2007 [DIRS 174109]). Appendices A and B discusses the acquisition of data related to geochemistry.

Subcriterion (4): Section 6.4 provides sufficient information to substantiate that the mathematical groundwater modeling approach and computational model are applicable to site conditions. Section 6.4.1 discusses the equations from the basic laws of flow that were applied and Section 6.4.2 describes the computational model used to solve those equations. Section 6.4.3 describes the inputs from data about the site, including the HFM (Section 6.4.3.1), grid generation (Section 6.4.3.2), hydrogeologic properties (Section 6.4.3.3), discrete features and regions (Section 6.4.3.7), boundary conditions (Section 6.4.3.8), and recharge (Section 6.4.3.9).

Section 6.5.1 provides sufficient information to substantiate that the mathematical groundwater model is calibrated. Section 6.5.1.1 describes the calibration process. Section 6.5.1.2 describes the parameter optimization procedure, Section 6.5.1.3 describes the calibration targets, and calibration parameters. Section 6.5.2 describes the calibration results for water levels (Section 6.5.2.1), fluxes (Section 6.5.2.2), flowpaths (Section 6.5.2.3), and specific discharge (Section 6.5.2.4).

Acceptance Criterion 3: ***Data Uncertainty Is Characterized and Propagated Through the Model Abstraction.***

Subcriterion (1): Section 6.5.1 explains how calibration is used to optimize the values of important model parameters in a way that is technically defensible, reasonably accounts for uncertainties and variabilities.

Subcriterion (2): The effect of climate on flowpaths is evaluated adequately in Section 6.6.4. Saturated zone modeling analyses considered in this report indicate that a rise in the water table will cause some of the flow paths from below the repository to the accessible environment to be in units with lower values of permeability than the ones saturated by the present-day water-table conditions. Furthermore, the approach used to estimate water-table rise to the north of the repository has little impact on the simulated flow system down gradient of Yucca Mountain in the SZ site-scale flow model. Results are presented in a data package (DTN: SN0702T0510106.006) for use by downstream users.

Subcriterion (3): Section 6.5.1 and 6.7 show how uncertainty has been adequately represented in the development of parameters for the model.

Subcriterion (4): The SZ flow Expert Elicitation Panel was conducted in accordance with instructions by Kotra et al. (1996 [DIRS 100909]) and addressed the following issues:

- Appropriateness of the horizontal to vertical anisotropy ratio of 10:1 (Section 6.6.1)
- Estimates of discharge from the volcanic aquifer (Section 6.7)
- Semiperched water as an explanation for the observed LHG (Section 6.3.1.4)
- Specific discharge near Yucca Mountain (Sections 6.5.1.3, 6.5.2.4, and 8).

Acceptance Criterion 4: ***Model Uncertainty Is Characterized and Propagated Through the Model Abstraction.***

Subcriterion (1): Several ACMs are identified in Sections 6.6.1 through 6.6.4. They are: (1) vertical anisotropies in hydraulic properties, with and without vertical anisotropy and varied horizontal anisotropy ratios (Section 6.6.1); (2) models for the LHG north of Yucca Mountain and variable anisotropy in the Solitario Canyon Fault (Section 6.6.2); and (3) water-table rise resulting from climate change (Section 6.6.4).

ACMs for vertical and horizontal anisotropies were considered (Section 6.6.1). The vertical anisotropy from expert elicitation is only a rule of thumb and removal of the vertical anisotropy from model calibration can affect the difference between the measured and computed heads. Horizontal anisotropy will be included in the TSPA analysis (Section 6). As discussed in Section 6.6.2, the LHG ACM and Solitario Canyon Fault ACM could significantly affect model results, so it is important to represent these features accurately in the conceptual model (i.e., they must be present in some fashion). Section 6.6.4 explains how the change in SZ flowpaths resulting from a rise in the water table need not be included in the TSPA because the use of scaling factors conservatively accounts for the impact of climate changes on SZ flow.

Subcriterion (2): Conceptual model uncertainties are adequately defined and documented in Sections 6.4 and 6.7 and Appendices H and I. These sections also include the proper assessment of the effects on conclusions regarding performance. Section 6.7 addresses uncertainty in the flowpaths due to alternative conceptualizations and model calibration.

Uncertainty in the quantification of specific discharge is discussed in Sections 6.7 and Appendix H. A nonlinear analysis is presented in Section 6.7.2 and Appendix I. There is general consistency between the specific discharge simulated by the model and the median of values of uncertainty ranges estimated by the SZ expert panel from testing data. Uncertainty in specific discharge is propagated forward to the TSPA.

Uncertainty in the hydrologic contacts is discussed in Section 6.7.3 and shown to have moderate effects in some cases. Accordingly, this uncertainty was determined not to warrant propagation to the TSPA. Additional uncertainties due to limitation in site data, conceptualization of the LHG, and representation of potentially perched water-level measurements, and fault conceptualizations are discussed in Sections 6.7.4 through 6.7.8. None of these uncertainties warrants propagation to TSPA.

Uncertainty due to scaling is discussed in Section 6.7.9 where it is concluded that such uncertainty does not significantly affect flow modeling.

Subcriterion (3): The conceptual model uncertainty considered in this report is consistent with available site characterization data and field measurements. The genesis of the conceptual model is discussed in Section 6.3. Alternative conceptual models are considered in Section 6.6. A thorough description of uncertainty, especially uncertainty associated with specific discharge estimates, is given in Section 6.7. Furthermore, an introduction on predictive variance uncertainty minimization and quantification is given in Appendix H. An extension of this theory to nonlinear predictive variance is outlined in Appendix I.

Subcriterion (4): Alternative modeling approaches are appropriate and consistent with available data and current scientific knowledge, and appropriately consider their results and limitations, using analyses that are sensitive to the processes modeled, as discussed above.

Acceptance Criteria from Section 2.2.1.1.3, *System Description and Demonstration of Multiple Barriers*

Acceptance Criterion 3: *Technical Basis for Barrier Capability is Adequately Presented.*

When considered together, reports associated with the saturated zone including this report, *Site-Scale Saturated Zone Transport* (SNL 2007 [DIRS 177392]), and *Saturated Zone Flow and Transport Model Abstraction* (SNL 2007 [DIRS 177390]) constitute an adequate description (including thorough discussions of uncertainty) of the saturated zone as a natural barrier to radionuclide release.

INTENTIONALLY LEFT BLANK

9. INPUTS AND REFERENCES

The following is a list of the references cited in this document. Column 1 contains the unique six-digit numerical identifiers (the Document Input Reference System numbers), which are placed in the text following the reference callout (e.g., Ahlers et al. 1999 [DIRS 109715]). The purpose of these numbers is to assist in locating a specific reference. Multiple sources by the same author (e.g., SNL 2007) are sorted alphabetically by title.

9.1 DOCUMENTS CITED

109715 Ahlers, C.F.; Finsterle, S.; and Bodvarsson, G.S. 1999. "Characterization and Prediction of Subsurface Pneumatic Response at Yucca Mountain, Nevada." *Journal of Contaminant Hydrology, 38,* (1-3), 47-68. New York, New York: Elsevier. TIC: 244160.

103750 Altman, W.D.; Donnelly, J.P.; and Kennedy, J.E. 1988. *Qualification of Existing Data for High-Level Nuclear Waste Repositories: Generic Technical Position.* NUREG-1298. Washington, D.C.: U.S. Nuclear Regulatory Commission. TIC: 200652.

103597 Altman, W.D.; Donnelly, J.P.; and Kennedy, J.E. 1988. *Peer Review for High-Level Nuclear Waste Repositories: Generic Technical Position.* NUREG-1297. Washington, D.C.: U.S. Nuclear Regulatory Commission. TIC: 200651.

105038 Bear, J. 1979. *Hydraulics of Groundwater.* New York, New York: McGraw-Hill. TIC: 217574.

173179 Belcher, W.R. 2004. *Death Valley Regional Ground-Water Flow System, Nevada and California - Hydrogeologic Framework and Transient Ground-Water Flow Model.* Scientific Investigations Report 2004-5205. Reston, Virginia: U.S. Geological Survey. ACC: MOL.20050323.0070.

104370 Benson, L. and Klieforth, H. 1989. "Stable Isotopes in Precipitation and Ground Water in the Yucca Mountain Region, Southern Nevada: Paleoclimatic Implications." *Aspects of Climate Variability in the Pacific and the Western Americas.* Peterson, D.H., ed.. Geophysical Monograph 55. Pages 41-59. Washington, D.C.: American Geophysical Union. TIC: 224413.

101036 Benson, L.V. and McKinley, P.W. 1985. *Chemical Composition of Ground Water in the Yucca Mountain Area, Nevada, 1971-84.* Open-File Report 85-484. Denver, Colorado: U.S. Geological Survey. ACC: NNA.19900207.0281.

101194 Bish, D.L. 1989. *Evaluation of Past and Future Alterations in Tuff at Yucca Mountain, Nevada, Based on the Clay Mineralogy of Drill Cores USW G-1, G-2, and G-3.* LA-10667-MS. Los Alamos, New Mexico: Los Alamos National Laboratory. ACC: NNA.19890126.0207.

101195 Bish, D.L. and Chipera, S.J. 1989. *Revised Mineralogic Summary of Yucca Mountain, Nevada.* LA-11497-MS. Los Alamos, New Mexico: Los Alamos National Laboratory. ACC: NNA.19891019.0029.

101233 Blankennagel, R.K. and Weir, J.E., Jr. 1973. *Geohydrology of the Eastern Part of Pahute Mesa, Nevada Test Site, Nye County, Nevada.* Professional Paper 712-B. Washington, D.C.: U.S. Geological Survey. TIC: 219642.

179072 Bower, K.M. and Zyvoloski, G. 1997. "A Numerical Model for Thermo-Hydro-Mechanical Coupling in Fractured Rock." *International Journal of Rock Mechanics and Mining Sciences & Geomechanics Abstracts, 34,* (8), 1201-1211. New York, New York: Pergamon. TIC: 259103.

149161 Bower, K.M.; Gable, C.W.; and Zyvoloski, G.A. 2000. *Effect of Grid Resolution on Control Volume Finite Element Groundwater Modeling of Realistic Geology.* LA-UR-001870. Los Alamos, New Mexico: Los Alamos National Laboratory. TIC: 248256.

102004 Broxton, D.E.; Bish, D.L.; and Warren, R.G. 1987. "Distribution and Chemistry of Diagenetic Minerals at Yucca Mountain, Nye County, Nevada." *Clays and Clay Minerals, 35,* (2), 89-110. Long Island City, New York: Pergamon Press. TIC: 203900.

143665 CRWMS M&O 2000. *Total System Performance Assessment for the Site Recommendation*. TDR-WIS-PA-000001 REV 00. Las Vegas, Nevada: CRWMS M&O. ACC: MOL.20001005.0282.

155974 BSC (Bechtel SAIC Company) 2001. *Calibration of the Site-Scale Saturated Zone Flow Model.* MDL-NBS-HS-000011 REV 00 ICN 01. Las Vegas, Nevada: Bechtel SAIC Company. ACC: MOL.20010713.0049.

157132 BSC 2001. *Input and Results of the Base Case Saturated Zone Flow and Transport Model for TSPA.* ANL-NBS-HS-000030 REV 00 ICN 01. Las Vegas, Nevada: Bechtel SAIC Company. ACC: MOL.20011112.0068.

160247 BSC 2002. *Analysis of Geochemical Data for the Unsaturated Zone.* ANL-NBS-HS-000017 REV 00 ICN 02. Las Vegas, Nevada: Bechtel SAIC Company. ACC: MOL.20020314.0051.

170029 BSC 2004. *Geologic Framework Model (GFM2000).* MDL-NBS-GS-000002 REV 02. Las Vegas, Nevada: Bechtel SAIC Company. ACC: DOC.20040827.0008.

170008 BSC 2004. *Hydrogeologic Framework Model for the Saturated Zone Site Scale Flow and Transport Model.* MDL-NBS-HS-000024 REV 00. Las Vegas, Nevada: Bechtel SAIC Company. ACC: DOC.20041118.0001.

170014 BSC 2004. *Probability Distribution for Flowing Interval Spacing.* ANL-NBS-MD-000003 REV 01. Las Vegas, Nevada: Bechtel SAIC Company. ACC: DOC.20040923.0003.

170015 BSC 2004. *Recharge and Lateral Groundwater Flow Boundary Conditions for the Saturated Zone Site-Scale Flow and Transport Model.* ANL-NBS-MD-000010 REV 01. Las Vegas, Nevada: Bechtel SAIC Company. ACC: DOC.20041008.0004.

170037 BSC 2004. *Saturated Zone Site-Scale Flow Model.* MDL-NBS-HS-000011 REV 02. Las Vegas, Nevada: Bechtel SAIC Company. ACC: DOC.20041122.0001.

169861 BSC 2004. *UZ Flow Models and Submodels.* MDL-NBS-HS-000006 REV 02. Las Vegas, Nevada: Bechtel SAIC Company. ACC: DOC.20041101.0004; DOC.20050629.0003.

170009 BSC 2004. *Water-Level Data Analysis for the Saturated Zone Site-Scale Flow and Transport Model.* ANL-NBS-HS-000034 REV 02. Las Vegas, Nevada: Bechtel SAIC Company. ACC: DOC.20041012.0002; DOC.20050214.0002.

169734 BSC 2004. *Yucca Mountain Site Description.* TDR-CRW-GS-000001 REV 02 ICN 01. Two volumes. Las Vegas, Nevada: Bechtel SAIC Company. ACC: DOC.20040504.0008.

179466 SNL 2007. *Total System Performance Assessment Data Input Package for Requirements Analysis for Subsurface Facilities*. TDR-TDIP-PA-000001 REV 00. Las Vegas, Nevada: Sandia National Laboratories.

175539 BSC 2005. *Q-List.* 000-30R-MGR0-00500-000-003. Las Vegas, Nevada: Bechtel SAIC Company. ACC: ENG.20050929.0008.

177375 BSC 2006. *Technical Work Plan for Saturated Zone Flow and Transport Modeling.* TWP-NBS-MD-000006 REV 02. Las Vegas, Nevada: Bechtel SAIC Company. ACC: DOC.20060519.0002.

100106 Buesch, D.C.; Spengler, R.W.; Moyer, T.C.; and Geslin, J.K. 1996. *Proposed Stratigraphic Nomenclature and Macroscopic Identification of Lithostratigraphic Units of the Paintbrush Group Exposed at Yucca Mountain, Nevada.* Open-File Report 94-469. Denver, Colorado: U.S. Geological Survey. ACC: MOL.19970205.0061.

162906 Burke, W.H.; Denison, R.E.; Hetherington, E.A.; Koepnick, R.B.; Nelson, H.F.; and Otto, J.B. 1982. "Variation of Seawater $^{87}Sr/^{86}Sr$ Throughout Phanerozoic Time." *Geology, 10,* 516-519. Boulder, Colorado: Geological Society of America. TIC: 255085.

126814 Campana, M.E. and Byer, R.M., Jr. 1996. "A Conceptual Evaluation of Regional Ground-Water Flow, Southern Nevada-California, USA." *Environmental and Engineering Geoscience, II,* (4), 465-478. Boulder, Colorado: Geological Society of America. TIC: 246651.

162940 Chapman, J.B. and Lyles, B.F. 1993. *Groundwater Chemistry at the Nevada Test Site: Data and Preliminary Interpretations.* DOE/NV/10845-16. Las Vegas, Nevada: U.S. Department of Energy, Nevada Operation Office. ACC: MOL.20031023.0087.

153475 Cheng, H.; Edwards, R.L.; Hoff, J.; Gallup, C.D.; Richards, D.A.; and Asmerom, Y. 2000. "The Half-Lives of Uranium-234 and Thorium-230." *Chemical Geology, 169,* 17-33. Amsterdam, The Netherlands: Elsevier. TIC: 249205.

105079 Chipera, S.J. and Bish, D.L. 1997. "Equilibrium Modeling of Clinoptilolite-Analcime Equilibria at Yucca Mountain, Nevada." *Clays and Clay Minerals, 45,* (2), 226-239. Long Island City, New York: Pergamon Press. TIC: 233948.

100025 Chipera, S.J.; Bish, D.L.; and Carlos, B.A. 1995. "Equilibrium Modeling of the Formation of Zeolites in Fractures at Yucca Mountain, Nevada." *Natural Zeolites '93: Occurrence, Properties, Use, Proceedings of the 4th International Conference on the Occurrence, Properties, and Utilization of Natural Zeolites, June 20-28, 1993, Boise, Idaho.* Ming, D.W. and Mumpton, F.A., eds. Pages 565-577. Brockport, New York: International Committee on Natural Zeolites. TIC: 243086.

101125 Claassen, H.C. 1985. *Sources and Mechanisms of Recharge for Ground Water in the West-Central Amargosa Desert, Nevada—A Geochemical Interpretation.* U.S. Geological Survey Professional Paper 712-F. Washington, D.C.: United States Government Printing Office. TIC: 204574.

105738 Clark, I.D. and Fritz, P. 1997. *Environmental Isotopes in Hydrogeology.* Boca Raton, Florida: Lewis Publishers. TIC: 233503.

178598 Cooley, R.L. and Christensen, S. 2006. "Bias and Uncertainty in Regression-Calibrated Models of Groundwater Flow in Heterogeneous Media." *Advances in Water Resources, 29,* 639-656. New York, New York: Elsevier. TIC: 259000.

178650 Cooley, R.L. 2004. *A Theory for Modeling Ground-Water Flow in Heterogeneous Media*. Professional Paper 1679. Reston, Virginia: U.S. Geological Survey. ACC: MOL.20070108.0003.

101040 Craig, R.W. and Robison, J.H. 1984. *Geohydrology of Rocks Penetrated by Test Well UE-25p#1, Yucca Mountain Area, Nye County, Nevada.* Water-Resources Investigations Report 84-4248. Denver, Colorado: U.S. Geological Survey. ACC: NNA.19890905.0209.

100353 CRWMS M&O 1998. *Saturated Zone Flow and Transport Expert Elicitation Project.* Deliverable SL5X4AM3. Las Vegas, Nevada: CRWMS M&O. ACC: MOL.19980825.0008.

139582 CRWMS M&O 2000. *Calibration of the Site-Scale Saturated Zone Flow Model.* MDL-NBS-HS-000011 REV 00. Las Vegas, Nevada: CRWMS M&O. ACC: MOL.20000825.0122.

153246 CRWMS M&O 2000. *Total System Performance Assessment for the Site Recommendation.* TDR-WIS-PA-000001 REV 00 ICN 01. Las Vegas, Nevada: CRWMS M&O. ACC: MOL.20001220.0045.

101043 Czarnecki, J.B. 1984. *Simulated Effects of Increased Recharge on the Ground-Water Flow System of Yucca Mountain and Vicinity, Nevada-California.* Water-Resources Investigations Report 84-4344. Denver, Colorado: U.S. Geological Survey. ACC: HQS.19880517.1750.

160149 Czarnecki, J.B. 1985. *Simulated Effects of Increased Recharge on the Ground-Water Flow System of Yucca Mountain and Vicinity, Nevada-California.* Water-Resources Investigations Report 84-4344. Denver, Colorado: U.S. Geological Survey. TIC: 203222.

100377 Czarnecki, J.B.; Faunt, C.C.; Gable, C.W.; and Zyvoloski, G.A. 1997. *Hydrogeology and Preliminary Calibration of a Preliminary Three-Dimensional Finite-Element Ground-Water Flow Model of the Site Saturated Zone, Yucca Mountain, Nevada.* Administrative Report. Denver, Colorado: U.S. Geological Survey. ACC: MOL.19980204.0519.

100131 D'Agnese, F.A.; Faunt, C.C.; Turner, A.K.; and Hill, M.C. 1997. *Hydrogeologic Evaluation and Numerical Simulation of the Death Valley Regional Ground-Water Flow System, Nevada and California.* Water-Resources Investigations Report 96-4300. Denver, Colorado: U.S. Geological Survey. ACC: MOL.19980306.0253.

120425 D'Agnese, F.A.; O'Brien, G.M.; Faunt, C.C.; and San Juan, C.A. 1999. *Simulated Effects of Climate Change on the Death Valley Regional Ground-Water Flow System, Nevada and California.* Water-Resources Investigations Report 98-4041. Denver, Colorado: U.S. Geological Survey. TIC: 243555.

158876 D'Agnese, F.A.; O'Brien, G.M.; Faunt, C.C.; Belcher, W.R.; and San Juan, C. 2002. *A Three-Dimensional Numerical Model of Predevelopment Conditions in the Death Valley Regional Ground-Water Flow System, Nevada and California.* Water-Resources Investigations Report 02-4102. Denver, Colorado: U.S. Geological Survey. TIC: 253754.

162939 Davisson, M.L.; Kenneally, J.M.; Smith, D.K.; Hudson, G.B.; Nimz, G.J.; and Rego, J.H. 1994. *Preliminary Report on the Isotope Hydrology Investigations at the Nevada Test Site: Hydrologic Resources Management Program, FY 1992-1993.* UCRL-ID-116122. Livermore, California: Lawrence Livermore National Laboratory, Nuclear Chemistry Division. TIC: 210954.

100027 Day, W.C.; Dickerson, R.P.; Potter, C.J.; Sweetkind, D.S.; San Juan, C.A.; Drake, R.M., II; and Fridrich, C.J. 1998. *Bedrock Geologic Map of the Yucca Mountain Area, Nye County, Nevada.* Geologic Investigations Series I-2627. Denver, Colorado: U.S. Geological Survey. ACC: MOL.19981014.0301.

101557 Day, W.C.; Potter, C.J.; Sweetkind, D.S.; Dickerson, R.P.; and San Juan, C.A. 1998. *Bedrock Geologic Map of the Central Block Area, Yucca Mountain, Nye County, Nevada.* Miscellaneous Investigations Series Map I-2601. Washington, D.C.: U.S. Geological Survey. ACC: MOL.19980611.0339.

100439 de Marsily, G. 1986. *Quantitative Hydrogeology: Groundwater Hydrology for Engineers.* San Diego, California: Academic Press. TIC: 208450.

105384 Dettinger, M.D. 1989. "Reconnaissance Estimates of Natural Recharge to Desert Basins in Nevada, U.S.A., by Using Chloride-Balance Calculations." *Journal of Hydrology, 106,* 55-78. Amsterdam, The Netherlands: Elsevier. TIC: 236967.

154690 Dettinger, M.D. 1989. *Distribution of Carbonate-Rock Aquifers in Southern Nevada and the Potential for Their Development, Summary of Findings, 1985-88.* Summary Report No. 1. Carson City, Nevada: State of Nevada. ACC: NNA.19940412.0056.

178613 Doherty, J. 2006. *Addendum to the PEST Manual.* Brisbane, Australia: Watermark Numerical Computing. ACC: MOL.20070111.0003.

118564 Drever, J.I. 1988. *The Geochemistry of Natural Waters.* 2nd Edition. Englewood Cliffs, New Jersey: Prentice-Hall. TIC: 242836.

103415 Dudley, W.W., Jr. and Larson, J.D. 1976. *Effect of Irrigation Pumping on Desert Pupfish Habitats in Ash Meadows, Nye County, Nevada.* Professional Paper 927. Washington, D.C.: U.S. Geological Survey. ACC: MOL.20010724.0312.

163577 Eddebbarh, A.A.; Zyvoloski, G.A.; Robinson, B.A.; Kwicklis, E.M.; Reimus, P.W.; Arnold, B.W.; Corbet, T.; Kuzio, S.P.; and Faunt, C. 2003. "The Saturated Zone at Yucca Mountain: An Overview of the Characterization and Assessment of the Saturated Zone as a Barrier to Potential Radionuclide Migration." *Journal of Contaminant Hydrology, 62-63,* 477-493. New York, New York: Elsevier. TIC: 254205.

100633 Ervin, E.M.; Luckey, R.R.; and Burkhardt, D.J. 1994. *Revised Potentiometric-Surface Map, Yucca Mountain and Vicinity, Nevada.* Water-Resources Investigations Report 93-4000. Denver, Colorado: U.S. Geological Survey. ACC: NNA.19930212.0018.

100146 Faunt, C.C. 1997. *Effect of Faulting on Ground-Water Movement in the Death Valley Region, Nevada and California.* Water-Resources Investigations Report 95-4132. Denver, Colorado: U.S. Geological Survey. ACC: MOL.19980429.0119.

105559 Faure, G. 1986. *Principles of Isotope Geology.* 2nd Edition. New York, New York: John Wiley & Sons. TIC: 237212.

100033 Flint, L.E. 1998. *Characterization of Hydrogeologic Units Using Matrix Properties, Yucca Mountain, Nevada.* Water-Resources Investigations Report 97-4243. Denver, Colorado: U.S. Geological Survey. ACC: MOL.19980429.0512.

109425 Forester, R.M.; Bradbury, J.P.; Carter, C.; Elvidge-Tuma, A.B.; Hemphill, M.L.; Lundstrom, S.C.; Mahan, S.A.; Marshall, B.D.; Neymark, L.A.; Paces, J.B.; Sharpe, S.E.; Whelan, J.F.; and Wigand, P.E. 1999. *The Climatic and Hydrologic History of Southern Nevada During the Late Quaternary.* Open-File Report 98-635. Denver, Colorado: U.S. Geological Survey. TIC: 245717.

144110 Forsyth, P.A. 1989. "A Control Volume Finite Element Method for Local Mesh Refinement." *Proceedings, Tenth. SPE Symposium on Reservoir Simulation, Houston, Texas, February 6-8, 1989.* SPE 18415. Pages 85-96. Richardson, Texas: Society of Petroleum Engineers. TIC: 247068.

101173 Freeze, R.A. and Cherry, J.A. 1979. *Groundwater.* Englewood Cliffs, New Jersey: Prentice-Hall. TIC: 217571.

178611 Freifeld, B.; Doughty, C.; and Finsterle, S. 2006. *Preliminary Estimates of Specific Discharge and Transport Velocities Near Borehole NC-EWDP-24PB.* LBNL-60740. Berkeley, California: Lawrence Berkeley National Laboratory. ACC: MOL.20070111.0001.

100575 Fridrich, C.J.; Dudley, W.W., Jr.; and Stuckless, J.S. 1994. "Hydrogeologic Analysis of the Saturated-Zone Ground-Water System, Under Yucca Mountain, Nevada." *Journal of Hydrology, 154,* 133-168. Amsterdam, The Netherlands: Elsevier. TIC: 224606.

178742 Futa, K.; Marshall, B.D.; and Peterman, Z.E. 2006. "Evidence for Ground-Water Stratification Near Yucca Mountain, Nevada." *Proceedings of the 11th International High-Level Radioactive Waste Management Conference (IHLRWM), April 30 - May 4, 2006, Las Vegas, Nevada.* Pages 301-306. La Grange Park, Illinois: American Nuclear Society. TIC: 258345.

127184 Gascoyne, M. 1992. "Geochemistry of the Actinides and Their Daughters." Chapter 2 of *Uranium-Series Disequilibrium: Applications to Earth, Marine, and Environmental Sciences.* Ivanovich, M. and Harmon, R.S., eds. 2nd Edition. New York, New York: Oxford University Press. TIC: 234680.

129721 Geldon, A.L.; Umari, A.M.A.; Earle, J.D.; Fahy, M.F.; Gemmell, J.M.; and Darnell, J. 1998. *Analysis of a Multiple-Well Interference Test in Miocene Tuffaceous Rocks at the C-Hole Complex, May-June 1995, Yucca Mountain, Nye County, Nevada.* Water-Resources Investigations Report 97-4166. Denver, Colorado: U.S. Geological Survey. TIC: 236724.

100397 Geldon, A.L.; Umari, A.M.A.; Fahy, M.F.; Earle, J.D.; Gemmell, J.M.; and Darnell, J. 1997. *Results of Hydraulic and Conservative Tracer Tests in Miocene Tuffaceous Rocks at the C-Hole Complex, 1995 to 1997, Yucca Mountain, Nye County, Nevada.* Milestone SP23PM3. Las Vegas, Nevada: U.S. Geological Survey. ACC: MOL.19980122.0412.

179104 Gilmore, K. 2006. "RE: Some Problems in Checking." E-mail to from K. Gilmore (Nye County) to C.L. Axness (SNL), July 26, 2006. ACC: LLR.20070228.0142.

155411 Graves, R.P. 1998. *Water Levels in the Yucca Mountain Area, Nevada, 1996.* Open-File Report 98-169. Denver, Colorado: U.S. Geological Survey. ACC: MOL.19981117.0340.

155197 Harbaugh, A.W.; Banta, E.R.; Hill, M.C.; and McDonald, M.G. 2000. *MODFLOW-2000, The U.S. Geological Survey Modular Ground-Water Model—User Guide to Modularization Concepts and the Ground-Water Flow Process.* Open-File Report 00-92. Reston, Virginia: U.S. Geological Survey. TIC: 250197.

178488 Harter, T. and Hopmans, J.W. 2004. "Role of Vadose-Zone Flow Processes in Regional-Scale Hydrology: Review, Opportunities and Challenges." In *Unsaturated-Zone Modeling,* Volume 6, Chapter 6 of *Wageningen UR Frontis Series.* Feddes, R.A.; de Rooij, G.H.; and van Dam, J.C., eds. Boston, Massachusetts: Kluwer Academic Publishers. TIC: 258894.

169681 Hevesi, J.A.; Flint, A.L.; and Flint, L.E. 2003. *Simulation of Net Infiltration and Potential Recharge Using a Distributed-Parameter Watershed Model of the Death Valley Region, Nevada and California*. Water-Resources Investigations Report 03-4090. Sacramento, California: U.S. Geological Survey. ACC: MOL.20031124.0212.

116809 Hevesi, J.A.; Flint, A.L.; and Istok, J.D. 1992. "Precipitation Estimation in Mountainous Terrain Using Multivariate Geostatistics. Part II: Isohyetal Maps." *Journal of Applied Meteorology, 31,* (7), 677-688. Boston, Massachusetts: American Meteorological Society. TIC: 225248.

158753 Hill, M.C.; Banta, E.R.; Harbaugh, A.W.; and Anderman, E.R. 2000. *MODFLOW-2000, The U.S. Geological Survey Modular Ground-Water Model — User Guide to the Observation, Sensitivity, and Parameter-Estimation Processes and Three Post-Processing Programs.* Open-File Report 00-184. Denver, Colorado: U.S. Geological Survey. TIC: 252581.

145088 Ingraham, N.L.; Lyles, B.F.; Jacobson, R.L.; and Hess, J.W. 1991. "Stable Isotopic Study of Precipitation and Spring Discharge in Southern Nevada." *Journal of Hydrology, 125,* 243-258. Amsterdam, The Netherlands: Elsevier. TIC: 238581.

103010 Kilroy, K.C. 1991. *Ground-Water Conditions in Amargosa Desert, Nevada-California, 1952-87.* Water-Resources Investigations Report 89-4101. Carson City, Nevada: U.S. Geological Survey. TIC: 209975.

178599 Kitanidis, P.K. 1996. "On the Geostatistical Approach to the Inverse Problem." *Advances in Water Resources, 19,* (6), 333-342. New York, New York: Elsevier. TIC: 259001.

100909 Kotra, J.P.; Lee, M.P.; Eisenberg, N.A.; and DeWispelare, A.R. 1996. *Branch Technical Position on the Use of Expert Elicitation in the High-Level Radioactive Waste Program.* NUREG-1563. Washington, D.C.: U.S. Nuclear Regulatory Commission. TIC: 226832.

103011 La Camera, R.J. and Locke, G.L. 1997. *Selected Ground-Water Data for Yucca Mountain Region, Southern Nevada and Eastern California, Through December 1996.* Open-File Report 97-821. Carson City, Nevada: U.S. Geological Survey. ACC: MOL.20010724.0311.

181434 LANL (Los Alamos National Laboratory) 2001. *Software Management Report (SMR) for CORPSCON Version 5.11.08*. SDN: 10547-SMR-5.11.08-00. Los Alamos, New Mexico: Los Alamos National Laboratory. ACC: MOL.20011011.0403.

103012 Laczniak, R.J.; Cole, J.C.; Sawyer, D.A.; and Trudeau, D.A. 1996. *Summary of Hydrogeologic Controls on Ground-Water Flow at the Nevada Test Site, Nye County, Nevada.* Water-Resources Investigations 96-4109. Carson City, Nevada: U.S. Geological Survey. TIC: 226157.

100051 Langmuir, D. 1997. *Aqueous Environmental Geochemistry.* Upper Saddle River, New Jersey: Prentice Hall. TIC: 237107.

100153 LeCain, G.D. 1997. *Air-Injection Testing in Vertical Boreholes in Welded and Nonwelded Tuff, Yucca Mountain, Nevada.* Water-Resources Investigations Report 96-4262. Denver, Colorado: U.S. Geological Survey. ACC: MOL.19980310.0148.

144612 LeCain, G.D.; Anna, L.O.; and Fahy, M.F. 2000. *Results from Geothermal Logging, Air and Core-Water Chemistry Sampling, Air-Injection Testing, and Tracer Testing in the Northern Ghost Dance Fault, Yucca Mountain, Nevada, November 1996 to August 1998.* Water-Resources Investigations Report 99-4210. Denver, Colorado: U.S. Geological Survey. TIC: 247708.

100053 Levy, S.S. 1991. "Mineralogic Alteration History and Paleohydrology at Yucca Mountain, Nevada." *High Level Radioactive Waste Management, Proceedings of the Second Annual International Conference, Las Vegas, Nevada, April 28-May 3, 1991. 1,* 477-485. La Grange Park, Illinois: American Nuclear Society. TIC: 204272.

100589 Lichty, R.W. and McKinley, P.W. 1995. *Estimates of Ground-Water Recharge Rates for Two Small Basins in Central Nevada.* Water-Resources Investigations Report 94-4104. Denver, Colorado: U.S. Geological Survey. ACC: MOL.19960924.0524.

101258 Loeven, C. 1993. *A Summary and Discussion of Hydrologic Data from the Calico Hills Nonwelded Hydrogeologic Unit at Yucca Mountain, Nevada.* LA-12376-MS. Los Alamos, New Mexico: Los Alamos National Laboratory. ACC: NNA.19921116.0001.

100465 Luckey, R.R.; Tucci, P.; Faunt, C.C.; Ervin, E.M.; Steinkampf, W.C.; D'Agnese, F.A.; and Patterson, G.L. 1996. *Status of Understanding of the Saturated-Zone Ground-Water Flow System at Yucca Mountain, Nevada, as of 1995.* Water-Resources Investigations Report 96-4077. Denver, Colorado: U.S. Geological Survey. ACC: MOL.19970513.0209.

101142 Marshall, B.D.; Peterman, Z.E.; and Stuckless, J.S. 1993. "Strontium Isotopic Evidence for a Higher Water Table at Yucca Mountain." *High Level Radioactive Waste Management, Proceedings of the Fourth Annual International Conference, Las Vegas, Nevada, April 26-30, 1993. 2,* 1948-1952. La Grange Park, Illinois: American Nuclear Society. TIC: 208542.

116222 McKinley, P.W.; Long, M.P.; and Benson, L.V. 1991. *Chemical Analyses of Water from Selected Wells and Springs in the Yucca Mountain Area, Nevada and Southeastern California.* Open-File Report 90-355. Denver, Colorado: U.S. Geological Survey. ACC: NNA.19901031.0004.

158813 Meijer, A. 2002. "Conceptual Model of the Controls on Natural Water Chemistry at Yucca Mountain, Nevada." *Applied Geochemistry, 17,* (6), 793-805. New York, New York: Elsevier. TIC: 252808.

126847 Merlivat, L. and Jouzel, J. 1979. "Global Climatic Interpretation of the Deuterium-Oxygen 18 Relationship for Precipitation." *Journal of Geophysical Research, 84,* (C8), 5029-5033. Washington, D.C.: American Geophysical Union. TIC: 247773.

178788 Moore, C. 2005. *The Use of Regularized Inversion in Groundwater Model Calibration and Prediction Uncertainty Analysis.* Ph.D. Thesis. Queensland, Australia: The University of Queensland. TIC: 259082.

178402 Moore, C. and Doherty, J. 2005. "Role of the Calibration Process in Reducing Model Predictive Error." *Water Resources Research, 41,* 1-14. Washington, D.C.: American Geophysical Union. TIC: 258856.

178403 Moore, C. and Doherty, J. 2006. "The Cost of Uniqueness in Groundwater Model Calibration." *Advances in Water Resources, 29,* 605-623. New York, New York: Elsevier. TIC: 258857.

150321 Neuman, S.P. 1975. "Analysis of Pumping Test Data from Anisotropic Unconfined Aquifers Considering Delayed Gravity Response." *Water Resources Research, 11,* (2), 329-342. Washington, D.C.: American Geophysical Union. TIC: 222414.

101464 Neuman, S.P. 1990. "Universal Scaling of Hydraulic Conductivities and Dispersivities in Geologic Media." *Water Resources Research, 26,* (8), 1749-1758. Washington, D.C.: American Geophysical Union. TIC: 237977.

147379 Norton, D. and Knapp, R.B. 1977. "Transport Phenomena in Hydrothermal Systems: The Nature of Porosity." *American Journal of Science, 277,* 913-936. New Haven, Connecticut: Yale University, Kline Geology Laboratory. TIC: 247599.

107770 NRC (U.S. Nuclear Regulatory Commission) 1998. "Proposed Rule: 10 CFR Part 63---'Disposal of High-Level Radioactive Wastes in a Proposed Geologic Repository at Yucca Mountain, Nevada'." SECY-98-225. Washington, D.C.: U.S. Nuclear Regulatory Commission. Accessed October 30, 1999. TIC: 240520. URL: http://www.nrc.gov/NRC/COMMISSION/SECYS/1998-225scy.html.

163274 NRC 2003. *Yucca Mountain Review Plan, Final Report.* NUREG-1804, Rev. 2. Washington, D.C.: U.S. Nuclear Regulatory Commission, Office of Nuclear Material Safety and Safeguards. TIC: 254568.

101278 O'Brien, G.M. 1998. *Analysis of Aquifer Tests Conducted in Borehole USW G-2, 1996, Yucca Mountain, Nevada.* Water-Resources Investigations Report 98-4063. Denver, Colorado: U.S. Geological Survey. ACC: MOL.19980904.0095.

149438 Oatfield, W.J. and Czarnecki, J.B. 1989. *Hydrogeologic Inferences from Drillers Logs and from Gravity and Resistivity Surveys in the Amargosa Desert, Southern Nevada.* Open-File Report 89-234. Denver, Colorado: U.S. Geological Survey. TIC: 200468.

100069 Oliver, T. and Root, T. 1997. *Hydrochemical Database for the Yucca Mountain Area, Nye County, Nevada.* Denver, Colorado: U.S. Geological Survey. ACC: MOL.19980302.0367.

145190 Osmond, J.K. and Cowart, J.B. 1992. "Ground Water." Chapter 9 of *Uranium-Series Disequilibrium: Applications to Earth, Marine, and Environmental Sciences.* Ivanovich, M. and Harmon, R.S., eds. 2nd Edition. New York, New York: Oxford University Press. TIC: 234680.

154724 Paces, J.B. and Whelan, J.F. 2001. "Water-Table Fluctuations in the Amargosa Desert, Nye County, Nevada." *"Back to the Future - Managing the Back End of the Nuclear Fuel Cycle to Create a More Secure Energy Future," Proceedings of the 9th International High-Level Radioactive Waste Management Conference (IHLRWM), Las Vegas, Nevada, April 29-May 3, 2001.* La Grange Park, Illinois: American Nuclear Society. TIC: 247873.

158817 Paces, J.B.; Ludwig, K.R.; Peterman, Z.E.; and Neymark, L.A. 2002. "$^{234}U/^{238}U$ Evidence for Local Recharge and Patterns of Ground-Water Flow in the Vicinity of Yucca Mountain, Nevada, USA." *Applied Geochemistry, 17,* (6), 751-779. New York, New York: Elsevier. TIC: 252809.

100072 Paces, J.B.; Ludwig, K.R.; Peterman, Z.E.; Neymark, L.A.; and Kenneally, J.M. 1998. "Anomalous Ground-Water $^{234}U/^{238}U$ Beneath Yucca Mountain: Evidence of Local Recharge?" *High-Level Radioactive Waste Management, Proceedings of the Eighth International Conference, Las Vegas, Nevada, May 11-14, 1998.* Pages 185-188. La Grange Park, Illinois: American Nuclear Society. TIC: 237082.

107408 Paces, J.B.; Neymark, L.A.; Marshall, B.D.; Whelan, J.F.; and Peterman, Z.E. 1998. "Inferences for Yucca Mountain Unsaturated-Zone Hydrology from Secondary Minerals." *High-Level Radioactive Waste Management, Proceedings of the Eighth International Conference, Las Vegas, Nevada, May 11-14, 1998.* Pages 36-39. La Grange Park, Illinois: American Nuclear Society. TIC: 237082.

156507 Paces, J.B.; Neymark, L.A.; Marshall, B.D.; Whelan, J.F.; and Peterman, Z.E. 2001. *Ages and Origins of Calcite and Opal in the Exploratory Studies Facility Tunnel, Yucca Mountain, Nevada.* Water-Resources Investigations Report 01-4049. Denver, Colorado: U.S. Geological Survey. TIC: 251284.

159511 Parkhurst, D.L. and Appelo, C.A.J. 1999. *User's Guide to PHREEQC (Version 2)—A Computer Program for Speciation, Batch-Reaction, One-Dimensional Transport, and Inverse Geochemical Calculations.* Water-Resources Investigations Report 99-4259. Denver, Colorado: U.S. Geological Survey. TIC: 253046.

158824 Patterson, G.L. 1999. "Occurrences of Perched Water in the Vicinity of the Exploratory Studies Facility North Ramp." *Hydrogeology of the Unsaturated Zone, North Ramp Area of the Exploratory Studies Facility, Yucca Mountain, Nevada.* Rousseau, J.P.; Kwicklis, E.M.; and Gillies, D.C., eds. Water-Resources Investigations Report 98-4050. Denver, Colorado: U.S. Geological Survey. ACC: MOL.19990419.0335.

178743 Patterson, G.L. and Striffler, P.S. 2006. "Vertical Variability in Saturated Zone Hydrochemistry Near Yucca Mountain, Nevada." *Proceedings of the 11th International High-Level Radioactive Waste Management Conference (IHLRWM), April 30 - May 4, 2006, Las Vegas, Nevada.* Pages 390-394. La Grange Park, Illinois: American Nuclear Society. TIC: 258345.

179459 Patterson, G.L. and Thomas, J. 2005. "Carbon-14 Groundwater Analysis." *Office of Science and Technology and International OSTI&I: Annual Report 2005*. DOE/RW-0581. Pages 183-184. Washington, D.C.: U.S. Department of Energy, Office of Science and Technology and International. ACC: HQO.20060322.0021.

107402 Patterson, G.L.; Peterman, Z.E.; and Paces, J.B. 1998. "Hydrochemical Evidence for the Existence of Perched Water at USW WT-24, Yucca Mountain, Nevada." *High-Level Radioactive Waste Management, Proceedings of the Eighth International Conference, Las Vegas, Nevada, May 11-14, 1998.* Pages 277-278. La Grange Park, Illinois: American Nuclear Society. TIC: 237082.

101149 Peterman, Z.E. and Stuckless, J.S. 1993. "Isotopic Evidence of Complex Ground-Water Flow at Yucca Mountain, Nevada, USA." *High Level Radioactive Waste Management, Proceedings of the Fourth Annual International Conference, Las Vegas, Nevada, April 26-30, 1993. 2,* 1559-1566. La Grange Park, Illinois: American Nuclear Society. TIC: 208542.

107034 Plummer, M.A.; Phillips, F.M.; Fabryka-Martin, J.; Turin, H.J.; Wigand, P.E.; and Sharma, P. 1997. "Chlorine-36 in Fossil Rat Urine: An Archive of Cosmogenic Nuclide Deposition During the Past 40,000 Years." *Science, 277,* 538-541. Washington, D.C.: American Association for the Advancement of Science. TIC: 237425.

101466 Pollock, D.W. 1988. "Semianalytical Computation of Path Lines for Finite-Difference Models." *Ground Water, 26,* (6), 743-750. Worthington, Ohio: National Water Well Association. TIC: 226464.

103316 Press, W.H.; Teukolsky, S.A.; Vetterling, W.T.; and Flannery, B.P. 1992. *Numerical Recipes in Fortran 77, The Art of Scientific Computing.* Volume 1 of *Fortran Numerical Recipes.* 2nd Edition. Cambridge, United Kingdom: Cambridge University Press. TIC: 243606.

100073 Quade, J. and Cerling, T.E. 1990. "Stable Isotopic Evidence for a Pedogenic Origin of Carbonates in Trench 14 Near Yucca Mountain, Nevada." *Science, 250,* 1549-1552. Washington, D.C.: American Association for the Advancement of Science. TIC: 222617.

154688 Rasmussen, T.C.; Evans, D.D.; Sheets, P.J.; and Blanford, J.H. 1993. "Permeability of Apache Leap Tuff: Borehole and Core Measurements Using Water and Air." *Water Resources Research, 29,* (7), 1997-2006. Washington, D.C.: American Geophysical Union. TIC: 245278.

101284 Rice, W.A. 1984. *Preliminary Two-Dimensional Regional Hydrologic Model of the Nevada Test Site and Vicinity.* SAND83-7466. Albuquerque, New Mexico: Sandia National Laboratories. ACC: NNA.19900810.0286.

165986 Robledo, A.R.; Ryder, P.L.; Fenelon, J.M.; and Paillet, F.L. 1998. *Geohydrology of Monitoring Wells Drilled in Oasis Valley near Beatty, Nye County, Nevada, 1997.* Water-Resources Investigations Report 98-4184. Carson City, Nevada: U.S. Geological Survey. ACC: MOL.20031027.0156.

162938 Rose, T.P.; Benedict, F.C., Jr.; Thomas, J.M.; Sicke, W.S.; Hershey, R.L.; Paces, J.B.; Farnham, I.M.; and Peterman, Z.E. 2002. *Preliminary, Geochemical Data Analysis and Interpretation of the Pahute Mesa-Oasis Valley Groundwater Flow System, Nye County, Nevada.* Las Vegas, Nevada: U.S. Department of Energy, Nevada Operations Office. ACC: MOL.20031208.0200.

144725 Rose, T.P.; Kenneally, J.M.; Smith, D.K.; Davisson, M.L.; Hudson, G.B.; and Rego, J.H. 1997. *Chemical and Isotopic Data for Groundwater in Southern Nevada.* UCRL-ID-128000. Livermore, California: Lawrence Livermore National Laboratory. TIC: 243649.

102097 Rousseau, J.P.; Kwicklis, E.M.; and Gillies, D.C., eds. 1999. *Hydrogeology of the Unsaturated Zone, North Ramp Area of the Exploratory Studies Facility, Yucca Mountain, Nevada.* Water-Resources Investigations Report 98-4050. Denver, Colorado: U.S. Geological Survey. ACC: MOL.19990419.0335.

100644 Sass, J.H.; Lachenbruch, A.H.; Dudley, W.W., Jr.; Priest, S.S.; and Munroe, R.J. 1988. *Temperature, Thermal Conductivity, and Heat Flow Near Yucca Mountain, Nevada: Some Tectonic and Hydrologic Implications.* Open-File Report 87-649. Denver, Colorado: U.S. Geological Survey. TIC: 203195.

102213 Savard, C.S. 1998. *Estimated Ground-Water Recharge from Streamflow in Fortymile Wash Near Yucca Mountain, Nevada.* Water-Resources Investigations Report 97-4273. Denver, Colorado: U.S. Geological Survey. TIC: 236848.

100075 Sawyer, D.A.; Fleck, R.J.; Lanphere, M.A.; Warren, R.G.; Broxton, D.E.; and Hudson, M.R. 1994. "Episodic Caldera Volcanism in the Miocene Southwestern Nevada Volcanic Field: Revised Stratigraphic Framework, $^{40}Ar/^{39}Ar$ Geochronology, and Implications for Magmatism and Extension." *Geological Society of America Bulletin, 106,* (10), 1304-1318. Boulder, Colorado: Geological Society of America. TIC: 222523.

161591 Sharpe, S. 2003. *Future Climate Analysis—10,000 Years to 1,000,000 Years After Present.* MOD-01-001 REV 01. Reno, Nevada: Desert Research Institute. ACC: MOL.20030407.0055.

101929 Simonds, F.W.; Whitney, J.W.; Fox, K.F.; Ramelli, A.R.; Yount, J.C.; Carr, M.D.; Menges, C.M.; Dickerson, R.P.; and Scott, R.B. 1995. *Map Showing Fault Activity in the Yucca Mountain Area, Nye County, Nevada.* Miscellaneous Investigations Series Map I-2520. Denver, Colorado: U.S. Geological Survey. TIC: 232483.

150228 Slate, J.L.; Berry, M.E.; Rowley, P.D.; Fridrich, C.J.; Morgan, K.S.; Workman, J.B.; Young, O.D.; Dixon, G.L.; Williams, V.S.; McKee, E.H.; Ponce, D.A.; Hildenbrand, T.G.; Swadley, W C; Lundstrom, S.C.; Ekren, E.B.; Warren, R.G.; Cole, J.C.; Fleck, R.J.; Lanphere, M.A.; Sawyer, D.A.; Minor, S.A.; Grunwald, D.J.; Laczniak, R.J.; Menges, C.M.; Yount, J.C.; Jayko, A.S.; Mankinen, E.A.; Davidson, J.G.; Morin, R.L.; and Blakely, R.J. 2000. *Digital Geologic Map of the Nevada Test Site and Vicinity, Nye, Lincoln and Clark Counties, Nevada, and Inyo County, California, Revision 4; Digital Aeromagnetic Map of the Nevada Test Site and Vicinity, Nye, Lincoln, and Clark Counties, Nevada, and Inyo County, California; and Digital Isostatic Gravity Map of the Nevada Test Site and Vicinity, Nye, Lincoln, and Clark Counties, Nevada, and Inyo County, California.* Open-File Report 99-554—A, —B, and —C. Denver, Colorado: U.S. Geological Survey. TIC: 248049; 251985; 251981.

174109 SNL 2007. *Hydrogeologic Framework Model for the Saturated Zone Site Scale Flow and Transport Model.* MDL-NBS-HS-000024 REV 01. Las Vegas, Nevada: Sandia National Laboratories.

177390 SNL 2007. *Saturated Zone Flow and Transport Model Abstraction.* MDL-NBS-HS-000021 REV 04. Las Vegas, Nevada: Sandia National Laboratories.

177394 SNL 2007. *Saturated Zone In-Situ Testing.* ANL-NBS-HS-000039 REV 02. Las Vegas, Nevada: Sandia National Laboratories. ACC: DOC.20070608.0004.

174294 SNL 2007. *Simulation of Net Infiltration for Present-Day and Potential Future Climates*. MDL-NBS-HS-000023 REV 01. Las Vegas, Nevada: Sandia National Laboratories.

177392 SNL 2007. *Site-Scale Saturated Zone Transport.* MDL-NBS-HS-000010 REV 03. Las Vegas, Nevada: Sandia National Laboratories.

178871 SNL 2007. *Total System Performance Assessment Model /Analysis for the License Application*. MDL-WIS-PA-000005 REV 00. Las Vegas, Nevada: Sandia National Laboratories.

175177 SNL 2007. *UZ Flow Models and Submodels.* MDL-NBS-HS-000006 REV 03. Las Vegas, Nevada: Sandia National Laboratories.

158818 Steinkampf, W.C. and Werrell, W.L. 2001. *Ground-Water Flow to Death Valley, as Inferred from the Chemistry and Geohydrology of Selected Springs in Death Valley National Park, California and Nevada.* Water-Resources Investigations Report 98-4114. Denver, Colorado: U.S. Geological Survey. TIC: 251734.

101159 Stuckless, J.S.; Whelan, J.F.; and Steinkampf, W.C. 1991. "Isotopic Discontinuities in Ground Water Beneath Yucca Mountain, Nevada." *High Level Radioactive Waste Management, Proceedings of the Second Annual International Conference, Las Vegas, Nevada, April 28-May 3, 1991. 2,* 1410-1415. La Grange Park, Illinois: American Nuclear Society. TIC: 204272.

101933 Thomas, J.M.; Welch, A.H.; and Dettinger, M.D. 1996. *Geochemistry and Isotope Hydrology of Representative Aquifers in the Great Basin Region of Nevada, Utah, and Adjacent States.* Professional Paper 1409-C. Denver, Colorado: U.S. Geological Survey. ACC: MOL.20010803.0369.

106585 Thordarson, W. 1965. *Perched Ground Water in Zeolitized-Bedded Tuff, Rainier Mesa and Vicinity, Nevada Test Site, Nevada.* TEI-862. Washington, D.C.: U.S. Geological Survey. ACC: NN1.19881021.0066.

126827 Thorstenson, D.C.; Weeks, E.P.; Haas, H.; Busenberg, E.; Plummer, L.N.; and Peters, C.A. 1998. "Chemistry of Unsaturated Zone Gases Sampled in Open Boreholes at the Crest of Yucca Mountain, Nevada: Data and Basic Concepts of Chemical and Physical Processes in the Mountain." *Water Resources Research, 34,* (6), 1507-1529. Washington, D.C.: American Geophysical Union. TIC: 246315.

101490 Tompson, A.F.B. and Gelhar, L.W. 1990. "Numerical Simulation of Solute Transport in Three-Dimensional, Randomly Heterogeneous Porous Media." *Water Resources Research, 26,* (10), 2541-2562. Washington, D.C.: American Geophysical Union. TIC: 224902.

178576 Tonkin, M.J. and Doherty, J. 2005. "A Hybrid Regularized Inversion Methodology for Highly Parameterized Environmental Models." *Water Resources Research, 41,* (W10412), 1-16. Washington, D.C.: American Geophysical Union. TIC: 258946.

179068 Tseng, P-H. and Zyvoloski, G.A. 2000. "A Reduced Degree of Freedom Method for Simulating Non-Isothermal Multi-Phase Flow in a Porous Medium." *Advances in Water Resources, 23,* 731-745. New York, New York: Elsevier. TIC: 254768.

101060 Tucci, P. and Burkhardt, D.J. 1995. *Potentiometric-Surface Map, 1993, Yucca Mountain and Vicinity, Nevada.* Water-Resources Investigations Report 95-4149. Denver, Colorado: U.S. Geological Survey. ACC: MOL.19960924.0517.

155410 Tucci, P. 2001. Segment of SN-USGS-SCI-126-V1: Revision of Water Level AMR (ANL-NBS-HS-000034, Rev 00/ICN 01). Scientific Notebook SN-USGS-SCI-126-V1. ACC: MOL.20010712.0271.

154625 USGS (U.S. Geological Survey) 2001. *Water-Level Data Analysis for the Saturated Zone Site-Scale Flow and Transport Model.* ANL-NBS-HS-000034 REV 00 ICN 01. Denver, Colorado: U.S. Geological Survey. ACC: MOL.20010405.0211.

168473 USGS 2004. *Water-Level Data Analysis for the Saturated Zone Site-Scale Flow and Transport Model.* ANL-NBS-HS-000034 REV 01 Errata 002. Denver, Colorado: U.S. Geological Survey. ACC: MOL.20020209.0058; MOL.20020917.0136; DOC.20040303.0006.

105946 Vaniman, D.T.; Bish, D.L.; Chipera, S.J.; Carlos, B.A.; and Guthrie, G.D., Jr. 1996. *Chemistry and Mineralogy of the Transport Environment at Yucca Mountain.* Volume I of *Summary and Synthesis Report on Mineralogy and Petrology Studies for the Yucca Mountain Site Characterization Project.* Milestone 3665. Los Alamos, New Mexico: Los Alamos National Laboratory. ACC: MOL.19961230.0037.

157427 Vaniman, D.T.; Chipera, S.J.; Bish, D.L.; Carey, J.W.; and Levy, S.S. 2001. "Quantification of Unsaturated-Zone Alteration and Cation Exchange in Zeolitized Tuffs at Yucca Mountain, Nevada, USA." *Geochimica et Cosmochimica Acta, 65,* (20), 3409-3433. New York, New York: Elsevier. TIC: 251574.

178577 Vecchia, A.V. and Cooley, R.L. 1987. "Simultaneous Confidence and Prediction Intervals for Nonlinear Regression Models with Application to a Groundwater Flow Model." *Water Resources Research, 23,* (7), 1237-1250. Washington, D.C.: American Geophysical Union. ACC: MOL.20070108.0002.

143606 Verma, S. and Aziz, K. 1997. "A Control Volume Scheme for Flexible Grids in Reservoir Simulation." *Proceedings, SPE Reservoir Simulation Symposium, 8-11, June 1997, Dallas, Texas.* SPE 37999. Pages 215-227. Richardson, Texas: Society of Petroleum Engineers. TIC: 247097.

154706 Vesselinov, V.V.; Illman, W.A.; Hyun, Y.; Neuman, S.P.; Di Federico, V.; and Tartakovsky, D.M. 2001. "Observation and Analysis of a Pronounced Permeability and Porosity Scale-Effect in Unsaturated Fractured Tuff." *Fractured Rock 2001, An International Conference Addressing Groundwater Flow, Solute Transport, Multiphase Flow, and Remediation in Fractured Rock, March 26-28, 2001, Toronto, Ontario, Canada.* Kueper, B.H.; Novakowski, K.S.; and Reynolds, D.A., eds. Smithville, Ontario, Canada: Smithville Phase IV. TIC: 249909.

101062 Waddell, R.K. 1982. *Two-Dimensional, Steady-State Model of Ground-Water Flow, Nevada Test Site and Vicinity, Nevada-California.* Water-Resources Investigations Report 82-4085. Denver, Colorado: U.S. Geological Survey. ACC: NNA.19870518.0055.

103022 Walker, G.E. and Eakin, T.E. 1963. *Geology and Ground Water of Amargosa Desert, Nevada-California.* Ground-Water Resources – Reconnaissance Series Report 14. Carson City, Nevada: State of Nevada, Department of Conservation and Natural Resources. TIC: 208665.

178643 Watermark Computing 2004. *Groundwater Data Utilities Part B: Program Descriptions*. Brisbane, Australia: Watermark Computing. ACC: MOL.20070115.0009.

178642 Watermark Numerical Computing 2003. *Groundwater Data Utilities Part A: Overview*. Brisbane, Australia: Watermark Numerical Computing. ACC: MOL.20070115.0008.

178612 Watermark Numerical Computing 2004. *PEST, Model-Independent Parameter Estimation User Manual.* 5th Edition. Brisbane, Australia: Watermark Numerical Computing. ACC: MOL.20070111.0002.

130510 Wen, X-H. and Gomez-Hernandez, J.J. 1996. "The Constant Displacement Scheme for Tracking Particles in Heterogeneous Aquifers." *Ground Water, 34,* (1), 135-142. Worthington, Ohio: Water Well Journal Publishing. TIC: 246656.

137305 Whelan, J.F.; Moscati, R.J.; Allerton, S.B.M.; and Marshall, B.D. 1998. *Applications of Isotope Geochemistry to the Reconstruction of Yucca Mountain, Nevada, Paleohydrology—Status of Investigations: June 1996.* Open-File Report 98-83. Denver, Colorado: U.S. Geological Survey. ACC: MOL.19981012.0740.

108865 Whelan, J.F.; Moscati, R.J.; Roedder, E.; and Marshall, B.D. 1998. "Secondary Mineral Evidence of Past Water Table Changes at Yucca Mountain, Nevada." *High-Level Radioactive Waste Management, Proceedings of the Eighth International Conference, Las Vegas, Nevada, May 11-14, 1998.* Pages 178-181. La Grange Park, Illinois: American Nuclear Society. TIC: 237082.

101165 White, A.F. 1979. *Geochemistry of Ground Water Associated with Tuffaceous Rocks, Oasis Valley, Nevada.* Professional Paper 712-E. Washington, D.C.: U.S. Geological Survey. TIC: 219633.

108871 White, A.F. and Chuma, N.J. 1987. "Carbon and Isotopic Mass Balance Models of Oasis Valley - Fortymile Canyon Groundwater Basin, Southern Nevada." *Water Resources Research, 23,* (4), 571-582. Washington, D.C.: American Geophysical Union. TIC: 237579.

101166 White, A.F.; Claassen, H.C.; and Benson, L.V. 1980. *The Effect of Dissolution of Volcanic Glass on the Water Chemistry in a Tuffaceous Aquifer, Rainier Mesa, Nevada.* Geochemistry of Water. Geological Survey Water-Supply Paper 1535-Q, Washington, D.C.: U.S. Government Printing Office. TIC: 221391.

155614 Wilson, C. 2001. *Data Qualification Report: Stratigraphic Data Supporting the Hydrogeologic Framework Model for Use on the Yucca Mountain Project.* TDR-NBS-HS-000013 REV 00. Las Vegas, Nevada: Bechtel SAIC Company. ACC: MOL.20010725.0225.

170977 Williams, N.H. 2003. "Contract No. DE-AC28-01RW12101 - Transmittal of Report Technical Basis Document No. 11: Saturated Zone Flow and Transport Revision 2 Addressing Twenty-Five Key Technical Issue (KTI) Agreements Related to Saturated Zone Flow and Transport." Letter from N.H. Williams (BSC) to C.M. Newbury (DOE/ORD), September 30, 2003, MP:cg - 0930038958, with enclosure. ACC: MOL.20040105.0270.

108882 Winograd, I.J. and Pearson, F.J., Jr. 1976. "Major Carbon 14 Anomaly in a Regional Carbonate Aquifer: Possible Evidence for Megascale Channeling, South Central Great Basin." *Water Resources Research, 12,* (6), 1125-1143. Washington, D.C.: American Geophysical Union. TIC: 217731.

101167 Winograd, I.J. and Thordarson, W. 1975. *Hydrogeologic and Hydrochemical Framework, South-Central Great Basin, Nevada-California, with Special Reference to the Nevada Test Site.* Geological Survey Professional Paper 712-C. Washington, D.C.: United States Government Printing Office. ACC: NNA.19870406.0201.

100094 Winograd, I.J.; Coplen, T.B.; Landwehr, J.M.; Riggs, A.C.; Ludwig, K.R.; Szabo, B.J.; Kolesar, P.T.; and Revesz, K.M. 1992. "Continuous 500,000-Year Climate Record from Vein Calcite in Devils Hole, Nevada." *Science, 258,* 255-260. Washington, D.C.: American Association for the Advancement of Science. TIC: 237563.

178405 Winterle, J. 2005. *Simulation of Spring Flows South of Yucca Mountain, Nevada, Following a Potential Future Water Table Rise.* San Antonio, Texas: Center for Nuclear Waste Regulatory Analyses. ACC: MOL.20061120.0234.

178404 Winterle, J.R. 2003. *Evaluation of Alternative Concepts for Saturated Zone Flow: Effects of Recharge and Water Table Rise on Flow Paths and Travel Times at Yucca Mountain.* San Antonio, Texas: Center for Nuclear Waste Regulatory Analyses. ACC: MOL.20061120.0233.

129796 Winterle, J.R. and La Femina, P.C. 1999. *Review and Analysis of Hydraulic and Tracer Testing at the C-Holes Complex Near Yucca Mountain, Nevada.* San Antonio, Texas: Center for Nuclear Waste Regulatory Analyses. TIC: 246623.

149596 Yang, I.C. and Peterman, Z.E. 1999. "Chemistry and Isotopic Content of Perched Water." In *Hydrogeology of the Unsaturated Zone, North Ramp Area of the Exploratory Studies Facility, Yucca Mountain, Nevada.* Rousseau, J.P.; Kwicklis, E.M.; and Gillies, D.C., eds. Water-Resources Investigations Report 98-4050. Denver, Colorado: U.S. Geological Survey. ACC: MOL.19990419.0335.

100194 Yang, I.C.; Rattray, G.W.; and Yu, P. 1996. *Interpretation of Chemical and Isotopic Data from Boreholes in the Unsaturated Zone at Yucca Mountain, Nevada.* Water-Resources Investigations Report 96-4058. Denver, Colorado: U.S. Geological Survey. ACC: MOL.19980528.0216.

101441 Yang, I.C.; Yu, P.; Rattray, G.W.; Ferarese, J.S.; and Ryan, J.N. 1998. *Hydrochemical Investigations in Characterizing the Unsaturated Zone at Yucca Mountain, Nevada.* Water-Resources Investigations Report 98-4132. Denver, Colorado: U.S. Geological Survey. ACC: MOL.19981012.0790.

179430 YMP (Yucca Mountain Site Characterization Project) 2001. Sample Collection Report, Characterization of the Yucca Mountain Unsaturated-Zone Percolation Surface-Based Studies, May 17, 1995 through May 18, 1995. Las Vegas, Nevada: Yucca Mountain Site Characterization Office. ACC: MOL.20011030.0681.

101171 Zyvoloski, G. 1983. "Finite Element Methods for Geothermal Reservoir Simulation." *International Journal for Numerical and Analytical Methods in Geomechanics, 7,* (1), 75-86. New York, New York: John Wiley & Sons. TIC: 224068.

163341 Zyvoloski, G.; Kwicklis, E.; Eddebbarh, A.A.; Arnold, B.; Faunt, C.; and Robinson, B.A. 2003. "The Site-Scale Saturated Zone Flow Model for Yucca Mountain: Calibration of Different Conceptual Models and their Impact on Flow Paths." *Journal of Contaminant Hydrology, 62-63,* 731-750. New York, New York: Elsevier. TIC: 254340.

9.2 CODES, STANDARDS, REGULATIONS, AND PROCEDURES

176567 10 CFR 50. 2006. Energy: Domestic Licensing of Production and Utilization Facilities. Internet Accessible.

176544 10 CFR 63. 2006. Energy: Disposal of High-Level Radioactive Wastes in a Geologic Repository at Yucca Mountain, Nevada. Internet Accessible.

AP-2.22Q, Rev. 1, ICN 1. *Classification Analyses and Maintenance of the Q-List.* Washington, D.C.: U.S. Department of Energy, Office of Civilian Radioactive Waste Management. ACC: DOC.20040714.0002.

AP-2.27Q, Rev. 1, ICN 5. *Planning for Science Activities.* Washington, D.C.: U.S. Department of Energy, Office of Civilian Radioactive Waste Management. ACC: DOC.20041014.0001.

AP-SI.1Q, Rev. 5, ICN 2. *Software Management.* Washington, D.C.: U.S. Department of Energy, Office of Civilian Radioactive Waste Management. ACC: DOC.20030902.0003.

AP-SIII.10Q, Rev. 2, ICN 7. *Models.* Washington, D.C.: U.S. Department of Energy, Office of Civilian Radioactive Waste Management. ACC: DOC.20040920.0002.

176399 ASME NQA-1-2004. 2004. Quality Assurance Requirements for Nuclear Facilities Applications. New York, New York: American Society of Mechanical Engineers. TIC: 256850.

177092 DOE (U.S. Department of Energy) 2006. *Quality Assurance Requirements and Description*. DOE/RW-0333P, Rev. 18. Washington, D.C.: U.S. Department of Energy, Office of Civilian Radioactive Waste Management. ACC: DOC.20060602.0001.

IT-PRO-0011, *Software Management*.

IT-PRO-0012, *Qualification of Software*.

IT-PRO-0013 *Software Independent Verification and Validation*.

LP-SI.11Q-BSC, Rev. 0, ICN 1. *Software Management.* Washington, D.C.: U.S. Department of Energy, Office of Civilian Radioactive Waste Management. ACC: DOC.20041005.0008.

LS-PRO-0203, *Q-List and Classification of Structures, Systems, and Components*.

SCI-PRO-001, *Qualification of Unqualified Data*.

SCI-PRO-003, Rev. 2, ICN 0. *Document Review.* Washington, D.C.: U.S. Department of Energy, Office of Civilian Radioactive Waste Management. ACC: DOC.20070418.0002.

SCI-PRO-006, *Models*.

9.3 SOURCE DATA, LISTED BY DATA TRACKING NUMBER

149155 GS000308312322.003. Preliminary Release of Field, Chemical, and Isotopic Data from the Nye County Early Warning Drilling Program (EWDP) Wells in Amargosa Valley, Nevada Collected Between 12/11/98 and 11/15/99. Submittal date: 03/16/2000.

149947 GS000508312332.001. Water-Level Data Analysis for the Saturated Zone Site-Scale Flow and Transport Model. Submittal date: 06/01/2000.

150842 GS000700012847.001. Chemical and Isotopic Data from Cind-R-Lite Well Samples Collected on 5/17/95 and 9/6/95. Submittal date: 07/10/2000.

171433 GS001208312312.009. Ground-Water Altitudes from Manual Depth-to-Water Measurements at Various Boreholes January through June 2000. Submittal date: 12/29/2000.

162908 GS010208312322.001. Uranium Concentrations and 234U/238U Activity Ratios Analyzed Between August, 1998 and April, 2000 for Saturated-Zone Well Water, Springs, and Runoff Collected between April, 1998 and November 1999. Submittal date: 03/30/2001.

162910 GS010308312322.002. Chemical and Isotopic Data from Wells in Yucca Mountain Area, Nye County, Nevada, Collected between 12/11/98 and 11/15/99. Submittal date: 03/29/2001.

154734 GS010308312322.003. Field, Chemical and Isotopic Data from Wells in Yucca Mountain Area, Nye County, Nevada, Collected Between 12/11/98 and 11/15/99. Submittal date: 03/29/2001.

155307 GS010608312332.001. Potentiometric-Surface Map, Assuming Perched Conditions North of Yucca Mountain, in the Saturated Site-Scale Model. Submittal date: 06/19/2001.

156187 GS010608315215.002. Uranium and Thorium Isotope Data for Waters Analyzed Between January 18, 1994 and September 14, 1996. Submittal date: 06/26/2001.

156007 GS010808312322.004. Uranium and Uranium Isotopic Data for Water Samples from Wells and Springs in the Yucca Mountain Vicinity Collected Between December 1996 and December 1997. Submittal date: 08/29/2001.

163555 GS010908312332.002. Borehole Data from Water-Level Data Analysis for the Saturated Zone Site-Scale Flow and Transport Model. Submittal date: 10/02/2001.

168699 GS010908312332.003. Vertical Head Differences from Water-Level Data Analysis for the Saturated Zone Site-Scale Flow and Transport Model. Submittal date: 10/20/2001.

162874 GS010908314221.001. Geologic Map of the Yucca Mountain Region, Nye County, Nevada. Submittal date: 01/23/2002.

158690 GS011008314211.001. Interpretation of the Lithostratigraphy in Deep Boreholes NC-EWDP-19D1 and NC-EWDP-2DB Nye County Early Warning Drilling Program. Submittal date: 01/16/2001.

162911 GS011108312322.006. Field and Chemical Data Collected between 1/20/00 and 4/24/01 and Isotopic Data Collected between 12/11/98 and 11/6/00 from Wells in the Yucca Mountain Area, Nye County, Nevada. Submittal date: 11/20/2001.

174112 GS020108314211.001. Interpretation of the Lithostratigraphy in Deep Boreholes, NC-EWDP-7SC and NC-EWDP-15P, Nye County Early Warning Drilling Program. Submittal date: 01/16/2001.

162913 GS021008312322.002. Stable Isotopic Data for Water Samples Collected between 02/20/98 and 08/20/98 in the Yucca Mountain Area, Nye County, Nevada. Submittal date: 11/12/2002.

163483 GS030108314211.001. Interpretation of the Lithostratigraphy in Deep Boreholes NC-EWDP-18P, NC-EWDP-22SA, NC-EWDP-10SA, NC-EWDP-23P, NC-EWDP-19IM1A, and NC-EWDP-19IM2A, Nye County Early Warning Drilling Program, Phase III. Submittal date: 02/11/2003.

166467 GS031108312322.003. Uranium Concentrations and $^{234}U/^{238}U$ Ratios for Ground-Water Samples from Boreholes ER-EC-7, ER-18-2, and UE-18R Collected between December 1999 and June 2000. Submittal date: 11/25/2003.

174113 GS031108314211.004. Interpretation of the Lithostratigraphy in Deep Boreholes NC-EWDP-16P, NC-EWDP-27P, and NC-EWDP-28P, Nye County Early Warning Drilling Program, Phase IV A. Submittal date: 11/26/2003.

179431 GS031208312322.004. Dissolved Organic Carbon-14 (DOC-14) Hydrochronology Data for Groundwater from Wells in the Yucca Mountain Area for Samples Analyzed through 1/30/2003. Submittal date: 01/26/2004.

179422 GS040108312322.001. Field and Chemical Data Collected Between 10/4/01 and 10/3/02 and Isotopic Data Collected Between 5/19/00 and 5/22/03 from Wells in the Yucca Mountain Area, Nye County, Nevada. Submittal date: 06/07/2004.

172396 GS040208312322.003. Uranium Concentrations and 234U/238U Ratios from Spring, Well, Runoff, and Rain Waters Collected from the Nevada Test Site and Death Valley Vicinities and Analyzed between 01/15/98 and 08/15/98. Submittal date: 04/01/2004.

179432 GS040708312322.004. Strontium Isotope Ratios and Strontium Concentrations on Groundwater Samples from Springs in the Area of Amargosa Valley and Desert. Submittal date: 09/08/2004.

179433 GS040808312322.005. Strontium Isotope Ratios and Strontium Concentrations on Groundwater Samples in Support of Nye Co. Early Warning Drilling Program (EWDP) and the Alluvial Tracer Complex (ATC). Submittal date: 09/20/2004.

179434 GS040808312322.006. Field, Chemical, and Isotope Data for Spring and Well Samples Collected Between 03/01/01 and 05/12/04 in the Yucca Mountain Area, Nye County, Nevada. Submittal date: 11/15/2004.

174114 GS040908314211.001. Interpretation of the Lithostratigraphy in Deep Boreholes NC-EWDP-24P and NC-EWDP-29P, Nye County Early Warning Drilling Program, Phase IV B. Submittal date: 10/26/2004.

179435 GS050708314211.001. Description and Interpretation of Core Samples from Alluvial Core Holes NC-EWDP-19PB and NC-EWDP-22PC, Nye County Early Warning Drilling Program. Submittal date: 07/27/2005.

105937 GS920408312321.003. Chemical Composition of Groundwater in the Yucca Mountain Area, Nevada 1971 - 1984. Submittal date: 04/24/1987.

148109 GS930108315213.002. Water Chemistry and Sample Documentation for Two Samples from Lathrop Wells Cone and USW VH-2. Submittal date: 01/15/1993.

145525 GS930108315213.004. Uranium Isotopic Analyses of Groundwaters from SW Nevada – SE California. Submittal date: 01/21/1993.

145530 GS930308312323.001. Chemical Composition of Groundwater and the Locations of Permeable Zones in the Yucca Mountain Area. Submittal date: 03/05/1993.

145404 GS930908312323.003. Hydrochemical Data from Field Test and Lab Analyses of Water Samples Collected at Field Stations: USW VH-1, JF3, UE-29 UZN#91, Virgin Spring, Nevares Spring, UE-25 J#12, UE-25 J#13, UE-22 ARMY#1, and USW UZ-14. Submittal date: 09/30/1993.

149611 GS931100121347.007. Selected Ground-Water Data for Yucca Mountain Region, Southern Nevada and Eastern California, Through December 1992. Submittal date: 11/30/1993.

164673 GS940908315213.005. U Concentrations and 234U/238U Ratios for Waters in Yucca Mountain Region. Submittal date: 09/22/1994.

106516 GS950708315131.003. Woodrat Midden Age Data in Radiocarbon Years Before Present. Submittal date: 07/21/1995.

148114 GS950808312322.001. Field, Chemical, and Isotopic Data Describing Water Samples Collected in Death Valley National Monument and at Various Boreholes in and Around Yucca Mountain, Nevada, Between 1992 and 1995. Submittal date: 08/16/1995.

151649 GS951208312272.002. Tritium Analyses of Porewater from USW UZ-14, USW NRG-6, USW NRG-7A and UE-25 UZ#16 and of Perched Water from USW SD-7, USW SD-9, USW UZ-14 and USW NRG-7A from 12/09/92 to 5/15/95. Submittal date: 12/15/1995.

106517 GS960308315131.001. Woodrat Midden Radiocarbon (C14). Submittal date: 03/07/1996.

162915 GS960408312323.002. Chemical and Isotopic Data Describing Water Samples Collected from 11 Springs and One Stream Within Death Valley National Park in 1993, 1994, and 1995. Submittal date: 04/02/1996.

114124 GS960908312232.012. Comparison of Air-Injection Permeability Values to Laboratory Permeability Values. Submittal date: 09/26/1996.

162916 GS960908312323.005. Hydrochemical Data Obtained from Water Samples Collected at Water Well ER-30-1 on 1/31/95 and 2/1/95. Submittal date: 09/10/1996.

145405 GS970708312323.001. Delta 18-O and Delta D Stable Isotope Analyses of a Bore-Hole Waters from GEXA Well 4 and VH-2. Submittal date: 07/22/1997.

164674 GS970708315215.008. Strontium Isotope Ratios and Isotope Dilution Data for Strontium for Two Samples Collected at UE-25 C#3, 12/4/96 and 2/19/97. Submittal date: 07/29/1997.

145921 GS970808315215.012. Uranium and Thorium Isotope Data from Secondary Minerals in the ESF Collected Between 02/15/97 and 09/15/97. Submittal date: 09/17/1997.

149617 GS980108312322.005. Water Chemistry Data from Samples Collected at Borehole USW WT-24, Between 10/06/97 and 12/10/97. Submittal date: 01/26/1998.

146065 GS980208312322.006. Uranium Isotopic Data for Saturated- and Unsaturated-Zone Waters Collected by Non-YMP Personnel Between May 1989 and August 1997. Submittal date: 02/03/1998.

145412 GS980908312322.008. Field, Chemical, and Isotopic Data from Precipitation Sample Collected Behind Service Station in Area 25 and Ground Water Samples Collected at Boreholes UE-25 C #2, UE-25 C #3, USW UZ-14, UE-25 WT #3, UE-25 WT #17, and USW WT-24, 10/06/97 to 07/01/98. Submittal date: 09/15/1998.

118977 GS980908312322.009. Uranium Concentrations and $^{234}U/^{238}U$ Ratios from Spring, Well, Runoff, and Rain Waters Collected from the Nevada Test Site and Death Valley Vicinities and Analyzed between 01/15/1998 and 08/15/1998. Submittal date: 09/23/1998.

145692 GS990308312272.002. Isotopic Composition of Pore Water from Boreholes USW UZ-14 and USW NRG-6. Submittal date: 03/02/1999.

149393 GS990808312322.001. Field and Isotopic Data From Ground Water Samples From Wells in the Amargosa Valley and NTS. Submittal date: 08/23/1999.

162917 GS990808312322.002. Chemical and Isotopic Data from Ground Water Samples Collected from Wells in the Amargosa. Submittal date: 08/23/1999.

145263 GS991208314221.001. Geologic Map of the Yucca Mountain Region. Submittal date: 12/01/1999.

147077 LA0002JF831222.001. Apparent Infiltration Rates in Alluvium from USW UZ-N37, USW UZ-N54, USW UZ-14 and UE-25 UZ#16, Calculated by Chloride Mass Balance Method. Submittal date: 02/25/2000.

147079 LA0002JF831222.002. Apparent Infiltration Rates in PTN Units from USW UZ-7A, USW UZ-N55, USW UZ-14, UE-25 UZ#16, USW NRG-6, USW NRG-7A, and USW SD-6, SD-7, SD-9 and SD-12 Calculated by the Chloride Mass Balance Method. Submittal date: 02/25/2000.

165507 LA0202EK831231.002. Calculation of Corrected and Uncorrected Groundwater Carbon-14 Ages. Submittal date: 02/25/2002.

180317 LA0202EK831231.004. Calculation of the Maximum Possible Percentage of 1000Year-Old Water Present in Selected Yucca Mountain Area Groundwater Samples. Submittal date: 02/25/2002.

163561 LA0303PR831231.002. Estimation of Groundwater Drift Velocity from Tracer Responses in Single-Well Tracer Tests at Alluvium Testing Complex. Submittal date: 03/18/2003.

163788 LA0304TM831231.002. SZ Site-Scale Flow Model, FEHM Files for Base Case. Submittal date: 04/14/2003.

171890 LA0308RR831233.001. Regional Groundwater Flow Pathways in the Yucca Mountain Area Inferred from Hydrochemical and Isotopic Data. Submittal date: 08/25/2003.

165471 LA0309EK831223.001. UTM Coordinates for Selected Amargosa Desert Wells. Submittal date: 09/05/2003.

171887 LA0309EK831231.001. SZ Flow and Transport Model, FEHM Files for Tracer Transport. Submittal date: 09/02/2003.

166546 LA0309RR831233.001. Regional Groundwater Hydrochemical Data in the Yucca Mountain Area Used as Direct Inputs for ANL-NBS-HS-000021, REV 01. Submittal date: 09/05/2003.

166548 LA0309RR831233.002. Regional Groundwater Hydrochemical Data in the Yucca Mountain Area Used as Corroborative Data for ANL-NBS-HS-000021, REV 01. Submittal date: 09/05/2003.

171889 LA0310EK831231.001. SZ Geochemical Calculations, Groundwater Travel Times for Selected Wells. Submittal date: 10/16/2003.

165995 LA0310EK831232.001. SZ Geochemical Models, PHREEQC Files for Selected Groundwater Parameters. Submittal date: 10/02/2003.

165985 LA0311EK831223.001. Well Completion Summary Information for the Nye County EWDP, Phases I and II. Submittal date: 11/04/2003.

166068 LA0311EK831232.001. Hydrochemical Data Obtained from GEOCHEM.02 Database. Submittal date: 11/06/2003.

166069 LA0311EK831232.002. Groundwater Hydrochemical Data from Nye County Early Warning Drilling Project Boreholes as Reported by Nye County. Submittal date: 11/04/2003.

122733 LA9909JF831222.010. Chloride, Bromide, Sulfate, and Chlorine-36 Analyses of ESF Porewaters. Submittal date: 09/29/1999.

122736 LA9909JF831222.012. Chloride, Bromide, and Sulfate Analyses of Porewater Extracted from ESF Niche 3566 (Niche #1) and ESF 3650 (Niche #2) Drillcore. Submittal date: 09/29/1999.

145401 LAJF831222AQ97.002. Chlorine-36 Analyses of Packrat Urine. Submittal date: 09/26/1997.

145402 LAJF831222AQ98.011. Chloride, Bromide, Sulfate and Chlorine-36 Analyses of Springs, Groundwater, Porewater, Perched Water and Surface Runoff. Submittal date: 09/10/1998.

163044 LB03023DSSCP9I.001. 3-D Site Scale UZ Flow Field Simulations for 9 Infiltration Scenarios. Submittal date: 02/28/2003.

148744 MO0003SZFWTEEP.000. Data Resulting from the Saturated Zone Flow and Transport Expert Elicitation Project. Submittal date: 03/06/2000.

151492 MO0007GNDWTRIS.002. Isotopic Content of Groundwater from Yucca Mountain Project Borehole, USW G-2, Extracted from ANL-NBS-HS-000021, Geochemical and Isotopic Constraints on Groundwater Flow Directions, Mixing and Recharge at Yucca Mountain, Nevada. Submittal date: 07/27/2000.

151493 MO0007GNDWTRIS.003. Isotopic Content of Groundwater from Yucca Mountain Project Boreholes UZ-14, WT-17, and WT #3, Extracted from ANL-NBS-HS-000021, Geochemical and Isotopic Constraints on Groundwater Flow Directions, Mixing and Recharge at Yucca Mountain, Nevada. Submittal date: 07/27/2000.

151494 MO0007GNDWTRIS.004. Isotopic Content of Groundwater from Borehole TW-5 Extracted from ANL-NBS-HS-000021, Geochemical and Isotopic Constraints on Groundwater Flow Directions, Mixing and Recharge at Yucca Mountain, Nevada. Submittal date: 07/27/2000.

151495 MO0007GNDWTRIS.005. Isotopic Content of Groundwater from Yucca Mountain Project Borehole JF #3, Extracted from ANL-NBS-HS-000021, Geochemical and Isotopic Constraints on Groundwater Flow Directions, Mixing and Recharge at Yucca Mountain, Nevada. Submittal date: 07/28/2000.

151496 MO0007GNDWTRIS.006. Isotopic Content of Groundwater from Selected Yucca Mountain Project WT Boreholes Extracted from ANL-NBS-HS-000021, Geochemical and Isotopic Constraints on Groundwater Flow Directions, Mixing and Recharge at Yucca Mountain, Nevada. Submittal date: 07/28/2000.

151497 MO0007GNDWTRIS.007. Isotopic Content of Groundwater from Yucca Mountain Project Boreholes WT #14, WT #15, and WT #12, Extracted from ANL-NBS-HS-000021, Geochemical and Isotopic Constraints on Groundwater Flow Directions, Mixing and Recharge at Yucca Mountain, Nevada. Submittal date: 07/28/2000.

151508 MO0007GNDWTRIS.008. Isotopic Content of Groundwater from Yucca Mountain Project Borehole UE-25 P #1 Extracted from ANL-NBS-HS-000021, Geochemical and Isotopic Constraints on Groundwater Flow Directions, Mixing and Recharge at Yucca Mountain, Nevada. Submittal date: 07/28/2000.

151509 MO0007GNDWTRIS.009. Isotopic Content of Groundwater from Selected Yucca Mountain Project Boreholes Extracted from ANL-NBS-HS-000021, Geochemical and Isotopic Constraints on Groundwater Flow Directions, Mixing and Recharge at Yucca Mountain, Nevada. Submittal date: 07/28/2000.

151500 MO0007GNDWTRIS.010. Isotopic Content of Groundwater from Selected Yucca Mountain Project Boreholes Extracted from ANL-NBS-HS-000021, Geochemical and Isotopic Constraints on Groundwater Flow Directions, Mixing and Recharge at Yucca Mountain, Nevada. Submittal date: 07/28/2000.

151501 MO0007GNDWTRIS.011. Isotopic Content of Groundwater from Selected Boreholes Not Drilled for the Yucca Mountain Project Extracted from ANL-NBS-HS-000021, Geochemical and Isotopic Constraints on Groundwater Flow Directions, Mixing and Recharge at Yucca Mountain, Nevada. Submittal date: 07/28/2000.

151504 MO0007GNDWTRIS.013. Isotopic Content of Perched Groundwater from Yucca Mountain Project Boreholes Extracted from ANL-NBS-HS-000021, Geochemical and Isotopic Constraints on Groundwater Flow Directions, Mixing and Recharge at Yucca Mountain, Nevada. Submittal date: 07/28/2000.

151507 MO0007MAJIONPH.002. Major Ion Content of Groundwater from Borehole TW-5 Extracted from ANL-NBS-HS-000021, Geochemical and Isotopic Constraints on Groundwater Flow Directions, Mixing and Recharge at Yucca Mountain, Nevada. Submittal date: 07/27/2000.

151513 MO0007MAJIONPH.003. Major Ion Content of Groundwater from Yucca Mountain Project Borehole USW G-2, Extracted from ANL-NBS-HS-000021, Geochemical and Isotopic Constraints on Groundwater Flow Directions, Mixing and Recharge at Yucca Mountain, Nevada. Submittal date: 07/27/2000.

151516 MO0007MAJIONPH.004. Major Ion Content of Groundwater from Borehole ONC #1, Extracted from ANL-NBS-HS-000021, Geochemical and Isotopic Constraints on Groundwater Flow Directions, Mixing and Recharge at Yucca Mountain, Nevada. Submittal date: 07/27/2000.

151517 MO0007MAJIONPH.005. Major Ion Content of Groundwater from Boreholes UZ-14, WT-17 and WT #3, Extracted from ANL-NBS-HS-000021, Geochemical and Isotopic Constraints on Groundwater Flow Directions, Mixing and Recharge at Yucca Mountain, Nevada. Submittal date: 07/27/2000.

151518 MO0007MAJIONPH.006. Major Ion Content of Groundwater from Selected Boreholes Not Drilled on the Yucca Mountain Project, Extracted from ANL-NBS-HS-000021, Geochemical and Isotopic Constraints on Groundwater Flow Directions, Mixing and Recharge at Yucca Mountain, Nevada. Submittal date: 07/25/2000.

151519 MO0007MAJIONPH.007. Major Ion Content of Groundwater from Yucca Mountain Project Borehole UE-25 UZ #16, Extracted from ANL-NBS-HS-000021, Geochemical and Isotopic Constraints on Groundwater Flow Directions, Mixing and Recharge at Yucca Mountain, Nevada. Submittal date: 07/27/2000.

151521 MO0007MAJIONPH.008. Major Ion Content of Groundwater from Selected YMP and Other Boreholes Extracted from ANL-NBS-HS-000021, Geochemical and Isotopic Constraints on Groundwater Flow Directions, Mixing and Recharge at Yucca Mountain, Nevada. Submittal date: 07/27/2000.

151522 MO0007MAJIONPH.009. Major Ion Content of Groundwater from Borehole NDOT Extracted from ANL-NBS-HS-000021, Geochemical and Isotopic Constraints on Groundwater Flow Directions, Mixing and Recharge at Yucca Mountain, Nevada. Submittal date: 07/27/2000.

151523 MO0007MAJIONPH.010. Major Ion Content of Groundwater from Borehole UE-25 P #1 Extracted from ANL-NBS-HS-000021, Geochemical and Isotopic Constraints on Groundwater Flow Directions, Mixing and Recharge at Yucca Mountain, Nevada. Submittal date: 07/27/2000.

151524 MO0007MAJIONPH.011. Major Ion Content of Groundwater from Selected Yucca Mountain Project Boreholes Extracted from ANL-NBS-HS-000021, Geochemical and Isotopic Constraints on Groundwater Flow Directions, Mixing and Recharge at Yucca Mountain, Nevada. Submittal date: 07/27/2000.

151529 MO0007MAJIONPH.012. Major Ion Content of Groundwater from Selected YMP and Other Boreholes Extracted from ANL-NBS-HS-000021, Geochemical and Isotopic Constraints on Groundwater Flow Directions, Mixing and Recharge at Yucca Mountain, Nevada. Submittal date: 07/27/2000.

151530 MO0007MAJIONPH.013. Major Ion Content of Groundwater from Selected YMP and Other Boreholes Extracted from ANL-NBS-HS-000021, Geochemical and Isotopic Constraints on Groundwater Flow Directions, Mixing and Recharge at Yucca Mountain, Nevada. Submittal date: 07/27/2000.

151531 MO0007MAJIONPH.014. Major Ion Content of Groundwater from Selected Boreholes Not Drilled on the Yucca Mountain Project Extracted from ANL-NBS-HS-000021, Geochemical and Isotopic Constraints on Groundwater Flow Directions, Mixing and Recharge at Yucca Mountain, Nevada. Submittal date: 07/27/2000.

151532 MO0007MAJIONPH.015. Major Ion Content of Groundwater from NC-EWDP Boreholes Extracted from ANL-NBS-HS-000021, Geochemical and Isotopic Constraints on Groundwater Flow Directions, Mixing and Recharge at Yucca Mountain, Nevada. Submittal date: 07/27/2000.

151533 MO0007MAJIONPH.016. Major Ion Content of Perched Groundwater from Selected YMP Boreholes with Perched Water Extracted from ANL-NBS-HS-000021, Geochemical and Isotopic Constraints on Groundwater Flow Directions, Mixing and Recharge at Yucca Mountain, Nevada. Submittal date: 07/28/2000.

151534 MO0008MAJIONPH.017. Major Ion Content of Groundwater from Selected WT Boreholes Drilled for the Yucca Mountain Project Extracted from ANL-NBS-HS-000021, Geochemical and Isotopic Constraints on Groundwater Flow Directions, Mixing and Recharge at Yucca Mountain, Nevada. Submittal date: 08/02/2000.

153777 MO0012MWDGFM02.002. Geologic Framework Model (GFM2000). Submittal date: 12/18/2000.

153384 MO0012URANISOT.000. Water - Selected Uranium Abundance and Isotope Ratios. Submittal date: 12/06/2000.

154733 MO0102DQRBTEMP.001. Temperature Data Collected from Boreholes Near Yucca Mountain in Early 1980's. Submittal date: 02/21/2001.

155523 MO0102DQRGWREC.001. Groundwater Recharge Rate Data for the Four Reaches of Fortymile Wash Near Yucca Mountain, Nevada. Submittal date: 02/26/2001

157187 MO0112DQRWLNYE.018. Well Completion Diagram for Borehole NC-EWDP-19D. Submittal date: 12/05/2001.

168375 MO0203GSC02034.000. As-Built Survey of Nye County Early Warning Drilling Program (EWDP) Phase III Boreholes NC-EWDP-10S, NC-EWDP-18P, and NC-EWDP-22S - Partial Phase III List. Submittal date: 03/21/2002.

168378 MO0206GSC02074.000. As-Built Survey of Nye County Early Warning Drilling Program (EWDP) Phase III Boreholes, Second Set. Submittal date: 06/03/2002.

179372 MO0206NYE04926.119. NC-EWDP-7SC Well Completion Diagram. Submittal date: 06/19/2002.

165876 MO0306NYE05259.165. Revised NC-EWDP-19IM1 Well Completion Diagram. Submittal date: 07/02/2003.

165877 MO0306NYE05260.166. Revised NC-EWDP-19IM2 Well Completion Diagram. Submittal date: 07/02/2003.

179373 MO0306NYE05261.167. Revised NC-EWDP-10S Well Completion Diagram. Submittal date: 07/03/2003.

179374 MO0306NYE05262.168. Revised NC-EWDP-10P Well Completion Diagram. Submittal date: 07/03/2003.

179375 MO0306NYE05263.169. Revised NC-EWDP-18P Well Completion Diagram. Submittal date: 07/03/2003.

170556 MO0307GSC03094.000. As-Built Survey of Nye County Early Warning Drilling Program Phase IV Boreholes EWDP-16P, EWDP-27P & EWDP-28P. Submittal date: 07/14/2003.

165529 MO0309THDPHRQC.000. Input Data File (PHREEQC.DAT) for Thermodynamic Data Software Code PHREEQC, Version 2.3. Submittal date: 09/22/2003.

174103 MO0312GSC03180.000. As-Built Survey of Nye County Early Warning Drilling Program, Phase IV Boreholes: NC-EWPD-24P & NC-EWDP-29P. Submittal date: 12/03/2003.

174102 MO0408GSC04123.000. Nye County Early Warning Drilling Program, Phase IV, As-Built Location of NC-EWDP-19PB Borehole. Submittal date: 08/12/2004.

179336 MO0409SEPPSMPC.000. Potentiometric-Surface Map Showing Possible Changes After Including EWDP Phases III and IV Wells. Submittal date: 09/23/2004.

179599 MO0505NYE06464.314. NC-EWDP-22PC Well Completion Diagram. Submittal date: 05/16/2005

177372 MO0507NYE06631.323. EWDP Manual Water Level Measurements through February 2005. Submittal date: 07/21/2005.

174523 MO0507SPAINHFM.000. Input Data for HFM - USGS-Supplied Data to Supplement Regional Hydrogeologic Framework Model. Submittal date: 02/22/2005.

177371 MO0602SPAMODAR.000. Model Archives from USGS Special Investigations Report 2004-5205, Death Valley Regional Ground-Water Flow System, Nevada and California-Hydrogeologic Framework and Transient Ground-Water Flow Model. Submittal date: 02/10/2006.

179352 MO0610MWDHFM06.002. Hydrogeologic Framework Model (HFM2006) Stratigraphic Horizon Grids. Submittal date: 11/01/2006.

179486 MO0612NYE07008.366. NC-EWDP-32P WELL COMPLETION DIAGRAM. Submittal date: 12/04/2006.

179487 MO0612NYE07011.368. NC-EWDP-33P WELL COMPLETION DIAGRAM. Submittal date: 12/04/2006.

179337 MO0612NYE07122.370. EWDP Manual Water Level Measurements through November 2006. Submittal date: 12/15/2006.

129714 SNT05082597001.003. TSPA-VA (Total System Performance Assessment-Viability Assessment) Saturated Zone (SZ) Base Case Modeling Analysis Results. Submittal date: 02/03/1998.

9.4 OUTPUT DATA, LISTED BY DATA TRACKING NUMBER

LA0612RR150304.001. UTM Coordinates for Selected Nye County Early Warning Drilling Program Boreholes: NC-EWDP-7SC and Phases III and IV. Submittal date: 12/18/2006.

LA0612RR150304.002. Hydrochemical Data Obtained from the Underground Test Area (UGTA) Program's Geochem05 Database. Submittal date: 12/18/2006.

LA0612RR150304.003. Geochemical and Isotopic Data for Selected NC-EWDP Wells, Phases II, III, and IV. Submittal date: 01/02/2007.

LA0612RR150304.004. Regional Groundwater Flow Pathways In The Yucca Mountain Area Inferred From Hydrochemical And Isotopic Data. Submittal date: 01/02/2007.

LA0612RR150304.005. Uranium Activity Ratios Calculated from Isotopic Ratios Reported for Nye County EWDP Boreholes and McCracken Well by Geochron Laboratories, for Samples Collected between November 1999 and June 2000. Submittal date: 12/21/2006.

LA0612TM831231.001. SZ Site-Scale Flow Model, LaGriT Files for Base-Case FEHM Grid. Submittal date: 12/21/2006.

MO0611SCALEFLW.000. Water Table for the Saturated Zone Site Scale Flow Model. Submittal date: 11/15/2006.

SN0610T0510106.001. Water Level Data, Well Location Data, and Open Well Interval Data. Submittal date: 10/02/2006.

SN0612T0510106.003. Recharge and Lateral Groundwater Flow Boundary Conditions for the Saturated Zone (SZ) Site-Scale Flow Model. Submittal date: 12/04/2006.

SN0612T0510106.004. Saturated Zone (SZ) Site-Scale Flow Model PEST and FEHM Files Using HFM2006. Submittal date: 01/17/2007.

SN0702T0510106.006. Saturated Zone (SZ) Site-Scale Flow Model with "Water Table Rise" Alternate Conceptual Model - FEHM Files Using HFM2006. Submittal date: 02/19/2007.

SN0702T0510106.007. Nye County Early Warning Drilling Program (EWDP) Well Data for Period 2/2001 through 11/2006 Used for Saturated Zone (SZ) Flow Model Potentiometric Surface, Calibration and Validation. Submittal date: 02/22/2007

SN0704T0510106.008. Flux, head and particle track output from the qualified, calibrated saturated zone (SZ) site-scale flow model. Submittal date: 05/01/2007.

SN0705T0510106.009. PEST V11.1 Predictive Uncertainty Analysis Including The Prediction Maximizer. Submittal date: 05/24/2007.

9.5 SOFTWARE CODES

155082 Software Code: CORPSCON V. 5.11.08. 2001. WINDOWS NT 4.0. STN: 10547-5.11.08-00.

167994 Software Code: EARTHVISION V. 5.1. 2000. IRIX 6.5. STN: 10174-5.1-00.

163072 Software Code: EXT_RECH V. 1.0. 2002. Sun O.S. 5.7. STN: 10958-1.0-00.

179539 Software Code: FEHM V. 2.24. 2006. SUN 9.S. 5.7 & 5.8, Windows XP, RedHat Linux 7.1. STN: 10086-2.24-02.

173140 Software Code: LaGriT V. 1.1. 2004. Sun OS 5.7, 5.8, 5.9, IRIX64 OS 6.5. STN: 10212-1.1-00.

164654 Software Code: fehm2tec VV 1.0. 2003. Sun, Solaris 2.7 and 2.8. 11092-1.0-00.

164653 Software Code: maketrac VV 1.1. 2003. Sun, SunOS 5.7 and 5.8. 11078-1.1-00.

157837 Software Code: PHREEQC VV2.3. 2002. PC. 10068-2.3-01.

164652 Software Code: reformat_sz VV 1.0. 2003. Sun, Solaris 2.7 and 2.8. 11079-1.0-00.

161564 PEST V. 5.5. 2002. SUN O.S. 5.7 & 5.8, WINDOWS 2000, RedHat 7.3. STN: 10289-5.5-00.

179480 PEST V11.1. 2007. Windows. 611582-11.1-00.

155323 PHREEQC V. 2.3. 2001. WINDOWS 95/98/NT, Redhat 6.2. STN: 10068-2.3-00.

163070 Software Code: Extract VV 1.0. 2002. Sun UltraSPARC - SunOS 5.7. 10955-1.0-00.

163071 Software Code: Extract VV 1.1. 2002. Sun UltraSPARC - SunOS 5.7. 10955-1.1-00.

163073 Software Code: Mult_Rech VV 1.0. 2002. Sun UltraSPARC - SunOS 5.7. 10959-1.0-00.

180546 Software Code: SPDIS.EXE VV0.0, Windows XP. 611598-00-00.

163074 Software Code: Xread_Distr_Rech VV 1.0. 2002. Sun UltraSPARC - SunOS 5.7. 10960-1.0-00.

163075 Software Code: Xread_Distr_Rech_-UZ VV 1.0. 2002. Sun UltraSPARC - SunOS 5.7. 10961-1.0-00.

163076 Software Code: Xread_Reaches VV 1.0. 2002. Sun UltraSPARC - SunOS 5.7. 10962-1.0-00.

163077 Software Code: Xwrite_Flow_New VV 1.0-125. 2002. Sun UltraSPARC - SunOS 5.7. 10963-1.0-125-00.

163078 Software Code: Zone VV 1.0. 2002. Sun UltraSPARC - SunOS 5.7. 10957-1.0-00.

INTENTIONALLY LEFT BLANK

APPENDIX A
GEOCHEMICAL AND ISOTOPIC CONSTRAINTS ON GROUNDWATER FLOW

A1. PURPOSE

The purpose of the work described in this appendix is to provide an analysis of groundwater recharge rates, flow directions and velocities, and mixing proportions of water from different source areas based on groundwater geochemical and isotopic data. The analysis of hydrochemical and isotopic data is intended to provide a basis for evaluating the hydrologic system at Yucca Mountain independently of evaluations that are based purely on hydraulic arguments. In this way, this appendix is intended as an independent corroboration of the saturated zone flow model presented in the main text of this report.

This appendix is based on the previous revision of this report (BSC 2004 [DIRS 170037]) in that many of the same analyses and techniques were used to estimate generalized flow directions from hydrochemical data. However, several updates are made to the analyses including:

1. Analyze new data to determine chemical reactions in the groundwater system, the evolution of groundwater as it moves from upgradient source areas to downgradient areas of potential groundwater withdrawal, groundwater mixing relationships, and chemical and isotopic distributions of strontium and uranium.

2. Correct groundwater ^{14}C ages for water/rock interactions.

3. Provide an analysis of groundwater recharge rates, flow directions and velocities, and mixing proportions of water from different source areas.

4. Compare patterns of groundwater movement produced by the SZ flow model with flow patterns inferred from hydrochemical and isotopic data.

Information supporting the resolution of several technical issues related to the saturated zone was also developed in this appendix:

1. Groundwater residence times based on ^{14}C

2. Flow path lengths in alluvium and tuff.

Addressing these and related issues will help in determining the performance of the saturated zone as a natural barrier to radionuclide migration by providing validation information for the SZ site-scale flow model.

The physical and hydrochemical parameters summarized in this appendix are important controls on the transport of dissolved and colloidal species in the saturated zone. This information can be used in the SZ site-scale flow and SZ transport models to simulate the transport of radionuclides as breakthrough curves. These breakthrough curves are then used as input in the TSPA-LA calculations.

This appendix was left largely untouched from the previous revision of this report (BSC 2004 [DIRS 170037]) and that it is presented here to provide historical context. Appendix B represents analyses of the latest geochemical data, none of which contradict the findings in this appendix.

A2. NOT USED

A3. SOFTWARE CODES

Software uses in this appendix are considered a corroboration activity that provides indirect support for validation of the SZ site-scale flow model as described in Section 7. The computer code, PHREEQC V2.3 (STN: 10068-2.3-00; [DIRS 155323]), used directly in this appendix, is public-domain geochemical software whose description is summarized in Table A3-1. The software was obtained from Software Configuration Management (SCM) and is appropriate for the license application. The code was used only within its range of validation as required by LP-SI.11Q-BSC, *Software Management*. Input files for this appendix are identified in Section A4; technical data numbers of the associated modeling results are listed in Section A7.2.

Table A3-1. Software Used in Support of this Scientific Analysis

Software Name and Version (V)	Software Tracking Number (STN)	Description/ Section Where Used	Computer and Platform Identification	Reference	Date Baselined
PHREEQC, V2.3	10068-2.3-00	Used to speciate elements in groundwater, calculate mineral saturation indices, and calculate mixing fractions and chemical reactions required to produce observed groundwater compositions. PHREEQC is a C-language program developed by the U.S. Geological Survey (USGS). Used in Sections A6.3.5 and A6.3.6.6.2, A6.3.8 and A6.3.9	Windows 95/98/NT; Compaq professional workstation AP400	[DIRS 155323]	03/29/01
FEHM V2.20*	10086-2.20-00	Flow modeling/flow and transport modeling used to illustrate groundwater flow paths. Used in Section A6.3.10.	Sun workstation SunOS v. 5.7-5.8	[DIRS 161725]	01/28/03
reformat_sz V1.0	11079-1.0-00	Used to reformat hydrochemical and isotopic data originally in a text format for input into PHREEQC. Written in Fortran 77. Used in Sections A6.3.5, A6.3.6.6.2, and A6.3.8.	Solaris 2.7, 2.8	[DIRS 164652]	05/21/03
maketrac V1.1	11078-1.1-00	Used to create *trac* macro for FEHM. Used in Section A6.3.10.	Sun workstation SunOS v. 5.7-5.8	[DIRS 164653]	07/02/03
fehm2tec V1.0	11092-1.0-00	Used to reformat FEHM output for plotting with TECPLOT, V 8.0. Used in Section A6.3.10.	Sun workstation Solaris 2.7, 2.8	[DIRS 164654]	06/26/03

*NOTE: FEHM v2.20 was used throughout Appendix A because the analyses documented in this Appendix were not updated for revision 03 of this modeling report. Reference to FEHM v2.20 and its modeling results as documented in revision 2 of the SZ site-scale flow model remain in this document for historical accuracy.

The range of hydrochemical and isotopic data used in PHREEQC V2.3 (STN: 10068-2.3-00; [DIRS 155323]) is indicated by Tables A6-1 and A6-2. The results of all calculations using PHREEQC were checked with order-of-magnitude estimations.

FEHM V2.20 (STN: 10086-2.20-00; [DIRS 161725]) was used to illustrate groundwater flow paths predicted by the SZ flow model (DTN: LA0304TM831231.002 [DIRS 163788]), as documented in *Saturated Zone Site-Scale Flow Model* (BSC 2004 [DIRS 170037]).. The reformat_sz was used to reformat hydrochemical and isotopic data for input into PHREEQC; output from reformat_sz V1.0 (STN: 11079-1.0-00; [DIRS 164652]) was verified by visual inspection. Maketrac V1.1 (STN: 11078-1.1-00; [DIRS 164653]) was used to help create the trac macro for FEHM, and fehm2tec V1.0 (STN: 11092-1.0-00; [DIRS 164654]) was used to reformat FEHM output for plotting with TECPLOT. The output from the maketrac and fehm2tec codes was verified by visual inspection of the FEHM results.

Software use documented in historical versions of Appendix A and listed above in Table A3-1 is not listed in Table 3-1 because it is indirect-use software for the hydrochemistry analysis to conduct a corroboration activity and provides only validation support to the SZ site-scale flow model.

A4. INPUTS

This appendix summarizes hydrochemistry data to ultimately derive hydrochemically inferred flow pathways. The data evaluations, including the derived flow pathways, are used to corroborate information put forth in the main body of this report. As such, this appendix does not require direct inputs nor does it produce qualified technical outputs. Output developed within this appendix is considered unqualified intermediary output.

Input data used in this appendix come from several sources, as summarized in Table A4-1 and Table A4-2. Table A4-3 lists the types of chemical and isotopic groundwater data presented by the sources in Table A4-1 and A4-2, including local data for the Yucca Mountain area and regional data for the Death Valley flow system and Nevada Test Site (NTS). The input data referenced in Tables A4-1, A4-2 and Table A4-3 represent geochemical and isotopic characteristics of perched water and groundwater near Yucca Mountain and hence are appropriate for the intended use. Data from the Death Valley flow system immediately surrounding Yucca Mountain are also presented to provide evidence for potential sources of groundwater found near Yucca Mountain and place the Yucca Mountain groundwater system within a regional perspective. The data presented for the area around Yucca Mountain within the SZ site-scale flow model domain (Figure A6-1) include representative historical data sets collected in the 1960s through the 1990s, as well as more recent data from newly drilled wells. In the immediate Yucca Mountain area, nearly all data collected since Yucca Mountain came under consideration as a repository were evaluated. Data from the outlying areas were selected to provide more complete geographic coverage but are not nearly as comprehensive as the data sets in the Yucca Mountain area. When both new data (1990s and later) and historical data sets were available in an area, emphasis was generally given to the newer data sets because they were typically more comprehensive in terms of the suite of chemicals and isotopes that were analyzed. This emphasis was especially true for the areas north of Yucca Mountain in the Timber Mountain, Beatty Wash, Fortymile Canyon and Oasis Valley areas. In the west-central Amargosa Desert, the data represent a blend of historic and recently collected data because of uncertainty in the effects of recent groundwater development on groundwater compositions. Elsewhere (for example, in Amargosa Flats), historical data sets were used where they provided the only representative hydrochemical data for an area.

Data contained in the DTNs and other sources listed in Tables A4-1, A4-2 and A4-3 are summarized for each sample/well location in Section A6.3 (Tables A6-1 and A6-2) where areal distributions and scatterplots of the hydrochemical and isotopic data are discussed and portrayed on figures. Where multiple sets of data were available for a location/sample, these data were averaged to derive the values shown in those tables, and it is these compiled values that are plotted in the figures of Section A6.3. Groundwater samples taken from different depth intervals in the same well were evaluated to examine the trends of groundwater composition with depth in the well (see Section A6.3.3). Groundwater sample depths and information on the geologic units present in the sampled interval are given in Table A4-3 to aid in understanding the causes of similarities or differences in groundwater compositions from particular geographic areas. Tables A4-1 to A4-3 provide the DTN links back to the original data used to generate the compiled and plotted values listed and shown in Section A6.

Table A4-1. Sources of Data

DTN Description	DTN	Tables Used[2]
Chemical and isotopic data from borehole TW-5	MO0007GNDWTRIS.004 [DIRS 151494] [1]	S00368_001
	MO0007MAJIONPH.002 [DIRS 151507] [1]	S00352_001
Chemical data from the Nye County EWDP Wells in Amargosa Valley, Nevada, collected between 12/11/98 and 11/15/99.	MO0007MAJIONPH.015 [DIRS 151532] [1]	S00365_001
Chemical data from borehole NDOT collected 5/17/95	MO0007MAJIONPH.009 [DIRS 151522] [1]	S00359_001
Chemical and isotopic data from boreholes WT-7, WT-10, WT#12, WT#14, and WT#15	MO0007GNDWTRIS.006 [DIRS 151496] [1]	S00370_001
	MO0008MAJIONPH.017 [DIRS 151534] [1]	S00383_001
Stable isotope ratios and radiocarbon data for WT#12, WT#14, and WT#15	MO0007GNDWTRIS.007 [DIRS 151497] [1]	S00371_001
Chemical and isotopic data from test well UE-25 p#1, Yucca Mountain area, Nye County, Nevada	MO0007GNDWTRIS.008 [DIRS 151508] [1]	S00372_001
	MO0007MAJIONPH.010 [DIRS 151523] [1]	S00360_001
Chemical and isotopic data for groundwater in the Yucca Mountain area, Nevada 1971 to 1984	MO0007GNDWTRIS.009 [DIRS 151509] [1]	S00373_001
	MO0007MAJIONPH.011 [DIRS 151524] [1]	S00361_001
	MO0007GNDWTRIS.010 [DIRS 151500] [1]	S00374_001
Chemical composition of groundwater from ONC#1	MO0007MAJIONPH.004 [DIRS 151516] [1]	S00354_001
Chemical and isotopic data from perched groundwater at selected YMP boreholes	MO0007MAJIONPH.016 [DIRS 151533]	S00378_001
	MO0007GNDWTRIS.013 [DIRS 151504] [1]	S00377_001
Chemical analyses of water from selected wells and springs in the Yucca Mountain area, Nevada, and southeastern California	MO0007MAJIONPH.012 [DIRS 151529] [1]	S00362_001
Chemical composition of groundwater in the Yucca Mountain area	MO0007MAJIONPH.013 [DIRS 151530] [1]	S00363_001
Chemical and isotopic data for groundwater in the west-central Amargosa Desert, Nevada	MO0007GNDWTRIS.011 [DIRS 151501] [1]	S00375_001
	MO0007MAJIONPH.014 [DIRS 151531] [1]	S00364_001
Selected groundwater data for Yucca Mountain region, southern Nevada, through December 1992	MO0007GNDWTRIS.005 [DIRS 151495] [1]	S00369_001
	MO0007MAJIONPH.008 [DIRS 151521] [1]	S00358_001
Hydrochemical database for the Death Valley Region	MO0007MAJIONPH.006 [DIRS 151518] [1]	S00356_001
Chemical and isotopic data for groundwater samples collected at boreholes USW UZ-14, UE-25 WT#3, and USW WT-17	MO0007GNDWTRIS.003 [DIRS 151493] [1]	S00367_001
	MO0007MAJIONPH.005 [DIRS 151517] [1]	S00355_001
Chemical composition of groundwater from UZ#16	MO0007MAJIONPH.007 [DIRS 151519] [1]	S00357_001
Chemical and isotopic data for borehole USW G-2	MO0007GNDWTRIS.002 [DIRS 151492] [1]	S00366_001
	MO0007MAJIONPH.003 [DIRS 151513] [1]	S00353_001
Chemical and isotopic data from the CIND-R-LITE well samples collected on 5/17/95 and 9/6/95	GS000700012847.001 [DIRS 150842] [1]	S00446_001

Table A4-1. Sources of Data (Continued)

DTN Description	DTN[1]	Tables Used[2]
Field, chemical, and isotopic data describing water samples collected in Death Valley National Monument and at various boreholes in and around Yucca Mountain, Nevada, between 1992 and 1995	GS950808312322.001 [DIRS 148114] [1]	S96068_001 to S96068_003, S96068_010, S96068_011, S96068_015 to S96068_018, S96068_032, S96068_036 to S96068_040, S96068_042, S96068_043
$\delta^{18}O$ and δD stable isotope analyses of borehole waters from GEXA Well 4 and VH-2	GS970708312323.001 [DIRS 145405] [1]	S97550_001 S97550_002
Uranium concentrations and $^{234}U/^{238}U$ ratios from spring, well, runoff, and rainwater collected from the NTS and Death Valley vicinities and analyzed between 01/15/98 and 08/15/98	GS980908312322.009 [DIRS 118977] [1]	S99222_001
Water chemistry and sample documentation for two samples from Amargosa Valley (formerly Lathrop Wells) cone and USW VH-2	GS930108315213.002 [DIRS 148109] [1]	S98045_002 to S98045_010, S98045_023, S98045_029
Uranium isotopic analyses of groundwater from SW Nevada–SE California	GS930108315213.004 [DIRS 145525] [1]	S96290_001 S96290_002
Stable isotopic data for water samples collected between 02/20/98 and 08/20/98 in the Yucca Mountain area, Nye County, Nevada	GS021008312322.002 [DIRS 162913] [1]	S02343_001 S02343_002
Field and isotopic data from groundwater samples from wells in the Amargosa Valley and NTS	GS990808312322.001 [DIRS 149393] [1]	S99384_001 S99384_002
Chemical and isotopic data from groundwater samples collected from wells in the Amargosa	GS990808312322.002 [DIRS 162917] [1]	S99385_001 S99385_002
Field, chemical, and isotopic data from wells in the Yucca Mountain area, Nye County, Nevada, collected between 12/11/98 and 11/15/99	GS010308312322.003 [DIRS 154734] [1]	S01053_001 S01053_002 S01053_004
Field and chemical data collected between 1/20/00 and 4/24/01 and isotopic data collected between 12/11/98 and 11/6/00 from wells in the Yucca Mountain area, Nye County Nevada	GS011108312322.006 [DIRS 162911] [1]	S01174_001 S01174_002
Uranium and thorium isotope data for waters analyzed between January 18, 1994, and September 14, 1996	GS010608315215.002 [DIRS 156187] [1]	S01134_001
Uranium and uranium isotope data for water samples from wells and springs in the Yucca Mountain vicinity collected between December 1996 and December 1997	GS010808312322.004 [DIRS 156007] [1]	S01132_001
Uranium concentrations and $^{234}U/^{238}U$ ratios for waters in Yucca Mountain region	GS940908315213.005 [DIRS 164673]	S96241_002 S96241_003

Table A4-1. Sources of Data (Continued)

DTN Description	DTN[1]	Tables Used[2]
Hydrochemical data obtained from water samples collected at water well ER-30-1 on 1/31/95 and 2/1/95	GS960908312323.005 [DIRS 162916] [1]	S97098_002 to S97098_005, S97098_013, S97098_017 to S97098_021, S97098_028 to S97098_031
Strontium isotope ratios and isotope dilution data for strontium for two samples collected at UE-25 c#3, 12/4/96 and 2/19/97	GS970708315215.008 [DIRS 164674] [1]	S97527_001 S97527_002
Tritium analyses of pore water from USW UZ-14, USW NRG-6, USW NRG-7A, and UE-25 UZ#16 and of perched water from USW SD-7, USW SD-9, USW UZ-14, and USW NRG-7A from 12/09/92 to 5/15/95	GS951208312272.002 [DIRS 151649]	S01175_002
Chloride, bromide, sulfate and chlorine-36 analyses of springs, groundwater, pore water, perched water, and surface runoff	LAJF831222AQ98.011 [DIRS 145402]	S98328_001
SZ site-scale flow model, FEHM files for SZ site-scale flow model	LA0304TM831231.002 [DIRS 163788]	—
Thermodynamic characteristics input file required to run PHREEQC	MO0309THDPHRQC.000 [DIRS 165529]	S03316_001
Uranium activity ratios of pore waters from upper lithophysal unit of Topopah Spring tuff	MO0012URANISOT.000 [DIRS 153384]	—
Field, chemical, and isotopic data from a precipitation sample collected behind the service station in area 25 and groundwater samples collected at boreholes UE-25 c#2, UE-25 c#3, USW UZ-14, UE-25 WT#3, USW WT-17, and USW WT-24, between 10/06/97 and 07/01/98	GS980908312322.008 [DIRS 145412]	S98383_001, 003, 005 to 007, 009, 014, 016, 018, 022, 024, 025, 028, 031, 038, 041 to 044, 046
Uranium Concentrations and 234U/238U Ratios from Spring, Well, Runoff, and Rain Waters Collected from the Nevada Test Site and Death Valley Vicinities and Analyzed between 01/15/98 and 08/15/98 (Only the data for Water Well 8 and c#3 were used as input from this DTN).	GS040208312322.003 [DIRS 172396]	S04101_001

[1]DTNs that reference this footnote are acquired-data sources used as input for developed-data DTN: LA0309RR831233.001 [DIRS 166546], which is cited as one of the sources for data shown in Tables A6-1 and A6-2. In this case, the acquired-data DTN has not been listed separately as a source for data in the footnotes of those two tables.

[2]Names of the tables within each DTN that were sources of data.

Table A4-2. Sources of Data and Other Information

Information Used	Reference (DTN)[1]	Source of Data Used
Chloride, bromide, sulfate, and chlorine-36 analyses of ESF porewaters	LA9909JF831222.010 [DIRS 122733]	S99410_001
Chloride, bromide, and sulfate analyses of pore water extracted from ESF Niche 3566 (Niche #1) and ESF 3650 (Niche #2) drill core	LA9909JF831222.012 [DIRS 122736]	S99412_001
Apparent infiltration rates in alluvium from USW UZ-N37, USW UZ-N54, USW UZ-14, and UE-25 UZ#16, calculated by chloride mass-balance method	LA0002JF831222.001 [DIRS 147077]	S00142_001
Apparent infiltration rates in PTn units from USW UZ-7A, USA UZ-N55, USW UZ-14, UE-25 UZ#16, USW NRG-6, USW NRG-7A, and USW SD-6, SD-7, SD-9, and SD-12 calculated by the chloride mass-balance method	LA0002JF831222.002 [DIRS 147079]	S00143_001 S00143_002 S00143_003
Uranium and thorium isotopic data from secondary minerals in the ESF collected between 02/15/97 and 09/15/97	GS970808315215.012 [DIRS 145921]	S97566_001 S97566_003 S97566_006
Chemical and isotopic data from wells in Yucca Mountain area, Nye County, Nevada collected between 12/11/98 and 11/15/99	GS010308312322.002 [DIRS 162910] [1]	S01052_001
Uranium concentrations and $^{234}U/^{238}U$ activity ratios analyzed between August 1998 and April 2000 for saturated-zone well water, springs, and runoff collected between April 1998 and November 1999	GS010208312322.001 [DIRS 162908] [1]	S01051_001
Chemical and isotopic data describing water samples collected from 11 springs and one stream within Death Valley National Park in 1993, 1994, and 1995	GS960408312323.002 [DIRS 162915] [1]	S00176_001
Field, chemical, and isotopic data from a precipitation sample collected behind the service station in area 25 and groundwater samples collected at boreholes UE-25 c#2, UE-25 c#3, USW UZ-14, UE-25 WT#3, USW WT-17, and USW WT-24, between 10/06/97 and 07/01/98	GS980908312322.008 [DIRS 145412] [1]	S98383_001, S98383_003, S98383_005, S98383_006, S98383_007, S98383_009, S98383_014, S98383_016, S98383_018, S98383_022, S98383_024, S98383_025, S98383_028, S98383_031, S98383_038, S98383_041 to S98383_044, S98383_046
Selected groundwater data for Yucca Mountain region, southern Nevada, and eastern California, through December 1992	GS931100121347.007 [DIRS 149611] [1]	S96375_006, S96375_007

Table A4-2. Sources of Data and Other Information (Continued)

Information Used	Reference (DTN) [1]	Source of Data Used
Water chemistry data from samples collected at borehole USW WT-24 between 10/06/97 and 12/10/97	GS980108312322.005 [DIRS 149617] [1]	S98308_001, S98308_006, S98308_007, S98308_009, S98308_010, S98308_015, S98308_019, S98308_026, S98308_027, S98308_029, S98308_031, S98308_033, S98308_036 S98308_038
Chemical composition of groundwater and the locations of permeable zones in the Yucca Mountain area	GS930308312323.001 [DIRS 145530] [1]	S97314_008, S97314_017, S97314_018
Chemical composition of groundwater in the Yucca Mountain area, Nevada, 1971 to 1984	GS920408312321.003 [DIRS 105937]	S97126_009, S97126_018, S97126_019
Selected groundwater hydrochemical and isotopic data from Geochem02.mdb—the Department of Energy's comprehensive water quality database for groundwater in the vicinity of the Nevada Test Site (Rev. 4)	LA0311EK831232.001 [DIRS 166068]	—
Hydrochemical data from field tests and lab analyses of water samples collected at field stations USW VH-1, JF3, UE-29 UZN#91, Virgin Spring, Nevares Spring, UE-25 J#12, UE-25 J#13, UE-22 Army#1, and USW UZ-14	GS930908312323.003 [DIRS 145404]	S96076_001
Isotopic compositions of pore water from boreholes USW UZ-14 and USW NRG-6	GS990308312272.002 [DIRS 145692]	S00254_001
Groundwater strontium isotope data from selected Nye County Early Warning Drilling Program borehole	LA0311EK831232.002 [DIRS 166069]	—
Chemical composition of groundwater in the Yucca Mountain area, Nevada, 1971-1984	Benson and McKinley 1985 [DIRS 101036]	Tables 1 and 5
Hydrochemical database for the Yucca Mountain area, Nye County, Nevada	Oliver and Root 1997 [DIRS 100069], *yucca.xls*	Hydrochemical, isotope and summary worksheets
$^{234}U/^{238}U$ evidence for local recharge and patterns of groundwater flow in the vicinity of Yucca Mountain	Paces et al. 2002 [DIRS 158817]	Table 1, Appendix A
Sources and mechanisms of recharge for groundwater in the west-central Amargosa Desert, Nevada—a geochemical interpretation	Claassen 1985 [DIRS 101125]	Table 1

Table A4-2. Sources of Data and Other Information (Continued)

Information Used	Reference (DTN)[1]	Source of Data Used
Chemical and isotopic data for groundwater in southern Nevada.	Rose et al. 1997 [DIRS 144725]	Tables 2, 3, and 4
Preliminary report on the isotope hydrology investigations at the Nevada Test Site: Hydrologic Resources Management Program, FY 1992–1993	Davisson et al. 1994 [DIRS 162939]	Tables 1 and 2
Groundwater chemistry at the Nevada Test Site: data and preliminary interpretations	Chapman and Lyles 1993 [DIRS 162940]	Appendix B, Figs. 10, 12, and 14
Well completion summary information for the Nye County EWDP, Phases I and II	LA0311EK831223.001 [DIRS 165985]	—
Well completion data and spring discharge area lithologies for the PM-OV area	Rose et al. 2002 [DIRS 162938]	Appendix A
UTM coordinates for selected Amargosa Desert wells	LA0309EK831223.001 [DIRS 165471]	spreadsheet Claassen_coord.xls
Borehole data from water-level analysis for the SZ site-scale flow and transport model	GS010908312332.002 [DIRS 163555][2]	*mean312411.xls* (columns C and D only)
Uranium isotopic data for saturated- and unsaturated-zone waters collected by non-YMP personnel between May 1989 and August 1997	GS980208312322.006 [DIRS 146065]	S98201_001 S98201_002
Uranium concentrations and $^{234}U/^{238}U$ ratios for groundwater samples from boreholes ER-EC-7, ER-18-2, and UE-18r, collected between December 1999 and June 2000	GS031108312322.003 [DIRS 166467]	—

[1]DTNs that reference this footnote are acquired-data sources used as input for developed-data DTN: LA0309RR831233.002 [DIRS 166548], which is cited as one of the sources for data shown in Tables A6-1 and A6-2. In this case, the acquired-data DTN has not been listed separately as a source for data in the footnotes of those two tables.

[2]This DTN was only used to establish well locations consistent with the flow model. Water-level data were not used to develop the geochemical flowpaths.

Table A4-3. Summary of Groundwater Wells and Data Sources

Well Identifier	Abbreviation Used in Appendix	Figure A6-5	UTM-X[a] (m)	UTM-Y[3] (m)	Area[b]		Approximate Interval Sampled (m)[e]	Geologic Unit[c,e]	Reference for Sampled Depth and Chemical (C) and Isotopic (I) Data[d]
Oasis Valley/Northwest Amargosa									
ER-EC-08	ER-EC-08	1	532764	4106142	OV/NWA	Oasis Valley/Northwest Amargosa	(192.6 to 320.0) (423.1 to 474.9) (495.6 to 606.6)[4]	Tfb Tmaw Tmap[4]	DTN: LA0311EK831232.001 [DIRS 166068], 7/23/99, 6/28/00 and 7/12/00 samples
ER-OV-01	ER-OV-01	2	528417	4104084	OV/NWA	Oasis Valley/Northwest Amargosa	(45.7 to 51.8)[8]	Tuff[8]	DTNs: LA0311EK831232.001 [DIRS 166068], 11/8/97 sample; GS010808312322.004 [DIRS 156007], U concentrations and isotopes
ER-OV-06a	ER-OV-06a	3	528417	4104084	OV/NWA	Oasis Valley/Northwest Amargosa	(154.2 to 160.3)[8]	Tuff[8]	DTNs: LA0311EK831232.001 [DIRS 166068], 11/7/97 and 11/8/97 samples; GS010808312322.004 [DIRS 156007], U concentrations and isotopes
ER-OV-05	ER-OV-05	4	520280	4099809	OV/NWA	Oasis Valley/Northwest Amargosa	(51.8 to 57.9)[8]	Alluvium[8]	DTN: LA0311EK831232.001 [DIRS 166068], 11/7/97 sample
ER-OV-02	ER-OV-02	5	526310	4098716	OV/NWA	Oasis Valley/Northwest Amargosa	(51.8 to 57.9)[8]	colluvial and alluvial gravel[8]	DTNs: LA0311EK831232.001 [DIRS 166068], 11/11/97 sample); GS010808312322.004 [DIRS 156007], U concentrations and isotopes
Springdale Upper Well (10S/47E-32adc)	Springdale Upper Well (10S/47E-32adc)	6	523522	4097506	OV/NWA	Oasis Valley/Northwest Amargosa	open borehold (depth not reported)	tuff breccia or alluvium[4]	DTNs: LA0311EK831232.001 [DIRS 166068], 11/12/97 sample; GS010808312322.004 [DIRS 156007], U concentrations and isotopes
Goss Springs North (11S/47E-10bad)	Goss Springs North (11S/47E-10bad)	7	526100	4094647	OV/NWA	Oasis Valley/Northwest Amargosa	0.0 (spring)	not reported	DTNs: LA0311EK831232.001 [DIRS 166068], 11/13/97 sample; GS010808312322.004 [DIRS 156007], U concentrations and isotopes

Table A4-3. Summary of Groundwater Wells and Data Sources (Continued)

Well Identifier	Abbreviation Used in Appendix	Figure A6-5	UTM-X[a] (m)	UTM-Y[3] (m)	Area[b]		Approximate Interval Sampled (m)[d]	Geologic Unit[c,d]	Reference for Sampled Depth and Chemical (C) and Isotopic (I) Data
Oasis Valley/Northwest Amargosa (Continued)									
ER-OV-03a	ER-OV-03a	8	526299	4094587	OV/NWA	Oasis Valley/Northwest Amargosa	(67.1 to 73.2)[8]	tuff[8]	DTNs: LA0311EK831232.001 [DIRS 166068], 11/9/97 sample; GS010808312322.004 [DIRS 156007], U concentrations and isotopes
ER-OV-03a3	ER-OV-03a3	9	526299	4094587	OV/NWA	Oasis Valley/Northwest Amargosa	(34.4 to 40.5)[8]	Tma, tuff[8]	DTNs: LA0311EK831232.001 [DIRS 166068], 11/9/97 sample; GS010808312322.004 [DIRS 156007], U concentrations and isotopes
ER-OV-03a2	ER-OV-03a2	10	526299	4094587	OV/NWA	Oasis Valley/Northwest Amargosa	(183.5 to 189.6)[8]	Not reported	DTNs: LA0311EK831232.001 [DIRS 166068], 11/9/97 sample; GS010808312322.004 [DIRS 156007], U concentrations and isotopes
Goss Spring (11S/47E-10bcc)	Goss Spring (11S/47E-10bcc)	11	526061	4093440	OV/NWA	Oasis Valley/Northwest Amargosa	0.0 (spring)[2]	Tv[2]	DTN: LA0311EK831232.001 [DIRS 166068], 9/7/95 sample
ER-OV-04a	ER-OV-04a	12	525671	4089316	OV/NWA	Oasis Valley/Northwest Amargosa	(33.8 to 39.9)[8]	Alluvium[8]	DTNs: LA0311EK831232.001 [DIRS 166068], 11/7/97 sample;GS010808312322.004 [DIRS 156007], U concentrations and isotopes
Beatty Well no. 1 (Wat&Sanit Distr)	Beatty Well no. 1 (Wat&Sanit Distr)	13	521378	4085329	OV/NWA	Oasis Valley/Northwest Amargosa	(30.0 to 48.8)	Not reported	DTN: LA0311EK831232.001 [DIRS 166068], 2/11/97 and 4/28/97 samples

Table A4-3. Summary of Groundwater Wells and Data Sources (Continued)

Well Identifier	Abbreviation Used in Appendix	Figure A6-5	UTM-X[a] (m)	UTM-Y[3] (m)	Area[b]		Approximate Interval Sampled (m)[d]	Geologic Unit[c,d]	Reference for Sampled Depth and Chemical (C) and Isotopic (I) Data
Oasis Valley/Northwest Amargosa (Continued)									
Bond Gold Mining #1	Bond Gold Mining #1	14	516203	4074502	OV/NWA	Oasis Valley/Northwest Amargosa	Not reported	Qal[13]	DTNs: GS010308312322.003 [DIRS 154734], T, pH, Alk, ions, $\delta^{18}O$, δD, $\delta^{13}C$); GS011108312322.006 [DIRS 162911], ^{14}C, $\delta^{18}O$, δD, $\delta^{13}C$, $\delta^{34}S$; GS010208312322.001 [DIRS 162908], U concentrations and isotopes; GS010308312322.002 [DIRS 162910], U concentrations
US Ecology MW-313	US Ecology MW-313	15	527666	4069293	OV/NWA	Oasis Valley/Northwest Amargosa	open borehole (depth not reported)	Qal[13]	DTNs: GS010308312322.003 [DIRS 154734], T, pH, Alk, ions, $\delta^{18}O$, δD, $\delta^{13}C$; GS011108312322.006 [DIRS 162911], ^{14}C, $\delta^{18}O$, δD, $\delta^{13}C$, $\delta^{34}S$; GS010208312322.001 [DIRS 162908], U concentrations and isotopes; GS010308312322.002 [DIRS 162910], U concentrations
US Ecology MW-600	US Ecology MW-600	16	527666	4069293	OV/NWA	Oasis Valley/Northwest Amargosa	open borehole (depth not reported)	Qal[13]	DTNs: GS010308312322.003 [DIRS 154734], T, pH, Alk, ions, $\delta^{18}O$, δD, $\delta^{13}C$; GS011108312322.006 [DIRS 162911], ^{14}C, $\delta^{18}O$, δD, $\delta^{13}C$, $\delta^{34}S$; GS010208312322.001 [DIRS 162908], U concentrations and isotopes; GS010308312322.002 [DIRS 162910], U concentrations

Table A4-3. Summary of Groundwater Wells and Data Sources (Continued)

Well Identifier	Abbreviation Used in Appendix	Figure A6-5	UTM-X[a] (m)	UTM-Y[3] (m)	Area[b]		Approximate Interval Sampled (m)[d]	Geologic Unit[c,d]	Reference for Sampled Depth and Chemical (C) and Isotopic (I) Data
Oasis Valley/Northwest Amargosa (Continued)									
Nucl. Eng. Co.	NEC Well	17	527519	4068738	OV/NWA	Oasis Valley/Northwest Amargosa	open borehole (86 to 180)[3]	QTal[2]	DTNs: MO0007GNDWTRIS.011 [DIRS 151501). $\delta^{13}C$, ^{14}C; MO0007MAJIONPH.014 [DIRS 151531], C
US Ecology MR-3	US Ecology MR-3	18	527395	4068707	OV/NWA	Oasis Valley/Northwest Amargosa	open borehole (depth not reported)	Qal[13]	DTNs: GS010308312322.003 [DIRS 154734], T, pH, Alk, $\delta^{18}O$, δD, $\delta^{13}C$; GS011108312322.006 [DIRS 162911], $\delta^{18}O$, δD, $\delta^{13}C$, $\delta^{34}S$; GS010308312322.003 [DIRS 154734], ^{14}C; GS010208312322.001 [DIRS 162908], U concentrations and isotopes
Timber Mountain									
UE-18r	UE-18r	19	549322	4109762	TM	Timber Mountain	509[4,6]	Tm, debris flow[4]	DTNs: LA0311EK831232.001 [DIRS 166068], 7/11/91,8/11/92 and 12/9/99 samples; GS031108312322.003 [DIRS 154734], U isotopes
ER-18-2	ER-18-2	20	555725	4106389	TM	Timber Mountain	(411.9 to 758.0)[4]	Tmar[4]	DTNs: LA0311EK831232.001 [DIRS 166068], 3/21/00 sample; GS031108312322.003 [DIRS 154734], U isotopes
ER-EC-05	ER-EC-05	21	538702	4106389	TM	Timber Mountain	(356.3 to 439.8) (559.3 to 654.1) (688.7 to 755.9)[4]	Ttc Tfbr,Tfbw Tmap[4]	DTNs: LA0311EK831232.001 [DIRS 166068], 7/8/99,5/4/00, and 5/25/00 samples; GS010808312322.004 [DIRS 156007], U concentrations and isotopes
Coffer's Ranch Windmill Well	Coffer's Ranch Windmill Well	22	539421	4095192	TM	Timber Mountain	(109.8 to 146.3)[4]	Not reported	DTNs: LA0311EK831232.001 [DIRS 166068], samples from 1994 through 1997; GS010808312322.004 [DIRS 156007], U concentrations and isotopes

Table A4-3. Summary of Groundwater Wells and Data Sources (Continued)

Well Identifier	Abbreviation Used in Appendix	Figure A6-5	UTM-X[a] (m)	UTM-Y[3] (m)	Area[b]		Approximate Interval Sampled (m)[d]	Geologic Unit[c,d]	Reference for Sampled Depth and Chemical (C) and Isotopic (I) Data
Timber Mountain (Continued)									
ER-OV-03c	ER-OV-03c	23	535494	4094374	TM	Timber Mountain	(156.1 to 162.2)[4,8]	Tma[4]	DTNs: LA0311EK831232.001 [DIRS 166068], 11/10/97 sample; GS010808312322.004 [DIRS 156007], U concentrations and isotopes
ER-EC-07	ER-EC-07	24	546484	40931217	TM	Timber Mountain	(272.8 to 312.4) (351.4 to 399.3)[4]	Tfb,Tfl[4]	DTNs: LA0311EK831232.001 [DIRS 166068], 8/7/99, 4/28/2000 and 6/5/00 samples; GS031108312322.003 [DIRS 166467], U isotopes
Fortymile Wash – North									
Water Well 8	Water Well 8	25	563113	4113275	FMW-N	Fortymile Wash – North	377[6]	Tv[2]	DTNs: LA0311EK831232.001 [DIRS 166068], 11/4/97 sample; GS040208312322.003 [DIRS 172396], U concentrations and isotopes
Test Well 1 (USGS HTH #1)	Test Well 1 (USGS HTH #1)	26	569000	4112499	FMW-N	Fortymile Wash – North	624[6]	Tv[5]	DTN: LA0311EK831232.001 [DIRS 166068], 8/13/92 sample
UE-18t	UE-18t	27	559591	4109095	FMW-N	Fortymile Wash – North	(577.9 to 792.5)[4]	Tm[4]	DTN: LA0311EK831232.001 [DIRS 166068], 9/23/88 sample
ER-30-1 (upper)	ER-30-1 (upper)	28	560805	4100463	FMW-N	Fortymile Wash – North	(179.1 to 185.2)[4]	Basaltic lava[4]	DTNs: GS960908312323.005 [DIRS 162916], ions and most isotopes; GS950808312322.001 [DIRS 148114], T, pH, Alkalinity, $^{87}Sr/^{86}Sr$
ER-30-1 (lower)	ER-30-1 (lower)	29	560805	4100463	FMW-N	Fortymile Wash – North	(227.2 to 233.3)[4]	Gravelly sand[4]	DTNs: GS960908312323.005 [DIRS 162916], ions and most isotopes; GS950808312322.001 [DIRS 148114], T, pH, Alkalinity, $^{87}Sr/^{86}Sr$

Table A4-3. Summary of Groundwater Wells and Data Sources (Continued)

Well Identifier	Abbreviation Used in Appendix	Figure A6-5	UTM-X[a] (m)	UTM-Y[3] (m)	Area[b]		Approximate Interval Sampled (m)[d]	Geologic Unit[c,d]	Reference for Sampled Depth and Chemical (C) and Isotopic (I) Data
Fortymile Wash – North (Continued)									
UE-29 a#2	a#2(dp)	30	555753	4088351	FMW-N	Fortymile Wash – North	247 to 354[1]	Th[2]	DTNs: MO0007GNDWTRIS.010 [DIRS 151500], $\delta^{18}O$, δD, $\delta^{13}C$, ^{14}C; MO0007MAJIONPH.013 [DIRS 151530], C; GS010808312322.004 [DIRS 156007], U concentrations and isotopes; GS930308312323.001 [DIRS 145530], T, F^-, $Sr2^+$
	a#2(sh)	31					87 to 213[1]	Th[2]	
UE-29a#1 HTH	UE-29a#1 HTH	32	555758	4088341	FMW-N	Fortymile Wash – North	(10.7 to 65.5)[4]	Rhyolite[4]	DTNs: LA0311EK831232.001 [DIRS 166068], 11/6/97 sample; GS010808312322.004 [DIRS 156007], U concentrations and isotopes
UE-25 WT#15	WT#15	33	554034	4078702	FMW-N	Fortymile Wash – North	Open borehole (354 to 415)[9]	Tpt[9]	DTNs: MO0007GNDWTRIS.007 [DIRS 151497], $\delta^{18}O$, δD, $\delta^{13}C$, ^{14}C; MO0007GNDWTRIS.006 [DIRS 151496], $\delta^{18}O$, δD, $\delta^{13}C$, ^{14}C; MO0008MAJIONPH.017 [DIRS 151534], C
UE-25 WT#14	WT#14	34	552630	4077330	FMW-N	Fortymile Wash – North	open borehole (346 to 399)[9]	Tpt,Tac[9]	
UE-25 J-13	J-13	35	554017	4073517	FMW-N	Fortymile Wash – North	(303 to 424) (820 to 1,009)[9]	Tpt Tct,Tlr[9]	DTNs: MO0007GNDWTRIS.010 [DIRS 151500). $\delta^{18}O$, δD, $\delta^{13}C$, ^{14}C; MO0007MAJIONPH.013 [DIRS 151530], C; GS930108315213.004 [DIRS 145525], U concentrations and isotopes; GS930308312323.001 [DIRS 145530], T, F^-, $Sr2^+$; LA0311EK831232.001 [DIRS 166068], 87Sr/86Sr
UE-25 J-12	J-12	36	554444	4068774	FMW-N	Fortymile Wash – North	open borehole (227 to 271)[9]	Tpt[9]	

Table A4-3. Summary of Groundwater Wells and Data Sources (Continued)

Well Identifier	Abbreviation Used in Appendix	Figure A6-5	UTM-X[a] (m)	UTM-Y[3] (m)	Area[b]		Approximate Interval Sampled (m)[d]	Geologic Unit[c,d]	Reference for Sampled Depth and Chemical (C) and Isotopic (I) Data
Fortymile Wash – North (Continued)									
UE-25 JF#3	JF#3	37	554498	4067974	FMW-N	Fortymile Wash – North	open borehole (216 to 347)[15]	Tv[15]	DTNs: MO0007GNDWTRIS.005 [DIRS 151495], $\delta^{18}O$, δD, $\delta^{13}C$, ^{14}C; MO0007MAJIONPH.008 [DIRS 151521], C; GS930908312323.003 [DIRS 145404], F^-, Sr^{2+}; GS930108315213.004 [DIRS 145525], U concentrations and isotopes; LA0311EK831232.001 [DIRS 166068], $^{87}Sr/^{86}Sr$
Solitario Canyon Wash									
USW H-6	H-6(bh)	38	546188	4077816	SCW	Solitario Canyon Wash	open borehole (526 to 1,220)[1]	Tcb/Tct[2]	DTNs: MO0007GNDWTRIS.010 [DIRS 151500], $\delta^{18}O$, δD, $\delta^{13}C$, ^{14}C; MO0007MAJIONPH.013 [DIRS 151530], C; GS930308312323.001 [DIRS 145530], (T, F^-, Sr^{2+});
	H-6(Tct)	39					753 to 835[1]	Tct[2]	DTN: MO0007GNDWTRIS.010 [DIRS 151500], ($\delta^{18}O$, δD, $\delta^{13}C$, ^{14}C); MO0007MAJIONPH.012 [DIRS 151529], (C);Benson and McKinley 1985 [DIRS 101036], T, F^-, Sr^{2+}
	H-6(Tcb)	40					608 to 646[1]	Tcb[2]	

Table A4-3. Summary of Groundwater Wells and Data Sources (Continued)

Well Identifier	Abbreviation Used in Appendix	Figure A6-5	UTM-X[a] (m)	UTM-Y[3] (m)	Area[b]		Approximate Interval Sampled (m)[d]	Geologic Unit[c,d]	Reference for Sampled Depth and Chemical (C) and Isotopic (I) Data
Solitario Canyon Wash (Continued)									
USW WT-7	WT-7	41	546151	4075474	SCW	Solitario Canyon Wash	open borehole (421 to 491)[9]	Tpt,Tcp[9]	DTNs: MO0007GNDWTRIS.006 [DIRS 151496], $\delta^{18}O$, $\delta^{13}C$; MO0008MAJIONPH.017 [DIRS 151534], C; LA0311EK831232.001 [DIRS 166068], F^-, Sr^{2+}, $^{87}Sr/^{86}Sr$; Paces et al. 2002 [DIRS 158817], Table 1, U concentrations and isotopes
USW WT-10	WT-10	42	545964	4073378	SCW	Solitario Canyon Wash	open borehole (347 to 431)[9]	Tpt[9]	DTNs: MO0007GNDWTRIS.006 [DIRS 151496], $\delta^{18}O$, δD, $\delta^{13}C$, ^{14}C; MO0008MAJIONPH.017 [DIRS 151534], C; DTN: LA0311EK831232.001 [DIRS 166068], (F^-, Sr^{2+}, $^{87}Sr/^{86}Sr$); Paces et al. 2002 [DIRS 158817], Table 1, U concentrations and isotopes
Yucca Mountain – Crest									
USW G-2	G-2	43	548143	4082542	YM-CR	Yucca Mountain – Crest	533 to 792[10]	Tpt,Tac[10]	DTNs: MO0007GNDWTRIS.002 [DIRS 151492], $\delta^{18}O$, δD, $\delta^{13}C$, ^{14}C; MO0007MAJIONPH.003 [DIRS 151513], C; GS010608315215.002 [DIRS 156187], U concentrations and isotopes; LA0311EK831232.001 [DIRS 166068], F^-, Sr^{2+}, $^{87}Sr/^{86}Sr$
USW WT-24	USW WT-24	44	548691	4081898	YM-CR	Yucca Mountain – Crest	688[11]	Not reported	DTN: GS980908312322.008 [DIRS 145412], 4/24/98 sample; Paces et al. 2002 [DIRS 158817], Table 1

Table A4-3. Summary of Groundwater Wells and Data Sources (Continued)

Well Identifier	Abbreviation Used in Appendix	Figure A6-5	UTM-X[a] (m)	UTM-Y[3] (m)	Area[b]		Approximate Interval Sampled (m)[d]	Geologic Unit[c,d]	Reference for Sampled Depth and Chemical (C) and Isotopic (I) Data
Yucca Mountain – Crest (Continued)									
USW UZ-14	UZ-14 (sh)	45	548032	4080260	YM-CR	Yucca Mountain – Crest	bailed (579)[11]	Tcp	DTNs: MO0007GNDWTRIS.003 [DIRS 151493], $\delta^{18}O$, δD, $\delta^{13}C$, ^{14}C; MO0007MAJIONPH.005 [DIRS 151517], C; GS980908312322.008 [DIRS 145412], T, F^-, Sr^{2+}, SiO_2, HCO_3^-, and $\delta^{34}S$
	UZ-14 (dp)	46					bailed (655)[11]	Tcb	
USW H-1	H-1(Tcp)	47	548727	4079926	YM-CR	Yucca Mountain – Crest	572-687[1]	Tcp[2]	DTNs: MO0007GNDWTRIS.010 [DIRS 151500], $\delta^{18}O$, δD, $\delta^{13}C$, ^{14}C; MO0007MAJIONPH.013 [DIRS 151530], C; GS930308312323.001 [DIRS 145530], T, F^-, Sr^{2+}
	H-1(Tcb)	48					687 to 1829[1]	Tcb[2]	
USW H-5	H-5	49	547668	4078841	YM-CR	Yucca Mountain – Crest	open borehole (704 to 1220)[1]	Tcb/Tct[2]	DTNs: MO0007GNDWTRIS.010 [DIRS 151500], $\delta^{18}O$, δD, $\delta^{13}C$, ^{14}C; MO0007MAJIONPH.013 [DIRS 151530], C; GS930308312323.001 [DIRS 145530], T, F^-, Sr^{2+}
USW SD-6	USW SD-6	50	547592	4077514	YM-CR	Yucca Mountain – Crest	open borehole (depth not reported)	Not reported	DTNs: GS010308312322.003 [DIRS 154734], T, pH, alkalinity, ions, $\delta^{18}O$, δD, $\delta^{13}C$; GS011108312322.006 [DIRS 162911], $\delta^{13}C$, $\delta^{34}S$; GS010208312322.001 [DIRS 162908], U concentrations and isotopes
USW H-3	H-3	51	547562	4075759	YM-CR	Yucca Mountain – Crest	open borehole (822 to 1,220)[1]	Tct[2]	DTNs: MO0007GNDWTRIS.009 [DIRS 151509], $\delta^{18}O$, δD, $\delta^{13}C$, ^{14}C; MO0007MAJIONPH.011 [DIRS 151524], C; MO0007MAJIONPH.012 [DIRS 151529], C; GS920408312321.003 [DIRS 105937], T, F^-, Sr^{2+}

Table A4-3. Summary of Groundwater Wells and Data Sources (Continued)

Well Identifier	Abbreviation Used in Appendix	Figure A6-5	UTM-X[a] (m)	UTM-Y[3] (m)	Area[b]		Approximate Interval Sampled (m)[d]	Geologic Unit[c,d]	Reference for Sampled Depth and Chemical (C) and Isotopic (I) Data
Yucca Mountain – Central									
USW G-4	G-4	52	548933	4078602	YM-C	Yucca Mountain – Central	open borehole (541 to 915)[1]	Tct	DTNs: MO0007GNDWTRIS.010 [DIRS 151500], $\delta^{18}O$, δD, $\delta^{13}C$, ^{14}C); MO0007MAJIONPH.013 [DIRS 151530], (C); GS930308312323.001 [DIRS 145530], (T, F^-, Sr^{2+})
UE-25 b#1	b#1(Tcb)	53	549949	4078423	YM-C	Yucca Mountain – Central	863-875[1]	Tcb[2]	DTNs: MO0007GNDWTRIS.010 [DIRS 151500], ($\delta^{18}O$, δD, $\delta^{13}C$, ^{14}C; MO0007MAJIONPH.013 [DIRS 151530], C; GS930308312323.001 [DIRS 145530], T, F^-, Sr^{2+}
	b#1(bh)	54					open borehole (470-1220)[1]	Th/Tct[2]	
USW H-4	H-4	55	549188	4077309	YM-C	Yucca Mountain – Central	open borehole (519 to 1,220)[1]	Tcb/Tct[2]	DTNs: MO0007GNDWTRIS.010 [DIRS 151500], $\delta^{18}O$, δD, $\delta^{13}C$, ^{14}C; MO0007MAJIONPH.013 [DIRS 151530], C; GS930308312323.001 [DIRS 145530], T, F^-, Sr^{2+}
UE-25 UZ#16	UZ#16	56	549484.9	4076986	YM-C	Yucca Mountain – Central	490 to 492	Tcp	DTN: MO0007MAJIONPH.007 [DIRS 151519], C
Yucca Mountain – Southeast									
UE-25 ONC#1	ONC#1	57	550479.9	4076608	YM-SE	Yucca Mountain – Southeast	open borehole (433 to 469)[15]	Th/Tcp[15]	DTN: MO0007MAJIONPH.004 [DIRS 151516], C; Oliver and Root 1997 [DIRS 100069], Sr^{2+} and $^{87}Sr/^{86}Sr$
UE-25 c#1	c#1	58	550955	4075933	YM-SE	Yucca Mountain – Southeast	open borehole (400 to 914)[1]	Tcb/Tct[2]	DTNs: MO0007GNDWTRIS.009 [DIRS 151509], $\delta^{18}O$, δD, $\delta^{13}C$, ^{14}C; MO0007MAJIONPH.011 [DIRS 151524], C; MO0007MAJIONPH.012 [DIRS 151529], C; GS920408312321.003 [DIRS 105937], T, F^-, Sr^{2+}; LA0311EK831232.001 [DIRS 166068], $^{87}Sr/^{86}Sr$ for c#1

Table A4-3. Summary of Groundwater Wells and Data Sources (Continued)

Well Identifier	Abbreviation Used in Appendix	Figure A6-5	UTM-X[a] (m)	UTM-Y[3] (m)	Area[b]		Approximate Interval Sampled (m)[d]	Geologic Unit[c,d]	Reference for Sampled Depth and Chemical (C) and Isotopic (I) Data
Yucca Mountain – Southeast (Continued)									
UE-25 c#3	c#3	59	550930	4075902	YM-SE	Yucca Mountain – Southeast	open borehole (402 to 913)[1]	Tcb/Tct[2]	DTNs: MO0007GNDWTRIS.009 [DIRS 151509], $\delta^{18}O$, δD, $\delta^{13}C$, ^{14}C; MO0007MAJIONPH.011 [DIRS 151524], C; MO0007MAJIONPH.012 [DIRS 151529], C; GS920408312321.003 [DIRS 105937], T, F^-, Sr^{2+}
	c#3(95-97)	60							DTNs: GS950808312322.001 [DIRS 148114], C, $\delta^{18}O$, δD; GS010808312322.004 [DIRS 156007); GS010608315215.002 [DIRS 156187]; GS040208312322.003 [DIRS 172396]; U concentrations and isotopes; [DIRS 172396] GS980908312322.008 [DIRS 145412], $\delta^{34}S$; GS970708315215.008 [DIRS 164674], $^{87}Sr/^{86}Sr$ for c#3
UE-25 c#2	c#2	61	550955	4075871	YM-SE	Yucca Mountain – Southeast	open borehole (401 to 913)[1]	Tcb[2]	DTNs: MO0007GNDWTRIS.009 [DIRS 151509], $\delta^{18}O$, δD, $\delta^{13}C$, ^{14}C; MO0007MAJIONPH.011 [DIRS 151524], C; MO0007MAJIONPH.012 [DIRS 151529], C; GS920408312321.003 [DIRS 105937], T, F^-, Sr^{2+}; GS980908312322.008 [DIRS 145412], $\delta^{34}S$ for c#2

Table A4-3. Summary of Groundwater Wells and Data Sources (Continued)

Well Identifier	Abbreviation Used in Appendix	Figure A6-5	UTM-X[a] (m)	UTM-Y[3] (m)	Area[b]		Approximate Interval Sampled (m)[d]	Geologic Unit[c,d]	Reference for Sampled Depth and Chemical (C) and Isotopic (I) Data
Yucca Mountain – Southeast (Continued)									
UE-25 p#1	p#1(v)	62	551501	4075659	YM-SE	Yucca Mountain – Southeast	381-1197[1]	tuff[2]	DTNs: MO0007GNDWTRIS.009 [DIRS 151509], $\delta^{18}O$, δD, $\delta^{13}C$, ^{14}C; MO0007MAJIONPH.011 [DIRS 151524], C; MO0007GNDWTRIS.008 [DIRS 151508], $\delta^{18}O$, δD, $\delta^{13}C$, ^{14}C; MO0007MAJIONPH.010 [DIRS 151523], C; GS930108315213.004 [DIRS 145525], U concentrations and isotopes; GS920408312321.003 [DIRS 105937], T, F^-, Sr^{2+}; LA0311EK831232.001 [DIRS 166068], $^{87}Sr/^{86}Sr$
	p#1(c)	63					1,297 to 1,805[1]	Srm/ DSlm[2]	
USW WT-17	WT-17	64	549905	4073307	YM-SE	Yucca Mountain – Southeast	open borehole (393 to 443)[9]	Tcp[9]	DTNs: MO0007GNDWTRIS.003 [DIRS 151493], $\delta^{18}O$, δD, $\delta^{13}C$, ^{14}C; MO0007MAJIONPH.005 [DIRS 151517], C; GS980908312322.008 [DIRS 145412], T, F^-, Sr^{2+}, and $\delta^{34}S$; GS980908312322.009 [DIRS 118977], U concentrations and isotopes
UE-25 WT#3	WT#3	65	552090	4072550	YM-SE	Yucca Mountain – Southeast	open borehole (301 to 348)[9]	Tcb[9]	DTNs: MO0007GNDWTRIS.003 [DIRS 151493], $\delta^{18}O$, δD, $\delta^{13}C$, ^{14}C; MO0007MAJIONPH.005 [DIRS 151517], C; GS980908312322.008 [DIRS 145412], T, F^-, Sr^{2+}, and $\delta^{34}S$); GS980908312322.009 [DIRS 118977], U concentrations and isotopes

Table A4-3. Summary of Groundwater Wells and Data Sources (Continued)

Well Identifier	Abbreviation Used in Appendix	Figure A6-5	UTM-X[a] (m)	UTM-Y[3] (m)	Area[b]		Approximate Interval Sampled (m)[d]	Geologic Unit[c,d]	Reference for Sampled Depth and Chemical (C) and Isotopic (I) Data
Yucca Mountain – Southeast (Continued)									
UE-25 WT#12	WT#12	66	550168	4070659	YM-SE	Yucca Mountain – Southeast	open borehole (345 to 399)[9]	Tpt/Tac[9]	DTNs: MO0007GNDWTRIS.007 [DIRS 151497], $\delta^{18}O$, δD, $\delta^{13}C$, ^{14}C; MO0007GNDWTRIS.006 [DIRS 151496], $\delta^{18}O$, δD, $\delta^{13}C$, ^{14}C; MO0008MAJIONPH.017 [DIRS 151534], C; GS010608315215.002 [DIRS 156187], U concentrations and isotopes; LA0311EK831232.001 [DIRS 166068], $^{87}Sr/^{86}Sr$; Oliver and Root 1997 [DIRS 100069], F^-, Sr^{2+}
Jackass Flats									
UE-25 J-11	UE-25 J-11	67	563798	4071073	JF	Jackass Flats	open borehole (317 to 405)[9]	Tb, Tpt[9]	DTNs: GS010308312322.003 [DIRS 154734], pH, alkalinity, $\delta^{18}O$, δD, $\delta^{13}C$, ^{14}C; GS011108312322.006 [DIRS 162911], $\delta^{34}S$; GS010308312322.002 [DIRS 162910], ions; GS010208312322.001 [DIRS 162908], U concentrations and isotopes
Crater Flat									
GEXA Well 4	GEXA Well 4	68	534069	4086110	CF	Crater Flat	(244 to 488)[4]	TV[4,15]	DTNs: GS970708312323.001 [DIRS 145405], $\delta^{18}O$, δD; MO0007MAJIONPH.008 [DIRS 151521], C; GS980208312322.006 [DIRS 146065], U concentrations and isotopes; Oliver and Root 1997 [DIRS 100069], T, F^-, Sr^{2+}, $^{87}Sr/^{86}Sr$

Table A4-3. Summary of Groundwater Wells and Data Sources (Continued)

Well Identifier	Abbreviation Used in Appendix	Figure A6-5	UTM-X[a] (m)	UTM-Y[3] (m)	Area[b]		Approximate Interval Sampled (m)[d]	Geologic Unit[c,d]	Reference for Sampled Depth and Chemical (C) and Isotopic (I) Data
Crater Flat (Continued)									
USW VH-1	VH-1	69	539976	4071714	CF	Crater Flat	open borehole (184 to 762)[1]	Tcb[2]	DTNs: MO0007GNDWTRIS.010 [DIRS 151500], $\delta^{18}O$, δD, $\delta^{13}C$, ^{14}C; MO0007MAJIONPH.013 [DIRS 151530], C; GS930308312323.001 [DIRS 145530], T, F^-, Sr^{2+}; LA0311EK831232.001 [DIRS 166068], $^{87}Sr/^{86}Sr$; Paces et al. 2002 [DIRS 158817], Table 1, U concentrations and isotopes
Crater Flat - Southwest									
USW-VH-2	VH-2	70	537738	4073214	CF-SW	Crater Flat – Southwest	open borehole (164 to 1,219)[15]	Tv[15]	DTNs: GS930108315213.002 [DIRS 148109], C; GS970708312323.001 [DIRS 145405], $\delta^{18}O$, δD; MO0007MAJIONPH.008 [DIRS 151521], C; GS930108315213.004 [DIRS 145525], U concentrations and isotopes; LA0311EK831232.001 [DIRS 166068], F^-, Sr^{2+}, $^{87}Sr/^{86}Sr$
NC-EWDP-7S	NC-EWDP-7S	71	539558	4064318	CF-SW	Crater Flat – Southwest	(8.5 to 12.2)[7]	Paleospring deposits[7]	DTN: GS011108312322.006 [DIRS 162911], T, pH, ions, ^{14}C, $\delta^{18}O$, δD, $\delta^{13}C$, $\delta^{34}S$
NC-EWDP-7SC	NC-EWDP-7SC	72	539558	4064320	CF-SW	Crater Flat – Southwest	Open borehole (7.6 to 237.3)[7]	Paleospring deposits, Tertiary sediments and volcanic rock[7]	DTN: GS011108312322.006 [DIRS 162911], T, pH, ions, ^{14}C, $\delta^{18}O$, δD, $\delta^{13}C$, $\delta^{34}S$

Table A4-3. Summary of Groundwater Wells and Data Sources (Continued)

Well Identifier	Abbreviation Used in Appendix	Figure A6-5	UTM-X[a] (m)	UTM-Y[3] (m)	Area[b]		Approximate Interval Sampled (m)[d]	Geologic Unit[c,d]	Reference for Sampled Depth and Chemical (C) and Isotopic (I) Data
Crater Flat – Southwest (Continued)									
NC-EWDP-1DX	NC-EWDP-1DX	73	536768	4062503	CF-SW	Crater Flat – Southwest	Open borehole (16.8 to 762)[7]	Paleospring deposits, alluvium, Tertiary sediments[7]	DTNs: GS010308312322.003 [DIRS 154734], T, pH, alkalinity, $\delta^{18}O$, δD, $\delta^{13}C$; GS011108312322.006 [DIRS 162911], $\delta^{34}S$; GS010308312322.002 [DIRS 162910], F^-, Sr^{2+}; MO0007MAJIONPH.015 [DIRS 151532], C; GS010208312322.001 [DIRS 162908], U concentrations and isotopes
NC-EWDP-1DX Zone 2	NC-EWDP-1DX Zone 2	74	536768	4062503	CF-SW	Crater Flat – Southwest	(658.4 to 682.8)[7]	Tertiary sediments[7]	DTNs: GS010308312322.003 [DIRS 154734], T, pH, alkalinity, ions, $\delta^{18}O$, δD, $\delta^{13}C$, ^{14}C; GS011108312322.006 [DIRS 162911], $\delta^{34}S$; GS010308312322.002 [DIRS 162910], U concentration data; GS010208312322.001 [DIRS 162908], U concentrations and isotopes; LA0311EK831232.002 [DIRS 166069], $^{87}Sr/^{86}Sr$
NC-EWDP-1S Zone 1	NC-EWDP-1S Zone 1	75	536771	4062499	CF-SW	Crater Flat – Southwest	(48.8 to 54.9)[7]	Tertiary welded tuff[7]	DTNs: GS010308312322.003 [DIRS 154734], T, pH, alkalinity, ions, $\delta^{18}O$, δD, $\delta^{13}C$, ^{14}C; GS011108312322.006 [DIRS 162911], $\delta^{34}S$; GS010308312322.002 [DIRS 162910], U concentration data; GS010208312322.001 [DIRS 162908], U concentrations and isotopes; LA0311EK831232.002 [DIRS 166069], $^{87}Sr/^{86}Sr$

Table A4-3. Summary of Groundwater Wells and Data Sources (Continued)

Well Identifier	Abbreviation Used in Appendix	Figure A6-5	UTM-X[a] (m)	UTM-Y[3] (m)	Area[b]		Approximate Interval Sampled (m)[d]	Geologic Unit[c,d]	Reference for Sampled Depth and Chemical (C) and Isotopic (I) Data
Crater Flat – Southwest (Continued)									
NC-EWDP-1S Zone 2	NC-EWDP-1S Zone 2	76	536771	4062499	CF-SW	Crater Flat – Southwest	(64.0 to 82.3)[7]	Tertiary welded tuff[7]	DTNs: GS010308312322.003 [DIRS 154734], T, pH, alkalinity, ions, $\delta^{18}O$, δD, $\delta^{13}C$, ^{14}C; GS011108312322.006 [DIRS 162911], $\delta^{34}S$; GS010308312322.002 [DIRS 162910], U concentration data; GS010208312322.001 [DIRS 162908], U concentrations and isotopes; LA0311EK831232.002 [DIRS 166069], $^{87}Sr/^{86}Sr$
NC-EWDP-1S	NC-EWDP-1S	77	536771	4062499	CF-SW	Crater Flat – Southwest	Open borehole (15.8 to 103.6)	Tertiary welded tuff[7]	DTNs: GS010308312322.003 [DIRS 154734], T, pH, alkalinity, $\delta^{18}O$, δD, $\delta^{13}C$; GS011108312322.006 [DIRS 162911], $\delta^{34}S$; GS010308312322.002 [DIRS 162910], ions; GS010208312322.001 [DIRS 162908], U concentrations and isotopes
NC-EWDP-12PA	NC-EWDP-12PA	78	536906	4060766	CF-SW	Crater Flat – Southwest	(99.0 to 117.2)[7]	Tertiary Reworked tuff[7]	DTNs: GS011108312322.006 [DIRS 162911], T, pH, ions, ^{14}C, $\delta^{18}O$, δD, $\delta^{13}C$, $\delta^{34}S$; LA0311EK831232.002 [DIRS 166069], $^{87}Sr/^{86}Sr$
NC-EWDP-12PB	NC-EWDP-12PB	79	536863	4060794	CF-SW	Crater Flat – Southwest	(99.1 to 117.3)[7]	Tertiary Reworked tuff[7]	DTNs: GS011108312322.006 [DIRS 162911], T, pH, ions, ^{14}C, $\delta^{18}O$, δD, $\delta^{13}C$, $\delta^{34}S$; LA0311EK831232.002 [DIRS 166069], $^{87}Sr/^{86}Sr$

Table A4-3. Summary of Groundwater Wells and Data Sources (Continued)

Well Identifier	Abbreviation Used in Appendix	Figure A6-5	UTM-X[a] (m)	UTM-Y[3] (m)	Area[b]		Approximate Interval Sampled (m)[d]	Geologic Unit[c,d]	Reference for Sampled Depth and Chemical (C) and Isotopic (I) Data
Crater Flat – Southwest (Continued)									
NC-EWDP-12PC	NC-EWDP-12PC	80	536872	4060809	CF-SW	Crater Flat – Southwest	(51.8 to 70.0)[7]	Alluvium[7]	DTNs: GS011108312322.006 [DIRS 162911], T, pH, ions, ^{14}C, $\delta^{18}O$, δD, $\delta^{13}C$, $\delta^{34}S$; LA0311EK831232.002 [DIRS 166069], $^{87}Sr/^{86}Sr$
Yucca Mountain - South									
NC-EWDP-09SX	NC-EWDP-09SX	81	539039	4061004	YM-S	Yucca Mountain – South	Open borehole (30.2 to 121.0)	Valley fill, Alluvium, Tertiary volcanic rock[7]	DTNs: GS010308312322.003 [DIRS 154734], T, pH, alkalinity, $\delta^{18}O$, δD, $\delta^{13}C$; GS011108312322.006 [DIRS 162911], $\delta^{13}C$, $\delta^{34}S$; MO0007MAJIONPH.015 [DIRS 151532], C; GS010308312322.002 [DIRS 162910], F^-, Sr^{2+}; GS010208312322.001 [DIRS 162908], U concentrations and isotopes; LA0311EK831232.002 [DIRS 166069], $^{87}Sr/^{86}Sr$
NC-EWDP-09SX Zone 1	NC-EWDP-09SX Zone 1	82	539040	4061006	YM-S	Yucca Mountain – South	(27.4 to 36.6)[7]	Alluvium[7]	DTNs: GS010308312322.003 [DIRS 154734], T, pH, alkalinity, ions, $\delta^{18}O$, δD, $\delta^{13}C$, ^{14}C; GS011108312322.006 [DIRS 162911], ^{14}C, $\delta^{34}S$; GS010308312322.002 [DIRS 162910], U concentration data; GS010208312322.001 [DIRS 162908], U concentrations and isotopes; LA0311EK831232.002 [DIRS 166069], $^{87}Sr/^{86}Sr$

Table A4-3. Summary of Groundwater Wells and Data Sources (Continued)

Well Identifier	Abbreviation Used in Appendix	Figure A6-5	UTM-X[a] (m)	UTM-Y[3] (m)	Area[b]		Approximate Interval Sampled (m)[d]	Geologic Unit[c,d]	Reference for Sampled Depth and Chemical (C) and Isotopic (I) Data
Yucca Mountain – South (Continued)									
NC-EWDP-09SX Zone 2	NC-EWDP-09SX Zone 2	83	539040	4061006	YM-S	Yucca Mountain – South	(42.7 to 48.8)[7]	Alluvium[7]	DTNs: GS010308312322.003 [DIRS 154734], T, pH, alkalinity, ions, $\delta^{18}O$, δD, $\delta^{13}C$, ^{14}C; GS011108312322.006 [DIRS 162911], $\delta^{34}S$; GS010308312322.002 [DIRS 162910], U concentration data; GS010208312322.001 [DIRS 162908], U concentrations and isotopes; LA0311EK831232.002 [DIRS 166069], $^{87}Sr/^{86}Sr$
NC-EWDP-09SX Zone 3	NC-EWDP-09SX Zone 3	84	539040	4064006	YM-S	Yucca Mountain – South	(76.2 to 88.4)[7]	Tertiary tuff[7]	DTNs: GS010308312322.003 [DIRS 154734], T, pH, alkalinity, ions, $\delta^{18}O$, δD, $\delta^{13}C$, ^{14}C; GS011108312322.006 [DIRS 162911], $\delta^{34}S$; GS010308312322.002 [DIRS 162910], U concentration data; GS010208312322.001 [DIRS 162908], U concentrations and isotopes; LA0311EK831232.002 [DIRS 166069], $^{87}Sr/^{86}Sr$
NC-EWDP-09SX Zone 4	NC-EWDP-09SX Zone 4	85	539040	4061006	YM-S	Yucca Mountain – South	(100.6 to 103.7)[7]	Tertiary tuff[7]	DTNs: GS010308312322.003 [DIRS 154734], T, pH, alkalinity, ions, $\delta^{18}O$, δD, $\delta^{13}C$, ^{14}C; GS011108312322.006 [DIRS 162911], $\delta^{34}S$; GS010308312322.002 [DIRS 162910], U concentration data; GS010208312322.001 [DIRS 162908], U concentrations and isotopes; LA0311EK831232.002 [DIRS 166069], $^{87}Sr/^{86}Sr$

Table A4-3. Summary of Groundwater Wells and Data Sources (Continued)

Well Identifier	Abbreviation Used in Appendix	Figure A6-5	UTM-X[a] (m)	UTM-Y[3] (m)	Area[b]		Approximate Interval Sampled (m)[d]	Geologic Unit[c,d]	Reference for Sampled Depth and Chemical (C) and Isotopic (I) Data
Yucca Mountain – South (Continued)									
NC-EWDP-03D	NC-EWDP-03D	86	541273	4059444	YM-S	Yucca Mountain – South	(159 to 292)[7]	Alluvium, Tertiary sedimentary and volcanic rocks[7]	DTNs: GS010308312322.003 [DIRS 154734], T, pH, alkalinity, $\delta^{18}O$, δD, $\delta^{13}C$, ^{14}C; GS011108312322.006 [DIRS 162911], $\delta^{34}S$; GS010308312322.002 [DIRS 162910], F^-, Sr^{2+}; MO0007MAJIONPH.015 [DIRS 151532], C; GS010208312322.001 [DIRS 162908], U concentrations and isotopes
NC-EWDP-3S Zone 2	NC-EWDP-3S Zone 2	87	541273	4059444	YM-S	Yucca Mountain – South	(103.6 to 128.0)[14]	Tertiary tuff and sediments[7]	DTNs: GS010308312322.003 [DIRS 154734], T, pH, alkalinity, ions, $\delta^{18}O$, δD, $\delta^{13}C$, ^{14}C; GS011108312322.006 [DIRS 162911], $\delta^{34}S$; GS010308312322.002 [DIRS 162910], U concentration data; GS010208312322.001 [DIRS 162908], U concentrations and isotopes; LA0311EK831232.002 [DIRS 166069], $^{87}Sr/^{86}Sr$
NC-EWDP-3S Zone 3	NC-EWDP-3S Zone 3	88	541273	4059444	YM-S	Yucca Mountain – South	(146.3 to 160.0)[14]	Tertiary tuff and sediments[7]	DTNs: GS010308312322.003 [DIRS 154734], T, pH, alkalinity, ions, $\delta^{18}O$, δD, $\delta^{13}C$, ^{14}C; GS011108312322.006 [DIRS 162911], $\delta^{18}O$, $\delta^{34}S$; GS010308312322.002 [DIRS 162910], U concentration data; GS010208312322.001 [DIRS 162908], U concentrations and isotopes; LA0311EK831232.002 [DIRS 166069], $^{87}Sr/^{86}Sr$

Table A4-3. Summary of Groundwater Wells and Data Sources (Continued)

Well Identifier	Abbreviation Used in Appendix	Figure A6-5	UTM-X[a] (m)	UTM-Y[3] (m)	Area[b]		Approximate Interval Sampled (m)[d]	Geologic Unit[c,d]	Reference for Sampled Depth and Chemical (C) and Isotopic (I) Data
Yucca Mountain – South (Continued)									
CIND-R-LITE	CIND-R-LITE	89	544027	4059809	YM-S	Yucca Mountain – South	not reported	Tv[15]	DTNs: GS930108315213.002 [DIRS 148109], C; MO0007MAJIONPH.006 [DIRS 151518], C; GS000700012847.001 [DIRS 150842], C, I; GS930108315213.004 [DIRS 145525], U concentrations and isotopes; LA0311EK831232.001 [DIRS 166068], F^-, Sr^{2+}, $^{87}Sr/^{86}Sr$
NC-EWDP-15P	NC-EWDP-15P	90	544848	4058158	YM-S	Yucca Mountain – South	(61.0 to 79.2)[7]	Alluvium[7]	DTNs: GS011108312322.006 [DIRS 162911], T, pH, ions, ^{14}C, $\delta^{18}O$, δD, $\delta^{13}C$, $\delta^{34}S$; LA0311EK831232.002 [DIRS 166069], $^{87}Sr/^{86}Sr$
NC-EWDP-02D	NC-EWDP-02D	91	547744	40571647	YM-S	Yucca Mountain – South	Open borehole (95.1 to 493.2)[7]	Alluvium[7]	DTNs: GS010308312322.003 [DIRS 154734], T, pH, alkalinity, $\delta^{18}O$, δD, $\delta^{13}C$, ^{14}C; GS011108312322.006 [DIRS 162911], $\delta^{34}S$; GS010308312322.002 [DIRS 162910], F^-, Sr^{2+}; MO0007MAJIONPH.015 [DIRS 151532], C; GS010208312322.001 [DIRS 162908], U concentrations and isotopes
NC-EWDP-19D	NC-EWDP-19D	92	549238	4058265	YM-S	Yucca Mountain – South	Open borehole (106.1 to 443.9)[7]	Alluvium, Tertiary tuff and sediments[7]	DTNs: GS011108312322.006 [DIRS 162911], T, pH, ions, ^{14}C, $\delta^{18}O$, δD, $\delta^{13}C$, $\delta^{34}S$; LA0311EK831232.002 [DIRS 166069], $^{87}Sr/^{86}Sr$

Table A4-3. Summary of Groundwater Wells and Data Sources (Continued)

Well Identifier	Abbreviation Used in Appendix	Figure A6-5	UTM-X[a] (m)	UTM-Y[3] (m)	Area[b]		Approximate Interval Sampled (m)[d]	Geologic Unit[c,d]	Reference for Sampled Depth and Chemical (C) and Isotopic (I) Data
Yucca Mountain – South (Continued)									
NC-EWDP-19P	NC-EWDP-19P	93	549250	4058287	YM-S	Yucca Mountain – South	(109.5 to 139.8)[7]	Alluvium[7]	DTNs: GS011108312322.006 [DIRS 162911], T, pH, ions, ^{14}C, $\delta^{18}O$, δD, $\delta^{13}C$, $\delta^{34}S$; LA0311EK831232.002 [DIRS 166069], $^{87}Sr/^{86}Sr$
NC-EWDP-19D (alluvial)	NC-EWDP-19D (alluvial)	94	549238	4058265	YM-S	Yucca Mountain – South	(125.9 to 242.4) (assumed to be combined depth range of screened intervals 1 to 4)	Alluvium[7]	DTN: GS011108312322.006 [DIRS 162911], T, pH, ions, ^{14}C, $\delta^{18}O$, δD, $\delta^{13}C$, $\delta^{34}S$
NC-EWDP-19D (zone #1)	NC-EWDP-19D (zone #1)	95	549238	4058265	YM-S	Yucca Mountain – South	(125.9 to 131.4)[7]	Alluvium[7]	DTN: GS011108312322.006 [DIRS 162911], T, pH, ions,^{14}C, $\delta^{18}O$, δD, $\delta^{13}C$, $\delta^{34}S$
NC-EWDP-19D (zone #2)	NC-EWDP-19D (zone #2)	96	549238	4058265	YM-S	Yucca Mountain – South	(151.8 to 157.3)[7]	Alluvium[7]	DTN: GS011108312322.006 [DIRS 162911], T, pH, ions,^{14}C, $\delta^{18}O$, δD, $\delta^{13}C$, $\delta^{34}S$
NC-EWDP-19D (zone #3)	NC-EWDP-19D (zone #3)	97	549238	4058265	YM-S	Yucca Mountain – South	(176.1 to 206.0)[7]	Alluvium[7]	DTN: GS011108312322.006 [DIRS 162911], T, pH, ions,^{14}C, $\delta^{18}O$, δD, $\delta^{13}C$, $\delta^{34}S$
NC-EWDP-19D (zone #4)	NC-EWDP-19D (zone #4)	98	549238	4058265	YM-S	Yucca Mountain – South	(220.2 to 242.4)[7]	Alluvium[7]	DTN: GS011108312322.006 [DIRS 162911], T, pH, ions,^{14}C, $\delta^{18}O$, δD, $\delta^{13}C$, $\delta^{34}S$
Amargosa Valley									
NC-EWDP-4PB	NC-EWDP-4PB	99	553202	4056768	LW	Amargosa Valley	(225.4 to 255.8)[7]	Alluvium[7]	DTNs: GS011108312322.006 [DIRS 162911], T, pH, ions, ^{14}C, $\delta^{18}O$, δD, $\delta^{13}C$, $\delta^{34}S$; LA0311EK831232.002 [DIRS 166069], $^{87}Sr/^{86}Sr$
NC-EWDP-4PA	NC-EWDP-4PA	100	553167	4056766	LW	Amargosa Valley	(123.5 to 147.9)[7]	Alluvium[7]	DTNs: GS011108312322.006 [DIRS 162911], T, pH, ions, ^{14}C, $\delta^{18}O$, δD, $\delta^{13}C$, $\delta^{34}S$; LA0311EK831232.002 [DIRS 166069], $^{87}Sr/^{86}Sr$

Table A4-3. Summary of Groundwater Wells and Data Sources (Continued)

Well Identifier	Abbreviation Used in Appendix	Figure A6-5	UTM-X[a] (m)	UTM-Y[3] (m)	Area[b]		Approximate Interval Sampled (m)[d]	Geologic Unit[c,d]	Reference for Sampled Depth and Chemical (C) and Isotopic (I) Data
Amargosa Valley (Continued)									
Desert Farms Garlic Plot	Desert Farms Garlic Plot	101	553295	4055305	LW	Amargosa Valley	open borehole (depth not reported)	Qal[13]	DTNs: GS990808312322.001 [DIRS 149393], T, pH, $\delta^{18}O$, δD, $\delta^{13}C$; GS990808312322.002 [DIRS 162917], ions and ^{14}C; GS021008312322.002 [DIRS 162913], $\delta^{34}S$; GS010208312322.001 [DIRS 162908], U concentrations and isotopes
15S/50E-18ccc	15S/50E-18ccc	103	553710	4055273	LW	Amargosa Valley	open borehole (105 to 102)[2]	Qal[2]	DTN: MO0007MAJIONPH.006 [DIRS 151518], C; Oliver and Root 1997 [DIRS 100069], F^-, Sr^{2+}
NDOT	NDOT	104	553685	4055242	LW	Amargosa Valley	open borehole (105 to 151)	Qal[13]	DTNs: MO0007MAJIONPH.008 [DIRS 151521], C; MO0007MAJIONPH.009 [DIRS 151522], C; GS940908315213.005 [DIRS 164673], U concentrations and isotopes; Oliver and Root 1997 [DIRS 100069], F^- and $^{87}Sr/^{86}Sr$
15S/50E-18cdc	15S/50E-18cdc	105	553934.3	4055151	LW	Amargosa Valley	open borehole (105 to 120)[2]	Qal[2]	DTN: MO0007MAJIONPH.006 [DIRS 151518], C; Claassen 1985 [DIRS 101125], Table 1, sample 34, T

Table A4-3. Summary of Groundwater Wells and Data Sources (Continued)

Well Identifier	Abbreviation Used in Appendix	Figure A6-5	UTM-X[a] (m)	UTM-Y[3] (m)	Area[b]		Approximate Interval Sampled (m)[d]	Geologic Unit[c,d]	Reference for Sampled Depth and Chemical (C) and Isotopic (I) Data
Amargosa Valley (Continued)									
Airport Well	Airport Well	106	552846	4054904	LW	Amargosa Valley	open borehole (76 to 229)[15]	Qal[15]	DTNs: GS990808312322.001 [DIRS 149393], T, pH, alkalinity); GS010308312322.003 [DIRS 154734], ions, δD, $\delta^{13}C$; GS990808312322.002 [DIRS 162917], ions and ^{14}C; GS011108312322.006 [DIRS 162911], $\delta^{34}S$; GS021008312322.002 [DIRS 162913], $\delta^{34}S$; Paces et al. 2002 [DIRS 158817], Table 1, U concentrations and isotopes
15S/50E-19b1	15S/50E-19b1	107	553862.5	4054720	LW	Amargosa Valley	open borehole (103 to 110)[15]	Qal[13]	DTN: MO0007MAJIONPH.006 [DIRS 151518], C
Amargosa River									
16S/48E-8ba	16S/48E-8ba	108	536979	4048129	AR	Amargosa River	open borehole (34-80)[2]	Qal[2]	DTN: MO0007MAJIONPH.012 [DIRS 151529], C; Claassen 1985 [DIRS 101125], Table 1, sample 45
16S/48E-7bba	16S/48E-7bba	109	534791	4048366	AR	Amargosa River	open borehole (0 to 38)[2]	Qal[2]	DTN: MO0007MAJIONPH.012 [DIRS 151529], C; Claassen 1985 [DIRS 101125], Table 1, sample 46, T
16S/48E-7cbc	16S/48E-7cbc	110	534546	4047441	AR	Amargosa River	open borehole (23 to 46)[2]	Qal[2]	DTNs: MO0007MAJIONPH.012 [DIRS 151529], C; MO0007GNDWTRIS.011 [DIRS 151501], $\delta^{18}O$, δD, $\delta^{13}C$, ^{14}C; MO0007MAJIONPH.014 [DIRS 151531], C; Claassen 1985 [DIRS 101125], Table 1, sample 47, T
16S/48E-18bcc	16S/48E-18bcc	111	534827	4045747	AR	Amargosa River	open borehole (27 to 110)[2]	Qal[2]	DTN: MO0007MAJIONPH.012 [DIRS 151529], C

Table A4-3. Summary of Groundwater Wells and Data Sources (Continued)

Well Identifier	Abbreviation Used in Appendix	Figure A6-5	UTM-X[a] (m)	UTM-Y[3] (m)	Area[b]		Approximate Interval Sampled (m)[d]	Geologic Unit[c,d]	Reference for Sampled Depth and Chemical (C) and Isotopic (I) Data
Amargosa River (Continued)									
16S/48E-17ccc	16S/48E-17ccc	112	536122	4045106	AR	Amargosa River	open borehole (depth not reported)	Qal[2]	DTN: MO0007MAJIONPH.012 [DIRS 151529], C
16S/48E-18dad	16S/48E-18dad	113	536069	4045814	AR	Amargosa River	open borehole (depth not reported)	Qal[13]	DTNs: MO0007MAJIONPH.012 [DIRS 151529], C; MO0007GNDWTRIS.011 [DIRS 151501], $\delta^{18}O$, δD, $\delta^{13}C$; MO0007MAJIONPH.014 [DIRS 151531], C
16S/48E-8cda	16S/48E-8cda	114	537063	4045941	AR	Amargosa River	open borehole (40 to unknown)[2]	Qal[2]	DTN: MO0007MAJIONPH.012 [DIRS 151529], C; Claassen 1985 [DIRS 101125], Table 1, sample 51, T
16S/48E-17abb	16S/48E-17abb	115	537035	4046681	AR	Amargosa River	open borehole (31 to 90)[3]	Qal[2]	DTN: MO0007MAJIONPH.012 [DIRS 151529], C; Claassen 1985 [DIRS 101125], Table 1, sample 52, T
Barrachman Dom/Irr.	Barrachman Dom/Irr.	116	534951	4048117	AR	Amargosa River	open borehole (depth not reported)	Qal[13]	DTNs: GS990808312322.001 [DIRS 149393], $\delta^{18}O$, δD, $\delta^{13}C$; GS990808312322.002 [DIRS 162917], ions and ^{14}C; GS021008312322.002 [DIRS 162913], $\delta^{34}S$; GS010208312322.001 [DIRS 162908], U concentrations and isotopes

Table A4-3. Summary of Groundwater Wells and Data Sources (Continued)

Well Identifier	Abbreviation Used in Appendix	Figure A6-5	UTM-X[a] (m)	UTM-Y[3] (m)	Area[b]		Approximate Interval Sampled (m)[d]	Geologic Unit[c,d]	Reference for Sampled Depth and Chemical (C) and Isotopic (I) Data
Amargosa River (Continued)									
McCracken Domestic	McCracken Domestic	117	537372	4047061	AR	Amargosa River	open borehole (depth not reported)	Qal[13]	DTNs: GS990808312322.001 [DIRS 149393], T, pH, alkalinity, $\delta^{18}O$, δD, $\delta^{13}C$; GS990808312322.002 [DIRS 162917], ions and ^{14}C; GS021008312322.002 [DIRS 162913], $\delta^{34}S$; GS010208312322.001 [DIRS 162908], U concentrations and isotopes; LA0311EK831232.002 [DIRS 166069], $^{87}Sr/^{86}Sr$
Fortymile Wash – West									
16S/48E-15ba	16S/48E-15ba	118	539670	4046693	FMW-W	Fortymile Wash – West	open borehole (30 to 50)[3]	Qal[13]	DTN: MO0007MAJIONPH.012 [DIRS 151529], C; Claassen 1985 [DIRS 101125], Table 1, sample 37, T
16S/48E-10cba	16S/48E-10cba	119	539766	4047463	FMW-W	Fortymile Wash – West	open borehole (depth not reported)	Qal[13]	DTNs: MO0007MAJIONPH.012 [DIRS 151529], C; MO0007GNDWTRIS.011 [DIRS 151501], $\delta^{18}O$, δD, $\delta^{13}C$, ^{14}C; MO0007MAJIONPH.014 [DIRS 151531], C; Claassen 1985 [DIRS 101125], Table 1, sample 25, T
16S/48E-15aaa	16S/48E-15aaa	120	540763	4046852	FMW-W	Fortymile Wash – West	open borehole (29 to 50)[3]	Qal[13]	DTNs: MO0007MAJIONPH.012 [DIRS 151529], C; MO0007GNDWTRIS.011 [DIRS 151501], $\delta^{18}O$, δD, $\delta^{13}C$, ^{14}C; MO0007MAJIONPH.014 [DIRS 151531], C; Claassen 1985 [DIRS 101125], Table 1, sample 23, T

Table A4-3. Summary of Groundwater Wells and Data Sources (Continued)

Well Identifier	Abbreviation Used in Appendix	Figure A6-5	UTM-X[a] (m)	UTM-Y[3] (m)	Area[b]		Approximate Interval Sampled (m)[d]	Geologic Unit[c,d]	Reference for Sampled Depth and Chemical (C) and Isotopic (I) Data
Fortymile Wash – West (Continued)									
Selbach Domestic	Selbach Domestic	121	539256	4046506	FMW-W	Fortymile Wash – West	open borehole (depth not reported)	Qal[13]	DTNs: GS990808312322.001 [DIRS 149393], T, pH, $\delta^{18}O$, δD, $\delta^{13}C$; GS990808312322.002 [DIRS 162917], ions and ^{14}C; GS021008312322.002 [DIRS 162913], $\delta^{34}S$; GS010208312322.001 [DIRS 162908], U concentrations and isotopes
16S/48E-15dda	16S/48E-15dda	122	540893	4045620	FMW-W	Fortymile Wash – West	open borehole (depth not reported)	Qal[13]	DTN: MO0007MAJIONPH.012 [DIRS 151529], C
16S/49E-23add	16S/49E-23add	123	551958	4045217	FMW-W	Fortymile Wash – West	open borehole (depth not reported)	Qal[13]	DTNs: MO0007MAJIONPH.012 [DIRS 151529], C; MO0007GNDWTRIS.011 [DIRS 151501], $\delta^{18}O$, δD, $\delta^{13}C$, ^{14}C; MO0007MAJIONPH.014 [DIRS 151531], C
16S/48E-23bdb	16S/48E-23bdb	124	541469	4044729	FMW-W	Fortymile Wash – West	open borehole (29 to 100)[3]	Qal[13]	DTN: MO0007MAJIONPH.012 [DIRS 151529], C; Claassen 1985 [DIRS 101125], Table 1, sample 24, T
16S/48E-23da	16S/48E-23da	125	542391	4044729	FMW-W	Fortymile Wash – West	open borehole (24 to 100)[3]	Qal[13]	DTN: MO0007MAJIONPH.006 [DIRS 151518], C; Claassen 1985 [DIRS 101125], Table 1, sample 53, T

Table A4-3. Summary of Groundwater Wells and Data Sources (Continued)

Well Identifier	Abbreviation Used in Appendix	Figure A6-5	UTM-X[a] (m)	UTM-Y[3] (m)	Area[b]		Approximate Interval Sampled (m)[d]	Geologic Unit[c,d]	Reference for Sampled Depth and Chemical (C) and Isotopic (I) Data
Fortymile Wash – West (Continued)									
Funeral Mountain Ranch Irrig	Funeral Mountain Ranch Irrig	126	541406	4043314	FMW-W	Fortymile Wash – West	open borehole (depth not reported)	Qal[13]	DTNs: GS990808312322.001 [DIRS 149393], T, pH, $\delta^{18}O$, δD, $\delta^{13}C$; GS990808312322.002 [DIRS 162917], ions and ^{14}C; GS021008312322.002 [DIRS 162913], $\delta^{34}S$; GS010208312322.001 [DIRS 162908], U concentrations and isotopes
Fortymile Wash – South									
16S/49E-05acc	16S/49E-05acc	127	546664.5	4049439	FMW-S	Fortymile Wash – South	open borehole (21 to 90)[3]	Qal[13]	DTNs: MO0007MAJIONPH.012 [DIRS 151529], C; MO0007GNDWTRIS.011 [DIRS 151501], $\delta^{18}O$, δD, $\delta^{13}C$, ^{14}C; MO0007MAJIONPH.014 [DIRS 151531], C; Oliver and Root 1997 [DIRS 100069], F^-, Sr^{2+}
16S/49E-8abb	16S/49E-8abb	128	546695	4048453	FMW-S	Fortymile Wash – South	open borehole (45 to 60)[3]	Qtal[3]	DTNs: MO0007MAJIONPH.012 [DIRS 151529], C; MO0007GNDWTRIS.011 [DIRS 151501], $\delta^{18}O$, δD, $\delta^{13}C$, ^{14}C; MO0007MAJIONPH.014 [DIRS 151531], C; Claassen 1985 [DIRS 101125], Table 1, sample 5, T
16S/49E-8acc	16S/49E-8acc	129	546723	4047806	FMW-S	Fortymile Wash – South	open borehole (45 to 60)[3]	Qtal[2]	DTN: MO0007MAJIONPH.012 [DIRS 151529], C; Claassen 1985 [DIRS 101125], Table 1, sample 6, T

Table A4-3. Summary of Groundwater Wells and Data Sources (Continued)

Well Identifier	Abbreviation Used in Appendix	Figure A6-5	UTM-X[a] (m)	UTM-Y[3] (m)	Area[b]		Approximate Interval Sampled (m)[d]	Geologic Unit[c,d]	Reference for Sampled Depth and Chemical (C) and Isotopic (I) Data
Fortymile Wash – South (Continued)									
16S/49E-18dc	16S/49E-18dc	130	545144	4045579	FMW-S	Fortymile Wash – South	open borehole (33 to 110)[3]	Qtal[2]	DTNs: MO0007MAJIONPH.012 [DIRS 151529], C; MO0007GNDWTRIS.011 [DIRS 151501], $\delta^{18}O$, δD, ^{14}C; MO0007MAJIONPH.014 [DIRS 151531], C
16S/48E-24aaa	16S/48E-24aaa	131	544077	4045235	FMW-S	Fortymile Wash – South	open borehole (29 to 150)[3]	Qtal[2]	DTN: MO0007MAJIONPH.012 [DIRS 151529], C; Claassen 1985 [DIRS 101125], Table 1, sample 12, T
16S/49E-19daa	16S/49E-19daa	132	545777	4044535	FMW-S	Fortymile Wash – South	open borehole (30 to 90)[3]	Qtal[2]	DTNs: MO0007MAJIONPH.012 [DIRS 151529], C; MO0007GNDWTRIS.011 [DIRS 151501], $\delta^{18}O$, δD, ^{14}C; MO0007MAJIONPH.014 [DIRS 151531], C; Claassen 1985 [DIRS 101125], Table 1, sample 11, T
DeLee Large Irrigation	DeLee Large Irrigation	133	544975	4043727	FMW-S	Fortymile Wash – South	open borehole (depth not reported)	Qal[13]	DTNs: GS990808312322.001 [DIRS 149393], T, pH, $\delta^{18}O$, δD, $\delta^{13}C$; GS990808312322.002 [DIRS 162917], ions and ^{14}C; GS021008312322.002 [DIRS 162913], $\delta^{34}S$; GS010208312322.001 [DIRS 162908], U concentrations and isotopes
16S/48E-25aa	16S/48E-25aa	134	544160	4043602	FMW-S	Fortymile Wash – South	open borehole (26 to 50)[3]	QTal[2]	DTNs: MO0007MAJIONPH.012 [DIRS 151529], C; MO0007GNDWTRIS.011 [DIRS 151501], $\delta^{18}O$, δD, ^{14}C; MO0007MAJIONPH.014 [DIRS 151531], C; Claassen 1985 [DIRS 101125], Table 1, sample 13, T

Table A4-3. Summary of Groundwater Wells and Data Sources (Continued)

Well Identifier	Abbreviation Used in Appendix	Figure A6-5	UTM-X[a] (m)	UTM-Y[3] (m)	Area[b]		Approximate Interval Sampled (m)[d]	Geologic Unit[c,d]	Reference for Sampled Depth and Chemical (C) and Isotopic (I) Data
Fortymile Wash – South (Continued)									
16S/48E-36aaa	16S/48E-36aaa	135	544168	4042031	FMW-S	Fortymile Wash – South	open borehole (21 to 50)[3]	Qal[2]	DTNs: MO0007MAJIONPH.012 [DIRS 151529], C, MO0007GNDWTRIS.011 [DIRS 151501], $\delta^{18}O$, δD, MO0007MAJIONPH.014 [DIRS 151531], C
Bray Domestic	Bray Domestic	136	546665	4040701	FMW-S	Fortymile Wash – South	open borehole (depth not reported)	Qal[13]	DTNs: GS990808312322.001 [DIRS 149393], T, pH, $\delta^{18}O$, δD, $\delta^{13}C$; GS990808312322.002 [DIRS 162917], ions and ^{14}C; GS021008312322.002 [DIRS 162913], $\delta^{34}S$; GS010208312322.001 [DIRS 162908], U concentrations and isotopes
Amargosa Estates #2	Amargosa Estates #2	137	544634	4040394	FMW-S	Fortymile Wash – South	open borehole (depth not reported)	Qal[13]	DTNs: GS990808312322.001 [DIRS 149393], T, $\delta^{18}O$, δD, $\delta^{13}C$; GS990808312322.002 [DIRS 162917], pH, ions and ^{14}C; GS021008312322.002 [DIRS 162913], $\delta^{34}S$; GS010208312322.001 [DIRS 162908], U concentrations and isotopes
17S/48E-1ab	17S/48E-1ab	138	544152	4040182	FMW-S	Fortymile Wash – South	open borehole (16 to 60)[3]	Qal[13]	DTNs: MO0007MAJIONPH.012 [DIRS 151529], C; MO0007GNDWTRIS.011 [DIRS 151501], $\delta^{18}O$, δD, ^{14}C; MO0007MAJIONPH.014 [DIRS 151531], C

Table A4-3. Summary of Groundwater Wells and Data Sources (Continued)

Well Identifier	Abbreviation Used in Appendix	Figure A6-5	UTM-X[a] (m)	UTM-Y[3] (m)	Area[b]		Approximate Interval Sampled (m)[d]	Geologic Unit[c,d]	Reference for Sampled Depth and Chemical (C) and Isotopic (I) Data
Fortymile Wash – South (Continued)									
17S/49E-7bb	17S/49E-7bb	139	544758	4038645	FMW-S	Fortymile Wash – South	open borehole (12 to 150)[3]	Qal[13]	DTNs: MO0007MAJIONPH.012 [DIRS 151529], C; MO0007GNDWTRIS.011 [DIRS 151501], $\delta^{18}O$, δD, ^{14}C; MO0007MAJIONPH.014 [DIRS 151531], C; Claassen 1985 [DIRS 101125], Table 1, sample 16, T
17S/49E-8ddb	17S/49E-8ddb	140	547575	4037612	FMW-S	Fortymile Wash – South	open borehole (15 to 100)[3]	Qal[13]	DTNs: MO0007MAJIONPH.012 [DIRS 151529], C; MO0007GNDWTRIS.011 [DIRS 151501], $\delta^{18}O$, δD, ^{14}C; MO0007MAJIONPH.014 [DIRS 151531], C; Claassen 1985 [DIRS 101125], Table 1, T
17S/49E-35ddd	17S/49E-35ddd	141	552739	4031202	FMW-S	Fortymile Wash – South	0.0 (Ash Tree Spring)[3]	Qal[13]	DTNs: MO0007MAJIONPH.012 [DIRS 151529], C; MO0007GNDWTRIS.011 [DIRS 151501], $\delta^{18}O$, δD, ^{14}C; MO0007MAJIONPH.014 [DIRS 151531], C; Claassen 1985 [DIRS 101125], Table 1, sample 20, T
Fortymile Wash – East									
15S/49E-22a1	15S/49E-22a1	142	550086.3	4054974	FMW-E	Fortymile Wash – East	open borehole (90 to 174)[15]	Qal[15]	DTN: MO0007MAJIONPH.006 [DIRS 151518], C; Oliver and Root 1997 [DIRS 100069], F^-
15S/49E-22dcc	15S/49E-22dcc	143	549672.5	4053523	FMW-E	Fortymile Wash – East	open borehole (78 to 148)[3]	Qal[13]	DTNs: MO0007MAJIONPH.006 [DIRS 151518], C; MO0007GNDWTRIS.011 [DIRS 151501], I, "Amargosa well 3"; Oliver and Root 1997 [DIRS 100069], F^-, Sr^{2+}

Table A4-3. Summary of Groundwater Wells and Data Sources (Continued)

Well Identifier	Abbreviation Used in Appendix	Figure A6-5	UTM-X[a] (m)	UTM-Y[3] (m)	Area[b]		Approximate Interval Sampled (m)[d]	Geologic Unit[c,d]	Reference for Sampled Depth and Chemical (C) and Isotopic (I) Data
Fortymile Wash – East (Continued)									
15S/49E-27acc	15S/49E-27acc	144	549552.9	4052722	FMW-E	Fortymile Wash – East	open borehole (73 to 467)[2]	Qal[13]	DTN: MO0007MAJIONPH.012 [DIRS 151529], C; Oliver and Root 1997 [DIRS 100069], F^-, Sr^{2+}
O'Neill Domestic	O'Neill Domestic	145	547304	4047893	FMW-E	Fortymile Wash – East	open borehole (depth not reported)	Qal[13]	DTNs: GS990808312322.001 [DIRS 149393], T, pH, $\delta^{18}O$, δD, $\delta^{13}C$; GS990808312322.002 [DIRS 162917], ions and ^{14}C; GS021008312322.002 [DIRS 162913], $\delta^{34}S$; GS010208312322.001 [DIRS 162908], U concentrations and isotopes
16S/49E-9cda	16S/49E-9cda	146	548168	4047291	FMW-E	Fortymile Wash – East	open borehole (46 to 90)[3]	Qal[2]	DTN: MO0007MAJIONPH.012 [DIRS 151529], C; Claassen 1985 [DIRS 101125], Table 1, sample 7, T
16S/49E-9dcc	16S/49E-9dcc	147	548343	4047045	FMW-E	Fortymile Wash – East	open borehole (49 to 60)[3]	Qal[2]	DTNs: MO0007MAJIONPH.012 [DIRS 151529], C; MO0007GNDWTRIS.011 [DIRS 151501], $\delta^{18}O$, δD, $\delta^{13}C$, ^{14}C; MO0007MAJIONPH.014 [DIRS 151531], C; Claassen 1985 [DIRS 101125], Table 1, sample 8, T
16S/49E-16ccc	16S/49E-16ccc	148	547508	4045222	FMW-E	Fortymile Wash – East	open borehole (depth not reported)	Qal[13]	DTNs: MO0007MAJIONPH.012 [DIRS 151529], C; MO0007GNDWTRIS.011 [DIRS 151501], $\delta^{18}O$, δD, $\delta^{13}C$, ^{14}C; MO0007MAJIONPH.014 [DIRS 151531], C

Table A4-3. Summary of Groundwater Wells and Data Sources (Continued)

Well Identifier	Abbreviation Used in Appendix	Figure A6-5	UTM-X[a] (m)	UTM-Y[3] (m)	Area[b]		Approximate Interval Sampled (m)[d]	Geologic Unit[c,d]	Reference for Sampled Depth and Chemical (C) and Isotopic (I) Data
Fortymile Wash – East (Continued)									
Ponderosa Dairy #1	Ponderosa Dairy #1	149	549382	4038747	FMW-E	Fortymile Wash – East	open borehole (depth not reported)	Qal[13]	DTNs: GS990808312322.001 [DIRS 149393], T, $\delta^{18}O$, δD, $\delta^{13}C$; GS990808312322.002 [DIRS 162917], ions and ^{14}C; GS021008312322.002 [DIRS 162913], $\delta^{34}S$; GS010208312322.001 [DIRS 162908], (U concentrations and isotopes
17S/49E-9aa	17S/49E-9aa	150	549382	4038262	FMW-E	Fortymile Wash – East	open borehole (5 to 6)[2]	Qal[2]	DTNs: MO0007MAJIONPH.012 [DIRS 151529], C; MO0007GNDWTRIS.011 [DIRS 151501], $\delta^{18}O$, δD, ^{14}C; MO0007MAJIONPH.014 [DIRS 151531], C
17S/49E-15bbd	17S/49E-15bbd	151	549843	4036855	FMW-E	Fortymile Wash – East	open borehole (17 to 110)[3]	Qal[13]	DTNs: MO0007MAJIONPH.012 [DIRS 151529], C; MO0007GNDWTRIS.011 [DIRS 151501], ^{14}C; MO0007MAJIONPH.014 [DIRS 151531], C; Claassen 1985 [DIRS 101125], Table 1, sample 19, T
M. Gilgan Well	M. Gilgan Well	152	549550	4036791	FMW-E	Fortymile Wash – East	open borehole (depth not reported)	Qal[13]	DTNs: GS990808312322.001 [DIRS 149393], T, pH, $\delta^{18}O$, δD, $\delta^{13}C$; GS990808312322.002 [DIRS 162917], ions and ^{14}C; GS021008312322.002 [DIRS 162913], $\delta^{34}S$; GS010208312322.001 [DIRS 162908], U concentrations and isotopes
17S/49E-15bc	17S/49E-15bc	153	549870	4036577	FMW-E	Fortymile Wash – East	open borehole (15 to 157)[2]	Qal[2]	DTN: MO0007MAJIONPH.012 [DIRS 151529], C; Claassen 1985 [DIRS 101125], Table 1, sample 38, T

Table A4-3. Summary of Groundwater Wells and Data Sources (Continued)

Well Identifier	Abbreviation Used in Appendix	Figure A6-5	UTM-X[a] (m)	UTM-Y[3] (m)	Area[b]		Approximate Interval Sampled (m)[d]	Geologic Unit[c,d]	Reference for Sampled Depth and Chemical (C) and Isotopic (I) Data
Gravity Fault									
NC-EWDP-5S	NC-EWDP-5S	154	555676	4058229	GF	Gravity fault	(183.3 to 237.7)[7]	Alluvium[7]	DTNs: GS010308312322.003 [DIRS 154734], T, $\delta^{18}O$, δD; GS010308312322.002 [DIRS 162910], F^-, Sr^{2+}, SiO_2; MO0007MAJIONPH.015 [DIRS 151532], pH, C; GS010208312322.001 [DIRS 162908], U concentrations and isotopes; LA0311EK831232.002 [DIRS 166069], $^{87}Sr/^{86}Sr$
NC-EWDP-5SB	NC-EWDP-5SB	155	555678	4058216	GF	Gravity fault	(115.6 to 149.0)[7]	Alluvium[7]	DTNs: GS011108312322.006 [DIRS 162911], T, pH, ions, ^{14}C, $\delta^{18}O$, δD, $\delta^{13}C$, $\delta^{34}S$; LA0311EK831232.002 [DIRS 166069], $^{87}Sr/^{86}Sr$
16S/50E-7bcd	16S/50E-7bcd	156	553932	4047540	GF	Gravity fault	open borehole (43 to 60)[3]	Qal[2]	DTNs: MO0007MAJIONPH.012 [DIRS 151529], C; MO0007GNDWTRIS.011 [DIRS 151501], $\delta^{18}O$, δD, $\delta^{13}C$, ^{14}C; MO0007MAJIONPH.014 [DIRS 151531], C
Nelson Domestic	Nelson Domestic	157	553683	4047702	GF	Gravity fault	open borehole (depth not reported)	Qal[13]	DTNs: GS990808312322.001 [DIRS 149393], T, pH, $\delta^{18}O$, δD, $\delta^{13}C$; GS990808312322.002 [DIRS 162917], ions and ^{14}C; GS021008312322.002 [DIRS 162913], $\delta^{34}S$; GS010208312322.001 [DIRS 162908], U concentrations and isotopes
16S/49E-12ddd	16S/49E-12ddd	158	553834	4047386	GF	Gravity fault	open borehole (depth not reported)	Qal[13]	DTN: MO0007MAJIONPH.012 [DIRS 151529], C

Table A4-3. Summary of Groundwater Wells and Data Sources (Continued)

Well Identifier	Abbreviation Used in Appendix	Figure A6-5	UTM-X[a] (m)	UTM-Y[3] (m)	Area[b]		Approximate Interval Sampled (m)[d]	Geologic Unit[c,d]	Reference for Sampled Depth and Chemical (C) and Isotopic (I) Data
Gravity Fault (Continued)									
Lowe Domestic	Lowe Domestic	159	552116	4047002	GF	Gravity fault	open borehole (depth not reported)	Qal[13]	DTNs: GS990808312322.001 [DIRS 149393], T, $\delta^{18}O$, δD, $\delta^{13}C$; GS990808312322.002 [DIRS 162917], ions and ^{14}C; GS021008312322.002 [DIRS 162913], $\delta^{34}S$; GS010208312322.001 [DIRS 162908], U concentrations and isotopes
16S/49E-15aaa	16S/49E-15aaa	160	550556	4046842	GF	Gravity fault	open borehole (51 to 120)[3]	Qal[2]	DTNs: MO0007MAJIONPH.012 [DIRS 151529], C; MO0007GNDWTRIS.011 [DIRS 151501], $\delta^{18}O$, δD, $\delta^{13}C$; MO0007MAJIONPH.014 [DIRS 151531], C; Claassen 1985 [DIRS 101125], Table 1, sample 29, T
Anvil Ranch Irrigation	Anvil Ranch Irrigation	161	548906	4043723	GF	Gravity fault	open borehole (depth not reported)	Qal[13]	DTNs: GS990808312322.001 [DIRS 149393], pH, $\delta^{18}O$, δD, $\delta^{13}C$; GS990808312322.002 [DIRS 162917], ions and ^{14}C; GS021008312322.002 [DIRS 162913], $\delta^{34}S$; GS010208312322.001 [DIRS 162908], U concentrations and isotopes
16S/49E-36aaa	16S/49E-36aaa	162	553569	4042053	GF	Gravity fault	open borehole (depth not reported)	Qal[13]	DTNs: MO0007GNDWTRIS.011 [DIRS 151501], $\delta^{18}O$, δD, $\delta^{13}C$, ^{14}C; MO0007MAJIONPH.014 [DIRS 151531], C
16S/49E-35baa	16S/49E-35baa	163	551307	4042040	GF	Gravity fault	open borehole (26 to 100)[3]	Qal[2]	DTN: MO0007MAJIONPH.012 [DIRS 151529], C; Claassen 1985 [DIRS 101125], Table 1, sample 33, T

Table A4-3. Summary of Groundwater Wells and Data Sources (Continued)

Well Identifier	Abbreviation Used in Appendix	Figure A6-5	UTM-X[a] (m)	UTM-Y[3] (m)	Area[b]		Approximate Interval Sampled (m)[d]	Geologic Unit[c,d]	Reference for Sampled Depth and Chemical (C) and Isotopic (I) Data
Gravity Fault (Continued)									
Payton Domestic	Payton Domestic	164	553134	4041977	GF	Gravity fault	open borehole (depth not reported)	Qal[13]	DTNs: GS990808312322.001 [DIRS 149393], T, pH, $\delta^{18}O$, δD, $\delta^{13}C$; GS990808312322.002 [DIRS 162917], ions and ^{14}C; GS021008312322.002 [DIRS 162913], $\delta^{34}S$; GS010208312322.001 [DIRS 162908], U concentrations and isotopes
16S/49E-36aba	16S/49E-36aba	165	553222	4041836	GF	Gravity fault	open borehole (depth not reported)	Qal[2]	DTN: MO0007MAJIONPH.012 [DIRS 151529], C
16S/49E-35aaa	16S/49E-35aaa	166	551980	4041520	GF	Gravity fault	open borehole (35 to 52)[2]	Qal[2]	DTN: MO0007MAJIONPH.012 [DIRS 151529], C
Oettinger Well	Oettinger Well	167	551698	4040954	GF	Gravity fault	open borehole (depth not reported)	Qal[13]	DTNs: GS990808312322.001 [DIRS 149393], T, pH, $\delta^{18}O$, δD, $\delta^{13}C$; GS990808312322.002 [DIRS 162917], ions and ^{14}C; GS021008312322.002 [DIRS 162913], $\delta^{34}S$; GS010208312322.001 [DIRS 162908], U concentrations and isotopes
Amargosa Motel (b)	Amargosa Motel (b)	168	551720	4038945	GF	Gravity fault	open borehole (depth not reported)	Qal[13]	DTNs: GS990808312322.001 [DIRS 149393], T, pH, $\delta^{18}O$, δD, $\delta^{13}C$; GS990808312322.002 [DIRS 162917], ions and ^{14}C; GS021008312322.002 [DIRS 162913], $\delta^{34}S$; GS010208312322.001 [DIRS 162908], U concentrations and isotopes

Table A4-3. Summary of Groundwater Wells and Data Sources (Continued)

Well Identifier	Abbreviation Used in Appendix	Figure A6-5	UTM-X[a] (m)	UTM-Y[3] (m)	Area[b]		Approximate Interval Sampled (m)[d]	Geologic Unit[c,d]	Reference for Sampled Depth and Chemical (C) and Isotopic (I) Data
Gravity Fault (Continued)									
17S/49E-11ba	17S/49E-11ba	169	551873	4038623	GF	Gravity fault	open borehole (20 to 56)[2]	Qal[2]	DTN: MO0007MAJIONPH.012 [DIRS 151529], C; Claassen 1985 [DIRS 101125], Table 1, sample 36, T
Spring Meadows Well #8	Spring Meadows Well #8	170	560913	4038129	GF	Gravity fault	open borehole (depth not reported)	Not reported	DTN: LA0311EK831232.001 [DIRS 166068], 10/15/70 sample
17S/50E-19aab	17S/50E-19aab	171	555998	4035691	GF	Gravity fault	open borehole (depth not reported)	Qal[13]	DTN: MO0007MAJIONPH.012 [DIRS 151529], C; Claassen 1985 [DIRS 101125], Table 1, sample 58, T
USFWS - Five Springs Well	USFWS - Five Springs Well	172	561126	4035571	GF	Gravity fault	open borehole (depth not reported)	Not reported	DTN: LA0311EK831232.001 [DIRS 166068], 8/24/90, 4/28/92, 8/18/92, and 9/22/96 samples; the 1990 and 1992 samples are also in DTN: GS931100121347.007 [DIRS 149611)
Spring Meadows Well #10	Spring Meadows Well #10	173	556916	4034042	GF	Gravity fault	open borehole (depth not reported)	Not reported	DTN: LA0311EK831232.001 [DIRS 166068], 8/15/62 sample
18S/49E-1aba	18S/49E-1aba	174	554035	4031056	GF	Gravity fault	0 (Spring)[3]	Qal[13]	DTN: MO0007MAJIONPH.014 [DIRS 151531], C; Claassen 1985 [DIRS 101125], Table 1, sample 40, T
18S/50E-6dac	18S/50E-6dac	175	556035	4029960	GF	Gravity fault	open borehole (depth not reported)	Qal[13]	DTN: MO0007MAJIONPH.012 [DIRS 151529], C
18S/50E-7aa	18S/50E-7aa	176	556040	4029158	GF	Gravity fault	open borehole (depth not reported)	Qal[13]	DTN: MO0007MAJIONPH.014 [DIRS 151531], C; Claassen 1985 [DIRS 101125], Table 1, sample 59, T

Table A4-3. Summary of Groundwater Wells and Data Sources (Continued)

Well Identifier	Abbreviation Used in Appendix	Figure A6-5	UTM-X[a] (m)	UTM-Y[3] (m)	Area[b]		Approximate Interval Sampled (m)[d]	Geologic Unit[c,d]	Reference for Sampled Depth and Chemical (C) and Isotopic (I) Data
Amargosa River/ Fortymile Wash									
16S/48E-36dcc	16S/48E-36dcc	177	543530	4040395	AR/FMW	Amargosa River/ Fortymile Wash	open borehole (13 to 120)[3]	Qal[2]	DTN: MO0007MAJIONPH.012 [DIRS 151529], C; Claassen 1985 [DIRS 101125], Table 1, sample 26, T
Crane Domestic	Crane Domestic	178	543587	4037930	AR/FMW	Amargosa River/ Fortymile Wash	open borehole (depth not reported)	Qal[13]	DTNs: GS990808312322.001 [DIRS 149393], T, pH, $\delta^{18}O$, δD, $\delta^{13}C$; GS990808312322.002 [DIRS 162917], ions and ^{14}C; GS021008312322.002 [DIRS 162913], $\delta^{34}S$; GS010208312322.001 [DIRS 162908], U concentrations and isotopes
27N/4E-27bbb	27N/4E-27bbb	179	541520	4034130	AR/FMW	Amargosa River/ Fortymile Wash	open borehole (14 to 90)[3]	Qal[2]	DTN: MO0007MAJIONPH.012 [DIRS 151529], C; Claassen 1985 [DIRS 101125], Table 1, sample 54, T
IMV on Windjammer	IMV on Windjammer	180	548115	4033603	AR/FMW	Amargosa River/ Fortymile Wash	open borehole (depth not reported)	Qal[13]	DTNs: GS990808312322.001 [DIRS 149393], T, pH, $\delta^{18}O$, δD, $\delta^{13}C$; GS990808312322.002 [DIRS 162917], ions and ^{14}C; GS021008312322.002 [DIRS 162913], $\delta^{34}S$; GS010208312322.001 [DIRS 162908], U concentrations and isotopes
17S/49E-29acc	17S/49E-29acc	181	547349	4033420	AR/FMW	Amargosa River/ Fortymile Wash	open borehole (depth not reported)	Qal[13]	DTN: MO0007MAJIONPH.012 [DIRS 151529], C; Claassen 1985 [DIRS 101125], Table 1, sample 44, T
17S/49E-28bcd	17S/49E-28bcd	182	548370	4033395	AR/FMW	Amargosa River/ Fortymile Wash	open borehole (depth not reported)	Qal[13]	DTN: MO0007MAJIONPH.012 [DIRS 151529], C

Table A4-3. Summary of Groundwater Wells and Data Sources (Continued)

Well Identifier	Abbreviation Used in Appendix	Figure A6-5	UTM-X[a] (m)	UTM-Y[3] (m)	Area[b]		Approximate Interval Sampled (m)[d]	Geologic Unit[c,d]	Reference for Sampled Depth and Chemical (C) and Isotopic (I) Data
Amargosa River/ Fortymile Wash (Continued)									
18S/49E-2cbc	18S/49E-2cbc	183	551377	4030023	AR/FMW	Amargosa River/ Fortymile Wash	open borehole (22 to 160)[3]	Qal[2]	DTN: MO0007MAJIONPH.012 [DIRS 151529], C; Claassen 1985 [DIRS 101125], Table 1, sample 41, T
Mom's Place	Mom's Place	184	551996	4029417	AR/FMW	Amargosa River/ Fortymile Wash	open borehole (depth not reported)	Qal[13]	DTNs: GS990808312322.001 [DIRS 149393], T, pH, $\delta^{18}O$, δD, $\delta^{13}C$; GS990808312322.002 [DIRS 162917], ions and ^{14}C; GS021008312322.002 [DIRS 162913], $\delta^{34}S$; GS010208312322.001 [DIRS 162908], U concentrations and isotopes
18S/49E-11bbb	18S/49E-11bbb	185	551307	4029283	AR/FMW	Amargosa River/ Fortymile Wash	open borehole (depth not reported)	Qal[13]	DTN: MO0007MAJIONPH.012 [DIRS 151529], C; Claassen 1985 [DIRS 101125], Table 1, sample 42, T
Skeleton Hills									
TW-5	TW-5	186	562604	4054686	SH	Skeleton Hills	open borehole (207 to 244)[15]	Protozoic clastic rocks[16]	DTNs: MO0007MAJIONPH.006 [DIRS 151518], C; MO0007GNDWTRIS.004 [DIRS 151494], $\delta^{18}O$, δD; MO0007MAJIONPH.002 [DIRS 151507], C; Oliver and Root 1997 [DIRS 100069], F^-, Sr^{2+}, $^{87}Sr/^{86}Sr$
Unnamed Well 15S/50E-22-7	Unnamed Well 15S/50E-22-7	187	559605	4053895	SH	Skeleton Hills	open borehole (depth not reported)	Not reported	DTN: LA0311EK831232.001 [DIRS 166068], 11/20/72 sample

Table A4-3. Summary of Groundwater Wells and Data Sources (Continued)

Well Identifier	Abbreviation Used in Appendix	Figure A6-5	UTM-X[a] (m)	UTM-Y[3] (m)	Area[b]		Approximate Interval Sampled (m)[d]	Geologic Unit[c,d]	Reference for Sampled Depth and Chemical (C) and Isotopic (I) Data
Amargosa Flat									
Amargosa Tracer Hole #2	Amargosa Tracer Hole #2	188	569158	4043531	AF	Amargosa Flat	open borehole (12 to 252)[2]	Paleozoic carbonate rocks[2]	DTN: LA0311EK831232.001 [DIRS 166068], 9/17/66, 10/7/67, 2/15/88 and 2/16/68 samples
Cherry Patch Well, 17S/52E-08cdb	Cherry Patch Well, 17S/52E-08cdb	189	576207	4038588	AF	Amargosa Flat	open borehole (10 to 122)[2]	Qal (limestone)[2]	DTN: LA0311EK831232.001 [DIRS 166068], 8/24/90, 3/24/92, 9/5/91,and 5/15/97 samples; the 1990 through 1992 data are also in DTN: GS931100121347.007 [DIRS 149611]
USDOE-MSH-C shallow Well	USDOE-MSH-C shallow Well	190	565396	4039700	AF	Amargosa Flat	open borehole (depth not reported)	Not reported	DTN: LA0311EK831232.001 [DIRS 166068], 9/27/96 sample
Mine Mountain									
UE-17a	UE-17a	191	574116	4103157	MM	Mine Mountain	Bailed from 254 Open borehole (194 to 354)[6]	Not reported	DTN: LA0311EK831232.001 [DIRS 166068], 6/9/93 sample; also in Rose et al. 1997 [DIRS 144725], samples 56 to 58
UE-1a	UE-1a	192	578395	4100387	MM	Mine Mountain	Bailed from 168 Open borehole (167 to 171)[6]	Tv[5]	DTN: LA0311EK831232.001 [DIRS 166068], 9/1/92 sample; also in Davisson et al. 1994 [DIRS 162939]; Rose et al. 1997 [DIRS 144725], sample 46
UE-1b	UE-1b	193	579004	4100389	MM	Mine Mountain	Bailed from 207 Open borehole (198 to 382)[6]	Paleozoic carbonate rocks[5]	DTN: LA0311EK831232.001 [DIRS 166068], 9/1/92 sample; also in Davisson et al. 1994 [DIRS 162939]; Rose et al. 1997 [DIRS 144725], sample 45
UE-16f	UE-16f	194	574100	4098960	MM	Mine Mountain	Bailed from 395 Open borehole (112 to 422)[6]	Eleana Fm.[5]	DTN: LA0311EK831232.001 [DIRS 166068], 7/12/93; Rose et al. 1997 [DIRS 144725], sample 42, sulfate, SO_4^{2-} and Na^+

Table A4-3. Summary of Groundwater Wells and Data Sources (Continued)

Well Identifier	Abbreviation Used in Appendix	Figure A6-5	UTM-X[a] (m)	UTM-Y[3] (m)	Area[b]		Approximate Interval Sampled (m)[d]	Geologic Unit[c,d]	Reference for Sampled Depth and Chemical (C) and Isotopic (I) Data
Mine Mountain (Continued)									
UE-14b	UE-14b	195	575427	4087304	MM	Mine Mountain	Not reported	Tv[5]	DTN: LA0311EK831232.001 [DIRS 166068], 9/1/88 and 7/24/91 samples; the 9/1/88 sample is in Chapman and Lyles 1993 [DIRS 162940], p. 39
Pluto 1	Pluto 1	196	579238	4075338	MM	Mine Mountain	Possibly perched[5]	Tv[5]	DTN: LA0311EK831232.001 [DIRS 166068], 11/2/84 sample; also in Chapman and Lyles 1993 [DIRS 162940], p. 38
Pluto 5	Pluto 5	197	579263	4074977	MM	Mine Mountain	Possibly perched[5]	Tv[5]	DTN: LA0311EK831232.001 [DIRS 166068], 9/26/88 sample; also in Chapman and Lyles 1993 [DIRS 162940], p. 38
USGS Test Well F (HTH)	USGS Test Well F (HTH)	198	578858	4068348	MM	Mine Mountain	Not reported	Tv[5]	DTN: LA0311EK831232.001 [DIRS 166068], 5/21/75,2/2/76, and 3/12/80 samples
Funeral Mountains									
Woodcamp Spring	Woodcamp Spring	199	502027	4091249	FMt	Funeral Mountains	0.0 (spring discharge)[12]	Tertiary volcanic rock[12]	DTN: GS960408312323.002 [DIRS 162915], C, I
Bond Gold Mining #13	Bond Gold Mining #13	200	519383	4059841	FMt	Funeral Mountains	open borehole (depth not reported)	Qal[13]	DTN: GS010308312322.003 [DIRS 154734], T, pH, alkalinity, ions, $\delta^{18}O$, δD, $\delta^{13}C$, ^{14}C; GS011108312322.006 [DIRS 162911], $\delta^{34}S$; GS010208312322.001 [DIRS 162908], U concentrations and isotopes; GS010308312322.002 [DIRS 162910], U concentrations; LA0311EK831232.002 [DIRS 166069], $^{87}Sr/^{86}Sr$

Table A4-3. Summary of Groundwater Wells and Data Sources (Continued)

Well Identifier	Abbreviation Used in Appendix	Figure A6-5	UTM-X[a] (m)	UTM-Y[3] (m)	Area[b]		Approximate Interval Sampled (m)[d]	Geologic Unit[c,d]	Reference for Sampled Depth and Chemical (C) and Isotopic (I) Data
Funeral Mountains (Continued)									
Nevares Spring	Nevares Spring	201	516068	516068	FMt	Funeral Mountains	0.0 (spring discharge)[12]	Travertine[12]	DTN: GS960408312323.002 [DIRS 162915], C, I
Travertine Spring	Travertine Spring	202	515211	4032657	FMt	Funeral Mountains	0.0 (spring discharge)[12]	Qal[12]	DTN: GS960408312323.002 [DIRS 162915], C, I

[a] Coordinate data are from (1) LA0311EK831232.001 [DIRS 166068], (2) GS010908312332.002 [DIRS 163555], (3) GS010208312322.001 [DIRS 162908], (4) Paces et al. 2002 [DIRS 158817], (5) GS010808312322.004 [DIRS 156007], and (6) LA0309EK831223.001 [DIRS 165471]. These sources do not always identify whether coordinates are reported relative to North American Datum (NAD) 1927 or 1983, and the coordinates listed may represent a mixture of both coordinate systems. Because of uncertainty in the reference system used in any source, an uncertainty of approximately 100 m results in the coordinates of boreholes listed. Because of the scale at which data are presented, this uncertainty has a negligible effect on the interpretation of groundwater geochemical patterns and flow paths given in this appendix.

[b] See Figure A6-5 and Section A6.3.2 for a definition of subareas near Yucca Mountain. The subareas used in this appendix may differ from subareas used in DTNs that begin MO000…, which are associated with the earlier analysis model report version of this appendix.

[c] Geologic units: Qal Quaternary alluvium; QTal Quaternary-Tertiary alluvium; Tv Tertiary volcanic rocks; Tb Tertiary basalts; Tpt Tertiary Topopah Spring Member of Paintbrush tuff; Tct Tertiary Crater Flat tuff; Th Tertiary tuffaceous beds of Calico Hills; Tac Tertiary Calico Hills Formation; Tcb Tertiary Bullfrog Member of Crater Flat tuff; Tcp Tertiary Prow Pass Member of Crater Flat tuff; Tlr Tertiary Lithic Ridge tuff; DSlm Devonian and Silurian Lone Mountain Dolomite; Srm Silurian Roberts Mountain Dolomite; Tfb (and its subunits Tfbr and Tfbw) are volcanic rocks of the Tertiary Beatty Wash Formation; Tm is the Tertiary Timber Mountain tuff; Tma (and its subunits Tmaw, Tmap and Tmar) are the Tertiary Ammonia Tanks tuff; Tft is a basalt; and Ttc is the Tertiary commendite of Ribbon Cliff). Geologic units are defined in Oliver and Root 1997 [DIRS 100069], p. 5; Buesch et al. 1996 [DIRS 100106], Table 4; McKinley et al. 1991 [DIRS 116222], pp. 5 to 6; Day et al. 1998 [DIRS 101557], map sheet 2; Slate et al. 1999 [DIRS 150228]. Also, see stratigraphic column in Figure A6-2.

[d] C: the DTN or reference was the source for chemical data for this well; I: the DTN or reference was the source for isotopic data for this well. References to sample identifiers in Claassen 1985 [DIRS 101125], Table 1 provide traceability between identifiers used in the listed DTNs and those listed in column 1 of this table. As indicated in footnotes for Tables A4-1 and Table A4-2, many of the data sources listed in this table were used as input for developed-data DTNs: LA0309RR831233.001 [DIRS 166546] and LA0309RR831233.002 [DIRS 166548], which are cited as the sources for the bulk of the data listed in Tables A6-1 and A6-2. In this case, the acquired-data sources have not been listed separately as sources for data in the footnotes of those two tables.

[e] Sources of data on interval depths and geologic units sampled are (1) Benson and McKinley 1985, [DIRS 101036], Table 1, (2) McKinley et al. 1991 [DIRS 116222], Tables 1 and 5, (3) Claassen 1985 [DIRS 101125], Table 1), (4) Rose et al. 2002 [DIRS 162938], Table A-1, (5) Chapman and Lyles 1993 [DIRS 162940], Figures 11, 13, 16), (6) Davisson et al. 1994 [DIRS 162939], Table 1, (7) DTN: LA0311EK831223.001 [DIRS 165985], (8) Robledo et al. 1998 [DIRS 165986], Tables 1 and 4, (9) Graves et al. 1998 [DIRS 155411], throughout report, (10) O'Brien 1998 [DIRS 101278], Table 2, (11) DTN: GS980908312322.008 [DIRS 145412], (12) Steinkampf and Werrell (2001 [DIRS 158818], pp. 11 to 14), (13) lithology estimated from Figure 1 of Claassen 1985 [DIRS 101125], (14) GS010308312322.003 [DIRS 154734], (15) Oliver and Root 1997 [DIRS 100069], *yucca.xls*, (16) Winograd and Thordarson 1975 [DIRS 101167], Plate 1).

A5. ASSUMPTIONS

The scientific analyses presented in this appendix sometimes required that assumptions be made about certain aspects of the hydrochemical or hydrologic system. Typically, these assumptions were made (1) to simplify a problem so that a solution could be approximated, (2) to obtain bounding estimates, or (3) because no relevant data were available at the time the analysis was made.

Table A5-1. Assumptions

	Assumption	Rationale for Assumption
1	To provide an initial assessment of flow directions indicated by the hydraulic gradient in Figure A6-3, flow vectors are drawn parallel to this gradient, implicitly assuming the hydraulic conductivity of the rocks is isotropic.	In spite of the likely anisotropy introduced by the presence of north and northwest trending faults in the Yucca Mountain area, this assumption was made to get an initial sense of the flow directions indicated by the hydraulic gradients. The likelihood that actual flow directions may be more aligned with fault orientations than indicated by these flow lines is acknowledged in the text. This assumption does not influence the conclusions herein that are based solely on groundwater geochemical and isotopic data.
2	The dissolved aluminum concentration of groundwater in the Yucca Mountain area is in equilibrium with kaolinite.	The assumption that groundwater aluminum concentrations are controlled by equilibrium with kaolinite was supported by calculating dissolved aluminum concentrations in equilibrium with a variety of secondary minerals with PHREEQC (Parkhurst and Appelo 1999 [DIRS 159511]) and comparing these calculated concentrations with concentrations measured at a subset of wells in the Yucca Mountain area (Figure A6-30). This assumption affects calculation of mineral saturation indices in Table A6.3-5.
3	For the purpose of calculating mineral saturation indices, the temperature of groundwater samples can be approximated either from published maps of water table temperatures at Yucca Mountain, or, in the Amargosa Desert, can be assumed to be 25°C.	The use of a contour map of water table temperatures (Fridrich et al. 1994 [DIRS 100575], Figure 8) to estimate groundwater sample temperatures at Yucca Mountain is an acceptable approximation because most of the samples for which this approximation was made are from the upper part of the saturated zone (see Table A4-3 for sampled depths and Figure A6-5 for locations of samples 33, 34, 41, 56, 57, and 66). Likewise, the assumption that groundwater samples in the Amargosa Desert with no measured temperatures are at 25°C is an acceptable approximation because most of the measured groundwater sample temperatures are in the range of 20°C to 30°C (see temperature data for samples from the Amargosa Valley (rows 99-107), Amargosa River (rows 108-117), Fortymile Wash—West (rows 118 to 126), Fortymile Wash—South (rows 127 to 141), Fortymile Wash—East (rows 142 to 153), Gravity Fault (rows 154 to 176), and Amargosa River/Fortymile Wash (rows 177-185) in Table A6-1).
4	The chemical and isotopic composition of the groundwater sample from the carbonate aquifer at borehole p#1 (sample p#1(c) in Tables A6-1 and A6-2) and, in particular, its Cl^- and SO_4^{2-} concentrations, are representative of the composition of groundwater in carbonate aquifer at Yucca Mountain.	Borehole p#1 is the only borehole near Yucca Mountain where groundwater was directly sampled from the carbonate aquifer, so this assumption is made out of necessity. The Cl^- and SO_4^{2-} concentrations of groundwater at p#1 (28 and 160 mg/L, respectively) are similar to the concentrations of these ions in groundwater from the carbonate aquifer at Ash Meadows where Cl^- ranges from 21 to 27 mg/L and SO_4^{2-} ranges from 80 to 111 mg/L (Winograd and Pearson 1976 [DIRS 108882], Table 1). The variability in the concentrations of Cl^- and SO_4^{2-} in the carbonate aquifer at Ash Meadows may indicate the extent of the variability that could be expected at Yucca Mountain.

Table A5-1. Assumptions (Continued)

	Assumption	Rationale for Assumption
5	The chloride mass-balance (CMB) method is assumed to be applicable to the estimation of recharge rates at Yucca Mountain. The CMB method assumes one-dimensional, downward piston flow in the soil zone, no run-on or runoff, no Cl^- source other than precipitation, and no Cl^- sink (e.g. the formation of halite is negligible).	The absence of chloride sources and sinks is indicated by the absence of halite or other chloride-bearing minerals in the soils and rocks at Yucca Mountain. The departures of actual flow conditions from the assumption of one-dimensional piston flow are mitigated somewhat for the calculations done on the basis of the saturated-zone chloride data. This result is because, for Yucca Mountain as a whole, flow can be assumed to be vertical between the ground surface and the water table, even though lateral flow in the unsaturated zone could redistribute water on a more local scale. Similarly, when using the saturated-zone data with the CMB method, the effects of nonpiston flow are mitigated because hydrodynamic mixing and mixing in the well bore when groundwater is pumped tend to average the Cl^- concentrations of fast- and slow-moving water percolating through fractures and matrix in the unsaturated zone. Run-on and runoff both can redistribute Cl^- locally at Yucca Mountain. However, although run-on is a factor to consider for wells near Fortymile Wash, run-on from other areas to Yucca Mountain does not occur, and so the total Cl^- balance for Yucca Mountain itself is not affected by this process. Runoff from Yucca Mountain to Fortymile Wash would tend to cause the actual Cl^--deposition rates at Yucca Mountain to be less than those assumed in the calculations and, thus, cause the estimated Yucca Mountain recharge to overestimate the actual recharge.
6	The estimated range of annual deposition rates for chloride at Yucca Mountain encompasses the present-day rate as well as the rates that prevailed when the sampled pore waters infiltrated below the soil zone.	Several independent lines of evidence support this assumption. First, the range of deposition rates assumed for Yucca Mountain reflect the present-day wet and dry chloride deposition rates estimated for sites at Red Rock Canyon and Kawich Range, Nevada (BSC 2002 [DIRS 160247]), which represent climates that are drier and wetter, respectively, than that prevailing at Yucca Mountain today. The second line of evidence is the constancy of the $^{36}Cl/Cl$ ratio throughout the Holocene, based on packrat midden data (Plummer et al. 1997 [DIRS 107034]). Finally, the nearly uniform Cl concentrations in the perched water and SZ groundwater beneath Yucca Mountain also support the assumption. Section A6.3.6.5 addresses the uncertainty in the deposition rate and propagation of that uncertainty through the resulting estimates of recharge obtained by the chloride mass-balance method.
7	The chemical and isotopic composition of deep-perched water from boreholes UZ-14 and SD-7 is representative of local recharge at Yucca Mountain.	A possible conceptual model for the formation of perched water at Yucca Mountain is that perched water originates when local infiltration rates exceed the hydraulic conductivity of the perching layer, so that deep infiltration begins to pond at the top of the layer. The perched water then moves toward the water table to become recharge either by (1) seeping slowly through the matrix of the perching layer, (2) moving laterally down-dip along the top of the perching layer, or (3) by draining down faults where these intersect the perching layer, depending on local structural conditions. Although some additional water/rock interactions such as cation exchange may occur in the deep UZ between the surface and perched-water horizons, the deep perched water already incorporates the effects of evaporative processes and water/rock/gas interactions in the soil zone that dominate the chemical and isotopic compositions of unsaturated-zone waters (Meijer 2002 [DIRS 158813]). The compositions of the deep-perched waters are therefore a good approximation of the water compositions of local recharge.

Table A5-1. Assumptions (Continued)

	Assumption	Rationale for Assumption
8	Carbon isotope exchange is not a significant process affecting ^{14}C activities of groundwater near Yucca Mountain.	The age-correction models (Section A6.3.6.6.2) did not consider the process of carbon-isotope exchange, a process that alters the carbon-isotope composition of groundwater without increasing the net concentrations of elements contained in the carbon-bearing solid phases. Isotope exchange is important to consider where the groundwater is already saturated with calcite and additional interaction between groundwater and calcite that might alter the isotopic composition (^{14}C and $\delta^{13}C$) of the dissolved carbon would not be reflected by a change in the concentration of the total dissolved carbon. The groundwater in the carbonate aquifer is already saturated with calcite, and thus, exchange reactions are important to consider in this environment. In the volcanic aquifer, almost all groundwater samples for which age corrections were made were under saturated with calcite. Any interaction between groundwater and calcite in the volcanic aquifer should, therefore, be reflected by an increase in the dissolved carbon concentrations in the groundwater, a process already considered by the mass-balance approach embedded in the modeling.
9	The $\delta^{13}C$ of calcite in alluvium is similar to the $\delta^{13}C$ of pedogenic calcite in the unsaturated zone of Yucca Mountain (about –4 per mil).	No data presently exists on the isotopic composition of calcite contained in alluvium south and southeast of the repository area at Yucca Mountain. Late-stage fracture-lining calcite from the unsaturated zone has a distribution with a mode of about –6 per mil, whereas intermediate-stage calcite is more uniformly distributed and has a mode of about –2 per mil (Whelan et al. 1998 [DIRS 108865], p. 179). An average value of –4 per mil approximates an average value for the intermediate and late-stage fracture-lining calcite in the unsaturated zone at Yucca Mountain.
10	It is assumed for the purpose of tracing flow lines from chemical and isotopic data that, once in the saturated-zone groundwater system, δD, $\delta^{18}O$, Cl^-, SO_4^{2-}, and $\delta^{34}S$ are sufficiently conservative (i.e., nonreactive) to identify likely flow paths and groundwater mixing relationships.	This assumption is sound for δD and $\delta^{18}O$ because these constitute the water molecule; thus, large amounts of water/rock interaction are required to alter their composition. This assumption is acknowledged in the text as an approximation for Cl^- and SO_4^{2-}. Changes in the input concentrations of these constituents as a result of climate change or modifications due to water/rock interaction will result in variability along a flow path. However, in most cases, this effect is expected to be small. Regardless, the areal contrast in concentrations between these constituents is large enough that meaningful inferences about flow directions can be made.
11	The chemical composition of groundwater at borehole J-11 is representative of groundwater in central Jackass Flats.	Because borehole J-11 is the only borehole that has been drilled and sampled in central Jackass Flats, this is a necessary assumption.
12	A straight-line distance was assumed in evaluating transport times between wells based on ^{14}C.	The straight-line distance assumption allows for straightforward calculation of transport times and results in the fastest transport time. It is therefore a conservative assumption.
13	No correction was made to estimated ^{14}C transport times in fractured volcanics for matrix diffusion.	Corrections for diffusion of ^{14}C into the matrix of fractured volcanics would tend to increase the calculated groundwater transport times because the matrix pore waters tend to have lower pmc values. However, detailed data on the ^{14}C content of pore waters along potential pathways are lacking.
14	No additional ^{14}C is added to groundwater from downgradient recharge as a groundwater moves from an upgradient to a downgradient well defining a flow-path segment.	The data on oxygen and hydrogen isotopes for groundwater sampled in downgradient wells generally indicate lighter isotope ratios as water is sampled from wells progressively further downgradient. The lighter isotope ratios represent older waters (Pleistocene). The lack of modern hydrogen and oxygen isotope ratios in downgradient locations is evidence of minimal modern recharge at these locations.

A.6. SCIENTIFIC ANALYSIS

A6.1 OBJECTIVES

The objective is to provide an analysis of groundwater recharge rates, flow directions and velocities, and mixing proportions of water from different source areas based on groundwater geochemical and isotopic data. An analysis of these processes based on geochemical data can provide an independent basis for evaluating the interpretation of the flow system provided by the SZ site-scale flow model.

The analysis is structured as follows: Section A6.2 provides background information regarding geographic, geologic and hydrologic setting as well as a summary of over twenty five years of geologic and hydrologic research that has taken place in the region. Information within these sections is continually used and evaluated throughout this appendix. Sections A6.3.1 through A6.3.5 provide an overview of the hydrochemical setting in the study area. A discussion of hydrochemical trends with depth for some boreholes provided in Section A6.3.3, areal distribution plots of hydrochemical and isotopic data discussed in Section A6.3.4, and calculated geochemical parameters presented in Section A6.3.5 provide the initial hydrochemical framework for evaluating the hydraulic system. Particular attention is provided in Section A6.3.6 to evaluate the sources and evolution of water beneath Yucca Mountain. Sections A6.3.7 through A6.3.10 then evaluate flow away from Yucca Mountain. Section A6.3.7 evaluates mixing patterns evident in some areas, and Section A6.3.8 describes PHREEQC models of groundwater mixing and evolution. Section A6.3.9 uses ^{14}C groundwater ages to evaluate flow velocities, and Section A6.3.10 confirms the consistency of flow models using FEHM and flow models derived from hydrochemical arguments. Finally, Section A6.3.11 integrates all the above sections to produce a map describing regional flow pathways.

A6.2 INTRODUCTION AND PREVIOUS WORK

A6.2.1 Geography, Geology, and Physical Hydrology

Yucca Mountain is located in the Great Basin about 150 km northwest of Las Vegas, Nevada. The mountain consists of a series of fault-bounded blocks of ash-flow and ash-fall tuffs and a smaller volume of lava deposited between 14 and 11 Ma (million years before present) from a series of calderas located a few to several tens of kilometers to the north in the vicinity of Timber Mountain (Sawyer et al. 1994 [DIRS 100075], Figure 1). Volcanic rocks erupted from these calderas typically thin to the south and eventually pinch out beneath alluvium in the Amargosa Desert (Figure A6-1). Yucca Mountain itself extends southward from Pinnacles Ridge toward the Amargosa Desert (Figure A6-1). Volcanic units on Yucca Mountain typically dip 5 to 10 degrees to the east. Crater Flat is west of Yucca Mountain and separated from it by Solitario Canyon, which is the surface expression of the Solitario Canyon fault—a steeply dipping scissors fault with down-to-the-west displacement of as much as 500 m in southern Yucca Mountain (Day et al. 1998 [DIRS 101557], pp. 6 and 7). Underlying Crater Flat is a thick sequence of alluvium, lava, and tuff that has been locally cut by faults and volcanic dikes. East of Yucca Mountain, and separated from it by Fortymile Wash, is Jackass Flats, which is also underlain by a thick sequence of alluvium and volcanic rocks. Timber Mountain, approximately 25 km to the

north of the repository area, is a resurgent dome within the larger caldera complex that erupted the tuffs at Yucca Mountain.

The central block of Yucca Mountain is bounded by Drill Hole Wash on the north, the Solitario Canyon fault on the west, the Bow Ridge fault on the east, and is dissected by the Ghost Dance and Dune Wash faults (Figure A6-1). Topography north of the central block at Yucca Mountain is controlled by long, northwest-trending, fault-controlled washes. Within and south of the central block, washes are shorter and trend eastward. Topography in the southern part of Yucca Mountain is controlled by south-trending faults.

Based on similarities in their core-scale hydrologic and mechanical properties, saturated volcanic units at Yucca Mountain were grouped into two confining layers and two aquifers by Luckey et al. (1996 [DIRS 100465], pp. 17 to 19) (Figure A6-2). Figure A6-2 represents a simplification of the more detailed hydrostratigraphic framework presented in DTN: GS030208312332.001 [DIRS 163087] and used in the SZ site-scale flow model DTN: LA0304TM831231.002 [DIRS 163788] and is shown here only to provide a broad overview of the site hydrostratigraphy. In general, the confining units are zeolitic, nonwelded tuffs and the uppermost aquifers are fractured, welded, and devitrified tuffs (the Upper Volcanic Aquifer) or include intervals of fractured, welded, and devitrified tuffs (the Lower Volcanic Aquifer). Most zeolite formation took place before approximately 11 Ma (Broxton et al. 1987 [DIRS 102004], p. 101; Bish 1989 [DIRS 101194], pp. 31 and 33) and was concentrated in the originally permeable, nonwelded vitric tuffs; zeolitization was less intense in the partly to densely welded, devitrified tuffs that are present in the interiors of the Prow Pass and Bullfrog tuffs of the Crater Flat group. Zeolitization and clay alteration is more intense and zeolite facies alteration occurs higher in the section in northern Yucca Mountain because of the high paleotemperature gradients that existed near the calderas (Broxton et al. 1987 [DIRS 102004], pp. 107 to 108; Bish 1989 [DIRS 101194], p. 35). Regionally, argillite of the Eleana Formation is a confining layer, and the Paleozoic carbonate rocks are an important aquifer (Winograd and Thordarson 1975 [DIRS 101167], Table 1, columns 6, 7; Laczniak et al. 1996 [DIRS 103012], Table 1). The Eleana Formation is inferred to be present in northern Yucca Mountain based on areal magnetic data (Luckey et al. 1996 [DIRS 100465], p. 20), though it has not been penetrated by drill core. The carbonate aquifer was penetrated at borehole p#1 (the correspondence between well identifiers and borehole abbreviations is given in Table A4-3), but its continuity and thickness in this part of southern Nevada, and consequently its importance as a regional aquifer, is thought to be less near Yucca Mountain than in areas farther to the east (Thomas et al. 1996 [DIRS 101933], Figure 17).

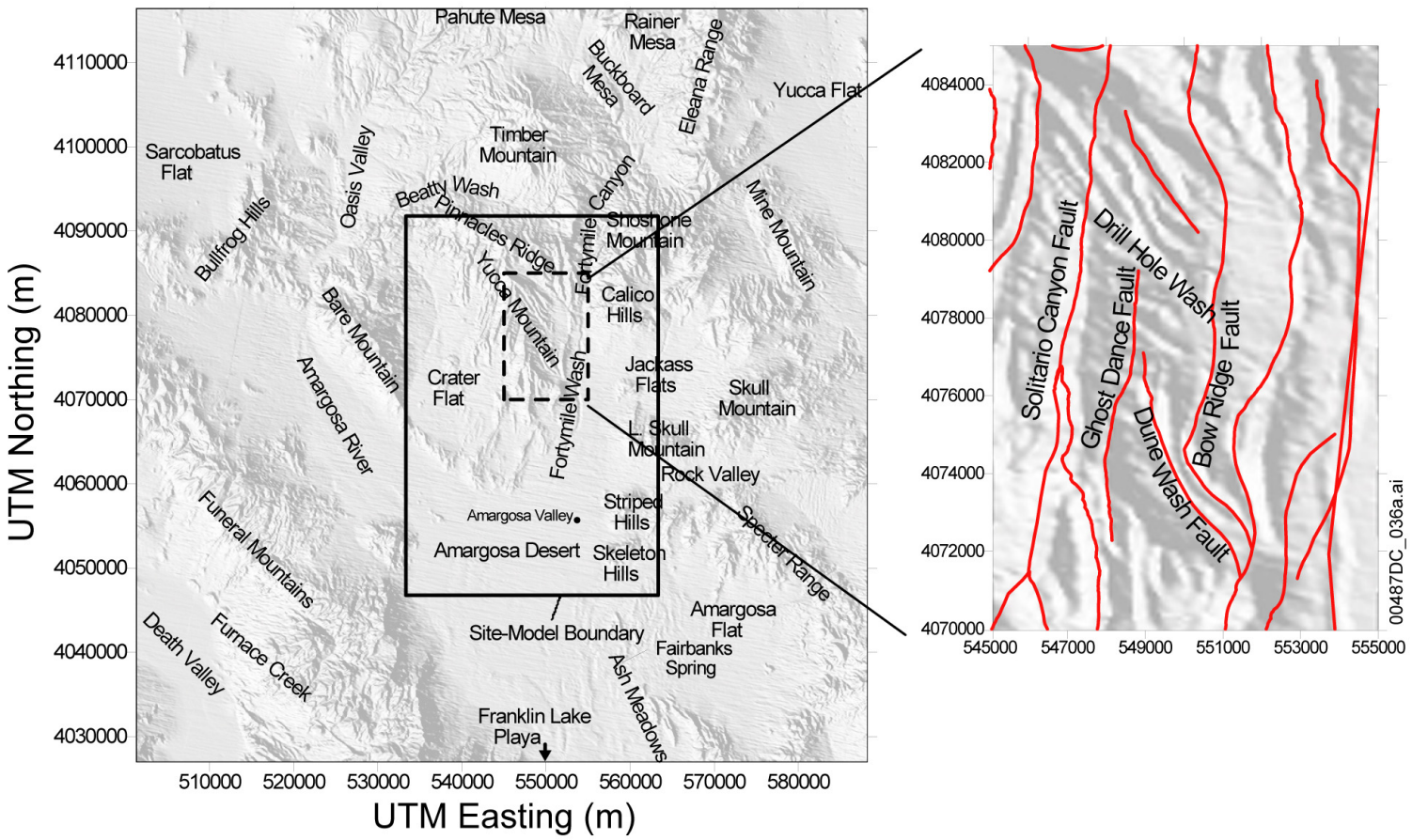

DTN: GS010908314221.001 [DIRS 145263] (Tertiary faults).

NOTE: The solid rectangle is the boundary of the SZ site-scale flow and transport model. UTM=Universal Transverse Mercator.

Figure A6-1. Important Physiographic Features near Yucca Mountain

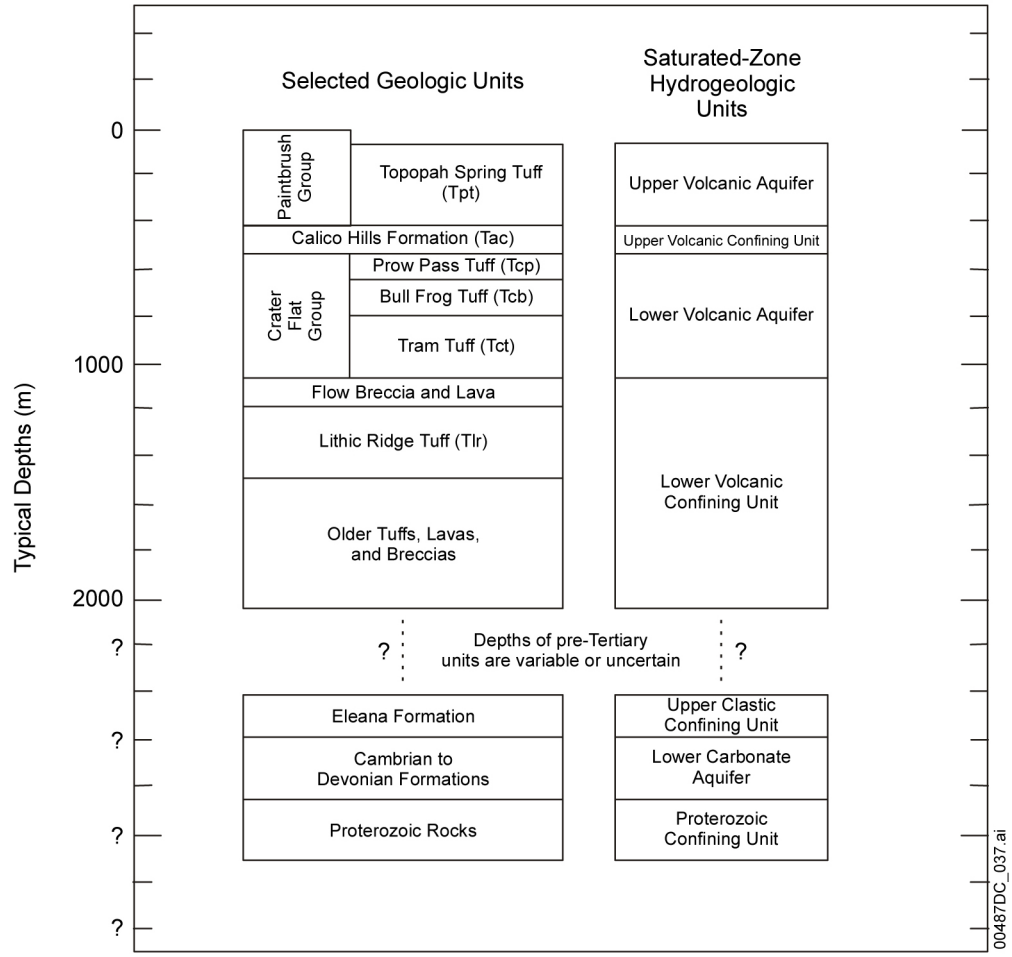

Source: Luckey et al. 1996 [DIRS 100465], Figure 7.

NOTE: Valley Fill of variable age, consisting of sands, gravels, clays, freshwater limestones, and basaltic lavas, overlies various units of the Tertiary volcanic rocks and pre-Tertiary rocks in basins to the west, east, and south of Yucca Mountain. For example, see Kilroy 1991 [DIRS 103010], Figure 3.

Figure A6-2. Selected Geologic and Hydrogeologic Units for the Saturated Zone at Yucca Mountain

A map of the potentiometric surface in the Yucca Mountain area was developed as part of an associated analysis report (USGS 2001 [DIRS 154625], Figure 1-2) based on average water–level data collected from 1985 to 1995 (Figure A6-3). The potentiometric-surface elevations at individual boreholes are based on composite water levels in the volcanic units or, at boreholes where heads were measured at multiple depths in the units, on the shallowest head measurement. (USGS 2001 [DIRS 154625], p. 18). The water levels have been influenced by local pumping in the southern part of the model area (USGS 2001 [DIRS 154625], p. 23).

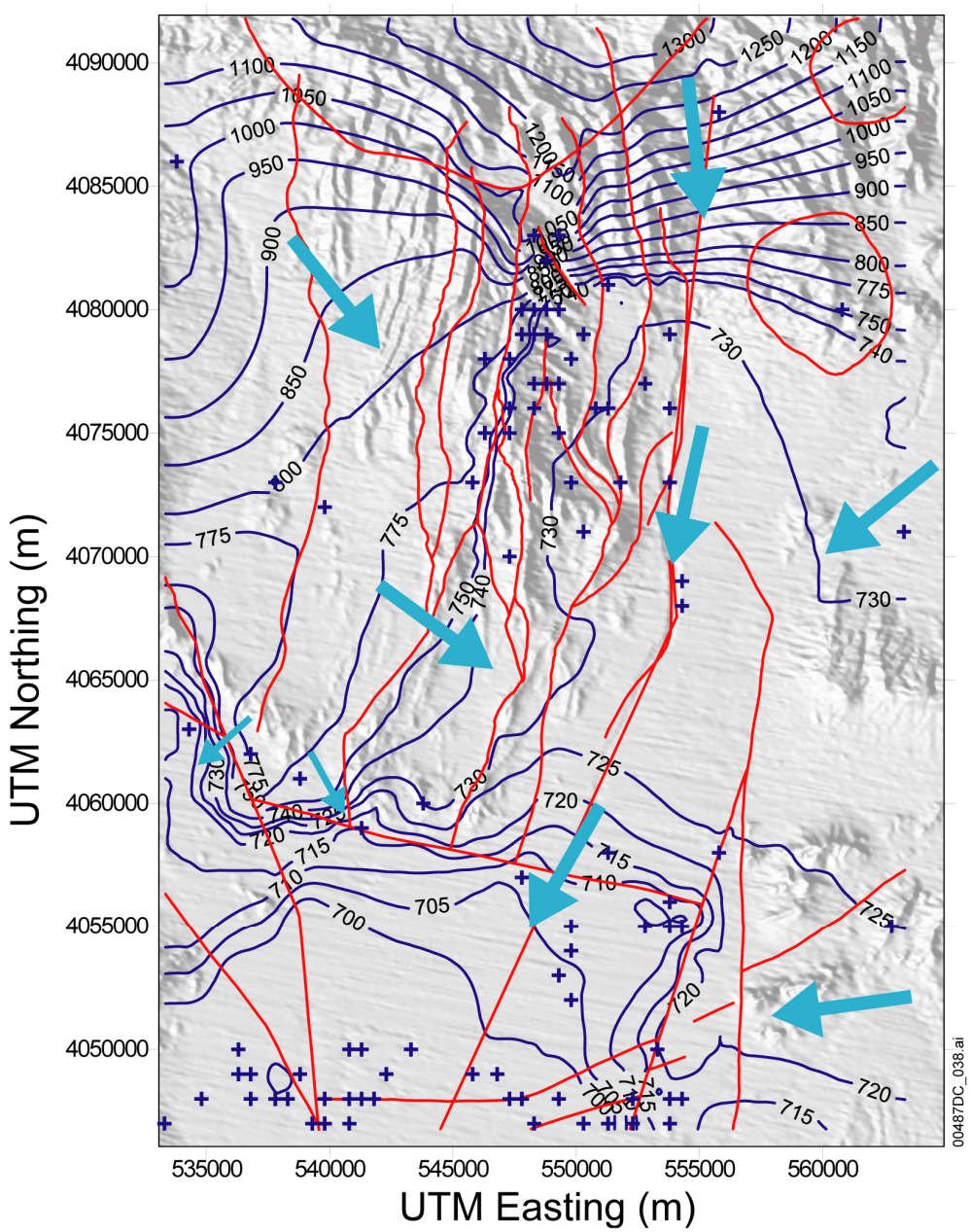

Source: USGS (2001 [DIRS 154625], Figure 1-2); DTNs: GS010908314221.001 [DIRS 145263] (Tertiary faults); GS000508312332.001 [DIRS 149947] (Water-level contours).

NOTE: The inferred groundwater flow directions are based on Assumption 1 in Table A5-1. The circular areas outlined in red near the Calico Hills in the northeast corner of the map are zones of hydrothermal alteration associated with granitic intrusions, and the semicircular area along the central northern portion of the map is the southern boundary of the Claim Canyon caldera (BSC 2004 ([DIRS 170037], Table 6-17; BSC 2004 [DIRS 170008], Figure 6-3; and Zyvoloski et al. 2003 [DIRS 163341], Figure 2b). The other red lines are selected faults; blue crosses indicated the location of hydraulic head measurements. Blue lines are contours showing elevation (in meters above sea level) of the potentiometric surface; contour intervals vary. UTM=Universal Transverse Mercator. For illustrative/historical perspective purposes only.

Figure A6-3. Potentiometric Surface and Inferred Flow Directions (light blue arrows) for Yucca Mountain and Vicinity

Several possible flow directions were defined by drawing arrows parallel to the gradient in the potentiometric surface (Figure A6-3). The flow directions were drawn under the assumption that hydraulic conductivity and transmissivity are isotropic (Assumption 1 in Table A5-1). In fractured-rock aquifers, such as those at Yucca Mountain, hydraulic conductivity probably is anisotropic (Luckey et al. 1996 [DIRS 100465], p. 36). Nonetheless, this assumption provides a starting point for evaluating the possible flow pathways of groundwater in the Yucca Mountain area. Groundwater models of the site that account for the effects of faults and anisotropy on the flow paths may indicate paths substantially different than those drawn from Figure A6-3.

The flow paths shown in Figure A6-3 indicate that water may flow from the north and northwest under Yucca Mountain. In Figure A6-3, some of the flow from the north is predicted to flow southeastward toward Fortymile Wash in northern Yucca Mountain, an area dominated by northwest-trending, fault-controlled washes. The inferred flow directions indicate that groundwater flows southeast from Yucca Mountain and southwest from Jackass Flats toward the Fortymile Wash area. Groundwater from the Fortymile Canyon area flows south and then southwest in the southern part of the site model area. Flow in the southern part of Yucca Mountain is predominantly southeastward toward Fortymile Wash rather than south toward the Amargosa Desert (Figure A6-3). The faults in the southern part of Yucca Mountain do not seem to exert an observable effect on the potentiometric surface, but this may reflect the sparseness of boreholes and small hydraulic gradient in this area.

A6.2.2 Previous Hydrochemical Investigations

Yucca Mountain has been under investigation as a repository site since the early 1980s, and an extensive body of literature exists concerning its groundwater hydrochemical and isotopic characteristics. The following summary of that literature is not exhaustive but represents the range of interpretations that have been made concerning groundwater flow at and near Yucca Mountain. Literature data were used to create and evaluate conceptual models, corroborate existing models, and to enhance the database of hydrochemistry data obtained by the Project.

Several published studies (White and Chuma 1987 [DIRS 108871]; Benson and Klieforth 1989 [DIRS 104370]; Stuckless et al. 1991 [DIRS 101159]; Fridrich et al. 1994 [DIRS 100575]; Luckey et al. 1996 [DIRS 100465]; Campana and Byer 1996 [DIRS 126814]; Paces et al. 2002 [DIRS 158817]) have focused on the origin and flow paths of groundwater in the vicinity of Yucca Mountain. These authors primarily differed with respect to the extent of recharge occurring through Yucca Mountain or along Fortymile Wash, the residence time of groundwater beneath Yucca Mountain, and the extent of mixing between the volcanic and carbonate aquifers.

Based on δD and $\delta^{18}O$ data for the Yucca Mountain region, Benson and Klieforth (1989 [DIRS 104370], p. 48) proposed that groundwater beneath Yucca Mountain could be a mixture of overland flow along Fortymile Wash and groundwater flow from upland areas to the north (Pahute Mesa). Benson and Klieforth (1989 [DIRS 104370], pp. 48 and 49, Figure 11) reported that the $\delta^{18}O$ values of groundwater in the vicinity of Yucca Mountain were lower for water with apparent ^{14}C ages between 18.5 and 9 ka (thousand years before present) and were higher and constant since then, a relation that was attributed to global climate change and accompanying changes in the paths of storms bringing moisture to southern Nevada prior to 9 ka. Benson and Klieforth (1989 [DIRS 104370], p. 42) also argued that groundwater ^{14}C ages in the

Yucca Mountain area do not require substantial correction to account for the dissolution of calcite, based on geochemical modeling of three wells in Fortymile Wash by White and Chuma (1987 [DIRS 108871], Table 2, Figure 23) and the observation that surface runoff in Fortymile Wash was saturated with calcite and yet still had a ^{14}C activity of 100% modern carbon (pmc).

Groundwater in the volcanic aquifers in the Yucca Mountain area was interpreted by Stuckless et al. (1991 [DIRS 101159], p. 1,414) to be a mixture of at least three end members. One source of groundwater in the volcanic aquifer, represented by groundwater from borehole UE-29 a#2 in Fortymile Canyon, is characterized by isotopically light ^{13}C ($\delta^{13}C$), a high ^{14}C activity, and isotopically heavy δD. This groundwater is either mixed with a second source of groundwater from the Paleozoic carbonate aquifer having an isotopically heavy $\delta^{13}C$ and a low ^{14}C activity or, alternatively, is modified by calcite derived from the carbonate aquifer with these isotopic characteristics. A third, poorly constrained end member with a $\delta^{13}C$ value and ^{14}C activity intermediate between that of the first and second sources and having a lighter δD value than the first source was hypothesized to explain the scatter in the $\delta^{13}C$ and ^{14}C about a possible mixing trend line (Stuckless et al. 1991 [DIRS 101159], Figure 4). Groundwater at Pahute Mesa from borehole UE-20 a#2 has these characteristics and it was suggested by Stuckless et al. (1991 [DIRS 101159], p. 1,414) as a possible third source for the groundwater at Yucca Mountain.

Fridrich et al. (1994 [DIRS 100575], pp. 153 to 159) used the spatial variability in $\delta^{13}C$, water table temperature, magnetic data, and unsaturated zone heat flux to infer that groundwater in the northern part of Yucca Mountain entered the deep carbonate aquifer and reemerged into the shallow volcanic aquifer along faults in the central and southern parts of the mountain. Luckey et al. (1996 [DIRS 100465], p. 44) noted the downgradient increase in the calcium-to-sodium ratio from west to east across Yucca Mountain and speculated that it might reflect either upwelling from the underlying carbonate aquifer through faults on the east side of Yucca Mountain or mixing of water flowing from the west with calcium-rich water recharged from Fortymile Wash.

Campana and Byer (1996 [DIRS 126814], p. 465) presented a steady-state mixing-cell model of the NTS regional groundwater flow system that used corrected ^{14}C ages to determine flow volumes and directions and recharge rates in the regional flow system. Their results indicated that between 28% and 88% of the groundwater beneath Yucca Mountain originated as local recharge, which was estimated to be between 1.9 mm/yr^{-1} to 4.2 mm/yr^{-1} as an annual average distributed evenly across the cell's surface area (Campana and Byer 1996 [DIRS 126814], p. 473). In their model, the remainder of the flow beneath Yucca Mountain originated from the west in Crater Flat. Flow from upland areas north of Yucca Mountain was diverted eastward toward Fortymile Canyon and Fortymile Wash before reaching Yucca Mountain. Groundwater beneath Yucca Mountain was interpreted by Campana and Byer (1996 [DIRS 126814], Figure 5) to be a mixture of groundwaters having different ^{14}C activities, with a mean age of 10.9- to 16.0-ka and a median age of 6.3- to 6.5-ka (Campana and Byer 1996 [DIRS 126814], Table 7). Approximately 20% to 25% of the total recharge in their regional model domain originated from the Fortymile Canyon and Wash area, where areally distributed recharge rates were estimated to be 26 to 32 mm/yr^{-1} (5.3×10^6 to 6.6×10^6 m^3/yr^{-1}) (Campana and Byer 1996 [DIRS 126814],

p. 476). Water in the Amargosa Desert originated from groundwater flow from Fortymile Canyon and Wash area and Crater Flat.

Based on $^{234}U/^{238}U$ activity ratios in perched water and the underlying groundwater, Paces et al. (2002 [DIRS 158817]) concluded that at least some of the shallow groundwater presently beneath Yucca Mountain appears to have been recharged locally. Paces et al. (2002 [DIRS 158817], p. 770) suggested a conceptual model that explains the presence of high $^{234}U/^{238}U$ data in the saturated zone beneath Yucca Mountain. The hydraulic barriers that cause the comparatively large hydraulic gradients in the northern and western parts of Yucca Mountain inhibit underflow from upgradient areas, thereby allowing the chemical and isotopic composition of a small amount of local recharge to exert a prominent influence on the isotopic and chemical composition of the groundwater. Likewise, because both the present-day recharge rates and rates of groundwater flow from upgradient areas are small, hydraulic gradients beneath Yucca Mountain are relatively flat and groundwater that was recharged at Yucca Mountain in the late Pleistocene continues to persist in the groundwater beneath the Yucca Mountain (Paces et al. 2002 [DIRS 158817], p. 770). The absence of high $^{234}U/^{238}U$ activity ratios in groundwater downgradient from Yucca Mountain could reflect the hydraulic isolation of Yucca Mountain, dilution by Fortymile Wash groundwater or other Yucca Mountain recharge with lower $^{234}U/^{238}U$ activity ratios (bulk-rock dissolution seems to have lowered $^{234}U/^{238}U$ activity ratios in perched water at borehole USW SD-7 (Paces et al. 2002 [DIRS 158817], p. 768)), water/rock interactions that incorporate other sources of uranium, or the upwelling of small amounts of groundwater from the carbonate aquifer.

Winograd and Thordarson (1975 [DIRS 101167], p. C111) concluded from chemical data that groundwater in the central Amargosa Desert (Figure A6-1) originates from at least three sources: (1) water dominated by calcium, magnesium, sodium, and bicarbonate that flows across the hydraulic barrier responsible for springs at Ash Meadows; (2) water southwest of Amargosa Valley (formerly, Lathrop Wells) dominated by sodium, potassium, and bicarbonate that probably flows from western Jackass Flats; and (3) water in the west-central and northwestern Amargosa Desert that flows from Oasis Valley. In addition, Winograd and Thordarson (1975 [DIRS 101167], p. C112) noted the dilute nature of the groundwater near Fortymile Wash and interpreted the low dissolved solids content of this water to indicate an origin from paleorecharge along the channel rather than underflow from areas north of Jackass Flats. Winograd and Thordarson (1975 [DIRS 101167], p. C112) also noted the higher dissolved solids content in wells at and south of Amargosa Valley, which they attributed to small amounts of groundwater leaking upward from the carbonate aquifer into the valley fill near the Gravity fault.

Claassen (1985 [DIRS 101125]) and White and Chuma (1987 [DIRS 108871]) presented different hypotheses regarding the origin of water in the northern Amargosa Desert near the present-day Fortymile Wash drainage. Claassen (1985 [DIRS 101125], p. F30) argued that groundwater near surface drainages was predominantly derived from surface runoff during the Pleistocene and the very early Holocene based on its apparent ^{14}C age (Claassen 1985 [DIRS 101125], Figure 15), and on the high ratio of calcium plus magnesium to sodium plus potassium [(Ca + Mg)/(Na + K)] of groundwater from the northern Amargosa Desert compared to groundwater from upgradient locations (Claassen 1985 [DIRS 101125], p. F13, Figure 9). The $^{234}U/^{238}U$ activity ratios and δD values of groundwater near Fortymile Wash in the northern Amargosa Desert were also later interpreted as supportive of this hypothesis (Paces et al. 2002

[DIRS 158817], p. 767). In contrast, White and Chuma (1987 [DIRS 108871], p. 578) argued that groundwater in the northern Amargosa Desert evolved chemically from groundwater that had recharged upgradient in Fortymile Canyon. The ^{14}C age of groundwater in the northern Amargosa was used to calculate groundwater velocities beneath Fortymile Wash of between 3 and 30 m yr^{-1} over an average distance of about 15 km extending southward from borehole J-13 to the north-central Amargosa Desert (White and Chuma 1987 [DIRS 108871], p. 578).

A6.3 ANALYSIS OF HYDROCHEMICAL AND ISOTOPIC DATA

This section presents the results of the analysis of the hydrochemical and isotopic data in the vicinity of Yucca Mountain in eleven major subsections. Section A6.3.1 discusses factors affecting the chemical and isotopic composition of groundwater. In section A6.3.2 all groundwater samples evaluated in this appendix are assigned to a specific grouping to facilitate interpretation and discussion. Section A6.3.3 discusses depth-dependent trends in the chemical and isotopic composition of groundwater. Section A6.3.4 presents areal distribution maps of hydrochemical data and discusses geographic trends shown by these data. Section A6.3.5 presents areal distribution maps showing calculated geochemical parameters such as mineral saturation indices. Section A6.3.6 presents an evaluation of the evidence regarding local recharge at Yucca Mountain. Also discussed in this subsection are evaluations of the evidence for the timing and magnitude of recharge. Section A6.3.7 presents an evaluation of mixing relations among groundwaters. Section A6.3.8 presents an analysis of mixing and water rock interactions using PHREEQC V2.3 (BSC 2001 [DIRS 155323]). Section A6.3.9 addresses groundwater flow velocities. Section A6.3.10 presents results of the site-scale saturated zone groundwater flow model for a portion of the study area. Section A6.3.11 presents an analysis of groundwater flow paths in the Yucca Mountain region based on cumulative evidence presented in the previous sections.

The data derived from the DTNs and other sources are summarized here for each sample/well location for the major ions (Table A6-1) and for the isotopes and trace elements (Table A6-2). Where multiple sets of data were available for a location/sample, these data were averaged to derive the values shown in these two tables, and the areal distribution of the hydrochemical and isotopic data discussed in this section and portrayed on figures of the area of study uses the compiled values of Tables A6-1 and A6-2. All analytical data have uncertainty associated with the individual values, as fully described in Sections A7.3.1 and A7.3.2. Because these samples were collected over a time-span of several decades by different organizations using different methods, analytical precision and accuracy may be variable for particular analytes. In many cases, the original data sources do not provide an indication of the precision or accuracy. However, a sense of the uncertainties associated with historic measurements can be obtained from data that are more recently collected; uncertainties in historic data are probably higher than the values listed below because of recent developments in measurement technology.

Analytical accuracy for recent measurements are (Section A7.3.1):

- Ten percent for major anions, cations and strontium concentration, except for fluoride, for which accuracy is estimated as better than ±15%. In some cases, strontium was determined by isotope dilution, mass spectrometry methods, for which data are more precise (e.g., ±0.5%)

- ±3.0 per mil for δD, ±0.2 per mil for $\delta^{18}O$, $\delta^{13}C$, and $\delta^{34}S$, and ±0.1 pmc for ^{14}C
- Better than 1% for uranium concentrations and from 0.09% to 4.5% (with a mean of 0.73%) for $^{234}U/^{238}U$
- ±0.00001 for $^{87}Sr/^{86}Sr$, which translates to an uncertainty of approximately 0.01 per mil in $\delta^{87}Sr$ units.

An additional guide to the reliability of individual water analyses is also provided by the calculated charge-balance errors listed in Table A6-3. Groundwaters from most sites used in this analysis, especially those near Yucca Mountain itself, have charge-balance errors less than ± 5%. However, groundwaters from some outlying areas that were used as data in this analysis have charge-balance errors as high as 10% to 20%. These sample sites are located primarily in the Mine Mountain group of samples and did not have a significant influence on the conclusions derived in this analysis.

Table A6-1. Field Parameters and Major Ion Composition

Well Name[a]	Figure A6-5 Sample	Temperature (°C)	pH	Ca^{2+} (mg/L)	Mg^{2+} (mg/L)	Na^{+} (mg/L)	K^{+} (mg/L)	Cl^{-} (mg/L)	SO_4^{2-} (mg/L)	HCO_3^{-} (mg/L)	CO_3^{2-} (mg/L)	F^{-} (mg/L)	SiO_2 (mg/L)
Oasis Valley/NW Amargosa													
ER-EC-08	1	38.2	8.0	10.3	0.9	120.0	5.6	50.7	84.8	176.8	—[d]	5.3	49.1
ER-OV-01	2	25.7	8.3	6.2	0.1	139.7	6.8	45.6	82.7	196.9	1.7	2.1	70.0
ER-OV-06a	3	28.6	8.3	2.1	0.7	144.5	7.5	48.5	80.0	197.9	3.0	3.1	52.9
ER-OV-05	4	21.9	7.8	21.5	4.4	103.5	10.0	37.7	55.6	235.6	—	1.7	82.4
ER-OV-02	5	18.9	8.2	14.3	0.6	143.0	4.1	51.2	88.1	227.1	—	2.3	57.4
Springdale Upper Well (10S/47E-32adc) (11/12/97)	6	23.6	7.7	22.0	4.1	130.0	8.7	37.2	67.7	292.8	—	2.1	69.9
Goss Springs North (11S/47E-10bad) (11/13/97)	7	17.7	8.2	16.4	1.2	107.0	5.0	43.0	76.4	180.1	—	2.4	53.2
Er-OV-03a	8	17.5	8.1	14.0	1.0	118.0	5.2	42.6	76.0	183.6	—	2.3	54.7
ER-OV-03a3	9	21.2	8.3	13.3	1.1	120.5	5.7	44.9	81.2	184.2	—	2.1	55.1
ER-OV-03a2	10	20.0	9.2	5.7	1.0	331.0	84.7	262.0	295.0	186.2	41.6	—	20.0
Goss Spring (11S/47E-10bcc)	11	22.0	7.7	17.5	1.3	116.5	5.1	45.0	78.1	181.0	—	2.8	50.4
ER-OV-04a (11/07/97)	12	23.7	8.4	8.7	0.1	98.8	7.8	28.2	59.9	162.4	2.2	2.8	68.9
Beatty Well no. 1 (Wat&Sanit Distr)	13	22.2	8.0	39.2	5.5	126.3	8.5	48.4	113.0	203.0	—	1.4	—
Bond Gold Mining #1	14	—	8.3	23.0	6.0	65.0	7.3	40.0	52.0	161.0	0.0	0.6	29.0
US Ecology MW-313	15	—	7.5	54.0	16.0	146.0	13.0	69.0	205.0	336.0	0.0	5.0	68.0
US Ecology MW-600	16	—	7.9	20.0	11.5	167.5	8.8	67.5	153.0	296.0	0.0	5.2	62.5
NECWell	17	—	7.6	54.9	14.1	170.1	10.2	79.1	190.2	328.3	0.0	—	70.3
US Ecology MR-3	18	—	7.7	—	—	—	—	—	—	325.0	0.0	—	—
Timber Mountain													
UE-18r	19	30.6	8.2	18.5	0.7	73.3	2.7	6.8	19.7	202.8	5.2	2.7	48.6
ER-18-2	20	55.2	7.6	5.8	0.2	351.7	3.1	13.2	54.0	730.0	—	12.8	42.8
ER-EC-05	21	29.9	8.0	20.3	0.6	73.9	1.7	16.2	35.5	176.8	—	4.7	40.9
Coffer's Ranch Windmill Well	22	20.1	8.3	16.2	0.2	70.6	0.9	7.5	30.2	184.0	—	3.4	40.2
ER-OV-03c	23	22.2	8.2	15.1	0.4	79.7	1.3	17.4	43.6	161.5	—	4.5	42.9
ER-EC-07	24	30.0	7.9	21.6	1.7	36.8	3.1	6.0	18.3	148.8	—	1.5	44.0

Table A6-1. Field Parameters and Major Ion Composition (Continued)

Well Name[a]	Figure A6-5 Sample	Temperature (°C)	pH	Ca^{2+} (mg/L)	Mg^{2+} (mg/L)	Na^{+} (mg/L)	K^{+} (mg/L)	Cl^{-} (mg/L)	SO_4^{2-} (mg/L)	HCO_3^{-} (mg/L)	CO_3^{2-} (mg/L)	F^{-} (mg/L)	SiO_2 (mg/L)
Fortymile Wash—North													
Water Well 8	25	24.2	7.3	7.9	1.2	31.1	3.3	7.3	15.0	78.0	—	0.7	50.0
Test Well 1 (USGS HTH #1)	26	26.6	8.7	1.2	0.0	51.3	0.5	3.2	8.7	104.0	—	—	19.5
UE-18t	27	—	8.6	22.2	1.0	141.0	8.2	64.4	10.8	331.0	—	—	7.0
ER-30-1 (upper)	28	22.9	9.4	3.5	0.1	62.0	1.8	6.2	12.0	87.5	22.1	1.7	29.0
ER-30-1 (lower)	29	24.3	9.2	2.1	0.1	65.0	1.0	6.5	9.9	106.3	11.1	1.4	25.0
a#2(dp)	30	25.1	7.2	10.0	0.2	44.0	1.1	11.0	22.0	107.0	0.0	1.0	44.0
a#2(sh)	31	22.7	7.0	10.0	0.3	44.0	1.3	8.8	21.0	107.0	0.0	0.9	44.0
UE-29a#1 HTH	32	22.9	7.6	15.0	2.3	36.5	4.1	7.9	16.2	108.9	0.0	0.6	57.2
WT#15	33	33.0[b]	7.5	12.0	1.7	62.0	4.6	12.0	16.0	166.0	0.0	—	52.0
WT#14	34	30.0[b]	7.3	10.0	0.8	45.0	5.0	8.2	22.0	119.0	0.0	—	57.0
J-13	35	31.0	7.2	12.0	2.1	42.0	5.0	7.1	17.0	124.0	0.0	2.4	57.0
J-12	36	27.0	7.1	14.0	2.1	38.0	5.1	7.3	22.0	119.0	0.0	2.1	54.0
JF#3	37	26.6	7.7	18.0	3.1	38.0	8.9	10.0	30.0	120.0	0.0	1.6	56.0
Solitario Canyon Wash													
H-6(bh)	38	37.8	8.1	4.1	0.1	86.0	1.3	7.6	29.0	182.0	0.0	4.7	48.0
H-6(Tct)	39	41.6	8.3	1.4	0.0	88.0	1.3	7.2	25.0	217.0	0.0	3.9	47.0
H-6(Tcb)	40	37.2	8.3	4.7	0.1	88.0	1.4	7.4	32.0	234.0	0.0	4.7	49.0
WT-7	41	34.0[b]	8.7	2.6	0.2	97.0	2.1	13.0	7.2	252.0	0.0	—	20.0
WT-10	42	38.5	8.4	2.6	0.1	94.5	1.0	7.8	33.5	186.0	0.0	3.7	46.5
Yucca Mountain—Crest													
G-2	43	34.2	7.5	7.7	0.5	46.0	5.3	6.5	15.0	121.0	0.0	1.0	51.0
USW WT-24	44	—	7.9	0.3	0.036	59.0	1.6	6.7	15.0	119.0	0.0	0.9	53.0
UZ-14(sh)	45	25.7	8.4	0.48	0.023	70.0	1.9	6.7	14.0	133	2.7	6.3	44
UZ-14(dp)	46	27.5	8.4	0.2	0.030	74.0	1.9	7.7	14.0	137.0	3.0	6.7	47
H-1(Tcp)	47	33.0	7.7	4.5	>01	51.0	2.4	5.7	18.0	115.0	0.0	1.2	47.0
H-1(Tcb)	48	34.7	7.7	6.2	>0.1	51.0	1.6	5.8	19.0	122.0	0.0	1.0	40.0
H-5	49	35.9	7.9	2.0	0.0	60.0	2.1	6.1	16.0	126.5	0.0	1.4	48.0

Table A6-1. Field Parameters and Major Ion Composition (Continued)

Well Name[a]	Figure A6-5 Sample	Temperature (°C)	pH	Ca^{2+} (mg/L)	Mg^{2+} (mg/L)	Na^{+} (mg/L)	K^{+} (mg/L)	Cl^{-} (mg/L)	SO_4^{2-} (mg/L)	HCO_3^{-} (mg/L)	CO_3^{2-} (mg/L)	F^{-} (mg/L)	SiO_2 (mg/L)
Yucca Mountain—Crest (Continued)													
USW SD-6	50	35.0	8.4	0.4	0.0	90.6	1.5	6.8	26.7	181.8	2.5	4.7	45.6
H-3	51	26.5	9.2	0.8	0.0	120.0	1.1	9.5	31.0	274.0	0.0	5.5	43.0
Yucca Mountain—Central													
G-4	52	35.6	7.7	13.0	0.2	57.0	2.1	5.9	19.0	139.0	0.0	2.5	45.0
b#1(Tcb)	53	37.2	7.1	18.0	0.7	46.0	2.8	7.5	21.0	133.0	0.0	1.6	51.0
b#1(bh)	54	36.0	7.3	18.0	0.7	49.5	3.6	10.8	23.0	156.0	0.0	1.6	52.5
H-4	55	34.8	7.4	17.0	0.3	73.0	2.6	6.9	26.0	173.0	0.0	4.6	46.0
UZ#16	56	30.0[b]	—	11.4	1.6	79.2	—	10.6	29.1	210.0	0.0	—	36.2
Yucca Mountain—Southeast													
ONC#1	57	31.0[b]	8.7	13.0	1.1	51.0	3.6	7.1	24.0	115.0	8.8	—	27.0
c#1	58	41.5	7.6	11.0	0.3	56.0	2.0	7.4	23.0	151.0	0.0	2.1	56.0
c#3	59	40.8	7.7	11.0	0.4	55.0	1.9	7.2	22.0	137.0	0.0	2.0	53.0
c#3(95-97)	60	40.8[c]	7.7	11.0	0.3	57.0	1.9	6.5	19.0	141.0	0.0	—	58.0
c#2	61	40.5	7.7	12.0	0.4	54.0	2.1	7.1	22.0	139.0	0.0	2.1	54.0
p#1(v)	62	44.3	6.8	37.0	10.0	92.0	5.6	13.0	38.0	344.0	0.0	3.4	49.0
p#1(c)	63	56.0	6.6	100.0	39.0	150.0	12.0	28.0	160.0	694.0	0.0	4.7	41.0
WT-17	64	28.7	7.1	8.9	0.9	49.0	2.6	6.4	17.5	129.5	0.0	2.0	39.0
WT#3	65	31.8	7.6	11.2	1.0	49.0	3.9	6.0	18.3	138.5	0.0	2.3	56.2
WT#12	66	33.0[b]	7.6	15.0	0.3	66.0	2.6	7.8	28.0	167.0	0.0	3.1	47.0
Jackass Flats													
UE-25 J-11	67	—	8.1	76.5	15.0	154.0	17.0	17.5	479.5	82.0	0.0	1.2	57.5
Crater Flat													
GEXA Well4	68	31.8	7.9	11.5	0.4	71.0	3.3	13.5	45.5	150.0	0.0	3.2	48.0
VH-1	69	35.4	7.6	10.3	1.5	79.0	1.9	10.3	44.3	164.7	0.0	2.7	49.7
Southwest Crater Flat													
VH-2	70	32.8	7.1	78.5	29.8	70.8	8.1	16.0	142.5	391.8	0.0	1.1	26.3
NC-EWDP-7S	71	21.5	7.3	77.0	37.0	86.0	8.2	19.5	167.0	420.0	0.0	1.0	23.0

Table A6-1. Field Parameters and Major Ion Composition (Continued)

Well Name[a]	Figure A6-5 Sample	Temperature (°C)	pH	Ca^{2+} (mg/L)	Mg^{2+} (mg/L)	Na^{+} (mg/L)	K^{+} (mg/L)	Cl^{-} (mg/L)	SO_4^{2-} (mg/L)	HCO_3^{-} (mg/L)	CO_3^{2-} (mg/L)	F^{-} (mg/L)	SiO_2 (mg/L)
Southwest Crater Flat (Continued)													
NC-EWDP-7SC	72	—	7.2	83.0	38.0	90.7	4.3	22.0	179.0	429.0	0.0	0.9	23.7
NC-EWDP-1DX	73	—	7.2	55.5	31.0	73.5	10.0	16.0	136.0	369.0	0.0	0.7	46.5
NC-EWDP-1DX Zone 2	74	28.6	6.7	40.0	11.0	329.7	6.2	49.7	112.3	1011.5	0.0	11.0	51.3
NC-EWDP-1S Zone 1	75	26.7	7.4	57.5	30.5	65.0	9.0	15.5	128.5	360.0	0.0	0.6	50.5
NC-EWDP-1S Zone 2	76	27.6	7.3	55.5	30.5	64.5	8.9	15.5	126.0	356.0	0.0	0.6	48.5
NC-EWDP-1S	77	27.8	7.3	59.0	31.0	67.5	8.6	15.0	127.0	358.0	0.0	0.6	55.0
NC-EWDP-12PA	78	28.5	6.8	30.3	8.2	146.0	27.0	14.0	102.3	414.5	0.0	4.1	69.3
NC-EWDP-12PB	79	29.3	6.9	30.5	8.2	140.5	27.0	14.0	105.0	396.5	0.0	4.2	68.0
NC-EWDP-12PC	80	28.6	7.5	53.0	27.5	72.0	10.0	14.0	123.5	323.0	0.0	1.0	55.5
Southern Yucca Mountain													
NC-EWDP-09SX	81	28.4	8.0	20.3	7.7	76	4.3	11.0	61.7	212.3	0.0	2.2	52.7
NC-EWDP-9SX Zone 1	82	26.0	8.3	17.5	5.8	76.5	5.5	15.0	57.5	193.5	1.9	2.2	40.5
NC-EWDP-9SX Zone 2	83	27.6	7.9	18.0	7.2	73.0	4.5	11.3	59.3	203.5	0.0	2.1	44.7
NC-EWDP-9SX Zone 3	84	27.5	8.1	17.5	7.1	71.5	4.2	10.0	58.0	207.0	0.0	2.2	42.5
NC-EWDP-9SX Zone 4	85	27.9	8.0	18.3	7.2	70.3	3.8	9.9	58.3	208.7	0.0	2.1	46.3
NC-EWDP-03D	86	34.3	8.4	0.5	0.1	113.0	3.0	9.0	45.0	223.3	6.2	2.9	54.0
NC-EWDP-3S Zone 2	87	32.2	8.7	0.8	0.1	127.5	1.8	18.0	47.5	224.5	11.7	3.0	59.0
NC-EWDP-3S Zone 3	88	32.4	8.9	0.8	0.1	134.7	3.0	10.2	47.3	255.5	23.5	4.2	47.7
CIND-R-LITE	89	50.0[b]	7.8	12.3	6.2	71.7	4.0	9.2	46.0	193.7	0.0	2.5	54.3
NC-EWDP-15P	90	29.9	7.8	10.0	2.5	80.0	3.3	8.7	44.0	188.0	0.0	2.2	49.3
NC-EWDP-02D	91	—	7.5	19.0	1.2	42.0	4.1	6.1	22.0	149.0	0.0	1.6	49.0
NC-EWDP-19D	92	30.2	8.7	1.8	0.1	107.8	3.6	6.2	27.8	219.3	13.5	2.2	61.0
NC-EWDP-19P	93	29.2	8.7	14.0	0.9	44.0	3.7	8.9	24.0	110.0	7.4	1.7	57.0
NC-EWDP-19D (alluvial)	94	30.9	8.6	2.3	0.2	96.5	3.4	6.3	22.0	202.5	17.5	2.2	57.0
NC-EWDP-19D (zone #1)	95	32.0	8.6	3.7	0.3	91.5	3.7	6.1	22.0	189.0	12.5	2.0	58.0
NC-EWDP-19D (zone #2)	96	28.9	8.3	10.7	1.0	60.5	3.8	6.3	21.5	153.0	0.0	1.7	60.5
NC-EWDP-19D (zone #3)	97	30.8	8.5	1.3	0.1	99.0	3.2	6.3	26.0	204.0	7.4	2.0	55.0

Table A6-1. Field Parameters and Major Ion Composition (Continued)

Well Name[a]	Figure A6-5 Sample	Temperature (°C)	pH	Ca^{2+} (mg/L)	Mg^{2+} (mg/L)	Na^{+} (mg/L)	K^{+} (mg/L)	Cl^{-} (mg/L)	SO_4^{2-} (mg/L)	HCO_3^{-} (mg/L)	CO_3^{2-} (mg/L)	F^{-} (mg/L)	SiO_2 (mg/L)
Southern Yucca Mountain (Continued)													
NC-EWDP-19D (zone #4)	98	31.3	8.9	0.9	0.0	107.3	3.4	5.6	18.7	212.0	21.5	2.7	59.7
Amargosa Valley													
NC-EWDP-4PB	99	24.2	9.5	6.7	0.0	67.0	1.9	5.5	34.7	63.0	40.7	1.7	32.0
NC-EWDP-4PA	100	24.3	8.2	12.5	0.3	55.0	2.9	7.4	52.5	108.5	0.0	1.2	32.5
Desert Farms Garlic Plot	101	26.2	7.8	30.0	2.1	71.0	5.1	13.0	117.0	125.0	0.0	0.8	40.0
15S/49E-13dda	102	—	—	—	—	—	—	—	—	—	—	—	—
15S/50E-18ccc	103	—	8.4	16.8	0.5	93.1	3.9	13.1	100	157	0.0	2.1	34.3
NDOT	104	27.3	8.0	16.3	0.8	101.3	3.8	14.7	110.0	160.0	0.0	1.9	43.7
15S/50E-18cdc	105	25.1	8.0	12.0	0.5	93.0	3.9	13.1	100.0	157.0	0.0	1.9	34.0
Airport Well	106	27.6	8.7	5.6	0.1	69.0	1.5	6.6	45.0	116.0	6.2	1.8	38.0
15S/50E-19b1	107	23.9	8.1	20.0	3.9	107.5	6.0	17.5	127.5	167.5	0.0	1.4	43.0
Amargosa River													
16S/48E-8ba	108	25.0	7.9	58.5	6.3	180.5	12.9	79.8	202.7	295.9	0.0	—	37.9
16S/48E-7bba	109	24.7	7.4	52.9	9.5	140.0	10.2	63.1	179.6	250.8	0.0	—	69.1
16S/48E-7cbc	110	24.2	7.7	46.9	16.0	130.1	9.4	62.0	179.6	239.2	0.0	—	64.3
16S/48E-18bcc	111	—	8.0	54.9	10.9	150.1	11.7	61.0	190.2	271.5	0.0	—	79.9
16S/48E-17ccc	112	—	7.7	66.1	10.9	169.9	12.1	83.0	235.3	239.2	0.0	—	77.5
16S/48E-18dad	113	—	7.7	52.9	8.5	149.9	10.6	63.1	187.3	236.1	0.0	—	76.9
16S/48E-8cda	114	23.3	7.6	48.1	6.8	160.0	10.2	67.0	179.6	264.2	0.0	—	67.9
16S/48E-17abb	115	24.0	7.4	60.1	7.8	157.0	12.1	69.1	178.7	302.0	0.0	—	75.1
Barrachman Dom/Irrigation	116	19.0	7.5	53.0	12.0	128.0	10.0	62.0	179.0	286.0	0.0	1.8	66.0
McCracken Domestic	117	21.7	7.5	83.0	12.0	194.0	12.0	123.0	266.0	243.0	0.0	1.7	73.0
Fortymile Wash—West													
16S/48E-15ba	118	25.0	8.0	60.1	7.8	147.1	9.8	65.6	198.8	264.2	0.0	—	37.3
16S/48E-10cba	119	24.5	8.3	9.2	3.9	60.9	5.5	8.2	32.7	166.0	0.0	—	64.3
16S/48E-15aaa	120	25.5	8.1	9.6	3.2	57.9	5.9	7.4	27.9	153.2	0.0	—	67.9
Selbach Domestic	121	23.9	8.0	23.0	8.1	90.0	6.6	36.0	96.0	178.0	0.0	1.4	68.0

Table A6-1. Field Parameters and Major Ion Composition (Continued)

Well Name[a]	Figure A6-5 Sample	Temperature (°C)	pH	Ca^{2+} (mg/L)	Mg^{2+} (mg/L)	Na^{+} (mg/L)	K^{+} (mg/L)	Cl^{-} (mg/L)	SO_4^{2-} (mg/L)	HCO_3^{-} (mg/L)	CO_3^{2-} (mg/L)	F^{-} (mg/L)	SiO_2 (mg/L)
Fortymile Wash—West (Continued)													
16S/48E-15dda	122	—	8.0	20.0	5.8	70.8	7.4	17.4	37.5	175.7	0.0	—	71.5
16S/49E-23add	123	—	8.2	16.0	1.7	55.9	6.6	8.9	34.6	126.9	0.0	—	76.3
16S/48E-23bdb	124	24.0	7.3	9.2	1.0	66.0	6.6	8.9	26.9	156.2	0.0	—	73.9
16S/48E-23da	125	27.8	8.2	22.0	2.2	69.0	6.6	26.6	67.2	134.2	0.0	—	—
Funeral Mountain Ranch Irrigation	126	22.2	8.2	12.0	2.4	80.0	7.0	12.0	43.0	200.0	0.0	2.3	87.0
Fortymile Wash—South													
16S/49E-05acc	127	—	8.1	29.0	2.2	35.0	5.1	6.0	26.0	135.0	0.0	1.0	62.0
16S/49E-8abb	128	23.0	7.5	30.1	2.7	37.0	5.5	7.8	29.8	151.9	0.0	—	54.1
16S/49E-8acc	129	25.8	7.9	22.8	2.4	37.0	6.6	6.0	28.8	137.9	0.0	—	58.3
16S/49E-18dc	130	—	8.1	20.0	2.7	42.1	9.0	7.4	27.9	150.1	0.0	—	58.9
16s/48E-24aaa	131	27.0	8.1	18.0	0.7	54.0	7.0	7.8	29.8	147.1	0.0	—	78.7
16S/49E-19daa	132	26.4	8.2	24.0	1.2	36.1	8.2	6.7	32.7	134.2	0.0	—	75.1
DeLee Large Irrigation	133	14.6	8.0	24.0	1.1	37.0	8.4	6.2	25.0	135.0	0.0	1.1	76.5
16S/48E-25aa	134	26.5	8.1	18.8	0.7	43.0	7.4	9.2	27.9	133.0	0.0	—	72.1
16S/48E-36aaa	135	—	8.4	16.8	1.9	40.0	6.3	6.7	25.0	133.0	0.0	—	78.7
Bray Domestic	136	20.9	8.0	22.0	1.8	35.0	8.8	7.9	25.0	131.0	0.0	1.0	74.0
Amargosa Estates #2	137	24.0	8.1	20.0	2.1	38.0	6.8	6.5	22.0	134.0	0.0	1.6	79.0
17S/48E-1ab	138	—	8.2	18.8	1.5	40.0	7.0	6.4	25.0	134.9	0.0	—	78.7
17S/49E-7bb	139	—	8.3	24.0	1.7	48.0	7.4	9.6	30.7	153.2	0.0	—	79.9
17S/49E-8ddb	140	24.0	8.4	20.8	2.7	36.1	7.4	6.4	26.9	123.3	0.0	—	80.8
17S/49E-35ddd	141	23.0	8.0	15.2	4.6	50.6	8.2	6.7	40.3	157.4	0.0	—	81.1
Fortymile Wash—East													
15S/49E-22a1	142	27.8	8.0	25.0	2.4	41.0	5.2	8.0	33.0	145.0	0.0	1.4	52.0
15S/49E-22dcc	143	29.5	6.7	27.0	2.0	43.0	4.6	8.5	33.0	149.0	0.0	1.0	49.0
15S/49E-27acc	144	44.1	7.8	22.0	1.6	48.0	2.9	7.3	36.0	151.0	0.0	0.9	19.0
O'Neill Domestic	145	19.5	7.9	26.0	2.4	44.0	7.6	7.4	43.0	141.0	0.0	0.8	65.0
16S/49E-9cda	146	24.0	7.6	30.5	3.4	51.0	8.6	12.1	64.4	143.4	0.0	—	65.5

Table A6-1. Field Parameters and Major Ion Composition (Continued)

Well Name[a]	Figure A6-5 Sample	Temperature (°C)	pH	Ca^{2+} (mg/L)	Mg^{2+} (mg/L)	Na^{+} (mg/L)	K^{+} (mg/L)	Cl^{-} (mg/L)	SO_4^{2-} (mg/L)	HCO_3^{-} (mg/L)	CO_3^{2-} (mg/L)	F^{-} (mg/L)	SiO_2 (mg/L)
Fortymile Wash—East (Continued)													
16S/49E-9dcc	147	23.3	8.2	22.8	2.7	56.1	9.0	9.9	67.2	140.9	0.0	—	72.1
16S/49E-16ccc	148	—	7.9	30.1	1.9	39.8	4.3	8.2	50.9	132.4	0.0	—	76.9
Ponderosa Dairy #1	149	28.3	8.0	30.0	4.5	59.0	11.0	16.0	93.0	145.0	0.0	1.2	74.0
17S/49E-9aa	150	—	8.0	24.8	3.6	48.0	9.8	9.9	69.2	131.2	0.0	—	70.3
17S/49E-15bbd	151	22.5	8.1	20.8	3.9	31.3	8.2	9.9	34.6	120.2	0.0	—	72.7
M. Gilgan Well	152	24.5	8.2	19.0	2.3	41.0	7.5	8.0	28.0	129.0	0.0	1.6	77.0
17S/49E-15bc	153	24.0	8.2	21.6	1.0	39.1	6.6	10.6	27.9	122.0	0.0	—	—
Gravity Fault													
NC-EWDP-5S	154	—	8.3	17.0	3.5	149.0	11.0	39.0	146.0	—	—	1.0	3.7
NC-EWDP-5SB	155	23.4	7.6	14.0	1.7	107.0	6.9	32.0	61.0	211.0	0.0	1.2	21.0
16S/50E-7bcd	156	30.6	7.6	47.7	17.5	111.5	12.9	29.1	151.8	291.7	0.0	—	28.8
Nelson Domestic	157	29.4	7.5	43.0	16.0	110.0	11.5	26.5	154.0	308.0	0.0	3.8	25.5
16S/49E-12ddd	158	—	7.6	45.7	17.0	120.0	4.3	24.1	160.4	288.6	0.0	—	20.4
Lowe Domestic	159	18.5	7.7	44.0	11.0	111.0	11.0	30.0	147.0	274.0	0.0	1.4	43.0
16S/49E-15aaa	160	23.8	7.7	40.9	7.5	80.0	9.8	23.0	129.7	195.3	0.0	—	46.3
Anvil Ranch Irrigation	161	20.5	7.9	47.0	5.8	68.0	13.0	40.0	120.0	138.0	0.0	1.1	71.0
16S/49E-36aaa	162	—	7.8	52.1	22.1	120.0	18.0	26.9	168.1	314.3	0.0	—	37.9
16S/49E-35baa	163	24.0	7.4	53.3	18.0	113.1	13.3	31.2	170.0	302.7	0.0	—	37.9
Payton Domestic	164	20.2	7.6	51.0	19.0	107.0	16.0	41.0	155.0	290.0	0.0	3.9	36.0
16S/49E-36aba	165	—	7.7	44.9	19.9	110.1	16.8	24.1	155.6	292.9	0.0	—	42.7
16S/49E-35aaa	166	—	7.7	44.1	16.0	120.0	16.0	29.1	147.9	271.5	0.0	—	36.7
Oettinger Well	167	25.2	7.5	50.0	16.0	103.0	15.0	29.0	157.0	291.0	0.0	3.3	39.0
Amargosa Motel (b)	168	24.0	7.6	49.5	18.0	97.5	14.0	27.0	151.0	286.0	0.0	3.0	43.5
17S/49E-11ba	169	22.0	8.1	40.1	14.1	97.0	14.1	28.0	160.4	209.9	0.0	—	52.9
Spring Meadows Well #8	170	21.0	—	22.0	10.9	110.0	14.9	21.9	73.9	295.8	—	2.1	31.0
17S/50E-19aab	171	16.0	8.6	7.6	8.5	252.0	27.4	69.8	175.8	415.5	0.0	—	42.7
USFWS – Five Springs Well	172	33.5	7.5	47.0	20.0	67.5	7.9	23.3	82.0	304.0	—	1.6	21.8

Table A6-1. Field Parameters and Major Ion Composition (Continued)

Well Name[a]	Figure A6-5 Sample	Temperature (°C)	pH	Ca^{2+} (mg/L)	Mg^{2+} (mg/L)	Na^{+} (mg/L)	K^{+} (mg/L)	Cl^{-} (mg/L)	SO_4^{2-} (mg/L)	HCO_3^{-} (mg/L)	CO_3^{2-} (mg/L)	F^{-} (mg/L)	SiO_2 (mg/L)
Gravity Fault (Continued)													
Spring Meadows Well #10	173	19.5	—	2.8	2.9	250.0	14.9	25.8	105.1	494.0	—	3.2	67.0
18S/49E-1aba	174	17.5	8.6	24.0	11.9	94.9	19.2	18.1	99.9	263.0	0.0	—	72.7
18S/50E-6dac	175	—	8.2	23.6	11.9	102.5	13.7	20.6	106.6	230.0	0.0	—	80.5
18S/50E-7aa	176	13.0	8.4	25.7	9.5	140.9	19.2	37.6	147.0	261.2	0.0	—	47.5
Amargosa River/Fortymile Wash													
16S/48E-36dcc	177	26.0	7.2	54.9	9.7	100.0	12.9	33.0	110.5	300.2	0.0	—	70.3
Crane Domestic	178	26.3	7.2	64.0	18.0	147.0	16.0	41.0	138.0	451.0	0.0	3.3	45.0
27N/4E-27bbb	179	22.0	7.8	58.1	19.0	134.0	19.2	31.9	106.6	438.1	0.0	—	72.1
IMV on Windjammer	180	23.5	7.5	45.0	9.9	100.0	11.0	30.5	89.0	303.0	0.0	2.8	67.5
17S/49E-29acc	181	21.0	7.6	54.1	15.1	160.0	19.9	69.8	186.4	275.8	0.0	—	72.1
17S/49E-28bcd	182	—	7.6	42.9	10.0	100.0	12.1	24.1	89.3	294.7	0.0	—	70.3
18S/49E-2cbc	183	23.8	7.8	28.9	11.9	120.0	9.8	19.9	74.0	352.1	0.0	—	58.9
Mom's Place	184	22.8	7.8	27.0	6.7	77.0	9.4	14.0	55.0	236.0	0.0	2.6	75.0
18S/49E-11bbb	185	25.0	7.6	34.1	8.5	99.1	11.7	30.8	90.3	224.6	0.0	—	78.1
Skeleton Hills													
TW-5	186	30.0	7.9	33.0	17.0	130.0	12.0	21.0	99.0	395.0	0.0	3.4	19.0
Unnamed Well 15S/50E-22-7	187	—	6.7	27.0	2.0	43.0	4.6	8.5	33.0	148.8	—	0.9	49.0
Amargosa Flat													
Amargosa Tracer Hole #2	188	30.5	8.0	42.8	18.5	63.8	7.5	21.0	68.7	279.2	—	1.9	22.0
Cherry Patch Well, 17S/52E-08cdb	189	26.2	7.3	76.0	38.8	272.5	9.6	122.5	485.0	344.7	—	1.7	25.5
USDOE-MSH-C shallow Well	190	20.5	8.0	16.0	17.0	81.0	9.4	17.0	58.0	261.0	—	1.7	34.0
Mine Mountain													
UE-17a	191	27.0	7.6	41.0	29.9	80.0	3.0	27.7	95.5	200.0	—	0.9	11.8
UE-1a	192	25.4	7.4	48.5	23.9	50.5	8.7	26.3	—	402.5		—	19.3
UE-1b	193	27.4	7.4	37.4	13.7	31.3	10.7	5.9	—	184.0		—	80.9
UE-16f	194	29.4	8.9	1.8	1.9	421.2	5.0	18.8	423.0	900.0	33.0	5.2	4.5
UE-14b	195	—	8.4	10.5	0.2	77.5	1.5	7.1	80.8	116.0		—	43.8

Table A6-1. Field Parameters and Major Ion Composition (Continued)

Well Name[a]	Figure A6-5 Sample	Temperature (°C)	pH	Ca^{2+} (mg/L)	Mg^{2+} (mg/L)	Na^{+} (mg/L)	K^{+} (mg/L)	Cl^{-} (mg/L)	SO_4^{2-} (mg/L)	HCO_3^{-} (mg/L)	CO_3^{2-} (mg/L)	F^{-} (mg/L)	SiO_2 (mg/L)
Mine Mountain (Continued)													
Pluto 1	196	—	8.0	40.5	9.8	36.2	7.7	23.7	46.9	150.0	—	—	54.0
Pluto 5	197	—	7.9	55.0	21.6	26.4	4.3	11.5	54.2	218.0	—	—	58.0
USGS Test Well F (HTH)	198	64.5	6.9	46.0	16.7	63.0	9.1	12.9	79.3	254.2	—	3.2	36.4
Funeral Mountains													
Woodcamp Spring	199	19.2	7.2	23.0	3.3	38.0	14.0	24.0	24.0	122.0	—	0.2	57.0
Bond Gold Mining #13	200	32.4	7.3	144.5	79.5	85.5	7.0	63.5	621.5	274.5	0.0	0.6	16.5
Nevares Spring	201	39.4	7.4	42.0	20.0	140.0	11.0	37.0	170.0	353.0	—	3.2	26.0
Travertine Spring	202	35.3	7.4	33.0	18.0	140.0	12.0	37.0	150.0	343.0	—	3.7	30.0

Sources: Primarily DTNs: LA0309RR831233.001 [DIRS 166546] and LA0309RR831233.002 [DIRS 166548]; and others as documented in Table A4-3.

[a] dp = deep sample, sh = shallow sample, Tcp = sample from Prow Pass tuff, Tcb = sample from Bullfrog tuff, bh = sample from entire borehole, ’95 = sample from 1995, v = sample from volcanic aquifer, c = sample from carbonate aquifer, Tct = sample from Tram Member or Crater Flat tuff. Where not otherwise indicated, sample is from entire open interval of borehole.

[b] The groundwater temperature was estimated from the map of water table temperature shown in Fridrich et al. 1994 [DIRS 100575], Figure 8.

[c] The groundwater temperature for this sample was assumed to be the same as for the c#3 sample.

[d] The symbol “—“ indicates the data are not available.

Table A6-2. Isotope and Trace Element Composition

Well Name	Figure A6-5 Sample	$\delta^{13}C$ (per mil)	^{14}C (pmc)	δD (per mil)	$\delta^{18}O$ (per mil)	$\delta^{34}S$ (per mil)	U (µg)	$^{234}U/^{238}U$ (AR)	Sr^{2+} (µg)	$^{87}Sr/^{86}Sr$ (ratio)	$\delta^{87}Sr$ (per mil)
Oasis Valley/NW Amargosa											
ER-EC-08	1	−1.0	8.7	−116.0	−14.8	—	4.4	—	—	0.70864	−0.8
ER-OV-01	2	−2.0	5.0	−112.5	−14.7	—	9.4	3.7	4.9	0.71058	1.9
ER-OV-06a	3	−2.2	6.0	−113.0	−14.7	—	5.2	3.3	10.6	0.70932	0.2
ER-OV-05	4	−3.1	17.3	−106.0	−13.7	—	2.2	2.8	192.0	0.70976	0.8
ER-OV-02	5	−2.6	16.2	−112.0	−14.7	—	18.3	2.5	46.0	0.71006	1.2
Springdale Upper Well (10S/47E-32adc)	6	−1.7	10.8	−104.0	−13.9	—	2.6	5.4	291.0	0.71026	1.5
Goss Springs North (11S/47E-10bad)	7	−2.9	21.8	−110.0	−14.7	—	9.23	2.9	88.0	0.71039	1.7
Er-OV-03a	8	−3.0	16.3	−111.0	−14.7	—	9.1	2.9	75.2	0.71029	1.5
ER-OV-03a3	9	−2.8	16.5	−110.0	−14.6	—	9.1	2.9	76.8	0.71003	1.2
ER-OV-03a2	10	−5.0	21.0	−109.0	−14.5	—	9.8	5.4	167.0	0.70809	−1.6
Goss Spring (11S/47E-10bcc)	11	—	20.8	−111.7	−14.7	—	9.2	2.9	90.0	0.71050	1.8
ER-OV-04a	12	−3.4	8.0	−109.5	−14.8	—	3.0	3.0	22.0	0.71006	1.2
Beatty Well no. 1 (Wat & Sanit Distr)	13	—	—	—	—	—	8.8	—	155.3	—	—
Bond Gold Mining #1	14	−8.8	12.8	−100.0	−13.8	15.7	0.1	3.5	150.0	—	—
US Ecology MW-313	15	−6.1	17.0	−109.0	−14.1	21.8	7.8	3.2	361.0	—	—
US Ecology MW-600	16	−8.4	19.3	−108.3	−14.4	19.5	4.9	2.5	340.0	—	—
NECWell	17	−5.9	28.8	—	—	—	—	—	—	—	—
US Ecology MR-3	18	−6.5	323.0	−109.0	−14.5	20.1	6.5	3.2	—	—	—
Timber Mountain											
UE-18r	19	−1.7	7.7	−110.0	−14.7	—	5.1	6.1	116.5	0.70903	−0.2
ER-18-2	20	−0.7	1.6	−112.0	−14.7	—	8.0	12.7	224.3	0.70872	−0.7
ER-EC-05	21	−2.5	6.3	−113.0	−14.9	—	3.2	6.4	140.1	0.70916	−0.1
Coffer's Ranch Windmill Well	22	−3.9	9.6	−103.9	−13.5	—	5.5	4.9	162.1	0.70922	0.0
ER-OV-03c	23	−3.2	6.8	−109.0	−14.7	—	4.2	5.4	99.0	0.70924	0.1
ER-EC-07	24	−6.3	36.5	−98.0	−13.2	—	1.8	7.2	123.1	0.70938	0.2
Fortymile Wash—North											
Water Well 8	25	−11.6	25.0	−103.0	−13.5	—	0.4	3.9	5.2	0.71025	1.5

Table A6-2. Isotope and Trace Element Composition (Continued)

Well Name	Figure A6-5 Sample	$\delta^{13}C$ (per mil)	^{14}C (pmc)	δD (per mil)	$\delta^{18}O$ (per mil)	$\delta^{34}S$ (per mil)	U (µg /L)	$^{234}U/^{238}U$ (AR)	Sr^{2+} (µg /L)	$^{87}Sr/^{86}Sr$ (ratio)	$\delta^{87}Sr$ (per mil)
Fortymile Wash—North (Continued)											
Test Well 1 (USGS HTH #1)	26	−10.2	30.1	—	−14.7	—	0.6	—	15.0	0.70892	−0.4
UE-18t	27	—	—	—	—	—	—	—	—	—	—
ER-30-1 (upper)	28	−6.3	—	−93.2	−12.4	—	—	—	13.0	0.70778	−2.0
ER-30-1 (lower)	29	−6.0	—	−86.7	−11.8	—	—	—	7.0	0.70807	−1.59
a#2(dp)	30	−12.6	62.3	−93.5	−12.8	—	—	—	39.0	—	—
a#2(sh)	31	−13.1	60.0	−93.0	−12.8	—	0.7	4.0	33.0	—	—
UE-29a#1 HTH	32	−10.5	75.7	−91.0	−12.6	—	1.5	3.6	54.7	0.71105	2.6
WT#15	33	−11.8	21.6	−97.5	−13.2	—	—	—	—	—	—
WT#14	34	−12.8	24.1	−97.5	−12.8	—	—	—	—	—	—
J-13	35	−7.3	29.2	−97.5	−13.0	—	0.6	7.2	20.0	0.71146	3.2
J-12	36	−7.9	32.2	−97.5	−12.8	—	0.3	5.5	10.0	0.71164	3.4
JF#3	37	−8.6	30.7	−97.0	−13.2	—	0.8	4.1	—	0.71133	3.0
Solitario Canyon Wash											
H-6(bh)	38	−7.5	16.3	−106.0	−13.8	—	—	—	8.0	—	—
H-6(Tct)	39	−7.3	10.0	−105.0	−14.0	—	—	—	3.0	—	—
H-6(Tcb)	40	−7.1	12.4	−107.0	−14.0	—	—	—	8.0	—	—
WT-7	41	−9.0	—	—	−14.0	—	0.1	4.8	—	0.71027	1.5
WT-10	42	−6.1	7.3	−103.0	−13.8	—	2.8	4.8	4.0	0.71007	1.2
Yucca Mountain—Crest											
G-2	43	−11.8	20.5	−98.8	−13.3	—	1.2	7.6	10.0	0.71070	2.1
USW WT-24	44	−10.6	27.3	−101.1	−13.2	—	1.1	6.4	1.5	—	—
UZ-14(sh)	45	−14.1	24.6	−100.4	−14.0	11.4	—	—	57.0	—	—
UZ-14(dp)	46	−14.4	21.1	−100.6	−14.0	—	—	—	32.0	—	—
H-1(Tcp)	47	—	19.9	−103.0	−13.4	—	—	—	5.0	—	—
H-1(Tcb)	48	−11.4	23.9	−101.0	−13.5	—	—	—	20.0	—	—
H-5	49	−10.3	19.8	−102.0	−13.6	—	—	—	6.5	—	—

Table A6-2. Isotope and Trace Element Composition (Continued)

Well Name	Figure A6-5 Sample	$\delta^{13}C$ (per mil)	^{14}C (pmc)	δD (per mil)	$\delta^{18}O$ (per mil)	$\delta^{34}S$ (per mil)	U (µg /L)	$^{234}U/^{238}U$ (AR)	Sr^{2+} (µg /L)	$^{87}Sr/^{86}Sr$ (ratio)	$\delta^{87}Sr$ (per mil)
Yucca Mountain—Crest (Continued)											
USW SD-6	50	−9.4	—	−105.3	−14.4	12.5	5.0	3.9	>1.0	—	—
H-3	51	−4.9	10.5	−101.0	−13.9	—	—	—	1.0	—	—
Yucca Mountain—Central											
G-4	52	−9.1	22.0	−103.0	−13.8	—	—	—	17.0	—	—
b#1(Tcb)	53	−8.6	18.9	−99.5	−13.5	—	—	—	47.0	—	—
b#1(bh)	54	−10.6	16.7	−100.3	−13.4	—	—	—	41.0	—	—
H-4	55	−7.4	11.8	−104.0	−14.0	—	—	—	27.0	—	—
UZ#16	56	—	—	—	—	—	—	—	—	—	—
Yucca Mountain—Southeast											
ONC#1	57	—	—	—	—	—	—	—	1720.0	0.71040	1.7
c#1	58	−7.1	15.0	−102.0	−13.5	—	—	—	30.0	0.71040	1.7
c#3	59	−7.5	15.7	−103.0	−13.5	—	—	—	44.0	—	—
c#3(95-97)	60	—	—	−99.7	−13.4	10.8	1.2	8.1	60.0	0.70981	0.9
c#2	61	−7.0	16.6	−100.0	−13.4	10.9	—	—	45.0	—	—
p#1(v)	62	−4.2	3.5	−106.0	−13.5	—	—	—	180.0	—	—
p#1(c)	63	−2.3	2.3	−106.0	−13.8	—	13.3	2.3	450.0	0.71177	3.6
WT-17	64	−8.3	16.2	−101.9	−13.7	10.5	1.1	7.6	—	—	—
WT#3	65	−8.2	22.3	−102.1	−13.6	10.8	0.8	7.2	32.0	—	—
WT#12	66	−8.1	11.4	−102.5	−13.8	—	2.5	7.2	23.0	0.70991	1.0
Jackass Flats											
UE-25 J-11	67	−11.0	12.3	−105.3	−13.5	8.8	2.0	1.5	264.0	—	—
Crater Flat											
GEXA Well4	68	—	—	−105.6	−14.1	—	3.0	5.1	34.0	0.70974	0.8
VH-1	69	−8.5	12.2	−108.0	−14.2	—	3.6	5.5	66.7	0.71096	2.5
Southwest Crater Flat											
VH-2	70	—	—	−99.5	−13.5	—	3.0	3.1	570.0	0.71300	5.4
NC-EWDP-7S	71	−4.9	8.4	−98.0	−13.0	14.3	—	—	630.0	—	—

Table A6-2. Isotope and Trace Element Composition (Continued)

Well Name	Figure A6-5 Sample	$\delta^{13}C$ (per mil)	^{14}C (pmc)	δD (per mil)	$\delta^{18}O$ (per mil)	$\delta^{34}S$ (per mil)	U (µg /L)	$^{234}U/^{238}U$ (AR)	Sr^{2+} (µg /L)	$^{87}Sr/^{86}Sr$ (ratio)	$\delta^{87}Sr$ (per mil)
Southwest Crater Flat (Continued)											
NC-EWDP-7SC	72	—	—	—	—	—	—	—	558.0	—	—
NC-EWDP-1DX	73	−4.5	—	−101.3	−13.5	14.6	5.1	3.9	510.0	—	—
NC-EWDP-1DX Zone 2	74	−2.1	2.5	−105.7	−14.7	28.3	0.0	3.0	981.0	0.71293	5.3
NC-EWDP-1S Zone 1	75	−5.8	7.7	−101.3	−13.6	14.8	8.6	4.5	568.0	0.71279	5.1
NC-EWDP-1S Zone 2	76	−5.6	7.2	−100.8	−13.7	15.2	7.6	4.5	533.0	0.71288	5.2
NC-EWDP-1S	77	−5.6	—	−99.6	−13.8	14.5	8.6	4.5	557.0	—	—
NC-EWDP-12PA	78	−3.4	4.7	−103.8	−13.6	16.9	—	—	302.0	0.71561	9.0
NC-EWDP-12PB	79	−3.6	4.5	−100.5	−13.6	16.7	—	—	296.0	0.71460	7.6
NC-EWDP-12PC	80	−5.3	9.0	−101.8	−13.4	14.7	—	—	462.0	0.71269	4.9
Southern Yucca Mountain											
NC-EWDP-09SX	81	−6.5	—	−104.2	−14.0	13.3	5.1	5.0	151.3	0.71250	4.7
NC-EWDP-9SX Zone 1	82	−7.1	12.2	−102.0	−14.3	14.2	4.6	4.9	129.0	0.71247	4.6
NC-EWDP-9SX Zone 2	83	−7.0	11.4	−104.7	−14.3	13.9	4.6	5.0	149.0	0.71239	4.5
NC-EWDP-9SX Zone 3	84	−6.8	10.9	−104.5	−14.1	14.4	4.4	5.0	144.5	0.71246	4.6
NC-EWDP-9SX Zone 4	85	−6.2	11.0	−105.0	−14.2	13.8	4.6	5.0	146.7	0.71254	4.7
NC-EWDP-03D	86	−6.8	10.0	−105.6	−14.4	11.2	2.0	3.4	1.3	—	—
NC-EWDP-3S Zone 2	87	−8.4	21.5	−104.8	−14.3	10.9	2.6	3.2	2.5	0.71032	1.6
NC-EWDP-3S Zone 3	88	−5.0	8.4	−106.2	−14.2	9.8	7.4	2.9	3.7	0.71100	2.5
CIND-R-LITE	89	—	—	−102.0	−13.6	—	2.8	4.7	108.0	0.71221	4.2
NC-EWDP-15P	90	−6.3	12.0	−106.3	−13.8	13.2	—	—	50.0	0.71222	4.3
NC-EWDP-02D	91	−8.3	23.5	−104.0	−14.1	11.9	1.2	4.8	53.0	—	—
NC-EWDP-19D	92	−7.6	12.4	−106.1	−13.8	9.0	—	—	3.5	0.71056	1.9
NC-EWDP-19P	93	−9.5	23.5	−103.5	−13.6	11.7	—	—	57.0	0.71133	3.0
NC-EWDP-19D (alluvial)	94	−7.1	12.4	−108.8	−13.8	10.7	—	—	7.5	—	—
NC-EWDP-19D(zone #1)	95	−7.0	17.6	−109.0	−13.9	10.1	—	—	15.0	—	—
NC-EWDP-19D(zone #2)	96	−7.6	21.0	−104.0	−13.6	10.6	—	—	36.0	—	—

Table A6-2. Isotope and Trace Element Composition (Continued)

Well Name	Figure A6-5 Sample	$\delta^{13}C$ (per mil)	^{14}C (pmc)	δD (per mil)	$\delta^{18}O$ (per mil)	$\delta^{34}S$ (per mil)	U (µg /L)	$^{234}U/^{238}U$ (AR)	Sr^{2+} (µg /L)	$^{87}Sr/^{86}Sr$ (ratio)	$\delta^{87}Sr$ (per mil)
Southern Yucca Mountain (Continued)											
NC-EWDP-19D(zone #3)	97	−9.4	12.5	−106.3	−13.5	10.9	—	—	3.0	—	—
NC-EWDP-19D(zone #4)	98	−6.4	11.2	−110.2	−13.9	11.7	—	—	2.0	—	—
Amargosa Valley											
NC-EWDP-4PB	99	−10.0	15.9	−108.5	−13.9	9.6	—	—	36.0	0.71021	1.4
NC-EWDP-4PA	100	−10.5	23.1	−101.3	−13.3	8.9	—	—	62.5	0.70949	0.4
Desert Farms Garlic Plot	101	−9.1	8.8	−106.4	−13.1	8.8	1.3	3.4	144.0	—	—
15S/49E-13dda	102	—	—	—	—	—	—	—	—	—	—
15S/50E-18ccc	103	—	—	—	—	—	—	—	80.0	—	—
NDOT	104	—	—	—	—	—	2.5	2.5	—	0.71081	2.3
15S/50E-18cdc	105	—	—	—	—	—	—	—	—	—	—
Airport Well	106	−10.3	10.5	−106.2	−13.2	8.7	0.6	3.1	24.0	—	—
15S/50E-19b1	107	—	—	—	—	—	—	—	—	—	—
Amargosa River											
16S/48E-8ba	108	—	—	—	—	—	—	—	—	—	—
16S/48E-7bba	109	—	—	—	—	—	—	—	—	—	—
16S/48E-7cbc	110	−6.2	31.4	−102.0	−13.1	—	—	—	—	—	—
16S/48E-18bcc	111	—	—	—	—	—	—	—	—	—	—
16S/48E-17ccc	112	—	—	—	—	—	—	—	—	—	—
16S/48E-18dad	113	−5.7	—	−104.0	−13.6	—	—	—	—	—	—
16S/48E-8cda	114	—	—	—	—	—	—	—	—	—	—
16S/48E-17abb	115	—	—	—	—	—	—	—	—	—	—
Barrachman Dom/Irr.	116	−5.8	17.9	−107.4	−13.5	20.9	5.2	3.4	473.0	—	—
McCracken Domestic	117	−12.1	32.9	−102.7	−12.9	18.5	5.2	3.3	600.0	0.71456	7.6
Fortymile Wash—West											
16S/48E-15ba	118	—	—	—	—	—	—	—	—	—	—
16S/48E-10cba	119	−5.6	15.6	−102.0	−13.4	—	—	—	—	—	—
16S/48E-15aaa	120	−7.1	17.1	−103.0	−13.4	—	—	—	—	—	—

Table A6-2. Isotope and Trace Element Composition (Continued)

Well Name	Figure A6-5 Sample	$\delta^{13}C$ (per mil)	^{14}C (pmc)	δD (per mil)	$\delta^{18}O$ (per mil)	$\delta^{34}S$ (per mil)	U (µg /L)	$^{234}U/^{238}U$ (AR)	Sr^{2+} (µg /L)	$^{87}Sr/^{86}Sr$ (ratio)	$\delta^{87}Sr$ (per mil)
Fortymile Wash—West (Continued)											
Selbach Domestic	121	−8.1	30.7	−103.2	−12.9	10.9	2.7	4.2	217.0	—	—
16S/48E-15dda	122	—	—	—	—	—	—	—	—	—	—
16S/49E-23add	123	−8.4	27.4	−99.0	−13.2	—	—	—	—	—	—
16S/48E-23bdb	124	—	—	—	—	—	—	—	—	—	—
16S/48E-23da	125	—	—	—	—	—	—	—	—	—	—
Funeral Mountain Ranch Irrigation	126	−5.5	6.5	−106.6	−13.7	13.2	1.3	2.9	114.0	—	—
Fortymile Wash—South											
16S/49E-05acc	127	−7.1	19.3	−103.0	−13.2	—	—	—	50.0	—	—
16S/49E-8abb	128	−6.8	21.4	−99.5	−13.2	—	—	—	—	—	—
16S/49E-8acc	129	—	—	—	—	—	—	—	—	—	—
16S/49E-18dc	130	—	28.4	−102.0	−12.6	—	—	—	—	—	—
16s/48E-24aaa	131	—	—	—	—	—	—	—	—	—	—
16S/49E-19daa	132	—	20.8	−101.0	−13.1	—	—	—	—	—	—
DeLee Large Irrigation	133	−8.4	20.5	−104.1	−13.3	9.5	1.5	3.2	109.5	—	—
16S/48E-25aa	134	—	19.3	−102.0	−13.0	—	—	—	—	—	—
16S/48E-36aaa	135	—	—	−98.5	−12.6	—	—	—	—	—	—
Bray Domestic	136	−10.0	23.5	−103.5	−13.2	9.3	1.5	3.1	101.0	—	—
Amargosa Estates #2	137	−10.6	21.6	−104.3	−13.1	10.2	1.3	3.0	129.0	—	—
17S/48E-1ab	138	—	18.4	−104.0	−13.0	—	—	—	—	—	—
17S/49E-7bb	139	—	10.0	−104.0	−12.7	—	—	—	—	—	—
17S/49E-8ddb	140	—	27.8	−102.0	−13.0	—	—	—	—	—	—
17S/49E-35ddd	141	—	13.8	−102.0	−12.4	—	—	—	—	—	—
Fortymile Wash—East											
15S/49E-22a1	142	—	—	—	—	—	—	—	—	—	—
15S/49E-22dcc	143	—	—	—	—	—	—	—	65.0	—	—
15S/49E-27acc	144	—	—	—	—	—	—	—	65.0	—	—
O'Neill Domestic	145	−6.7	17.7	−101.8	−13.2	9.6	1.7	2.8	109.0	—	—

Table A6-2. Isotope and Trace Element Composition (Continued)

Well Name	Figure A6-5 Sample	$\delta^{13}C$ (per mil)	^{14}C (pmc)	δD (per mil)	$\delta^{18}O$ (per mil)	$\delta^{34}S$ (per mil)	U (µg /L)	$^{234}U/^{238}U$ (AR)	Sr^{2+} (µg /L)	$^{87}Sr/^{86}Sr$ (ratio)	$\delta^{87}Sr$ (per mil)
Fortymile Wash—East (Continued)											
16S/49E-9cda	146	—	—	—	—	—	—	—	—	—	—
16S/49E-9dcc	147	−7.3	21.9	−103.0	−13.4	—	—	—	—	—	—
16S/49E-16ccc	148	−5.2	24.8	−97.5	−13.2	—	—	—	—	—	—
Ponderosa Dairy #1	149	−7.2	14.2	−105.5	−13.3	16.6	2.3	2.9	248.0	—	—
17S/49E-9aa	150	—	18.9	−105.0	−12.8	—	—	—	—	—	—
17S/49E-15bbd	151	—	40.3	—	—	—	—	—	—	—	—
M. Gilgan Well	152	−9.0	27.9	−100.1	−13.0	9.4	0.8	3.0	155.0	—	—
17S/49E-15bc	153	—	—	—	—	—	—	—	—	—	—
Gravity Fault											
NC-EWDP-5S	154	—	—	−107.0	−14.0	—	0.04	6.7	361.0	0.71206	4.0
NC-EWDP-5SB	155	−1.5	4.0	−107.0	−13.3	17.8	—	—	204.0	0.71232	4.4
16S/50E-7bcd	156	−3.6	7.0	−105.0	−13.8	—	—	—	—	—	—
Nelson Domestic	157	−2.0	0.9	−110.2	−13.8	22.6	1.7	3.2	829.5	—	—
16S/49E-12ddd	158	—	—	—	—	—	—	—	—	—	—
Lowe Domestic	159	−3.0	1.2	−103.7	−13.8	21.5	2.8	3.3	724.0	—	—
16S/49E-15aaa	160	−3.4	—	−105.0	−13.8	—	—	—	—	—	—
Anvil Ranch Irrigation	161	−10.4	11.8	−103.3	−13.1	13.2	2.1	2.8	319.0	—	—
16S/49E-36aaa	162	−4.4	10.3	−104.0	−13.7	—	—	—	—	—	—
16S/49E-35baa	163	—	—	—	—	—	—	—	—	—	—
Payton Domestic	164	−2.7	3.3	−109.7	−13.8	21.7	1.0	3.6	1069.0	—	—
16S/49E-36aba	165	—	—	—	—	—	—	—	—	—	—
16S/49E-35aaa	166	—	—	—	—	—	—	—	—	—	—
Oettinger Well	167	−2.6	1.4	−108.5	−13.8	21.8	1.5	3.3	915.0	—	—
Amargosa Motel (b)	168	−3.0	1.9	−109.0	−13.7	22.0	1.6	3.2	954.0	—	—
17S/49E-11ba	169	—	—	—	—	—	—	—	—	—	—
Spring Meadows Well #8	170	—	—	—	—	—	—	—	—	—	—
17S/50E-19aab	171	—	—	—	—	—	—	—	—	—	—

Table A6-2. Isotope and Trace Element Composition (Continued)

Well Name	Figure A6-5 Sample	$\delta^{13}C$ (per mil)	^{14}C (pmc)	δD (per mil)	$\delta^{18}O$ (per mil)	$\delta^{34}S$ (per mil)	U (µg /L)	$^{234}U/^{238}U$ (AR)	Sr^{2+} (µg /L)	$^{87}Sr/^{86}Sr$ (ratio)	$\delta^{87}Sr$ (per mil)
Gravity Fault (Continued)											
USFWS – Five Springs Well	172	—	—	−104.0	−13.6	—	—	—	860.0	—	—
Spring Meadows Well #10	173	—	—	—	—	—	—	—	—	—	—
18S/49E-1aba	174	—	—	—	—	—	—	—	—	—	—
18S/50E-6dac	175	—	—	—	—	—	—	—	—	—	—
18S/50E-7aa	176	—	—	—	—	—	—	—	—	—	—
Amargosa River/Fortymile Wash											
16S/48E-36dcc	177	—	—	—	—	—	—	—	—	—	—
Crane Domestic	178	−4.3	7.9	−108.8	−13.4	22.3	4.0	3.3	674.0	—	—
27N/4E-27bbb	179	—	—	—	—	—	—	—	—	—	—
IMV on Windjammer	180	−5.0	6.6	−104.0	−13.4	19.3	3.6	3.0	430.0	—	—
17S/49E-29acc	181	—	—	—	—	—	—	—	—	—	—
17S/49E-28bcd	182	—	—	—	—	—	—	—	—	—	—
18S/49E-2cbc	183	—	—	—	—	—	—	—	—	—	—
Mom's Place	184	−4.9	11.4	−105.5	−13.2	17.1	1.9	3.0	346.0	—	—
18S/49E-11bbb	185	—	—	—	—	—	—	—	—	—	—
Skeleton Hills											
TW-5	186	—	—	−113.2	−15.4	—	—	—	1509.0	0.71505	8.2
Unnamed Well 15S/50E-22-7	187	—	—	—	—	—	—	—	80.0	—	—
Amargosa Flat											
Amargosa Tracer Hole #2	188	−6.0	4.6	—	−13.6	—	—	—	790.0	—	—
Cherry Patch Well, 17S/52E-08cdb	189	—	—	—	—	—	1.8	2.9	1500.0	—	—
USDOE-MSH-C shallow Well	190	—	—	−108.0	−14.1	—	—	—	540.0	—	—
Mine Mountain											
UE-17a	191	−9.9	4.9	−100.0	−13.3	—	0.4	—	829.0	0.71020	1.5
UE-1a	192	−8.6	60.5	−103.0	−13.5	—	4.3	—	630.0	0.70957	0.5
UE-1b	193	−4.5	16.0	−105.0	—	—	4.3	—	470.0	0.70950	0.4
UE-16f	194	−11.7	3.4	−104.0	−13.5	—	—	—	550.0	0.71138	3.1

Table A6-2. Isotope and Trace Element Composition (Continued)

Well Name	Figure A6-5 Sample	$\delta^{13}C$ (per mil)	^{14}C (pmc)	δD (per mil)	$\delta^{18}O$ (per mil)	$\delta^{34}S$ (per mil)	U (µg /L)	$^{234}U/^{238}U$ (AR)	Sr^{2+} (µg /L)	$^{87}Sr/^{86}Sr$ (ratio)	$\delta^{87}Sr$ (per mil)
Mine Mountain (Continued)											
UE-14b	195	—	—	—	—	—	—	—	—	—	—
Pluto 1	196	—	—	—	—	—	—	—	—	—	—
Pluto 5	197	—	—	—	—	—	—	—	—	—	—
USGS Test Well F (HTH)	198	—	—	—	—	—	—	—	570.0	—	—
Funeral Mountains											
Woodcamp Spring	199	−12.2	78.0	−91.6	−12.4	—	—	—	20.0	0.70871	−0.7
Bond Gold Mining #13	200	−7.5	8.1	−100.6	−13.3	29.3	8.1	1.9	2140.0	0.72732	25.5
Nevares Spring	201	−5.5	3.0	−101.0	−13.5	—	1.3	2.1	1100.0	0.71679	10.7
Travertine Spring	202	−3.8	3.3	−102.0	−13.5	—	3.3	2.4	1100.0	0.71734	11.5

Sources: Primarily DTNs: LA0309RR831233.001[DIRS 166546]; LA0309RR831233.002 [DIRS 166548], and LA0311EK831232.002 [DIRS 166069]; and others as documented in Table A4-3.

AR = activity ratio

A6.3.1 Factors Affecting the Chemical and Isotopic Composition of Groundwater

This section will summarize the study of Meijer (2002 [DIRS 158813]) that describes the effects of: (1) precipitation composition, (2) evaporation, (3) precipitation/dissolution reactions, (4) adsorption and ion-exchange reactions, and (5) climate change on the chemical composition of groundwater. Additional details are presented in Meijer (2002 [DIRS 158813]) and in the *Yucca Mountain Site Description* (BSC 2004 [DIRS 169734], Sections 5.2.2, 8.2.7, and 8.3.6).

A6.3.1.1 Factors Affecting the Chemical Composition of Groundwater

The main processes that control groundwater chemistry are:

- Precipitation (atmospheric) quantities and compositions
- Surface water quantities and compositions in recharge areas and along stream courses
- Soil-zone processes in recharge areas and along flow paths between the soil and saturated zone
- Rock-water interactions in the unsaturated zone
- Rock-water interactions in the saturated zone
- Temperature and pressure effects in the unsaturated and saturated zones
- Mixing of groundwater from different flow systems.

Although all the processes listed above may affect the groundwater chemistry, mixing and rock-water interactions generally are the most dominant in determining changes to the major-ion composition of recharge after it has reached the saturated zone.

Processes that affect infiltrating waters in the soil zone or the unsaturated zone include evapotranspiration, mineral and gas dissolution reactions, gas ex-solution and mineral-precipitation reactions, and ion-exchange reactions. The dominant changes to the water compositions that result from these processes in the volcanic rock in the Yucca Mountain area are increases in the concentration of all chemical species and major relative increases in SiO_2, Na^+, and HCO_3^- compared to the composition of precipitation.

The dominant water-rock reactions that impact the water chemistry after the shallow unsaturated-zone or soil-zone reactions are SiO_2-precipitation reactions and ion-exchange reactions involving minerals such as zeolites and clays. The cation-hydrogen ion-exchange reaction will also continue to be of significance. The ion-exchange reactions lead to increased Na^+ concentrations and decreased Ca^{2+}, Mg^{2+}, and K^+ concentrations in the waters. However, changes in the concentrations of these ions will only occur if zeolites and/or clays are present in adequate quantities in rock units through which the waters migrate. The Na^+–H^+ ion-exchange reaction will continue to increase the Na^+ content of the waters until thermodynamic equilibrium is achieved with the host rock.

The primary controls on the pH of groundwater in the saturated zone are the partial pressure of CO_2 and the rate at which hydrogen ions are consumed by the rock-mineral matrix. In the saturated zone, access to the CO_2 reservoir in the gas phase of the unsaturated zone becomes progressively more difficult with depth. Therefore, unless a secondary source of H_2CO_3 or another source of acidity (e.g., sulfide minerals) exists in the saturated zone, the reaction of hydrogen ions with the rock mineral matrix will eventually consume the available acidity, leading to increased pH.

Winograd and Thordarson (1975 [DIRS 101167], pp. C97 to C102, Plate C) identified six hydrochemical facies in the vicinity of the Nevada Test Site. Where the host rocks are limestone and dolomite, as in the case of the carbonate aquifer, the dominant ions are Ca^{2+}, Mg^{2+}, and HCO_3^-. Tuffaceous aquifers are characterized by groundwater having Na^+, K^+ and HCO_3^- as the dominant ions. Groundwater of mixed compositions occurs where groundwater flows from one aquifer type into another, or from alluvium derived from one rock type into alluvium derived from another rock type. Groundwater mixing can also produce groundwaters that are intermediate in compositions between the carbonate and tuffaceous aquifers. In the alluvial valley fill deposits, the host rocks consist of fragments that reflect the rock composition in the upland sediment source areas. For example, in the west central Amargosa Desert, a central region of predominantly tuffaceous valley fill is flanked to the east and west by zones containing significant proportions of carbonate-rock detritus (Claassen 1985 [DIRS 101125], p. F5, Figure 1), which greatly affect the major-ion composition of the groundwater. This lateral sedimentary facies relationship is further complicated in the Amargosa Desert by the local presence of playa deposits (Claassen 1985 [DIRS 101125], pp. F5 and F30). Groundwater in the vicinity of playa deposits typically contains greater concentrations of SO_4^{2-} and Cl^-, which were concentrated in the playa deposits through earlier cycles of evaporation (Claassen 1985 [DIRS 101125], p. F18).

A6.3.1.2 Factors Affecting the Isotopic Composition of Groundwater

The main processes that control the isotopic chemistry of SZ groundwaters have some common ground with those that control major-ion chemistry; however, major differences exist between these chemical regimes. As with major-ion content, precipitation quantity and composition are the starting point for the isotopic evolution of groundwater.

A6.3.1.2.1 Hydrogen and Oxygen

Hydrogen and oxygen isotope ratios are useful for tracing groundwater movement where spatial differences in their concentrations exist. Both hydrogen and oxygen are composed of more than one stable isotope. The stable hydrogen isotopes of interest here are ^1H and ^2H. The latter isotope is commonly referred to as deuterium with the chemical symbol D. The ratio of these two isotopes is measured and is generally reported in δ notation as follows, with units of per mil:

$$\delta D = [(D/^1H)_{sample}/(D/^1H)_{standard} - 1] \times 1{,}000 \qquad \text{(Eq. A6-1)}$$

The standard used for these measurements is known as Vienna Standard Mean Ocean Water (Clark and Fritz 1997 [DIRS 105738], p. 8).

The stable oxygen isotopes of interest here are ^{16}O and ^{18}O. The ratio of these isotopes is measured and also reported in δ notation as follows, with units of per mil:

$$\delta^{18}O = [(^{18}O/^{16}O)_{sample}/(^{18}O/^{16}O)_{standard} - 1] \times 1{,}000 \quad \text{(Eq. A6-2)}$$

Vienna Standard Mean Ocean Water is also used as the standard for oxygen isotope measurements (Clark and Fritz 1997 [DIRS 105738], p. 8).

The ^{2}H and ^{18}O atoms are part of the water molecule and, at low temperatures, are generally unaffected by water-rock interactions. The values of δD and $\delta^{18}O$ in precipitation, fresh surface water, and groundwater are typically negative because of fractionation between the heavy and light isotopes of hydrogen and oxygen during evaporation over the initial moisture source area and because the residual water vapor becomes progressively more depleted in the heavier isotopes (^{2}H and ^{18}O) during successive precipitation events. A detailed discussion of all the processes affecting the isotopic composition of precipitation and recharge, and possible effects of water-rock interactions, is beyond the scope of this report. A summary of these processes is available in textbooks, such as Clark and Fritz (1997 [DIRS 105738], Sections 2 to 4, 9). Some of the net effects of these processes are depicted in Figure A6-4.

The values of δD and $\delta^{18}O$ in precipitation are strongly correlated on a global basis. This correlation has been termed the "global meteoric water line." The equation for this line is $\delta D = 8\ \delta^{18}O + 10$ (Clark and Fritz 1997 [DIRS 105738], p. 36). The slope of the line is related to the ratio of the equilibrium fractionation factors for ^{2}H and ^{18}O, which are approximately 8.2 at 25ºC (Clark and Fritz 1997 [DIRS 105738], p. 50). Locally, the isotopic composition of precipitation may follow a line with a somewhat different slope and intercept. Such lines have been referred to as the "local meteoric water line." The deuterium "excess" is the intercept in the meteoric water line when the slope is eight. This "excess" is inversely related to the relative humidity of the air in the moisture source area (Clark and Fritz 1997 [DIRS 105738], p. 45; Merlivat and Jouzel 1979 [DIRS 126847], p. 5,029).

One of the primary factors affecting the isotopic composition of precipitation is condensation temperature, which is a function of season, elevation, and climate. Precipitation falling during periods when temperatures are low has more negative ("depleted") δD and $\delta^{18}O$ values than precipitation falling during warm periods. Because average surface temperatures are correlated with elevation, precipitation falling at higher elevations tends to have more negative isotope ratios than precipitation falling at lower elevations. Late Pleistocene groundwater, identified by ^{14}C age dating or other techniques, is often more isotopically depleted compared to modern waters because it was recharged under conditions that were cooler than at present. Also, because of the inverse relation between the value for the deuterium excess and relative humidity of the moisture source areas, data for old groundwaters recharged during pluvial periods in the Pleistocene sometimes plot below the present-day global or local meteoric water line (Clark and Fritz 1997 [DIRS 105738], pp. 198 to 199, Figure 8-2).

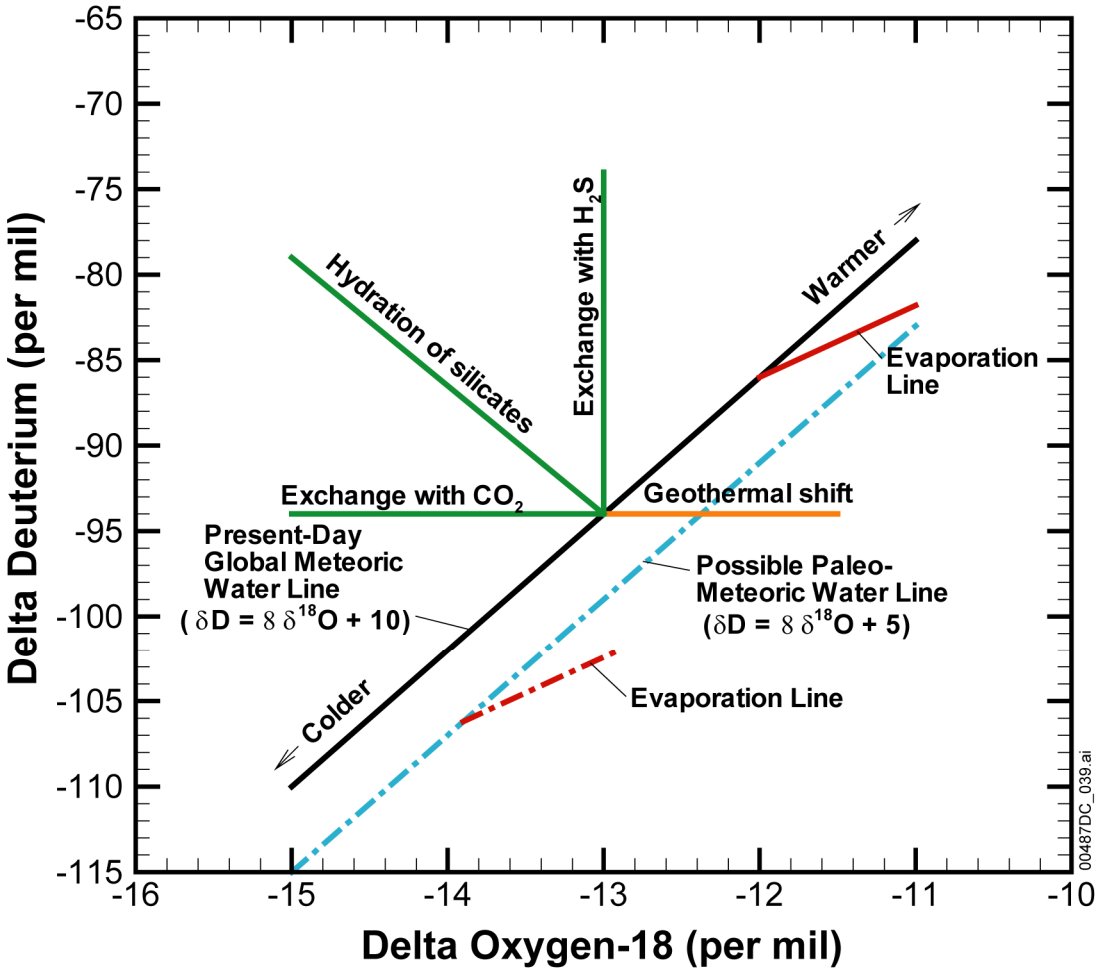

Source: Based on Clark and Fritz 1997 [DIRS 105738], Figures 2-1, 2-9, 2-11, and 9-1.

NOTE: The possible paleometeoric water line for the Amargosa Desert area is based on arguments of White and Chuma 1987 [DIRS 108871], p. 573.

Figure A6-4. Effects of Different Processes on Delta Deuterium and Delta Oxygen-18 Composition of Subsurface Water

Despite seasonal variations in the δD and $\delta^{18}O$ composition of precipitation, the isotopic composition of the recharge water in humid regions is generally close to the average volume-weighted isotopic composition of precipitation. In arid climates, the isotopic composition of the recharge can be substantially different from the average volume-weighted isotopic composition of precipitation because of the preferential recharge of winter precipitation (see, for example, Ingraham et al. 1991 [DIRS 145088], p. 256) and because of evaporation prior to recharge. Generally, evaporation shifts the δD and $\delta^{18}O$ composition of the infiltrating water to the right of the meteoric water line. The slope of the evaporation line increases with increasing relative humidity of the air (Clark and Fritz 1997 [DIRS 105738], Figure 2-8). The slope of the evaporation line ranges between 3.9 and 4.5 for relative humidities between 0 and 50%, which encompasses the range of relative humidities typical of Yucca Mountain during the summer months. Like evaporation, transpiration by plants increases the salinity of soil moisture; however, transpiration is a nonfractionating process and does not result in isotopic enrichment of

the residual soil moisture (Clark and Fritz [DIRS 105738], pp. 80 and 94). The relative importance of evaporation and transpiration on soil water loss can be evaluated by examining if increases in soil-water salinity are accompanied by corresponding increases in δD and $\delta^{18}O$ compositions along an evaporation trend.

Once in the ground, interaction between groundwater and the solid surfaces in soil or rock can cause the $\delta^{18}O$ composition of groundwater to be shifted horizontally to the right of the meteoric water line. This interaction is facilitated by high temperatures such as those associated with known geothermal fields (Clark and Fritz 1997 [DIRS 105738], pp. 250 to 255). At low temperatures, these interactions are kinetically inhibited. However, under special circumstances, interactions between groundwater and silicate minerals, or between groundwater and subsurface gases, may cause the isotopic compositions of groundwater to be shifted to the left of the meteoric water line (Clark and Fritz 1997 [DIRS 105738], Figure 9-1). The special circumstances typically involve alteration of rock to clays at high rock/water ratios or, in the case of gases, proximity to gas vents associated with volcanoes. Note that hydrogen isotope ratios are not generally affected as much by water/rock interactions as oxygen isotope ratios because rocks generally contain much less hydrogen than water on a volume-to-volume basis.

A6.3.1.2.2 Carbon

Carbon has two stable isotopes ^{12}C and ^{13}C and a third isotope, ^{14}C, which is radioactive. Carbon-14 is produced in the atmosphere by interactions of nitrogen and cosmic rays that bombard the earth constantly. The reaction can be described as ^{14}N (n,p) $\Rightarrow$ ^{14}C. ^{14}C is rapidly mixed in the atmosphere and incorporated into the CO_2 molecule where it is then available for incorporation into terrestrial carbonaceous material. The radioactive decay of ^{14}C, with a half-life ($t_{1/2}$) of 5,730 years (Clark and Fritz 1997 [DIRS 105738], Table 1-3), forms the basis for radiocarbon dating. The ^{14}C age of a sample is calculated by the following equation:

$$t = (-1/\lambda) \ln ({}^{14}A/{}^{14}A_0) \quad \text{(Eq. A6-3)}$$

where

t is the mean groundwater age (yr)

λ is the radioactive decay constant, equal to $\ln (2)/t_{1/2}$: 1.21×10^{-4} yr^{-1} (Clark and Fritz 1997 [DIRS 105738], p. 201)

^{14}A is the measured ^{14}C activity

$^{14}A_0$ is the assumed initial activity.

^{14}C ages are typically expressed in percent modern carbon (pmc). A ^{14}C activity of 100 pmc is taken as the ^{14}C activity of the atmosphere in the year 1890, before the natural ^{14}A of the atmosphere was diluted by large amounts of ^{14}C-free carbon-dioxide gas from the burning of fossil fuel (Clark and Fritz 1997 [DIRS 105738], p. 18).

Theoretically, the activity of ^{14}C in a groundwater sample reflects the time at which the water was recharged. Unfortunately, precipitation is generally very dilute and has a high affinity for dissolution of solid phases in the soil zone, unsaturated zone, and/or saturated zone. In particular, in the transition from precipitation compositions to groundwater compositions, the bicarbonate + carbonate concentration in the water commonly increases by orders of magnitude (Langmuir 1997 [DIRS 100051], p. 292, Table 8.7; Meijer 2002 [DIRS 158813]). Because bicarbonate is the principal ^{14}C-containing species in most groundwaters, the source of this additional bicarbonate can have a major impact on the "age" calculated from the ^{14}C activity of a given water sample. If the source is primarily decaying plant material in an active soil zone, the calculated "age" for the water sample should be close to the real age. On the other hand, if the source of the bicarbonate is dissolution of old ($\geq 10^4$ yr) calcite with low ^{14}C activity, the calculated age for the sample will be too old.

A useful measure of the source of the carbon in a water sample is the $\delta^{13}C$ value of the sample because this value is different for organic materials compared to calcites. The $\delta^{13}C$ value is defined as follows, and expressed in units of per mil:

$$\delta^{13}C = [(^{13}C/^{12}C)_{sample}/(^{13}C/^{12}C)_{standard} - 1] \times 1000 \quad \text{(Eq. A6-4)}$$

The standard used for reporting stable carbon isotope measurements is carbon from a belemnite fossil from the Cretaceous Pee Dee Formation in South Carolina (Clark and Fritz 1997 [DIRS 105738], p. 9).

The $\delta^{13}C$ values of carbon species typical of the soil waters in arid environments range from –25 to –13 per mil (Forester et al. 1999 [DIRS 109425], p. 36). At Yucca Mountain, pedogenic carbonate minerals have $\delta^{13}C$ values that generally are between –8 and –4 per mil, although early formed calcites are also present that have $\delta^{13}C$ values greater than 0 per mil (Forester et al. 1999 [DIRS 109425], Figure 16; Whelan et al. 1998 [DIRS 137305], Figure 5). Paleozoic carbonate rocks typically have $\delta^{13}C$ values close to 0 per mil (Forester et al. 1999 [DIRS 109425], Figure 16; Whelan et al. 1998 [DIRS 137305], Figure 5).

A6.3.1.2.3 Sulfur

Four stable isotopes of sulfur occur in nature; of these ^{32}S and ^{34}S are the most abundant. The sulfur isotopes are fractionated as a result of reduction of sulfate and by isotope exchange reactions. The isotopic composition of sulfur is expressed in terms of delta-^{34}S ($\delta^{34}S$) as defined by:

$$\delta^{34}S = [(^{34}S/^{32}S)_{sample}/(^{34}S/^{32}S)_{standard} - 1] \times 1{,}000 \quad \text{(Eq. A6-5)}$$

The standard used for reporting $\delta^{34}S$ is the troilite (FeS) phase of the Canon Diablo meteorite (CDT), which has a $^{34}S/^{32}S$ ratio of 0.0450. Analytical precision is generally greater than ±0.3 per mil (Clark and Fritz 1997 [DIRS 105738], p. 11).

In groundwater, sulfur is transported principally as the conservative ion SO_4^{2-} and thus is a potentially useful indicator of groundwater mixing. Dissolution of solids containing sulfur can also readily change the $\delta^{34}S$ of groundwater. Of particular importance for this study is the fact

the early Paleozoic marine carbonate that forms the carbonate aquifer near Yucca Mountain and, presumably, the groundwater from this aquifer, should both have distinctly high $\delta^{34}S$ values (25 to 30 per mil) compared to volcanic aquifer groundwater (Clark and Fritz 1997 [DIRS 105738], pp. 138 to 148, Figures 6-1 and 6-2). The $\delta^{34}S$ in volcanic environments is about 0 ±2 per mil where the sulfur is in a reduced oxidation state and ranges from about 3 to 15 per mil in more oxidizing environments (Clark and Fritz 1997 [DIRS 105738], Figure 6-1).

A6.3.1.2.4 Uranium

^{234}U ($t_{1/2}$ = 2.45 × 10^5 yr) (Cheng et al. 2000 [DIRS 153475], p. 17) is part of the ^{238}U ($t_{1/2}$ = 4.47 × 10^9 yr) radioactive decay series (Clark and Fritz 1997 [DIRS 105738], Table 1-3). The $^{234}U/^{238}U$ activity ratio in rocks is generally close to the secular equilibrium value 1. However, ^{234}U is typically enriched relative to ^{238}U in groundwater (Activity ratios > 1; Osmond and Cowart 1992 [DIRS 145190], Figure 9.1). The primary causes for this enrichment are: preferential dissolution of ^{234}U from crystallographic defects caused by alpha decay; the tendency for ^{234}U atoms to be converted to the more soluble uranyl ion due to the effects of radiation-induced ionization (Gascoyne 1992 [DIRS 127184], Section 2.5.1), and direct ejection of ^{234}Th (which decays in about 24 days to ^{234}U) into groundwater by alpha recoil. Uranium activity ratios may be lowered by release of uranium from rock and minerals with $^{234}U/^{238}U$ ratios near secular equilibrium through dissolution. Consequently, the $^{234}U/^{238}U$ activity ratios are the result of the competing effects of enrichment processes and dissolution of uranium-bearing material. Given the long half-life of ^{234}U relative to groundwater ages in this region, changes in the $^{234}U/^{238}U$ activity ratio due to ^{234}U decay are insignificant. Removal of uranium from solution by precipitation or sorption decrease U concentrations, but these processes do not affect the isotopic ratio. Therefore, the isotopic ratio should be relatively constant along a groundwater pathway unless additional U is added to the groundwater through mixing or by mineral or glass dissolution, or recoil-related processes.

A6.3.1.2.5 Strontium

Strontium is a trace constituent in groundwaters, with concentrations typically ranging from 10 µg/L to 1,000 µg/L. Strontium has four naturally occurring isotopes, ^{84}Sr, ^{86}Sr, ^{87}Sr and ^{88}Sr, all of which are stable. The absolute abundances of ^{84}Sr, ^{86}Sr and ^{88}Sr do not change. In contrast, the absolute abundance of ^{87}Sr is continually increasing because this nuclide is produced from decay of ^{87}Rb. Therefore, the $^{87}Sr/^{86}Sr$ ratios of rocks and minerals continually increase; the present day $^{87}Sr/^{86}Sr$ ratio depends on the relative abundances of Rb to Sr and on their age (Faure 1986 [DIRS 105559], Section 8). Strontium in groundwater is acquired from the materials through which the water passes. The $^{87}Sr/^{86}Sr$ ratios in groundwater will evolve toward the isotopic composition of the host material along its flow path as water-rock reaction progresses. Strontium isotope ratios can therefore provide a record of groundwater sources, flow pathways, and water-rock interaction.

Strontium isotope ratios are commonly expressed using the delta notation relative to a standard value according to the equation:

$$\delta^{87}Sr = [(^{87}Sr/^{86}Sr)_{sample}/(^{87}Sr/^{86}Sr)_{standard} - 1] \times 1{,}000 \quad \text{(Eq. A6-6)}$$

where the $(^{87}Sr/^{86}Sr)_{standard}$ value is modern seawater with a ratio of 0.7092.

Strontium in the oceans has a residence time of about 5,000,000 years, considerably longer than oceanic mixing times, which are on the order of 1,000 yrs (Faure 1986 [DIRS 105559], Section 11). As a result, the $^{87}Sr/^{86}Sr$ ratio of strontium in the open oceans is consistent globally. This ratio, however, has changed throughout the Phanerozoic in response to the relative contributions of the different rock types that are exposed to chemical weathering. The variations of the $^{87}Sr/^{86}Sr$ ratios throughout the Phanerozoic have been determined by analyzing unaltered samples of marine carbonate (e.g., Burke et al. 1982 [DIRS 162906]). This work and subsequent refinements by a number of other studies have produced a detailed history of the variations in oceanic $^{87}Sr/^{86}Sr$ ratios throughout the Phanerozoic. Such information can be quite useful when interpreting $^{87}Sr/^{86}Sr$ ratios of groundwater that has interacted with marine carbonate rock.

A6.3.2 Assignment and Description of Hydrochemical Groupings in the Vicinity of Yucca Mountain

Hydrochemical and isotopic data from over 200 groundwater samples are presented in this appendix. The locations of wells cited in this section are shown in Figure A6-5, with insets to show greater detail. As these maps show, the data are unevenly distributed throughout the Yucca Mountain region, with clusters of wells in central and northern Yucca Mountain, farming areas of the Amargosa Desert, and along U.S. Highway 95. Elsewhere, data are relatively sparse, particularly to the west and east of Yucca Mountain in Crater Flat and Jackass Flats, respectively. An important data gap also exists at Yucca Mountain itself, between the cluster of wells in central and northern Yucca Mountain, and the line of wells along U.S. Highway 95. The potential impact of these gaps in data coverage is to make mixing trends among groundwaters separated by the gaps less obvious.

To facilitate interpretation and discussion, these samples are assigned to 22 different groups. Each group is identified by a unique symbol and color, which are used in plots throughout. Samples are numbered sequentially within groups. Numbering within and between groups generally increases from north to south, with the exception of the last three groups, Mine Mountain, Amargosa Flat, and Funeral Mountains. All groupings are based largely on geographic distribution, or geographic affiliation. Hydrochemical similarities and/or trends were also considered in the group assignments. Accordingly, some groups show a relatively uniform hydrochemical composition, whereas others show a spread in hydrochemistry and were grouped to emphasize this transition. A brief geographic and hydrochemical description of each group follows. Hydrochemistry of all samples is shown on trilinear (Piper) and scatter plots (Figures A6-6 through A6-8), with the groups divided into three separate figures for clarity.

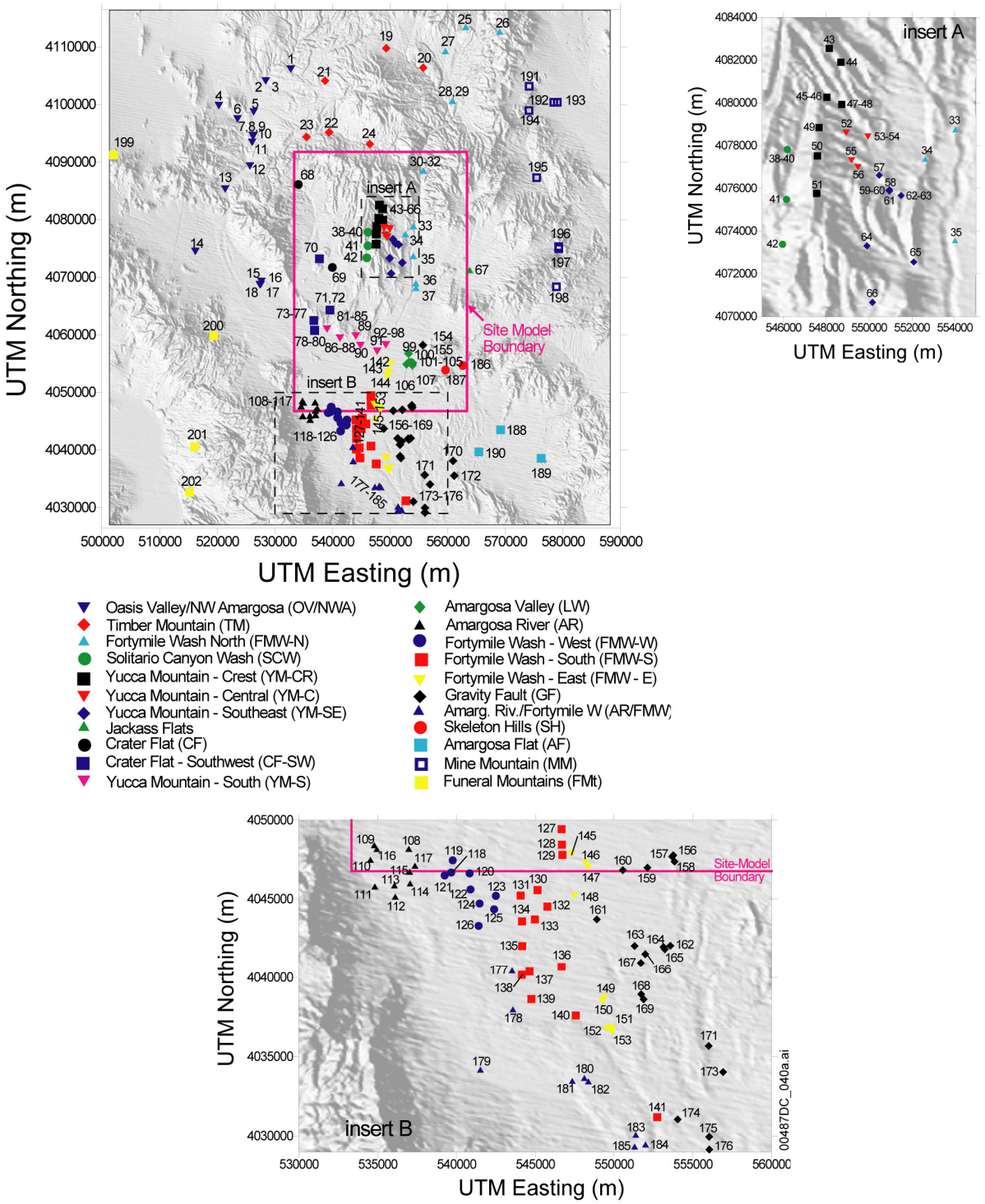

NOTES: The figure has color-coded data points and should not be read in a black and white version. The upper right panel corresponds to the area marked "insert A"; the lower panel corresponds to the area marked "insert B." Borehole numbers correspond to the names in Table A6-2.

UTM = Universal Transverse Mercator.

Figure A6-5. Locations of Boreholes in the Vicinity of Yucca Mountain and the Northern Amargosa Desert

The Oasis Valley/northwest Amargosa Desert group (OV/NWA) comprises boreholes located from the northern part of Oasis Valley extending southward along the course of the Amargosa River to the west and south of Bare Mountain. Boreholes drilled as part of the Nye County Early Warning Drilling Program (NC-EWDP) are located along the southern edge of Crater Flat and extend southeasterly into Fortymile Wash. Most of these wells have been assigned into two groupings, Crater Flat–southwest (CF-SW) and Yucca Mountain-south (YM-S), on the basis of geographic position and hydrochemistry. Two boreholes with similar chemistry comprise the Crater Flat group (CF). Boreholes to the north of Yucca Mountain are assigned to the Timber Mountain group (TM). A single borehole, though one with unique hydrochemical characteristics comprises the Jackass Flats group. Several tightly grouped boreholes along U.S. Highway 95 are assigned to the Amargosa Valley (formerly Lathrop Wells) group (LW). Finally, the boreholes in the northeast part of the study area are assigned to the Mine Mountain group.

Most groundwaters from these regions are a sodium-bicarbonate type (Figure A6-6). Notable exceptions are those samples from the SW Crater Flat Group and the Mine Mountain Group, which contain greater Ca^{2+} + Mg^{2+} relative to Na^{+} + K^{+}. These groundwaters either originate from the regional carbonate aquifer or have contacted alluvium derived from carbonate rocks and their greater Ca^{2+} + Mg^{2+} contents reflect the composition of these rock. The hydrochemical characteristics of groundwater beneath the broad area of Jackass Flats are represented by data from a single borehole (J-11), which has a unique chemical signature that may or may not be representative of regional groundwater flow in this area.

Boreholes at Yucca Mountain were divided into (1) a western group designated Solitario Canyon Wash (SCW), which includes samples from west of the Solitario Canyon fault, (2) a group of samples that encompasses the crest of Yucca Mountain (Yucca Mountain-Crest YM-CR), (3) a central group (Yucca Mountain Central, YM-C), which includes boreholes located within the central block of Yucca Mountain, and (4) a southeastern group (Yucca Mountain-Southeast, YM-SE), which includes boreholes along and south of Dune Wash. Boreholes near Fortymile Wash east and northeast of Yucca Mountain are assigned to a northern Fortymile Wash North group (FMW-N), distinguishing them from samples along the course of the Fortymile Wash in the Amargosa Desert (discussed below).

These groundwater are mostly sodium-bicarbonate water, typically with low total dissolved solids (TDS) (Figure A6-7). An important exception to this is the borehole p#1(c) sample from the YM-SE group (site 63), which penetrates to the carbonate aquifer. This sample is distinct from those from the volcanic aquifer in that it has higher calcium, magnesium, and TDS. The contribution of carbonate water in sample p#1(v) from the volcanic aquifer (site 62) is also evident in Figure A6-7. It was estimated that about 28.6% of the groundwater in this sample originated from upward flow in the borehole from the carbonate aquifer (Craig and Robison 1984 [DIRS 101040], p. 49).

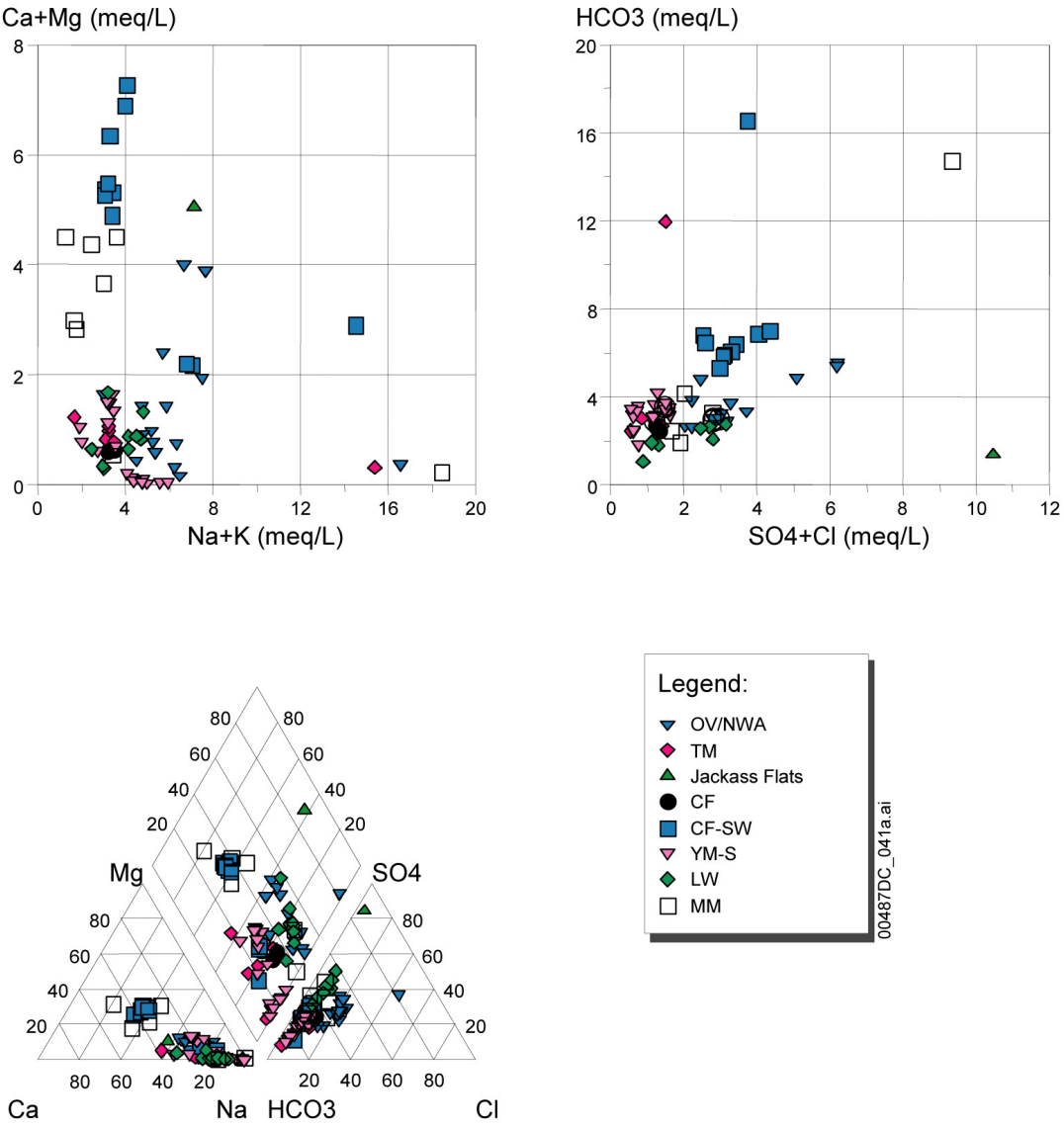

Source: Table A6-1.

NOTE: Units for the trilinear plots are percent milliequivalents per liter. Legend explained in Figure A6-5.

Figure A6-6. Trilinear and Scatter Plots for Samples that Surround Yucca Mountain But Are Generally North of the Amargosa Valley

Figure A6-8 shows hydrochemical characteristics from boreholes located south of U.S. Highway 95. The Amargosa River (AR) and Gravity fault (GF) groupings constitute boreholes located on the west and east sides of the Amargosa Desert, respectively. Groundwater from these groupings is typically sodium-calcium-bicarbonate-sulfate water type with higher TDS than samples in the central Amargosa Desert. Boreholes located along and near the main channel of Fortymile Wash in the Amargosa Desert are assigned to the Fortymile Wash-south (FMW-S) grouping. These are relatively dilute sodium-bicarbonate waters. The Amargosa River, Gravity fault and FMW-S groups, in general, represent three end-members of the hydrochemistry displayed in the Amargosa Desert region. Boreholes of the

Fortymile Wash-East (FMW-E), Fortymile Wash-West (FMW-W) and Amargosa River/Fortymile Wash (AR/FMW) groupings are transitional between these end members. Boreholes near the Skeleton Hills and Specter Range Thrust fault are grouped together as Skeleton Hills (SH). Boreholes in the far east of the study area are assigned to the Amargosa Flat group (AF), and finally, the widely spaced samples along the western part of the study area are grouped as the Funeral Mountains (FMt) group.

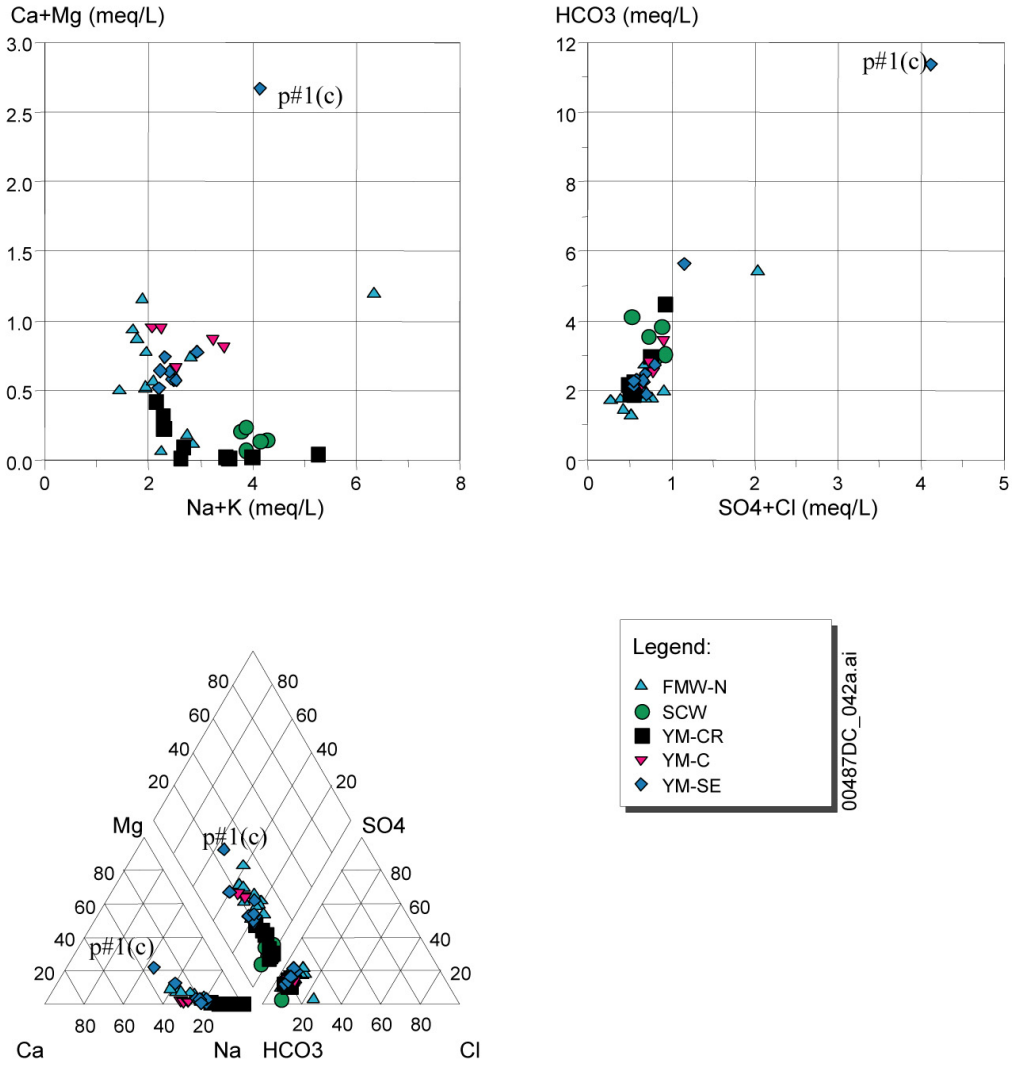

Source: Table A6-1.

NOTE: Units for the trilinear plots are percent milliequivalents per liter. Legend explained in Figure A6-5.

Figure A6-7. Trilinear and Scatter Plots for Samples from the Yucca Mountain Area

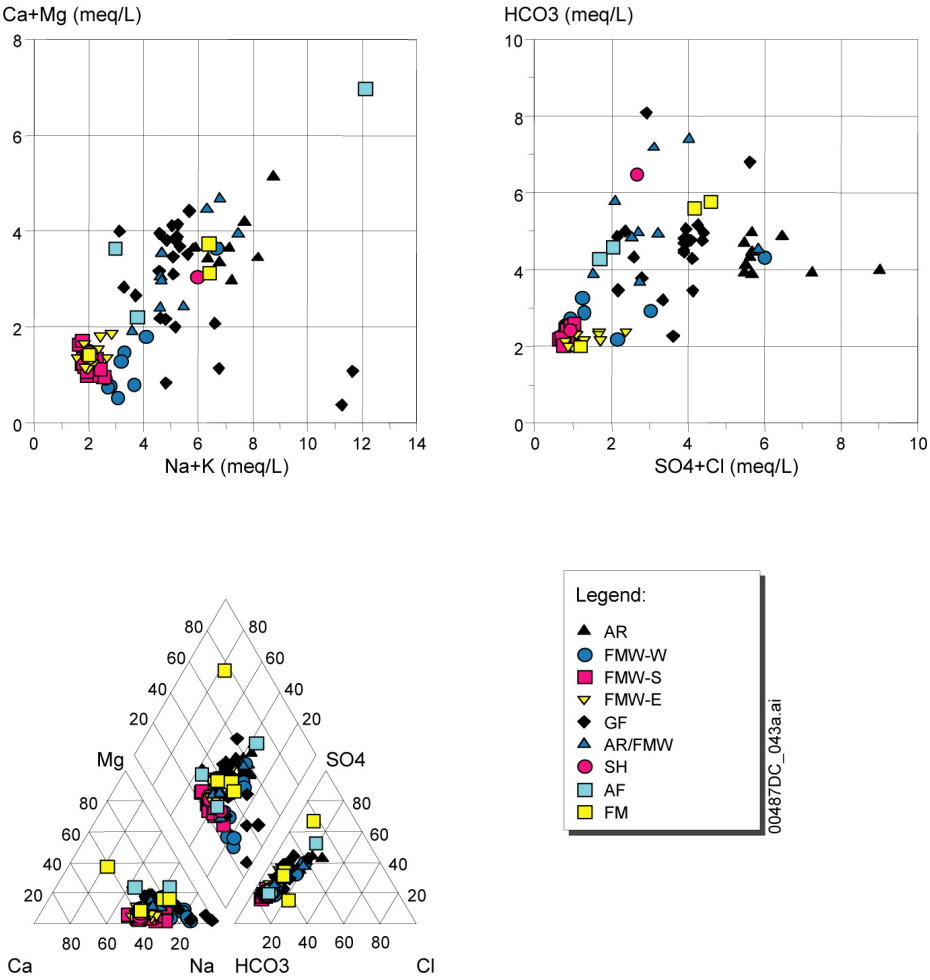

Source: Table A6-1.

NOTE: Units for the trilinear plots are percent milliequivalents per liter. Legend explained in Figure A6-5.

Figure A6-8. Trilinear and Scatter Plots for Samples from Groupings in the Amargosa Desert Region

A6.3.3 Depth-Dependent Trends in the Chemical and Isotopic Composition of Groundwater

This section describes groundwater samples from different depth intervals in single well or closely spaced wells to evaluate the relationship between hydrochemistry and depth and/or aquifer rock type. For most wells in the Yucca Mountain area, groundwater samples were obtained by pumping from an open borehole. In some boreholes, flow logs made during pumping indicate that much of the groundwater came from a relatively narrow depth interval, whereas in other boreholes, flow logs indicate the mixing of groundwater from different depth intervals. Sampling groundwater from an open borehole produces a groundwater composition that is naturally weighted by the permeability of the producing zones and which may be representative of the average composition of groundwater flowing past the open interval of the borehole (see Section A6.3.4). However, it may also result in artificial mixing of groundwaters that would not otherwise mix and thereby obscure compositional differences that reflect different groundwater sources and rates of groundwater movement. This section examines data from the

NC-EWDP wells obtained from discrete-interval sampling or from closely spaced wells and piezometers completed at different depths to assess the magnitude and importance of these differences.

A6.3.3.1 Boreholes NC-EWDP-19D and -19P

Groundwater samples were collected at borehole NC-EWDP-19D (Site 92) from the open borehole ("composite" sample), from the saturated alluvial section (Site 94), from zones 1 to 4 at different depth intervals within the alluvium (Sites 95–98), and from the alluvium at nearby piezometer NC-EWDP-19P (Site 93). The screened interval in NC-EWDP-19P (109.5– to 139.8-m depth) is slightly higher but overlaps with Zone 1 of NC-EWDP-19D (125.9 –131.4 m). The open borehole sample from NC-EWDP-19D included contributions from a lithic ash flow tuff between depths of 251 and 379 m, whereas the remainder of the groundwater samples originated from the alluvium overlying the tuffs (DTN: LA0311EK831223.001 [DIRS 165985]). The compositions of groundwater from the open-hole and the composite alluvial interval likely reflect the relative amounts of inflow from different zones into the borehole during pumping.

All of the groundwater samples from NC-EWDP-19D and -19P are characterized by low Cl-concentrations compared to Crater Flat area groundwater and very light $\delta^{18}O$ compared to northern Fortymile Wash area (FMW-N) groundwater found at boreholes J-13, J-12, and JF-3 (Tables A6-1 and A6-2). Samples from wells NC-EWDP-19P and -19D (Zone 2) have higher concentrations of Ca^{2+} and Sr^{2+} (not shown, see Table A6-2), lower concentrations of Na^{+} and HCO_3^{-}, heavier δD, and higher ^{14}C activity compared to other alluvial groundwater from well NC-EWDP-19D (Figure A6-9). These compositional characteristics are compatible with less water-rock interaction and short residence times of groundwater in this interval compared with other intervals in the alluvium. However, hydraulic testing (BSC 2004 [DIRS 170010]) at NC-EWDP-19D indicated that Zone 4 was the most permeable zone in the immediate vicinity of the borehole.

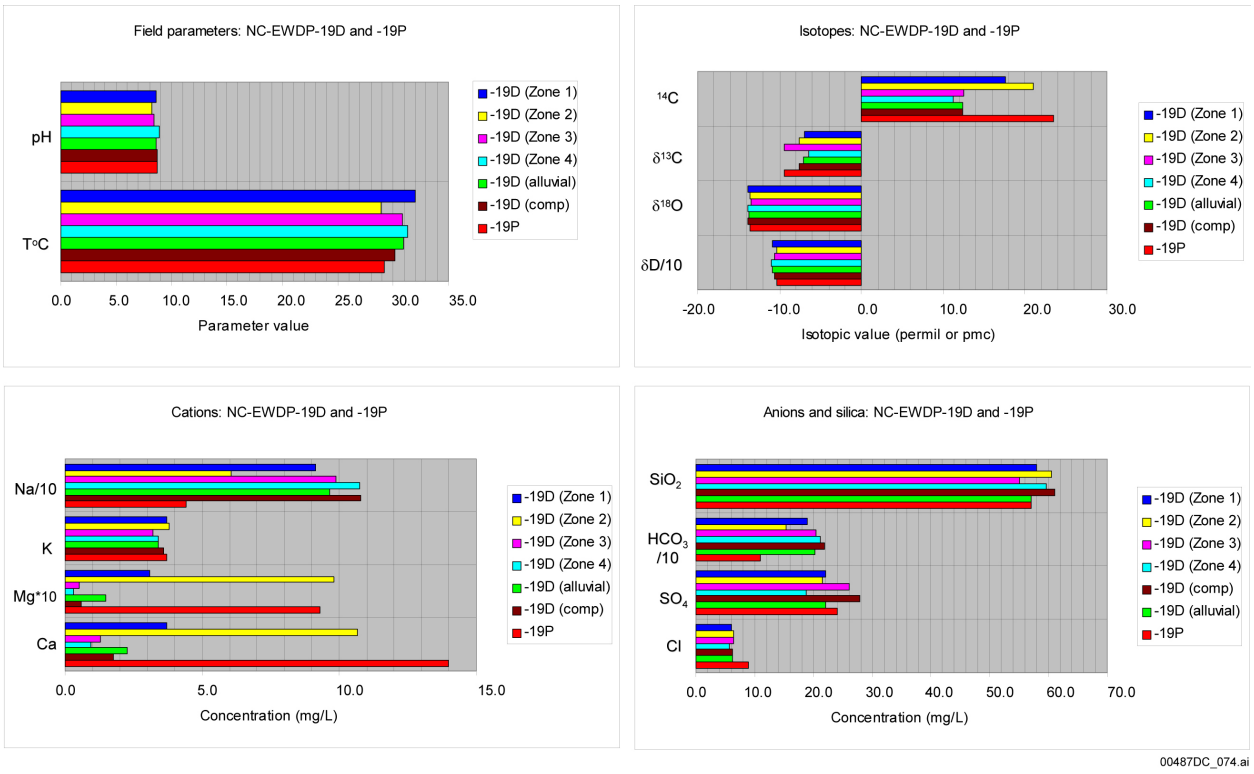

Source: Tables A6-1 and A6-2.

NOTE: For plotting purposes only, Mg^{2+} concentration has been multiplied by 10, and the values for Na^{+}, δD, and HCO_3^{-} have been divided by 10.

Figure A6-9. Plots of Selected Hydrochemical Constituents for the Different Depth Intervals of Boreholes NC-EWDP-19D and -19P

A6.3.3.2 Borehole NC-EWDP-9SX

Groundwater from four depth intervals in borehole NC-EWDP-9SX (Sites 82 to 85) originates from the upper 91 m of the SZ just south of Crater Flat. The groundwater over this relatively narrow depth range is similar in all four-depth intervals (Figure A6-10). In general, ^{14}C, $\delta^{13}C$, δD, Na^{+}, K^{+}, and Cl^{-} decrease slightly and HCO_3^{-} increases with depth in the borehole, but overall, there is relatively little chemical or isotopic variability within the depth range spanned by sampling Zones 1 to 4. In addition to the data shown in Figure A6-10, the Sr^{2+} concentration in Zone 1 is slightly less than in the other zones, but the $\delta^{87}Sr$, $\delta^{34}S$, and $^{234}U/^{238}U$ activity ratio data are very similar in all four zones (Table A6-2). The composite sample from borehole NC-EWDP-9SX (Site 81) has a composition that is similar to that of the individual zones but with slightly higher concentrations of Ca^{2+}, Mg^{2+}, Na^{+}, SO_4^{2-}, SiO_2, and Sr^{2+}. The remainder of the chemical and isotopic species of the composite sample is similar or intermediate to those of the four individual zones.

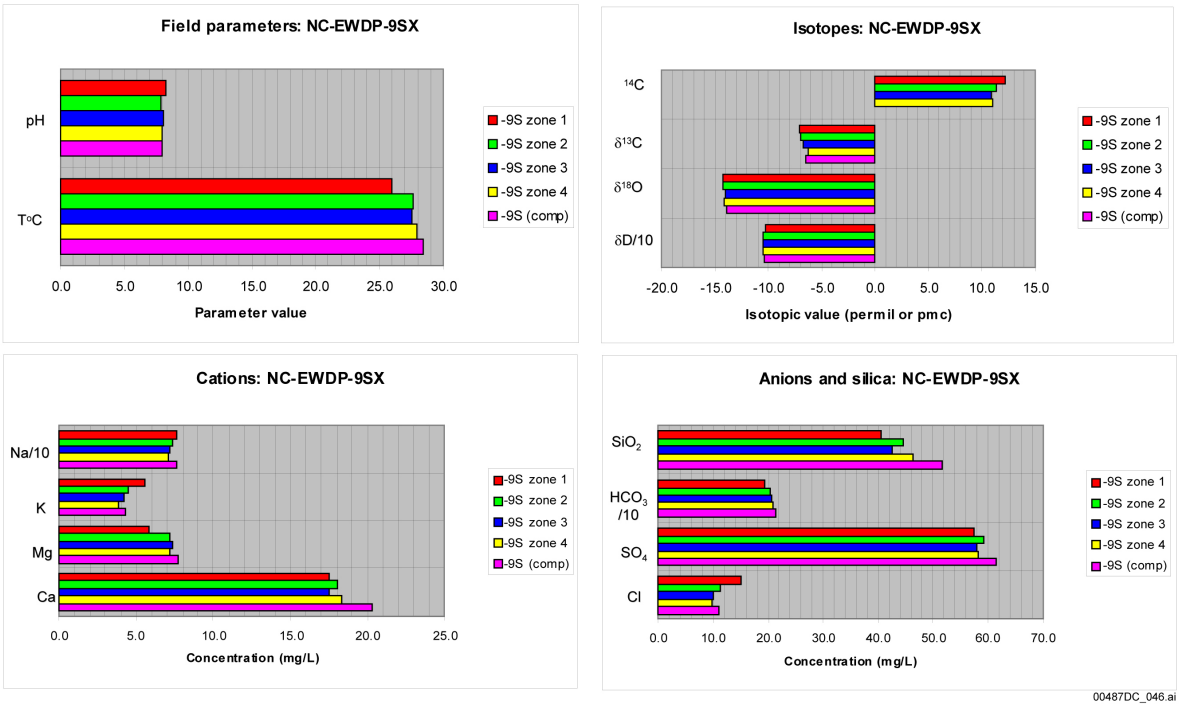

Sources: Tables A6-1 and A6-2.

NOTE: For plotting purposes only, the values for Na^+, δD, and HCO_3^- have been divided by 10.

Figure A6-10. Plots of Selected Hydrochemical Constituents for the Different Depth Intervals of Borehole NC-EWDP-9SX

A6.3.3.3 Boreholes NC-EWDP-1DX and -1S

Groundwater from shallow intervals (48.8–54.9 and 64.0–82.3 m) in borehole NC-EWDP-1S (Sites 75 to 76) shows large differences in both chemical and isotopic composition compared to deep groundwater (658.4 to 682.8 m) from Zone 2 (Site 74) in borehole NC-EWDP-1DX (Figure A6-11). Chemically, groundwater from Zone 2 in NC-EWDP-1DX has much higher Na^+, Sr^{2+} (not shown, see Table A6-2), Cl^-, F^- (not shown, see Table A6-2), and HCO_3^- concentrations and has lower pH and lower Ca^{2+} and SO_4^{2-} concentrations than the shallower groundwater from NC-EWDP-1S. The deep groundwater from Zone 2 of borehole NC-EWDP-1DX is heavier in $\delta^{13}C$ and $\delta^{34}S$ (not shown, see Table A6-2), lighter in $\delta^{18}O$ and δD, and has a lower $^{234}U/^{238}U$ activity ratio (not shown, see Table A6-2) than the shallow zones in NC-EWDP-1S (Figure A6-11 and Table A6-2). The composite groundwater samples from boreholes NC-EWDP-1S (Site 77) and NC-EWDP-1DX (Site 73) have similar isotopic and chemical compositions to the shallow groundwater samples from NC-EWDP-1S.

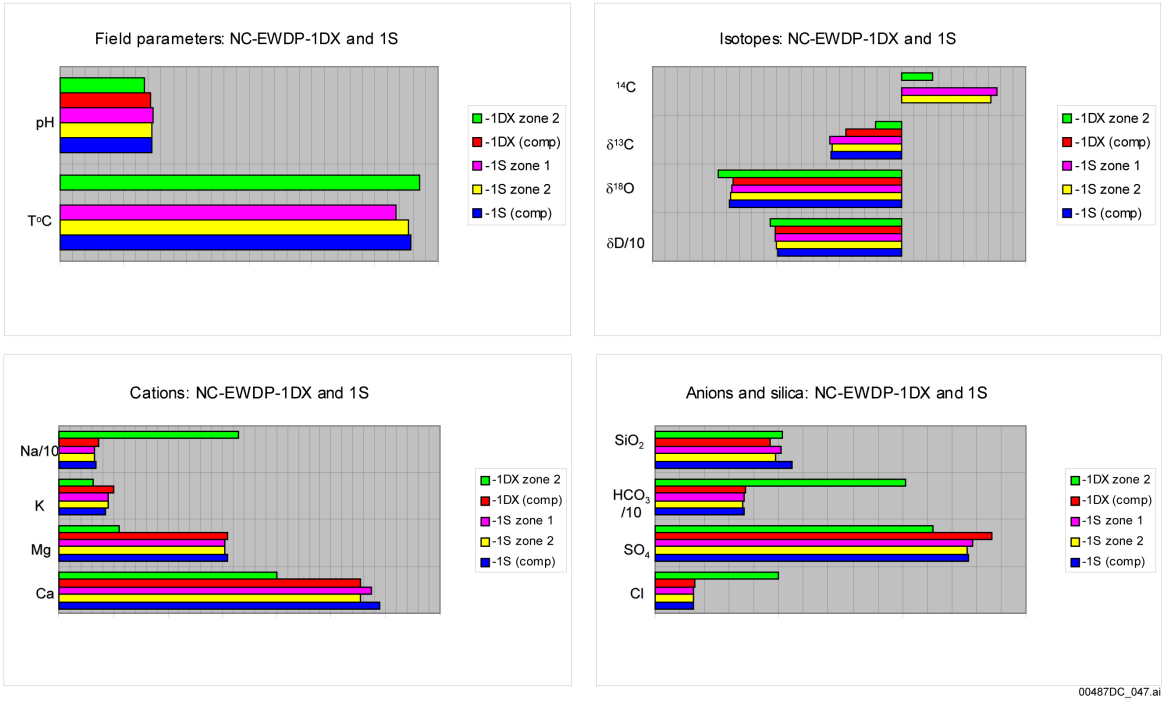

Sources: Tables A6-1 and A6-2.

NOTE: For plotting purposes only, the values for Na^+, δD, and HCO_3^- have been divided by 10.

Figure A6-11. Plots of Selected Hydrochemical Constituents for the Different Depth Intervals of Boreholes NC-EWDP-1S and -1DX

A6.3.3.4 Boreholes NC-EWDP-3D and -3S

Groundwater at NC-EWDP-3S was sampled from Zone 2 between depths of 103.6 and 128.0 m (site 87) and from Zone 3 between depths of 146.3 and 160.0 m (Site 88) (DTN: GS010308312322.003 [DIRS 154734]). Well NC-EWDP-3D (Site 86) was drilled to 762 m but was open between 159 to 292 m (DTN: LA0311EK831223.001 [DIRS 165985]). The groundwaters from these three sample locations have similar concentrations in most major ions with the exception that the sample from Zone 2 of NC-EWDP-3S is higher in Cl^- concentration, has higher ^{14}C, and is lighter in $\delta^{13}C$ compared to the other two samples (Figure A6-12). Compared to other wells in the YM-S group, groundwater samples from NC-EWDP-3D and -3S are very low in divalent cations, including Ca^{2+}, Mg^{2+}, and Sr^{2+} (not shown, see Table A6-2).

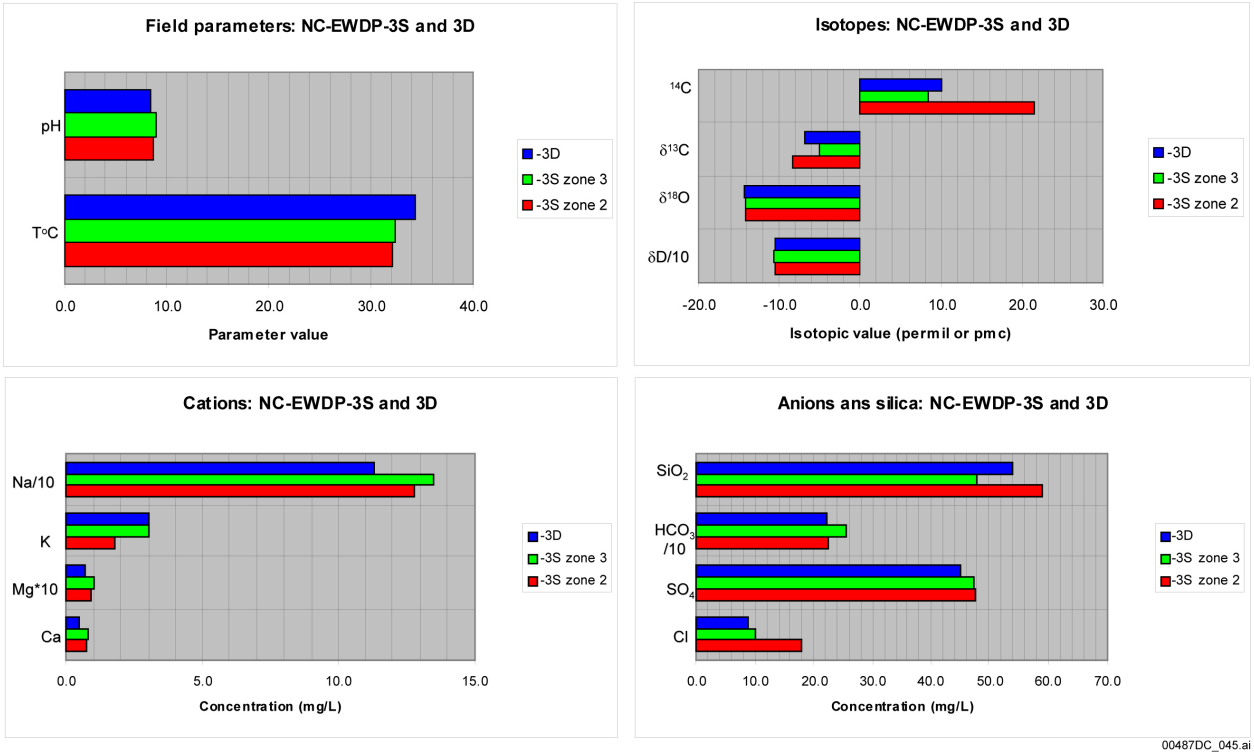

Sources: Tables A6-1 and A6-2.

NOTE: For plotting purposes only, Mg^{2+} concentration has been multiplied by 10, and the values for Na^{+}, δD, and HCO_3^{-} have been divided by 10.

Figure A6-12. Plots of Selected Hydrochemical Constituents for the Different Depth Intervals of Boreholes NC-EWDP-3S and -3D

A6.3.3.5 Boreholes NC-EWDP-12PA, -12PB, and -12PC

Boreholes NC-EWDP-12PA (Site 78), -12PB (Site 79), and -12PC (Site 80) form a piezometer nest in the northern Amargosa Desert just south of western Crater Flat. As shown in Table A4-3, the open intervals of the piezometers in boreholes NC-EWDP-12PA and NC-EWDP-12PB are located about 46 m below the open interval in NC-EWDP-12PC. Groundwater from boreholes NC-EWDP-12PA and NC-EWDP-12PB is very similar with respect to almost all chemical species and isotopes (Figure A6-13). The shallower groundwater from NC-EWDP-12PC is higher in ^{14}C, Ca^{2+}, Mg^{2+}, and SO_4^{2-}, lower in K^{+}, Na^{+}, HCO_3^{-}, F^{-} (not shown, see Table A6-2), and SiO_2, and lighter in $\delta^{13}C$ than groundwater from the other boreholes. The lower ^{14}C and heavier $\delta^{13}C$ of the groundwater in boreholes NC-EWDP-12PA and -12PB indicates the deep groundwater has interacted with more carbonate rocks. The geologic map of the NTS and vicinity shows that a slide block of carbonate sedimentary rock from Bare Mountain outcrops along the low ridge bordering southern Crater Flat just north of these boreholes (Slate et al. 2000 [DIRS 150228], Plate 1, p. 13). The groundwater at all three boreholes has similar $\delta^{18}O$ and δD to groundwater at borehole VH-2 in western Crater Flat (Table A6-2).

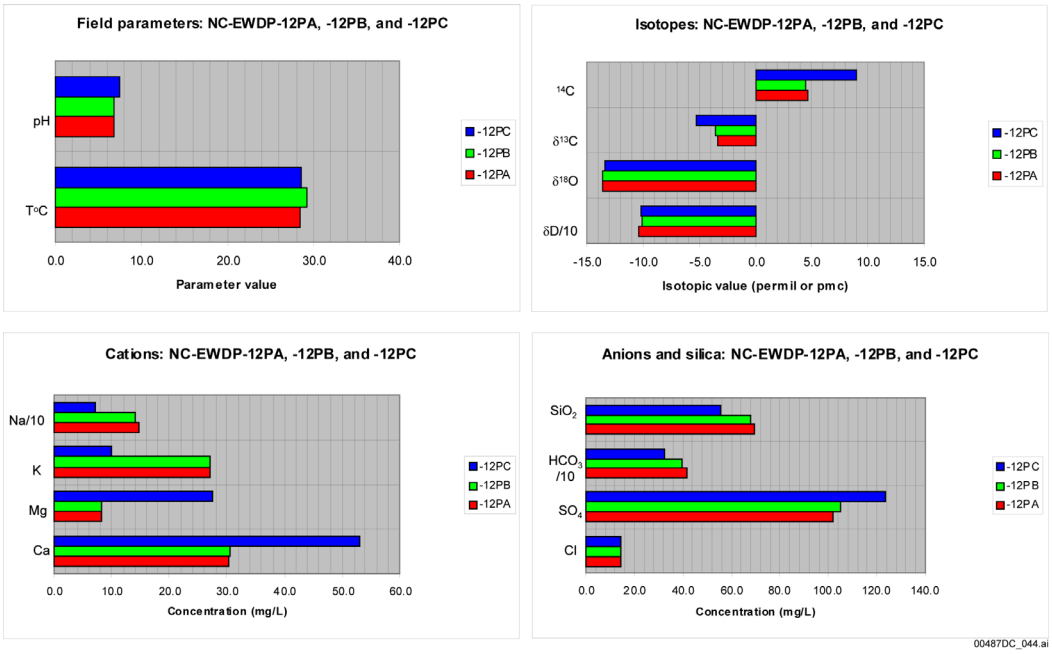

Sources: Tables A6-1 and A6-2.

NOTE: For plotting purposes only, the values for Na^+, δD, and HCO_3^- have been divided by 10.

Figure A6-13. Plots of Selected Hydrochemical Constituents for the Different Depth Intervals of Boreholes NC-EWDP-12PA, -12PB and -12PC

A6.3.3.6 Summary of Depth-Dependent Trends in Groundwater Compositions

Groundwater geochemical and isotopic data from five groups of NC-EWDP wells and piezometers along U.S. Highway 95 were examined to determine the extent of compositional changes with sampling depth. The changes with depth for most constituents were small at wells NC-EWDP-9SX, piezometers NC-EWDP-12PA, NC-EWDP-12PB and NC-EWDP-12PC, and wells NC-EWDP-3D and NC-EWDP-3S. This may be due, in part, to the relatively small range of depths sampled within each of these groups. For these groups, the composition of the groundwater sampled from the open borehole within the group does not substantially differ from any of the samples taken from a narrower depth interval. For wells NC-EWD-1DX and NC-EWD-1S, the deep (658.4–682.8 m) sample from Zone 2 of NC-EWDP-1DX (Site 74) is very different from the other samples in this group. However, groundwater from Zone 2 does not appear to contribute significantly to the composition of groundwater pumped from the open interval of NC-EWDP-1DX (Site 73), which more closely resembles shallow groundwater from nearby well NC-EWDP-1S. This observation indicates that the deep groundwater from Zone 2 at NC-EWDP-1DX may be relatively stagnant and not representative of the flowing groundwater composition at this location. Groundwaters from wells NC-EWDP-19D and NC-EWDP-19P have significant compositional variations with depth that indicate possible differences in groundwater sources, flow rates, or extent of water/rock interactions. The shallow groundwater from piezometer NC-EWDP-19P (Site 93) represents the composition of the shallowest and, perhaps, youngest groundwater in this area. The composite alluvial sample from well NC-EWDP-19D (Site 94) approximates the average composition of alluvial groundwater in this area.

A6.3.4 Areal Distributions of Chemical and Isotopic Species

In this section, areal distributions of values measured for the concentrations of major cations and anions and for isotopic ratios are presented, along with some preliminary analysis. The discussions of areal trends in individual chemical and isotopic constituents presented in this section are intended to be somewhat general in character. More detailed discussions are presented below. Many boreholes, particularly the Nye County-EWDP boreholes along U.S. Highway 95 (Yucca Mountain-South grouping) have numerous sampled intervals as discussed previously. In these cases, one value, which is considered to best represent the average value for that borehole and to best represent regional hydrochemical trends is plotted. Typically, data for groundwater samples pumped from the entire open interval of borehole are plotted in figures in Sections A6.3.4 and A6.3.5. Thus, the sampled groundwater compositions are naturally weighted toward the compositions in the most permeable intervals of the well, and the compositions of groundwater from less permeable zones attain less emphasis. These composite samples thus provide a good indication of the flux-weighted composition of groundwater actually moving past the well in the aquifer. (Note: One exception to this generalization exists in the case of NC-EWDP-19D, where the composite alluvial sample, rather than the composite borehole sample, was used.) Nonetheless, vertical heterogeneity displayed among the samples is recognized as an important element in evaluating the flow system. Although groundwater pumped from the open interval of a borehole may be representative of the average flowing composition, more detailed depth sampling, like that available for well NC-EWDP-19D (Section A6.3.3.1), does suggest that in some locations groundwaters may originate from different sources, travel at different velocities, or undergo different degrees of water/rock interaction. These groundwaters can become artificially mixed in samples pumped from large open intervals, partially obscuring details of the flow system.

A6.3.4.1 pH

Groundwater pH at Yucca Mountain varies between about 7 and 9 (Figure A6-14). Some of the higher pH values are found in the vicinity of Yucca Crest, with similarly high pH values found in groundwater associated with Solitario Canyon Wash. Groundwater in the carbonate aquifer at borehole p#1 (Site 63) has a distinctly lower pH value (6.6) compared to groundwater in the volcanic aquifer at Yucca Mountain. Groundwater to the north and northeast of Yucca Mountain also has a pH range of 7 to 9, with the highest values present in the northernmost part of Fortymile Wash. South of the northern boundary of the site model, groundwater pH along Fortymile Wash shows an overall increase from values of about 7.2 to 7.6 directly east of Yucca Mountain to values greater than 8 near Fortymile Wash in the Amargosa Desert. Groundwater pH values less than 8 generally are typical of the groundwater associated with the Amargosa River and Gravity fault areas (Figure A6-14).

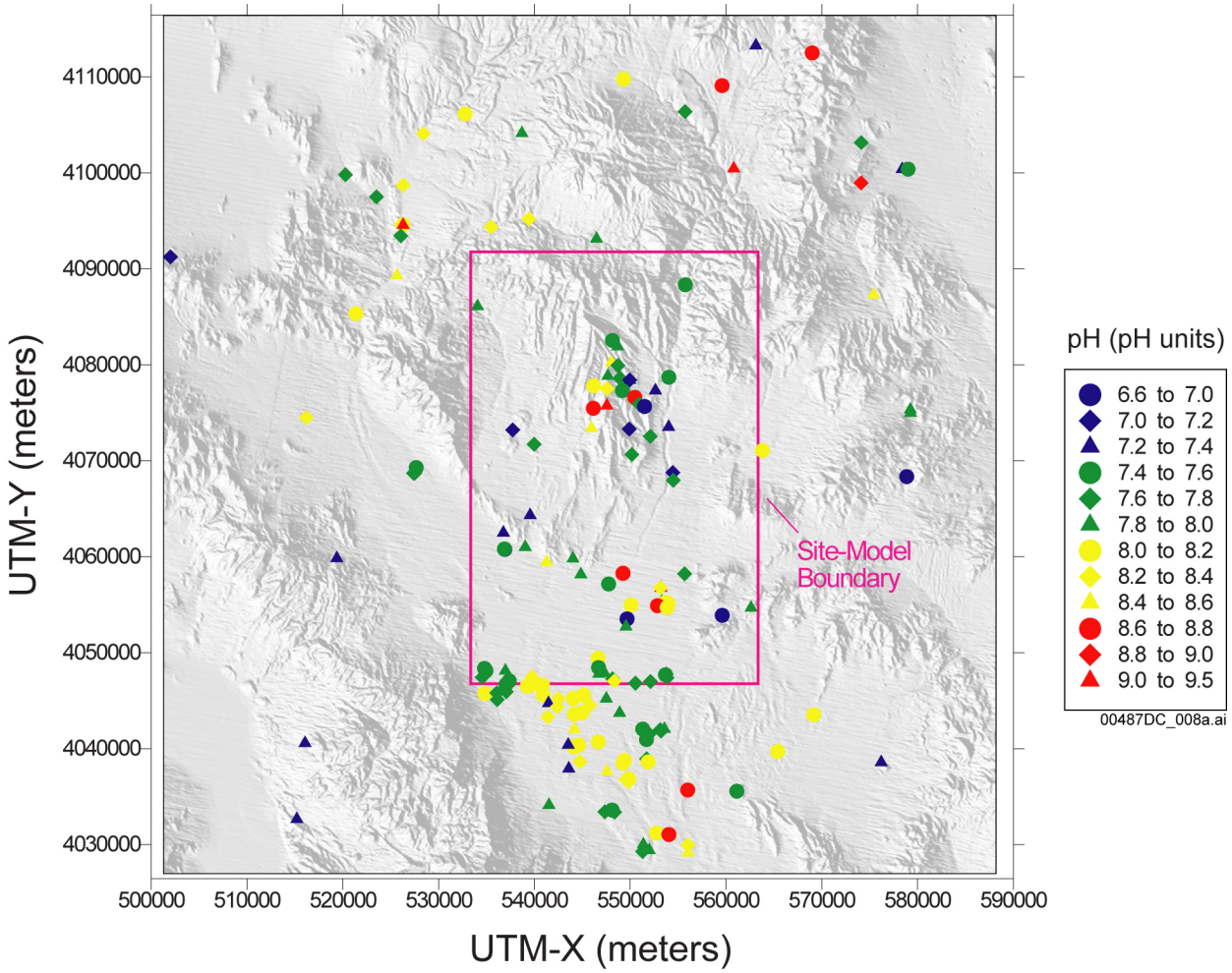

Source: Table A6-1.

NOTES: This figure has color-coded data points and should not be read in a black and white version. The pH is $-\log[H^+]$ where $[H^+]$ is the activity of hydrogen ion in moles/L.

UTM-X = UTM-Easting; UTM-Y = UTM-Northing; UTM = Universal Transverse Mercator.

Figure A6-14. Areal Distribution of pH in Groundwater

A6.3.4.2 Chloride

The chloride (Cl^-) concentrations of groundwater samples in the Yucca Mountain vicinity are shown in Figure A6-15. The areal distribution clearly shows coherent spatial patterns in Cl^-concentrations. Except for borehole p#1, where groundwater was sampled from the carbonate aquifer (Site 62) and from deep in the volcanic section (Site 62) where groundwater seems to be mixed with groundwater from the carbonate aquifer, the Cl^- concentrations of groundwater in the Yucca Mountain area generally are low (less than 9 mg/L) compared to areas to the west and east. Several wells to the north of Yucca Mountain in the Timber Mountain area have similarly low Cl^- concentrations. Groundwater from the Oasis Valley to the northwest of the site model area generally has Cl^- concentrations of 20 to 50 mg/L. These concentrations are slightly lower than the Cl^- concentrations of 50 mg/L or more measured in groundwater near the Nuclear Engineering Company (NEC) wells west of Bare Mountain or in groundwater in the southwest

corner of the site model boundary. Groundwater to the northeast and east of the site model boundary shows considerable variability between closely spaced wells, so that it is difficult to make generalizations about Cl^- concentrations in these areas.

Groundwater in eastern Crater Flat has low Cl^- concentrations compared to groundwater in western Crater Flat, a distinction that is preserved at the south end of Crater Flat at the NC-EWDP boreholes. One borehole at the southern end of Crater Flat (Site 71 – NC-EWDP-7S) has a relatively high Cl^- concentration of 18 to 20 mg/L. The depth to groundwater at this borehole is only about 7 m and groundwater in this area, like the shallow groundwater in Oasis Valley, may have been affected by evapotranspiration. Low Cl^- concentrations associated with the Fortymile Wash area east of Yucca Mountain extend southward into the Amargosa Desert, where the low-concentration zone is bounded by areas having substantially higher Cl^- concentrations.

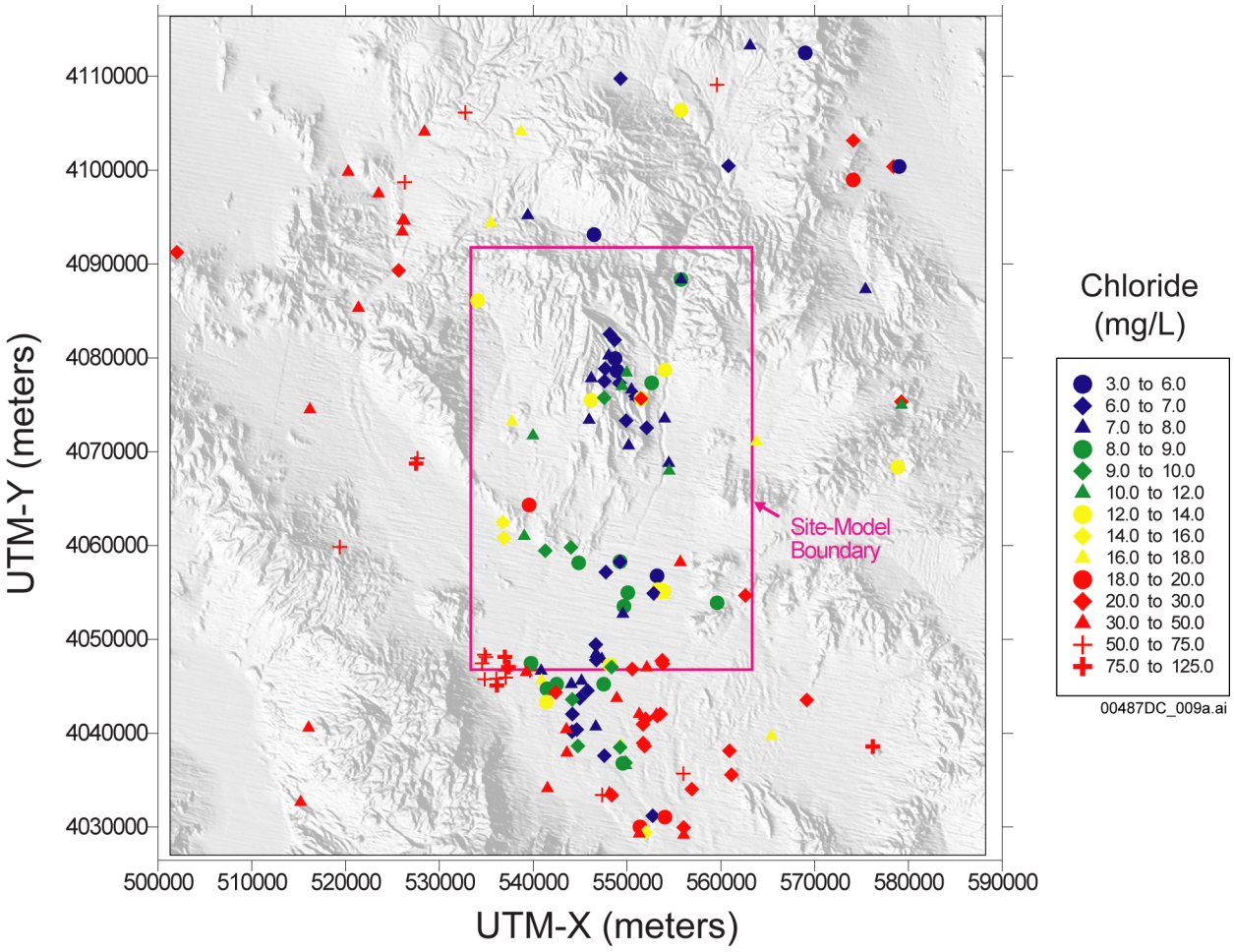

Source: Table A6-1.

NOTE: This figure has color-coded data points and should not be read in a black and white version.
UTM-X = UTM-Easting; UTM-Y = UTM-Northing; UTM = Universal Transverse Mercator.

Figure A6-15. Areal Distribution of Chloride in Groundwater

A6.3.4.3 Sulfate

The areal distribution of sulfate (SO_4^{2-}) (Figure A6-16) has patterns similar to those described for Cl^- (Figure A6-15). Except at borehole p#1 where the SO_4^{2-} concentrations are much higher, groundwater at Yucca Mountain generally has SO_4^{2-} concentrations less than 35 mg/L, whereas SO_4^{2-} concentrations west and east of Yucca Mountain are moderately to substantially higher. Borehole J-11 (Site 67) in central Jackass Flat has a SO_4^{2-} concentration of 479 mg/L. Groundwater north of Yucca Mountain at Timber Mountain and in the upper part of Fortymile Wash near Rainer Mesa has SO_4^{2-} concentrations in the same range as those found at Yucca Mountain. Groundwater SO_4^{2-} concentrations north of the site model area increase toward Oasis Valley. The compositional differences between groundwater in western and eastern Crater Flat observed in Cl^- concentrations are also evident in SO_4^{2-} concentrations, with the difference that the SO_4^{2-} concentration at Gexa Well 4 (Site 68) in the northwest corner of the site model area more closely resembles groundwater in eastern Crater Flat at borehole VH-1 (Site 69) rather than western Crater Flat at borehole VH-2 (Site 70). As is the case for Cl^-, the low SO_4^{2-} groundwater associated with Fortymile Wash east of Yucca Mountain also extends southward into the Amargosa Desert, where it is surrounded by groundwater having distinctly higher SO_4^{2-} concentrations. Unlike Cl^-, however, groundwater SO_4^{2-} concentrations increase toward the south along Fortymile Wash.

The groundwater with high Cl^- concentrations near the southwest corner of the site model area also has relatively high (100 to 200 mg/L) SO_4^{2-} concentrations. Groundwater to the north of this area in western Crater Flat and to the northwest in southern Oasis Valley has similarly high SO_4^{2-} concentrations.

A6.3.4.4 Bicarbonate

The areal distribution of bicarbonate (HCO_3^-) is shown in Figure A6-17. The areal patterns for HCO_3^- are similar to those described for SO_4^{2-} and Cl^- with some differences. Groundwater with high (greater than 200 mg/L) HCO_3^- concentrations is present in easternmost Crater Flat and western Yucca Mountain near Solitario Canyon. Elsewhere at Yucca Mountain, groundwater generally has HCO_3^- concentrations less than 175 mg/L. Groundwater near the Fortymile Wash drainage in the Amargosa Desert (FMW-S group) has much lower (less than 160 mg/L) HCO_3^- concentrations than groundwater in the surrounding areas in the GF, AR, and AR/FMW groups but has slightly higher HCO_3^- concentrations than groundwater upgradient along Fortymile Wash (FMW-N group).

Most groundwater in the TM group has HCO_3^- concentrations of 170 mg/L or greater with the exception of Site 24 (well ER-EC-07) in Beatty Wash, which has a concentration (148.8 mg/L) similar to that typically found in northern Yucca Mountain (120 to 140 mg/L). The moderately high HCO_3^- concentrations found in the Oasis Valley area increase southeastward along the Amargosa River toward the AR and AR/FMW group wells.

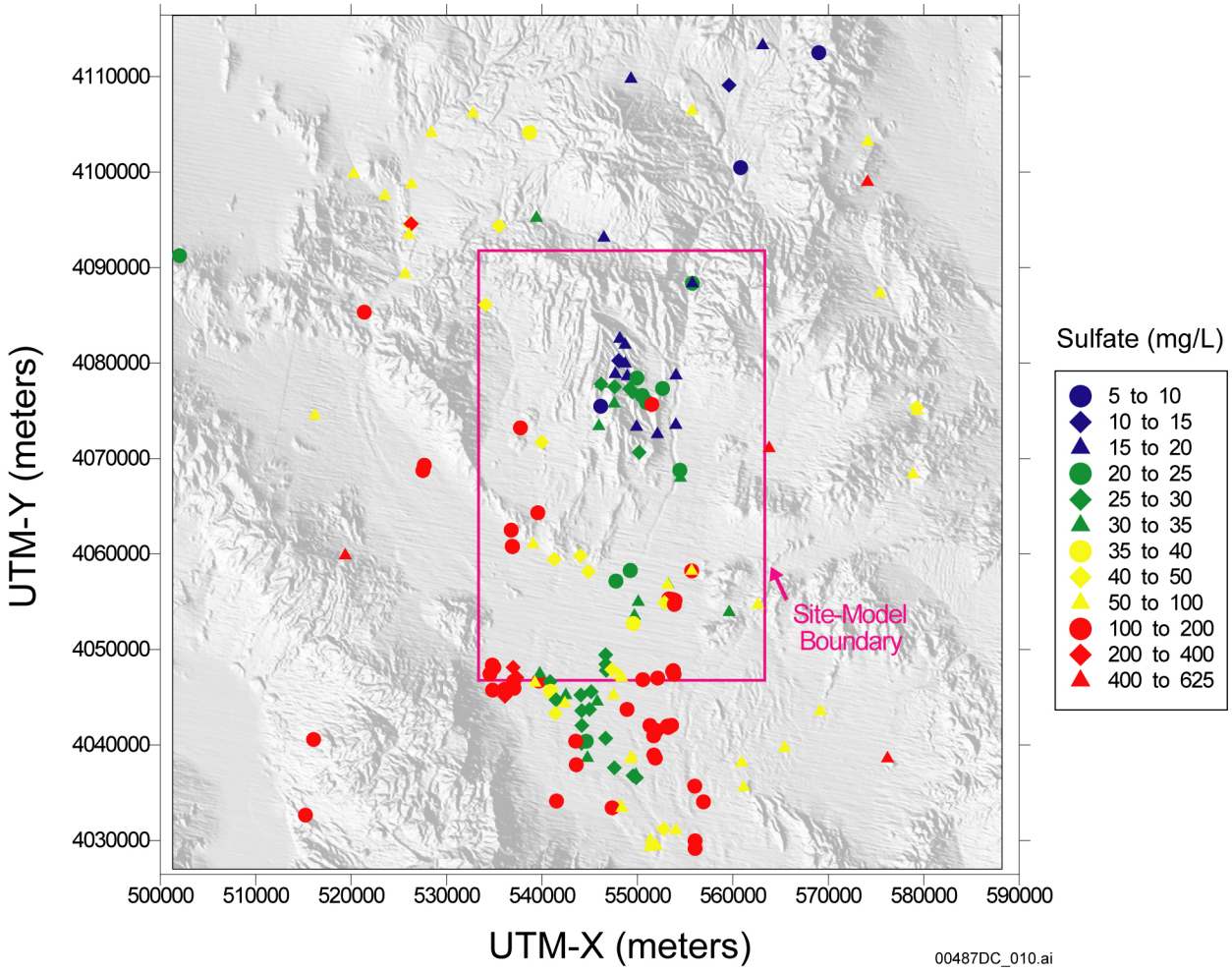

Source: Table A6-1.

NOTE: This figure has color-coded data points and should not be read in a black and white version.

UTM-X = UTM-Easting and UTM-Y = UTM-Northing. UTM = Universal Transverse Mercator.

Figure A6-16. Areal Distribution of Sulfate in Groundwater

Groundwater in southwestern Crater Flat (CF-SW group) has higher HCO_3^- than groundwater in the CF grouping. Bicarbonate concentrations at site NC-EWDP-7S (Site 71) are particularly high, possibly reflecting the location of this well in a paleospring deposit or evaporative effects associated with a shallow water table (Table A6-1). Groundwater in central Jackass Flats at borehole J-11 (Site 67), where the high SO_4^{2-} was noted previously, has one of the lowest HCO_3^- concentrations (82 mg/L) in the map area. Similarly low HCO_3^- concentrations are found in some of the LW group wells to the southwest of borehole J-11.

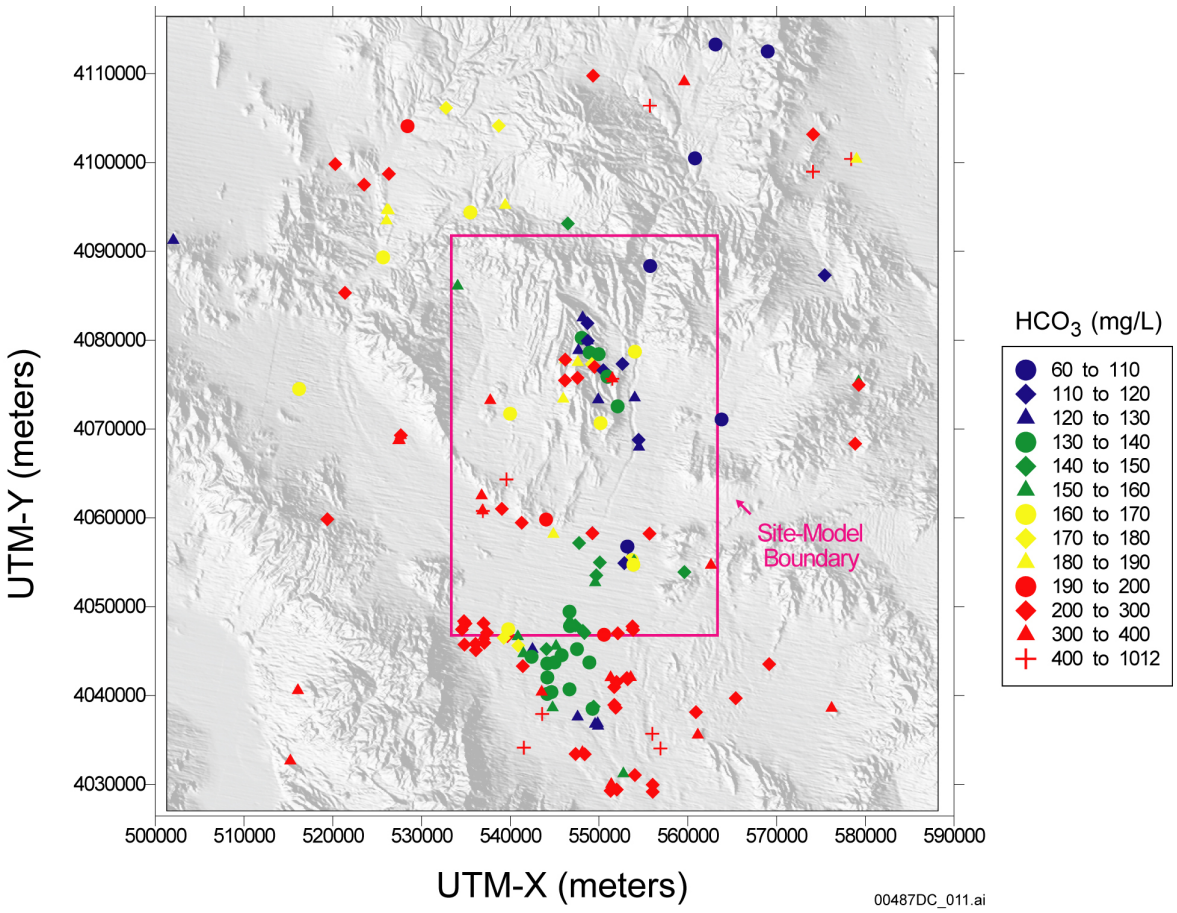

Source: Table A6-1.

NOTE: This figure has color-coded data points and should not be read in a black and white version.

UTM-X = UTM-Easting; UTM-Y = UTM-Northing; UTM = Universal Transverse Mercator.

Figure A6-17. Areal Distribution of Bicarbonate in Groundwater

A6.3.4.5 Fluoride

Few data for F^- concentrations are available for the Yucca Mountain. (Figure A6-18). These data are consistent with the concentration distributions for other anions like Cl^- (Figure A6-15) in this area, with dilute concentrations found near Fortymile Wash and concentrations that increase to the west and east of the wash. Groundwater fluoride concentrations at Yucca Mountain have a variability that is comparable to the variability found in the Yucca Mountain region as a whole (Figure A6-18). The F^- concentrations in northern Yucca Mountain are low compared to other areas of Yucca Mountain. Relatively high F^- concentrations of 4.5 to 13.0 mg/L are found in groundwater at several wells along Yucca Crest (YM-CR group), in the Solitario Canyon Wash (SWC) group, and in the carbonate aquifer at well p#1 (Sites 62 and 63). Groundwater along Fortymile Wash has F^- concentrations that generally vary between 1 and 2 mg/L, with no systematic north–south variations evident. Groundwater in southwest Crater Flat has lower F^- concentrations than groundwater in eastern Crater Flat or in the NC-EWDP wells farther to the east.

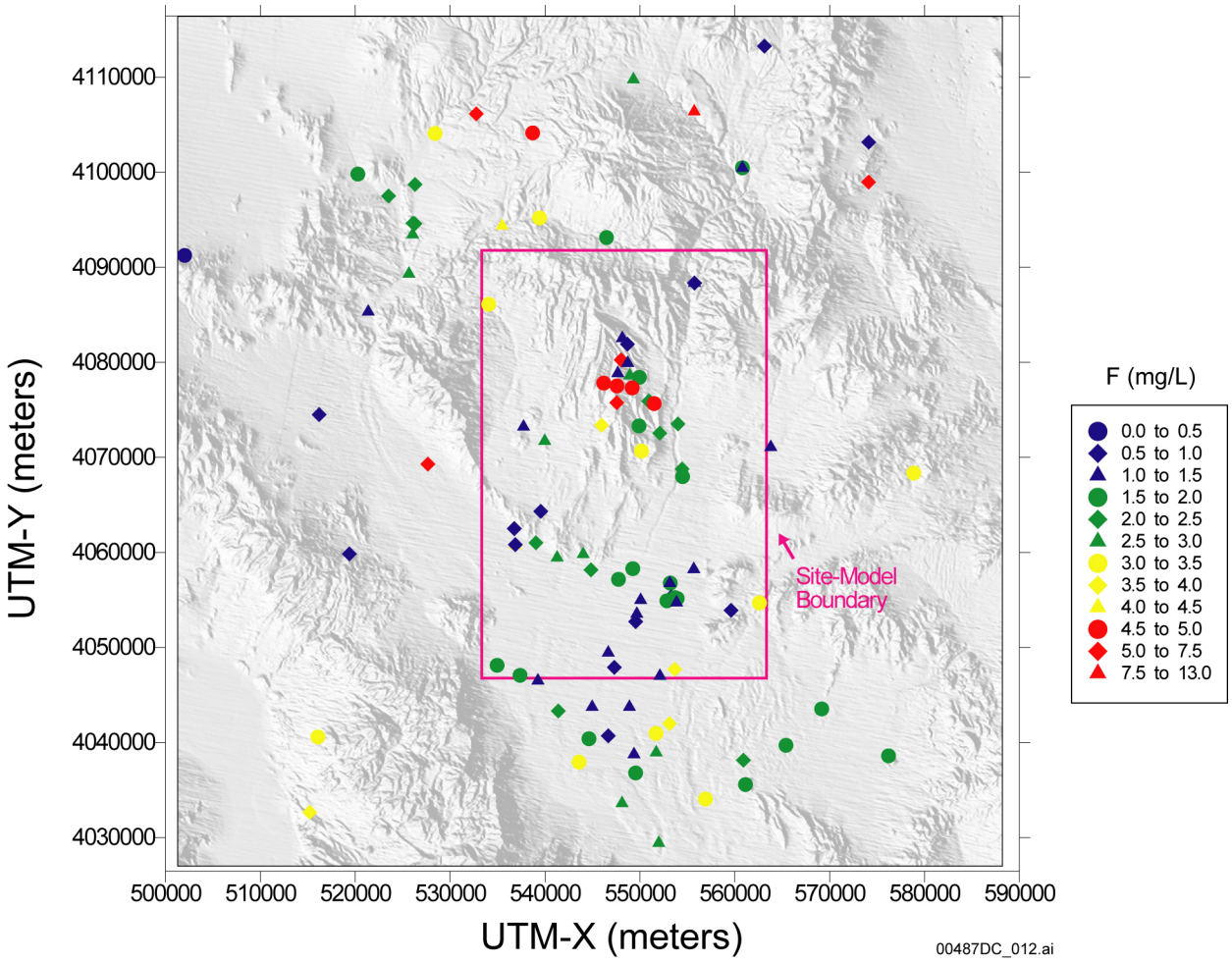

Source: Table A6-1.

NOTE: This figure has color-coded data points and should not be read in a black and white version.

UTM-X = UTM-Easting; UTM-Y = UTM-Northing; UTM = Universal Transverse Mercator.

Figure A6-18. Areal Distribution of Fluoride in Groundwater

A6.3.4.6 Silica

Groundwater in northern and central Yucca Mountain has SiO_2 concentrations that range from 30 to 60 mg/L (Figure A6-19). Groundwater beneath Fortymile Wash east of Yucca Mountain has SiO_2 concentrations that are approximately 50 to 60 mg/L. Southward from Yucca Mountain and along Fortymile Wash, SiO_2 concentrations in groundwater near the southern site model boundary increase abruptly. Relatively high SiO_2 concentrations (65 to 90 mg/L) characterize groundwater throughout most of Amargosa Desert and can also be traced southeastward from the Oasis Valley area through the northwest Amargosa Desert. An exception to this general trend is the area near the Gravity fault where SiO_2 concentrations are considerably lower. Most groundwater in the alluvium near the Gravity Fault is thought to originate from the lower carbonate aquifer where this aquifer abuts low permeability alluvium along the Gravity Fault. Groundwater from the carbonate aquifer typically contains lower SiO_2 concentrations (median, 8 to 31 mg/L) compared to groundwater in the volcanic aquifer (median, 44 to 85 mg/L)

(comparison of SiO_2 in Facies I and III to that in Facies II, Winograd and Thordarson 1975 [DIRS 101167], Table 8). This interpretation is also consistent with the generally higher bicarbonate, Ca, and Mg concentrations, and heavier stable carbon isotope ratios, in groundwater in the alluvium near the fault (as discussed in Sections A6.3.4.4, A6.3.4.7, A6.3.4.8, and A6.3.4.14, respectively).

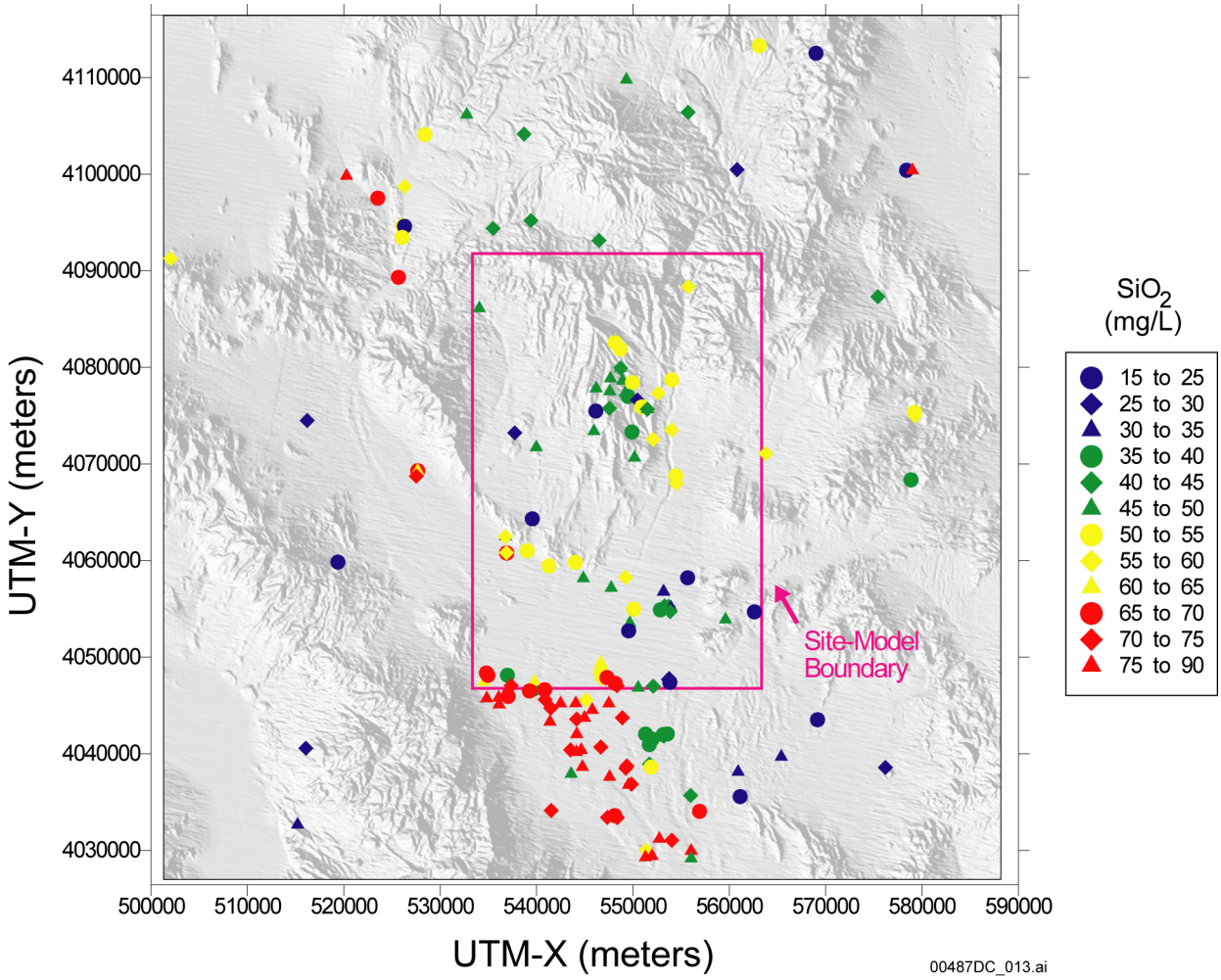

Source: Table A6-1.

NOTE: This figure has color-coded data points and should not be read in a black and white version.

UTM-X = UTM-Easting; UTM-Y = UTM-Northing; UTM = Universal Transverse Mercator.

Figure A6-19. Areal Distribution of Silica in Groundwater

A6.3.4.7 Calcium

The calcium (Ca^{2+}) concentrations of groundwater at Yucca Mountain are generally less than 20 mg/L (Figure A6-20), except at borehole p#1 (Site 63), where groundwater from the carbonate aquifer has a concentration of 100 mg/L. Along the eastern edge of Crater Flat and in western Yucca Mountain, Ca^{2+} concentrations are less than 5 mg/L. The Ca^{2+} concentration is higher in western Crater Flat at borehole VH-2 (Site 70) than in eastern Crater Flat at borehole

VH-1 (Site 69). The Ca^{2+} concentration at Gexa Well 4 in the northwest corner of the site model area is similar to the value at VH-1 and at NC-EWDP wells southeast of Crater Flat (Yucca Mountain-South group). The Ca^{2+} concentration is relatively high (82 mg/L) at borehole J-11 (Site 67) in central Jackass Flats, where SO_4^{2-} is also relatively high (Figure A6-16). The Ca^{2+} concentration along Fortymile Wash is between 10 and 20 mg/L east and northeast of Yucca Mountain and increases to values generally between 20 and 30 mg/L in the Amargosa Desert.

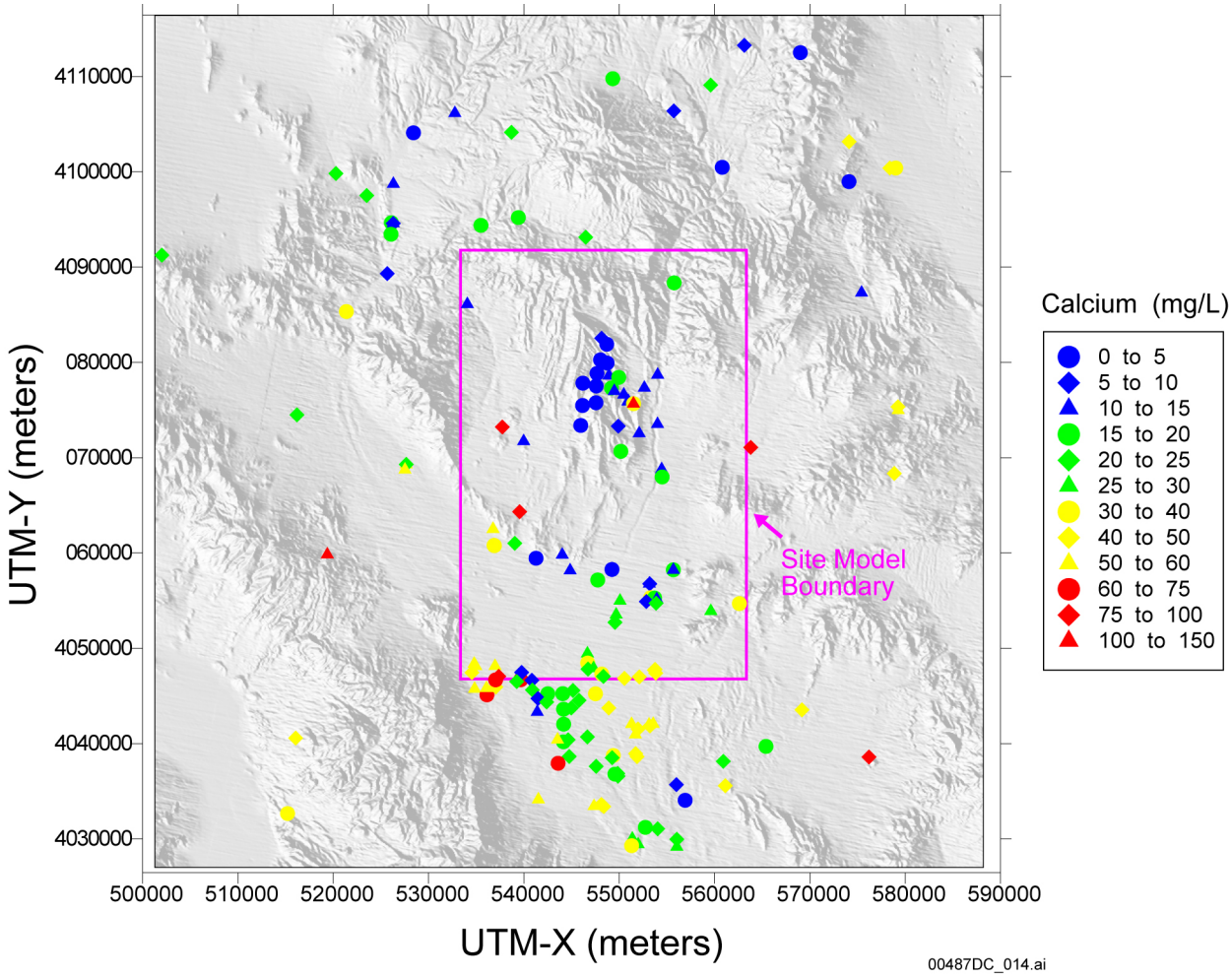

Source: Table A6-1.

NOTE: This figure has color-coded data points and should not be read in a black and white version.

UTM-X = UTM-Easting; UTM-Y = UTM-Northing; UTM = Universal Transverse Mercator.

Figure A6-20. Areal Distribution of Calcium in Groundwater

The Ca^{2+} concentration increases to the west and the east of Fortymile Wash in the Amargosa Desert. Groundwater Ca^{2+} concentrations in the southwest corner of the site model area (Amargosa River group) are generally higher than Ca^{2+} concentrations in upgradient areas in western Crater Flat, west of Bare Mountain, and in the Oasis Valley.

A6.3.4.8 Magnesium

The areal distribution of magnesium (Mg^{2+}) concentrations (Figure A6-21) display a pattern that is similar, in terms of relative concentrations, to that of Ca^{2+}. Magnesium concentrations in groundwater at Yucca Mountain range from 0.1 to 1.6 mg/L, except at borehole p#1 where the Mg^{2+} concentration is 10 mg/L in the volcanic aquifer and 39 mg/L in the carbonate aquifer. The Mg^{2+} concentration in groundwater in western Crater Flat at borehole VH-2 (Site 70) is high (30 mg/L) compared to the concentration of 1.5 mg/L measured in groundwater at borehole VH-1 (Site 69). In Nye County-EWDP wells south and southeast of Crater Flat (SW Crater Flat and Yucca Mountain-South groups), Mg^{2+} concentrations are quite variable with concentrations generally increasing to the northwest. Concentrations of Mg^{2+} are generally low (less than 1.5 mg/L) at Timber Mountain and in upper Fortymile Canyon, but are generally between 2 and 3 mg/L along the length of Fortymile Wash east of Yucca Mountain and in the Amargosa Desert. Magnesium concentrations on the east and west side of the Amargosa Desert are considerably higher with values typically between 5 and 20 mg/L. In the southwest corner of the model area (Amargosa River group), Mg^{2+} concentrations generally are between 5 to 10 mg/L, but a few samples have concentrations between 10 and 20 mg/L, similar to the concentration of groundwater at the sites 15 to 17 west of Bare Mountain (11.5 to 16 mg/L), but higher than those in Oasis Valley. The concentration of Mg^{2+} is 13 mg/L at borehole J-11 (Site 67) in central Jackass Flats.

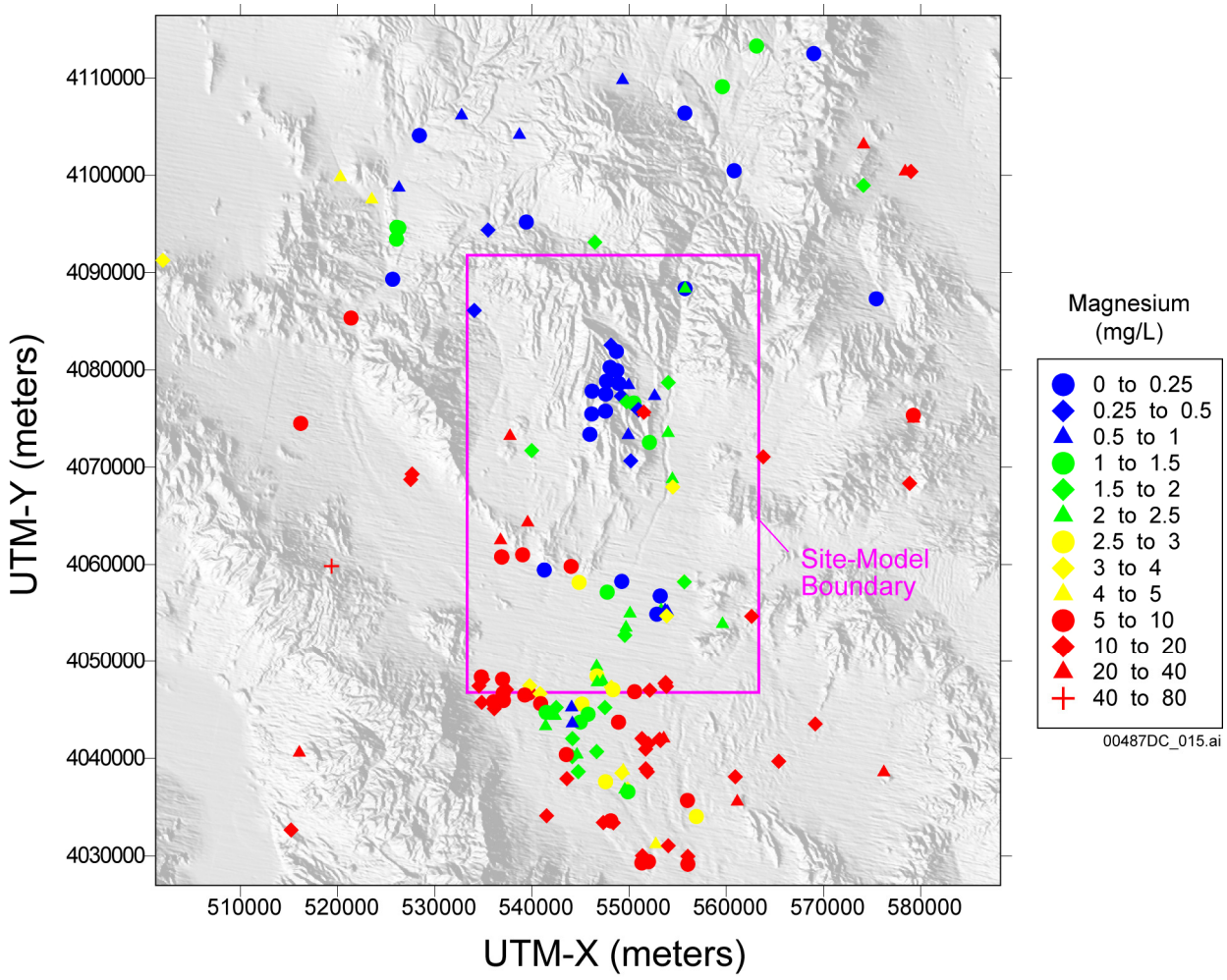

Source: Table A6-1.

NOTE: This figure has color-coded data points and should not be read in a black and white version.

UTM-X = UTM-Easting; UTM-Y = UTM-Northing; UTM = Universal Transverse Mercator.

Figure A6-21. Areal Distribution of Magnesium in Groundwater

A6.3.4.9 Sodium

The areal distribution of sodium (Na^+) is shown in Figure A6-22. Excluding data from the carbonate aquifer (borehole p#1), the Na^+ concentrations of groundwater at Yucca Mountain range between 46 and 130 mg/L with the higher values from samples in the western part of Yucca Mountain (Solitario Canyon Wash and Yucca Crest groups). A zone of relatively low Na^+ concentrations (less than 60 mg/L) extends southeastward from northern Yucca Mountain toward lower Dune Wash and Fortymile Wash. The Na^+ concentrations of groundwater in the NC-EWDP boreholes west of Fortymile Wash are generally between 40 and 100 mg/L, except at boreholes NC-EWDP-3D and NC-EWDP-3S (Sites 86 to 88) where the Na^+ concentration was anomalously high (113 to 135 mg/L). The Na^+ concentrations of groundwater at borehole NC-EWDP-5S (Site 154) west of the Striped Hills and at well J-11 (Site 67) in central Jackass Flats are also high (149 and 154 mg/L, respectively [Table A6-1]). Note that the value of

149 mg/L at NC-EWDP-5S listed in Table A6-1 is obscured in Figure A6-22 by the somewhat lower value of 107 mg/L at nearby Site 155. Most of the groundwater samples along Fortymile Wash have Na^+ concentrations between 35 and 50 mg/L; there are not any obvious trends in the Na^+ concentrations of groundwater beneath Fortymile Wash east of Yucca Mountain and beneath the wash in the Amargosa Desert. In the Amargosa Desert, Na^+ concentrations in groundwater increase away from Fortymile Wash in both eastward and westward directions. Groundwater in the southwest corner of the site model area (Amargosa River group) has high Na^+ concentrations (130 to 180 mg/L), similar to those of sites 15 to 17 west of Bare Mountain and groundwater in Oasis Valley.

A6.3.4.10 Potassium

Potassium (Figure A6-23) concentrations in groundwater at Yucca Mountain range between 1 and 6 mg/L, except in the carbonate aquifer at borehole p#1 (Site 63) where the K^+ concentration is 12 mg/L. Groundwater from the Solitario Canyon and Yucca Crest groups typically has smaller K^+ concentration when compared to groundwater farther east at Yucca Mountain in the FMW-N group. The K^+ concentrations in groundwater in western Crater Flat at borehole VH-2 (Site 70) is high (8 mg/L). Similarly high K^+ concentrations are found south of VH-2 in Nye County-EWDP wells 1S (Site 77) and 1DX (Site 73) and even higher concentrations exist at NC-EWDP-12PA (Site 78) and -12PB (Site 79). Concentrations of K^+ are generally low (less than 5 mg/L) in northern Fortymile Canyon but are generally between 5 and 8 mg/L along the length of Fortymile Wash east of Yucca Mountain and in the Amargosa Desert. In the eastern and western parts of the Amargosa Desert, K^+ concentrations are typically higher than those in groundwater near the adjacent reach of Fortymile Wash. However, even among the FMW-S samples along Fortymile Wash, K^+ concentrations are two to three times higher than K^+ concentrations in upgradient areas in the southern Yucca Mountain (YM-S) group. Potassium concentrations in the Amargosa River (AR) group are similar to those of groundwater at Sites 15 through 17 west of Bare Mountain and somewhat higher than those found in Oasis Valley.

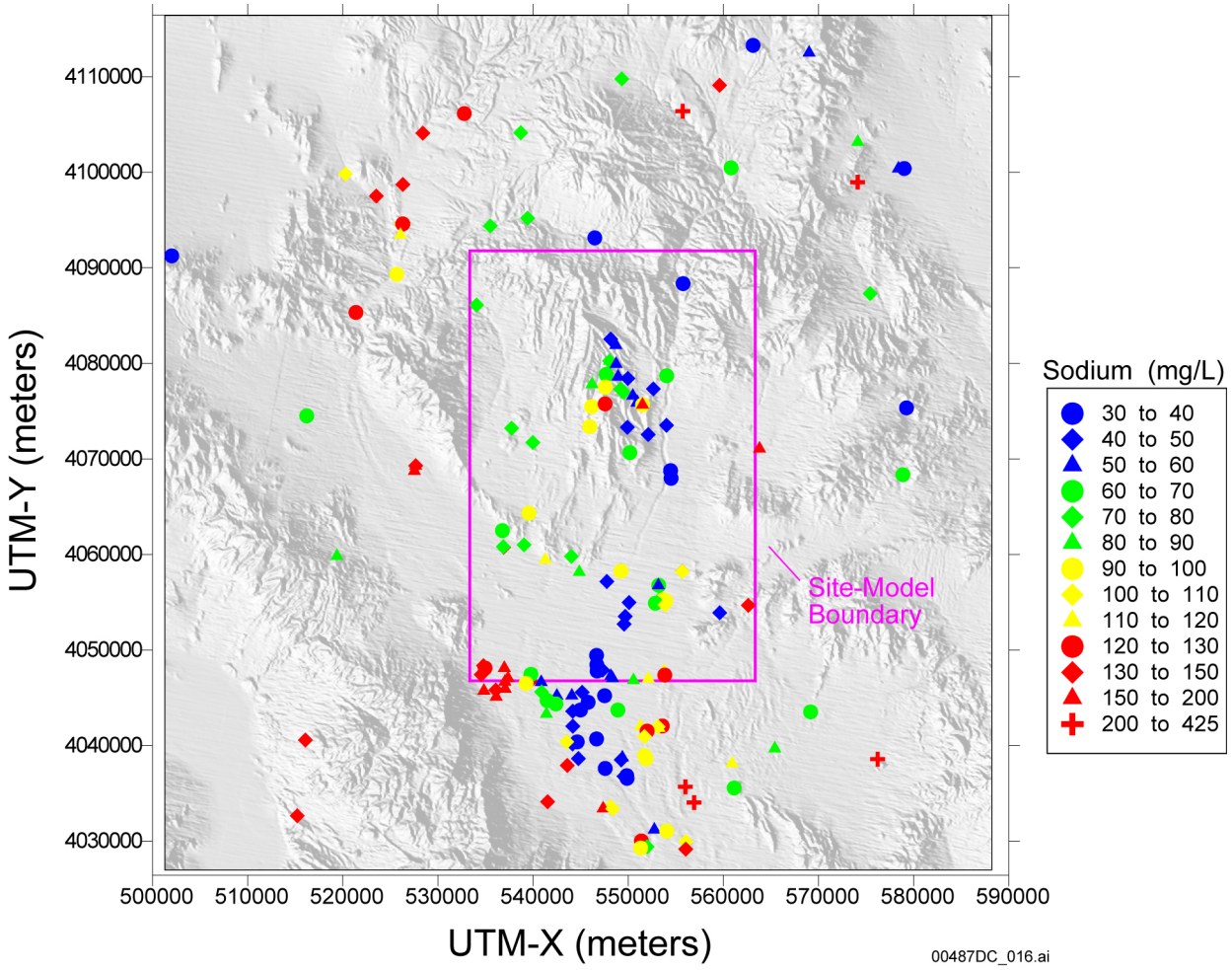

Source: Table A6-1.

NOTE: This figure has color-coded data points and should not be read in a black and white version.

UTM-X = UTM-Easting; UTM-Y = UTM-Northing; UTM = Universal Transverse Mercator.

Figure A6-22. Areal Distribution of Sodium in Groundwater

A6.3.4.11 Delta Deuterium

The areal distribution of delta deuterium (δD) values is shown in Figure A6-24 (this isotopic parameter is defined and discussed in Section A6.3.1.2). The δD values in groundwaters from the Yucca Mountain area range from about –105 per mil at borehole USW SD-6 (Site 50) to about –99 per mil at borehole G-2 (Site 43). In Crater Flat, the δD values of –108 and –106 per mil measured in water from borehole VH-1 (Site 69) and from Gexa Well 4 (Site 68) are substantially lighter (i.e., more negative) than the δD value of –99 per mil measured in groundwater from borehole VH-2 (Site 70), but similar to the extremely light values found in Oasis Valley and lower Beatty Wash. The δD values at borehole NC-EWDP-1DX (Site 73) of –101.3 per mil and at borehole NC-EWDP-3D (Site 86) of –105.6 per mil are generally similar to the values at upgradient boreholes VH-2 and VH-1 (–99.5 and –108.0, respectively).

The groundwater δD value of –98.0 per mil at Site 71 (NC-EWDP-7S) is also relatively heavy and comparable to the value at borehole VH-2.

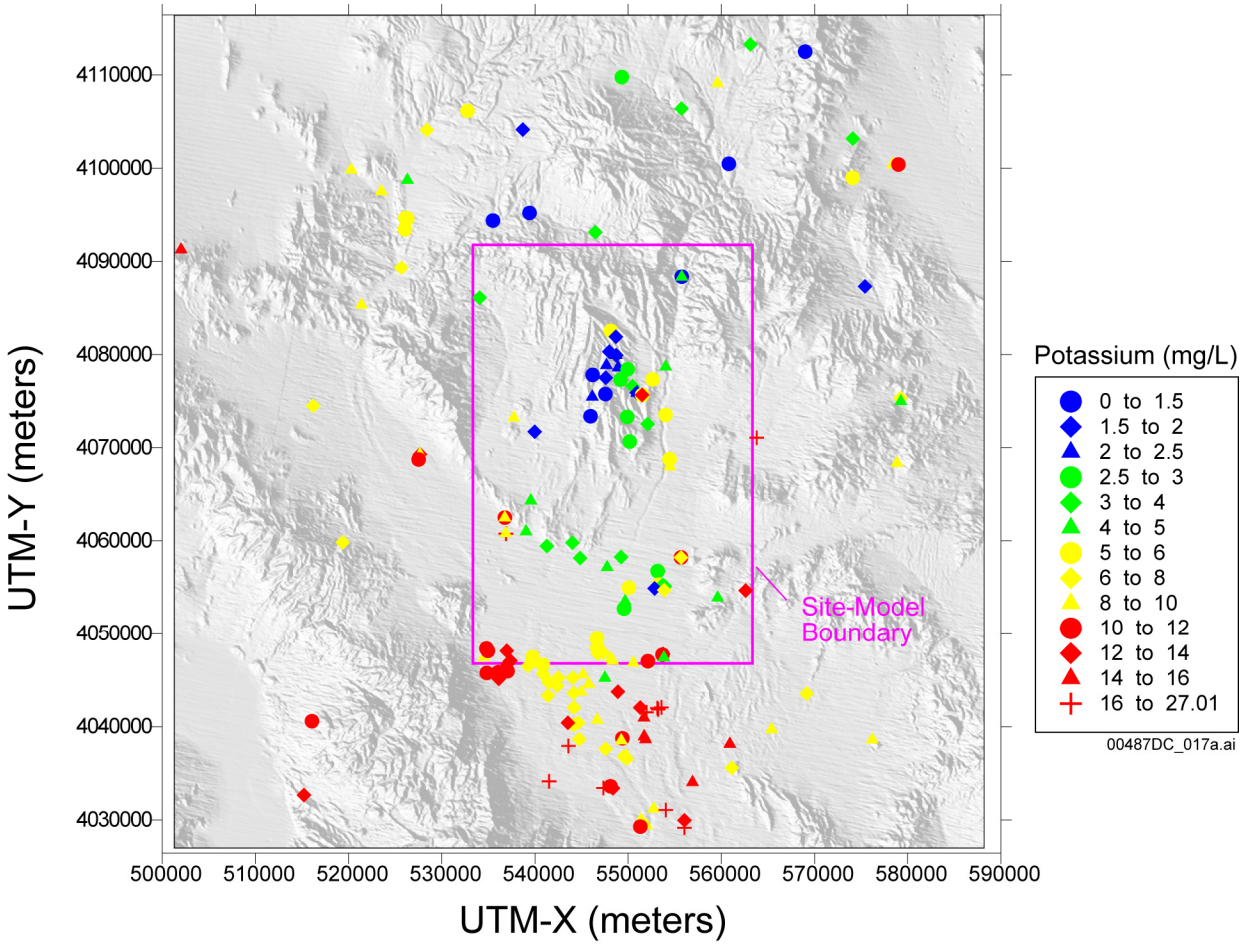

Source: Table A6-1.

NOTE: This figure has color-coded data points and should not be read in a black and white version.

UTM-X = UTM-Easting; UTM-Y = UTM-Northing; UTM = Universal Transverse Mercator.

Figure A6-23. Areal Distribution of Potassium in Groundwater

The δD values of groundwater near Fortymile Wash show a general trend toward more depleted values from north to south, ranging from about –93 to –91 per mil at boreholes UE-29 a#1 and a#2 (Sites 30 to 32) near the northern boundary of the site model area to values that are generally –100 per mil or less near the southern boundary of the model area. East of Yucca Mountain, groundwater beneath Fortymile Wash has δD values of about –97 per mil. The δD values of –104 per mil of groundwater at boreholes NC-EWDP-2D (Site 91)) and δD values of –110 to –104 per mil at well NC-EWDP-19D (Sites 92 and 94 to 98) are substantially lighter than in groundwater associated with Fortymile Wash in the FMW-N group. Groundwater in the Amargosa Desert has variable values, and spatial patterns are not as regular as for other chemical species, but groundwater in the eastern part of the Amargosa Desert is generally lighter in δD than groundwater farther to the west near Fortymile Wash.

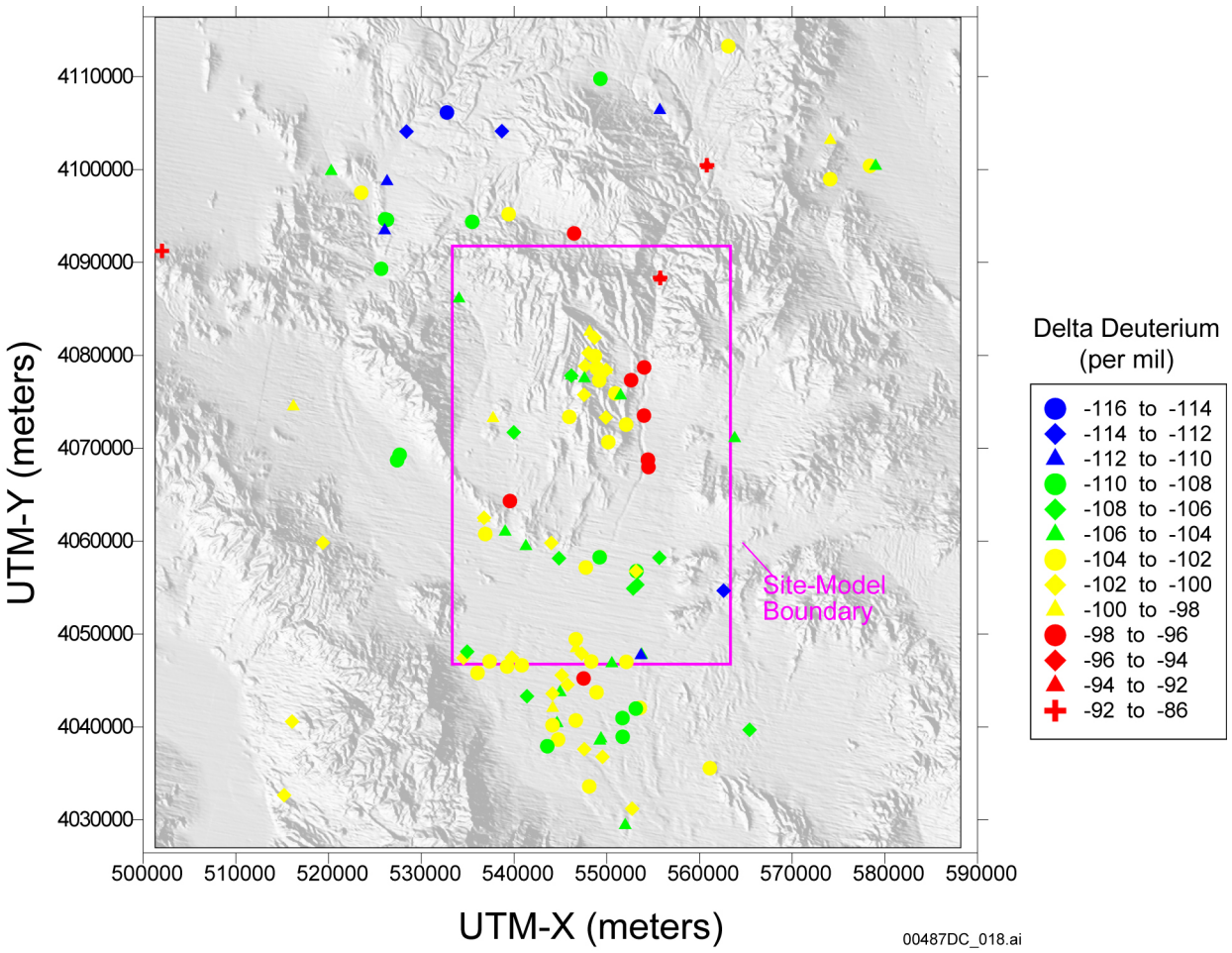

Source: Table A6-2.

NOTE: This figure has color-coded data points and should not be read in a black and white version.

UTM-X = UTM-Easting; UTM-Y = UTM-Northing; UTM = Universal Transverse Mercator.

Figure A6-24. Areal Distribution of Delta Deuterium in Groundwater

Groundwater δD values at Timber Mountain are quite variable, ranging from about –114 to -96 per mil, with the heaviest value found in upper Beatty Wash at Site 24 (well ER-EC-07). The groundwater δD values near Oasis Valley are among the lightest in the vicinity of Yucca Mountain (–116 to –108 per mil). Groundwater δD values lighter than –108 per mil are also found at sites 15 to 18 (Figure A6-5) west of Bare Mountain in the northwest Amargosa Desert. Southeast of these sites along the Amargosa River, groundwater from the AR and AR/FMW well groups has δD values that are typically heavier than values from wells to the northwest.

A6.3.4.12 Delta ^{18}O

Figure A6-25 shows the areal distribution of $\delta^{18}O$ values for the Yucca Mountain area (this isotopic parameter is defined and discussed in Section A6.3.1.2). Groundwater at Yucca Mountain has $\delta^{18}O$ values between –13.3 and –14.4 per mil, with groundwater in western Yucca

Mountain near Solitario Canyon having values that fall toward the lighter end of this range. Groundwater at borehole VH-1 (Site 69) in Crater Flat has a $\delta^{18}O$ value of –14.2 per mil, similar to the $\delta^{18}O$ value of –14.1 per mil of groundwater at Gexa Well 4 (Site 68) and at Site 23 (well ER-OV-03c) in lower Beatty Wash. Groundwater in southwestern Crater Flat has substantially heavier $\delta^{18}O$ values, with groundwater at VH-2 (Site 70) having a $\delta^{18}O$ value of –13.4 per mil. Groundwaters sampled from the NC-EWDP wells along the southern edge of Crater Flat generally have $\delta^{18}O$ values that are similar to those in wells directly to the north at boreholes VH-1 and VH-2. However, the groundwater $\delta^{18}O$ value at site 71 (NC-EWDP-7S) has a somewhat heavier $\delta^{18}O$ value than upgradient groundwater, perhaps reflecting the effects of evapotranspiration due to the shallow water table (7 m) at this well.

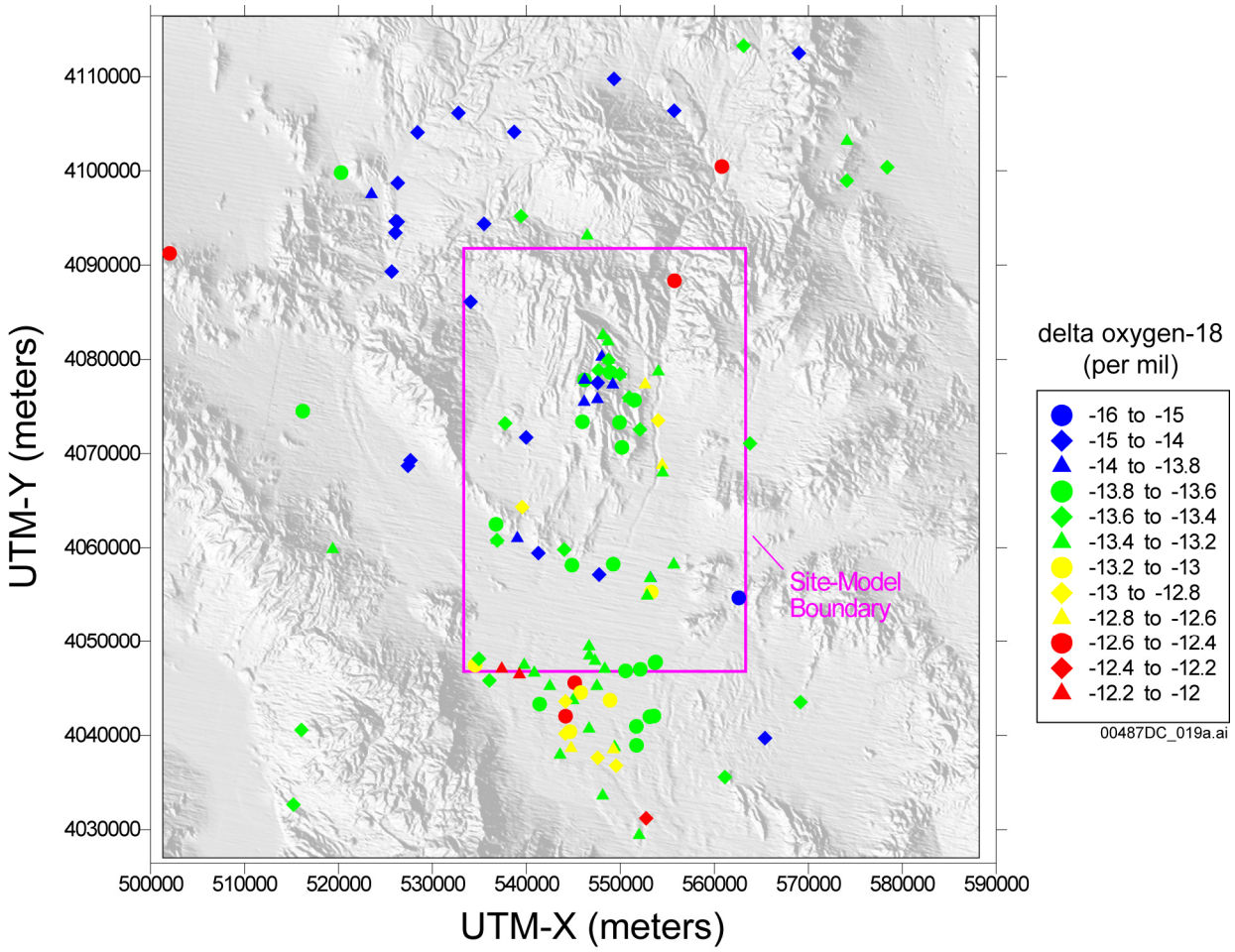

Source: Table A6-2.

NOTE: This figure has color-coded data points and should not be read in a black and white version.

UTM-X = UTM-Easting; UTM-Y = UTM-Northing; UTM = Universal Transverse Mercator.

Figure A6-25. Areal Distribution of $\delta^{18}O$ in Groundwater

The groundwater $\delta^{18}O$ values at Sites 28 to 32 (Figure A6-5) in the FMW-N group are relatively heavy (–12.8 to –11.8 per mil) compared to wells to the south within this group and to most groundwater in the FMW-S group (Table A6-2). (The apparent range of values on Figure A6-25 is somewhat less because not all data are evident in the figure). Groundwater within the FMW-N group is distinctly heavier in $\delta^{18}O$ than groundwater to the west at Yucca Mountain. In the Amargosa Desert, the $\delta^{18}O$ of groundwaters near Fortymile Wash generally are distinct from those of groundwater farther east or west from the Wash, although near the southern boundary of the site model area, this distinction becomes less well defined.

The groundwater $\delta^{18}O$ at Timber Mountain are generally lighter than most groundwater found at Yucca Mountain, except for groundwater found directly north of Yucca Mountain in upper Beatty Wash. Groundwater $\delta^{18}O$ values become lighter toward the west in Beatty Wash. Relatively light groundwater $\delta^{18}O$ values are found in Oasis Valley and in the northwest Amargosa Desert west of Bare Mountain at Sites 15 to 18. As with δD values, groundwater $\delta^{18}O$ increase downstream along the Amargosa River toward the AR and AR/FMW sites.

A6.3.4.13 Delta ^{34}S

Groundwater data for $\delta^{34}S$ were not collected from the Yucca Mountain area and Amargosa Desert before the late 1990s, nor have they been collected in areas north of Yucca Mountain. Consequently, areal coverage is not as complete as for most other ions and isotopes. The limited data from Yucca Mountain shows that groundwater from two wells along Yucca Crest have higher $\delta^{34}S$ values than groundwater in the YM-SE grouping near Dune Wash (Figure A6-26). Groundwater from wells in the CF-SW and YM-S groupings near U.S. Highway 95 generally show an overall increase toward the west. Groundwaters in the easternmost wells of the YM-S grouping (wells NC-EWDP-2D, NC-EWDP-19D, and NC-EWDP-19P) have $\delta^{34}S$ values that span a range similar to that defined by the groundwater samples from Yucca Crest and Dune Wash. In the Amargosa Desert, groundwater associated with the Amargosa River and the Gravity fault has substantially higher $\delta^{34}S$ values than groundwater associated with Fortymile Wash, perhaps reflecting the presence of alluvium derived from carbonate rocks in these areas. As discussed in Section A6.3.1.2.3, marine sulfates from the early Paleozoic have $\delta^{34}S$ values near 30 per mil, values that are considerably higher than the values of 0 to 15 typical of sulfur of a volcanic origin. Some of the lowest groundwater $\delta^{34}S$ values are found in Jackass Flat at well J-11 (Site 67) and in several of the LW-group wells in the Amargosa Valley area.

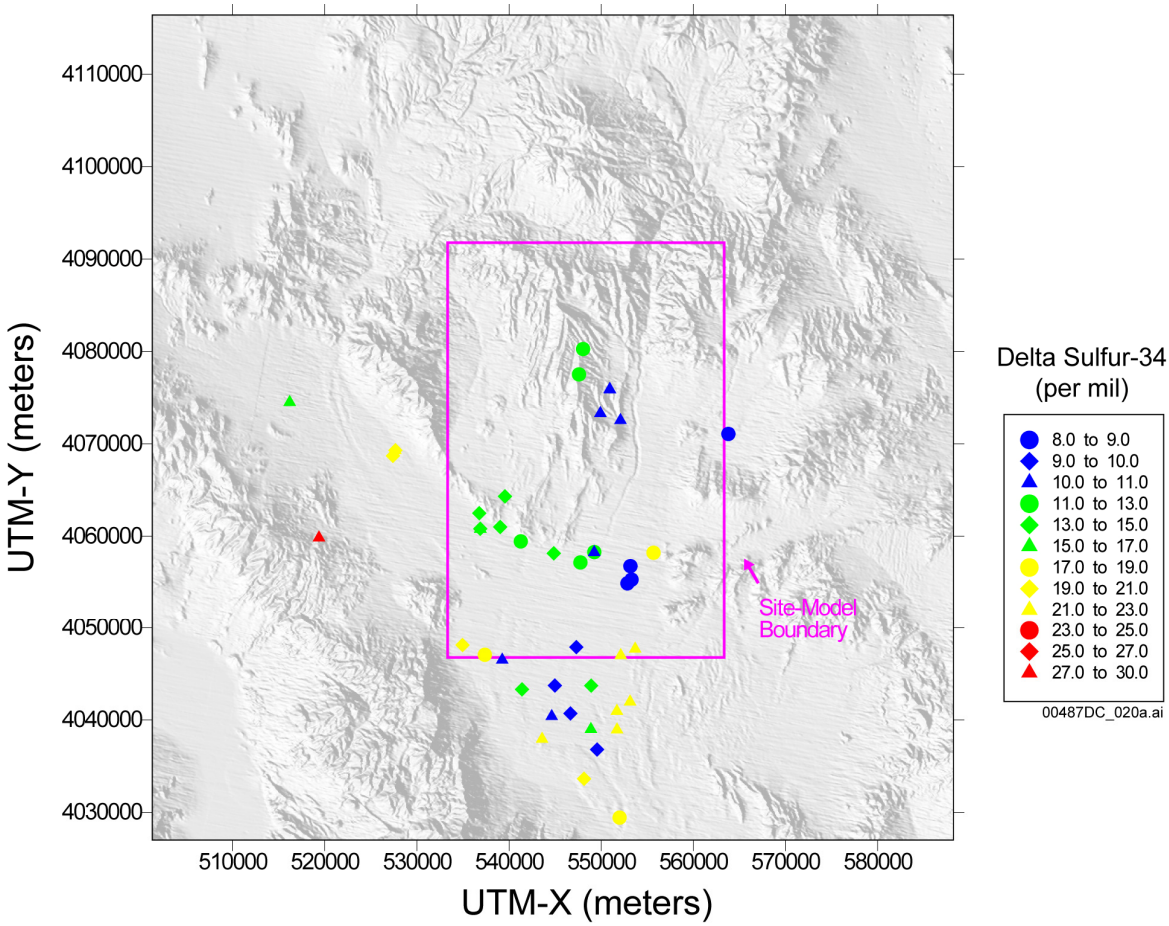

Source: Table A6-2.

NOTE: This figure has color-coded data points and should not be read in a black and white version.

UTM-X = UTM-Easting; UTM-Y = UTM-Northing; UTM = Universal Transverse Mercator.

Figure A6-26. Areal Distribution of $\delta^{34}S$ in Groundwater

A6.3.4.14 Delta ^{13}C

The areal distribution of $\delta^{13}C$ values is shown in Figure A6-27 (this isotopic parameter is defined and discussed in Section A6.3.1.2). Excluding the data from borehole p#1 (Sites 62 and 63), where groundwater has $\delta^{13}C$ values of –2.3 per mil in the carbonate aquifer and –4.2 per mil in the volcanic aquifer, the $\delta^{13}C$ values of groundwater at Yucca Mountain vary between –14.4 per mil at borehole UZ-14 (Sites 45 and 46) to –4.9 per mil at borehole H-3 (Site 51). Although patterns are complex on a borehole-by-borehole basis, groundwater in the northern most part of Yucca Mountain is generally lighter in $\delta^{13}C$ than groundwaters found toward the central and southern parts of the mountain. North of Yucca Mountain, groundwater $\delta^{13}C$ values are generally considerably heavier than the groundwater $\delta^{13}C$ values found at Yucca Mountain. Only groundwater from well ER-EC-07 (Site 24) in Beatty Wash has a $\delta^{13}C$ within the range of values found at Yucca Mountain, in the Solitario Canyon Wash area, or in Crater Flat at borehole VH-1 (Site 69). Overall, the $\delta^{13}C$ values of groundwater in the Nye County-EWDP boreholes at

the southern edge of Crater Flat increase toward the west, reflecting the increasing proximity of groundwater to carbonate rocks with relatively heavy $\delta^{13}C$ values.

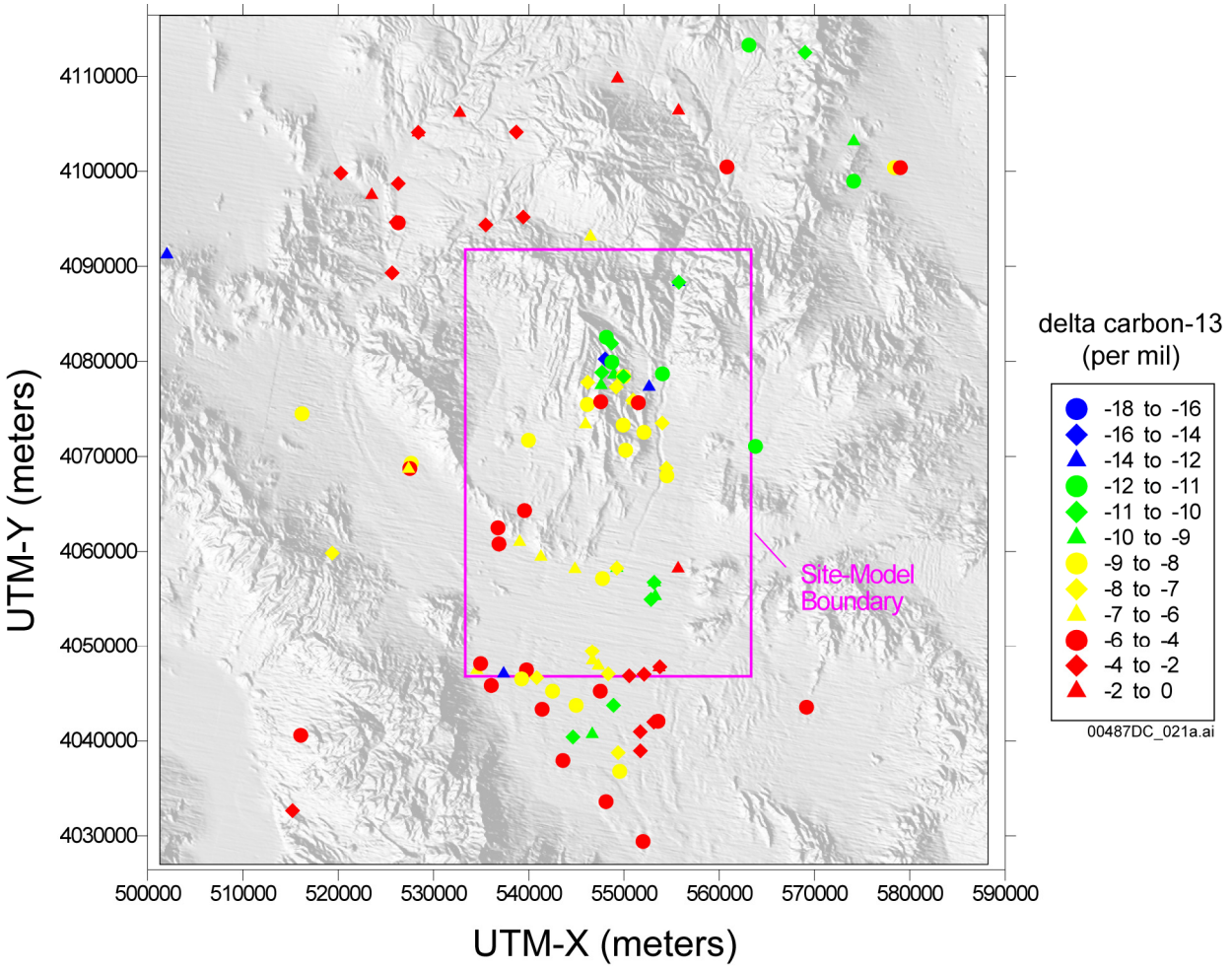

Source: Table A6-2.

NOTE: This figure has color-coded data points and should not be read in a black and white version.

UTM-X = UTM-Easting; UTM-Y = UTM-Northing; UTM = Universal Transverse Mercator.

Figure A6-27. Areal Distribution of $\delta^{13}C$ in Groundwater

The $\delta^{13}C$ values of groundwater near Fortymile Wash generally increase between the north and south boundaries of the site model area, although local reversals in this trend are evident. The groundwater $\delta^{13}C$ values near Fortymile Wash are generally lower than the $\delta^{13}C$ values toward the western and eastern parts of the Amargosa Desert, where groundwater $\delta^{13}C$ values reflect the proximity to carbonate rocks of the southern Funeral Mountains and discharge from the carbonate aquifer across the Gravity fault, respectively. Several of the $\delta^{13}C$ values of groundwater near the southwest corner of the site model area are similar to the values measured in groundwater at sites 15 to 18 west of Bare Mountain and in wells and springs in Oasis Valley. Groundwater in Jackass Flats and some groundwater at Amargosa Valley have relatively light

$\delta^{13}C$ values, despite the proximity of the Amargosa Valley (LW) group to groundwater near the Gravity fault with considerably heavier $\delta^{13}C$ values.

A6.3.4.15 ^{14}C Activity

The areal distribution of ^{14}C activity in pmc is shown in Figure A6-28. This hydrochemical parameter is discussed in Section A6.3.1.2. Excluding groundwater from borehole p#1 (Sites 62 and 63), which has a ^{14}C activity of 2.3 pmc in the carbonate aquifer and 3.5 pmc in the volcanic aquifer, the ^{14}C activity of groundwater at Yucca Mountain ranges from 10.5 pmc at borehole H-3 (Site 51) to 27 pmc at borehole WT-24 (Site 44) in northern Yucca Mountain. Groundwater at the eastern edge of Crater Flat near Solitario Canyon has some of the lowest ^{14}C activities of groundwater in the map area, with values as low as 7.3 pmc at borehole WT-10 (Site 42) and 10 pmc in a sample from borehole H-6 (Site 34). Groundwater ^{14}C activities are slightly higher (12 pmc) farther to the west in Crater Flat at borehole VH-1 (Site 69). Groundwater at several Nye County-EWDP wells in the YM-S grouping to the south of borehole VH-1 has similar ^{14}C activities. The groundwater at boreholes NC-EWDP-2D (Site 91), NC-EWDP-19P (Site 93), and some zones in NC-EWDP-19D (i.e. Site 96) have ^{14}C activities of 20 pmc or more, similar to the ^{14}C activities of groundwater in Dune Wash and Fortymile Wash.

Groundwater near Fortymile Wash has ^{14}C activities that range from about 76 pmc at borehole a#1 (Site 32) near the northern boundary of the model area to values less than 20 pmc near the southern boundary of the model area, with local reversals in this overall trend among the FMW-N group of samples. Southward from this area along Fortymile Wash, groundwater ^{14}C activities are lower but also do not show an obvious north-to-south trend. South of the southern boundary of the site model area, groundwater ^{14}C activities near Fortymile Wash range from 10 to 40 pmc. Elsewhere in the Amargosa Desert, several groundwater ^{14}C activities measured in the southwest corner of the site model area are approximately 30 pmc, which is considerably higher than the values of groundwater to the north and moderately higher than the values measured to the northwest at sites 15 to 18 west of Bare Mountain and in Oasis Valley.

In general, it can be noted that where relatively high groundwater $\delta^{13}C$ values indicate water/rock interactions with isotopically heavy carbonate rock (Figure A6-27), the groundwater ^{14}C activities are generally low compared to other areas. These carbonate-rock-affected groundwaters are present at Timber Mountain, near Bare Mountain in the CF-SW area, near the southern Funeral Mountains in some AR and AR/FMW groundwaters, and near the GF samples. The highest ^{14}C activities are associated with major drainages, including the Amargosa River in the southwest corner of the site model area, upper Beatty Wash, and along Fortymile Wash, suggesting that these major washes are important areas of Holocene recharge.

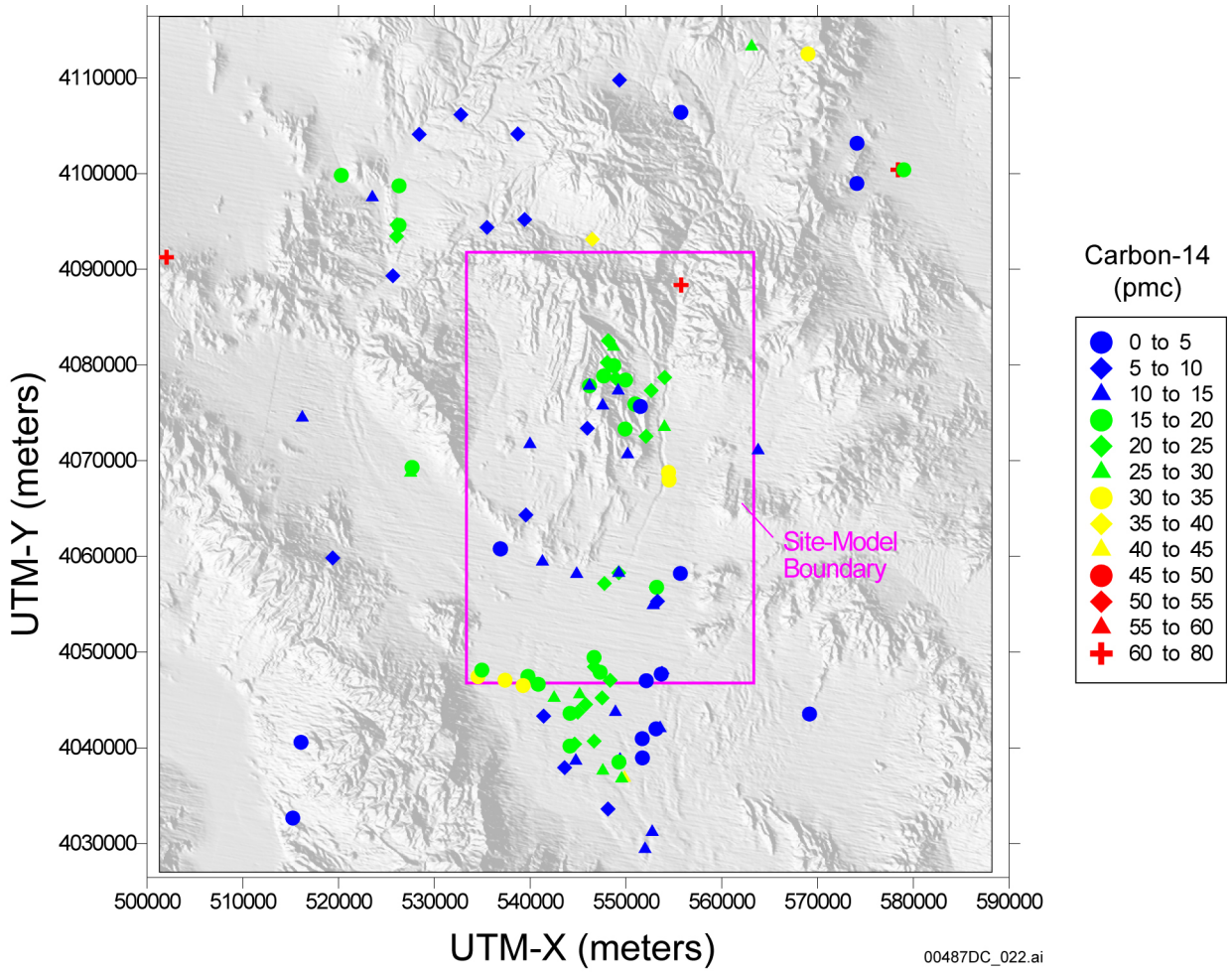

Source: Table A6-2.

NOTE: This figure has color-coded data points and should not be read in a black and white version.

UTM-X = UTM-Easting; UTM-Y = UTM-Northing; UTM = Universal Transverse Mercator.

Figure A6-28. Areal Distribution of ^{14}C in Groundwater

A6.3.4.16 Uranium Concentration and $^{234}U/^{238}U$ Activity Ratios

Uranium concentration and $^{234}U/^{238}U$ activity ratio data are shown in Figures A6-29 and A6-30 respectively. Processes affecting uranium concentrations and $^{234}U/^{238}U$ activity ratios are discussed in Section A6.3.1.2 and in Paces et al (2002 [DIRS 158817]). Some of the highest activity ratios in the region are found at Timber Mountain (TM group) and in northern and southeastern Yucca Mountain (YM-CR and YM-SE groups). Samples in the YM-CR and YM-SE with these elevated $^{234}U/^{238}U$ activity ratios also have relatively small uranium concentrations (less than 2.5 µg/L, but most approximately 1 µg/L), whereas groundwaters from the TM group (except for Site 24 in upper Beatty Wash) have somewhat higher uranium concentrations (Figure A6-29). In addition to different uranium concentrations, other hydrochemical attributes of the Timber Mountain and Yucca Mountain groundwaters, such as Na^+ (Figure A6-22), HCO_3^- (Figure A6-17), and $\delta^{13}C$ (Figure A6-27), are also generally

different, suggesting the groundwaters from these areas are not necessarily related, despite their similar $^{234}U/^{238}U$ activity ratios. Data from borehole p#1 (Site 63) at Yucca Mountain indicate the carbonate aquifer has comparatively high uranium concentrations (13.3 µg/L) and low $^{234}U/^{238}U$ activity ratios (2.3) compared to some shallow groundwater at Yucca Mountain.

Uranium activity ratios decrease southward along Fortymile Wash from a value as high as 7 at well J-13 (Site 35) to values below 3.0 in the northern Amargosa Desert. Paces et al. (2002 [DIRS 158817], p. 769) suggested that significant groundwater pumping from well J-13 and nearby well J-12 (Site 36) may have disrupted natural flow patterns and induced Yucca Mountain groundwater with high $^{234}U/^{238}U$ activity ratios to flow eastward toward Fortymile Wash. Measurements of archived water samples from well J-12 indicated its $^{234}U/^{238}U$ activity ratio in 1971 was 5.5, supporting the authors' contention that the $^{234}U/^{238}U$ activity ratios at well J-13 may have initially been lower than recent measurement at that well have indicated.

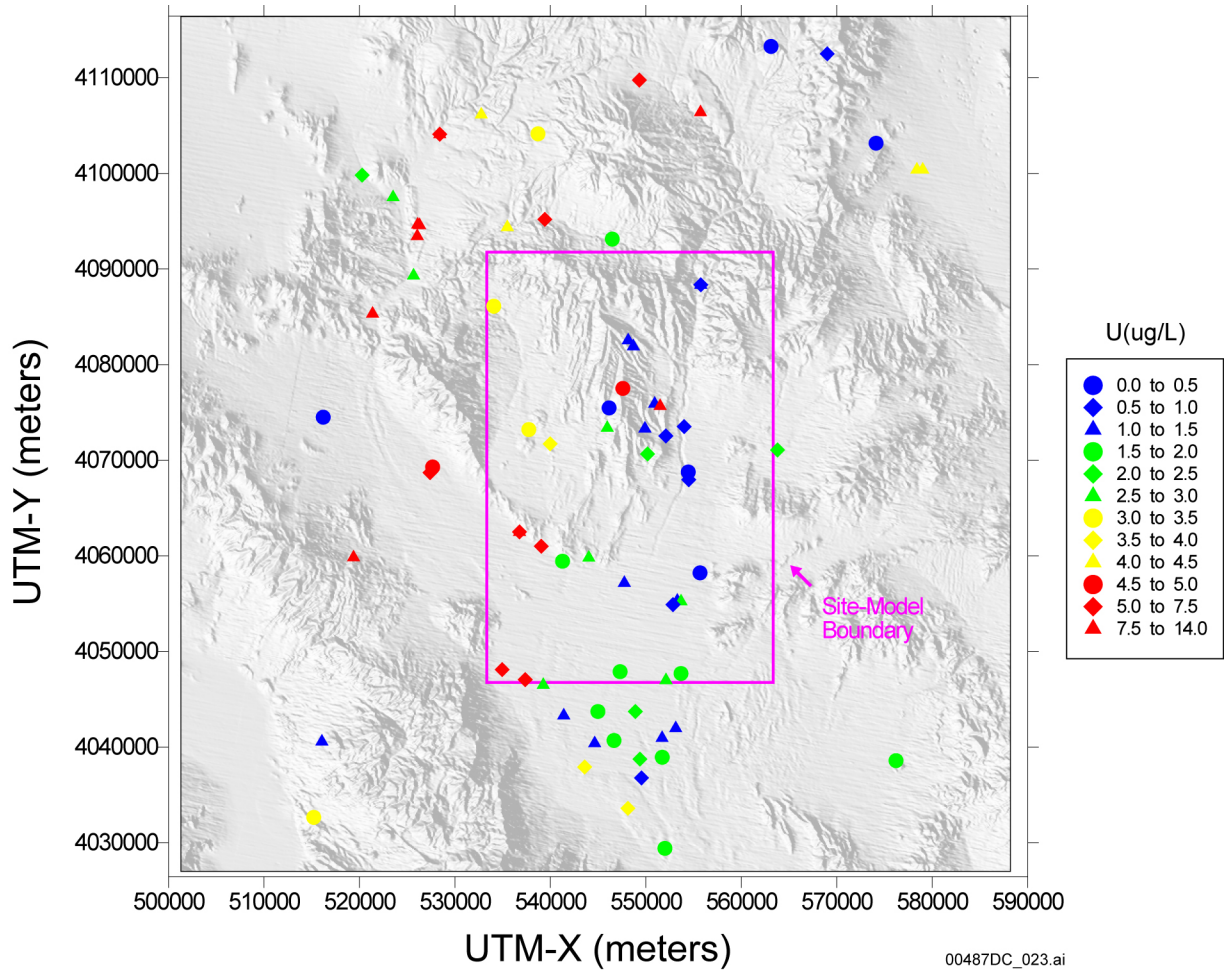

Source: Table A6-2.

NOTE: This figure has color-coded data points and should not be read in a black and white version.

UTM-X = UTM-Easting; UTM-Y = UTM-Northing; UTM = Universal Transverse Mercator.

Figure A6-29. Areal Distribution of Uranium in Groundwater

Uranium concentrations and $^{234}U/^{238}U$ activity ratios in the Amargosa Desert region have a relatively narrow range with concentrations typically between 1 and 4 µg/L and activity ratios mostly between 2.5 and 3.5. Borehole NC-EWDP-5S (Site 154) has an anomalously high $^{234}U/^{238}U$ activity ratio for this location of 6.6 and a very low uranium concentration of 0.04 µg/L. From east to west of Yucca Mountain through the Crater Flat area into the Oasis Valley, $^{234}U/^{238}U$ activity ratios generally decrease whereas uranium concentrations increase.

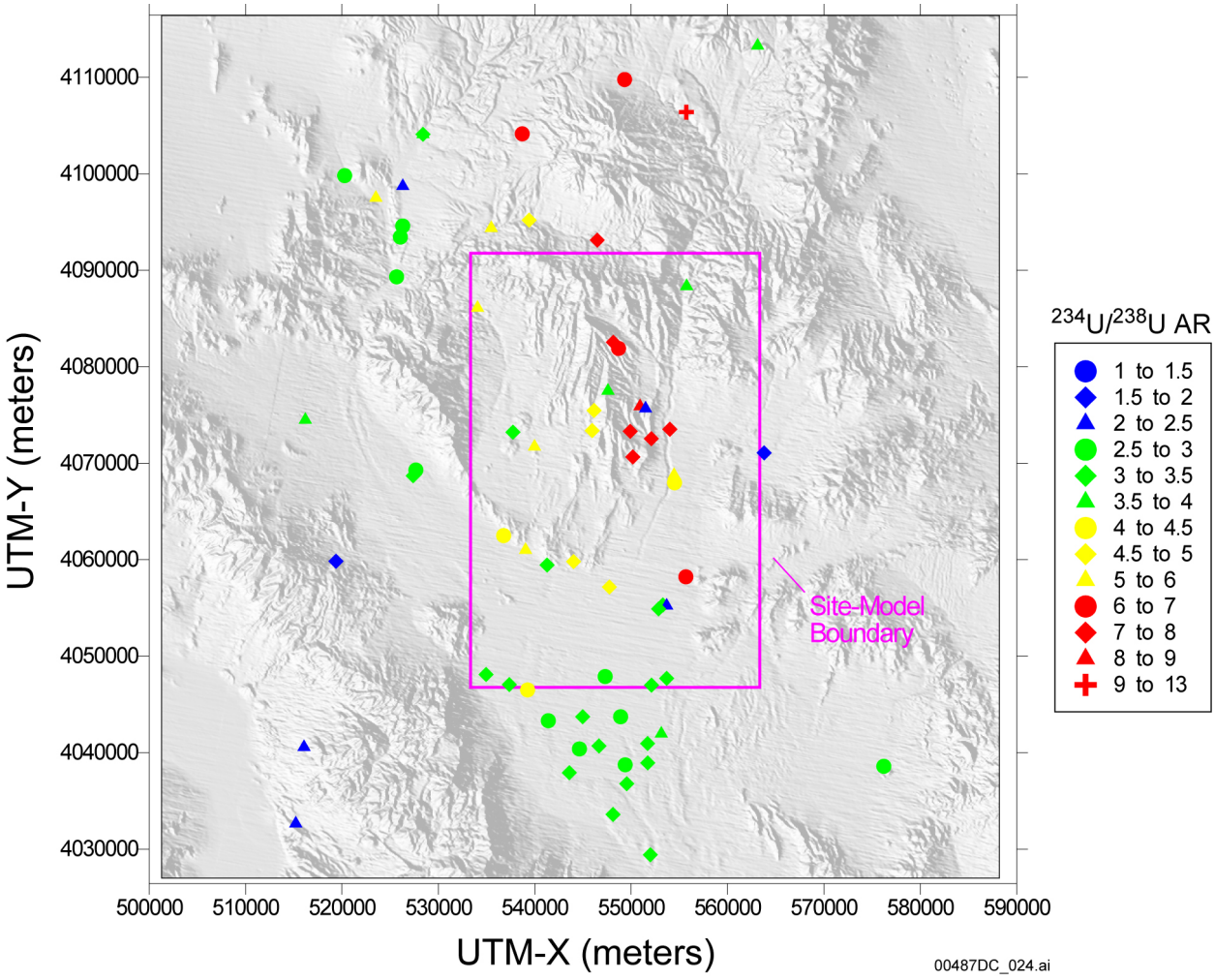

Source: Table A6-2.

NOTE: This figure has color-coded data points and should not be read in a black and white version.

UTM-X = UTM-Easting; UTM-Y = UTM-Northing; UTM = Universal Transverse Mercator.

Figure A6-30. Areal Distribution of $^{234}U/^{238}U$ Activity Ratios in Groundwater

A6.3.4.17 Strontium Concentrations and Delta Strontium-87

Strontium concentrations from groundwater at Yucca Mountain vary considerably with values between 1.0 and 1,720 µg/L; most values, however, are between 10 and 50 µg/L. In general, groundwater near Fortymile Wash has lower Sr^{2+} concentrations than groundwater to the east or west of the wash. Strontium concentrations in the FMW-N group are low (values mostly less

than 50 µg/L) relative to those in the FMW-S group (most values greater than 100 µg/L). Sr^{2+} concentrations in Beatty Wash are one-to-two orders of magnitude higher that Sr^{2+} concentrations in northern Yucca Mountain in the YM-CR group, which are among the lowest in the region. Groundwater from p#1(c) has a relatively high Sr^{2+} concentration of 450 µg/L. Similarly high values also characterize groundwater that is likely to have contacted Paleozoic carbonate rocks elsewhere in the area (e.g., samples from SW Crater Flat, Gravity fault, Funeral Mountains, and Amargosa Flat groupings). Groundwater in the Timber Mountain area has Sr^{2+} concentrations between about 99 and 224 µg/L.

Strontium isotope-ratio data (expressed as $\delta^{87}Sr$) are unevenly distributed throughout the area with numerous values to the north of Yucca Mountain, some in the Yucca Mountain area and along U.S. Highway 95, and none in the Amargosa Desert region. Very low $\delta^{87}Sr$ values are found in groundwater in Beatty Wash, in the Timber Mountain area, and in Oasis Valley (less than 1.8 per mil, with some negative values). Generally higher values exist to the south of the TM and upper FMW-N groups, although some Yucca Mountain groundwaters also have comparably low $\delta^{87}Sr$ values. Interestingly, $\delta^{87}Sr$ values of groundwater from the carbonate aquifer or from boreholes that have a component of water from the carbonate aquifer (e.g. p#1(c), SW Crater Flat, Funeral Mountains) have high $\delta^{87}Sr$. These waters also typically have high strontium concentrations. Reaction with the Paleozoic carbonate aquifer rock cannot explain this trend as these rocks are expected to have $\delta^{87}Sr$ values of less than zero. A possible explanation is that these waters have reacted with Paleozoic or Precambrian clastic rocks, which are expected to have high $\delta^{87}Sr$ due to their composition and age of the original detrital material (Peterman and Stuckless 1993 [DIRS 101149], p. 1,561).

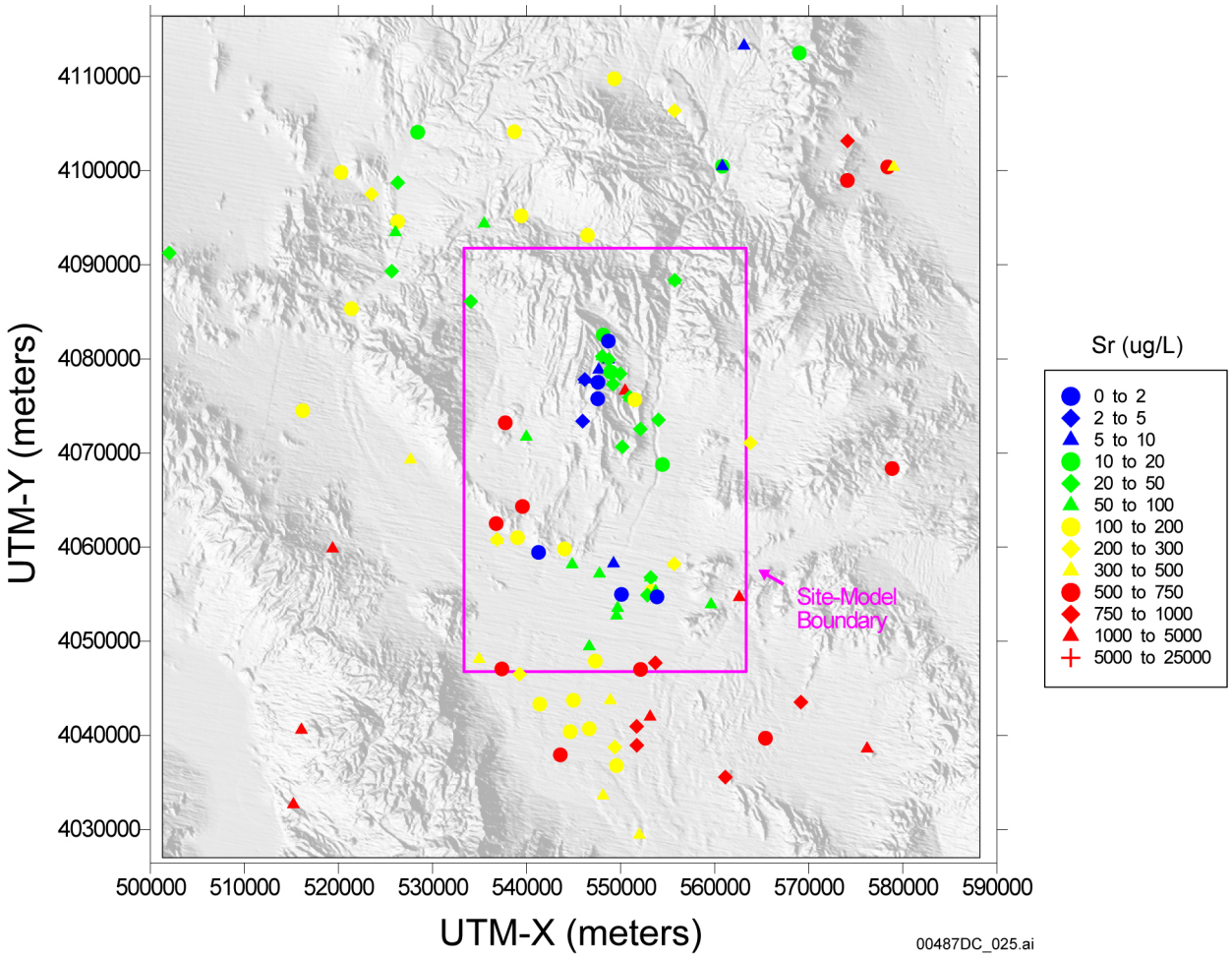

Source: Table A6-2.

NOTE: This figure has color-coded data points and should not be read in a black and white version.

UTM-X = UTM-Easting; UTM-Y = UTM-Northing; UTM = Universal Transverse Mercator.

Figure A6-31. Areal Distribution of Strontium in Groundwater

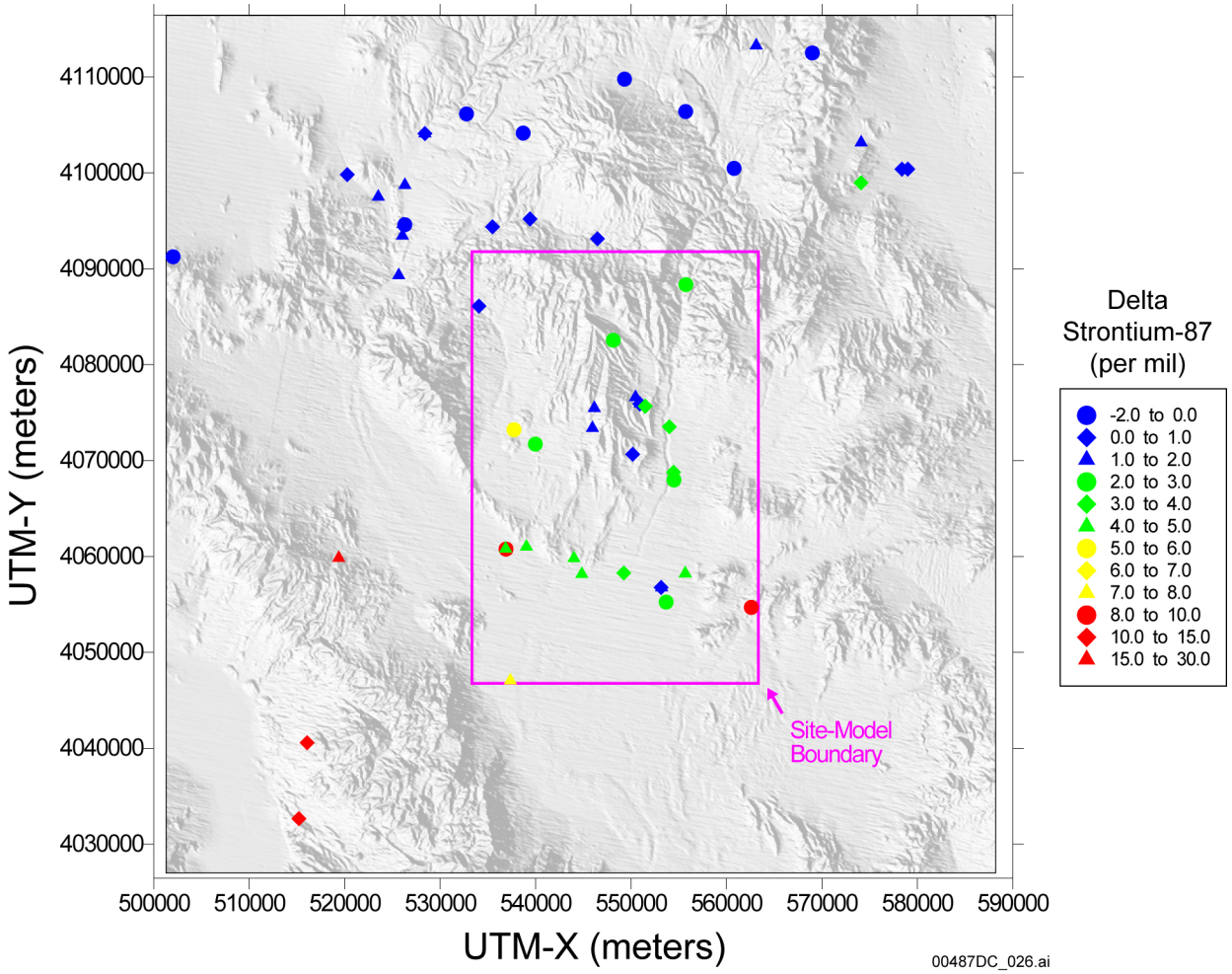

Source: Table A6-2.

NOTE: This figure has color-coded data points and should not be read in a black and white version.

UTM-X = UTM-Easting, UTM-Y = UTM-Northing; UTM = Universal Transverse Mercator.

Figure A6-32. Areal Distribution of $\delta^{87}Sr$ in Groundwater

A6.3.5 Areal Distribution of Calculated Geochemical Parameters

The following subsections describe the areal distribution of the calculated geochemical parameters, including a brief summary of how the calculated parameters would be expected to reflect the relative state of evolution of the groundwater. A number of geochemical parameters were calculated with PHREEQC V2.3 (STN: 10068-2.3-00 [DIRS 155323]; Parkhurst and Appelo 1999 [DIRS 159511]) to further characterize groundwater in the Yucca Mountain area. These parameters include charge balance error, ionic strength, dissolved inorganic carbon (DIC), the logarithm of dissolved carbon-dioxide partial pressure (log P_{CO_2}), and the saturation indices of many minerals identified at Yucca Mountain (Table A6-3 below). The charge-balance errors are helpful in evaluating the reliability of hydrochemical analyses given in Table A6-1 of this report. The calculated DIC concentrations are used for evaluating the extent of calcite dissolution Yucca Mountain recharge undergoes as it moves through the saturated zone

(Section A6.3.6.6) and in mixing models involving ^{14}C (Sections A6.3.6.7 and A7.3.6). The saturation indices are used to help constrain the possible reactions in inverse mixing and water/rock interaction models presented in Section A6.3.8.

The saturation indices of many common minerals such as K-feldspar, amorphous silica [SiO_2(a)], and calcite were based on thermodynamic data contained in the *phreeqc.dat* database provided with PHREEQC (Parkhurst and Appelo 1999 [DIRS 159511], Table 55). In addition, the specific chemical formulas and thermodynamic data for Ca- and Na-clinoptilolite and smectite that have been identified at Yucca Mountain were used in PHREEQC to compute saturation indices. The chemical formulas of these minerals and the Gibbs free-energies **(ΔG^O_f)** and enthalpies **(ΔH^O_f)** of formation estimated for these minerals are listed in Table A6-4.

For the purpose of calculating mineral saturation indices, when field temperature measurements are unavailable, the temperature of groundwater samples was approximated either from published maps of water table temperatures at Yucca Mountain or, in the Amargosa Desert, was assumed to be 25°C. The use of a contour map of water table temperatures (Fridrich et al. 1994 [DIRS 100575], Figure 8) to estimate groundwater sample temperatures at Yucca Mountain is an acceptable approximation because most of the samples for which this approximation was made are from the upper part of the saturated zone (see Table A4-3 for sampled depths and Figure A6-5 for locations of samples 33, 34, 41, 57, and 66). Likewise, the assumption that groundwater samples in the Amargosa Desert with no measured temperatures are at 25°C is an acceptable approximation because most of the measured groundwater sample temperatures are in the range of 25°C to 30°C (see temperature data for samples from the Amargosa Valley (rows 99 to 107), Amargosa River (rows 108 to 117), Fortymile Wash—West (rows 118 to 126), Fortymile Wash—South (rows 127 to 141), Fortymile Wash—East (rows 142 to 153), Gravity Fault (rows 154 to 176), and Amargosa River/Fortymile Wash (rows 177 to 185) in Table A6-1.

The calculation of saturation indices for alumino-silicate minerals such as those listed in Table A6-4 requires measurements of dissolved Al^{3+} concentrations in the groundwater. Although recent groundwater samples from the Yucca Mountain area have reported dissolved Al^{3+} concentrations, historic data from the Yucca Mountain area are generally lacking this information. To get an estimate of the saturation indices of alumino-silicate minerals throughout the Yucca Mountain area, dissolved Al^{3+} concentrations for each sample were assumed to be in equilibrium with kaolinite (see Table A5-1, Assumption 2). This assumption provides estimates of dissolved Al^{3+} concentrations that are in good agreement with measured Al^{3+} concentrations at sites where these data are available (Figure A6-33). Estimates of Al concentrations made by assuming groundwater equilibrium with other Al^{3+}-bearing minerals such as gibbsite, smectite, clinoptilolite, and K-feldspar did not produce nearly as good a match to the available Al^{3+} data. Other factors affecting the calculated saturation indices are discussed in Section A7.3.2. These factors include uncertainty in thermodynamic data use to calculate the mineral solubility constants, variability in mineral compositions and particle sizes, and slow reaction rates relative to the groundwater residence times.

Table A6-3. Calculated Geochemical Parameters of Groundwater Samples Used in this Report

Well	Figure A6-5 Sample	Ionic Strength	Charge Balance Error (%)[1]	DIC as (mg/L HCO_3^-)	log P_{CO2} (atm)	Mineral Saturation Indices[2,3]							
						Calcite	Smectite	Ca-Clino.	SiO_2 (a)	Fluorite	Albite	K-Feldspar	Dolomite
Oasis Valley/NW Amargosa													
ER-EC-08	1	7.18×10^{-3}	–3.5	176.8	–2.68	–0.06	4.00	16.11	–0.49	–0.53	–1.51	–0.65	–0.73
ER-OV-01	2	7.43×10^{-3}	1.3	197.2	–3.02	–0.10	6.16	29.11	–0.24	–1.43	–0.80	0.22	–1.64
ER-OV-06a	3	7.46×10^{-3}	0.8	201.0	–2.99	–0.53	5.32	23.90	–0.39	–1.59	–1.04	–0.03	–1.14
ER-OV-05	4	7.27×10^{-3}	0.2	241.5	–2.46	–0.01	6.81	31.43	–0.13	–1.01	–1.25	0.11	–0.41
ER-OV-02	5	8.24×10^{-3}	–0.2	226.6	–2.90	0.12	6.80	30.85	–0.26	–0.91	–1.03	–0.16	–0.87
Springdale Upper Well (10S/47E-32adc)	6	8.51×10^{-3}	–0.3	303.0	–2.26	0.00	6.31	27.98	–0.21	–0.86	–1.40	–0.22	–0.41
Goss Springs North (11S/47E-10bad)	7	6.88×10^{-3}	–1.6	179.7	–3.01	0.08	6.88	31.04	–0.29	–0.77	-1.22	–0.12	–0.72
Er-OV-03a	8	7.02×10^{-3}	1.1	184.6	–2.90	–0.08	6.90	30.91	–0.27	–0.87	–1.25	–0.17	–1.06
ER-OV-03a3	9	7.19×10^{-3}	0.5	182.0	–3.08	0.14	6.47	29.69	–0.31	–1.03	–1.05	0.01	–0.50
ER-OV-03a2	10	2.06×10^{-2}	–3.0	241.6	–3.92	0.54	5.39	26.20	–0.81	—	–0.76	1.05	0.64
Goss Spring (11S/47E-10bcc)	11	7.21×10^{-3}	1.4	187.6	–2.47	–0.32	6.04	24.88	–0.34	–0.67	–1.73	–0.71	–1.46
ER-OV-04a	12	5.71×10^{-3}	0.2	162.7	–3.21	0.06	6.46	30.96	–0.23	–0.97	–0.86	0.40	–1.48
Beatty Well no. 1 (Wat&Sanit Distr)	13	—	—	—	—	—	—	—	—	—	—	—	—
Bond Gold Mining #1	14	5.90×10^{-3}	–2.4	158.7	–3.12	0.39	5.10	20.82	–0.62	–1.91	–1.89	–0.50	0.55
US Ecology MW-313	15	1.42×10^{-2}	–6.0	355.2	–2.00	0.18	6.08	26.48	–0.23	0.16	–1.59	–0.30	0.18
US Ecology MW-600	16	1.18×10^{-2}	–4.0	300.4	–2.45	0.12	6.04	27.07	–0.28	–0.20	–1.21	–0.15	0.34
Nucl. Eng. Co. Well	17	1.43×10^{-2}	–0.1	342.4	–2.11	0.28	6.15	27.23	–0.22	—	–1.40	–0.28	0.32
US Ecology MR-3	18	—	—	—	—	—	—	—	—	—	—	—	—
Timber Mountain													
UE-18r	19	4.84×10^{-3}	0.0	211.2	–2.85	0.42	5.01	21.03	–0.44	–0.73	–1.50	–0.66	–0.17
ER-18-2	20	1.54×10^{-2}	5.3	755.1	–1.55	0.02	1.65	2.43	–0.67	–0.29	–1.64	–1.68	–0.91
ER-EC-05	21	4.84×10^{-3}	6.5	144.8	–2.82	0.09	4.78	18.13	–0.50	–0.20	–1.84	–1.19	–0.95

Table A6-3. Calculated Geochemical Parameters of Groundwater Samples Used in this Report (Continued)

Well	Figure A6-5 Sample	Ionic Strength	Charge Balance Error (%)[1]	DIC as (mg/L HCO_3^-)	log P_{CO2} (atm)	Mineral Saturation Indices[2,3]							
						Calcite	Smectite	Ca-Clino.	SiO_2 (a)	Fluorite	Albite	K-Feldspar	Dolomite
Timber Mountain (Continued)													
Coffer's Ranch Windmill Well	22	4.63×10^{-3}	–1.4	182.4	–3.08	0.26	6.11	25.06	–0.43	–0.45	–1.55	–1.04	–1.10
ER-OV-03c	23	5.03×10^{-3}	0.1	160.8	–3.02	0.10	5.90	24.21	–0.42	–0.28	–1.54	–0.95	–1.07
ER-EC-07	24	3.69×10^{-3}	–2.9	150.6	–2.70	0.06	4.86	18.66	–0.47	–1.13	–2.17	–0.96	–0.58
Fortymile Wash—North													
Water Well 8	25	2.26×10^{-3}	2.6	86.1	–2.40	–1.29	5.51	19.66	–0.36	–2.12	–2.70	–1.32	–3.06
Test Well 1 (USGS HTH #1)	26	2.29×10^{-3}	7.7	99.6	–3.70	–0.60	4.15	13.12	–0.82	—	–1.97	–1.66	—
UE-18t	27	8.09×10^{-3}	0.5	320.8	–3.12	0.93	3.21	7.90	–1.25	—	–2.52	–1.41	0.89
ER-30-1 (upper)	28	3.17×10^{-3}	4.4	108.9	–4.43	0.43	5.26	23.32	–0.72	–1.78	–1.04	–0.21	–0.34
ER-30-1 (lower)	29	3.04×10^{-3}	7.1	113.2	–4.18	0.09	4.86	19.81	–0.76	–2.17	–1.27	–0.73	–0.79
a#2 (dp)	30	2.96×10^{-3}	–2.3	121.0	–2.16	–1.16	5.14	16.23	–0.42	–1.74	–2.76	–2.03	–3.66
a#2 (sh)	31	2.92×10^{-3}	–0.3	130.2	–1.98	–1.39	5.39	16.75	–0.40	–1.80	–2.95	–2.12	–3.98
UE-29a#1 HTH	32	3.09×10^{-3}	5.2	114.1	–2.57	–0.61	6.04	24.28	–0.29	–1.98	–2.21	–0.80	–1.71
WT#15	33	3.95×10^{-3}	2.3	175.2	–2.23	–0.50	4.55	16.64	–0.42	—	–2.20	–1.08	–1.42
WT#14	34	3.11×10^{-3}	0.2	130.5	–2.19	–0.95	4.97	18.11	–0.35	—	–2.45	–1.12	–2.59
J-13	35	3.23×10^{-3}	0.3	139.0	–2.06	–0.94	4.82	16.97	–0.36	–0.97	–2.58	–1.23	–2.22
J-12	36	3.29×10^{-3}	–1.3	138.1	–2.01	–1.04	5.22	18.33	–0.35	–0.98	–2.75	–1.31	–2.54
JF#3	37	3.78×10^{-3}	1.3	123.8	–2.61	–0.36	5.60	23.21	–0.33	–1.12	–2.13	–0.44	–1.11
Solitario Canyon Wash													
H-6(bh)	38	4.41×10^{-3}	–0.8	181.1	–2.76	–0.30	3.93	14.51	–0.50	–0.97	–1.57	–1.20	–1.75
H-6(Tct)	39	4.52×10^{-3}	–6.6	212.4	–2.87	–0.47	3.43	12.50	–0.55	–1.65	–1.41	–1.09	—
H-6(Tcb)	40	4.97×10^{-3}	-9.5	229.7	–2.87	0.03	4.10	16.23	–0.49	–0.93	–1.35	–0.95	–1.15
WT-7	41	4.76×10^{-3}	–2.5	241.0	–3.27	0.13	3.31	10.76	–0.88	—	–1.73	–1.16	–0.39
WT-10	42	4.64×10^{-3}	1.4	180.3	–3.06	–0.21	3.84	14.76	–0.53	–1.40	–1.28	–1.08	–1.36

Table A6-3. Calculated Geochemical Parameters of Groundwater Samples Used in this Report (Continued)

Well	Figure A6-5 Sample	Ionic Strength	Charge Balance Error (%)[1]	DIC as (mg/L HCO_3^-)	log P_{CO2} (atm)	Mineral Saturation Indices[2,3]							
						Calcite	Smectite	Ca-Clino.	SiO_2 (a)	Fluorite	Albite	K-Feldspar	Dolomite
Yucca Mountain—Crest													
G-2	43	2.89×10^{-3}	0.6	127.6	–2.35	–0.79	4.35	15.53	–0.44	–1.95	–2.35	–1.05	–2.33
USW WT-24	44	2.73×10^{-3}	2.4	120.9	–2.82	–1.93	5.49	21.06	–0.35	–3.34	–1.78	–1.01	—
UZ-14(sh)	45	3.41×10^{-3}	8.1	129.2	–3.29	–1.41	5.31	21.74	–0.45	–1.69	–1.35	–0.61	–2.95
UZ-14(dp)	46	3.53×10^{-3}	6.3	133.8	–3.26	–1.55	5.14	21.26	–0.43	–1.84	–1.29	–0.50	–3.04
H-1(Tcp)	47	2.78×10^{-3}	0.6	118.5	–2.58	–0.86	4.40	15.47	–0.46	–2.01	–2.17	–1.25	–2.95
H-1(Tcb)	48	2.93×10^{-3}	–0.7	125.7	–2.55	–0.68	3.96	12.49	–0.55	–2.05	–2.32	–1.60	–2.71
H-5	49	2.92×10^{-3}	2.1	127.8	–2.73	–0.95	4.08	14.59	–0.48	–2.26	–1.90	–1.14	—
USW SD-6	50	4.35×10^{-3}	–0.7	182.1	–3.08	–1.05	4.16	16.13	–0.51	–1.96	–1.30	–0.86	—
H-3	51	6.12×10^{-3}	–3.7	240.9	–3.85	–0.09	5.23	23.60	–0.55	–1.55	–0.57	–0.28	—
Yucca Mountain—Central													
G-4	52	3.56×10^{-3}	3.7	143.0	–2.49	–0.31	4.07	13.89	–0.50	–0.96	–2.18	–1.39	–1.98
b#1(Tcb)	53	3.59×10^{-3}	2.0	152.4	–1.89	–0.76	3.85	11.12	–0.46	–1.22	–2.76	–1.78	–2.47
b#1(bh)	54	3.94×10^{-3}	–3.4	170.1	–2.03	–0.51	4.13	13.61	–0.44	–1.22	–2.50	–1.43	–1.99
H-4	55	4.58×10^{-3}	3.9	185.2	–2.10	–0.42	4.11	13.31	–0.48	–0.33	–2.34	–1.57	–2.16
UZ#16	56	5.79×10^{-3}	10.8	185.9	–3.75	0.85	—	—	–0.62	—	–1.05	—	2.27
Yucca Mountain—Southeast													
ONC#1	57	3.40×10^{-3}	9.1	107.8	–3.64	0.49	4.24	16.99	–0.72	—	–1.72	–0.60	0.33
c#1	58	3.63×10^{-3}	–3.4	156.6	–2.31	–0.37	3.61	12.00	–0.45	–1.25	–2.12	–1.41	–1.82
c#3	59	3.48×10^{-3}	0.2	140.5	–2.46	–0.32	3.65	12.34	–0.47	–1.28	–2.07	–1.37	–1.60
c#3(95-97)	60	3.43×10^{-3}	3.6	144.5	–2.45	–0.30	3.78	13.30	–0.43	—	–1.98	–1.29	–1.69
c#2	61	3.53×10^{-3}	–0.2	142.5	–2.45	–0.28	3.72	12.85	–0.46	–1.20	–2.06	–1.31	–1.56
p#1(v)	62	8.25×10^{-3}	–1.2	438.7	–1.14	–0.32	2.90	6.20	–0.53	–0.44	–2.83	–1.93	–0.72
p#1(c)	63	1.85×10^{-2}	–2.5	976.6	–0.58	0.22	1.35	–1.76	–0.68	–0.02	–3.04	–2.14	0.53
WT-17	64	3.15×10^{-3}	–1.0	150.1	–1.96	–1.18	4.50	13.04	–0.51	–1.23	–2.93	–1.91	–2.96
WT#3	65	3.37×10^{-3}	–1.2	144.3	–2.41	–0.52	4.83	18.44	–0.37	–1.05	–2.13	–0.97	–1.66
WT#12	66	4.30×10^{-3}	0.1	174.0	–2.33	–0.31	4.43	15.67	–0.46	–0.71	–2.16	–1.32	–1.90

Table A6-3. Calculated Geochemical Parameters of Groundwater Samples Used in this Report (Continued)

Well	Figure A6-5 Sample	Ionic Strength	Charge Balance Error (%)[1]	DIC as (mg/L HCO_3^-)	log P_{CO2} (atm)	Mineral Saturation Indices[2,3]							
						Calcite	Smectite	Ca-Clino.	SiO_2 (a)	Fluorite	Albite	K-Feldspar	Dolomite
Jackass Flats													
J-11	67	1.69×10^{-2}	1.4	80.6	–3.23	0.24	6.09	28.57	–0.31	–1.00	–1.13	0.25	0.10
Crater Flat													
GEXA Well 4	68	4.56×10^{-3}	–2.3	151.8	–2.69	–0.21	4.72	18.48	–0.45	–0.80	–1.82	–0.89	–1.46
VH-1	69	4.77×10^{-3}	0.9	171.3	–2.32	–0.47	4.18	14.35	–0.46	–1.03	–2.05	–1.45	–1.33
Crater Flat—Southwest													
VH-2	70	1.29×10^{-2}	–1.3	446.9	–1.48	0.14	3.60	8.75	–0.71	–1.08	–3.15	–1.85	0.28
NC-EWDP-7S	71	1.44×10^{-2}	–0.6	461.8	–1.73	0.19	4.96	15.69	–0.68	–1.06	–2.95	–1.59	0.37
NC-EWDP-7SC	72	1.50×10^{-2}	–0.4	480.4	–1.60	0.18	4.47	12.52	–0.69	–1.17	–3.01	–2.00	0.36
NC-EWDP-1DX	73	1.19×10^{-2}	–3.5	414.1	–1.66	–0.03	5.42	20.19	–0.40	–1.52	–2.51	–1.04	0.03
NC-EWDP-1DX Zone 2	74	2.09×10^{-2}	–9.3	1,385.6	–0.70	–0.26	4.86	15.91	–0.38	0.62	–2.30	–1.72	–0.70
NC-EWDP-01S Zone 1	75	1.15×10^{-2}	–3.7	386.1	–1.86	0.20	5.39	21.01	–0.38	–1.65	–2.30	–0.84	0.49
NC-EWDP-01S Zone 2	76	1.14×10^{-2}	–3.8	389.0	–1.75	0.09	5.17	19.40	–0.40	–1.68	–2.44	–0.99	0.30
NC-EWDP-01S	77	1.16×10^{-2}	–1.9	390.9	–1.75	0.12	5.32	20.60	–0.35	–1.66	–2.31	–0.90	0.34
NC-EWDP-12PA	78	1.10×10^{-2}	–1.6	540.6	–1.18	–0.58	5.37	20.88	–0.25	–0.25	–2.28	–0.71	–1.35
NC-EWDP-12PB	79	1.08×10^{-2}	–1.7	491.4	–1.29	–0.48	5.28	20.77	–0.27	–0.23	–2.21	–0.64	–1.15
NC-EWDP-12PC	80	1.09×10^{-2}	0.0	340.5	–1.99	0.25	5.31	21.52	–0.35	–1.26	–2.08	–0.64	0.60

Table A6-3. Calculated Geochemical Parameters of Groundwater Samples Used in this Report (Continued)

Well	Figure A6-5 Sample	Ionic Strength	Charge Balance Error (%)[1]	DIC as (mg/L HCO_3^-)	log P_{CO2} (atm)	Mineral Saturation Indices[2,3]							
						Calcite	Smectite	Ca-Clino.	SiO_2 (a)	Fluorite	Albite	K-Feldspar	Dolomite
Yucca Mountain—South													
NC-EWDP-09SX	81	6.32×10^{-3}	–1.1	213.3	–2.67	0.21	5.33	22.48	–0.39	–0.89	–1.62	–0.57	0.37
NC-EWDP-9SX Zone 1	82	5.95×10^{-3}	–1.6	194.5	–3.02	0.37	5.41	23.28	–0.48	–0.92	–1.53	–0.35	0.62
NC-EWDP-9SX Zone 2	83	6.01×10^{-3}	–2.3	206.4	–2.59	0.03	5.20	20.88	–0.44	–0.96	–1.86	–0.76	0.04
NC-EWDP-9SX Zone 3	84	5.94×10^{-3}	–3.2	206.8	–2.78	0.22	5.20	21.43	–0.47	–0.93	–1.72	–0.64	0.44
NC-EWDP-9SX Zone 4	85	5.95×10^{-3}	–3.8	209.9	–2.68	0.15	5.23	21.43	–0.43	–0.96	–1.75	–0.71	0.28
NC-EWDP-03D	86	5.63×10^{-3}	–1.8	230.1	–2.99	–0.90	4.52	19.24	–0.43	–2.31	–1.06	–0.40	–2.05
NC-EWDP-3S Zone 2	87	6.27×10^{-3}	–0.7	234.5	–3.30	–0.45	4.97	22.47	–0.40	–2.09	–0.66	–0.26	–1.36
NC-EWDP-3S Zone 3	88	6.90×10^{-3}	–3.9	279.9	–3.44	–0.22	4.67	21.29	–0.51	–1.85	–0.67	–0.07	–0.89
CIND-R-LITE	89	5.26×10^{-3}	–2.0	195.9	–2.35	0.04	2.69	8.92	–0.53	–1.18	–1.88	–1.08	0.29
NC-EWDP-15P	90	5.02×10^{-3}	–1.0	192.2	–2.50	–0.30	4.95	19.33	–0.42	–1.17	–1.83	–0.94	–0.81
NC-EWDP-02D	91	3.74×10^{-3}	–2.9	158.2	–2.33	–0.45	5.52	20.90	–0.38	–1.07	–2.39	–1.06	–1.76
NC-EWDP-19D	92	5.31×10^{-3}	–0.4	233.7	–3.31	–0.10	5.36	25.23	–0.36	–1.96	–0.69	0.11	–1.03
NC-EWDP-19P	93	3.40×10^{-3}	–1.9	115.4	–3.62	0.53	5.52	25.93	–0.38	–1.22	–1.13	0.09	0.26
NC-EWDP-19D (alluvial)	94	4.88×10^{-3}	–2.6	228.2	–3.22	–0.08	5.17	23.71	–0.39	–1.84	–0.88	–0.07	–0.79
NC-EWDP-19D (zone #1)	95	4.63×10^{-3}	0.4	204.5	–3.26	0.10	5.08	23.52	–0.39	–1.72	–0.90	–0.03	–0.45
NC-EWDP-19D (zone #2)	96	3.77×10^{-3}	1.9	149.8	–3.11	0.13	5.54	24.92	–0.33	–1.33	–1.29	–0.20	–0.37
NC-EWDP-19D (zone #3)	97	4.78×10^{-3}	0.5	212.1	–3.15	–0.44	5.08	22.61	–0.40	–2.16	–0.99	–0.21	–1.58
NC-EWDP-19D (zone #4)	98	5.20×10^{-3}	–0.8	234.4	–3.51	–0.22	5.14	24.52	–0.40	–2.11	–0.56	0.21	—

Table A6-3. Calculated Geochemical Parameters of Groundwater Samples Used in this Report (Continued)

Well	Figure A6-5 Sample	Ionic Strength	Charge Balance Error (%)[1]	DIC as (mg/L HCO_3^-)	log P_{CO2} (atm)	Mineral Saturation Indices[2,3]							
						Calcite	Smectite	Ca-Clino.	SiO_2 (a)	Fluorite	Albite	K-Feldspar	Dolomite
Amargosa Valley													
NC-EWDP-4PB	99	3.98×10^{-3}	–0.9	113.6	–4.53	0.78	5.18	23.61	–0.73	–1.56	–0.90	–0.10	—
NC-EWDP-4PA	100	3.91×10^{-3}	–0.4	107.8	–3.18	–0.11	5.25	20.58	–0.56	–1.51	–1.95	–0.88	–1.51
Desert Farms Garlic Plot	101	6.54×10^{-3}	0.0	127.7	–2.71	–0.09	5.22	20.39	–0.48	–1.58	–2.06	–0.88	–0.99
15S/49E-13dda	102	—	—	—	—	—	—	—	—	—	—	—	—
15S/50E-18ccc	103	6.35×10^{-3}	–1.0	153.5	–3.23	0.32	5.32	22.38	–0.55	–0.97	–1.50	–0.53	–0.54
NDOT	104	6.76×10^{-3}	–0.4	161.0	–2.80	–0.04	5.22	21.28	–0.45	–1.11	–1.64	–0.75	–1.03
15S/50E-18cdc	105	6.16×10^{-3}	–3.5	158.4	–2.81	–0.20	5.15	19.90	–0.54	–1.20	–1.88	–0.92	–1.44
Airport Well	106	3.93×10^{-3}	0.0	121.5	–3.61	0.12	5.08	21.47	–0.54	–1.56	–1.28	–0.63	–1.14
15S/50E-19b1	107	7.69×10^{-3}	1.5	167.5	–2.90	0.10	5.72	24.44	–0.43	–1.26	–1.52	–0.42	–0.18
Amargosa River													
16S/48E-8ba	108	1.42×10^{-2}	1.4	299.8	–2.46	0.56	5.42	22.83	–0.49	—	–1.61	–0.42	0.49
16S/48E-7bba	109	1.23×10^{-2}	0.8	269.6	–2.02	–0.03	6.09	25.98	–0.23	—	–1.69	–0.48	–0.47
16S/48E-7cbc	110	1.21×10^{-2}	0.8	246.8	–2.35	0.18	6.16	27.12	–0.25	—	–1.49	–0.28	0.24
16S/48E-18bcc	111	1.30×10^{-2}	1.7	272.1	–2.60	0.60	6.48	30.96	–0.17	—	–0.95	0.28	0.84
16S/48E-17ccc	112	1.47×10^{-2}	3.4	246.3	–2.35	0.31	6.34	29.10	–0.18	—	–1.21	–0.02	0.19
16S/48E-18dad	113	1.25×10^{-2}	3.1	243.3	–2.35	0.24	6.32	28.73	–0.18	—	–1.27	–0.08	0.02
16S/48E-8cda	114	1.25×10^{-2}	1.2	276.1	–2.21	0.12	6.32	27.88	–0.22	—	–1.44	–0.28	–0.28
16S/48E-17abb	115	1.33×10^{-2}	0.8	324.8	–1.95	0.08	6.31	27.59	–0.18	—	–1.57	–0.33	–0.39
Barrachman Dom/Irr.	116	1.26×10^{-2}	–4.2	304.4	–2.10	0.04	6.83	29.73	–0.20	–0.63	–1.65	–0.35	–0.29
McCracken Domestic	117	1.71×10^{-2}	3.2	257.3	–2.17	0.16	6.64	29.58	–0.18	–0.57	–1.40	–0.23	–0.22

Table A6-3. Calculated Geochemical Parameters of Groundwater Samples Used in this Report (Continued)

Well	Figure A6-5 Sample	Ionic Strength	Charge Balance Error (%)[1]	DIC as (mg/L HCO_3^-)	log P_{CO2} (atm)	Mineral Saturation Indices[2,3]							
						Calcite	Smectite	Ca-Clino.	SiO_2 (a)	Fluorite	Albite	K-Feldspar	Dolomite
Fortymile Wash—West													
16S/48E-15ba	118	1.30×10^{-2}	–0.2	265.4	–2.61	0.62	5.42	22.86	–0.50	—	–1.62	–0.45	0.71
16S/48E-10cba	119	4.25×10^{-3}	–0.9	163.3	–3.10	0.03	6.21	28.67	–0.27	—	–1.22	0.08	0.04
16S/48E-15aaa	120	3.95×10^{-3}	1.7	152.8	–2.92	–0.15	6.10	27.61	–0.25	—	–1.39	–0.04	–0.43
Selbach Domestic	121	7.48×10^{-3}	–0.9	178.9	–2.77	0.10	6.33	28.77	–0.23	–1.19	–1.29	–0.08	0.08
16S/48E-15dda	122	5.41×10^{-3}	6.8	176.5	–2.77	0.10	6.26	28.59	–0.22	—	–1.35	0.01	0.00
16S/49E-23add	123	4.02×10^{-3}	7.5	125.0	–3.11	0.07	6.39	30.06	–0.19	—	–1.20	0.21	–0.48
16S/48E-23bdb	124	3.97×10^{-3}	3.0	172.3	–2.11	–0.97	6.12	24.99	–0.19	—	–2.04	–0.68	–2.56
16S/48E-23da	125	—	—	—	—	—	—	—	—	—	—	—	—
Funeral Mountain Ranch Irrig.	126	5.29×10^{-3}	–2.0	198.4	–2.93	0.08	6.94	33.28	–0.11	–0.97	–0.93	0.39	–0.22
Fortymile Wash—South													
16S/49E-05acc	127	4.07×10^{-3}	5.0	134.3	–2.98	0.26	6.09	27.16	–0.28	–1.31	–1.68	–0.18	–0.24
16S/49E-8abb	128	4.42×10^{-3}	2.2	161.4	–2.33	–0.29	5.96	23.69	–0.32	—	–2.36	–0.82	–1.30
16S/49E-8acc	129	3.91×10^{-3}	1.4	139.7	–2.76	–0.01	5.83	25.07	–0.31	—	–1.91	–0.33	–0.64
16S/49E-18dc	130	4.05×10^{-3}	0.5	149.7	–2.93	0.15	6.03	27.13	–0.30	—	–1.65	0.02	–0.22
16s/48E-24aaa	131	4.06×10^{-3}	3.5	146.1	–2.93	0.12	6.15	28.67	–0.20	—	–1.29	0.13	–0.80
16S/49E-19daa	132	3.92×10^{-3}	0.1	131.9	–3.08	0.29	6.22	29.24	–0.21	—	–1.41	0.27	–0.35
DeLee Large Irrigation	133	3.85×10^{-3}	2.5	136.6	–2.94	–0.06	7.79	36.15	–0.10	–1.16	–1.54	0.29	–1.25
16S/48E-25aa	134	3.73×10^{-3}	0.6	132.1	–2.98	0.10	6.10	28.06	–0.23	—	–1.47	0.09	–0.87
16S/48E-36aaa	135	3.56×10^{-3}	0.1	128.3	–3.30	0.31	6.50	31.26	–0.19	—	–1.13	0.41	0.03
Bray Domestic	136	3.75×10^{-3}	0.9	131.8	–2.91	–0.01	6.87	31.56	–0.17	–1.37	–1.61	0.18	–0.82
Amargosa Estates #2	137	3.68×10^{-3}	1.4	133.3	–2.99	0.09	6.56	30.50	–0.17	–1.04	–1.43	0.17	–0.45
17S/48E-1ab	138	3.65×10^{-3}	1.2	134.1	–2.98	0.08	6.42	29.84	–0.18	—	–1.42	0.17	–0.58
17S/49E-7bb	139	4.37×10^{-3}	2.8	149.5	–3.14	0.42	6.52	31.32	–0.18	—	–1.14	0.39	0.04
17S/49E-8ddb	140	3.68×10^{-3}	4.6	118.6	–3.34	0.35	6.69	32.46	–0.17	—	–1.15	0.52	0.16
17S/49E-35ddd	141	4.43×10^{-3}	–0.9	158.3	–2.82	–0.09	6.68	31.02	–0.15	—	–1.38	0.19	–0.36

Table A6-3. Calculated Geochemical Parameters of Groundwater Samples Used in this Report (Continued)

Well	Figure A6-5 Sample	Ionic Strength	Charge Balance Error (%)[1]	DIC as (mg/L HCO_3^-)	log P_{CO2} (atm)	Mineral Saturation Indices[2,3]							
						Calcite	Smectite	Ca-Clino.	SiO_2 (a)	Fluorite	Albite	K-Feldspar	Dolomite
Fortymile Wash—East													
15S/49E-22a1	142	4.27×10^{-3}	0.0	145.5	–2.83	0.17	5.44	23.00	–0.38	–1.12	–1.87	–0.46	–0.31
15S/49E-22dcc	143	4.41×10^{-3}	1.2	207.6	–1.50	–1.05	4.64	13.63	–0.41	–1.40	–3.20	–1.88	–2.84
15S/49E-27acc	144	4.26×10^{-3}	–1.3	153.3	–2.50	0.14	1.93	1.05	–0.94	–1.73	–2.94	–2.04	–0.37
O'Neill Domestic	145	4.56×10^{-3}	2.2	143.4	–2.79	–0.05	6.84	30.57	–0.21	–1.50	–1.72	–0.07	–0.85
16S/49E-9cda	146	5.43×10^{-3}	2.6	149.9	–2.46	–0.22	6.15	26.24	–0.24	—	–1.96	–0.38	–1.06
16S/49E-9dcc	147	5.16×10^{-3}	0.5	139.2	–3.08	0.22	6.57	31.04	–0.20	—	–1.25	0.32	–0.16
16S/49E-16ccc	148	4.62×10^{-3}	0.6	133.8	–2.79	0.06	6.32	28.15	–0.19	—	–1.64	–0.26	–0.73
Ponderosa Dairy #1	149	6.29×10^{-3}	–1.2	153.1	–2.33	–0.29	5.72	24.50	–0.23	–1.24	–1.91	–0.34	–1.02
17S/49E-9aa	150	5.10×10^{-3}	0.0	131.5	–2.90	0.06	6.25	28.64	–0.23	—	–1.54	0.11	–0.38
17S/49E-15bbd	151	3.85×10^{-3}	–0.7	119.6	–3.05	0.04	6.65	30.72	–0.19	—	–1.58	0.21	–0.34
M. Gilgan Well	152	3.82×10^{-3}	1.8	127.0	–3.11	0.15	6.49	30.56	–0.19	–1.08	–1.33	0.28	–0.27
17S/49E-15bc	153	—	—	—	—	—	—	—	—	—	—	—	—
Gravity Fault													
NC-EWDP-5S	154	—	—	—	—	—	—	—	—	—	—	—	—
NC-EWDP-5SB	155	6.60×10^{-3}	–0.2	221.3	–2.29	–0.42	4.59	14.45	–0.73	–1.50	–2.63	–1.46	–1.42
16S/50E-7bcd	156	1.13×10^{-2}	1.4	303.4	–2.12	0.27	4.19	14.45	–0.65	—	–2.37	–1.03	0.51
Nelson Domestic	157	1.12×10^{-2}	–3.8	325.0	–2.00	0.14	4.12	13.15	–0.70	–0.20	–2.58	–1.27	0.23
16S/49E-12ddd	158	1.14×10^{-2}	1.6	301.5	–2.16	0.18	4.39	13.17	–0.76	—	–2.62	–1.72	0.27
Lowe Domestic	159	1.07×10^{-2}	–1.5	284.4	–2.32	0.16	6.38	26.74	–0.38	–0.90	–1.88	–0.47	–0.03
16S/49E-15aaa	160	8.50×10^{-3}	–1.3	201.8	–2.43	0.08	5.75	23.76	–0.39	—	–1.97	–0.53	–0.25
Anvil Ranch Irrigation	161	8.09×10^{-3}	1.5	139.8	–2.81	0.15	6.88	31.83	–0.18	–1.06	–1.47	0.21	–0.33
16S/49E-36aaa	162	1.25×10^{-2}	3.8	321.1	–2.33	0.45	5.39	22.40	–0.49	—	–1.89	–0.37	0.88
16S/49E-35baa	163	1.21×10^{-2}	0.1	325.8	–1.95	0.04	5.36	20.36	–0.48	—	–2.30	–0.88	–0.05
Payton Domestic	164	1.19×10^{-2}	–0.8	304.0	–2.19	0.16	5.88	23.63	–0.47	0.01	–2.16	–0.59	0.17
16S/49E-36aba	165	1.14×10^{-2}	2.3	302.3	–2.26	0.27	5.51	22.89	–0.44	—	–1.92	–0.39	0.54
16S/49E-35aaa	166	1.11×10^{-2}	4.8	280.3	–2.29	0.24	5.29	21.29	–0.50	—	–2.01	–0.54	0.38
Oettinger Well	167	1.14×10^{-2}	–2.0	307.9	–2.06	0.12	5.28	20.55	–0.48	–0.20	–2.22	–0.72	0.09

Table A6-3. Calculated Geochemical Parameters of Groundwater Samples Used in this Report (Continued)

Well	Figure A6-5 Sample	Ionic Strength	Charge Balance Error (%)[1]	DIC as (mg/L HCO_3^-)	log P_{CO2} (atm)	Mineral Saturation Indices[2,3]							
						Calcite	Smectite	Ca-Clino.	SiO_2 (a)	Fluorite	Albite	K-Feldspar	Dolomite
Gravity Fault (Continued)													
Amargosa Motel (b)	168	1.12×10^{-2}	–1.1	298.8	–2.17	0.20	5.63	22.94	–0.42	–0.27	–2.05	–0.54	0.28
17S/49E-11ba	169	1.00×10^{-2}	1.2	209.6	–2.82	0.44	6.34	29.04	–0.33	—	–1.38	0.16	0.74
Spring Meadows Well #8	170	—	—	—	—	—	—	—	—	—	—	—	—
17S/50E-19aab	171	1.46×10^{-2}	1.2	405.5	–3.08	0.35	6.95	33.70	–0.38	—	–0.67	0.82	0.99
USFWS - Five Springs Well	172	8.94×10^{-3}	4.9	261.4	–2.07	0.18	3.38	8.48	–0.80	–0.91	–2.93	–1.63	0.42
Spring Meadows Well #10	173	—	—	—	—	—	—	—	—	—	—	—	—
18S/49E-1aba	174	8.51×10^{-3}	–0.8	253.0	–3.27	0.75	7.53	38.08	–0.16	—	–0.62	1.11	1.44
18S/50E-6dac	175	8.45×10^{-3}	3.1	227.2	–2.87	0.41	6.52	31.77	–0.17	—	–0.91	0.56	0.87
18S/50E-7aa	176	1.06×10^{-2}	1.7	258.0	–3.08	0.50	7.53	35.92	–0.30	—	–1.00	0.63	0.75
Amargosa River/Fortymile Wash													
16S/48E-36dcc	177	1.04×10^{-2}	0.4	336.8	–1.73	–0.09	5.88	24.31	–0.23	—	–2.02	–0.58	–0.57
Crane Domestic	178	1.42×10^{-2}	–0.5	504.9	–1.56	0.12	5.24	19.91	–0.42	–0.14	–2.25	–0.89	0.04
27N/4E-27bbb	179	1.30×10^{-2}	2.4	448.3	–2.21	0.61	6.70	31.22	–0.19	—	–1.27	0.26	1.05
IMV on Windjammer	180	9.65×10^{-3}	–0.8	321.2	–2.05	0.10	6.25	26.99	–0.23	–0.32	–1.75	–0.35	–0.12
17S/49E-29acc	181	1.37×10^{-2}	5.0	288.6	–2.21	0.15	6.75	30.78	–0.18	—	–1.39	0.10	0.05
17S/49E-28bcd	182	9.34×10^{-3}	1.8	307.7	–2.15	0.19	6.15	27.12	–0.22	—	–1.62	–0.20	0.10
18S/49E-2cbc	183	9.42×10^{-3}	0.1	360.7	–2.28	0.28	6.11	26.86	–0.29	—	–1.49	–0.23	0.51
Mom's Place	184	6.77×10^{-3}	–0.5	241.7	–2.45	0.10	6.57	29.79	–0.18	–0.55	–1.47	–0.01	–0.08
18S/49E-11bbb	185	8.40×10^{-3}	4.5	234.5	–2.26	–0.01	6.28	28.08	–0.18	—	–1.53	–0.12	–0.28
Skeleton Hills													
TW-5	186	1.10×10^{-2}	–1.5	400.0	–2.30	0.54	3.77	12.02	–0.83	–0.41	–2.37	–1.12	1.19
Unnamed Well 15S/50E-22-7	187	4.19×10^{-3}	8.6	171.5	–1.62	–1.20	5.23	16.45	–0.38	–1.43	–3.18	–1.81	–3.18

Table A6-3. Calculated Geochemical Parameters of Groundwater Samples Used in this Report (Continued)

Well	Figure A6-5 Sample	Ionic Strength	Charge Balance Error (%)[1]	DIC as (mg/L HCO_3^-)	log P_{CO2} (atm)	Mineral Saturation Indices[2,3]							
						Calcite	Smectite	Ca-Clino.	SiO_2 (a)	Fluorite	Albite	K-Feldspar	Dolomite
Amargosa Flat													
Amargosa Tracer Hole #2	188	8.57×10^{-3}	–0.4	279.8	–2.54	0.64	3.94	13.13	–0.78	–0.77	–2.45	–1.11	1.32
Cherry Patch Well, 17S/52E-08cdb	189	2.37×10^{-2}	2.5	307.4	–1.88	–0.02	4.48	14.33	–0.67	–0.77	–2.39	–1.52	0.01
USDOE-MSH-C shallow Well	190	7.40×10^{-3}	–0.7	263.9	–2.63	0.07	5.82	23.92	–0.50	–1.14	–1.93	–0.47	0.46
Mine Mountain													
UE-17a	191	9.51×10^{-3}	14.9	208.5	–2.31	0.03	3.34	5.62	–1.01	–1.42	–3.27	–2.38	0.30
UE-1a	192	9.02×10^{-3}	–3.7	432.9	–1.81	0.21	4.21	11.64	–0.79	—	–3.24	–1.66	0.48
UE-1b	193	5.32×10^{-3}	18.9	197.6	–2.13	–0.15	5.94	25.26	–0.18	—	–2.20	–0.35	–0.37
UE-16f	194	2.66×10^{-2}	–15.7	902.7	–2.98	0.31	1.82	–0.30	–1.51	–1.59	–2.25	–1.88	1.08
UE-14b	195	4.87×10^{-3}	2.2	113.0	–3.36	0.01	5.59	23.60	–0.44	—	–1.36	–0.73	–1.35
Pluto 1	196	5.92×10^{-3}	5.9	150.4	–2.84	0.32	5.90	25.75	–0.34	—	–1.89	–0.22	0.38
Pluto 5	197	7.65×10^{-3}	7.4	220.2	–2.59	0.49	5.95	25.27	–0.31	—	–2.07	–0.51	0.93
USGS Test Well F (HTH)	198	7.90×10^{-3}	9.4	252.6	–1.31	–0.11	0.35	–6.49	–0.79	–0.57	–3.24	–2.17	–0.19

Table A6-3. Calculated Geochemical Parameters of Groundwater Samples Used in this Report (Continued)

Well	Figure A6-5 Sample	Ionic Strength	Charge Balance Error (%)[1]	DIC as (mg/L HCO_3^-)	log P_{CO2} (atm)	Mineral Saturation Indices[2,3]							
						Calcite	Smectite	Ca-Clino.	SiO_2 (a)	Fluorite	Albite	K-Feldspar	Dolomite
Funeral Mountains													
Woodcamp Spring	199	4.17×10^{-3}	3.7	139.1	–2.15	–0.84	6.45	25.84	–0.26	–2.73	–2.59	–0.61	–2.26
Bond Gold Mining #13	200	2.44×10^{-2}	-5.3	296.7	–1.86	0.30	3.09	5.38	–0.91	–1.53	–3.29	–2.13	0.74
Nevares Spring	201	1.27×10^{-2}	–2.1	375.7	–1.78	0.20	2.87	6.81	–0.77	–0.49	–2.59	–1.53	0.53
Travertine Spring	202	1.19×10^{-2}	–2.3	366.1	–1.82	0.04	3.55	10.70	–0.67	–0.41	–2.45	–1.30	0.25

Source: DTN: LA0310EK831232.001 [DIRS 165995].

[1] PHREEQC calculates percent error in the selected output file as 100 x (*cations* - |*anions*|)/(*cations* + |*anions*|), where *cations* is the electrical charge of the cations in equivalents per liter and *anions* is the electrical charge of the anions in equivalents per liter (Parkhurst and Appelo 1999 [DIRS 159511], p. 140).

[2] The saturation index of a mineral phase is calculated as the base-ten logarithm of the ratio of the ion activity product (IAP) to the solubility constant (K_{sp}) of the mineral at the prevailing temperature: log (IAP/K_{sp}). Values of log (IAP/K_{sp}) less than zero indicate the groundwater is undersaturated with that mineral. Conversely, values of log (IAP/K_{sp}) greater than zero indicate the groundwater is oversaturated with that mineral. Values of log (IAP/K_{sp}) equal to zero indicate the groundwater is at equilibrium with the mineral (Langmuir 1997 [DIRS 100051], p. 8).

[3] The log P_{CO2} and saturation indices for calcite, SiO_2(a), fluorite, albite and K-feldspar were calculated using the database *phreeqc.dat* (Parkhurst and Appelo 1999 [DIRS 159511], Table 55). The saturation indices for smectite and Ca-clinoptilolite were calculated based on the Gibbs free-energy data listed in Table A6-4 of this report.

Clino. = Clinoptilolite.

Table A6-4. Yucca Mountain Mineral Phase Compositions and Thermodynamic Data Used in PHREEQC Analyses

Phase	Formula	ΔG^{O}_{f} (kJ/mol-°K)	ΔH^{O}_{f} (kJ/mol)	Reference
Smectite	$K_{0.1}Na_{0.02}Ca_{0.14}Al_{4.4}Si_{7.6}O_{20}(OH)_4 \cdot 4H_2O$	–11,619.6	–12,595.6	Chipera et al. (1995 [DIRS 100025], Table 1)
Ca-Clinoptilolite	$K_{2.5}Na_{1.1}Ca_{1.2}Al_{6.0}Si_{30.0}O_{72.0} \cdot 26.8\ H_2O$	-39,067.7	-42,491.3	Chipera and Bish (1997 [DIRS 105079], Tables 1 to 2)
Na-Clinoptilolite	$K_{2.8}Na_{1.5}Ca_{0.9}Al_{6.1}Si_{29.9}O_{72.0} \cdot 26.8\ H_2O$	-39,093.8	-42,512.1	Chipera and Bish (1997 [DIRS 105079], Tables 1 to 2)

The geochemical parameters calculated in this section provide an indication of which minerals are potentially dissolving or precipitating in Yucca Mountain groundwater and, thus, provide important constraints on groundwater mixing and reaction models. Table A6-3 indicates that groundwater in the Yucca Mountain area is generally slightly undersaturated with amorphous silica [SiO_2(a)], fluorite, and albite and greatly supersaturated with Ca-clinoptilolite and smectite typical of Yucca Mountain. The spatial distribution of saturation indices of minerals whose saturation state in groundwater are more variable are discussed in more detail in the following subsections.

In addition to the saturation indices shown in Table A6-3, saturation indices were also calculated for other common minerals (DTN: LA0310EK831232.001 [DIRS 165995]). The calculated Na-clinoptilolite saturation indices generally are similar to those shown in Table A6-3 for Ca-clinoptilolite. All groundwaters in the Yucca Mountain area are significantly undersaturated with gypsum and halite and slightly oversaturated with quartz (chalcedony). Yucca Mountain area groundwaters are generally undersaturated with respect to sepiolite ($Mg_2Si_3O_{7.5}(OH) \cdot 3H_2O$), except in areas of the Amargosa Desert such as the Gravity fault area where Si-rich groundwater from the volcanic alluvium mixes with Mg-rich discharge from the carbonate aquifer. Kaolinite saturation indices are zero in all cases because of the assumption (Table A5-1, Assumption 2) that all groundwaters are in equilibrium with kaolinite.

A6.3.5.1 Ionic Strength

Ionic strength (I) is a measure of the interionic effects resulting from the electrical attraction and repulsion between various ions in solution. It is defined by $I = 1/2 \sum_i C_i Z_i^2$ (Langmuir 1997 [DIRS 100051], p. 123), where C_i is the concentration (mol/kg solution) and Z_i is the charge of ion i. Ionic strength is expressed in this report as moles per kilogram of groundwater.

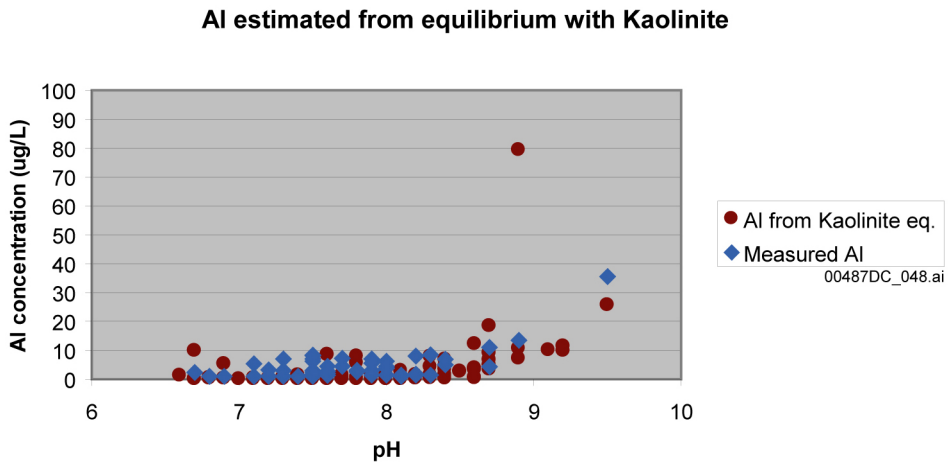

DTNs: GS980908312322.008 [DIRS 145412; GS990808312322.002 [DIRS 162917]; GS010308312322.002 [DIRS 162910]; GS011108312322.006 [DIRS 162911].

NOTE: The single, large calculated Al value is from a sample with very small SiO2 value (UE-16f, sample 194).

Figure A6-33. Comparison between Measured Dissolved Aluminum Concentrations and Dissolved Aluminum Concentrations Calculated by PHREEQC Assuming Equilibrium with Kaolinite

Excluding groundwater from the carbonate aquifer at borehole p#1, groundwater at Yucca Mountain has an ionic strength that ranges from about 2.2×10^{-3} to 4.8×10^{-3} mole/kg (Figure A6-34). A single groundwater from the Yucca Crest area from borehole H-3 (Site 51) has a somewhat higher value (6.12×10^{-3} mole/kg). The ionic strength of groundwater at the NC-EWDP wells in southern Yucca Mountain and south of Crater Flat increases toward the west, reflecting the differences in the ionic strength of the groundwater to the north and west of these wells. North of Yucca Mountain, groundwater shows a westward increase in ionic strength from the northern Fortymile Wash area through Timber Mountain and toward Oasis Valley. The highest ionic strength groundwaters are associated with the southwestern Crater Flat, the Amargosa River, the Gravity fault area, and central Jackass Flats.

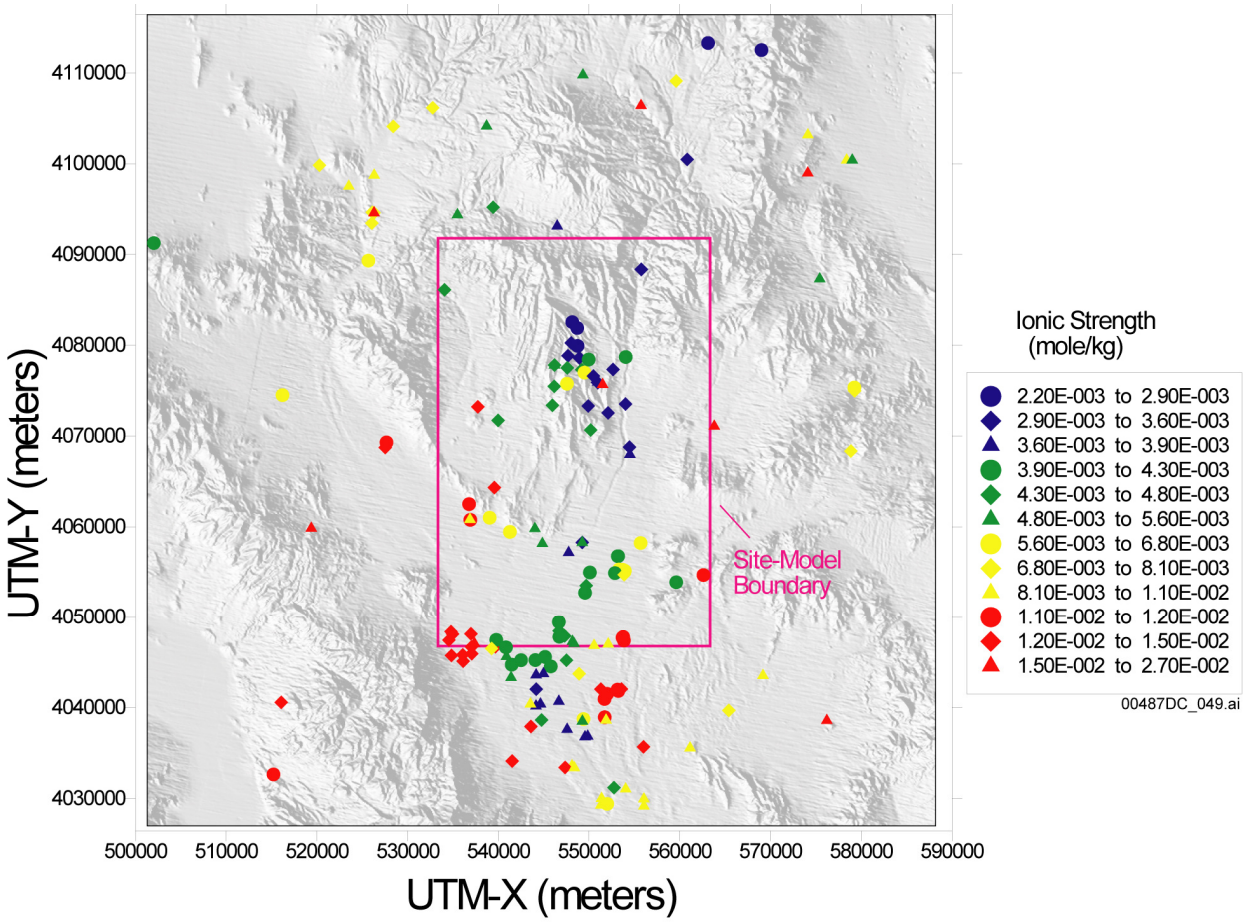

Sources: Table A6-1; DTN: LA0310EK831232.001 [DIRS 165995].

NOTE: This figure has color-coded data points and should not be read in a black and white version.

UTM-X = UTM-Easting; UTM-Y = UTM-Northing; and UTM=Universal Transverse Mercator.

Figure A6-34. Areal Distribution of Ionic Strength in Groundwater

A6.3.5.2 Dissolved Inorganic Carbon

Dissolved inorganic carbon (DIC) represents the total amount of carbon present in all dissolved carbon species, including H_2CO_3, HCO_3^-, and CO_3^{2-}. It is expressed in Table A6-6 and Figure A6-35 as the mg/L HCO_3^- having the same number of moles of carbon per liter. Although alkalinity changes can result from groundwater interactions with noncarbonate rocks, the DIC of groundwater can change only if the groundwater: (1) mixes with groundwater having different DIC concentrations, (2) dissolves carbon-bearing minerals such as calcite or dolomite, (3) precipitates calcite, or (4) interacts with CO_2(g) in the overlying unsaturated zone. The last process tends to be of limited importance due to the very low diffusion of CO_2(g) in water. Hence, in the absence of mixing, downgradient increases in DIC are a good indicator of contact between groundwater and either calcite or dolomite.

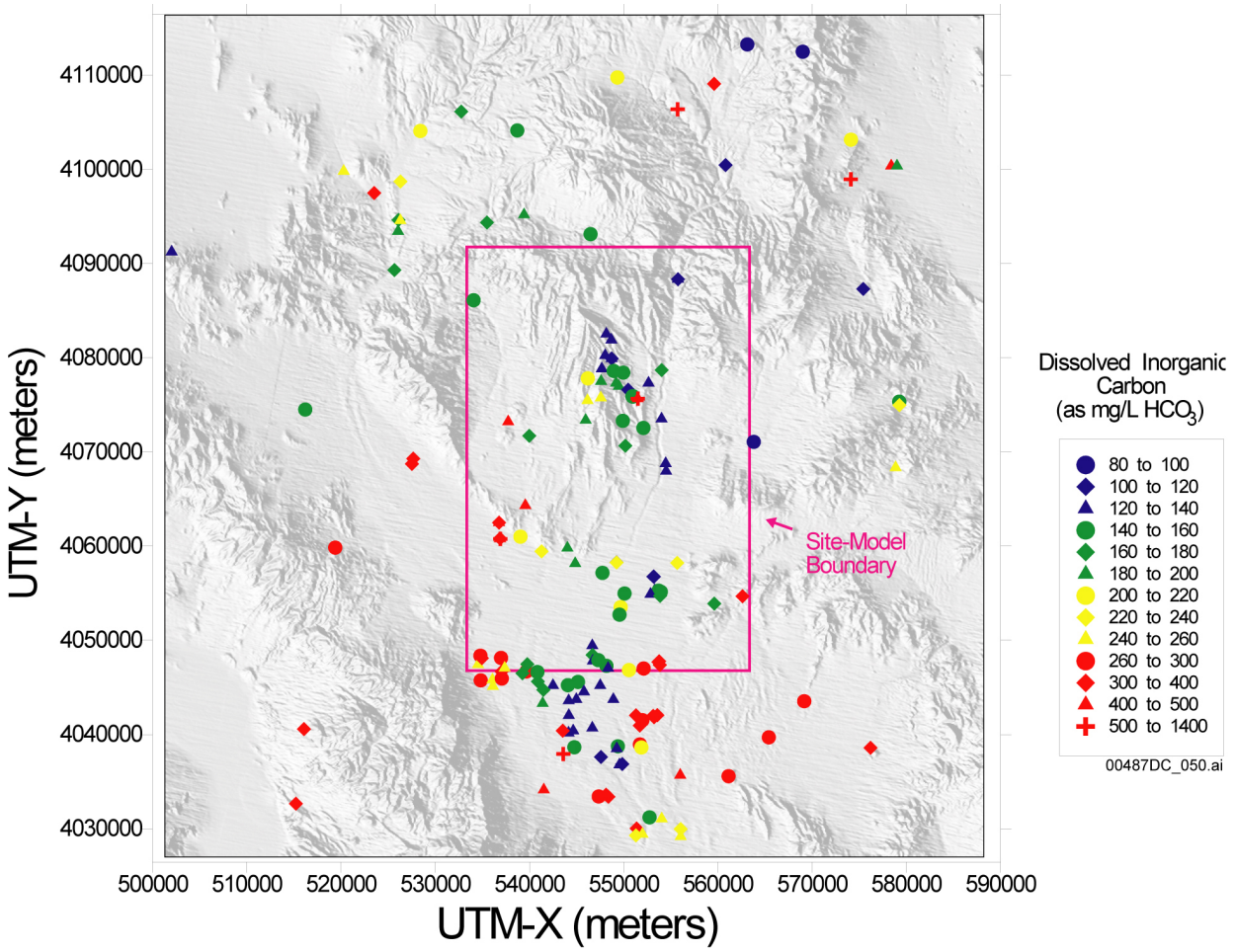

Sources: Table A6-1; DTN: LA0310EK831232.001 [DIRS 165995].

NOTE: This figure has color-coded data points and should not be read in a black and white version.

UTM-X = UTM-Easting; UTM-Y = UTM-Northing; and UTM=Universal Transverse Mercator.

Figure A6-35. Areal Distribution of Dissolved Inorganic Carbon in Groundwater

Groundwater in the northern part of Yucca Mountain has relatively low concentrations of DIC (Figure A6-35). Somewhat higher DIC concentrations are found near Solitario Canyon in some of the SCW and YM-CR wells. Groundwater DIC concentrations increase toward the south at Yucca Mountain. The groundwater in Beatty Wash directly north of Yucca Mountain at well ER-EC-07 (Site 24) has similarly low DIC concentrations as northern Yucca Mountain, as does groundwater at most of the FMW-N wells northeast and east of Yucca Mountain. Southward along Fortymile Wash, the DIC concentrations of groundwater in the FMW-S wells increases and then decreases slightly but are generally low compared to the higher values found in groundwater in the surrounding AR, AR/FMW, and GF area wells. Groundwater in several of the wells in the Amargosa Valley area (LW group) has DIC concentrations that are nearly as low as that found at well J-11 (Site 67) in Jackass Flats. Groundwater in western and southwestern Crater Flat has much higher DIC concentrations than groundwater in the eastern part of the Crater Flat area, reflecting the presence of carbonate rocks at Bare Mountain.

A6.3.5.3 Dissolved Carbon-Dioxide Partial Pressure

The logarithm of dissolved carbon-dioxide partial pressure [log P_{CO_2} (atm)] is generally higher than expected due to equilibrium with the atmosphere (log P_{CO_2} = –3.5 atm) because of the much higher carbon-dioxide partial pressures found in the soil zone through which the water recharging the groundwater has passed. Soil-zone log P_{CO_2} values can be –2.0 atm or greater depending on climate and vegetation cover. Unsaturated-zone log P_{CO_2} at Yucca Mountain under the present climate is about –3.0 atm (Yang et al. 1996 [DIRS 100194]; Thorstenson et al. 1998 [DIRS 126827]). However, CO_2(g) production rates in the soil zones depend on climate, which has changed over time and presently changes with elevation and latitude (Quade and Cerling 1990 [DIRS 100073]), so unsaturated zone log P_{CO_2} values could have been higher under past wetter climates. Most Yucca Mountain area groundwaters have log P_{CO_2} values that are higher than are found in the unsaturated zone at Yucca Mountain.

In the absence of climate change, the tendency in groundwater is for log P_{CO_2} values to decrease downgradient from the recharge area as hydrogen ions and dissolved CO_2 react with the rock to form secondary minerals and HCO_3^- (Drever 1988 [DIRS 118564]). However, as stated above, climate change and other conditions particular to the recharge area can complicate this simple model.

At Yucca Mountain, groundwater in the Solitario Canyon and Yucca Crest area generally has lower log P_{CO_2} values than groundwater further to the east at Yucca Mountain (Figure A6-36). Along Fortymile Wash, groundwater log P_{CO_2} values show an overall southward decrease between the FMW-N and FMW-S area wells. Groundwater log P_{CO_2} values for well J-11 (Site 67) in Jackass Flats and at some LW area wells are also relatively low, whereas log P_{CO_2} values are relatively high at wells in southwest Crater Flat and AR and AR/FMW area wells.

A6.3.5.4 Calcite Saturation Index

In general, calcite saturation indices ($SI_{calcite}$) are expected to increase along a flow path as H^+ ions and dissolved CO_2 are converted to HCO_3^- and CO_3^{2-} during silicate weathering reactions or Ca^{2+} and HCO_3^- are added to the groundwater from calcite dissolution. Downgradient decreases in $SI_{calcite}$ could result from loss of Ca^{2+} through mineral precipitation or ion exchange.

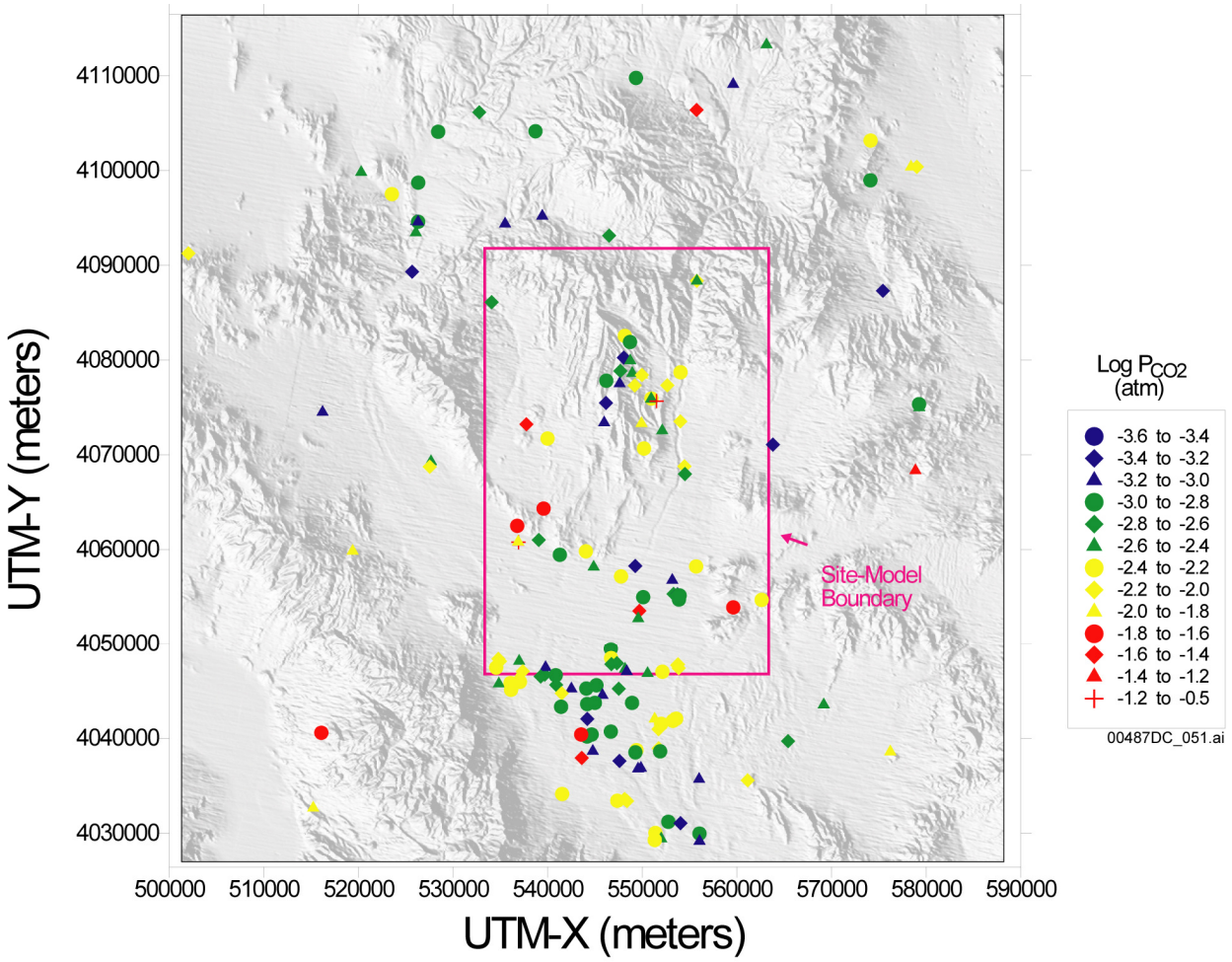

Sources: Table A6-1; DTN: LA0310EK831232.001 [DIRS 165995].

NOTE: This figure has color-coded data points and should not be read in a black and white version.

UTM-X = UTM-Easting; UTM-Y = UTM-Northing; and UTM=Universal Transverse Mercator.

Figure A6-36. Areal Distribution of Dissolved Carbon-Dioxide Partial Pressure in Groundwater

Groundwater north and northwest of Yucca Mountain in the Timber Mountain and Oasis Valley/Northwest Amargosa areas is generally saturated or supersaturated with calcite (Figure A6-37). Groundwater throughout most of Yucca Mountain is undersaturated with calcite, with the most undersaturated groundwater present in northern Yucca Mountain. Along Fortymile Wash, groundwater shows a southward increase in $SI_{Calcite}$. Almost all groundwater in the Amargosa Desert south of U.S. Highway 95 is saturated or supersaturated with calcite. Groundwater in most of the Crater Flat area is saturated or supersaturated with calcite.

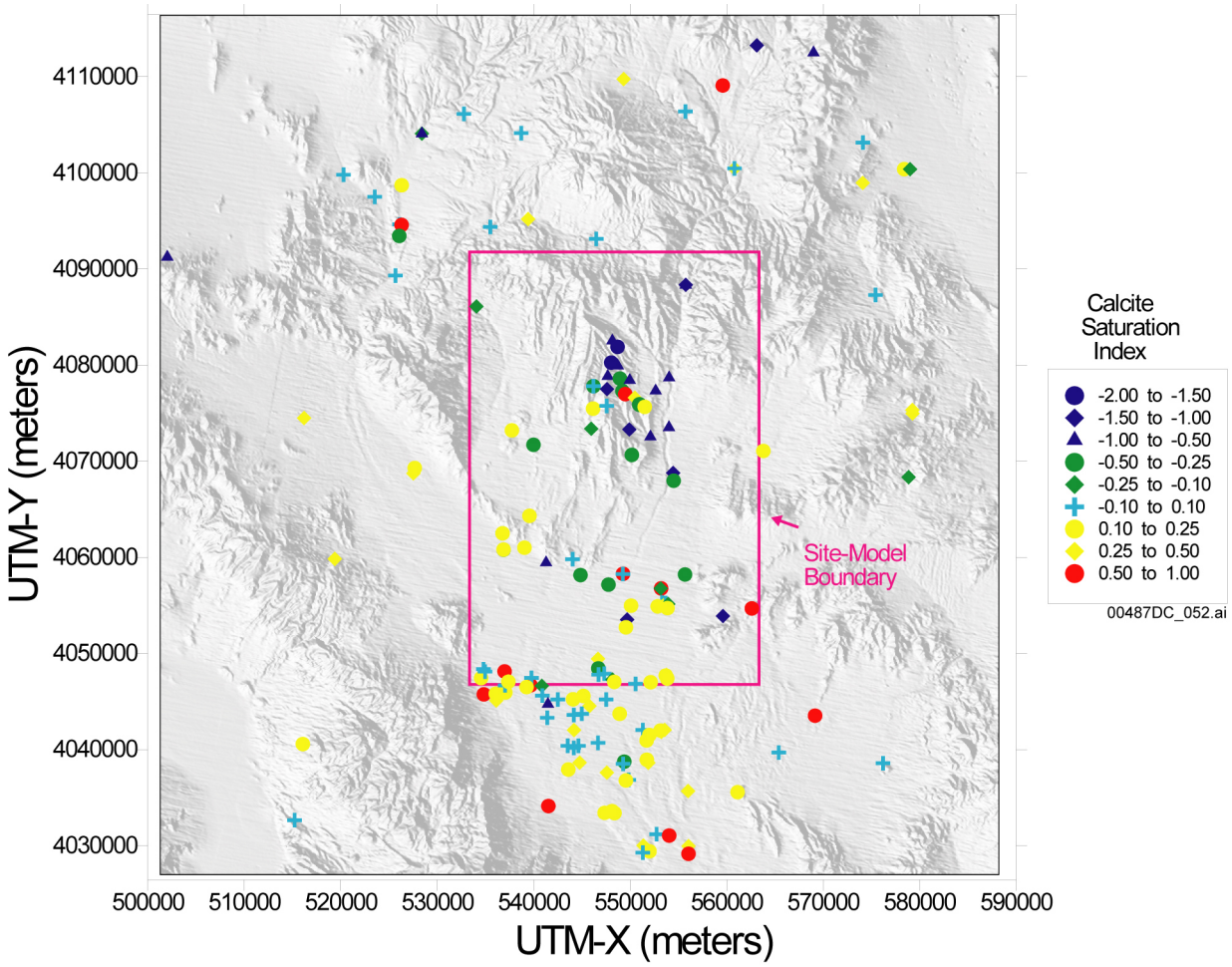

Sources: Table A6-1; DTN: LA0310EK831232.001 [DIRS 165995].

NOTE: This figure has color-coded data points and should not be read in a black and white version.

UTM-X = UTM-Easting; UTM-Y = UTM-Northing; and UTM=Universal Transverse Mercator.

Figure A6-37. Areal Distribution of Calcite Saturation Index in Groundwater

A6.3.5.5 Smectite Saturation Index

Except for a few samples in the Mine Mountain area, groundwater throughout the Yucca Mountain region is supersaturated with smectite (Figure A6-38). The degree of supersaturation increases southward from Yucca Mountain toward the Amargosa Desert. If groundwater from Yucca Mountain and Fortymile Wash flows southward toward the Amargosa Desert, the southward increase in smectite saturation indices suggests that silicate-weathering reactions are providing ions to the groundwater faster than they can be removed by smectite precipitation.

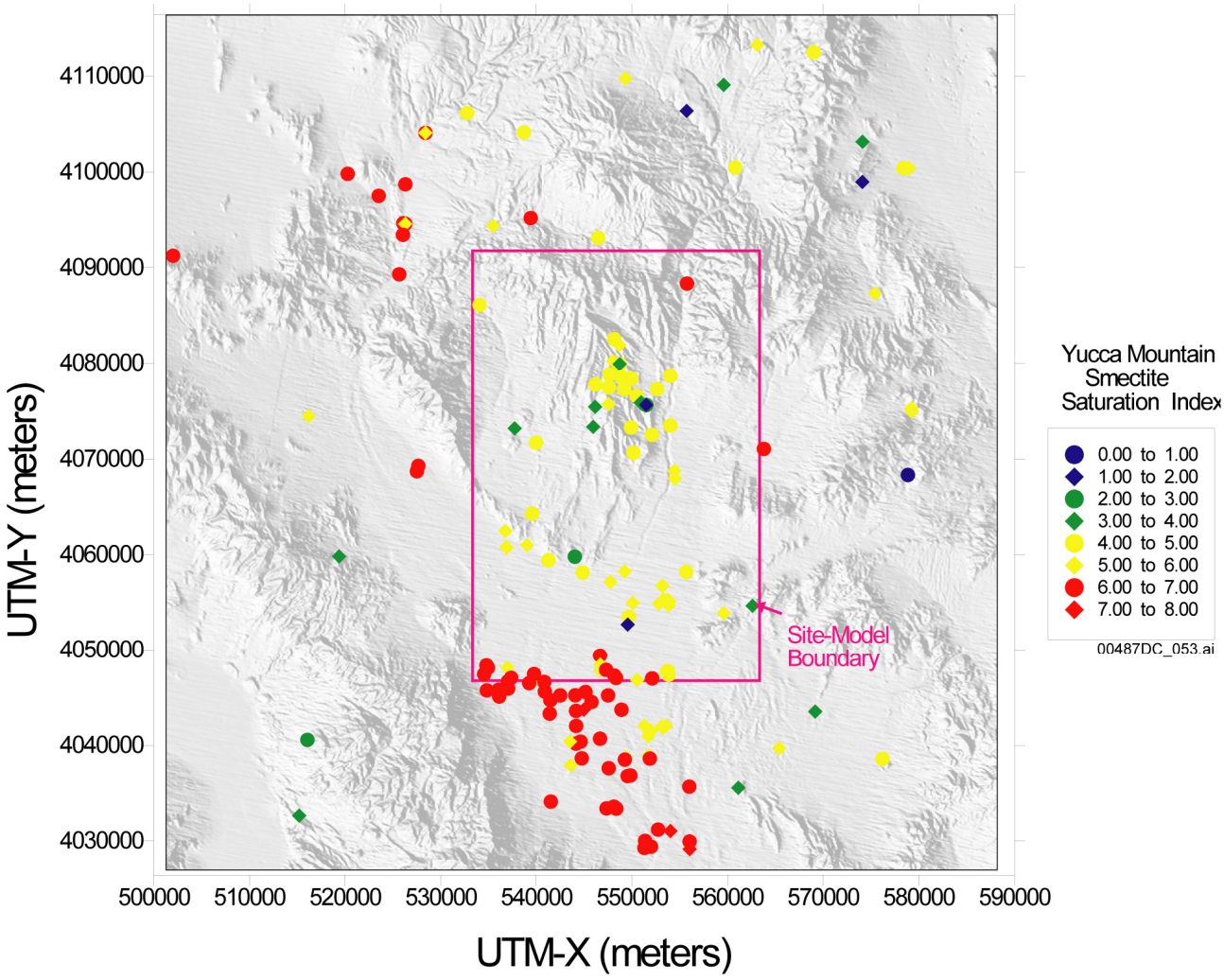

Sources: Table A6-1; DTN: LA0310EK831232.001 [DIRS 165995].

NOTE: This figure has color-coded data points and should not be read in a black and white version.

UTM-X = UTM-Easting; UTM-Y = UTM-Northing; and UTM=Universal Transverse Mercator.

Figure A6-38. Areal Distribution of Smectite Saturation Index in Groundwater

A6.3.5.6 Calcium Clinoptilolite Saturation Index

Throughout most of the Yucca Mountain region, groundwater is also supersaturated with Ca-clinoptilolite (Figure A6-39). As is the case for smectite, the degree of supersaturation increases southward from the Yucca Mountain area toward the Amargosa Desert.

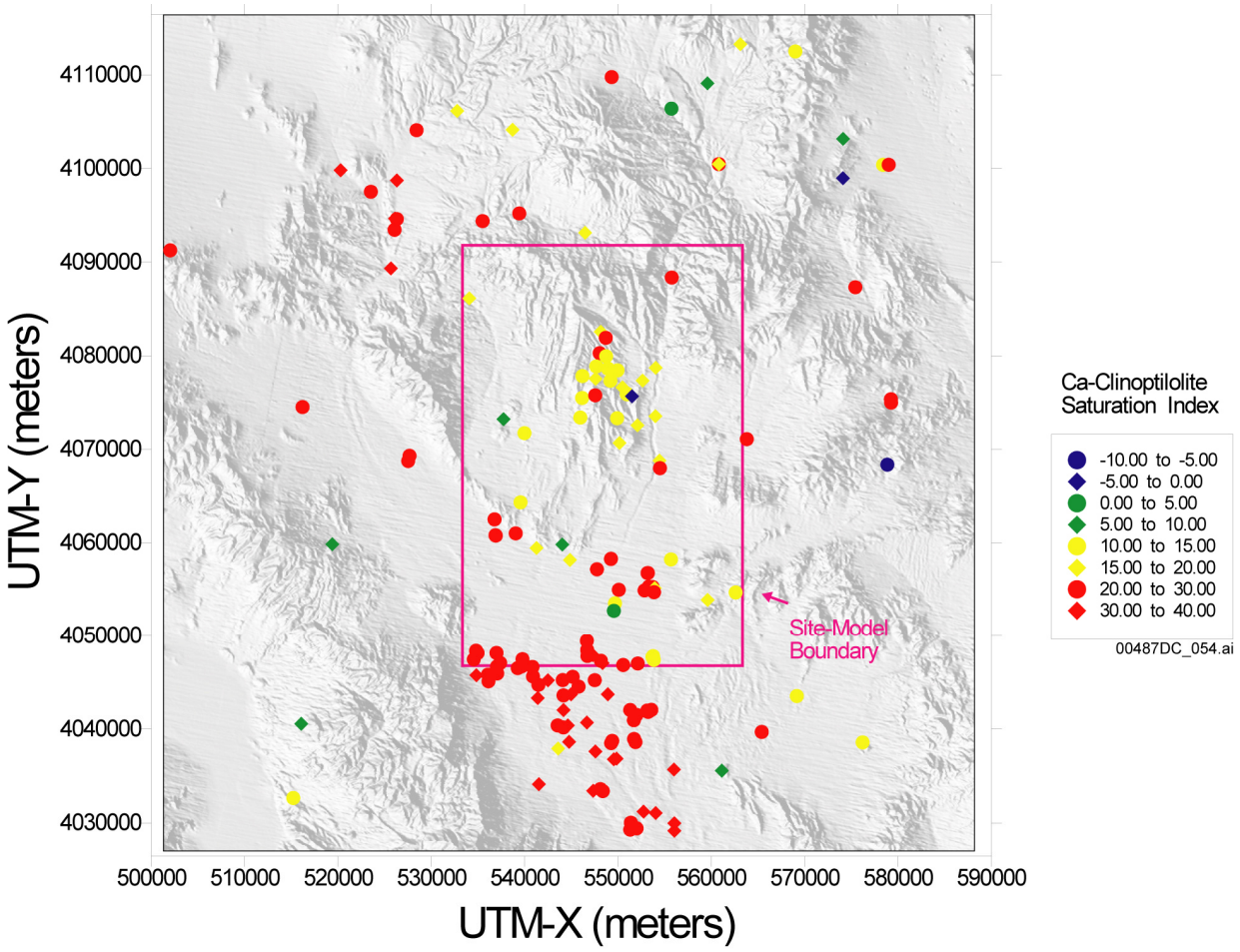

Sources: Table A6-1; DTN: LA0310EK831232.001 [DIRS 165995].

NOTE: This figure has color-coded data points and should not be read in a black and white version.

UTM-X = UTM-Easting; UTM-Y = UTM-Northing; and UTM=Universal Transverse Mercator.

Figure A6-39. Areal Distribution of Calcium Clinoptilolite Saturation Index in Groundwater

A6.3.5.7 Potassium Feldspar Saturation Index

Except for some wells in the Oasis Valley area, the groundwater at most wells along or north of U.S. Highway 95 are undersaturated with K-feldspar (Figure A6-40). Conversely, south of the site model area, most groundwater along or adjacent to Fortymile Wash is saturated or slightly supersaturated with K-feldspar, reflecting the much higher K and dissolved SiO_2 concentrations of groundwater in these areas.

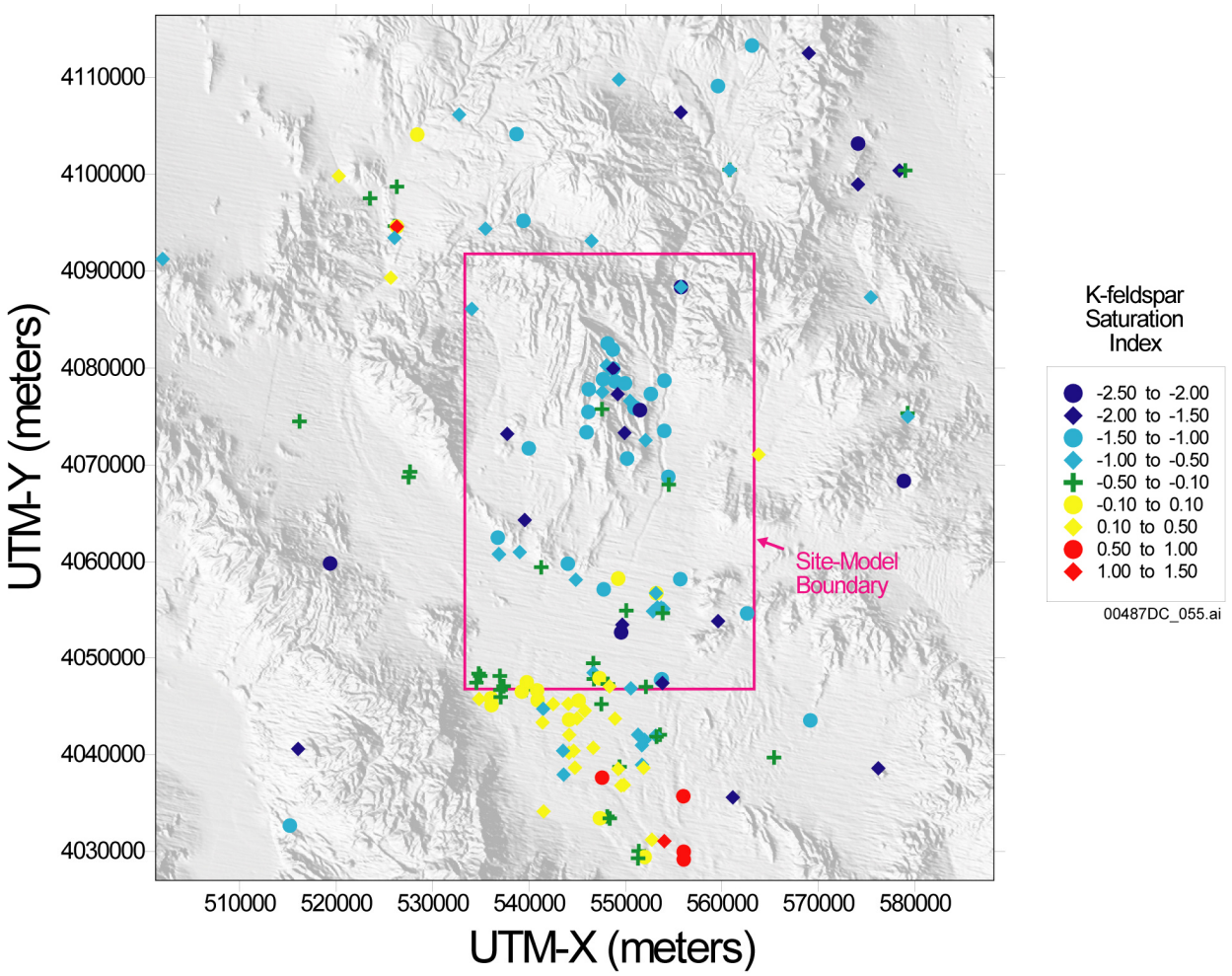

Sources: Table A6-1; DTN: LA0310EK831232.001 [DIRS 165995].

NOTE: This figure has color-coded data points and should not be read in a black and white version.

UTM-X = UTM-Easting; UTM-Y = UTM-Northing; and UTM=Universal Transverse Mercator.

Figure A6-40. Areal Distribution of K-Feldspar Saturation Index in Groundwater

A6.3.5.8 Summary of Areal Distribution of Calculated Geochemical Parameters

If groundwater is moving southward from Yucca Mountain and Fortymile Wash into the northern Amargosa Desert, the areal distributions of calculated geochemical parameters presented in Table A6-3 and shown in Figures A6-34 to A6-40, combined with the areal distribution plots shown in Section A6.3.4, provide some insight into the potential reactions affecting groundwater compositions. Groundwater in these areas has low and relatively constant Cl^- concentrations (6 to 8 mg/L) compared to surrounding areas, and so downgradient changes in composition and in saturation indices can be attributed to water/rock interaction rather then evaporation.

Silicate weathering reactions are indicated by the overall increase in dissolved SiO_2 near the southern boundary of the SZ site model (Figure A6–3.6) and increases in pH (Figure A6–3.1), HCO_3^- (Figure A6–3.4), and $SI_{calcite}$ (Figure A6-37). Weathering of primary silicate minerals like plagioclase or K-feldspar typically involves the consumption of H^+ ions and dissolved CO_2 and the production of cations, HCO_3^-, dissolved SiO_2, and secondary minerals like kaolinite or smectite, consistent with these trends (Drever 1988 [DIRS 118564], p. 151; Langmuir 1997 [DIRS 100051], p. 325). The overall southward increase in $SI_{K\text{-}feldspar}$ (Figure A6-40) and accompanying increase in $SI_{Smectite}$ (Figure A6-38) and $SI_{Ca\text{-}clinoptilolite}$ (Figure A6-39) indicate that, if secondary minerals are precipitated, the primary silicate dissolution reactions may be faster than the precipitation rates for the secondary minerals. The extreme supersaturation of smectite and Ca-clinoptilolite may be indicating that these precipitation reactions are kinetically inhibited.

The saturation indices of alumino-silicate minerals are based on the apparent control of Al^{3+} concentrations by kaolinite (Figure A6-33). Kaolinite has been documented only in trace amounts in the Yucca Mountain area, unlike zeolites, which are prevalent throughout the saturated zone near Yucca Mountain (Vaniman et al. 1996 [DIRS 105946]). Although this assumption is somewhat empirical (see Table A5-1, Assumption 2), it is reasonable because reaction pathways represented on phase-stability diagrams typically represent kaolinite as an intermediate weathering product that is eventually replaced by more stable secondary phases (Drever 1988 [DIRS 118564], Figure 8-8, pp. 156 to 158; Langmuir 1997 [DIRS 100051], Figure 9.14).

A6.3.6 Sources and Evolution of Groundwater beneath Yucca Mountain

The following sections provide an analysis of the origin and evolution of groundwater at Yucca Mountain. Data on perched water from the unsaturated zone at Yucca Mountain are presented in Section A6.3.6.1. Perched water compositions are taken to approximate the composition of local recharge from Yucca Mountain itself. Perched water compositions and other groundwaters upgradient from Yucca Mountain are compared to groundwater presently beneath Yucca Mountain evaluate the possible sources of Yucca Mountain groundwaters.

A6.3.6.1 Description of Perched-Water Data

Perched water was encountered in at least five boreholes at Yucca Mountain: USW UZ-14, USW NRG-7a, USW SD-9, USW SD-7, and USW WT-24. The perched-water samples were obtained by bailing or by pumping, depending on factors related to the drilling of the borehole. In general, it is believed that pumping produces a water sample that is more likely to represent in situ chemical and isotopic conditions for the following reasons. Drilling may affect the chemical and isotopic composition of water in the borehole by introducing foreign drilling fluids (generally air) into the water and by grinding the rock, thereby exposing fresh, unaltered rock surfaces that may react with the water. To minimize these drilling effects, a borehole is typically purged of water present in the borehole, and many additional borehole water volumes are pumped from the formation before sampling. This process increases confidence that the water sample represents actual hydrochemical conditions in the formation. In cases for which a water sample is bailed without first pumping the borehole, the water sample may not be representative of in situ hydrochemical conditions.

Of the perched-water samples considered in this analysis, samples from boreholes SD-9 and NRG-7a (Table A6-5) were obtained exclusively by bailing (Yang and Peterman 1999 [DIRS 149596], Table 19) during a hiatus in drilling following the encounter with the perched water. No pumping was done prior to sample collection at these boreholes.

Perched-water samples from UZ-14 (Table A6-5) obtained prior to August 17, 1993, were obtained without first pumping the borehole. Pumped samples were obtained between August 17 and August 27, and an additional bailed sample was taken after pumping on August 31, 1993. A time series of delta strontium-87 ($\delta^{87}Sr$) versus water production showed that $\delta^{87}Sr$ values continued to change until about 12,000 liters had been pumped from the borehole, or sometime after August 25, 1993 (Yang and Peterman 1999 [DIRS 149596], Table 19, Figure 113). Therefore, the $\delta^{87}Sr$ data, and likely other data, obtained from samples collected from UZ-14 after this date probably best represent in situ conditions. These samples include UZ-14 PT-4 and UZ-14 D (Table A6-5).

Perched water from borehole SD-7 sampled on March 8, 1995, was obtained by bailing prior to pumping. Perched-water samples obtained from borehole SD-7 between March 16 and March 21, 1995, were obtained by pumping (Yang et al. 1996 [DIRS 100194], p. 37).

Perched water was sampled by pumping from borehole WT-24. However, according to Patterson et al. (1998 [DIRS 107402], p. 277), the isotopic data obtained prior to the end of the 24-hour pumping test conducted on October 21 to 22, 1997, were collected during what the authors considered a clean-out period. Only data collected from borehole WT-24 following this clean-out period are presented in this report.

In summary, the perched-water data are thought to represent in situ conditions to varying degrees, depending on whether the samples were bailed or pumped and the extent to which the borehole was cleaned out prior to sampling. The data collected from borehole SD-7 on or after March 16, 1995, from borehole UZ-14 after August 25, 1993, and from borehole WT-24 on or after October 22, 1997, are thought to best represent the actual chemical and isotopic conditions of the perched water at Yucca Mountain. These samples are weighted more heavily than the remaining samples in developing the conclusions of this report.

Table A6-5. Chemical and Isotopic Composition of Perched Water at Yucca Mountain

Water Sample	Depth (m)	Sampling Method	Date	pH	Chemical Concentrations (mg/L)								^{13}C(‰)	^{14}C(pmc)	^{3}H[a] (TU)	δD (‰)	$\delta^{18}O$ (‰)	$^{234}U/^{238}U$ Activity Ratio	$^{36}Cl/Cl$ (x 10^{-15})
					Ca^{2+}	Mg^{2+}	Na^{+}	K^{+}	Cl^{-}	SO_4^{2-}	HCO_3^{-}	SiO_2							
SD-7	479.76	Bailed	03-08-95	—	14.2	0.13	45.5	5.3	4.4	9.1	112	62.3	–10.4	34.4	6.2	–99.8	–13.4	—	511
	488.29	Pumped	03-16-95	8.1	13.3	0.13	45.5	5.3	4.1	9.1	128	57.4	–9.4	28.6	—	–99.7	–13.3	—	—
	488.29	Pumped	03-17-95	8.2	12.8	0.08	45.8	5.5	4.1	8.6	130	50.9	–9.5	28.4	—	–99.6	–13.4	3.504	657
	488.29	Pumped	03-20-95	8.0	12.9	0.07	45.5	5.4	4.1	8.5	127	55	–9.5	27.9	—	–99.6	–13.4	3.58	—
	488.29	Pumped	03-21-95	8.2	13.5	0.08	44.6	5.5	4.1	10.3	128	55.9	–9.5	28.4	< 0.3	–99.6	–13.3	3.69	609, 635
SD-9	—	Bailed	03-07-94	—	—	—	—	—	—	—	—	—	–14.4	41.8	0	–97.8	–13.3	—	—
	—	Bailed	07-07-94	—	—	—	—	—	—	—	—	—	—	—	—	—	—	2.42[b]	—
	453.85	Bailed	07-17-94	8.6	2.9	0.2	98	9.8	5.6	27.6	197[c]	64.2	–14.4	41.8	0	–97.8	–13.3	—	449
	—	Bailed	09-12-94	—	—	—	—	—	—	—	—	—	—	—	—	—	—	2.42[b]	497
UZ-14 A	384.60	Bailed	08-02-93	7.6	23	1.8	39	5.6	7.9	14.3	150	34.2	–10.2	41.7	0.3	–98.6	–13.8	—	559
UZ-14 A2	384.60	Bailed	08-02-93	7.8	24	1.8	38	3.9	9.1	13.8	148.8	36.4	–10.1	40.6	3.1	–97.5	–13.5	—	538
UZ-14 B	387.68	Bailed	08-03-93	8.1	31	2.7	40	4.4	8.3	16.3	147.6	51.4	–9.5	36.6	0	–97.1	–13.4	—	566
UZ-14 C	390.75	Bailed	08-05-93	8.3	45	4.1	88	5.8	15.5	223	106.1	7.7	–9.2	66.8	0.4	–87.4	–12.1	—	389
UZ-14 PT-1	390.75	Pumped	08-17-93	—	37	3.1	40	6.3	7.2	57.3	144	21.4	–9.8	32.3	1.8	–97.8	–13.3	—	644
UZ-14 PT-2	390.75	Pumped	08-19-93	—	30	2.4	35	3.3	7.0	22.9	144	25.7	—	28.9	3.1	–97.9	–13.4	—	656
UZ-14 PT-4	390.75	Pumped	08-27-93	—	27	2.1	34	1.8	6.7	14.1	141.5	32.1	–9.6	27.2	0	–97.3	–13.4	7.56	675
UZ-14 D	390.75	Bailed	08-31-93	7.8	31	2.5	35	4.1	7.0	24.2	146.4	40.7	–11.3	29.2	0	–97.6	–13.1	—	690

Table A6-5. Chemical and Isotopic Composition of Perched Water at Yucca Mountain (Continued)

Water Sample	Depth (m)	Sampling Method	Date	pH	Chemical Concentrations (mg/L)								^{13}C(‰)	^{14}C (pmc)	^{3}H[a] (TU)	δD (‰)	$\delta^{18}O$ (‰)	$^{234}U/^{238}U$ Activity Ratio	$^{36}Cl/Cl$ (× 10^{-15})
					Ca^{2+}	Mg^{2+}	Na^{+}	K^{+}	Cl^{-}	SO_4^{2-}	HCO_3^{-}	SiO_2							
WT-24[d]	—	Pumped	10-22-97	8.1	23	1.4	37	2.4	9.0	16	135	46	–11.8	29.6	<0.3	–99.4	–13.5	8.34	596
		Pumped	12-10-97	8.6	18.0	1.3	37.5	2.9	8.9	16.0	121.0	36.5	–10.8	—	—	–100.6	–13.5	8.12	—
NRG-7a	—	Bailed	03-04-94	—	—	—	—	—	—	—	—	—	—	—	—	—	—	5.17[b]	518
	460.25	Bailed	03-07-94	8.7	3	0	42	6.8	7	4	114	9	–16.6	66.9	10	–93.9	–12.8	—	491
	—	Bailed	03-08-94	—	—	—	—	—	—	—	—	—	—	—	—	—	—	—	474

Sources: DTNs: GS980108312322.005 [DIRS 149617] (ions, pH, $\delta^{13}C$, δD, $\delta^{18}O$, ^{3}H)[d], GS950808312322.001[DIRS 148114] (^{3}H), GS010808312322.004 [DIRS 156007] ($^{234}U/^{238}U$ activity ratios), GS951208312272.002 [DIRS 151649] (^{3}H), LAJF831222AQ98.011[DIRS 145402] ($^{36}Cl/Cl$), MO0007GNDWTRIS.013 [DIRS 151504] ($\delta^{13}C$, δD, $\delta^{18}O$, ^{14}C), MO0007MAJIONPH.016 [DIRS 151533] (ions and pH), GS980908312322.008 [DIRS 145412] (^{14}C)[d].

NOTES: "—" not available.

[a] Tritium analyses have an accuracy of plus or minus 12 TU.
[b] These results are not representative of in situ conditions due to sample contamination.
[c] This sample also contains 10 mg/L CO_3^{2-}.
[d] Average values of samples collected on the indicated date.

A6.3.6.2 Evidence from $^{234}U/^{238}U$ Activity Ratios for Local Recharge

Precipitation typically contains low concentrations of solutes, including uranium. As the precipitation infiltrates through the soil, uranium is dissolved from the readily soluble soil components. Measured $^{234}U/^{238}U$ activity ratios in secondary minerals formed in soil zones on Yucca Mountain range from 1.4 to 1.8 reflecting both enrichment and dissolution processes (DTNs: GS010608315215.002 [DIRS 156187], GS970808315215.012 [DIRS 145921], and GS980908312322.009 [DIRS 118977]). Pore waters extracted from a small number of core samples from the unsaturated zone at Yucca Mountain have $^{234}U/^{238}U$ activity ratios that range from 1.5 to 3.8. Pore waters extracted from the top of the Paintbrush tuff nonwelded hydrogeologic unit (PTn) have $^{234}U/^{238}U$ activity ratios of 1.5 to 2.5, whereas pore waters from the stratigraphically lower upper lithophysal unit of the welded Topopah Spring tuff (Tpt) have $^{234}U/^{238}U$ activity ratios of 2.5 to 3.8 (DTN: MO0012URANISOT.000 [DIRS 153384], pp. 1 to 4). These data, as well as data from fracture-lining minerals (Paces et al. 1998 [DIRS 107408], Figure 3), suggest a general increase in $^{234}U/^{238}U$ activity ratios in pore waters from the soil zone down through the upper unsaturated zone.

Activity ratios of $^{234}U/^{238}U$ in perched-water samples range from 3.5 at borehole SD-7 to 8.4 at borehole WT-24 (DTNs: GS010608315215.002 [DIRS 156187] and GS010808312322.004 [DIRS 156007]). The values at the high end of this range are unusual and suggest the existence of certain flow conditions. In particular, the high ratios require that the ^{234}U enrichment processes discussed in Section A6.3.1.2.4 dominate over dissolution of uranium-bearing minerals. This situation suggests small water-to-rock ratios. For the unsaturated zone at Yucca Mountain, the high $^{234}U/^{238}U$ ratios are consistent with small water fluxes passing through a fracture network. In fractures with small, and probably intermittent water fluxes, ^{234}U will accumulate over time whereas the relative amount of ^{238}U that may be incorporated into the water via dissolution will likely be small. In this way, a small flux of water flowing through a fracture may preferentially incorporate ^{234}U relative to ^{238}U, resulting in water with an elevated $^{234}U/^{238}U$ ratio, as suggested by Paces et al. (2001 [DIRS 156507] and 2002 [DIRS 158817]). The progressive accumulation of such small water fluxes could result in perched water with the observed high $^{234}U/^{238}U$ ratios. The changes to the $^{234}U/^{238}U$ activity ratios that would occur over time within the perched water depend on the ^{238}U content of the host rock, the weathering characteristics of the rock, the water volume to rock surface area, redox conditions, and other factors (Clark and Fritz 1997 [DIRS 105738], pp. 238 to 240). The $^{234}U/^{238}U$ activity ratio of the perched water may either increase or decrease with time, depending on the relative importance of these factors.

The elevated $^{234}U/^{238}U$ activity ratios found in Yucca Mountain perched water and shallow groundwater are attributable to unsaturated zone flow through the thick sequence of fractured, welded tuffs that constitute the Topopah Spring tuff. Figure A6-41 summarizes the change in $^{234}U/^{238}U$ ratios with depth in the vicinity of Yucca Mountain. In surface water and pore water from the nonwelded PTn, $^{234}U/^{238}U$ activity ratios are small, reflecting the relatively important contribution of ^{238}U from dissolution. Deeper in the subsurface, calcite and opal from the ESF have higher, though variable $^{234}U/^{238}U$ activity ratios. The variability of these ratios is attributed to precipitation of these materials from waters that have experienced variable transport times and paths through the unsaturated zone (Paces et al. 2001 [DIRS 156507], p. 63). Permeable vitric tuffs are absent beneath the Topopah Spring tuff in the northern part of Yucca Mountain

(Rousseau et al. 1999 [DIRS 102097], Figure 16) where perched water has high $^{234}U/^{238}U$. In this part of the mountain, recharge to the saturated zone is estimated to occur mainly along faults and other preferential pathways due to the low permeability of the underlying zeolitic tuffs (BSC 2004 [DIRS 169861], Appendix A and Figure 6.6-3). Toward the southern part of the central block, however, thick permeable vitric intervals are present beneath the Topopah Spring Tuff, and recharge to the saturated zone is expected to take place primarily through these permeable vitric tuffs. Matrix flow through the vitric tuffs may lower the $^{234}U/^{238}U$ activity ratios through bulk−rock dissolution. Support for this hypothesis is provided by comparing the $^{234}U/^{238}U$ activity ratios and U concentrations in perched water below vitric tuffs at borehole SD-7 in southern Yucca Mountain to the $^{234}U/^{238}U$ activity ratios and uranium in perched water at boreholes UZ-14 and WT-24 in northern Yucca Mountain, where vitric tuffs are thin or absent. The relatively low $^{234}U/^{238}U$ activity ratio (3.5) and higher uranium concentrations for perched water at borehole SD-7 compared to perched water in boreholes WT-24 and UZ-14 (Paces et al. 2002 [DIRS 158817], Table 2) are consistent with this conceptual model.

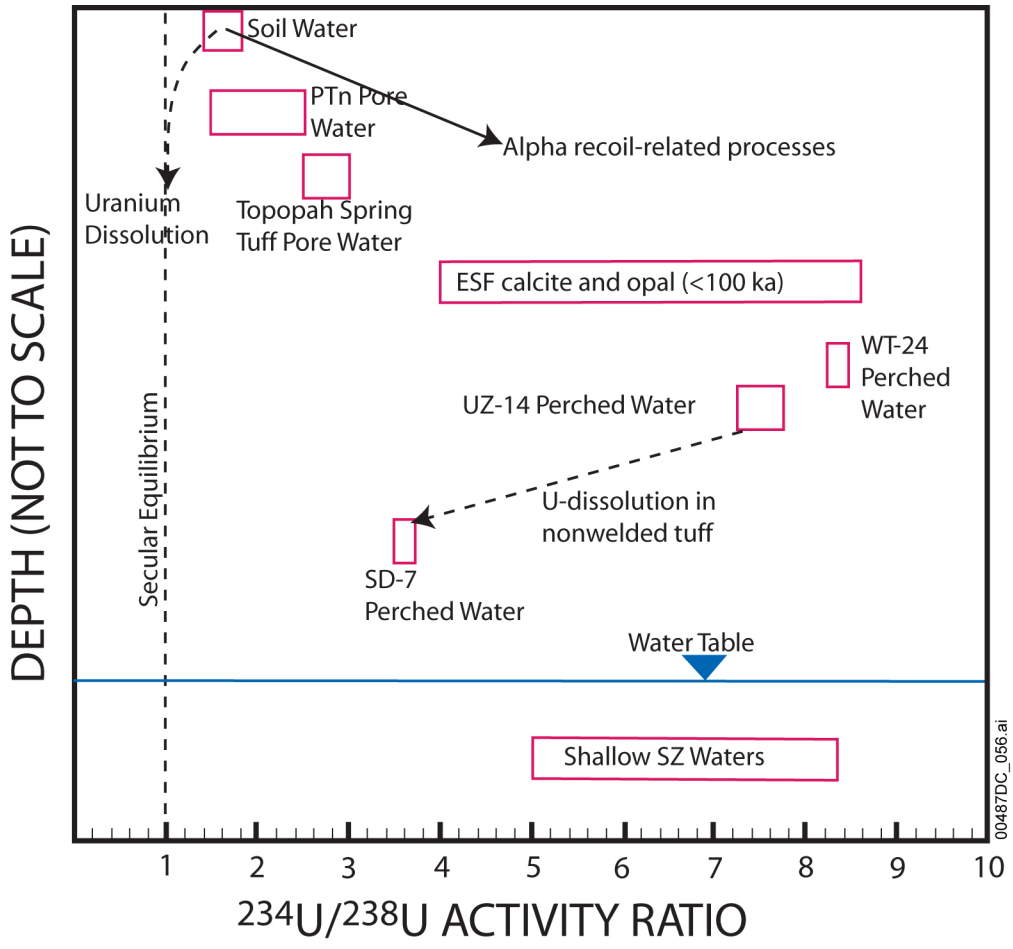

Source: Modified from Paces et al. 2001 [DIRS 156507], Figure 37.

Figure A6-41. Uranium Isotopic Compositions and Schematic Evolutionary Trends at Yucca Mountain

In summary, the high $^{234}U/^{238}U$ activity ratios found in some Yucca Mountain perched water are interpreted to be due to percolation of groundwater through a very thick unsaturated interval of fractured, welded tuff. In the northern part of Yucca Mountain where deep, permeable vitric tuffs are absent and recharge occurs by preferential flow along faults, the relatively high $^{234}U/^{238}U$ activities are unmodified by further bulk-rock dissolution. In the southern part of Yucca Mountain where deep unsaturated flow takes place through the matrix of vitric, nonwelded tuffs, bulk-rock dissolution may reduce the high $^{234}U/^{238}U$ activity ratios acquired by fracture flow through the welded tuffs. One inference of this conceptual model is that the high $^{234}U/^{238}U$ activity ratios found in groundwater near Dune Wash at boreholes WT-3, WT-12, and WT-17 may reflect recharge through areas where deep vitric tuffs are absent, such as north of the Drill Hole Wash area (the reader should note that in this appendix the location WT-3 refers to UE-25 WT #3 and WT-12 refers to UE-25 WT #12). However, the necessary data from the deep unsaturated zone are too few to fully substantiate this hypothesis at this time.

A6.3.6.3 Evidence for Local Recharge from Other Chemical Constituents

This section compares other chemical and isotopic characteristics of perched water and groundwater to further evaluate the concept that Yucca Mountain recharge, as represented by perched water, is the principal source of groundwater beneath Yucca Mountain. Comparisons of perched water analyses from Table A6-5 with SZ groundwater from Yucca Mountain (YM-CR, YM-C, YM-SE, and YM-S groups) and groundwater upgradient from Yucca Mountain in the TM, FMW-N, SCW, and CF groups are shown in Figures A6-42 to A6-46.

The scatter plot of SO_4^{2-} versus Cl^- (Figure A6-42) shows that perched waters pumped from boreholes UZ-14, WT-24, and SD-7 have SO_4^{2-} and Cl^- concentrations that are similar to those of groundwaters at many YM-CR area wells. These concentrations plot near a line, termed the Southern Nevada Precipitation line that was derived by considering how the SO_4^{2-} and Cl^- concentrations measured in precipitation from the Kawich Range, just north of the Nevada Test Site, would change with progressive evaporation. With progressive evaporation, the dissolved SO_4^{2-} and Cl^- concentrations in the remaining water would increase and plot along a line with a slope (2.7) equal to the ratio of their concentrations in precipitation (96 and 35 mg/L, respectively) (Meijer 2002 [DIRS 158813], Table 1). Groundwaters that plot on or near the Southern Nevada Precipitation line are likely to have had most of their SO_4^{2-} and Cl^- derived from atmospheric deposition of salts composed of these ions.

In contrast, other Yucca Mountain groundwaters, particularly groundwaters at some YM-S sites, show elevated SO_4^{2-} concentrations relative to perched water and appear to trend from the perched-water data toward the p#1 mixing line. This line (slope = 5.7) is defined by the origin and groundwater SO_4^{2-} and Cl^- concentrations from the carbonate aquifer at borehole p#1 (160 and 28 mg/L, respectively). Groundwaters that included a component of groundwater from the carbonate aquifer would be expected to trend toward this line, depending on the concentrations of SO_4^{2-} and Cl^- dissolved in the groundwater before mixing occurred. Elevated groundwater SO_4^{2-} concentrations relative to the Southern Nevada Precipitation line could also indicate the addition of SO_4^{2-} through the dissolution of S-bearing minerals like gypsum, pyrite, or alunite.

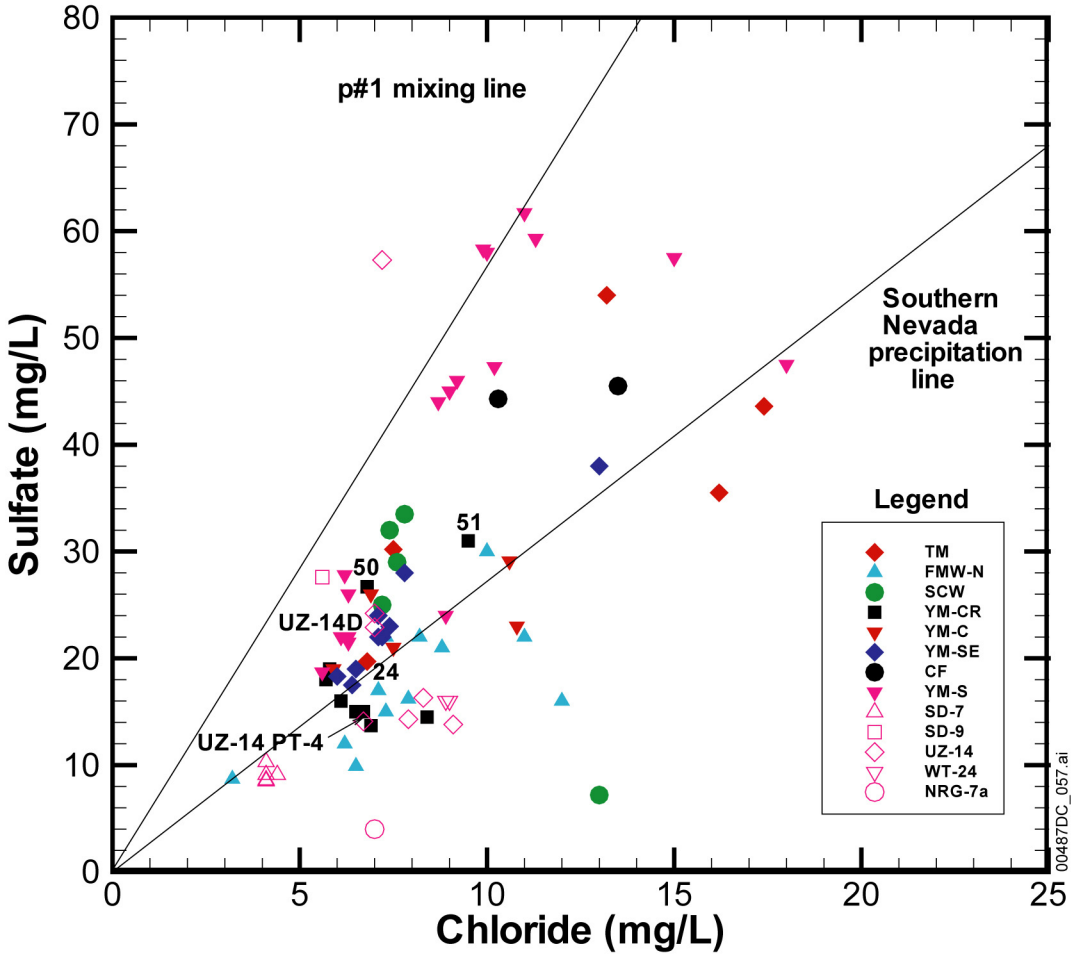

Sources: Tables A6-1 and A6-5.

NOTES: Sample p#1 plots well above limits of the figure. This figure has color-coded data points and should not be read in a black and white version. Perched water data are represented by open symbols. The more representative samples of perched water from borehole UZ-14 are labeled in the figure.

Figure A6-42. Scatter Plot Comparing Sulfate and Chloride Compositions of Perched Waters and Saturated Zone Groundwaters

The scatter plot of $\delta^{13}C$ versus 1/DIC (Figure A6-43) shows that perched water at Yucca Mountain is generally more dilute in DIC and has lighter $\delta^{13}C$ than most Yucca Mountain groundwater, although some groundwater from the YM-CR group in northern Yucca Mountain has comparable DIC and $\delta^{13}C$ values. No systematic differences between the northern (boreholes UZ-14 and WT-24) and central Yucca Mountain perched water (borehole SD-7) compositions are evident in $\delta^{13}C$ and DIC compositions, suggesting the relative uniformity of recharge compositions throughout Yucca Mountain. The Yucca Mountain groundwater shows an overall southward trend toward heavier $\delta^{13}C$ and higher DIC concentrations (lower 1/DIC).

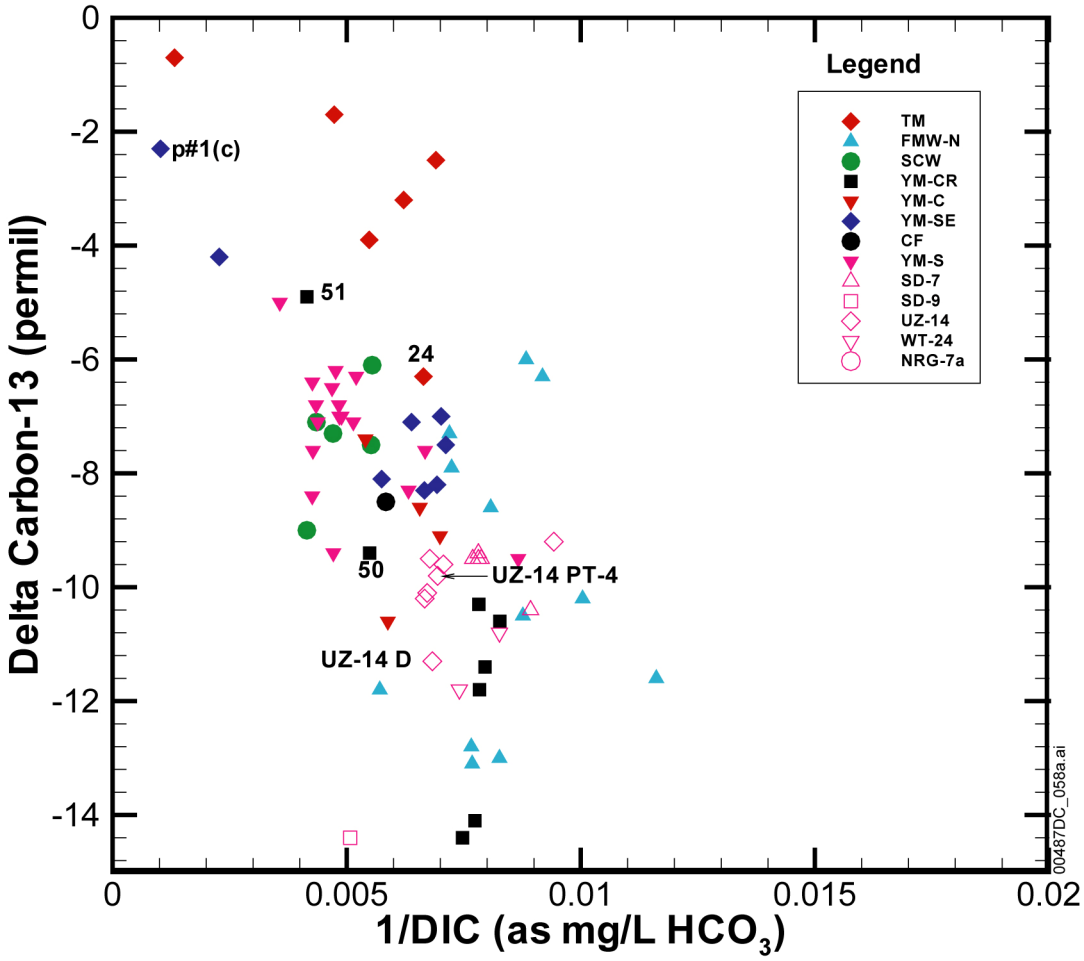

Sources: Tables A6-2, A6-3, and A6-5.

NOTES: This figure has color-coded data points and should not be read in a black and white version. Perched water data are represented by open symbols. The more representative samples of perched water from borehole UZ-14 are labeled in the figure.

Figure A6-43. Scatter Plot Comparing Delta Carbon-13 and Dissolved Inorganic Carbon Compositions of Perched Waters and Saturated Zone Groundwaters

Perched groundwater at Yucca Mountain has $\delta^{18}O$ and δD compositions that are slightly heavier in δD but generally similar to many YM-CR groundwaters (Figure A6-44). Elsewhere at Yucca Mountain, groundwaters tend to be lighter in δD than the perched water. There is an overall southward trend toward lighter δD among the YM-CR, YM-C, YM-SE and YM-S groups.

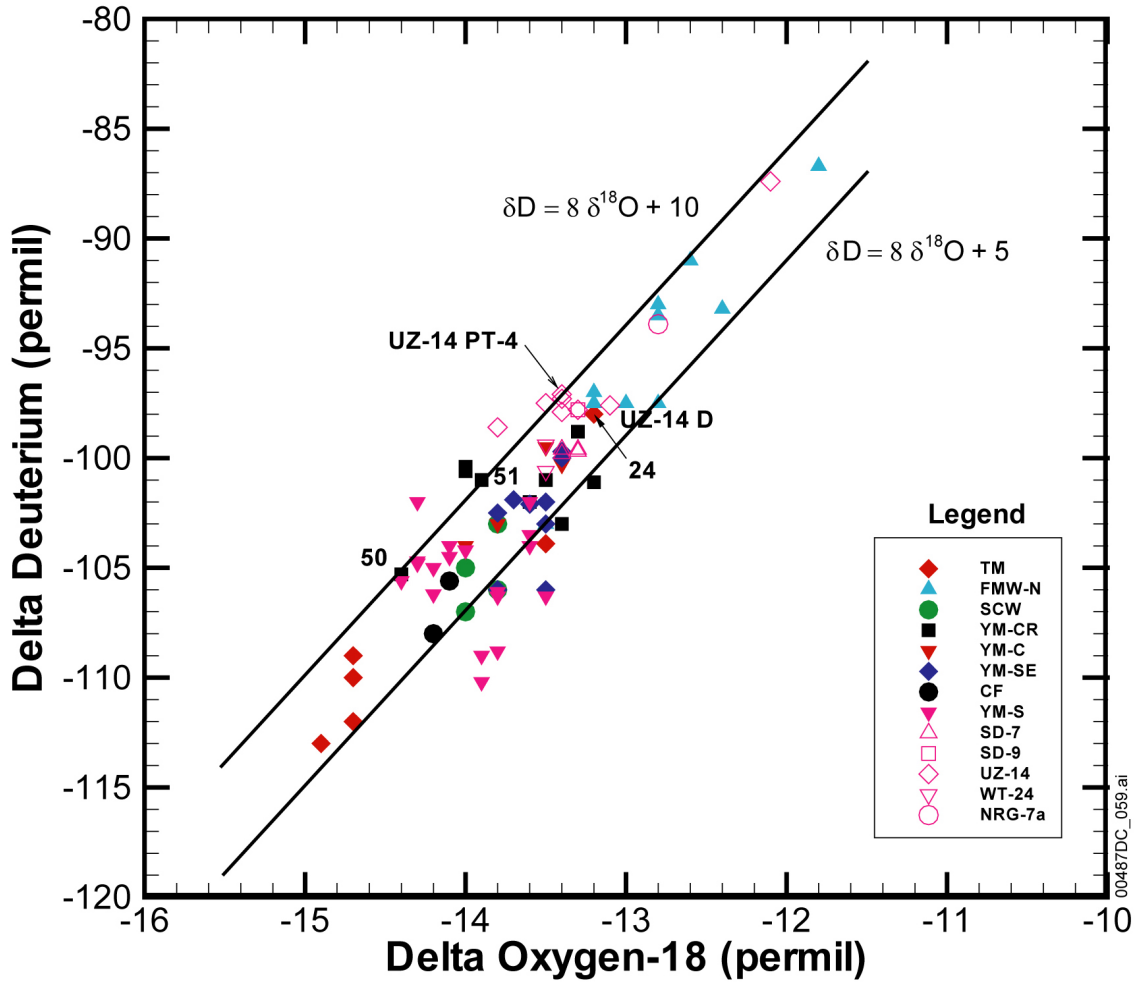

Sources: Tables A6-2 and A6-5.

NOTE: This figure has color-coded data points and should not be read in a black and white version. The solid lines are the global meteoric water line ($\delta D = 8\ \delta^{18}O + 10$) (Clark and Fritz 1997 [DIRS 105738], p. 36) and a possible paleometeoric water line for southern Nevada ($\delta D = 8\ \delta^{18}O + 5$) (White and Chuma 1987 [DIRS 108871], pp. 573 to 574). Perched water data are represented by open symbols. The more representative samples of perched water from borehole UZ-14 are labeled in the figure.

Figure A6-44. Scatter Plot Comparing Delta Deuterium and Delta Oxygen-18 Data for Perched Water and Groundwater near Yucca Mountain

Perched waters at Yucca Mountain have ^{14}C activities that are higher than most Yucca Mountain area groundwaters (Figure A6-45). As discussed in connection with Figure A6-43, the $\delta^{13}C$ values of perched water are comparable to or lighter than all but a few of the Yucca Mountain area groundwaters. These groundwaters show a southward trend toward heavier $\delta^{13}C$ and lower ^{14}C activities.

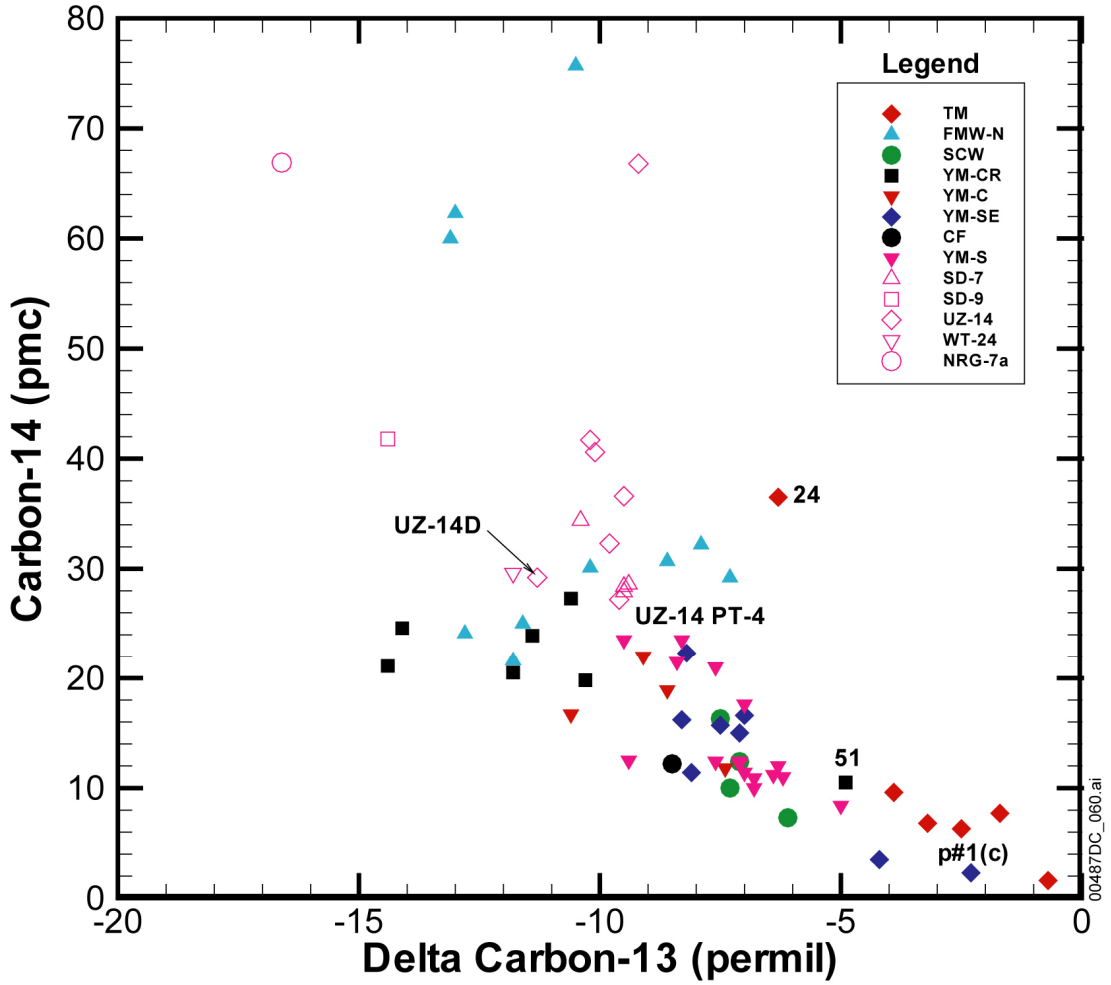

Sources: Tables A6-2 and A6-5.

NOTE: This figure has color-coded data points and should not be read in a black and white version. Perched water data are represented by open symbols. The more representative samples of perched water from borehole UZ-14 are labeled in the figure.

Figure A6-45. ^{14}C Activity versus Delta ^{13}C of Perched Water and Groundwater near Yucca Mountain

Perched waters at Yucca Mountain have higher Ca^{2+} and lower Na^{+} concentrations than most Yucca Mountain groundwaters (Figure A6-46). The YM-C and YM-SE area groundwaters are most similar to the perched water with regard to Ca^{2+} and Na^{+} concentrations, whereas most YM-CR and YM-S groundwater have substantially less Ca^{2+} and more Na^{+} than the perched water. Some YM-S groundwaters and one YM-C groundwater (from well H-4) also appear to be affected by mixing with carbonate aquifer groundwater like that found at borehole p#1, indicated by increased Ca^{2+} and Na^{+} concentrations in these groundwaters along a mixing trend defined by the groundwaters from well p#1.

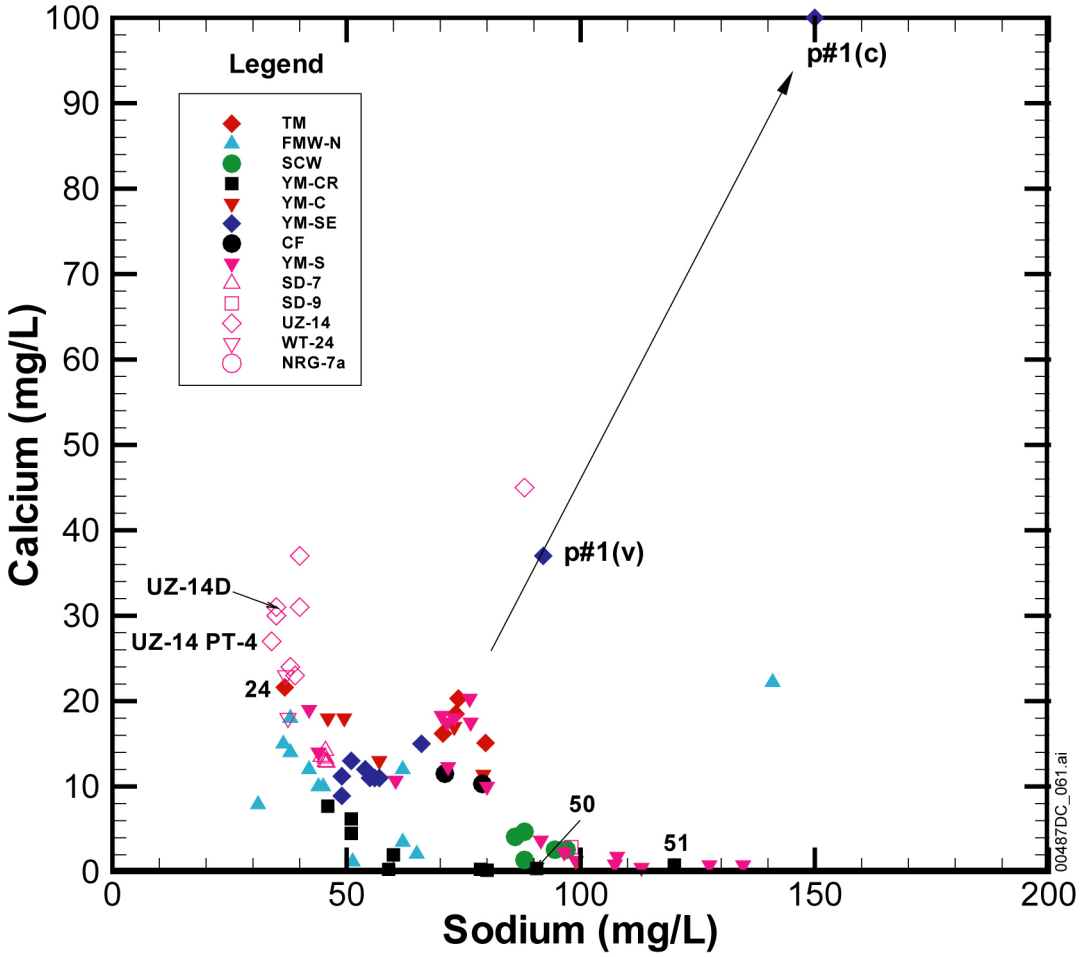

Sources: Tables A6-1 and A6-5.

NOTE: This figure has color-coded data points and should not be read in a black and white version. Perched water data are represented by open symbols. The more representative samples of perched water from borehole UZ-14 are labeled in the figure.

Figure A6-46. Scatter Plot Comparing Calcium and Sodium Compositions of Perched Waters and Saturated Zone Groundwaters

In summary, groundwater chemical and isotopic compositions at Yucca Mountain are compatible with the hypothesis that much or most of the groundwater is derived from local recharge. The perched-water and groundwater Cl^- and SO_4^{2-} concentrations are similar, although southward increases in groundwater SO_4^{2-} concentrations require some additional sources of SO_4^{2-} through water-rock interaction or mixing with groundwater having higher SO_4^{2-} concentrations. Similarly, the $\delta^{13}C$ and DIC concentrations of perched water are similar to those of groundwater in northern Yucca Mountain, but water-rock interactions involving isotopically heavy calcite or mixing with small amounts of a groundwater having high DIC concentrations and heavy $\delta^{13}C$ is required to explain the southward increases in $\delta^{13}C$ and DIC. Perched water $\delta^{18}O$ and δD compositions are similar to those found in groundwater in northern Yucca Mountain but are slightly heavier than those found toward the southern end of the mountain. Because climate change has probably affected the $\delta^{18}O$ and δD composition of recharge over time (see

Section A6.3.1.2), the differences between the perched water $\delta^{18}O$ and δD compositions and groundwater $\delta^{18}O$ and δD compositions elsewhere at Yucca Mountain do not rule out local recharge as a source for these groundwaters. The higher ^{14}C activities of the perched water compared to Yucca Mountain groundwater are compatible with the hypotheses that Yucca Mountain groundwater is derived from local recharge. Groundwater is expected to be older than the recharge from which it is derived. Similarly, the fact that perched water has high Ca^{2+} and lower Na^{+} than the underlying groundwater is compatible with local recharge being the source of the groundwater. Pore-water analyses from the deep unsaturated zone indicate that Ca^{2+} is exchanged for Na^{+} on minerals in the deep unsaturated zone (Meijer 2002 [DIRS 158813], p. 799), consistent with the observed relation between Ca^{2+} and Na^{+} in the perched and SZ waters. Likewise, it appears that other divalent cations like Mg^{2+} and Sr^{2+}, as well as Ca^{2+}, are selectively removed by zeolites in exchange for Na^{+} (and perhaps for K^{+}) in the deep unsaturated zone (Vaniman et al. 2001 [DIRS 157427], Table 2).

A6.3.6.4 Evaluation of Saturated Zone Flow beneath Yucca Mountain

The steep gradient in the potentiometric surface to the north and along the west side of Yucca Mountain requires flow in southerly or easterly directions beneath Yucca Mountain. The N-S and NW-SE fault orientations in the area may also focus flow in these directions. Therefore, if SZ groundwater does contribute to flow beneath Yucca Mountain, then this groundwater would most likely originate from the north, northwest or west. These possibilities are evaluated below.

For the most part, the hydrochemistry of groundwater north of Yucca Mountain that was sampled as part of the NTS Underground Test Area Restoration Project (DTN: LA0311EK831232.001 [DIRS 166068]) differs from that of SZ groundwater beneath Yucca Mountain. As shown in Figures A6-32, A6-33, and A6-42, the Cl^{-} and SO_4^{2-} concentrations of most samples in the Timber Mountain group are substantially higher than those for Yucca Mountain groundwater. Similarly, $\delta^{13}C$ are generally too heavy and the ^{14}C too low for groundwater near Timber Mountain to be the primary source of Yucca Mountain groundwater (Figure A6-45). Only one well (ER-EC-07, Sample 24) in Beatty Wash has Cl^{-}, SO_4^{2-}, $\delta^{13}C$, and ^{14}C values that suggest it could be a major component of the groundwater beneath Yucca Mountain (Figures A6-42 and A6-45). Although limited data for $\delta^{87}Sr$ are available from Yucca Mountain, the $\delta^{87}Sr$ in groundwater from the northernmost well at Yucca Mountain (G-2) is too high for this groundwater to have originated from groundwater at well ER-EC-07 (Figure A6-49). The much higher Sr^{2+} concentrations in groundwater at well ER-EC-07 compared to all northern Yucca Mountain groundwater (Figure A6-48) indicates that acquisition of more radiogenic strontium through water-rock interaction during flow between wells ER-EC-07 and G-2 is not a likely explanation for the difference in $\delta^{87}Sr$ values at these wells.

It has been suggested that water may upwell from the carbonate aquifer into the tuff aquifer of Yucca Mountain (Stuckless et al. 1991 [DIRS 101159]). The Cl^{-} and SO_4^{2-} concentrations in groundwater from borehole p#1(c) are substantially elevated over those of the tuff aquifer, as discussed above. The Cl^{-} and SO_4^{2-} concentrations of groundwater at borehole p#1 are similar to those of groundwater from other areas where carbonate rocks are present (e.g., Crater Flat–SW), suggesting that groundwater from borehole p#1 may be representative of compositions in the carbonate aquifer beneath Yucca Mountain. Groundwater from sample p#1(c) also has much

higher $\delta^{13}C$, lower ^{14}C, and much higher concentrations of DIC, Ca^{2+}, and Na^{+} (Figures A6-43 A6-46) when compared to the tuff aquifer. As is evident from Figures A6-42 to A6-46, most of the groundwater samples from the volcanic aquifer do not resemble the groundwater sampled at p#1(c). These data clearly indicate that groundwater from the carbonate aquifer does not constitute a major part of the groundwater beneath Yucca Mountain. However, the higher Cl^{-} and SO_4^{2-} concentration as well as other constituents (Figure A6-46) of sample p#1(v) are readily explained by mixing between groundwater from the carbonate and volcanic aquifers within the borehole. It is estimated from flow logs that the p#1(v) sample received about 28.6% of its water from the carbonate aquifer as a result of upward flow in the borehole, despite an attempt to isolate the volcanic and carbonate aquifers from each other with a temporary plug (Craig and Robison 1984 [DIRS 101040], p. 49).

Carbon isotope data can be used to limit the amount of mixing of waters in the volcanic and Paleozoic aquifers, as follows. The $\delta^{13}C$ and DIC of the carbonate aquifer at p#1(c) are –2.3 per mil (Table A6-2) and 976.6 mg/L as HCO_3^{-} (Table A6-3), respectively. In contrast, for groundwater samples where uranium isotopes indicate only Yucca Mountain recharge exists (i.e., samples 43, 44, 60, 64, 65, and 66) the average DIC concentration is about 143.6 ± 18.6 mg/L as HCO_3^{-} and the average $\delta^{13}C$ is -9.1 ± 1.4 per mil (Note: uncertainty is given as 1 standard deviation and the $\delta^{13}C$ of sample 59 was used for sample 60). Mixing calculations were done using the composition for sample p#1(c) and the average composition of Yucca Mountain recharge from samples 43, 44, 60, 64, 65, and 66 as end members. The calculations employed the relations $DIC_{mix} = X_c \bullet DIC_c + (1\text{-}X_c) \bullet DIC_v$ and $\delta^{13}C_{mix} \bullet DIC_{mix} = X_c \bullet \delta^{13}C_c \bullet DIC_c + (1\text{-}X_c) \bullet \delta^{13}C_v \bullet DIC_v$, where X_c is the fraction of groundwater from the carbonate aquifer in the mixture and the subscripts *mix, c*, and *v* indicate that the variables pertain to the mixture, carbonate aquifer, and volcanic aquifer, respectively. These calculations indicate that the presence of 10% carbonate aquifer water would increase the DIC and $\delta^{13}C$ of Yucca Mountain recharge water to 227 and –6.2 per mil, respectively; similarly, the presence of 20% carbonate aquifer water in the mixture would increase DIC and $\delta^{13}C$ to 310 and –4.8 per mil, respectively. On the basis of these calculations, groundwater from borehole USW H-3 (Site 51) with a DIC concentration of 240.9 mg/L HCO_3 and a $\delta^{13}C$ of –4.9 per mil may have approximately 10% to 20% carbonate aquifer water. However, all other samples from the Yucca Mountain block have less than 5% carbonate aquifer water. These relatively small amounts of carbonate aquifer water in the volcanic aquifer probably form upper limits because isotopically heavy calcite is present in the volcanic aquifer that, if dissolved, would result in effects on DIC and $\delta^{13}C$ compositions similar to those produced by mixing.

Groundwater from the Solitario Canyon Wash (SCW) area wells is similar with respect to most chemical and isotopic constituents to groundwater in the southern Yucca Mountain (YM-S) well grouping and to groundwater from wells H-3 (Site 51) and SD-6 (Site 50) in the Yucca Crest (YM-CR) grouping (Figures A6-42 to A6-46). The chemical and isotopic similarities between the SCW and YM-S groupings indicates the generally southward flow of groundwater from the SCW area wells, whereas the chemical and isotopic similarities between groundwaters at wells H-3 and SD-6 and SCW area groundwater is compatible with at least a small amount of groundwater leakage eastward across the Solitario Canyon fault. However, because the vast majority of YM-C and YM-SE area groundwaters appear to be unrelated to groundwater from

the Solitario Canyon area, groundwater leakage from Solitario Canyon to these areas must be relatively small compared to other groundwater sources, such as local recharge.

In summary, considerable hydrochemical evidence exists to support the hypothesis that the bulk of the SZ water beneath Yucca Mountain was derived from local recharge. Similarly, evidence in support of groundwater flow to Yucca Mountain from upgradient areas is weak. Exceptions to this are leakage of groundwater from the Solitario Canyon area into groundwater at wells SD-6 and H-3, and potentially wells in southern Yucca Mountain, including those near Fortymile Wash. Local upwelling of relatively small amounts (generally less than 5%) of carbonate aquifer water into the volcanic aquifer is permitted by the groundwater data from most YM-CR, YM-C, and YM-SE area wells.

On the basis of the above discussions, groundwater beneath Yucca Mountain is best characterized by generally low concentrations of dissolved solids and by high $^{234}U/^{238}U$ activity ratios. Lower $^{234}U/^{238}U$ ratios do not, however, exclude the presence of Yucca Mountain recharge in the groundwater. Low $^{234}U/^{238}U$ activity ratios (less than 6) in downgradient groundwater can result from recharge in southern Yucca Mountain with a lower $^{234}U/^{238}U$ activity ratio, mixing of Yucca Mountain recharge with groundwater from other sources, and water-rock interactions that add dissolved uranium to the groundwater.

A6.3.6.5 Evaluation of Evidence for the Magnitude of Recharge at Yucca Mountain

The magnitude of recharge at Yucca Mountain is estimated in this section on the basis of the concentrations of constituents such as chloride that are considered conservative in groundwater systems of the type present at Yucca Mountain. In particular, the chloride mass balance (CMB) method will be used for this purpose. This method is based on the premise that the flux of Cl^-deposited at the surface equals the flux of Cl^- carried beneath the root zone by infiltrating water. With increasing depth in the root zone, Cl^- concentrations in soil waters increase and apparent infiltration rates decrease as water is extracted by the processes of evapotranspiration (Figure A6-47). However, once soil waters move below the zone of evapotranspiration, they become net infiltration, and their Cl^- concentrations are assumed to remain constant. It is these Cl^- concentrations that are used to calculate net infiltration rates and, ultimately, recharge rates.

The CMB method (e.g., Dettinger 1989 [DIRS 105384], p. 59) uses the following equation to calculate the infiltration rate (I, in mm) when runoff or run-on is negligible:

$$I = (P\ C_0)/C_p \qquad \text{(Eq. A6-7)}$$

where

P is average annual precipitation (mm)

C_0 is average Cl^- concentration in precipitation, including the contribution from dry fallout (mg/L)

C_p is the measured Cl^- concentration in groundwaters (mg/L).

The CMB method (Figure A6-47) assumes steady one-dimensional, downward piston flow, constant average annual precipitation rate, constant average annual Cl^- deposition rate (PC_0), no run-on or run-off, no Cl^- source other than precipitation (e.g., it is assumed that the concentrations of Cl^- brought in by surface runoff and Cl^- released from weathering of surface rocks are negligible), and no Cl^- sink (Table A5-1, Assumption 5). When these conditions are met, the estimates of infiltration rate are equal to the recharge rate at the water table; the terms infiltration rate and recharge rate are used interchangeably in the remainder of this section.

Estimates of recharge using the CMB technique for 15 groundwater basins in Nevada were found to be in fairly good agreement with estimates obtained by the Maxey-Eakin linear step function (Dettinger 1989 [DIRS 105384], p. 75). Using a 6-year study of two upland basins selected as analogue wetter climate sites for Yucca Mountain, Lichty and McKinley (1995 [DIRS 100589], p. 1) showed the CMB method to be more robust than a water-balance modeling approach using a deterministic watershed model for estimating basin-wide recharge for two comparatively wet sites in the Kawich Range north of Yucca Mountain. They attributed the robustness of the CMB method to the small number of measured parameters required as compared to the number of parameters needed for defining a deterministic watershed model.

Point estimates of net infiltration or recharge using the CMB method tend to be less robust than basin-wide estimates because of additional assumptions concerning vertical groundwater flow and surface water flow. Conditions under which these assumptions may not be valid at Yucca Mountain are discussed in another scientific analysis report (BSC 2001 [DIRS 160247], Section A6.9.2.2). Values of net infiltration estimated at Yucca Mountain using the CMB method range from less than 0.5 mm/yr in washes to a maximum of nearly 20 mm/yr beneath ridgetops and side slopes (based on data and calculations in DTNs: LA0002JF831222.001, [DIRS 147077]; LA0002JF831222.002 [DIRS 147079]; LA9909JF831222.010 [DIRS 122733]; LA9909JF831222.012 [DIRS 122736]; and BSC 2001 [DIRS 160247], Section A6.9.2.4), depending on the Cl^- deposition rate assumed in the calculation.

Table A6-6 lists recharge rates calculated from measured groundwater Cl^- concentrations using the CMB method. This method requires that the Cl^- deposition rate, which is the product of precipitation and effective Cl^- concentration in precipitation (including both wet and dry fallout), be known. The average annual precipitation rate for Yucca Mountain is 170 mm (Hevesi et al. 1992 [DIRS 116809], p. 677), and estimates of average Cl^- concentrations in precipitation at Yucca Mountain range from 0.3 to 0.6 mg/L (BSC 2001 [DIRS 160247], Section A6.9.2.3). To bound the recharge rate estimates, Rate 1 in Table A6-6 is calculated using the lower estimate for Cl^- concentration whereas Rate 2 is calculated using the higher estimate. The CMB recharge estimates average 7 ± 1 mm/yr for Rate 1 and 14 ± 2 mm/yr for Rate 2 (Table A6-6). The much narrower range of fluxes estimated for the saturated-zone samples compared to the unsaturated zone samples can probably be attributed to the greater volume averaging of the SZ samples, as well as to mixing in the aquifer and in the borehole when the SZ samples were pumped.

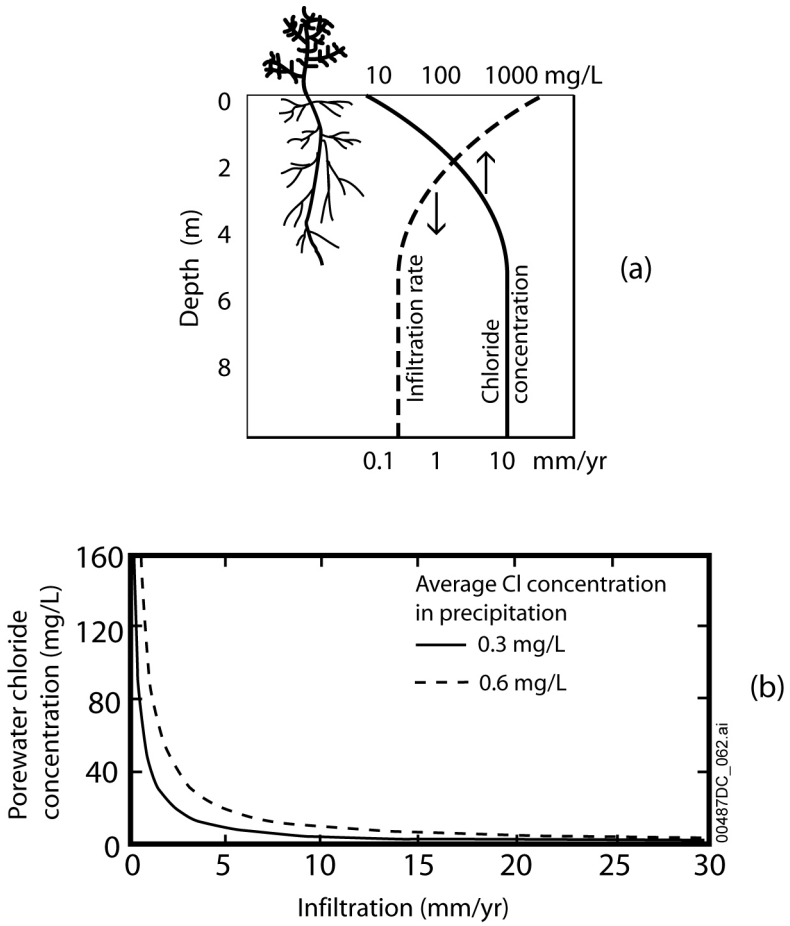

For illustration only.

NOTES: Part (a) illustrates the underlying basis of the CMB method. Part (b) shows porewater Cl^- concentrations as a function of infiltration, assuming a range of chloride deposition rates (106 to 183 mg porewater $Cl^-/(m^2$ year). Using an average annual precipitation rate of 170 mm (Hevesi et al. 1992 [DIRS 116809], p. 677), these deposition rates correspond to effective Cl^- concentrations of 0.62 mg/L to 1.07 mg/L in local precipitation.

Figure A6-47. Chloride Mass-Balance Method for Estimating Infiltration

As indicated in the following section, it appears from interpretations of both stable isotope (δD and $\delta^{18}O$) and ^{14}C data that most of the groundwater presently beneath Yucca Mountain infiltrated in the late Pleistocene, when precipitation and Cl^- deposition rates were potentially different from present conditions. It is estimated from wood rat midden data that mean annual precipitation during the Pleistocene was 1.9 times present precipitation at a 1,500-m elevation and 1.3 times present precipitation at a 750-m elevation (Forester et al. 1999 [DIRS 109425], p. 32). For the elevation range of 1,000 to 1,500-m that encompasses the surface elevations of most wells listed in Table A6-6 (DTN: GS010908312332.002 [DIRS 163555]), an average increase in Pleistocene precipitation of 1.7 times present precipitation can be estimated for Yucca Mountain. However, it is not clear if Cl^- concentrations in precipitation were the same during the Pleistocene or if Cl^- concentrations decreased so that Cl^- deposition rates (the product of P and C_0) were constant or even lower than today. If Cl^- concentrations in precipitation were similar in the late Pleistocene to those of the present day, Pleistocene infiltration rates may have

been approximately 70% higher, on average, than the rates listed in Table A6-6 using present-day precipitation rates and Cl^- concentrations. On the other hand, if Cl^- deposition rates in the Pleistocene were approximately the same as today, as inferred by (Plummer et al. 1997 [DIRS 107034], p. 540) from $^{36}Cl/Cl$ ratios in packrat middens, the infiltration rates listed in Table A6-8 using present-day Cl^- deposition rates are valid.

A6.3.6.6 Evaluation of Evidence for Timing of Recharge

Hydrochemical data that bear on the question of the age or timing of local recharge include hydrogen and oxygen isotope ratios and ^{14}C activities. Hydrogen and oxygen isotope ratios may contain age information because the numerical values of these ratios in groundwaters reflect the climate under which the waters were infiltrated. Therefore, if waters were recharged in a climatic regime different from the current regime, this fact should be reflected in the isotope ratios of the groundwaters.

The activity of ^{14}C in a particular groundwater sample potentially offers a more direct indication of the time at which that groundwater was recharged. In general, the older the sample, the lower the ^{14}C activity. However, the interpretation of the age of a groundwater sample from ^{14}C activity data is complicated by the fact that groundwaters can undergo soil-water-rock-gas interactions that can alter the proportions of carbon isotopes in a groundwater sample. This process, in turn, can lead to modification of the age calculated for the sample based on ^{14}C activity as discussed further below.

Table A6-6. Recharge Rates Based on the Chloride Mass Balance Method

Well Identifier	Chloride concentration (mg/L)	Apparent Recharge Rate[a] (mm/yr)	
		Rate 1	Rate 2
G-2	6.5	7.8	15.7
UZ-14 (sh)	6.9	7.4	14.8
H-1 (Tcp)	5.7	8.9	17.9
b#1(bh)	10.8	4.7	9.4
c#1	7.4	6.9	13.8
c#2	7.1	7.2	14.4
c#3	7.2	7.1	14.2
c#3('95-97)	6.5	7.8	15.7
ONC#1	7.1	7.2	14.4
p#1(v)[b]	13.0	3.9	7.8
G-4	5.9	8.6	17.3
H-3	9.5	5.4	10.7
H-4	6.9	7.4	14.8
H-5	6.1	8.4	16.7
UZ#16	10.6	4.8	9.6
WT#12	7.8	6.5	13.1

Table A6-6. Recharge Rates Based on the Chloride Mass Balance Method (Continued)

Well Identifier	Chloride concentration (mg/L)	Apparent Recharge Rate[a] (mm/yr)	
		Rate 1	Rate 2
WT-17	6.4	7.7	15.5
WT#3	6.0	8.2	16.5

Source: Table A6-1.

[a] Infiltration rates were calculated based on equation (7). Rate 1 is calculated using the lower estimate for Cl^- concentration in precipitation (0.3 g/L); Rate 2 is calculated using the higher estimate (0.6 mg/L). Recharge estimates obtained by the CMB method are based on Table A5-1, Assumption 5.

[b] Approximately 28.6% of the water in this sample is from upward flow in the borehole from the carbonate aquifer (Craig and Robison 1984 [DIRS 101040], p. 49).

A6.3.6.6.1 Evidence for the Timing of Recharge from Hydrogen and Oxygen Isotope Ratios

Many of the effects of seasonal and long-term temperature changes on hydrogen and oxygen values in groundwater described in Section A6.3.1.2.1 have been reported for the Yucca Mountain area. Benson and Klieforth (1989 [DIRS 104370], Figure 11) noted a correlation between $\delta^{18}O$ values and the ^{14}C age of groundwaters near Yucca Mountain. Waters are lighter in $\delta^{18}O$ with increasing age between 9,000 and 18,500 years ago, a trend they attributed to the colder temperatures existing at the time the older water was recharged. Variations in the $\delta^{18}O$ compositions of groundwater discharging in the Ash Meadows area at Devils Hole 55-km southeast of Yucca Mountain were preserved in calcites deposited between 570,000 and 60,000 years before the present (Winograd et al. 1992 [DIRS 100094], Figures 2 and 3). These variations were shown to correlate well with known glacial and interglacial episodes during the period of record, with $\delta^{18}O$ decreasing, on average, by 1.9 per mil during glacial periods.

The δD and $\delta^{18}O$ values of regional groundwater samples and perched-water samples at Yucca Mountain are plotted in Figure A6-48. The modern global meteoric water line ($\delta D = 8\ \delta^{18}O + 10.0$) shown on Figure A6-48 is approximately equal to the local Yucca Mountain meteoric water line ($\delta D = 8\ \delta^{18}O + 8.9$) as defined by Benson and Klieforth (1989 [DIRS 104370], Figure 14) from snow samples obtained from Yucca Mountain. Snow samples were used to define the local meteoric water line because these samples were less likely to be affected by evaporation than rain samples, especially samples of light summer rains that can have a substantial fraction of their volume evaporated before reaching the ground. A paleometeoric water line of $\delta D = 8\ \delta^{18}O + 5.0$ was suggested by White and Chuma (1987 [DIRS 108871], pp. 573 to 574) to fit data from the Amargosa Desert and Oasis Valley.

Although considerable variability in δD and $\delta^{18}O$ values is evident in Figure A6-48, much of this variability is attributable to the heavy δD and $\delta^{18}O$ values of the FMW-N samples and the light δD and $\delta^{18}O$ values of the TM samples. The Yucca Mountain groundwaters (YM groupings only) and most perched waters (excluding NRG-7a and one UZ-14 sample) vary in δD by about 13 per mil and in $\delta^{18}O$ by about 1 per mil. The high ^{14}C activities associated with the

FMW-N groundwater and the low ^{14}C activities associated with the TM groundwater suggest that some of the differences between the δD and $\delta^{18}O$ values in these groups is attributable to changes in the δD and $\delta^{18}O$ composition in response to climate change, with the heavy values representing the composition of groundwater recharged under the modern climate.

Because the groundwaters shown in Figure A6-48 probably originated from different recharge areas and recharge elevations, the effects of climate-induced changes and these other factors are mixed. The effects of time- and climate-induced changes on δD and $\delta^{18}O$ composition can be isolated from these other effects by examining the changes in the composition of pore and perched water with depth in the unsaturated zone at Yucca Mountain (Figure A6-48). In this case, because all of the perched and porewater data from borehole UZ-14 probably originated close to the borehole, the effects of spatial and elevation distributions of recharge are minimal. At borehole UZ-14, the porewater data from borehole UZ-14 show a general trend of lighter δD and $\delta^{18}O$ in the deeper (Tac and Tcp) pore waters and heavier δD and $\delta^{18}O$ in shallow pore waters (PTn). The shallow pore water that results from infiltration at Yucca Mountain is similar in δD and $\delta^{18}O$ composition to the modern groundwater from upper Fortymile Canyon, suggesting that the δD and $\delta^{18}O$ composition of modern precipitation is similar in both locations. Note that none of the porewater data in Figure A6-48 show systematic trends that indicate evaporative effects (Section A6.3.1.2.1, Figure A6-4). This observation suggests that the relatively high porewater salinities observed in the shallow part of this borehole (Yang et al. 1996 [DIRS 100194], Table 3), and perhaps other parts of Yucca Mountain, are due to plant transpiration rather than evaporation (Section A6.3.1.2.1). Other groundwaters from the Yucca Mountain area, like those in the FMW-S group, may indicate more significant evaporative effects (Figure A6-48).

Perched waters from UZ-14 have δD and $\delta^{18}O$ compositions that are intermediate between the shallow and deep pore waters. The deep pore water from the relatively impermeable Tac unit is lighter than the pore water from the underlying, but more permeable Tcp unit, suggesting that it has been more difficult to flush the older, lighter pore water in the Tac with younger water (Yang et al. 1998 [DIRS 101441]). The porewater data indicate that groundwater from the YM-C and YM-SE is similar in composition to the deep pore water from the Tac unit at borehole UZ-14, supportive of their possible origin from local recharge. The decrease in $\delta^{18}O$ composition of about 2 per mil between the shallow pore water and the deep porewater and Yucca Mountain groundwater compositions from the YM-CR, YM-C, and YM-SE groupings is comparable to the approximately 1.9 per mil differences in calcite $\delta^{18}O$ composition at Devils Hole (Winograd et al. 1992 [DIRS 100094], Figure 2) for glacial and subsequent interglacial periods, suggesting the deep pore water and Yucca Mountain groundwater were recharged under a paleoclimatic conditions that existed until the late Pleistocene.

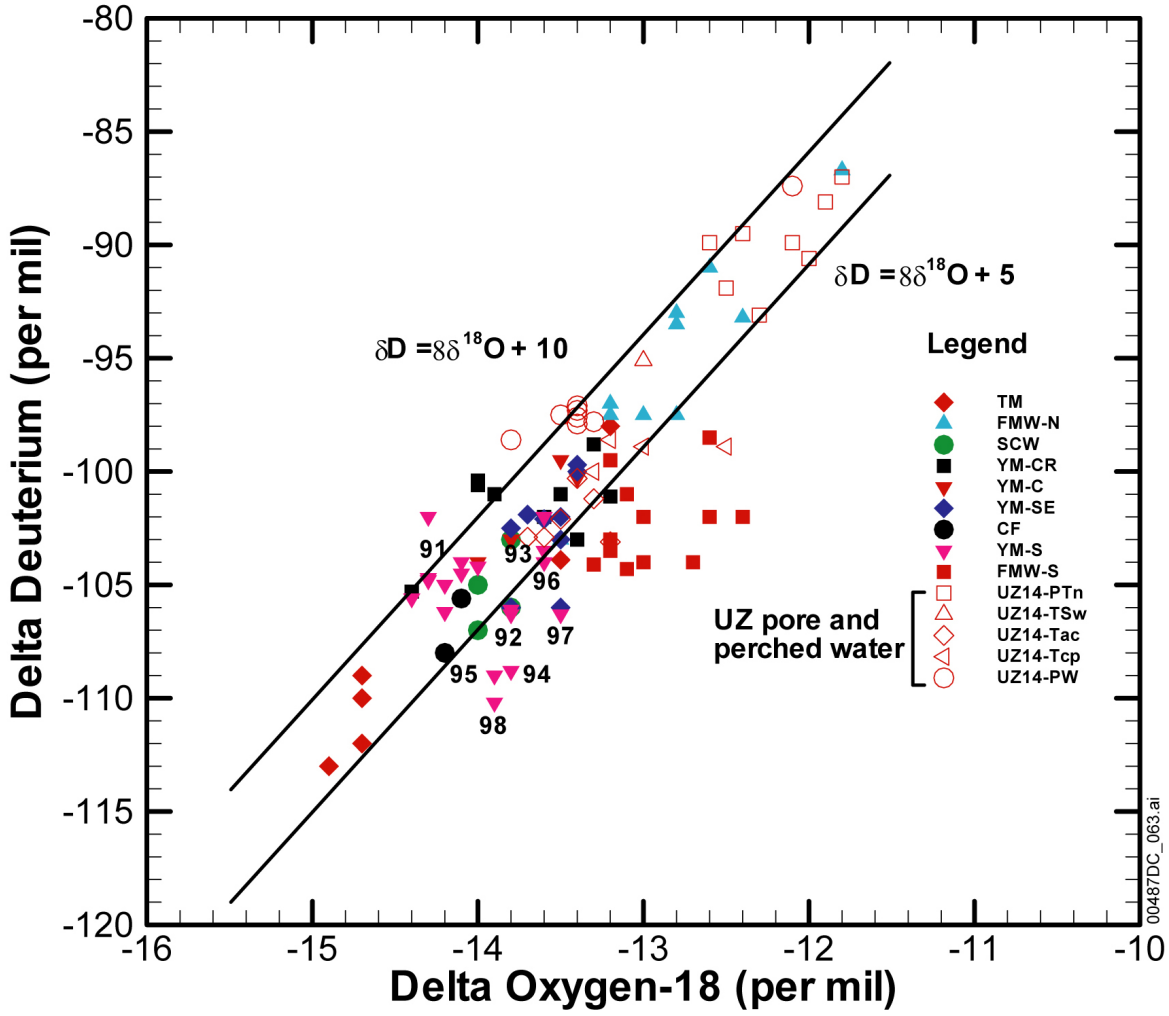

Source: DTN: GS990308312272.002 [DIRS 145692]; Tables A6-2 and A6-5; porewater data for borehole UZ-14 are from Yang et al. 1998 [DIRS 101441] Tables 9–12.

NOTE: This figure has color-coded data points and should not be read in a black and white version. The solid lines are the global meteoric water line (δD = 8 δ^{18}O + 10) (Clark and Fritz 1997 [DIRS 105738], p. 36) and a possible paleometeoric water line for southern Nevada (δD = 8 δ^{18}O + 5) (White and Chuma 1987 [DIRS 108871], pp. 573 to 574).

Figure A6-48. Delta Deuterium and Delta ^{18}O Data for Borehole UZ-14 Unsaturated Zone Pore Water, Perched Water, and Groundwater near Yucca Mountain

In contrast, some of the YM-S area groundwater does not overlap with the deep porewater data from the borehole, raising doubts as to whether it originated predominantly from Yucca Mountain recharge. Many groundwaters from the YM-S group, including Sites 91 (NC-EWDP-2D) and 92 (NC-EWDP-19D composite) near Fortymile Wash are isotopically similar to groundwaters in the Crater Flat (CF) and Solitario Canyon Wash (SCW) groups. Groundwaters from Sites 93 (NC-EWDP-19P) and 96 (NC-EWDP-19D Zone 2) plot nearer to the deep pore water from borehole UZ-14. The remaining groundwater samples from NC-EWDP-19D (Sites 94, 95, 97, and 98) have no clear affinity with groundwater from other areas. In general, it does not appear likely from the δD and δ^{18}O compositions that groundwater

from wells NC-EWDP-2D or NC-EWDP-19D originated from present or paleorecharge along Fortymile Wash, based on the lack of overlap between data from these sites and data from the FMW-N and FMW-S groups. However, for groundwaters from Sites 93 (NC-EWDP-19P) and 96 (NC-EWDP-19D Zone 2), the δD and $\delta^{18}O$ data do not obviously rule out an origin from paleorecharge along Fortymile Wash.

A6.3.6.6.2 Evidence for the Timing of Recharge from Carbon Isotope Data

As is discussed in Section A6.3.1, the ^{14}C ages of groundwater are susceptible to modification through water-rock reactions. Nonetheless, various observations indicate that the ^{14}C ages of the perched-water samples do not require substantial correction for the dissolution of carbonate. First, the ratios of ^{36}Cl to stable chlorine ($^{36}Cl/Cl$) of the perched-water samples are similar to those expected for their uncorrected ^{14}C age, based on reconstructions of $^{36}Cl/Cl$ ratios in precipitation throughout the late Pleistocene and Holocene from packrat midden data (Plummer et al. 1997 [DIRS 107034], Figure 3; DTNs: LAJF831222AQ97.002 [DIRS 145401]; GS950708315131.003 [DIRS 106516]; GS960308315131.001 [DIRS 106517]). Second, Winograd et al. (1992 [DIRS 100094], Figure 2) presented data from calcite deposits that indicated the $\delta^{18}O$ values in precipitation during the Pleistocene were, on average, 1.9 per mil more depleted during pluvial periods compared to interpluvial periods. The $\delta^{18}O$ values of the perched-water samples generally are more depleted than porewater samples from the shallow unsaturated zone at Yucca Mountain by more than 1.0 per mil (Figure A6-48). This consistent difference suggests that, at some boreholes, the perched water may contain a substantial component of water from the Pleistocene.

Values for $\delta^{13}C$ and ^{14}C in perched waters and groundwaters from the Yucca Mountain area are plotted in Figure A6-45. Excluding the perched-water and the Fortymile Wash area (FMW-N) samples, the $\delta^{13}C$ and ^{14}C values reported for the groundwater samples are negatively correlated. In the absence of chemical reactions and/or mixing, waters moving from source areas to Yucca Mountain should experience no change in $\delta^{13}C$, but their ^{14}C activity should decrease with time. If waters infiltrating into the source area had more or less constant $\delta^{13}C$ values, data points for waters infiltrated at different times would form a vertical trend in Figure A6-45. The fact that the data points in the figure do not form a vertical trend suggests either that the $\delta^{13}C$ of waters infiltrated at the source areas are not constant or that chemical reactions or mixing have affected the carbon isotope values. If waters that infiltrate into the source areas have randomly variable $\delta^{13}C$ ratios, then a random relation between $\delta^{13}C$ and ^{14}C values would be expected. Rather the $\delta^{13}C$ and ^{14}C values for Yucca Mountain and Crater Flat groundwaters are well correlated as shown in Figure A6-45.

It has been noted that $\delta^{13}C$ values in infiltrating waters reflect the types of vegetation present at the infiltration point. According to the data of Quade and Cerling (1990 [DIRS 100073], p. 1,550), the $\delta^{13}C$ of modern water infiltrated in cooler climates (for example, at higher elevations) is more negative than for modern water infiltrated in warmer climates (for example, at lower elevations). The change from a relatively wet, cool climate to a relatively warm, dry climate at the end of the Pleistocene would be expected to exert a similar effect on the $\delta^{13}C$ of infiltration as elevation does on modern infiltration. In other words, Pleistocene infiltration would be expected to have lighter $\delta^{13}C$ than modern infiltration at the same elevation. However,

both a climate induced change in $\delta^{13}C$ values, or recharge from a distant, high-elevation source would result in a positive correlation in Figure A6-45 because the older samples (that is, lowest pmc) plotted would tend to have the most negative $\delta^{13}C$ (that is, they infiltrated when the climate was cooler than it is now or in distant, high-elevation areas). Because the observed correlation in the groundwater values is negative instead of positive, the primary cause of the correlation must involve some other process(es). Both calcite dissolution and mixing with groundwater from the carbonate aquifer are possible explanations for this observed trend. Both of these processes would tend to introduce DIC with heavy $\delta^{13}C$ and little ^{14}C. The importance of each process probably varies spatially and can be assessed by determining if increases in other ions and isotopes present at high concentrations in the carbonate aquifer are evident in the groundwater.

A likely cause of the negative correlation evident in Figure A6-45 is the dissolution of carbonate minerals such as calcite. For example, calcite with a $\delta^{13}C$ value of –4 per mil and a ^{14}C activity of zero could readily explain the correlation if it were being dissolved by infiltrating soil waters. This explanation assumes that points on the regression line are of the same age but that the water dissolved different amounts of calcite. In this explanation, the scatter of points about the regression line could represent samples of slightly different ages. For example, δD and $\delta^{18}O$ data suggest that groundwaters from the northern part of Fortymile Wash (FMW-N) and the perched waters have younger ages than most Yucca Mountain groundwaters. This observation is consistent with the data plotted in Figure A6-45.

The data points for groundwater from the FMW-N grouping with high ^{14}C activities (Sites 30 to 32) are of particular interest because they represent recent infiltration based on their high tritium and ^{36}Cl-to-chloride ratios (DTN: LAJF831222AQ98.011 [DIRS 145402]). As shown in Figure A6-45, the ^{14}C activities in these samples vary between 60 and 75 pmc. This result suggests these samples obtained a significant fraction of their bicarbonate concentrations from a source with little or no ^{14}C activity. Interestingly, these samples have lower $\delta^{13}C$ values than most groundwaters from the Yucca Mountain area. This result suggests the bicarbonate source was not calcite typical of the soil zone on Yucca Mountain, as these have $\delta^{13}C$ values between −2 and −8 per mil (Whelan et al. 1998 [DIRS 137305], Figure 5).

In instances where the recharge source for a groundwater can be identified, it is possible to estimate the extent to which the ^{14}C activity of the groundwater has been lowered through water/rock interactions in the saturated zone by comparing the DIC concentrations of the recharge (DIC_{rech}) and the downgradient groundwater (DIC_{gw}) (Clark and Fritz 1997 [DIRS 105738], Chapter 8). The downgradient increase in DIC_{gw} relative to DIC_{rech} represents the extent to which mineral sources of carbon have been added to the groundwater. These mineral sources of carbon may have diluted the initial ^{14}C activity of the recharge by the addition of ^{14}C-free carbon. The extent of this dilution and its effect on the calculated groundwater ^{14}C age can be represented by a correction factor ($q_{DIC} = DIC_{rech}/DIC_{gw}$) which is then applied to the radioactive decay equation to calculate the corrected ^{14}C age, as indicated in footnote (b) to Table A6-9. The basis for the equations given in footnote (b) and their limitations are described in more detail in Section A6.3.9.

As described in Sections A6.3.6.2 to A6.3.6.4, evidence exists that some groundwater samples from Yucca Mountain originated almost exclusively from recharge through Yucca Mountain

itself. Corrections were made to groundwater ^{14}C ages at locations within 18-km of the repository where groundwater had been identified from anomalously high $^{234}U/^{238}U$ ratios as having originated mostly from local recharge (Paces et al. 1998 [DIRS 100072]; see also Table A6-5). Corrections were also made to the ^{14}C ages of groundwater from several locations for which $^{234}U/^{238}U$ activity ratios were not measured, but which may contain substantial fractions of local Yucca Mountain recharge based on proximity to groundwater with high $^{234}U/^{238}U$ activity ratios. For these samples, total DIC concentrations, calcite saturation indices, and logarithms of the partial pressure of carbon dioxide (log P_{CO_2}) were computed with PHREEQC (DTN: MO0309THDPHRQC.000 [DIRS 165529]). In these corrections, the values of DIC_{rech} are allowed to vary between 128.3 and 144 mg/L bicarbonate (HCO_3^-), based on values measured in perched water at Yucca Mountain (Yang et al. 1996 [DIRS 100194], Table A6-5). The correction factor q_{DIC} ranges from 0.74 at borehole WT#12 to 1.0 at several boreholes (Table A6-5). Corrected groundwater ^{14}C ages range from 11,430 years at borehole WT#3 to 16,390 years at borehole WT#12 (Table A6-7). These calculations show that only minor corrections to the groundwater ^{14}C ages are necessary for samples located along the estimated flow path from the repository (see below).

Table A6-7. Chemistry and Ages of Groundwaters from Seven Boreholes at Yucca Mountain

Borehole	$^{234}U/^{238}U$ Activity Ratio	^{14}C Activity (pmc)	*DIC*, as HCO_3^- (mg/L)	log P_{CO_2} (atm)	log (IAP/K_{cal})[a]	Factor q_{DIC}	Corrected ^{14}C Age(yr)[b]	Uncorrected ^{14}C Age (yr)[c]
G-2	7.6	20.5	127.6	–2.352	–0.791	1	13,100	13,100
WT-17	7.6	16.2	150.0	–1.958	–1.175	0.86 to 0.96	13,750 to 14,710	15,040
WT#3	7.2	22.3	144.3	–2.413	–0.515	0.89 to 1.0	11,430 to 12,380	12,400
WT#12	7.2	11.4	173.9	–2.327	–0.313	0.74 to 0.83	15,430 to 16,390	17,950
c#3	8.1	15.7	140.2	–2.458	–0.319	0.92 to 1.0	14,570 to 15,300	15,300
b#1 (Tcb)[d]	—	18.9	152.3	–1.892	–0.757	0.84 to 0.95	12,350 to 13,300	13,770
G-4	—	22.0	142.8	–2.490	–0.305	0.90 to 1.0	11,630 to 12,510	12,500

Source: DTN: LA0202EK831231.002 [DIRS 165507]; Tables A6-1 and A6-2.

[a] log (IAP/K_{cal}) is the calcite saturation index. Negative values indicate undersaturation with calcite.

[b] The corrected age is calculated by multiplying the initial ^{14}C activity ($^{14}A_0$) in Equation A6-3 by q_{DIC}: $t = (-1/\lambda) \ln (^{14}A/(^{14}A_0\, q_{DIC}))$. The factor q_{DIC} is calculated as $q_{DIC} = DIC_{rech}/DIC_{gw}$, where the subscripts *rech* and *gw* indicate the DIC of recharge and downgradient groundwater.

[c] Calculated from Equation A6-3.

[d] The sample from borehole b#1 came from the Bullfrog tuff (Tcb).

A6.3.6.7 Calculations to Determine the Fraction of Young Water in Yucca Mountain Recharge

Given that groundwater samples at Yucca Mountain were often pumped over large depth intervals that mixed shallow and deep water (Table A4-3), it may be difficult to demonstrate conclusively that groundwater does not contain a small fraction of young water. In this section, however, calculations are performed to bound the maximum percentage of young water that could be present in the sampled groundwater.

Recharge at Yucca Mountain has probably been continuous in time, so that the measured groundwater ^{14}C activities result from the mixing of recharge (and possibly groundwater from other areas) having a broad range of ages (Campana and Byer 1996 [DIRS 126814], Figure 5). However, because data on the temporal distribution of recharge, mixing depth, and storage volume required for more detailed analyses are lacking, the fraction of young water in a groundwater sample is calculated in this section by idealizing individual groundwater samples as a binary mixture of younger and older groundwaters. Young water is arbitrarily defined as having a ^{14}C age, or residence time, of less than 1,000 years. In a binary mixture, the total number of ^{14}C atoms in the mixture depends on the ^{14}C activities, volume fractions, and total DIC concentrations of the two components, which in this case, are taken to be young and old waters:

$$(^{14}C_{\text{mix}})(DIC_{\text{mix}}) = (X_{\text{young}})(^{14}C_{\text{young}})(DIC_{\text{young}}) + (X_{\text{old}})(^{14}C_{\text{old}})(DIC_{\text{old}}) \qquad \text{(Eq. A6-8)}$$

where

^{14}C = the ^{14}C activity (in pmc)
DIC_i = dissolved inorganic carbon concentration (mg/L) of component i
X_i = the volume fraction of component i
mix, young, and old = mixed, young, and old components of the groundwater.

The volume fractions sum to one, so that $X_{\text{old}} = 1 - X_{\text{young}}$. Equation A6-8 can be solved for X_{young}:

$$X_{\text{young}} = \frac{(^{14}C_{\text{mix}})\,(DIC_{\text{mix}}) \;-\; (^{14}C_{\text{old}})\,(DIC_{\text{old}})}{(^{14}C_{\text{young}})\,(DIC_{\text{young}}) \;-\; (^{14}C_{\text{old}})\,(DIC_{\text{old}})} \qquad \text{(Eq. A6-9)}$$

The ^{14}C activity of 1,000-yr-old water with an initial ^{14}C activity of 100 pmc is equal to 88.6 pmc. DIC_{young} is expressed in these calculations as equivalent to mg/L HCO^-_3 and is assigned a value of 130 mg/L based on the typical alkalinity of many perched-water samples (Table A6-5). For samples with pH values above 7, which include perched water from the unsaturated zone at Yucca Mountain, alkalinity is approximately equal to the total DIC (Drever 1988 [DIRS 118564], p. 51). The value for $^{14}C_{\text{old}}$ was assigned a value of 10 pmc, which is approximately the lowest value measured in groundwater from the volcanic aquifer at Yucca Mountain (boreholes H-3 (10.5 pmc) and H-4 (11.8 pmc)).

Calculations of the possible fraction of young water in a sample (age less than 1,000 years) considered various *DIC* concentrations for the old component in the mixed water (Table A6-8). In Case 1, the *DIC* concentrations of the water components (mixed, old, and young) are assigned to be essentially equal, so that X_{young} depends only on values of ^{14}C. In Case 2, a moderately high value of 175 mg/L HCO_3^- was assigned for DIC_{old}. In Case 3, a value of 225 mg/L HCO_3^- was assigned for DIC_{old}. For Case 1, the calculated values of X_{young} range from about 0.02 (borehole WT#12) to 0.16 (boreholes WT#3 and G-4). For Case 2, the range of values for X_{young} is similar to, but slightly lower than, those from Case 1. In Case 3, the calculated values for X_{young} were lower than those from Cases 1 and 2, and three values were negative, which indicates that the value of 225 mg/L HCO_3^- for DIC_{old} was too high to be generally applicable.

Table A6-8. Sensitivity of the Permissible Fraction of Young Water Present in Groundwater to Dissolved Inorganic Carbon Concentration Assumed for the Old Component of the Mixed Groundwater

Borehole	Sample ^{14}C (pmc)	Sample *DIC* (mg/L HCO_3^-)	X_{young} (Case 1)	X_{young} (Case 2)	X_{young} (Case 3)
G-2	20.5	127.6	0.134	0.089	0.039
WT#12	11.4	173.9	0.018	0.024	–0.029
WT-17	16.2	150.0	0.079	0.070	–0.019
WT#3	22.3	144.3	0.156	0.150	0.104
c#3	15.7	140.2	0.073	0.046	–0.005
b#1 (Tcb)	18.9	152.3	0.113	0.116	0.068
G-4	22.0	142.8	0.153	0.142	0.096

Sources: DTN: LA0202EK831231.004 [DIRS 180317]; calculated using data from Tables A6-1 and A6-2.

NOTES: Table values were calculated based on data in Tables A6-1 and A6-2, Equation A6-9, and parameter values given in the text. Young groundwater is defined as less than 1,000 years old.
Case 1: $DIC_{old} = DIC_{young} = DIC_{mix}$; Case 2: DIC_{old} = 175 mg/L HCO_3^-; Case 3: DIC_{old} = 225 mg/L HCO_3^-.

Sensitivity studies were conducted to examine the effects of assigning variable values of $^{14}C_{old}$ with DIC_{old} = 175 mg/L HCO_3^-. Results of these studies show that the calculated values of X_{young} are somewhat sensitive to the value of $^{14}C_{old}$ (Table A6-9). Using $^{14}C_{old}$ = 5 pmc (Case 4) more than doubles the calculated value of X_{young} at many boreholes; however, values less than 10 pmc have not been observed at Yucca Mountain, so a value for $^{14}C_{old}$ of 5 pmc is considered unrealistic. A value for $^{14}C_{old}$ of 15 pmc (Case 5) is also generally unrealistic, given the many negative values calculated for X_{young}.

In summary, it is possible that a small fraction of young water (less than 1,000 years old) is present in the saturated zone downgradient from the repository area. Estimates range from a low of about 0.02 at borehole WT#12 to more than 0.15 at boreholes WT#3 and G-4. Smaller fractions of young water would be estimated to be present if water younger than 1,000 years old were assumed in the calculations.

Table A6-9. Sensitivity of the Permissible Fraction of Young Water Present in Groundwater to the Assumed ^{14}C Activity of the Old Component of the Mixed Groundwater

Borehole	Sample ^{14}C (pmc)	Sample *DIC* (mg/L HCO_3^-)	X_{young} (Case 4)	X_{young} (Case 2)	X_{young} (Case 5)
G-2	20.5	127.6	0.164	0.089	–0.001
WT#12	11.4	173.9	0.104	0.024	–0.072
WT-17	16.2	150.0	0.146	0.070	–0.022
WT#3	22.3	144.3	0.220	0.150	0.067
c#3	15.7	140.2	0.125	0.046	–0.048
B#1 (Tcb)	18.9	152.3	0.188	0.116	0.029
G-4	22.0	142.8	0.213	0.142	0.058

Sources: DTN: LA0202EK831231.004 [DIRS 180317]; calculated using data from Tables A6-1 and A6-2.

NOTES: Table values were calculated based on data in Tables A6-3 and A6-4, Equation A6-9, and assumptions given in the text. Young groundwater is defined as less than 1,000 years old. Case 4: $^{14}C_{old}$ = 5 pmc; Case 2: $^{14}C_{old}$ = 10 pmc; Case 5: $^{14}C_{old}$ = 15 pmc.

A6.3.7 Hydrochemical Evidence for Mixing of Groundwater

Groundwater chemical and isotopic compositions in the Yucca Mountain area exhibit both gradual and relatively abrupt spatial variability (Section A6.3.4) that may be related to mixing. Mixing may occur when: (1) groundwater from adjacent flow paths is spread by dispersion and diffusion, (2) the groundwater passes beneath a recharge area, (3) deep groundwater moves upward because of head gradients, faults, or hydraulic barriers, or (4) groundwater from different areas converges toward either natural discharge areas or toward wells. Preliminary mixing relations are investigated in this section through scatterplots involving relatively nonreactive chemical and isotopic species like Cl^-, SO_4^{2-}, δD, and $\delta^{34}S$. Potential mixing relations identified through these scatterplots are further explored through the use of inverse geochemical models in Section A6.3.8 that seek to quantitatively explain groundwater chemical and isotopic evolution in terms of mixing and water-rock interactions.

A6.3.7.1 Mixing Relations South of Yucca Mountain

Groundwater samples from boreholes located south of Yucca Mountain that constitute the YM-S, CF, and CF-SW groupings show a wide range of solute concentrations that generally increase to the northwest. Scatter plots (Figure A6-49) illustrate the distinct hydrochemistry of groundwater affected by carbonate rocks (CF-SW, p#1(c)) when compared to groundwater from the volcanic or tuff-derived alluvial aquifers. In fact, samples from the CF-SW group define a trend with a dilute end member intersecting typical groundwater compositions of the volcanic aquifer at Yucca Mountain. Importantly, some samples from the YM-S group fall along this line. In the YM-S group, groundwaters from borehole NC-EWDP-9SX (Samples 81 to 85) are most similar to samples from the CF-SW group chemically and are also geographically proximal to the CF-SW wells to the north and west. It is interpreted that the hydrochemistry of samples from borehole NC-EWDP-9SX represents a mix of carbonate aquifer-like water from southwest Crater Flat and dilute groundwater from the volcanic aquifer. Samples 89 and 90 also plot along mixing lines between the volcanic aquifer and the carbonate aquifer-like groundwaters. Given the geographic position of these wells, it is unclear as to whether this carbonate aquifer-like water enters the system via upward gradient flow from depth or if it could be due to dispersive

mixing of groundwater from the CF-SW Group. On the Cl^- versus δD plot (Figure A6-49) groundwater from the YM-S group define a trend toward the CF-SW group, not toward the composition of p#1 or deep groundwater from NC-EWDP-1DX Zone 2 (Site 74), indicating dispersive mixing rather than groundwater upwelling as the more likely hypothesis. The Cl^- versus δD plot (Figure A6-49) also helps to eliminate the possibility that the compositional trends defined by these samples are due to water/rock interaction with alluvium that is increasingly dominated by carbonate detritus derived from Bare Mountain because δD is not affected by this process.

A6.3.7.2 Evaluation of Mixing Relationships in the Amargosa Desert Region

The different groundwater groupings in the Amargosa Desert display a great contrast in solute concentration and isotopic data (Section A6.3.4). Indeed, much of the hydrochemical variation displayed in areal plots of chemical and isotopic species is contained in the relatively small area of the Amargosa Desert. This pronounced contrast in hydrochemistry, along with the relatively dense sample distribution allows for detailed evaluation of possible mixing patterns.

Groundwater in the AR grouping is chemically quite distinct with relatively large concentrations of solutes compared to groundwater to the east in Amargosa Desert, and thus, it is readily distinguishable and traceable. East and southeast of the AR grouping the consistent and distinct character of this groundwater is absent. Mixing with the dilute groundwater that constitutes the FMW-W and FMW-S groupings readily explains this observation. On a plot of the conservative solutes Cl^- and SO_4^{2-} (Figure A6-50) the hydrochemically distinct groupings of the AR and FMW-S groupings is evident along with the trend displayed by some samples of the FMW-W group and all of the samples from the AR/FMW grouping. This relationship is taken as sound evidence that intermediate Cl^- and SO_4^{2-} compositions of FMW-W and AR/FMW are a result of mixing of Amargosa Desert groundwater with dilute groundwater of the FMW-W grouping and/or FMW-S grouping (shown as mixing line 1, Mix 1, in Figure A6-50). This hypothesis is also supported by cross plots of other constituents. For example, although the number of samples is limited, Figure A6-51 shows the mixing relationships on a plot of $\delta^{34}S$ versus $1/SO_4^{2-}$. On this plot, the few samples from FMW-W and AR/FMW are near the mixing line drawn between the FMW-S and AR samples (Mix 1). Scatter plots of other constituents show similar relations, although some deviations from the consistent trend displayed in Figure A6-50 suggest that water-rock interaction has modified the hydrochemistry in some samples. Hydrochemical data are interpreted to indicate that samples 121, 122, 125, and 126 (FMW-W) and most samples from the AR/FMW group represent mixtures of AR groundwater with FMW-S and/or dilute groundwater from FMW-W. Samples 139 and 134 from FMW-S also plot along mixing line 1 (Figure A6-50) suggesting that these samples also contain a small fraction of AR groundwater. These samples are among the more westerly in this grouping; thus, the geographic position is consistent with this mixing hypothesis.

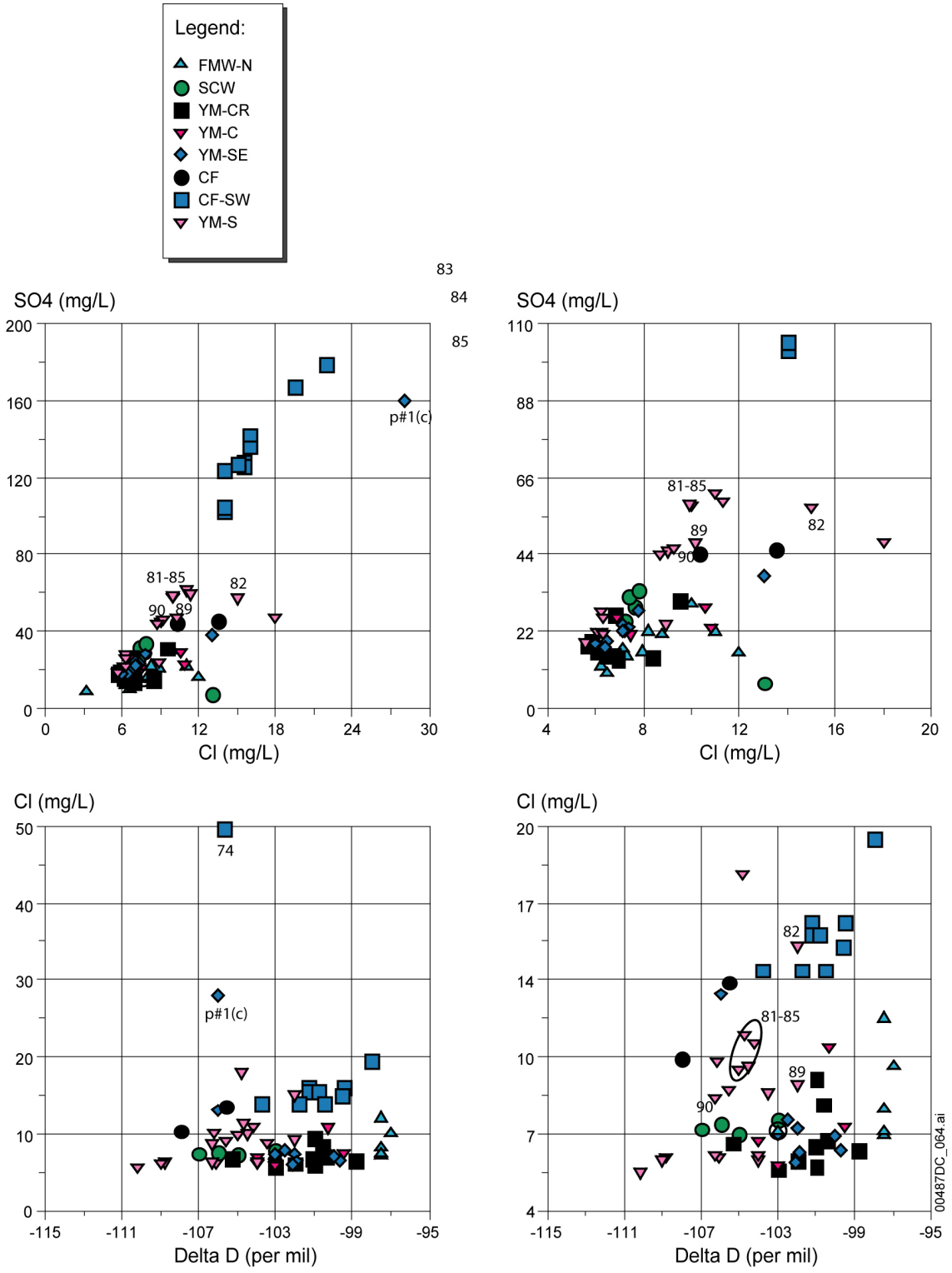

Sources: Tables A6-1 and A6-2.

NOTE: The plots on the right side of this figure have expanded scales compared to similar plots directly to their left to better display details in the tightly clustered data.

Figure A6-49. Scatter Plots Showing Mixing in Southern Yucca Mountain

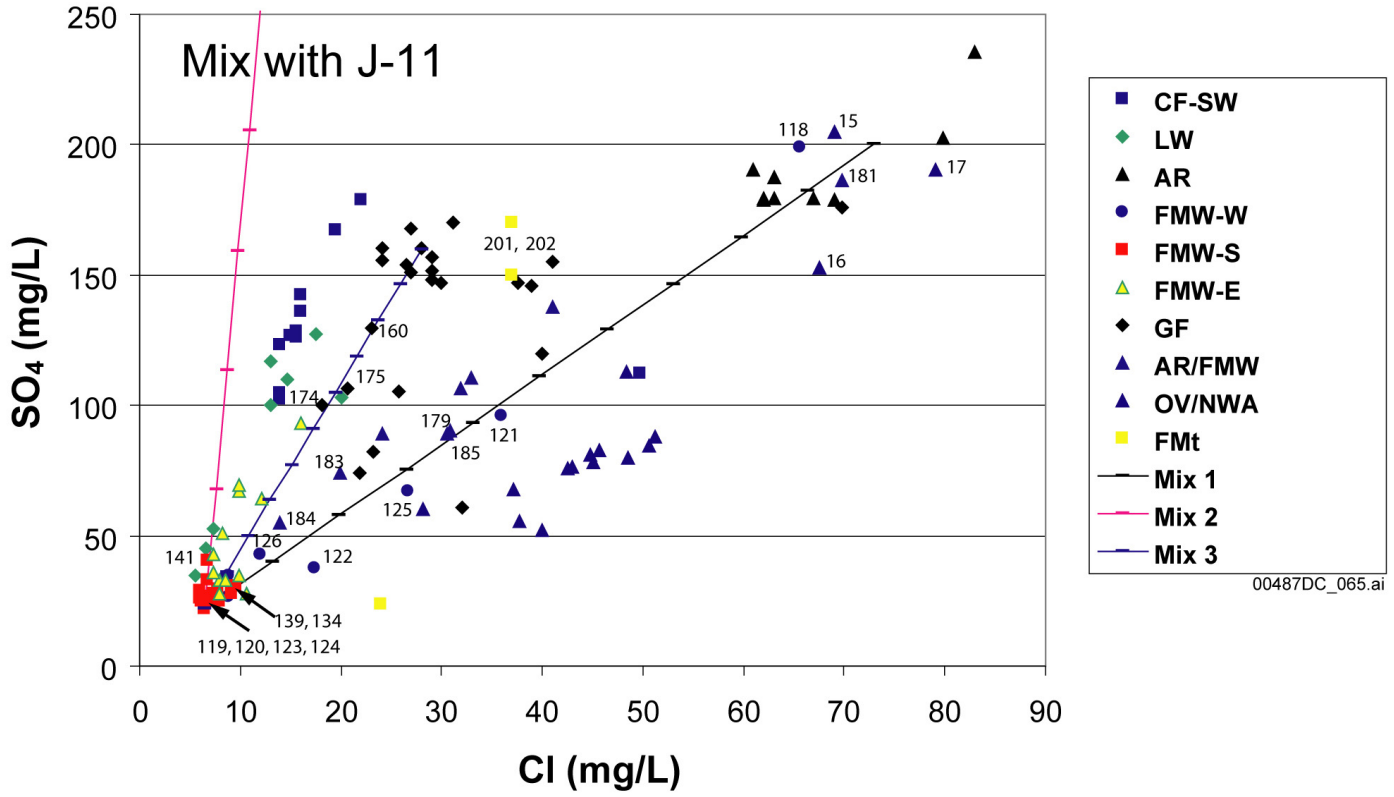

Source: Table A6-1.

NOTES: Mixing lines show 10% increments. End members for the mixing lines are: dilute end member for all mixing lines is 6.5 mg/L Cl^- and 22 mg/L SO_4^{2-}. Mixing line 1 (Mix 1) upper end member is the average of the AR Group of 73 mg/L Cl^- and 200 mg/L SO_4^{2-}. Mixing line 2 (Mix 2) upper end member corresponds to Cl^- and SO_4^{2-} values for J-11 of 17.5 mg/L and 480 mg/L, respectively. Mixing line 3 (Mix 3) upper end member is the visual average of the tight cluster displayed by the GF Group (Cl^- and SO_4^{2-} concentration of 28 mg/L and 160 mg/L, respectively). Mixing lines are drawn by plotting calculated values for Cl^- and SO_4^{2-} obtained by the mixing equation: $[Cl^-]_{mix} = F \bullet [Cl^-]_A + (1 - F) \bullet [Cl^-]_B$, where F is the fraction of component A in the mix. The SO_4^{2-} concentration is determined by substituting values for SO_4^{2-} into the equation.

Figure A6-50. Cross Correlation Plot of Sulfate versus Chloride for Samples in the Amargosa Desert Region

Samples 119, 120, 123, and 124 are the most dilute groundwaters from the FMW-West grouping. Three of four of these are also the most northeasterly wells of the grouping, furthest from the flow pathway of the AR group groundwater. Samples 118, 121, 122, 125, and 126 are located to the south or southwest of the dilute samples and show variable amounts of mixing with Amargosa River groundwater. This pattern is consistent with southeastward groundwater flow from the vicinity of the AR group. The relative amounts of mixed Amargosa River water are not entirely consistent with geographic position, however. Similar to the FMW-W grouping, the mixing percentages for wells of the AR/FMW group do not correlate with geographic position. In fact, the Cl^- and SO_4^{2-} concentrations of samples 118 and 181 are essentially identical to those of the AR group, and these are located adjacent to wells with significantly different anion concentrations. This inconsistency in detailed correlation between hydrochemistry and geographic position may be due to factors that are unknown or poorly understood including well completion, well pumping history, and vertical and horizontal anisotropy in the flow system. The similar hydrochemistry of well 181 compared to that of the AR group suggests a continuous flow pathway between these areas. Doing so, however, isolates sample 179, which clearly plots as a mixed sample with most of this water similar to the dilute water of the FMW-S group, and geographically separates a mixed sample from one of its presumed sources. Again, this inconsistency may be related to vertical heterogeneities or potentially points to another dilute groundwater source in southwestern Amargosa Desert. Although a pristine AR end member groundwater has not been sampled south of well 181, the mixing relationship demonstrated by samples 183 to 185 allows continuation of the flow pathway to the west of these samples.

Groundwater from the Gravity fault group also has a distinct Cl^- and SO_4^{2-} concentrations, although the group does show some variability (Figure A6-50). A mixing line between average Cl^- and SO_4^{2-} concentrations for the tight cluster of the GF and FMW-S group samples is shown on Figure A6-50 (Mix 3). Groundwaters from the LW and FMW-E groups define an array along, though slightly above, this mixing line. These two groups of wells also lie geographically between the two hydrochemical end-member groups. This relationship suggests that the intermediate chemical compositions of the LW and the FMW-E groups may be due to mixing of variable amounts of dilute water from the Fortymile Wash and groundwater from the GF group. Analysis of other constituents, however, suggests that an additional component may be present. As mentioned, samples of the LW and FMW-E groups plot along *but above* the mixing line between the GF samples and the FMW-S samples. In fact, these samples plot intermediate between this mixing line (Mix 3) and a mixing line (Mix 2) between the FMW-S samples and well J-11, which has Cl^- and SO_4^{2-} concentrations of 17.5 mg/L and 480 mg/L, respectively (Figures A6-32 and A6-33, Table A6-1). It is possible, given this relationship and the relative geographic position of these well groupings that some groundwater from the vicinity of well J-11 (Site 67) has mixed with these samples. On the plot of $\delta^{34}S$ and $1/SO_4^{2-}$ (Figure A6-51), the few samples from the LW group and the FMW-E group form a trend between the FMW-S samples and groundwater from well J-11. This trend is strongly suggestive of a mixing relationship between these samples. Mixing calculations using Cl^-, SO_4^{2-}, and $\delta^{34}S$ indicate that a maximum of approximately 20% J-11 well water is present in one of these samples (site 101—the Desert Farms Garlic Plot well). Sample 141 (FMW-S) contains elevated SO_4^{2-} for the measured Cl^- concentration and plots along mixing line 3. The geographic position and hydrochemistry of this sample are consistent with it containing a small percentage of J-11-like water. The data plotted in Figure A6-51 do not support the hypothesis that

groundwater from the LW and FMW-E groups contains a component of GF water, although the data set for $\delta^{34}S$ is incomplete.

Many of the GF samples are also collinear with some samples from FMW-E and LW groups (Figure A6-50). For example, samples 160, 174, and 175 plot intermediate between the tight cluster of GF samples and dilute groundwater of the FMW-S, FMW-E, and LW groups. These samples are also among the more westerly of the GF samples, located geographically between groundwater that defines the tight cluster of GF samples and the FMW-E samples. These samples are also interpreted to be mixtures of GF groundwater and more dilute water of the FMW-E group.

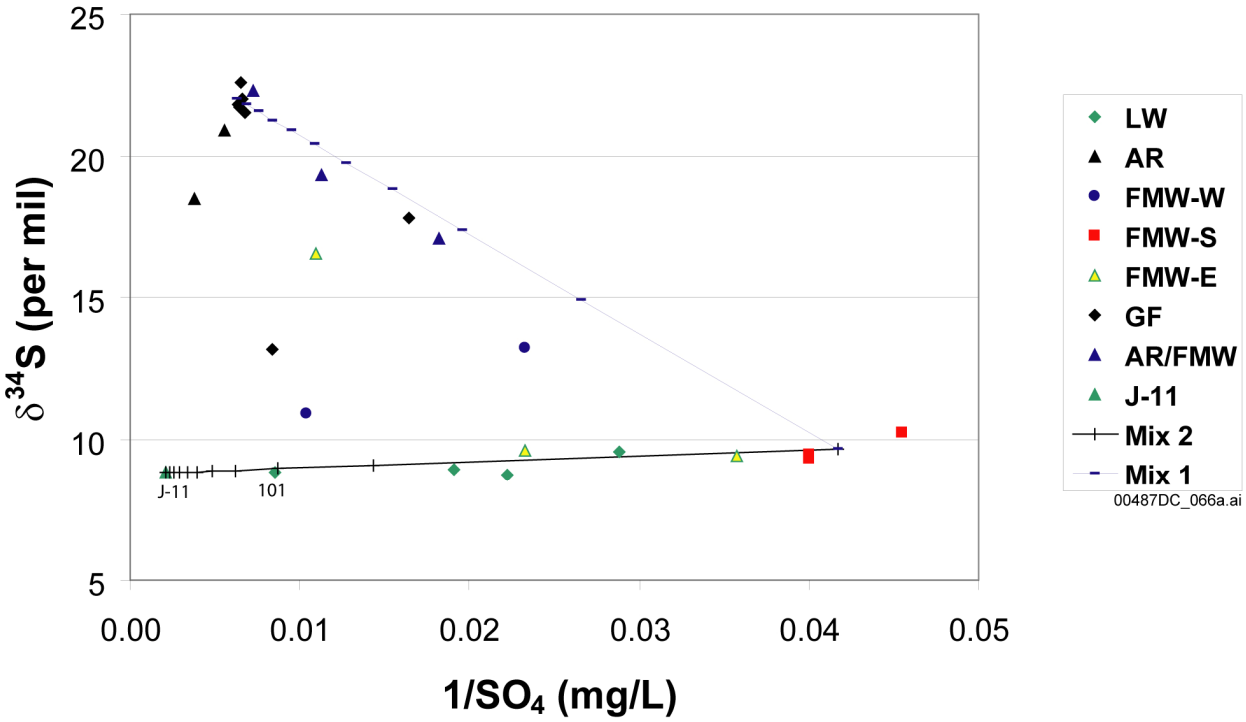

Sources: Tables A6-1 and A6-2.

NOTES: On this diagram, a mixture plots as a straight line. Mixing lines show 10% increments. End members for the mixing lines are: 24 mg/L SO_4^{2-} and 9.65 per mil $\delta^{34}S$ for the dilute end member. Mixing line 1 (Mix 1) upper end member is the visual average of the AR group samples of 160 mg/L SO_4^{2-} and 22 per mil $\delta^{34}S$. Mixing line 2 (Mix 2) upper end members corresponds to SO_4^{2-} and $\delta^{34}S$ values for J-11 of 480 mg/L and 8.8 per mil, respectively. Mixing lines are drawn by plotting calculated values for SO_4^{2-} and $\delta^{34}S$ obtained by the mixing equations: $[SO_4^{2-}]_{mix} = F \bullet [SO_4^{2-}]_A + (1 - F) \bullet [SO_4^{2-}]_B$, where F is the fraction of component A in the mix. Delta sulfur-34 is determined by: $[\delta^{34}S]_{mix} = (F \bullet [SO_4^{2-}]_A \bullet \delta^{34}S_A + (1 - F) \bullet [SO_4^{2-}]_B \bullet \delta^{34}S_B)/[SO_4^{2-}]_{mix}$.

Figure A6-51. Scatter Plot of Delta ^{34}S versus Inverse Sulfate for Samples in the Amargosa Desert Region

A6.3.8 Groundwater Mixing and Reaction Analyses Using PHREEQC

In general, the chemical and isotopic composition of groundwater results from the mixing of groundwater from various upgradient locations as well as water-rock interaction along the individual flow paths. Groundwater mixing can occur naturally as a result of hydrodynamic dispersion and can also be induced during groundwater pumping. In either case, however, groundwater mixing can result in real or apparent changes in the composition of even nonreactive chemical and isotopic species in a downgradient direction.

A number of inverse groundwater mixing and reaction analyses were performed to help identify both the upgradient groundwaters that could be present in a downgradient groundwater and the chemical reactions required to explain the downgradient changes in the composition of reactive species. The groundwaters that are considered as potential components in the downgradient groundwater are identified from relatively nonreactive species such as Cl^-, SO_4^{2-}, δD, $\delta^{18}O$, and $\delta^{34}S$. The composition of these species in the downgradient groundwater is assumed to result only from mixing of upgradient groundwaters. The remainder of the chemical and isotopic species, including other major and minor ions, dissolved SiO_2, and dissolved carbon isotopes, are considered in these models to result both from mixing and from water-rock interaction. After first determining the mixing fractions of the potential components from the nonreactive species, PHREEQC adjusts the amounts of reactive chemical and isotopic species in the mixture by finding some combination of the allowable reactions that satisfy the mass balance constraints for each chemical and isotopic species. The consideration of reactive species limits the number of potential mixing analyses to those for which plausible chemical reactions can also be found.

The potential groundwater components in the mixture were identified from contour maps of hydraulic heads (Figure A6.5-1) and areal plots and scatterplots between the aforementioned nonreactive chemical and isotopic species. For groundwaters in the volcanic or alluvial aquifers, upgradient groundwater could include recharge as well as groundwater in the carbonate aquifer, which at Yucca Mountain has a higher hydraulic head than groundwater in the volcanic aquifer.

The geographic distribution of one or more nonreactive species in a downgradient direction as shown on maps in Section A6.3.4 suggests an initial combination of groundwaters that may lie along a flow path. In some parts of the Yucca Mountain area where only slight differences in solute concentrations exist among wells, scatterplots of both nonreactive and reactive species were used to suggest possible combinations of groundwaters that may be involved in a mixture (Sections A6.3.6.3 and A6.3.7).

The chemical reactions considered in these PHREEQC (DTN: MO0309THDPHRQC.000 [DIRS 165529]) mixing and reaction analyses are restricted to those that are consistent with known ion-exchange reactions and mineral saturation indices. Generally, porewater data from Yucca Mountain (Yang et al. 1996 [DIRS 100194], 1998 [DIRS 101441]) and Rainier Mesa (White et al. 1980 [DIRS 101166]) indicate that Ca^{2+}, Mg^{2+}, and K^+ in solution are exchanged for Na^+ initially on the exchange sites of minerals. The saturation indices calculated in Section A6.3.5 indicate that Ca-clinoptilolite, Na-clinoptilolite, and smectite may precipitate from groundwater in some areas. Conversely, plagioclase, K-feldspar, calcite, fluorite, kaolinite, and amorphous silica are potentially dissolved by groundwater in certain parts of the Yucca Mountain area. Measurements of $CO_2(g)$ in the unsaturated zone at Yucca Mountain indicate a

log P_{CO_2} of about –3.0 (Yang et al. 1996 [DIRS 100194], Figure 18b). Groundwater with calculated log P_{CO_2} greater than –3.0 will therefore potentially degas into the overlying unsaturated zone when the log P_{CO_2} of the groundwater is greater than –3.0 and vice-versa.

A summary of the mineral phases considered in the PHREEQC analyses, their chemical formulas, and any constraints imposed on their precipitation or dissolution is summarized in Table A6-10. Unless otherwise noted in Table A6-12, all mineral phases were considered as potential reactants or products in each PHREEQC analyses discussed in this section.

The inverse analyses identified by PHREEQC are required to simultaneously satisfy mass-balance constraints for pH and for each element contained in the phases listed in Table A6-10. Where the inverse analyses consider groundwater mixing, the proportions of groundwater from various upgradient wells in the mixture are identified from nonreactive elements or isotopes that, by definition, are not contained in the list of reactive phases. These additional nonreactive elements and isotopes include Cl^- and, depending on the model, δD and $\delta^{18}O$. Many of the inverse models were also required to satisfy mass-balance constraints for $\delta^{13}C$, which made it necessary to specify values of ^{14}C and $\delta^{13}C$ for the C-bearing phases in these models (Table A6-10, Note 7).

The groundwater concentrations and isotopic compositions, as well as the isotopic compositions of the gas and mineral phases, are assumed by PHREEQC to be somewhat uncertain because of laboratory analytical error and because of uncertainty associated with the effects of well drilling, completion, and development on groundwater sample compositions. The specified uncertainties varied, depending on the parameter and the model. In general, the specified uncertainties were as follows: pH (0.05 pH units), ions (10% of the measured concentrations), $\delta^{13}C$ (0.1 per mil), $\delta^{18}O$ (0.1 per mil), and δD (1.0 per mil). These uncertainties determined the amount by which the measured chemical or isotopic parameters in each solution could be adjusted by PHREEQC to obtain mass balance for that parameter. In some cases, however, if no convergent analyses were identified because of a mass imbalance for a single chemical or isotopic species, the specified uncertainties for that species were increased from their typical values until a model, or set of models, could be found. For example, in one set of models, the specified uncertainty for $\delta^{13}C$ was increased to 0.5 per mil, and in another set, the uncertainty in $\delta^{18}O$ was increased to 0.4 per mil. In several sets of analyses, it was necessary to increase the uncertainty in F^- to 20% or more of the measured concentrations, effectively eliminating F^- as a chemical constraint for that set of models. For a subset of models, it was necessary to consider dissolution of kaolinite to balance Al^{3+} concentrations; generally, however, Al^{3+} concentrations could be balanced using the other alumino-silicate minerals.

Additional uncertainty associated with these analyses results from the variability in mineral compositions, nonideal chemical compositions for common rock forming minerals like K-feldspar and calcites, and the nonuniqueness of the inverse models themselves. As demonstrated in the following sections, it is often possible to find several combinations of wells and sets of water/rock interactions that can explain the chemical and isotopic composition of groundwater in the downgradient well.

Table A6-10. Mineral Phases and Exchange Reactions Considered in the PHREEQC Inverse Analyses

Phase or Exchange Cation	Formula in PHREEQC Analyses[1]	Constraint	Formula Reference
Carbon dioxide[7]	CO_2	Exsolution only	Parkhurst and Appelo 1999 [DIRS 159511], Table 55
Calcite[7]	$CaCO_3$	Dissolution or precipitation[2]	Parkhurst and Appelo 1999 [DIRS 159511], Table 55
Plagioclase	$Na_{0.8}Ca_{0.2}Al_{1.2}Si_{2.8}O_8$	Dissolution only	Vaniman et al. 1996 [DIRS 105946], Figure 1.22
K-feldspar	$KAlSi_3O_8$	Dissolution only	Parkhurst and Appelo 1999 [DIRS 159511], Table 55
Ca exchange	CaX_2	Sorption only	Parkhurst and Appelo 1999 [DIRS 159511], Table 55
Mg exchange	MgX_2	Sorption only	Parkhurst and Appelo 1999 [DIRS 159511], Table 55
Na exchange	NaX	De-sorption only	Parkhurst and Appelo 1999 [DIRS 159511], Table 55
K exchange	KX	None	Parkhurst and Appelo 1999 [DIRS 159511], Table 55
Amorphous silica	SiO_2	Dissolution only	Parkhurst and Appelo 1999 [DIRS 159511], Table 55
Kaolinite	$Al_2Si_2O_5(OH)_4$	None[3]	Parkhurst and Appelo 1999 [DIRS 159511], Table 55
Smectite	$K_{0.1}Na_{0.02}Ca_{0.14}Al_{4.4}Si_{7.6}O_{20}(OH)_4 \bullet 4H_2O$	Precipitation only	Chipera et al. 1995 [DIRS 100025], Table 1
Ca-Clinoptilolite[4]	$K_{2.5}Na_{1.1}Ca_{1.2}Al_{6.0}Si_{30.0}O_{72.0} \bullet 26.8\ H_2O$	Precipitation only	Chipera and Bish 1997 [DIRS 105079], Tables 1 to 2
Na-Clinoptilolite[4]	$K_{2.8}Na_{1.5}Ca_{0.9}Al_{6.1}Si_{29.9}O_{72.0} \bullet 26.8\ H_2O$	Precipitation only	Chipera and Bish 1997 [DIRS 105079], Tables 1 to 2
Pyrite	FeS_2	Dissolution only	Parkhurst and Appelo 1999 [DIRS 159511], Table 55
Biotite	$KMg_2FeAlSi_3O_{10}(OH)_2$	Dissolution only	Vaniman et al. 1996 [DIRS 105946], Figure 1.22
Gypsum	$CaSO_4 \bullet 2H_2O$	Dissolution only	Parkhurst and Appelo 1999 [DIRS 159511], Table 55
Oxygen	O_2	None[3]	Parkhurst and Appelo 1999 [DIRS 159511], Table 55
Ferrihydrite	$Fe(OH)_3$ (a)	Precipitation	Parkhurst and Appelo 1999 [DIRS 159511], Table 55

Table A6-10. Mineral Phases and Exchange Reactions Considered in the PHREEQC Inverse Analyses (Continued)

Phase or Exchange Cation	Formula in PHREEQC Analyses[1]	Constraint	Formula Reference
Fluorite[5]	CaF_2	Dissolution only	Parkhurst and Appelo 1999 [DIRS 159511], Table 55
Dolomite[6,7]	$CaMg(CO_3)_2$	Dissolution only	Parkhurst and Appelo 1999 [DIRS 159511], Table 55

[1] An X in a formula in this column represents the exchange site.
[2] A dissolution constraint for calcite was imposed for all inverse models except for models involving the Desert Farms Garlic Plot well, for which a precipitation constraint was imposed for calcite.
[3] Although no precipitation (or exsolution) or dissolution constraints were imposed, none of the inverse models required the precipitation of kaolinite or the exsolution of O_2. Kaolinite dissolution was considered only in models for wells NC-EWDP-3D, WT-3, and certain depth intervals of NC-EWDP-19D, for which it was necessary to balance Al^{3+} concentrations in the inverse models. Although groundwaters are assumed to be in equilibrium with kaolinite, kaolinite dissolution can be driven by the precipitation of smectite and clinoptilolite phases from the groundwater.
[4] Either Ca-clinoptilolite or Na-clinoptilolite, but not both, were considered in each inverse model. In the inverse models, the relevant clinoptilolite composition was determined by geography, with models for wells having potential upgradient sources in Crater Flat or Solitario Canyon assigned Na-clinoptilolite as a possible secondary phase and inverse models involving wells in central or eastern Yucca Mountain or near Fortymile Wash assigned Ca-clinoptilolite as a potential secondary phase. These choices were based on trends in clinoptilolite composition noted by Broxton et al. (1987 [DIRS 102004], Figure 8).
[5] Fluorite dissolution was considered only in a subset of inverse models, including those models with wells VH-1, WT-3, NC-EWDP-15P, GEXA Well 4, NC-EWDP-3D, and NC-EWDP-1S as the downgradient wells.
[6] Dolomite dissolution was considered only in a subset of inverse models where the proximity to dolomite outcrops or to alluvium derived from these outcrops had a possible influence on groundwater composition. These inverse models included those models with wells VH-1, GEXA Well 4, NC-EWDP-9S, NC-EWDP-3D, or NC-EWDP-1S as the downgradient well.
[7] The inclusion of $\delta^{13}C$ as a mass-balance constraint requires that the ^{14}C and $\delta^{13}C$ of carbon-bearing phases (CO_2, calcite, and dolomite) be defined. The ^{14}C activity of any CO_2 de-gassing from groundwater was set equal to the ^{14}C of the groundwater at the downgradient well, and the ^{14}C of the calcite and dolomite (if present) were set to 0. The $\delta^{13}C$ of CO_2 de-gassing from the groundwater was assumed to be -18 ± 2 per mil, based on measurements of the $\delta^{13}C$ of CO_2 in the unsaturated zone at Yucca Mountain (Yang et al. 1996 [DIRS 100194], Figure 19). Except for the WT-3 models for which $\delta^{13}C$ was set to -1 ± 3 per mil, the $\delta^{13}C$ of saturated-zone calcite in the volcanic and alluvial aquifers was set to -4 ± 3 per mil, and the $\delta^{13}C$ of dolomite was set to 0 ± 2 per mil, based on data for SZ calcites contained in Whelan et al. (1998 [DIRS 108865], p. 179 and Figure 2).

A6.3.8.1 Desert Farms Garlic Plot

The PHREEQC analyses investigated if groundwater at the Desert Farms Garlic Plot (DFGP) well (Site 101) could be produced by a mixture of groundwater from Fortymile Wash at borehole JF-3 (Site 37) and groundwater from Jackass Flats at well J-11 (Site 67). This PHREEQC analyses was motivated by the similar $\delta^{34}S$ and $\delta^{13}C$ ratios and low HCO_3^- at both J-11 and the DFGP well, and by the mixing relation estimated from $\delta^{34}S$ versus $1/SO_4^{2-}$, which indicated well J-11 and wells from the FMW-S area as potential mixing end members (Figures A6-50 and A6-51). The 6 analyses identified by PHREEQC are of the form:

DFGP well = X_1 JF-3 + X_2 J-11 – calcite + plagioclase + SiO_2(a) + K-feldspar – smectite – Ca-clinoptilolite + biotite + pyrite + O_2 (g) – $Fe(OH)_3$(a) – MgX_2 – KX + NaX

where the fraction of well JF-3 groundwater (X_1) is between 0.76 and 0.77 and the fraction of well J-11 groundwater (X_2) is between 0.23 and 0.24. (Note that in these PHREEQC analyses the "+" indicates the phase was taken in solution along the flow path and "–" indicates the phase left the solution along the flow path. The "X" indicates phases on exchange sites.) Subsets of the phases indicated in the preceding reaction were identified in 6 reaction analyses by PHREEQC for this group of wells. Calcite precipitation was considered as a possible reaction because the groundwater at well J-11 is saturated with calcite (Figure A6.3-34). These mixing analyses did not use $\delta^{34}S$ as a constraint, but these mixing fractions are nonetheless in good agreement with the mixing fractions for Fortymile Wash area groundwaters and well J-11 groundwater estimated using mixing trends based on $\delta^{34}S$ versus $1/SO_4^{2-}$ (Figure A6-51). However, the PHREEQC analyses could not match groundwater F^- or δD data at the DFGP well. The inability to match the δD data could reflect differences in the ages of waters actually mixed to produce the DPGP water. The J-11 water could not be directly mixed with JF-3 because these two wells are kilometers apart. Instead, a water similar to J-11 could have been mixed with a water similar to JF-3 to produce the DFGP water. The actual waters mixed could have been different from J-11 or JF-3 in age. The inability to match the F^- data may reflect analytical errors in the F^- analyses or water/rock interactions not specified in the PHREEQC calculations (e.g., dissolution of fluorite (CaF_2)).

A6.3.8.2 Well 16S/49E-05acc

The PHREEQC analyses investigated whether groundwater at the northernmost well in the FMW-S group (well 16S/49E-05acc) (Site 127) could be produced from groundwater in the southern part of the FMW-N group at well J-12 (Site 37). Groundwater from the JF well J-11 (Site 67) was also included as a potential mixing member. The inclusion of well J-11 as a potential mixing member was motivated by the higher SO_4^{2-} of groundwater in the FMW-S group compared to the FMW-N group and the very high SO_4^{2-} at well J-11 (Figure A6-33). However, no PHREEQC analyses were identified that included well J-11 groundwater at well 16S/49E-05acc. The 3 PHREEQC analyses for well 16S/49E-05acc were of the form:

16S/49E-05acc = J-12 + calcite + plagioclase + K-feldspar + gypsum – Ca-clinoptilolite + biotite + pyrite + O_2 (g) – $Fe(OH)_3$(a)

Subsets of the phases indicated in the preceding reaction were identified in 3 reaction analyses by PHREEQC for this pair of wells. The PHREEQC analyses were able to match the $\delta^{13}C$ at well 16S/49E-05acc but not the $\delta^{18}O$ and δD values. The δD between the FMW-N and FMW-S groups is significantly different (Figure A6-41). The cause of this difference is probably climate change, which has resulted in the upgradient groundwater in the FMW-N group being of more recent origin compared to the downgradient groundwater in the FMW-S group (Figure A6-41). The groundwater in the FMW-S group is older and contains a greater percentage of cooler Pleistocene recharge, which in turn, has lighter δD.

A6.3.8.3 GEXA Well 4

The groundwater at GEXA well 4 (Site 68) was modeled as a mixture of the groundwater in lower Beatty Wash at well ER-OV-03c (Site 23) and local recharge from surface runoff. Recharge from surface runoff is likely because GEXA well 4 is located in a major drainage in

northwest Crater Flat (Figure A6-4). Because the chemical and isotopic characteristics of local recharge from surface runoff have not been measured in this area, the chemical and isotopic characteristics of the local recharge represented by groundwater from 29a#2 (Site 31) in Fortymile Canyon was used. The 9 models identified by PHREEQC were of the form:

GEXA Well 4 $= X_1$ ER-OV-03c + X_2 recharge from runoff + calcite + dolomite + plagioclase + SiO_2(a) + K-feldspar – smectite – Na-clinoptilolite + pyrite + O_2 (g) – $Fe(OH)_3$(a) – CaX_2 – MgX_2 – KX + NaX

where the fraction of well ER-OV-03c groundwater (X_1) ranged from about 0.68 to 0.79 and the fraction of recharge from surface runoff (X_2) ranged from about 0.21 to 0.32. Subsets of the phases indicated in the preceding reaction were identified in 9 reaction analyses by PHREEQC for the group of wells. Dolomite was considered a potentially reactive phase due to the presence of Paleozoic dolomites at Bare Mountain. The PHREEQC analyses successfully matched the $\delta^{18}O$ and δD of groundwater at GEXA well 4 in addition to the ion composition.

A6.3.8.4 Borehole VH-1

The groundwater at borehole VH-1 (site 69) was modeled as a potential mixture of groundwater from GEXA Well 4 (Site 68) and groundwater from Beatty Wash at well ER-OV-03c (Site 23), Coffer Ranch Windmill Well (CRWW) (Site 22), and ER-EC-07 (Site 24). These wells were chosen as potential mixing components because they are all upgradient from borehole VH-1. Furthermore, these upgradient wells spanned a considerable range in Cl^-, SO_4^{2-}, $\delta^{18}O$, and δD (Section A6.3.4), which collectively bounded the values in groundwater at borehole VH-1. The 6 analyses identified by PHREEQC were of the form:

VH-1 = X_1 ER-OV-03c + X_2 CRWW + X_3 ER-OV-07 + X_4 GEXA well 4 + dolomite + plagioclase + SiO_2(a) + K-feldspar – smectite – Na-clinoptilolite + pyrite + O_2(g) – $Fe(OH)_3$(a) – CaX_2 – KX + NaX

where X_1 is the fraction of groundwater from well ER-OV-03c, X_2 is the fraction of groundwater from the CRWW, X_3 is the fraction of groundwater from well ER-OV-07, and X_4 is the fraction of groundwater from GEXA well 4. Subsets of the phases indicated in the preceding reaction were identified in 6 reaction analyses by PHREEQC for this set of wells. Four of the six analyses were two component-mixing models involving roughly equal amounts of ER-OV-03c and CRWW groundwater. Of the two remaining analyses, one model was a three-component mixing model involving roughly equal amounts of ER-OV-03c (X_1 = 0.34), CRWW (X_2 = 0.29), and GEXA well 4 (X_4 = 0.37) groundwater, and one model involved about 10% of groundwater from ER-EC-07 with subequal amounts of ER-OV-03c (X_1 = 0.39) and CRWW (X_2 = 0.53) groundwater. The models collectively indicate that most of the groundwater originates from lower Beatty Wash, with at most, a small component from upper Beatty Wash at well ER-EC-07. In light of the PHREEQC analyses for GEXA well 4 groundwater that indicate a component of local recharge from surface runoff, the groundwater at well VH-1 may also include a small component of local recharge from surface runoff in the northwest corner of Crater Flat. In addition to explaining the ion composition of groundwater at VH-1, the PHREEQC analyses accurately replicate the $\delta^{18}O$ and δD of groundwater at VH-1. However, attempts to

simultaneously model the relatively light $\delta^{13}C$ (–8.5 per mil) of groundwater at borehole VH-1 were unsuccessful.

A6.3.8.5 Well NC-EWDP-1S (Composite)

Groundwater at well NC-EWDP-1S (composite) (Site 77) was evaluated as a potential mixture of groundwater at upgradient wells VH-1 (Site 69) and VH-2 (Site 70). These components were suggested by the hydraulic gradient and fault orientations (Figure A6.5-1) and by the fact that many chemical and isotopic species in groundwater at well NC-EWDP-1S (composite) are very similar in composition to the groundwater at borehole VH-2 (Section A6.3.4). The 9 models identified by PHREEQC were of the form:

NC-EWDP-1S (composite) = X_1 VH-1 + X_2 VH-2 + dolomite – calcite + Plagioclase + SiO_2(a) + K-feldspar – Na-clinoptilolite – smectite – KX + NaX

where the fraction of well VH-1 groundwater (X_1) ranged from about 0.14 to 0.16 and the fraction of groundwater from well VH-2 (X_2) ranged from about 0.84 to 0.86. Subsets of the phases indicated in the preceding reaction were identified in the 9 reaction models by PHREEQC for group of wells. Note that in southwestern Crater Flat, the groundwater is saturated with calcite (Figure A6.3-34), so that calcite precipitation rather than dissolution is likely. In addition to reproducing the ion compositions, the PHREEQC analyses were also able to reproduce the $\delta^{18}O$ and δD compositions of groundwater at NC-EWDP-1S (composite) with a high degree of accuracy. These models indicate that groundwater at NC-EWDP-1S (composite) originates dominantly from groundwater at well VH-2.

A6.3.8.6 Well NC-EWDP-9SX (Composite)

Groundwater at well NC-EWDP-9SX (composite) (Site 81) was evaluated as a potential mixture of groundwater at upgradient wells VH-1 (Site 69) and VH-2 (Site 70). These components were suggested by the hydraulic gradient and fault orientations (Figure A6.5-1) and by the fact that many chemical and isotopic species in groundwater at well NC-EWDP-9SX (composite) are intermediate in composition between the groundwaters at boreholes VH-1 and VH-2 (Section A6.3.7.1). The 3 models identified by PHREEQC were of the form:

NC-EWDP-9SX (composite) = X_1 VH-1 + X_2 VH-2 + plagioclase + SiO_2(a) + K-feldspar – Na-clinoptilolite – smectite – CaX_2 – KX + NaX

where the fraction of well VH-1 groundwater (X_1) ranged from about 0.78 to 0.79 and the fraction of groundwater from well VH-2 (X_2) ranged from about 0.21 and 0.22. Subsets of the phases indicated in the preceding reaction were identified in the 3 reaction models identified by PHREEQC for this group of wells. In addition to reproducing the ion compositions, the PHREEQC analyses were also able to reproduce the $\delta^{18}O$ and δD compositions of groundwater at NC-EWDP-9SX (composite) with a high degree of accuracy. These models are consistent with the interpretation that groundwater at NC-EWDP-9S originates dominantly from groundwater at well VH-1.

A6.3.8.7 Well NC-EWDP-3D (Composite)

Groundwater at well NC-EWDP-3D (composite) (Site 86) was evaluated as a potential mixture of groundwater at upgradient wells VH-1 (Site 69) and WT-10 (Site 42). These components were suggested by the hydraulic gradient and fault orientations (Figure A6.5-1) and by the fact that many chemical and isotopic species in groundwater at well NC-EWDP-3D (composite) are intermediate in composition between the groundwaters at boreholes VH-1 and WT-10 (Section A6.3.4). The 1 model identified by PHREEQC was of the form:

NC-EWDP-3D (composite) = X_1 VH-1 + X_2 WT-10 + calcite + plagioclase + SiO_2(a) + K-feldspar + kaolinite – Na-clinoptilolite – MgX_2 + NaX

with the fraction of well VH-1 groundwater (X_1) equal to 0.80 and the fraction of groundwater from well WT-10 (X_2) equal to 0.20. In addition to reproducing the ion compositions, the PHREEQC models were also able to reproduce the $\delta^{18}O$, δD, and $\delta^{13}C$ compositions of groundwater at NC-EWDP-3D (composite) with a high degree of accuracy. These models indicate that groundwater at NC-EWDP-3D originates dominantly from groundwater at well VH-1.

A6.3.8.8 Well NC-EWDP-15P

The groundwater at well NC-EWDP-15P (Site 90) was modeled as a potential mixture of groundwaters from upgradient wells VH-1 (Site 69) and WT-10 (Site 42). The carbonate-aquifer-like groundwater from borehole VH-2 (Site 70) was also considered as a potential component based on head gradients in southern Crater Flat and Yucca Mountain and on mixing trends that suggested a carbonate-aquifer component in the groundwater in this area (see Section A6.3.7.1). The 2 PHREEQC analyses found for well NC-EWDP-15P took the form:

NC-EWDP-15P = X_1 WT-10 + X_2 VH-2 + X_3 VH-1 + SiO_2(a) + K-feldspar +gypsum – Na-clinoptilolite – smectite

where the fraction of well WT-10 groundwater (X_1) was approximately 0.45 to 0.49, the fraction of carbonate aquifer groundwater from borehole VH-2 (X_2) was 0.05 to 0.06, and the fraction of groundwater from well VH-1 (X_3) was about 0.45 to 0.49. The 2 PHREEQC analyses were able to successfully match the $\delta^{18}O$ and δD at well NC-EWDP-15P with a high degree of accuracy. The $\delta^{13}C$ of groundwater at NC-EWDP-15P was not estimated by the inverse models because no groundwater $\delta^{13}C$ data were available from borehole VH-2. The PHREEQC analyses support the hypothesis that groundwater flows from eastern Crater Flat through wells in southern Yucca Mountain.

A6.3.8.9 Borehole WT-3

The PHREEQC models investigated whether groundwater at borehole WT-3 (Site 65) could have evolved from groundwater in northern Yucca Mountain at borehole WT-24 (Site 44). This possible flow path was suggested by fault orientations and the hydraulic gradient in the northern Yucca Mountain area, the high $^{234}U/^{238}U$ activity ratio at both boreholes, and the fact that groundwater at borehole WT-24 is the only location upgradient from borehole WT-3 with a

higher ^{14}C activity. The reaction models for these wells assumed that calcite dissolved along the flow path had a $\delta^{13}C$ of –1.0 ± 3 per mil because this is a common value measured in saturated zone calcite (Whelan et al. 1998 [DIRS 108865], Figure 3). The reactions identified by PHREEQC for this flow path were of the general form:

WT-3 = WT-24 + calcite + fluorite + SiO_2(a) + K-feldspar + kaolinite – smectite – Ca-clinoptilolite + biotite + O_2(g) – $Fe(OH)_3$(a) – CaX_2 – MgX_2

Subsets of the phases indicated in the preceding reaction were identified in 6 reaction models identified by PHREEQC for this pair of wells. The results of the reaction models confirm this as a plausible flow path.

A6.3.8.10 Well NC-EWDP-19D and -19P

Groundwater at well NC-EWDP-19D (Sites 92 and 94 to 98) was sampled from several different zones in alluvium as well as from longer intervals spanning the depth of the alluvium or the entire well. The chemistry and isotopic compositions of these zones exhibited substantial differences in both chemical and isotopic compositions (see Section A6.3.3). Although cation, bicarbonate, and isotope compositions varied substantially among different zones, the groundwater Cl^- and SO_4^{2-} compositions within almost all zones are uniformly low. The similarity of groundwater Cl^- and SO_4^{2-} compositions in well NC-EWDP-19D and upgradient well WT-3 (Site 65) suggests a flow path between these two wells, in spite of the differences in other chemical and isotopic species. Groundwater at well WT-3 is also the only upgradient groundwater with ^{14}C activity high enough to explain the high ^{14}C activities of some zones in well NC-EWDP-19D. One group of models for well NC-EWDP-19D therefore attempts to explain the compositional difference between wells WT-3 and various zones within well NC-EWDP-19D as the result of water rock interactions along the flow path between the wells. The same set of reactions are applied to varying extents to explain the differences in compositions between various depth intervals in well NC-EWDP-19D:

NC-EWDP-19D (various zones) = WT-3 + calcite + SiO_2(a) + K-feldspar + kaolinite + plagioclase + gypsum – smectite – Ca-clinoptilolite + biotite + pyrite + O_2 (g) – $Fe(OH)_3$(a) – CaX_2 – MgX_2 ± KX + NaX

Scatter plots (Figures A6-42 to A6-46) show that some groundwaters in the SCW group are similar to groundwater at well NC-EWDP-19D. Although slightly higher in Cl^- and SO_4^{2-}, groundwater in the SCW group is similar to groundwater at well NC-EWDP-19D with respect to cation compositions, DIC, and $\delta^{13}C$. However, the groundwater ^{14}C activities in the SCW area are far too low for this groundwater to be the source of groundwater at NC-EWDP-19D unless the SCW groundwater mixes with younger groundwater along its flow path. This younger water is assumed to be local recharge from Yucca Mountain itself, as represented by perched water from borehole SD-7. Some component of local recharge in southern Yucca Mountain is consistent with the hypothesis that much of the groundwater at Yucca Mountain is derived from local recharge (Section A6.3.6). The local recharge represented by perched water from SD-7

also has lower Cl^- and SO_4^{2-} concentrations than the well NC-EWDP-19D, making it a suitable mixing end member. This group of models can be represented as:

NC-EWDP-19D (various zones) = X_1 WT-10 + X_2 local recharge (SD-7 perched water) + calcite + SiO_2(a) + K-feldspar + kaolinite + plagioclase + gypsum – smectite – Ca-clinoptilolite + biotite + pyrite + O_2(g) – $Fe(OH)_3$(a) – CaX_2 – MgX_2 ± KX + NaX

where X_1 is the fraction of groundwater from SCW well WT-10 (Site 42), X_2 is the fraction of local recharge (as represented by perched water from borehole SD-7). Similar chemical processes but different sources are invoked in the two sets of PHREEQC models to explain the composition of groundwater within different zones in well NC-EWDP-19D. Both sets of models are able to explain the chemical compositions and $\delta^{13}C$ values of groundwater in various zones at well NC-EWDP-19D, but neither set of models adequately explains the extremely light $\delta^{18}O$ and δD compositions in some of these zones.

The PHREEQC analyses for groundwater at well NC-EWDP-19P (Site 93) use the same set of reactions as for -19D but consider groundwater flow from well WT-3 and well JF-3 in the FMW-N group as possible sources of groundwater at well NC-EWDP-19P. The PHREEQC analyses results indicate that 80% to 100% of the shallow groundwater in well NC-EWDP-19P originates from the area of well JF-3.

A6.3.9 Evaluation of Groundwater Velocities in the Yucca Mountain Region

In this section, groundwater velocities are estimated along various flow-path segments using the ^{14}C activities of the groundwater along the flow path. The measured ^{14}C activities at the upgradient well defining the segment are adjusted to account for decreases in the ^{14}C activity that result from water-rock interactions the groundwater undergoes between wells, as identified by the PHREEQC mixing and chemical reaction models described in Section A6.3.8. This adjustment to the initial ^{14}C activity at the upgradient well is necessary to distinguish between the decrease in ^{14}C activity caused by water-rock interaction and the decrease in ^{14}C activity due to transit time between the wells. After determining the transit time between wells, linear groundwater velocities are determined by dividing the distance between the wells by the transit time.

The transit time between wells is calculated from the radioactive decay equation for ^{14}C (Section A6.3.1.2.2). A variety of methods have been used to estimate the value of $^{14}A_0$ to use with the radioactive decay law (Clark and Fritz 1997 [DIRS 105738], Chapter 8). One simple method that can be used to correct for the effects of calcite (or dolomite) dissolution in the case where the downgradient groundwater evolves from a single upgradient source is to compare the total DIC in the upgradient well (DIC_u) with the DIC of the downgradient groundwater (DIC_d) (Clark and Fritz 1997 [DIRS 105738], p. 209):

$$q_{DIC} = \frac{DIC_u}{DIC_d} \qquad \text{(Eq. 6-10)}$$

where q_{DIC} represents the fraction of the DIC in the downgradient that originated from the upgradient well, with the remainder acquired from water-rock-gas interactions. Therefore, the

initial value of $^{14}A_0$ is the product of q_{DIC} and the measured ^{14}C activity at the upgradient well ($^{14}A_u$):

$$^{14}A_0 = {}^{14}A_u \bullet q_{DIC} \quad \text{(Eq. 6-11)}$$

Several assumptions are made to simplify this calculation. The method assumes that after infiltration reaches the SZ and becomes recharge, the water is effectively isolated from further interaction with carbon dioxide gas in the unsaturated zone, so that any downgradient increases in the DIC of the groundwater are a result of interactions with carbon-bearing minerals. These minerals are assumed to be depleted in ^{14}C, which is probably the case because most SZ calcite was formed either during a 10-million-year-old hydrothermal event or under unsaturated conditions at a time when the water table was lower than today (Whelan et al. 1998 [DIRS 108865], p. 180). Thus, although the proportions of dissolved carbon-dioxide gas, bicarbonate, and carbonate may change with pH as the groundwater interacts with the rock, the total DIC is fixed unless the groundwater reacts with calcite. This method would not account for any interactions between groundwater and calcite once the groundwater had become saturated with calcite (Table A5-1, Assumption 8), nor would it account for the effects of groundwater mixing. This method was applied to obtain a preliminary estimate for the case that the upgradient groundwater was undersaturated with calcite and mixing was not considered an important process based on the PHREEQC inverse analyses.

Additional simplifying assumptions in evaluating transport times based on ^{14}C ages along flow paths include: groundwater flows along the straight-line distance between wells. This is a necessary, though likely inaccurate, assumption since the quantitative data for a particular nonlinear travel path are lacking. Using the straight-line distance yields the highest flow velocity. Also, the effects of matrix diffusion are not accounted for, though they are likely. Matrix diffusion may add older DIC to the groundwater. Corrections to account for this older component would also increase the calculated flow velocity.

For flow path segments in which PHREEQC inverse analyses indicate the downgradient groundwater evolves from a single upgradient well, the value of $^{14}A_U$ is simply groundwater ^{14}A at the upgradient well and the expression for q_{DIC} is computed as follows:

$$q_{DIC} = (DIC_u)/(DIC_u + DIC_{carbonate}) \quad \text{(Eq. 6-12)}$$

where DIC_u is the DIC at the upgradient well and $DIC_{carbonate}$ is the amount of carbon contributed by water-rock interactions involving carbonate rocks. The denominator in Equation 12 was expressed as $DIC_u + DIC_{carbonate}$ rather than simply as the measured value of DIC_d to allow for the possibility that the measured DIC concentrations were affected by $CO_2(g)$ de-gassing either during flow or during sampling.

For flow path segments for which the PHREEQC inverse analyses identified mixing as an important control on the downgradient groundwater chemistry, the values of $^{14}A_u$ and q_{DIC} were calculated as follows:

$$^{14}Au = (f_1\ {}^{14}A_1\ DIC_1 + f_2\ {}^{14}A_2\ DIC_2 + \ldots + f_i\ {}^{14}A_i\ DIC_i)/(f_1\ DIC_1 + f_2\ DIC_2 + \ldots + f_i\ DIC_i)$$

(Eq. 6-13)

and

$$q_{DIC} = (f_1\, DIC_1 + f_2\, DIC_2 + \ldots + f_i\, DIC_i)/(f_1\, DIC_1 + f_2\, DIC_2 + \ldots + f_i\, DIC_i + DIC_{carbonate})$$

(Eq. 6-14)

where f_i is the fraction of upgradient component i in the mixture. The equations do not consider the effects of CO_2 degassing or dissolution, or calcite precipitation on ^{14}C activity. This omission is an acceptable simplification because the fractionation factor for ^{14}C is small (Clark and Fritz 1997 [DIRS 105738], inside front cover), and the ^{14}C in the CO_2 or calcite exiting the groundwater should leave the ^{14}C in the groundwater relatively unchanged. Gas dissolution by the groundwater should not occur in most instances because the log P_{CO_2} of the groundwater is higher than that of the overlying unsaturated zone (see Section A6.3.8).

It is important to recognize that the hydrogeologic environment at Yucca Mountain represents a departure from the ideal circumstances under which ^{14}C activities can be reliably used to calculate groundwater velocities. Ideally, the ^{14}C method should be used where recharge is added at a known location and moves through a confined aquifer, isolated from the effects of groundwater mixing or downgradient additions of recharge. The degree of confinement of the aquifers at Yucca Mountain is not known, and mixing and downgradient additions of recharge are possible that could cause conditions to depart from the ideal circumstances. The PHREEQC analyses that have identified groundwater mixing as a process affecting groundwater compositions can, in theory, help to calculate the effects of groundwater mixing on ^{14}C activities, as described in Equations 6-13 and 6-14. However, in the Yucca Mountain area, the calculation of groundwater velocities based on ^{14}C activities is made more complicated by the possible presence of multiple, distributed recharge areas. If relatively young recharge were added along a flow path, the ^{14}C activity of the mixed groundwater would be higher, and the calculated transit times shorter, than for the premixed groundwater without the downgradient recharge. Unfortunately, the chemical and isotopic characteristics of the recharge from various areas at Yucca Mountain may not be sufficiently distinct to identify separate sources of local recharge in the groundwater.

Despite these nonideal conditions, groundwater velocities were calculated for several possible flow paths south of the repository in the Yucca Mountain area. The results of the calculations are described in the following subsections. These results should be viewed in light of the reservations noted above.

A6.3.9.1 Flow-Path Segment from Well WT-3 to Well NC-EWDP-19D

The PHREEQC inverse analyses (Section A6.3.8) indicate that groundwater sampled from various zones in well NC-EWDP-19D (Sites 92 and 94 to 98) could have evolved from groundwater at well WT-3 (Site 65). Table A6-11 shows the transit times calculated by using the DIC of groundwater at well WT-3 and PHREEQC estimates of the carbon dissolved by this groundwater as it moves toward various zones at well NC-EWDP-19D (Equation 6-12). The third column of Table A6-11 refers to the transit time estimate made from the measured DIC at well WT-3 and that particular zone in well NC-EWDP-19D. The differences between the transit times based on the PHREEQC analyses results (Table A6-11, Column 2) and the transit times based on the measured differences in DIC concentrations (Table A6-11, Column 3) arise from

the fact that the PHREEQC analyses allow the DIC concentrations at each of the 2 wells to vary within 10% of their measured values, resulting in slightly different estimates of the amount of calcite dissolution along this flow path. These small differences in the estimates of calcite dissolution can cause transit times to vary from positive to negative and vice versa when the differences in ^{14}C activity between the upgradient and downgradient wells are small, as in the models involving zones 1 and 2 of NC-EWDP-19D (sites 95 and 96).

As Table A6-11 indicates, groundwater in the composite well and alluvial groundwaters require approximately 1,000 years to travel the approximately 15-km distance between wells WT-3 and NC-EWDP-19D. This transport time equates to linear groundwater velocities of approximately 15-m/yr. The groundwater in the deeper alluvial zones (Zones 3 and 4) requires approximately 1,500 to 3,000 years and, thus, travels at a linear groundwater velocity of 5 to 10-m/yr. In contrast, the transit times calculated for groundwater from shallow Zones 1 and 2 have transit times that range from 0 to about 350 years. Many of the calculated groundwater transit times were negative, indicating that the differences between ^{14}C activities in groundwater at well WT-3 and these zones in well NC-EWDP-19D were too small, and the uncertainty in DIC reactions estimated by PHREEQC too large, to adequately resolve the transit times. Using the upper transit time of 188 years, groundwater flow from well WT-3 to Zone 2 in well NC-EWDP-19D is about 80-m/yr. Likewise, using the upper transit time of 535 years, groundwater flow from WT-3 to zone 1 of NC-EWDP-19D is about 28 m/yr. These relatively high velocities may indicate that some of the shallow groundwater at well WT-3 moves along major faults like the Paintbrush Canyon fault, the effects of regionally convergent groundwater flow indicated by the hydraulic gradient (Figure A6.5-1), or they may simply reflect uncertainty in some assumptions implicit in this method, as discussed above in Section A6.3.9.

Table A6-11. Calculated Groundwater Transit Times (in years) Between Well WT-3 and Various Depth Zones in Well NC-EWDP-19D

Zone in NC-EWDP-19D	Mean transit time based on PHREEQC analyses (years)[a]	Transit time based on $q_{DIC} = DIC_U/DIC_D$ (years)
1	535 ± 1	-926[b]
2	–115 ± 112[b]	188
3	3110[c]	1601
4	1684 ± 2	1681
alluvial zone	1065 ± 2	1063
Composite (combined alluvial and volcanic zones)	870 ± 2	866

Sources: DTNs: LA0310EK831232.001 [DIRS 165995] (inverse analyses); LA0310EK831231.001 [DIRS 171889] (calculated travel times); Table A6-2 (^{14}C data); Table A6-3 (DIC concentrations).

[a] Uncertainties are 1 standard deviation of the times estimated using the model results.
[b] Negative transit times were calculated because of small differences in the ^{14}C activities of the upgradient and downgradient wells and uncertainty in the DIC concentrations and PHREEQC reaction analyses.
[c] No standard deviation was calculated because only 1 model for this zone was identified.

A6.3.9.2 Flow Path Segment from Well WT-24 to Well WT-3

The transit times calculated by using the DIC of groundwater at well WT-24 (Site 44) and PHREEQC estimates of the carbon dissolved by this groundwater as it moves toward well WT-3 (site 65) averaged -499 ± 147 years. The transit time estimate based on the measured differences in DIC of groundwater at wells WT-24 and WT-3 is 216 years. The differences in the estimates arise from the fact that the PHREEQC analyses allow an uncertainty of 10% in the DIC concentrations at each of the wells, which allows a slightly larger amount of calcite to be dissolved in the models (33 to 39 mg/L in the PHREEQC analyses versus 23 mg/L based on the measured DIC values). Using the estimate of transit time based on the measured DIC values and a linear distance between wells WT-24 and WT-3 of 10-km results in a linear groundwater velocity of 46-m/yr.

A6.3.10 Groundwater Flow Patterns Simulated with the Saturated Zone Flow Model

The saturated zone site-scale flow model (DTN: LA0304TM831231.002 [DIRS 163788]), or simply, the SZ flow model, was used to simulate the movement of a conservative tracer through various features in the model. The location of these hydrogeologic features and their numerical designations in the model are described and shown in *Saturated Zone Site-Scale Flow Model* (BSC 2004 [DIRS 170037], Figure 6-5 and Table 6-17), *Hydrogeologic Framework Model for the Saturated Zone Site Scale Flow and Transport Model* (BSC 2004 [DIRS 170008], Figure 6-3), and the journal article by Zyvoloski et al. (2003 [DIRS 163341], Figure 2b). The goal of these simulations was to provide an understanding of where groundwater at any location in the flow system may have originated and to what extent groundwaters originating from various locations may mix. These simulation results are then qualitatively evaluated in the context of the understanding gained from the analysis of the hydrochemical and isotopic data discussed in the previous sections.

The simulations performed with FEHM used the advection-dispersion (trac) macro embedded in that code to simulate the steady-state distribution of a tracer originating from most boundary segments and from Yucca Mountain and Fortymile Wash recharge. In each simulation, an assigned longitudinal dispersivity of 10 m and a transverse dispersivity of 1 m were used. Small dispersivities were assumed to better observe the effects of heterogeneities on groundwater mixing and dilution. Nonetheless, as in most simulations that use the advection-dispersion equation, some numerical dispersion due to the mesh discretization may also have affected the tracer simulation results. For this reason, the simulation results are not analyzed quantitatively, and comparisons to the geochemical data are qualitative in nature.

The flow-system behavior illustrated by these simulations is partly the result of the distributions of aquifers and confining units in the model (Figure A6-52). Where an aquifer exists along the boundary of the model, relatively large amounts of water enter the model along that boundary segment and the tracer originating from that segment dominates the character of the downgradient groundwater for a considerable distance. Conversely, where confining units are present along the boundary, groundwater inflow is small, and the tracer originating from that segment is readily diluted by the relatively larger amounts of untraced groundwater entering the model along the neighboring boundary segments.

Two simulations were done for each boundary segment considered. The first simulation for each segment examined the steady-state distribution of inflow along the pre-Tertiary rocks contained within that boundary segment. These pre-Tertiary rocks include the granitic rocks, the Lower Clastic Confining Unit, the Lower Carbonate Aquifer, the Upper Clastic Confining unit, the Lower Carbonate Aquifer Thrust, and the Upper Carbonate Aquifer Thrust. The Tertiary rocks (and sediment) include the remainder of the model units shown on Figure A6-52. The Prow Pass tuff, the Bullfrog tuff, and the Tram tuff, although not explicitly identified as aquifers in Figure A6-52, comprise the Lower Volcanic Aquifer of Luckey et al. (1996 [DIRS 100465], Figure 7).

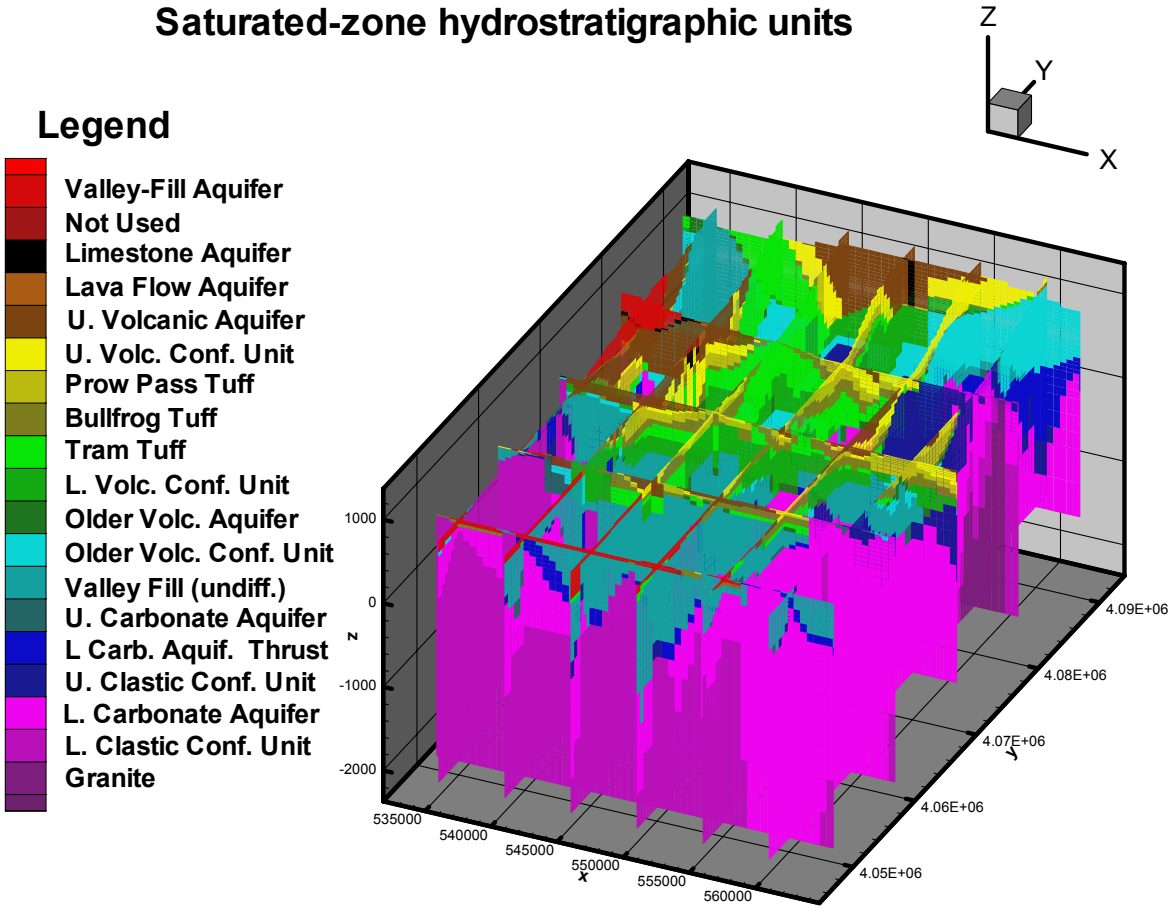

Sources: DTNs: LA0304TM831231.002 [DIRS 163788]; LA0309EK831231.001 [DIRS 171887].

NOTES: The X and Y coordinates are Universal Trans-Mercator Projection (UTM) coordinates in meters. The Z coordinate is elevation relative to sea level in meters. X = UTM-Easting and Y = UTM-Northing.

Figure A6-52. Geologic Units Defined in the Saturated Zone Flow Model

The first simulation result presented here shows the steady-state distribution of Yucca Mountain recharge in the model (Figure A6-53). Also shown in the figure are the locations of the boreholes that provided head data used in the calibration of the SZ flow model. Some key boreholes that figured prominently in the earlier discussions of the hydrochemistry are labeled in this and subsequent figures. The boreholes extend from ground surface (not shown) through the water table, which in this case, coincides with the top of the model. The plotted length of each borehole in these figures, from ground surface to the top of the model (the water table), thus approximates the thickness of the unsaturated zone at that location.

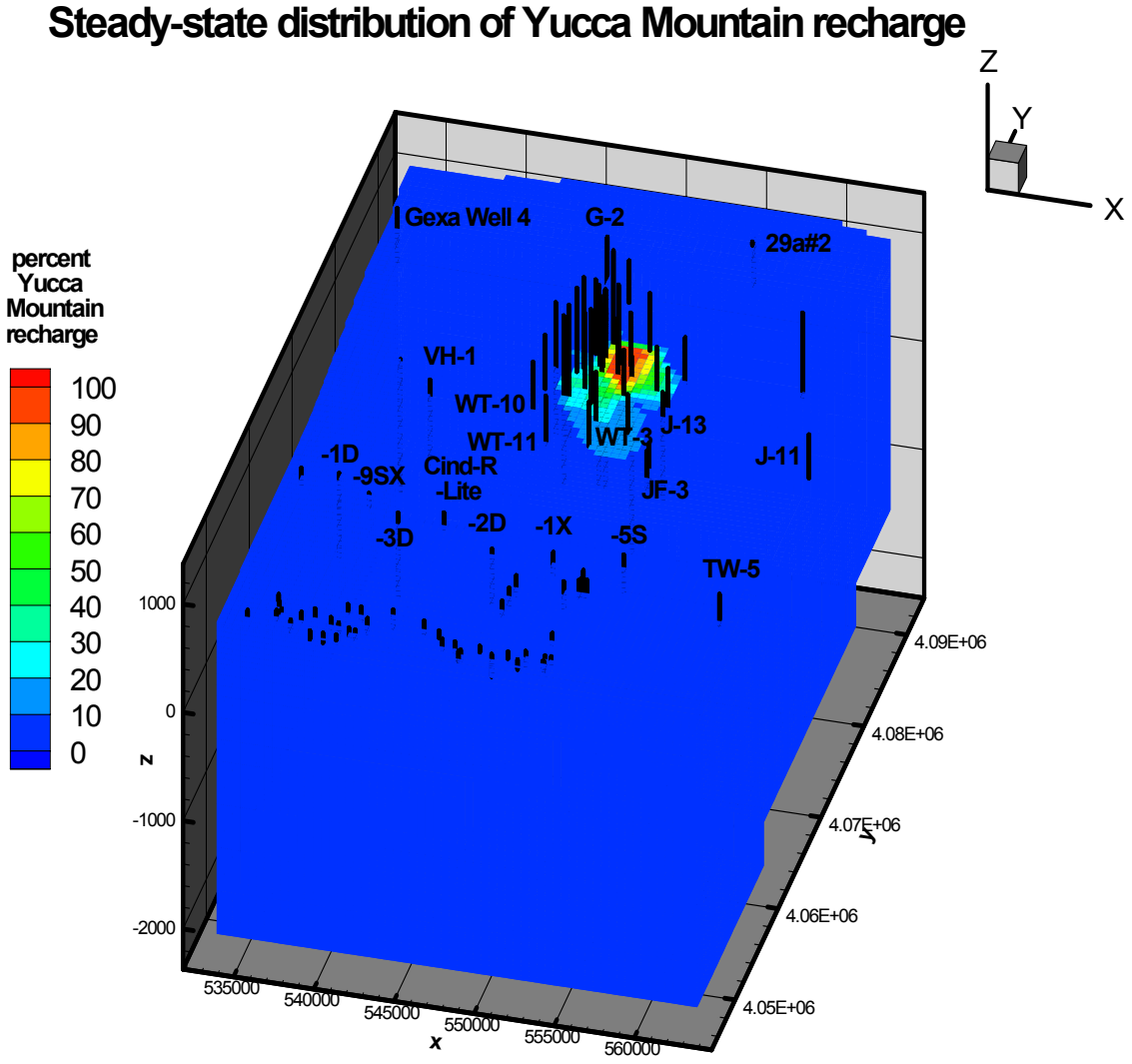

Sources: DTNs: LA0304TM831231.002 [DIRS 163788]; LA0309EK831231.001 [DIRS 171887].

NOTES: The X and Y coordinates are Universal Trans-Mercator Projection (UTM) coordinates in meters. The Z coordinate is elevation relative to sea level in meters. X = UTM-Easting and Y = UTM-Northing.

Figure A6-53. Steady-State Distribution of the Percentage of Yucca Mountain Recharge in Downgradient Groundwater Calculated Using the Saturated Zone Flow Model

The longest boreholes are located along Yucca Crest where the unsaturated zone thickness can reach 750 m.

The Yucca Mountain recharge entering the model was tagged with a concentration of 100 units, whereas all other water entering the model was given a tracer concentration of 0 units. The percentage of Yucca Mountain recharge at any location in the model is therefore equivalent to the tracer concentration at that location. The simulation results indicate that Yucca Mountain recharge is substantially diluted by groundwater flowing from adjacent parts of the flow system by the time it passes the Dune Wash area near well WT-3 (Site 65). The percentage of Yucca Mountain recharge in the groundwater is less than 10% near well NC-EWDP-2D (Site 91) along U.S. Highway 95. The downgradient decrease in tracer concentrations associated with Yucca Mountain recharge cannot be explained by spreading of the plume due to numerical dispersion because, in this case, the plume tends to become narrower and more focused in the downgradient direction. A more likely explanation is that as Yucca Mountain recharge moves downgradient, it is mixed and diluted by groundwater moving from more active parts of the flow system. These results are consistent with observed hydrochemical patterns and help to explain the difficulty in identifying Yucca Mountain recharge in groundwater near and south of U.S. Highway 95.

The flow entering along the northern boundary of the model (zone 61) in northwest Crater Flat is shown in Figures A6-54 to A6-56. The flow through the pre-Tertiary rocks is predicted to emerge into the shallow part of the flow system in several points of the model, including the central part of Crater Flat near borehole VH-1 (Site 69) and the southern part of Crater Flat near well NC-EWDP-3D (Site 86) and the NC-EWDP-15P well (Site 90). The groundwater at borehole VH-2 (Site 70) in central Crater Flat does appear to have many of the characteristics of groundwater from the carbonate aquifer, and groundwater at well NC-EWDP-3D (Site 86) and the NC-EWDP-15P well (Site 90) were analyzed with the PHREEQC code to be partially derived from the carbonate aquifer, in agreement with these results. The deep groundwater flowing through Crater Flat is apparently forced both upward and to the east by a buried ridge formed by the low-permeability Lower Clastic Confining unit (compare Figures A6-52 and A6-55). The groundwater entering Crater Flat through the undifferentiated Valley Fill in zone 61 dominates the shallow flow system in most of Crater Flat, except for the westernmost part of Crater Flat where the groundwater enters from the western boundary along Bare Mountain. Although most of the groundwater entering the undifferentiated Valley Fill in northwest Crater Flat flows southward from borehole VH-1 (Site 69) to wells NC-EWDP-9SX (Sites 81–85) and NC-EWDP-3D (Site 86), as analyzed with the PHREEQC calculations (Sections A6.3.8.6 and A6.3.8.7), a part of this groundwater flows southeastward past well WT-10 (Site 42) and into southern Yucca Mountain to become a component of the groundwater near the NC-EWDP-15P well (Site 90) and NC-EWDP-2D (Site 91). PHREEQC calculations for these well NC-EWDP-15P and for nearby well NC-EWDP-19D indicated that groundwater from well WT-10 (Site 42) could constitute a significant fraction of the groundwater at these wells (Sections A6.3.8.8 and A6.3.8.10).

Because of the very low permeability of the pre-Tertiary rocks near Zone 62 at Timber Mountain, very little groundwater enters the model from this area and tracer concentrations indicate that inflow from this area exerts little influence on the downgradient water chemistry (figure not shown). The Tertiary rocks from Zone 62 include the relatively permeable upper volcanic aquifer, which permits a considerably greater amount of groundwater to enter the model

than the pre-Tertiary rocks in this zone. The steady-state distribution of tracer concentrations (Figure A6-57) indicates that groundwater entering through the Tertiary rocks of Zone 62 flows southward through Yucca Mountain and forms a component of the groundwater throughout the Yucca Mountain area, including southeastern Crater Flat at wells WT-10 (Site 42), NC-EWDP-3D (Site 86), the Cind-R-Lite well (Site 89), and wells NC-EWDP-2D (Site 91) and NC-EWDP-19D (Sites 92 and 94 to 98) in southern Yucca Mountain near Fortymile Wash. The $\delta^{13}C$ of shallow groundwater in the northernmost part of Yucca Mountain is too light for that groundwater to have originated from groundwater directly to the north at well ER-EC-07 (Site 24) in Beatty Wash. However, the increase in groundwater $\delta^{13}C$ southward at Yucca Mountain is consistent with an increasing component of groundwater from the area of well ER-EC-07 (Site 24) present in the Yucca Mountain groundwater.

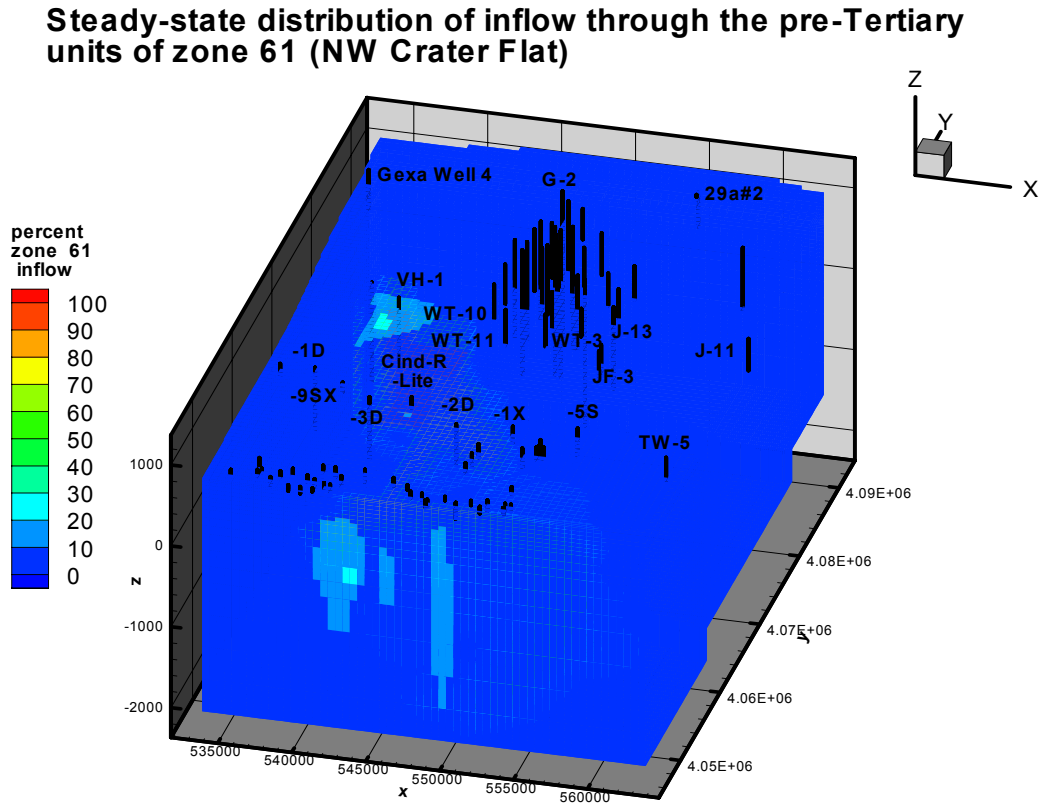

Sources: DTNs: LA0304TM831231.002 [DIRS 163788]; LA0309EK831231.001 [DIRS 171887].

NOTES: The X and Y coordinates are Universal Trans-Mercator Projection (UTM) coordinates in meters. The Z coordinate is elevation relative to sea level in meters. X = UTM-Easting and Y = UTM-Northing.

Figure A6-54. Map View of Steady-State Distribution of the Percentage of Inflow through the Pre-Tertiary Units of Northwest Crater Flat Groundwater Calculated Using the Saturated Zone Flow Model

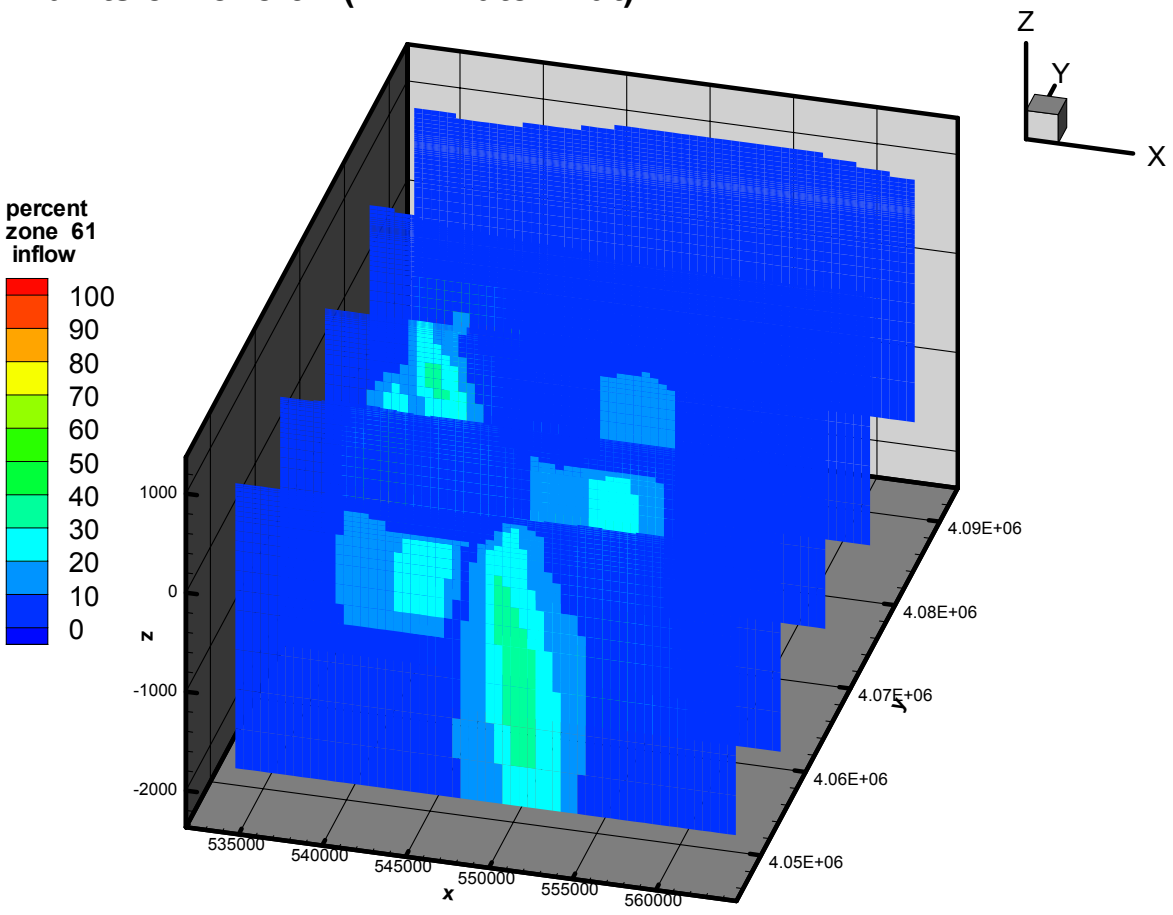

Sources: DTNs: LA0304TM831231.002 [DIRS 163788]; LA0309EK831231.001 [DIRS 171887].

NOTES: The X and Y coordinates are Universal Trans-Mercator Projection (UTM) coordinates in meters. The Z coordinate is elevation relative to sea level in meters. X = UTM-Easting and Y = UTM-Northing.

Figure A6-55. Cross Sectional View of Steady-State Distribution of the Percentage of Inflow through the Pre-Tertiary Units of Northwest Crater Flat Groundwater Calculated Using the Saturated Zone Flow Model

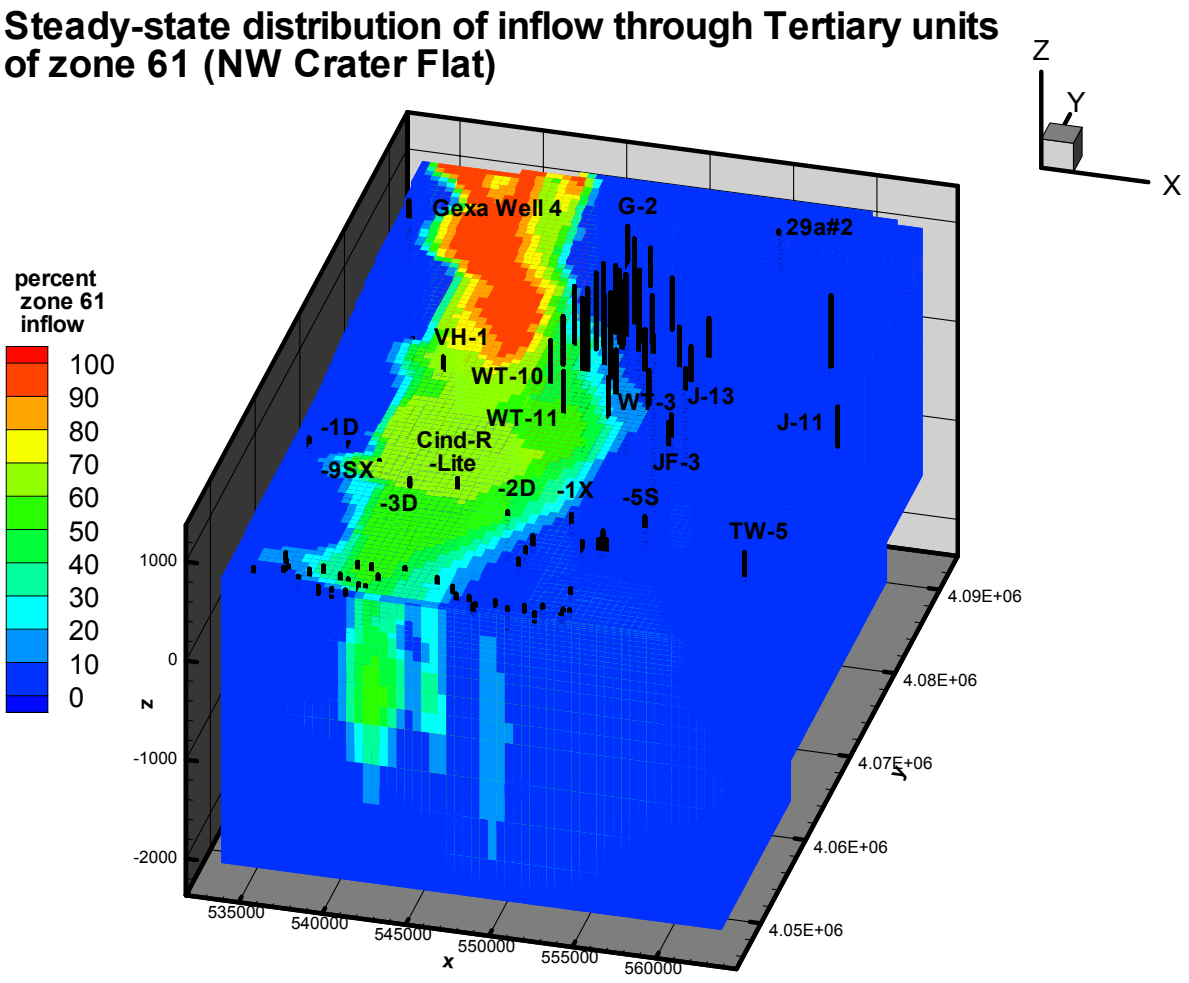

Sources: DTNs: LA0304TM831231.002 [DIRS 163788]; LA0309EK831231.001 [DIRS 171887].

NOTES: The X and Y coordinates are Universal Trans-Mercator Projection (UTM) coordinates in meters. The Z coordinate is elevation relative to sea level in meters. X = UTM-Easting and Y = UTM-Northing.

Figure A6-56. Steady-State Distribution of the Percentage of Inflow through the Tertiary Units of Northwest Crater Flat Groundwater Calculated Using the Saturated Zone Flow Model

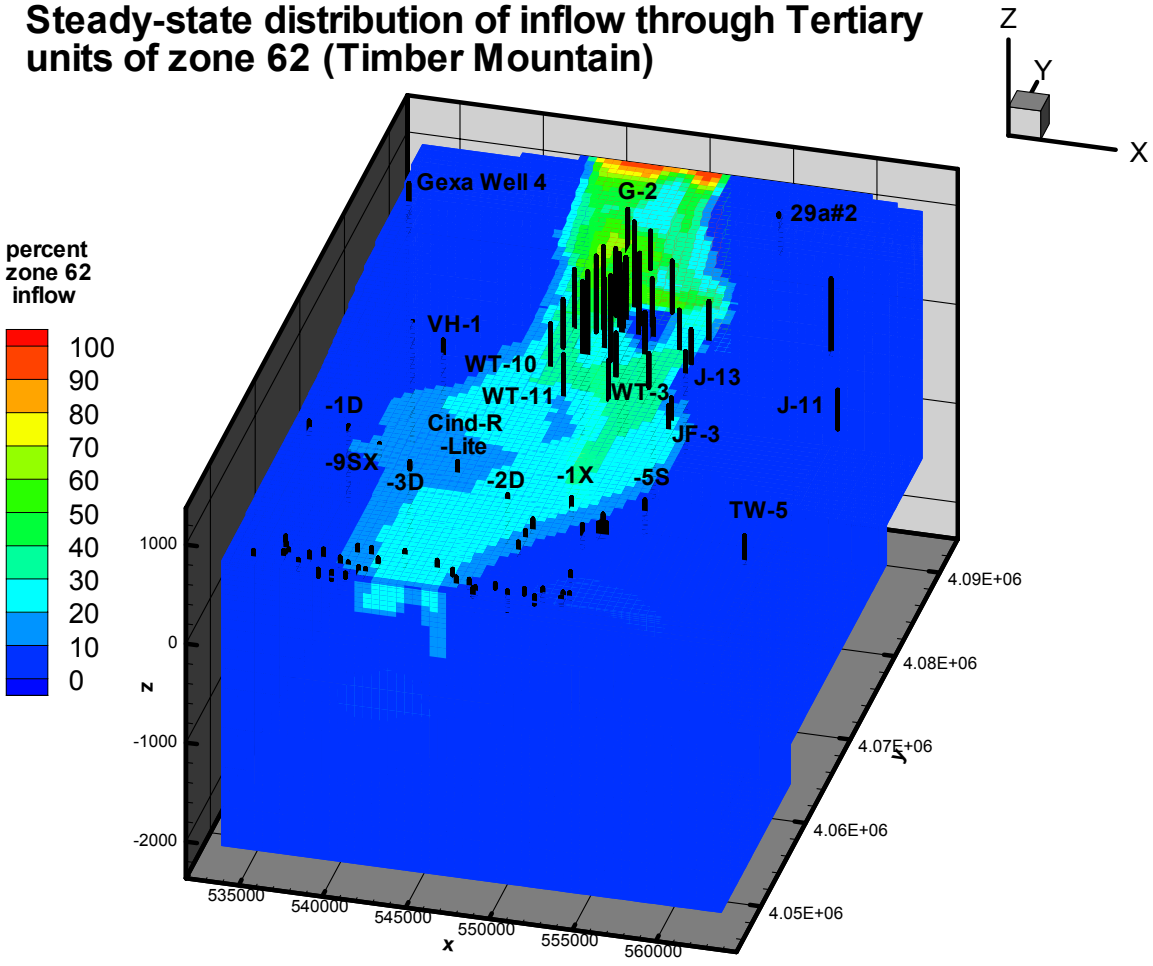

Sources: DTNs: LA0304TM831231.002 [DIRS 163788]; LA0309EK831231.001 [DIRS 171887].

NOTES: The X and Y coordinates are Universal Trans-Mercator Projection (UTM) coordinates in meters. The Z coordinate is elevation relative to sea level in meters. X = UTM-Easting and Y = UTM-Northing.

Figure A6-57. Steady-State Distribution of the Percentage of Shallow Timber Mountain Area Groundwater through the Tertiary Units Calculated Using the Saturated Zone Flow Model

Groundwater entering the model domain from the pre-Tertiary rocks of Zone 63 near Fortymile Canyon follows a sinuous pathway through the Fortymile Wash area and western Jackass Flats as it moves southward through the model (Figures A6-58 and A6-59). The sinuous movement of this tracer plume in the model may be related to the deflection of groundwater eastward around the buried ridge of the Lower Clastic Confining unit in the southwestern part of the model (Figure A6-52) and, later, by the large amount of inflow from Zone 81 in the southeast part of the model (see below). Groundwater from the pre-Tertiary rocks of Zone 63 is predicted by the SZ flow model to be a small component of the shallow groundwater at borehole JF-3 (Site 37) and other Fortymile Wash area boreholes in the northern Amargosa Desert and in the Amargosa Valley area. The groundwater from the pre-Tertiary rocks of Zone 63 could be the component of groundwater from western Jackass Flats predicted from an analysis of sulfur isotopes to be present in minor amounts in some LW and FMW-E groundwaters (Figure A6-51).

The steady-state distribution of groundwater entering the Fortymile Canyon area of the model through the Tertiary rocks of Zone 63 indicates that this groundwater is diluted by groundwater from other areas, including Yucca Mountain (Figure A6-60) by the time it has reached well J-13 (Site 35) in Fortymile Wash. The shallow groundwater entering Zone 63 again becomes a small component of the groundwater southward along Fortymile Wash near JF-3 (Site 37) and in southern Yucca Mountain near well NC-EWDP-2D (Site 91), but does not persist as an identifiable part of the groundwater in the FMW-S area wells. Dilution of the shallow inflow from Zone 63 by downgradient recharge along Fortymile Wash is not a plausible explanation for the dilution of the Zone 63 in flow, given the small amount of Fortymile Wash recharge present in the model. The geochemical and isotopic data from the FMW-N and FMW-S wells indicate a much more significant component of inflow from Zone 63, and perhaps of recharge along the wash, than is indicated by the SZ flow model.

Like groundwater from the pre-Tertiary units of Zone 63, the groundwater entering the northern boundary through the pre-Tertiary rocks of Zone 64 beneath Shoshone Mountain follows a sinuous trajectory through western Jackass Flats and emerges into the shallow flow system in the vicinity of well NC-EWDP-5S (Site 154) of the Amargosa Valley area (figure not shown). Some of the groundwater entering the model through Zone 64 leaves the model along its eastern boundary. The model results suggest that the deep groundwater from Zone 64 could also be the component of groundwater from western Jackass Flats identified from $\delta^{34}S$ analysis to be present in some of the LW and FMW-E area wells. The Tertiary rocks of Zone 64 are comprised of confining units (Figure A6-52) and virtually no groundwater enters the model through these rocks.

The groundwater in the southeast corner of the model near the Skeleton Hills area is dominated by inflow from pre-Tertiary rocks of Zone 81 (Figure A6-61). The model results are consistent with the geochemical and isotopic data from this area, which suggest that the groundwaters near the Gravity fault, and as far west as NC-EWDP-5S (Site 154) and some LW- and FMW-E area wells, contain a component of groundwater from the carbonate aquifer leaking into the alluvium across the Gravity fault.

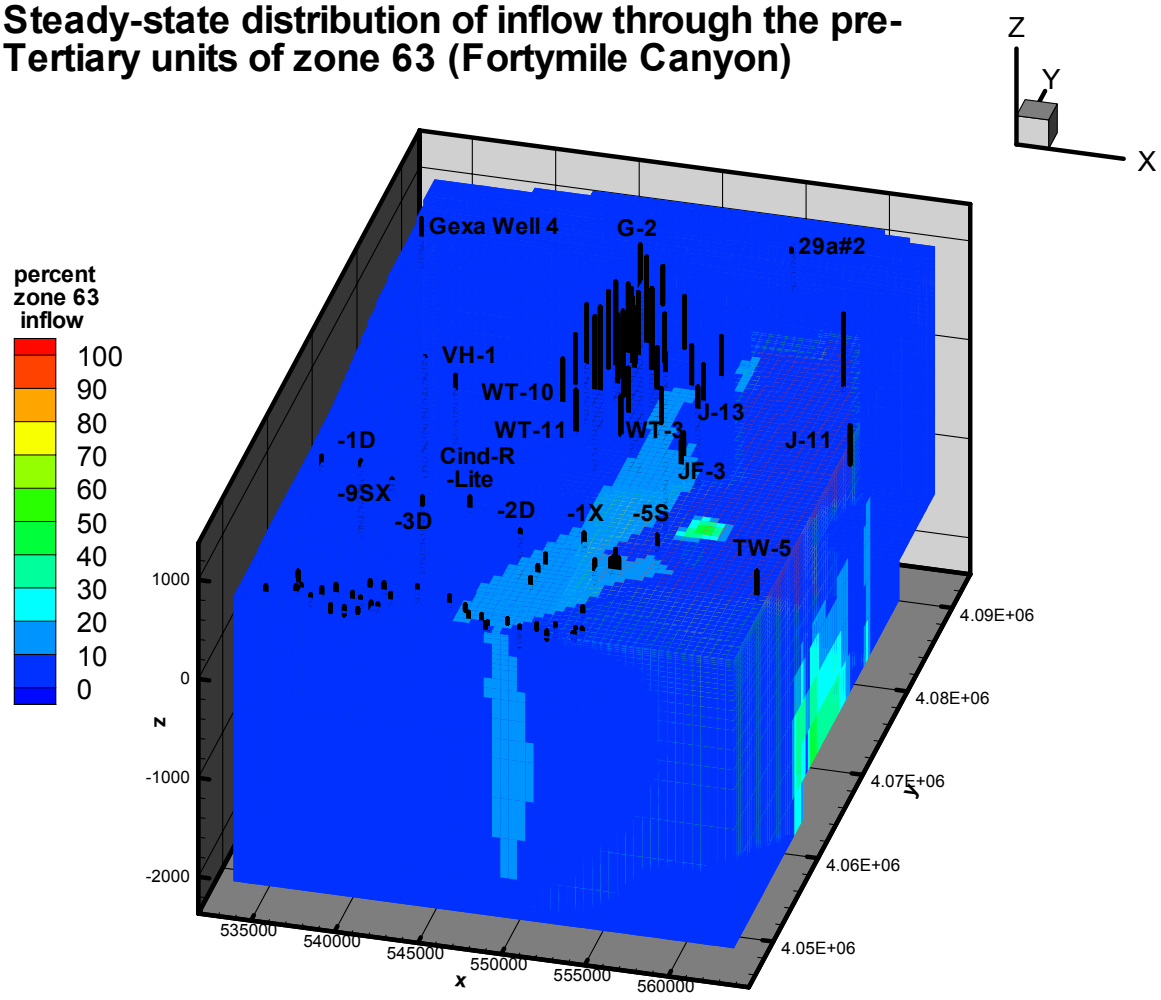

Sources: DTNs: LA0304TM831231.002 [DIRS 163788]; LA0309EK831231.001 [DIRS 171887].

NOTES: The X and Y coordinates are Universal Trans-Mercator Projection (UTM) coordinates in meters. The Z coordinate is elevation relative to sea level in meters.

Figure A6-58. Map View of Steady-State Distribution of the Percentage of Shallow Upper Fortymile Wash Area Groundwater through the Pre-Tertiary Units Calculated Using the Saturated Zone Flow Model

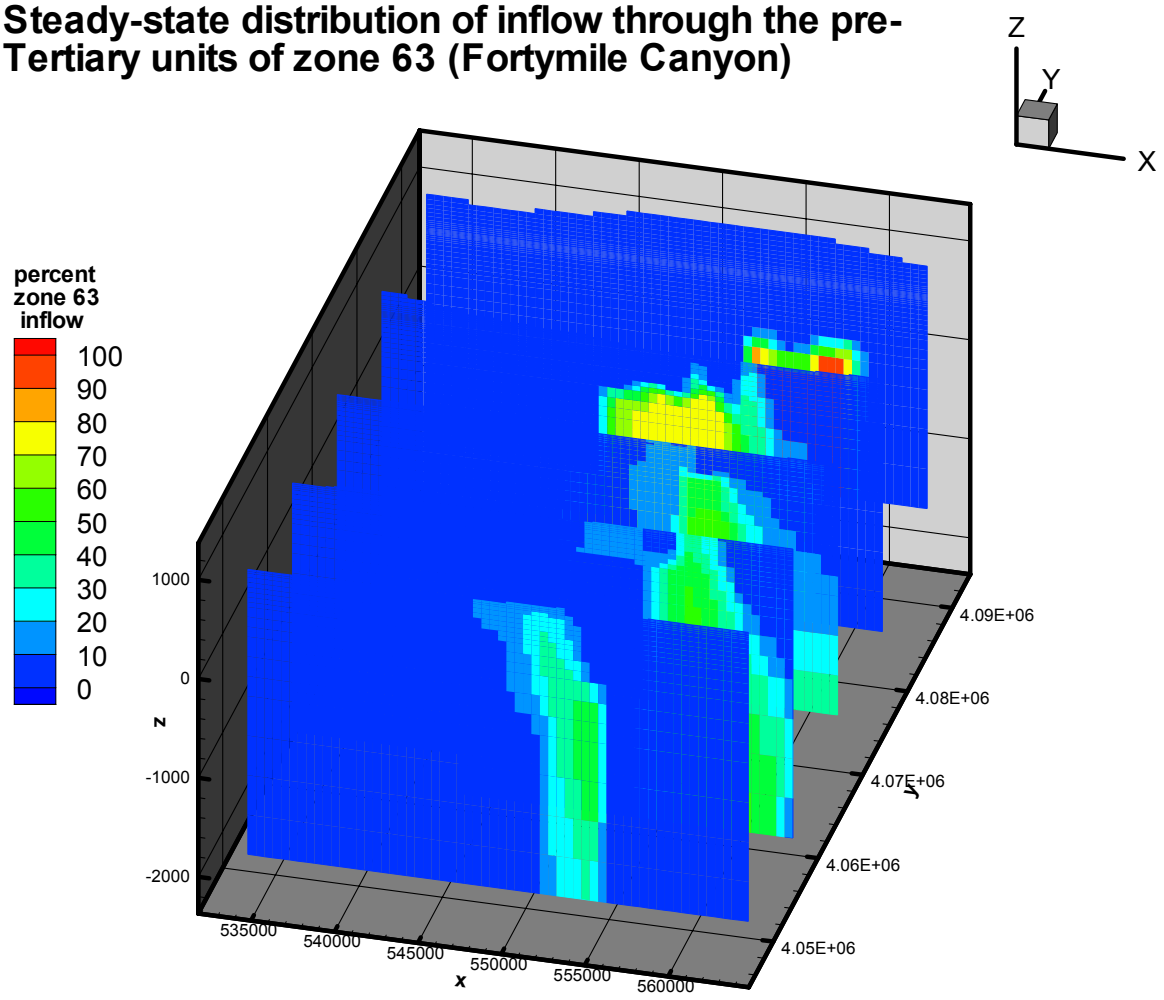

Sources: DTNs: LA0304TM831231.002 [DIRS 163788]; LA0309EK831231.001 [DIRS 171887].

NOTES: The X and Y coordinates are Universal Trans-Mercator Projection (UTM) coordinates in meters. The Z coordinate is elevation relative to sea level in meters.

Figure A6-59. Cross Sectional View of Steady-State Distribution of the Percentage of Shallow Upper Fortymile Wash Area Groundwater through the Pre-Tertiary Units Calculated Using the Saturated Zone Flow Model

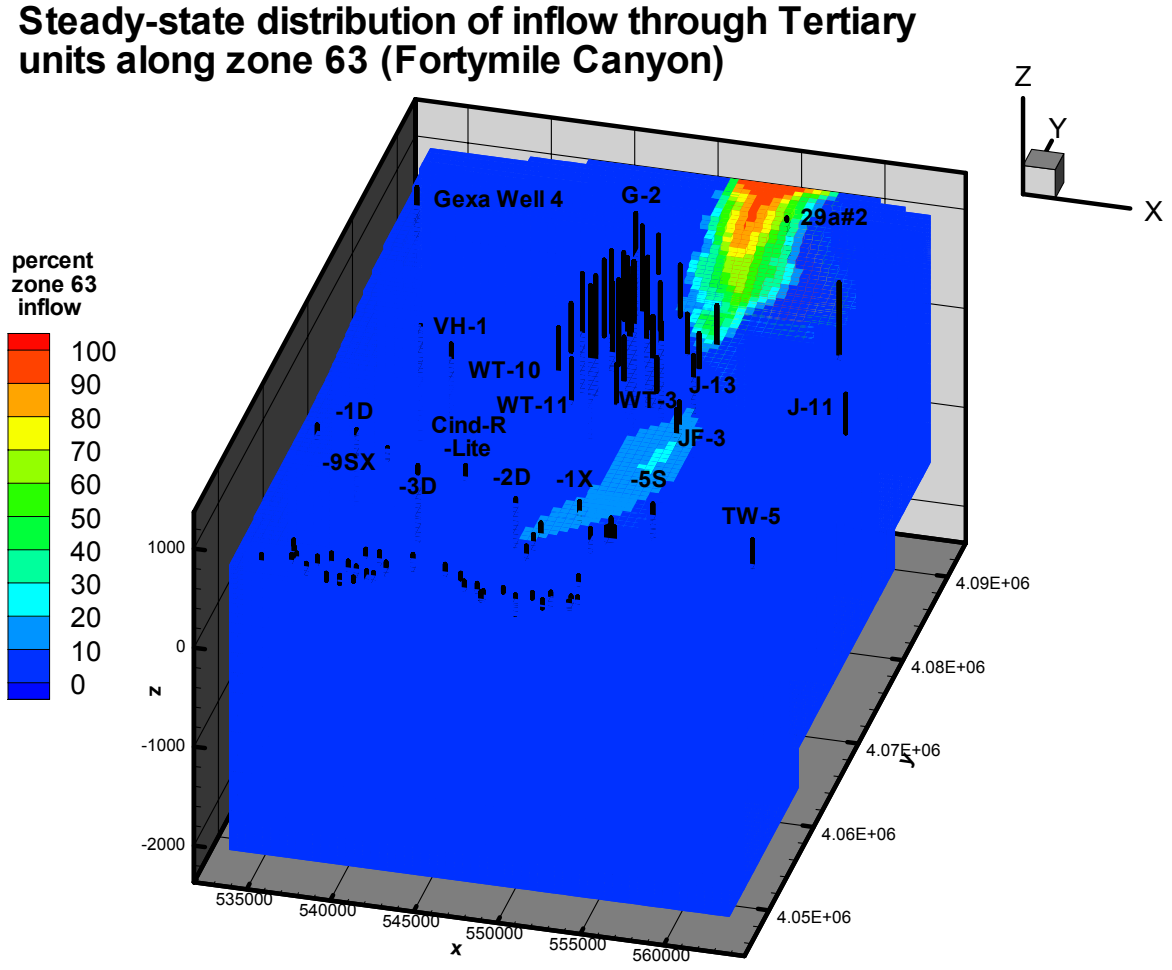

Sources: DTNs: LA0304TM831231.002 [DIRS 163788]; LA0309EK831231.001 [DIRS 171887].

NOTES: The X and Y coordinates are Universal Trans-Mercator Projection (UTM) coordinates in meters. The Z coordinate is elevation relative to sea level in meters.

Figure A6-60. Steady-State Distribution of the Percentage of Shallow Upper Fortymile Wash Area Groundwater through the Tertiary Units Calculated Using the Saturated Zone Flow Model

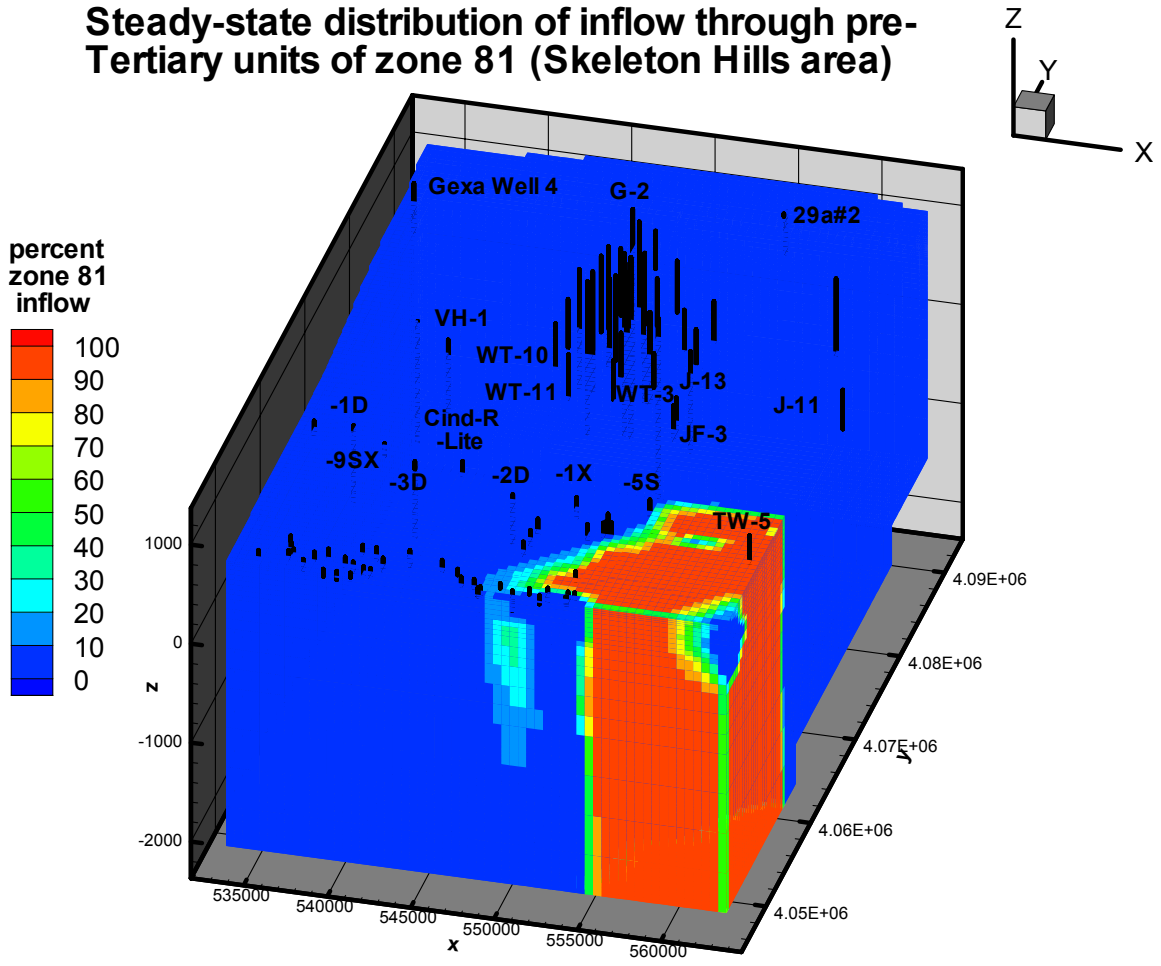

Sources: DTNs: LA0304TM831231.002 [DIRS 163788]; LA0309EK831231.001 [DIRS 171887].

NOTES: The X and Y coordinates are Universal Trans-Mercator Projection (UTM) coordinates in meters. The Z coordinate is elevation relative to sea level in meters.

Figure A6-61. Steady-State Distribution of the Percentage of Pre-Tertiary Rocks of the Skeleton Hills Area Groundwater Calculated Using the Saturated Zone Flow Model

In summary, the flow patterns and mixing relations identified with the SZ flow model are similar in many ways to the flow patterns and mixing relations inferred from the hydrochemical and isotopic data for the area. Of particular importance are the simulations of movement of recharge from the Yucca Mountain area. These simulations indicate that groundwater from Yucca Mountain may not be easily identifiable in groundwaters south of Yucca Mountain because of dilution by groundwater from other, more active parts of the flow system. The SZ flow model appears to underestimate the quantity of inflow from the Fortymile Canyon area through the Tertiary units. This conclusion is based on the observation that groundwater along Fortymile Wash through Jackass Flats and the Amargosa Desert is chemically and isotopically unique

compared to the surrounding groundwaters, but the tracer simulations indicate that groundwater inflow from Fortymile Canyon or from downgradient recharge along the wash is present only in dilute amounts along Fortymile Wash. Some of the discrepancy between the simulations and the data for the Fortymile Wash area may be due to recharge of some or most of this chemically distinct groundwater during wetter climate periods.

A6.3.11 Regional Flow Paths Inferred from Hydrochemical Data

Groundwater flow paths and mixing zones are identified on the basis of the preceding discussions of measured and calculated geochemical and isotopic parameters. The hydraulic gradient shown on the potentiometric surface map (Figure A6-3) is used to constrain flow directions only insofar as groundwater cannot flow from areas of lower hydraulic head to areas of higher hydraulic head. Chemical and isotopic composition of groundwater were then used to locate flow pathways in the context of the hydraulic gradient and considering the possibility that flow paths can be oblique to the potentiometric gradient because of anisotropy in permeability.

The analysis of flow paths that follows assumes that Cl^- and SO_4^{2-} values are conservative and that changes to these are due to mixing along flow paths. This same assumption holds for isotopes of hydrogen and oxygen; however, because recharge waters have almost certainly changed over time, it is to be expected that isotopic variability in these constituents will occur in groundwaters of different ages (Benson and Klieforth 1989 [DIRS 104370], Figure 11; Winograd et al. 1992 [DIRS 100094], Figure 2). In spite of the potential reactive nature of Na and Ca, the contrast in concentrations between some areas is great enough that meaningful inferences about flow directions can be made.

Flow paths can be traced using conservative constituents only where compositional differences exist that allow some directions to be eliminated as possible flow directions. Some chemical and isotopic species in some areas have relatively uniform compositions and, thus, provide no information about flow paths. In other areas, they show more distinct compositional differences and, thus, can be used to infer flow directions. Because no single chemical or isotopic species varies sufficiently to determine flow paths everywhere in the study area, multiple lines of evidence were used to construct the flow paths inferred in this section. This evidence includes the areal distribution of chemical and isotopic species, sources of recharge, groundwater ages and evaluation of mixing/groundwater evolution through scatterplots, and inverse mixing and reaction models as presented in the previous sections.

Flow path 1 (Figure A6-62) traces the movement of groundwater southeastward from Oasis Valley (OV/NWA group) through the Amargosa Desert along the axis of the Amargosa River (AR and AR/FMW groups) to its confluence with Fortymile Wash (FMW-S group). This flow path is identified from areal plots of chloride (Figure A6-15) and scatterplots of SO_4^{2-} versus Cl^- (Figure A6-50) that support this flow path. It is inferred from Figure A6-50 that the more dilute groundwater from the Oasis Valley area (OV/NWA group) became concentrated by evapotranspiration as it moves from the Oasis Valley area into the northwestern Amargosa Desert toward sites 15 to 17. This inference is based on the common trend of the OV/NWA and AR groups in Figure A6-50, which indicates that the composition of the AR group can be derived by concentrating groundwater from the OV/NWA group through evapotranspiration downgradient from the Oasis Valley sample locations. Data contained in White (1979

[DIRS 101165], Table 2, sample sites 28 and 29) corroborate this interpretation. These data show that groundwater exiting Oasis Valley through Beatty Narrows into the NW Amargosa Desert has a Cl^- concentration of between 76.9 and 100.0 mg/L and SO_4^{2-} concentrations of between 183.5 and 249.8 mg/L. The more dilute solute concentration of these two samples is nearly identical to that from Sites 15 to 17. The data in Figure A6-50 also indicate that groundwater in the CF-SW group has a much lower Cl^- concentration than groundwater in the AR group, making it unlikely that groundwater from the CF-SW wells is a major component of groundwater in the AR and FMW-W wells. Groundwater along flow path 1 becomes more dilute in the AR/FMW wells as it becomes increasingly mixed with FMS-S group groundwater near Fortymile Wash (see below). Northwest of this mixing zone, high groundwater ^{14}C activities (Figure A6-28) and variable δD (Figure A6-24) and $\delta^{18}O$ (Figure A6-25) compositions at the AR wells indicate the presence of relatively young recharge in the groundwater due to runoff or irrigation in the area.

Flow path 2 (Figure A6-62) traces the movement of groundwater from the Fortymile Canyon area southward along the axis of Fortymile Wash into the Amargosa Desert. This flow pathway is drawn on the basis of similar anion and cation concentrations along the flow line and dissimilarities compared to regions to the east and west (see, for example, Figures A6-15, A6-16, and A6-22). Groundwater along the northern part of this flow path (FMW-N groups samples) is distinguished from groundwater at Yucca Mountain by δD and $\delta^{18}O$ compositions that are heavier and/or more offset from the global meteoric water line ($\delta D = 8\ \delta^{18}O + 10$) than the groundwater found under Yucca Mountain (Figure A6-48). It is inferred that the groundwater found along the FMW-S wells in the Amargosa Desert is derived, in part, from groundwater flow from the FMW-N wells, based on the similarly dilute SO_4^{2-} (Figure A6-16) and Cl^- (Figure A6-15) compositions of these groundwaters. Differences in the δD compositions of the FMW-N and FMW-S groundwaters (Figure A6-24) are attributed to the effects of changing climatic conditions on the δD composition of recharge (see Section A6.3.6.6.1). Groundwater flow from the FMW-N area wells southward into the Amargosa Desert along the axis of the wash is also compatible with expected and observed chemical evolution trends between the two areas, such as downgradient increases in pH (Figure A6-14), calcite saturation indices (Figure A6-37), and HCO_3^- (Figure A6-17) and SiO_2 (Figure A6-1) concentrations. Some part of the groundwater along Fortymile Wash may also be derived by recharge from overland flow, based on the observation that ^{14}C activities do not decrease systematically southward in either the northern or southern segments of the wash (Figure A6-28). Groundwater flow from the eastern and western parts of the Amargosa Desert toward Fortymile Wash is relatively minor, however, based on the much higher solute contents (Figures A6-15 to A6-17, and A6-34) and distinct isotopic compositions (Figures A6-26 and A6-27) of groundwaters adjacent to the FMW-S area wells.

Flow path 3 (Figure A6-62) traces the movement of groundwater from Jackass Flats in the vicinity of well J-11 (Site 67) as it moves along the western edge of the Amargosa Valley (LW) area wells and arcs southward through the FMW-E area wells. The identification of groundwater from Jackass Flats in this mixture of groundwaters is possible because the high SO_4^{2-} and low $\delta^{34}S$ characteristics of groundwater from well J-11 distinguish it from the high SO_4^{2-} and high $\delta^{34}S$ groundwater characteristic of the Gravity fault (GF group) and the low SO_4^{2-} and low $\delta^{34}S$ groundwater of the Fortymile Wash area (FMW-S group) on scatterplots of $\delta^{34}S$ versus $1/SO_4^{2-}$

concentration (Figure A6-51). A source for this high SO_4^{2-} groundwater from Jackass Flats rather than the Gravity fault area is also indicated by the similarly light $\delta^{13}C$ of groundwater along this flow path (Figure A6-27).

Flow path 4 (Figure A6-62) traces the movement of groundwater from the lower Beatty Wash area (southern TM group samples) into northwestern Crater Flat. This groundwater flows predominantly southward in Crater Flat through Sites 69 (borehole VH-1) and Site 86 (NC-EWDP-3D). The chemistry and isotopic composition of this groundwater appears to be a mixture of subequal amounts of groundwater from Sites 22 and 23 in lower Beatty Wash, with much smaller amounts of recharge from local runoff in Crater Flat or groundwater flow from Site 24 (Section A6.3.8.4). Dashed lines are used to illustrate these relationships on Figure A6-62. Groundwater from Site 68 (GEXA Well 4), which may be groundwater from Site 23 modified by recharge from surface runoff (Section A6.3.8.3), also contributes groundwater to this flow path. Scatterplots and PHREEQC inverse models (Sections A6.3.8.3 and A6.3.8.4) show that a mixture of groundwater from Sites 22 and 23 is required to account for both the relatively low Cl^- and the light $\delta^{18}O$ and δD activity ratios characteristic of this flow path, whereas small amounts of recharge from local runoff or flow from Site 24 are needed to decrease the $\delta^{13}C$ of the lower Beatty Wash groundwater.

Most groundwater at Timber Mountain north of Yucca Mountain (TM group) is characterized by $\delta^{13}C$ values that are too heavy (–6 to 0 per mil) and ^{14}C values that are too low for it to be a major source of groundwater at Yucca Mountain (Figure A6-45). The absence of significant amounts of Timber Mountain groundwater beneath Yucca Mountain is also indicated by the extremely low $\delta^{87}Sr$ and high Sr^{2+} concentration of the Timber Mountain groundwater compared to Yucca Mountain (Figure A6-32 and A6-31). The extremely light $\delta^{13}C$ (Figures A6-27 and A6-45) and high $\delta^{87}Sr$ (Figure A6-32) of groundwater in northern Yucca Mountain (YM-CR group) compared to Timber Mountain (TM group) groundwater indicates that groundwater from the Timber Mountain/Beatty Wash area does not flow south through northern Yucca Mountain. One well in upper Beatty Wash (Site 24 - ER-EC-07) has a high ^{14}C activity (Figure A-28), and $\delta^{13}C$ (Figure A6-27) and $\delta^{87}Sr$ values (Figure A6-32) similar to those of groundwaters in the Solitario Canyon Wash area (SCW group) and to groundwater south of Drill Hole Wash at Yucca Mountain. Based on Figure A6-45, some groundwater from the area of well ER-EC-07 in upper Beatty Wash could be present in Yucca Mountain groundwater south of Drill Hole Wash (YM-C, YM-SE, and YM-S groups) and along Solitario Canyon Wash (SCW group) if sorption on rock removed most of the Sr^{2+} from the Beatty Wash area along its flow path.

Flow path 5 (Figure A6-62) traces groundwater with a distinct chemical composition that comprises the SW Crater Flat (CF-SW) Group. Groundwater from site 70 (borehole VH-2) is chemically and isotopically distinct from groundwater that characterizes flow path 4, with higher concentrations of many major ions (Figures A6-15 to A6-17) (but lower concentrations of F (Figure A6-18) and SiO_2 (Figure A6-19)) and relatively high $\delta^{18}O$ (Figure A6-25) and δD (Figures A6-24 and A6-49) values. The $\delta^{18}O$ and δD of groundwater from borehole VH-2 is similar to groundwater from Species Spring (Rose et al. 1997 [DIRS 144725]), a perched spring at Bare Mountain, suggesting that groundwater at borehole VH-2 and other CF-SW group wells are derived principally from local recharge and runoff from Bare Mountain. Dashed east and southeast-oriented lines schematically illustrate this

flow (Figure A6-62). Groundwater in Oasis valley has some of the lightest groundwater δD and $\delta^{18}O$ values in the Yucca Mountain area (Figures A6-24 and A6-25), eliminating flow from Oasis Valley under Bare Mountain as a possible source of groundwater in southwest Crater Flat. The similar chemical and isotopic characteristics between groundwater from borehole VH-2 and other southwest Crater Flat boreholes (Section A6.3.4) and PHREEQC models of Sites 77 and 81 (Sections A6.3.8.5 and A6.3.8.6) indicate a dominantly north-south flow along this flow path as far south as these sites. Importantly, the chemically distinct groundwater along this flow pathway is not observed in boreholes to the south in the Amargosa Desert (AR and FMW-S groups) (for example, see Figure A6-50). Mixing relationships discussed in connection with Figure A6-49, and PHREEQC models of Sites 86 and 90 (Sections A6.3.8.7 and A6.3.8.8), suggest that this groundwater likely flows to the east and southeast and mixes with wells from the YM-S group (Figure A6-49).

Flow path 6 (Figure A6-62) traces the movement of groundwater from Site 42 (well WT-10) southward toward Sites 89 (Cind-R-Lite well) and 90 (well NC-EWDP-15P). This flow path is identified from PHREEQC models that indicate that groundwater from well NC-EWDP-15P is formed from subequal amounts of groundwater from Sites 69 (well VH-1) and 42 (well WT-10), with a minor component (5%) of groundwater like that from Site 70 (well VH-2) (see Section A6.3.8.8). Mixing trends indicated by plots of Cl versus δD (Figure A6-49) also suggest leakage from Crater Flat toward the YM-S group in southern Yucca Mountain. Although the predominant direction of flow from the Solitario Canyon (SCW group) area is southward along the Solitario Canyon fault, evidence for the leakage of small amounts of groundwater eastward across the fault is also provided by similarities in the ion concentrations and isotopic values of groundwaters in the SCW and YM-CR area wells (Section A6.3.6.3, Figures A6-42 to A6-46). This chemical and isotopic similarity indicates that groundwater as far east as borehole NC-EWDP-19D may have some component of groundwater from the Solitario Canyon Wash area. The short southeast-oriented dashed lines from Solitario Canyon group wells schematically illustrate this leakage.

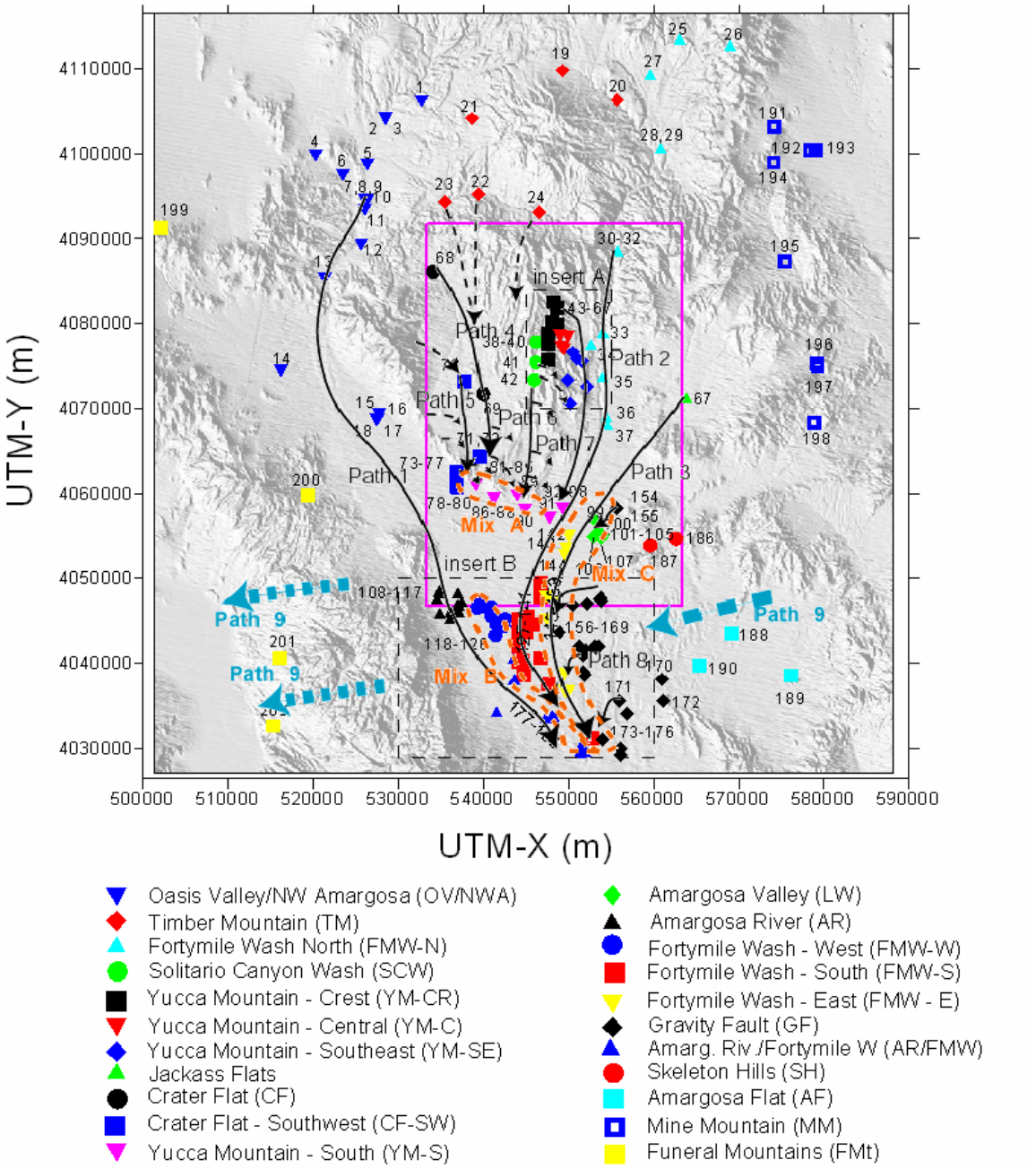

Source: DTN: LA0308RR831233.001 [DIRS 171890].

NOTES: This figure has color-coded data points and should not be read in a black and white version. Solid lines indicate a relatively high degree of confidence in the interpretations; dashed flow paths indicate relatively less confidence. Base map shows borehole designators and inserts; for reference see Figure A6-5 and Table A4-3.

UTM-X = UTM-Easting, UTM-Y = UTM-Northing; UTM = Universal Transverse Mercator.

Figure A6-62. Regional Flow Paths Inferred from Hydrochemical and Isotopic Data

Flow path 7 (Figure A6-62) traces the movement of groundwater from northern Yucca Mountain southeastward toward YM-SE wells in the Dune Wash area and then southwestward along the western edge of Fortymile Wash. The upper segment of this flow path is motivated by the high groundwater $^{234}U/^{238}U$ activity ratios found in the northern Yucca Mountain and Dune Wash areas (Figure A6-47). High $^{234}U/^{238}U$ activity ratios (greater than 7) typify both perched water and groundwater along and north of Drill Hole Wash but not groundwater along Yucca Crest at borehole SD-6 (Site 50) or perched water at borehole SD-7. Based on the conceptual model for the evolution of $^{234}U/^{238}U$ activity ratios described in Section A6.3.6.2, dissolution of thick vitric tuffs that underlie the Topopah Spring welded tuff along Yucca Crest south of Drill Hole Wash would be expected to decrease the $^{234}U/^{238}U$ activity ratios of deep unsaturated zone percolation south of the Wash. High $^{234}U/^{238}U$ activity ratios are expected only where these vitric tuffs are absent, as in northern Yucca Mountain. Results of a PHREEQC analysis of the evolution of groundwater between site 44 (well WT-24) in northern Yucca Mountain and Site 65 (well WT-3) in the Dune Wash area are consistent with this segment of flow path 7 (Section A6.3.8.9). The southern segment of flow path 7 is based on PHREEQC analyses of groundwater evolution between well WT-3 and various depth intervals of well NC-EWDP-19D (Sites 92 and 94 to 98) (Section A6.3.8.10). Groundwater at well NC-EWDP-19D has low Cl^- (Figure A6-15) and SO_4^{2-} (Figure A6-16) concentrations that are characteristic of groundwater at well WT–3. The light $\delta^{18}O$ and δD values eliminate Fortymile Wash as a possible source of the dilute groundwater at well NC-EWDP-19D (Figures A6-24, A6-25, A6-44 and A6-48). An alternative set of PHREEQC analyses was developed that interprets the groundwater at NC-EWDP-19D to be a result of the mixing of groundwater from well WT-10 and local southern Yucca Mountain recharge, as represented by perched water from borehole SD-7 (Section A6.3.8.10). Both sets of models explain the major-ion chemistry and $\delta^{13}C$ values of groundwater at NC-EWDP-19D. The arrows leading from flow path 6 toward NC-EWDP-19D (Figure A6-62) reflect this alternative groundwater path. It should also be noted that the $\delta^{18}O$ and δD values of groundwater at well NC-EWDP-19D are substantially lighter than for groundwater at either wells WT-3 or WT-10, requiring that climate change be invoked as a possible explanation for their differences.

Flow Path 8 (Figure A6-62) schematically illustrates leakage of groundwater from the carbonate aquifer (GF and AF Groups) across the Gravity fault. Hydrogeologists and geochemists have recognized this leakage across the fault for many years (Winograd and Thordarson 1975 [DIRS 101167]; Claassen 1985 [DIRS 101125]). These hypotheses are also compatible with the hydraulic gradient and our understanding of the regional groundwater flow patterns (Lacziak et al. 1996 [DIRS 103012]). The carbonate aquifer component in this groundwater is recognized by many of the same chemical and isotopic characteristics that typify groundwater discharging from the carbonate aquifer at Ash Meadows. These characteristics include high concentrations of Ca^{2+} (Figure A6-20) and Mg^{2+} (Figure A6-21), low SiO_2 (Figure A6-19), heavy $\delta^{13}C$ values (Figure A6-27), low ^{14}C activity (Figure 6-28), and comparable $\delta^{18}O$ and δD values as the Ash Meadows groundwater. Westward seepage of this groundwater mixes with the southward flow of groundwater along path 3 to produce groundwater with compositions intermediate between the two (Section A6.3.7.2). Evidence for these flow paths is best defined in groundwater compositions of some of the more westerly samples of the GF group such as samples 160, 175, and 175 (Figure 6-50).

Flow path 9 (Figure A6-62) is drawn to schematically illustrate deep underflow of groundwater from the carbonate aquifer, east of and including the GF and AF groups, beneath the Amargosa Desert and Funeral Mountains to the discharge points in Death Valley. The similarity in the chemical and isotopic characteristics of groundwater found in the Gravity fault area and groundwater that discharges from springs at sites 201 (Nevares Spring) and 202 (Travertine Spring) support this interpretation. The dissimilarity in Cl^- (Figure A6-15), Mg^{2+} (Figure A6-21), and SiO_2 (Figure A6-19) concentrations in these springs compared to the groundwater from the alluvial aquifer along the Amargosa River suggests that this alluvial groundwater is not the predominant source of the spring discharge in Death Valley.

A6.3.11.1 Mixing Zones

Figure A6-62 also highlights three zones (Mix A, B, and C) within which there is good evidence for mixing as demonstrated by trends of multiple solutes and isotope ratios on cross-correlation plots. Details of the mixing relations were given in Section A6.3.7.

Mixing zone A is defined by YM-S and CF-SW samples along U.S. Highway 95. The mixing zone is indicated by groundwater compositions of samples 78 to 85, 89, and 90 that are intermediate between the compositionally distinct groundwater of the CF-SW group and dilute groundwater of the YM-S group that is interpreted to have originated in the Yucca Mountain area (see Figure A6-49 and the discussion of flow paths 6 and 7 in Section A6.3.11). The location of the southernmost CF-SW samples coincides with a steep hydraulic gradient (Figure A6-3), which remains steep to the west but decreases to the east. Evidence for the distinct groundwater of the CF-SW group in boreholes to the south in the Amargosa Desert is lacking (for example, Figure A6-50). Thus, hydrochemical data and the hydraulic gradient suggest that southward flow indicated by flow path 5 is effectively blocked to the south. This flow is at least partly diverted to the east where it mixes with more dilute groundwater of the YM-S group to the east.

Mixing zone B consists of samples from the FMW-W and AR/FMW groups and a few samples from the FMW-S groups. The zone highlights groundwater with compositions that are intermediate between the distinct and consistent groundwater compositions of the AR group and the dilute groundwater of the FMW-S group (Figure A6-50). Flow path 1 is drawn to skirt the edge of mixing zone B and to connect the groundwater from the Amargosa River group to sample 181, which has a similar groundwater composition and is interpreted to represent undiluted groundwater from the AR group.

Mixing zone C consists of all samples from the LW and FMW-E groups, a few of the more westerly samples form the GF group, and at least one sample (141) from the FMW-S group. The mixing zone is characterized by small percentages of the distinctively high SO_4^{2-} groundwater from borehole J-11 (Figure A6-51) in groundwater near flow path 3. This distinct hydrochemical signature persists in variable percentages as far south as borehole 150. Groundwater with this distinctive signature is mixed to variable degrees with dilute water from the FMW-S group to the west or groundwater from the carbonate aquifer (GF Group) to the east.

An important conclusion derived from identification of these mixing zones is that they qualitatively illustrate the extent of transverse dispersivity along certain flow pathways. The mixing zones also illustrate that, although some flow pathways may remain intact for great distances (e.g., paths 1 and 2), even these most-persistent flow paths eventually loose their distinct character, largely through mixing. This effect is best illustrated in southern Amargosa desert where flow paths 1, 2, and 3, with contributions from 8, converge and mix. The distinct end member groundwater of the AR and FMW-S groups, representing flow paths 1 and 2, appears to be absent at the southern boundary of the study area. Whereas it is possible that these end member groundwaters have not yet been sampled, the proximity of mixed groundwater samples in the southern part of the study area (samples 141, 174, 175, 183, 184, and 185) leaves little room for unmixed (end member) groundwater to move through the area. The hydrochemical data are interpreted to indicate that groundwaters from distinct sources that merge in the Amargosa Desert eventually lose their hydrochemically distinct character and flow southward as partially mixed groundwater.

A7. SUMMARY, DATA TRACKING NUMBERS, AND UNCERTAINTIES

A7.1 SUMMARY

Hydrochemical data from the saturated zone in the Yucca Mountain region were compiled, documented, and analyzed in this appendix. The hydrochemical data are used together with physical hydraulic data to evaluate the local and regional flow system at Yucca Mountain. This report provides an independent assessment of the flow patterns (Section A6.3.11) and recharge rates (Section A6.3.6) near Yucca Mountain that can be compared with flow paths and recharge rates associated with the SZ site-scale flow model documented in *Water-Level Data Analysis for the Saturated Zone Site-Scale Flow and Transport Model* (BSC 2004 [DIRS 170008]), and for which the model input/output files are in DTN: LA0304TM831231.002 [DIRS 163788]. This report also provides an independent basis for calculating groundwater residence times (Section A6.3.9) that can be compared with particle breakthrough curves calculated using the site-scale SZ transport model. Additionally, this appendix contributes to the resolution of technical issues associated with groundwater residence times and flow path lengths in alluvium and tuff, as discussed below. The methods used in this appendix are widely accepted, the data are sufficient and the analysis appropriate for the intended use if this document.

A7.1.1 Summary of Overview Sections (Sections A6.3.1 to A6.3.5)

Areal distributions of chemical and isotopic data as well as calculated parameters show many consistent patterns throughout the study area. Groundwater that has low concentration of most solutes characterizes groundwater beneath Yucca Mountain and in Fortymile Wash. Dilute groundwaters characterize the northern part of Fortymile Wash as well as the southern part in the Amargosa Desert. Increases in most solute concentrations occur to the west of Yucca Mountain and along the southern margin of Yucca Mountain near U.S. Highway 95. Dilute groundwaters are flanked by less dilute groundwaters to the east and west in the Amargosa Desert. Hydrochemical data presented in these sections provide first-order constraints on flow pathways. Groundwater beneath Yucca Mountain and in Fortymile Wash is characterized by low concentrations of most solutes.

Section A6.3.3 reveals that some wells display significant hydrochemical variability with depth. An important example is illustrated in the data from wells NC-EWDP-19D and -19P, which show that groundwater in all zones is similar to groundwater from the volcanic aquifer at Yucca Mountain, whereas groundwater in -19P is more chemically similar to groundwater in Fortymile Wash. These data illustrate potentially important information regarding flow pathways that may be obscured when only groundwater samples from open boreholes are available, as is the case for most data in this report. In the absence of additional discrete vertical sampling data, the two-dimensional analysis will form the basis of the flow-path analysis described herein.

A7.1.2 Summary of Sources and Evolution of Recharge at Yucca Mountain (Section A6.3.6)

Particular attention is given to this topic to set the stage for evaluation of flow from Yucca Mountain. Hydrochemistry of perched water is considered a reliable surrogate for potential recharge water. The hydrochemistry of perched groundwater is quite similar to that of groundwater beneath Yucca Mountain. Some perched water and groundwater beneath Yucca Mountain has similarly elevated $^{234}U/^{238}U$ activity ratios and relatively small uranium concentrations. Depth-dependent trends in uranium activity ratios of unsaturated-zone pore water and perched water are also consistent with a model for local recharge. Local recharge of groundwater beneath Yucca Mountain is also supported by hydrochemical evaluation of potential upgradient sources of groundwater. Significant hydrochemical differences between most of these waters argue against the possibility that significant percentages of upgradient groundwater are present at Yucca Mountain. It is therefore concluded that much of the water present beneath Yucca Mountain was derived from local recharge.

Estimates of the magnitude of recharge at Yucca Mountain were obtained using the chloride mass balance method. For groundwaters within the immediate vicinity of Yucca Mountain, chloride concentrations range from 5.7 to 10.8 mg/L (excluding p#1-v), indicating local recharge rates between 4.7 and 17.9 mm/yr using an average, present-day precipitation rate of 170 mm/yr and an estimated range of Cl^- concentrations in precipitation of 0.3 to 0.6 mg/L.

The timing of recharge at Yucca Mountain was evaluated using hydrogen and oxygen isotopes as well as ^{14}C ages. Although the hydrogen and oxygen isotope data do not place an absolute age on the groundwater, they do indicate that the groundwater was recharged under paleoclimatic conditions that existed until the late Pleistocene. Corrected groundwater ^{14}C ages range from 11,430 years at borehole UE-25 WT#3 to 16,390 years at borehole UE-25 WT#12. These calculations are based on the averaged, that is, mixed age, of the groundwater sample. Calculations are also presented to bound the fraction of young water present in Yucca Mountain recharge. Estimates using an age of 1,000 years for the young component range from a low of about 0.02 at borehole UE-25 WT#12 to more than 0.15 at boreholes UE-25 WT#3 and USW G-4. Smaller fractions of young water would be present if water younger than 1,000-year-old were assumed in the calculations.

A7.1.3 Summary of Groundwater Flow and Evolution Away From Yucca Mountain (Sections A6.3.7 to A6.3.10)

Areal distribution plots reveal regions where steep gradients in solute concentrations and isotopic signatures exist. Based on evaluating elemental and isotopic correlation and PHREEQC analyses, it is concluded that mixing does readily explain compositional gradients in some areas. For example, mixing explains the compositional gradient displayed by the Nye County wells along U.S. Highway 95 where dilute groundwater to the southeast mixes with groundwater with high solute concentrations present to the northwest. Mixing also readily accounts for many of the groundwater compositions found in the Amargosa Desert. Here, dilute groundwater present along the Fortymile Wash drainage in the central part of the Amargosa Desert mixes with groundwater to the east and west to produce intermediate compositions. It is also concluded that sulfate-rich groundwater similar to that found in well J-11 is present in the Amargosa Desert. PHREEQC analyses help to confirm mixing relationships and define other components that must be added or removed through water-rock interaction to achieve observed groundwater compositions.

In Section A6.3.9, groundwater velocities are estimated along a selected flow path south of the repository in the Yucca Mountain area. Velocities are estimated by evaluating the ^{14}C activities of the groundwater along the flow path in context with PHREEQC analyses of groundwater evolution. Estimated groundwater velocities along a linear flow path from WT-24 to WT-3 are 46 m/yr or higher. Groundwater velocities were also estimated along a flow path from WT-3 to the various zones sampled at NC-EWDP-19D. These velocities range from approximately 80 m/yr to 5 m/yr. The faster velocities are suggested to indicate that some of the shallow groundwater at well WT-3 moves along major faults such as the Paintbrush Canyon fault.

The site-scale saturated zone flow model (or, simply, SZ flow model) was used to simulate the movement of a conservative tracer from various segments along the boundaries in the model (Section A6.3.10). Flow patterns and mixing relations identified with the SZ flow model were generally consistent with flow patterns and mixing relations inferred from the hydrochemical and isotopic data for the area. Of particular importance are simulations of the movement of recharge from the Yucca Mountain area. These simulations indicate that groundwater from Yucca Mountain may not be easily identifiable in groundwaters south of Yucca Mountain because of dilution by groundwater from other, more active parts of the flow system. This groundwater mixture includes contributions from northwest Crater Flat, Timber Mountain, and Fortymile Canyon. In some other respects, the SZ flow model differs from what is inferred from the geochemical data. For instance, the SZ flow model appears to underestimate the quantity of inflow from the Fortymile Canyon area through the Tertiary units. This conclusion is based on the observation that groundwater along Fortymile Wash through Jackass Flats and the Amargosa Desert is chemically and isotopically unique compared to the surrounding groundwaters, but the tracer simulations indicate that groundwater inflow from Fortymile Canyon or from downgradient recharge along the wash is present only in dilute amounts along Fortymile Wash. Some of the discrepancy between the simulations and the data for the Fortymile Wash area may be due to recharge of some or most of this chemically distinct groundwater during wetter climate periods.

A7.1.4 Summary of Flow Pathways (Section A6.3.11)

Flow paths can be traced using areal plots and scatterplots of geochemical and isotopic data, inverse mixing and water/rock interaction analyses involving PHREEQC, and simulations done with the SZ flow model. Because no single chemical or isotopic species varies sufficiently to determine flow paths everywhere in the study area, multiple chemical and isotopic species were considered.

Flow Path 1 (Figure A6-62) shows groundwater moving roughly parallel to the Amargosa River from an area west of Bare Mountain toward the southwest corner of the site model area. Flow Path 2 indicates that groundwater flows parallel to Fortymile Wash to connect upgradient areas in Fortymile Canyon with downgradient areas in the Amargosa Desert. Groundwater following Flow Path 3 flows from central Jackass Flats near well J-11 through the eastern part of the Amargosa Desert. Flow Paths 4 and 5 shows groundwater moving predominantly south-southeast through Crater Flat. Mixing relations and modeling suggest that these groundwaters leak across a region with a steep hydraulic gradient to mix with more dilute groundwaters to the southeast. Flow Paths 6 and 7 show groundwater flow from the Solitario Canyon area to the south. Again, leakage to the southeast across a steep hydraulic gradient coincident with the Solitario Canyon fault is suggested by hydrochemical trends. Groundwater from northern Yucca Mountain is interpreted to flow southeast toward lower Dune Wash and then southwestward toward wells located west of Fortymile Wash near U.S. Highway 95 (Flow Path 7). The location of Flow Path 7 implies that groundwater from the repository area will flow further to the west of this path. Flow Path 8 illustrates leakage to the east across the hydrologic boundary between the carbonate aquifer to the east and the alluvial aquifer in Amargosa Desert. Flow Path 9 schematically illustrates deep underflow of groundwater from the carbonate aquifer, east of and including the GF and AF groups, beneath the Amargosa Desert and Funeral Mountains to the discharge points in Death Valley.

Regions where mixing relations are strongly suggested by hydrochemical data are also shown in Figure A6-62. An important conclusion derived from drawing these mixing zones is that they document and qualitatively illustrate the extent of transverse dispersivity along certain flow pathways. The mixing zones also illustrate that although some flow pathways may remain intact for great distances (e.g., Paths 1 and 2), even these most persistent flow paths eventually lose their distinct character largely through mixing as is demonstrated in southern Amargosa Desert along the southern border of the map area.

A7.2 DATA TRACKING NUMBERS

Several data tracking numbers (DTNs), generated in this appendix are cited elsewhere in this report where they are used as indirect input. These intermediary output DTNs are listed below in an order that coincides with the structure of the appendix. These results are not qualified and cannot be used as direct input without qualification:

- Regional groundwater hydrochemical data: DTNs: LA0309RR831233.001 [DIRS 166546] and LA0309RR831233.002 [DIRS 166548]

- Calculated hydrochemical parameters: DTN: LA0310EK831232.001 [DIRS 165995]

- Calculation of corrected and uncorrected groundwater ^{14}C ages: DTN: LA0202EK831231.002 [DIRS 165507]

- Calculations of fractions of young water in selected Yucca Mountain groundwaters: DTN: LA0202EK831231.004 [DIRS 180317]

- Groundwater travel-time calculations for selected wells: DTN: LA0310EK831231.001 [DIRS 171889]

- FEHM groundwater models of nonreactive tracer transport in the Yucca Mountain area: DTN: LA0309EK831231.001 [DIRS 171887]

- A map of groundwater flow paths in the Yucca Mountain area: DTN: LA0308RR831233.001 [DIRS 171890].

A7.3 UNCERTAINTIES AND RESTRICTIONS

The evaluations and conclusions presented in this appendix are interpretive in nature. The overall uncertainty of these interpretations is a function of the analytical uncertainty of the data on which the interpretations were based, the distribution of data both areally and with depth, the representativeness of these data for various parts of the groundwater system, and the uncertainty in the conceptual models that formed the framework for the interpretations.

Results presented in this appendix are affected to different degrees by each of these uncertainties. The following sections list the key uncertainties associated with each of the DTNs cited in Section A7.2.

A7.3.1 Compilation of Hydrochemical Data

The uncertainty associated with the DTNs results primarily from the analytical uncertainty associated with the measurements and the representativeness of the data for those parts of the aquifer from which the groundwater samples were taken. Ideally, groundwater samples are taken after the well has been pumped for some time after drilling so that the effects of foreign drilling fluids and borehole cuttings on in situ groundwater compositions have been mitigated. Although this is true of the vast majority of the samples used in this report, a small number of samples used in this report originated from wells in which the samples were bailed prior to a "clean-out" period. This approach may have caused the chemical characteristics of these samples to change somewhat relative to in situ groundwater. In general, bailed samples were used in this report only if later pumped samples were not available from a particular well. The representativeness of sampled groundwater of in situ groundwater compositions is also related to the depth interval over which the sample was taken. Most hydrochemical data reported here are from single-interval boreholes, the hydrochemistry of which will represent an average of the sampled depth intervals. Hydrochemical data for discrete depth intervals are presented in Section 6.7.3.

The representativeness of sampled groundwater of in situ conditions may also be affected by the sampling method. For example, choice of container or prolonged exposure to atmosphere may

affect groundwater chemistry. Most sample data presented herein were collected by the United States Geological Survey (or by their contractors), who have a long and proven record of groundwater sampling using proven techniques. Furthermore, Yucca Mountain Project Quality Assurance Programs also govern many of these sampling procedures. This program is designed to assure that methods utilized are appropriate for the desired purpose. Thus, the data are accepted to be representative of in situ conditions. All analytical data presented herein have uncertainty associated with the individual values. These uncertainties reflect limits of precision of the analytical technique combined with accuracy of the measurement, which is typically determined by replicate analysis of samples (standards) with known values. The data presented herein were determined using a variety of analytical techniques by a number of laboratories, collected over a span of more than 20 years, during which time analytical techniques and associated uncertainties have changed. In some cases, uncertainties for individual analytes or groups of analytes are presented in the original data sources, however, in other data sets analytical uncertainties are neither given nor discussed. Some examples of stated uncertainties are presented below.

The National Water Quality Laboratory produced many of the data presented herein for the Yucca Mountain Program at the United States Geological Survey and uncertainties are stated in some of the DTNs. For example, accuracy for major anions, cations and strontium concentration is estimated to be better than 10% except for fluoride, which is estimated at 15% (DTN: GS000308312322.003 [DIRS 149155]). Uncertainty in concentration of major anions and cations as well as strontium concentration is quoted at less than 10% in DTN: GS011108312322.006 [DIRS 162911]. This DTN also presents uncertainties for isotopic measurements as follows (all given in per mil): deuterium 3.0, ^{18}O 0.2, ^{13}C 0.2, and ^{34}S 0.2. In some cases, strontium was determined by isotope dilution, mass spectrometry methods, for which data are more precise (e.g. 0.5%, DTN: GS970708315215.008 [DIRS 164674]). Uncertainties for ^{14}C are 0.1 pmc for data presented in DTN: GS011108312322.006 [DIRS 162911]. Uncertainties for uranium concentration are given as better than 1% (Paces et al. 2002 [DIRS 158817]). Uncertainties in uranium isotope ratios ($^{234}U/^{238}U$) are typically given with each individual analysis in the original data source. For example, uncertainties presented in Paces et al. (2002 [DIRS 158817], Table 2) range from 0.09% to 4.5% with a mean of 0.73% (with the exception of a single analysis of a rainfall sample with small U concentration for which uncertainty in the $^{234}U/^{238}U$ ratio is 9.8%). Uncertainties for strontium isotope ratios ($^{87}Sr/^{86}Sr$) are typically quoted at 0.00001 for absolute values (e.g., DTN: GS011108312322.006 [DIRS 162911] and for Nye County wells), which translates to an uncertainty of approximately 0.01 in $\delta^{87}Sr$ units.

For the purpose of this report, uncertainties assigned to analytical data are based on one or more of the following: (1) stated uncertainties in the original data set; (2) consideration that data produced by the same facility, for which no uncertainties are stated, are likely to have similar uncertainties to data with stated uncertainties; (3) typical uncertainties given in the literature; or (4) the authors' personal experience with typical uncertainties associated for various analytical techniques and analytes. Where uncertainties are not stated, the following uncertainties are assigned to the analytical data: Major anions and anions and strontium concentration: 10 %; fluoride concentration: 15%; stable isotopes of hydrogen, oxygen, sulfur, and carbon (expressed as δH, δO, δS, and δC in per mil): 0.2; and ^{14}C: 0.2 pmc. Uncertainties in uranium concentration and uranium and strontium isotope ratios are given in the original data sets.

In addition to analytical errors, many of the samples in the portion of the data set that had no prior DTNs may have an additional uncertainty in that they were obtained from a database (geochem02.mdb) that does not represent the primary source of the data. Hence, the possibility of transcription errors is compounded. Where original published sources could be found and checked against that database, some transcription errors in the database were evident. This uncertainty affects only groundwater samples at locations to the west, north, and east of the site model area, outside of the site model area.

It is prudent to point out that most of the evaluations presented herein are based on hydrochemical groupings and general data trends displayed within and among these groupings as opposed to any one analysis or data set from any one sample. Generally, the range of analytical values displayed within a single hydrochemical grouping is greater than the analytical uncertainty for any individual analysis. Hydrochemical groupings and data trends remain valid and essentially unaffected by considerations of analytical uncertainty.

A7.3.2 Calculated Hydrochemical Parameters

The uncertainty in the calculated hydrochemical parameters reflects the analytical uncertainty of the measurements, the representativeness of these measurements of in situ groundwater conditions, and uncertainty in the solubility constants of the minerals for which saturation indices were calculated. Uncertainty in the applicability of the solubility constants arises from (1) inaccurate, incomplete or inconsistent thermodynamic data, (2) nonstoichiometric or variable mineral compositions, (3) differences in the particle sizes of minerals that produced the thermodynamic data and particle sizes of minerals to which the data were applied, (4) model assumptions and limitations, such as which aqueous complexes are considered in the model, and (5) kinetic effects arising from slow reaction rates relative to groundwater residence times (Langmuir 1997 [DIRS 100051], p. 221). In addition, because solubility constants are a function of temperature, uncertainty in groundwater temperatures affects the calculated saturation indices. Measured groundwater temperatures were used to calculate saturation indices for most wells considered in this report. For a relatively small number of wells in the Yucca Mountain area, groundwater temperatures were estimated from published maps of water table temperatures. Groundwaters in the Amargosa Desert with no temperature data were assumed to be at 25°C based on the measured groundwater temperatures of nearby wells. A sensitivity analysis to examine the effect of temperature changes on log P_{CO2} and mineral saturation indices for groundwater from well J-13 indicated the following uncertainties as assumed temperatures were varied by ±5°C around 25°C: log P_{CO2} (±0.06), $SI_{calcite}$ (±0.04), $SI_{smectite}$ (±1.72), $SI_{Ca\text{-}clinoptilolite}$ (±4.77), $SI_{SiO2(a)}$ (±0.04), $SI_{fluorite}$ (±0.06), SI_{albite} (±0.28), $SI_{K\text{-}feldspar}$ (±0.34), and $SI_{dolomite}$ (±0.14). Saturation indices for calcite and dolomite and log P_{CO2} increase with temperature, but the remaining saturation indices decrease with temperature. The saturation indices of smectite and Ca-clinoptilolite are particularly sensitive to temperature because of the large enthalpies estimated for these minerals (Table A6-4); however, groundwaters in the Amargosa Desert are typically very supersaturated with these minerals (Figures A6-38 and A6-39), so that a temperature uncertainty of ±5°C does not change the fundamental conclusion that groundwaters in the Amargosa Desert are supersaturated with these minerals. For other minerals, uncertainty in groundwater temperatures of 25 ±5°C introduces less absolute uncertainty into the calculated saturation indices.

Another source of uncertainty in the calculated saturation indices of alumino-silicate minerals concerns the assumption that total dissolved Al^{3+} concentrations are in equilibrium with kaolinite. This assumption was based on an empirical fit to dissolved Al^{3+} concentrations from a subset of the Yucca Mountain area wells for which dissolved Al^{3+} data exist (see Section A6.3.5). Estimates of Al^{3+} concentrations that rely on assumed equilibrium with kaolinite underestimate measured Al^{3+} concentrations by –3.0 ±2.9 ppb. If the actual Al^{3+} concentrations were approximately 3 ppb higher than was estimated for the Yucca Mountain area, the saturation indices of all Al-bearing minerals would increase. Assuming Al^{3+} equilibrium with kaolinite, most groundwaters in the Yucca Mountain area are estimated to be saturated with smectite and Ca-clinoptilolite (Figures A6-38 and A6-39). With higher Al^{3+} concentrations, these groundwaters would be even more supersaturated with these minerals. Groundwaters in the Yucca Mountain area are presently estimated to be both undersaturated and supersaturated with K-feldspar (Figure A6-37). With higher Al^{3+} concentrations, some groundwaters that are estimated to be undersaturated with K-feldspar might be calculated to be saturated or supersaturated with K-feldspar.

A7.3.3 Calculated ^{14}C Ages

The calculations of ^{14}C ages used the downgradient increase in the DIC concentrations of selected Yucca Mountain area groundwaters, relative to the DIC concentrations of Yucca Mountain perched waters to estimate the extent of ^{14}C dilution by calcite dissolution in the saturated zone (Section A6.3.6.6.2). The selected groundwater samples were chosen because they, like the perched water samples, had high $^{234}U/^{238}U$ activity ratios relative to many Yucca Mountain area groundwaters, thus indicating the likelihood of a common origin. The estimated increases in the DIC concentrations of the groundwaters were then used to reduce the initial ^{14}C activities to below their original atmospheric values to calculate a "corrected" ^{14}C age for the groundwater. The critical assumptions in this analysis are that (1) the perched water itself required no age corrections and (2) that the measured increases in groundwater DIC relative to perched water limit the amount of ^{14}C dilution by calcite. Assumption (1) appears to be valid based on the historic variations of $^{36}Cl/Cl$ and ^{14}C activities measured on organic carbon in pack-rat middens and similar relations between $^{36}Cl/Cl$ and ^{14}C activities measured for inorganic carbon in perched water. Assumption (2) requires that no reductions in groundwater DIC concentrations take place through exsolution of CO_2 during groundwater flow or during sampling. Although CO_2 losses from groundwater to the unsaturated zone are estimated to be small because of the low diffusion of CO_2 in groundwater, exsolution of CO_2 during groundwater sampling may be a more significant effect. However, groundwater at the wells where ^{14}C age corrections were made typically had relatively low (< 7.8) pH values, indicating that the effects of degassing on DIC concentrations during sample collection were minimal.

A7.3.4 Calculations of the Fractions of "Young" Water in Yucca Mountain Groundwaters

These calculations interpret the measured ^{14}C activities of groundwater beneath Yucca Mountain to result from the mixing of groundwater that has been recharged at different times from the unsaturated zone at Yucca Mountain. Although recharge may have been added continuously over time at varying rates to Yucca Mountain groundwater, the calculations simplify the actual distribution by assuming that the measured ^{14}C activities result from the mixing of an "old"

component and a "young" component that are widely separated in time. This approach effectively replaces the actual (but unknown) distribution of groundwater ages by a bimodal distribution of ages with the same mean age. This idealized distribution of ages places more emphasis on the very young and very old groundwaters than the actual age distribution would indicate. This method provides upper bounds to the fraction of young groundwater in the mixture, which is the quantity of interest in these calculations.

A7.3.5 PHREEQC Inverse Models of Groundwater Mixing and Water-Rock Interaction

The PHREEQC inverse models of groundwater mixing and water-rock interaction described in Section A6.3.8 are affected by uncertainties in the accuracy and representativeness of groundwater compositions (see Section A7.3.1), uncertainties in mineral-phase compositions, and uncertainties in the conceptual model. The uncertainties in the accuracy and representativeness of groundwater compositions are accounted for in the PHREEQC models through user-specified uncertainty criteria. Generally, uncertainties specified in the PHREEQC models were 10% or less of the measured concentrations for major and minor ions, 0.1 per mil for $\delta^{18}O$, 1.0 per mil for δD, 0.1 per mil for $\delta^{13}C$, and 0.05 pH units for pH. These uncertainties were intended to reflect not only analytical uncertainty in the measurements (See Section A7.3.1) but also the representativeness of the groundwater samples in light of the chemical and isotopic heterogeneity that exists in groundwaters from closely spaced wells. It was necessary to specify some uncertainty in these models in order to simultaneously satisfy the multiple mass-balance constraints involved in any particular model. There is also some variability in mineral phase compositions from Yucca Mountain and, hence, some uncertainty in specifying a single representative phase composition for the entire area. This variability is particularly true of clinoptilolites, which are known to have east-to-west chemical variations across the Yucca Mountain area (Broxton et al. 1987 [DIRS 102004]). Generally, clinoptilolite compositions used in any particular model were chosen to be representative of the area near the wells considered by that model. For reactions involving the dissolution or precipitation of calcite (or dolomite), it was necessary to specify the $\delta^{13}C$ composition of the calcite. The $\delta^{13}C$ compositions are variable in SZ calcites and, therefore, some uncertainty exists in choosing a single representative value. Calcite in the volcanic aquifers was assumed to have $\delta^{13}C$ values of between -4 ± 3 and -1 ± 3 per mil, whereas calcite in the alluvial aquifers near Fortymile Wash was assumed to be -4 ± 3 per mil. Although the values of $\delta^{13}C$ used for the volcanic aquifer are in agreement with measured values (Whelan et al. 1998 [DIRS 137305]), the isotopic characteristics of calcite in alluvium have not been measured at Yucca Mountain. The calcite in alluvium was assumed to have isotopic characteristics ($\delta^{13}C = -4$ per mil) similar to pedogenic calcite at the surface of Yucca Mountain (Table A5-1 in Assumption 9).

The specified uncertainty in solution compositions and in the isotopic composition of the minerals is propagated through the PHREEQC inverse models so that, for each model, upper and lower bounds are also estimated for the mixing ratios and amounts of each mineral phase dissolved. However, although quantitative measures of uncertainty are provided for each model discussed in this report (DTN: LA0310EK831232.001 [DIRS 165995]), these uncertainty estimates do not consider the other combinations of mineral reactions and mixing end members present in alternative models identified by PHREEQC. Additionally, these uncertainty estimates do not consider the conceptual model uncertainty.

Conceptual-model uncertainty includes the choice of mineral phases to be considered in a particular model, any constraints on the precipitation/dissolution or exchange reactions imposed on these phases, and the choice of groundwaters considered in these models as potential mixing components. The rationale behind selection of these various parameters is discussed in Section A6.3.8. It is acknowledged; however, that all possible combinations of these parameters were not exhaustively evaluated. Other combinations of end-member mixing components and reaction history could possibly be modeled to yield a particular downgradient water chemistry. Given all the potential combinations of mixing end members and reaction models, it is impossible to quantify uncertainty related to uncertainties in the conceptual model.

A7.3.6 Groundwater Velocities

The groundwater velocities calculated in Section A6.3.9 were based on the measured groundwater ^{14}C activities at wells defining a flow path segment, the linear distance between the wells, and the water-rock interactions identified by the PHREEQC models for that flow-path segment. The calculated velocities are, therefore, affected by the accuracy and representativeness of the groundwater ^{14}C measurements (see Section A7.3.1), the assumption that groundwater flows along a straight path between the wells defining the flow-path segment, and the uncertainties associated with the PHREEQC models, as described in Section A7.3.5. An indication of the quantitative uncertainty associated with transit times is provided by the standard deviations associated with transport times based on the PHREEQC models and differences between the means of these estimates and estimates made based on downgradient increases in DIC concentrations (Table A6-11). An additional uncertainty that may impact these calculations concerns the implicit assumption that no additional ^{14}C is added to the groundwater from downgradient recharge as the groundwater moves from the upgradient to downgradient wells defining a flow-path segment. Recharge at Yucca Mountain may not vary enough spatially to guarantee that upgradient and downgradient recharge could be recognized in a mixture.

A7.3.7 FEHM Groundwater Models of Nonreactive Tracer Transport in the Yucca Mountain Area

The FEHM simulations of nonreactive tracer transport described in Section A6.3.10 used the Yucca Mountain site-scale saturated zone flow model documented in *Water-Level Data Analysis for the Saturated Zone Site-Scale Flow and Transport Model* (BSC 2004 [DIRS 170008]), using the model input/output files in DTN: LA0304TM831231.002 [DIRS 163788]. Uncertainty in flow modeling arises from a number of sources including, but not limited to, the conceptual model of the processes affecting groundwater flow, water–level measurements and simplifications of the model geometry, boundary conditions, hydrogeologic unit extent and depth, and the values of permeability assigned to hydrogeologic units. Such uncertainties associated with this flow model are identified and quantified in *Saturated Zone Site-Scale Flow Model* (BSC 2004 [DIRS 170037], Section 6.8). An additional uncertainty that pertains to the tracer simulations but not the flow model itself concerns numerical dispersion associated with the advection/dispersion equation. Numerical dispersion would tend to cause greater apparent mixing and dilution than would be present solely because of hydraulic conductivity variations in the model. These effects are likely to have influenced the tracer concentration distributions shown in Section A6.3.10 and, in particular, the relatively dilute concentrations near the edges of these tracer plumes may be an artifact of this numerical dispersion.

A7.3.8 A Map of Groundwater Flow Paths for the Yucca Mountain Area

The map of groundwater flow paths in the Yucca Mountain area (Figure A6-62) was developed on the basis of areal variations of chemical and isotopic species (Section A6.3.4), scatterplots that indicated mixing between groundwaters from different areas (Section A6.3.7), and PHREEQC models of groundwater mixing and chemical evolution (Section A6.3.8). The flow-path map is affected, therefore, by the uncertainties already described for these associated technical data products in Sections A7.3.1, A7.3.2, and A7.3.5.

Possibly, the most important uncertainty in the flow path map relates to the source of the groundwater at well NC-EWDP-19D (Sites 92 and 94 to 98). Two equally plausible sets of groundwater mixing and reaction models were developed with PHREEQC for groundwater at well NC-EWDP-19D, each of which implies a different direction for groundwater flow from the repository area in southern Yucca Mountain. The first set of models indicates that groundwater from various depths at NC-EWDP-19D originates from groundwater in the Dune Wash area (represented by groundwater from well WT-3) and a set of water-rock-gas reactions. These results are represented on the flow-path map as the southern part of Flow Path 7. Groundwater from the repository area would be constrained by the southern part of Flow Path 7 to move predominantly southward or southwestward through southern Yucca Mountain, thereby avoiding most of the alluvium north of U.S. Highway 95. The second group of PHREEQC models for groundwater from various zones in well NC-EWDP-19D indicated that these groundwaters are a mixture of groundwaters from the Solitario Canyon Wash area (represented by groundwater from well WT-10) and local Yucca Mountain recharge (represented by perched water from borehole SD-7), plus a set of water-rock reactions. This origin for the groundwater at well NC-EWDP-19D indicates that groundwater from the repository area will follow a more southeasterly trajectory and would probably encounter more of the alluvium west of Fortymile Wash than is indicated by Flow Path 7. The leakage of groundwater from the Solitario Canyon area across the Solitario Canyon fault beneath Yucca Mountain is indicated by the southeast-trending arrows originating from Flow Path A6.

INTENTIONALLY LEFT BLANK

APPENDIX B
REEVALUATION OF CONSTRAINTS ON GROUNDWATER FLOW USING GEOCHEMICAL AND ISOTOPIC DATA FROM NYE COUNTY EARLY WARNING DRILLING PROGRAM WELLS

B1. PURPOSE

The purpose of this appendix is to provide an analysis of flow directions and velocities, and mixing proportions of water from different source areas based on groundwater geochemical and isotopic data. The analysis of hydrochemical and isotopic data is intended to provide a basis for evaluating the hydrologic system at Yucca Mountain independently of evaluations that are based purely on hydraulic arguments. In this way, this appendix is intended as an independent corroboration of the saturated zone flow model presented in the main text of this report.

This appendix provides a focused update of *Appendix A—Geochemical and Isotopic Constraints on Groundwater Flow* in *Saturated Zone Site-Scale Model* (BSC 2004 [DIRS 170037). Since the issuance of *Saturated Zone Site-Scale Flow Model* (BSC 2004 [DIRS 170037], Appendix A), several new boreholes have been drilled, and groundwater samples from these boreholes have been analyzed for hydrochemical and isotopic constituents. In addition, new hydrochemical data have also been obtained from several of the previously existing boreholes. This update primarily involves the incorporation of new data on major ion chemistry, $^{234}U/^{238}U$ activity ratios, and ^{14}C available as of September 2006. These new hydrochemical data are evaluated to determine their impacts on inferences about groundwater flowpaths and travel times from beneath the repository established in Appendix A. In so doing, this appendix also addresses condition report (CR) 6767, which asked if any new hydrochemical and isotopic data from Nye County wells, particularly ^{14}C activities and $^{234}U/^{238}U$ activity ratios, suggested trends counter to the conclusions and interpretations of groundwater flowpaths and travel times as documented in Appendix A of this report. This appendix analyzes the latest hydrochemical and isotopic data and confirms that none of it contradicts the conclusions and analyses in Appendix A.

Addressing these and related issues will help in determining the performance of the saturated zone as a natural barrier to radionuclide migration. The physical and hydrochemical parameters summarized in Appendix A and augmented by this appendix are important controls on the transport of dissolved and colloidal species in the saturated zone. This information can be used in the SZ site-scale flow and SZ transport models to simulate the transport of radionuclides as breakthrough curves. These breakthrough curves are then used as input in the TSPA-LA calculations.

This report is governed by the Office of Civilian Radioactive Waste Management *Technical Work Plan for Saturated Zone Flow and Transport Modeling* (BSC 2006 [DIRS 177375]). Activities listed in the TWP (BSC 2006 [DIRS 177375], Sections 1.2.2 and 1.2.7) that are appropriate to this appendix are documented in this report.

B2. QUALITY ASSURANCE

Planning and preparation of this appendix was initiated under the Bechtel SAIC Company (BSC) Quality Assurance Program. Therefore, forms and associated documentation prepared prior to October 2, 2006, the date this work transitioned to the Lead Laboratory, were completed in accordance with BSC procedures. Forms and associated documentation executed on or after October 2, 2006, were prepared in accordance with Lead Laboratory procedures.

Development of this appendix is subject to the Office of Civilian Radioactive Waste Management quality assurance program as indicated in the TWP (BSC 2006 [DIRS 177375]. Approved quality assurance procedures identified in Section 4 of the TWP (BSC 2006 [DIRS 177375]) have been used to conduct and document the activities described in this appendix:

- LP-7.5Q-OCRWM, *Establishing Deliverable Acceptance Criteria and Submitting and Reviewing Deliverables*
- DM-PRO-002, *Records Management*
- IT-PRO-0011, *Software Management*
- LS-PRO-001, *Technical Reports*
- SCI-PRO-003, *Document Review*
- SCI-PRO-004, *Managing Technical Product Inputs*
- SCI-PRO-006, *Models*
- TST-PRO-001, *Submittal and Incorporation of Data to the Technical Data Management System.*

These procedures are a deviation from the TWP (BSC 2006 [DIRS 177375]) and reflect the change to corresponding Sandia National Laboratories Lead Laboratory procedures. Section 8 of the TWP (BSC 2006 [DIRS 177375]) also identifies the methods used to control the electronic management of data.

B3. USE OF SOFTWARE

YMP-qualified software (CORPSCON V.5.11.08, STN: 10547-5.11.08-00 [DIRS 155082]) was used to convert borehole survey results from Nevada State Plane coordinates to UTM coordinates in NAD-27 (see Appendix F). The converted coordinates are reported in the following DTN:

- Output DTN: LA0612RR150304.001, UTM Coordinates for Selected Nye County Early Warning Drilling Program Boreholes: NC-EWDP-7SC and Phases III and IV.

Commercial, off-the-shelf software used in support of this analysis to create data plots is exempt from the qualification requirements of IM-PRO-003, but meets the acceptance criteria of being able to correctly produce plots of acceptable graphic quality in formats suitable for incorporation into this report.

- *EXCEL 2003* was used to preprocess data from DTNs to obtain representative average values. The calculation of basic statistics was used with standard functions only.

- *Adobe Illustrator CS2* was used to visualize and illustrate data to create flowpath maps.

- *AqQA* V3.7, was used to create trilinear diagrams showing proportions of major ions in groundwater and *x-y* scatter plots.

Outputs from *EXCEL*, *Adobe Illustrator*, and *AqQA* were visually checked for correctness. The data used to produce the outputs can be found in the Technical Data Management System (TDMS) within data packages that have been assigned data tracking numbers (DTN). The DTNs are identified in appropriate places throughout this appendix to allow the independent reviewer to reproduce or verify results by visual inspection or hand calculation.

B4. INPUTS

This appendix summarizes hydrochemistry data to ultimately derive hydrochemically inferred flow pathways. The data evaluations, including the derived flow pathways, are used to corroborate information put forth in the main body of this report. As such, this appendix does not require direct inputs nor does it produce qualified technical outputs. Output developed within this appendix is considered unqualified intermediary output.

Newly available geochemical and isotopic data are presented in Tables B4-1 through B4-9. These data inputs are listed below in three general categories: (a) geographic and depth-related data for new NC-EWDP wells (Table B4-1), (b) geochemical and isotopic data for these new wells (Tables B4-2 and B4-3), and (c) geochemical and isotopic data that fill data gaps for existing well locations from Appendix A (Tables B4-4 to B4-9). The new geochemical and isotopic data that were obtained from the TDMS were acquired primarily by the U.S. Geological Survey (USGS), the NC-EWDP, and the Nevada System of Higher Education through its cooperative agreement with the U.S. Department of Energy Yucca Mountain Site Characterization Office. The latter data source is signified by the use of UCC (shortened acronym for the University and Community College System of Nevada) in the source DTN identifiers listed below. Additional acquired data not found in the TDMS were extracted from the Underground Test Area (UGTA) Program's publicly available geochemical database (intermediary output DTN: LA0612RR150304.003). The relevant data in this database were acquired by the USGS, the Nye County Nuclear Waste Repository Program (NWRPO), the Harry Reid Center for Environmental Studies, the Desert Research Institute, and Lawrence Livermore National Laboratory.

Geographic coordinates, screen depths, and lithologies for the new Nye County wells and samples are listed in Table B4-1, which was compiled from the following DTNs:

- Output DTN (developed in Appendix F): LA0612RR150304.001, UTM Coordinates for Selected Nye County Early Warning Drilling Program Boreholes: NC-EWDP-7SC and Phases III and IV

- GS010908312332.002 [DIRS 163555], Borehole Data from Water-Level Data Analysis for the Saturated Zone Site-Scale Flow and Transport Model

- GS011008314211.001 [DIRS 158690], Interpretation of the Lithostratigraphy in Deep Boreholes NC-EWDP-19D1 and NC-EWDP-2DB Nye County Early Warning Drilling Program
- GS020108314211.001 [DIRS 174112], Interpretation of the Lithostratigraphy in Deep Boreholes, NC-EWDP-7SC and NC-EWDP-15D, Nye County Early Warning Drilling Program
- GS030108314211.001 [DIRS 163483], Interpretation of the Lithostratigraphy in Deep Boreholes NC-EWDP-18P, NC-EWDP-22SA, NC-EWDP-10SA, NC-EWDP-23P, NC-EWDP-19IM1A, and NC-EWDP-19IM2A, Nye County Early Warning Drilling Program, Phase III
- GS031108314211.004 [DIRS 174113], Interpretation of the Lithostratigraphy in Deep Boreholes NC-EWDP-16P, NC-EWDP-27P, and NC-EWDP-28P, Nye County Early Warning Drilling Program, Phase IV A
- GS040908314211.001 [DIRS 174114], Interpretation of the Lithostratigraphy in Deep Boreholes NC-EWDP-24P and NC-EWDP-29P, Nye County Early Warning Drilling Program, Phase IV B
- GS050708314211.001 [DIRS 179435], Description and Interpretation of Core Samples from Alluvial Core Holes NC-EWDP-19PB and NC-EWDP-22PC, Nye County Early Warning Drilling Program
- MO0112DQRWLNYE.014 [DIRS 157184], Well Completion Diagram for Borehole NC-EWDP-19P
- MO0112DQRWLNYE.018 [DIRS 157187], Well Completion Diagram for Borehole NC-EWDP-19D
- MO0110NYE03848.087 [DIRS 179436], NC-EWDP-Washburn-1X Well Completion Diagram
- MO0206NYE04926.119 [DIRS 179372], NC-EWDP-7SC Well Completion Diagram
- MO0306NYE05259.165 [DIRS 165876], Revised NC-EWDP-19IM1 Well Completion Diagram
- MO0306NYE05260.166 [DIRS 165877], Revised NC-EWDP-19IM2 Well Completion Diagram
- MO0306NYE05261.167 [DIRS 179373], Revised NC-EWDP-10S Well Completion Diagram
- MO0306NYE05262.168 [DIRS 179374], Revised NC-EWDP-10P Well Completion Diagram

- MO0306NYE05263.169 [DIRS 179375], Revised NC-EWDP-18P Well Completion Diagram
- MO0306NYE05264.170 [DIRS 179376], Revised NC-EWDP-22S Well Completion Diagram
- MO0306NYE05265.171 [DIRS 179377], Revised NC-EWDP-22PA Well Completion Diagram
- MO0306NYE05266.172 [DIRS 179378], Revised NC-EWDP-22PB Well Completion Diagram
- MO0306NYE05267.173 [DIRS 179379], Revised NC-EWDP-23P Well Completion Diagram
- MO0312NYE05716.204 [DIRS 179380], NC-EWDP-27P Well Completion Diagram
- MO0312NYE05718.202 [DIRS 179381], NC-EWDP-28P Well Completion Diagram
- MO0409NYE06093.241 [DIRS 179382], NC-EWDP-29P Well Completion Diagram
- MO0409NYE06096.242 [DIRS 179383], NC-EWDP-24P Well Completion Diagram
- MO0409NYE06101.246 [DIRS 179384], NC-EWDP-19PB Well Completion Diagram
- MO0702NYE05714.375 [DIRS 179443], NC-EWDP-16P Well Completion Diagram.

Geochemical and isotopic compositions for the new Nye County wells (Tables B4-2 and B4-3) derive from a large number of DTNs as well as from sources outside the YMP. The source data are compiled, evaluated, developed and averaged in the following intermediary output DTNs:

- LA0612RR150304.002, Hydrochemical Data Obtained from the Underground Test Area (UGTA) Program's Geochem05 Database
- LA0612RR150304.003, Geochemical and Isotopic Data for Selected NC-EWDP Wells, Phases II, III, and IV
- LA0612RR150304.005, Uranium Activity Ratios Calculated from Isotopic Ratios Reported for Nye County EWDP Boreholes and McCracken Well by Geochron Laboratories, for Samples Collected between November 1999 and June 2000.

Some new geochemical and isotopic data were considered inappropriate for use in this analysis. Reasons for considering data inappropriate include water samples collected prior to well completion, samples with problems noted during collection, samples with inadequate specification of the sampled depth interval in the source DTN, and outliers. These reasons and other considerations are documented in the supporting documentation for the above DTNs.

New geochemical and isotopic data for existing wells (Tables B4-4 to B4-9, Figure B6-14) are taken from the following acquired and developed DTNs:

- GS010608315215.002 [DIRS 156187], Uranium and Thorium Isotope Data for Waters Analyzed between January 18, 1994 and September 14, 1996
- GS031208312322.004 [DIRS 179431], Dissolved Organic Carbon-14 (DOC-14) Hydrochronology Data for Groundwater from Wells in the Yucca Mountain Area for Samples Analyzed through 1/30/2003
- GS040108312322.001 [DIRS 179422], Field and Chemical Data Collected between 10/4/01 and 10/3/02 and Isotope Data Collected between 5/19/00 and 5/22/03 from Wells in the Yucca Mountain Area, Nye County, Nevada
- GS040708312322.004 [DIRS 179432], Strontium Isotope Ratios and Strontium Concentrations on Groundwater Samples from Springs in the Area of Amargosa Valley and Desert
- GS040808312322.005 [DIRS 179433], Strontium Isotope Ratios and Strontium Concentrations on Groundwater Samples in Support of Nye Co. Early Warning Drilling Program (EWDP) and the Alluvial Tracer Complex (ATC)
- GS040808312322.006 [DIRS 179434], Field, Chemical, and Isotope Data for Spring and Well Samples Collected between 03/01/01 and 05/12/04 in the Yucca Mountain Area, Nye County, Nevada
- Output DTN: LA0612RR150304.002, Hydrochemical Data Obtained from the Underground Test Area (UGTA) Program's Geochem05 Database
- Output DTN: LA0612RR150304.005, Uranium Activity Ratios Calculated from Isotopic Ratios Reported for Nye County EWDP Boreholes and McCracken Well by Geochron Laboratories, for Samples Collected between November 1999 and June 2000
- MO0310UCC008IF.003 [DIRS 179440], Major Cation, Major Anion, and Trace Element Concentrations in Groundwater Collected from the October 2000 Sampling of Phase II and III Wells of the Nye County Early Warning Drilling Program (NC-EWDP)
- MO0311UCC008IF.007 [DIRS 179441], Major Cation, Major Anion, and Trace Element Concentrations in Groundwater Collected during the May 2000 Sampling of Phase I and II Wells of the Nye County Early Warning Drilling Program (NC-EWDP)
- UN0010SPA008KS.001 [DIRS 179442], Major Cation, Major Anion, and Trace Element Concentrations in Groundwaters Collected from Bond Gold Well, SD-6ST1, and the May 99 Sampling of the Phase I Wells of the Nye County Early Warning Drilling Program (EWDP).

Table B4-1. Geographic and Geologic Data Sources for New Nye County Boreholes and Zones

Well Identifier[a]	Assigned Sample ID[a]	UTM-X[b] (m)	UTM-Y[b] (m)	Area[c]	Interval Sampled	Geologic Unit[d]	DTN References for Sampled Depth and Geologic Unit
NC-EWDP-07SC Zone 1	203	539632	4064317	CF-SW Crater Flat—Southwest	80.0 to 90.0 ft 24.4 to 27.4 m (screen)	QTu	MO0206NYE04926.119 [DIRS 179372] GS020108314211.001 [DIRS 174112]
NC-EWDP-07SC Zone 2	204	539632	4064317	CF-SW Crater Flat—Southwest	180.0 to 210.0 ft 54.9 to 64.0 m (screen)	QTu	
NC-EWDP-07SC Zone 3	205	539632	4064317	CF-SW Crater Flat—Southwest	270.0 to 370.0 ft 82.3 to 112.8 m (screen)	Tmr	
NC-EWDP-07SC Zone 4	206	539632	4064317	CF-SW Crater Flat—Southwest	429.8 to 449.8 ft 131.0 to 137.1 m (screen)	Tmr	
NC-EWDP-07SC Zone 5	207	539632	4064317	CF-SW Crater Flat—Southwest	470.0 to 778.5 ft 143.2 to 237.3 m (bottom of borehole, filled with natural fill and drill cuttings)	Tmr, Tpt, Tcp, Tcb	
NC-EWDP-10P Zone 1	208	553149	4064916	FMW-N Fortymile Wash—North	660.1 to 699.3 ft 201.2 to 213.1 m (screen)	QTu[e]	MO0306NYE05262.168 [DIRS 179374] GS030108314211.001 [DIRS 163483]
NC-EWDP-10P Zone 2	209	553149	4064916	FMW-N Fortymile Wash—North	801.2 to 860.0 ft 244.2 to 262.1 m (screen)	Tab[e]	
NC-EWDP-10S composite	210	553140	4064899	FMW-N Fortymile Wash—North	660.0 to 860.0 ft 201.2 to 262.1 m (screen)	QTu, Tab	MO0306NYE05261.167 [DIRS 179373] GS030108314211.001 [DIRS 163483]
NC-EWDP-10S Zone 1	211	553140	4064899	FMW-N Fortymile Wash—North	660.0 to 700.0 ft 201.2 to 213.3 m (screen)	QTu	
NC-EWDP-10S Zone 2	212	553140	4064899	FMW-N Fortymile Wash—North	800.0 to 860.0 ft 243.8 to 262.1 m (screen)	Tab	

Table B4-1. Geographic and Geologic Data Sources for New Nye County Boreholes and Zones (Continued)

Well Identifier[a]	Assigned Sample ID[a]	UTM-X[b] (m)	UTM-Y[b] (m)	Area[c]	Interval Sampled[a]	Geologic Unit[d]	DTN References for Sampled Depth and Geologic Unit
NC-EWDP-16P composite	213	545665	4064263	YM-S Yucca Mountain—South	489.4 to 549.4 ft 149.2 to 167.4 m (screen)	Tmr	MO0702NYE05714.375 [DIRS 179443] GS031108314211.004 [DIRS 174113]
NC-EWDP-18P composite	214	549416	4067233	YM-S Yucca Mountain--South	835.8 to 885.0 ft 254.7 to 269.7 m (screen)	Tpts	MO0306NYE05263.169 [DIRS 179375] GS030108314211.001 [DIRS 163483]
NC-EWDP-19D Zones 5-7	215	549317	4058270	YM-S Yucca Mountain—South	882.2 to 980.3 ft 268.9 to 298.8 m 1122.1 to 1219.6 ft 342.0 to 371.6 m 1296.7 to 1379.7 ft 395.2 to 420.5 m (3 screens)	Tpt, Tpts, Tge	MO0112DQRWLNYE.018 [DIRS 157187] GS011008314211.001 [DIRS 158690]
NC-EWDP-19IM1 Composite	216	549317	4058291	YM-S Yucca Mountain—South	Not reported	QTu, Tpt	MO0306NYE05259.165 [DIRS 165876] GS030108314211.001 [DIRS 163483]
NC-EWDP-19IM1 Zone 1	217	549317	4058291	YM-S Yucca Mountain—South	410.0 to 430.0 ft 125.0 to 131.1 m (screen)	QTu	
NC-EWDP-19IM1 Zone 2	218	549317	4058291	YM-S Yucca Mountain—South	515.0 to 535.0 ft 157.0 to 163.1 m (screen)	QTu	
NC-EWDP-19IM1 Zone 3	219	549317	4058291	YM-S Yucca Mountain—South	574.9 to 674.9 ft 175.2 to 205.7 m (screen)	QTu	
NC-EWDP-19IM1 Zone 4	220	549317	4058291	YM-S Yucca Mountain—South	724.9 to 784.8 ft 220.9 to 239.2 m (screen)	QTu	
NC-EWDP-19IM1 Zone 5	221	549317	4058291	YM-S Yucca Mountain—South	849.5 to 949.3 ft 258.9 to 289.3 m (screen)	Tpt	
NC-EWDP-19IM2 Composite	222	549337	4058291	YM-S Yucca Mountain—South	Not reported	QTu, Tpt	MO0306NYE05260.166 [DIRS 165877] GS030108314211.001 [DIRS 163483]

Table B4-1. Geographic and Geologic Data Sources for New Nye County Boreholes and Zones (Continued)

Well Identifier[a]	Assigned Sample ID[a]	UTM-X[b] (m)	UTM-Y[b] (m)	Area[c]	Interval Sampled[a]	Geologic Unit[d]	DTN References for Sampled Depth and Geologic Unit
NC-EWDP-19P	223	549329	4058292	YM-S Yucca Mountain—South	359.2 to 458.6 ft 109.5 to 139.8 m (screen)	QTu[f]	MO0112DQRWLNYE.014 [DIRS 157184] GS011008314211.001 [DIRS 158690]
NC-EWDP-19PB Zone 1	224	549337	4058316	YM-S Yucca Mountain—South	375.0 to 395.0 ft 114.3 to 120.4 m (screen)	QTu	MO0409NYE06101.246 [DIRS 179384] GS050708314211.001 [DIRS 179435]
NC-EWDP-19PB Zone 2	225	549337	4058316	YM-S Yucca Mountain—South	514.7 to 534.7 ft 156.9 to 163.0 m (screen)	QTu	
NC-EWDP-22PA Zone 1	226	552020	4062038	FMW-N Fortymile Wash—North	520.7 to 579.7 ft 158.7 to 176.7 m (screen)	QTu[g]	MO0306NYE05265.171 [DIRS 179377] GS030108314211.001 [DIRS 163483]
NC-EWDP-22PA Zone 2	227	552020	4062038	FMW-N Fortymile Wash—North	661.5 to 759.8 ft 201.6 to 231.6 m (screen)	QTu[g]	
NC-EWDP-22PB Zone 1	228	552038	4062037	FMW-N Fortymile Wash—North	881.3 to 979.7 ft 268.8 to 298.6 m (screen)	QTu[g]	MO0306NYE05266.172 [DIRS 179378] GS030108314211.001 [DIRS 163483]
NC-EWDP-22PB Zone 2	229	552038	4062037	FMW-N Fortymile Wash—North	1,140.3 to 1,179.7 ft 347.5 to 359.6 m (screen)	QTu[g]	
NC-EWDP-22S Zone 1	230	552019	4062020	FMW-N Fortymile Wash—North	521.5 to 581.3 ft 159.1 to 176.7 m (screen)	QTu	MO0306NYE05264.170 [DIRS 179376] GS030108314211.001 [DIRS 163483]

Table B4-1. Geographic and Geologic Data Sources for New Nye County Boreholes and Zones (Continued)

Well Identifier[a]	Assigned Sample ID[a]	UTM-X[b] (m)	UTM-Y[b] (m)	Area[c]	Interval Sampled[a]	Geologic Unit[d]	DTN References for Sampled Depth and Geologic Unit
NC-EWDP-22S Zone 2	231	552019	4062020	FMW-N Fortymile Wash—North	661.2 to 760.6 ft 201.8 to 231.5 m (screen)	QTu	
NC-EWDP-22S Zone 3	232	552019	4062020	FMW-N Fortymile Wash—North	880.2 to 980.0 ft 268.8 to 298.5 m (screen)	QTu	
NC-EWDP-22S Zone 4	233	552019	4062020	FMW-N Fortymile Wash—North	1,140.0 to 1,180.0 ft 348.1 to 359.5 m (screen)	Tab	
NC-EWDP-23P Zone 1	234	553924	4059875	LW Amargosa Valley	460.9 to 519.9 ft 140.2 to 158.5 m (screen)	QTu	MO0306NYE05267.173 [DIRS 179379] GS030108314211.001 [DIRS 163483]
NC-EWDP-23P Zone 2	235	553924	4059875	LW Amargosa Valley	650.5 to 689.8 ft 198.1 to 210.3 m (screen)	QTu	
NC-EWDP-24P	236	549386	4062055	YM-S Yucca Mountain—South	400.0 to 440.0 ft 121.9 to 134.1 m (screen)	Tcb	MO0409NYE06096.242 [DIRS 179383] GS040908314211.001 [DIRS 174114]
NC-EWDP-27P	237	544935	4065276	YM-S Yucca Mountain—South	580.7 to 620.6 ft 177.0 to 189.1 m (screen)	Tpt	MO0312NYE05716.204 [DIRS 179380] GS031108314211.004 [DIRS 174113]
NC-EWDP-28P	238	545746	4062393	YM-S Yucca Mountain—South	370.0 to 449.0 ft 112.8 to 136.8 m (screen)	Tma, Tmabt	MO0312NYE05718.202 [DIRS 179381] GS031108314211.004 [DIRS 174113]

Table B4-1. Geographic and Geologic Data Sources for New Nye County Boreholes and Zones (Continued)

Well Identifier[a]	Assigned Sample ID[a]	UTM-X[b] (m)	UTM-Y[b] (m)	Area[c]	Interval Sampled[a]	Geologic Unit[d]	DTN References for Sampled Depth and Geologic Unit
NC-EWDP-29P	239	549396	4059606	YM-S Yucca Mountain—South	340.0 to 390.0 ft 103.6 to 118.9 m (screen)	Tpc, Tpbt4	MO0409NYE06093.241 [DIRS 179382] GS040908314211.001 [DIRS 174114]
NC-EWDP-Washburn-1X[h] Zone 2	240	551465	4057563	FMW-N Fortymile Wash—North	420.0 to 480.0 ft 128.0 to 146.3 m (screen)	unknown	MO0110NYE03848.087 [DIRS 179436] NA

UTM = Universal Transverse Mercator.

[a] The well identifier includes the designator "Zone" to indicate that the sample derives from a discrete portion of the borehole length, usually a screened interval. The borehole interval included in a specified zone is defined in the table column labeled "Interval Sampled." Sample IDs are assigned to these new samples sequentially, starting with the number immediately following the last one assigned in Table A4-3. Sample locations are labeled with their assigned sample identifiers in Figure B6-1.

[b] Data source for UTM coordinates: DTN: GS010908312332.002 [DIRS 163555] for NC-EWDP-19D, NC-EWDP-19P and NC-EWDP-Washburn-1X; Output DTN: LA0612RR150304.001 for all others (developed in Appendix F). Throughout this appendix, UTM-X is used to refer to UTM-Easting, and UTM-Y refers to UTM-Northing.

[c] See Figure A6-5 and Section A6.7.2 for a definition of these subareas, or hydrochemical groups, in the vicinity of Yucca Mountain. Section B6.2 describes the basis used to assign each new groundwater sample to one of these subareas.

[d] Geologic units: QTu, Quaternary and Tertiary alluvium (undivided); Tab Tertiary sedimentary rocks; Tge Pre-volcanic Tertiary sedimentary rocks; Tma Ammonia Tanks Tuff; Tmabt, Pre-Ammonia Tanks Tuff bedded tuff; Tmr Rainier Mesa Tuff; Tpbt4 Pre-Tiva Canyon Tuff; Tpc Tiva Canyon Tuff; Tpt Topopah Spring Tuff; Tpts Pre-Topopah Spring Sedimentary Rocks.

[e] The identification of geologic units for zones 1 and 2 in NC-EWDP-10P is extrapolated from those reported for these depths in the nearby borehole NC-EWDP-10SA in DTN: GS030108314211.001 [DIRS 163483].

[f] The identification of geologic units for NC-EWDP-19P is extrapolated from those reported for these depths in the nearby borehole NC-EWDP-19D1 in DTN: GS011008314211.001 [DIRS 158690].

[g] The identification of geologic units for zones 1 and 2 in NC-EWDP-22PA and zones 1 and 2 in NC-EWDP-22PB is extrapolated from those reported for these depths in the nearby borehole NC-EWDP-22SA in DTN: GS030108314211.001 [DIRS 163483].

[h] DTNs are inconsistent in the use of a hole name for NC-EWDP-Washburn-1X with or without "EWDP." In this appendix, it was judged best to maintain a uniform usage of the inclusion of "EWDP" in the identifier.

Table B4-2. Field Parameters and Average Major Ion Compositions for New Wells

Well Identifier	Sample ID Assigned in Table B4-1	Sample Temperature (°C)	pH	Ca^{2+} (mg/L)	Mg^{2+} (mg/L)	Na^{+} (mg/L)	K^{+} (mg/L)	Cl^{-} (mg/L)	SO_4^{2-} (mg/L)	HCO_3^{-} (mg/L)	CO_3^{2-} (mg/L)	F^{-} (mg/L)	SiO_2 (mg/L)
NC-EWDP-07SC Zone 1	203	19, 33	7.5	76	37	84	5.9	15.1	151	418	0	0.8	22
NC-EWDP-07SC Zone 2	204	14, 23	7.3	77	37	84	6.0	15.2	153	438	0	0.8	22
NC-EWDP-07SC Zone 3	205	20, 23	7.7	69	37	87	7.3	16.7	146	435	0	0.8	27
NC-EWDP-07SC Zone 4	206	—	8.2	28	28	85	8.6	15.9	128	288	0	0.8	28
NC-EWDP-07SC Zone 5	207	—	—	—	—	—	—	—	—	—	—	—	—
NC-EWDP-10P Zone 1	208	26	7.6	14	2.2	44	5.8	6.6	20	134	0	2.1	58
NC-EWDP-10P Zone 2	209	22, 30	7.6	15	2.3	41	5.7	6.3	19	130	0	2.1	60
NC-EWDP-10S composite	210	28	7.8	15	2.4	41	5.8	6.3	20	126	0	1.9	59
NC-EWDP-10S Zone 1	211	22, 30	7.8	14	2.4	42	5.9	6.6	19	135	0	2.1	59
NC-EWDP-10S Zone 2	212	22, 31	7.9	11	1.7	51	5.4	6.7	20	147	0	2.0	54
NC-EWDP-16P composite	213	—	8.5	0.8	0.08	106	1.7	8.5	55	190	5	2.7	44
NC-EWDP-18P composite	214	27, 34	8.1	9.8	0.1	68	1.8	7.0	21	174	0	2.5	48
NC-EWDP-19D Zones 5-7	215	31	9.0	0.6	0.03	113	3.5	5.5	20	224	22	2.2	60
NC-EWDP-19IM1 composite[a]	216	—	8.7	2.9	0.2	96	3.3	6.3	26	206	6	2.0	57
NC-EWDP-19IM1 Zone 1	217	18	8.7	2.1	0.3	95	3.2	5.3	17	216	10	2.2	58
NC-EWDP-19IM1 Zone 2[a]	218	29	8.5	5.9	0.5	77	3.3	6.0	22	193	4	2.0	56
NC-EWDP-19IM1 Zone 3[a]	219	30	8.6	1.1	0.03	101	3.4	6.2	25	218	9	2.0	57
NC-EWDP-19IM1 Zone 4[a]	220	31	9.1	0.7	0.02	107	3.2	5.5	17	209	23	2.3	59
NC-EWDP-19IM1 Zone 5	221	31	8.8	0.5	0.04	98	2.9	5.2	16	206	16	2.1	62
NC-EWDP-19IM2 composite	222	32	8.8	0.3	0.02	100	3.1	5.2	16	217	12	2.1	62
NC-EWDP-19P	223	—	7.7	18	1.5	45	3.8	6.4	20	143	0	1.7	53
NC-EWDP-19PB Zone 1	224	—	8.3	14	1.4	56	3.9	6.5	29	149	0	1.7	47
NC-EWDP-19PB Zone 2	225	—	8.4	7.8	0.6	80	3.1	5.7	23	203	1	1.5	56
NC-EWDP-22PA Zone 1	226	28	7.5	15	2.5	43	5.4	6.4	19	126	0	2.0	53
NC-EWDP-22PA Zone 2	227	24, 28	7.4	20	2.9	37	5.1	6.5	21	131	0	1.6	58
NC-EWDP-22PB Zone 1	228	29	7.9	25	3.3	39	5.6	6.3	22	157	0	1.0	56
NC-EWDP-22PB Zone 2	229	28	7.9	23	3.0	46	5.0	6.1	27	157	0	0.9	44

Table B4-2. Field Parameters and Average Major Ion Compositions for New Wells (Continued)

Well Identifier	Sample ID assigned in Table B4-1	Sample Temperature (°C)	pH	Ca^{2+} (mg/L)	Mg^{2+} (mg/L)	Na^{+} (mg/L)	K^{+} (mg/L)	Cl^{-} (mg/L)	SO_4^{2-} (mg/L)	HCO_3^{-} (mg/L)	CO_3^{2-} (mg/L)	F^{-} (mg/L)	SiO_2 (mg/L)
NC-EWDP-22S Zone 1	230	28	7.6	15	2.6	39	5.3	6.3	18	124	0	1.7	54
NC-EWDP-22S Zone 2	231	28	7.8	18	2.8	37	5.2	6.4	21	138	0	1.4	48
NC-EWDP-22S Zone 3	232	28	7.9	22	3.1	37	5.5	6.4	19	141	0	1.1	52
NC-EWDP-22S Zone 4	233	29	8.0	20	2.6	41	5.1	5.9	20	142	0	1.0	51
NC-EWDP-23P Zone 1	234	25	7.9	25	5.2	90	8.2	13.6	127	173	0	1.4	41
NC-EWDP-23P Zone 2	235	25	8.4	16	0.9	119	4.2	10.8	155	149	4	1.1	35
NC-EWDP-24P	236	32	7.9	15	0.9	53	3.1	6.7	24	164	—	2.2	38[b]
NC-EWDP-27P	237	—	8.4	5.0	1.0	102	3.7	9.0	39	222	5	3.7	39
NC-EWDP-28P	238	29	8.6	3.7	0.4	101	4.2	7.6	32	213	10	2.1	67
NC-EWDP-29P	239	26	8.1	16	1.2	52	4.3	6.3	21	151	—	2.1	60[b]
NC-EWDP-Washburn-1X Zone 2	240	—	7.7	20	2.7	37	4.8	6.9	27	127	0	1.4	55

Source: Output DTN: LA0612RR150304.003.

[a] The only water-quality sample available for this interval was collected less than 3 months after well completion, and may not be representative of undisturbed chemistry.

[b] Analyses for this analyte are only available for a sample that was collected less than 3 months after well completion, and may not be representative of undisturbed chemistry.

Table B4-3. Average Isotope and Trace Element Compositions for New Wells

Well Identifier	Sample ID assigned in Table B4-1	δ^{13}C-DIC (per mil)	^{14}C-DIC (pmc)	δD (per mil)	δ^{18}O (per mil)	δ^{34}S (per mil)	U (µg/L)	^{234}U/^{238}U Activity Ratio	Sr^{2+} (µg/L)	^{87}Sr/^{86}Sr (ratio)	δ^{87}Sr (per mil)
NC-EWDP-07SC Zone 1	203	−4.8	5.6	−98.8	−13.3	14.3	5.5	—	510	0.71351	6.1
NC-EWDP-07SC Zone 2	204	−4.7	5.5	−98.3	−13.3	14.3	5.5	—	522	0.71334	5.8
NC-EWDP-07SC Zone 3	205	−4.8	6.0	−98.0	−13.3	16.1	3.0	—	549	0.71287	5.2
NC-EWDP-07SC Zone 4	206	−5.7	6.9	−97.8	−13.4	21.7	0.2	—	365	0.71229	4.4
NC-EWDP-07SC Zone 5	207	—	—	—	—	—	—	—	—	—	—
NC-EWDP-10P Zone 1	208	−10.2	24.7	−98.5	−13.1	9.6	0.9	—	62	0.71122	2.8
NC-EWDP-10P Zone 2	209	−10.0	24.1	−96.8	−13.2	9.7	0.9	—	60	0.71122	2.8
NC-EWDP-10S composite	210	−8.8	26.2	−100.0	−12.7	9.7	0.7	—	53	—	—
NC-EWDP-10S Zone 1	211	−9.1	24.3	−99.5	−13.1	9.9	0.7	—	62	0.71103	2.6
NC-EWDP-10S Zone 2	212	−8.4	24.4	−97.3	−13.2	9.2	0.9	—	55	0.71047	1.8
NC-EWDP-16P composite	213	−8.5	16.8	−99.5	−13.6	4.7	3.9	—	8.8	—	—
NC-EWDP-18P composite	214	−8.1	21.0	−102.3	−13.7	12.2	2.5	—	25	0.70931	0.2
NC-EWDP-19D Zones 5-7	215	−7.1	9.2	−106.0	−13.2	9.6	2.6	—	1.1	0.71025	1.5
NC-EWDP-19IM1 composite [a]	216	−8.9	—	−104.5	−13.4	9.3	1.7	—	8.2	0.71081	2.3
NC-EWDP-19IM1 Zone 1 [a]	217	−6.0	12.5	−105.0	−14.0	11.2	2.8	—	17	0.70970	0.7
NC-EWDP-19IM1 Zone 2 [a]	218	−9.5	14.9	−100.0	−11.8	9.2	2.0	—	18	0.71069	2.1
NC-EWDP-19IM1 Zone 3 [a]	219	−7.0	11.4	−103.0	−13.0	9.8	1.9	—	2.0	0.71043	1.7
NC-EWDP-19IM1 Zone 4 [a]	220	−7.5	9.0	−101.5	−12.1	11.2	1.6	—	1.4	0.70990	1.0
NC-EWDP-19IM1 Zone 5 [a]	221	−6.8	6.4	−104.5	−13.8	11.6	2.0	—	1.9	0.71000	1.1
NC-EWDP-19IM2 composite	222	−7.0	5.9	−104.5	−13.9	11.9	2.2	—	1.0	0.71117	2.8
NC-EWDP-19P	223	−7.9	20.3	−100.0	−13.5	11.3	0.8	5.1	61	0.71143	3.1
NC-EWDP-19PB Zone 1	224	−8.4	20.6	—	—	8.0	2.0	—	81	0.71007	1.2
NC-EWDP-19PB Zone 2	225	−6.8	10.9	—	—	9.8	3.1	—	36	0.71002	1.2
NC-EWDP-22PA Zone 1	226	−10.5	24.1	−99.0	−13.1	8.2	0.9	—	65	0.71090	2.4
NC-EWDP-22PA Zone 2	227	−10.0	21.7	−97.5	−13.3	9.5	0.5	—	70	0.71060	2.0
NC-EWDP-22PB Zone 1	228	−9.5	20.3	−97.8	−13.2	9.1	1.1	—	101	0.71036	1.6
NC-EWDP-22PB Zone 2	229	−10.7	21.8	−96.8	−13.1	8.3	1.6	—	79	0.71059	2.0
NC-EWDP-22S Zone 1	230	−9.1	22.7	−98.3	−13.1	9.5	0.4	—	59	0.71093	2.4
NC-EWDP-22S Zone 2	231	−7.6	20.9	−98.4	−13.1	9.9	0.5	—	73	0.71047	1.8

Table B4-3. Average Isotope and Trace Element Compositions for New Wells (Continued)

Well Name	Sample ID assigned in Table B4-1	δ^{13}C-DIC (per mil)	^{14}C-DIC (pmc)	δD (per mil)	δ^{18}O (per mil)	δ^{34}S (per mil)	U (µg/L)	^{234}U/^{238}U Activity Ratio	Sr^{2+} (µg/L)	^{87}Sr/^{86}Sr (ratio)	δ^{87}Sr (per mil)
NC-EWDP-22S Zone 3	232	−8.1	19.6	−98.8	−13.1	9.9	0.7	—	92	0.71044	1.8
NC-EWDP-22S Zone 4	233	−8.8	20.2	−98.5	−13.0	8.9	0.7	—	78	0.71038	1.7
NC-EWDP-23P Zone 1	234	−10.5	23.6	−101.0	−13.1	5.1	5.9	—	132	0.71054	1.9
NC-EWDP-23P Zone 2	235	−10.6	20.8	−104.3	−13.3	2.1	3.7	—	134	0.70944	0.3
NC-EWDP-24P [a]	236	−8.1	17.2	−104.0	−13.6	12.3	0.8	—	68	—	—
NC-EWDP-27P	237	−7.3	12.4	−102.0	−13.6	11.1	4.4	—	45	—	—
NC-EWDP-28P	238	−11.6	16.0	−101.5	−13.5	8.9	4.7	—	33	—	—
NC-EWDP-29P [a]	239	−8.8	20.2	−102.0	−13.3	10.2	1.0	—	70	0.71040	1.7
NC-EWDP-Washburn-1X Zone 2	240	−9.4	21.3	−101.3	−13.2	9.3	0.7	—	70	0.71009	1.3

Sources: Output DTNs: LA0612RR150304.002, LA0612RR150304.003, LA0612RR150304.005.

DIC = dissolved inorganic carbon; pmc = percent modern carbon.

[a] The only water-quality sample available for this well was collected less than 3 months after well completion, and may not be representative of undisturbed chemistry.

Table B4-4. Additional Data on Field Parameters and Major Ion Compositions for Well Cited in Appendix A

Well Identifier	Sample ID on Figure A6-5	Temperature (°C)	pH	Ca^{2+} (mg/L)	Mg^{2+} (mg/L)	Na^{+} (mg/L)	K^{+} (mg/L)	Cl^{-} (mg/L)	SO_4^{2-} (mg/L)	HCO_3^{-} (mg/L)	CO_3^{2-} (mg/L)	F^{-} (mg/L)	SiO_2 (mg/L)
U.S. Ecology MR-3 (Bond Gold Mining Well #12 (BGMW12)) (16-Aug-89, 18-May-99)	18	—	7.7[a]	47.5	18	161	10.5	80	195	325.0[a]	0.0[a]	3.2	67.5

Source: Output DTN: LA0612RR150304.002.

[a] Value from Table A6-1.

Table B4-5. Additional Data on Strontium Isotopic Compositions for Wells Cited in Appendix A

Well Identifier	Sample ID on Figure A6-5	Sr^{2+} (µg/L)	$^{87}Sr/^{86}Sr$ (ratio)	$\delta\ ^{87}Sr$ (per mil)[a]	Source DTN[a]
ER-EC-08	1	2.2	0.70864[c]	−0.8	LA0612RR150304.002 (Output DTN)
Bond Gold Mining #1 (BGMW1)[d]	14	157	0.71028	1.5	GS040708312322.004 [DIRS 179432]
US Ecology MW-313	15	398	0.71197	3.9	GS040708312322.004 [DIRS 179432]
US Ecology MW-600[b]	16	363	0.71202	4.0	GS040708312322.004 [DIRS 179432]
U.S. Ecology MR-3 (Bond Gold Mining Well #12 (BGMW12))[d]	18	390	0.71196	3.9	GS040708312322.004 [DIRS 179432]
USW SD-6	50	0.4	0.71106	2.6	LA0612RR150304.002 (Output DTN) UN0010SPA008KS.001 [DIRS 179442]
J-11	67	264[c]	0.70935	0.2	LA0612RR150304.002 (Output DTN)
NC-EWDP-07S	71	641	0.71322	5.7	GS040808312322.005 [DIRS 179433]
NC-EWDP-07SC[b,e]	72	562	0.71329	5.8	GS040808312322.005 [DIRS 179433]
NC-EWDP-01DX (borehole)	73	510[c]	0.71280	5.1	LA0612RR150304.002 (Output DTN)
NC-EWDP-01S[b,e]	77	557[c]	0.71288	5.2	GS040808312322.005 [DIRS 179433]
NC-EWDP-03D (SMF Barcode 537190)[b]	86	2.5	0.71016	1.4	GS040808312322.005 [DIRS 179433]
NC-EWDP-02D	91	53.0[c]	0.71161	3.4	GS040808312322.005 [DIRS 179433]
NC-EWDP-19D (alluvial; Zones 1 to 4)[b,e]	94	7.5[c]	0.71100	2.5	GS040808312322.005 [DIRS 179433]
NC-EWDP-19D (Zone 1) (SMF Barcode 571011)[b]	95	34	0.71129	3.0	GS040808312322.005 [DIRS 179433]
NC-EWDP-19D (Zone 2) (SMF Barcode 554583)[b]	96	39	0.71120	2.8	GS040808312322.005 [DIRS 179433]
NC-EWDP-19D (Zone 3) (SMF Barcode 554543)[b]	97	2.2	0.71052	1.9	GS040808312322.005 [DIRS 179433]
NC-EWDP-19D (Zone 4) (SMF Barcode 553974)[b]	98	2.2	0.71107	2.6	GS040808312322.005 [DIRS 179433]
Desert Farms Garlic Plot (DFGP)[d]	101	144[c]	0.70973	0.8	GS040708312322.004 [DIRS 179432]
Airport Well[b]	106	24.0[c]	0.70984	0.9	GS040708312322.004 [DIRS 179432]
Barrachman Domestic / Irrigation	116	473[c]	0.71770	12.0	GS040708312322.004 [DIRS 179432]
Selbach Domestic	121	217[c]	0.71472	7.8	GS040708312322.004 [DIRS 179432]
Funeral Mountain Ranch Irrig	126	114[c]	0.71664	10.5	GS040708312322.004 [DIRS 179432]
DeLee Large Irrigation	133	110[c]	0.71169	3.5	GS040708312322.004 [DIRS 179432]
Bray Domestic	136	101[c]	0.71163	3.4	GS040708312322.004 [DIRS 179432]
Amargosa Estates #2[d]	137	129[c]	0.71286	5.2	GS040708312322.004 [DIRS 179432]
O'Neill Domestic	145	109[c]	0.71136	3.0	GS040708312322.004 [DIRS 179432]
Ponderosa Dairy	149	248[c]	0.71216	4.2	GS040708312322.004 [DIRS 179432]
M. Gilgan Well[d]	152	155[c]	0.71287	5.2	GS040708312322.004 [DIRS 179432]
Nelson Domestic	157	830[c]	0.71309	5.5	GS040708312322.004 [DIRS 179432]

Table B4-5. Additional Data on Strontium Isotopic Compositions for Wells Cited in Appendix A (Continued)

Well Identifier	Sample ID on Figure A6-5	Sr^{2+} (µg/L)	$^{87}Sr/^{86}Sr$ (ratio)	$\delta^{87}Sr$ (per mil)[a]	Source DTN [a]
Lowe Domestic	159	724[c]	0.71305	5.4	GS040708312322.004 [DIRS 179432]
Anvil Ranch Irrigation	161	319[c]	0.71191	3.8	GS040708312322.004 [DIRS 179432]
Payton Domestic	164	1,069[c]	0.71327	5.7	GS040708312322.004 [DIRS 179432]
Oettinger Well	167	915[c]	0.71325	5.7	GS040708312322.004 [DIRS 179432]
Amargosa Motel (B)	168	954[c]	0.71316	5.6	GS040708312322.004 [DIRS 179432]
Crane Domestic	178	674[c]	0.71835	12.9	GS040708312322.004 [DIRS 179432]
IMV on Windjammer [b]	180	430[c]	0.71668	10.5	GS040708312322.004 [DIRS 179432]
Moms Place	184	346[c]	0.71652	10.3	GS040708312322.004 [DIRS 179432]

NOTE: Unless noted otherwise, data presented here are limited to those for samples collected at least 3 months following well completion.

[a] With the exception of Output DTN: LA0612RR150304.002, the cited DTNs that report $^{87}Sr/^{86}Sr$ ratios do not report $\delta^{87}Sr$ values. In these cases, the $\delta^{87}Sr$ values shown in this table were calculated by the equation: $[(R_x / 0.70920) - 1] \times 1{,}000$, in which R_x is the sample's $^{87}Sr/^{86}Sr$ ratio and 0.70920 is the present-day strontium isotopic ratio assumed for the USGS seawater standard EN1 (Futa et al. 2006 [DIRS 178742], p. 302).

[b] When more than one analysis was reported for a particular location (other than the NC-EWDP wells), then the results shown above are averages of the available data; such is the case for sample IDs 16, 106, and 180. For NC-EWDP wells, because these were drilled and completed so recently, the values reported in the table above are either for the most recent sample collected (sample IDs 86 and 95 to 98, SMF barcode is listed next to the well's identifier), or an average of results from all sampling events reported in the source DTN (sample IDs 72, 77 and 94). Although sampling dates are not included in DTNs: GS040708312232.004 [DIRS 179432] and GS040808312322.005 [DIRS 179433], these dates are documented in sample collection reports that are traceable through SMF barcode numbers reported in these DTNs. Sample collection dates for the NC-EWDP samples in this table are reported on the sample collection forms (YMP 2001 [DIRS 179430], pp. 18 to 20, 34, 42, 44, 46, 53, 55, 57, 63, 69, 72, 75, and 78).

[c] Data from Table A6-2.

[d] The source DTNs show minor inconsistencies in the well identifier used for this location. In this appendix, it was judged best to maintain a uniform usage with the identifier used in Table A4-3.

[e] The only strontium isotopic data available for this interval are for samples collected less than 3 months after well completion, and may not be representative of undisturbed chemistry.

SMF = Sample Management Facility.

Table B4-6. Additional Data on Uranium Isotope Values for Wells Cited in Appendix A

Well Identifier	Sample ID in Figure A6-5	U (µg/L)[a]	$^{234}U/^{238}U$ Activity Ratio[a]	Source DTN [b]
ER-EC-08	1	4.8	5.1	LA0612RR150304.002 (Output DTN)—U, AR
ER-30-1 (upper)	28	1.9	2.0	LA0612RR150304.002 (Output DTN)—U, AR
ER-30-1 (lower)	29	1.6	2.5	LA0612RR150304.002 (Output DTN)—U, AR
USW UZ-14 (pump test #4) [c]	46	0.02	7.4	GS010608315215.002 [DIRS 156187]—U, AR
UE-25c #1 HTH	58	0.6	5.7	LA0612RR150304.002 (Output DTN)—U, AR
NC-EWDP-07S (24-Oct-00)	71	6.2	—	MO0310UCC008IF.003 [DIRS 179440]—U
NC-EWDP-12PA	78	1.1	7.5	LA0612RR150304.002 (Output DTN)—U LA0612RR150304.005 (Output DTN)—AR MO0310UCC008IF.003 [DIRS 179440]—U MO0311UCC008IF.007 [DIRS 179441]—U
NC-EWDP-12PB	79	0.95	6.5	LA0612RR150304.002 (Output DTN)—U LA0612RR150304.005 (Output DTN)—AR MO0310UCC008IF.003 [DIRS 179440]—U MO0311UCC008IF.007 [DIRS 179441]—U
NC-EWDP-12PC	80	9.0	4.4	LA0612RR150304.002 (Output DTN)—U LA0612RR150304.005 (Output DTN)—AR MO0310UCC008IF.003 [DIRS 179440]—U MO0311UCC008IF.007 [DIRS 179441]—U
NC-EWDP-15P	90	3.3	5.2	LA0612RR150304.002 (Output DTN) —U LA0612RR150304.005 (Output DTN)—AR MO0310UCC008IF.003 [DIRS 179440]—U MO0311UCC008IF.007 [DIRS 179441]—U
NC-EWDP-19D (open hole; 7 zones)	92	1.8	3.6	LA0612RR150304.002 (Output DTN)—U LA0612RR150304.005 (Output DTN)—AR
NC-EWDP-19P	93	—	5.1	LA0612RR150304.005 (Output DTN)—AR
NC-EWDP-19D (alluvial; Zones 1 to 4)	94	1.7	—	LA0612RR150304.002 (Output DTN)—U
NC-EWDP-19D (Zone 1)	95	1.5	—	LA0612RR150304.002 (Output DTN)—U
NC-EWDP-19D (Zone 2)	96	1.2	—	LA0612RR150304.002 (Output DTN)—U
NC-EWDP-19D (Zone 3)	97	1.7	—	LA0612RR150304.002 (Output DTN)—U
NC-EWDP-19D (Zone 4)	98	1.7	—	LA0612RR150304.002 (Output DTN)—U
NC-EWDP-04PB	99	0.5	2.5	LA0612RR150304.002 (Output DTN)—U LA0612RR150304.005 (Output DTN)—AR MO0310UCC008IF.003 [DIRS 179440]—U MO0311UCC008IF.007 [DIRS 179441]—U GS040808312322.006 [DIRS 179434]—U

Table B4-6. Additional Data on Uranium Isotope Values for Wells Cited in Appendix A (Continued)

Well Identifier	Sample ID in Figure A6-5	U (µg/L)[a]	$^{234}U/^{238}U$ Activity Ratio[a]	Source DTN [b]
NC-EWDP-04PA	100	0.8	2.7	LA0612RR150304.002 (Output DTN)—U LA0612RR150304.005 (Output DTN)—AR
NC-EWDP-05SB	155	0.15	4.1	LA0612RR150304.002 (Output DTN)—U LA0612RR150304.005 (Output DTN)—AR MO0310UCC008IF.003 [DIRS 179440]—U

[a] When more than one analysis was reported for a particular location, then the results shown above are averages of the available data.

[b] Each source DTN is identified as a source of uranium concentrations (U) and/or activity ratios (AR) in the last column.

[c] Average values for the last 6 samples collected from pump test #4, on August 25 to 27, 1993. (Note: The date is embedded in the sample name listed for this sampling event in DTN: GS010608315215.002 [DIRS 156187], in the format YrMoDy (Year-Month-Day).) Based on the variably elevated uranium concentrations observed for earlier samples, these later samples are considered more likely to be representative of the perched water at this location.

Table B4-7. Additional Data on Sulfur Isotope Values for Wells Cited in Appendix A

Well Identifier	Sample ID in Figure A6-5	$\delta^{34}S$ (per mil)[a]
J-13	35	10.5
VH-2	70	14.7
VH-1	69	13.0
NC-EWDP-07SC (composite, 28/29-Mar-01)	72	13.5

Source: DTN: GS040108312322.001 [DIRS 179422].

[a] When more than one analysis was reported for a particular location, then the results shown above are averages of the available data. This was the case for J-13, VH-1 and NC-EWDP-07SC.

Table B4-8. Additional Data on Carbon Isotope Values for Wells Cited in Appendix A

Well name	Sample ID in Figure A6-5	$\delta^{13}C$ (per mil)	^{14}C (pmc)	Source DTN
U.S. Ecology MR-3 (Bond Gold Mining Well #12 (BGMW12)), 16-Aug-89	18	−6.7	26.2	LA0612RR150304.002 (Output DTN)
ER-30-1 (upper)	28	−8.1	33.9	LA0612RR150304.002 (Output DTN)
ER-30-1 (lower)	29	−8.2	43.6	LA0612RR150304.002 (Output DTN)
USW SD-6	50	−9.4 [a]	15.0	LA0612RR150304.002 (Output DTN)
VH-1	69	−7.3 [b]	14.5 [b]	GS040108312322.001 [DIRS 179422] GS040808312322.006 [DIRS 179434]

Table B4-8. Additional Data on Carbon Isotope Values for Wells Cited in Appendix A (Continued)

Well name	Sample ID in Figure A6-5	$\delta^{13}C$ (per mil)	^{14}C (pmc)	Source DTN
VH-2	70	−4.8	7.0	GS040108312322.001 [DIRS 179422]
NC-EWDP-07SC	72	−4.9	6.5	GS040108312322.001 [DIRS 179422]
NC-EWDP-03S	87	−8.4[a]	61.2	GS040808312322.006 [DIRS 179434]
NC-EWDP-19D	95	−7.0[a]	19.4	GS040108312322.001 [DIRS 179422]
NC-EWDP-04PB	99	−10.0[a]	8.7	GS040808312322.006 [DIRS 179434]
NC-EWDP-05SB	155	−1.0	1.48	GS040108312322.001 [DIRS 179422]

[a] Data from Table A6-2.

[b] Values reported for VH-1 are averages of data from two different sampling events at this location. Equal weight is given to each sampling event by "averaging the averages" from each event.

pmc = percent modern carbon.

Table B4-9. Additional Data on Stable Hydrogen and Oxygen Isotope Values for Wells Cited in Appendix A

Well Name	Sample ID in Figure A6-5	δD (per mil)	$\delta^{18}O$ (per mil)	Source DTN
NEC well a	17	−107.7	−14.0	LA0612RR150304.002 (Output DTN)
Test Well #1	26	−110.3	−14.7[b]	LA0612RR150304.002 (Output DTN)
VH-2	70	−105.0	−13.6	GS040108312322.001 [DIRS 179422]
NC-EWDP-07SC	72	−100.0[c]	−13.5[c]	GS040108312322.001 [DIRS 179422]

[a] DTNs are slightly inconsistent in the use of a unique well identifier for this location. In this appendix, it was judged best to maintain a uniform usage with the identifier used in Table A4-3.

[b] Data from Table A6-2.

[c] The reported value represents the average of several analyses reported for this well in the source DTN.

B5. ASSUMPTIONS

A list of the assumptions used in Sections B6 and B7 is provided in Section A5 of Appendix A, and is augmented by the following additional assumptions:

1. Borehole coordinates used in this analysis are sufficiently accurate for the intended purpose of delineating regional flowpaths based on areal distributions of hydrochemical and isotopic species. The rationale for this assumption is presented in Section 6.2.1 of *Water-Level Data Analysis for the Saturated Zone Site-Scale Flow and Transport Model* (BSC 2004 [DIRS 170009]).

2. Averaged hydrochemical and isotopic analyses provide values representative of natural, steady-state conditions in the flow system. In general, groundwater samples were collected from boreholes from which many borehole volumes of groundwater had been pumped prior to sampling. In many cases, data were available from sampling events at different times, such that the dataset could be evaluated for outliers and/or temporal trends to determine the validity of this assumption. Because these data are used in this report to define broad regional patterns, geochemical anomalies that may be due to

violations of this assumption can be distinguished from regional trends and are not used to define regional geochemical patterns and flow pathways. Anomalous values are excluded for reasons provided in the supporting documentation for the source DTNs, and in table footnotes.

3. Hydrochemical and isotopic compositions from the uppermost open interval of each borehole represent the uppermost part of the saturated zone (i.e., the water table). The rationale for this assumption is presented in Section 6.2.1 of *Water-Level Data Analysis for the Saturated Zone Site-Scale Flow and Transport Model* (BSC 2004 [DIRS 170009]).

B6. ANALYSIS OF NEW HYDROCHEMICAL AND ISOTOPIC DATA

B6.1 OBJECTIVES

The specific objectives of this appendix as outlined in *Technical Work Plan for Saturated Zone Flow and Transport Modeling* (BSC 2006 [DIRS 177375], Section 1.2.2, p. 7) are to incorporate new data on major ion chemistry, uranium series and ^{14}C and to evaluate the impact of these data on inferred groundwater flow pathways and travel times. Appendix A is a compilation and interpretation performed by the YMP of hydrochemical and isotopic data, for data that were available through 2003. Since then, several new boreholes have been drilled, and data from these boreholes as well as new data from existing boreholes have become available. This appendix presents and evaluates new data that were available as of September 2006.

New analytical methods have been used to obtain some of the ^{14}C data evaluated herein. These methods involve the measurement of ^{14}C on the organic fraction of carbon present in the groundwater. This method was not employed to collect data reported in Appendix A, and therefore a brief description of methodology is presented in Section B6.5.

B6.2 New Nye County EWDP Wells

Locations of 19 boreholes with 35 sampled intervals or zones cited in this appendix are shown in Figure B6-1. The new wells are located south of the Yucca Mountain repository, partially filling the previous gap in borehole distribution between the cluster of wells in central and northern Yucca Mountain, and the line of wells along U.S. Highway 95.

In Appendix A, each groundwater sample was assigned to one of 22 different hydrochemical groups. This convention is continued for the new groundwater samples presented in this update, with each new borehole being assigned to one of the existing groups; no new hydrochemical groupings are necessary to categorize the new data. Each group is identified by a unique symbol and color, which are then used in plots throughout Appendices A and B. Groupings are based largely on geographic distribution or common physiographic feature, as well as on hydrochemical similarities and/or trends. A brief geographic and hydrochemical description of the groups to which the new EWDP wells have been assigned follows. Hydrochemical trends of the new EWDP well samples are shown on trilinear (Piper) plots (Figure B6-2). The group assignments for the new wells are listed in Table B4-1 and shown in Figure B6-3. Sections B6.3 and B6.4 incorporate these new data into updated maps showing areal distributions of individual chemical species and in updated scatter plots addressing the implications of the new data for

groundwater mixing relationships. Throughout this appendix, borehole designations may be shortened by dropping the Nye County prefixes. For example, most Nye County boreholes identified by NC-EWDP-xxx are shortened to read -xxx. Each borehole identifier is followed by the sample number(s) assigned to it in Table B4-1, and as shown in Figure B6-1.

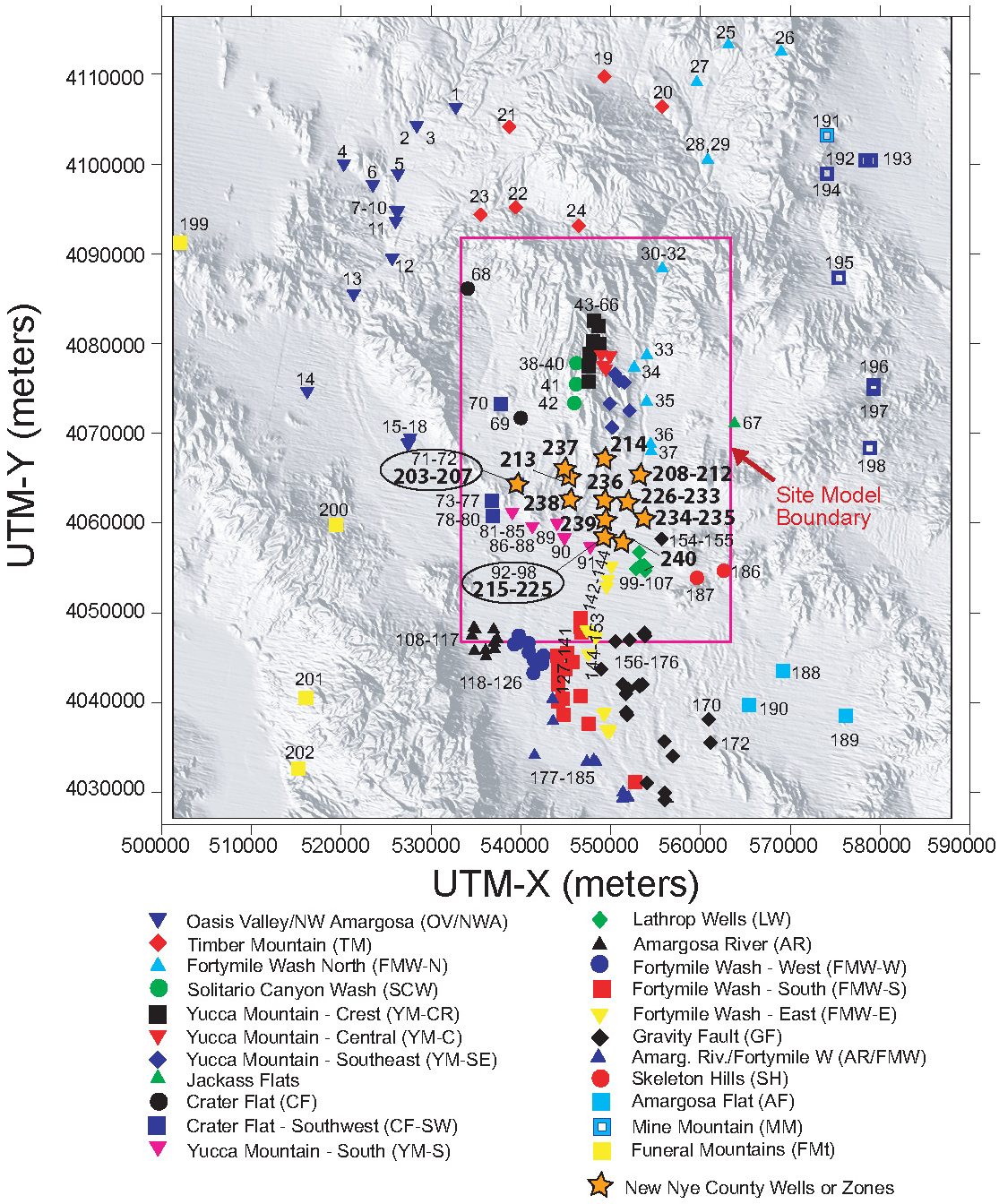

Sources: Figure A6-5, Tables A4-3 and B4-1.

NOTES: This figure has color-coded data points and should not be read in a black and white version.

UTM-X = UTM-Easting; UTM-Y = UTM-Northing; UTM = Universal Transverse Mercator.

The new borehole locations, 203 through 240, are defined in Table B4-1, which is a continuation of the sample number sequence listed in Table A4-3.

Figure B6-1. Map Showing Locations of New Nye County Boreholes in the Vicinity of the Northern Amargosa Desert

Borehole NC-EWDP-7SC (samples 203 to 207) was drilled proximal to borehole NC-EWDP-7S (sample 71). Borehole -7SC contains four screens. The chemistry of the upper three zones of -7SC is very similar to that of -7S, with these four samples plotting nearly on top of one another on the trilinear diagram in Figure B6-2, as well as to data previously presented for the composite sample of -7SC (sample 72). Both -7S and -07SC were assigned to the Crater Flat—Southwest (CF-SW) hydrochemical group in Appendix A. Accordingly, borehole -7SC is also assigned to the CF-SW group.

Hydrochemistry data are available for several boreholes drilled in new locations in the region between the repository and U.S. Highway 95. These include boreholes NC-EWDP-16P, -18P, -24P, -27P, -28P, and -29P (samples 213, 214, 236, 237, 238, and 239, respectively). In addition to these six new boreholes, new hydrochemistry data have become available for five boreholes at the NC-EWDP-19 complex (-19D, -19IM1, -19IM2, -19P, and -19PB; samples 215–225). All of these boreholes are provisionally assigned to the Yucca Mountain—South (YM-S) hydrochemical grouping, primarily on the basis of geographic distribution although this assignment is also supported by the general similarity between their geochemical signatures and those of other boreholes in the YM-S group (Figure B6-2). Patterson and Striffler (2006 [DIRS 178743], Figure 1) assigned three of these boreholes (-16P, -27P, and -28P) to their Western hydrochemical facies, distinguishing these from boreholes to the east, which were assigned to their Eastern hydrochemical facies. The grouping presented here is strictly for convenience, and is not meant to connote genetic relationships among different groundwaters or to guide interpretation of flow pathways. As more boreholes become available in this region and as additional hydrochemical data are made available for evaluation, the YM-S group may warrant finer subdivision.

Multiple new boreholes were drilled at two new locations along Fortymile Wash. Hydrochemical data are available for two new boreholes at the NC-EWDP-10 location (-10P and -10S; samples 208 to 212), and for three new boreholes at the NC-EWDP-22 location (-22PA, -22PB, and -22S; samples 226 to 233). These boreholes contain multiple screened intervals, some of which show chemical characteristics that differ slightly from those in other zones of the same borehole (Figure B6-2). Nonetheless, the general hydrochemistry of these boreholes and most of their individual zones is sufficiently consistent to justify assigning all of them to a single group, the Fortymile Wash—North (FMW-N) grouping.

As pointed out by Patterson and Striffler (2006 [DIRS 178743], p. 393) and by Futa et al. (2006 [DIRS 178742], p. 305), geochemical data for groundwater from NC-EWDP-19PB and -22S show evidence supporting the possibility of vertical stratification in this part of the flow system. This interpretation is based mostly on chemical and isotopic data obtained from a detailed vertical sampling of groundwater extracted from aquifer material collected during drilling. The main conclusion of these studies is that groundwater derived primarily from recharge along Fortymile Wash may overlie older groundwater derived from regions to the north, closer to the repository footprint.

Borehole Washburn-1X (sample 240) is located due south of NC-EWDP-22 (assigned to the FMW-N group), and midway between boreholes of the NC-EWDP-19 complex (assigned to the YM-S group) and boreholes of the NC-EWDP-4PA, -4PA, and -4PC complex (assigned to the Amargosa Valley group (LW, reflecting that this area was formerly called Lathrop Wells). The chemistry of Washburn-1X is not distinctly different from any of these three locations, but most closely resembles groundwater in the FMW-N grouping (Figure B6-2), to which it is therefore assigned.

Groundwater from borehole NC-EWDP-23P (samples 234 and 235) has a fairly distinctive chemistry with relatively high SO_4, low $\delta^{34}S$, and other geochemical characteristics most similar to those of groundwater from well J-11 (sample 67) in Jackass Flats (Figure B6-2). Borehole -23P also lies along Flow Path 3 (Figure A6-62, updated in Section B6.6), which originates at well J-11 and passes through other boreholes assigned to the Amargosa Valley (LW, Lathrop Wells) grouping. Accordingly, borehole -23P is also assigned to the LW group.

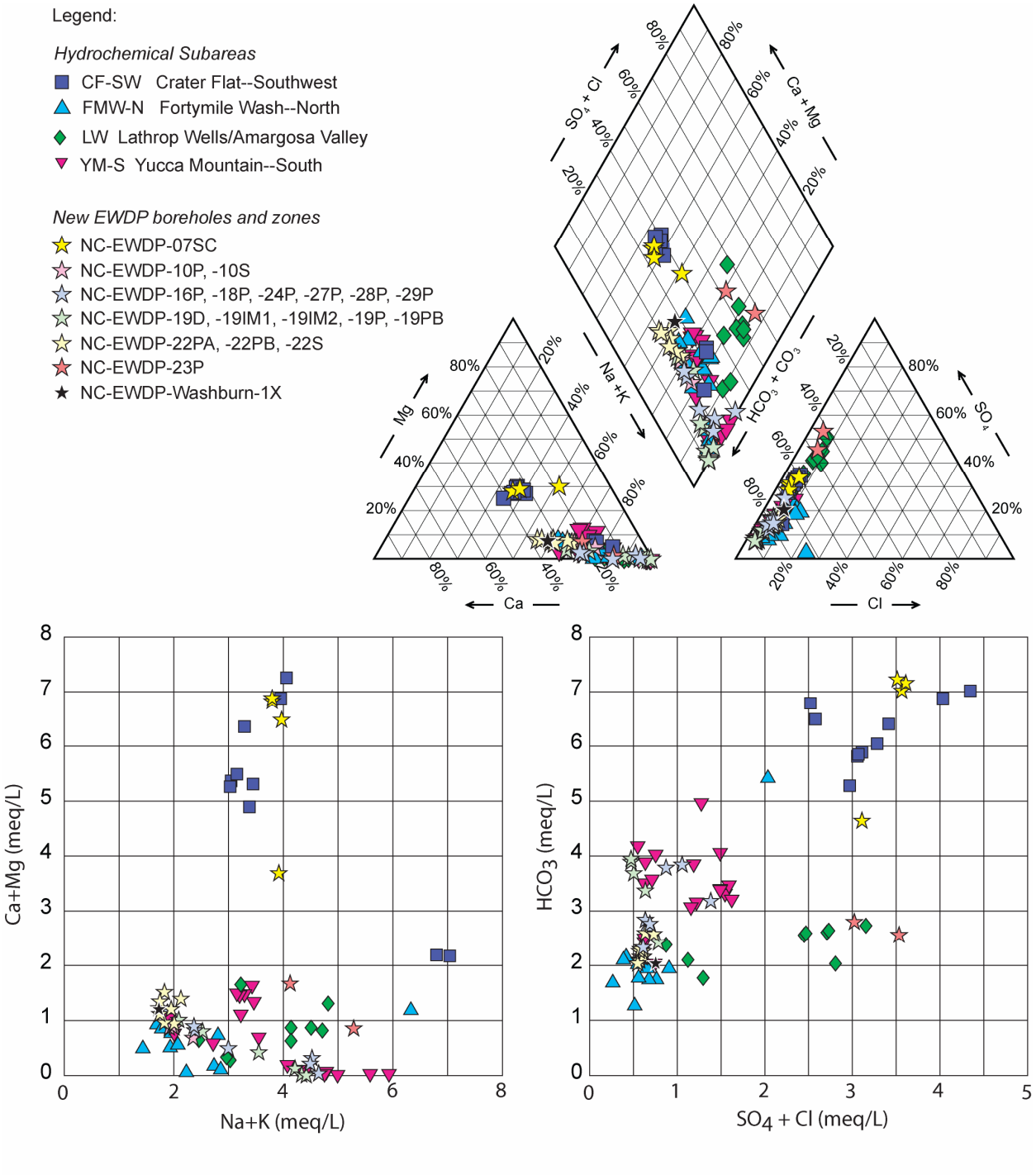

Sources: Tables A6-1 and B4-2.

NOTES: Units for the trilinear plot are percent milliequivalents (meq) per liter.

Figure B6-2. Trilinear and Scatter plots for New Nye County Boreholes and Zones

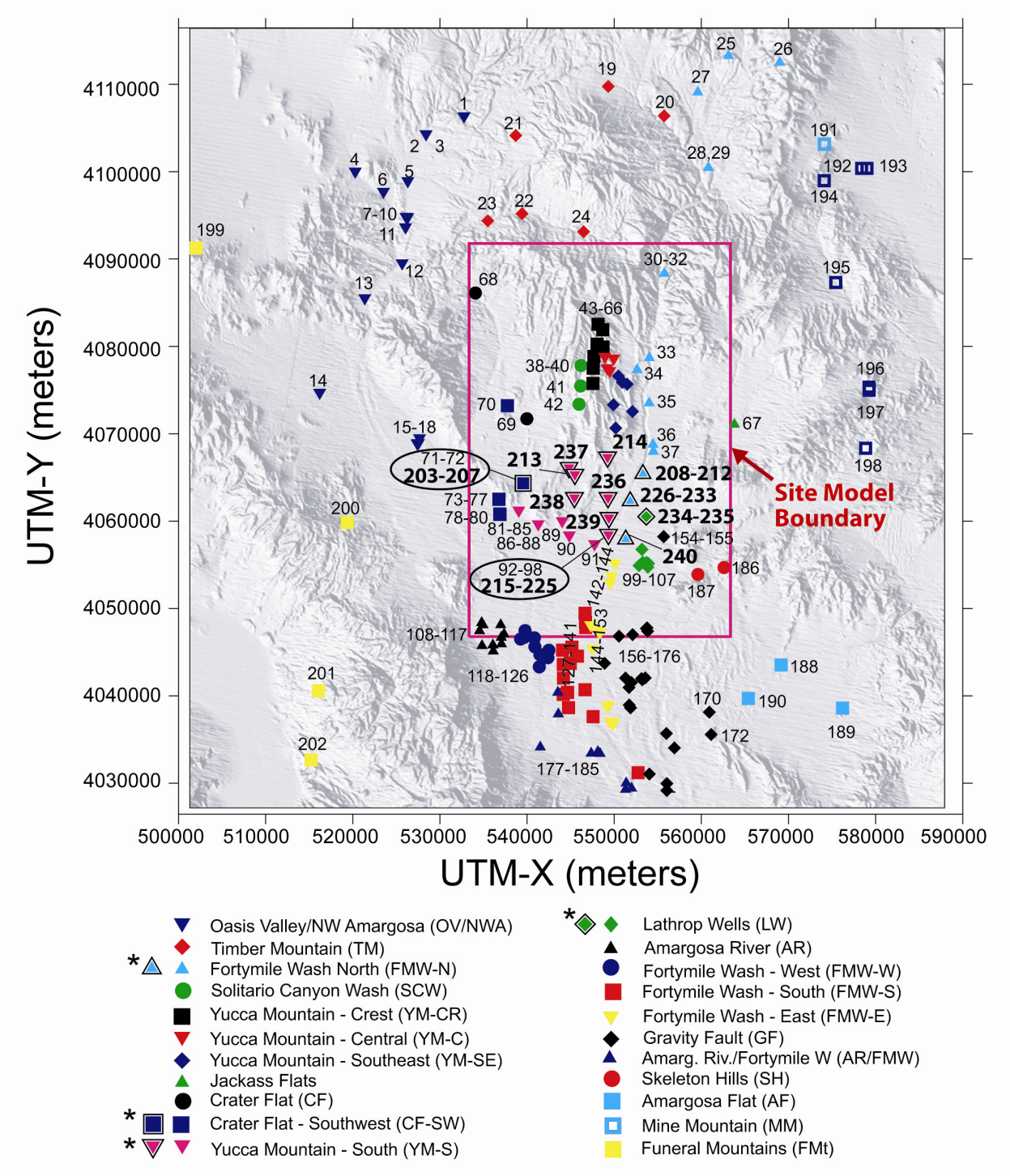

NOTES: This figure has color-coded data points and should not be read in a black and white version.

A black and white border around a plotted symbol (such as those marked with an asterisk in the legend) identifies new Nye County boreholes and zones, which are overlaid on the map from Figure A6-5. The numbers assigned to these new locations, 203 through 240, are defined in Table B4-1, which is a continuation of the sample number sequence listed in Table A4-3.

UTM-X = UTM-Easting; UTM-Y = UTM-Northing; UTM = Universal Transverse Mercator.

Figure B6-3. Map Showing Assignment of New Nye County Boreholes to Hydrochemical Groupings

B6.3 ANALYSIS OF AREAL DISTRIBUTIONS OF NEW HYDROCHEMICAL AND ISOTOPIC DATA

Maps showing the areal distributions of selected chemical species are presented in this section. Selection of these chemical species follows that in the TWP (BSC 2006 [DIRS 177375], Section 2.1.2.2) and is supported by the following rationale. Chloride, sulfate and bicarbonate are plotted because they are major groundwater constituents and because chloride and sulfate, in particular, tend to behave as conservative species and therefore are potentially very informative for tracing groundwater flow pathways. Calcium is plotted to illustrate the distribution of this major divalent cation, and sodium is plotted as the major monovalent cation. One of the objectives of this appendix, as established in the TWP (BSC 2006 [DIRS 177375], Section 2.1.2.2), is to qualitatively evaluate new carbon isotope data with respect to their implications for transport velocities. As described in Section A6.3.1.2.2, interpretation of ^{14}C groundwater ages is aided by knowledge of $\delta^{13}C$ as well as the ^{14}C values. Accordingly, spatial distributions are shown for both stable and radioactive carbon isotopes.

The following maps of areal distributions plot the new data with distinctive white and black outlines surrounding the symbols coded by shape and color to represent different concentration ranges. Many locations have multiple boreholes, as well as multiple sampled zones for a single borehole. It is difficult in these two-dimensional maps to illustrate ranges of values. Therefore, the presentation of data in this section follows the practice described in Section A6.3.4, by selecting one or in some cases two values considered to best represent the average groundwater composition at each mapped location. Data from uppermost intervals are given slightly more weight than those from deeper intervals because the higher zones are considered more likely to describe the transport flowpaths from the repository (with the possible exception of boreholes in the Fortymile Wash area, as discussed in the previous section). As described in Section A6.3.4, vertical heterogeneity is recognized as being present and undoubtedly complicates this two-dimensional evaluation of flow pathways.

A number of the new samples in this appendix are from one of the boreholes that had previously produced a sample (from a different interval than the new one) that was included in Appendix A. A sample in this appendix is plotted as “new data” as described above only if its concentration differs significantly from that of the previous sample from this borehole. For example, borehole NC-EWDP-7SC was completed with four screened intervals after Appendix A was prepared in 2003. The chemistry of the upper three zones of -7SC is very similar to that of -7S as well as to data previously presented for the composite interval of -7SC. No changes to the symbols used for this location in Appendix A are required for many solutes and therefore only new data that differ significantly from older data are shown as “new” in the following plots. Interpretations based on data presented for borehole -7SC in Appendix A are not affected by the new data. The borehole complex at NC-EWDP-19 contains three new boreholes, most with multiple sampled intervals. These new data were examined for consistency with data presented in Appendix A, with emphasis placed on data from upper intervals in these new wells. The symbols plotted at the -19 location were modified only for those few cases in which the new data extended the range of values previously displayed. Consistent values were not changed. The new data do not affect this two-dimensional analysis, although they do further define the range of vertical anisotropy at this site.

B6.3.1 Areal Distribution of Chloride in Groundwater (Figure B6-4)

Chloride concentration data are shown in Figure B6-4. Most new samples in the YM-S and FMW-N groupings show low chloride concentrations (< 7 mg/L) typical of this region and of boreholes further north near the repository footprint. Exceptions to this trend are boreholes NC-EWDP-16P, -27P, and -28P (samples 213, 237, and 238), with slightly higher chloride concentrations (8.5 mg/L, 9.0 mg/L, and 7.6 mg/L, respectively). This slight increase may reflect small amounts of flow contributed from the west or northwest. Borehole Washburn-1X (sample 240) has a low chloride value (6.9 mg/L) typical of surrounding groundwater. The two screens in borehole -23P (samples 234 and 235) have significantly higher chloride values (10.8 mg/L and 13.6 mg/L), which likely reflect addition of groundwater from the northeast as discussed in the next section.

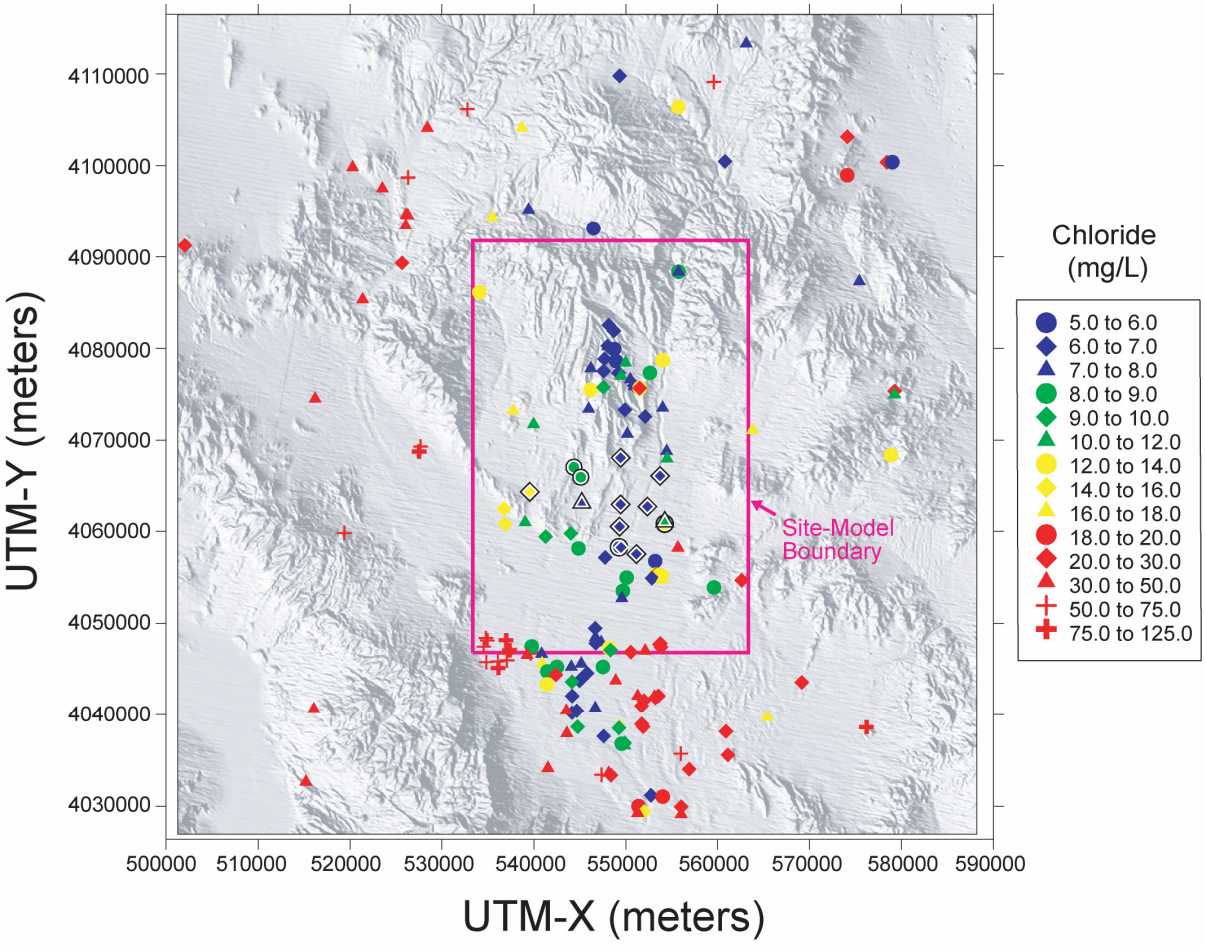

Sources: Tables A6-1 and B4-2.

NOTES: This figure has color-coded data points and should not be read in a black and white version.

A black and white border around a plotted symbol (such as those marked with an asterisk in the legend) identifies new Nye County boreholes and zones, as well as any existing locations for which new data support reassignment to a different concentration category than was used in Figure A6-15.

UTM-X = UTM-Easting; UTM-Y = UTM-Northing; UTM = Universal Transverse Mercator.

Figure B6-4. Areal Distribution of Chloride in Groundwater

B6.3.2 Areal Distribution of Sulfate in Groundwater (Figure B6-5)

Sulfate concentrations are shown in Figure B6-5. Samples NC-EWDP-18P, -24, -29 (samples 214, 236, and 239) as well as those from new boreholes along Fortymile Wash (-10 complex, samples 208 to 212; -22 complex, samples 226 to 233) have consistent sulfate concentrations (19 mg/L to 27 mg/L) that are typical of groundwater to the north. Boreholes -16P, -27P, and -28P (samples 213, 237, and 238) have slightly elevated sulfate concentrations (55 mg/L, 39 mg/L, and 32 mg/L, respectively) that, similar to the interpretation of the chloride values, may indicate contribution of groundwater from the northwest or west in Crater Flat, which have consistently higher sulfate concentrations compared to boreholes nearer the repository footprint to the north. Sulfate concentrations in borehole -23P (samples 234 and 235) are relatively high (127 mg/L and 155 mg/L), which is likely to reflect flow from the northeast or east. Washburn-1X (sample 240) has a sulfate concentration (27 mg/L) that is intermediate between sulfate concentrations of boreholes located to the north and west and those located to the east. This intermediate sulfate concentration may indicate flow of groundwater from the northeast or east through the Washburn-1X locality.

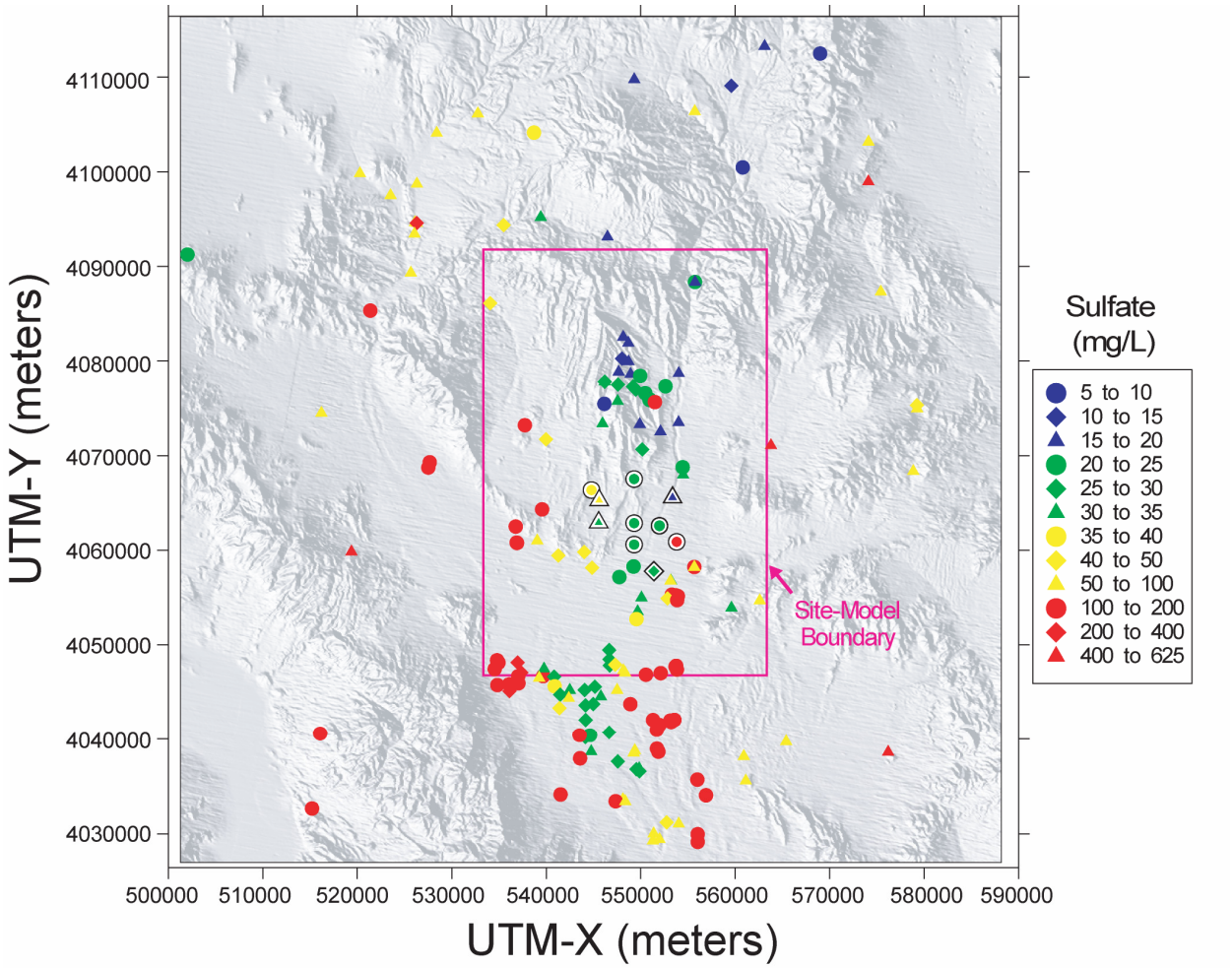

Sources: Tables A6-1 and B4-2.

NOTES: This figure has color-coded data points and should not be read in a black and white version.

A black and white border around a plotted symbol identifies new Nye County boreholes and zones, as well as any existing locations for which new data support reassignment to a different concentration category than was used in Figure A6-16.

UTM-X = UTM-Easting; UTM-Y = UTM-Northing; UTM = Universal Transverse Mercator.

Figure B6-5. Areal Distribution of Sulfate in Groundwater

B6.3.3 Areal Distribution of Bicarbonate in Groundwater (Figure B6-6)

Bicarbonate concentrations are shown in Figure B6-6. Samples NC-EWDP-16P, -27P, and -28P (samples 213, 237, and 238) have bicarbonate concentrations (190, 222, and 213 mg/L) that are higher relative to samples to the east, but which are typical of samples to the north and west. The rest of the samples from the new Nye County boreholes have slightly variable bicarbonate concentrations ranging between 125 to 173 mg/L. This concentration range is within the range of samples to the north.

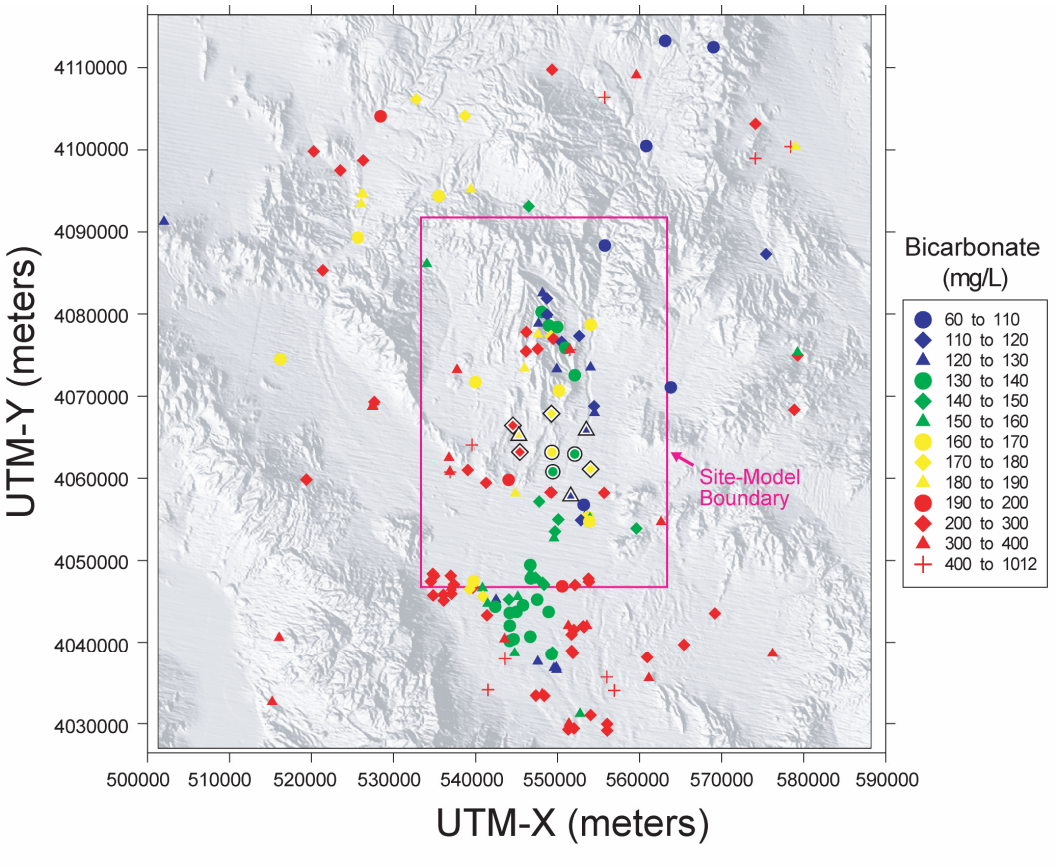

Sources: Tables A6-1 and B4-2.

NOTES: This figure has color-coded data points and should not be read in a black and white version.

A black and white border around a plotted symbol identifies new Nye County boreholes and zones, as well as any existing locations for which new data support reassignment to a different concentration category than was used in Figure A6-17.

UTM-X = UTM-Easting; UTM-Y = UTM-Northing; UTM = Universal Transverse Mercator.

Figure B6-6. Areal Distribution of Bicarbonate in Groundwater

B6.3.4 Areal Distribution of Calcium in Groundwater (Figure B6-7)

Calcium concentrations are shown in Figure B6-7. Samples -16P, -27P, and -28P (samples 213, 237, and 238) have low calcium concentrations (≤ 5 mg/L), similar to samples from the Solitario Canyon Wash and Yucca Crest groupings to the north. Samples -23P (samples 234 and 235) and Washburn-1X (sample 240) have calcium concentrations (16 to 25 mg/L) that are higher relative to most samples to the west and north. The only upgradient location in the region with higher calcium concentrations than these two boreholes is borehole J-11 (sample 67 in Table A6-1, 76.5 mg/L). The remaining samples have low to intermediate calcium concentrations (mostly < 20 mg/L) typical of locations to the north.

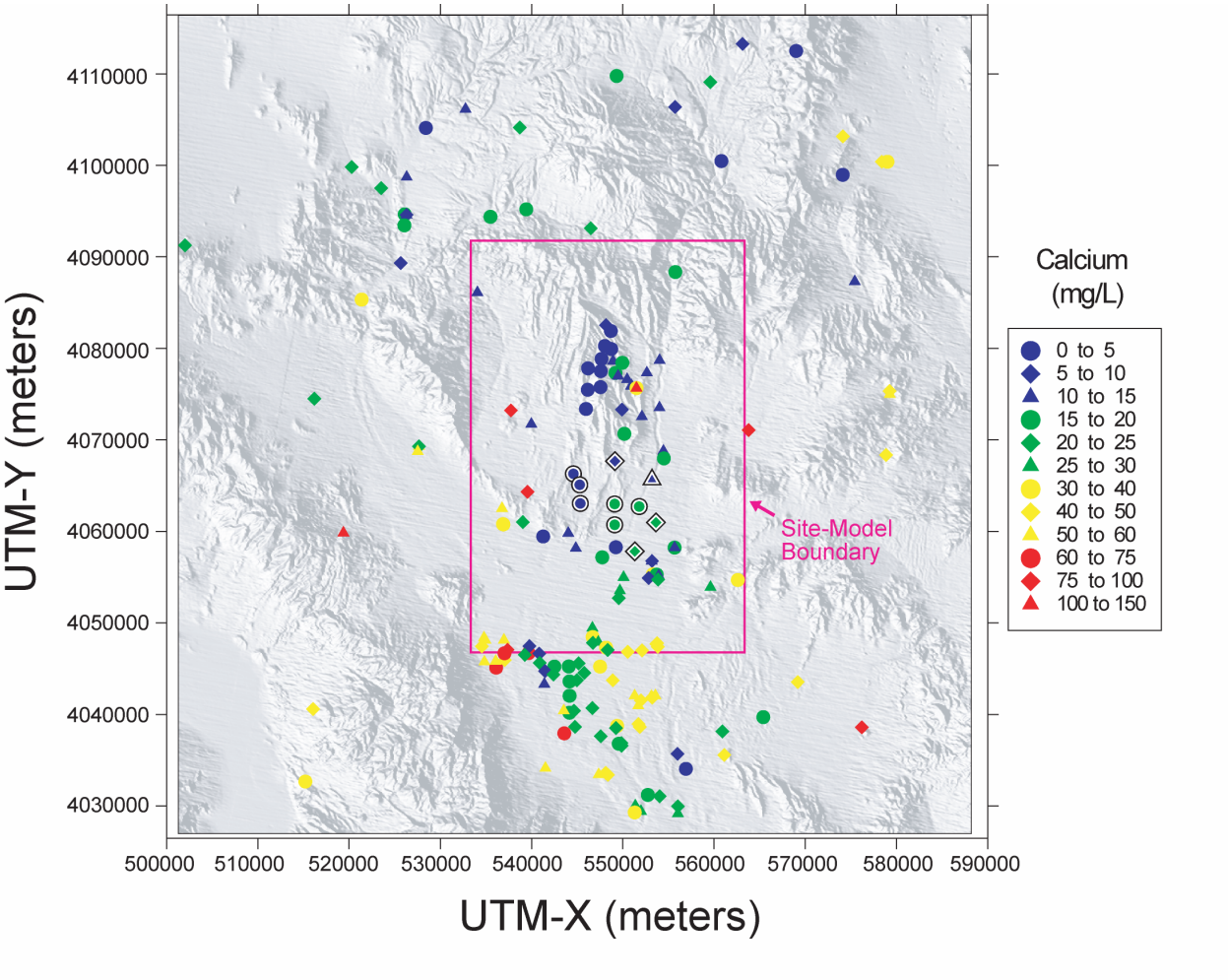

Sources: Tables A6-1 and B4-2.

NOTES: This figure has color-coded data points and should not be read in a black and white version.

A black and white border around a plotted symbol identifies new Nye County boreholes and zones, as well as any existing locations for which new data support reassignment to a different concentration category than was used in Figure A6-20.

UTM-X = UTM-Easting; UTM-Y = UTM-Northing; UTM = Universal Transverse Mercator.

Figure B6-7. Areal Distribution of Calcium in Groundwater

B6.3.5 Areal Distribution of Sodium in Groundwater (Figure B6-8)

Sodium concentrations are shown in Figure B6-8. Sodium concentrations in samples -16P, -27P, and -28P (samples 213, 237, and 238; 101 mg/L to 106 mg/L) are higher relative to most samples to the northwest; however, they are similar to some boreholes in the Solitario Canyon Wash and Yucca Crest groupings. Sodium concentrations in sample -23P (samples 234 and 235, 90 and 119 mg/L) are intermediate between that for sample J-11 (154 mg/L, sample 67 in Table A6-1) and samples to the north. The remaining samples have low sodium concentrations mostly within a range of 37 to 80 mg/L, typical of samples to the north.

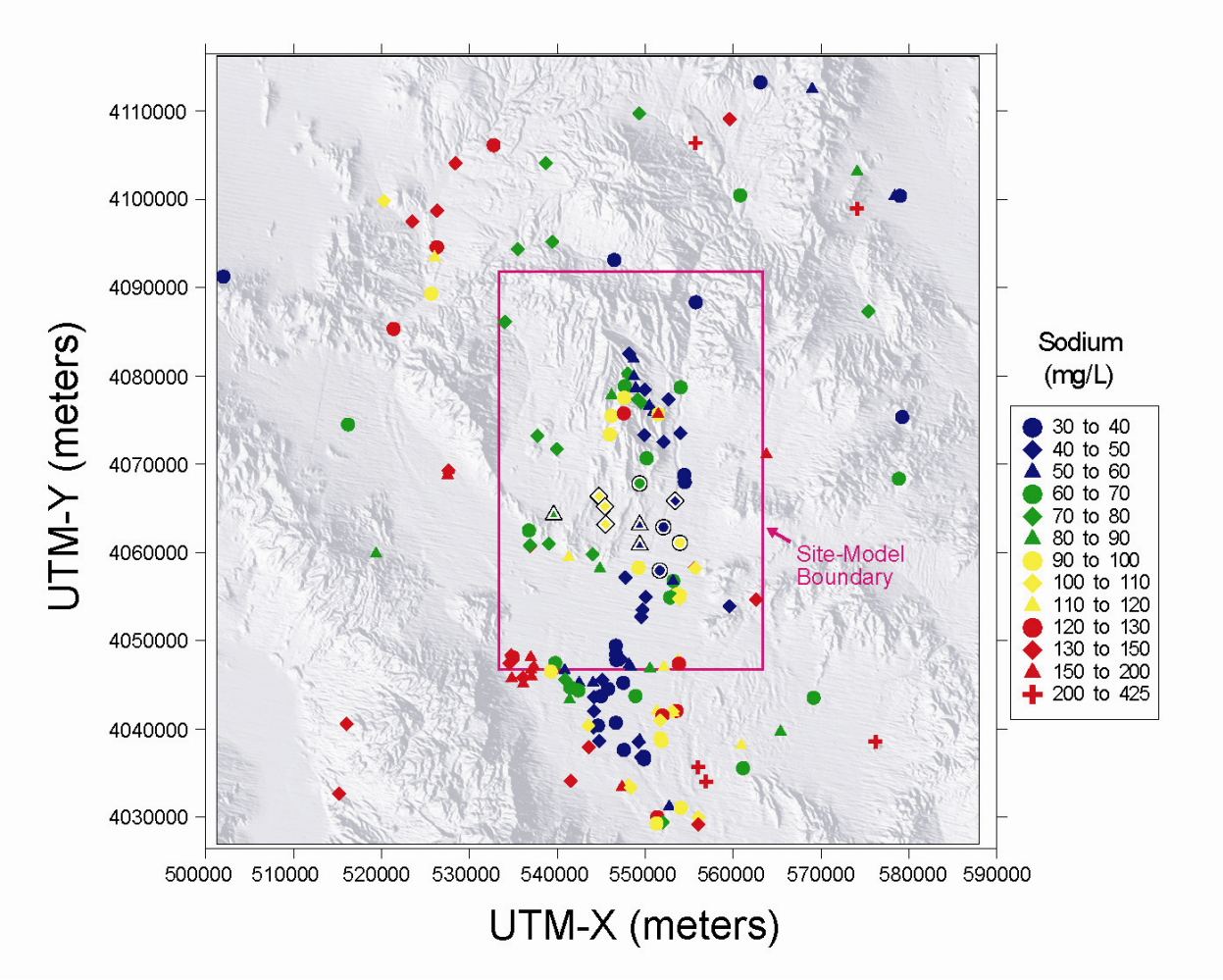

Sources: Tables A6-1 and B4-2.

NOTES: This figure has color-coded data points and should not be read in a black and white version.

A black and white border around a plotted symbol identifies new Nye County boreholes and zones, as well as any existing locations for which new data support reassignment to a different concentration category than was used in Figure A6-22.

UTM-X = UTM-Easting; UTM-Y = UTM-Northing; UTM = Universal Transverse Mercator.

Figure B6-8. Areal Distribution of Sodium in Groundwater

B6.3.6 Areal Distribution of Delta ^{13}C in Groundwater (Figure B6-9)

The areal distribution of $\delta^{13}C$ values is shown in Figure B6-9. The new samples show a range of values that is generally typical of values documented in upgradient areas to the north. The shallowmost sample from each of the new boreholes located adjacent to Fortymile Wash (-10P Zone 1, -10S Zone 1, -22PA Zone 1, -22PB Zone 1, -22S Zone 1, and Washburn-1X; samples 208, 211, 226, 228, 230, and 240, respectively), have slightly lighter (more negative) values (−9.1 to −10.5 per mil, Table B4-3) compared to deeper samples from the same boreholes or samples from wells immediately to the north (−7.9 and −8.6 per mil for J-12 and JF#3, samples 36 and 37 in Table A6-2). This lighter isotopic signal has been cited as evidence for more recent recharge of water via Fortymile Wash (Patterson and Striffler 2006 [DIRS 178743], p. 392). To

the east of Fortymile Wash, sample -23P also has light $\delta^{13}C$ values (–10.5 and –10.6 per mil, samples 234 and 235 in Table B4-3) that are similar to those for borehole J-11 (–11.0 per mil, sample 67 in Table A6-2) and the Amargosa Valley (LW, Lathrop Wells) grouping (–9.1 to –10.5 per mil, samples 99, 100, 101, and 106 in Table A6-2).

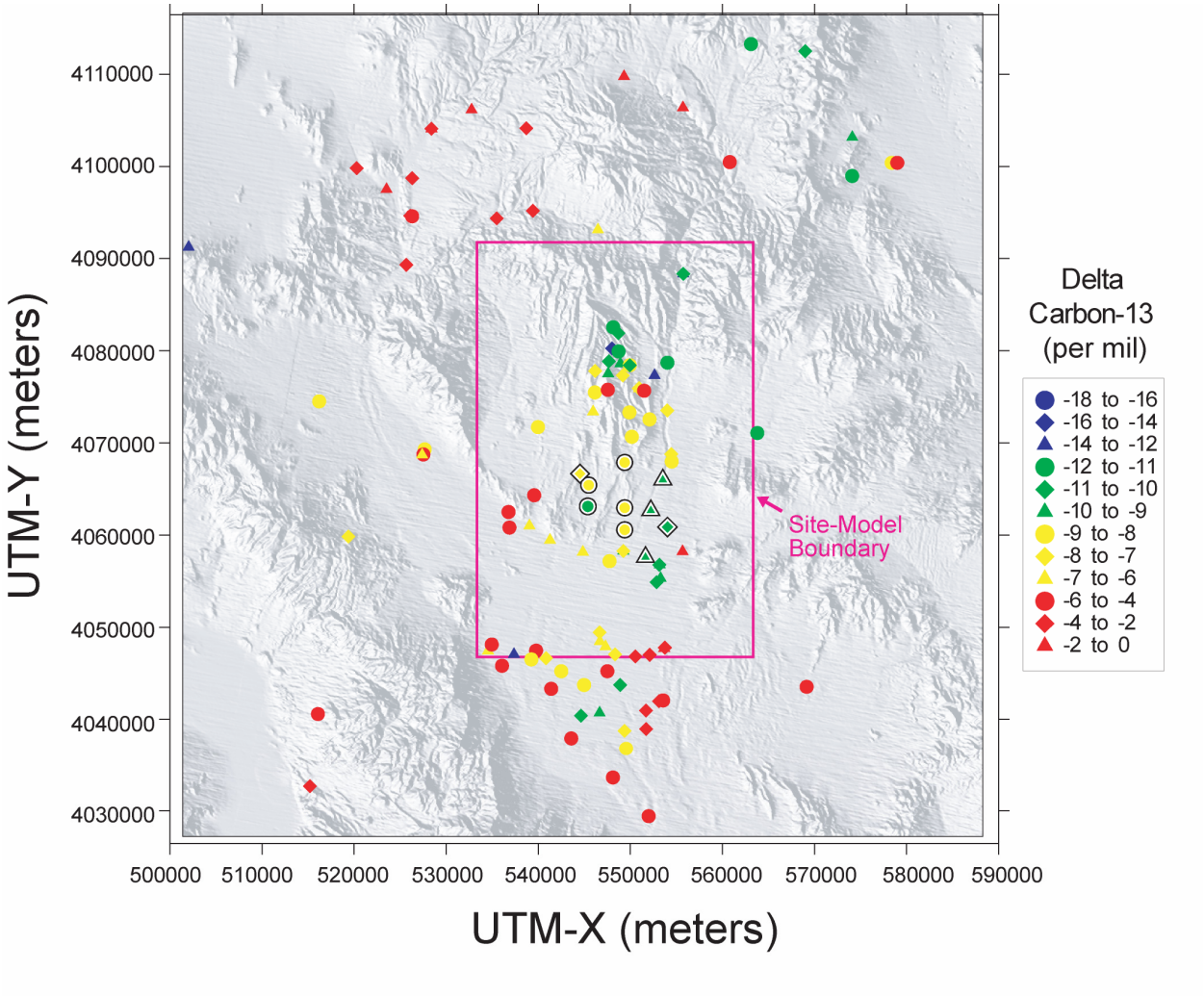

Sources: Tables A6-2 and B4-3.

NOTES: This figure has color-coded data points and should not be read in a black and white version.

A black and white border around a plotted symbol identifies new Nye County boreholes and zones, as well as any existing locations for which new data support reassignment to a different isotopic category than was used in Figure A6-27.

UTM-X = UTM-Easting; UTM-Y = UTM-Northing; UTM = Universal Transverse Mercator.

Figure B6-9. Areal Distribution of Delta ^{13}C in Groundwater

B6.3.7 Areal Distribution of ^{14}C in Groundwater (Figure B6-10)

The areal distribution of ^{14}C activities is shown in Figure B6-10. Data from new samples show a trend that is generally consistent with that of previously reported samples. The new samples show a general increase in ^{14}C activity from west to east. Samples -16P, -27P, and -28P (samples 213, 237, and 238) have ^{14}C activities between 12 and 17 pmc, values that are common

to the north and west. A central group of samples (-18P, -24P, and -29P) have slightly higher activities between 17 and 21 pmc (samples 214, 236, and 239 in Table B4-3). Samples along Fortymile Wash from -10, -22, and Washburn-1X have values generally between 20 and 25 pmc. The ^{14}C activity for borehole VH-2 (7.0 pmc, sample 70 in Table B4-8), which had not previously been included in Appendix A, is also plotted. This value is consistent with other values for the CF-SW grouping.

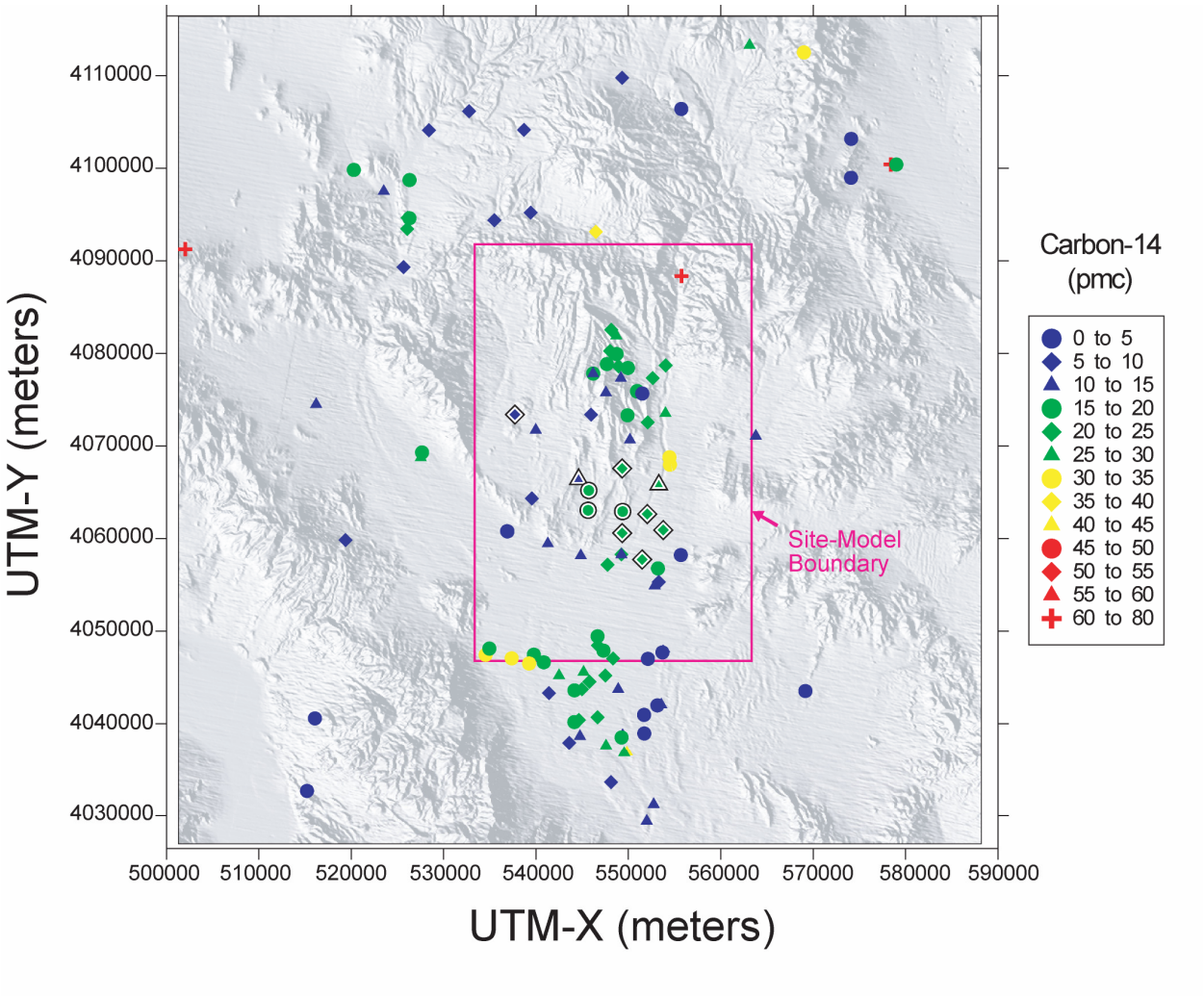

Sources: Tables A6-2 and B4-3.

NOTES: This figure has color-coded data points and should not be read in a black and white version.

A black and white border around a plotted symbol identifies new Nye County boreholes and zones, as well as any existing locations for which new data support reassignment to a different radiocarbon activity category than was used in Figure A6-28.

UTM-X = UTM-Easting; UTM-Y = UTM-Northing; UTM = Universal Transverse Mercator.

Figure B6-10. Areal Distribution of ^{14}C in Groundwater

B6.3.8 Areal Distribution of $^{234}U/^{238}U$ Activity Ratios in Groundwater (No Figure)

Few new uranium isotopic data have become available since production of Appendix A. New uranium isotopic data are presented in Table B4-6. Taken as a whole, the dataset helps to better define regional variations in uranium activity ratios. Activity ratios for groundwater to the north of Yucca Mountain (ER-EC-08, ER-30-1 upper and lower; 5.1, 2.0, and 2.5, respectively; Table B4-6) plot within the range of ratios previously observed in those respective regions. The activity ratio in groundwater from perched water in USW-UZ-14 (7.3, Table B4-6) is typical of values in the Yucca Mountain potential repository area. The ratio for UE-25c#1 (5.7) is lower than the only other value reported for that well complex in Appendix A (8.1 for UE-25c#3, sample 60 in Table A6-2). This result indicates greater variation in uranium activity ratios in this area than was previously recognized. Data from boreholes to the south of Yucca Mountain are generally consistent with values previously reported for the region with a few exceptions. The activity ratio of 7.5 for borehole NC-EWDP-12PA is larger than previously observed for this grouping (CF-SW). The activity ratio reported for borehole NC-EWDP-05SB (4.1, sample 155, Table B4-6) is less than that measured in adjacent borehole -5S (6.7, sample 154, Table A6-2). Activity ratios determined for closely spaced boreholes -12PA, -12PB, and -12PC (7.5, 6.5, 4.4, respectively, Table B4-6) differ significantly and indicate vertical heterogeneity in this borehole.

B6.4 ANALYSIS OF NEW EVIDENCE FOR MIXING RELATIONS BETWEEN WATER OF DIFFERENT SOURCES

Examination of areal distribution Figures B6-4 to B6-10 reveals some consistent patterns. For example, samples from boreholes -16P, -27P, and -28P share similar chemical and isotopic characteristics that are also similar to some samples to the north and/or west, but notably dissimilar to samples to the northeast and east. The chemical and isotopic characteristics of samples from borehole -23P are generally unique when compared to those of the most proximal boreholes, but show similarities to borehole J-11 located to the northeast. In the following section these patterns are analyzed to evaluate mixing of different groundwater. This information is then integrated into the delineation of groundwater flow pathways.

As discussed in Section A6.3.7.1, most solute concentrations in groundwater in the YM-S grouping increase to the west, from low values typical of the dilute groundwater near Fortymile Wash and regions to the north, to higher values more typical of the CF-SW grouping to the west. This same general geochemical pattern is also demonstrated with boreholes -16P, -27P, and -28P, which typically have solute concentrations that are intermediate between those of groundwater to the east and those to the west. On a plot of sulfate vs. chloride concentrations (Figure B6-11), these three boreholes plot along a mixing line between samples from the Solitario Canyon Wash grouping and groundwater from either the CF-SW grouping or the CF grouping (borehole VH-1). The trend defined by samples -27P, -28P, and VH-1 (Figure B6-11) suggests mixing with Crater Flat-type water in this area. However, comparison of chloride vs δD (Figure B6-11) as well as of chloride and bicarbonate values suggests that groundwater similar to that of CF-SW grouping is the more likely candidate for mixing. Although an unambiguous distinction cannot be made with the available data, the new data for boreholes -16P, -27P, and -28P increase confidence in the hypothesis that groundwater similar to that of the Solitario Canyon Wash grouping to the north mixes with groundwater derived from the northwest or west in this region.

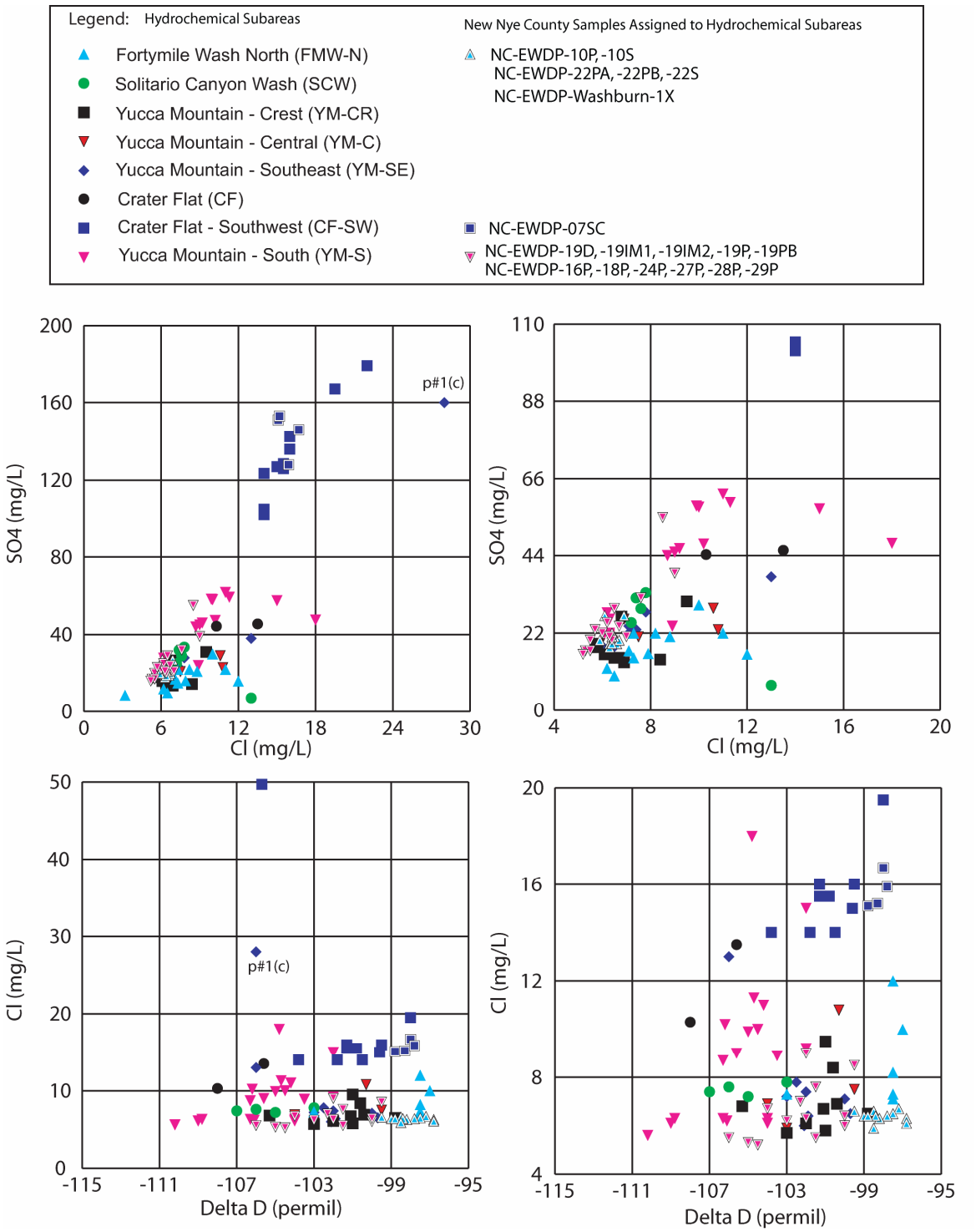

Sources: Tables A6-1, A6-2, B4-2, and B4-3.

NOTE: The plots on the right side of this figure have expanded scale compared to similar plots directly to their left to better display details in the tightly clustered data.

Figure B6-11. Scatter Plots Showing Mixing in Southern Yucca Mountain

In contrast with Figure B6-11, Figure B6-12 focuses specifically on the use of sulfate and chloride concentrations for evaluating mixing endmembers for groundwaters within the site model boundaries, and only to the south and east of Yucca Mountain (i.e. this figure excludes data for groundwater samples to the west or further south). Compared to its nearest neighbors (-27 and -28), groundwater from borehole -16P has an elevated sulfate concentration (55 mg/L, Table B4-2) and plots distinctly above the mixing trend defined by samples -27P and -28P in Figure B6-12, despite the fact that -16P is located roughly halfway between these two wells. This sample also has an anomalously low $\delta^{34}S$ value (4.7 per mil, Table B4-3) (Figure B6-13). Taken together, these data indicate that groundwater in this borehole has a different sulfate source compared to adjacent boreholes.

Groundwater from borehole -23P, which lies east of Fortymile Wash and due north of Amargosa Valley (formerly Lathrop Wells), typically has solute concentrations and isotopic values that are intermediate between proximal samples to the west and south (i.e., samples in the Yucca Mountain—South and Fortymile Wash—East hydrochemical subareas) and those of groundwater from borehole J-11 to the northeast (Figure B6-12). As shown on Figure B6-12, groundwater from Zone 2 of borehole -23P (10.8 mg/L Cl and 155 mg/L SO_4, Table B4-2) plots near the mixing line between dilute samples to the south and west and borehole J-11. Groundwater from Zone 1 (13.6 mg/L Cl and 127 mg/L SO_4, Table B4-2) plots off of this trend and towards the mixing lines formed between the dilute end-member and samples in the Amargosa Valley (Lathrop Wells) group and/or the Gravity Fault Group, suggesting a possible contribution from the east. As shown on Figure B6-13, the source of some of the sulfate in samples from -23P has a lower $\delta^{34}S$ value compared to that from any other borehole plotted on this figure, including the potential upgradient end-member, borehole J-11 (8.8 per mil). As for the case of -16P, these trends also indicate that groundwater in this borehole has a different sulfate source compared to other boreholes in the regional flow system.

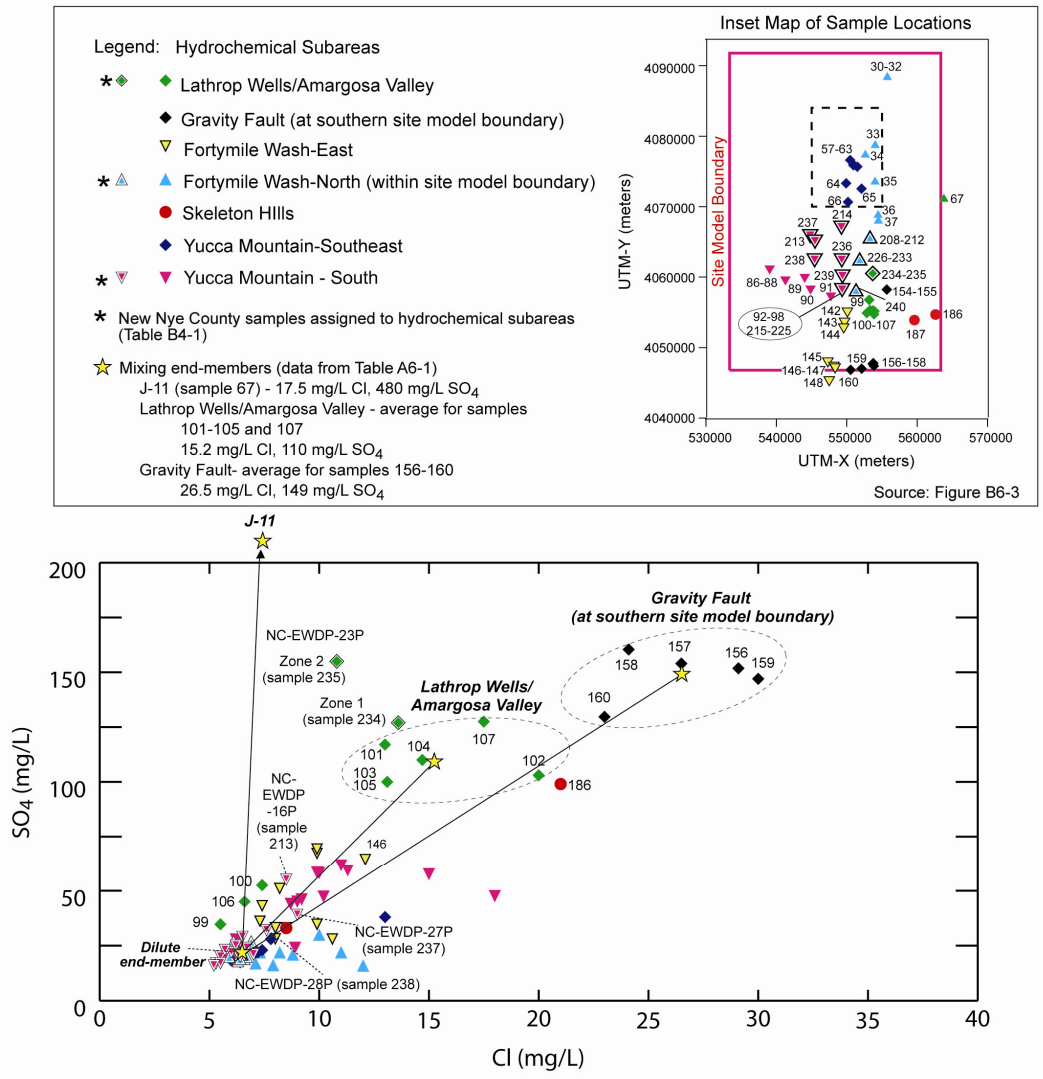

Sources: Tables A6-1 and B4-3.

NOTE: The dilute endmember for all three mixing lines is 6.5 mg/L Cl^- and 22 mg/L SO_4^{2-} and the compositions of the upper endmembers are listed in the legend.

Figure B6-12. Cross Correlation Plot of Sulfate versus Chloride for Groundwaters within the Boundaries of the Site Model, and South and East of Yucca Mountain

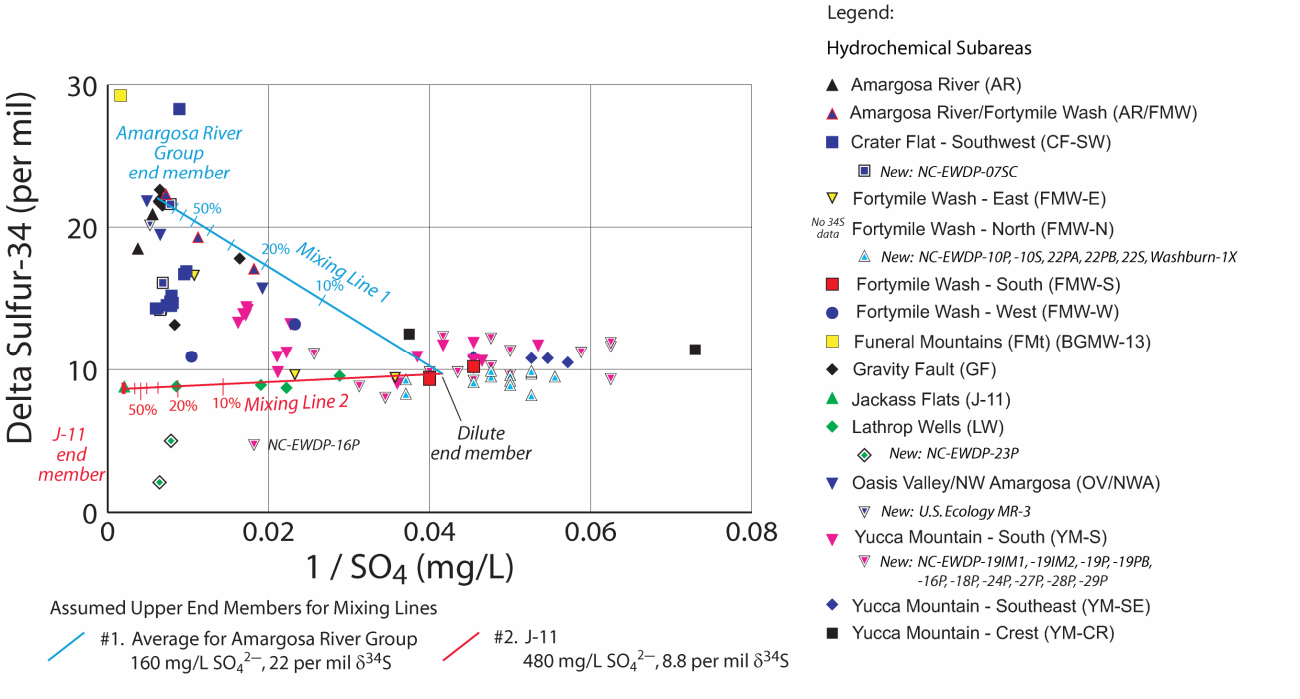

Sources: Tables A6-1, A6-2, B4-2, and B4-3.

NOTE: In this diagram, a mixture plots as a straight line. Mixing lines show tic marks at 10% increments. The dilute endmember for both mixing lines is 24 mg/L SO_4^{2-} and 9.65 per mil $\delta^{34}S$. The compositions of the upper endmembers are listed in the legend. Mixing lines are drawn by plotting calculated values for SO_4^{2-} and $\delta^{34}S$ obtained using the mixing equation: $[\delta^{34}S]_{mix} = \{F \bullet [SO_4^{2-}]_A + (1-F) \bullet [SO_4^{2-}]_B$, where F is the fraction of component A in the mix. $\delta^{34}S$ is determined by: $[\delta^{34}S]_{mix} = \{F \bullet [SO_4^{2-}]_A \bullet \delta^{34}S_A + (1-F) \bullet [SO_4^{2-}]_B \bullet \delta^{34}S_B) / [SO_4^{2-}]_{mix}$.

Figure B6-13. Scatter Plot of $\delta^{34}S$ versus Inverse Sulfur for Samples in the Vicinity of Yucca Mountain and the Amargosa Desert Region

B6.5 ANALYSIS OF NEW EVIDENCE FOR GROUNDWATER TRAVEL TIMES BASED ON ^{14}C

Groundwater travel times based on ^{14}C activities in dissolved inorganic carbon (DIC) can be calculated based on the extent of decrease in ^{14}C activities along a flowpath. However, some proportion of the radiocarbon reduction (expressed as a percentage) may be attributable to its dilution by inorganic carbon sources along the flowpath that contain no measurable ^{14}C activity ("dead" carbon). The result is that the radiocarbon-based travel times may be longer than the actual travel times. A variety of models exist for estimating and correcting for such dilution, based on shifts in stable carbon isotope ratios and in DIC concentrations. These models were reviewed in Section A6.3.9. An alternative approach proposed for obtaining more reliable groundwater travel time estimates is to measure ^{14}C activities in fractions of dissolved organic carbon (DOC). As precipitation infiltrates through the soil zone, it acquires much or most of its carbon (including ^{14}C) from the soil zone. This carbon will be a mixture of "old" carbon, for example from dissolution or exchange with carbonate minerals, and contemporary carbon in the form of decaying organic matter. In this case, the calculated "age" based solely on ^{14}C measurements for DOC fractions will theoretically reflect the actual time of infiltration of the

groundwater. In contrast, "ages" based on total inorganic carbon may require corrections based on assumed models of water-rock interaction (Patterson and Thomas 2005 [DIRS 179459]).

New data that bear on groundwater travel times including ^{14}C, ^{13}C, and DIC values are available for most of the new Nye County Wells. DIC and DOC radiocarbon measurements in groundwater from the Yucca Mountain vicinity are also presented by Patterson and Thomas (2005 [DIRS 179459], Figure 3). These new data are summarized in Figure B6-14 and discussed below.

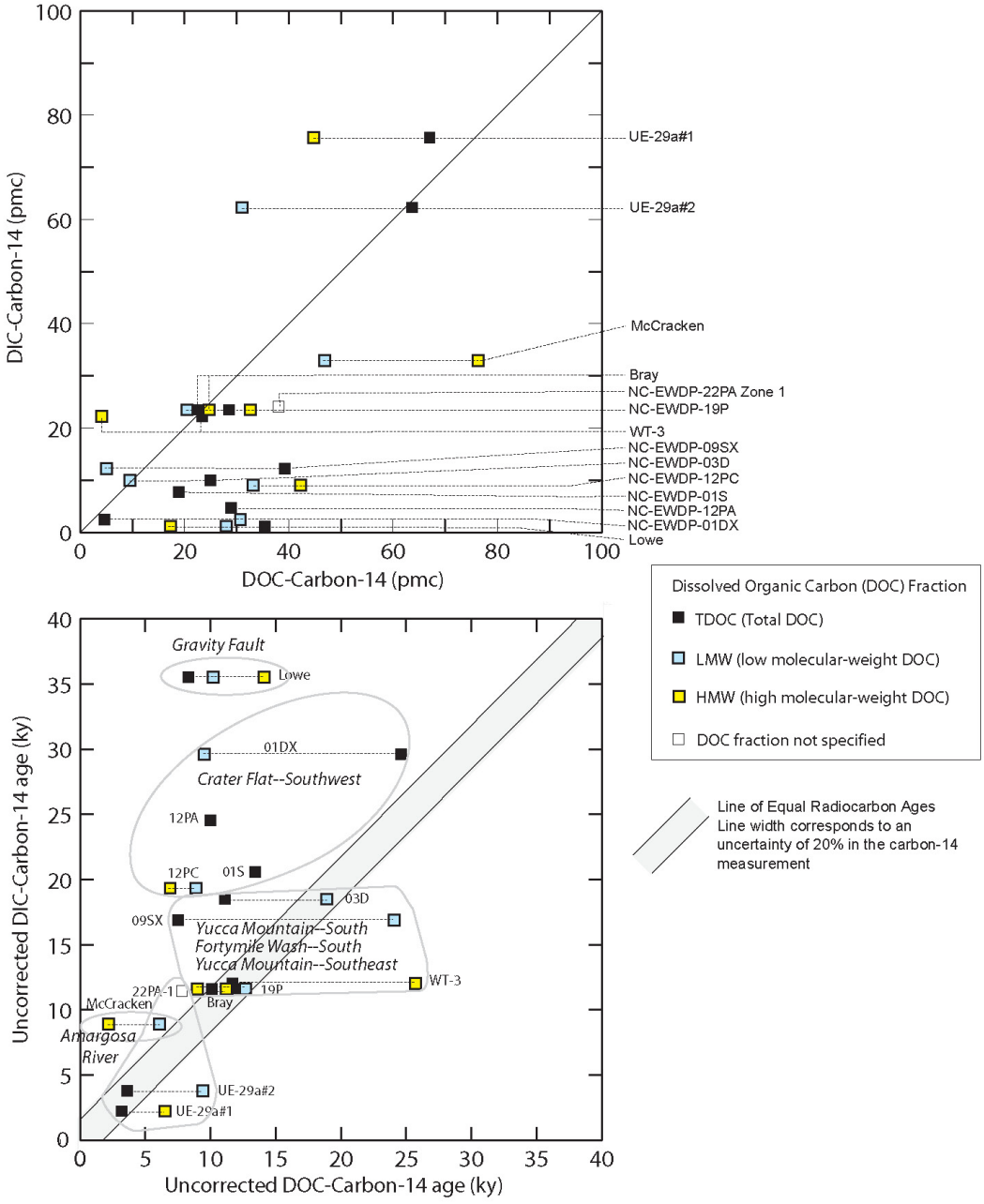

Sources: Tables A6-2 and B6-4, for DIC-14; DTN: GS031208312322.004 [DIRS 179431], for DOC-14.

Figure B6-14. Comparison of Radiocarbon Measurements of Inorganic and Organic Dissolved ^{14}C in Groundwater Samples from the Yucca Mountain Vicinity

Areal distributions of bicarbonate (as a surrogate for DIC), $\delta^{13}C$, and ^{14}C (measured on the DIC fraction) are shown in Figures B6-6, B6-9, and B6-10, respectively. These new inorganic-carbon data are generally consistent with data presented in Appendix A. Although these new data do not show consistent north to south trends, there is a general west to east increase in ^{14}C activity among the new Nye County boreholes (Figure B6-10). This shift corresponds to a decrease in bicarbonate concentration and decrease in $\delta^{13}C$ values. These data are consistent with a greater component of carbonate-derived groundwater in the west compared to the east and a greater component of more recently recharged water along Fortymile Wash.

Preliminary results of uncorrected radiocarbon ages based on ^{14}C activities measured for the total DOC fraction of several groundwaters are reported in DTN: GS031208312322.004 [DIRS 179431]. Figure B6-14 compares these uncorrected ^{14}C-TDOC ages, along with uncorrected radiocarbon ages calculated from separate analyses of the light and heavy molecular-weight DOC fractions, to uncorrected ^{14}C-DIC ages.

^{14}C ages determined from ^{14}C activities in DIC and TDOC fractions are in reasonable agreement for samples UE-29a#1, UE-29a#2, -22PA-1 (although the DOC fraction used for the -22PA-1 age estimate was not specified), -19P, and WT-3, all of which are located near Fortymile Wash. However, ^{14}C ages for these same samples determined from the low or high molecular weight fractions are in poor agreement with ages determined using ^{14}C-DIC. These data plot in fields that indicate a smaller percentage of ^{14}C activity (relative to that in modern carbon) in the DOC fraction relative to that in the DIC fraction and correspondingly older ^{14}C ages. The reason for this shift is unknown at this time. Several other samples plot in fields indicating smaller DIC percentages compared to those of TDOC, which yield older uncorrected ^{14}C ages based on DIC. Many of these samples (-1DX, -12PA, -12PC, and -9SX) are located in the CF-SW region, which hosts groundwater with a distinct carbonate signature. The age relationship noted is consistent with addition of dead carbon as inorganic carbon.

B6.6 REGIONAL FLOWPATHS INFERRED FROM HYDROCHEMICAL DATA

Hydrochemical data from the new boreholes presented above validate many of the flow pathways presented previously (Figure A6-62) and also allow minor refinements of that figure. The new boreholes are located in the region bounded between Flow Path 4 and Flow Path 3. A slightly modified version of the regional flowpath figure (Figure A6-62) is presented in Figure B6-15. The rationale underlying each modification is described below.

New hydrochemical data from -23P further validate Flow Path 3. In particular, sulfate/chloride ratios and high sulfate concentrations in -23P are similar to those from borehole J-11 (Jackass Flat grouping), strengthening the argument that water from Jackass Flat flows southwesterly to this region. Boreholes -23P and Washburn-1X constrain the position of Flow Path 3. Only minor adjustments were made to this flowpath. Based on interpretation of new data from -23P, mixing zone C was extended slightly to the north, and an additional arrow indicating eastward flow of Flow Path 8 was added.

New hydrochemical data from boreholes -27P, -16P, and -28P confirm a southerly flow from the Solitario Canyon Wash (Grouping SCW) area along Flow Path 6. Slightly elevated sulfate and chloride values in two samples suggest that groundwater from regions to the northwest and/or

west are added along this flowpath. The exact source of these groundwaters is not well constrained by the available data. Accordingly, Flow Path 4 was shortened to allow the possibility that groundwater from the CF-SW group, or from the direction of VH-1, or possibly a mix of these waters, flows southeast to the region of the -27P, -16P, and -28P boreholes.

New hydrochemical data from boreholes in and immediately west of Fortymile Wash are generally dilute, consistent with groundwater to the north. No changes to Flow Paths 2 or 7 are required by the data.

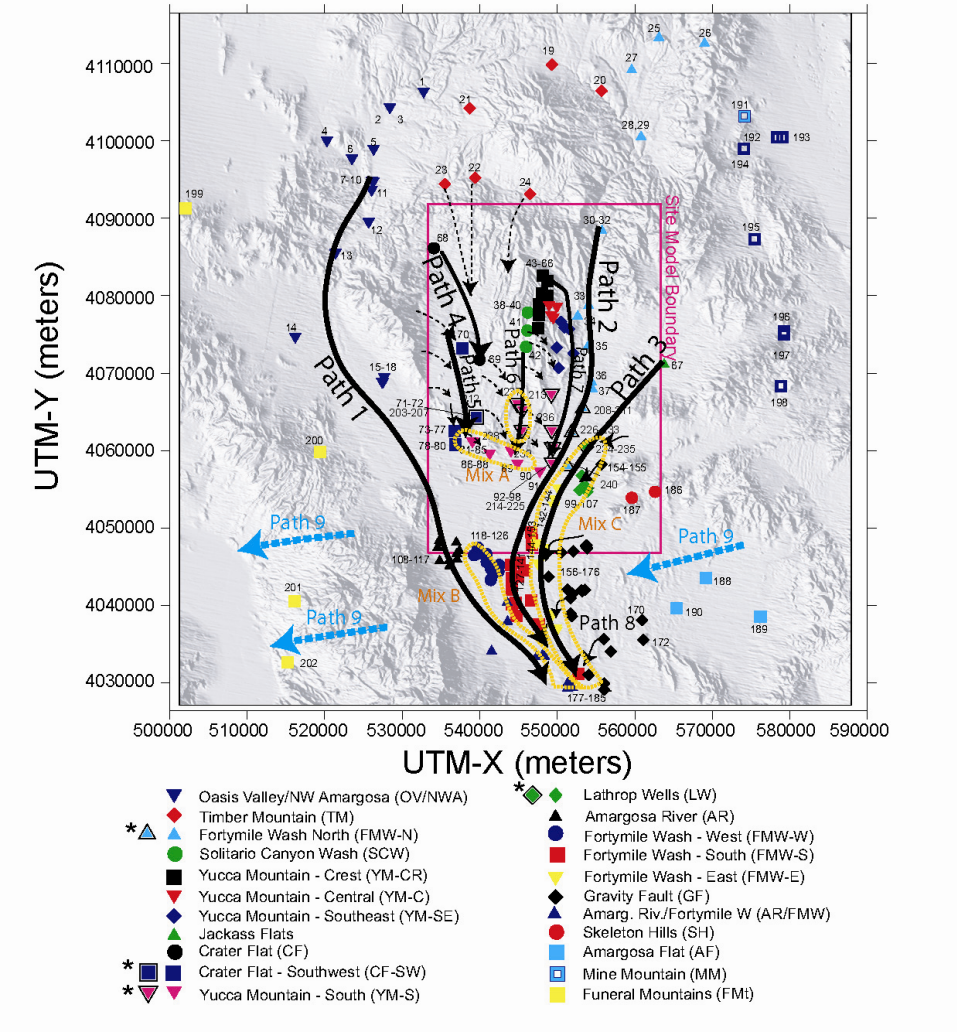

Output DTN: LA0612RR150304.004.

NOTES: This figure has color-coded data points and should not be read in a black and white version.

Solid lines indicate a relatively high degree of confidence in the interpretations; dashed flow paths indicate relatively less confidence. Base map shows borehole designators and inserts; see Figure A6-5 and Table A4-3. A black and white border around a plotted symbol (such as those marked with an asterisk in the legend) identifies new Nye County boreholes and zones, which are overlaid on the map from Figure A6-5. The numbers assigned to these new locations, 203 through 240, are defined in Table B4-1, which is a continuation of the sample number sequence listed in Table A4-3.

UTM-X = UTM-Easting; UTM-Y = UTM-Northing; UTM = Universal Transverse Mercator.

Figure B6-15. Regional Flow Paths Inferred from Hydrochemical and Isotopic Data

B7. CONCLUSIONS

Analysis of new hydrochemical data largely confirm and strengthen hypotheses presented previously in Appendix A. The probable flow pathway from the repository remains dominantly to the south. New carbon isotope data do not contradict calculations of travel times performed in Appendix A. In fact, these new carbon isotope data strengthen suggestions that dilutions in original ^{14}C activity can be reasonably accounted for by correction using dissolved inorganic carbon as outlined in Appendix A. The sparse new uranium isotopic data are in general agreement with data previously reported. These new uranium data do not require any modifications to the previously proposed flowpaths.

APPENDIX C
DATA SUITABILITY EVALUATION – THE 2004 DEATH VALLEY REGIONAL GROUNDWATER FLOW SYSTEM MODEL

C1. INTRODUCTION

SCI-PRO-006 establishes the process for documenting performance assessment modeling activities. It states in Section 6.2.1(L) that:

> "Data obtained from external sources that are not established fact must be qualified for intended use either in accordance with SCI-PRO-001 or within the specific model by doing the following:
>
> 1. Plan and document the qualification process in the model report. Documentation will include:
>
>   - Description of unqualified external source data evaluated
>   - Data qualification method(s) used (as specified in Attachment 3 of SCI-PRO-001) and rationale for selection of method(s)
>   - Acceptance criteria used to determine if the data are qualified (as related to the attributes in Attachment 4 of SCI-PRO-001)
>   - The decision as to the qualification of the data
>
> 2. If relevant data from external sources are evaluated against any of the above factors and determined not to meet a criterion, describe the basis for this conclusion. Also document whether the data were justified using an alternative factor (i.e., acceptance criteria) and included as direct input to the technical product, or excluded from the technical product."

The plan for this appendix is to demonstrate (based on the above-mentioned criteria) that inputs to and outputs of the DVRFS model (Belcher 2004 [DIRS 173179]) are suitable for use in the SZ site-scale flow model with emphasis on the recharge input data and flux output data. To facilitate this plan, this appendix uses technical assessment methods, as discussed in SCI-PRO-001 to evaluate the appropriateness of unqualified DVRFS data, the applicable portions of the data are qualified for intended use in this report in accordance with the requirements of SCI-PRO-006. While selected methodologies of SCI-PRO-001 were incorporated because they provide a sound, well established framework for demonstrating suitability of the DVRFS data for their intended use, SCI-PRO-006 is the governing procedure used to qualify the data for use within this technical product only. The data will remain unqualified for all other uses unless it is separately qualified outside this report.

The DVRFS model was prepared by the USGS and has been published as a Scientific Investigations Report. Inputs to the regional model were used to identify recharge to the upper surface of the SZ site-scale flow and transport model, and outputs from the regional model were used to identify flux targets across the lateral boundaries of the site-scale model. Specifically, the data to be evaluated for suitability (*cbcf.asc*) are found in DTN: MO0602SPAMODAR.000 [DIRS 177371], which contains all the input and output files from the DVRFS (Belcher 2004 [DIRS 173179]). The SZ flow model boundary data extracted from the DVRFS model are the

subject of Output DTN: SN0612T0510106.003. These data include information from several input files related to recharge (infiltration) and the output cell-by-cell flux file. The extracted flux data are used to calibrate the SZ flow model lateral boundaries fluxes (see Sections 6.3.1.6 and 6.3.1.7). This appendix demonstrates the suitability of these data for use in this model using arguments supporting the data reliability, qualifications of the organization, and prior uses of the data.

Executive Summary

The Evaluation Team found the DVRFS model database to be well researched, the model to be appropriately constructed, and the resulting output to provide a reasonable simulation of regional flow. The net infiltration model, INFILV3 (Hevesi et al. 2003 [DIRS 169681]), was calibrated to available surface water flow measurements and constrained by prior estimates of recharge and discharge. The INFILV3 model simulated a mean annual potential recharge to the model domain of about 125×10^6 m^3 for the period 1950 to 1999 (Belcher 2004 [DIRS 173179], p. 132). Within the area of the SZ site-scale model, the recharge fluxes from the regional model are consistent with similar-magnitude fluxes independently estimated from the unsaturated zone flow model and from focused recharge through Fortymile Wash. The INFILV3 model and method are used and accepted by the technical community and it is appropriate for use with the regional model.

The simulated hydraulic heads of the final calibrated transient model fit observed heads reasonably well (residuals with absolute values less than 10 m) with two exceptions: in most areas of nearly flat hydraulic gradient the fit is considered moderate (residuals with absolute values of 10 to 20 m), and in areas of steep hydraulic gradient, such as Indian Springs, western Yucca Flat, and the southern part of the Bullfrog Hills, the fit is poor (residuals with absolute values greater than 20 m, Belcher 2004 [DIRS 173179], pp. 1 and 334).

The Evaluation Team considers this overall goodness-of-fit to be acceptable for use in this report. Because the goodness-of-fit is a measure of the model's accuracy, a degree of uncertainty must be associated with the regional model outputs used to identify lateral flux boundary conditions for the site-scale model. These uncertainties were adequately addressed by using the regional model fluxes not as absolute values, but as target boundary conditions during site-scale model calibration. Specifying the fluxes absolutely would also over-constrain the site-scale model and interferes with its calibration.

The Evaluation Team has concluded that the DVRFS model provides a suitable source of data for establishing recharge and lateral flux boundary conditions for the SZ site-scale flow and transport model. In accordance with SCI-PRO-006, this finding qualifies these data only for their intended uses in this report. The regional model source DTN: MO0602SPAMODAR.000 [DIRS 177371] will remain unqualified.

C1.1 PURPOSE

This appendix evaluates the appropriateness of unqualified data from the USGS flow model of the DVRFS for use in the SZ site-scale flow model. The regional flow model was developed in part to support site-scale modeling for the YMP. Inputs to the regional model were used in this

report to identify recharge across the upper surface of the site-scale model and outputs from the regional model were used to identify flow targets across the lateral boundaries of the site-scale model. This evaluation was performed in accordance with the data requirements of SCI-PRO-006, Section 6.2.1(L). A finding that the regional model is suitable for this specific application means that it is qualified to support the license application, but only for the uses made in this report. The appropriateness and limitations of the data with respect to intended use are addressed in this appendix.

C1.2 SCOPE

This data suitability evaluation identifies one data tracking number (DTN) containing unqualified, developed hydrogeological data associated with the DVRFS model. These data were collected by the USGS and are cited in a USGS Scientific Investigations Report by Belcher (2004 [DIRS 173179]). The data evaluated in the plan are presented in DTN: MO0602SPAMODAR.000 [DIRS 177371], "Model Archives from USGS Special Investigations Report 2004-5204, Death Valley Regional Ground-Water Flow System, Nevada and California – Hydrogeologic Framework and Transient Ground-Water Flow Model."

The aforementioned DTN is unqualified because it summarizes a study performed for the YMP and contains data collected by non-YMP personnel. MODFLOW-2000 (Harbaugh et al. 2000 [DIRS 155197]) had not been qualified as of the writing of this report. In addition to the recharge and lateral flow data used in this report, the data set contains other information that was not directly used here and is not within the scope of this evaluation activity. However, the larger body of data is used in the DVRFS model and must also be evaluated for the model outputs to be considered suitable for use in the SZ site-scale flow model. This appendix focuses on the specific data selected to support the SZ site-scale flow model. To the extent that only subsets of data within this DTN were used (e.g., cell-by-cell fluxes were extracted from the 2004 DVRFS model at positions corresponding to the boundaries of the SZ site-scale flow model), only those data are evaluated for suitability.

C1.3 DATA EVALUATION TEAM

The Chairperson for this data evaluation is Scott C. James.

The team member for this data evaluation is David K. Rudeen.

C1.4 BACKGROUND

C1.4.1 DVRFS

In the early 1990s, two numerical models of the DVRFS were developed by the DOE to support investigations at the Nevada Test Site (NTS), where nuclear tests were conducted from 1951 to 1992, and at Yucca Mountain. In general, the two models were based on the same hydrologic data set. However, the models differed in the details of their implementation and calibration techniques. These differences yielded somewhat different flowpaths and flux results between the two models.

An earlier version of the DVRFS was used to provide boundary conditions for the previous revision of the SZ site-scale flow model (BSC 2004 [DIRS 170015], Appendix B). Much of the justification used is still relevant even though some methods, data interpretations, software and inputs have changed. Many of these changes are due to expanded input databases, better interpretation methods, and model refinements rather than corrections to erroneous or faulty data and models. Therefore, evaluations here are expansions on the justifications presented earlier (BSC 2004 [DIRS 170015], Appendix B).

In 1998, the DOE requested that the USGS begin a 5-year project to develop an improved model of the DVRFS to support NNSA/NSO and YMP programs. This work was performed by the USGS in cooperation with the DOE under Interagency Agreements. Newly available data and modeling tools were used and the data and results of the previous regional-scale model were built upon. During this effort, the USGS cooperated with other Federal, State, and local entities in the region, including the National Park Service, the Fish and Wildlife Service, the Bureau of Land Management, and county governments in Nevada and California to benefit from their expertise. The ultimate objective of the DVRFS model project is the construction and calibration of a model that simulates the transient flow conditions throughout the model domain.

The hydrogeology, conceptual hydrologic model, and the hydrologic system inputs and outputs were used to construct a regional hydrogeologic framework model (HFM) and a transient numerical flow model. The flow model simulates transient conditions from 1913 through 1998 using the modular code, MODFLOW-2000 (Harbaugh et al. 2000 [DIRS 155197]) and yields the simulated steady-state head distribution representing prepumping conditions. Transient stresses imposed on the regional groundwater flow system include pumpage that occurred from 1913 through 1998, and flows from springs affected by pumping. Simulated areal recharge was held constant at average annual values.

The DVRFS model domain encompasses approximately 100,000 km^2 in Nevada and California and is bounded by latitudes 35°00'N and 38°15'N and by longitudes 115°00'W and 118°00'W (Belcher 2004 [DIRS 173179], p. 9).

C1.4.2 SZ Site-Scale Flow

The data from DTN: MO0602SPAMODAR.000 [DIRS 177371] are presented in *Death Valley Regional Ground-Water Flow System, Nevada and California – Hydrogeologic Framework and Transient Ground-Water Flow Model* (SIR 2004-5205) (Belcher 2004 [DIRS 173179]). Although that report is unqualified, the model was developed and reviewed in accordance with USGS policy and the model results were formally published in a Scientific Investigations Report after receiving USGS Director approval.

The domain of the SZ site-scale flow and transport model lies entirely within the larger domain of the regional-scale flow model. Three sources are used to develop estimates of recharge across the upper surface of the SZ site-scale model: (1) distributed recharge as used in the 2004 DVRFS, (2) flux at the bottom boundary of the 2003 UZ site-scale flow model (DTN: LB03023DSSCP9I.001 [DIRS 163044]), (3) and data from infiltration through Fortymile Wash (Savard 1998 [DIRS 102213]). Only the first of these data sources, the 2004 DVRFS model, is addressed in this appendix. Outflow from the UZ model is technical product output,

and the estimates of recharge from Fortymile Wash have been separately qualified (Wilson 2001 [DIRS 155614]; DTN: MO0102DQRGWREC.001 [DIRS 155523]).

Output from the regional model was used to develop estimates of flow across the lateral boundaries of the base-case SZ site-scale flow model. The SZ site-scale flow model uses a nested modeling approach, where uncertainties in boundary conditions for the smaller model are reduced by developing them from internal flow patterns calculated within a larger model. The increased precision and accuracy required in a site-specific study requires fine grid resolution, which is computationally expensive. To increase computational efficiency, the SZ flow model domain is reduced in size (area of model footprint) with the consequence that the model boundaries are often not optimally located where flow conditions are well understood. Thus, it is common to develop the boundary conditions from a larger, lower-resolution model that has optimally located boundaries (e.g., at groundwater divides). This is the process followed when using the regional model to develop boundary conditions for the SZ site-scale model.

C2. SUITABILITY EVALUATION APPROACH

C2.1 SUITABILITY EVALUATION METHODS

The regional model is unqualified because its input data and software are unqualified. The regional hydrologic and geologic data required for the model were collected outside the YMP. However, model construction and review were performed in accordance with accepted YMP quality assurance procedures and USGS policy (Belcher 2004 [DIRS 173179]). In view of these conditions and the unique status of the model in depicting regional flow, the data evaluation was guided by Method 5, *Technical Assessment*, of SCI-PRO-001, Attachment 3*, Considerations for Determining Qualification Methods*. This methodology was used as a guideline because of it provides well established framework for the suitability evaluation.

The Evaluation Team evaluated the appropriateness and accuracy of the methods used by the USGS to develop the regional model inputs and outputs. Technical assessments focused on the methodology used to prepare the model inputs and perform the modeling. The assessments also considered the appropriateness of the model results for the applied uses in this report and the accuracy requirements associated with those uses. Because the modeling was performed on a regional basis in an area with unevenly distributed data and complex hydrogeology, the modeling results are necessarily approximate. Such results can be appropriately used so long as consideration is given to limitations on their accuracy, precision, and representativeness for intended use.

C2.2 PLAN FOR QUALIFYING THE DATA

A technical assessment of the data will be undertaken in this data qualification process. It will be demonstrated that the processes used to generate the data were generated by qualified professionals, are reliable, and that there are prior uses of these type of data.

Evaluation Criteria: The unqualified data were evaluated for use in this report based on consideration of the following criteria. These criteria were selected to incorporate the

considerations in SCI-PRO-001, *Attachment 3, Considerations for Determining Qualification Methods*, and *Attachment 4, Qualification Process Attributes*.

1. Are the methods used to develop the regional-scale model reasonable and generally accepted by the technical community?

2. Are the methods used to develop boundary conditions for the SZ site-scale model from the regional-scale flow model results reasonable and generally accepted by the technical community?

3. Are there more appropriate sources of information for developing the SZ site-scale model boundary conditions?

4. Are the boundary condition data and their associated uncertainties acceptable for their intended use by the SZ site-scale flow model?

Other considerations:

1. Appropriateness of data acquisition and subsequent data development relative to intended use

2. Similar application or uses of data, model, or results

3. The qualifications of personnel and organization performing the work

4. The quality and reliability of the measurement control program

5. Peer and/or professional reviews of the data, model and results

6. Extent and reliability of the documentation.

Recommendation Criteria: A recommendation for suitability is based on the satisfactory resolution of the evaluation criteria. Although these criteria are considered in determining whether the data are appropriate for their intended use in the SZ site-scale flow model, the final conclusions of the Evaluation Team are based on expert judgment, and not all of the evaluation criteria may be applied.

C3. EVALUATION RESULTS

A technical assessment of the DVRFS model (Belcher 2004 [DIRS 173179]) was performed by evaluating the approach used to develop the model's input database, the code selection and model development processes, and the assessment of the model output. Each of these elements of the review is discussed in the following sections of this appendix. These sections summarize the data evaluated by the evaluation team, demonstrate the depth of data sources used and/or developed by the USGS and demonstrate the effort and diligence the USGS (Belcher 2004 [DIRS 173179]) put into the development of the DVRFS model.

C3.1 INPUT DATABASE

The methods used to compile the regional model's input database were reviewed with special emphasis on the recharge data that were directly used as the boundary condition at the water table in the SZ site-scale flow model. The model was constructed using methods that have been widely accepted within the technical community. The model was based primarily on existing data, accompanied by extensive analysis and synthesis. In compiling the input database, heavy reliance was placed on the USGS National Water Information System database and on formal USGS publications, such as professional papers, water resources (or scientific) investigations reports, and water supply papers. Because the USGS uses standard scientific work practices and rigorous procedural controls for data collection, these data sources are considered to be reliable. New methods of storage, retrieval, and analysis of the complex input database were used that take advantage of recent advances in the technology of Geoscientific Information Systems (GSIS). Emphasis on the input database focused on identifying regional discharge, recharge, the regional hydrogeologic framework, and the regional patterns of groundwater movement.

The USGS (Belcher 2004 [DIRS 173179], p. 103) conducted a series of studies to reassess previous estimates of the major flow components and hydraulic properties of the DVRFS region to improve the data for the conceptual model and for model calibration as part of the DVRFS investigation. These studies focused on refining estimates of natural groundwater discharge by developing local estimates of evapotranspiration, and compiling and making additional spring-flow measurements; compiling groundwater pumpage information to estimate the history of groundwater development; estimating groundwater recharge from numerical simulations of net infiltration; estimating boundary inflow and outflow by using regional hydraulic gradients and water budgets of areas adjacent to the DVRFS model domain; estimating hydraulic properties from available literature and aquifer-test data; and evaluating available water-level data to estimate representative pre- and post-pumping hydraulic head information. In general, existing and newly acquired data were evaluated using current technology and concepts, analyses were refined or new algorithms were implemented for making interpretations, and values appropriate for the regional extent and scale of the model were estimated.

C3.1.1 Discharge Component

Estimates of natural groundwater discharge were evaluated for Death Valley, Oasis Valley, and the other major discharge areas in the DVRFS model domain by the USGS (Belcher 2004 [DIRS 173179], p. 132). Natural groundwater discharge was estimated from evaporation from open water and moist, bare soil and from transpiration by the phreatophytes growing in the discharge area. Discharge from the many regional springs in these discharge areas was accounted for because most spring flow eventually is evapotranspired. In Pahrump and Penoyer Valleys, where groundwater is discharged both naturally and by pumping, natural discharge estimates were based on published sources and were assumed to vary with local pumping. In discharge areas not affected by pumping, rates of natural groundwater discharge were assumed to remain fairly constant, presuming no major changes in climate. Mean annual discharge from evapotranspiration for the model domain is estimated at about 115.5×10^6 m^3 (Belcher 2004 [DIRS 173179], p. 132).

The evapotranspiration investigations did not account for spring flow where springs supported narrow bands of riparian habitat along the valley margins or where local pumping had decreased spring flow. Previously published spring-discharge rates and some additional measurements of discharge from selected springs were compiled. Annual natural discharge from springs not accounted for in evapotranspiration studies is estimated at about 16.8×10^6 m^3 (Belcher 2004 [DIRS 173179], p. 132).

The local pumping of groundwater for large-scale agricultural use in Pahrump Valley caused Bennetts Spring to stop flowing in 1959 and Manse Spring to stop flowing around 1977. A history of groundwater use for the DVRFS (1913 to 1998) was developed by compiling available information and using various estimation methods to fill gaps where data were missing. In 1913, groundwater used to support agriculture in Pahrump Valley was estimated at less than 5×10^6 m^3. Groundwater pumping remained relatively constant through 1944 and thereafter increased steadily in response to agricultural expansion. The estimated total volume of groundwater pumped from the DVRFS model domain from 1913 to 1998 is about 3.276×10^6 m^3 and in 1998 about 93.5×10^6 m^3. These estimates are not adjusted for water potentially returned to the groundwater flow system (Belcher 2004 [DIRS 173179], p. 132).

C3.1.2 Recharge Component

Groundwater recharge is defined as water that infiltrates downward through the unsaturated zone into the water table. Most of the groundwater recharge originates from precipitation that falls on mountainous areas throughout the DVRFS. The distribution and quantification of recharge for basins in the DVRFS were evaluated by the USGS using empirical, water-balance, chloride mass-balance, and distributed-parameter methods (Belcher 2004 [DIRS 173179], p. 115).

Recharge in the DVRFS was estimated from net infiltration using a distributed-parameter, deterministic watershed model, INFILv3, documented in the USGS Water Resources Investigations Report 03-4090 (Hevesi et al. 2003 [DIRS 169681]). The INFILv3 model was developed by the USGS specifically for estimating the magnitude and the spatial and temporal distribution of net infiltration in the Death Valley region. In the INFILv3 model, net infiltration equals the sum of snowmelt, precipitation, and infiltrating surface flow minus the sum of evapotranspiration, runoff, and changes in root-zone storage. The approach simulated daily climate changes and numerous near surface processes controlling infiltration. The INFILv3 model was calibrated to available surface-water flow measurements and constrained by prior estimates of recharge and discharge. The INFILv3 model simulated a mean annual potential recharge to the model domain of about 125×10^6 m^3 from 1950 to 1999 (Belcher 2004 [DIRS 173179], p. 132).

The recharge fluxes from the regional model are consistent with similar magnitude fluxes independently estimated from the 2003 UZ site-scale flow model (DTN: LB03023DSSCP9I.001 [DIRS 163044]) and from the focused recharge through Fortymile Wash (Savard 1998 [DIRS 102213]). The correlation between topography and recharge is similar in the regional and the UZ models, both of which show decreasing recharge with decreasing elevations to the south. The magnitudes of recharge are also similar, ranging from near zero to 1,262 mm/yr beneath a stream channel with an average net recharge over the entire model domain of 2.8 mm/yr (Belcher 2004 [DIRS 173179], p. 115). In addition, the more refined UZ site-scale flow model

and Fortymile Wash analysis supplement the coarser, regional-scale analysis. The regional model focus is on broad topographical and vegetal considerations. It does not account for the refined topography of Yucca Mountain captured in the UZ site-scale flow model, nor does it specifically account for localized recharge from runoff in Fortymile Wash. Although residual uncertainties affect the recharge data, the total recharge mass fluxes of about 61.2 kg/s into the site scale SZ flow model from the 2004 DVRFS is small compared to the total lateral mass influx of about 617 kg/s calculated for the lateral boundaries of the model. Residual uncertainties in the recharge will therefore have relatively little impact on the overall modeling results. However, it is noted that beneath the repository site, where vertical seepage may be an important transport mechanism for migrating radionuclides, the recharge is comprehensively defined and integrated into the upper boundary of the SZ site-scale flow and transport model.

C3.1.2.1 Lateral Flow

Areas of potential inflow and outflow, or lateral flow, along the DVRFS model boundary were defined for prepumped conditions. Hydraulic gradients determined from a regional potentiometric map indicate that one boundary segment has no flow and that flow occurs across 11 of 12 lateral boundary segments of the model domain—8 boundary segments have inflow and 3 have outflow (Belcher 2004 [DIRS 173179], p. 118).

Lateral flow across the boundary of the DVRFS model domain was estimated. Flows from water-budget studies were compared to Darcy calculations by using hydraulic gradients obtained from a regional potentiometric surface map (Belcher 2004 [DIRS 173179], Appendix 1) and estimated hydraulic conductivities of the hydrogeologic units (HGUs) along the model boundary. The estimated mean annual groundwater flow into the model domain is about 18.4×10^6 m^3 and out of the model domain is about 9.5×10^6 m^3 (Belcher 2004 [DIRS 173179], pp. 118 and 132).

C3.1.2.2 Balance of Components

A water budget is used to assess the significance of individual flow components in the groundwater system and to evaluate the balance between inflows and outflows.

A water budget for the prepumping period (before 1913) computed for the DVRFS model domain was balanced to within about 7%. For prepumped conditions, annual recharge accounted for about 87% of the total inflow and natural discharge (evapotranspiration and spring flow) accounted for about 93% of the total outflow. Although natural discharge by evapotranspiration was assumed to represent prepumped conditions, actual discharge may have been reduced by local pumpage. The remainder of the inflow and outflow is accounted for by lateral flows into and out of the model domain (Belcher 2004 [DIRS 173179], p. 132).

The water budget for pumped conditions for the DVRFS model domain is incomplete because accurate estimates for the major hydrologic components are not available. Pumpage in 1998 was about 70% of the total outflow estimated for prepumped conditions. A likely source of most of the water being pumped from the DVRFS region is groundwater in storage. This water, when removed from the flow system, decreases the hydraulic head within aquifers and decreases natural discharge through evapotranspiration and from spring flow. These decreases are partly

reflected by declining water-level measurements in areas of pumping and by estimates showing declining spring discharge in Pahrump Valley (Belcher 2004 [DIRS 173179], p. 132).

C3.1.2.3 Hydraulic Properties

Previously developed reasonable ranges of hydraulic properties, primarily horizontal hydraulic conductivity, were used for the major HGUs of the DVRFS. Fracturing appears to have the greatest influence on the permeability of bedrock HGUs; the greater the degree of fracturing, the greater the permeability. In the Cenozoic volcanic rocks, alteration decreases hydraulic conductivity and welding forms brittle rocks that fracture more easily and increase hydraulic conductivity. Storage coefficients from the literature were used because field data necessary to develop HGU-specific values were extremely limited (Belcher 2004 [DIRS 173179], p. 133).

The average depth for hydraulic-conductivity estimates within the model domain is 700 m with a maximum depth of 3,600 m. Using these limited data, hydraulic conductivity decreased with depth. A rigorous quantification of a depth-decay function was prevented by the variability in available hydraulic-conductivity data (Belcher 2004 [DIRS 173179], p. 133).

C3.1.2.4 Hydraulic Head

Nearly 40,000 water levels measured since 1907 in about 2,100 wells were evaluated as part of the DVRFS investigation. Almost 100 wells in the DVRFS model domain have a record of 20 years or longer. Head observations representing steady-state, prepumped conditions were computed from about 12,000 water levels averaged at 700 wells in the DVRFS model domain. Head observations range from about 2,500 m above sea level in the Spring Mountains to nearly 100 m below sea level in Death Valley. Transient, pumped conditions were represented by head observations computed from nearly 15,000 water levels measured in about 350 wells. Water-level records for individual wells spanned periods from 1 to about 50 years. Each head observation was assigned an uncertainty based on potential errors related to uncertainties in the altitude measurement of a water level and fluctuations introduced by climate variations or any other non-simulated transient stress (Belcher 2004 [DIRS 173179], p. 133).

C3.1.3 Regional Hydrogeologic Framework

The regional HFM accounts for the influences of stratigraphy and geologic structure on groundwater movement, the hydrologic properties of the HGU, and the regional potentiometric surface. The framework is a geometrical configuration of the regional hydrogeologic structure designed to support the regional model. A regional digital elevation model was combined with geologic maps to provide a three-dimensional series of points locating the outcrops of individual geologic formations, geologic cross sections, and borehole lithologic logs. The surface and subsurface data were then interpolated to define the tops of HGUs.

A three-dimensional digital HFM was constructed to interpret the regional hydrogeology of the DVRFS. The HFM integrates existing and new geologic information developed in the DVRFS and describes the geometry and extent of the HGUs that control groundwater flow. It is a required information source for the DVRFS numerical groundwater flow model. The primary data sources used to develop the HFM are: digital elevation models, geologic maps, borehole

lithologic logs, geologic and hydrogeologic cross sections, local three-dimensional hydrogeologic framework models, and hydrostructural information. The geologic data from geologic maps, cross sections, and borehole lithologic logs were correlated into 27 HGUs. Gridded surfaces from other three-dimensional HFMs constructed for the NTS and Yucca Mountain were also used. The HFM defines regional-scale hydrogeology and structures to a depth of 4,000 m below sea level. The model has 1,500-m horizontal resolution and variable vertical thickness for the HGUs. The faults thought to be hydrologically significant were used for offsetting HGUs in the three-dimensional model (Belcher 2004 [DIRS 173179], p. 253).

The HFM was evaluated for accuracy by visual inspection and by analysis of the gridded surfaces for HGU extent and thickness. The HFM was compared to the known extent of HGUs, input cross sections, and other three-dimensional framework models. Evaluations of the HFM show that it generally portrays the regional hydrogeology. During flow-model calibration, in some locations the HFM did not allow accurate simulations. In such locations, the HFM was examined and the uncertainty in the existing interpretations considered; where alternative interpretations were appropriate and deemed necessary, the HFM was modified (Belcher 2004 [DIRS 173179], pp. 184 and 253).

C3.1.4 Discussion

The Evaluation Team found that the regional model's input database was diligently compiled using appropriate methodologies that take into account the difficulties of handling large amounts of data for a large and complex region, as well as the uncertainties that are present in much of the developed information. Data collection methods were based on standard scientific work practices using USGS procedures.

Discharges from evapotranspiration, playa evaporation, spring flow, and pumping were well researched, particularly the evapotranspiration component, which constituted the largest single source of discharge. Recharge was dominated by infiltration of precipitation, which remained somewhat uncertain despite significant efforts to quantify it. The average estimated regional recharge from infiltration of 125×10^6 m^3/yr (Belcher 2004 [DIRS 173179], pp. 132 to 133) amounts to over 87 percent of the total regional inflow. Although the general magnitude of the simulated net-infiltration volume was consistent with prior discharge and recharge estimates for the DVRFS region, substantial differences were observed in some local basins. Nonetheless, the spatial distribution of estimated net infiltration was considered a reasonable indication of the spatial distribution of the potential recharge across the model domain under current climate conditions (Belcher 2004 [DIRS 173179], p. 118).

C3.2 CODE SELECTION AND MODEL DEVELOPMENT

As of November 2006, *MODFLOW-2000* (Hill et al. 2000 [DIRS 158753]; Harbaugh et al. 2001 [DIRS 155197]) was used to simulate the DVRFS. This code is currently being added to the YMP software baseline and is expected to be available for use in qualified calculations. *MODFLOW-2000* incorporates a nonlinear least squares regression technique that is used to estimate aquifer parameters that yield the best fit to measured heads and discharges (Belcher 2004 [DIRS 173179], p. 346). Although more refined interim databases were developed, the final model was constructed with 16 layers with $1,500 \times 1,500$-m^2 grid spacing,

consisting of 27 HGUs through which groundwater flows (Belcher 2004 [DIRS 173179], p. 349). Belcher (2004 [DIRS 173179], p. 350) found this configuration appropriate for evaluation of regional-scale processes. These include the assessment of boundary conditions of local-scale models, the evaluation of alternative conceptual models, the approximation of aspects of regional-scale advective transport of contaminants, and the analysis of the consequences of changed system stresses, such as those that would be imposed on the system by increased pumping.

C3.2.1 Model Construction

The three-dimensional hydrogeologic data sets for the DVRFS described previously were discretized to develop the input arrays required for the model. Because the data sets were developed at grid cell resolutions ranging from 100 to 1,500 m, their discretization to a common, larger grid cell resolution inevitably results in further simplification of the flow-system conceptual model and HFM. This resampling and simplification of the three-dimensional hydrogeologic data sets were apparent in definition of the model grid, assignment of boundary conditions, and definition of model parameters (Belcher 2004 [DIRS 173179], p. 265).

A GSIS was used to ensure accurate spatial control of physical features and the finite-difference model grid. GSIS also was used during calibration to manipulate and compare model input data sets with model output (Belcher 2004 [DIRS 173179], p. 265).

C3.2.2 Hydraulic Properties

HGUs are the basis for assigning horizontal hydraulic conductivity, vertical anisotropy, depth decay of hydraulic conductivity, and storage characteristics to model grid. Model input arrays also were used to account for variations in the hydraulic properties within HGUs by zonation (Belcher 2004 [DIRS 173179], pp. 266 to 268).

To incorporate the hypothesis that hydraulic conductivity decreases with depth, exponential decay was implemented to yield HGUs that are relatively impermeable at depth and relatively permeable near the land surface (Belcher 2004 [DIRS 173179], p. 268).

Vertical anisotropy (the ratio of horizontal to vertical hydraulic conductivity) is defined for each HGU. Because of their layered nature, basin-fill sediments are likely to have significant vertical anisotropy. The assumed presence of solution features in carbonate rocks would indicate that these rocks have relatively small vertical anisotropy. The vertical anisotropy of other rocks and sediments would be expected to fall somewhere between these two extremes (Belcher 2004 [DIRS 173179], p. 268).

Model layers were simulated as confined, and the storage consequences of water-table changes over time were simulated using a storage coefficient in the top model layer that was equivalent to a specific yield. The top model layer was defined as the simulated potentiometric surface in the unconfined part of the system (Belcher 2004 [DIRS 173179], p. 268).

C3.2.3 Observations Used In Model Calibration

Poorly quantified or unquantified characteristics of the system can be constrained on the basis of observations. Observations used to calibrate the DVRFS model were those of hydraulic heads (water levels), changes in head over time due to pumpage, and discharge by evapotranspiration and spring flow. Estimated boundary flows (simulated as constant-head boundaries) were treated like observations but are less accurate than other observation types and were given less weight in the simulation (Belcher 2004 [DIRS 173179], p. 279).

For the prepumped, steady-state stress period, all observations were considered representative of steady-state conditions. For the pumped, transient stress periods, some hydraulic-head and discharge observations are not influenced by pumping and thus were also considered representative of long-term steady-state conditions. Hydraulic-head observations influenced by pumping were treated as head-change observations. Natural discharge from evapotranspiration and springs was considered to be constant and not influenced by pumping, with some exceptions. It was assumed that constant-head observations used to simulate flow into and out of the model boundary were not influenced by pumping (Belcher 2004 [DIRS 173179], p. 279).

C3.2.4 Hydraulic Head

Water levels measured in boreholes and wells located within the model domain were used to develop hydraulic-head and head-change observations for calibration of the regional flow model. Only those water levels considered representative of regional groundwater conditions were used to calculate head observations (Belcher 2004 [DIRS 173179], p. 279).

C3.2.5 Groundwater Discharge Observations and Errors

Discharge observations were developed primarily from discharge estimates that were derived from evapotranspiration estimates and spring-flow measurements discussed above. Uncertainty in the discharge from each area was also estimated (Belcher 2004 [DIRS 173179], p. 283).

C3.2.6 Boundary Flow Observations and Errors

The boundary flow observations were obtained from Belcher (2004 [DIRS 173179], Appendix 2) that estimates potential flow through 7 segments of the boundary of the DVRFS model domain. These values have a great deal of uncertainty associated with them, but were used as observations during calibration (Belcher 2004 [DIRS 173179], p. 283).

C3.2.7 Model Calibration

Model calibration is the process of changing model input values in an attempt to match simulated and actual conditions. Models typically are calibrated either by trial and error or by using formal parameter-estimation methods. Calibration of parameter values of the DVRFS model primarily relied on the parameter-estimation techniques available in MODFLOW-2000 and was achieved using a two-step process. First, the model was calibrated to prepumped (steady-state) flow conditions. Once calibrated, this model formed the initial condition for the transient flow model. The model was calibrated again to simulate transient flow conditions for 1913 to 1998 (Belcher 2004 [DIRS 173179], p. 283).

Sensitivity analyses were used to evaluate the information provided by the observations for the estimation of all defined parameters, and nonlinear regression was used to estimate parameter values that produced the best fit to observed hydraulic heads and discharges. For the DVRFS model, 100 parameters are used and more than 90 were estimated at some point during the modeling process. The maximum number of parameters estimated by nonlinear regression peaked at around 30 (Belcher 2004 [DIRS 173179], p. 283).

Uncertain aspects of the hydrogeology were evaluated by constructing models with different hydraulic property distributions and different methods to simulate evapotranspiration, spring flow, recharge, and the boundary conditions. These models were evaluated through sensitivity analyses and nonlinear regression methods. Also discussed was how model errors were detected when estimated parameter values were found to be unreasonable (Belcher 2004 [DIRS 173179], p. 283).

C3.2.8 Conceptual Model Variations

During calibration, a number of conceptual models were evaluated using regression methods within *MODFLOW-2000*. A best fit to hydraulic head, groundwater discharge, and boundary-flow observations was calculated for each conceptual model. Evidence of model errors or data problems was investigated after each model run. These analyses were used in conjunction with hydrogeologic data to modify and improve the existing conceptual model, observation data sets, and weighting (Belcher 2004 [DIRS 173179], p. 287). Model parameters that were varied include: horizontal hydraulic conductivity depth of decay of hydraulic conductivity, vertical anisotropy, storage properties hydrogeologic structures, recharge and discharge.

C3.2.9 Discussion

The Evaluation Team considers use of *MODFLOW-2000* to be appropriate. *MODFLOW* has been the industry standard for simulating flow. The advantages of *MODFLOW-2000* in simplifying the parameter estimation and calibration process and evaluation of the model results are clearly explained (Belcher 2004 [DIRS 173179], pp. 283 to 327). No model modifications were made without supporting hydrogeologic criteria. Also, hydraulic parameter values were maintained within reasonable bounds.

C3.3 MODEL EVALUATION

The final calibration was evaluated to assess the accuracy of simulated results by comparing measured and expected values to simulated values. The fit of simulated heads to observed hydraulic heads is generally good (residuals with absolute values less than 10 m) in most areas of nearly flat hydraulic gradients, and moderate (residuals with absolute values of 10 to 20 m) in the remainder of the areas of nearly flat hydraulic gradients. The poorest fit of simulated heads to observed hydraulic heads (residuals with absolute values greater than 20 m) is in steep hydraulic-gradient areas in the vicinity of Indian Springs, western Yucca Flat, and the southern Bullfrog Hills. Most of these inaccuracies can be attributed to: (1) insufficient representation of the hydrogeology in the HFM, (2) misinterpretation of water levels, and (3) model error associated with grid cell size (Belcher 2004 [DIRS 173179], p. 349).

Groundwater discharge residuals are fairly random, with as many areas in which simulated discharges are less than observed discharges as areas in which simulated discharges are greater than observed. The largest unweighted groundwater discharge residuals are in Death Valley and Sarcobatus Flat (northeastern area). The two major discharge areas that contribute the largest volumetric error to the model are the Shoshone/Tecopa area and Death Valley. Positive weighted residuals were computed in transient simulations of the Pahrump Valley that may indicate a poor definition of hydraulic properties and discharge estimates, especially near Bennetts Spring (Belcher 2004 [DIRS 173179], p. 349).

Parameter values estimated by the regression analyses were within the range of expected values. As with any model, uncertainties and errors remain, but this model is considered an improvement on previous representations of the flow system (Belcher 2004 [DIRS 173179], p. 350).

Inherent limitations result from uncertainty in three basic aspects of the model inadequacies or inaccuracies: in observations used to calibrate the model, in the representation of geologic complexity in the HFM, and in representation of the groundwater flow system in the flow model. It is important to understand how these characteristics limit the use of the model. These basic aspects of the model are represented at a regional scale, and the use of the model to address regional-scale issues or questions is the most appropriate use of the model (Belcher 2004 [DIRS 173179], p. 350).

C3.4 DISCUSSION

The Evaluation Team concurs with Belcher (2004 [DIRS 173179], p. 349) that this model provides a generally good simulation of the DVRFS. Considering the large size of the region, the hydrogeologic complexity, and the sparse data, achieving any better overall validation accuracy would have been surprising. The team found that the DVRFS model database was well researched, the model was appropriately constructed, and the resulting output provides a reasonable simulation of regional flow. Fitting techniques used by Belcher (2004 [DIRS 173179]) were considered state-of-the-art when the report was published. The calibration process and the uncertain aspects of the hydrogeology that were evaluated through the sensitivity analyses and nonlinear regression methods are well described (Belcher 2004 [DIRS 173179], pp. 283 to 327). Uncertainties in the model output are of potential concern to the Evaluation Team because the simulated fluxes along the boundaries of the SZ site-scale flow models account for most of the flow through this model. Fluxes are dependent on the adopted hydraulic properties and the DVRFS adopted hydraulic properties are technically reasonable for the given units and rock types. The model assumption that conductivity decreases with respect to depth is reasonable for the given rock type. In the SZ site-scale flow model, the fluxes in the 16 regional model layers are combined to provide total flow across the boundary for vertical panels of various widths extending from the water table to a depth of 4,000 m below the water table. Uncertainties are incorporated into the SZ site-scale models by treating the fluxes as target values during model calibration. Fixed-head boundary conditions were assigned to the perimeter of the SZ site-scale models from regional water level and head data, where heads were varied laterally along the model perimeter but were held constant in the vertical direction. Other targets were also considered during base-case SZ site-scale flow model calibration that affect fluxes, including rock permeabilities and specific discharge estimates given by the Expert Elicitation Panel (see Section 6.5.1.3). A comparison of the resulting calibrated boundary fluxes of the

site-scale model with those determined from the regional model shows a reasonable matching of total boundary fluxes but greater differences, some on the order of 100%, for individual boundary segments (Section 6.5.2.2). The reasons for these differences are primarily attributed to the increased resolution of the site-scale model. In addition, the pumping wells modeled in the 2004 DVRFS are not considered in the SZ site-scale flow model. These discharges are effectively replaced by additional flux through the southern boundary of the SZ site-scale flow model because constant head boundary conditions reflect drawdown due to pumping. Use of the regional model flux data as target rather than absolute values in the site-scale model is appropriate considering the uncertainties inherent in those data and the fact that DVRFS model does not necessarily match estimated regional recharge/discharge fluxes.

Upon review of the alternative models (e.g., Waddell 1982 [DIRS 101062]; Rice 1984 [DIRS 101284]), the DVRFS model was found to be the most appropriate source of information for both distributed recharge and lateral flow boundary conditions for the SZ site-scale flow and transport model.

C3.5 SUMMARY OF EVALUATION RESULTS

The Evaluation Team found the DVRFS model database to be well researched, the model to be appropriately constructed, and the resulting output to provide a reasonable simulation of regional flow. Sound methodologies were used during the calibration process, in that, the model was not modified without supporting hydrogeologic criteria and hydraulic parameter values were maintained within reasonable bounds.

Quantification of the recharge component of flow was reviewed in particular detail because of the direct use of those data in the SZ site-scale flow model. Recharge in the DVRFS region was estimated from net infiltration using a deterministic mass-balance method. The approach, using INFIL V3, simulated daily climate changes and numerous near surface processes controlling infiltration. As expected, recharge was dominated by infiltration of precipitation. Within the domain of the SZ site-scale flow and transport model, the recharge fluxes from the regional model are consistent with estimates from the 2003 UZ site-scale flow model and with focused recharge from Fortymile Wash. Discharges from evapotranspiration, playa evaporation, spring flow, and pumping were well researched, particularly the evapotranspiration component, which constituted the largest single source of discharge. The Evaluation Team considers use of the *MODFLOW-2000* code in constructing the model to be appropriate. The MODFLOW codes have become industry standards and the advantages of the *MODFLOW-2000* adaptation in simplifying the calibration process and evaluating the model results were important.

The simulated hydraulic heads of the final calibrated transient model generally fit observed heads reasonably well (residuals with absolute values less than 10 m) with two exceptions: in most areas of nearly flat hydraulic gradient the fit is considered moderate (residuals with absolute values of 10 to 20 m), and in areas of steep hydraulic gradient, the fit is poor (residuals with absolute values greater than 20 m). The Evaluation Team considers the overall goodness-of-fit of the regional model to be good, although in some cases a significant degree of uncertainty is associated with the model outputs. Nevertheless, the output from the 2004 DVRFS model is relevant and appropriate for its intended use.

Uncertainties in the simulated fluxes along the lateral boundaries of the SZ site-scale flow model are potentially significant because these fluxes constitute the greatest sources of flow through the SZ site-scale model and they are not independently corroborated. However, these uncertainties were recognized in calibrating the site-scale model by using the regional model fluxes along with other data sources in a generalized manner as calibration targets rather than as fixed model inputs. Actual boundary conditions in the site-scale model were defined by fixed heads, which are better known than the boundary fluxes. This approach made the fluxes largely a function of the calibrated model permeabilities. A comparison of the resulting calibrated regional and site-scale model boundary fluxes shows reasonable matching of total fluxes but greater differences, some on the order of 100%, for individual boundary segments. These observations indicate that the use of the regional model flux data in the site-scale model is appropriately generalized considering the uncertainties inherent in those data.

C4. EVALUATION CONCLUSIONS

The conclusions of the Evaluation Team review of the regional model are presented below in terms of the primary evaluation criteria presented in Section C2.2.

1. *Are the methods used to develop the regional-scale model reasonable and generally accepted by the technical community?*

   The methods used to develop the database, the choice of models, the methods of calibration, and the analysis of the results are all reasonable and generally accepted by the technical community. The use of GSIS to store, manipulate, and analyze the data is also accepted by the technical community.

2. *Are the methods used to develop boundary conditions for the SZ site-scale model from the regional-scale flow model results reasonable and generally accepted by the technical community?*

   The nested model approach for obtaining lateral flux boundary conditions for smaller models is well established and accepted by the technical community. The recharge boundary for the regional model was obtained from a net-infiltration model, INFIL V3, which was calibrated to available surface-water flow measurements and constrained by prior estimates of recharge and discharge. The model and method are also well established and accepted by the technical community.

3. *Are there more appropriate sources of information for developing the SZ site-scale model boundary conditions?*

   Other sources of similar information are older and less well developed than the 2004 DVRFS model. The regional model was developed in part to support site-scale modeling. It provides a reasonable and comprehensive simulation of regional flow, and is an appropriate source of information for developing hydrologic boundary conditions for the SZ site-scale model.

4. *Are the boundary condition data and their associated uncertainties acceptable for their intended use by the SZ site-scale flow model?*

   Uncertainties in the lateral boundary condition data have been appropriately addressed by using them as target values for SZ site-scale flow model calibration. The calibration has been successfully completed using this approach, indicating that the boundary condition data have been successfully used and are therefore appropriate for their intended use. In addition, much of the source data for the regional model are YMP-accepted data, the *MODFLOW-2000* code is currently being qualified for project use, the regional model has been validated and residual uncertainties have been identified, and the modeling effort was adequately reviewed and documented. Furthermore, it should be noted that differences between the 1997 DVRFS (D'Agnese et al. 1997 [DIRS 100131]) and the 2001 DVRFS (D'Agnese et al. 2002 [DIRS 158876]) models, while not extraordinary, can largely be attributed to the fact that the 1997 DVRFS model simulates conditions found in the early 1990s (includes pumping) and the 2001 DVRFS model simulates predevelopment conditions (no pumping). The 2004 DVRFS, with extensive modeling enhancements, combines both the predevelopment condition in the initial steady state step and groundwater pumping in subsequent transient steps.

C5. RECOMMENDATIONS

The Evaluation Team has concluded that the Death Valley regional flow model database was well researched, the model was appropriately constructed, and the resulting output provides a reasonable simulation of regional flow based on application of all evaluation criteria. At the time of publication of this report, this model was the most recent and best-supported SZ flow model of the Yucca Mountain region. It incorporates updated geological and hydrogeological data, it benefits from contemporary geological and hydrogeological conceptual models, and it provides a three-dimensional representation of the region. Upon review of the alternatives, the DVRFS model was found to be an appropriate source of information for both recharge and lateral flux boundary conditions for the SZ site-scale flow and transport model.

Based on the foregoing evaluation, the Evaluation Team has concluded that the 2004 DVRFS model provides a suitable source of data for establishing recharge and lateral flux boundary conditions for the SZ site-scale flow and transport model. In accordance with SCI-PRO-006, this finding qualifies these data only for their intended uses in this report. The source DTN: MO0602SPAMODAR.000 [DIRS 177371] will remain unqualified for other uses.

APPENDIX D
DATA SUITABILITY EVALUATION – NYE COUNTY EARLY WARNING DRILLING PROGRAM (NC-EWDP) WELL DATA

D1. INTRODUCTION

SCI-PRO-006, Section 6.2.1(L), establishes the process for documenting performance assessment modeling activities:

> "Data obtained from external sources that are not established fact must be qualified for intended use either in accordance with SCI-PRO-001 or within the specific model by doing the following:
>
> 1. Plan and document the qualification process in the model report. Documentation will include:
>
>   - Description of unqualified external source data evaluated
>
>   - Data qualification method(s) used (as specified in Attachment 3 of SCI-PRO-001) and rationale for selection of method(s)
>
>   - Acceptance criteria used to determine if the data are qualified (as related to the attributes in Attachment 4 of SCI-PRO-001)
>
>   - The decision as to the qualification of the data
>
> 2. If relevant data from external sources are evaluated against any of the above factors and determined not to meet a criterion, describe the basis for this conclusion. Also document whether the data were justified using an alternative factor (i.e., acceptance criteria) and included as direct input to the technical product, or excluded from the technical product."

D1.1 PURPOSE

The plan for this appendix is to evaluate the suitability (based on the above-mentioned criteria) of unqualified Nye County well data for use in the SZ site-scale flow model. The well data are used in developing the potentiometric surface and to calibrate and validate the SZ site-scale flow model. Specifically, these data are the coordinates of the well head (UTM), average depths of the open intervals, and measured water levels. The well data were developed from the NC-EWDP, which is considered an outside source and they are not established fact and, therefore, the data are considered unqualified.

To facilitate this plan, this evaluation uses the methodologies of SCI-PRO-001 as a guideline to qualify applicable portions of a dataset for intended use in this report in accordance with the requirements of SCI-PRO-006, Section 6.2.1(L) (see above). Some of the methodologies of SCI-PRO-001 were incorporated because they provide a sound, well established framework for demonstrating suitability of the NC-EWDP well data for intended use within this product only. However, SCI-PRO-006 is the governing procedure used to qualify the data for use within this technical product only. The data will remain unqualified for all other uses, unless it is separately qualified outside of this report. A finding that the data from Nye County wells are suitable for

intended use means that they are qualified to support the license application, but only for the uses made in this report. The appropriateness and limitations of the data with respect to intended use are addressed in this appendix. This appendix demonstrates the suitability of these data for use in this model using arguments supporting the data reliability, qualifications of the organization, and prior uses of the data.

D1.2 SCOPE

This appendix identifies one DTN containing unqualified data associated with the Nye County well dataset. These data were collected by the Early Warning Drilling Program. The data also reside in the TDMS for use by the YMP. The data evaluated in this appendix consisting of dozens of DTNs, were obtained from TDMS and consolidated into a single model Output DTN: SN0702T0510106.007. The consolidated DTN consists of acquired survey data in geographic (latitude-longitude) coordinates, water-level measurement open-intervals, water-level histories and time averaged water-levels for wells 7SC, 10P, 10S, 16P, 18P, 19IM1, 19IM2, 19PB, 22PA, 22PB, 22S, 23P, 24P, 27P, 28P, and 29P, and Phase V wells 13P, 22PC, 24PB, 32P, and 33P. Well locations in terms of UTM coordinates for 7SC through 29P are provided in Output DTN: LA0612RR150304.001 and are discussed in Appendix F. Well locations for Phase V wells are developed in Output DTN: SN0702T0510106.007. The aforementioned DTN is unqualified because it contains data collected by non-YMP personnel under QA procedures that are different than YMP QA procedures. This qualification report focuses on the specific data selected to support the SZ site-scale flow model. To the extent that only subsets of data within this DTN were used, only those data are evaluated for suitability (see Table D-2).

D1.3 DATA EVALUATION TEAM

The chairperson for this evaluation is Scott C. James, SNL, Department 8757.

The team member for this evaluation is David K. Rudeen, RHYM,Inc. (SNL, Department 6781).

D2. EVAUATION APPROACH

D2.1 EVAUATION METHODS

The Nye County well data are unqualified because they were collected outside the YMP. However, these data were evaluated for use in this report because the data source is considered reliable, the data have been used in previous revision of this report, and there are available corroborating data from qualified sources (proximally located qualified water levels). Also, Nye County has a rigorous Quality Assurance Program (QAP). In view of these conditions the data were evaluated for their intended use using a combination of Method 1, *Equivalent QA Program*, and Method 2, *Corroborating Data,* from SCI-PRO-001, Attachment 3, *Considerations for Determining Qualification Methods*, as a guide. SCI-PRO-001 methodologies are only used as framework for the suitability evaluation because, they are sound and well established.

D2.2 PLAN FOR QUALIFYING THE DATA

A technical assessment of the data will be undertaken in this data qualification process. It will be demonstrated that the processes used to generate the data were generated by qualified professionals, are reliable and there is available corroborating data.

The NC-EWDP data were evaluated for use in this report based on consideration of the following evaluation criteria. These criteria were selected to incorporate the considerations in SCI-PRO-001, Attachment 3*, Considerations for Determining Qualification Methods* and Attachment 4*, Qualification Process Attributes*.

1. Is there functional equivalence of the data-gathering process to applicable QARD concepts (qualification of personnel, technical adequacy of equipment and procedures, quality and reliability of measurement control and audits)?

2. Is the data addressed in this appendix consistent with corroborating data?

3. Are the methods used to incorporate the data into the SZ site-scale model reasonable and generally accepted by the technical community?

4. Are there more appropriate sources of the required SZ site-scale model data?

5. Are the associated uncertainties acceptable for their intended use by the SZ site-scale flow model?

A recommendation of suitable for intended use is based on the satisfactory resolution of the evaluation criteria. Although these criteria are considered in determining whether the data are appropriate for their intended use in the SZ site-scale flow model, the final conclusions of the Evaluation Team are based on expert judgment, and not all of the evaluation criteria may be applied.

D3. EVALUATION RESULTS

The data from several Nye County wells will be used to develop the potentiometric surface and to calibrate and validate the SZ site-scale flow model. As such, the wells need to be located with an accuracy on the order of 10 m and water levels and open interval should be measured to the nearest 1 m. Nye County well data meet these criteria. The suitability of these data is, therefore, justified for this specific application. These data are considered acceptable for use in this report because the personnel (Nye County geologists) and organization (the Early Warning Drilling Program, EWDP) collecting the data are qualified to do so, the data have been used in previous revisions of this report, and there are available corroborating data from qualified sources (proximally located qualified water levels). Most importantly, Nye County has a rigorous Quality Assurance Program that governs the development and implementation of procedures used for sample collection and data production and, while it is not necessarily equivalent to the Yucca Mountain Quality Assurance Program, it meets the highest standard required under their Quality Assurance Program, which adds confidence to the initial quality of the data.

D3.1 QA PROGRAM

The NWRPO QAP provides assurance that data gathered from Nye County nuclear waste oversight and investigation programs are of the highest quality. The QA program ensures that NWRPO scientific activities proceed in a systematic and technically sound manner. The QAP uses documented instructions and procedures to ensure the validity, integrity, preservation and retrievability of all data generated by NWRPO programs. Comprehensiveness of the Nye County QAP is illustrated by the index shown in Figure D-1.

Nye County policy requires the NWRPO to establish and maintain a documented Quality Assurance Program for the purpose of ensuring the NWRPO will continually achieve quality of performance in all areas of its responsibilities, through the application of effective management systems and in conformance with its mission. The NWRPO QAP meets the requirements of ANSI/ASME NQA-1 [DIRS 176399] and the criteria at 10 CFR Part 50 [DIRS 176567], Appendix B.

All NWRPO personnel and contractors or subcontractors who perform or manage quality-affecting functions, work under the procedures outlined in the QAP. The NWRPO Project Manager is responsible for assuring all work performed under his or her direction complies with the requirements of the QAP. The YMP Quality Assurance Officer is responsible for establishing, implementing and verifying the QAP complies with this policy.

The QAP provides assurance that data derived from NWRPO oversight and investigation programs are of the highest quality. The QAP ensures NWRPO scientific activities proceed in a systematic manner, using documented instructions and procedures that ensure the validity, integrity, preservation, and retrievability of data generated.

Revision 11, 03-31-04

NYE COUNTY NUCLEAR WASTE REPOSITORY PROJECT OFFICE
QUALITY ASSURANCE NUMERICAL INDEX

Number	Title	Revision	Date	Change Notices
	Policy Documents			
QAPP	Quality Assurance Program Plan	4	6-15-03	
	Quality Administrative Procedures			
QAP-3.1	Independent Technical Review	1	3-31-04	
QAP-3.2	Documentation of Technical Investigations	2	3-31-04	
QAP-5.1	Preparation of Quality Administrative Procedures	1	3-31-04	
QAP 5.2	Preparation of Work Plans, Test Plans, and Technical Procedures	2	3-31-04	
QAP-6.1	Issue and Control of Quality Assurance Documents	1	3-31-04	
QAP-7.1	Procurement of Items and Services	1	3-31-04	
QAP-8.1	Sample Management	1	3-31-04	
QAP-12.1	Control of Measuring and Test Equipment	2	3-31-04	
QAP-15.1	Control of Nonconforming Items or Activities	1	3-31-04	
QAP-16.1	Corrective Action	1	3-31-04	
QAP-17.1	Records Management	2	3-31-04	
QAP-18.1	Audits and Surveillances	1	3-31-04	

Figure D-1. Snapshot of Index Nye County QAP

The NWRPO QAP is based on the interpretation of Federal requirements (ANSI/ASME NQA-1 [DIRS 176399]), 10 CFR Part 50, Appendix B [DIRS 176567]) for nuclear power plants, adapted for waste repository research. The program also establishes procedures for controlling activities that ultimately affect the final product of NWRPO oversight and investigation. The extent to which this QAP deals with quality assurance and the responsibilities outlined within the range of NWRPO activities, is consistent with the importance of individual tasks. NWRPO QA program components include: (1) impact monitoring and assessment, (2) suitability evaluation and compliance, (3) employment and procurement outreach, and (4) public involvement and education.

The current NWRPO QAP was reinitiated in March of 1997 after being in hiatus since October of 1996. The program focuses on the establishment of fundamental elements of the quality assurance program, including creation of a measuring and test equipment control system and refinement of a quality assurance records management system.

The primary issue facing the NWRPO QAP is ensuring the traceability and validity of data gathered by the program. The QA applied to the gathering and analysis of data must be sufficient to ensure their conformance to regulatory controls. In addition, as NWRPO technical activity increases, QA audits, surveillance, and evaluation actions also increase. As additional technical and administrative staff is added, it is necessary to communicate relevant. QA responsibilities and provide proper training to enable project participants to perform appropriate QA.

D3.2 CORROBORATING DATA

Unqualified Nye County well data is compared with existing qualified Nye County and private well data in Table D-1. Well locations used for comparison are sometimes hundreds to thousands of meters separated, so exact comparisons are not expected. The comparison is made with nearest qualified well or a well that is expected to be in a comparable head region given the understood head gradient in the region. Differences tend to be well within the range of residuals seen from the calibration and consistent regions of flat gradients (lower residuals) just south of the repository and high gradients (higher residuals) in the region hear U.S. Highway 95 Fault. The largest difference (–37.8) is for the deepest open interval (Z4) at well NC-EWDP-7SC for which the qualified well did not have a corresponding open interval. Overall the new Nye County EWDP well data is very consistent with existing qualified data and is deemed appropriate for use as calibration targets and development of the potentiometric surface.

Table D-1. Comparison of New Nye County Well Data with Corroborating Data

Well ID	X-UTM (m)	Y-UTM (m)	Elevation (m)	Measured Head (m)	Qualified Well ID	X-UTM (m)	Y-UTM (m)	Qualified Head (m)	Difference (m)
NC-EWDP-7SC	539632	4064317	704.5	828.5	NC-EWDP-7S	539638	4064323	830.3	–1.8
NC-EWDP-7SC-Z1	539632	4064317	812.6	830.3	NC-EWDP-7S	539638	4064323	830.3	0
NC-EWDP-7SC-Z2	539632	4064317	779.1	830.4	NC-EWDP-7S	539638	4064323	830.3	0.1
NC-EWDP-7SC-Z3	539632	4064317	741	821.7	NC-EWDP-7S	539638	4064323	830.3	–8.6
NC-EWDP-7SC-Z4	539632	4064316	704.5	792.5	NC-EWDP-7S	539638	4064323	830.3	–37.8
NC-EWDP-10P Deep	553149	4064916	650.4	726.9	UE-25 J-12	554444	4068774	727.9	–1.0
NC-EWDP-10P Shallow	553149	4064916	696.4	726.9	UE-25 J-12	554444	4068774	727.9	–1.0
NC-EWDP-10S-Z1	553140	4064899	696	727	UE-25 J-12	554444	4068774	727.9	–0.9
NC-EWDP-10S-Z2	553140	4064899	650.3	727.5	UE-25 J-12	554444	4068774	727.9	–0.4
NC-EWDP-18P	549416	4067233	702.3	711.2	NC-EWDP-2DB	547800	4057196	712.6	–1.4
NC-EWDP-19IM1-Z1	549317	4058291	691.1	711.9	NC-EWDP-19D	549317	4058271	711.8	0.1
NC-EWDP-19IM1-Z2	549317	4058291	659.1	712.1	NC-EWDP-19D	549317	4058271	711.8	0.3
NC_EWDP-19IM1-Z3	549317	4058291	628.6	712.5	NC-EWDP-19D	549317	4058271	711.8	0.7
NC_EWDP-19IM1-Z4	549317	4058291	589	713.3	NC-EWDP-19D	549317	4058271	711.8	1.5
NC_EWDP-19IM1-Z5	549317	4058291	545	711.8	NC-EWDP-19D	549317	4058271	711.8	0.0
NC_EWDP-19IM2	549337	4058291	599.2	723.3	NC-EWDP-19D	549317	4058271	711.8	11.5
NC_EWDP-22PA Deep	552020	4062038	652	724.8	NC-EWDP-4PB	553281	4056774	723.5	1.3
NC_EWDP-22PA Shallow	552020	4062038	700.9	724.8	NC-EWDP-4PB	553281	4056774	723.5	1.3
NC_EWDP-22PB Deep	552038	4062037	514.9	724.8	NC-EWDP-4PB	553281	4056774	723.5	1.3
NC_EWDP-22PB Shallow	552038	4062037	584.9	724.8	NC-EWDP-4PB	553281	4056774	723.5	1.3
NC_EWDP-22S-Z1	552019	4062020	700.3	724.9	NC-EWDP-4PB	553281	4056774	723.5	1.4
NC_EWDP-22S-Z2	552019	4062020	651.7	724.9	NC-EWDP-4PB	553281	4056774	723.5	1.4
NC_EWDP-22S-Z3	552019	4062020	584.9	724.9	NC-EWDP-4PB	553281	4056774	723.5	1.4
NC_EWDP-22S-Z4	552019	4062020	514.8	724.9	NC-EWDP-4PB	553281	4056774	723.5	1.4
NC_EWDP-23P Deep	553923	4059875	649.2	724.3	NC-EWDP-4PB	553281	4056774	723.5	0.8

Table D-1. Comparison of New Nye County Well Data with Corroborating Data (Continued)

Well ID	X-UTM (m)	Y-UTM (m)	Elevation (m)	Measured Head (m)	Qualified Well ID	X-UTM (m)	Y-UTM (m)	Qualified Head (m)	Difference (m)
NC_EWDP-23P Shallow	553923	4059875	704	724.2	NC-EWDP-4PB	553281	4056774	723.5	0.7
NC_EWDP-16P	545665	4064263	722.3	729.4	Cind-R-Lite Well	544027	4059809	729.8	–0.4
NC_EWDP-19PB Deep	549337	4058316	659.5	707.9	NC-EWDP-19D	549317	4058271	711.8	–3.9
NC_EWDP-19PB Shallow	549337	4058316	702.1	707.4	NC-EWDP-19D	549317	4058271	711.8	–4.4
NC_EWDP-24P	549386	4062055	786.4	727.1	USW WT-11	547542	4070428	730.7	–3.6
NC_EWDP-27P	544935	4065276	728.2	728.6	Cind-R-Lite Well	544027	4059809	729.8	–1.2
NC_EWDP-28P	545746	4062393	718.7	729.3	Cind-R-Lite Well	544027	4059809	729.8	–0.5
NC_EWDP-29P	549396	4059606	719.2	724.8	NC-EWDP-15P	544927	4058163	722.4	2.4
13P	543471	4066433	759.5	764.4	NC-EWDP-9SX,P1	539118	4061010	766.4	–2.0
22PC-Z1	552037	4062019	702.3	724.9	NC-EWDP-4PB	553281	4056774	723.5	1.4
22PC-Z2	552037	4062019	651.8	724.9	NC-EWDP-4PB	553281	4056774	723.5	1.4
24PB	549387	4062025	621.6	727.2	USW WT-11	547542	4070428	730.7	–3.6
32P-Z1	546184	4054789	697.1	701.7	NC-EWDP-2D	547823	4057170	706.1	–4.4
32P-Z2	546184	4054789	631.5	701.0	NC-EWDP-2D	547823	4057170	706.1	–5.1
32P-Z3	546184	4054789	558.2	701.1	NC-EWDP-2D	547823	4057170	706.1	–5.0
33P-Z1	545117	4057146	713.1	720.8	NC-EWDP 15P	544927	4058163	722.4	–1.6
33P-Z2	545117	4057146	629.7	721.9	NC-EWDP 15P	544927	4058163	722.4	–0.5
33P-Z3	545117	4057146	594.2	721.8	NC-EWDP 15P	544927	4058163	722.4	–0.6

Sources: DTNs: GS010908312332.002 [DIRS 163555], Output DTNs: LA0612RR150304.001, see Appendix F; SN0702T0510106.007. See Table D-2 for well to DTN mapping.

D4. EVALUATION CONCLUSIONS

The conclusions of the Evaluation Team review of the Nye County well data are presented below in terms of the evaluation criteria presented in Section D2.2.

1. *Is there functional equivalence of the data-gathering process to applicable QARD concepts (qualification of personnel, technical adequacy of equipment and procedures, quality and reliability of measurement control and audits)?*

The evaluation in Section D3 found the Nye County QAP (index shown in Figure D-1) to be functionally equivalent to applicable QARD concepts. The Nye Count QA program ensures NWRPO scientific programs, including the EWDP, proceed in a systematic and technically sound manner. The documented instructions and procedures ensure the qualification of personnel, the technical adequacy of equipment and testing procedures and the validity, integrity, preservation and retrievability of data generated by the NWRPO programs.

2. *Are the data addressed in this appendix consistent with corroborating data?*

The data addressed in this appendix is consistent with the corroborating data presented above. Measurements from wells in close proximity and in same formations agree to within expectations and requirements of the intended use.

3. *Are the methods used to incorporate the data into the SZ site-scale model reasonable and generally accepted by the technical community?*

The use of well data in both the construction of the potentiometric surface and as calibration targets in the SZ site-scale flow model is well established and accepted by the technical community.

4. *Are there more appropriate sources of the required SZ site-scale model data?*

Other sources of similar information are older and less well developed than the recently obtained well data. The Nye County well data was obtained in part to support YMP ground flow monitoring and modeling. It provides a reasonable and most comprehensive source of head data and is an appropriate source of information for developing hydrologic data for the SZ site-scale model.

5. *Are the associated uncertainties acceptable for their intended use by the SZ site-scale flow model?*

Uncertainties in the well data have been appropriately addressed by using them as target values for SZ site-scale flow model calibration. The calibration has been successfully completed using this approach, indicating that the well data have been successfully used and are therefore appropriate for their intended use.

Based on the assessment of the NWRPO QAP and corroborating data presented above, the Nye County well data are considered suitable for use in both the construction of the potentiometric surface and as calibration targets for the SZ site-scale flow model. In accordance with criteria established in Section D2.2, this finding qualifies these data only for their intended uses in this report. The Output DTN: SN0702T0510106.007 will remain unqualified for other uses.

D6. DATA SOURCE AND DEVELOPMENT

This section describes the data sources compiled into Output DTN: SN0702T0510106.007 as well as documents the qualified software and basic MS-Excel spreadsheet calculations used to convert the NC-EWDP well data into a form suitable for use in the SZ site-scale flow model.

A list of Nye County wells with data to be qualified in this appendix and their corresponding DTNs are presented in Table D-2. YMP qualified software (CORPSCON V.5.11.08, STN: 10547-5.11.08-00 [DIRS 155082]) was used to convert the GPS latitude and longitude coordinates into UTM (m) coordinates for modeling purposes in Output DTN: LA0612RR150304.001 (see Appendix F) and for Phase V wells in Output DTN: SN0702T0510106.007. These data are summarized in Table D-3. To calibrate the SZ site-scale flow model, in addition to the UTM coordinates of the well and water level, the measurement point is also needed. This measurement point corresponds to the midpoint of the open interval of the well screen. The land surface elevations, distances to the tops and bottoms of the open interval well screens and measurement points are presented in Table D-4. Water-level data are provided in Tables D-5 and D-6. The measurement point elevations (or reference elevations) listed in Table D-5 are different than the ground surface elevations presented in Table D-3 and the open interval measurement points listed in Table D-4.

The data listed in Tables D-3 through D-6 were developed as follows:

DTNs (Table D-2) are available for GPS survey summary reports and well completion reports for most of the NC-EWDP wells discussed in this appendix. Data discussed in this appendix were developed from the reports as follows:

- Well locations in UTM coordinates consistent with the SZ Flow model were calculated from longitude/latitude geographic coordinates obtained from the DTNs listed in Table D-2. UTM coordinates for calibration wells NC-EWDP-7SC through -29P were provided by Output DTN: LA0612RR150304.001, which is discussed in Appendix F. The Phase V UTM well locations used in validation were calculated using CORPSCON V.5.11.08 (STN: 10547-5.11.08-00 [DIRS 155082]) and are included in Output DTN: SN0702T0510106.007.

- Screened intervals used in water level measurements were obtained from the well completion reports listed in Table D-2. The screened intervals were converted from feet relative to a surface marker to elevations (amsl) in meters using basic MS Excel spreadsheet functions. The midpoint elevation (m) for each screened interval was also calculated and is used as the measurement location. The spreadsheet calculations are included in Output DTN: SN0702T0510106.007. For water level measurements that fell below the top of the screened interval, new measurement locations were calculated

as the midpoint between the water level elevation and the bottom elevation of the interval.

- Time-averaged water-level data were developed from the water level DTNs shown in Table D-2 also using a MS Excel spreadsheet. There are two different water level DTNs representing the two different time frames of the SZ Flow model development. The well data used for SZ Flow model calibration includes well data through February 2005; the second is well data used for validation that did not become available until December 2006, which includes water-level data through November 2006. Generally, variability of measured water levels with time falls within expected values (< 1 m).

All developed data and sources, including the MS Excel workbook, have been stored under Output DTN: SN0702T0510106.007.

Table D-2. Nye County Wells with Data to Be Evaluated and Corresponding Data Sources

Well	Phase	Summary GPS Survey DTN	Well Completion Report DTN
Phase II, III, and IV Wells used in SZ Flow Calibration			
7SC	II	MO0206GSC02074.000 [DIRS 168378]	MO0206NYE04926.119 [DIRS 179372]
10P	III	MO0206GSC02074.000 [DIRS 168378]	MO0306NYE05262.168 [DIRS 179374]
10S	III	MO0203GSC02034.000 [DIRS 168375]	MO0306NYE05261.167 [DIRS 179373]
16P	IV	MO0307GSC03094.000 [DIRS 170556]	MO0702NYE05714.375 [DIRS 179443]
18P	III	MO0203GSC02034.000 [DIRS 168375]	MO0306NYE05263.169 [DIRS 179375]
19IM1	III	MO0206GSC02074.000 [DIRS 168378]	MO0306NYE05259.165 [DIRS 165876]
19IM2	III	MO0206GSC02074.000 [DIRS 168378]	MO0306NYE05260.166 [DIRS 165877]
19PB	IV	MO0408GSC04123.000 [DIRS 174102]	MO0409NYE06101.246 [DIRS 179384]
22PA	III	MO0206GSC02074.000 [DIRS 168378]	MO0306NYE05265.171 [DIRS 179377]
22PB	III	MO0206GSC02074.000 [DIRS 168378]	MO0306NYE05266.172 [DIRS 179378]
22S	III	MO0203GSC02034.000 [DIRS 168375]	MO0306NYE05264.170 [DIRS 179376]
23P	III	MO0206GSC02074.000 [DIRS 168378]	MO0306NYE05267.173 [DIRS 179379]
24P	IV	MO0312GSC03180.000 [DIRS 174103]	MO0409NYE06096.242 [DIRS 179383]
27P	IV	MO0307GSC03094.000 [DIRS 170556]	MO0312NYE05716.204 [DIRS 179380]
28P	IV	MO0307GSC03094.000 [DIRS 170556]	MO0312NYE05718.202 [DIRS 179381]
29P	IV	MO0312GSC03180.000 [DIRS 174103]	MO0409NYE06093.241 [DIRS 179382]
Phase V Wells used for SZ Flow Validation			
13P	V	MO0606ABLNCPVB.000 [DIRS 180020]	MO0611NYE06947.344 [DIRS 180022]
22PC	V	MO0503GSC05025.000 [DIRS 175275]	MO0505NYE06464.314 [DIRS 179599]
24PB	V	MO0608ABEWDPPV.000 [DIRS 180021]	MO0606NYE06949.340 [DIRS 180023]
32P	V	MO0608ABEWDPPV.000 [DIRS 180021]	MO0612NYE07008.366 [DIRS 179486]
33P	V	MO0608ABEWDPPV.000 [DIRS 180021]	MO0612NYE07011.368 [DIRS 179487]
Water-Level Data			
Calibration Wells	II-IV	MO0507NYE06631.323 [DIRS 177372]	
Validation wells	V	MO0612NYE07122.370 [DIRS 179337]	

Table D-3. Nye County Wells with GPS Locations

Well	NC-EWDP Phase	Latitude	Longitude	Northing (m)	Easting (m)
7SC	II	36° 43' 31.822"	116° 33' 25.425"	4064317	539632
10P	III	36° 43' 48.874"	116° 24' 20.362"	4064916	553149
10S	III	36° 43' 48.339"	116° 24' 20.725"	4064899	553140
16P	IV	36° 43' 29.089"	116° 29' 22.219"	4064263	545665
18P	III	36° 45' 04.797"	116° 25' 50.340"	4067233	549416
19IM1	III	36° 40' 14.615"	116° 26' 56.397"	4058291	549317
19IM2	III	36° 40' 14.614"	116° 26' 55.597"	4058291	549337
19PB	IV	36° 40' 15.440"	116° 26' 55.593"	4058316	549337
22PA	III	36° 42' 15.712"	116° 25' 06.581"	4062038	552020
22PB	III	36° 42' 15.665"	116° 25' 05.863"	4062037	552038
22S	III	36° 42' 15.132"	116° 25' 06.636"	4062020	552019
23P	III	36° 41' 05.137"	116° 23' 50.412"	4059875	553923
24P	IV	36° 42' 16.775"	116° 26' 52.756"	4062055	549386
27P	IV	36° 44' 02.072"	116° 29' 51.436"	4065276	544935
28P	IV	36° 42' 28.386"	116° 29' 19.390"	4062393	545746
29P	IV	36° 40' 57.297"	116° 26' 52.884"	4059606	549396
13P	V	36° 44' 39.866"	116° 30' 50.235"	4066433	543471
22PC	V	36° 42' 15.090"	116° 25' 05.906"	4062019	552037
24PB	V	36° 42' 15.777"	116° 26' 52.692"	4062025	549387
32P	V	36° 38' 21.544"	116° 29' 03.381"	4054789	546184
33P	V	36° 39' 38.210"	116° 29' 45.814"	4057146	545117

Source : Output DTNs: LA0612RR150304.001 (see Appendix F) ; Phase V: SN0702T0510106.007.

Table D-4. Land Surface Elevation and the Top and Bottom of the Open Intervals for Nye County Wells

Well NC-EWDP	Elevation (ft)	Top (ft)	Bottom (ft)		Elevation (m)	Top (m)	Bottom (m)	Measurement Point (m)
7SC	2751.0	429.8	449.8		838.5	131.0	137.1	704.5
7SC-Z1	2751.0	80.0	90.0		838.5	24.4	27.4	812.6
7SC-Z2	2751.0	180.0	210.0		838.5	54.9	64.0	779.1
7SC-Z3	2751.0	270.0	370.0		838.5	82.3	112.8	741.0
7SC-Z4	2751.0	429.8	449.8		838.5	131.0	137.1	704.5
10P Shallow	2964.6	660.0	700.0		903.6	201.2	213.4	696.3
10P Deep	2964.6	800.0	860.0		903.6	243.8	262.1	650.6
10S-Z1	2963.5	660.1	699.3		903.3	201.2	213.1	696.1
10S-Z2	2963.5	801.2	860.0		903.3	244.2	262.1	650.1
16P	2889.1	489.4	549.4		880.6	149.2	167.5	722.3
18P	3164.5	835.8	885.0		964.5	254.8	269.7	702.3

Table D-4. Land Surface Elevation and the Top and Bottom of the Open Intervals for Nye County Wells (Continued)

Well NC-EWDP	Elevation (ft)	Top (ft)	Bottom (ft)		Elevation (m)	Top (m)	Bottom (m)	Measurement Point (m)
19IM1-Z1	2687.3	410.0	430.0		819.1	125.0	131.1	691.1
19IM1-Z2	2687.3	515.0	535.0		819.1	157.0	163.1	659.1
19IM1-Z3	2687.3	574.9	674.9		819.1	175.2	205.7	628.6
19IM1-Z4	2687.3	724.9	784.8		819.1	220.9	239.2	589.0
19IM1-Z5	2687.3	849.5	949.3		819.1	258.9	289.3	545.0
19IM2	2688.1	410.2	950.1		819.3	125.0	131.1	691.3
19PB Shallow	2688.7	375.0	395.0		819.5	114.3	120.4	702.2
19PB Deep	2688.7	514.7	534.7		819.5	156.9	163.0	659.6
22PA Shallow	2849.9	520.7	579.7		868.6	158.7	176.7	700.9
22PA Deep	2849.9	661.5	759.8		868.6	201.6	231.6	652.0
22PB Shallow	2849.3	881.3	979.7		868.5	268.6	298.6	584.9
22PB Deep	2849.3	1140.3	1179.7		868.5	347.6	359.6	514.9
22S-Z1	2849.0	521.5	581.3		868.4	159.0	177.2	700.3
22S-Z2	2849.0	661.2	760.6		868.4	201.5	231.8	651.7
22S-Z3	2849.0	880.2	980.0		868.4	268.3	298.7	584.9
22S-Z4	2849.0	1140.0	1180.0		868.4	347.5	359.7	514.8
23P Shallow	2800.2	460.9	519.9		853.5	140.5	158.5	704.0
23P Deep	2800.2	650.5	689.8		853.5	198.3	210.3	649.2
24P	2790.2	400.0	440.0		850.4	121.9	134.1	722.4
27P	2973.6	580.7	620.6		853.5	177.0	189.2	670.4
28P	2767.5	370.0	449.0		843.5	112.8	136.9	718.7
29P	2726.2	340.0	390.0		830.9	103.6	118.9	719.7
13P	2937.8	426.0	466.0		895.5	765.6	753.4	759.5
22PC-Z1	2848.9	510.0	579.8		868.3	712.9	691.6	702.3
22PC-Z2	2848.8	665.4	755.0		868.3	665.5	638.2	651.8
24PB	2788.8	729.2	769.9		850.0	627.8	615.4	621.6
32P-Z1	2545.3	238.7	277.9		775.8	703.1	691.1	697.1
32P-Z2	2545.3	463.7	483.3		775.8	634.5	628.5	631.5
32P-Z3	2545.3	697.9	730.0		775.8	563.1	553.3	558.2
33P-Z1	2570.1	210.8	249.9		783.4	719.1	707.2	713.1
33P-Z2	2570.1	484.5	523.6		783.4	635.7	623.8	629.7
33P-Z3	2570.1	600.9	640.0		783.4	600.2	588.3	594.2

Source: Output DTN: SN0702T0510106.007.

Table D-5. Nye County Water Level Measurements through 2/2005

Well NC-EWDP	Phase	Date	Time	Groundwater Elevation (ft amsl)	MP Elevation (ft amsl)	Depth to Water (ft)	Sounder
7SC	II	2/14/2001	9:00	2717.63	2749.68	32.05	NWRPO-500
7SC	II	2/21/2001	10:15	2713.88	2749.68	35.80	NWRPO-500
7SC	II	2/28/2001	11:40	2717.63	2749.68	32.05	NWRPO-500
7SC	II	3/26/2001	15:08	2711.97	2749.68	37.71	NWRPO-500
7SC	II	3/27/2001	14:18	2722.30	2749.68	27.38	NWRPO-500
7SC	II	3/30/2001	11:35	2721.97	2749.68	27.71	NWRPO-500
7SC	II	4/2/2001	10:15	2721.97	2749.68	27.71	NWRPO-500
7SC-Z1	II	3/19/2003	11:53	2724.29	2749.68	25.39	NWRPO-500-2
7SC-Z1	II	2/17/2004	11:54	2723.93	2749.68	25.75	NWRPO-1000-7
7SC-Z1	II	9/29/2004	14:36	2724.21	2749.68	25.47	NWRPO-500-8
7SC-Z2	II	9/13/2002	9:54	2724.27	2749.68	25.41	NWRPO-1000-4
7SC-Z2	II	9/13/2002	12:30	2724.1	2749.68	25.58	NWRPO-1000-4
7SC-Z2	II	3/19/2003	12:14	2724.32	2749.68	25.36	NWRPO-500-2
7SC-Z2	II	2/17/2004	12:28	2724.34	2749.68	25.34	NWRPO-1000-7
7SC-Z2	II	9/29/2004	15:06	2724.47	2749.68	25.21	NWRPO-500-8
7SC-Z3	II	9/12/2002	15:45	2695.40	2749.68	54.28	NWRPO-1000-4
7SC-Z3	II	9/13/2002	9:24	2694.61	2749.68	55.07	NWRPO-1000-4
7SC-Z3	II	3/21/2003	9:23	2696.82	2749.68	52.86	NWRPO-500-2
7SC-Z3	II	3/10/2004	9:17	2696.78	2749.68	52.90	NWRPO-500-1
7SC-Z4	II	3/28/2003	11:55	2613.73	2749.68	135.95	NWRPO-500-2
7SC-Z4	II	3/15/2004	10:42	2586.37	2749.68	163.31	NWRPO-500-1
10P Deep	III	1/28/2002	8:23	2384.93	2966.65	581.72	NWRPO-1000-4
10P Deep	III	2/5/2002	15:47	2384.83	2966.65	581.82	NWRPO-1000-4
10P Deep	III	2/11/2002	10:55	2384.75	2966.65	581.90	NWRPO-1000-4
10P Deep	III	3/25/2002	6:29	2384.69	2966.65	581.96	NWRPO-1000-4
10P Deep	III	4/25/2002	10:48	2384.88	2966.65	581.77	NWRPO-1000-4
10P Deep	III	5/21/2002	10:16	2384.68	2966.65	581.97	NWRPO-1000-4

Table D-5. Nye County Water Level Measurements through 2/2005 (Continued)

Well NC-EWDP	Phase	Date	Time	Groundwater Elevation (ft amsl)	MP Elevation (ft amsl)	Depth to Water (ft)	Sounder
10P Deep	III	6/27/2002	7:01	2384.83	2966.65	581.82	NWRPO-1000-4
10P Deep	III	7/24/2002	9:15	2384.67	2966.65	581.98	NWRPO-1000-5
10P Deep	III	7/25/2002	7:07	2384.81	2966.65	581.84	NWRPO-1000-4
10P Deep	III	8/22/2002	7:08	2384.77	2966.65	581.88	NWRPO-1000-4
10P Deep	III	8/22/2002	7:35	2384.70	2966.65	581.95	NWRPO-1000-5
10P Deep	III	8/27/2002	8:15	2384.97	2966.65	581.68	NWRPO-1000-4
10P Deep	III	8/27/2002	16:45	2385.05	2966.65	581.60	NWRPO-1000-4
10P Deep	III	9/25/2002	8:19	2384.98	2966.65	581.67	NWRPO-1000-4
10P Deep	III	10/16/2002		2384.98	2966.65	581.67	NWRPO-1000-5
10P Deep	III	11/18/2002	11:13	2384.63	2966.65	582.02	NWRPO-1000-5
10P Deep	III	12/23/2002	11:05	2384.85	2966.65	581.80	NWRPO-1000-5
10P Deep	III	1/30/2003	10:43	2384.72	2966.65	581.93	NWRPO-1000-5
10P Deep	III	2/24/2003	9:25	2385.09	2966.65	581.56	NWRPO-1000-5
10P Deep	III	3/12/2003	8:58	2384.86	2966.65	581.79	NWRPO-1000-5
10P Deep	III	4/17/2003	9:45	2385.08	2966.65	581.57	NWRPO-1000-4
10P Deep	III	4/17/2003	9:36	2384.96	2966.65	581.69	NWRPO-1000-5
10P Deep	III	4/17/2003	9:55	2384.99	2966.65	581.66	NWRPO-1000-6
10P Deep	III	5/15/2003	9:01	2384.84	2966.65	581.81	NWRPO-1000-5
10P Deep	III	6/16/2003	8:57	2384.83	2966.65	581.82	NWRPO-1000-5
10P Deep	III	7/17/2003	7:25	2384.79	2966.65	581.86	NWRPO-1000-5
10P Deep	III	8/18/2003	6:33	2384.94	2966.65	581.71	NWRPO-1000-5
10P Deep	III	9/15/2003	7:22	2384.88	2966.65	581.77	NWRPO-1000-5
10P Deep	III	10/21/2003	8:45	2384.72	2966.65	581.93	NWRPO-1000-5
10P Deep	III	11/13/2003	8:19	2384.79	2966.65	581.86	NWRPO-1000-5
10P Deep	III	1/19/2004	10:57	2384.87	2966.65	581.78	NWRPO-1000-5
10P Deep	III	2/15/2004	8:26	2384.90	2966.65	581.75	NWRPO-1000-5
10P Deep	III	2/25/2004	8:26	2384.72	2966.65	581.93	NWRPO-1000-5
10P Deep	III	3/25/2004	8:02	2384.84	2966.65	581.81	NWRPO-1000-5
10P Deep	III	5/17/2004	8:05	2384.93	2966.65	581.72	NWRPO-1000-5

Table D-5. Nye County Water Level Measurements through 2/2005 (Continued)

Well NC-EWDP	Phase	Date	Time	Groundwater Elevation (ft amsl)	MP Elevation (ft amsl)	Depth to Water (ft)	Sounder
10P Deep	III	6/28/2004	7:21	2384.86	2966.65	581.79	NWRPO-1000-5
10P Deep	III	7/26/2004	7:20	2384.85	2966.65	581.80	NWRPO-1000-5
10P Deep	III	8/23/2004	10:35	2384.93	2966.65	581.72	NWRPO-1000-5
10P Deep	III	9/20/2004	8:20	2384.65	2966.65	582.00	NWRPO-1000-5
10P Deep	III	10/11/2004	8:25	2384.81	2966.65	581.84	NWRPO-1000-5
10P Shallow	III	1/28/2002	8:14	2385.11	2966.65	581.54	NWRPO-1000-4
10P Shallow	III	2/5/2002	15:36	2384.96	2966.65	581.69	NWRPO-1000-4
10P Shallow	III	2/11/2002	11:05	2384.86	2966.65	581.79	NWRPO-1000-4
10P Shallow	III	3/25/2002	6:36	2384.86	2966.65	581.79	NWRPO-1000-4
10P Shallow	III	4/25/2002	10:38	2385.01	2966.65	581.64	NWRPO-1000-4
10P Shallow	III	5/21/2002	10:01	2384.82	2966.65	581.83	NWRPO-1000-4
10P Shallow	III	6/27/2002	6:52	2384.96	2966.65	581.69	NWRPO-1000-4
10P Shallow	III	7/24/2002	9:24	2384.82	2966.65	581.83	NWRPO-1000-5
10P Shallow	III	7/25/2002	6:57	2384.93	2966.65	581.72	NWRPO-1000-4
10P Shallow	III	8/22/2002	7:03	2384.88	2966.65	581.77	NWRPO-1000-4
10P Shallow	III	8/22/2002	7:21	2384.81	2966.65	581.84	NWRPO-1000-5
10P Shallow	III	8/26/2002	15:45	2385.18	2966.65	581.47	NWRPO-1000-4
10P Shallow	III	8/27/2002	10:45	2385.08	2966.65	581.57	NWRPO-1000-4
10P Shallow	III	9/25/2002	8:07	2385.13	2966.65	581.52	NWRPO-1000-4
10p Shallow	III	10/16/2002	11:35	2385.14	2966.65	581.51	NWRPO-1000-6
10p Shallow	III	10/16/2002	11:48	2385.24	2966.65	581.41	NWRPO-1000-4
10p Shallow	III	10/16/2002	11:58	2385.14	2966.65	581.51	NWRPO-1000-5
10p Shallow	III	11/18/2002	11:02	2384.77	2966.65	581.88	NWRPO-1000-5
10p Shallow	III	12/23/2002	10:54	2385.00	2966.65	581.65	NWRPO-1000-5
10P Shallow	III	1/30/2003	10:32	2384.85	2966.65	581.80	NWRPO-1000-5
10P Shallow	III	2/24/2003	9:13	2385.18	2966.65	581.47	NWRPO-1000-5
10P Shallow	III	3/12/2003	8:46	2385.01	2966.65	581.64	NWRPO-1000-5
10P Shallow	III	4/17/2003	9:24	2385.12	2966.65	581.53	NWRPO-1000-5
10P Shallow	III	5/15/2003	8:49	2385.02	2966.65	581.63	NWRPO-1000-5

Table D-5. Nye County Water Level Measurements through 2/2005 (Continued)

Well NC-EWDP	Phase	Date	Time	Groundwater Elevation (ft amsl)	MP Elevation (ft amsl)	Depth to Water (ft)	Sounder
10P Shallow	III	6/16/2003	8:46	2384.97	2966.65	581.68	NWRPO-1000-5
10P Shallow	III	7/17/2003	7:12	2384.94	2966.65	581.71	NWRPO-1000-5
10P Shallow	III	8/18/2003	6:33	2385.09	2966.65	581.56	NWRPO-1000-5
10P Shallow	III	9/15/2003	7:10	2385.00	2966.65	581.65	NWRPO-1000-5
10P Shallow	III	10/21/2003	8:34	2384.87	2966.65	581.78	NWRPO-1000-5
10P Shallow	III	11/13/2003	8:07	2384.95	2966.65	581.70	NWRPO-1000-5
10P Shallow	III	1/19/2004	10:46	2385.01	2966.65	581.64	NWRPO-1000-5
10P Shallow	III	2/25/2004	8:14	2384.87	2966.65	581.78	NWRPO-1000-5
10P Shallow	III	3/25/2004	7:50	2385.01	2966.65	581.64	NWRPO-1000-5
10P Shallow	III	5/17/2004	7:55	2385.11	2966.65	581.54	NWRPO-1000-5
10P Shallow	III	6/28/2004	7:10	2385.03	2966.65	581.62	NWRPO-1000-5
10P Shallow	III	7/26/2004	7:09	2385.00	2966.65	581.65	NWRPO-1000-5
10P Shallow	III	8/23/2004	10:20	2385.13	2966.65	581.52	NWRPO-1000-5
10P Shallow	III	9/20/2004	8:09	2384.84	2966.65	581.81	NWRPO-1000-5
10P Shallow	III	10/11/2004	8:15	2385.00	2966.65	581.65	NWRPO-1000-5
10P Shallow	III	2/14/2005	8:14	2385.04	2966.65	581.61	NWRPO-1000-5
10S-Z1	III	7/24/2002	11:24	2385.07	2966.27	581.20	NWRPO-1000-5
10S-Z1	III	9/12/2002	7:00	2385.28	2966.27	580.99	NWRPO-1000-4
10S-Z1	III	9/12/2002	10:25	2385.23	2966.27	581.04	NWRPO-1000-4
10S-Z1	III	6/10/2003	13:40	2385.32	2966.27	580.95	NWRPO-1000-5
10S-Z1	III	11/6/2003	8:34	2385.11	2966.27	581.16	NWRPO-1000-7
10S-Z1	III	6/29/2004	11:10	2385.32	2966.27	580.95	NWRPO-1000-7
10S-Z2	III	7/24/2002	9:36	2384.87	2966.27	581.40	NWRPO-1000-5
10S-Z2	III	9/11/2002	12:10	2385.10	2966.27	581.17	NWRPO-1000-4
10S-Z2	III	9/11/2002	16:25	2385.24	2966.27	581.03	NWRPO-1000-4
10S-Z2	III	6/10/2003	12:50	2385.07	2966.27	581.20	NWRPO-1000-5
10S-Z2	III	11/7/2003	16:35	2385.16	2966.27	581.11	NWRPO-1000-7
10S-Z2	III	6/29/2004	10:11	2385.09	2966.27	581.18	NWRPO-1000-7
18P	III	11/9/2001	9:50	2386.93	3166.56	779.63	NWRPO-1000-4

Table D-5. Nye County Water Level Measurements through 2/2005 (Continued)

Well NC-EWDP	Phase	Date	Time	Groundwater Elevation (ft amsl)	MP Elevation (ft amsl)	Depth to Water (ft)	Sounder
18P	III	1/2/2002	11:21	2386.96	3166.56	779.60	NWRPO-1000-4
18P	III	1/28/2002	7:35	2386.91	3166.56	779.65	NWRPO-1000-4
18P	III	2/25/2002	7:02	2386.79	3166.56	779.77	NWRPO-1000-4
18P	III	3/25/2002	7:07	2386.86	3166.56	779.70	NWRPO-1000-4
18P	III	5/21/2002	9:16	2386.82	3166.56	779.74	NWRPO-1000-4
18P	III	6/27/2002	8:05	2386.79	3166.56	779.77	NWRPO-1000-4
18P	III	7/25/2002	8:03	2386.95	3166.56	779.61	NWRPO-1000-4
18P	III	8/22/2002	8:23	2386.91	3166.56	779.65	NWRPO-1000-4
18P	III	8/22/2002	8:37	2386.81	3166.56	779.75	NWRPO-1000-5
18P	III	10/16/2002	9:38	2386.84	3166.56	779.72	NWRPO-1000-6
18P	III	10/16/2002	10:11	2386.92	3166.56	779.64	NWRPO-1000-5
18P	III	11/18/2002	11:52	2386.62	3166.56	779.94	NWRPO-1000-5
18P	III	12/23/2002	10:15	2386.79	3166.56	779.77	NWRPO-1000-5
18P	III	1/30/2003	11:48	2386.90	3166.56	779.66	NWRPO-1000-5
18P	III	2/24/2003	10:13	2387.16	3166.56	779.40	NWRPO-1000-5
18P	III	3/12/2003	9:42	2386.89	3166.56	779.67	NWRPO-1000-5
18P	III	4/17/2003	10:54	2387.09	3166.56	779.47	NWRPO-1000-4
18P	III	4/17/2003	10:42	2386.99	3166.56	779.57	NWRPO-1000-5
18P	III	4/17/2003	11:07	2387.01	3166.56	779.55	NWRPO-1000-6
18P	III	5/15/2003	9:45	2386.89	3166.56	779.67	NWRPO-1000-5
18P	III	6/16/2003	9:50	2386.95	3166.56	779.61	NWRPO-1000-5
18P	III	7/17/2003	8:15	2386.91	3166.56	779.65	NWRPO-1000-5
18P	III	8/18/2003	7:20	2386.95	3166.56	779.61	NWRPO-1000-5
18P	III	9/15/2003	8:06	2386.96	3166.56	779.60	NWRPO-1000-5
18P	III	10/21/2003	9:44	2386.92	3166.56	779.64	NWRPO-1000-4
18P	III	10/21/2003	9:30	2386.80	3166.56	779.76	NWRPO-1000-5
18P	III	10/21/2003	10:00	2386.85	3166.56	779.71	NWRPO-1000-6
18P	III	10/21/2003	10:17	2386.86	3166.56	779.70	NWRPO-1000-7
18P	III	11/13/2003	8:52	2386.76	3166.56	779.80	NWRPO-1000-5

Table D-5. Nye County Water Level Measurements through 2/2005 (Continued)

Well NC-EWDP	Phase	Date	Time	Groundwater Elevation (ft amsl)	MP Elevation (ft amsl)	Depth to Water (ft)	Sounder
18P	III	1/19/2004	11:33	2386.90	3166.56	779.66	NWRPO-1000-5
18P	III	2/25/2004	9:02	2386.81	3166.56	779.75	NWRPO-1000-5
18P	III	3/25/2004	8:36	2386.85	3166.56	779.71	NWRPO-1000-5
18P	III	5/17/2004	8:32	2386.92	3166.56	779.64	NWRPO-1000-5
18P	III	5/17/2004	8:46	2386.97	3166.56	779.59	NWRPO-1000-6
18P	III	5/17/2004	8:57	2386.99	3166.56	779.57	NWRPO-1000-7
18P	III	6/28/2004	8:07	2386.90	3166.56	779.66	NWRPO-1000-5
18P	III	8/23/2004	11:25	2386.95	3166.56	779.61	NWRPO-1000-5
18P	III	9/20/2004	8:50	2386.76	3166.56	779.80	NWRPO-1000-5
18P	III	10/11/2004	8:50	2386.85	3166.56	779.71	NWRPO-1000-5
18P	III	10/11/2004	9:00	2386.90	3166.56	779.66	NWRPO-1000-7
18P	III	10/11/2004	9:11	2386.89	3166.56	779.67	NWRPO-1000-6
18P	III	2/14/2005	7:40	2386.99	3166.56	779.57	NWRPO-1000-5
19IM1-Z1	III	11/14/2001	9:10	2321.09	2689.64	368.55	NWRPO-500-3
19IM1-Z1	III	1/23/2003	14:46	2322.9	2689.64	366.74	NWRPO-1000-5
19IM1-Z1	III	7/10/2003	11:35	2330	2689.64	359.64	NWRPO-1000-5
19IM1-Z1	III	2/17/2004	9:44	2332.17	2689.64	357.47	NWRPO-500-2
19IM1-Z1	III	9/20/2004	9:34	2333.17	2689.64	356.47	NWRPO-500-8
19IM1-Z2	III	11/14/2001	16:05	2321.36	2689.64	368.28	NWRPO-500-3
19IM1-Z2	III	1/23/2003	14:04	2327.18	2689.64	362.46	NWRPO-1000-5
19IM1-Z2	III	7/10/2003		2331.31	2689.64	358.33	NWRPO-1000-5
19IM1-Z2	III	2/17/2004	9:04	2333.95	2689.64	355.69	NWRPO-500-2
19IM1-Z2	III	9/16/2004	13:29	2335.67	2689.64	353.97	NWRPO-500-8
19IM1-Z3	III	11/14/2001	10:10	2328.96	2689.64	360.68	NWRPO-500-3
19IM1-Z3	III	1/23/2003	13:15	2329.24	2689.64	360.40	NWRPO-1000-5
19IM1-Z3	III	7/10/2003	9:50	2332.37	2689.64	357.27	NWRPO-1000-5
19IM1-Z3	III	2/12/2004	11:53	2334.25	2689.64	355.39	NWRPO-500-2
19IM1-Z3	III	9/16/2004	12:41	2336.25	2689.64	353.39	NWRPO-500-8
19IM1-Z4	III	11/14/2001	13:45	2329.61	2689.64	360.03	NWRPO-500-3

Table D-5. Nye County Water Level Measurements through 2/2005 (Continued)

Well NC-EWDP	Phase	Date	Time	Groundwater Elevation (ft amsl)	MP Elevation (ft amsl)	Depth to Water (ft)	Sounder
19IM1-Z4	III	1/23/2003	12:20	2332.63	2689.64	357.01	NWRPO-1000-5
19IM1-Z4	III	7/9/2003		2334.51	2689.64	355.13	NWRPO-1000-5
19IM1-Z4	III	2/12/2004	11:04	2335.41	2689.64	354.23	NWRPO-500-2
19IM1-Z4	III	9/16/2004	11:40	2337.63	2689.64	352.01	NWRPO-500-8
19IM1-Z5	III	11/14/2001	8:55	2337.18	2689.64	352.46	NWRPO-500-3
19IM1-Z5	III	1/23/2003	11:10	2336.63	2689.64	353.01	NWRPO-1000-5
19IM1-Z5	III	7/9/2003	12:35	2337.23	2689.64	352.41	NWRPO-1000-5
19IM1-Z5	III	2/12/2004	10:10	2337.42	2689.64	352.22	NWRPO-500-2
19IM1-Z5	III	9/8/2004	14:00	2340.36	2689.64	349.28	NWRPO-500-8
19IM1-Z5	III	9/9/2004	9:17	2340.30	2689.64	349.34	NWRPO-500-8
19IM2	III	1/29/2003	8:17	2333.85	2690.00	356.15	NWRPO-1000-5
19IM2	III	2/24/2003	7:31	2334.75	2690.00	355.25	NWRPO-1000-4
19IM2	III	3/11/2003	7:33	2334.72	2690.00	355.28	NWRPO-1000-5
19IM2	III	4/15/2003	9:20	2334.89	2690.00	355.11	NWRPO-1000-5
19IM2	III	5/14/2003	7:39	2334.83	2690.00	355.17	NWRPO-1000-5
19IM2	III	6/14/2003	6:36	2334.82	2690.00	355.18	NWRPO-1000-5
19IM2	III	7/17/2003	10:02	2335.38	2690.00	354.62	NWRPO-1000-5
19IM2	III	8/17/2003	7:17	2335.75	2690.00	354.25	NWRPO-1000-5
19IM2	III	9/13/2003	7:51	2335.87	2690.00	354.13	NWRPO-1000-5
19IM2	III	10/20/2003	12:14	2336.03	2690.00	353.97	NWRPO-1000-5
19IM2	III	11/14/2003	7:48	2336.13	2690.00	353.87	NWRPO-1000-5
19IM2	III	1/19/2004	8:27	2336.03	2690.00	353.97	NWRPO-1000-5
22PA Deep	III	2/11/2002	12:04	2377.75	2852.15	474.40	NWRPO-1000-4
22PA Deep	III	2/25/2002	7:43	2377.68	2852.15	474.47	NWRPO-1000-4
22PA Deep	III	3/25/2002	6:08	2377.73	2852.15	474.42	NWRPO-1000-4
22PA Deep	III	4/23/2002	6:44	2377.97	2852.15	474.18	NWRPO-500-3
22PA Deep	III	5/21/2002	10:55	2377.78	2852.15	474.37	NWRPO-500-3
22PA Deep	III	6/27/2002	6:07	2377.95	2852.15	474.20	NWRPO-500-3
22PA Deep	III	7/25/2002	6:10	2377.94	2852.15	474.21	NWRPO-500-3

Table D-5. Nye County Water Level Measurements through 2/2005 (Continued)

Well NC-EWDP	Phase	Date	Time	Groundwater Elevation (ft amsl)	MP Elevation (ft amsl)	Depth to Water (ft)	Sounder
22PA Deep	III	7/25/2002	9:35	2378.15	2852.15	474.00	NWRPO-1000-5
22PA Deep	III	8/22/2002	6:31	2377.86	2852.15	474.29	NWRPO-1000-4
22PA Deep	III	8/28/2002	6:30	2377.99	2852.15	474.16	NWRPO-500-3
22PA Deep	III	8/28/2002	13:00	2378.01	2852.15	474.14	NWRPO-500-3
22PA Deep	III	9/25/2002	7:26	2378.17	2852.15	473.98	NWRPO-1000-4
22PA Deep	III	10/16/2002	14:52	2378.30	2852.15	473.85	NWRPO-1000-5
22PA Deep	III	11/18/2002	10:17	2377.96	2852.15	474.19	NWRPO-1000-5
22PA Deep	III	12/23/2002	11:38	2378.15	2852.15	474.00	NWRPO-1000-5
22PA Deep	III	1/30/2003	9:45	2378.06	2852.15	474.09	NWRPO-1000-5
22PA Deep	III	2/24/2003	8:22	2378.25	2852.15	473.90	NWRPO-1000-5
22PA Deep	III	3/12/2003	7:53	2378.12	2852.15	474.03	NWRPO-1000-5
22PA Deep	III	4/17/2003	8:35	2378.28	2852.15	473.87	NWRPO-1000-5
22PA Deep	III	5/15/2003	7:46	2378.12	2852.15	474.03	NWRPO-1000-5
22PA Deep	III	6/16/2003	7:55	2378.15	2852.15	474.00	NWRPO-1000-5
22PA Deep	III	7/17/2003	6:20	2378.11	2852.15	474.04	NWRPO-1000-5
22PA Deep	III	7/31/2003	8:30	2378.08	2852.15	474.07	NWRPO-1000-5
22PA Deep	III	10/21/2003	7:45	2378.09	2852.15	474.06	NWRPO-1000-5
22PA Deep	III	11/13/2003	7:12	2378.12	2852.15	474.03	NWRPO-1000-5
22PA Deep	III	1/19/2004	9:56	2378.17	2852.15	473.98	NWRPO-1000-5
22PA Deep	III	2/25/2004	7:23	2378.11	2852.15	474.04	NWRPO-1000-5
22PA Deep	III	3/25/2004	7:01	2378.16	2852.15	473.99	NWRPO-1000-5
22PA Deep	III	5/17/2004	7:10	2378.20	2852.15	473.95	NWRPO-1000-5
22PA Deep	III	6/28/2004	6:27	2378.15	2852.15	474.00	NWRPO-1000-5
22PA Deep	III	7/26/2004	6:26	2378.16	2852.15	473.99	NWRPO-1000-5
22PA Deep	III	8/23/2004	9:25	2378.17	2852.15	473.98	NWRPO-1000-5
22PA Deep	III	9/20/2004	7:19	2377.92	2852.15	474.23	NWRPO-1000-5
22PA Deep	III	10/11/2004	7:33	2378.10	2852.15	474.05	NWRPO-1000-5
22PA Shallow	III	2/11/2002	12:12	2378.32	2852.15	473.83	NWRPO-1000-4
22PA Shallow	III	2/25/2002	7:52	2377.96	2852.15	474.19	NWRPO-1000-4

Table D-5. Nye County Water Level Measurements through 2/2005 (Continued)

Well NC-EWDP	Phase	Date	Time	Groundwater Elevation (ft amsl)	MP Elevation (ft amsl)	Depth to Water (ft)	Sounder
22PA Shallow	III	3/29/2002	6:06	2377.87	2852.15	474.28	NWRPO-1000-4
22PA Shallow	III	4/23/2002	6:38	2377.93	2852.15	474.22	NWRPO-500-3
22PA Shallow	III	5/21/2002	10:44	2377.73	2852.15	474.42	NWRPO-500-3
22PA Shallow	III	6/27/2002	5:59	2377.90	2852.15	474.25	NWRPO-500-3
22PA Shallow	III	7/25/2002	6:01	2377.91	2852.15	474.24	NWRPO-500-3
22PA Shallow	III	7/25/2002	9:47	2378.13	2852.15	474.02	NWRPO-1000-5
22PA Shallow	III	8/22/2002	6:26	2377.80	2852.15	474.35	NWRPO-1000-4
22PA Shallow	III	8/28/2002	11:53	2377.96	2852.15	474.19	NWRPO-500-3
22PA Shallow	III	8/28/2002	17:00	2377.97	2852.15	474.18	NWRPO-500-3
22PA Shallow	III	9/25/2002	7:18	2378.12	2852.15	474.03	NWRPO-1000-4
22PA Shallow	III	10/16/2002	14:41	2378.24	2852.15	473.91	NWRPO-1000-5
22PA Shallow	III	10/16/2002	14:41	2378.24	2852.15	473.91	NWRPO-1000-5
22PA Shallow	III	11/18/2002	10:08	2377.91	2852.15	474.24	NWRPO-1000-5
22PA Shallow	III	11/18/2002	10:08	2377.91	2852.15	474.24	NWRPO-1000-5
22PA Shallow	III	12/23/2002	11:29	2378.11	2852.15	474.04	NWRPO-1000-5
22PA Shallow	III	12/23/2002	11:29	2378.11	2852.15	474.04	NWRPO-1000-5
22PA Shallow	III	1/30/2003	9:34	2378.04	2852.15	474.11	NWRPO-1000-5
22PA Shallow	III	2/24/2003	8:22	2378.50	2852.15	473.65	NWRPO-1000-5
22PA Shallow	III	3/12/2003	8:07	2378.09	2852.15	474.06	NWRPO-1000-5
22PA Shallow	III	4/17/2003	8:25	2378.26	2852.15	473.89	NWRPO-1000-5
22PA Shallow	III	5/15/2003	7:56	2378.07	2852.15	474.08	NWRPO-1000-5
22PA Shallow	III	6/16/2003	7:44	2378.13	2852.15	474.02	NWRPO-1000-5
22PA Shallow	III	7/17/2003	6:08	2378.09	2852.15	474.06	NWRPO-1000-5
22PA Shallow	III	7/31/2003	8:45	2378.03	2852.15	474.12	NWRPO-1000-5
22PA Shallow	III	10/21/2003	8:07	2378.06	2852.15	474.09	NWRPO-1000-5
22PA Shallow	III	11/13/2003	6:59	2378.11	2852.15	474.04	NWRPO-1000-5
22PA Shallow	III	1/19/2004	9:46	2378.14	2852.15	474.01	NWRPO-1000-5
22PA Shallow	III	2/25/2004	7:12	2378.07	2852.15	474.08	NWRPO-1000-5
22PA Shallow	III	3/25/2004	6:50	2378.10	2852.15	474.05	NWRPO-1000-5

Table D-5. Nye County Water Level Measurements through 2/2005 (Continued)

Well NC-EWDP	Phase	Date	Time	Groundwater Elevation (ft amsl)	MP Elevation (ft amsl)	Depth to Water (ft)	Sounder
22PA Shallow	III	5/17/2004	7:02	2378.14	2852.15	474.01	NWRPO-1000-5
22PA Shallow	III	6/28/2004	6:20	2378.11	2852.15	474.04	NWRPO-1000-5
22PA Shallow	III	7/26/2004	6:18	2378.17	2852.15	473.98	NWRPO-1000-5
22PA Shallow	III	8/23/2004	9:10	2378.14	2852.15	474.01	NWRPO-1000-5
22PA Shallow	III	9/20/2004	7:08	2377.88	2852.15	474.27	NWRPO-1000-5
22PA Shallow	III	10/11/2004	7:23	2378.04	2852.15	474.11	NWRPO-1000-5
22PB Deep	III	3/29/2002	5:53	2377.71	2851.79	474.08	NWRPO-500-3
22PB Deep	III	4/23/2002	7:02	2377.76	2851.79	474.03	NWRPO-500-3
22PB Deep	III	5/21/2002	11:14	2377.60	2851.79	474.19	NWRPO-500-3
22PB Deep	III	6/27/2002	6:23	2377.76	2851.79	474.03	NWRPO-500-3
22PB Deep	III	7/25/2002	6:31	2377.75	2851.79	474.04	NWRPO-500-3
22PB Deep	III	7/25/2002	10:21	2377.94	2851.79	473.85	NWRPO-1000-5
22PB Deep	III	8/22/2002	6:42	2377.68	2851.79	474.11	NWRPO-1000-4
22PB Deep	III	8/29/2002	14:20	2377.69	2851.79	474.10	NWRPO-500-3
22PB Deep	III	8/30/2002	13:00	2378.09	2851.79	473.70	NWRPO-1000-4
22PB Deep	III	9/25/2002	7:42	2378.11	2851.79	473.68	NWRPO-1000-4
22PB Deep	III	10/16/2002	15:16	2378.11	2851.79	473.68	NWRPO-1000-5
22PB Deep	III	11/18/2002	10:35	2377.78	2851.79	474.01	NWRPO-1000-5
22PB Deep	III	12/23/2002	11:57	2377.99	2851.79	473.80	NWRPO-1000-5
22PB Deep	III	1/30/2003	10:06	2377.89	2851.79	473.90	NWRPO-1000-5
22PB Deep	III	2/24/2003	8:49	2378.08	2851.79	473.71	NWRPO-1000-5
22PB Deep	III	3/12/2003	7:53	2377.97	2851.79	473.82	NWRPO-1000-5
22PB Deep	III	4/17/2003	8:57	2378.10	2851.79	473.69	NWRPO-1000-5
22PB Deep	III	5/15/2003	8:19	2377.95	2851.79	473.84	NWRPO-1000-5
22PB Deep	III	6/16/2003	8:19	2378.00	2851.79	473.79	NWRPO-1000-5
22PB Deep	III	7/17/2003	6:45	2377.96	2851.79	473.83	NWRPO-1000-5
22PB Deep	III	7/31/2003	9:00	2377.92	2851.79	473.87	NWRPO-1000-5
22PB Deep	III	10/21/2003	7:57	2377.91	2851.79	473.88	NWRPO-1000-5
22PB Deep	III	11/13/2003	7:40	2377.98	2851.79	473.81	NWRPO-1000-5

Table D-5. Nye County Water Level Measurements through 2/2005 (Continued)

Well NC-EWDP	Phase	Date	Time	Groundwater Elevation (ft amsl)	MP Elevation (ft amsl)	Depth to Water (ft)	Sounder
22PB Deep	III	1/19/2004	10:21	2378.00	2851.79	473.79	NWRPO-1000-5
22PB Deep	III	2/25/2004	7:49	2377.94	2851.79	473.85	NWRPO-1000-5
22PB Deep	III	3/25/2004	7:25	2378.00	2851.79	473.79	NWRPO-1000-5
22PB Deep	III	5/17/2004	7:31	2378.04	2851.79	473.75	NWRPO-1000-5
22PB Deep	III	6/28/2004	6:44	2377.98	2851.79	473.81	NWRPO-1000-5
22PB Deep	III	7/26/2004	6:44	2377.98	2851.79	473.81	NWRPO-1000-5
22PB Deep	III	8/23/2004	9:50	2378.03	2851.79	473.76	NWRPO-1000-5
22PB Deep	III	9/20/2004	7:44	2377.81	2851.79	473.98	NWRPO-1000-5
22PB Deep	III	10/11/2004	7:52	2377.92	2851.79	473.87	NWRPO-1000-5
22PB Shallow	III	3/29/2002	5:58	2377.78	2851.79	474.01	NWRPO-500-3
22PB Shallow	III	4/23/2002	6:57	2377.85	2851.79	473.94	NWRPO-500-3
22PB Shallow	III	5/21/2002	11:04	2377.67	2851.79	474.12	NWRPO-500-3
22PB Shallow	III	6/27/2002	6:15	2377.84	2851.79	473.95	NWRPO-500-3
22PB Shallow	III	7/25/2002	6:22	2377.83	2851.79	473.96	NWRPO-500-3
22PB Shallow	III	7/25/2002	10:31	2377.99	2851.79	473.80	NWRPO-1000-5
22PB Shallow	III	8/22/2002	6:38	2377.74	2851.79	474.05	NWRPO-1000-4
22PB Shallow	III	8/28/2002	14:25	2377.89	2851.79	473.90	NWRPO-500-3
22PB Shallow	III	1/30/2003	9:57	2377.98	2851.79	473.81	NWRPO-1000-5
22PB Shallow	III	2/24/2003	8:40	2378.14	2851.79	473.65	NWRPO-1000-5
22PB Shallow	III	3/12/2003	8:07	2378.04	2851.79	473.75	NWRPO-1000-5
22PB Shallow	III	4/17/2003	8:47	2378.18	2851.79	473.61	NWRPO-1000-5
22PB Shallow	III	5/15/2003	8:08	2378.02	2851.79	473.77	NWRPO-1000-5
22PB Shallow	III	6/16/2003	8:08	2378.08	2851.79	473.71	NWRPO-1000-5
22PB Shallow	III	7/17/2003	6:33	2378.03	2851.79	473.76	NWRPO-1000-5
22PB Shallow	III	7/31/2003	9:10	2377.98	2851.79	473.81	NWRPO-1000-5
22PB Shallow	III	10/21/2003	8:07	2377.99	2851.79	473.80	NWRPO-1000-5
22PB Shallow	III	11/13/2003	7:29	2378.03	2851.79	473.76	NWRPO-1000-5
22PB Shallow	III	1/19/2004	10:11	2378.07	2851.79	473.72	NWRPO-1000-5
22PB Shallow	III	2/25/2004	7:37	2378.00	2851.79	473.79	NWRPO-1000-5

Table D-5. Nye County Water Level Measurements through 2/2005 (Continued)

Well NC-EWDP	Phase	Date	Time	Groundwater Elevation (ft amsl)	MP Elevation (ft amsl)	Depth to Water (ft)	Sounder
22PB Shallow	III	3/25/2004	7:14	2378.03	2851.79	473.76	NWRPO-1000-5
22PB Shallow	III	5/17/2004	7:21	2378.09	2851.79	473.70	NWRPO-1000-5
22PB Shallow	III	6/28/2004	6:37	2378.04	2851.79	473.75	NWRPO-1000-5
22PB Shallow	III	7/26/2004	6:36	2378.06	2851.79	473.73	NWRPO-1000-5
22PB Shallow	III	8/23/2004	9:40	2378.09	2851.79	473.70	NWRPO-1000-5
22PB Shallow	III	9/20/2004	7:32	2377.84	2851.79	473.95	NWRPO-1000-5
22PB Shallow	III	10/11/2004	7:44	2377.97	2851.79	473.82	NWRPO-1000-5
22S-Z1	III	7/25/2002	14:33	2378.30	2851.51	473.21	NWRPO-1000-5
22S-Z1	III	9/10/2002	16:20	2378.46	2851.51	473.05	NWRPO-1000-4
22S-Z1	III	9/11/2002	9:40	2378.31	2851.51	473.20	NWRPO-1000-4
22S-Z1	III	3/25/2003	14:48	2378.31	2851.51	473.20	NWRPO-500-2
22S-Z1	III	6/17/2003	13:35	2378.25	2851.51	473.26	NWRPO-1000-5
22S-Z1	III	7/31/2003	13:30	2378.16	2851.51	473.35	NWRPO-1000-5
22S-Z1	III	4/21/2004	14:29	2378.57	2851.51	472.94	NWRPO-1000-4
22S-Z2	III	7/25/2002	13:31	2378.27	2851.51	473.24	NWRPO-1000-5
22S-Z2	III	9/10/2002	11:20	2378.41	2851.51	473.10	NWRPO-1000-4
22S-Z2	III	9/10/2002	15:20	2378.52	2851.51	472.99	NWRPO-1000-4
22S-Z2	III	3/25/2003	14:00	2378.31	2851.51	473.20	NWRPO-500-2
22S-Z2	III	6/17/2003	12:45	2378.27	2851.51	473.24	NWRPO-1000-5
22S-Z2	III	8/7/2003	11:30	2378.24	2851.51	473.27	NWRPO-1000-5
22S-Z2	III	4/21/2004	13:36	2378.57	2851.51	472.94	NWRPO-1000-4
22S-Z3	III	7/25/2002	12:39	2378.24	2851.51	473.27	NWRPO-1000-5
22S-Z3	III	9/9/2002	16:15	2378.41	2851.51	473.10	NWRPO-1000-4
22S-Z3	III	9/10/2002	10:20	2378.41	2851.51	473.10	NWRPO-1000-4
22S-Z3	III	3/25/2003	12:58	2378.33	2851.51	473.18	NWRPO-500-2
22S-Z3	III	4/24/2003	9:15	2378.30	2851.51	473.21	NWRPO-1000-5
22S-Z3	III	6/17/2003	11:25	2378.30	2851.51	473.21	NWRPO-1000-5
22S-Z3	III	4/21/2004	12:16	2378.53	2851.51	472.98	NWRPO-1000-5
22S-Z4	III	7/25/2002	10:01	2378.21	2851.51	473.30	NWRPO-1000-5

Table D-5. Nye County Water Level Measurements through 2/2005 (Continued)

Well NC-EWDP	Phase	Date	Time	Groundwater Elevation (ft amsl)	MP Elevation (ft amsl)	Depth to Water (ft)	Sounder
22S-Z4	III	9/9/2002	14:40	2378.38	2851.51	473.13	NWRPO-1000-4
22S-Z4	III	3/25/2003	8:32	2378.18	2851.51	473.33	NWRPO-500-2
22S-Z4	III	4/23/2003	11:25	2378.11	2851.51	473.40	NWRPO-1000-5
22S-Z4	III	6/17/2003	10:25	2378.23	2851.51	473.28	NWRPO-1000-5
22S-Z4	III	4/21/2004	10:58	2378.43	2851.51	473.08	NWRPO-1000-7
23P Deep	III	4/23/2002	7:30	2375.66	2802.65	426.99	NWRPO-500-3
23P Deep	III	5/21/2002	8:20	2375.89	2802.65	426.76	NWRPO-1000-4
23P Deep	III	6/27/2002	5:41	2375.97	2802.65	426.68	NWRPO-1000-4
23P Deep	III	7/25/2002	5:42	2375.96	2802.65	426.69	NWRPO-1000-4
23P Deep	III	9/30/2002	7:50	2376.01	2802.65	426.64	NWRPO-1000-4
23P Deep	III	10/1/2002	10:25	2375.95	2802.65	426.70	NWRPO-1000-4
23P Deep	III	10/16/2002	13:52	2376.30	2802.65	426.35	NWRPO-1000-5
23P Deep	III	11/16/2002	9:28	2375.95	2802.65	426.70	NWRPO-1000-5
23P Deep	III	12/23/2002	12:25	2376.21	2802.65	426.44	NWRPO-1000-5
23P Deep	III	1/30/2003	9:12	2376.07	2802.65	426.58	NWRPO-1000-5
23P Deep	III	2/24/2003	8:04	2376.33	2802.65	426.32	NWRPO-1000-5
23P Deep	III	3/12/2003	7:19	2376.18	2802.65	426.47	NWRPO-1000-5
23P Deep	III	4/17/2003	7:42	2376.36	2802.65	426.29	NWRPO-500-1
23P Deep	III	4/17/2003	7:49	2376.36	2802.65	426.29	NWRPO-500-2
23P Deep	III	4/17/2003	7:57	2376.37	2802.65	426.28	NWRPO-1000-4
23P Deep	III	4/17/2003	7:34	2376.30	2802.65	426.35	NWRPO-1000-5
23P Deep	III	4/17/2003	8:04	2376.32	2802.65	426.33	NWRPO-1000-6
23P Deep	III	5/15/2003	7:08	2376.20	2802.65	426.45	NWRPO-1000-5
23P Deep	III	6/16/2003	7:17	2376.17	2802.65	426.48	NWRPO-1000-5
23P Deep	III	7/17/2003	5:42	2376.11	2802.65	426.54	NWRPO-1000-5
23P Deep	III	8/18/2003	5:57	2376.24	2802.65	426.41	NWRPO-1000-5
23P Deep	III	9/15/2003	6:36	2376.18	2802.65	426.47	NWRPO-1000-5
23P Deep	III	10/21/2003	6:50	2376.13	2802.65	426.52	NWRPO-500-1
23P Deep	III	10/21/2003	6:57	2376.13	2802.65	426.52	NWRPO-500-2

Table D-5. Nye County Water Level Measurements through 2/2005 (Continued)

Well NC-EWDP	Phase	Date	Time	Groundwater Elevation (ft amsl)	MP Elevation (ft amsl)	Depth to Water (ft)	Sounder
23P Deep	III	10/21/2003	7:04	2376.13	2802.65	426.52	NWRPO-1000-4
23P Deep	III	10/21/2003	6:42	2376.07	2802.65	426.58	NWRPO-1000-5
23P Deep	III	10/21/2003	7:11	2376.09	2802.65	426.56	NWRPO-1000-6
23P Deep	III	10/21/2003	7:17	2376.10	2802.65	426.55	NWRPO-1000-7
23P Deep	III	11/13/2003	6:29	2376.14	2802.65	426.51	NWRPO-1000-5
23P Deep	III	1/19/2004	9:17	2376.16	2802.65	426.49	NWRPO-1000-5
23P Deep	III	2/25/2004	6:44	2376.06	2802.65	426.59	NWRPO-1000-5
23P Deep	III	3/25/2004	6:24	2376.17	2802.65	426.48	NWRPO-1000-5
23P Deep	III	5/17/2004	6:20	2376.25	2802.65	426.40	NWRPO-1000-5
23P Deep	III	5/17/2004	6:27	2376.34	2802.65	426.31	NWRPO-500-2
23P Deep	III	5/17/2004	6:36	2376.35	2802.65	426.30	NWRPO-1000-6
23P Deep	III	5/17/2004	6:41	2376.30	2802.65	426.35	NWRPO-1000-7
23P Deep	III	6/28/2004	5:54	2376.16	2802.65	426.49	NWRPO-1000-5
23P Deep	III	7/26/2004	5:59	2376.13	2802.65	426.52	NWRPO-1000-5
23P Deep	III	8/23/2004	8:50	2376.19	2802.65	426.46	NWRPO-1000-5
23P Deep	III	9/20/2004	6:50	2375.99	2802.65	426.66	NWRPO-1000-5
23P Deep	III	10/11/2004	6:29	2376.12	2802.65	426.53	NWRPO-1000-5
23P Deep	III	10/11/2004	6:58	2376.15	2802.65	426.50	NWRPO-500-1
23P Deep	III	10/11/2004	7:05	2376.16	2802.65	426.49	NWRPO-500-2
23P Deep	III	10/11/2004	6:45	2376.15	2802.65	426.50	NWRPO-1000-7
23P Deep	III	10/11/2004	6:51	2376.15	2802.65	426.50	NWRPO-1000-6
23P Deep	III	2/14/2005	8:54	2376.18	2802.65	426.47	NWRPO-1000-5
23P Shallow	III	4/23/2002	7:24	2375.94	2802.65	426.71	NWRPO-500-3
23P Shallow	III	5/21/2002	8:11	2375.83	2802.65	426.82	NWRPO-500-3
23P Shallow	III	6/27/2002	5:33	2375.96	2802.65	426.69	NWRPO-500-3
23P Shallow	III	7/25/2002	5:34	2375.97	2802.65	426.68	NWRPO-500-3
23P Shallow	III	8/22/2002	6:07	2375.90	2802.65	426.75	NWRPO-1000-4
23P Shallow	III	9/25/2002	6:36	2376.28	2802.65	426.37	NWRPO-1000-4
23P Shallow	III	10/1/2002	8:50	2376.18	2802.65	426.47	NWRPO-1000-4

Table D-5. Nye County Water Level Measurements through 2/2005 (Continued)

Well NC-EWDP	Phase	Date	Time	Groundwater Elevation (ft amsl)	MP Elevation (ft amsl)	Depth to Water (ft)	Sounder
23P Shallow	III	10/1/2002	14:10	2376.25	2802.65	426.40	NWRPO-1000-4
23P Shallow	III	10/16/2002	13:26	2376.32	2802.65	426.33	NWRPO-1000-6
23P Shallow	III	10/16/2002	13:37	2376.41	2802.65	426.24	NWRPO-1000-4
23P Shallow	III	10/16/2002	13:42	2376.31	2802.65	426.34	NWRPO-1000-5
23P Shallow	III	11/18/2002	9:20	2375.94	2802.65	426.71	NWRPO-1000-5
23P Shallow	III	12/23/2002	12:16	2376.20	2802.65	426.45	NWRPO-1000-5
23P Shallow	III	1/30/2003	9:04	2376.06	2802.65	426.59	NWRPO-1000-5
23P Shallow	III	2/24/2003	7:52	2376.29	2802.65	426.36	NWRPO-1000-5
23P Shallow	III	3/12/2003	7:06	2376.14	2802.65	426.51	NWRPO-1000-5
23P Shallow	III	4/17/2003	7:26	2376.30	2802.65	426.35	NWRPO-1000-5
23P Shallow	III	5/15/2003	7:17	2376.15	2802.65	426.50	NWRPO-1000-5
23P Shallow	III	6/16/2003	7:06	2376.15	2802.65	426.50	NWRPO-1000-5
23P Shallow	III	7/17/2003	5:32	2376.10	2802.65	426.55	NWRPO-1000-5
23P Shallow	III	8/18/2003	5:46	2376.23	2802.65	426.42	NWRPO-1000-5
23P Shallow	III	9/15/2003	6:25	2376.18	2802.65	426.47	NWRPO-1000-5
23P Shallow	III	10/21/2003	6:31	2376.06	2802.65	426.59	NWRPO-1000-5
23P Shallow	III	11/13/2003	6:17	2376.13	2802.65	426.52	NWRPO-1000-5
23P Shallow	III	1/19/2004	9:04	2376.15	2802.65	426.50	NWRPO-1000-5
23P Shallow	III	2/25/2004	6:31	2376.07	2802.65	426.58	NWRPO-1000-5
23P Shallow	III	3/25/2004	6:10	2376.14	2802.65	426.51	NWRPO-1000-5
23P Shallow	III	5/17/2004	6:10	2376.21	2802.65	426.44	NWRPO-1000-5
23P Shallow	III	6/28/2004	5:42	2376.14	2802.65	426.51	NWRPO-1000-5
23P Shallow	III	7/26/2004	5:46	2376.13	2802.65	426.52	NWRPO-1000-5
23P Shallow	III	8/23/2004	8:30	2376.17	2802.65	426.48	NWRPO-1000-5
23P Shallow	III	9/20/2004	6:36	2375.92	2802.65	426.73	NWRPO-1000-5
23P Shallow	III	10/11/2004	6:37	2376.12	2802.65	426.53	NWRPO-1000-5
23P Shallow	III	2/14/2005	8:43	2376.17	2802.65	426.48	NWRPO-1000-5
16P	IV	1/30/2003	14:27	2392.76	2891.57	498.81	NWRPO-1000-5
16P	IV	2/26/2003	6:51	2392.82	2891.57	498.75	NWRPO-1000-5

Table D-5. Nye County Water Level Measurements through 2/2005 (Continued)

Well NC-EWDP	Phase	Date	Time	Groundwater Elevation (ft amsl)	MP Elevation (ft amsl)	Depth to Water (ft)	Sounder
16P	IV	3/11/2003	8:54	2392.94	2891.57	498.63	NWRPO-1000-5
16P	IV	4/15/2003	10:55	2392.78	2891.57	498.79	NWRPO-1000-5
16P	IV	5/14/2003	8:45	2392.92	2891.57	498.65	NWRPO-1000-5
16P	IV	6/14/2003	7:50	2392.80	2891.57	498.77	NWRPO-1000-5
16P	IV	7/20/2003	6:27	2392.86	2891.57	498.71	NWRPO-1000-5
16P	IV	8/17/2003	8:22	2392.91	2891.57	498.66	NWRPO-1000-5
16P	IV	10/20/2003	9:29	2392.77	2891.57	498.80	NWRPO-1000-5
16P	IV	11/14/2003	8:54	2392.82	2891.57	498.75	NWRPO-1000-5
16P	IV	1/16/2004	10:47	2392.93	2891.57	498.64	NWRPO-1000-5
16P	IV	2/24/2004	12:49	2392.78	2891.57	498.79	NWRPO-1000-5
16P	IV	3/24/2004	8:36	2392.90	2891.57	498.67	NWRPO-1000-5
16P	IV	5/16/2004	8:28	2392.99	2891.57	498.58	NWRPO-1000-5
16P	IV	6/25/2004	6:51	2392.92	2891.57	498.65	NWRPO-1000-5
16P	IV	7/23/2004	7:29	2392.96	2891.57	498.61	NWRPO-1000-5
16P	IV	8/20/2004	7:18	2392.94	2891.57	498.63	NWRPO-1000-5
16P	IV	9/17/2004	8:04	2392.96	2891.57	498.61	NWRPO-1000-5
16P	IV	10/10/2004	8:23	2393.04	2891.57	498.53	NWRPO-1000-5
16P	IV	12/16/2004	8:33	2392.79	2891.57	498.78	NWRPO-1000-5
16P	IV	2/24/2005	9:06	2392.91	2891.57	498.66	NWRPO-1000-5
19PB Deep	IV	1/19/2004		2322.10	2690.30	368.20	NWRPO-1000-5
19PB Deep	IV	2/24/2004	11:16	2322.43	2690.30	367.87	NWRPO-1000-5
19PB Deep	IV	3/24/2004	10:06	2322.62	2690.30	367.68	NWRPO-1000-5
19PB Deep	IV	6/25/2004	8:21	2322.80	2690.30	367.50	NWRPO-1000-5
19PB Deep	IV	7/23/2004	8:55	2323.02	2690.30	367.28	NWRPO-1000-5
19PB Deep	IV	8/20/2004	8:50	2322.96	2690.30	367.34	NWRPO-1000-5
19PB Shallow	IV	1/19/2004		2321.06	2690.30	369.24	NWRPO-1000-5
19PB Shallow	IV	2/24/2004	11:06	2320.86	2690.30	369.44	NWRPO-1000-5
19PB Shallow	IV	3/24/2004	9:57	2320.99	2690.30	369.31	NWRPO-1000-5
19PB Shallow	IV	6/25/2004	8:15	2320.90	2690.30	369.40	NWRPO-1000-5

Table D-5. Nye County Water Level Measurements through 2/2005 (Continued)

Well NC-EWDP	Phase	Date	Time	Groundwater Elevation (ft amsl)	MP Elevation (ft amsl)	Depth to Water (ft)	Sounder
19PB Shallow	IV	7/23/2004	8:48	2320.95	2690.30	369.35	NWRPO-1000-5
19PB Shallow	IV	8/20/2004	8:42	2320.90	2690.30	369.40	NWRPO-1000-5
19PB Shallow	IV	12/16/2004	10:01	2320.64	2690.30	369.66	NWRPO-1000-5
19PB Shallow	IV	2/24/2005	7:50	2320.78	2690.30	369.52	NWRPO-1000-5
24P	IV	10/20/2003	12:31	2385.53	2792.28	406.75	NWRPO-1000-5
24P	IV	11/14/2003	7:12	2385.49	2792.28	406.79	NWRPO-1000-5
24P	IV	1/19/2004	7:48	2385.58	2792.28	406.70	NWRPO-1000-5
24P	IV	2/24/2004	11:37	2385.41	2792.28	406.87	NWRPO-1000-5
24P	IV	3/24/2004	9:30	2385.52	2792.28	406.76	NWRPO-1000-5
24P	IV	5/16/2004	9:34	2385.64	2792.28	406.64	NWRPO-1000-5
24P	IV	6/25/2004	7:46	2385.56	2792.28	406.72	NWRPO-1000-5
24P	IV	7/23/2004	8:21	2385.58	2792.28	406.70	NWRPO-1000-5
24P	IV	8/20/2004	8:17	2385.55	2792.28	406.73	NWRPO-1000-5
24P	IV	9/17/2004	9:03	2385.61	2792.28	406.67	NWRPO-1000-5
24P	IV	10/10/2004	9:31	2385.67	2792.28	406.61	NWRPO-1000-5
24P	IV	12/16/2004	9:32	2385.38	2792.28	406.90	NWRPO-1000-5
24P	IV	2/24/2005	7:22	2385.54	2792.28	406.74	NWRPO-1000-5
27P	IV	2/6/2003	10:30	2390.48	2976.10	585.62	NWRPO-1000-4
27P	IV	3/11/2003	8:28	2390.58	2976.10	585.52	NWRPO-1000-5
27P	IV	4/15/2003	10:36	2390.33	2976.10	585.77	NWRPO-1000-5
27P	IV	5/14/2003	8:24	2390.54	2976.10	585.56	NWRPO-1000-5
27P	IV	6/14/2003	7:22	2390.41	2976.10	585.69	NWRPO-1000-5
27P	IV	7/20/2003	6:01	2390.47	2976.10	585.63	NWRPO-1000-5
27P	IV	8/17/2003	8:01	2390.51	2976.10	585.59	NWRPO-1000-5
27P	IV	9/13/2003	8:35	2390.45	2976.10	585.65	NWRPO-1000-5
27P	IV	10/20/2003	9:09	2390.35	2976.10	585.75	NWRPO-1000-5
27P	IV	11/14/2003	8:35	2390.46	2976.10	585.64	NWRPO-1000-5
27P	IV	1/16/2004	10:27	2390.49	2976.10	585.61	NWRPO-1000-5
27P	IV	2/24/2004	12:28	2390.34	2976.10	585.76	NWRPO-1000-5

Table D-5. Nye County Water Level Measurements through 2/2005 (Continued)

Well NC-EWDP	Phase	Date	Time	Groundwater Elevation (ft amsl)	MP Elevation (ft amsl)	Depth to Water (ft)	Sounder
27P	IV	3/24/2004	8:15	2390.48	2976.10	585.62	NWRPO-1000-5
27P	IV	5/16/2004	8:08	2390.60	2976.10	585.50	NWRPO-1000-5
27P	IV	6/25/2004	6:30	2390.50	2976.10	585.60	NWRPO-1000-5
27P	IV	7/23/2004	7:09	2390.53	2976.10	585.57	NWRPO-1000-5
27P	IV	8/20/2004	6:59	2390.49	2976.10	585.61	NWRPO-1000-5
27P	IV	9/17/2004	7:45	2390.54	2976.10	585.56	NWRPO-1000-5
27P	IV	10/10/2004	8:05	2390.60	2976.10	585.50	NWRPO-1000-5
27P	IV	12/16/2004	8:12	2390.32	2976.10	585.78	NWRPO-1000-5
27P	IV	2/24/2005	8:44	2390.50	2976.10	585.60	NWRPO-1000-5
28P	IV	1/30/2003	15:04	2392.34	2770.09	377.75	NWRPO-1000-5
28P	IV	2/26/2003	7:07	2392.76	2770.09	377.33	NWRPO-1000-5
28P	IV	3/11/2003	9:17	2392.88	2770.09	377.21	NWRPO-1000-5
28P	IV	4/15/2003	11:12	2392.67	2770.09	377.42	NWRPO-1000-5
28P	IV	5/14/2003	9:04	2392.83	2770.09	377.26	NWRPO-1000-5
28P	IV	6/14/2003	8:07	2392.68	2770.09	377.41	NWRPO-1000-5
28P	IV	7/20/2003	6:53	2392.76	2770.09	377.33	NWRPO-1000-5
28P	IV	8/17/2003	8:39	2392.82	2770.09	377.27	NWRPO-1000-5
28P	IV	9/13/2003	9:10	2392.78	2770.09	377.31	NWRPO-1000-5
28P	IV	10/20/2003	9:45	2392.72	2770.09	377.37	NWRPO-1000-5
28P	IV	11/14/2003	9:11	2392.76	2770.09	377.33	NWRPO-1000-5
28P	IV	1/16/2004	11:03	2392.90	2770.09	377.19	NWRPO-1000-5
28P	IV	2/24/2004	13:04	2392.67	2770.09	377.42	NWRPO-1000-5
28P	IV	3/24/2004	8:51	2392.81	2770.09	377.28	NWRPO-1000-5
28P	IV	5/16/2004	8:44	2392.92	2770.09	377.17	NWRPO-1000-5
28P	IV	6/25/2004	7:06	2392.79	2770.09	377.30	NWRPO-1000-5
28P	IV	7/23/2004	7:44	2392.87	2770.09	377.22	NWRPO-1000-5
28P	IV	8/20/2004	7:33	2392.84	2770.09	377.25	NWRPO-1000-5
28P	IV	9/17/2004	8:21	2392.87	2770.09	377.22	NWRPO-1000-5
28P	IV	10/10/2004	8:38	2392.99	2770.09	377.10	NWRPO-1000-5

Table D-5. Nye County Water Level Measurements through 2/2005 (Continued)

Well NC-EWDP	Phase	Date	Time	Groundwater Elevation (ft amsl)	MP Elevation (ft amsl)	Depth to Water (ft)	Sounder
28P	IV	12/16/2004	8:49	2392.63	2770.09	377.46	NWRPO-1000-5
28P	IV	2/24/2005	9:21	2392.79	2770.09	377.30	NWRPO-1000-5
29P	IV	10/20/2003	12:45	2377.96	2726.12	348.16	NWRPO-1000-5
29P	IV	11/14/2003	7:27	2377.92	2726.12	348.20	NWRPO-1000-5
29P	IV	1/19/2004	8:04	2377.94	2726.12	348.18	NWRPO-1000-5
29P	IV	2/24/2004	11:51	2377.96	2726.12	348.16	NWRPO-1000-5
29P	IV	3/24/2004	9:46	2377.99	2726.12	348.13	NWRPO-1000-5
29P	IV	5/16/2004	9:51	2378.01	2726.12	348.11	NWRPO-1000-5
29P	IV	6/25/2004	8:01	2377.99	2726.12	348.13	NWRPO-1000-5
29P	IV	7/23/2004	8:35	2378.01	2726.12	348.11	NWRPO-1000-5
29P	IV	8/20/2004	8:31	2378.00	2726.12	348.12	NWRPO-1000-5
29P	IV	9/17/2004	9:16	2378.01	2726.12	348.11	NWRPO-1000-5
29P	IV	10/10/2004	9:44	2378.01	2726.12	348.11	NWRPO-1000-5
29P	IV	12/16/2004	9:47	2377.93	2726.12	348.19	NWRPO-1000-5
29P	IV	2/24/2005	7:37	2377.94	2726.12	348.18	NWRPO-1000-5

Source: Output DTN: SN0702T0510106.007.

MP = measurement point.

Table D-6. Nye County Water Level Measurements for Phase V Wells through 11/2006

Well Name	Phase	Date	Time	Groundwater Elevation (ft amsl)	MP Elevation (ft amsl)	Depth to Water (ft)	Sounder
13P	V	8/17/2005	11:40	2507.94	2940.46	432.52	NWRPO-500-1
13P	V	9/11/2005	6:42	2507.84	2940.46	432.62	NWRPO-1000-5
13P	V	10/10/2005	7:36	2507.69	2940.46	432.77	NWRPO-1000-5
13P	V	10/10/2005	7:44	2507.68	2940.46	432.78	NWRPO-1000-6
13P	V	10/10/2005	7:52	2507.69	2940.46	432.77	NWRPO-1000-7
13P	V	10/10/2005	8:00	2507.70	2940.46	432.76	NWRPO-500-8
13P	V	11/9/2005	9:00	2507.80	2940.46	432.66	NWRPO-500-8
13P	V	12/7/2005	10:28	2507.73	2940.46	432.73	NWRPO-500-8
13P	V	1/21/2006	8:25	2507.65	2940.46	432.81	NWRPO-1000-5
13P	V	4/19/2006	13:51	2507.81	2940.46	432.65	NWRPO-500-8
13P	V	4/19/2006	13:47	2507.79	2940.46	432.67	NWRPO-1000-6
13P	V	6/1/2006	13:54	2507.82	2940.46	432.64	NWRPO-500-8
13P	V	7/3/2006	12:38	2507.81	2940.46	432.65	NWRPO-500-8
13P	V	8/9/2006	15:25	2507.91	2940.46	432.55	NWRPO-500-8
13P	V	9/20/2006	12:34	2507.88	2940.46	432.58	NWRPO-500-8
13P	V	9/27/2006	12:16	2507.73	2940.46	432.73	NWRPO-500-1
13P	V	10/30/2006	13:22	2507.97	2940.46	432.49	NWRPO-500-1
13P	V	11/27/2006	11:56	2508.12	2940.46	432.34	NWRPO-500-8
22PC Deep	V	4/18/2006	12:15	2378.17	2850.59	472.42	NWRPO-500-2
22PC Deep	V	5/30/2006	13:36	2378.26	2850.59	472.33	NWRPO-1000-5
22PC Shallow	V	4/18/2006	12:11	2378.18	2850.61	472.43	NWRPO-500-2
22PC Shallow	V	5/30/2006	13:45	2378.28	2850.61	472.33	NWRPO-1000-5
22PC Shallow	V	9/13/2006	11:27	2378.42	2850.61	472.19	NWRPO-500-8
24PB	V	10/30/2006	15:42	2385.74	2790.57	404.83	NWRPO-500-1
24PB	V	11/27/2006	9:02	2385.57	2790.57	405.00	NWRPO-500-8
32P Deep	V	6/2/2006	13:44	2300.21	2547.29	247.08	NWRPO-1000-7
32P Deep	V	7/7/2006	7:56	2299.93	2547.29	247.36	NWRPO-500-1
32P Deep	V	8/9/2006	14:32	2300.07	2547.29	247.22	NWRPO-500-8
32P Deep	V	10/30/2006	14:54	2300.15	2547.29	247.14	NWRPO-500-1

Table D-6. Nye County Water Level Measurements for Phase V Wells through 11/2006 (Continued)

Well Name	Phase	Date	Time	Groundwater Elevation (ft amsl)	MP Elevation (ft amsl)	Depth to Water (ft)	Sounder
32P Deep	V	11/27/2006	14:15	2300.19	2547.29	247.10	NWRPO-500-8
32P Intermediate	V	6/2/2006	13:40	2299.93	2547.29	247.36	NWRPO-1000-7
32P Intermediate	V	7/7/2006	8:04	2299.84	2547.29	247.45	NWRPO-500-1
32P Intermediate	V	8/9/2006	14:36	2299.82	2547.29	247.47	NWRPO-500-8
32P Intermediate	V	10/30/2006	14:54	2299.97	2547.29	247.32	NWRPO-500-1
32P Intermediate	V	11/27/2006	14:11	2300.08	2547.29	247.21	NWRPO-500-8
32P Shallow	V	6/2/2006	13:30	2302.20	2547.29	245.09	NWRPO-1000-7
32P Shallow	V	7/7/2006	8:12	2301.79	2547.29	245.50	NWRPO-500-1
32P Shallow	V	8/9/2006	14:45		2547.29		NWRPO-500-8
32P Shallow	V	11/27/2006	14:07		2547.29		NWRPO-500-8
33P Deep	V	4/19/2006	12:27	2368.20	2572.18	203.98	NWRPO-1000-6
33P Deep	V	4/19/2006	12:22	2368.20	2572.18	203.98	NWRPO-500-8
33P Deep	V	6/2/2006	14:22	2368.20	2572.18	203.98	NWRPO-1000-7
33P Deep	V	7/3/2006	13:30	2368.17	2572.18	204.01	NWRPO-500-1
33P Deep	V	8/9/2006	13:25	2368.20	2572.18	203.98	NWRPO-500-8
33P Deep	V	10/30/2006	13:13	2368.32	2572.18	203.86	NWRPO-500-1
33P Deep	V	11/27/2006	13:36	2368.40	2572.18	203.78	NWRPO-500-8
33P Intermediate	V	4/19/2006	12:16	2368.31	2572.18	203.87	NWRPO-1000-6
33P Intermediate	V	4/19/2006	12:14	2368.32	2572.18	203.86	NWRPO-500-8
33P Intermediate	V	6/2/2006	14:19	2368.36	2572.18	203.82	NWRPO-1000-7
33P Intermediate	V	7/3/2006	13:38	2368.31	2572.18	203.87	NWRPO-500-1
33P Intermediate	V	8/9/2006	13:32	2368.33	2572.18	203.85	NWRPO-500-8
33P Intermediate	V	10/30/2006	13:11	2368.47	2572.18	203.71	NWRPO-500-1
33P Intermediate	V	11/27/2006	13:34	2368.53	2572.18	203.65	NWRPO-500-8
33P Shallow	V	4/19/2006	11:56	2364.78	2572.18	207.40	NWRPO-1000-6
33P Shallow	V	4/19/2006	12:06	2364.77	2572.18	207.41	NWRPO-500-8
33P Shallow	V	6/2/2006	14:16	2365.10	2572.18	207.08	NWRPO-1000-7
33P Shallow	V	7/3/2006	13:33	2365.05	2572.18	207.13	NWRPO-500-1

Table D-6. Nye County Water Level Measurements for Phase V Wells through 11/2006 (Continued)

Well Name	Phase	Date	Time	Groundwater Elevation (ft amsl)	MP Elevation (ft amsl)	Depth to Water (ft)	Sounder
33P Shallow	V	8/9/2006	13:30	2364.99	2572.18	207.19	NWRPO-500-8
33P Shallow	V	10/30/2006	15:09	2365.03	2572.18	207.15	NWRPO-500-1
33P Shallow	V	11/27/2006	13:32	2365.05	2572.18	207.13	NWRPO-500-8

Source: Output DTN : SN0702T0510106.007.

INTENTIONALLY LEFT BLANK

APPENDIX E
POTENTIOMETRIC SURFACE FOR THE SATURATED ZONE SITE-SCALE FLOW MODEL

E1. PURPOSE

The purpose of this appendix is to describe the potentiometric surface developed for use with the SZ Site-scale flow model described within this report. Also included is the process used to develop or construct the potentiometric surface. The description includes background, software used, inputs, analysis with uncertainty and limitations, and conclusions.

Previous potentiometric surfaces and analyses have been presented by *Water-Level Data Analysis for the Saturated Zone Site-Scale Flow and Transport Model* (USGS 2001 [DIRS 154625], 2004 [DIRS 168473]; BSC 2004 [DIRS 170009]). The initial version of the potentiometric surface (USGS 2001 [DIRS 154625]) was used for the calibration of the SZ site-scale flow model (BSC 2004 [DIRS 170037]).

The USGS (2004 [DIRS 168473]) used updated water-level data for selected wells through the year 2000 as the basis for estimating water-level altitudes and the potentiometric surface in the SZ site-scale flow and transport model domain based on an alternative interpretation of perched water conditions. The updated water-level data presented by the USGS (2004 [DIRS 168473]) include data obtained from the NC-EWDP Phases I and II and data from USW WT-24. That revision developed computer files containing:

- Water-level data within the model area (DTN: GS010908312332.002 [DIRS 163555])
- A table of known vertical head differences (DTN: GS010908312332.003 [DIRS 168699])
- A potentiometric-surface map (DTN: GS010608312332.001 [DIRS 155307]) using an alternative concept from that presented by the USGS (2001 [DIRS 154625]) for the area north of Yucca Mountain.

The water-level data analysis (BSC 2004 [DIRS 170009]) was based on work by the USGS (2004 [DIRS 168473]) and includes an analysis of the impact of more recent water-level data and the impact of adding data from the NC-EWDP Phases III and IV wells. It also expands the discussion of uncertainty in the potentiometric-surface map.

The current potentiometric surface presented in this appendix builds on the potentiometric surface as represented by contour lines presented by the USGS (2004 [DIRS 168473], Figure 6-1) as modified by *Water-Level Data Analysis for the Saturated Zone Site-Scale Flow and Transport Model* (BSC 2004 [DIRS 170009], Figure 6-2), which includes data from two additional recently completed wells, NC-EWDP-24P and NC-EWDP-29P, and is contained in DTN: MO0409SEPPSMPC.000 [DIRS 179336] and illustrated in Figure 6-16.

Output DTN: MO0611SCALEFLW.000 represents the current potentiometric surface and includes representations of the surface in addition to the contours as shown in Figure 6-4.

E2. USE OF SOFTWARE

The potentiometric surface was constructed primarily using EarthVision 5.1 (STN: 10174-5.1-000, [DIRS 167994],) on a Silicon Graphics Octane workstation running IRIX 6.5. EarthVision is a product of Dynamic Graphics, Inc. and is designed for the preparation of three-dimensional geologic surfaces and models. The use of EarthVision to prepare this surface is consistent with the intended use of the software. There are no limitations on the use of this potentiometric surface due to the use of EarthVision.

EarthVision 5.1 can create regularly spaced grids from irregularly spaced data points to create surfaces that represent the top of specific hydrogeological units or the saturated zone. Up to 10,000,000 data points can be used to produce a grid with dimensions up to 1,201 × 1,201 (*GS_EV_5_0.pdf*, pp. 22 and 24). The surface constructed was within the range of these limits.

Several commercially available software packages (exempt per IM-PRO-003) were also used for data handling, formatting, and data visualization in the preparation of the potentiometric surface. These software packages were Microsoft Access (97 and 2000), Microsoft Excel (97 and 2003), AutoCad (2002), EarthVision (7.5.2), and UltraEdit (11.10) by IDM Computer Solutions, Inc. Each of these software packages were used on the Windows 2000 platform. No calculations were performed by these commercial software packages and the only output was in the form of visualizations. AutoCad and EarthVision 7.5.2 were used for data visualization and are therefore exempt per IM-PRO-003. Access, Excel, and UltraEdit were used for formatting data and were also exempt per IM-PRO-003. Each of these exempt software packages is controlled by YMP Software Configuration Management.

E3. INPUTS

The inputs for the construction of the potentiometric surface consist of water level measurements and the contour lines from previous potentiometric surfaces as shown in DTN: MO0409SEPPSMPC.000 [DIRS 179336].

Water level measurements used for the construction of the latest potentiometric surface were obtained from Output DTN: SN0610T0510106.001. In some cases, more than one water-level value is given for a single well and some wells and intervals are not considered appropriate for use in construction of a potentiometric surface. Table A-2 of *Water-Level Data Analysis for the Saturated Zone Site-Scale Flow and Transport Model* (BSC 2004 [DIRS 170009]) was used to determine which wells and intervals were appropriate for use in the construction of the potentiometric surface. For wells or intervals not included in Appendix A of *Water-Level Data Analysis for the Saturated Zone Site-Scale Flow and Transport Model* (BSC 2004 [DIRS 170009]), the value for the uppermost interval found in Output DTN: SN0610T0510106.001 was used.

Contour lines from Figure 6-2 of *Water-Level Data Analysis for the Saturated Zone Site-Scale Flow and Transport Model* (BSC 2004 [DIRS 170009]) and found in DTN: MO0409SEPPSMPC.000 [DIRS 179336] were digitized and included as input data except in the immediate vicinity of the two recently completed wells, NC-EWDP-24P and NC-EWDP-29P.

E4. ANALYSIS

The potentiometric surface discussed herein is intended to be suitable for the needs of the saturated zone site-scale flow model described in this report. The area for which this potentiometric surface was constructed is identical to the area of the Hydrogeologic Framework Model HFM2006 (SNL 2007 [DIRS 174109]) and the SZ site-scale flow model of this report. The area covers about 1,350 km^2 and extends from 533,000 m to 563,000 m (west to east) and 4,046,500 m to 4,091,500 m (south to north), UTM (Zone 11, North American Datum 1927). The resolution, horizontal spacing, of the potentiometric surface was also established to match the Hydrogeologic Framework Model HFM2006 (SNL 2007 [DIRS 174109]) at 125 m.

The minimum tension method, generally recognized as providing geologically reasonable surfaces except where very steep surfaces are encountered (vertical distances many times greater than the horizontal data spacing), was used to construct the potentiometric surface. Control points were used to limit the tendency to overshoot in areas of very steep gradients. Some smoothing was also applied to minimize the effects of uneven data distribution.

The resulting potentiometric surface was checked at the water level measurement locations by determining the absolute value of the difference between the input value and the value indicated by the new potentiometric surface. The median difference was 0.2 m with a standard deviation of 1.9 m. This difference was determined to be suitable for use with the flow model described in this report. The potentiometric surface is intended for use with the SZ site-scale flow model and may not be suitable for other purposes. This surface does not replicate the input data exactly.

The uncertainty in the previously developed potentiometric surface map discussed in Section 6.5 of *Water-Level Data Analysis for the Saturated Zone Site-Scale Flow and Transport Model* (BSC 2004 [DIRS 170009]) is applicable to the current potentiometric surface. Uncertainty within the potentiometric surface is mostly related to the accuracy of the water-level measurements, distribution of data and relative variations of the surface. In areas of limited data and steep gradients, such as in the northwest portion of the model, uncertainty is greater than in the immediate vicinity of the repository. In general, the relatively flat portion of the potentiometric surface located just south of the repository is relatively less uncertain due to more wells located in the area. This area, from the repository extending to the south, is the most likely general direction of groundwater flow and is of more interest than the northwest portion of the model area.

The potentiometric surface intended for use with the SZ site-scale flow model is contained in Output DTN: MO0611SCALEFLW.000.

E5 CONCLUSIONS

The potentiometric surface found in Output DTN: MO0611SCALEFLW.000 has been prepared using the previous potentiometric surface (BSC 2004 [DIRS 170009]) and the most recently available water level information to create a surface suitable for use in the SZ site-scale flow model.

INTENTIONALLY LEFT BLANK

APPENDIX F
CONVERSION OF SURVEY COORDINATES FOR SELECTED NYE COUNTY EARLY WARNING DRILLING PROGRAM BOREHOLES, THROUGH PHASE IV

F1. PURPOSE

The purpose of these calculations is to convert qualified survey coordinates from Nevada State Plan (NSP) to UTM coordinates for selected NC-EWDP boreholes. Qualified borehole coordinates are required to support development of the new site-scale saturated-zone flow model.

The scope of these calculations covers NC-EWDP boreholes, through Phase IV, for which qualified UTM coordinates do not already exist in the Technical Data Management System (TDMS).

This activity is conducted under *Technical Work Plan for Saturated Zone Flow and Transport Modeling* (BSC 2006 [DIRS 177375]). It is a deviation from this TWP insofar as the conversion software used to conduct the activity is not identified in Section 9 of the TWP as software to be used for performing calculations, modeling or analyses for the work covered by the TWP. However, the software used for this activity is qualified, and the software package used to conduct the work was obtained from Software Configuration Management.

F2. QUALITY ASSURANCE

All activities in the governing TWP (BSC 2006 [DIRS 177375]) have been determined to be subject to *Quality Assurance Requirements and Description* (QARD) (DOE 2006 [DIRS 177092]), except for administrative activities. The calculations presented in this report are considered to be an analysis of data to support performance assessment and is therefore subject to the QARD (DOE 2006 [DIRS 177092]). No new data have been collected as part of this work scope. A prerequisite for this task is that all necessary qualified data are obtained from the TDMS.

In addition to the QARD (DOE 2006 [DIRS 177092]), the following procedures are used to perform this task:

- DM-PRO-001, *Document Control*
- DM-PRO-002, *Records Management*
- IM-PRO-002, *Control of the Electronic Management of Information*
- IM-PRO-003, *Software Management*
- RM-PRO-2001, *Document Control*
- SCI-PRO-004, *Managing Technical Product Inputs*
- SCI-PRO-006, *Models*
- TST-PRO-001, *Submittal and Incorporation of Data to the Technical Data Management System*.

Methods used to control the electronic management of data are specified in Section 8.4 of the TWP (BSC 2006 [DIRS 177375]). Specifically, the work described in this report involved the use of a personal computer which was subject to the following requirements:

- Files will be saved to backup disks or backup drives on a weekly basis
- At the completion of the analyses, models, or calculation reports, the developed data files will be transferred to the TDMS in accordance with TST-PRO-001
- Computers and workstations are controlled with passwords, and access to equipment is restricted to YMP trained personnel
- Disks and all other removable backup media will be labeled with the following: generating program, originator, date, document number, and content description.

Electronic files and data transfers will be checked for alteration either visually or by using file comparison software (e.g., signature generation and compare routing) to compare compressed and uncompressed files file-sizes.

The data package submitted to the TDMS will be prepared by outputting the data from the database through a spreadsheet.

The requirements of IM-PRO-002 were met by the following additional measures:

- Computers used for processing and storing information are password-protected
- All files are backed up on magnetic media monthly or more often, as appropriate
- Backup media will be labeled with the date and time of backup, DOE serial number of the computer backed up, system utility used to perform the backup, and format of the magnetic media
- Information transfers from one computer to another are done by magnetic media, Internet, or local network using file transfer protocol or attachments to e-mail
- Where possible, file transfers were verified by visually comparing the name, date, and file size
- ASCII files were also verified by visual comparison of the data.

F3. USE OF SOFTWARE

Software used for performing this calculation was qualified in accordance with LP-SI.12Q-BSC, *Qualification of Software*. The following software package was obtained from the Software Configuration Management Library in Las Vegas, Nevada for this task:

Software:	CORPSCON V.5.11.08
Software Tracking Number (STN):	10547-5.11.08.00 [DIRS 155082]
Status:	Qualified
Software range of use:	State of Nevada
Operating environment:	Dell Precision 420, Pentium III Serial Number JFYRF01 LANL Property Number 1091797 Operated under Windows NT 4.0
Computer location:	EES-6, TA-3, Building 43, Room A2, Los Alamos National Laboratory, Los Alamos NM 87545.

This software was selected because it was qualified and had been used to convert survey data to UTM coordinates for borehole and well locations in this report.

Commercial software (Microsoft Excel) was used without qualification in accordance with Section 2 of IM-PRO-003.

F4. INPUTS

F4.1 DIRECT INPUTS

The following DTNs are directly used to develop the list of well coordinate locations:

- MO0203GSC02034.000. As-Built Survey of Nye County Early Warning Drilling Program (EWDP) Phase III Boreholes NC-EWDP-10S, NC-EWDP-18P, and NC-EWDP-22S - Partial Phase III List. [DIRS 168375]
- MO0206GSC02074.000. As-Built Survey of Nye County Early Warning Drilling Program (EWDP) Phase III Boreholes, Second Set. [DIRS 168378]
- MO0307GSC03094.000. As-Built Survey of Nye County Early Warning Drilling Program Phase IV Boreholes EWDP-16P, EWDP-27P & EWDP-28P. [DIRS 170556]
- MO0312GSC03180.000. As-Built Survey of Nye County Early Warning Drilling Program, Phase IV Boreholes: NC-EWDP-24P & NC-EWDP-29P. [DIRS 174103]
- MO0408GSC04123.000. Nye County Early Warning Drilling Program, Phase IV, As-Built Location of NC-EWDP-19PB Borehole. [DIRS 174102]

F4.2 CRITERIA

The input data are selected to meet the following criteria:

- Acquired survey data are in the TDMS
- Survey data are qualified
- The accuracy and precision of the survey data are sufficient for their intended use in the saturated zone site-scale flow model
- Supporting documentation for the survey data clearly state the data uncertainties, so that these uncertainties can be characterized and propagated through any modeling or other calculations using them, as appropriate.

F4.3 CODES, STANDARDS, AND REGULATIONS

No codes, standards, or regulations are applicable to this task.

F5. ASSUMPTIONS

The input survey data and the coordinate conversion software produce results with adequate accuracy and precision for the intended use in the saturated zone site-scale flow model.

F6. SCIENTIFIC ANALYSIS DISCUSSION

F6.1 CALCULATION

Description and source of mathematical formulations, equations, algorithms, and numerical methods used in the calculation are described in *Software Management Report (SMR) for CORPSCON Version 5.11.08* (LANL 2001 [DIRS 181434]).

The steps taken to convert coordinates, and to verify the conversions, are described below:

1. A formatted data input file (*gscinp.txt*) was prepared for CORPSCON:

NC-EWDP-7SC, 532379.34, 719071.91
NC-EWDP-10P, 576745.41, 720883.49
NC-EWDP-10S, 576716, 720829.32
NC-EWDP-16P, 552178.64, 718826.37
NC-EWDP-18P, 564519.85, 728530.5
NC-EWDP-19IM1, 564093.9, 699185.01
NC-EWDP-19IM2, 564159.05, 699185.13
NC-EWDP-19PB, 564159.18, 699268.66
NC-EWDP-22PA, 573007.77, 711452.61
NC-EWDP-22PB, 573066.18, 711447.98
NC-EWDP-22S, 573003.45, 711393.91
NC-EWDP-23P, 579229.94, 704332.62
NC-EWDP-24P, 564362.13, 711538.96
NC-EWDP-27P, 549794.33, 722157.45
NC-EWDP-28P, 552420.36, 712688.26
NC-EWDP-29P, 564370.14, 703501.85

2. Conversion settings were specified for the input and output CORPSCON files:

	Input Settings	Output Settings
System	2 – State Plane	3 – UTM
Datum	1927 – NAD 27	1927 – NAD 27
Zone	2702 – Nevada Central	11 – 120W to 114W
Units	1 – US Survey Foot	3 – Meter
Vertical Datum	0 - None	0 – None

3. The following output file (*gscout.txt*) was generated by CORPSCON:

```
NC-EWDP-7SC,539632.058,4064316.681
NC-EWDP-10P,553149.116,4064915.731
NC-EWDP-10S,553140.212,4064899.193
NC-EWDP-16P,545665.433,4064262.850
NC-EWDP-18P,549415.690,4067232.928
NC-EWDP-19IM1,549316.995,4058290.464
NC-EWDP-19IM2,549336.848,4058290.570
NC-EWDP-19PB,549336.799,4058316.023
NC-EWDP-22PA,552020.195,4062038.031
NC-EWDP-22PB,552037.998,4062036.683
NC-EWDP-22S,552018.941,4062020.140
NC-EWDP-23P,553923.731,4059875.049
NC-EWDP-24P,549385.644,4062055.183
NC-EWDP-27P,544935.369,4065275.350
NC-EWDP-28P,545745.594,4062392.737
NC-EWDP-29P,549396.599,4059606.163
```

4. The output data were formatted for submission to the TDMS as a DTN (see Section F7).

F6.2 CORROBORATION

Before using the software to convert the borehole coordinates, the output of the CORPSCON conversion routine was first corroborated by executing the validation test case from the Software Management Report (CORPSCON, STN: 10547-5.11.08-00 [DIRS 155082], Section 2). Figure F-1 shows the screen shot of the CORPSCON input and output data used in the successful validation test.

The input DTNs also report acquired survey data in geographic (Latitude-Longitude) coordinates. As a secondary confirmatory action, the coordinates converted from NSP to UTM as described above were compared to those converted from geographic coordinates to UTM. Geographic coordinates were first converted from degree-minute-second format to decimal-degree format using (Equation F-1), producing the results listed in the rightmost columns of Table F-1:

$$\text{decimal degrees} = \text{degrees} + (\text{minutes}/60\ \text{min-deg}^{-1}) + (\text{s}/3{,}600\ \text{s-degree}^{-1}) \quad \text{(Eq. F-1)}$$

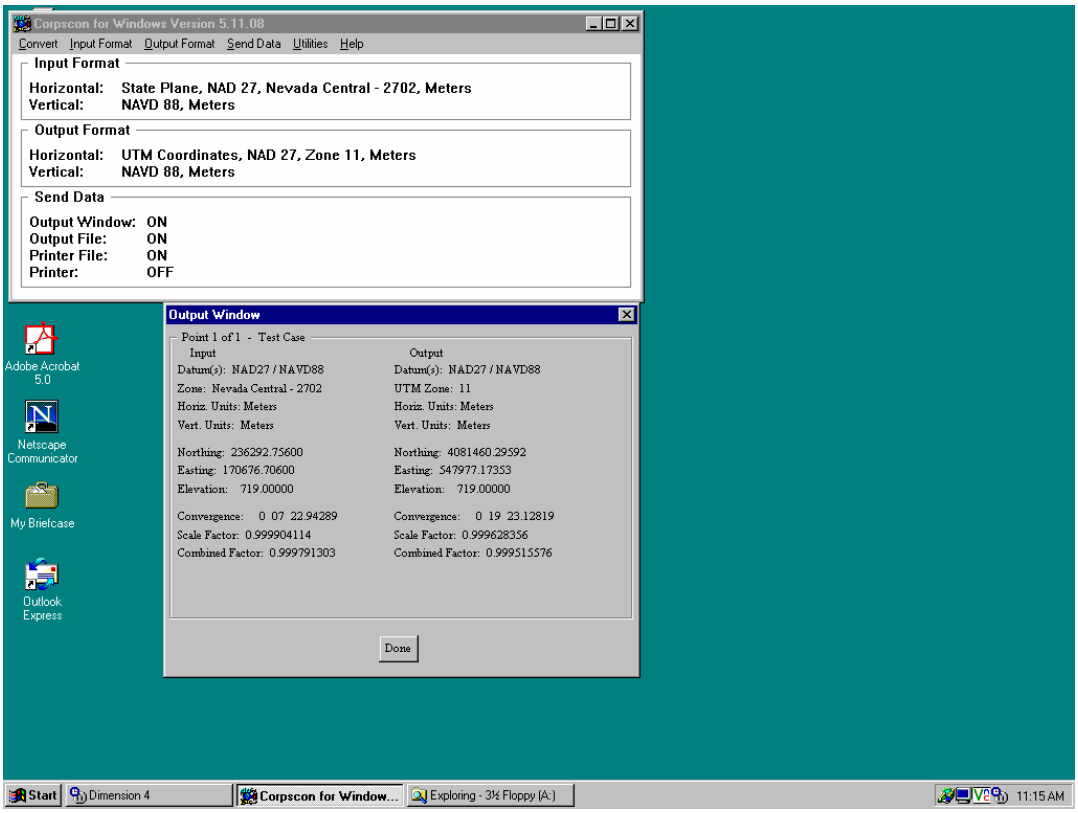

Figure F-1. Screen Shot of the Validation Test Case for CORPSCON Version 5.11.08

Table F-1. Acquired Survey Data used to Create Input File for Verification Calculations

WELL_ID	Source DTN for Geographic Coordinates	Latitude-North (Degree-Min-Sec) (NAD-83)	Longitude-West (Degree-Min-Sec) (NAD-83)	Latitude-North (Decimal degrees) (NAD-83)	Longitude-West (Decimal degrees) (NAD-83)
NC-EWDP-7SC	MO0206GSC02074.000 [DIRS 168378]	36 43 31.812	116 33 25.439	36.72550	116.55707
NC-EWDP-10P	MO0206GSC02074.000 [DIRS 168378]	36 43 48.874	116 24 20.362	36.73024	116.40566
NC-EWDP-10S	MO0203GSC02034.000 [DIRS 168375]	36 43 48.339	116 24 20.725	36.73009	116.40576
NC-EWDP-16P	MO0307GSC03094.000 [DIRS 170556]	36 43 29.089	116 29 22.219	36.72475	116.48951
NC-EWDP-18P	MO0203GSC02034.000 [DIRS 168375]	36 45 04.797	116 26 50.340	36.75133	116.44732
NC-EWDP-19IM1	MO0206GSC02074.000 [DIRS 168378]	36 40 14.615	116 26 56.397	36.67073	116.44900
NC-EWDP-19IM2	MO0206GSC02074.000 [DIRS 168378]	36 40 14.614	116 26 55.597	36.67073	116.44878
NC-EWDP-19PB	MO0408GSC04123.000 [DIRS 174102]	36 40 15.440	116 26 55.593	36.67096	116.44878

Table F-1. Acquired Survey Data used to Create Input File for Verification Calculations (Continued)

WELL_ID	Source DTN for Geographic Coordinates	Latitude-North (Degree-Min-Sec) (NAD-83)	Longitude-West (Degree-Min-Sec) (NAD-83)	Latitude-North (Decimal degrees) (NAD-83)	Longitude-West (Decimal degrees) (NAD-83)
NC-EWDP-22PA	MO0206GSC02074.000[DIRS 168378]	36 42 15.712	116 25 06.581	36.70436	116.41849
NC-EWDP-22PB	MO0206GSC02074.000[DIRS 168378]	36 42 15.665	116 25 05.863	36.70435	116.41830
NC-EWDP-22S	MO0203GSC02034.000 [DIRS 168375]	36 42 15.132	116 25 06.636	36.70420	116.41851
NC-EWDP-23P	MO0206GSC02074.000 [DIRS 168378]	36 41 05.137	116 23 50.412	36.68476	116.39734
NC-EWDP-24P	MO0312GSC03180.000 [DIRS 174103]	36 42 16.775	116 26 52.756	36.70466	116.44799
NC-EWDP-27P	MO0307GSC03094.000 [DIRS 170556]	36 44 02.072	116 29 51.436	36.73391	116.49762
NC-EWDP-28P	MO0307GSC03094.000 [DIRS 170556]	36 42 28.386	116 29 19.390	36.70789	116.48872
NC-EWDP-29P	MO0312GSC03180.000 [DIRS 174103]	36 40 57.297	116 26 52.884	36.68258	116.44802

Source: Output DTN: LA0612RR150304.001.

Conversion settings were then specified for the input and output CORPSCON files:

	Input Settings	Output Settings
System	1 – Geographic	3 – UTM
Datum	1983 – NAD 83(86)	1927 – NAD 27
Zone	NA	11 – 120W to 114W
Units	NA	3 – Meter
Vertical Datum	0 - None	0 – None

NA = not applicable.

Using decimal-degree coordinates in the input file and the above settings, CORPSCON generated the UTM coordinates presented in Table F-2. The difference between the two sets of converted coordinates was calculated using:

$$\text{Difference} = [(\text{UTM-N}_{NSP}\text{-UTM-N}_{GEO})^2 + (\text{UTM-E}_{NSP}\text{-UTM-E}_{GEO})^2]^{0.5} \qquad \text{(Eq. F-2)}$$

where UTM-N_{NSP} and UTM-E_{NSP} are UTM-Northing and UTM-Easting coordinates calculated using Nevada State Plane coordinates for the input data; and UTM-N_{GEO} and UTM-E_{GEO} are UTM-Northing and UTM-Easting coordinates calculated using geographic coordinates for the input data. The consistently small difference of 0.3 m confirms the validity of the conversion process described in Section F6.1.

Table F-2. Comparison of UTM Coordinates Obtained from Conversion of NSP and Geographic Coordinates

	Converted From NSP		Converted From Geographic Coordinates		
Well ID	UTM-Northing (m)	UTM-Easting (m)	UTM-Northing (m)	UTM-Easting (m)	Difference (m)
NC-EWDP-7SC	4064316.68	539632.06	4064316.98	539631.95	0.32
NC-EWDP-10P	4064915.73	553149.12	4064915.88	553148.92	0.25
NC-EWDP-10S	4064899.19	553140.21	4064899.34	553140.01	0.25
NC-EWDP-16P	4064262.85	545665.43	4064263.06	545665.36	0.22
NC-EWDP-18P	4067232.93	549415.69	4067233.04	549415.59	0.15
NC-EWDP-19IM1	4058290.46	549317.00	4058290.76	549316.79	0.36
NC-EWDP-19IM2	4058290.57	549336.85	4058290.84	549336.65	0.34
NC-EWDP-19PB	4058316.02	549336.80	4058316.30	549336.60	0.34
NC-EWDP-22PA	4062038.03	552020.20	4062038.22	552019.98	0.29
NC-EWDP-22PB	4062036.68	552038.00	4062036.88	552037.81	0.28
NC-EWDP-22S	4062020.14	552018.94	4062020.34	552018.73	0.29
NC-EWDP-23P	4059875.05	553923.73	4059875.26	553923.47	0.34
NC-EWDP-24P	4062055.18	549385.64	4062055.40	549385.50	0.26
NC-EWDP-27P	4065275.35	544935.37	4065275.54	544935.33	0.19
NC-EWDP-28P	4062392.74	545745.59	4062392.99	545745.50	0.26
NC-EWDP-29P	4059606.16	549396.60	4059606.42	549396.42	0.31

Source: Output DTN: LA0612RR150304.001.

F7. CONCLUSIONS

Table F-3 summarizes results of this coordinate-conversion calculation.

Table F-3. UTM Coordinates for Selected Nye County EWDP Boreholes, Converted Using CORPSCON V.5.11.08

Borehole Identifier	UTM-Northing (m)	UTM-Easting (m)
NC-EWDP-7SC	4,064,316.68	539,632.06
NC-EWDP-10P	4,064,915.73	553,149.12
NC-EWDP-10S	4,064,899.19	553,140.21
NC-EWDP-16P	4,064,262.85	545,665.43
NC-EWDP-18P	4,067,232.93	549,415.69
NC-EWDP-19IM1	4,058,290.46	549,317.00
NC-EWDP-19IM2	4,058,290.57	549,336.85
NC-EWDP-19PB	4,058,316.02	549,336.80
NC-EWDP-22PA	4,062,038.03	552,020.20
NC-EWDP-22PB	4,062,036.68	552,038.00
NC-EWDP-22S	4,062,020.14	552,018.94
NC-EWDP-23P	4,059,875.05	553,923.73
NC-EWDP-24P	4,062,055.18	549,385.64
NC-EWDP-27P	4,065,275.35	544,935.37
NC-EWDP-28P	4,062,392.74	545,745.59
NC-EWDP-29P	4,059,606.16	549,396.60

Source: Output DTN: LA0612RR150304.001.

INTENTIONALLY LEFT BLANK

APPENDIX G
DISTRIBUTION AND ELEVATIONS OF HYDROGEOLOGIC UNITS IN THE SZ COMPUTATIONAL GRID

G1. PURPOSE

This appendix serves as a visual check of how well the modeled geological units match the HFM. Appendix G presents 23 figures (Figures G-1 through G-23) showing the extent and elevation for each of the 23 units among the 28 hydrogeologic units included in the computational grid. The figures show the distribution of grid nodes for material units 2 through 28, with exception of units 10, 13, 22, and 25, which are not present in the site-scale saturated zone flow model domain. The view is looking down at the top of the unit with North at the top of the page and nodes are colored by their elevation in meters. The white space shows where grid nodes do not exist for a particular unit. The left panel of each figure shows the distribution of units over the full model domain, the right panel shows the resulting distribution when the grid units are truncated by the water table surface (only that portion of the hydrogeologic unit below the water table is illustrated). When the right and left panels are the same, the entire geological unit is saturated (under the water table). The figures differ only when portions of the visualized unit lie above the water table and in these cases, the additional white space in the figure on the right hand side represents only portions of that unit above the water. Along with the figures showing grid node distribution, the number of nodes for the unit is also given in Table 6-5. See the main report for details and text regarding the assignment of the material units.

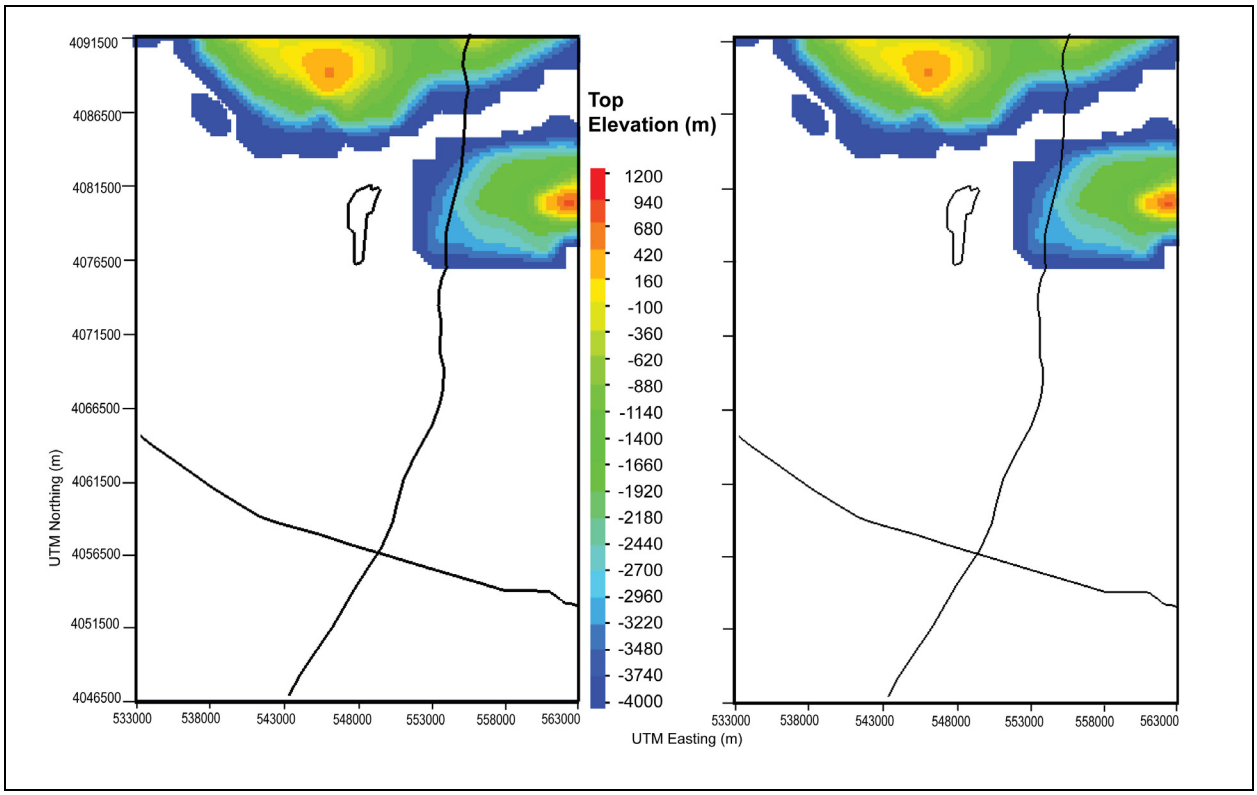

Sources: DTN: MO0610MWDHFM06.002 [DIRS 179352] (HFM2006); SNL 2007 [DIRS 179466] (repository outline).

Output DTNs: MO0611SCALEFLW.000 (potentiometric surface); LA0612TM831231.001.

NOTES: Hydrogeologic properties for unit defined by HFM for computational grid with 20,708 nodes total (left panel) and 20,708 nodes under water table (right panel). Coordinates in UTM, Zone 11, NAD27 meters. Black lines show repository outline, U.S. Highway 95 running East-West, and trace of Fortymile Wash running North-South. Elevation is in meters above mean sea level. For illustration purposes only.

HFM = Hydrogeologic Framework Model; UTM = Universal Transverse Mercator.

Figure G-1. Distribution and Elevations of ICU, Intrusive Confining Unit (2)

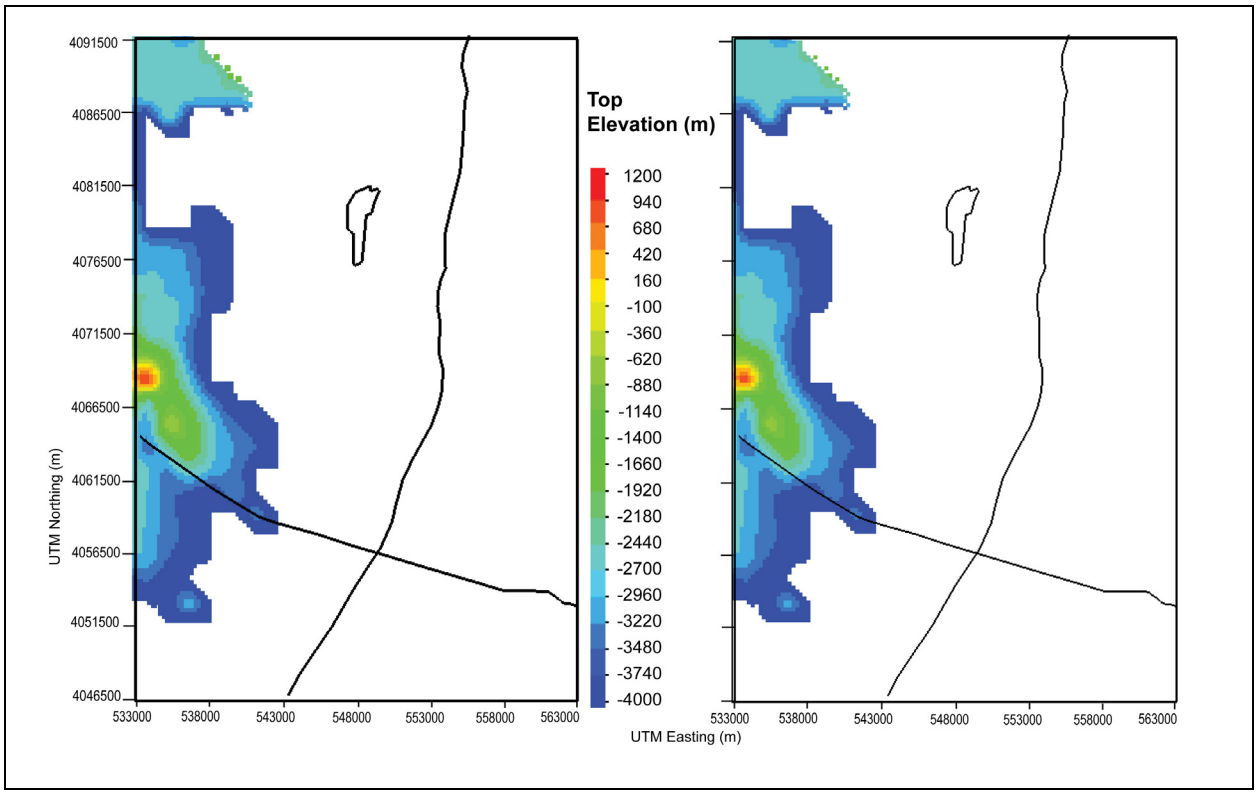

Sources: DTN: MO0610MWDHFM06.002 [DIRS 179352] (HFM2006); SNL 2007 [DIRS 179466] (repository outline).

Output DTNs: MO0611SCALEFLW.000 (potentiometric surface); LA0612TM831231.001.

NOTES: Hydrogeologic properties for unit defined by HFM for computational grid with 10,018 nodes total (left panel) and 10,015 nodes under water table (right panel). Coordinates in UTM, Zone 11, NAD27 meters. Black lines show repository outline, U.S. Highway 95 running East-West, and trace of Fortymile Wash running North-South. Elevation is in meters above mean sea level. For illustration purposes only.

HFM = Hydrogeologic Framework Model; UTM = Universal Transverse Mercator.

Figure G-2. Distribution and Elevations of XCU, Crystalline-Rock Confining Unit (3)

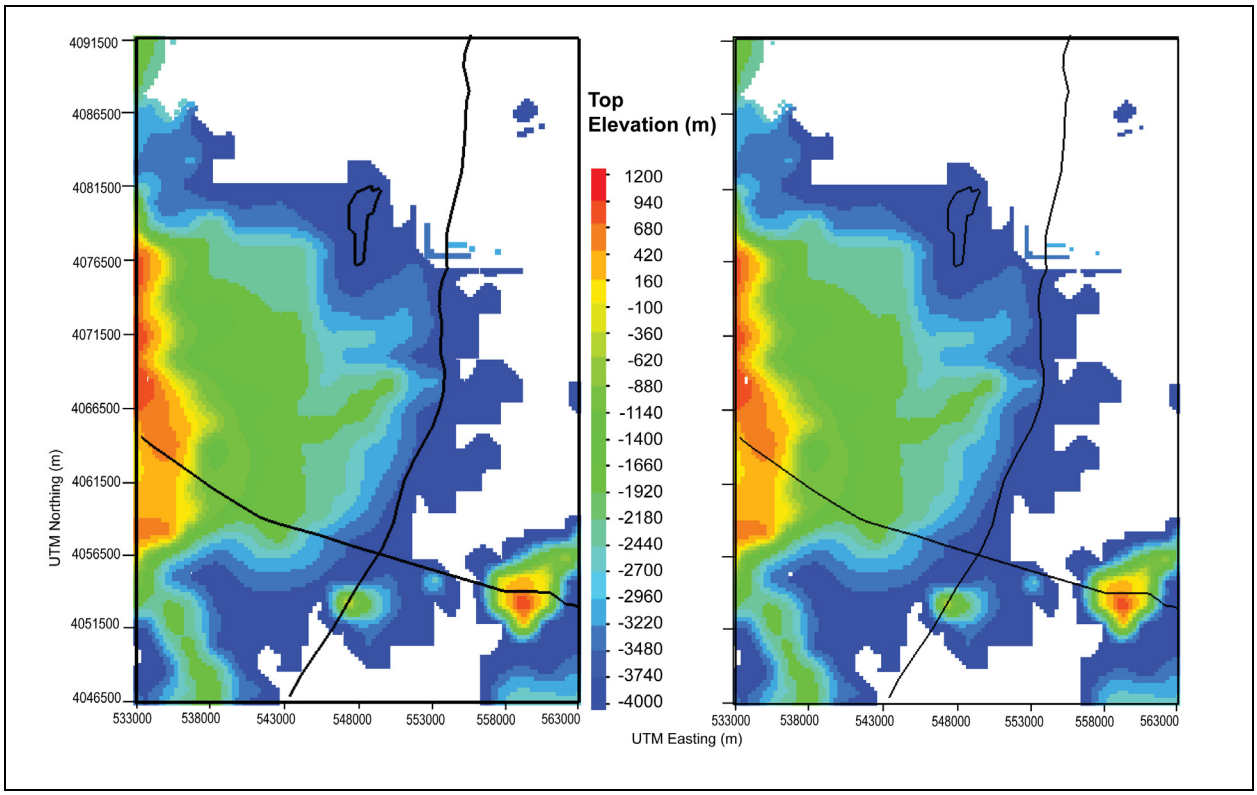

Sources: DTN: MO0610MWDHFM06.002 [DIRS 179352] (HFM2006); SNL 2007 [DIRS 179466] (repository outline).

Output DTNs: MO0611SCALEFLW.000 (potentiometric surface); LA0612TM831231.001.

NOTES: Hydrogeologic properties for unit defined by HFM for computational grid with 52,891 nodes total (left panel) and 52,745 nodes under water table (right panel). Coordinates in UTM, Zone 11, NAD27 meters. Black lines show repository outline, U.S. Highway 95 running East-West, and trace of Fortymile Wash running North-South. Elevation is in meters above mean sea level. For illustration purposes only.

HFM = Hydrogeologic Framework Model; UTM = Universal Transverse Mercator.

Figure G-3. Distribution and Elevations of LCCU, Lower Clastic-Rock Confining Unit (4)

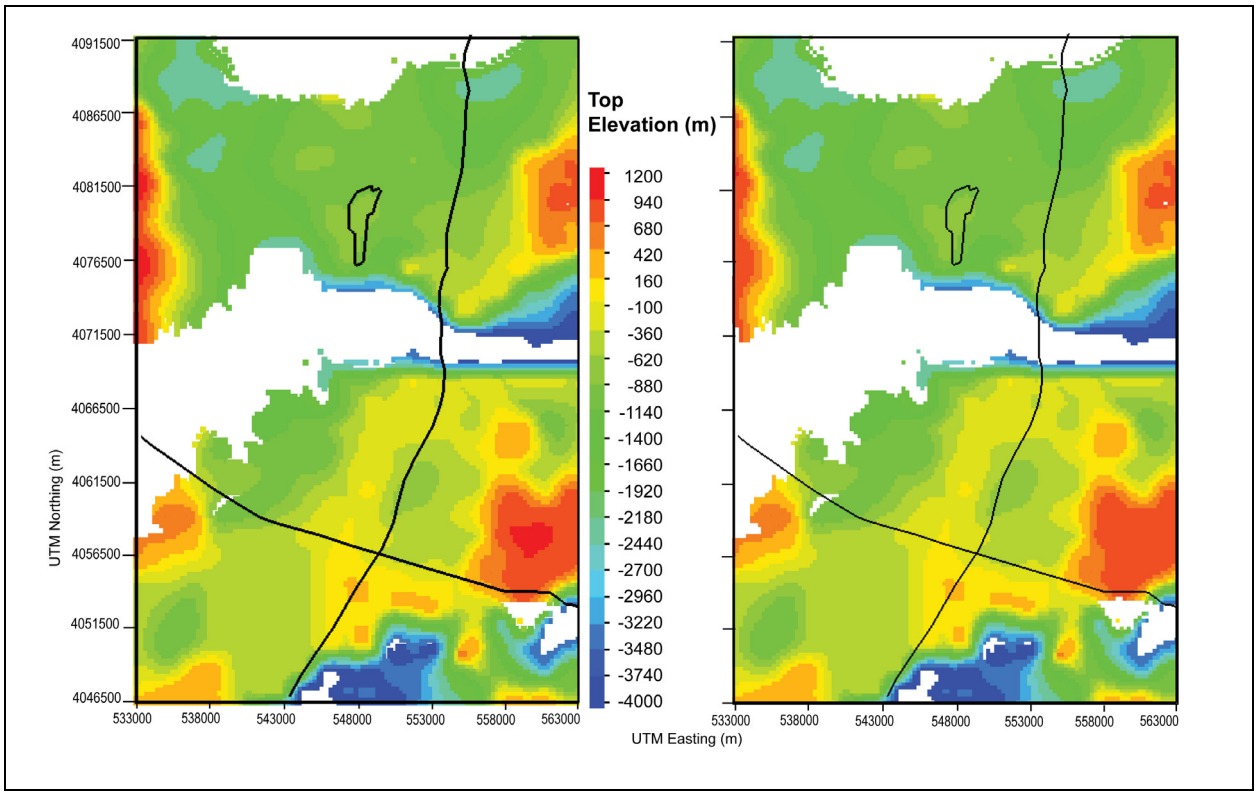

Sources: DTN: MO0610MWDHFM06.002 [DIRS 179352] (HFM2006); SNL 2007 [DIRS 179466] (repository outline).

Output DTNs: MO0611SCALEFLW.000 (potentiometric surface); LA0612TM831231.001.

NOTES: Hydrogeologic properties for unit defined by HFM for computational grid with 135,186 nodes total (left panel) and 131,312 nodes under water table (right panel). Coordinates in UTM, Zone 11, NAD27 meters. Black lines show repository outline, U.S. Highway 95 running East-West, and trace of Fortymile Wash running North-South. Elevation is in meters above mean sea level. For illustration purposes only.

HFM = Hydrogeologic Framework Model; UTM = Universal Transverse Mercator.

Figure G-4. Distribution and Elevations of LCA, Lower Carbonate-Rock Aquifer (5)

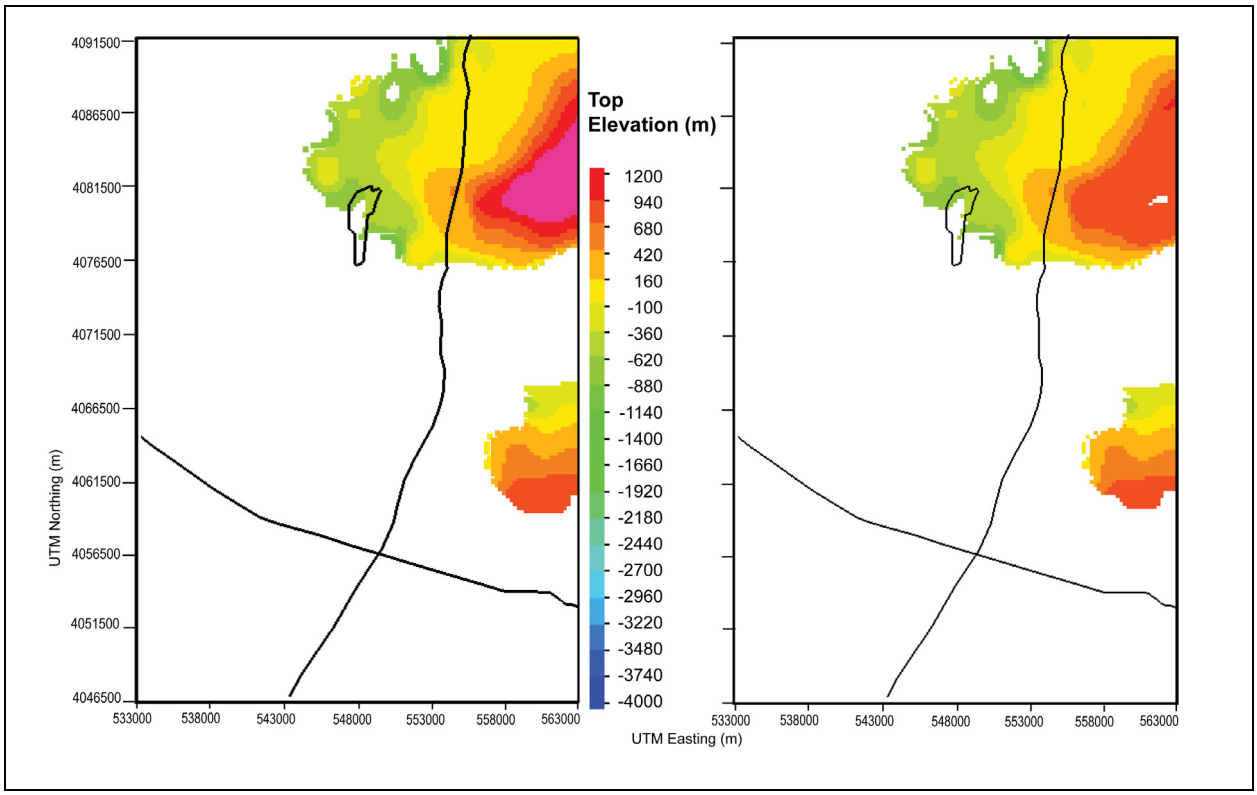

Sources: DTN: MO0610MWDHFM06.002 [DIRS 179352] (HFM2006); SNL 2007 [DIRS 179466] (repository outline).

Output DTNs: MO0611SCALEFLW.000 (potentiometric surface); LA0612TM831231.001.

NOTES: Hydrogeologic properties for unit defined by HFM for computational grid with 40,842 nodes total (left panel) and 33,533 nodes under water table (right panel). Coordinates in UTM, Zone 11, NAD27 meters. Black lines show repository outline, U.S. Highway 95 running East-West, and trace of Fortymile Wash running North-South. Elevation is in meters above mean sea level. For illustration purposes only.

HFM = Hydrogeologic Framework Model; UTM = Universal Transverse Mercator.

Figure G-5. Distribution and Elevations of UCCU, Upper Clastic-Rock Confining Unit (6)

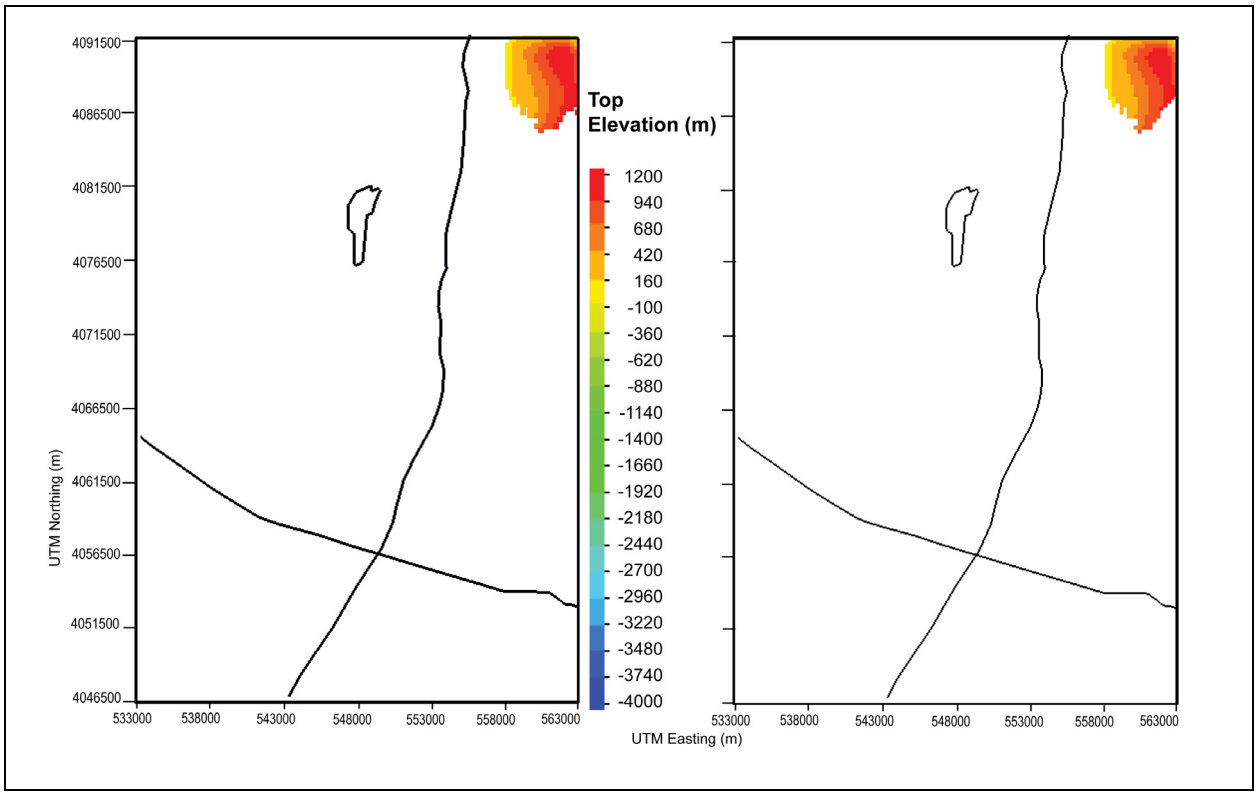

Sources: DTN: MO0610MWDHFM06.002 [DIRS 179352] (HFM2006); SNL 2007 [DIRS 179466] (repository outline).

Output DTNs: MO0611SCALEFLW.000 (potentiometric surface); LA0612TM831231.001.

NOTES: Hydrogeologic properties for unit defined by HFM for computational grid with 4,228 nodes total (left panel) and 4,201 nodes under water table (right panel). Coordinates in UTM, Zone 11, NAD27 meters. Black lines show repository outline, U.S. Highway 95 running East-West, and trace of Fortymile Wash running North-South. Elevation is in meters above mean sea level. For illustration purposes only.

HFM = Hydrogeologic Framework Model; UTM = Universal Transverse Mercator.

Figure G-6. Distribution and Elevations of UCA, Upper Carbonate-Rock Aquifer (7)

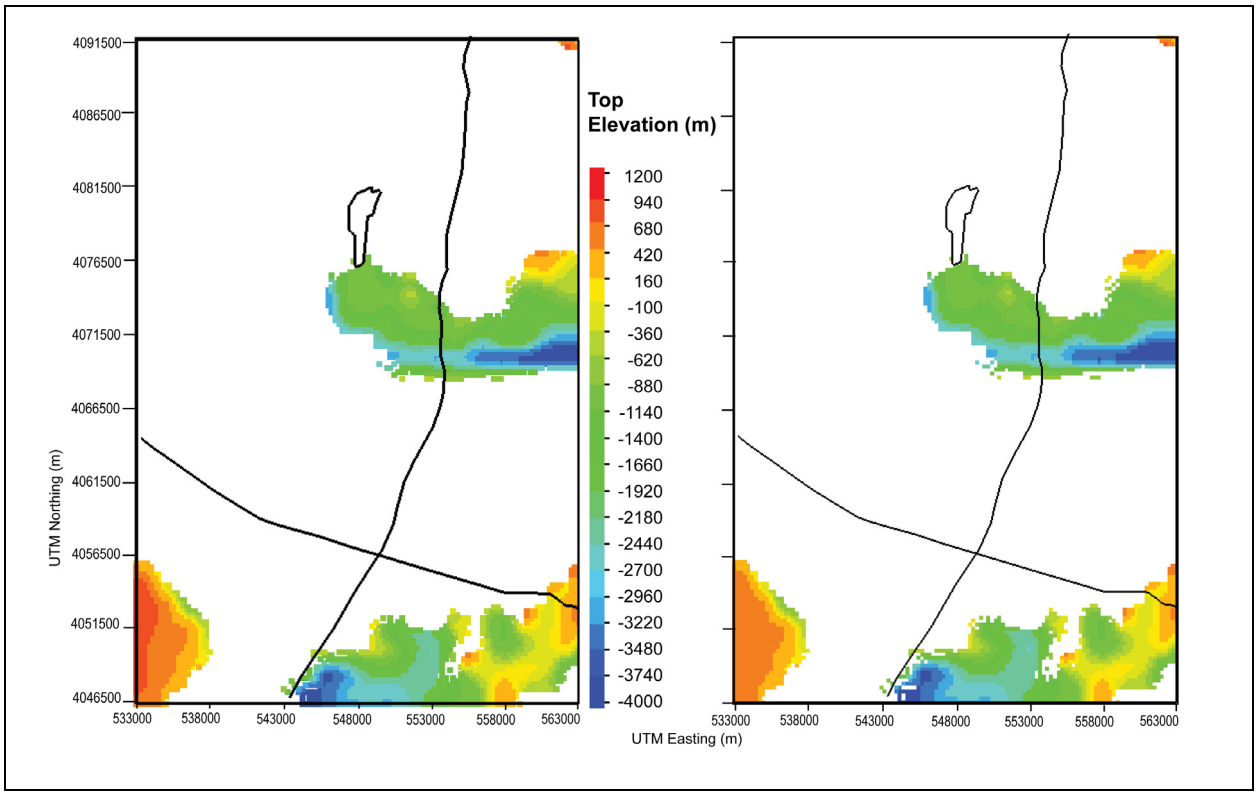

Sources: DTN: MO0610MWDHFM06.002 [DIRS 179352] (HFM2006); SNL 2007 [DIRS 179466] (repository outline).

Output DTNs: MO0611SCALEFLW.000 (potentiometric surface); LA0612TM831231.001.

NOTES: Hydrogeologic properties for unit defined by HFM for computational grid with 17,848 nodes total (left panel) and 17,053 nodes under water table (right panel). Coordinates in UTM, Zone 11, NAD27 meters. Black lines show repository outline, U.S. Highway 95 running East-West, and trace of Fortymile Wash running North-South. Elevation is in meters above mean sea level. For illustration purposes only.

HFM = Hydrogeologic Framework Model; UTM = Universal Transverse Mercator.

Figure G-7. Distribution and Elevations of LCCU-T1, Lower Clastic Confining Unit – Thrust (8)

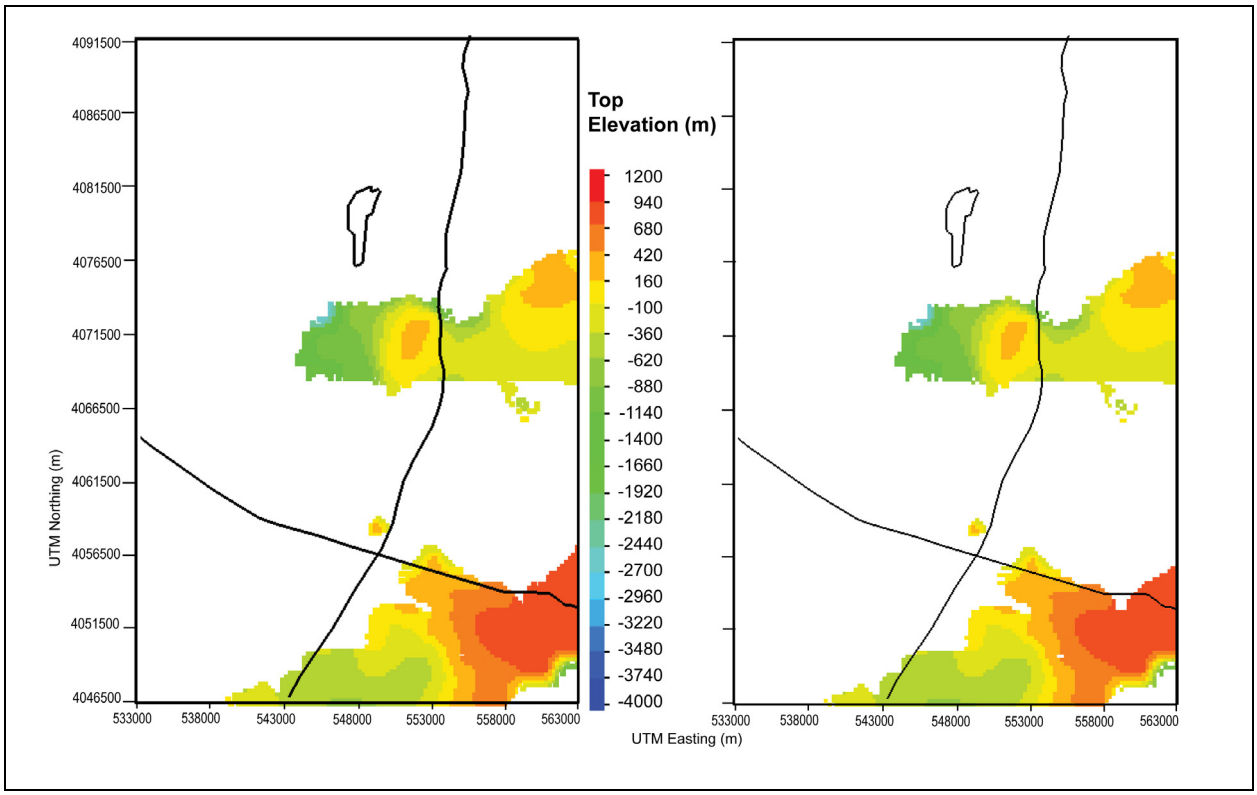

Sources: DTN: MO0610MWDHFM06.002 [DIRS 179352] (HFM2006); SNL 2007 [DIRS 179466] (repository outline).

Output DTNs: MO0611SCALEFLW.000 (potentiometric surface); LA0612TM831231.001.

NOTES: Hydrogeologic properties for unit defined by HFM for computational grid with 31,608 nodes total (left panel) and 28,588 nodes under water table (right panel). Coordinates in UTM, Zone 11, NAD27 meters. Black lines show repository outline, U.S. Highway 95 running East-West, and trace of Fortymile Wash running North-South. Elevation is in meters above mean sea level. For illustration purposes only.

HFM = Hydrogeologic Framework Model; UTM = Universal Transverse Mercator.

Figure G-8. Distribution and Elevations of LCA-T1, Lower Carbonate Aquifer – Thrust (9)

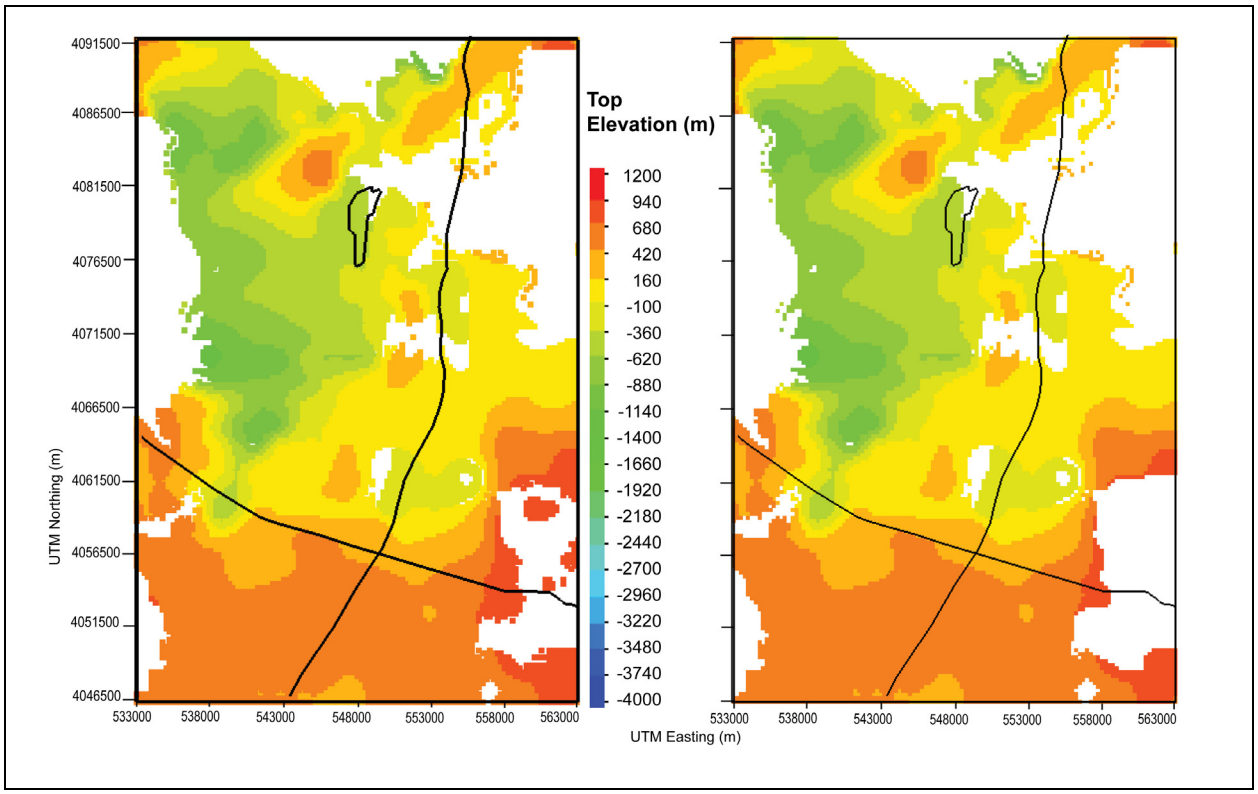

Sources: DTN: MO0610MWDHFM06.002 [DIRS 179352] (HFM2006); SNL 2007 [DIRS 179466] (repository outline).

Output DTNs: MO0611SCALEFLW.000 (potentiometric surface); LA0612TM831231.001.

NOTES: Hydrogeologic properties for unit defined by HFM for computational grid with 78,182 nodes total (left panel) and 76,856 nodes under water table (right panel). Coordinates in UTM, Zone 11, NAD27 meters. Black lines show repository outline, U.S. Highway 95 running East-West, and trace of Fortymile Wash running North-South. Elevation is in meters above mean sea level. For illustration purposes only.

HFM = Hydrogeologic Framework Model; UTM = Universal Transverse Mercator.

Figure G-9. Distribution and Elevations of VSU-Lower, Lower Volcanic and Sedimentary Units (11)

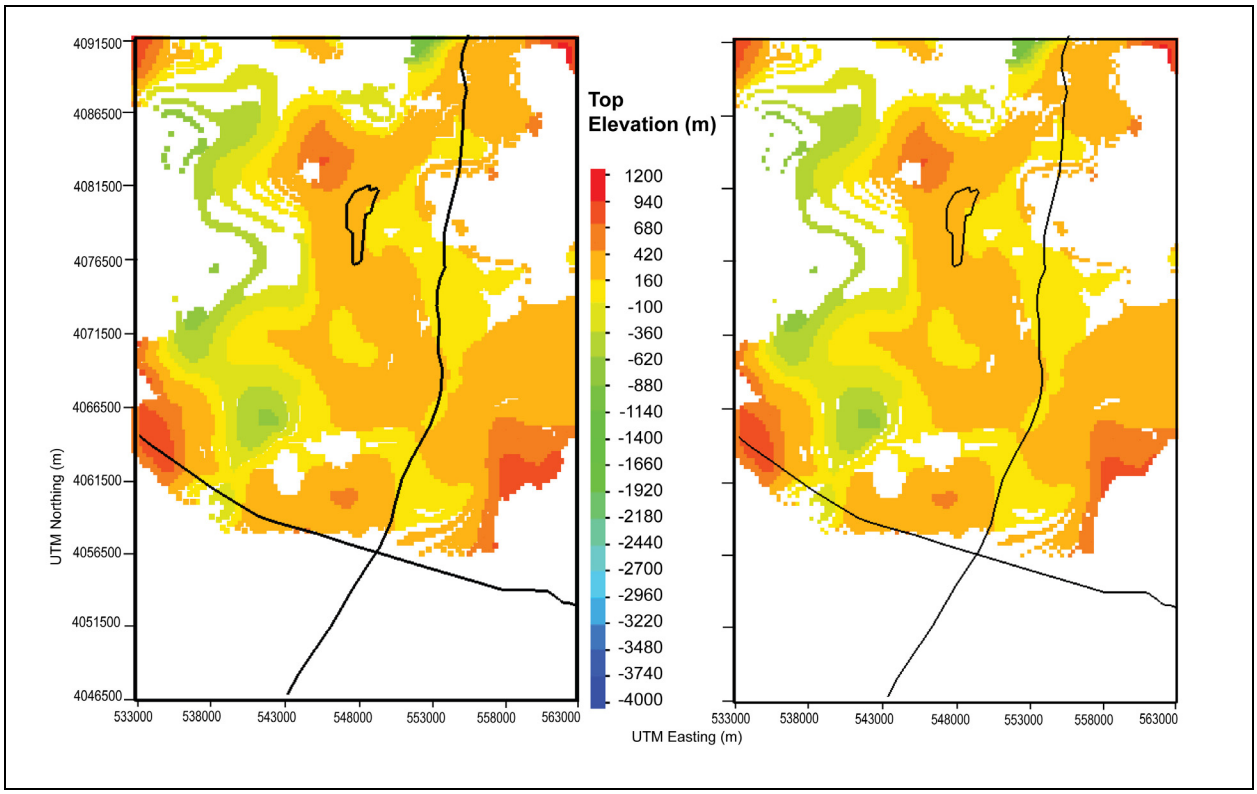

Sources: DTN: MO0610MWDHFM06.002 [DIRS 179352] (HFM2006); SNL 2007 [DIRS 179466] (repository outline).

Output DTNs: MO0611SCALEFLW.000 (potentiometric surface); LA0612TM831231.001.

NOTES: Hydrogeologic properties for unit defined by HFM for computational grid with 27,152 nodes total (left panel) and 26,691 nodes under water table (right panel). Coordinates in UTM, Zone 11, NAD27 meters. Black lines show repository outline, U.S. Highway 95 running East-West, and trace of Fortymile Wash running North-South. Elevation is in meters above mean sea level. For illustration purposes only.

HFM = Hydrogeologic Framework Model; UTM = Universal Transverse Mercator.

Figure G-10. Distribution and Elevations of OVU, Older Volcanic Units (12)

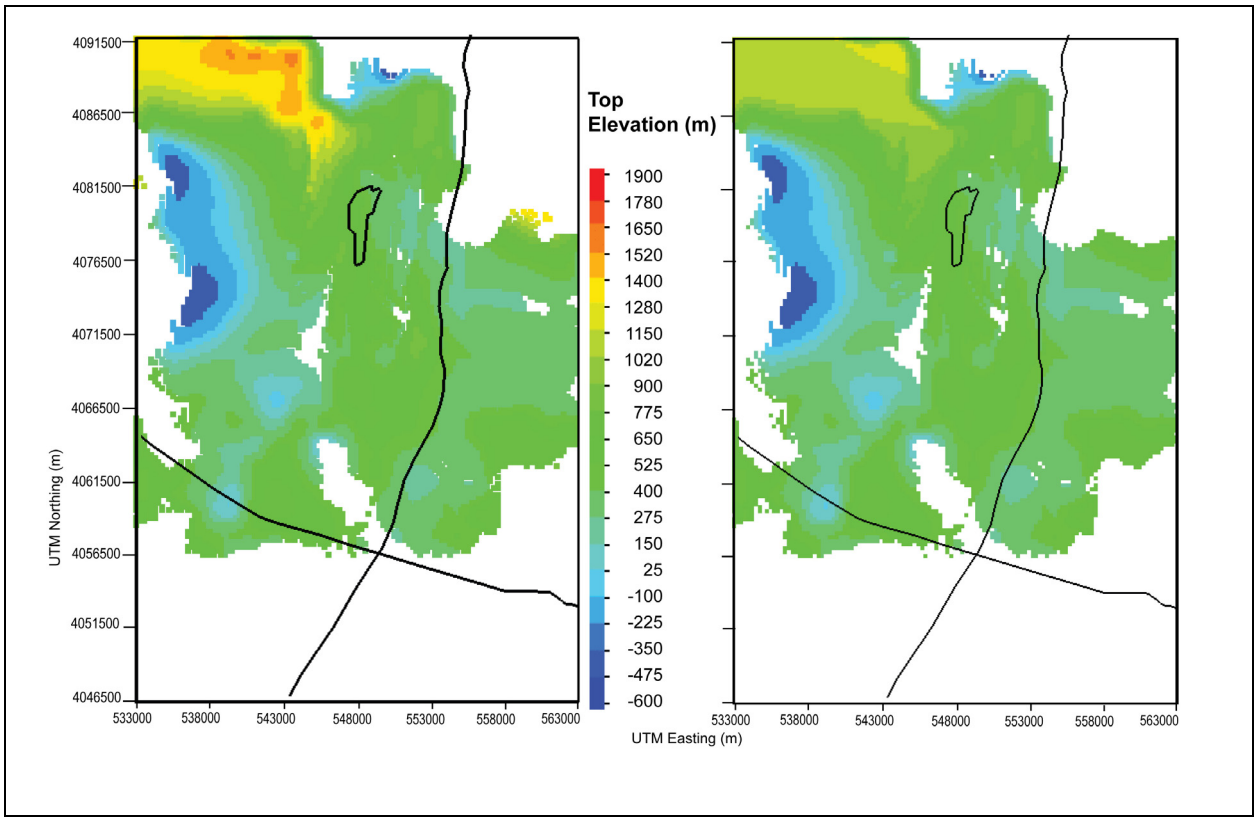

Sources: DTN: MO0610MWDHFM06.002 [DIRS 179352] (HFM2006); SNL 2007 [DIRS 179466] (repository outline).

Output DTNs: MO0611SCALEFLW.000 (potentiometric surface); LA0612TM831231.001.

NOTES: Hydrogeologic properties for unit defined by HFM for computational grid with 98,162 nodes total (left panel) and 93,327 nodes under water table (right panel). Coordinates in UTM, Zone 11, NAD27 meters. Black lines show repository outline, U.S. Highway 95 running East-West, and trace of Fortymile Wash running North-South. Elevation is in meters above mean sea level. For illustration purposes only.

HFM = Hydrogeologic Framework Model; UTM = Universal Transverse Mercator.

Figure G-11. Distribution and Elevations of CFTA, Crater Flat Tram Aquifer (14)

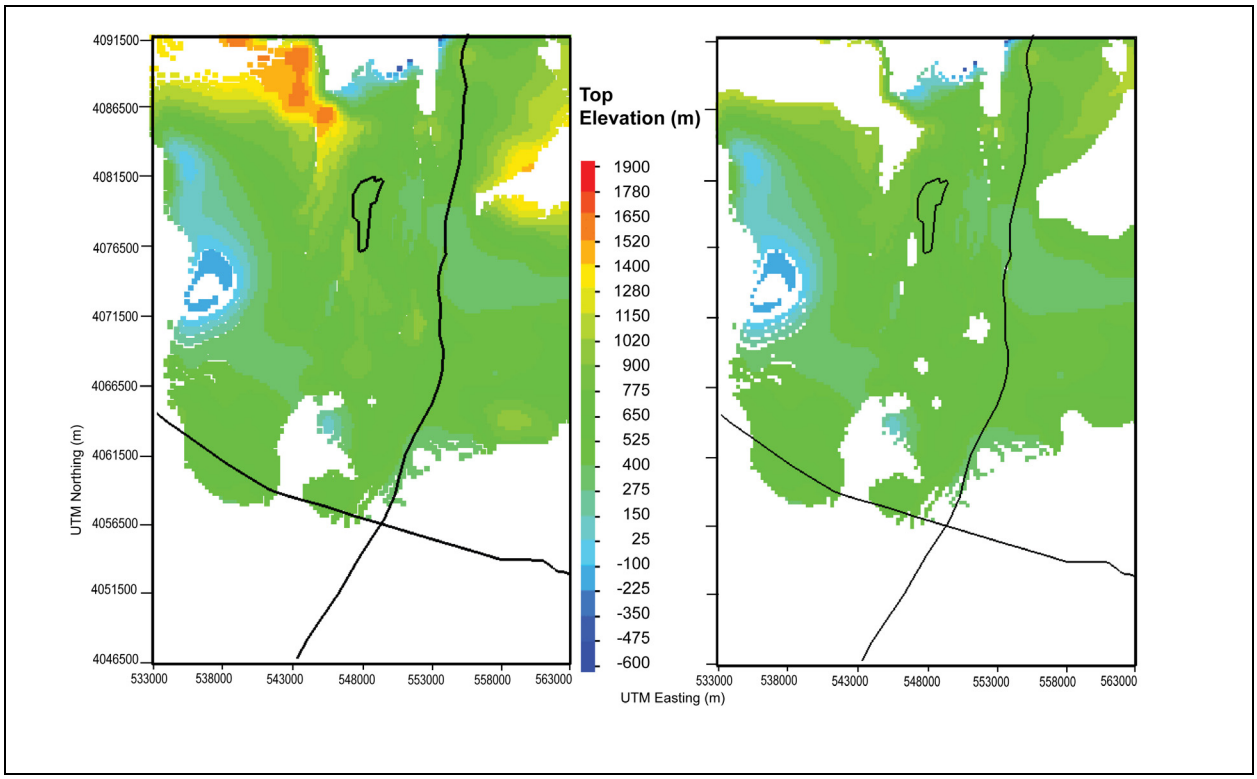

Sources: DTN: MO0610MWDHFM06.002 [DIRS 179352] (HFM2006); SNL 2007 [DIRS 179466] (repository outline).

Output DTNs: MO0611SCALEFLW.000 (potentiometric surface); LA0612TM831231.001.

NOTES: Hydrogeologic properties for unit defined by HFM for computational grid with 73,939 nodes total (left panel) and 67,436 nodes under water table (right panel). Coordinates in UTM, Zone 11, NAD27 meters. Black lines show repository outline, U.S. Highway 95 running East-West, and trace of Fortymile Wash running North-South. For illustration purposes only. Elevation is in meters above mean sea level.

HFM = Hydrogeologic Framework Model; UTM = Universal Transverse Mercator.

Figure G-12. Distribution and Elevations of CFBCU, Crater Flat Bullfrog Confining Unit (15)

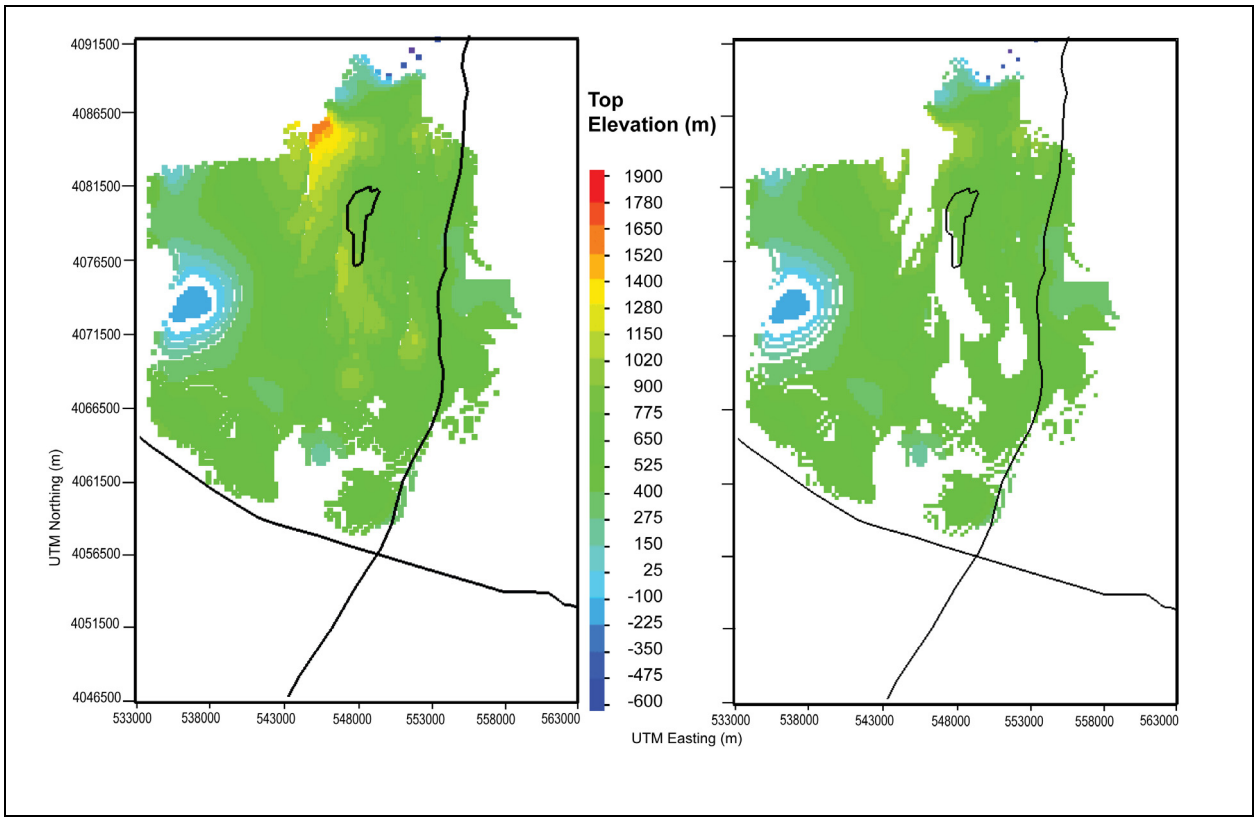

Sources: DTN: MO0610MWDHFM06.002 [DIRS 179352] (HFM2006); SNL 2007 [DIRS 179466] (repository outline).

Output DTNs: MO0611SCALEFLW.000 (potentiometric surface); LA0612TM831231.001.

NOTES: Hydrogeologic properties for unit defined by HFM for computational grid with 23,461 nodes total (left panel) and 20,242 nodes under water table (right panel). Coordinates in UTM, Zone 11, NAD27 meters. Black lines show repository outline, U.S. Highway 95 running East-West, and trace of Fortymile Wash running North-South. Elevation is in meters above mean sea level. For illustration purposes only.

HFM = Hydrogeologic Framework Model; UTM = Universal Transverse Mercator.

Figure G-13. Distribution and Elevations of CFPPA, Crater Flat Prow Pass Aquifer (16)

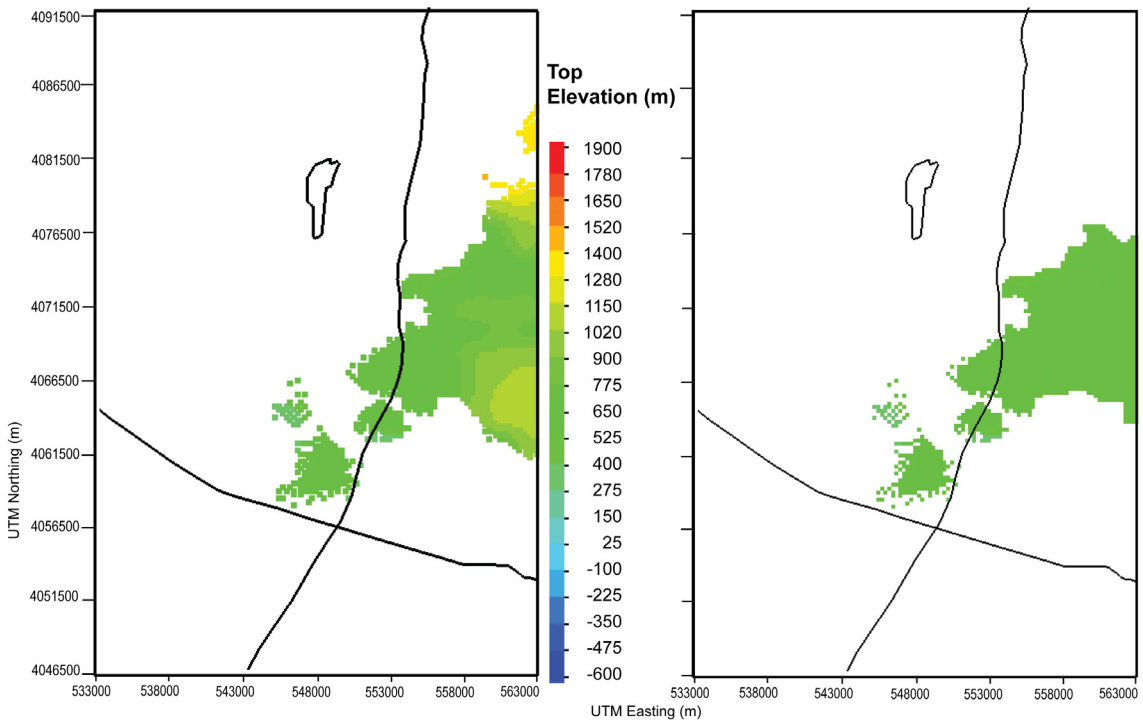

Sources: DTN: MO0610MWDHFM06.002 [DIRS 179352] (HFM2006); SNL 2007 [DIRS 179466] (repository outline).

Output DTNs: MO0611SCALEFLW.000 (potentiometric surface); LA0612TM831231.001.

NOTES: Hydrogeologic properties for unit defined by HFM for computational grid with 21,116 nodes total (left panel) and 14,576 nodes under water table (right panel). Coordinates in UTM, Zone 11, NAD27 meters. Black lines show repository outline, U.S. Highway 95 running East-West, and trace of Fortymile Wash running North-South. Elevation is in meters above mean sea level. For illustration purposes only.

HFM = Hydrogeologic Framework Model; UTM = Universal Transverse Mercator.

Figure G-14. Distribution and Elevations of WVU, Wahmonie Volcanic Unit (17)

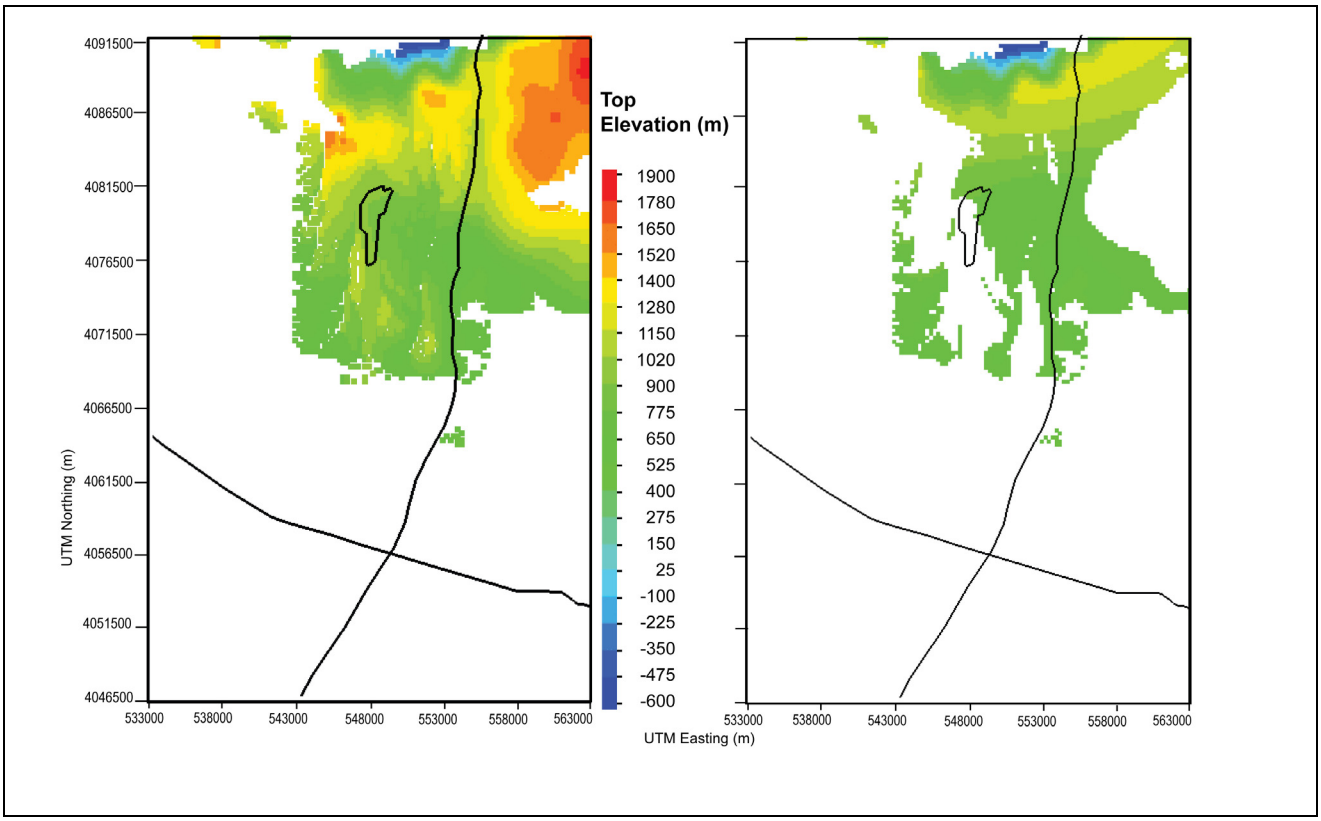

Sources: DTN: MO0610MWDHFM06.002 [DIRS 179352] (HFM2006); SNL 2007 [DIRS 179466] (repository outline).

Output DTNs: MO0611SCALEFLW.000 (potentiometric surface); LA0612TM831231.001.

NOTES: Hydrogeologic properties for unit defined by HFM for computational grid with 47,905 nodes total (left panel) and 29,189 nodes under water table (right panel). Coordinates in UTM, Zone 11, NAD27 meters. Black lines show repository outline, U.S. Highway 95 running East-West, and trace of Fortymile Wash running North-South. Elevation is in meters above mean sea level. For illustration purposes only.

HFM = Hydrogeologic Framework Model; UTM = Universal Transverse Mercator.

Figure G-15. Distribution and Elevations of CHVU, Calico Hills Volcanic Unit (18)

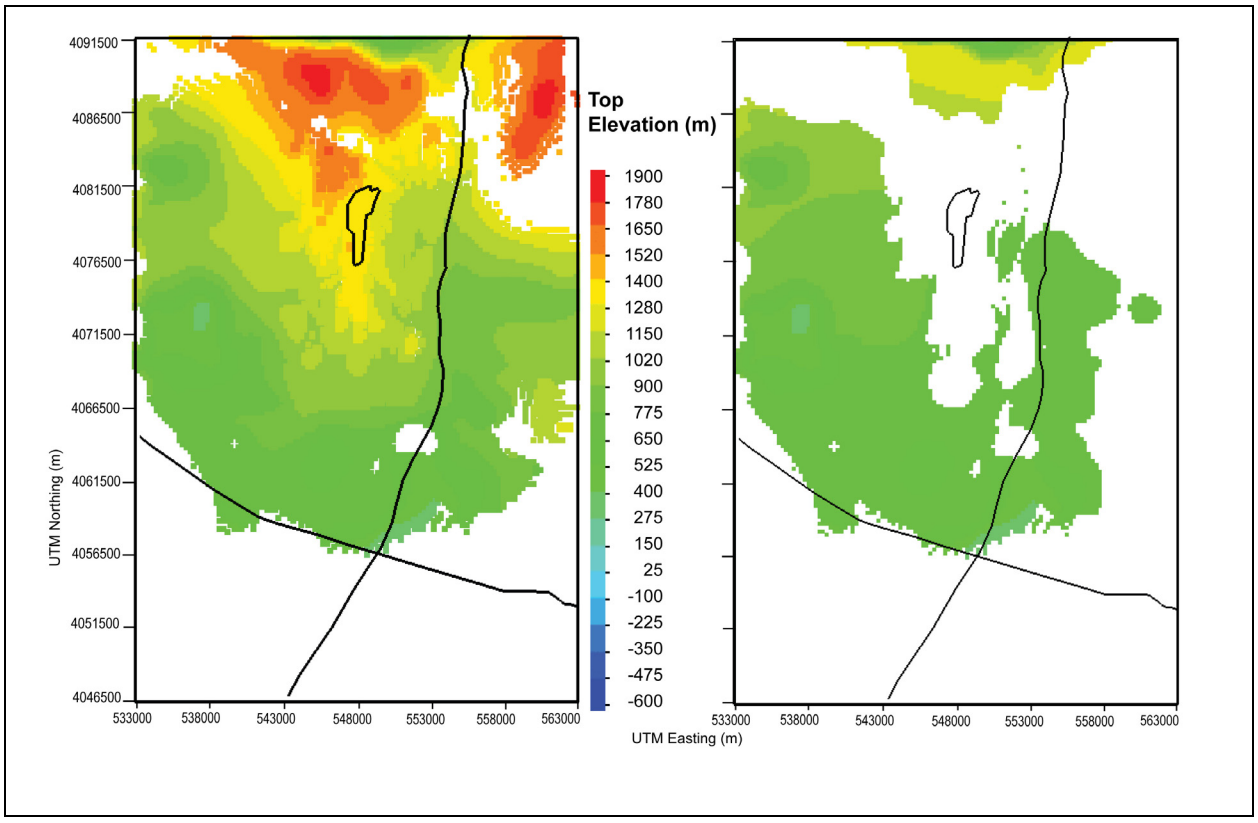

Sources: DTN: MO0610MWDHFM06.002 [DIRS 179352] (HFM2006); SNL 2007 [DIRS 179466] (repository outline).

Output DTNs: MO0611SCALEFLW.000 (potentiometric surface); LA0612TM831231.001.

NOTES: Hydrogeologic properties for unit defined by HFM for computational grid with 143,658 nodes total (left panel) and 94,149 nodes under water table (right panel). Coordinates in UTM, Zone 11, NAD27 meters. Black lines show repository outline, U.S. Highway 95 running East-West, and trace of Fortymile Wash running North-South. Elevation is in meters above mean sea level. For illustration purposes only.

HFM = Hydrogeologic Framework Model; UTM = Universal Transverse Mercator.

Figure G-16. Distribution and Elevations PVA, Paintbrush Volcanic Aquifer (19)

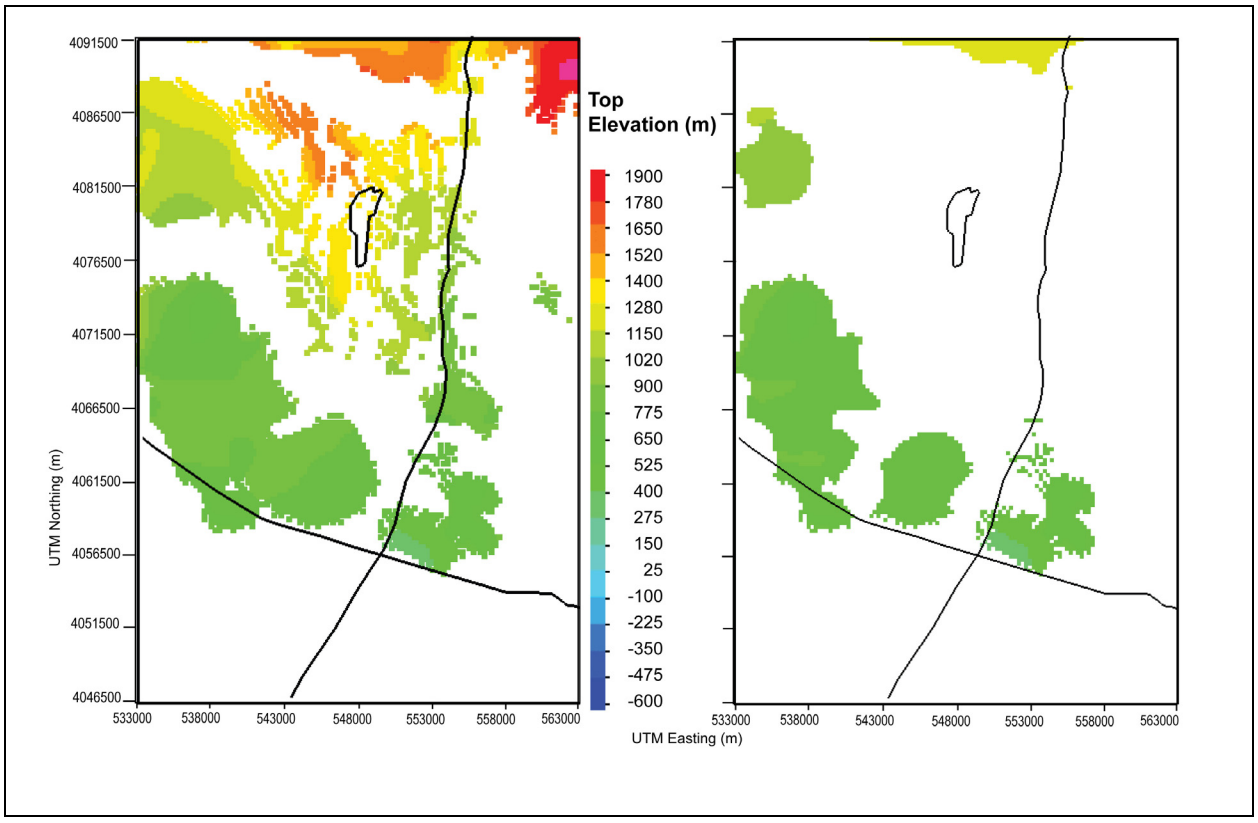

Sources: DTN: MO0610MWDHFM06.002 [DIRS 179352] (HFM2006); SNL 2007 [DIRS 179466] (repository outline).

Output DTNs: MO0611SCALEFLW.000 (potentiometric surface); LA0612TM831231.001.

NOTES: Hydrogeologic properties for unit defined by HFM for computational grid with 27,940 nodes total (left panel) and 18,131 nodes under water table (right panel). Coordinates in UTM, Zone 11, NAD27 meters. Black lines show repository outline, U.S. Highway 95 running East-West, and trace of Fortymile Wash running North-South. Elevation is in meters above mean sea level. For illustration purposes only.

HFM = Hydrogeologic Framework Model; UTM = Universal Transverse Mercator.

Figure G-17. Distribution and Elevations of TMVA, Timber Mountain Volcanic Aquifer (20)

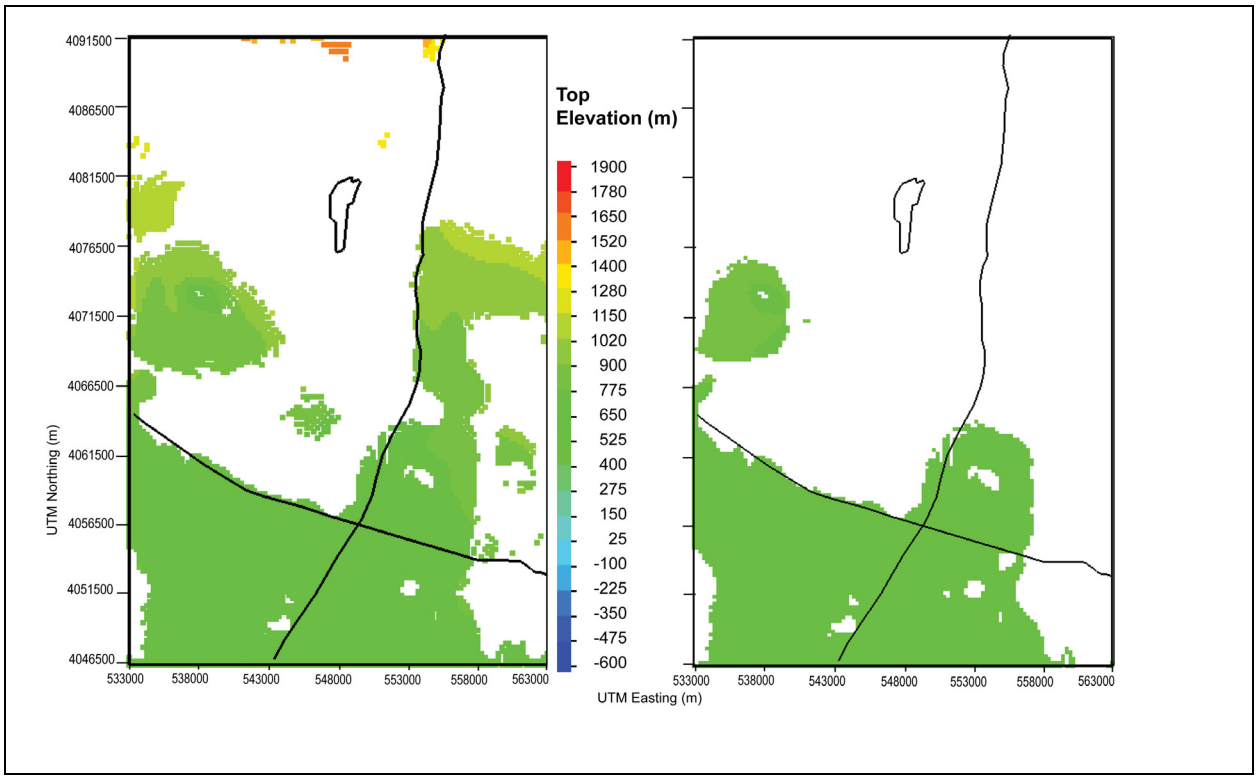

Sources: DTN: MO0610MWDHFM06.002 [DIRS 179352] (HFM2006); SNL 2007 [DIRS 179466] (repository outline).

Output DTNs: MO0611SCALEFLW.000 (potentiometric surface); LA0612TM831231.001.

NOTES: Hydrogeologic properties for unit defined by HFM for computational grid with 53,911 nodes total (left panel) and 42,717 nodes under water table (right panel). Coordinates in UTM, Zone 11, NAD27 meters. Black lines show repository outline, U.S. Highway 95 running East-West, and trace of Fortymile Wash running North-South. Elevation is in meters above mean sea level. For illustration purposes only.

HFM = Hydrogeologic Framework Model; UTM = Universal Transverse Mercator.

Figure G-18. Distribution and Elevation of VSU, Volcanic and Sedimentary Unit (Upper) (21)

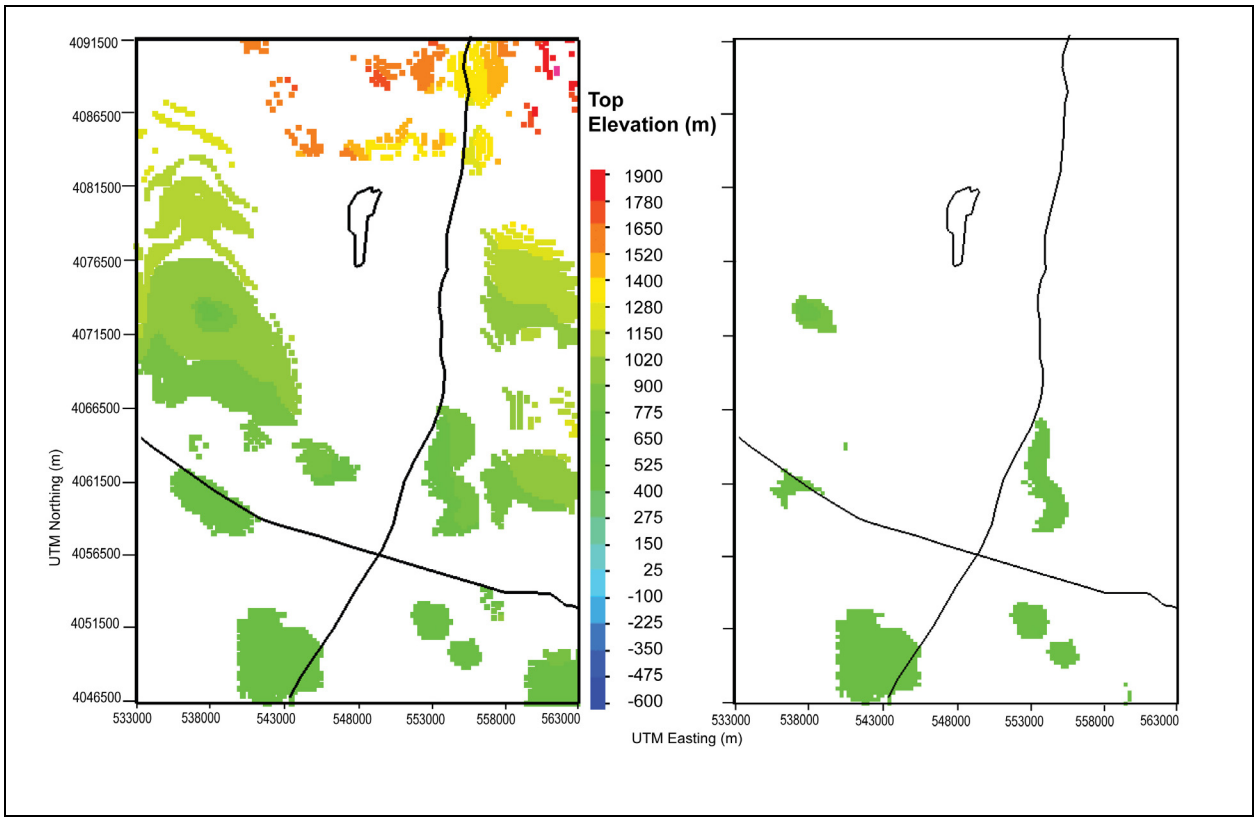

Sources: DTN: MO0610MWDHFM06.002 [DIRS 179352] (HFM2006); SNL 2007 [DIRS 179466] (repository outline).

Output DTNs: MO0611SCALEFLW.000 (potentiometric surface); LA0612TM831231.001.

NOTES: Hydrogeologic properties for unit defined by HFM for computational grid with 8,608 nodes total (left panel) and 2,751 nodes under water table (right panel). Coordinates in UTM, Zone 11, NAD27 meters. Black lines show repository outline, U.S. Highway 95 running East-West, and trace of Fortymile Wash running North-South. Elevation is in meters above mean sea level. For illustration purposes only.

HFM = Hydrogeologic Framework Model; UTM = Universal Transverse Mercator.

Figure G-19. Distribution and Elevations of LFU, Lava Flow Unit (23)

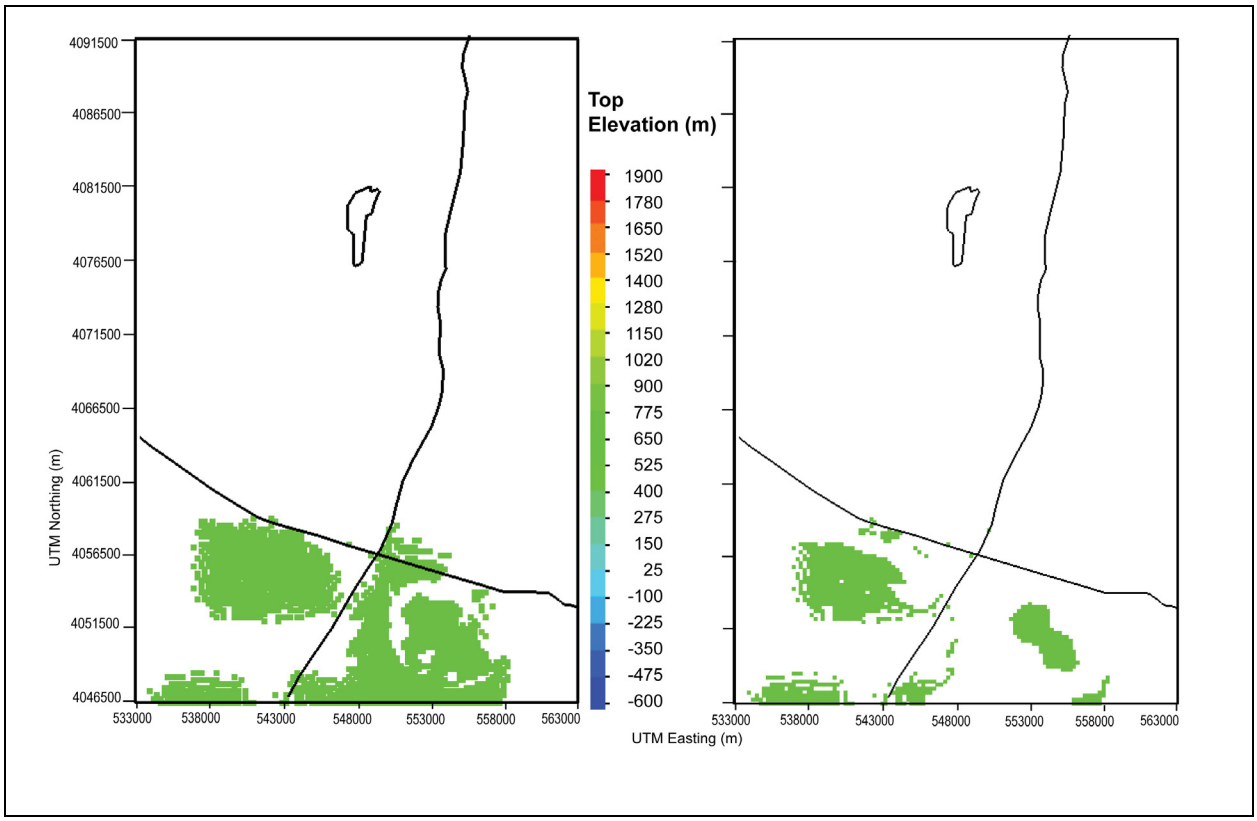

Sources: DTN: MO0610MWDHFM06.002 [DIRS 179352] (HFM2006); SNL 2007 [DIRS 179466] (repository outline).

Output DTNs: MO0611SCALEFLW.000 (potentiometric surface); LA0612TM831231.001.

NOTES: Hydrogeologic properties for unit defined by HFM for computational grid with 3,289 nodes total (left panel) and 1,387 nodes under water table (right panel). Coordinates in UTM, Zone 11, NAD27 meters. Black lines show repository outline, U.S. Highway 95 running East-West, and trace of Fortymile Wash running North-South. Elevation is in meters above mean sea level. For illustration purposes only.

HFM = Hydrogeologic Framework Model; UTM = Universal Transverse Mercator.

Figure G-20. Distribution and Elevations of LA, Limestone Aquifer (24)

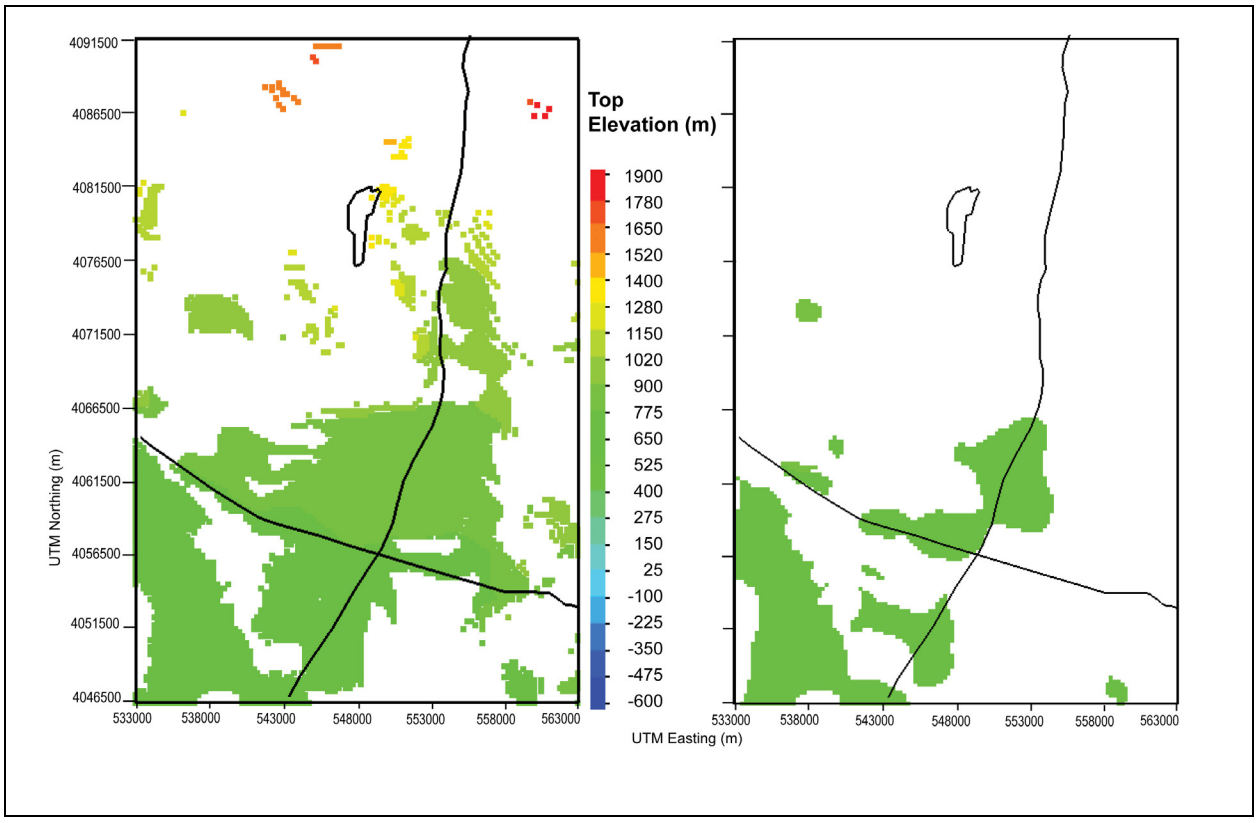

Sources: DTN: MO0610MWDHFM06.002 [DIRS 179352] (HFM2006); SNL 2007 [DIRS 179466] (repository outline).

Output DTNs: MO0611SCALEFLW.000 (potentiometric surface); LA0612TM831231.001.

NOTES: Hydrogeologic properties for unit defined by HFM for computational grid with 24,148 nodes total (left panel) and 10,637 nodes under water table (right panel). Coordinates in UTM, Zone 11, NAD27 meters. Black lines show repository outline, U.S. Highway 95 running East-West, and trace of Fortymile Wash running North-South. Elevation is in meters above mean sea level. For illustration purposes only.

HFM = Hydrogeologic Framework Model; UTM = Universal Transverse Mercator.

Figure G-21. Distribution and Elevations of OAA, Older Alluvial Aquifer (26)

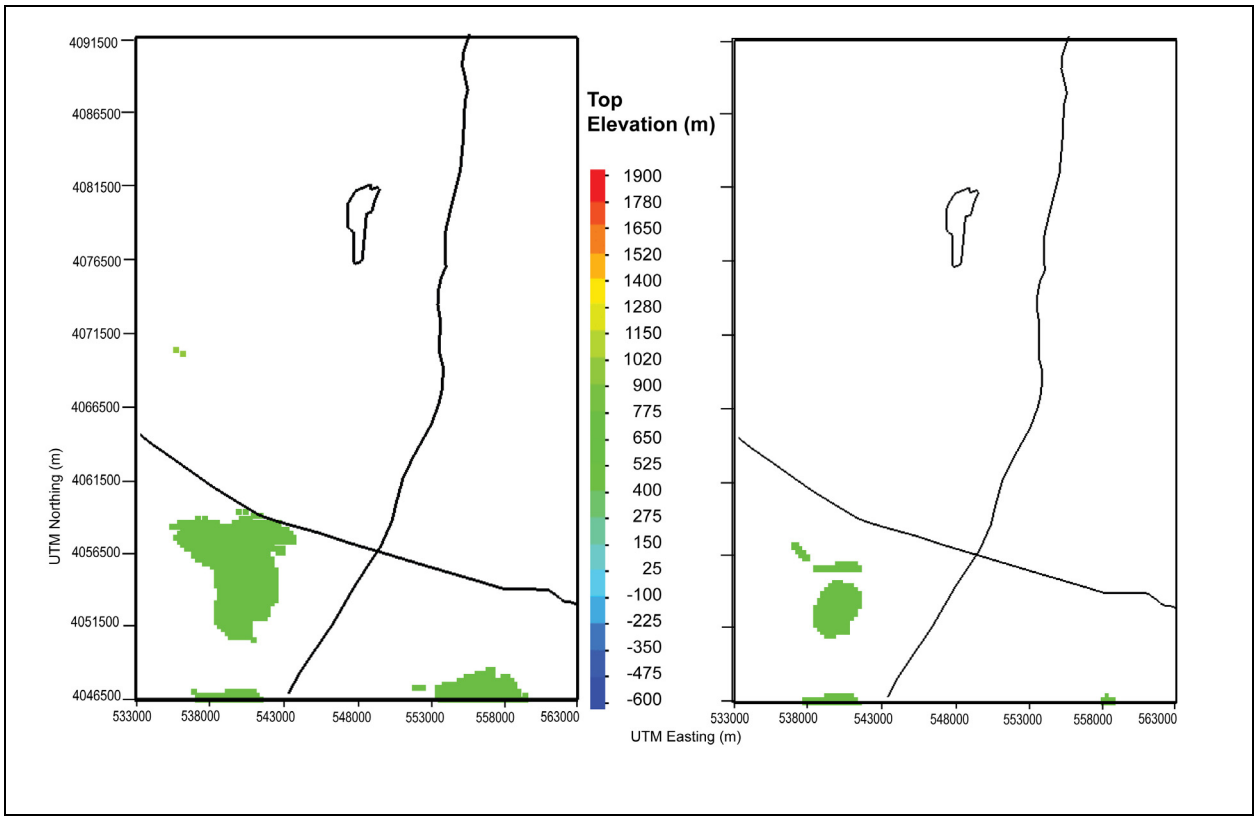

Sources: DTN: MO0610MWDHFM06.002 [DIRS 179352] (HFM2006); SNL 2007 [DIRS 179466] (repository outline).

Output DTNs: MO0611SCALEFLW.000 (potentiometric surface); LA0612TM831231.001.

NOTES: Hydrogeologic properties for unit defined by HFM for computational grid with 1,580 nodes total (left panel) and 247 nodes under water table (right panel). Coordinates in UTM, Zone 11, NAD27 meters. Black lines show repository outline, U.S. Highway 95 running East-West, and trace of Fortymile Wash running North-South. Elevation is in meters above mean sea level. For illustration purposes only.

HFM = Hydrogeologic Framework Model; UTM = Universal Transverse Mercator.

Figure G-22. Distribution and Elevations of YACU, Young Alluvial Confining Unit (27)

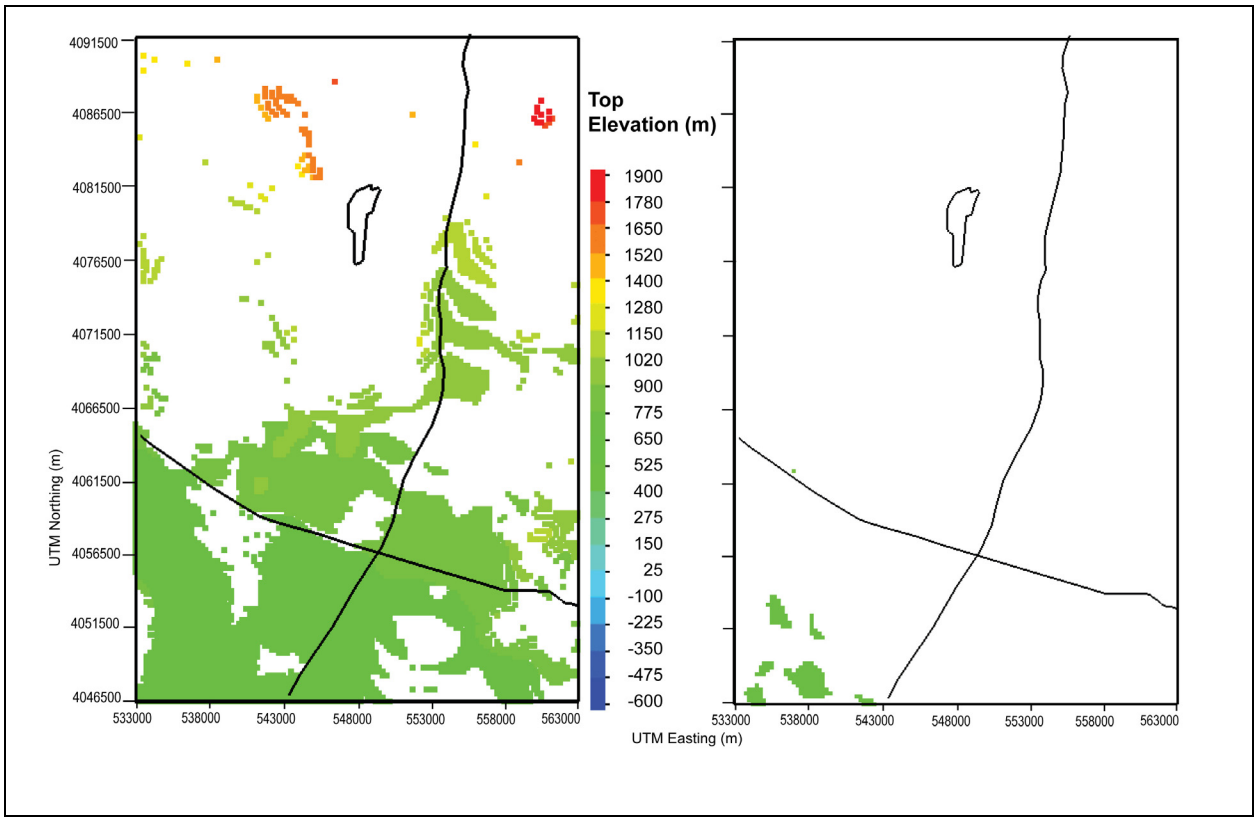

Sources: DTN: MO0610MWDHFM06.002 [DIRS 179352] (HFM2006); SNL 2007 [DIRS 179466] (repository outline).

Output DTNs: MO0611SCALEFLW.000 (potentiometric surface); LA0612TM831231.001.

NOTES: Hydrogeologic properties for unit defined by HFM for computational grid with 9,965 nodes total (left panel) and 197 nodes under water table (right panel). Coordinates in UTM, Zone 11, NAD27 meters. Black lines show repository outline, U.S. Highway 95 running East-West, and trace of Fortymile Wash running North-South. Elevation is in meters above mean sea level. For illustration purposes only.

HFM = Hydrogeologic Framework Model; UTM = Universal Transverse Mercator.

Figure G-23. Distribution and Elevations of YAA, Young Alluvial Aquifer (28)

APPENDIX H
REGULARIZED INVERSION AS A BASIS FOR MODEL CALIBRATION AND PREDICTIVE UNCERTAINTY ANALYSIS: AN EXPLANATION

H1. INTRODUCTION

Models are calibrated so that they make better predictions than if they were not calibrated. Unfortunately, calibrated model predictions can still be wrong. Furthermore, it is now being fully understood that a calibrated model can make even worse predictions than it did before calibration. With traditional approaches to model calibration, there is no way to find out: (1) whether a calibrated model's predictions are better than those before calibration, (2) if the predictions are better how much better they are, and (3) if their predictions are wrong how wrong they are. Traditional approaches to calibration are not able to ensure that calibrated models minimize "potential predictive wrongness" while quantifying the remaining uncertainty in the potential predictive wrongness.

The traditional approach to model calibration follows the tenet of the "principal of parsimony" espoused in many modeling texts and guidelines. First, the dimensionality of the calibration problem is reduced to facilitate a tractable model (i.e., few enough parameters are used to ensure their unique estimability) given the dataset available for calibration. The parameters values are then estimated through implicitly or explicitly maximizing some goodness-of-fit criterion. When the fit is judged to be "sufficient" (usually through minimization of an objective function), the model is deemed to be "calibrated" and therefore suitable for the making of predictions – predictions that may lay the groundwork for performance assessment calculations.

If automatic parameter estimation software is used in the calibration process, some estimates of parameter uncertainty are available. Estimates of the uncertainty of key model predictions can then be made based on the dependence of these predictions on the estimated parameters and their uncertainties.

The objective of this appendix is to show that calibrating a model and exploring the potential error of model predictions based on the theory of mathematical regularization, used in portions of this report, are better than methods based on the traditional approach to model calibration and predictive error analysis based on the principle of parsimony, which is not always effective or accurate. This same theory of mathematical regularization is regularly applied in many other branches of science where the analysis of costly and important data demands that maximum information be extracted (e.g., geophysical exploration and medical imaging). For example, a kidney is not defined prior to processing the data contained within a medical image; instead the location of the kidney "emerges" as a natural part of the data interpretation process. The same process should be used in groundwater data interpretation (which is what model calibration is) now that software that implements these methods efficiently in the groundwater modeling context are available. Public domain software that implements modern calibration and predictive uncertainty analysis based on regularized inversion is now available through the PEST package and its supporting utilities (Doherty 2003 [DIRS 178642], 2004 [DIRS 178643], 2006 [DIRS 178613]; PEST 2003 [DIRS 161564]). The groundwater industry will have to cross the same threshold that has been crossed in other industries, through application of regularized inversion as a methodology for model calibration and uncertainty analysis as a matter of course.

H2. TRADITIONAL MODEL CALIBRATION

Even with automatic optimization software, the task of calibrating a model can be unsatisfying and frustrating. Often a complex model of the groundwater system is developed. Its level of complexity is based on intuition and should be commensurate with available data available. This is an important point: whenever a model is built, it is based on some preconceived notion underpinning its construction related to the predictions it must make. Decisions regarding many aspects of the construction of that model must, of course, be made for the purpose of enhancing (and certainly not eroding) the model's ability to make that prediction.

Model complexity should be commensurate with the predictions it makes; no processes salient to those predictions should be omitted if the integrity of those predictions would be eroded by their omission. The same thing holds for parameters; no parameter salient to model prediction should be dropped or otherwise lumped into other parameters. Following the principle of parsimony, the dimensionality of the calibration is reduced to a tractable level, perhaps at the expense of compromising prediction validity by draping this simplistic parameterization scheme (based on a relatively small number of parameters) over what are often a set of complex processes. Then, with a certain sense of disquiet, it is assumed that values (that the model must employ for a vast number of parameter types and boundary conditions) have merit only because they are "reasonable." Next, a calibration methodology is defined that requires that the values of only a few parameters (normally defined to encompass considerable portions of the model domain) be estimated on the basis of field measurements. Hence, huge simplifications inevitably compromise a model's ability to estimate reality (e.g., assuming that large areas of the model domain subtended by artificial, rectilinear boundaries are homogeneous or that neighboring nodes within a geological unit possess exactly the same hydraulic properties). The fact that significant heterogeneity exists within a study area is ignored because unique assignment of values to the parameterization associated with this possible heterogeneity is simply beyond the reach of a limited calibration dataset.

Clearly heterogeneity is a foregone conclusion in subsurface formations even if ignoring heterogeneity during model calibration is justified on the basis that parameters pertaining to this heterogeneity cannot be estimated. Unfortunately, it is not equally justifiable that heterogeneity be ignored when the model is used to make a prediction. If a prediction is sensitive to actual system heterogeneity – heterogeneity that, of necessity, "falls between the cracks" of the calibration process – then that prediction may be seriously in error, despite the fact that the model may be "well calibrated" (i.e., a good fit between model outputs and field observations was obtained on the basis of a parameter simple enough to allow unique estimation of parameters, but which possesses just enough complexity to obtain this good fit).

Similar considerations apply to assumptions made for parameters with "fixed values" (e.g., vertical anisotropy). A good fit between model outputs and historical measurements of system state with these parameters fixed at "reasonable" values does not prove that these values are correct because it is quite possible that other reasonable values could also have been provided for these parameters. In fact, it is likely that adjustable parameters assigned "calibrated" values are (to some degree) incorrect to compensate for erroneous values assigned to fixed parameters. Despite the fact that the model may be "well-calibrated," a prediction will be in error if it is

sensitive either to an erroneously assigned fixed parameter, or to any parameter whose value has been misestimated to compensate for the erroneous value assigned to the fixed parameter.

As well as the above conceptual problems, the traditional approach to model calibration is fraught with practical difficulties. For example, parameter zonation will often start with a geological map; however such maps have varying accuracy and varying degrees of hydrogeologic relevance. Even where a map is available, ability to infer the disposition of geological units with depth is often limited. Furthermore, the salience of structural features such as faults or gravel beds (whose existence or whereabouts are estimated) to groundwater and contaminant movement is often difficult to judge. Nevertheless, model calibration is still based on a simplified zonation pattern, often with only a subset of zone-based parameters actually estimated. Hence, one of two things invariably occurs. On the one hand, it may become obvious that the zonation scheme is not properly reflective of subsurface hydraulic property spatial variability due to an inability to obtain a good fit between model outputs and site data. More zones may be needed or zone boundaries may need adjustment – both of which require that subjective and unsatisfying decisions be made on where to place rectilinear zone boundaries, and both inciting the modeler to wonder how sensitive different predictions may be to *ad hoc* decisions to emplace particular boundaries here and not there. On the other hand, where geological data are plentiful, and where groundwater head data are scarce (as is often the case where deep groundwater and contaminant movement is simulated as part of waste disposal and other studies), too many zones may have been introduced to allow unique assignment of parameter values through the calibration process. In this case, the modeler must decide which zones should be eradicated through amalgamation with neighboring zones, and/or which zonal hydraulic properties should be fixed at questionable values. Both of these procedures will effect model predictions, leaving the modeler with the sure knowledge that these predictions are in error. However, ability to assess the possible magnitude of this error is entirely lacking with this approach to parameter definition and estimation.

H3. TWO INESCAPABLE FACTS AND TWO FUNDAMENTAL PRINCIPLES

Some important facts must be acknowledged. And then, taking these as the starting point, an alternative approach to model parameterization and calibration based on these two fundamental principles is developed:

1. If a model is to be "calibrated" then its parameterization must be simplified so that the "inverse problem" (the calibration process) of assigning values to model parameters on the basis of an (often limited) calibration dataset has a unique solution. Traditionally, such simplification is undertaken prior to model calibration through adoption of a simplified parameter scheme as discussed above (e.g., an effective permeability applied to an entire geologic unit). However, as will be described below, other approaches to calibration are needed so that simplifications undertaken during the calibration process itself are far less subjective. Nevertheless, the fact remains that pursuit of the "calibrated model" requires sufficient parameterization simplification to yield a (simplification-dependent) unique set of estimated parameters. Because it is impossible to infer parameterization detail to the same level that hydraulic property detail really exists, the cost of obtaining a calibrated model is therefore a parameter field that *must be* locally in error, even if it is roughly correct in an average sense. See

Moore and Doherty (2006 [DIRS 178403]), and papers cited therein, for a more complete discussion of this topic.

2. Parameter error leads to predictive error. Furthermore, to the extent that a prediction depends on hydraulic property heterogeneity that "falls between the cracks" of the calibration process, the potential magnitude of its error grows. In general, predictions different from those comprising the calibration dataset (e.g., specific discharge predictions and hydraulic head calibration data) are more likely to be in error because they may depend on hydraulic properties that were fixed or grossly averaged over the model domain due to a paucity of information on these properties within the calibration dataset. Unfortunately, this introduces a contradiction because the reason for employing a complex physically based model in the first place is because predictions of just these types (different from the dataset) need to be made (otherwise the prediction would simply be directly measured at the site).

Armed with these facts, two fundamental criteria are defined that can, and should, enlighten the pursuit of a good strategy for model calibration:

1. The calibration process should aim to provide a model with a set of parameters that allows it to make predictions with minimized potential error.

2. The extent of this potential error should be quantified.

An approach to model calibration that goes a long way towards achieving these two fundamental objectives is outlined below.

H4. REGULARIZED INVERSION

"Regularization" is a word that mathematicians use to describe the parameter simplification process necessary to achieve a unique solution to an inverse problem (such as that of model calibration). In general, with fewer available data, more regularization must be undertaken (and hence a greater degree of parameter simplification). Regularization can be implemented using manual parsimonizing methods such as zonal definitions. As demonstrated below, parameter parsimony can also be implemented mathematically such that it is optimized to the calibration dataset and hence extracts maximum information from that dataset. This satisfies the first of the above principles.

The point of departure of calibration methods based on regularized inversion from traditional approaches is that the former are designed for the estimation of many parameters (possibly numbering in the hundreds or even thousands) rather than just a few. Thus we introduce to the model domain a parameterization density that is commensurate with whatever hydrogeological or process complexity that it is necessary for model prediction accuracy. It should be noted that this does not eliminate parameter error (and hence model predictive error) because parameter simplification in one form or another is an unavoidable precursor to model calibration. What it does provide however, is the ability to *quantify* potential parameter and predictive error. Because parameter complexity is not sustainable in a model due to inherent limitations in the calibration dataset, this complexity can be readily reintroduced where predictive "wiggle room"

is tested as part of a predictive error analysis procedure. Thus, the second of the above principles is respected.

Parameters whose values are estimated through regularized inversion can be defined on the basis of a large number of small zones of piecewise constancy, through devices such as pilot points (Doherty 2003 [DIRS 178642], 2004 [DIRS 178643]), through local or global basis functions, through combinations of these, or using other methodologies. The point is that if potential variability of hydraulic properties over a certain area is relevant to a prediction, such variability should be recognized in the model's parameterization (and thus included in the calibration and subsequent predictive error analysis). Inclusion in the calibration process ensures that maximum information is extracted from a calibration dataset; inclusion in the predictive error analysis ensures that the level of potential error associated with important model predictions is quantified. To the extent that simplification is required to achieve a unique solution to the inverse problem, mathematical regularization ensures that the calibration dataset is used optimally. Essentially, this produces "smoothed" or "blurred" parameter fields that are no "smoother" and no more "blurred" than necessary. To the extent that a prediction depends on hydraulic property detail that cannot be represented in these smoothed fields, the effect of smoothing on potential predictive error is quantified. Meanwhile, agonizing decisions such as how to supplement, reduce, or adjust an often artificial rectilinear zonation scheme do not need to be made, thus making calibration a far less subjective process.

Some may complain that the use of so many parameters may lead to "over-fitting" to a calibration dataset, pointing out that a close fit between model outputs and historical measurements can indeed be obtained when many parameters are estimated, but that predictive error may be consequently increased. The reader can be assured that this is easily avoided because regularized inversion, no matter how it is implemented, allows the modeler to vary the extent to which improved model-to-measurement fit is traded against the potential for model predictive error. In fact, because the potential for such error can now be quantified, it can also be minimized once the level of measurement noise and the level of geological heterogeneity are estimated.

H5. REGULARIZATION METHODS

H5.1 GENERAL

A brief description of some regularization methodologies is now presented while a few mathematical details are provided in Section H8. The reader is referred to literature cited herein for more details. Note that all methodologies described herein are available through the PEST suite of software (Watermark Computing 2004 [DIRS 178612]; Doherty 2006 [DIRS 178613]).

Two broad approaches to regularized inversion have been applied to groundwater model calibration: "Tikhonov" and "subspace" methodologies. Each has its advantages and disadvantages; however, certain hybrid schemes are able to combine the strengths of both of these without compromising computational efficiency. Complex models with long run times can be assigned thousands of parameters while their calibration can be achieved within a number of model runs less than twice the number of parameters actually used in the model. Linear and nonlinear predictive error analysis can then be undertaken with similar computational efficiency.

H5.2 TIKHONOV METHODS

Tikhonov regularization is implemented by reformulating the inverse problem of model calibration as a constrained minimization problem. First, a "preferred condition" is defined for all parameters used in the model. This can comprise preferred values for these parameters or preferred relationships between them (e.g., estimated or measured hydraulic property homogeneity). A set of parameter values is sought that achieves a certain (user-specified) level of model-to-measurement fit; this level of fit is set in accord with expected levels of measurement noise. Uniqueness is achieved by finding values for parameters that achieve this fit with minimal departure from the preferred parameter condition. If preferred parameter conditions are sensibly defined on the basis of site characterization studies, a realistic set of parameters is thereby achieved.

H5.3 SUBSPACE METHODS

The use of subspace methods recognizes the fact that most calibration datasets are best equipped to provide unique estimates of combinations of parameters and not individual parameters. Mathematical tools (singular value decomposition) determine what these combinations are and how many such combinations are estimable while inestimable parameter combinations retain their original values. By working with parameter combinations rather than individual parameters (combinations that are orthogonal in parameter space), the dimensionality of the "calibration solution space" (i.e., the number of parameter combinations that are actually estimated) can be optimized in accord with the level of measurement noise. That is, these combinations are assembled to provide optimal "receptacles" for the information content of the calibration dataset. If initial parameter estimates provided to the inversion process are based upon site characterization studies, then the fact that parameter combinations comprising the inestimable "calibration null space" (which is orthogonal to the calibration solution space) remain unchanged during calibration ensures reasonable parameter values in the calibrated model. The optimal dimensionality of the calibration solution and null spaces depends on the level of model-to-measurement fit desired, which should be set in accordance with measurement noise.

H5.4 HYBRID METHODS

There is no reason why both Tikhonov and subspace methods cannot be used in the same regularized calibration process as is done using the "SVD-assist" scheme implemented in PEST (Doherty 2006 [DIRS 178613]). Not only does this scheme combine the strengths of both of these methods; it carries another significant advantage. Through predefinition of estimable parameter combinations (using singular value decomposition or some related methodology), and through maintenance of these combinations through the calibration process as "super parameters," the number of effective parameters is reduced to one comprising the optimal dimensionality of the calibration solution space. The number of model runs required per calibration iteration is thereby reduced to the number of super parameters employed in the inversion process, as derivatives are computed with respect to these super parameters rather than with respect to individual model parameters. As Tonkin and Doherty (2005 [DIRS 178576]) show, the model run efficiency of the calibration process may be increased enormously.

H5.5 DISCUSSION

Regardless of the regularization method used, the advantages of developing many parameters to characterize hydraulic property complexity and heterogeneity over a model domain, rather than just a few parameters, are considerable. The parameter estimation process is free to be maximally responsive to the calibration dataset, introducing heterogeneity to estimated spatial parameter fields where the data suggest that such heterogeneity exists, or producing smooth or uniform parameter fields where there are no data to suggest otherwise. Thus, heterogeneity exists within the calibrated model "where it has to exist" because regularized inversion will introduce heterogeneity only where it is stipulated by the data. However, because model representation of heterogeneity may be considerably smoothed compared to what actually exists, parameter and predictive error may still abound. The question remains: how is predictive error quantified?

But before answering, it is important to point out that regularized inversion based on large numbers of parameters does not preclude the use of zones inspired by geological mapping. In fact, both of these parameterization schemes can comfortably coexist within the same model domain. Regularization allows all known geologic zones to be retained, even if unique estimates of the hydraulic properties associated with each zone cannot be extracted from the calibration dataset. Zones can also be combined with the use of finer scale parameterization devices such as pilot points. Furthermore, during the regularized inversion process (model calibration), heterogeneity can be preferentially introduced at zone boundaries, while the introduction of intrazonal heterogeneity is restricted only to those locations necessitated by the data.

H6. PREDICTIVE ERROR ANALYSIS

Because hydraulic properties in any real-world system are much more complex and heterogeneous than the calibrated model parameter fields that represent them, model parameters cannot help but be locally in error. So, too, will be many model predictions, particularly those that depend on hydraulic property detail. Thus, as has already been discussed, an unavoidable consequence of building and calibrating a model is the introduction of parameter and predictive error with most of this error arising from differences between model and real-world hydraulic property fields. These differences represent the hydraulic property detail that "slips between the cracks" of the calibration process.

Where the number of parameters used in a model is commensurate with potential hydraulic property complexity, predictive error can be quantified. Through site characterization studies, or simply through geological insight, information will always be available on the range of hydraulic properties that may exist within a study site or region, and on the degree of spatial correlation that these properties may show. Sometimes this information may be encapsulated in geostatistical descriptors such as a variogram. Regardless, reasonable estimates of hydraulic property variability can always be made; after all, a geologist will quickly identify aspects of model parameterization that seem unbelievable. These ideas can be approximately encapsulated in a spatial covariance matrix of hydraulic properties, which provides both a brief statistical summary of the innate variably of hydraulic properties in a study area and the likely continuity of these properties. Often, such a matrix can be built easily for most sites. Its approximate nature does not matter because approximation infers uncertainty. High uncertainty infers potentially

high hydraulic property variance, which is justifiably translated into potentially high levels of model predictive uncertainty if hydraulic property details are inestimable through the calibration process and predictions of interest are sensitive to them. Using basic matrix manipulation methods, such a probabilistic description of the "heterogeneity that may exist" within the subsurface, when compared with the "heterogeneity which must exist" as represented by the calibrated model parameter field, allows a probabilistic description of model predictive error to be developed, based on the difference between the two.

Subspace regularization methods provide particularly useful insights into the sources of model predictive error. As already stated, certain combinations of parameters are estimable through the calibration process; however, these estimates are contaminated by measurement noise in the calibration dataset. This is one source of potential predictive error. The other source of error arises from inestimable parameter combinations comprising the calibration null space. Thus, to the extent that a prediction depends on the null space (orthogonal) combinations of parameters, its potential error is in no way decreased during the calibration process. The potential wrongness of model predictions that depends on these parameter combinations is thus a function of the innate variability of system hydraulic properties described by the user-supplied covariance matrix. Total predictive error is computed by combining this term (null space error) with the measurement noise term (see Moore and Doherty 2005 [DIRS 178402] for more details).

Model predictive error analysis is a routine adjunct to regularized inversion using the PEST suite of software. Linear analysis (in which the action of the model on its parameters is approximated by a sensitivity matrix of appropriate dimensions) yields: (1) approximations to true predictive error variance, (2) contributions made by different parameter types to the potential error of key model predictions, and (3) optimization of yet-to-be-acquired data (based on the premise that the best data reduce predictive error variance the most). Such analysis is far superior to methods such as OPR-PPR that ignore the role of extra data in increasing the dimensionality of the calibration solution space, and hence can lead to erroneous conclusions regarding the relative benefits of future site characterization efforts.

Nonlinear predictive error analysis is more computationally expensive than linear analysis, but is more accurate. Moore (2006 [DIRS 178788]) shows how the constrained predictive maximization/minimization methodology of Vecchia and Cooley (1987 [DIRS 178577]) can be extended to the realm of regularized inversion based on large numbers of parameters. Despite the potentially large number of parameters involved in such a maximization/minimization process, it can nevertheless be efficiently undertaken if parameter variation is restricted to a "predictive subspace" encompassing only linear combinations of parameters to which the prediction of interest is most sensitive. Meanwhile, calibration constraints (which ensure that the model remains calibrated) and reality constraints (which ensure that parameters remain realistic) are applied to all model parameters, regardless of whether they belong to the predictive solution or null spaces.

"Calibration-constrained Monte Carlo" analysis is rapidly and cheaply implemented as another adjunct to regularized inversion. Information forthcoming from the regularized inversion process facilitates generation of stochastic parameter fields that minimally affect the calibrated status of a model. By adding these parameter variations to the calibrated parameter field (using precalculated sensitivities to eliminate the need for extra model runs and by correcting for

model-to-measurement misfit incurred by model nonlinearity through minor adjustment of parameter combinations comprising the calibration solution space), a suite of parameter fields that calibrate the model while encompassing the innate complexity of hydraulic property reality is generated. Model predictions made with all fields span the variance of that prediction.

H7. CONCLUSIONS

This appendix outlines the advantages of model calibration through regularized inversion over traditional methodologies based on the use of a small number of parameters in accordance with the "principle of parsimony." In fact, all calibration requires parameter simplification and parsimonizing. However, where regularization is undertaken by mathematical means, such simplification is optimally tuned to the calibration dataset, thus extracting maximum information from that dataset. This results in a calibrated parameter field that is indeed a simplified or smoothed version of reality, but are no simpler and no smoother than necessary. Furthermore, the difference between the heterogeneity that *must* exist to explain the data, and that which *may* exist in accordance with geological considerations, is explicitly accommodated in a predictive error analysis process during the regularized calibration process. As a result of this, the two basic principles of model calibration espoused above are respected (see Section H3).

In addition to its mathematical superiority, regularized inversion has other benefits. In most cases, it is far easier to implement than traditional parameter estimation. A modeler need no longer agonize over whether an artificial parameterization scheme is appropriate or not, or wonder whether it needs to be made more or less parsimonious. Model parameterization is now a far simpler matter, based on the tenet that "if it may affect the prediction, then include it as a parameter" (the same rule that applies to processes simulated by the model). Problems of parameter identifiability simply disappear because irrelevant parameters are combined during regularization. Thus, a modeler can never contrive too many parameters because the complexity of the estimated parameter field will be reduced to the level sustainable by the calibration dataset. Good fits between model outputs and field data can be achieved on the basis of aesthetically pleasing and geologically reasonable parameter fields, unencumbered by artificialities (such as geologically unsupported rectilinear zones arbitrarily emplaced at locations) contrived to lead to a better fit between model outputs and field measurements. Overall, a modeler will be satisfied that data have been treated with respect, and endowed with a worth equal to its cost because maximum information is extracted from it to make predictions whose potential wrongness is minimized.

H8. POST SCRIPTUM: SOME THEORY

H8.1 GENERAL

The purpose of this section is to briefly present some equations that underpin the points raised in a more qualitative manner in the above discussion. For simplicity, model linearity is assumed although extension of this theory to nonlinear systems is found in see many of the references previously cited.

Let the vector, $\mathbf{h}$, represent a set of system state measurements (dataset, e.g., groundwater heads), and let the vector, $\boldsymbol{\varepsilon}$, represent the noise associated with these measurements. Let the matrix, $\mathbf{X}$,

represent the action of the model (under calibration conditions) on a set of parameters **p**. Then, ignoring offsets:

$$\mathbf{h} = \mathbf{X}\mathbf{p} + \boldsymbol{\varepsilon}. \quad \text{(Eq. H-1)}$$

The noise, **ε**, associated with a particular set of measurements cannot be known. However, it is assumed that statistical structure is encapsulated in a known covariance matrix, $C(\boldsymbol{\varepsilon})$.

Let, s (a scalar), represent a model prediction of interest whose sensitivities to model parameters **p** is described by the vector, **y**. Then, for a linear model:

$$s = \mathbf{y}^T\mathbf{p}, \quad \text{(Eq. H-2)}$$

where the superscript T indicates the transpose. If the covariance matrix, $C(\mathbf{p})$, provides a stochastic description of innate parameter variability (taking account of the conditioning provided by direct or indirect measurements of hydraulic properties already available prior to the calibration process), then the variance σ_s^2 of the uncertainty associated with the model prediction, s, is:

$$\sigma_s^2 = \mathbf{y}^T C(\mathbf{p})\mathbf{y}. \quad \text{(Eq. H-3)}$$

Equation H-3 also characterizes the "error variance" of s. For an uncalibrated model, "uncertainty" and "error variance" are equivalent.

H8.2 OVER-DETERMINED PARAMETER ESTIMATION

Suppose that the system represented by **X** is a simple one, requiring only a few parameters for its characterization. Suppose further that these parameters are uniquely estimable on the basis of the calibration dataset comprising **h**. If measurement noise, **ε**, has a Gaussian distribution, then the best estimate, $\underline{\mathbf{p}}$, of the parameter set, **p**, can be computed using the equation:

$$\underline{\mathbf{p}} = \left(\mathbf{X}^T\mathbf{Q}\mathbf{X}\right)^{-1}\mathbf{X}^T\mathbf{Q}\mathbf{h}, \quad \text{(Eq. H-4)}$$

obtained by minimizing the following objective function:

$$\boldsymbol{\Phi} = (\mathbf{h} - \mathbf{X}\mathbf{p})^T\mathbf{Q}(\mathbf{h} - \mathbf{X}\mathbf{p}), \quad \text{(Eq. H-5)}$$

where **Q** is:

$$\mathbf{Q} = C^{-1}(\boldsymbol{\varepsilon}). \quad \text{(Eq. H-6)}$$

The prediction, as calculated by the calibrated model, is:

$$\underline{s} = \mathbf{y}^T\underline{\mathbf{p}}. \quad \text{(Eq. H-7)}$$

Model predictive error is thus:

$$s - \underline{s} = \mathbf{y}^T \left(\mathbf{p} - \underline{\mathbf{p}} \right) = \mathbf{y}^T \left[\mathbf{p} - \left(\mathbf{X}^T \mathbf{Q} \mathbf{X} \right)^{-1} \mathbf{X}^T \mathbf{Q} \mathbf{h} \right]. \quad \text{(Eq. H-8)}$$

Substituting Equation H-1 for **h** into Equation H-8 yields:

$$s - \underline{s} = -\mathbf{y}^T \left(\mathbf{X}^T \mathbf{Q} \mathbf{X} \right)^{-1} \mathbf{X}^T \mathbf{Q} \boldsymbol{\varepsilon}, \quad \text{(Eq. H-9)}$$

the variance of which is [recalling Equation H-6]:

$$\sigma^2_{s-\underline{s}} = \mathbf{y}^T \left(\mathbf{X}^T \mathbf{Q} \mathbf{X} \right)^{-1} \mathbf{y}. \quad \text{(Eq. H-10)}$$

In this case too, predictive error and predictive uncertainty are equivalent. Equation H-10 proves that the stochastic distribution of model predictive error (as encapsulated in its variance, $\sigma^2_{s-\underline{s}}$) is ultimately calculable from the stochastic distribution of measurement noise as encapsulated in **Q** through Equation H-6.

H8.3 UNDER-DETERMINED PARAMETER ESTIMATION

Suppose that the $\mathbf{X}^T\mathbf{Q}\mathbf{X}$ matrix of equation 4 cannot be inverted, or that it is so ill-conditioned that estimates of predictive error variance calculated using Equation H-10 exceed those calculated using Equation H -3. In the former case a generalized inverse of $\mathbf{X}^T\mathbf{Q}\mathbf{X}$ may be used in Equation H-4 to minimize **Φ** of Equation H-5. Thus:

$$\mathbf{p} = \left(\mathbf{X}^T \mathbf{Q} \mathbf{X} \right)^{-} \mathbf{X}^T \mathbf{Q} \mathbf{h}, \quad \text{(Eq. H-11)}$$

where the "–" rather than "−1" suffix indicates the generalized rather than unique matrix inverse. Because a rank-deficient matrix possesses an infinite number of generalized inverses, it is no longer possible to obtain a unique solution to the inverse problem solely through minimization of **Φ** (thus maximizing model-to-measurement goodness of fit). In fact, in most cases it is not appropriate to minimize this function at all because this will probably result in greater predictive error variance than that calculated using Equation H-3. Hence, definition of a set of "calibrated parameters," **p**, is a more difficult process and it must be undertaken carefully to avoid excessive transferal of measurement noise to the estimated parameter field (and to predictions that depend on it). In fact, as stated in the body of this document, the set of parameters, **p**, that should ideally be selected as the "calibrated parameter set" is that which minimizes the potential error of key model predictions. This will probably differ from the parameter set calculated through Equation H-11, because that parameter set allows a sufficient fit between model outputs and field data. This fit has as much information as possible extracted from calibration dataset, but it is not "over fitted" where estimated parameters and model predictions are not unduly contaminated by measurement noise. Moore and Doherty (2005 [DIRS 178402]) demonstrate how such a parameter set can be calculated.

In general, a calibrated parameter set, **p**, is computed from field measurements, **h**, as:

$$\underline{\mathbf{p}} = \mathbf{G}\mathbf{h}. \quad \text{(Eq. H-12)}$$

The nature of the matrix, **G**, depends on the type of regularization used during model calibration. Use of Tikhonov regularization yields:

$$\mathbf{G} = \left(\mathbf{X}^T\mathbf{Q}\mathbf{X} + \beta^2\mathbf{Z}^T\mathbf{R}\mathbf{Z}\right)^{-1}\mathbf{X}^T\mathbf{Q}, \quad \text{(Eq. H-13)}$$

where **Z** is a matrix of "regularization constraints" on parameter values which collectively stipulate a "preferred parameter condition." **R** is a suitable "regularization weight matrix." The "regularization weight factor," β^2, is calculated during the calibration process as that which leads to a user-specified level of model-to-measurement fit when the calibrated parameter field, **p**, is employed by the model.

When singular value decomposition is used, **G** is given by:

$$\mathbf{G} = \left(\mathbf{V}_1\mathbf{E}_1^{-1}\mathbf{V}^T\right)\mathbf{X}^T\mathbf{Q}, \quad \text{(Eq. H-14)}$$

where $\mathbf{V}_1$ is an orthogonal matrix whose columns are the eigenvectors of the $\mathbf{X}^T\mathbf{Q}\mathbf{X}$ matrix which span the calibration solution space and $\mathbf{E}_1$ is a diagonal matrix whose elements comprise corresponding eigenvalues of $\mathbf{X}^T\mathbf{Q}\mathbf{X}$. The calibration null space is spanned by vectors comprising the columns of another orthogonal matrix $\mathbf{V}_2$ (which is also orthogonal to $\mathbf{V}_1$). Eigenvalues of $\mathbf{X}^T\mathbf{Q}\mathbf{X}$ associated with the $\mathbf{V}_1$ eigenvectors are higher than those associated with the $\mathbf{V}_2$ eigenvectors (many of which can be zero). Ideally, the cutoff point between the two is selected by the user as that for which predictive error variance is reduced to a minimum. Alternatively, it is selected on the basis that model-to-measurement misfit is commensurate with measurement noise.

For hybrid regularization schemes that combine Tikhonov and subspace methods, the equations for **G** are slightly more complex; the reader is referred to *Addendum to the PEST Manual* (Doherty 2006 [DIRS 178613]) for details.

H8.4 MODEL PREDICTIVE ERROR ANALYSIS

Substitution of Equation H-1 into Equation H-12 yields:

$$\mathbf{p} = \mathbf{G}\mathbf{X}\mathbf{p} + \mathbf{G}\boldsymbol{\varepsilon} = \mathbf{R}\mathbf{p} + \mathbf{G}\boldsymbol{\varepsilon}, \quad \text{(Eq. H-15)}$$

where **R** in Equation H-15 is often referred to as the "resolution matrix." If no measurement noise accompanies the calibration dataset, the elements of each row of this matrix represent "averaging weights" through which the individual estimated parameters comprising the elements of **p** are computed from their real-world counterparts comprising the elements of **p**. A "perfect" resolution matrix would be the identity matrix, **I**, because then all model parameters would be equal to the real-world hydraulic properties that they represent. However, where calibration is under-determined, **R** is rank-deficient (a reflection of the fact that the inverse problem of model

calibration is ill-posed), and hence cannot be the identity matrix. The best that can be hoped for is that its diagonal elements dominate other row elements, thereby ensuring that each estimated parameter is more reflective of its real-world counterpart than it is of other model parameters. Unfortunately, off-diagonal elements are often high when calibrating real-world models against real-world datasets. Recall that a calibrated parameter assigned to a point or to an area of limited spatial extent within the domain of a calibrated model is actually a spatial integration of real-world hydraulic properties over a much larger area. Furthermore, this averaging process will often cross parameter boundaries where more than one type of parameter comprises **p**. The averaging process described by the resolution matrix, **R**, is responsible for smoothing of parameter fields assigned to a calibrated model during the regularized inversion process. As discussed previously, parameter simplification through spatial integration of heterogeneous real-world hydraulic properties is also partly responsible for model predictive error. Unfortunately, however, it is an unavoidable consequence of the quest for uniqueness in the calibrated model.

On the basis of Equation H-15, parameter error is described by:

$$\mathbf{p} - \underline{\mathbf{p}} = (\mathbf{I} - \mathbf{R})\mathbf{p} - \mathbf{G}\boldsymbol{\varepsilon}. \qquad \text{(Eq. H-16)}$$

Predictive error is then given by:

$$s - \underline{s} = \mathbf{y}^T(\mathbf{p} - \underline{\mathbf{p}}) = \mathbf{y}^T(\mathbf{I} - \mathbf{R})\mathbf{p} - \mathbf{y}^T\mathbf{G}\boldsymbol{\varepsilon}. \qquad \text{(Eq. H-17)}$$

Because **p** and **ε** are never known (only $\underline{\mathbf{p}}$, **R**, and **G** are known), model predictive error cannot be known. However, if $C(\mathbf{p})$ and $C(\boldsymbol{\varepsilon})$ are known (or guessed), model predictive error variance can be computed using the equation:

$$\sigma^2_{s-\underline{s}} = \mathbf{y}^T(\mathbf{I} - \mathbf{R})C(\mathbf{p})(\mathbf{I} - \mathbf{R})^T\mathbf{y} + \mathbf{y}^T\mathbf{G}C(\boldsymbol{\varepsilon})\mathbf{G}^T\mathbf{y}. \qquad \text{(Eq. H-18)}$$

Equation H-18 forms the basis of linear model predictive error variance analysis. It is apparent that model predictive error is dependent not just on one, but on two stochastic distributions, viz. $C(\boldsymbol{\varepsilon})$, which characterizes measurement noise, and $C(\mathbf{p})$, which characterizes real-world hydraulic property variability. Thus, there are two contributors to model predictive error that arise from 1) differences between hydraulic properties represented in the calibrated model and those that exist in reality, and 2) the fact that parameter estimation takes place on the basis of a dataset contaminated by measurement noise. The first term of Equation H-18 represents the contribution to model predictive error variance made by the calibration null space (anecdotally, this is often the dominant contributor to predictive error), while the second constitutes the contribution to predictive error variance made by the calibration solution space. Note that, as is obvious from Equation H-10, the first term is ignored in traditional model calibration and predictive error analysis.

It is important to note that *a priori* simplification of parameters employed by a model of a complex system, undertaken to formulate an over-determined inverse problem, does not eliminate the first term of Equation H-18 (Moore and Doherty 2006 [DIRS 178403]). Such a process is indeed a form of regularization and, as such, can be ascribed a resolution matrix (normally a less-than-optimal resolution matrix). Strictly speaking, Equation H-10 can only be

used for computation of predictive error variance at study sites where the earth is as simple as the model or when a correction is made to the computed predictive error variance to accommodate a priori regularization undertaken in this manner (Cooley 2004 [DIRS 178650]; Cooley and Christensen 2006 [DIRS 178598]). However, while such a strategy can indeed accommodate the contribution made to potential model predictive error due to parsimonized reality (thus satisfying the second of the precepts outlined in Section H.3), it does not necessarily result in minimization of that potential error (thus violating the first of these precepts).

H8.5 MODEL PREDICTIVE UNCERTAINTY ANALYSIS

Equation Equation H-18 allows computation of "potential model predictive wrongness," that is, the variance of $s - \underline{s}$. Model predictive uncertainty is a slightly different concept, requiring a Bayesian approach for its computation.

Combining Equations H-1 and H-2 into a single equation yields:

$$\begin{bmatrix} s \\ \mathbf{h} \end{bmatrix} = \begin{bmatrix} \mathbf{y}^T & \mathbf{0} \\ \mathbf{X} & \mathbf{I} \end{bmatrix} \begin{bmatrix} \mathbf{p} \\ \boldsymbol{\varepsilon} \end{bmatrix}. \quad \text{(Eq. H-19)}$$

Using standard matrix relationships for propagation of covariance:

$$\begin{aligned} C\left(\begin{bmatrix} s \\ \mathbf{h} \end{bmatrix}\right) &= \begin{bmatrix} \mathbf{y}^T & \mathbf{0} \\ \mathbf{X} & \mathbf{I} \end{bmatrix} \begin{bmatrix} C(\mathbf{p}) & \mathbf{0} \\ \mathbf{0} & C(\boldsymbol{\varepsilon}) \end{bmatrix} \begin{bmatrix} \mathbf{y} & \mathbf{X}^T \\ \mathbf{0} & \mathbf{I} \end{bmatrix} \\ &= \begin{bmatrix} \mathbf{y}^T C(\mathbf{p}) \mathbf{y} & \mathbf{y} C(\mathbf{p}) \mathbf{y}^T \\ \mathbf{X} C(\mathbf{p}) \mathbf{y} & \mathbf{X} C(\mathbf{p}) \mathbf{X}^T + C(\boldsymbol{\varepsilon}) \end{bmatrix}. \end{aligned} \quad \text{(Eq. H-20)}$$

Now suppose that an arbitrary vector $\mathbf{x}$ is partitioned into two separate vectors $\mathbf{x}_1$ and $\mathbf{x}_2$. That is:

$$\mathbf{x} = \begin{bmatrix} \mathbf{x}_1 \\ \mathbf{x}_2 \end{bmatrix}. \quad \text{(Eq. H-21)}$$

Let $C(\mathbf{x})$, the covariance matrix of $\mathbf{x}$, be correspondingly partitioned as:

$$C(\mathbf{x}) = \begin{bmatrix} \mathbf{C}_{11} & \mathbf{C}_{12} \\ \mathbf{C}_{21} & \mathbf{C}_{22} \end{bmatrix}. \quad \text{(Eq. H-22)}$$

Suppose further that the elements of $\mathbf{x}_2$ are known. Then, if there is correlation between at least some members of $\mathbf{x}_2$ and some members of $\mathbf{x}_1$ (this resulting in non-null $\mathbf{C}_{12}$ and $\mathbf{C}_{21}$ submatrices), the conditioned $\mathbf{C}_{11}$ matrix $\mathbf{C}'_{11}$ is calculable as:

$$\mathbf{C}'_{11} = \mathbf{C}_{12} - \mathbf{C}_{12}\mathbf{C}_{22}^{-1}\mathbf{C}_{21}, \quad \text{(Eq. H-23)}$$

provided **x** has a multi-Gaussian probability distribution. Applying this to Equation H-20, the conditional variance of the prediction *s* given the acquisition of calibration data, **h**, is:

$$\sigma_s^2 = \mathbf{y}^T C(\mathbf{p})\mathbf{y} - \mathbf{y}^T C(\mathbf{p})\mathbf{X}^T \left[\mathbf{X}C(\mathbf{p})\mathbf{X}^T + C(\boldsymbol{\varepsilon})\right]^{-1} \mathbf{X}C(\mathbf{p})\mathbf{y}. \qquad \text{(Eq. H-24)}$$

σ_s^2 of Equation H-24 is the variance of uncertainty of the prediction, *s*. Using methodologies such as those described by Kitanidis (1996 [DIRS 178599]), calibration can be undertaken in such a manner that σ_s^2 and $\sigma_{s-\underline{s}}^2$ are equal (thus ensuring that $\underline{s}$ provides us with a minimum error variance prediction of system behavior). In practice, if regularized inversion is properly undertaken, the difference between σ_s^2 and $\sigma_{s-\underline{s}}^2$ is normally small. Furthermore, where parameter and calibration datasets are large, regularized inversion based on the methods briefly outlined above, are made unconditionally numerically stable and computationally inexpensive, no matter how ill-posed the inverse problem is.

Versions of PEST from 11.1 onwards provide utility software to compute both model predictive error variance and model predictive uncertainty based on Equations H-18 and H-24, respectively.

INTENTIONALLY LEFT BLANK

APPENDIX I
PREDICTIVE ERROR ANALYSIS THROUGH CONSTRAINED PREDICTION MAXIMIZATION/MINIMIZATION

I1 THEORY – OVER DETERMINED CASE

Vecchia and Cooley (1987 [DIRS 178577]) present a method for exploration of the confidence interval of a prediction made by a calibrated model, which accommodates the fact that the relationships between model outputs and parameters may not be linear. The methodology is based on a constrained optimization technique. The prediction of interest is maximized or minimized while parameters are constrained such that the model remains in a calibrated state at a certain confidence level. This confidence level is then equated to the confidence level of the prediction. Confidence is assessed in terms of the rise in the objective function that is incurred through maximizing or minimizing the prediction (and thereby incurring alterations to parameter values such that they no longer minimize that function). The relationship between objective function rise and parameter/predictive confidence interval is assessed in terms of the stochastic distribution that is assumed to pertain to measurement noise, together with a multiplier for this distribution (the so-called "reference variance") that is estimated through the calibration process.

Figure I-1 shows this process schematically. The dashed lines show contours of a prediction as a function of two parameters; let it be supposed that the value of the prediction increases to the upper right of this figure. The full line is a single contour of the objective function. The minimum of this objective function (which defines the values of parameters which calibrate the model) is within this contour. The contour itself defines the value of the objective function at which the model is no longer calibrated at a certain confidence level. The "critical points" A and B define locations in parameter space (and hence parameter values) at which the prediction of interest is minimized and maximized respectively at the same confidence level as that which applies to the contour. The difference between the corresponding model predictions defines the confidence interval of the prediction.

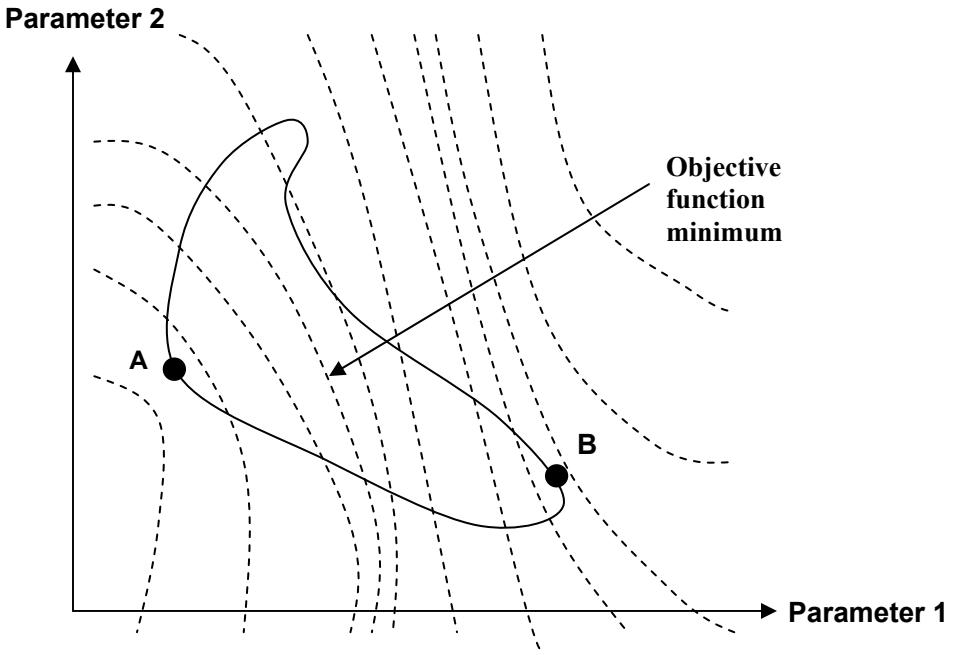

Figure I-1. Points in Parameter Space Corresponding to Maximum/Minimum Values of a Prediction at a Certain Confidence Level

Let δ refer to the difference between the objective function at the contour depicted in Figure I-1 and the minimized objective function. At a confidence level of 1 – α, δ is given by:

$$\delta = m\sigma_r^2 F_\alpha (m, n-m), \quad \text{(Eq. I-25)}$$

where $F(.,.)$ signifies an F distribution, n is the number of observations comprising the calibration dataset and m is the number of parameters being estimated. The reference variance σ_r^2 is given by:

$$\sigma_r^2 = \frac{\Phi_{\min}}{n-m}, \quad \text{(Eq. I-26)}$$

where $\Phi_{\min}$ is the minimized objective function as achieved through the calibration process. The objective function is defined as the sum of weighted squared differences between model outputs and field measurements. Derivation of Equation I-1 assumes that n is reasonably large.

For a linear model, the constrained maximization/minimization problem through which the points A and B of Figure I-1 must be obtained can be formulated as follows.

Find a parameter set **p** such as to maximize (minimize) $\mathbf{y}^T\mathbf{p}$ subject to:

$$(\mathbf{h} - \mathbf{X}\mathbf{p})^T \mathbf{Q} (\mathbf{h} - \mathbf{X}\mathbf{p}) = \Phi_0, \quad \text{(Eq. I-27)}$$

where

$$\Phi_0 = \Phi_{\min} + \delta. \quad \text{(Eq. I-28)}$$

In Equation I-3, **X** is the matrix representing the relationship between model outputs, **h**, and parameters, **p**, under calibration conditions, **y** encapsulates the sensitivity of a prediction s to the parameters **p**, and **Q** is the observation weight matrix, which is assumed to be inversely proportional to the measurement noise covariance matrix C(**ε**). Φ_0 is the objective function pertaining to a certain level of confidence as described by Equation I-1.

It can be shown that the solution to this problem is given by:

$$\mathbf{p} = \left(\mathbf{X}^T\mathbf{Q}\mathbf{X}\right)^{-1}\left(\mathbf{X}^T\mathbf{Q}\mathbf{h} - \frac{\mathbf{y}}{2\lambda}\right), \quad \text{(Eq. I-29)}$$

where λ is defined by:

$$\left(\frac{1}{2\lambda}\right)^2 = \frac{\Phi_0 - \mathbf{h}^T\mathbf{Q}\mathbf{h} + \mathbf{h}^T\mathbf{Q}\mathbf{X}\left(\mathbf{X}^T\mathbf{Q}\mathbf{X}\right)^{-1}\mathbf{X}^T\mathbf{Q}\mathbf{h}}{\mathbf{y}^T\left(\mathbf{X}^T\mathbf{Q}\mathbf{X}\right)^{-1}\mathbf{y}}. \quad \text{(Eq. I-30)}$$

Note that solution of the calibration problem through which parameters corresponding to Φ_{min} are computed, is achieved through an equation of somewhat similar form to Equation I-5, viz.:

$$\mathbf{p} = \left(\mathbf{X}^T\mathbf{Q}\mathbf{X}\right)^{-1}\mathbf{X}^T\mathbf{Q}\mathbf{h}. \quad \text{(Eq. I-31)}$$

When predictive analysis is carried out for a nonlinear model, the same equations are used. However in this case, **X** is replaced by the model Jacobian matrix, **J**, and a parameter upgrade vector is calculated instead of a solution vector. The solution process is then an iterative one in which the true solution is approached by repeated calculation of an upgrade vector based on repeated linearization of the problem through determination of a Jacobian matrix that is updated every iteration. For further details see Vecchia and Cooley (1987 [DIRS 178577]).

I2 UNDER-DETERMINED CASE

Use of the above theory assumes that the inverse problem of model calibration is unique; that is, it assumes that all contours about the minimum of the objective function are closed. Unfortunately, this is not the case for the SZ flow model, where the same objective function can be obtained using many different sets of parameters.

Fortunately, as Doherty (2006 [DIRS 178613]) and Moore (2006 [DIRS 178788]) show, the theory can be extended to the case of under-determined parameter estimation without too much difficulty.

For underdetermined parameter estimation there is no unique solution to Equation I-7. Hence, some form of regularisation must be introduced to the inverse problem. This often takes the form of a subspace method such as truncated singular value decomposition, or a Tikhonov method in which an optimal parameter set is defined as that which departs minimally from a preferred parameter condition. In either case, an optimised parameter set $\underline{\mathbf{p}}$ is computed as:

$$\underline{\mathbf{p}} = \mathbf{G}\mathbf{h}. \quad \text{(Eq. I-32)}$$

Now if the action of the model can be replaced by its linear matrix approximation, **X**, then (assuming zero offsets for simplicity):

$$\mathbf{h} = \mathbf{X}\mathbf{p} + \boldsymbol{\varepsilon}, \quad \text{(Eq. I-33)}$$

where **p** in Equation I-9 signifies the set of "real" system parameter values (can never be known), and **h** is, once again, the calibration dataset.

Thus:

$$\underline{\mathbf{p}} = \mathbf{R}\mathbf{p} + \mathbf{G}\boldsymbol{\varepsilon}, \quad \text{(Eq. I-34)}$$

where **R** is the "resolution matrix." Where noise is zero or minimal, each row of this matrix represents averaging weights through which calibrated parameter values contained in $\underline{\mathbf{p}}$ are obtained as functions of real parameter values contained in **p**. For under-determined inversion, **R** is always a rank-diminished matrix. Its null space defines the subspace of parameter space

from which any parameter realisation can be added or subtracted from the true set of parameters **p**, and that will still result in the same calibrated parameter set **p**. This space spans the "details that fit between the cracks" of the calibration process – these being parameter combinations that it is impossible to infer on the basis of the calibration dataset.

To the extent that a prediction of interest depends on parameter combinations occupying the "calibration solution space" (the orthogonal compliment to the calibration null space), constraints on this prediction are enforced by the fact that the model must remain calibrated. In fact, if a prediction depends only on these parameter combinations, then the above theory for over-determined predictive confidence interval determination could be employed subsequent to parameter reformulated as linear combinations of native model parameters lying entirely within the calibration solution space. Though some account would need to be taken of the fact that any kind of parsimonizing (including the projection of parameters onto the calibration solution space) incurs some degree of structural noise (see, for example, Moore and Doherty 2006 [DIRS 178403]), this could be simply accommodated by appropriate redefinition of measurement weights encapsulated in the **Q** matrix as proportional to the inverse covariance matrix of this noise as shown by Cooley (2004 [DIRS 178650]).

If a prediction is at least partially sensitive to linear combinations of parameters which occupy the calibration null space, the problem becomes a little more difficult, for separate constraints must be employed on these null space parameter combinations as a prediction is maximized or minimized. Suppose that singular value decomposition of the resolution matrix **R** yields:

$$\mathbf{R} = \mathbf{U}\mathbf{S}\mathbf{V}^T. \qquad \text{(Eq. I-35)}$$

Suppose also that the orthogonal matrix, **V**, can be represented as:

$$\mathbf{V} = [\mathbf{V}_1\ \mathbf{V}_2], \qquad \text{(Eq. I-36)}$$

where the columns of $\mathbf{V}_2$ represent orthogonal axes spanning the calibration null space, this corresponding to zero and near-zero values of the diagonal singular value matrix **S**. Define:

$$\begin{aligned} \mathbf{p}_1 &= \mathbf{V}_1\mathbf{V}_1^T\mathbf{p}, \\ \mathbf{p}_2 &= \mathbf{V}_2\mathbf{V}_2^T\mathbf{p}. \end{aligned} \qquad \text{(Eq. I-37)}$$

Then $\mathbf{p}_2$ represents the projection of the (unknown) real-world parameters **p** onto the calibration null space while $\mathbf{p}_1$ represents the projections of these same parameters onto the calibration solution space.

As a prediction is either maximized or minimized to determine its confidence interval, constraints on $\mathbf{p}_1$ are exerted through the necessity for the model to remain calibrated, just as for over-determined parameter estimation. Constraints on $\mathbf{p}_2$ however must be exerted in other ways, for these have no effect on the calibrated status of the model. Constraints on these parameters must, in fact, be "reality constraints;" that is, the parameters must remain realistic at a certain level of confidence. This level of confidence must be assessed in terms of their assumed probability distribution.

Let C(**p**) be a covariance matrix which describes the stochastic character of parameters represented in a model. Diagonal elements of this matrix describe the innate variability of individual parameters; off-diagonal elements described spatial parameter correlation. Based on $\mathbf{p}_2$ in Equation I-13, the stochastic nature of $\mathbf{p}_2$ projections onto the calibration null space can then be described by:

$$\mathrm{C}(\mathbf{p}_2) = \mathbf{V}_2\mathbf{V}_2^T\mathrm{C}(\mathbf{p})\mathbf{V}_2\mathbf{V}_2^T. \qquad \text{(Eq. I-38)}$$

The maximization/minimisation problem through which predictive confidence limits in the over-determined case are computed can now be formulated as follows.

Find a parameter set **p** such as to maximize (minimize) $\mathbf{y}^T\mathbf{p}$ Equation I-14 subject to:

$$(\mathbf{h}-\mathbf{X}\mathbf{p})^T\mathbf{Q}(\mathbf{h}-\mathbf{X}\mathbf{p}) + \mathbf{p}^T\mathbf{V}_2\mathbf{V}_2^T\mathbf{C}_2^{-1}(\mathbf{p})\mathbf{V}_2\mathbf{V}_2^T\mathbf{p} = \Phi_{\mathbf{0}}, \qquad \text{(Eq. I-39)}$$

where Φ_0 is chosen on the basis of a desired level of confidence. The objective function defined by Equation I-15 includes both of the above-mentioned constraints on parameter values, viz. those on calibration solution space projections enforced by the necessity for the model to remain calibrated (the first term), and those on calibration null space parameter projections, enforced by the necessity for parameters to remain realistic (the second term). With definition of this new objective function, maximization/minimization of the prediction *s* can be implemented using the same maximization/minimization algorithm as that described above.

In practice, it is better to work with parameter and model output differences than native parameter values when implementing the above procedure. Thus, **p** now represents differences between parameters obtained through the maximization/minimization process and those which are assumed to calibrate the model in Equation I-8. The objective function under calibration conditions with this new formulation is thus zero. If measurement noise and parameters are assumed to be describable by multi-Gaussian stochastic distributions, and if **Q** is formulated $\mathrm{C}^{-1}(\boldsymbol{\varepsilon})$ (where C(**ε**) is the covariance matrix of measurement noise), values for Φ_0 at different confidence levels are expressible as the square of normal deviates. For example, setting Φ_0 to 4 (square of 2) and maximizing and then minimizing the prediction *s*, results in definition of the 95.4% confidence interval for that prediction.

Approximations employed in this approach include the following:

1. Measurement noise is assumed to be represented by a user-supplied C(**ε**) covariance matrix. In practice most "measurement noise" is actually structural noise. Furthermore, as stated above, some of this structural noise is regularisation-induced. The latter can be computed (using, for example, paired stochastic model runs as described by Cooley (2004 [DIRS 178650]) and accommodated through appropriate definition of **Q**. However, if there are many parameters involved in the parameter estimation process, and if the fit between model outputs and field measurements is reasonably good, it may be possible to ignore the structural component of this term. In the case of the Yucca Mountain model this will probably not be the case. (It must be said, however, that the structural noise term is universally ignored elsewhere, in both general and academic groundwater modelling practice.)

2. The magnitude of structural noise associated with the calibration dataset (whether this be parsimonization-induced or a result of other model inadequacies) is normally assessed through the calibration process using a "reference variance" term. However, the estimation of this quantity has uncertainty associated with it. It is shown in most textbooks on parameter estimation that, even if measurement noise possesses a Gaussian distribution, parameter and predictive probabilities acquire a Student-t distribution for their characterization because of this. This will apply to the first term of Equation I-15 but not the second. Thus, use of the square of a normal variate for the total objective function as a means of assessing confidence will be somewhat in error.

QA: QA

Model
Administrative Change Notice

Complete only applicable items.

1. Document Number:	MDL-NBS-HS-000011	2. Revision:	03	3. ACN:	01
4. Title:	Saturated Zone Site-Scale Flow Model				
5. No. of Pages Attached	99				

6. Approvals:

Preparer:	Scott James (Print name and sign)	9/27/07 (Date)
Checker:	Carl Axness (Print name and sign)	9/28/07 (Date)
QCS/Lead Lab QA Reviewer:	Robert E. Spencer (Print name and sign)	09/28/07 (Date)
Independent Technical Reviewer:	Ming Zhu (Print name and sign)	10/1/07 (Date)
Responsible Manager:	Stephanie Kuzio for Kenneth Rehfeldt (Print name and sign)	10/1/07 (Date)

7. Affected Pages	8. Description of Change:
p. ix	Updated TOC to reflect changes in reference section.
p. xxi	Added ASCII to acronyms list.
p. xxia	Page rollover from change to acronyms list.
p. 1-1	Updated DIRS number and title for the Saturated Zone Flow and Transport Model Abstraction from 177390 to 181650.
p. 1-2	Updated Figure 1-1.
p. 1-5	Added explanations for CRs 8758 and 10893.
p. 6-1, p. 6-1a	Updated the FEPs reference to MO0706SPAFEPLA.001 [DIRS 181613]).
p. 6-3	Deleted redundant sentence at the beginning of 2nd paragraph, replaced "when" with "whose" in last line of 2nd paragraph, and deleted reference citation to Figure 6-1 in the last paragraph..
p. 6-19	Updated the reference from Table 6-5 to (SNL 2007 [DIRS 174109], Table 6-3)
p. 6-20	Updated DIRS number for the Saturated Zone Flow and Transport Model Abstraction from 177390 to 181650 and also called out sections specific to the Addendum.
p. 6-21	Corrected typo from "that" to "than"
p. 6-23	Updated DIRS number for the Saturated Zone Flow and Transport Model Abstraction from 177390 to 181650 and also the section specific to the Addendum.
p. 6-26	Updated DIRS number for the Saturated Zone Flow and Transport Model Abstraction from 177390 to 181650 and also the section specific to the Addendum.
p. 6-29	Updated DIRS number for the Saturated Zone Flow and Transport Model Abstraction from 177390 to 181650 and also the section specific to the Addendum.
p. 6-39	Changed "nodes" to "tetrahedral elements" and "as shown" with "which becomes evident"
p. 6-40	Changed m to superscript m^3 in Table 6-5.

Model
Administrative Change Notice

Complete only applicable items.

1. Document Number:	MDL-NBS-HS-000011	2. Revision:	03	3. ACN:	01
4. Title:	Saturated Zone Site-Scale Flow Model				

p. 6-42	Elevations added to Figure 6-10 per DOE comment and removed x-axis label.
p. 6-43	Replaced “Top” from Table 6-6, column three title with “Land”.
p. 6-44	Deleted “surface and below.”
p. 6-45	Updated DIRS number for the Saturated Zone Flow and Transport Model Abstraction from 177390 to 181650.
p. 6-47	Removed phrase, “with geometry described in Table 6-7” in last paragraph.
p. 6-48	Update Figure 6-12 caption to read “Altered Northern Region.”
p. 6-56	Replaced “Watermark Computing” with “STN: 10289-5.5-00.”
p. 6-66	Changed “zone” to “zones.”
p. 6-68	Corrected reference from Table 6-8 to Table 6-10.
p. 6-70	Changed “780-m to 730-m” to “780 to 730-m (~50-m).”
p. 6-75	Changed distance to 4,073,761 and made slight modification as follows “approximately 5 km south of the midpoint of the repository.”
p. 6-75	Deleted the sentence starting with “Mass balance….”
p. 6-77	Updated DIRS number for the Saturated Zone Flow and Transport Model Abstraction from 177390 to 181650 and also the portion specific to the addendum.
p. 6-83	Changed “will results” to “results.”
p. 6-93	Updated DIRS number for the Saturated Zone Flow and Transport Model Abstraction from 177390 to 181650 and also the portion specific to the addendum.
p. 6-93	Removed an extraneous semicolon.
p. 6-93	Added STN and PEST reference as follows “STN: 10289-5.5-00; [DIRS 161564], Watermark Numerical Computing 2004 [DIRS 178612]”
p. 6-96	Updated DIRS number for the Saturated Zone Flow and Transport Model Abstraction from 177390 to 181650 and also the portion specific to the Addendum.
p. 6-96	Corrected reference from “Watermark Computing” to “Doherty.”
p. 6-98	Corrected typo from “is” to “in.”
p. 6-99	Inserted “is” before “50-m” in the third paragraph.
p. 6-100	Updated DIRS number for the Saturated Zone Flow and Transport Model Abstraction from 177390 to 181650 and also the portion specific to the addendum.
p. 6-101	Updated DIRS number for the Saturated Zone Flow and Transport Model Abstraction from 177390 to 181650 and also the portion specific to the addendum.
p. 6-101	Reorganized sentence to improve readability.
p. 7-7	Corrected typo from “that” to “than.”
p. 7-12	Deleted extraneous “to”
p. 7-14	Changed "... percolation through..." with "... infiltrating into..."
p. 7-14	Changed “average” to “range” and updated numbers
p. 7-14	Replaced obsolete Flint reference with that of SNL 2007 to reflect the latest understanding of infiltration.
p. 7-14	Replaced the second Flint reference with a qualified DTN.
p. 7-16	Deleted extraneous Flint reference.

Model
Administrative Change Notice

Complete only applicable items.

1. Document Number:	MDL-NBS-HS-000011	**2. Revision**:	03	**3. ACN**:	01
4. Title:	Saturated Zone Site-Scale Flow Model				

p. 7-32	Updated sentence to improve readability as follows: "Specific discharge across the 18-km compliance boundary (see the green line on Figure 6-17) and discussed throughout other documents (SNL 2007 [DIRS 177392]) is…."
p. 7-34	Updated DIRS number for the Saturated Zone Flow and Transport Model Abstraction from 177390 to 181650 and also the portion specific to the addendum.
p. 7-34	Corrected typo from "theses" to "these."
p. 8-5	Updated DIRS number for the Saturated Zone Flow and Transport Model Abstraction from 177390 to 181650 and also the portion specific to the addendum.
p. 8-6	Updated DIRS number for the Saturated Zone Flow and Transport Model Abstraction from 177390 to 181650 and also the portion specific to the addendum.
p. 8-7	Updated DIRS number for the Saturated Zone Flow and Transport Model Abstraction from 177390 to 181650 and also the portion specific to the addendum.
p. 8-7	Uncapitalized "recharge" and "discharge"
p. 8-11	Updated DIRS number for the Saturated Zone Flow and Transport Model Abstraction from 177390 to 181650. Changed "hydrologic" to "hydrogeologic" in the first sentence of the second paragraph.
pp. 9-1 to 9-36	Rebuilt references section to address the condition identified in CR 10893.
p. A-59	Deleted unnecessary reference to BSC 2004.
p. A-215	Typo in DIRS 170008 changed to 170009.
p. A-218	Corrected "east" to "west" in second paragraph – "Flow Path 8 illustrates leakage to the west across the hydrologic boundary…"
p. A-220	Changes in spacing made (no space between number and %) and non-breaking space added.
p. A-222	Non-breaking space removed.
p. A-224	Typo in DIRS 170008 changed to 170009.
p. B-44	Corrected "eastward" to "westward" in fifth paragraph – "…and an additional arrow indicating westward flow of Flow Path 8 was added."
p. E-1	Minor typos like spacing (or addition of a non-breaking space) corrected.
p. E-2	Minor typos like spacing (or addition of a non-breaking space) corrected.
p. E-3	Minor typos like spacing (or addition of a non-breaking space) corrected.
p. F-1	Added "e" to "Plan."
p. H-1	Corrected date from 2003 to 2002.
p. I-1, I-1a	Added an introductory paragraph.
p. I-3	Corrected date from 2006 to 2005.
p. I-6	Italicized "t."
p. I-6	Added comma after Equation I-15
p. I-6	Added a concluding paragraph.

CONTENTS (Continued)

Page

ACRONYMS AND ABBREVIATIONS

ACC	accession number
ACM	alternative conceptual model
ASCII	American Standard Code for Information Interchange
AR	Amargosa River: group of boreholes located on the west side of Amargosa Desert
AR/FMW	Group of boreholes located near the confluence of the Amargosa River and Fortymile Wash drainages
ASCII	American Standard Code for Information Interchange
ATC	Alluvial Testing Complex
BSC	Bechtel SAIC Company, LLC
CFR	code of federal regulations
CF-SW	Crater Flat Southwest
CMB	chloride mass balance
CR	condition report
CRWW	Coffer Ranch Windmill Well
CVFE	control-volume finite element
DFGP	Desert Farms Garlic Plot
DIC	Dissolved inorganic carbon
DIRS	document reference system
DOC	dissolved organic carbon
DOE	Department of Energy
DOS	disk operating system
DTN	data tracking number
DVRFS	Death Valley Regional (ground water) Flow System
ESF	Exploratory Studies Facility
EWDP	Early Warning Drilling Program
FEHM	finite-element heat and mass transfer numerical analysis computer code
FEPs	features, events, and processes
FMW-E	Fortymile Wash-East: group of boreholes in the Amargosa Desert east of Fortymile Wash
FMW-N	Fortymile Wash-North: group of boreholes east and northeast of Yucca Mountain
FMW-S	Fortymile Wash-South: group of boreholes along or near the main channel of Fortymile Wash in Amargosa Desert
FMW-W	Fortymile Wash-West: group of boreholes in the Amargosa Desert west of Fortymile Wash
GF	Gravity Fault: group of boreholes located on east side of the Amargosa Desert
GSIS	geoscientific information system

HFM	hydrogeologic framework model
HFM2006	revised hydrogeologic framework model

1. PURPOSE

The purpose of this model report is to document revision of *Saturated Zone (SZ) Site-scale Flow Model* (BSC 2004 [DIRS 170037]) for Yucca Mountain, Nevada, in accordance with SCI-PRO-006, *Models*. This report provides validation and confidence in the flow model developed in support of the total system performance assessment (TSPA) for the license application (LA). The output from this report provides the flow model used in *Site-Scale Saturated Zone Transport Model*, (SNL 2007 [DIRS 177392]), which in turn provides output to the *Saturated Zone Flow and Transport Model Abstraction* (SNL 2007 [DIRS 181650]). In particular, the output from the SZ site-scale flow model is used by the SZ site-scale transport model to simulate the groundwater flow pathways and radionuclide transport to the accessible environment for use in *Saturated Zone Flow and Transport Model Abstraction* (SNL 2007 [DIRS 181650]), which feeds the TSPA calculations. Figure 1-1 shows the relationship of this report to other saturated zone reports that also pertain to SZ flow and transport. The figure also depicts the relationship between SZ models and analyses. It should be noted that Figure 1-1 does not contain a complete representation of the data and parameter inputs and outputs of all saturated zone reports, nor does it show inputs external to this suite of saturated zone reports.

Since the development, calibration, and validation of the SZ site-scale flow model (CRWMS M&O 2000 [DIRS 139582]), more data have been gathered and analyses have been completed. The data include new stratigraphic and water–level data from Nye County wells, single- and multiple-well hydraulic testing data (SNL 2007 [DIRS 177394]), and new hydrochemistry data (Appendix B). New analyses include the 2004 transient Death Valley Regional (ground water) Flow System (DVRFS) model (Belcher 2004 [DIRS 173179]), the creation of a new hydrogeologic framework model (HFM), called HFM2006 (SNL 2007 [DIRS 174109], DTN: MO0610MWDHFM06.002 [DIRS 179352]), and the 2003 unsaturated zone (UZ) flow model (BSC 2004 [DIRS 169861]). The new data and analyses were used to construct the SZ site-scale flow model presented in this report to support TSPA-LA. The intended use of this work is to provide a flow model that generates flow fields that are used to simulate radionuclide transport in saturated volcanic rock and alluvium under natural-gradient flow conditions. Simulations of water-table rise were also conducted for use in downstream transport and abstraction modeling. The SZ site-scale flow model simulations were completed using the three-dimensional, finite-element heat and mass transfer computer code, FEHM V2.24, STN: 10086-2.24-02 [DIRS 179539]. Concurrently, the process-level transport model and methodology for calculating radionuclide transport in the SZ at Yucca Mountain using FEHM are described in *Site-Scale Saturated Zone Transport* (SNL 2007 [DIRS 177392]). The velocity fields are calculated by the flow model, described herein, independent of the transport processes, and are then used as inputs to the transport model. Justification for this abstraction is presented in *Saturated Zone Flow and Transport Model Abstraction* (SNL 2007 [DIRS 181650]).

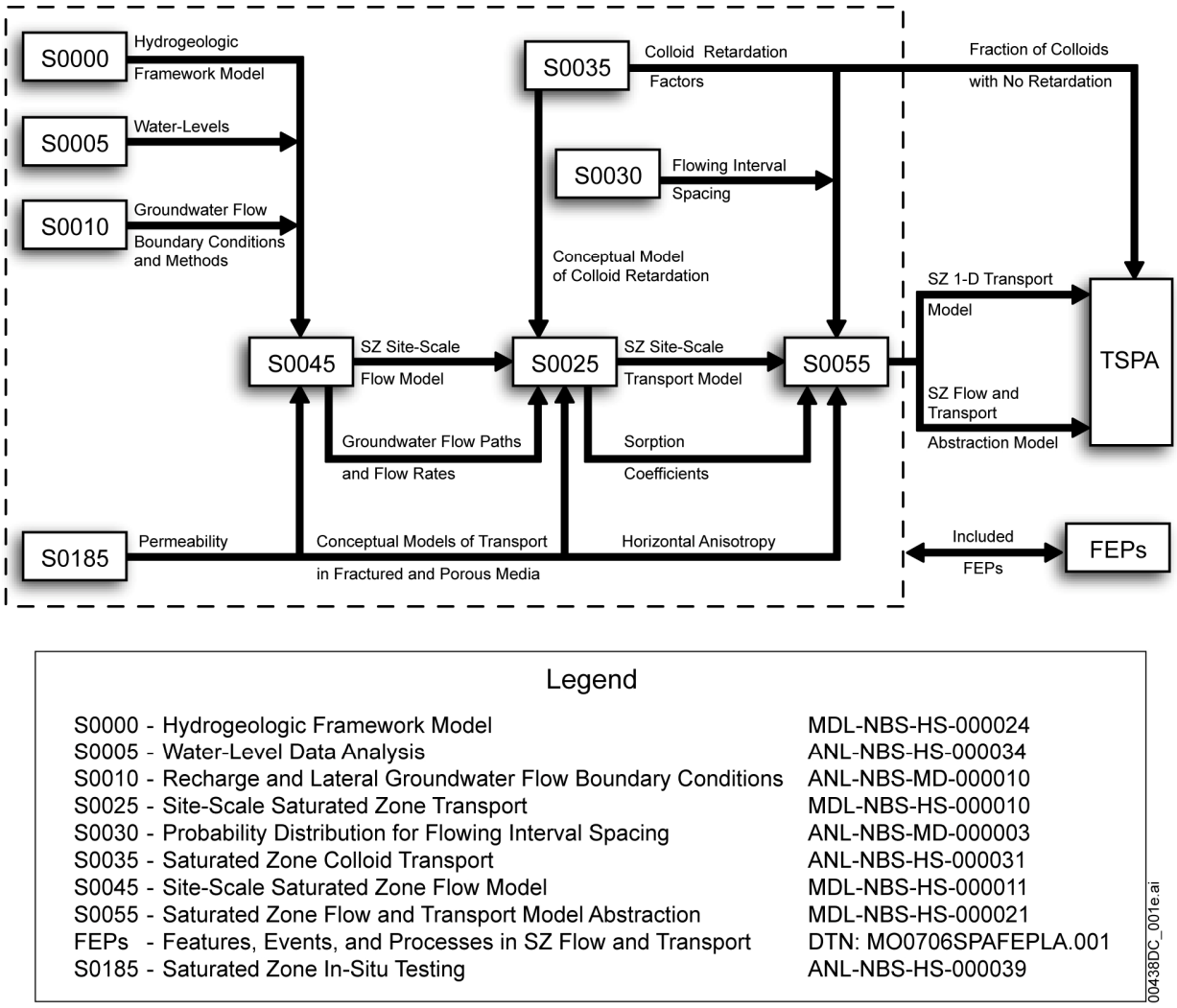

NOTE: This figure is a simplified representation of the flow of information among SZ reports. See the most recent revision of each report for a complete listing of data and parameter inputs. This figure does not show inputs external to this suite of SZ reports.

FEPs = features, events, and processes; SZ = saturated zone; TSPA = total system performance assessment.

Figure 1-1. Generalized Flow of Information among Reports Pertaining to Flow and Transport in the SZ

This model report is governed by *Technical Work Plan: Saturated Zone Flow and Transport Modeling* (BSC 2006 [DIRS 177375]). All activities listed in the technical work plan (TWP) that are appropriate to the SZ site-scale flow model are documented in this report. The TWP (BSC 2006 [DIRS 177375]) cites procedures that were in effect at the time the work described in this report was planned and approved. Following the transition of the science work scope from Bechtel SAIC Company, LLC (BSC) to Sandia National Laboratories (SNL), new procedures have been issued since October 2, 2006.

6. MODEL DISCUSSION

6.1 MODELING OBJECTIVES

The purpose of the SZ site-scale flow model is to describe the steady-state flow of groundwater as it moves from the water table below the repository, through the SZ, and to the accessible environment. The flow model estimates the SZ advective processes that control the movement of groundwater and dissolved radionuclides and colloidal particles that might be present.

The previous versions of the SZ site-scale flow model were developed in support of the TSPA-SR (CRWMS M&O 2000 [DIRS 153246]) and the TSPA-LA (BSC 2004 [DIRS 170037]). This model revision includes the following modifications to: (1) reflect the current understanding of SZ flow, (2) enhance model validation and uncertainty analyses, (3) improve locations and definitions of fault zones, (4) enhance grid resolution (500-m grid spacing to 250-m grid spacing), and (5) incorporate new data collected since the TSPA-SR:

- Implementation of the updated hydrogeologic framework model (HFM) that incorporates recent geologic data obtained from the Nye County Early Warning Drilling Program (DTN: MO0610MWDHFM06.002 [DIRS 179352]) and the 2004 DVRFS (Belcher 2004 [DIRS 173179])

- A potentiometric surface updated with water-level data from Phases III and IV of the NC-EWDP (Output DTN: MO0611SCALEFLW.000)

- Additional water-level calibration target data from Phases III and IV of the Nye County Early Warning Drilling Program (Output DTN: SN0702T0510106.007)

- Boundary volumetric/mass flow rates and recharge data from the 2004 DVRFS (Belcher 2004 [DIRS 173179]) and the 2003 UZ flow model (BSC 2004 [DIRS 169861])

- Use of field and laboratory tests (hydraulic and tracer data collected since TSPA-SR) to establish and confirm the conceptual model for flow, constrain model parameter calibration, and provide data for model validation and confidence building (SNL 2007 [DIRS 177394], Section 6).

This modeling analysis is a direct feed to *Site-Scale Saturated Zone Transport* (SNL 2007 [DIRS 177392]) because it provides the SZ flow fields for transport calculations.

6.2 FEATURES, EVENTS, AND PROCESSES CONSIDERED IN THE MODEL

As stipulated in *Technical Work Plan for: Saturated Zone Flow and Transport Modeling* (BSC 2006 [DIRS 177375]), this model report addresses the FEPs pertaining to SZ flow that are included (i.e., Included FEPs) for TSPA-LA listed in Table 6-1. SZ FEPs that were excluded (i.e., Excluded FEPs) for TSPA-LA are described in *Features, Events, and Processes for the Total System Performance Assessment* (SNL 2007 [DIRS 179476]). Table 6-1 provides a list of FEPs that are relevant to this model analysis in accordance with their assignment in the LA FEP

list (DTN: MO0706SPAFEPLA.001 [DIRS 181613]). Specific reference to the various sections

6.3 THE CONCEPTUAL MODEL

Yucca Mountain is located in the Great Basin about 150 km northwest of Las Vegas, Nevada. The mountain consists of a series of fault-bounded blocks of ash-flow and ash-fall tuffs and a smaller volume of lava deposited between 14 and 11 Ma (one million years (refers to age)) from a series of calderas located a few to several tens of kilometers to the north (Sawyer et al. 1994 [DIRS 100075]). Yucca Mountain itself extends southward from the Pinnacles Ridge toward the Amargosa Desert, where the tuffs thin and pinch out beneath the alluvium (Figure 6-1). The tuffs dip 5 to 10 degrees to the east over most of Yucca Mountain.

Crater Flat is west of Yucca Mountain and separated from it by Solitario Canyon, which is the surface expression of the Solitario Canyon Fault—a steeply dipping scissors fault with down-to-the-west displacement of as much as 500 m in southern Yucca Mountain (Day et al. 1998 [DIRS 100027], pp. 6 to 7). Underlying Crater Flat are thick sequences of alluvia, lavas, and tuffs that have been locally cut by faults and volcanic dikes. East of Yucca Mountain, and separated from it by Fortymile Wash, is Jackass Flats, which is underlain by a thick sequence of alluvium and volcanic rocks. Timber Mountain, approximately 25 km to the north of the repository area, is a resurgent dome within the larger caldera complex whose eruptions supplied the tuffs at Yucca Mountain.

The SZ site-scale flow model presented in this report describes our current state of knowledge of the saturated flow system. The boundaries of the numerical model for SZ flow and transport are indicated on Figure 6-1 in blue. The domain was selected to be: (1) coincident with grid cells of the DVRFS model (DTN: MO0602SPAMODAR.000 [DIRS 177371]) where site-scale model (FEHM) nodes correspond to regional model (MODFLOW-2000) cell corners in the horizontal plane; (2) sufficiently large to reduce the effects of boundary conditions on estimating permeabilities and calculated flow fields near Yucca Mountain; (3) sufficiently large to assess groundwater flow at distances beyond the 18-km compliance boundary from the repository area; (4) small enough to minimize the model size for computational efficiency and to include structural feature detail affecting flow; (5) thick enough to include part of the regional Paleozoic carbonate aquifer (the bottoms of the site- and regional-scale models are equal at −4,000 m below sea level); and (6) large enough to include borehole data from the Amargosa Desert at the southern end of the modeled area. The hydrogeologic setting of the SZ flow system in the vicinity of Yucca Mountain was summarized by Luckey et al. (1996 [DIRS 100465], p. 13). Yucca Mountain is part of the Alkali Flat-Furnace Creek sub-basin of the Death Valley groundwater basin (Waddell 1982 [DIRS 101062], pp. 15 to 16). Discharge within the sub-basin occurs at Alkali Flat (Franklin Lake Playa) and, possibly, Furnace Creek in Death Valley. Water inputs to the sub-basin include groundwater inflow/outflow along the northern, eastern, and western boundaries of the sub-basin, recharge from precipitation in high-elevation areas of the sub-basin, and recharge from surface runoff in Fortymile Canyon and Fortymile Wash. North and northeast of Yucca Mountain, recharge from precipitation also occurs at Timber Mountain, Pahute Mesa, Rainier Mesa, and Shoshone Mountain (Luckey et al. 1996 [DIRS 100465], p. 13).

porosity, and commonly constitute confining units. Ash fall tuffs have high primary porosity and moderate to low permeability, and they generally act as confining units.

As the tuff deposits cooled, they were subjected to secondary processes, including formation of cooling fractures, recrystallization or devitrification, and alteration of the initial glassy fragments to zeolite minerals and clay minerals, all of which affect the hydrologic properties of the rocks. Beginning with deposition and throughout their subsequent history, the rocks have been subjected to tectonic forces resulting in further fracturing and faulting. They also have been subject to changes in the position of the water table, which greatly affects the degree of alteration of the initially glassy deposits.

The forms of secondary heterogeneity most affecting the SZ are fracturing, faulting, and alteration of glassy materials to zeolites and clay minerals. Fractures, where interconnected, transmit water readily and account for the permeable character of the welded tuffs. Cooling fractures, which are pervasive in welded tuffs, tend to be strata-bound and confined to welded portions of flows, whereas tectonic fractures tend to cut through stratigraphic units, as do faults.

Nonwelded deposits are less subject to fracturing and more subject to alteration of the initial glassy deposits to zeolites and clay minerals, both of which reduce permeability. The presence of perched-water bodies in the UZ is attributed to the ubiquitous presence of a smectite-zeolite interval at the base of the Topopah Spring tuff, which, in the absence of through-going fractures, essentially stops the vertical movement of water (Luckey et al. 1996 [DIRS 100465], p. 46).

The heterogeneity in permeability of different types of deposits led to the subdivision of the Yucca Mountain geologic section into five basic SZ hydrologic units: upper volcanic aquifer, upper volcanic confining unit, lower volcanic aquifer, lower volcanic confining unit, and lower carbonate aquifer. To accommodate the more extensive area of the SZ flow model, HFM2006 (SNL 2007 [DIRS 174109], Table 6-3) includes 22 additional units above and below these basic five units. Near Yucca Mountain, volcanic deposits generally form laterally extensive stratigraphic units; however, due to physical heterogeneity, porosity and permeability are highly variable both laterally and vertically.

In the southern part of the SZ site-scale flow model domain, the volcanic deposits thin and inter-finger with valley fill deposits. The latter are heterogeneous (sand and gravel) because of their mode of deposition (Walker and Eakin 1963 [DIRS 103022], p. 14), but are not subject to the fracturing, faulting, and alteration types of heterogeneity that affect the volcanic rocks.

Within the SZ site-scale model area, little specific information is available on the lower carbonate aquifer. However, information from nearby areas (D'Agnese et al. 1997 [DIRS 100131], p. 90, Figures 46 and 47) suggests that the lower carbonate aquifer is minimally heterogeneous with reasonably high permeability attributed to pervasive solution-enlarged fractures.

Heterogeneity in material properties is a common characteristic of hydrogeologic units at the Yucca Mountain site and it exists at scales ranging from pore scale to regional scale. The larger-scale heterogeneity, at scales of kilometers to tens of kilometers, is effectively addressed via the different units within HFM2006, incorporation of specific hydrogeologic features

(e.g., faults and structural zones), and anisotropy. The pore scale heterogeneities are averaged via the concept of macroscopic parameters defined on the basis of a representative elementary volume (Freeze and Cherry 1979 [DIRS 101173], pp. 69 to 70). Groundwater flow equations use parameters defined on the basis of the representative elementary volume. For predominantly porous units such as bedded tuffs and alluvia, the size of the representative elementary volume may be on the order of a few cubic centimeters (de Marsily 1986 [DIRS 100439], p. 15). For fractured rocks (volcanics and carbonates), the size of the representative elementary volume is less well defined, but is typically related to the density of fracturing and is generally much larger than for granular material (Freeze and Cherry 1979 [DIRS 101173], p. 73). The 250-m grid spacing used for the flow model is sufficiently large to allow the use of representative-elementary-volume-defined parameters for groundwater flow. In fact, the grid spacing is large enough that subgrid scale heterogeneity needs to be considered with regard to radionuclide transport. Subgrid heterogeneity leads to enhanced dispersion with increasing scales of transport (de Marsily 1986 [DIRS 100439], pp. 247 to 248). Additionally, the uncertainty in the density of fracturing at the subgrid scale leads to uncertainty in the groundwater velocity and matrix diffusion. Flow modeling accounts for subgrid heterogeneity by defining scaled dispersivities and flowing interval spacing (BSC 2004 [DIRS 170014]) in the transport abstraction modeling (SNL 2007 [DIRS 181650], Section 6.5.2[a]) as random variables characterized by probability density functions.

Heterogeneity at intermediate scales between the grid size of 250 m and the large-scale features of the HFM are addressed using uncertainty in the anisotropy of hydraulic conductivity. A primary concern related to intermediate scale heterogeneity is the possibility of a fast pathway (Freifeld et al. 2006 [DIRS 178611], Table 4) along a relatively continuous path. In the fractured volcanic aquifers beneath Yucca Mountain, the fast path, if it exists, is likely to be related to a fracture or structural feature. The hydraulic testing at the C-wells complex (SNL 2007 [DIRS 177394], Section 6.2) suggest that at a large scale (about 1 km^2), hydraulic conductivity can be characterized as homogeneous, but anisotropic. The direction of anisotropy is primarily related to the dominant direction of fractures and faulting. The impact of possible fast paths at an intermediate scale of heterogeneity is incorporated in the transport simulations through probability distributions of specific discharge, horizontal anisotropy in permeability, and flowing interval spacing (SNL 2007 [DIRS 181650], Section 6.5.2[a]). The aggregate uncertainty in these and other parameters related to radionuclide transport yield simulated SZ transport times for nonsorbing species on the order of 100 years in some Latin Hypercube Sampled realizations of the SZ system (SNL 2007 [DIRS 181650], Figure 6-6[a]).

As noted previously, the properties of each hydrogeologic unit in the model are assumed uniform, but uncertain, with the value assigned during the calibration process. Nevertheless, heterogeneity of material properties at a variety of scales is included in the model via several different mechanisms. First, large-scale heterogeneity is defined by the distribution of units in HFM2006 and the discrete hydrogeologic features incorporated in the SZ site-scale flow model (Table 6-7). Subgrid heterogeneity is included in the transport simulations through the probability distributions for flowing interval spacing and dispersivity. Finally, intermediate scale heterogeneity, which is most likely to be reflected in possible fast paths at scales up to several kilometers, is included as uncertainty in anisotropy. Uncertainty in the HFM is discussed in Section 6.4.3.1.

6.3.1.10 Role of Faults

Faults and fault zones are hydrogeologic features that require special treatment in the SZ site-scale flow and transport models. Faulting and fracturing are pervasive at Yucca Mountain and they affect groundwater flow patterns because they may act as preferred conduits or barriers to groundwater flow. The role that faults play in facilitating or inhibiting groundwater flow depends on the nature of the fault (i.e., whether the faults are in tension, compression, or shear) and other factors such as the juxtaposition of varying geologic units along the fault plane, the rock types involved, fault zone materials, secondary mineralization, and depth below land surface.

Faunt (1997 [DIRS 100146]) investigated the effect of faulting on groundwater movement in the Death Valley region and developed a map of fault traces (Faunt 1997 [DIRS 100146], Figure 10) including diagrams (Faunt 1997 [DIRS 100146], Figure 11) showing the orientation of faults within the principal structural provinces of the region. Faunt (1997 [DIRS 100146], p. 38) grouped the faults into three categories depending on their orientations relative to the present-day stress field (i.e., those in relative tension, compression, or shear).

Faults in relative tension are more likely to be preferential conduits for groundwater, and faults in shear or compression are more likely to impede groundwater movements. Faults modeled to have the most evident effects on groundwater movement, such as effects on potentiometric contours, include the Solitario Canyon, U.S. Highway 95, Crater Flat, and Bare Mountain Faults (see Figure 6-4), all of which appear to act as barriers to groundwater flow. The following features are afforded special consideration in the SZ site-scale flow model: the Crater Flat Fault, the Solitario Canyon (with Windy Wash and Stage Coach splays), the U.S. Highway 95, the Bare Mountain, and Sever Wash Faults. In addition, zones are developed for the Fortymile Wash Structure and Lower Fortymile Wash alluvial regions that appear to act as conduits that focus flow. Other than the Fortymile Wash faults, these features are assigned anisotropic permeabilities that are 10 times more permeable in both directions parallel to the fault (*x*-*z* or *y*-*z* directions).

6.3.1.11 Altered Northern Region

The Claim Canyon caldera is an area of extensive alteration that seems to have resulted in a generalized reduction in permeability in many of the hydrogeologic units in this area (this area is hereinafter referred to as the altered northern region). The concept of the altered northern region allows different permeabilities to be assigned to the same geologic unit depending on whether or not a unit resides within the altered northern region (see Section 6.4.3.7). Deeper units (including the intrusive, crystalline, and lower clastic confining units and the lower carbonate aquifer) are excluded from this alteration because the caldera complex was not present during their genesis. Conceptually, this facilitates modeling of the LHG and it also makes intuitive sense because it is unlikely that permeabilities even within the same geologic unit would have identical values when they are separated by many kilometers (across the model domain from north to south). In the SZ site-scale model formulation, faults that fall within the altered northern region may have diminished impact on the model and could reasonably be removed from consideration here. A notable exception is Sever Wash Fault that retains a distinct permeability

- Horizontal anisotropy in permeability is adequately represented by a permeability tensor that is oriented in the north-south and east-west directions. In support of the TSPA-LA, horizontal anisotropy is considered for radionuclide transport in the SZ (SNL 2007 [DIRS 177394], Section 6.2.6). The numerical grid of the SZ site-scale flow model is aligned north-south and east-west, and values of permeability are specified in directions parallel to the grid. One analysis of the probable direction of horizontal anisotropy shows that the direction of maximum transmissivity is N 33°E (Winterle and La Femina 1999 [DIRS 129796], p. iii), indicating that the anisotropy applied on the SZ site-scale model grid is within approximately 30° of the inferred anisotropy. A detailed description of the horizontal anisotropy calculations is found in *Saturated Zone In-Situ Testing* (BSC 2006 [DIRS 177394], Appendix C6). Sensitivity analyses were performed to assess the impact of uncertainty in the anisotropy and are presented in *Saturated Zone Flow and Transport Model Abstraction* (SNL 2007 [DIRS 181650], Figure 6-1[a]).

- Horizontal anisotropy in permeability may apply to the fractured and faulted volcanic units of the SZ system along the groundwater flowpaths that run from the repository to points south and east of Yucca Mountain. The inferred flowpath from beneath the repository extends to the south and east. This is the area in which potential anisotropy could have an impact on radionuclide transport in the SZ. Given the conceptual basis for the anisotropy model, it is appropriate to apply anisotropy only to those hydrogeologic units that are dominated by groundwater flow in fractures. A more detailed discussion of anisotropy is provided in Section 6.4.3.11.

- Changes in the water-table elevation (due to future climate changes) will have negligible effect on the direction of the groundwater flow near Yucca Mountain although the magnitude of the groundwater flux will change. This supposition has been studied at regional (D'Agnese et al. 1999 [DIRS 120425]; Winterle 2003 [DIRS 178404]; Winterle 2005 [DIRS 178405]) and subregional scales (Czarnecki 1984 [DIRS 101043]). These studies found that the flow direction did not change significantly under increased recharge scenarios. The studies were based on confined aquifer models that did not take into account the free surface boundary at the water table or the saturation of geological units that currently are in the UZ overlying the present-day SZ. These UZ tuffs generally have a lower permeability than those in the SZ, and as such, UZ units that become saturated are not likely to yield faster fluxes in the SZ (BSC 2004 [DIRS 169861], Appendix A).

- Future water supply wells that might be drilled near Yucca Mountain (including outside the regulatory boundary) will have a negligible effect on the hydraulic gradient. Water levels at the southern boundary of the SZ site-scale flow and transport models (in the Amargosa Valley) currently reflect the effect of well pumpage (Luckey et al. 1996 [DIRS 100465], p. 41).

- In the analysis presented in this report, temperature is modeled to be proportional to the depth below the ground surface. Modeling a uniform temperature gradient with depth is equivalent to a model of uniform geothermal heat flux through a medium of homogeneous thermal conductivity. In addition, the temperature at the ground surface is held constant. Data indicate that the temperature gradients generally become more

and that permeability values derived from those tests were considered in the validation of the numerical model. It is not expected that the model can reproduce the transient tests, largely due to the 250-m-gridblock sizes. Because transient pumping is not used in any Yucca Mountain radionuclide migration simulations and steady-state gradients are modeled accurately with the model, this does not invalidate the steady-state assumption. Climate change and other transient impacts are incorporated in the SZ flow and transport abstractions (SNL 2007 [DIRS 181650], Tables 6-1[a] and 6-4[a]). Furthermore, the effects of water table rise on flowpaths are investigated here in Section 6.6.4.

The conceptual model of the long-term groundwater flow in this region includes the hypothesis that recharge rates and, consequently, the elevation of the water table and groundwater flow rates, were larger during the last glacial pluvial period. The time required for the flow system to equilibrate to a more arid climate depends primarily on the hydraulic conductivity of the rocks and the amount of water that must be drained from storage to lower the water table.

It is likely that equilibration to the drier climate has occurred given: (1) the long time (thousands of years) since the climate change was completed, (2) the relatively small amount of water stored (small specific yield) in fractured volcanic rocks that make up much of the model domain near the water table, and (3) the relatively large hydraulic conductivity of the fractured volcanic rocks.

The time required for the flow field to arrive at steady-state with respect to pumping from wells is much shorter than the time required for equilibration to climate change. It depends primarily upon the time required for changes in water level to be transmitted through the SZ. Fast transmittal is expected in fractured volcanic rock because of their relatively large hydraulic conductivity and small specific storage. The fact that the modern-day flow system on the scale of this model domain has equilibrated to pumping is supported by the lack of consistent, large-magnitude variations in water levels observed in wells near Yucca Mountain (Luckey et al. 1996 [DIRS 100465], pp. 29 to 32). A transient response to pumping would be expected, instead, to result in a continued decrease in water levels. Overall, pumping rates are typically negligible compared to the total mass of fluid in the system, which is on the order of 10^{16} kg.

6.4.2 Computational Model

The FEHM V2.24 (STN: 10086-2.24-02; [DIRS 179539]) software code is used for SZ site-scale modeling to obtain a numerical solution to the mathematical equation describing groundwater flow, Equation (6-5). FEHM is a nonisothermal, multiphase flow and transport code that simulates the flow of water and air and the transport of heat and solutes in two- and three-dimensional saturated or partially saturated heterogeneous porous media. The code includes comprehensive reactive geochemistry and transport modules and a particle-tracking capability. Fractured media can be simulated using equivalent-continuum, discrete-fracture, dual-porosity, or dual-permeability approaches. A subset of the FEHM code capabilities was used in the SZ site-scale flow model because only a single-phase, isothermal flow model is solved.

Particle tracking is a numerical technique that simulates the transport of fluid "particles." Particle-tracking techniques have a long history of use in similar applications (e.g., Pollock 1988

units (Table 6-2) provide a geometric representation of hydrogeology and structure and are used as a basis for assigning hydrologic properties within the SZ site-scale flow model domain.

The DVRFS HFM consists of 28 surfaces representing the top elevation of each of the 27 hydrogeologic units plus the base at −4,000-m elevation, and a horizontal grid consisting of a rectangular array of nodes with 125-m spacing (SNL 2007 [DIRS 174109], Section 6). HFM2006 consists of 24 surfaces because unit IDs 10, 13, 22, and 25 are not present in its model area (SNL 2007 [DIRS 174109], Tables 6-2 and 6-3). An important goal of the HFM2006 was to match geologic units with the regional DVRFS HFM. This match allows more direct comparisons with the regional conditions and parameters, without a transition at the site-scale model boundary, and facilitates use of boundary volumetric/mass flow rates extracted from the regional-scale model for use as target boundary conditions during site-scale model calibration. Permeabilities (hydraulic conductivities for the regional model) may not match across model boundaries because these parameters are calibrated independently. The HFM2006 surface grids exactly reproduce the DVRFS Model grid nodes except where more detailed data are available, primarily within the domain of the Geologic Framework Model (GFM) (DTN: MO0012MWDGFM02.002 [DIRS 153777]) and near NC-EWDP boreholes area. These more detailed areas are important considerations in understanding the SZ flow system and they help define the boundaries of the fractured tuff aquifers immediately beneath and down gradient from Yucca Mountain, and the alluvial aquifer from which groundwater discharges in the Amargosa Valley. Data from the NC-EWDP investigations better constrain the location of the tuff-alluvium contact at the water table and better characterize the thickness and lateral extent of the alluvial aquifer north of U.S. Highway 95 (SNL 2007 [DIRS 181650], Section 6.5.2.2[a]).

Recent NC-EWDP drilling revealed a larger formation of alluvial material (Unit 26) in HFM2006 replacing volcanic and sedimentary unit previously thought to be present. It also revealed more of Unit 20 (Timber Mountain Volcanics) to the south of the GFM area than was previously indicated.

This report describes SZ flow modeling using HFM2006, which incorporates the newer DVRFS HFM (Belcher 2004 [DIRS 173179]), GFM2000 (DTN: MO0012MWDGFM02.002 [DIRS 153777]), and all NC-EWDP data through Phase IV.

Table 6-2. Hydrogeologic Units for the Hydrogeologic Framework Model

Hydrogeologic Units in HFM2006				
Unit ID	**Abbreviation**	**Unit Name**	**Description**	**Stacking Order**
28	YAA	Younger alluvial aquifer	Pliocene to Holocene coarse-grained basin-fill deposits	27
27	YACU	Younger alluvial confining unit	Pliocene to Holocene playa and fine-grained basin-fill deposits	26
26	OAA	Older alluvial aquifer	Pliocene to Holocene coarse-grained basin-fill deposits	25
25	OACU	Older alluvial confining unit	Pliocene to Holocene playa and fine-grained basin-fill deposits (not in HFM2006 domain)	24
24	LA	Limestone aquifer	Cenozoic limestone, undivided	23

6.4.3.3 Hydrogeologic Properties

HFM2006 provides the hydrogeologically-defined geometry for SZ flow and transport process models and is used to assign geologic properties to the nodes of the computational grid. The physical hydrogeologic unit present at each node in the computational grid was established during the computational grid construction. The HFM2006 surface files represent the top surface of each hydrogeologic layer in the model framework and were imported into LaGriT to identify the hydrogeologic layer designation for each node and cell of the computational grid. Cells above the ground surface were identified using the HFM2006 surfaces, then they were removed from the grid. Quality checks were performed to ensure that the final grid is correct. These include histograms of element volume and element aspect ratio as described by Bower et al. (2000 [DIRS 149161]). Once the grid geometry was evaluated and the material units conform as needed to the input HFM, FEHM modeling input files are generated. These files include the mesh geometry, lists of nodes on external boundaries, and node lists sorted by material property.

All nodes were automatically and visually checked to ensure that they were assigned the correct material identification corresponding to the input HFM. Lists of the number of nodes associated with each material were compared to the volume of each material in the EARTHVISION framework to confirm that the hydrogeologic units are identified correctly.

When evaluating the computational grid for SZ flow and transport, the hydrogeologic properties of the grid are compared to the hydrogeologic framework used as input. It is expected that the grid units will differ slightly from the HFM due to differences in grid spacing (i.e., 250 versus 125 m). The grid units should still resemble the input HFM and areas of importance should be replicated accurately. The flow pathways are expected to leave the repository and travel in a south-southeasterly direction towards Fortymile Wash and the 18-km compliance boundary. From the 18-km boundary to the end of the model, the flowpaths should trend to the south-southwest and generally follow Fortymile Wash. Outlines of the repository, Fortymile Wash, and U.S. Highway 95 are included on Figure 6-5 as reference to these areas.

6.4.3.4 Evaluation of Hydrogeology represented in the SZ Computational Grid

All nodes were automatically and visually checked to ensure that they were assigned the correct material. The number of tetrahedral elements assigned to each hydrogeologic unit and their associated element volumes are presented in Table 6-5. Lists of the number of nodes associated with each material were compared to the volume of each material in the HFM2006 to confirm that the hydrogeologic units are identified correctly. To check that hydrogeologic properties are being assigned in accord with the HFM2006, relative unit volumes are compared. Differences will occur between the HFM and grid units due to variations in grid element sizes in the computational grid. Volumes represented by the HFM2006 surfaces are included for comparison. Large grid elements less accurately capture thin layers, which becomes evident when comparing unit volumes. Figures showing the grid units are supplied in Appendix G to confirm that differences are reasonable and acceptable.

Table 6-5. SZ Computational Grid and HFM2006 Volume Comparisons by Unit

Unit	Names	SZ Computational Grid			HFM2006 Surfaces	
		Tetrahedral Elements Number	Volume of Elements per Unit (m^3)	% Fractional Volume	Volume between Surfaces (m^3)	% Fractional Volume
28	YAA	32,106	4.75×10^9	0.07	1.15×10^{10}	0.17
27	YACU	7,788	8.11×10^8	0.01	9.89×10^8	0.01
26	OAA	137,772	2.09×10^{10}	0.31	2.35×10^{10}	0.34
24	LA	18,834	2.08×10^9	0.03	2.18×10^9	0.03
23	LFU	38,208	8.56×10^9	0.13	1.48×10^{10}	0.22
21	Upper VSU	316,716	5.53×10^{10}	0.81	5.58×10^{10}	0.82
20	TMVA	152,586	3.77×10^{10}	0.56	4.38×10^{10}	0.64
19	PVA	838,668	2.35×10^{11}	3.47	2.45×10^{11}	3.59
18	CHVU	280,368	9.29×10^{10}	1.37	9.45×10^{10}	1.38
17	WVU	122,802	2.52×10^{10}	0.37	2.57×10^{10}	0.38
16	CFPPA	140,064	3.38×10^{10}	0.56	3.78×10^{10}	0.55
15	CFBCU	439,698	1.35×10^{11}	1.98	1.35×10^{11}	1.98
14	CFTA	584,232	2.85×10^{11}	4.20	2.85×10^{11}	4.17
12	OVU	158,982	1.68×10^{11}	2.47	1.69×10^{11}	2.48
11	Lower VSU	461,478	5.97×10^{11}	8.78	5.96×10^{11}	8.72
9	LCA_T1	185,736	3.00×10^{11}	4.42	3.00×10^{11}	4.39
8	LCCU_T1	101,550	2.63×10^{11}	3.87	2.64×10^{11}	3.86
7	UCA	24,900	8.33×10^9	0.12	8.83×10^9	0.12
6	UCCU	238,248	2.18×10^{11}	3.21	2.21×10^{11}	3.24
5	LCA	793,620	2.55×10^{12}	37.59	2.54×10^{12}	37.13
4	LCCU	275,532	1.07×10^{12}	15.77	1.08×10^{12}	15.79
3	XCU	47,490	2.23×10^{11}	3.28	2.26×10^{11}	3.30
2	ICU	106,974	4.50×10^{11}	6.62	4.55×10^{11}	6.67
Totals		5,504,352	Element Volume 6.79×10^{12}		Sum Volume 6.83×10^{12}	

Source: Output DTN: LA0612TM831231.001.

NOTES: HFM2006 volumes represent the best achievable volumes when matching surface resolutions. The computational grid lengths are 250 m in the horizontal and depths range from 10 to 600 m in the vertical. Units 10, 13, 22, and 25 are not found within the domain of the SZ site-scale flow model.

Figures 6-8 through 6-10 represent sections cut through the computational grid and can be compared to matching sections cut through HFM2006 (SNL 2007 [DIRS 174109], Figures 6-5 and 6-6). The first figure is a north-to-south vertical section cut at an easting of 552,500 m. This section was selected because it is located approximately along the flowpath from Yucca Mountain to the south. The second figure is a west-to-east vertical section cut at a northing of 4,064,000 m and it is located within the area of the newest NC-EWDP well data used in HFM2006. This section cuts across most of the faulting in the area and demonstrates where the faulting is represented in the more widely spaced data of the regional model, which served as the basis for HFM2006. As can be seen in this figure, some of the offsets on the faults are preserved through changes in altitude of a given hydrogeologic unit. Given the depth to which the model extends and the lack of information in most of the modeled volume, this seems to be a rational simplification (SNL 2007 [DIRS 174109], Section 6).

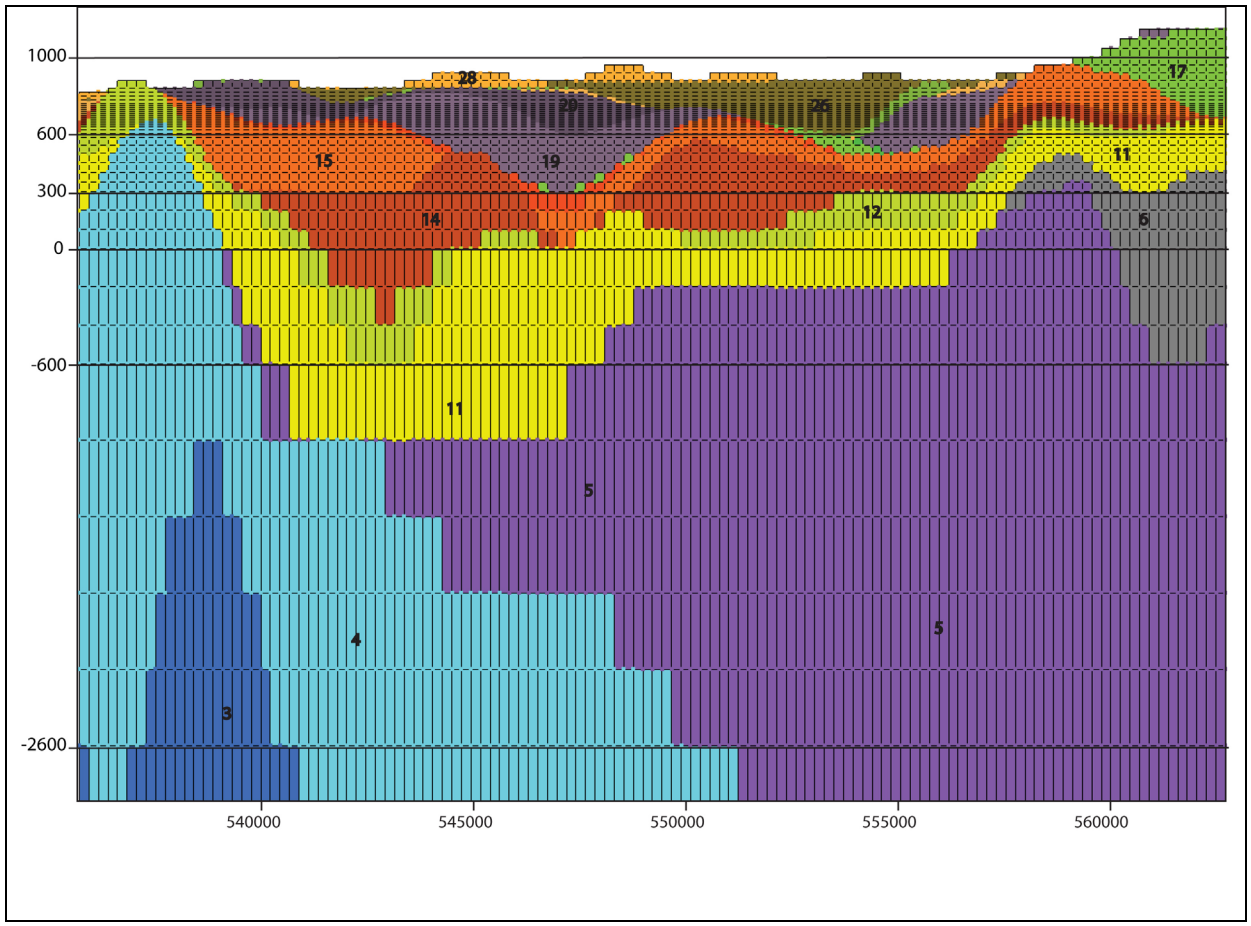

Source: Output DTN: LA0612TM831231.001.

NOTE: Coordinates in UTM, Zone 11, NAD27 meters, 5× vertical exaggeration. Unit numbers are the hydrogeologic numbers defined by HFM2006 in Table 6-2. This image shows the spacing of the grid in the vertical direction. The grid nodes used in FEHM flow modeling are shown here at the vertices of each grid block. Grid nodes and volumes are colored according to HFM2006 hydrogeology. The colors correspond to those in the legend for Figure 6-7.

UTM = Universal Transverse Mercator.

Figure 6-10. Hydrogeologic Grid Nodes and Spacing at West-East Cross Section in the SZ Computational Grid at UTM Northing = 4,064,000 m

6.4.3.5 Hydrogeology at the Water Table

A new water-table surface is used in conjunction with HFM2006 and is discussed in Appendix E. The water-table surface defines which grid nodes are below and above the water table, those that are above the water table are inactivated in the FEHM flow model. This results in node elevations at the top of the flow model that range from ~1,200 m in the north to ~700 m in the south. The hydrogeologic units at the water table top are shown in Figure 6-11, which compares well with HFM2006 view at the water table (SNL 2007 [DIRS 174109], Figure 6-7c). Table 6-6 lists the numbers of FEHM nodes in the entire model domain (below the land surface) and the number of saturated nodes below the water table.

Table 6-6. SZ Computational Grid Nodes by Unit

Unit	Abbreviation	Nodes per Unit Under Land Surface	Nodes per Unit Under Water Table Surface
28	YAA	9,965	197
27	YACU	1,580	247
26	OAA	24,148	10,637
24	LA	3,289	1,387
23	LFU	8,608	2,751
21	Upper VSU	53,911	42717
20	TMVA	27,940	18,131
19	PVA	143,658	94,149
18	CHVU	47,905	29,189
17	WVU	21,116	14,576
16	CFPPA	23,461	20,242
15	CFBCU	73,939	67,436
14	CFTA	98,162	93,327
12	OVU	27,152	26,691
11	Lower VSU	78,182	76,856
9	LCA_T1	31,608	28,588
8	LCCU_T1	17,848	17,053
7	UCA	4,228	4,201
6	UCCU	40,842	33,533
5	LCA	135,186	131,312
4	LCCU	52,891	52,745
3	XCU	10,018	10,015
2	ICU	20,708	20,708
	Totals	956,345	774,177

Source: Output DTN: LA0612TM831231.001.

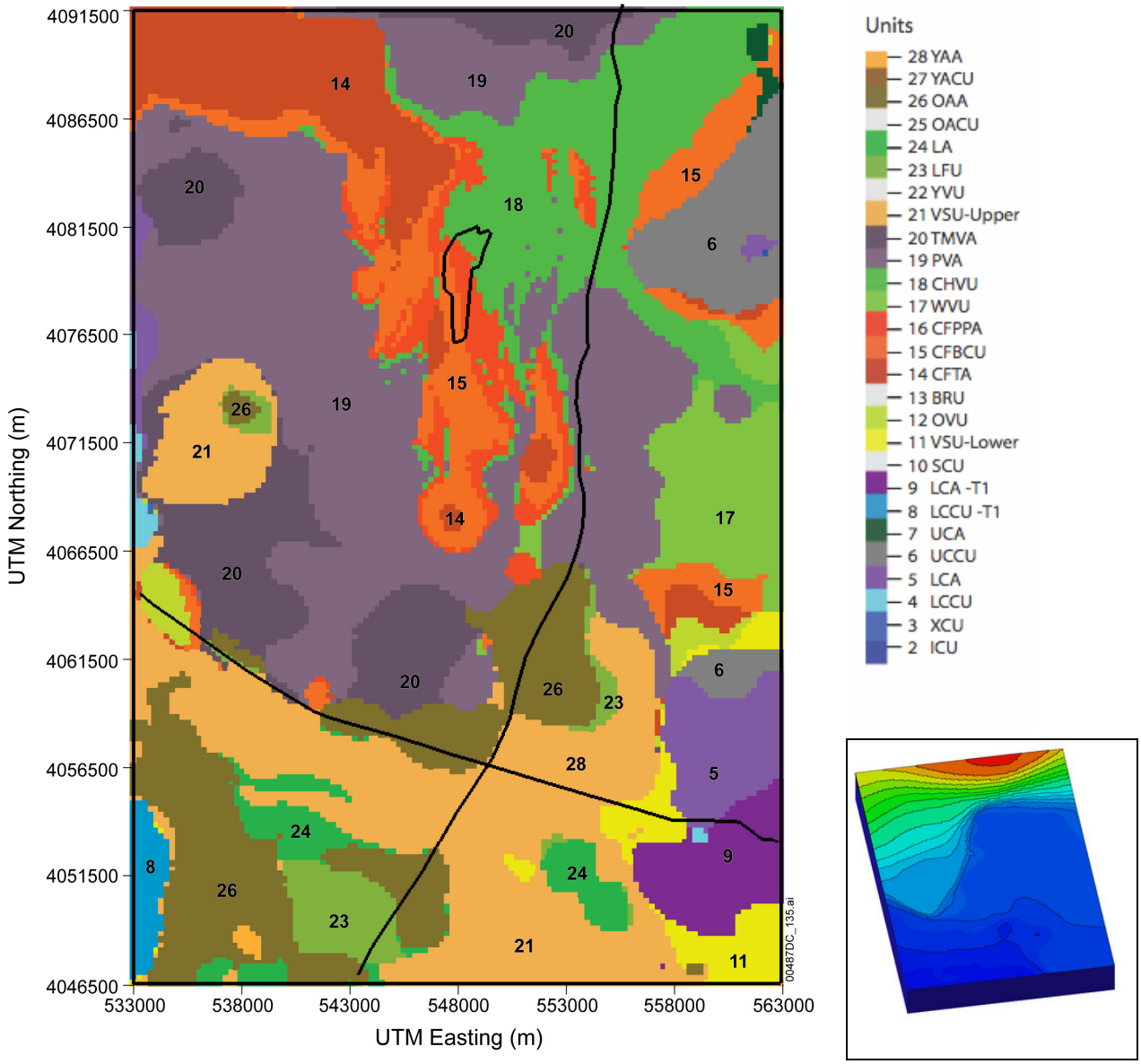

Source: Output DTN: LA0612TM831231.001.

NOTE: For illustration purposes only. The figure depicts grid points at the water-table surface. The black lines are used for reference and are the repository outline (SNL 2007 [DIRS 179466]), U.S. Highway 95, and Fortymile Wash. The inset shows the computational grid colored by the water table elevations ranging from 680 m in the south to 1,230 m in the north.

UTM = Universal Transverse Mercator.

Figure 6-11. Hydrogeologic Units Present at the Water-Table Surface in the SZ Computational Grid

The resolution of the computational grid was designed to have the smallest vertical spacing in the vicinity of the water-table below the repository. Therefore, the computational grid honors the hydrogeology of the HFM2006 as can be seen in these figures. Updates to the HFM2006 show differences most evident in the southern part of the model where the volcanic and sedimentary unit replaces the valley-fill aquifer as the most pervasive unit. Updates to the HFM2006 also include increased abundance of the Crater Flat group to the west of Yucca Mountain and the

occurrence of Lava Flow unit to the east of Fortymile Wash and to the north of U.S. Highway 95. These changes may have influence on the calibration and specific discharge simulations of the flow model.

Further comparisons can be made across each unit by comparing HFM2006 layer thickness and distribution maps (SNL 2007 [DIRS 174109], Appendix C) to the distribution of grid nodes for each hydrogeologic unit (SNL 2007 [DIRS 174109], Appendix A) and are presented in Appendix G. Figures for each grid unit include the distribution of each unit for the full model domain, and a second figure showing the grid units truncated by the water table surface. The truncated grid units show the active grid nodes for the FEHM modeling domain. Both sets of images are views looking directly down at the top, with south toward the page bottom and showing the horizontal distribution for each unit 1 through 28. The shapes of the HFM2006 maps (SNL 2007 [DIRS 174109], Appendix C) and the grid units (SNL 2007 [DIRS 174109], Appendix A) compare reasonably given that the grid resolution is 250 m and the HFM2006 is 125 m and that vertical grid resolution varies from 10 to 600 m.

6.4.3.6 Uncertainty

Uncertainty in the SZ computational grid is a function of HFM2006 and the resolution of the grid in relation to the flowpaths. Large grid spacing and associated loss of hydrogeologic unit shape accuracy are chosen to correspond with areas deep in the model and beyond the flowpath regions. Areas of highest resolution were chosen in the shallow units and in the area of the water table below the repository. Uncertainties in the HFM2006 relate most importantly to the quantity and location of available qualified data, and secondly to the interpretation of surfaces and the representation of important faults and structures. Uncertainties due to the definition of the hydrogeologic units are propagated through the flow and transport model abstraction (SNL 2007 [DIRS 181650]).

Model uncertainties in the HFM2006 can be attributed to interpretations and simplifications driven largely by the distribution and availability of data. The data distribution over the SZ area is uneven, much of the volume is unsampled, and many of the inputs are interpretations. As a result, the expected error in the HFM2006 varies significantly over the model area. Some of the surfaces, such as that of the upper volcanic aquifer in the area of the repository, are relatively well defined by more than one data set (derived from the surface hydrogeologic unit map and borehole lithologic logs). Others, especially the units that crop out less commonly, are less well defined and are extrapolated from sparse data. In the area of the repository, the unit locations are relatively well known. Even in this area, however, only one borehole penetrates the Paleozoic rocks. Data uncertainty increases with depth and distance from the repository as data become sparse and the effects of faults deeper in the system become unknown. As a result, the model contains an inherent level of uncertainty that is a function of data distribution and geologic complexity. Additional limitations include data-poor regions in the deeper Paleozoic carbonate region (SNL 2007 [DIRS 174109], Section 6.4.3).

HFM2006 is constructed with a horizontal grid spacing of 125 m, but most of the model domain does not contain sufficient geologic detail to support this resolution. This results in smoothly interpreted or interpolated surfaces at a resolution finer than justified by the geologic data. This finer resolution does not add any additional error. Specific borehole data and other measured

volcanic units (Units 12, 14, 15, 16, 17, 18, 19, 20, and 25), and to provide boundaries for a zone of enhanced permeabilitiy in the Crater Flat tuffs to better approximate the small haydraulic gradient in the region. The zone was defined based on responses of USW H-4, UE-25 C#1, UE-25 WT#14, and UE-25 WT#3 to pumping at the C-holes from May 1996 to November 1997. Furthermore, this zone did not include wells USW H-5, G-1, and UZ-14 because, although these wells are located east of the Solitario Canyon Fault, they showed anomlaous heads closer to those observed in wells located west of Solitario Canyon Fault (USW H-6, WT-7, and WT-14). This indicates that some non-characterized feature or process is impacting the water levels just to the east of Solitario Canyon Fault and the newly defined zone allows the model to better represent these data The quadrilateral is defined to encompass the small-gradient area southeast of the repository between Solitario Canyon and Fortymile Wash Faults without including wells USW H-5, G-1, and UZ-14, but including wells USW H-4, UE-25 C#1, UE-25 WT#14, and UE-25 WT#3.

Most hydrogeologic units (the 19 units with areal extents that reach into the north of the model including all units except the lower clastic confining unit thrust, lower carbonate aquifer thrust, Wahmonie volcanic unit, limestone aquifer, and the young alluvial confining unit) have been divided into northern and southern zones near the Claim Canyon caldera boundary to represent the altered northern zone (see Section 6.3.1.11). This zone of decreased permeability facilitates model representation of the LHG north of Yucca Mountain. Except for Sever Wash Fault, fault nodes do not reside in this region. The altered northern region is defined with an arc that intersects the model domain and it is defined by a circle with center 546,500; 4,102,400 (UTM easting and northing) and radius 21,100 m. This designation was selected such that the defining circle roughly corresponds to the center of the caldera complex and the radial extent includes wells: GEXA Well #4, UE-29 a#2, UE-29 UNZ#91, UE-25 WT#6, USW G-2, and USW WT-24. Breaking the hydrogeologic units into independent northern and southern zones yields 19 additional calibration parameters. Figure 6-13 illustrates the radial extent of the altered northern region.

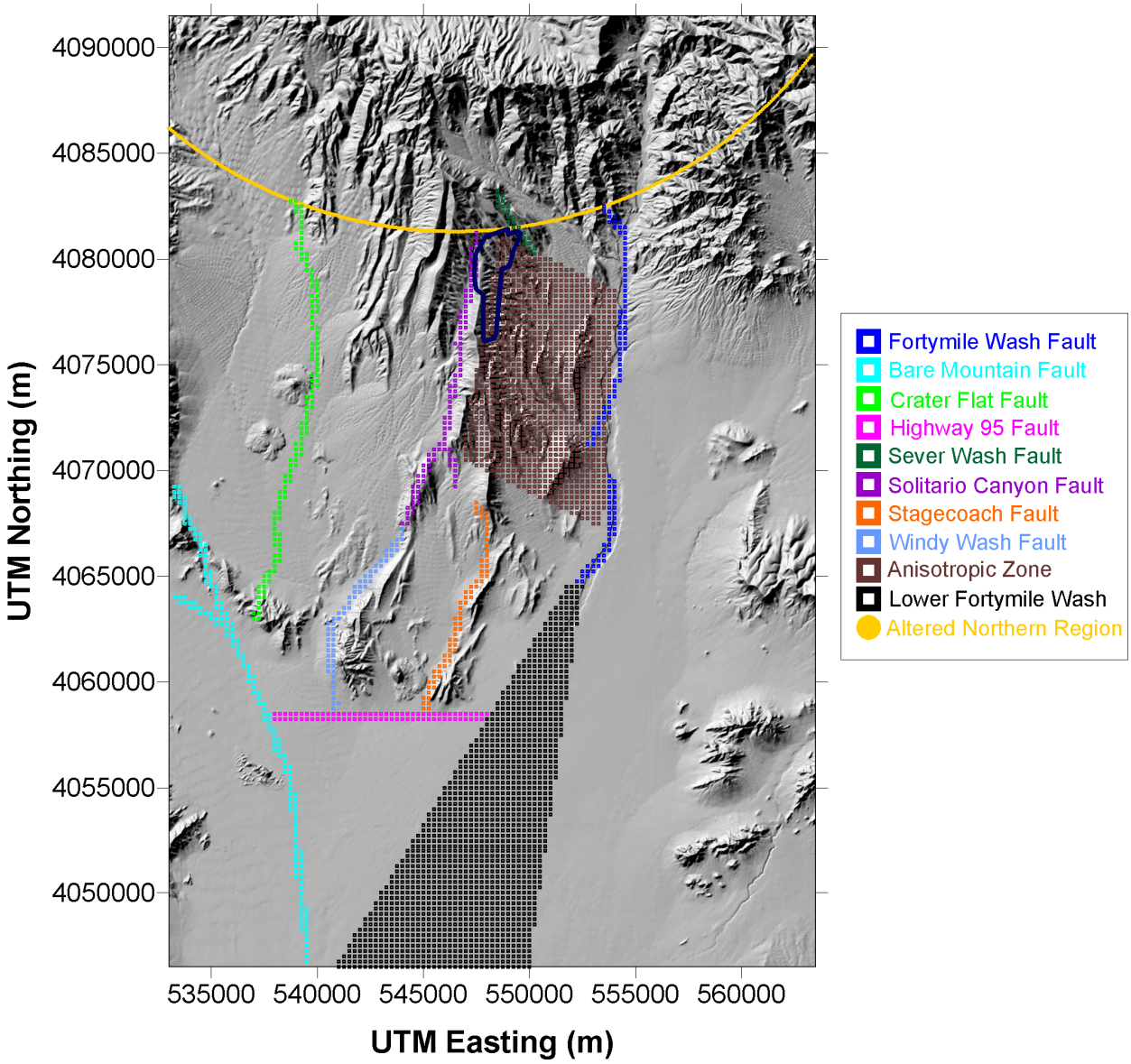

Source: Output DTN: SN0612T0510106.004, *feature_set.zonn* and *aniso.zonn*).

NOTE: Source for repository outline: SNL 2007 [DIRS 179466]. Fault traces are labeled in the legend. FEHM zone number correspond to the following regions: 39 – Anisotropic zone; 40 – Fortymile Wash Fault; 41 – Bare Mountain Fault; 42 – Crater Flat Fault; 43 – U.S. Highway 95 Fault; 44 – the Solitario Canyon Fault; 45 – Sever Wash Fault; 46 – Stagecoach Fault; 47 – Windy Wash Fault; 50 – Lower Fortymile Wash.

UTM = Universal Transverse Mercator.

Figure 6-12. Geologic Features Included in the SZ Site-Scale Flow Model

and vertical) multiplied by 10 (e.g., Solitario Canyon fault permeabilities in the *y*- and *z*-directions are 10 times that in the cross-fault direction). The permeabilities of major faults are used as calibration parameters; however, the anisotropy ratios were constant during the calibration process. A 10:1 horizontal to vertical anisotropy was also assigned in the Lower Fortymile Wash Alluvial Zone.

6.5 SZ SITE-SCALE FLOW MODEL RESULTS

6.5.1 Model Calibration

Calibration is the process by which values of important model parameters are estimated and optimized to produce the best fit between model output and observed data. Calibration is generally accomplished by adjusting model input parameters (e.g., permeabilities) to minimize the difference between observed and simulated conditions (in this case, comparing simulated and observed head values and lateral boundary volumetric/mass flow rates). Model calibration may be performed manually or through automated optimization procedures. Automated optimization procedures generally employ a carefully prescribed mathematical process that selects the optimal set of parameters based on minimizing an objective function describing the difference between observed and simulated conditions. These procedures typically provide the most structured and thorough means of calibrating a model, and, frequently, they provide useful additional information regarding model sensitivity to parameters and other useful statistical measures. Consequently, an automated optimization procedure is used to calibrate the SZ site-scale flow model. However, manual adjustments to the calibration are also performed to ensure accurate representation of the small hydraulic gradient region southeast of the repository by ensuring that simulated particle pathlines do not contradict flow directions inferred from the potentiometric map.

A description of the calibration technique includes discussions of: optimization procedures; model outputs, whose differences between observed values (calibration targets) were minimized; and parameters that were varied during calibration.

6.5.1.1 Calibration Criteria

Proper calibration of the SZ site-scale flow model requires consideration of the full range of available data, which include field data for water levels and hydraulic heads, permeability data from field and laboratory tests, locations of known faults and other geologic data, and hydrochemical data. Opinions expressed by the Expert Elicitation Panel (CRWMS M&O 1998 [DIRS 100353]) must also be considered. The goal during development of the SZ site-scale flow model was to deliver to performance assessment a model that, given data sparseness, is as realistic as possible.

6.5.1.2 Parameter Optimization Procedure

The SZ site-scale flow model was calibrated with the commercial parameter estimation code, PEST (STN: 10289-5.5-00; [DIRS 161564]). PEST is a Levenberg-Marquardt (LM)-based optimization algorithm. The LM package is a well-established algorithm (Press et al. 1992 [DIRS 103316], pp. 678 to 683), it is robust, and widely applicable. It will search for the minima of a multidimensional function. In this case, the

features or faults. The zone sizes were fixed based on data from HFM2006. Uncertainty associated with geologic contacts is discussed in Section 6.7.3.

Recall that vertical anisotropy is assigned a value of 10:1 (horizontal to vertical) in the volcanic and valley-fill units (above Unit 9). Lower permeability in the vertical direction than in the horizontal direction typically occurs in stratified media, and the ratio of 10:1 is in the generally accepted range (CRWMS M&O 1998 [DIRS 100353], Table 3-2). For a site-specific example, the relatively high vertical gradient observed in well UE-25 p#1 suggests that vertical permeability is lower than horizontal permeability (minimal hydraulic connectivity). Nine wells (see Section 6.3.1.5) exhibited vertical gradients (BSC 2004 [DIRS 170009], Table 6-4). The uncertainty associated with the vertical anisotropy is discussed in Section 6.7.2.

Specific hydrogeologic features thought to potentially impact groundwater flow are classified as distinct permeability zones. The permeability variable or permeability multiplication factor used for a specific feature was assigned to all of the nodes within that feature. The hydrogeologic features for which special permeability zones were established are primarily faults, fault zones, and areas of hydrogeologic alteration (Section 6.5.2). As previously discussed, these features are distinct from the subhorizontal hydrogeologic units identified in HFM2006. Each of the identified hydrogeologic features includes multiple geologic formations and represents a zone of altered permeability within individual formations.

Twenty-three permeability zones were established based on the geologic units within the SZ site-scale model domain from HFM2006 for model calibration. Additional (usually low) permeability zones reflecting altered northern region were added to the model to help establish known system characteristics (like the LHG). These were established by dividing existing (base) geologic units into altered northern regions with permeabilities defined by multipliers. These permeability multipliers are calibration parameters that modify the permeability values assigned to geologic units in the altered northern regions. Eight additional zones representing faults and the Lower Fortymile Wash alluvium were established because they were identified as important structural features (e.g., the Solitario Canyon Fault) or were necessary for some conceptual feature, such as the LHG north of Yucca Mountain (which is partially established in the model domain with help from the altered northern region).

As required by PEST, upper and lower bounds were placed on each permeability variable during parameter optimization with limits chosen to reflect maximum and minimum field values (permeability) or a realistic range of values (permeability multipliers). A list identifying permeability zones, its calibrated permeability parameter, and the upper and lower bounds specified for the parameter is provided in Table 6-9.

Table 6-9. Calibration Parameters Used in the SZ Site-Scale Flow Model

Parameter Name (zone number)	Geologic Unit or Feature	Calibrated Value (m^2)	Minimum Value (m^2)	Maximum Value (m^2)
ICU (2)	Intrusive Confining Unit (granite)	9.9×10^{-17}	1.0×10^{-19}	1.0×10^{-10}
XCU (3)	Crystalline Confining Unit (granite)	1.0×10^{-16}	1.0×10^{-19}	1.0×10^{-10}
LCCU (4)	Lower Clastic Confining Unit	9.7×10^{-17}	1.0×10^{-19}	1.0×10^{-10}
LCA (5)	Lower Carbonate Aquifer	9.7×10^{-15}	2.0×10^{-15}	1.0×10^{-10}

Table 6-9. Calibration Parameters Used in the SZ Site-Scale Flow Model (Continued)

Parameter Name (zone number)	Geologic Unit or Feature	Calibrated Value (m^2)	Minimum Value (m^2)	Maximum Value (m^2)
wwfz (47)	Windy Wash Fault Zone	4.8×10^{-16}	1.0×10^{-19}	1.0×10^{-10}
wash (50)	Lower Fortymile Wash	2.0×10^{-11}	1.0×10^{-19}	1.0×10^{-10}

Output DTN: SN0612T0510106.004, *sz_site_2006.pst*.

In addition to the PEST optimization described above, several manual adjustments were made to improve the model in ways that were not possible during the PEST run. Specifically, during calibration, only water levels (and lateral volumetric/mass flows) were considered in the objective function and hence head gradients or important head differences between wells were not explicitly considered. Manual adjustments were made to ensure that the flow direction southeast of the repository (in the small-gradient, anisotropic region) matched the direction inferred from the range and distribution of head values in this area. These adjustments modified the direction of particle paths emanating from the repository (to match the direction inferred from differences in the measured water levels) while maintaining good calibration (low objective function and low weighted RMSE for heads). The specific discharge was adjusted by changing the permeability of several units as listed in Table 6-10. Specific discharges were manipulated without adversely affecting the heads or gradient in the small hydraulic gradient area near Yucca Mountain. Table 6-10 shows the units that were adjusted during hand calibration, their PEST-optimized permeability values, and their hand calibrated values. It should be noted that an additional zone corresponding to the Bullfrog Tuff within the quadrilateral defined by the Yucca Mountain zone was added during hand calibration with a permeability of 5×10^{-13} m^2 to ensure that the small hydraulic gradient region observed southeast of the repository is honored by the model and the flow paths from below the repository did not terminate along the eastern model boundary.

Table 6-10. Hand Calibration Results used in the SZ Site-Scale Flow Model

Parameter Name (unit/zone number)	Geologic Unit or Feature	Hand-Calibrated Value (m^2)	PEST-Calibrated Value (m^2)
LCAT1 (9)	Lower Carbonate Aquifer	5.6×10^{-12}	5.6×10^{-14}
CFBCU (15)	Bullfrog Tuff	$5.2. \times 10^{-14}$	5.2×10^{-14}
CFPPA (16)	Prow Pass Tuff	3.1×10^{-12}	1.1×10^{-13}
PVA (19)	Paintbrush Volcanic Aquifer	6.5×10^{-14}	2.5×10^{-13}
VSU (21)	Volcanic and Sedimentary Unit	8.7×10^{-13}	8.7×10^{-16}
OAA (26)	Older Alluvial Aquifer	1.5×10^{-13}	8.8×10^{-13}
CFPPAm (116)	Prow Pass Tuff Multiplier	1.4×10^{-3}	9.4×10^{-3}
CHVUm (117)	Crater Hills Volcanic Unit Multiplier	2.3×10^{-3}	2.3×10^{-3}
4wfz (40)	Fortymile Wash Fault Zone	1.4×10^{-10}	6.4×10^{-11}
wash (50)	Lower Fortymile Wash Alluvial Zone	2.0×10^{-11}	5.2×10^{-13}

Output DTN: SN0612T0510106.004, *sz_site_2006_calibrated.pst*.

RMSE for calibrated model is only 18% worse than the best-fit potentiometric surface (24.39 m compared to 20.70 m). Moreover, the weighted RMSE of the calibrated model is an order of magnitude better than the best-fit potentiometric surface and this indicates excellent model agreement in high weight areas of the model domain—areas felt to be the most important to get accurate model simulations (i.e., downgradient from the repository). Because of the 10-m minimum layer thickness, head differences of less than this magnitude are within the uncertainty range of the model.

As can be seen in Figure 6-15, the largest head residuals (~100 m) are in the northern part of the model in the altered northern region and in the vicinity of the moderate hydraulic gradient. These residuals are largely the result of the low weighting factor of (0.1) and the possibility that they reflect perched conditions (see Section 6.5.2.1 for a description and Section 6.7.7 for a discussion of perched water effects). In the figure, a negative residual means that the calibrated value was lower than the target data (note that the PEST record file shows opposite signs; a negative residual means that the calibrated value was higher than observed). The next highest head residuals border the Crater Flat and Solitario Canyon Faults. These residuals (~25 m) are most likely the result of 250-m grid blocks not being able to resolve the 780 to 730-m (~50-m) drop in head in the short distance just east of the above-mentioned features. There may be additional complicating factors such as varied hydrologic characteristics in the Solitario Canyon Fault along its north-south transect. In the model, the fault acts as a barrier, but is defined with only one calibration parameter. This may not be adequate to represent the local behavior of such a long feature. For example, well USW G-1, about 1,000 m from the Solitario Canyon fault, shows an 8-m difference between measured and simulated heads. The measured head for this well (754 m), located on the east side of the fault, is closer to measured head values on the west side of the fault. Because the majority of wells on the east side have heads of approximately 745 m, the simulated head for USW G-1 has a calibrated result close to that value. Overall results indicate that the model adequately represents the water table near Yucca Mountain. In the vicinity of the 18-km compliance boundary and south, the modeled potentiometric surface is typically on the order of 5 m higher than the observed water levels although the estimated gradients match well (see Section 7.2.1).

6.5.2.4 Specific Discharge

Using the calibrated SZ site-scale flow model, specific discharge was estimated as the average over 100 particles. These particles were randomly distributed below the repository and tracked until they traveled across UTM Northing 4,073,761 m (approximately 5 km south of the midpoint of the repository). Pathlength divided by travel time yields the specific discharge for a particle and the average across 100 particles was 0.36 m/yr (1.08 ft/yr) for the calibrated model. End members of the 100-particle plume had specific discharges of 0.11 and 0.66 m/yr. The Expert Elicitation Panel (CRWMS M&O 1998 [DIRS 100353], Figure 3-2e) estimated a median specific discharge of 0.6 m/yr (2.0 ft/yr) for the 5-km (3-mile) distance. Thus, reasonable agreement is found between the specific discharge simulated by the calibrated SZ site-scale flow model and that estimated by the Expert Elicitation Panel (CRWMS M&O 1998 [DIRS 100353]).

6.6 CONSIDERATION OF ALTERNATIVE CONCEPTUAL MODELS

The SZ site-scale flow model propagates information through the SZ flow and transport model abstraction (SNL 2007 [DIRS 181650]) to the performance assessment calculations, which are used to evaluate potential risks to groundwater users downgradient from the repository area. The results of these performance assessment calculations depend upon the specific discharge of groundwater leaving the repository area as well as on the flow paths and the distribution of flow among the various hydrostratigraphic units that carry, deflect, or otherwise affect the flow. For this report only, the specific discharge was evaluated with SPDIS.EXE (STN: 611598-00-00 [DIRS 180546]), which calculates the average travel distance divided by corresponding travel time to reach a specified northing location (e.g., 5 km downgradient) across 100 particles. It is important to note that SPDIS.EXE yields a convenient metric to compare specific discharges, which represents surrogates for flow fields generated from the model. The alternative conceptual models (ACMs) presented here were investigated because they represented a hydrologic concern such as water table rise due to climate change or were related to a model feature (anisotropy) that had a possibility of affecting the specific discharge calculations. This section presents analyses of the ACMs, their representation in the numerical model, and a discussion about possible impacts on the model outputs. ACMs affecting model outputs are discussed here, although this uncertainty is not directly propagated to the radionuclide breakthrough curves in the TSPA calculations. Specifically, it should be noted that the SZ flow and transport abstraction model does not use the SZ site-scale flow model as a source of direct input to the assessment of uncertainty in groundwater specific discharge. The two direct inputs used to establish the groundwater specific discharge multiplier are DTNs: MO0003SZFWTEEP.000 [DIRS 148744] and LA0303PR831231.002 [DIRS 163561] (SNL 2007 [DIRS 181650], Figure 6-2[a]).

The calibrated SZ site-scale flow model described in detail in Section 6.5 also provides the basis for the ACMs discussed here. That is, the same numerical grid and HFM were used throughout this section. Various parameterization schemes were used to define the ACMs (e.g., change in potentiometric surface). The following ACMs were evaluated:

- Removal of vertical anisotropy: This ACM relates to removal of vertical anisotropy in permeability
- Removal of horizontal anisotropy: This ACM relates to removal of horizontal anisotropy in the volcanic units downgradient from Yucca Mountain
- Removal of the altered northern region: This ACM relates to removal of the permeability multipliers that reduce the permeability in the northern region, which help the model honor the observed high head
- Increase in permeability in the *z*-direction for the Solitario Canyon Fault
- Water table rise: This ACM relates to future water table rise.

unsaturated and saturated zones at Yucca Mountain indicated previous water-table elevations of 85 m (279 ft) higher than present (Marshall et al. 1993 [DIRS 101142], p. 1,948). Recently completed wells at paleospring discharge locations near the southern end of Crater Flat, which are inactive sites of Pleistocene spring discharge, revealed shallower-than-expected groundwater with depths of only 17 to 30 m (56 to 100 ft) to the water table (Paces and Whelan 2001 [DIRS 154724]; BSC 2004 [DIRS 168473], Table I-1). These findings indicate that the water-table rise during the Pleistocene at these paleospring locations could not have been more than about 30 m (100 feet) due to formation of discharge locations. The results of the mineralogical and geochemical studies showing a maximum water-table rise of up to 85 m reflect evolution of past climates for the last 1 million years, which included the effects of glacial climates. The maximum water-table rise under monsoon and glacial-transition climates is, therefore, expected to be less than 85 m because the monsoon and glacial-transition climates are warmer and dryer than the glacial climate (Sharpe 2003 [DIRS 161591]).

Interpretation of the water levels in wells at the southern end of Crater Flat, in relation to water-table rise, is complicated by several factors. The paleospring discharge locations at the southern end of Crater Flat are not along the flow path from Yucca Mountain. Also, a higher groundwater flow rate (increased hydraulic gradient) is expected under future wetter climatic conditions. However, the principles of hydrogeology specify that a uniform rise in the water table could only occur if the increased saturated thickness (and its effect on transmissivity) accommodates the additional groundwater flow through the aquifer. For the geology within the model domain, an increase in gradient to accommodate the increase in flow results in a nonuniform water-table rise with higher increases upgradient of flow. A higher groundwater flow rate implies a higher hydraulic gradient, a larger transmissivity, or both along any given flow line. Thus, the water table at upgradient locations would be expected to rise more than the water table at downgradient locations, resulting in a nonuniform rise in the water table across the flow system.

Two-dimensional groundwater flow modeling of the response to doubling mean annual precipitation indicated a maximum water table rise of 130 m (430 ft) in the vicinity of Yucca Mountain (Czarnecki 1985 [DIRS 160149]). This result is potentially overestimated because the analysis by Czarnecki (1985 [DIRS 160149]) was limited to two dimensions. In addition, average precipitation under monsoon and glacial-transition climates is less than twice the present-day value in the Yucca Mountain area, and the percolation flux resulting from the precipitation increase was also conservatively modeled (Czarnecki 1985 [DIRS 160149]). More recent groundwater flow modeling of the regional flow system under paleoclimate conditions (the DVRFS) simulated water levels of 60 to 150 m (200 to 490 ft) higher than present below Yucca Mountain (D'Agnese et al. 1999 [DIRS 120425], p. 2). Coarse resolution of the numerical grid in this model is believed to have resulted in potential overestimation of water table rise (150 m).

The uncertainty in water-table rise has been evaluated by considering these multiple lines of evidence and new geochemical data using a multidisciplinary workshop approach, as documented by *Total System Performance Assessment Model/Analysis for the License Application* (SNL 2007 [DIRS 178871]). Given that these various sources of information on water-table rise result in significant variations in the estimate and that none of the sources is clearly definitive, a subjective approach to quantifying uncertainty was used and a consensus

6.7 UNCERTAINTY

Characterizing and understanding the flow through the saturated zone is important for assessing the overall containment strategy for safely sequestering radioactive materials at the Yucca Mountain repository. Uncertainty in flow modeling arises from a number of sources including, but not limited to, the conceptual model of the processes affecting groundwater flow, water–level measurements and simplifications of the model geometry, boundary conditions, hydrogeologic unit extent and depth, and the values of permeability assigned to hydrogeologic units. This section discusses and attempts to quantify uncertainties in the SZ site-scale flow model because all uncertainty contributes to inaccuracy in system representation and response (uncertainty in model predictions). Such uncertainty is an inescapable aspect of geologic modeling. In addition to the discussion in this section, parameter uncertainty is addressed in the model abstraction document (SNL 2007 [DIRS 181650], Table 6-7[a]) and a thorough discussion of uncertainty analysis is given in Appendices H and I. *Saturated Zone Flow and Transport Model Abstraction* (SNL 2007 [DIRS 181650], Sections 6.5.2.1 and Figure 6-2[a]) includes additional quantitative analysis on horizontal anisotropy in permeability and groundwater specific discharge. *Saturated Zone In-Situ Testing* (SNL 2007 [DIRS 177394]) addresses the uncertainty related to the spatial distribution of the observation wells. Overall, it is understood that model predictions are always uncertain, thus it is important to minimize and quantify this uncertainty. It should be noted that the uses of PEST V11.1 (STN: 611582-11.1-00; [DIRS 179480]) and SPDIS (STN: 611598-00-00; [DIRS 180546]) are non-quality affecting analyses of the qualified results produced by PEST V5.5 (STN: 10289-5.5-00 [DIRS 161564]) and that they in no way change the conclusions of this report. Instead, this analysis sheds light on some of the details going on behind the scenes during the calibration process (e.g., differentiating null from solution space errors and evaluating data worth and parameter importance).

Estimating uncertainty in a modeled process is a wide ranging field of active research spanning many disciplines including hydrologic modeling, surface water flow and transport, medical imaging, geophysics, etc. A fundamental aspect of geologic modeling is the calibration phase where model parameters (in this case permeabilities) are adjusted until the model's replication of historical field measurements is judged to be "reasonably good." It is then assumed that this constitutes sufficient justification to use the model to make predictions to be used in site management. For the SZ site-scale flow model developed here, PEST (STN: 10289-5.5-00; [DIRS 161564], Watermark Numerical Computing 2004 [DIRS 178612]) was used to minimize the objective function comprising a weighted sum of squares of water-level measurements and fluxes across the lateral model boundaries (minimize the differences between measured and modeled data). Additional information was also used to hand calibrate the model, namely gradients that indicate that flowpaths emanating from below the repository should travel in a southeasterly direction. Future efforts could explicitly include soft data (e.g., local specific discharge estimates from well tests or elicitation) in the PEST calibration process.

When performing an uncertainty assessment on model results, which are solely dependent upon the parameter values supplied to the model, it is important to recognize two fundamental types of uncertainty in a model: null space and solution space uncertainties (see Appendix H). Null space uncertainty is that which arises in a calibrated model prediction due to the necessary simplifications made during model development (e.g., using a predefined HFM, applying constant BCs, representing heterogeneity with a homogenized geologic unit, single porosity

significantly different predicted model metrics, like specific discharge). Thus, null space uncertainty is the uncertainty in the prediction from a calibrated model due to the inability of the calibrating data set to inform those parameters that contribute to the model output metric (in this case, prediction of specific discharge). Recent advances in uncertainty assessment facilitate quantification of the null space error despite the inability to reduce it (given a specified, calibrated model and data set).

6.7.1 Uncertainty in Specific Discharge

In previous flow and transport and abstraction models of the SZ, the specific discharge was varied from one-tenth of its nominal value to ten times its nominal value in performance assessment calculations (BSC 2001 [DIRS 157132], Section 6.2.5). Based on recent calibration experience and the evaluation of permeability data from Yucca Mountain and other sites, the range was reduced to 1/8.93 times its nominal value to 8.93 times the nominal value (SNL 2007 [DIRS 181650], Figure 6-2[a]). The nominal value is obtained from a predictive run of the calibrated SZ site-scale flow model (Section 6.5). It should be noted that because the numerical model is linear, the calibration of the model can be preserved by scaling the fluxes, recharge, and permeabilities by exactly the same ratio. A new uncertainty analysis procedure is available in recent releases of the PEST software. Although PEST V11.1 is not qualified, it is still extremely useful in analyzing and describing the results from qualified codes. A general introduction and discussion of the latest techniques in uncertainty and sensitivity analyses is presented in Appendices H and I.

The PEST V11.1 (STN: 611582-11.1-00; [DIRS 179480]) PREDVAR suite of codes (Doherty 2006 [DIRS 178613]) was used to analyze FEHM's predictive uncertainty for specific discharge. First, null space and solution space uncertainties are quantified. This analysis, if done a priori, can help to determine if calibrating the conceptual model to the existing dataset will significantly reduce uncertainty in the selected predictive model metric. The effect of calibrating each model parameter (or each set of parameters when considering the permeability multipliers for the altered northern region, which were lumped) in reducing uncertainty in specific discharge 5 km from the repository is presented in Figure 6-26. Red bars are normalized contributions to uncertainty (they have unit sum) in specific discharge from uncalibrated parameters and blue bars are the same contribution from calibrated parameters. This figure can be interpreted as the answer to the following question: Assuming perfect knowledge of a parameter, how do the rest contribute to reduction in uncertainty of a prediction? Specifically, the contribution of calibrating each parameter with respect to reducing uncertainty in specific discharge is illustrated. There is seemingly little value gained in reducing uncertainty in specific discharge across the 5-km boundary through the calibration process. The uncertainty for specific discharge decreased 56% after calibration. It is not surprising to see such a small reduction in predictive uncertainty for specific discharge because calibration data did not include an estimate for specific discharge. If a specific discharge measurement was explicitly included in the automatic calibration process, a greater reduction in uncertainty would be expected. In these figures, a parameter's "contribution" to uncertainty is assessed through repeating the predictive uncertainty analysis under an assumption of perfect knowledge of that parameter type and measuring the decrease in predictive error thereby incurred. That is, each parameter is sequentially assigned it calibrated value with zero error bars and the resulting impact on decreased uncertainty in a prediction is assessed. In some circumstances, post-calibration

analysis of its potential worth to the calibration process. Figure 6-27 shows the relative worth of groups of observations for reducing specific discharge uncertainty. Not surprisingly, observation groups NYE COUNTY, CRATER FLAT, and FLUX are important observations for reducing predictive uncertainty in specific discharge. FLUX is important because it directly impacts overall flows through the model and should therefore be important to specific discharges throughout the model domain. Head observations in the altered northern region (HIGH HEAD), along the inferred flow path (PATH), and those considered perched (PERCHED) are of lesser importance in reducing uncertainty in specific discharge.

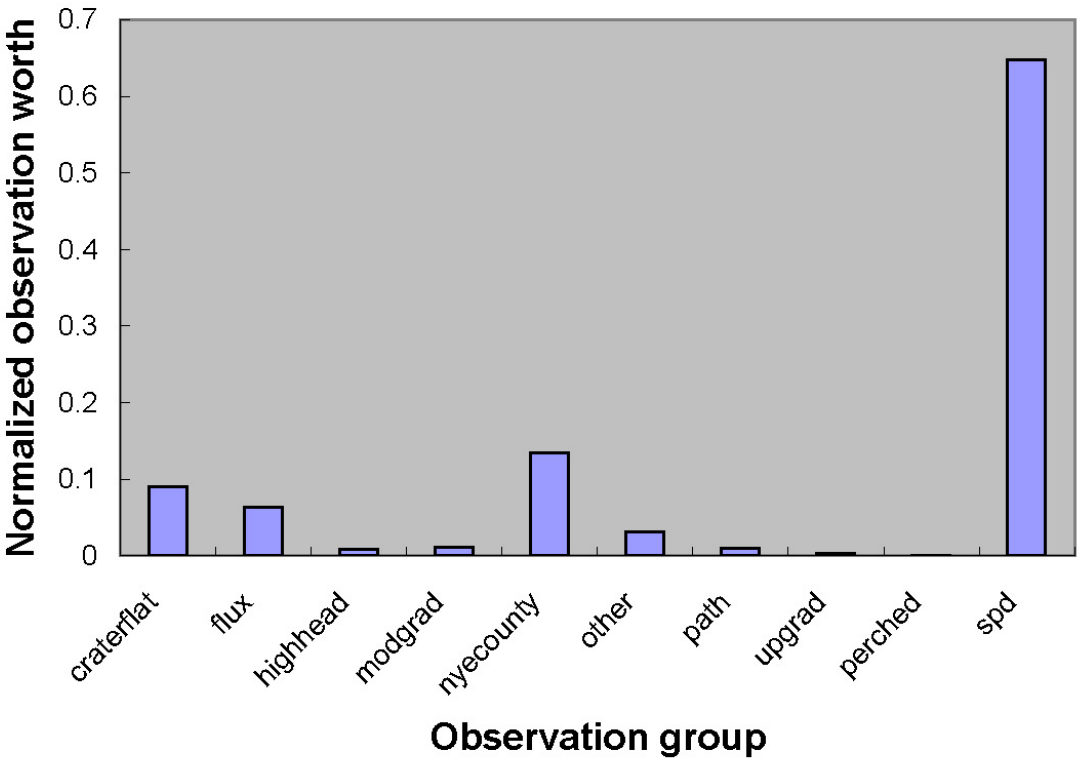

Source: Output DTN: SN0705T0510106.009.

NOTE: Observation groups are listed and defined in Table 6-9, "flux" are the boundary flux target observations and "spd" Is a hypothetical specific discharge observation that could be used in calibration.

Figure 6-27. Value of Observation Group to Reducing Uncertainty in Specific Discharge

6.7.2 Nonlinear Analysis

A methodology for nonlinear analysis of predictive error was applied to the Yucca Mountain model. Its theoretical basis is described in Appendix I. Applying the nonlinear analysis to the specific discharge prediction made by the SZ flow model yielded a maximum of 1.60 m/yr across the 5-km boundary (less than a factor of three times the maximum value of 0.66 m/yr). The nonlinear analysis is undertaken such that model calibration is maintained and only the null space is modified. By changing combinations of parameters that make no impact on the calibration objective function (weighted RMSE between modeled and measured head data and

boundary fluxes), the specific discharge was maximized to a value of 1.60 m/yr (Output DTN: SN0705T0510106.009). This indicates that even a model maintaining calibration can have significant "wiggle room" in its predictions. Note also that this maximization process was undertaken with the specific intent of seeing just how high the specific discharge could go for a nominally calibrated model. The chances for the exact combination of (null space) parameters required to make this happen in real life is low and this maximized specific discharge therefore represents a reasonable upper bound for this calibrated model. Furthermore, visualization of the flow field arising from this combination of permeabilities yielded an unrealistic scenario where flow exited the eastern boundary of the model.

6.7.3 Discussion of the Effect of Hydrogeologic Contact Uncertainty on Specific Discharge

The HFM conceptual model for the SZ site-scale flow model was created from a variety of field data and exists in electronic form as Earthvision surfaces (SNL 2007 [DIRS 174109]). There is uncertainty in the spatial positions of these surfaces primarily due to lack of data. These surfaces were used to generate the finite-element mesh such that each element is assigned those hydrogeologic properties found at the center of the element as discussed in Section 6.4.3.1. There is interest in how uncertainties in the representation of hydrogeologic-unit horizontal locations affect flux or specific discharge calculations. Due to the coarseness of the finite-element mesh, some horizontal uncertainty in the HFM can be entertained. As long as the horizontal spatial ambiguity in the location of hydrogeologic contacts is less than 125 m (one-half the grid block dimension), there is essentially zero impact on model specific discharge or flux calculations.

Because flow leaving the repository area is confined to a few of the most permeable units, the vertical dimension deserves special consideration. From the SZ site-scale flow model, it is known that the fluid leaves the repository area through the Crater Flat Tuffs and migrates to alluvial units. The flow paths in areal and vertical views are reproduced in Figure 6-17. Note that the vertical thickness of the flowing zone varies between 25 and 400 m, and the elevation changes from 400 to 700 m above sea level. From Table 6-4, the spacing in this part of the finite element mesh varies from 10 to 50 m. Consider, for example, that the uncertainty in the vertical location of a geologic contact is 50 m in the portion of the model where the flow path is 400 m thick. Changing a single element's hydrogeologic designation, either to or from one unit to another could not result in a change to the average local specific discharge by more than a factor of 50/400 (13%). This is well within the overall specific discharge uncertainty range (Section 6.7.1). The vertically thin flow path south of UTM Northing coordinates 4,065,000 m (Figure 6-17) results in a greater impact from geologic uncertainty. Here the fluid flow is vertically constrained to about 25 m. If the bottom contact of the local hydrogeologic unit were to change by 10 m (the thickness of a single layer), this could result in a change to the average specific discharge in that area of up to 40%. Integrated specific discharge calculations will be affected to a lesser degree. A study of the impacts of hydrogeologic contact location uncertainty reveals:

- Sensitivity to uncertainty in the hydrogeologic contact surfaces in the horizontal directions is much less than in the vertical direction due to the averaging effect of 250-m grid block spacing

- The change in specific discharge due to the 50-m uncertainty in the vertical hydrogeologic surface can produce up to a 13% change in the local specific discharge near the repository and in the alluvial flow regions

- 10-m uncertainty in the vertical hydrogeologic surface can produce up to a 40% change in the local specific discharge in the transitional zone (south of UTM Northing 4,065,000 m).

Because of the averaging effect across elements in the integrated specific-discharge calculations (0 to 18 km), a 50% regional change in a relatively small portion of the 0- to 18-km compliance boundary affects model results only moderately. The range of uncertainty considered for specific discharge in the SZ flow and transport abstractions model is significantly greater than the uncertainty in the HFM (SNL 2007 [DIRS 174109], Section 6.4.3).

6.7.4 Site Data

In the 18-km compliance region (green line on Figure 6-17), performance assessment calculations are also strongly influenced by travel of fluid in the alluvial aquifer. Estimates of groundwater specific discharge in the SZ have been obtained from field-testing at the ATC (SNL 2007 [DIRS 177394], Section 6.4.5). The ATC is approximately located at the boundary of the accessible environment, as specified in regulations for the Yucca Mountain Project, 10 CFR 63.302 [DIRS 176544]. The location of the ATC is approximately 18 km from Yucca Mountain, and testing was performed in the alluvium aquifer. Estimates of groundwater specific discharge at the ATC range from 0.47 to 5.4 m/yr (DTN: LA0303PR831231.002 [DIRS 163561]; SNL 2007 [DIRS 177394], Table 6.5-6). From the calibrated SZ site-scale flow model, the specific discharge to the 18-km compliance boundary is 0.55 m/yr. This calculation integrates transport through all volcanic and alluvial units from introduction below the repository to the 18-km compliance boundary and its relatively low value can partially be attributed to slow flows through the volcanic units.

In addition to the information from the Expert Elicitation Panel (CRWMS M&O 1998 [DIRS 100353]) (related to specific discharge in the volcanics), other data are available for specific discharge in the alluvium (SNL 2007 [DIRS 177394], Tables 6.5-5 and 6.5-6). The measured specific discharge at the ATC spans a factor of 7.8 (i.e., 1.2 to 9.4 m/yr) while at NC-EWDP-22S the range was 11.5 (0.47 to 5.4 m/yr). There are no site data available for specific discharge in volcanic units, but the Expert Elicitation Panel (CRWMS M&O 1998 [DIRS 100353], p. 3-43) typically suggested larger ranges (approximately two orders of magnitude or more). A factor of 1/8.93 to 8.93 times the nominal value that combines volcanic and alluvial uncertainties with Bayesian updating is used as a multiplier for the specific discharge throughout the model domain in the latest performance assessment calculations (SNL 2007 [DIRS 181650], Figure 6-2[a]). It is worth noting that the specific discharge is variable along any given flowpath and that it can either increase or decrease locally due to flow focusing, hence significant variability and uncertainty is expected locally, but these fluctuations are smoothed when averaged over kilometer-scale portions of the model domain. For example, across the 100 flow paths in the calibrated model, the range of specific discharges spans approximately an order of magnitude across both the 5- and 18-km boundaries. Nevertheless, the overarching criterion that the range in uncertainty of specific discharge encapsulate

uncertainty within the domain (with minimal overestimation) is met by TSPA. Historical details of the specific discharge multiplier distribution and associated sampling techniques, including figures, are contained in *Saturated Zone Flow and Transport Model Abstraction* (SNL 2007 [DIRS 181650], Figure 6-2[a]) and no differentiation is made between specific discharge in the volcanics or alluvium.

6.7.5 Remaining Uncertainties in Specific Discharge Estimates

The analyses and corresponding assignment of an uncertainty range for the groundwater specific discharge assume that the porous continuum approach is appropriate for the fractured volcanic tuffs. A remaining uncertainty is whether or not the continuum approach can be employed at the scale of the model. An alternative conceptual model not yet explicitly examined is one in which most of the flow from Yucca Mountain moves through faults rather than through the unfaulted rock. To test this alternative model, the known faults need to be included explicitly in the numerical grid of the SZ site-scale flow and transport models. Although the grid-generation and flow-calculation capabilities exist to do this, the need to calibrate the model efficiently and perform particle-tracking transport simulations has taken priority and led to the adoption of structured grids that make explicit inclusion of faults difficult. Important faults are included in the model to capture their impact on flow and transport. Furthermore, the adoption of a range that includes larger specific discharge values and smaller effective porosities introduces realizations that replicate the behavior of a fault-dominated flow and transport system. Therefore, the suite of performance assessment transport simulations currently used likely encompasses the range of behavior that would be obtained with a fault-based flow and transport model.

Finally, it is noted that model linearity assures that a global, constant-multiplier increase in permeability and corresponding increase in infiltration will yield an equal increase in specific discharge throughout the model domain without impacting the head RMSE. Although the net infiltration was defined by specified data sets (Belcher 2004 [DIRS 173179]; BSC 2004 [DIRS 169861]; Savard 1998 [DIRS 102213]), model permeabilities could be globally adjusted such that flux through the southern boundary increased to match that of the regional model (discussed in Section 6.5.2.2). The resulting 23% increase in specific discharge throughout the model domain is still within the uncertainty range of the entire SZ site-scale flow model and well within the specific discharge multiplier used in TSPA (SNL 2007 [DIRS 181650]); also see Sections 6.7.1, 6.7.4, 7.2.3, and 8.3.1 of this document).

6.7.6 Effect of Perched Water on Flow Paths and Specific Discharge

Perched water was not explicitly modeled in the SZ site-scale flow model because the weights applied to these observations were insignificant (0.1). It is noted that the conceptualization of the LHG through introduction of the altered northern region yielded water levels in wells UE-25 WT#6 and USW G-2 (suspected to be perched) that were much lower than the reported water levels. From Table 6-8, it can be seen that some modeled water levels are about 150 m lower than the data in this area to the north of Yucca Mountain; but this is consistent with the perched water-level interpretation in that area (BSC 2004 [DIRS 170009], Section 5). The area of suspected perched water is near the steepest hydraulic gradient in the model and these hydraulic gradients occur over only a few model elements. Thus, if there is some specific reason

7.1.3 Confidence Building After Model Development to Support the Scientific Basis of the Model

Model validation requires that mathematical models be validated by one or more of several methods given in Section 6.3.2 (1st and 9th bullets) of SCI-PRO-006. Validation of the SZ site-scale flow model as related to the procedural requirements mandates the following:

1. SCI-PRO-006, Section 6.3.2 (1st bullet): Corroboration of model results with the laboratory, field experiments, analog studies, or other relevant observations, not previously used to develop or calibrate the model.

   The SZ site-scale flow model was validated by comparing results from this model with the laboratory and field experiment and other observations. The validation criteria, testing, and results are described in detail in Section 7.2 of this report. Based on material presented in these sections, this criterion is considered satisfied.

2. SCI-PRO-006, Section 6.3.2 (9th bullet): Technical review through publication in a refereed professional journal. Although this is not required by the TWP, this post-development model validation activity adds to the confidence in the SZ site-scale flow model.

   A previous version of the SZ site-scale flow model and its results are described in the referenced professional publications by Eddebbarh et al. (2003 [DIRS 163577]) and Zyvoloski et al. (2003 [DIRS 163341]). These publications demonstrate additional confidence in the model, when taken in conjunction with the model validation activity described in Item 1 above because the same modeling techniques were used in this report. Moreover, this revision is based on an improved and updated HFM with more accurate fault locations, more than four times as many grid nodes, and a calibration that yielded a lower residual (weighted RMSE).

7.2 VALIDATION RESULTS

The validation activities for the SZ site-scale flow model are carried out according to *Technical Work Plan for Saturated Zone Flow and Transport Modeling* (SNL 2007 [DIRS 177375], Section 2.2), which requires Level II model validation of the SZ site-scale flow model based on its relative importance to the performance assessment for the repository. The TWP states that the validation will include confidence building activities implemented during model development. In addition, it states that post-development model validation will consist of a comparison of simulated flowpaths to those derived from hydrochemistry and isotope analyses, plus two or more other comparisons as indicated in the technical work plan.

Water levels and gradients. For purposes of postdevelopment model validation, a comparison of simulated and observed water levels for all new water-level data is presented in Section 7.2.1. This comparison focuses on the NC-EWDP Phase V water-level data (DTN: MO0612NYE07122.370 [DIRS 179337]). A comparison of simulated and observed gradients along the flowpath from the repository is also presented to evaluate the impact of the difference between observed and simulated water levels on the estimates of specific discharge. Specific discharge is directly proportional to the hydraulic gradient. As previously established in

To further validate the SZ site-scale flow model, a comparison was made of the hydraulic gradients along the flowpath using water-level data from two wells that were not used during calibration (NC-EWDP-22PC and -32P). Table 7-3 presents gradients calculated for postdevelopment model validation. Predicted gradients are about a factor of two lower than observed because the model does not capture the rapid water level change near U.S. Highway 95 fault. However, this region is south of the region of primary interest and, as discussed in Section 7.1.3, the model reproduces observed gradients over the relevant portion of the flowpath from the repository through Fortymile Wash to U.S. Highway 95 quite well. The validation is considered successful because the simulated hydraulic gradient agrees to within 50% with gradient calculations from data.

Table 7-3. Predicted and Observed Hydraulic Gradients for Post-Development Validation

Flow Segment	$\Delta H/\Delta L$ (Measured)	$\Delta H/\Delta L$ (Simulated)	Relative Error
NC-EWDP-24PB to NC-EWDP-32P	3.22×10^{-3}	1.81×10^{-3}	−0.44
NC-EWDP-22PC to NC-EWDP-32P	2.49×10^{-3}	1.39×10^{-3}	−0.44

Sources: DTNs: GS010908312332.002 [DIRS 163555] (non-NC-EWDP wells); SN0612T0510106.004 (modeled heads).

Output DTN: SN0702T0510106.007 (NC-EWDP aggregated Phase III, IV, and V well data).

NOTE: Calculations are from data in Table 7-2.

7.2.2 Comparison of Calibrated Effective Permeabilities to Field Test Results

The numerical model was calibrated by adjusting permeability values for individual hydrogeologic units in the model until the sum of the weighted residuals squared (the objective function) was minimized. The residuals include the differences between the measured and simulated hydraulic heads and the differences between the groundwater fluxes simulated with the SZ regional- and the site-scale models. Permeabilities estimated from hydraulic tests were neither formally included in the calibration nor considered in the calculation of the objective function. The field-derived permeabilities were instead used to check on the reasonableness of the final permeability estimates produced by the calibration.

Discussions of the permeability data from the Yucca Mountain area and nearby NTS as well as the Apache Leap site in Arizona are presented in the following subsections. A discussion of the general inferences about permeability that can be drawn from regional observations is also presented. Following these discussions, a comparison of calibrated effective permeabilities with the 95% confidence interval on the mean of measured permeability values is presented, including the analysis of the potential impact of calibrated permeability values on groundwater specific discharge.

7.2.2.1 General Permeability Data

Many factors affect the permeability of volcanic rocks at Yucca Mountain including: (1) the tendency of the rock either to fracture or to deform plastically in response to stress; (2) the ability of the rock to maintain open fractures, which is a function of the strength of the rock and overburden stress; (3) proximity to major zones of deformation, such as fault zones; and, (4) the degree of mineralization or alteration that would tend to seal fractures and faults. Other factors

(Patterson 1999 [DIRS 158824]) indicates that the formation generally has low permeability compared to the rate of water infiltrating into the unsaturated zone, which has been estimated to range between 1.5 and 48.2 mm/yr in the vicinity of the repository under the present climate (SNL 2007 [DIRS 174294], Table 6.5.7.1-2). Water flowing under a unit gradient at a rate of 10 mm/yr (3.17×10^{-10} m/s) would seep through a rock having a permeability of $0.0000323 \times 10^{-12}$ m^2 (assuming a viscosity of 0.001 N-s/m^2 and a water density of 1,000 kg/m^3); so the field-scale vertical permeability of the Calico Hills Formation, which includes the effects of fracturing, presumably has permeabilities less than this value. Based on core measurements, the geometric-mean hydraulic conductivity for the zeolitic Calico Hills Formation is 2.2×10^{-11} m/s (DTN: MO0605SPAFABRP.004 [DIRS 180539], file: *Analysis of source data.zip*), which is significantly higher than the low permeability ($0.0000323 \times 10^{-12}$ m^2) thought necessary for perched water. The calibrated effective permeability for the Calico Hills Volcanic unit was 0.46×10^{-12} m^2, which is on par with results from cross-hole testing.

7.2.2.1.2 Alluvial Testing Complex

From July through November 2000, pumping tests were conducted in well NC-EWDP-19D. The first test involved production from the entire saturated thickness of 136 m. The results indicated a transmissivity of about 21 m^2/day and an average hydraulic conductivity of 0.15 m/day, approximately equivalent to a permeability of 0.2×10^{-12} m^2 (SNL 2007 [DIRS 177394], Section 6.4.5 and Appendix F7). Subsequently, four screened intervals having a combined thickness of 84 m were tested individually. The combined transmissivities of these intervals totaled about 145 m^2/day, greatly exceeding the transmissivity determined for the initial open-hole test. There are at least two likely causes for the discrepancy. First, pumping apparently resulted in further well development, as fine materials were drawn into the well and discharged with the water. Second, the screened intervals are probably interconnected hydraulically, consistent with the complexity of fluvial-alluvial depositional environments, so that actual thicknesses of the producing zones were significantly greater than the screened intervals. The average permeability of the section is probably greater than the initial permeability determined from the open-hole test (0.2×10^{-12} m^2) but less than those calculated for the two deeper screened intervals, 1.5×10^{-12} and 3.3×10^{-12} m^2. Although thin, discontinuous zones may locally have higher permeabilities, these results indicate that significantly thick (greater than 10 m) and areally extensive zones at NC-EWDP-19D probably have average permeabilities between 0.1×10^{-12} and 1×10^{-12} m^2 (SNL 2007 [DIRS 177394], Sections 6.4.5 and Appendix F7).

7.2.2.1.3 Apache Leap

Fractured welded tuffs and relatively unfractured nonwelded tuffs occur both above and below the water table. Permeabilities measured in the unsaturated zone at Yucca Mountain using air may, therefore, have some relevance to the permeability values of similar rocks located below the water table. In the unsaturated zone, air-injection tests have been conducted from surface-based boreholes in both welded and nonwelded tuffs (LeCain 1997 [DIRS 100153]) and from test alcoves in and adjacent to the Ghost Dance Fault zone in the densely welded Topopah Spring tuff (LeCain et al. 2000 [DIRS 144612]). At Yucca Mountain, no water-injection tests were done in these same intervals to directly compare to the results of the air-injection tests. However, some understanding of the probable relation between permeabilities estimated from

account for heterogeneity and departures of the actual flow field from the assumed flow geometry.

7.2.2.1.4 Tuffaceous Formations

The Prow Pass, Bullfrog, and Tram tuffs of the Crater Flat group contain both nonwelded to partially welded margins and partially to densely welded interiors (Bish and Chipera 1989 [DIRS 101195]; Loeven 1993 [DIRS 101258]). The initially vitric nonwelded to partially welded margins of these units have been largely altered to zeolites during hydrothermal events as a result of their thermodynamically unstable glass composition and their initially high permeabilities (Broxton et al. 1987 [DIRS 102004]). The partially to densely welded parts of these units have devitrified to mostly quartz and feldspar and have higher matrix permeabilities than the nonwelded to partially welded zeolitized margins (Loeven 1993 [DIRS 101258]). Additionally, because the welded parts of the tuffs have a greater tendency to fracture, the densely welded parts of these units generally have higher secondary permeability. Thus, unless faults are locally present, the densely welded parts of the Prow Pass, Bullfrog, and Tram tuffs are expected to have substantially higher permeability than the nonwelded margins.

The densely welded parts of the Prow Pass, Bullfrog, and Tram tuffs are likely to have mean permeabilities that are less than the mean air permeabilities of the Tiva Canyon ($k = 4.7 \times 10^{-12}$ m^2) or Topopah Spring ($k = 0.75 \times 10^{-12}$ m^2) tuffs estimated from air-permeability tests (see Section 7.2.2.1.3). This likelihood is because greater lithostatic stresses at depth tend to close fractures and successive hydrothermal events have caused increasing degrees of alteration with depth (Broxton et al. 1987 [DIRS 102004]). Figure 7-3 shows the geometric-mean permeabilities from the single-hole air-permeability tests for the Tiva Canyon and Topopah Spring tuffs and the geometric-mean single-hole water permeabilities calculated for the Calico Hills Formation and the Prow Pass, Bullfrog, Tram, and Lithic Ridge tuffs. The single-hole permeabilities show the expected trends of decreasing permeability with depth. Conversely, the trends in the cross-hole permeability data from the C-wells (see Section 7.2.2.3.2 and Section 7.2.2.6, Figure 7-4) are exactly opposite those expected based on geologic reasoning; these trends could, however, reflect the proximity of each hydrogeologic unit to the Midway Valley fault, which intersects the C-wells in the upper part of the Tram tuff (Geldon et al. 1998 [DIRS 129721], Figure 3). Thus, it appears that permeability trends with depth at the C-wells are controlled by local conditions and do not reflect general trends in permeability established by the single-hole tests and expected from geologic reasoning.

permeability, the Lower Carbonate Aquifer remained the primary water bearing unit in the model.

Overall, the calibrated effective permeabilities show trends consistent with permeability data from Yucca Mountain and elsewhere at the NTS. The calibrated effective permeability of the three Crater Flat tuffs and Calico Hills formation are all within the values measured in the field. The relatively high permeability estimated for the Tram tuff from the cross-hole tests may be at least partially attributable to local conditions at the site of these tests. A breccia zone is present in the Tram tuff at boreholes UE-25 c#2 and UE-25 c#3 (Geldon et al. 1997 [DIRS 100397], Figure 3) that may have contributed to a local enhancement in the permeability of the Tram tuff.

Calibrated effective permeabilities for units corresponding to the Lava Flow Aquifer and the valley fill aquifer are within the range of measured permeabilities. The calibrated effective permeabilities of units corresponding to the Welded Tuff Aquifer are more than an order of magnitude lower than field estimates, but no confidence intervals are available and calibrated values would probably fall within these limits if they were available.

7.2.3 Specific Discharge

Although the calibrated permeabilities of any geologic unit or feature in the SZ site-scale flow model indirectly influence the simulated specific discharge, those geologic units along the flowpath from the repository to the compliance boundary directly determine the simulated specific discharge. Particle tracking using the SZ site-scale model (see Section 6.5.2.4) indicates that fluid particles migrating from the repository generally enter the SZ in the Crater Flat units (see Figure 6-22). Because of the high permeabilities of these units and the small hydraulic gradient, the particles remain in those units until reaching their southern ends. At this point, flow generally enters the alluvial portion of the flow system after briefly transitioning through the Paintbrush Volcanic Aquifer. The flowpath through the alluvial deposits is represented in the SZ site-scale model by the Lower Fortymile Wash alluvium. Thus, those calibrated permeabilities that most directly control the simulation of specific discharge by the SZ site-scale model are those for the Crater Flat units and the Lower Fortymile Wash alluvia.

Specific discharge across the 18-km compliance boundary (see the green line on Figure 6-17) and discussed throughout other documents (SNL 2007 [DIRS 177392]) is strongly influenced by groundwater flow in alluvium. Estimates of specific discharge in the SZ were recently obtained from field-testing at the ATC (SNL 2007 [DIRS 177394], Section 6.5.5). The ATC is located approximately 18 km from Yucca Mountain at the boundary of the accessible environment as specified at 10 CFR 63.302 [DIRS 176544]. The specific discharge from the repository to the 18-km compliance boundary was 0.55 m/yr (average across all flowpath lengths divided by travel times), although much of the time along this flowpath is spent in the slower flowing volcanic units indicating that the specific discharge in the alluvial material is higher than in the volcanics. The technique used to estimate specific discharge at locations within the SZ site-scale flow model corresponding to the locations where measurements are available (UE-25 c#3, NC-EWDP-22S, and NC-EWDP-19P) was to isolate a cubic volume within 1,000 m of the well location extended to 10 m above and below the entire open interval and to calculate the average specific discharge across all flowing nodes. The ATC testing was performed in the alluvium aquifer and estimates of groundwater specific discharge at the ATC range from 0.5 to 12 m/yr.

The simulated average specific discharge across the 5-km boundary ranges from 0.35 to 0.38 m/yr for differing values of horizontal anisotropy in permeability ranging from 20 to 0.05 (0.36 m/yr for the expected horizontal anisotropy values of 5:1 N-S to E-W with end members of the 100-particle distribution of 0.11 to 0.66 m/yr). This compares to the 0.6 m/yr derived by the Expert Elicitation Panel (CRWMS M&O 1998 [DIRS 100353], Section 3.2) and is also within their range, which actually spans nearly five orders of magnitude. The data from ATC field testing yielded specific discharge estimates ranging from 1.2 to 9.4 m/yr while testing at NC-EWDP-22S ranged from 0.47 to 5.4 m/yr. A distribution of specific discharge multipliers was developed (SNL 2007 [DIRS 181650], Figure 6-7) that ranged from 1/30th to 10 times the nominal value. Recently, that range was reduced to 1/8.93 and 8.93 times nominal specific discharge (SNL 2007 [DIRS 181650], Figure 6-2[a]). In addition to a distribution in specific discharge, uncertainty in effective porosity (variable effective porosity in conjunction with specific discharge can result in highly variable flow velocities through the SZ) is implemented through the use of a truncated normal distribution in the SZ transport abstraction model (SNL 2007 [DIRS 181650], Section 6.5.2.3). The details of the uncertainty distributions of specific discharge multiplier and effective porosity in the alluvium and their associated sampling techniques are contained in the SZ flow and transport abstraction model (SNL 2007 [DIRS 181650], Table 6-7[a]).

7.2.4 Comparison of Hydrochemical Data Trends with Calculated Particle Pathways

Groundwater flowpaths and mixing zones were identified in Appendices A and B in the analyses of the areal distributions of measured and calculated geochemical and isotopic parameters, scatter plots, and inverse mixing and reaction models Flowpaths of tracer particles were calculated with the SZ site-scale flow model. The particles were started below the repository footprint and allowed to transport downstream to the model boundary. These flow pathways are compared to flowpaths deduced from hydrochemical data shown in Figure 7-5. These flowpaths must be evaluated in the context of the hydraulic gradient while considering the possibility that flowpaths can be oblique to the potentiometric gradient because of anisotropy in permeability. These flowpaths were drawn by first using chemical and isotopic constituents generally considered to behave conservatively in groundwater such as chloride (Cl^-) and sulfate (SO_4^{2-}) ions. However, because no single chemical or isotopic species varies sufficiently to determine flowpaths everywhere in the study area, multiple lines of evidence were used to construct the flowpaths. This evidence includes the areal distribution of chemical and isotopic species, sources of recharge, groundwater ages and evaluation of mixing/groundwater evolution through scatter plots, and inverse mixing and reaction models as presented in Appendices A and B. The derivation of flow pathways from hydrochemical data is developed in detail in Appendices A and B and summarized in Sections B6.6 and B7.

Of particular interest are the Flow Paths 2 and 7 from this analysis. As shown in Figure 7-5, Flow Path 7 originates in the vicinity of the repository footprint and overlaps the model-calculated flowpaths. Flow Path 2 is also of interest, although it originates northeast of the repository, because it closely bounds Flow Path 7 to the east. Although flow pathways derived from hydrochemical data do not originate in the same location as particle tracks derived from the site-scale model, the paths converge east and south of the repository.

Table 8-1. Output Data

DTN	Intermediary?	Description
LA0612RR150304.001	Yes	NC-EWDP UTM coordinates
LA0612RR150304.002	Yes	Underground Testing Area geochemical data
LA0612RR150304.003	Yes	NC-EWDP geochemical data
LA0612RR150304.004	Yes	Hydrochemical flowpaths
LA0612RR150304.005	Yes	Uranium activity ratios for groundwaters
LA0612TM831231.001	No	LaGriT HFM2006 surfaces
MO0611SCALEFLW.000	No	Potentiometric surface
SN0610T0510106.001	Yes	NC-EWDP well location and water-level data
SN0612T0510106.003	Yes	Infiltration data
SN0612T0510106.004	No	SZ site-scale flow model output
SN0702T0510106.006	No	FEHM model of water table rise
SN0702T0510106.007	Yes	NC-EWDP well data used for SZ flow model potentiometric surface, calibration and validation
SN0704T0510106.008	No	Water-level and particle-track output from the calibrated model
SN0705T0510106.009	Yes	PEST v11.1 analyses

8.3 OUTPUT UNCERTAINTY

This section describes remaining uncertainties associated with the nominal flow field. Specifically, the section recommends how the uncertainty in metrics associated with model outputs (specific discharge and flowpaths) should be considered.

8.3.1 Specific Discharge Uncertainty Range

Because uncertainty in permeability translates into uncertainty in specific discharge (given a constant head gradient), insight gained when investigating permeability values during calibration has relevance to specific discharge estimates. Also, recall that for linear models such as this, calibration to hydraulic heads is preserved when scaling the fluxes, recharge, and permeabilities proportionally. The 95% confidence interval for calibrated permeabilities (Output DTN: SN0612T0510106.004, *sz_site_2006.rec*) typically spans 3 or more orders of magnitude. While this range could yield major changes in specific discharge in a homogeneous system, no single change in permeability by up to an order of magnitude yielded even a factor of 2 change in specific discharge because surrounding permeability values strongly impact the flow into/out of the altered unit. It can be concluded that even if calibrated permeabilities are in error by more than an order of magnitude for any given unit, the specific discharge output from the model will remain within the uncertainty limits developed elsewhere for use in TSPA (e.g., 1/8.93 to 8.93 times nominal value (SNL 2007 [DIRS 181650], Figure 6-2[a])). Experience with the calibrated SZ site-scale flow model indicates that the range of specific discharges used for TSPA is large enough to encapsulate all the uncertainties assumed during the development and calibration of this model.

The specific discharge from the repository to the 18-km compliance boundary is 0.55 m/yr, although much of the distance along this flowpath is in the slower flowing volcanic units indicating that the specific discharge in the alluvial material is higher than in the volcanics. The technique used to estimate specific discharge at locations within the SZ site-scale flow model alluvial material corresponding to the locations where measurements are available (NC-EWDP-22S, and NC-EWDP-19P) was to isolate a cubic volume within 1,000 m of the well location extending 10 m above and below the entire open interval and to calculate the average specific discharge across all flowing nodes. Measured groundwater specific discharges from alluvial pump tests range from 0.47 to 9.4 m/yr (SNL 2007 [DIRS 177394], Tables 6.5-5 and 6.5-6). For the expected flow porosity in the alluvium of 0.18 (SNL 2007 [DIRS 177394], Section 6.4), the field-test-derived specific discharges ranged from 0.89 m/yr at NC-EWDP-22S to 7.3 m/yr at NC-EWDP-19P. Model-simulated specific discharges at NC-EWDP-22S and -19P are 20.97 and 11.75 m/yr, respectively. These relatively high modeled values correspond to the high effective permeability assigned to the model unit for the Lower Fortymile Wash alluvium, but they are still within the factor of 3 of the upper end of test-derived expected value (7.3 m/yr) and therefore meet the validation criterion established by the TWP (BSC 2006 [DIRS 177375, Section 2.2.2.1). Comparatively little sensitivity was seen to horizontal anisotropy in the volcanics; the modeled average specific discharge across the 5-km boundary ranges from 0.35 to 0.38 m/yr for values of N-S to E-W horizontal anisotropy in permeability of 0.05 to 20, respectively (SNL 2007 [DIRS 177394], Section 6.2.6). Although there were no specific discharge measurements from the C-wells tests, the modeled value was estimated at 1.75 m/yr within 1,000 m of the C-wells. Finally, the nonlinear maximum calibrated specific discharge estimated across the 5-km boundary downgradient from the repository is 1.60 m/yr (Section 6.7.2 and Appendix I), which is just less than 3 times the maximum value of 0.66 m/yr. This combination of permeabilities was specifically selected to maximize specific discharge, which is still well within the range established by the specific discharge multiplier used in SZ abstraction models. That is, an uncertainty distribution in specific discharge is constructed where the nominal specific discharge is multiplied by 1/8.93 and 8.93 (SNL 2007 [DIRS 181650], Figure 6-2[a]). The details of the uncertainty distributions of specific discharge and effective porosity in the alluvium and their associated sampling techniques are outlined in the SZ abstraction model (SNL 2007 [DIRS 181650], Table 6-7[a]).

8.3.2 Flowpaths Uncertainty

The flowpaths from the water table beneath the repository to the accessible environment directly affect breakthrough curves and associated radionuclide transport times (recall that flowpath length is used to calculate specific discharge). Because the flowpaths are close to the water table and transition from the volcanic tuffs to the alluvium, flowpath uncertainty directly affects the length of flow in the volcanic tuffs and in the alluvium.

Uncertainty in flowpaths is affected by anisotropy in hydraulic properties of the volcanic tuffs. Large-scale anisotropy and heterogeneity were implemented in the SZ site-scale flow model through direct incorporation of known hydraulic features, faults, and fractures (see Section 6.7.10). Horizontal anisotropy in the volcanic units was derived from analysis of hydraulic testing at the C-wells (SNL 2007 [DIRS 177394], Section 6.2.6 and Appendix C6). This scientific analysis report also recommends an uncertainty range in anisotropy that should be used in the SZ site-scale flow model to account for uncertainty in the flowpaths and this

parameter was carried forward through to SZ abstraction modeling (SNL 2007 [DIRS 181650], Figure 6-2[a]). For isotropic permeability, average flowpath length to the 18-km compliance boundary is approximately 22.9 km. For anisotropy ratios of 20:1 and 0.05:1 (N-S:E-W), average flowpath lengths are 29.7 and 22.8 km, respectively. This is an acceptable range of variability in model results in light of the bounds established by geochemical analyses (Figure 7-5). Also, recall that 5 km of this difference can be attributed solely to the random initial distribution of particles below the repository.

The model is adequate for its intended use of providing flow-field simulations as input to the SZ site-scale transport model necessary to generate radionuclide breakthrough curves.

8.4 HOW THE APPLICABLE ACCEPTANCE CRITERIA ARE ADDRESSED

This section describes how the acceptance criteria in the YMRP (NRC 2003 [DIRS 163274], Section 2.2.1.3.8.3), *Flowpaths in the Saturated Zone*, are addressed by this report.

Acceptance Criteria from Section 2.2.1.3.8.3, *Flowpaths in the Saturated Zone*

Acceptance Criterion 1: *System Description and Model Integration Are Adequate.*

Subcriterion (1): Section 1 explains that this model generates SZ velocity fields which are used as inputs for the model of transport in the SZ and are abstracted in the TSPA. The important physical phenomena are adequately incorporated in the SZ abstraction process as described in the following subsections: hydraulic gradients (Section 6.3.1.4); vertical gradients (Section 6.3.1.5); lateral boundary conditions (Section 6.3.1.6); recharge (Section 6.3.1.7); discharge (Section 6.3.1.8); heterogeneity (Section 6.3.1.9); faults (Section 6.3.1.10); and groundwater flow processes (Section 6.3.2.). The discussion of groundwater table rise in Section 6.6.4 uses consistent and appropriate assumptions about climate change.

Subcriterion (2): Aspects of hydrology, geology and geochemistry that may affect flowpaths in the SZ are described adequately in Section 6.3 and Appendices A and B.

Subcriterion (4): Section 6.3.1.7 states that the recharge to the flow model was derived from three sources: regional-scale SZ model (Belcher 2004 [DIRS 173179]), 2003 UZ flow model (BSC 2004 [DIRS 169861]), and Fortymile Wash data (Savard 1998 [DIRS 102213]). Recharge from the UZ site-scale model (percolation flux) was taken as the flow through the base of that model, the domain of which includes approximately 40 km^2 (19.3 mi^2) that encompasses an area only slightly larger than the footprint of Yucca Mountain, a small fraction of the SZ model domain. The SZ site-scale flow model uses appropriate recharge values from flow in the unsaturated zone.

Subcriterion (5): Section 6.2 provides a road map to sections and FEPs document where sufficient data and technical bases to assess the degree to which FEPs have been included in the flowpaths.

Uncertainty in the quantification of specific discharge is discussed in Sections 6.7 and Appendix H. A nonlinear analysis is presented in Section 6.7.2 and Appendix I. There is general consistency between the specific discharge simulated by the model and the median of values of uncertainty ranges estimated by the SZ expert panel from testing data. Uncertainty in specific discharge is propagated forward to the TSPA.

Uncertainty in the hydrogeologic contacts is discussed in Section 6.7.3 and shown to have moderate effects in some cases. Accordingly, this uncertainty was determined not to warrant propagation to the TSPA. Additional uncertainties due to limitation in site data, conceptualization of the LHG, and representation of potentially perched water-level measurements, and fault conceptualizations are discussed in Sections 6.7.4 through 6.7.8. None of these uncertainties warrants propagation to TSPA.

Uncertainty due to scaling is discussed in Section 6.7.9 where it is concluded that such uncertainty does not significantly affect flow modeling.

Subcriterion (3): The conceptual model uncertainty considered in this report is consistent with available site characterization data and field measurements. The genesis of the conceptual model is discussed in Section 6.3. Alternative conceptual models are considered in Section 6.6. A thorough description of uncertainty, especially uncertainty associated with specific discharge estimates, is given in Section 6.7. Furthermore, an introduction on predictive variance uncertainty minimization and quantification is given in Appendix H. An extension of this theory to nonlinear predictive variance is outlined in Appendix I.

Subcriterion (4): Alternative modeling approaches are appropriate and consistent with available data and current scientific knowledge, and appropriately consider their results and limitations, using analyses that are sensitive to the processes modeled, as discussed above.

Acceptance Criteria from Section 2.2.1.1.3, *System Description and Demonstration of Multiple Barriers*

Acceptance Criterion 3: *Technical Basis for Barrier Capability is Adequately Presented.*

When considered together, reports associated with the saturated zone including this report, *Site-Scale Saturated Zone Transport* (SNL 2007 [DIRS 177392]), and *Saturated Zone Flow and Transport Model Abstraction* (SNL 2007 [DIRS 181650]) constitute an adequate description (including thorough discussions of uncertainty) of the saturated zone as a natural barrier to radionuclide release.

9. INPUTS AND REFERENCES

The following is a list of the references cited in this document. Column 1 contains the unique six-digit numerical identifiers (the Document Input Reference System numbers), which are placed in the text following the reference callout (e.g., Ahlers et al. 1999 [DIRS 109715]). The purpose of these numbers is to assist in locating a specific reference. Multiple sources by the same author (e.g., SNL 2007) are sorted alphabetically by title.

9.1 DOCUMENTS CITED

109715 Ahlers, C.F.; Finsterle, S.; and Bodvarsson, G.S. 1999. "Characterization and Prediction of Subsurface Pneumatic Response at Yucca Mountain, Nevada." *Journal of Contaminant Hydrology, 38,* (1-3), 47-68. New York, New York: Elsevier. TIC: 244160.

103750 Altman, W.D.; Donnelly, J.P.; and Kennedy, J.E. 1988. *Qualification of Existing Data for High-Level Nuclear Waste Repositories: Generic Technical Position.* NUREG-1298. Washington, D.C.: U.S. Nuclear Regulatory Commission. TIC: 200652.

103597 Altman, W.D.; Donnelly, J.P.; and Kennedy, J.E. 1988. *Peer Review for High-Level Nuclear Waste Repositories: Generic Technical Position.* NUREG-1297. Washington, D.C.: U.S. Nuclear Regulatory Commission. TIC: 200651.

156269 Bear, J. 1972. *Dynamics of Fluids in Porous Media.* Environmental Science Series. Biswas, A.K., ed. New York, New York: Elsevier. TIC: 217356.

105038 Bear, J. 1979. *Hydraulics of Groundwater.* New York, New York: McGraw-Hill. TIC: 217574.

173179 Belcher, W.R. 2004. Death Valley Regional Ground-Water Flow System, Nevada and California - Hydrogeologic Framework and Transient Ground-Water Flow Model. Scientific Investigations Report 2004-5205. Reston, Virginia: U.S. Geological Survey. ACC: MOL.20050323.0070.

104370 Benson, L. and Klieforth, H. 1989. "Stable Isotopes in Precipitation and Ground Water in the Yucca Mountain Region, Southern Nevada: Paleoclimatic Implications." *Aspects of Climate Variability in the Pacific and the Western Americas.* Peterson, D.H., ed.. Geophysical Monograph 55. Pages 41-59. Washington, D.C.: American Geophysical Union. TIC: 224413.

101036 Benson, L.V. and McKinley, P.W. 1985. *Chemical Composition of Ground Water in the Yucca Mountain Area, Nevada, 1971-84.* Open-File Report 85-484. Denver, Colorado: U.S. Geological Survey. ACC: NNA.19900207.0281.

101194 Bish, D.L. 1989. *Evaluation of Past and Future Alterations in Tuff at Yucca Mountain, Nevada, Based on the Clay Mineralogy of Drill Cores USW G-1, G-2, and G-3*. LA-10667-MS. Los Alamos, New Mexico: Los Alamos National Laboratory. ACC: NNA.19890126.0207.

101195 Bish, D.L. and Chipera, S.J. 1989. *Revised Mineralogic Summary of Yucca Mountain, Nevada.* LA-11497-MS. Los Alamos, New Mexico: Los Alamos National Laboratory. ACC: NNA.19891019.0029.

101233 Blankennagel, R.K. and Weir, J.E., Jr. 1973. *Geohydrology of the Eastern Part of Pahute Mesa, Nevada Test Site, Nye County, Nevada.* Professional Paper 712-B. Washington, D.C.: U.S. Geological Survey. TIC: 219642.

149161 Bower, K.M.; Gable, C.W.; and Zyvoloski, G.A. 2000. *Effect of Grid Resolution on Control Volume Finite Element Groundwater Modeling of Realistic Geology.* LA-UR-001870. Los Alamos, New Mexico: Los Alamos National Laboratory. TIC: 248256.

102004 Broxton, D.E.; Bish, D.L.; and Warren, R.G. 1987. "Distribution and Chemistry of Diagenetic Minerals at Yucca Mountain, Nye County, Nevada." *Clays and Clay Minerals, 35,* (2), 89-110. Long Island City, New York: Pergamon Press. TIC: 203900.

155974 BSC (Bechtel SAIC Company) 2001. *Calibration of the Site-Scale Saturated Zone Flow Model.* MDL-NBS-HS-000011 REV 00 ICN 01. Las Vegas, Nevada: Bechtel SAIC Company. ACC: MOL.20010713.0049.

157132 BSC 2001. *Input and Results of the Base Case Saturated Zone Flow and Transport Model for TSPA.* ANL-NBS-HS-000030 REV 00 ICN 01. Las Vegas, Nevada: Bechtel SAIC Company. ACC: MOL.20011112.0068.

160247 BSC 2002. *Analysis of Geochemical Data for the Unsaturated Zone.* ANL-NBS-HS-000017 REV 00 ICN 02. Las Vegas, Nevada: Bechtel SAIC Company. ACC: MOL.20020314.0051.

170029 BSC 2004. *Geologic Framework Model (GFM2000).* MDL-NBS-GS-000002 REV 02. Las Vegas, Nevada: Bechtel SAIC Company. ACC: DOC.20040827.0008.

170008 BSC 2004. *Hydrogeologic Framework Model for the Saturated Zone Site Scale Flow and Transport Model.* MDL-NBS-HS-000024 REV 00. Las Vegas, Nevada: Bechtel SAIC Company. ACC: DOC.20041118.0001.

170014 BSC 2004. *Probability Distribution for Flowing Interval Spacing.* ANL-NBS-MD-000003 REV 01. Las Vegas, Nevada: Bechtel SAIC Company. ACC: DOC.20040923.0003.

170015 BSC 2004. *Recharge and Lateral Groundwater Flow Boundary Conditions for the Saturated Zone Site-Scale Flow and Transport Model.* ANL-NBS-MD-000010 REV 01. Las Vegas, Nevada: Bechtel SAIC Company. ACC: DOC.20041008.0004.

170010 BSC 2004. *Saturated Zone In-Situ Testing.* ANL-NBS-HS-000039 REV 01. Las Vegas, Nevada: Bechtel SAIC Company. ACC: DOC.20041115.0008; DOC.20060116.0006.

170037 BSC 2004. *Saturated Zone Site-Scale Flow Model.* MDL-NBS-HS-000011 REV 02. Las Vegas, Nevada: Bechtel SAIC Company. ACC: DOC.20041122.0001.

169861 BSC 2004. *UZ Flow Models and Submodels.* MDL-NBS-HS-000006 REV 02. Las Vegas, Nevada: Bechtel SAIC Company. ACC: DOC.20041101.0004; DOC.20050629.0003.

170009 BSC 2004. *Water-Level Data Analysis for the Saturated Zone Site-Scale Flow and Transport Model.* ANL-NBS-HS-000034 REV 02. Las Vegas, Nevada: Bechtel SAIC Company. ACC: DOC.20041012.0002; DOC.20050214.0002.

169734 BSC 2004. *Yucca Mountain Site Description.* TDR-CRW-GS-000001 REV 02 ICN 01. Two volumes. Las Vegas, Nevada: Bechtel SAIC Company. ACC: DOC.20040504.0008.

175539 BSC 2005. *Q-List.* 000-30R-MGR0-00500-000-003. Las Vegas, Nevada: Bechtel SAIC Company. ACC: ENG.20050929.0008.

177375 BSC 2006. *Technical Work Plan for Saturated Zone Flow and Transport Modeling.* TWP-NBS-MD-000006 REV 02. Las Vegas, Nevada: Bechtel SAIC Company. ACC: DOC.20060519.0002.

100106 Buesch, D.C.; Spengler, R.W.; Moyer, T.C.; and Geslin, J.K. 1996. *Proposed Stratigraphic Nomenclature and Macroscopic Identification of Lithostratigraphic Units of the Paintbrush Group Exposed at Yucca Mountain, Nevada*. Open-File Report 94-469. Denver, Colorado: U.S. Geological Survey. ACC: MOL.19970205.0061.

162906 Burke, W.H.; Denison, R.E.; Hetherington, E.A.; Koepnick, R.B.; Nelson, H.F.; and Otto, J.B. 1982. "Variation of Seawater $^{87}Sr/^{86}Sr$ Throughout Phanerozoic Time." *Geology, 10,* 516-519. Boulder, Colorado: Geological Society of America. TIC: 255085.

126814 Campana, M.E. and Byer, R.M., Jr. 1996. "A Conceptual Evaluation of Regional Ground-Water Flow, Southern Nevada-California, USA." *Environmental and Engineering Geoscience, II,* (4), 465-478. Boulder, Colorado: Geological Society of America. TIC: 246651.

162940 Chapman, J.B. and Lyles, B.F. 1993. *Groundwater Chemistry at the Nevada Test Site: Data and Preliminary Interpretations.* DOE/NV/10845-16. Las Vegas, Nevada: U.S. Department of Energy, Nevada Operation Office. ACC: MOL.20031023.0087.

153475 Cheng, H.; Edwards, R.L.; Hoff, J.; Gallup, C.D.; Richards, D.A.; and Asmerom, Y. 2000. "The Half-Lives of Uranium-234 and Thorium-230." *Chemical Geology, 169,* 17-33. Amsterdam, The Netherlands: Elsevier. TIC: 249205.

105079 Chipera, S.J. and Bish, D.L. 1997. "Equilibrium Modeling of Clinoptilolite-Analcime Equilibria at Yucca Mountain, Nevada." *Clays and Clay Minerals, 45,* (2), 226-239. Long Island City, New York: Pergamon Press. TIC: 233948.

100025 Chipera, S.J.; Bish, D.L.; and Carlos, B.A. 1995. "Equilibrium Modeling of the Formation of Zeolites in Fractures at Yucca Mountain, Nevada." *Natural Zeolites '93: Occurrence, Properties, Use, Proceedings of the 4th International Conference on the Occurrence, Properties, and Utilization of Natural Zeolites, June 20-28, 1993, Boise, Idaho.* Ming, D.W. and Mumpton, F.A., eds. Pages 565-577. Brockport, New York: International Committee on Natural Zeolites. TIC: 243086.

101125 Claassen, H.C. 1985. *Sources and Mechanisms of Recharge for Ground Water in the West-Central Amargosa Desert, Nevada—A Geochemical Interpretation.* U.S. Geological Survey Professional Paper 712-F. Washington, D.C.: United States Government Printing Office. TIC: 204574.

105738 Clark, I.D. and Fritz, P. 1997. *Environmental Isotopes in Hydrogeology.* Boca Raton, Florida: Lewis Publishers. TIC: 233503.

178650 Cooley, R.L. 2004. *A Theory for Modeling Ground-Water Flow in Heterogeneous Media.* Professional Paper 1679. Reston, Virginia: U.S. Geological Survey. ACC: MOL.20070108.0003.

178598 Cooley, R.L. and Christensen, S. 2006. "Bias and Uncertainty in Regression-Calibrated Models of Groundwater Flow in Heterogeneous Media." *Advances in Water Resources, 29,* 639-656. New York, New York: Elsevier. TIC: 259000.

101040 Craig, R.W. and Robison, J.H. 1984. *Geohydrology of Rocks Penetrated by Test Well UE-25p#1, Yucca Mountain Area, Nye County, Nevada.* Water-Resources Investigations Report 84-4248. Denver, Colorado: U.S. Geological Survey. ACC: NNA.19890905.0209.

100353 CRWMS M&O 1998. *Saturated Zone Flow and Transport Expert Elicitation Project.* Deliverable SL5X4AM3. Las Vegas, Nevada: CRWMS M&O. ACC: MOL.19980825.0008.

139582 CRWMS M&O 2000. *Calibration of the Site-Scale Saturated Zone Flow Model.* MDL-NBS-HS-000011 REV 00. Las Vegas, Nevada: CRWMS M&O. ACC: MOL.20000825.0122.

153246 CRWMS M&O 2000. *Total System Performance Assessment for the Site Recommendation.* TDR-WIS-PA-000001 REV 00 ICN 01. Las Vegas, Nevada: CRWMS M&O. ACC: MOL.20001220.0045.

143665 CRWMS M&O 2000. *Total System Performance Assessment for the Site Recommendation.* TDR-WIS-PA-000001 REV 00. Las Vegas, Nevada: CRWMS M&O. ACC: MOL.20001005.0282.

101043 Czarnecki, J.B. 1984. *Simulated Effects of Increased Recharge on the Ground-Water Flow System of Yucca Mountain and Vicinity, Nevada-California.* Water-Resources Investigations Report 84-4344. Denver, Colorado: U.S. Geological Survey. ACC: HQS.19880517.1750.

160149 Czarnecki, J.B. 1985. *Simulated Effects of Increased Recharge on the Ground-Water Flow System of Yucca Mountain and Vicinity, Nevada-California.* Water-Resources Investigations Report 84-4344. Denver, Colorado: U.S. Geological Survey. TIC: 203222.

100377 Czarnecki, J.B.; Faunt, C.C.; Gable, C.W.; and Zyvoloski, G.A. 1997. Hydrogeology and Preliminary Calibration of a Preliminary Three-Dimensional Finite-Element Ground-Water Flow Model of the Site Saturated Zone, Yucca Mountain, Nevada. Administrative Report. Denver, Colorado: U.S. Geological Survey. ACC: MOL.19980204.0519.

100131 D'Agnese, F.A.; Faunt, C.C.; Turner, A.K.; and Hill, M.C. 1997. *Hydrogeologic Evaluation and Numerical Simulation of the Death Valley Regional Ground-Water Flow System, Nevada and California.* Water-Resources Investigations Report 96-4300. Denver, Colorado: U.S. Geological Survey. ACC: MOL.19980306.0253.

120425 D'Agnese, F.A.; O'Brien, G.M.; Faunt, C.C.; and San Juan, C.A. 1999. *Simulated Effects of Climate Change on the Death Valley Regional Ground-Water Flow System, Nevada and California.* Water-Resources Investigations Report 98-4041. Denver, Colorado: U.S. Geological Survey. TIC: 243555.

158876 D'Agnese, F.A.; O'Brien, G.M.; Faunt, C.C.; Belcher, W.R.; and San Juan, C. 2002. A Three-Dimensional Numerical Model of Predevelopment Conditions in the Death Valley Regional Ground-Water Flow System, Nevada and California. Water-Resources Investigations Report 02-4102. Denver, Colorado: U.S. Geological Survey. TIC: 253754.

162939 Davisson, M.L.; Kenneally, J.M.; Smith, D.K.; Hudson, G.B.; Nimz, G.J.; and Rego, J.H. 1994. Preliminary Report on the Isotope Hydrology Investigations at the Nevada Test Site: Hydrologic Resources Management Program, FY 1992-1993. UCRL-ID-116122. Livermore, California: Lawrence Livermore National Laboratory, Nuclear Chemistry Division. TIC: 210954.

100027 Day, W.C.; Dickerson, R.P.; Potter, C.J.; Sweetkind, D.S.; San Juan, C.A.; Drake, R.M., II; and Fridrich, C.J. 1998. *Bedrock Geologic Map of the Yucca Mountain Area, Nye County, Nevada.* Geologic Investigations Series I-2627. Denver, Colorado: U.S. Geological Survey. ACC: MOL.19981014.0301.

101557 Day, W.C.; Potter, C.J.; Sweetkind, D.S.; Dickerson, R.P.; and San Juan, C.A. 1998. *Bedrock Geologic Map of the Central Block Area, Yucca Mountain, Nye County, Nevada.* Miscellaneous Investigations Series Map I-2601. Washington, D.C.: U.S. Geological Survey. ACC: MOL.19980611.0339.

100439 de Marsily, G. 1986. *Quantitative Hydrogeology: Groundwater Hydrology for Engineers.* San Diego, California: Academic Press. TIC: 208450.

105384 Dettinger, M.D. 1989. "Reconnaissance Estimates of Natural Recharge to Desert Basins in Nevada, U.S.A., by Using Chloride-Balance Calculations." *Journal of Hydrology, 106,* 55-78. Amsterdam, The Netherlands: Elsevier. TIC: 236967.

154690 Dettinger, M.D. 1989. *Distribution of Carbonate-Rock Aquifers in Southern Nevada and the Potential for Their Development, Summary of Findings, 1985-88*. Summary Report No. 1. Carson City, Nevada: State of Nevada. ACC: NNA.19940412.0056.

178613 Doherty, J. 2006. *Addendum to the PEST Manual.* Brisbane, Australia: Watermark Numerical Computing. ACC: MOL.20070111.0002; MOL.20070111.0003.

118564 Drever, J.I. 1988. *The Geochemistry of Natural Waters.* 2nd Edition. Englewood Cliffs, New Jersey: Prentice-Hall. TIC: 242836.

103415 Dudley, W.W., Jr. and Larson, J.D. 1976. *Effect of Irrigation Pumping on Desert Pupfish Habitats in Ash Meadows, Nye County, Nevada.* Professional Paper 927. Washington, D.C.: U.S. Geological Survey. ACC: MOL.20010724.0312.

163577 Eddebbarh, A.A.; Zyvoloski, G.A.; Robinson, B.A.; Kwicklis, E.M.; Reimus, P.W.; Arnold, B.W.; Corbet, T.; Kuzio, S.P.; and Faunt, C. 2003. "The Saturated Zone at Yucca Mountain: An Overview of the Characterization and Assessment of the Saturated Zone as a Barrier to Potential Radionuclide Migration." *Journal of Contaminant Hydrology, 62-63,* 477-493. New York, New York: Elsevier. TIC: 254205.

100633 Ervin, E.M.; Luckey, R.R.; and Burkhardt, D.J. 1994. *Revised Potentiometric-Surface Map, Yucca Mountain and Vicinity, Nevada.* Water-Resources Investigations Report 93-4000. Denver, Colorado: U.S. Geological Survey. ACC: NNA.19930212.0018.

100146 Faunt, C.C. 1997. *Effect of Faulting on Ground-Water Movement in the Death Valley Region, Nevada and California.* Water-Resources Investigations Report 95-4132. Denver, Colorado: U.S. Geological Survey. ACC: MOL.19980429.0119.

105559 Faure, G. 1986. *Principles of Isotope Geology.* 2nd Edition. New York, New York: John Wiley & Sons. TIC: 237212.

109425 Forester, R.M.; Bradbury, J.P.; Carter, C.; Elvidge-Tuma, A.B.; Hemphill, M.L.; Lundstrom, S.C.; Mahan, S.A.; Marshall, B.D.; Neymark, L.A.; Paces, J.B.; Sharpe, S.E.; Whelan, J.F.; and Wigand, P.E. 1999. *The Climatic and Hydrologic History of Southern Nevada During the Late Quaternary.* Open-File Report 98-635. Denver, Colorado: U.S. Geological Survey. TIC: 245717.

144110 Forsyth, P.A. 1989. "A Control Volume Finite Element Method for Local Mesh Refinement." *Proceedings, Tenth SPE Symposium on Reservoir Simulation, Houston, Texas, February 6-8, 1989.* SPE 18415. Pages 85-96. Richardson, Texas: Society of Petroleum Engineers. TIC: 247068.

101173 Freeze, R.A. and Cherry, J.A. 1979. *Groundwater.* Englewood Cliffs, New Jersey: Prentice-Hall. TIC: 217571.

178611 Freifeld, B.; Doughty, C.; and Finsterle, S. 2006. *Preliminary Estimates of Specific Discharge and Transport Velocities Near Borehole NC-EWDP-24PB.* LBNL-60740. Berkeley, California: Lawrence Berkeley National Laboratory. ACC: MOL.20070111.0001.

100575 Fridrich, C.J.; Dudley, W.W., Jr.; and Stuckless, J.S. 1994. "Hydrogeologic Analysis of the Saturated-Zone Ground-Water System, Under Yucca Mountain, Nevada." *Journal of Hydrology, 154,* 133-168. Amsterdam, The Netherlands: Elsevier. TIC: 224606.

178742 Futa, K.; Marshall, B.D.; and Peterman, Z.E. 2006. "Evidence for Ground-Water Stratification Near Yucca Mountain, Nevada." *Proceedings of the 11th International High-Level Radioactive Waste Management Conference (IHLRWM), April 30 - May 4, 2006, Las Vegas, Nevada.* Pages 301-306. La Grange Park, Illinois: American Nuclear Society. TIC: 258345.

127184 Gascoyne, M. 1992. "Geochemistry of the Actinides and Their Daughters." Chapter 2 of *Uranium-Series Disequilibrium: Applications to Earth, Marine, and Environmental Sciences.* Ivanovich, M. and Harmon, R.S., eds. 2nd Edition. New York, New York: Oxford University Press. TIC: 234680.

129721 Geldon, A.L.; Umari, A.M.A.; Earle, J.D.; Fahy, M.F.; Gemmell, J.M.; and Darnell, J. 1998. *Analysis of a Multiple-Well Interference Test in Miocene Tuffaceous Rocks at the C-Hole Complex, May-June 1995, Yucca Mountain, Nye County, Nevada*. Water-Resources Investigations Report 97-4166. Denver, Colorado: U.S. Geological Survey. TIC: 236724.

100397 Geldon, A.L.; Umari, A.M.A.; Fahy, M.F.; Earle, J.D.; Gemmell, J.M.; and Darnell, J. 1997. *Results of Hydraulic and Conservative Tracer Tests in Miocene Tuffaceous Rocks at the C-Hole Complex, 1995 to 1997, Yucca Mountain, Nye County, Nevada*. Milestone SP23PM3. Las Vegas, Nevada: U.S. Geological Survey. ACC: MOL.19980122.0412.

179104 Gilmore, K. 2006. "RE: Some Problems in Checking." E-mail to from K. Gilmore (Nye County) to C.L. Axness (SNL), July 26, 2006. ACC: LLR.20070228.0142.

155411 Graves, R.P. 1998. *Water Levels in the Yucca Mountain Area, Nevada, 1996.* Open-File Report 98-169. Denver, Colorado: U.S. Geological Survey. ACC: MOL.19981117.0340.

155197 Harbaugh, A.W.; Banta, E.R.; Hill, M.C.; and McDonald, M.G. 2000. *MODFLOW-2000, The U.S. Geological Survey Modular Ground-Water Model—User Guide to Modularization Concepts and the Ground-Water Flow Process*. Open-File Report 00-92. Reston, Virginia: U.S. Geological Survey. TIC: 250197.

178488 Harter, T. and Hopmans, J.W. 2004. "Role of Vadose-Zone Flow Processes in Regional-Scale Hydrology: Review, Opportunities and Challenges." In *Unsaturated-Zone Modeling,* Volume 6, Chapter 6 of *Wageningen UR Frontis Series.* Feddes, R.A.; de Rooij, G.H.; and van Dam, J.C., eds. Boston, Massachusetts: Kluwer Academic Publishers. TIC: 258894.

169681 Hevesi, J.A.; Flint, A.L.; and Flint, L.E. 2003. *Simulation of Net Infiltration and Potential Recharge Using a Distributed-Parameter Watershed Model of the Death Valley Region, Nevada and California*. Water-Resources Investigations Report 03-4090. Sacramento, California: U.S. Geological Survey. ACC: MOL.20031124.0212.

116809 Hevesi, J.A.; Flint, A.L.; and Istok, J.D. 1992. "Precipitation Estimation in Mountainous Terrain Using Multivariate Geostatistics. Part II: Isohyetal Maps." *Journal of Applied Meteorology, 31,* (7), 677-688. Boston, Massachusetts: American Meteorological Society. TIC: 225248.

158753 Hill, M.C.; Banta, E.R.; Harbaugh, A.W.; and Anderman, E.R. 2000. *MODFLOW-2000, The U.S. Geological Survey Modular Ground-Water Model — User Guide to the Observation, Sensitivity, and Parameter-Estimation Processes and Three Post-Processing Programs*. Open-File Report 00-184. Denver, Colorado: U.S. Geological Survey. TIC: 252581.

145088 Ingraham, N.L.; Lyles, B.F.; Jacobson, R.L.; and Hess, J.W. 1991. "Stable Isotopic Study of Precipitation and Spring Discharge in Southern Nevada." *Journal of Hydrology, 125,* 243-258. Amsterdam, The Netherlands: Elsevier. TIC: 238581.

103010 Kilroy, K.C. 1991. *Ground-Water Conditions in Amargosa Desert, Nevada-California, 1952-87.* Water-Resources Investigations Report 89-4101. Carson City, Nevada: U.S. Geological Survey. TIC: 209975.

178599 Kitanidis, P.K. 1996. "On the Geostatistical Approach to the Inverse Problem." *Advances in Water Resources, 19,* (6), 333-342. New York, New York: Elsevier. TIC: 259001.

100909 Kotra, J.P.; Lee, M.P.; Eisenberg, N.A.; and DeWispelare, A.R. 1996. *Branch Technical Position on the Use of Expert Elicitation in the High-Level Radioactive Waste Program.* NUREG-1563. Washington, D.C.: U.S. Nuclear Regulatory Commission. TIC: 226832.

103011 La Camera, R.J. and Locke, G.L. 1997. *Selected Ground-Water Data for Yucca Mountain Region, Southern Nevada and Eastern California, Through December 1996.* Open-File Report 97-821. Carson City, Nevada: U.S. Geological Survey. ACC: MOL.20010724.0311.

103012 Laczniak, R.J.; Cole, J.C.; Sawyer, D.A.; and Trudeau, D.A. 1996. *Summary of Hydrogeologic Controls on Ground-Water Flow at the Nevada Test Site, Nye County, Nevada.* Water-Resources Investigations 96-4109. Carson City, Nevada: U.S. Geological Survey. TIC: 226157.

100051 Langmuir, D. 1997. *Aqueous Environmental Geochemistry.* Upper Saddle River, New Jersey: Prentice Hall. TIC: 237107.

181434 LANL (Los Alamos National Laboratory) 2001. *Software Management Report (SMR) for CORPSCON Version 5.11.08.* SDN: 10547-SMR-5.11.08-00. Los Alamos, New Mexico: Los Alamos National Laboratory. ACC: MOL.20011011.0403.

100153 LeCain, G.D. 1997. *Air-Injection Testing in Vertical Boreholes in Welded and Nonwelded Tuff, Yucca Mountain, Nevada.* Water-Resources Investigations Report 96-4262. Denver, Colorado: U.S. Geological Survey. ACC: MOL.19980310.0148.

144612 LeCain, G.D.; Anna, L.O.; and Fahy, M.F. 2000. *Results from Geothermal Logging, Air and Core-Water Chemistry Sampling, Air-Injection Testing, and Tracer Testing in the Northern Ghost Dance Fault, Yucca Mountain, Nevada, November 1996 to August 1998*. Water-Resources Investigations Report 99-4210. Denver, Colorado: U.S. Geological Survey. TIC: 247708.

100053 Levy, S.S. 1991. "Mineralogic Alteration History and Paleohydrology at Yucca Mountain, Nevada." *High Level Radioactive Waste Management, Proceedings of the Second Annual International Conference, Las Vegas, Nevada, April 28-May 3, 1991. 1,* 477-485. La Grange Park, Illinois: American Nuclear Society. TIC: 204272.

100589 Lichty, R.W. and McKinley, P.W. 1995. *Estimates of Ground-Water Recharge Rates for Two Small Basins in Central Nevada.* Water-Resources Investigations Report 94-4104. Denver, Colorado: U.S. Geological Survey. ACC: MOL.19960924.0524.

101258 Loeven, C. 1993. *A Summary and Discussion of Hydrologic Data from the Calico Hills Nonwelded Hydrogeologic Unit at Yucca Mountain, Nevada*. LA-12376-MS. Los Alamos, New Mexico: Los Alamos National Laboratory. ACC: NNA.19921116.0001.

100465 Luckey, R.R.; Tucci, P.; Faunt, C.C.; Ervin, E.M.; Steinkampf, W.C.; D'Agnese, F.A.; and Patterson, G.L. 1996. *Status of Understanding of the Saturated-Zone Ground-Water Flow System at Yucca Mountain, Nevada, as of 1995.* Water-Resources Investigations Report 96-4077. Denver, Colorado: U.S. Geological Survey. ACC: MOL.19970513.0209.

101142 Marshall, B.D.; Peterman, Z.E.; and Stuckless, J.S. 1993. "Strontium Isotopic Evidence for a Higher Water Table at Yucca Mountain." *High Level Radioactive Waste Management, Proceedings of the Fourth Annual International Conference, Las Vegas, Nevada, April 26-30, 1993. 2,* 1948-1952. La Grange Park, Illinois: American Nuclear Society. TIC: 208542.

116222 McKinley, P.W.; Long, M.P.; and Benson, L.V. 1991. *Chemical Analyses of Water from Selected Wells and Springs in the Yucca Mountain Area, Nevada and Southeastern California.* Open-File Report 90-355. Denver, Colorado: U.S. Geological Survey. ACC: NNA.19901031.0004.

158813 Meijer, A. 2002. "Conceptual Model of the Controls on Natural Water Chemistry at Yucca Mountain, Nevada." *Applied Geochemistry, 17,* (6), 793-805. New York, New York: Elsevier. TIC: 252808.

126847 Merlivat, L. and Jouzel, J. 1979. "Global Climatic Interpretation of the Deuterium-Oxygen 18 Relationship for Precipitation." *Journal of Geophysical Research, 84,* (C8), 5029-5033. Washington, D.C.: American Geophysical Union. TIC: 247773.

178788 Moore, C. 2005. *The Use of Regularized Inversion in Groundwater Model Calibration and Prediction Uncertainty Analysis.* Ph.D. Thesis. Queensland, Australia: The University of Queensland. TIC: 259082.

178402 Moore, C. and Doherty, J. 2005. "Role of the Calibration Process in Reducing Model Predictive Error." *Water Resources Research, 41,* 1-14. Washington, D.C.: American Geophysical Union. TIC: 258856.

178403 Moore, C. and Doherty, J. 2006. "The Cost of Uniqueness in Groundwater Model Calibration." *Advances in Water Resources, 29,* 605-623. New York, New York: Elsevier. TIC: 258857.

150321 Neuman, S.P. 1975. "Analysis of Pumping Test Data from Anisotropic Unconfined Aquifers Considering Delayed Gravity Response." *Water Resources Research, 11,* (2), 329-342. Washington, D.C.: American Geophysical Union. TIC: 222414.

101464 Neuman, S.P. 1990. "Universal Scaling of Hydraulic Conductivities and Dispersivities in Geologic Media." *Water Resources Research, 26,* (8), 1749-1758. Washington, D.C.: American Geophysical Union. TIC: 237977.

147379 Norton, D. and Knapp, R.B. 1977. "Transport Phenomena in Hydrothermal Systems: The Nature of Porosity." *American Journal of Science, 277,* 913-936. New Haven, Connecticut: Yale University, Kline Geology Laboratory. TIC: 247599.

163274 NRC (U.S. Nuclear Regulatory Commission) 2003. *Yucca Mountain Review Plan, Final Report.* NUREG-1804, Rev. 2. Washington, D.C.: U.S. Nuclear Regulatory Commission, Office of Nuclear Material Safety and Safeguards. TIC: 254568.

107770 NRC 1998. "Proposed Rule: 10 CFR Part 63---'Disposal of High-Level Radioactive Wastes in a Proposed Geologic Repository at Yucca Mountain, Nevada'." SECY-98-225. Washington, D.C.: U.S. Nuclear Regulatory Commission. Accessed October 30, 1999. TIC: 240520.
URL: http://www.nrc.gov/NRC/COMMISSION/SECYS/1998-225scy.html

101278 O'Brien, G.M. 1998. *Analysis of Aquifer Tests Conducted in Borehole USW G-2, 1996, Yucca Mountain, Nevada.* Water-Resources Investigations Report 98-4063. Denver, Colorado: U.S. Geological Survey. ACC: MOL.19980904.0095.

149438 Oatfield, W.J. and Czarnecki, J.B. 1989. *Hydrogeologic Inferences from Drillers Logs and from Gravity and Resistivity Surveys in the Amargosa Desert, Southern Nevada.* Open-File Report 89-234. Denver, Colorado: U.S. Geological Survey. TIC: 200468.

100069 Oliver, T. and Root, T. 1997. *Hydrochemical Database for the Yucca Mountain Area, Nye County, Nevada.* Denver, Colorado: U.S. Geological Survey. ACC: MOL.19980302.0367.

145190 Osmond, J.K. and Cowart, J.B. 1992. "Ground Water." Chapter 9 of *Uranium-Series Disequilibrium: Applications to Earth, Marine, and Environmental Sciences.* Ivanovich, M. and Harmon, R.S., eds. 2nd Edition. New York, New York: Oxford University Press. TIC: 234680.

154724 Paces, J.B. and Whelan, J.F. 2001. "Water-Table Fluctuations in the Amargosa Desert, Nye County, Nevada." *"Back to the Future - Managing the Back End of the Nuclear Fuel Cycle to Create a More Secure Energy Future," Proceedings of the 9th International High-Level Radioactive Waste Management Conference (IHLRWM), Las Vegas, Nevada, April 29-May 3, 2001*. La Grange Park, Illinois: American Nuclear Society. TIC: 247873.

158817 Paces, J.B.; Ludwig, K.R.; Peterman, Z.E.; and Neymark, L.A. 2002. "$^{234}U/^{238}U$ Evidence for Local Recharge and Patterns of Ground-Water Flow in the Vicinity of Yucca Mountain, Nevada, USA." *Applied Geochemistry, 17,* (6), 751-779. New York, New York: Elsevier. TIC: 252809.

100072 Paces, J.B.; Ludwig, K.R.; Peterman, Z.E.; Neymark, L.A.; and Kenneally, J.M. 1998. "Anomalous Ground-Water $^{234}U/^{238}U$ Beneath Yucca Mountain: Evidence of Local Recharge?" *High-Level Radioactive Waste Management, Proceedings of the Eighth International Conference, Las Vegas, Nevada, May 11-14, 1998.* Pages 185-188. La Grange Park, Illinois: American Nuclear Society. TIC: 237082.

107408 Paces, J.B.; Neymark, L.A.; Marshall, B.D.; Whelan, J.F.; and Peterman, Z.E. 1998. "Inferences for Yucca Mountain Unsaturated-Zone Hydrology from Secondary Minerals." *High-Level Radioactive Waste Management, Proceedings of the Eighth International Conference, Las Vegas, Nevada, May 11-14, 1998.* Pages 36-39. La Grange Park, Illinois: American Nuclear Society. TIC: 237082.

156507 Paces, J.B.; Neymark, L.A.; Marshall, B.D.; Whelan, J.F.; and Peterman, Z.E. 2001. *Ages and Origins of Calcite and Opal in the Exploratory Studies Facility Tunnel, Yucca Mountain, Nevada.* Water-Resources Investigations Report 01-4049. Denver, Colorado: U.S. Geological Survey. TIC: 251284.

159511 Parkhurst, D.L. and Appelo, C.A.J. 1999. *User's Guide to PHREEQC (Version 2)—A Computer Program for Speciation, Batch-Reaction, One-Dimensional Transport, and Inverse Geochemical Calculations*. Water-Resources Investigations Report 99-4259. Denver, Colorado: U.S. Geological Survey. TIC: 253046.

158824 Patterson, G.L. 1999. "Occurrences of Perched Water in the Vicinity of the Exploratory Studies Facility North Ramp." *Hydrogeology of the Unsaturated Zone, North Ramp Area of the Exploratory Studies Facility, Yucca Mountain, Nevada.* Rousseau, J.P.; Kwicklis, E.M.; and Gillies, D.C., eds. Water-Resources Investigations Report 98-4050. Denver, Colorado: U.S. Geological Survey. ACC: MOL.19990419.0335.

178743 Patterson, G.L. and Striffler, P.S. 2006. "Vertical Variability in Saturated Zone Hydrochemistry Near Yucca Mountain, Nevada." *Proceedings of the 11th International High-Level Radioactive Waste Management Conference (IHLRWM), April 30 - May 4, 2006, Las Vegas, Nevada.* Pages 390-394. La Grange Park, Illinois: American Nuclear Society. TIC: 258345.

179459 Patterson, G.L. and Thomas, J. 2005. "Carbon-14 Groundwater Analysis." *Office of Science and Technology and International OSTI&I: Annual Report 2005.* DOE/RW-0581. Pages 183-184. Washington, D.C.: U.S. Department of Energy, Office of Science and Technology and International. ACC: HQO.20060322.0021.

107402 Patterson, G.L.; Peterman, Z.E.; and Paces, J.B. 1998. "Hydrochemical Evidence for the Existence of Perched Water at USW WT-24, Yucca Mountain, Nevada." *High-Level Radioactive Waste Management, Proceedings of the Eighth International Conference, Las Vegas, Nevada, May 11-14, 1998.* Pages 277-278. La Grange Park, Illinois: American Nuclear Society. TIC: 237082.

101149 Peterman, Z.E. and Stuckless, J.S. 1993. "Isotopic Evidence of Complex Ground-Water Flow at Yucca Mountain, Nevada, USA." *High Level Radioactive Waste Management, Proceedings of the Fourth Annual International Conference, Las Vegas, Nevada, April 26-30, 1993. 2,* 1559-1566. La Grange Park, Illinois: American Nuclear Society. TIC: 208542.

107034 Plummer, M.A.; Phillips, F.M.; Fabryka-Martin, J.; Turin, H.J.; Wigand, P.E.; and Sharma, P. 1997. "Chlorine-36 in Fossil Rat Urine: An Archive of Cosmogenic Nuclide Deposition During the Past 40,000 Years." *Science, 277,* 538-541. Washington, D.C.: American Association for the Advancement of Science. TIC: 237425.

101466 Pollock, D.W. 1988. "Semianalytical Computation of Path Lines for Finite-Difference Models." *Ground Water, 26,* (6), 743-750. Worthington, Ohio: National Water Well Association. TIC: 226464.

103316 Press, W.H.; Teukolsky, S.A.; Vetterling, W.T.; and Flannery, B.P. 1992. *Numerical Recipes in Fortran 77, The Art of Scientific Computing.* Volume 1 of *Fortran Numerical Recipes.* 2nd Edition. Cambridge, United Kingdom: Cambridge University Press. TIC: 243606.

100073 Quade, J. and Cerling, T.E. 1990. "Stable Isotopic Evidence for a Pedogenic Origin of Carbonates in Trench 14 Near Yucca Mountain, Nevada." *Science, 250,* 1549-1552. Washington, D.C.: American Association for the Advancement of Science. TIC: 222617.

154688 Rasmussen, T.C.; Evans, D.D.; Sheets, P.J.; and Blanford, J.H. 1993. "Permeability of Apache Leap Tuff: Borehole and Core Measurements Using Water and Air." *Water Resources Research, 29,* (7), 1997-2006. Washington, D.C.: American Geophysical Union. TIC: 245278.

101284 Rice, W.A. 1984. *Preliminary Two-Dimensional Regional Hydrologic Model of the Nevada Test Site and Vicinity.* SAND83-7466. Albuquerque, New Mexico: Sandia National Laboratories. ACC: NNA.19900810.0286.

165986 Robledo, A.R.; Ryder, P.L.; Fenelon, J.M.; and Paillet, F.L. 1998. *Geohydrology of Monitoring Wells Drilled in Oasis Valley near Beatty, Nye County, Nevada, 1997.* Water-Resources Investigations Report 98-4184. Carson City, Nevada: U.S. Geological Survey. ACC: MOL.20031027.0156.

162938 Rose, T.P.; Benedict, F.C., Jr.; Thomas, J.M.; Sicke, W.S.; Hershey, R.L.; Paces, J.B.; Farnham, I.M.; and Peterman, Z.E. 2002. *Preliminary, Geochemical Data Analysis and Interpretation of the Pahute Mesa-Oasis Valley Groundwater Flow System, Nye County, Nevada.* Las Vegas, Nevada: U.S. Department of Energy, Nevada Operations Office. ACC: MOL.20031208.0200.

144725 Rose, T.P.; Kenneally, J.M.; Smith, D.K.; Davisson, M.L.; Hudson, G.B.; and Rego, J.H. 1997. *Chemical and Isotopic Data for Groundwater in Southern Nevada.* UCRL-ID-128000. Livermore, California: Lawrence Livermore National Laboratory. TIC: 243649.

102097 Rousseau, J.P.; Kwicklis, E.M.; and Gillies, D.C., eds. 1999. *Hydrogeology of the Unsaturated Zone, North Ramp Area of the Exploratory Studies Facility, Yucca Mountain, Nevada.* Water-Resources Investigations Report 98-4050. Denver, Colorado: U.S. Geological Survey. ACC: MOL.19990419.0335.

100644 Sass, J.H.; Lachenbruch, A.H.; Dudley, W.W., Jr.; Priest, S.S.; and Munroe, R.J. 1988. *Temperature, Thermal Conductivity, and Heat Flow Near Yucca Mountain, Nevada: Some Tectonic and Hydrologic Implications.* Open-File Report 87-649. Denver, Colorado: U.S. Geological Survey. TIC: 203195.

102213 Savard, C.S. 1998. *Estimated Ground-Water Recharge from Streamflow in Fortymile Wash Near Yucca Mountain, Nevada.* Water-Resources Investigations Report 97-4273. Denver, Colorado: U.S. Geological Survey. TIC: 236848.

100075 Sawyer, D.A.; Fleck, R.J.; Lanphere, M.A.; Warren, R.G.; Broxton, D.E.; and Hudson, M.R. 1994. "Episodic Caldera Volcanism in the Miocene Southwestern Nevada Volcanic Field: Revised Stratigraphic Framework, $^{40}Ar/^{39}Ar$ Geochronology, and Implications for Magmatism and Extension." *Geological Society of America Bulletin, 106,* (10), 1304-1318. Boulder, Colorado: Geological Society of America. TIC: 222523.

161591 Sharpe, S. 2003. *Future Climate Analysis—10,000 Years to 1,000,000 Years After Present.* MOD-01-001 REV 01. Reno, Nevada: Desert Research Institute. ACC: MOL.20030407.0055.

101929 Simonds, F.W.; Whitney, J.W.; Fox, K.F.; Ramelli, A.R.; Yount, J.C.; Carr, M.D.; Menges, C.M.; Dickerson, R.P.; and Scott, R.B. 1995. *Map Showing Fault Activity in the Yucca Mountain Area, Nye County, Nevada.* Miscellaneous Investigations Series Map I-2520. Denver, Colorado: U.S. Geological Survey. TIC: 232483.

150228 Slate, J.L.; Berry, M.E.; Rowley, P.D.; Fridrich, C.J.; Morgan, K.S.; Workman, J.B.; Young, O.D.; Dixon, G.L.; Williams, V.S.; McKee, E.H.; Ponce, D.A.; Hildenbrand, T.G.; Swadley, W C; Lundstrom, S.C.; Ekren, E.B.; Warren, R.G.; Cole, J.C.; Fleck, R.J.; Lanphere, M.A.; Sawyer, D.A.; Minor, S.A.; Grunwald, D.J.; Laczniak, R.J.; Menges, C.M.; Yount, J.C.; Jayko, A.S.; Mankinen, E.A.; Davidson, J.G.; Morin, R.L.; and Blakely, R.J. 2000. *Digital Geologic Map of the Nevada Test Site and Vicinity, Nye, Lincoln and Clark Counties, Nevada, and Inyo County, California, Revision 4; Digital Aeromagnetic Map of the Nevada Test Site and Vicinity, Nye, Lincoln, and Clark Counties, Nevada, and Inyo County, California; and Digital Isostatic Gravity Map of the Nevada Test Site and Vicinity, Nye, Lincoln, and Clark Counties, Nevada, and Inyo County, California.* Open-File Report 99-554—A, —B, and —C. Denver, Colorado: U.S. Geological Survey. TIC: 248049; 251985; 251981.

179476 SNL (Sandia National Laboratories) 2007. *Features, Events, and Processes for the Total System Performance Assessment.* ANL-WIS-MD-000026 REV 00. Las Vegas, Nevada: Sandia National Laboratories.

174109 SNL 2007. *Hydrogeologic Framework Model for the Saturated Zone Site-Scale Flow and Transport Model.* MDL-NBS-HS-000024 REV 01. Las Vegas, Nevada: Sandia National Laboratories. ACC: DOC.20070411.0003.

181650 SNL 2007. *Saturated Zone Flow and Transport Model Abstraction.* MDL-NBS-HS-000021 REV 03 AD 01. Las Vegas, Nevada: Sandia National Laboratories.

177394 SNL 2007. *Saturated Zone In-Situ Testing.* ANL-NBS-HS-000039 REV 02. Las Vegas, Nevada: Sandia National Laboratories. ACC: DOC.20070608.0004.

174294 SNL 2007. *Simulation of Net Infiltration for Present-Day and Potential Future Climates.* MDL-NBS-HS-000023 REV 01. Las Vegas, Nevada: Sandia National Laboratories. ACC: DOC.20070530.0014.

177392 SNL 2007. *Site-Scale Saturated Zone Transport.* MDL-NBS-HS-000010 REV 03. Las Vegas, Nevada: Sandia National Laboratories. ACC: DOC.20070822.0003.

179466 SNL 2007. *Total System Performance Assessment Data Input Package for Requirements Analysis for Subsurface Facilities.* TDR-TDIP-PA-000001 REV 00. Las Vegas, Nevada: Sandia National Laboratories.

175177 SNL 2007. *UZ Flow Models and Submodels.* MDL-NBS-HS-000006 REV 03. Las Vegas, Nevada: Sandia National Laboratories.

178871 SNL 2007. *Total System Performance Assessment Model /Analysis for the License Application.* MDL-WIS-PA-000005 REV 00. Las Vegas, Nevada: Sandia National Laboratories.

158818 Steinkampf, W.C. and Werrell, W.L. 2001. *Ground-Water Flow to Death Valley, as Inferred from the Chemistry and Geohydrology of Selected Springs in Death Valley National Park, California and Nevada*. Water-Resources Investigations Report 98-4114. Denver, Colorado: U.S. Geological Survey. TIC: 251734.

101159 Stuckless, J.S.; Whelan, J.F.; and Steinkampf, W.C. 1991. "Isotopic Discontinuities in Ground Water Beneath Yucca Mountain, Nevada." *High Level Radioactive Waste Management, Proceedings of the Second Annual International Conference, Las Vegas, Nevada, April 28-May 3, 1991. 2,* 1410-1415. La Grange Park, Illinois: American Nuclear Society. TIC: 204272.

101933 Thomas, J.M.; Welch, A.H.; and Dettinger, M.D. 1996. *Geochemistry and Isotope Hydrology of Representative Aquifers in the Great Basin Region of Nevada, Utah, and Adjacent States.* Professional Paper 1409-C. Denver, Colorado: U.S. Geological Survey. ACC: MOL.20010803.0369.

106585 Thordarson, W. 1965. *Perched Ground Water in Zeolitized-Bedded Tuff, Rainier Mesa and Vicinity, Nevada Test Site, Nevada.* TEI-862. Washington, D.C.: U.S. Geological Survey. ACC: NN1.19881021.0066.

126827 Thorstenson, D.C.; Weeks, E.P.; Haas, H.; Busenberg, E.; Plummer, L.N.; and Peters, C.A. 1998. "Chemistry of Unsaturated Zone Gases Sampled in Open Boreholes at the Crest of Yucca Mountain, Nevada: Data and Basic Concepts of Chemical and Physical Processes in the Mountain." *Water Resources Research, 34,* (6), 1507-1529. Washington, D.C.: American Geophysical Union. TIC: 246315.

101490 Tompson, A.F.B. and Gelhar, L.W. 1990. "Numerical Simulation of Solute Transport in Three-Dimensional, Randomly Heterogeneous Porous Media." *Water Resources Research, 26,* (10), 2541-2562. Washington, D.C.: American Geophysical Union. TIC: 224902.

178576 Tonkin, M.J. and Doherty, J. 2005. "A Hybrid Regularized Inversion Methodology for Highly Parameterized Environmental Models." *Water Resources Research, 41,* (W10412), 1-16. Washington, D.C.: American Geophysical Union. TIC: 258946.

179068 Tseng, P-H. and Zyvoloski, G.A. 2000. "A Reduced Degree of Freedom Method for Simulating Non-Isothermal Multi-Phase Flow in a Porous Medium." *Advances in Water Resources, 23,* 731-745. New York, New York: Elsevier. TIC: 254768.

155410 Tucci, P. 2001. Segment of SN-USGS-SCI-126-V1: Revision of Water Level AMR (ANL-NBS-HS-000034, Rev 00/ICN 01). Scientific Notebook SN-USGS-SCI-126-V1. ACC: MOL.20010712.0271.

101060 Tucci, P. and Burkhardt, D.J. 1995. *Potentiometric-Surface Map, 1993, Yucca Mountain and Vicinity, Nevada.* Water-Resources Investigations Report 95-4149. Denver, Colorado: U.S. Geological Survey. ACC: MOL.19960924.0517.

154625 USGS (U.S. Geological Survey) 2001. *Water-Level Data Analysis for the Saturated Zone Site-Scale Flow and Transport Model.* ANL-NBS-HS-000034 REV 00 ICN 01. Denver, Colorado: U.S. Geological Survey. ACC: MOL.20010405.0211.

168473 USGS 2004. *Water-Level Data Analysis for the Saturated Zone Site-Scale Flow and Transport Model.* ANL-NBS-HS-000034 REV 01 Errata 002. Denver, Colorado: U.S. Geological Survey. ACC: MOL.20020209.0058; MOL.20020917.0136; DOC.20040303.0006.

105946 Vaniman, D.T.; Bish, D.L.; Chipera, S.J.; Carlos, B.A.; and Guthrie, G.D., Jr. 1996. *Chemistry and Mineralogy of the Transport Environment at Yucca Mountain*. Volume I of *Summary and Synthesis Report on Mineralogy and Petrology Studies for the Yucca Mountain Site Characterization Project*. Milestone 3665. Los Alamos, New Mexico: Los Alamos National Laboratory. ACC: MOL.19961230.0037.

157427 Vaniman, D.T.; Chipera, S.J.; Bish, D.L.; Carey, J.W.; and Levy, S.S. 2001. "Quantification of Unsaturated-Zone Alteration and Cation Exchange in Zeolitized Tuffs at Yucca Mountain, Nevada, USA." *Geochimica et Cosmochimica Acta, 65,* (20), 3409-3433. New York, New York: Elsevier. TIC: 251574.

178577 Vecchia, A.V. and Cooley, R.L. 1987. "Simultaneous Confidence and Prediction Intervals for Nonlinear Regression Models with Application to a Groundwater Flow Model." *Water Resources Research, 23,* (7), 1237-1250. Washington, D.C.: American Geophysical Union. ACC: MOL.20070108.0002.

143606 Verma, S. and Aziz, K. 1997. "A Control Volume Scheme for Flexible Grids in Reservoir Simulation." *Proceedings, SPE Reservoir Simulation Symposium, 8-11, June 1997, Dallas, Texas.* SPE 37999. Pages 215-227. Richardson, Texas: Society of Petroleum Engineers. TIC: 247097.

154706 Vesselinov, V.V.; Illman, W.A.; Hyun, Y.; Neuman, S.P.; Di Federico, V.; and Tartakovsky, D.M. 2001. "Observation and Analysis of a Pronounced Permeability and Porosity Scale-Effect in Unsaturated Fractured Tuff." *Fractured Rock 2001, An International Conference Addressing Groundwater Flow, Solute Transport, Multiphase Flow, and Remediation in Fractured Rock, March 26-28, 2001, Toronto, Ontario, Canada.* Kueper, B.H.; Novakowski, K.S.; and Reynolds, D.A., eds. Smithville, Ontario, Canada: Smithville Phase IV. TIC: 249909.

101062 Waddell, R.K. 1982. *Two-Dimensional, Steady-State Model of Ground-Water Flow, Nevada Test Site and Vicinity, Nevada-California.* Water-Resources Investigations Report 82-4085. Denver, Colorado: U.S. Geological Survey. ACC: NNA.19870518.0055.

103022 Walker, G.E. and Eakin, T.E. 1963. *Geology and Ground Water of Amargosa Desert, Nevada-California.* Ground-Water Resources – Reconnaissance Series Report 14. Carson City, Nevada: State of Nevada, Department of Conservation and Natural Resources. TIC: 208665.

178643 Watermark Computing 2004. *Groundwater Data Utilities Part B: Program Descriptions.* Brisbane, Australia: Watermark Computing. ACC: MOL.20070115.0009.

178642 Watermark Numerical Computing 2003. *Groundwater Data Utilities Part A: Overview.* Brisbane, Australia: Watermark Numerical Computing. ACC: MOL.20070115.0008.

178612 Watermark Numerical Computing 2004. *PEST, Model-Independent Parameter Estimation User Manual.* 5th Edition. Brisbane, Australia: Watermark Numerical Computing. ACC: MOL.20070111.0002.

130510 Wen, X-H. and Gomez-Hernandez, J.J. 1996. "The Constant Displacement Scheme for Tracking Particles in Heterogeneous Aquifers." *Ground Water, 34,* (1), 135-142. Worthington, Ohio: Water Well Journal Publishing. TIC: 246656.

137305 Whelan, J.F.; Moscati, R.J.; Allerton, S.B.M.; and Marshall, B.D. 1998. *Applications of Isotope Geochemistry to the Reconstruction of Yucca Mountain, Nevada, Paleohydrology—Status of Investigations: June 1996*. Open-File Report 98-83. Denver, Colorado: U.S. Geological Survey. ACC: MOL.19981012.0740.

108865 Whelan, J.F.; Moscati, R.J.; Roedder, E.; and Marshall, B.D. 1998. "Secondary Mineral Evidence of Past Water Table Changes at Yucca Mountain, Nevada." *High-Level Radioactive Waste Management, Proceedings of the Eighth International Conference, Las Vegas, Nevada, May 11-14, 1998.* Pages 178-181. La Grange Park, Illinois: American Nuclear Society. TIC: 237082.

101165 White, A.F. 1979. *Geochemistry of Ground Water Associated with Tuffaceous Rocks, Oasis Valley, Nevada.* Professional Paper 712-E. Washington, D.C.: U.S. Geological Survey. TIC: 219633.

108871 White, A.F. and Chuma, N.J. 1987. "Carbon and Isotopic Mass Balance Models of Oasis Valley - Fortymile Canyon Groundwater Basin, Southern Nevada." *Water Resources Research, 23,* (4), 571-582. Washington, D.C.: American Geophysical Union. TIC: 237579.

101166 White, A.F.; Claassen, H.C.; and Benson, L.V. 1980. *The Effect of Dissolution of Volcanic Glass on the Water Chemistry in a Tuffaceous Aquifer, Rainier Mesa, Nevada.* Geochemistry of Water. Geological Survey Water-Supply Paper 1535-Q, Washington, D.C.: U.S. Government Printing Office. TIC: 221391.

170977 Williams, N.H. 2003. "Contract No. DE-AC28-01RW12101 - Transmittal of Report Technical Basis Document No. 11: Saturated Zone Flow and Transport Revision 2 Addressing Twenty-Five Key Technical Issue (KTI) Agreements Related to Saturated Zone Flow and Transport." Letter from N.H. Williams (BSC) to C.M. Newbury (DOE/ORD), September 30, 2003, MP:cg - 0930038958, with enclosure. ACC: MOL.20040105.0270.

155614 Wilson, C. 2001. *Data Qualification Report: Stratigraphic Data Supporting the Hydrogeologic Framework Model for Use on the Yucca Mountain Project*. TDR-NBS-HS-000013 REV 00. Las Vegas, Nevada: Bechtel SAIC Company. ACC: MOL.20010725.0225.

108882 Winograd, I.J. and Pearson, F.J., Jr. 1976. "Major Carbon 14 Anomaly in a Regional Carbonate Aquifer: Possible Evidence for Megascale Channeling, South Central Great Basin." *Water Resources Research, 12,* (6), 1125-1143. Washington, D.C.: American Geophysical Union. TIC: 217731.

101167 Winograd, I.J. and Thordarson, W. 1975. *Hydrogeologic and Hydrochemical Framework, South-Central Great Basin, Nevada-California, with Special Reference to the Nevada Test Site*. Geological Survey Professional Paper 712-C. Washington, D.C.: United States Government Printing Office. ACC: NNA.19870406.0201.

100094 Winograd, I.J.; Coplen, T.B.; Landwehr, J.M.; Riggs, A.C.; Ludwig, K.R.; Szabo, B.J.; Kolesar, P.T.; and Revesz, K.M. 1992. "Continuous 500,000-Year Climate Record from Vein Calcite in Devils Hole, Nevada." *Science, 258,* 255-260. Washington, D.C.: American Association for the Advancement of Science. TIC: 237563.

178405 Winterle, J. 2005. *Simulation of Spring Flows South of Yucca Mountain, Nevada, Following a Potential Future Water Table Rise.* San Antonio, Texas: Center for Nuclear Waste Regulatory Analyses. ACC: MOL.20061120.0234.

178404 Winterle, J.R. 2003. *Evaluation of Alternative Concepts for Saturated Zone Flow: Effects of Recharge and Water Table Rise on Flow Paths and Travel Times at Yucca Mountain*. San Antonio, Texas: Center for Nuclear Waste Regulatory Analyses. ACC: MOL.20061120.0233.

129796 Winterle, J.R. and La Femina, P.C. 1999. *Review and Analysis of Hydraulic and Tracer Testing at the C-Holes Complex Near Yucca Mountain, Nevada.* San Antonio, Texas: Center for Nuclear Waste Regulatory Analyses. TIC: 246623.

149596 Yang, I.C. and Peterman, Z.E. 1999. "Chemistry and Isotopic Content of Perched Water." In *Hydrogeology of the Unsaturated Zone, North Ramp Area of the Exploratory Studies Facility, Yucca Mountain, Nevada.* Rousseau, J.P.; Kwicklis, E.M.; and Gillies, D.C., eds. Water-Resources Investigations Report 98-4050. Denver, Colorado: U.S. Geological Survey. ACC: MOL.19990419.0335.

100194 Yang, I.C.; Rattray, G.W.; and Yu, P. 1996. *Interpretation of Chemical and Isotopic Data from Boreholes in the Unsaturated Zone at Yucca Mountain, Nevada.* Water-Resources Investigations Report 96-4058. Denver, Colorado: U.S. Geological Survey. ACC: MOL.19980528.0216.

101441 Yang, I.C.; Yu, P.; Rattray, G.W.; Ferarese, J.S.; and Ryan, J.N. 1998. *Hydrochemical Investigations in Characterizing the Unsaturated Zone at Yucca Mountain, Nevada.* Water-Resources Investigations Report 98-4132. Denver, Colorado: U.S. Geological Survey. ACC: MOL.19981012.0790.

179430 YMP (Yucca Mountain Site Characterization Project) 2001. Sample Collection Report, Characterization of the Yucca Mountain Unsaturated-Zone Percolation Surface-Based Studies, May 17, 1995 through May 18, 1995. Las Vegas, Nevada: Yucca Mountain Site Characterization Office. ACC: MOL.20011030.0681.

101171 Zyvoloski, G. 1983. "Finite Element Methods for Geothermal Reservoir Simulation." *International Journal for Numerical and Analytical Methods in Geomechanics, 7,* (1), 75-86. New York, New York: John Wiley & Sons. TIC: 224068.

163341 Zyvoloski, G.; Kwicklis, E.; Eddebbarh, A.A.; Arnold, B.; Faunt, C.; and Robinson, B.A. 2003. "The Site-Scale Saturated Zone Flow Model for Yucca Mountain: Calibration of Different Conceptual Models and their Impact on Flow Paths." *Journal of Contaminant Hydrology, 62-63,* 731-750. New York, New York: Elsevier. TIC: 254340.

9.2 CODES, STANDARDS, REGULATIONS, AND PROCEDURES

176567 10 CFR 50. 2006. Energy: Domestic Licensing of Production and Utilization Facilities. Internet Accessible.

176544 10 CFR 63. 2006. Energy: Disposal of High-Level Radioactive Wastes in a Geologic Repository at Yucca Mountain, Nevada. Internet Accessible.

AP-2.22Q, Rev. 1, ICN 1. *Classification Analyses and Maintenance of the Q-List.* Washington, D.C.: U.S. Department of Energy, Office of Civilian Radioactive Waste Management. ACC: DOC.20040714.0002.

AP-2.27Q, Rev. 1, ICN 5. *Planning for Science Activities.* Washington, D.C.: U.S. Department of Energy, Office of Civilian Radioactive Waste Management. ACC: DOC.20041014.0001.

AP-SI.1Q, Rev. 5, ICN 2. *Software Management.* Washington, D.C.: U.S. Department of Energy, Office of Civilian Radioactive Waste Management. ACC: DOC.20030902.0003.

AP-SIII.10Q, Rev. 2, ICN 7. *Models.* Washington, D.C.: U.S. Department of Energy, Office of Civilian Radioactive Waste Management. ACC: DOC.20040920.0002.

176399 ASME NQA-1-2004. 2004. Quality Assurance Requirements for Nuclear Facilities Applications. New York, New York: American Society of Mechanical Engineers. TIC: 256850.

177092 DOE (U.S. Department of Energy) 2006. *Quality Assurance Requirements and Description*. DOE/RW-0333P, Rev. 18. Washington, D.C.: U.S. Department of Energy, Office of Civilian Radioactive Waste Management. ACC: DOC.20060602.0001.

IT-PRO-0011, *Software Management*.

IT-PRO-0012, *Qualification of Software*.

IT-PRO-0013 *Software Independent Verification and Validation*.

LP-SI.11Q-BSC, Rev. 0, ICN 1. *Software Management.* Washington, D.C.: U.S. Department of Energy, Office of Civilian Radioactive Waste Management. ACC: DOC.20041005.0008.

LS-PRO-0203, *Q-List and Classification of Structures, Systems, and Components*.

SCI-PRO-001, *Qualification of Unqualified Data*.

SCI-PRO-003, Rev. 2, ICN 0. *Document Review.* Washington, D.C.: U.S. Department of Energy, Office of Civilian Radioactive Waste Management. ACC: DOC.20070418.0002.

SCI-PRO-006, *Models*.

9.3 SOURCE DATA, LISTED BY DATA TRACKING NUMBER

149155 GS000308312322.003. Preliminary Release of Field, Chemical, and Isotopic Data from the Nye County Early Warning Drilling Program (EWDP) Wells in Amargosa Valley, Nevada Collected Between 12/11/98 and 11/15/99. Submittal date: 03/16/2000.

149947 GS000508312332.001. Water-Level Data Analysis for the Saturated Zone Site-Scale Flow and Transport Model. Submittal date: 06/01/2000.

150842 GS000700012847.001. Chemical and Isotopic Data from Cind-R-Lite Well Samples Collected on 5/17/95 and 9/6/95. Submittal date: 07/10/2000.

155270 GS000808312312.007. Ground-Water Altitudes from Manual Depth-to-Water Measurements at Various Boreholes November 1998 through December 1999. Submittal date: 08/21/2000.

171433 GS001208312312.009. Ground-Water Altitudes from Manual Depth-to-Water Measurements at Various Boreholes January through June 2000. Submittal date: 12/29/2000.

162908 GS010208312322.001. Uranium Concentrations and 234U/238U Activity Ratios Analyzed Between August, 1998 and April, 2000 for Saturated-Zone Well Water, Springs, and Runoff Collected between April, 1998 and November 1999. Submittal date: 03/30/2001.

162910 GS010308312322.002. Chemical and Isotopic Data from Wells in Yucca Mountain Area, Nye County, Nevada, Collected between 12/11/98 and 11/15/99. Submittal date: 03/29/2001.

154734 GS010308312322.003. Field, Chemical and Isotopic Data from Wells in Yucca Mountain Area, Nye County, Nevada, Collected Between 12/11/98 and 11/15/99. Submittal date: 03/29/2001.

155307 GS010608312332.001. Potentiometric-Surface Map, Assuming Perched Conditions North of Yucca Mountain, in the Saturated Site-Scale Model. Submittal date: 06/19/2001.

156187 GS010608315215.002. Uranium and Thorium Isotope Data for Waters Analyzed Between January 18, 1994 and September 14, 1996. Submittal date: 06/26/2001.

156007 GS010808312322.004. Uranium and Uranium Isotopic Data for Water Samples from Wells and Springs in the Yucca Mountain Vicinity Collected Between December 1996 and December 1997. Submittal date: 08/29/2001.

163555 GS010908312332.002. Borehole Data from Water-Level Data Analysis for the Saturated Zone Site-Scale Flow and Transport Model. Submittal date: 10/02/2001.

168699 GS010908312332.003. Vertical Head Differences from Water-Level Data Analysis for the Saturated Zone Site-Scale Flow and Transport Model. Submittal date: 10/20/2001.

162874 GS010908314221.001. Geologic Map of the Yucca Mountain Region, Nye County, Nevada. Submittal date: 01/23/2002.

158690 GS011008314211.001. Interpretation of the Lithostratigraphy in Deep Boreholes NC-EWDP-19D1 and NC-EWDP-2DB Nye County Early Warning Drilling Program. Submittal date: 01/16/2001.

162911 GS011108312322.006. Field and Chemical Data Collected between 1/20/00 and 4/24/01 and Isotopic Data Collected between 12/11/98 and 11/6/00 from Wells in the Yucca Mountain Area, Nye County, Nevada. Submittal date: 11/20/2001.

174112 GS020108314211.001. Interpretation of the Lithostratigraphy in Deep Boreholes, NC-EWDP-7SC and NC EWDP-15P, Nye County Early Warning Drilling Program. Submittal date: 01/16/2001.

162913 GS021008312322.002. Stable Isotopic Data for Water Samples Collected between 02/20/98 and 08/20/98 in the Yucca Mountain Area, Nye County, Nevada. Submittal date: 11/12/2002.

163483 GS030108314211.001. Interpretation of the Lithostratigraphy in Deep Boreholes NC-EWDP-18P, NC-EWDP-22SA, NC-EWDP-10SA, NC-EWDP-23P, NC-EWDP-19IM1A, and NC-EWDP-19IM2A, Nye County Early Warning Drilling Program, Phase III. Submittal date: 02/11/2003.

163087 GS030208312332.001. HFM Final Output - Hydrogeologic Framework Model for the Saturated-Zone Site-Scale Flow and Transport Model. Submittal date: 02/10/2003.

166467 GS031108312322.003. Uranium Concentrations and 234U/238U Ratios for Ground-Water Samples from Boreholes ER-EC-7, ER-18-2, and UE-18R Collected between December 1999 and June 2000. Submittal date: 11/25/2003.

174113 GS031108314211.004. Interpretation of the Lithostratigraphy in Deep Boreholes NC-EWDP-16P, NC-EWDP-27P, and NC-EWDP-28P, Nye County Early Warning Drilling Program, Phase IV A. Submittal date: 11/26/2003.

179431 GS031208312322.004. Dissolved Organic Carbon-14 (DOC-14) Hydrochronology Data for Groundwater from Wells in the Yucca Mountain Area for Samples Analyzed through 1/30/2003. Submittal date: 01/26/2004.

179422 GS040108312322.001. Field and Chemical Data Collected Between 10/4/01 and 10/3/02 and Isotopic Data Collected Between 5/19/00 and 5/22/03 from Wells in the Yucca Mountain Area, Nye County, Nevada. Submittal date: 06/07/2004.

172396 GS040208312322.003. Uranium Concentrations and 234U/238U Ratios from Spring, Well, Runoff, and Rain Waters Collected from the Nevada Test Site and Death Valley Vicinities and Analyzed between 01/15/98 and 08/15/98. Submittal date: 04/01/2004.

179432 GS040708312322.004. Strontium Isotope Ratios and Strontium Concentrations on Groundwater Samples from Springs in the Area of Amargosa Valley and Desert. Submittal date: 09/08/2004.

179433 GS040808312322.005. Strontium Isotope Ratios and Strontium Concentrations on Groundwater Samples in Support of Nye Co. Early Warning Drilling Program (EWDP) and the Alluvial Tracer Complex (ATC). Submittal date: 09/20/2004.

179434 GS040808312322.006. Field, Chemical, and Isotope Data for Spring and Well Samples Collected Between 03/01/01 and 05/12/04 in the Yucca Mountain Area, Nye County, Nevada. Submittal date: 11/15/2004.

174114 GS040908314211.001. Interpretation of the Lithostratigraphy in Deep Boreholes NC-EWDP-24P and NC-EWDP-29P, Nye County Early Warning Drilling Program, Phase IV B. Submittal date: 10/26/2004.

179435 GS050708314211.001. Description and Interpretation of Core Samples from Alluvial Core Holes NC-EWDP-19PB and NC-EWDP-22PC, Nye County Early Warning Drilling Program. Submittal date: 07/27/2005.

105937 GS920408312321.003. Chemical Composition of Groundwater in the Yucca Mountain Area, Nevada 1971 - 1984. Submittal date: 04/24/1987.

148109 GS930108315213.002. Water Chemistry and Sample Documentation for Two Samples from Lathrop Wells Cone and USW VH-2. Submittal date: 01/15/1993.

145525 GS930108315213.004. Uranium Isotopic Analyses of Groundwaters from SW Nevada – SE California. Submittal date: 01/21/1993.

145530 GS930308312323.001. Chemical Composition of Groundwater and the Locations of Permeable Zones in the Yucca Mountain Area. Submittal date: 03/05/1993.

145404 GS930908312323.003. Hydrochemical Data from Field Test and Lab Analyses of Water Samples Collected at Field Stations: USW VH-1, JF3, UE-29 UZN#91, Virgin Spring, Nevares Spring, UE-25 J#12, UE-25 J#13, UE-22 ARMY#1, and USW UZ-14. Submittal date: 09/30/1993.

149611 GS931100121347.007. Selected Ground-Water Data for Yucca Mountain Region, Southern Nevada and Eastern California, Through December 1992. Submittal date: 11/30/1993.

164673 GS940908315213.005. U Concentrations and 234U/238U Ratios for Waters in Yucca Mountain Region. Submittal date: 09/22/1994.

106516 GS950708315131.003. Woodrat Midden Age Data in Radiocarbon Years Before Present. Submittal date: 07/21/1995.

148114 GS950808312322.001. Field, Chemical, and Isotopic Data Describing Water Samples Collected in Death Valley National Monument and at Various Boreholes in and Around Yucca Mountain, Nevada, Between 1992 and 1995. Submittal date: 08/16/1995.

151649 GS951208312272.002. Tritium Analyses of Porewater from USW UZ-14, USW NRG-6, USW NRG-7A and UE-25 UZ#16 and of Perched Water from USW SD-7, USW SD-9, USW UZ-14 and USW NRG-7A from 12/09/92 to 5/15/95. Submittal date: 12/15/1995.

106517 GS960308315131.001. Woodrat Midden Radiocarbon (C14). Submittal date: 03/07/1996.

162915 GS960408312323.002. Chemical and Isotopic Data Describing Water Samples Collected from 11 Springs and One Stream Within Death Valley National Park in 1993, 1994, and 1995. Submittal date: 04/02/1996.

114124 GS960908312232.012. Comparison of Air-Injection Permeability Values to Laboratory Permeability Values. Submittal date: 09/26/1996.

162916 GS960908312323.005. Hydrochemical Data Obtained from Water Samples Collected at Water Well ER-30-1 on 1/31/95 and 2/1/95. Submittal date: 09/10/1996.

145405 GS970708312323.001. Delta 18-O and Delta D Stable Isotope Analyses of a Bore-Hole Waters from GEXA Well 4 and VH-2. Submittal date: 07/22/1997.

164674 GS970708315215.008. Strontium Isotope Ratios and Isotope Dilution Data for Strontium for Two Samples Collected at UE-25 C#3, 12/4/96 and 2/19/97. Submittal date: 07/29/1997.

145921 GS970808315215.012. Uranium and Thorium Isotope Data from Secondary Minerals in the ESF Collected Between 02/15/97 and 09/15/97. Submittal date: 09/17/1997.

149617 GS980108312322.005. Water Chemistry Data from Samples Collected at Borehole USW WT-24, Between 10/06/97 and 12/10/97. Submittal date: 01/26/1998.

146065 GS980208312322.006. Uranium Isotopic Data for Saturated- and Unsaturated-Zone Waters Collected by Non-YMP Personnel Between May 1989 and August 1997. Submittal date: 02/03/1998.

145412 GS980908312322.008. Field, Chemical, and Isotopic Data from Precipitation Sample Collected Behind Service Station in Area 25 and Ground Water Samples Collected at Boreholes UE-25 C #2, UE-25 C #3, USW UZ-14, UE-25 WT #3, UE-25 WT #17, and USW WT-24, 10/06/97 to 07/01/98. Submittal date: 09/15/1998.

118977 GS980908312322.009. Uranium Concentrations and {superscript 234}U/{superscript 238}U Ratios from Spring, Well, Runoff, and Rain Waters Collected from the Nevada Test Site and Death Valley Vicinities and Analyzed between 01/15/1998 and 08/15/1998. Submittal date: 09/23/1998.

145692 GS990308312272.002. Isotopic Composition of Pore Water from Boreholes USW UZ-14 and USW NRG-6. Submittal date: 03/02/1999.

149393 GS990808312322.001. Field and Isotopic Data From Ground Water Samples From Wells in the Amargosa Valley and NTS. Submittal date: 08/23/1999.

162917 GS990808312322.002. Chemical and Isotopic Data from Ground Water Samples Collected from Wells in the Amargosa. Submittal date: 08/23/1999.

145263 GS991208314221.001. Geologic Map of the Yucca Mountain Region. Submittal date: 12/01/1999.

147077 LA0002JF831222.001. Apparent Infiltration Rates in Alluvium from USW UZ-N37, USW UZ-N54, USW UZ-14 and UE-25 UZ#16, Calculated by Chloride Mass Balance Method. Submittal date: 02/25/2000.

147079 LA0002JF831222.002. Apparent Infiltration Rates in PTN Units from USW UZ-7A, USW UZ-N55, USW UZ-14, UE-25 UZ#16, USW NRG-6, USW NRG-7A, and USW SD-6, SD-7, SD-9 and SD-12 Calculated by the Chloride Mass Balance Method. Submittal date: 02/25/2000.

165507 LA0202EK831231.002. Calculation of Corrected and Uncorrected Groundwater Carbon-14 Ages. Submittal date: 02/25/2002.

180317 LA0202EK831231.004. Calculation of the Maximum Possible Percentage of 1000 Year-Old Water Present in Selected Yucca Mountain Area Groundwater Samples. Submittal date: 02/25/2002.

163561 LA0303PR831231.002. Estimation of Groundwater Drift Velocity from Tracer Responses in Single-Well Tracer Tests at Alluvium Testing Complex. Submittal date: 03/18/2003.

163788 LA0304TM831231.002. SZ Site-Scale Flow Model, FEHM Files for Base Case. Submittal date: 04/14/2003.

171890 LA0308RR831233.001. Regional Groundwater Flow Pathways in the Yucca Mountain Area Inferred from Hydrochemical and Isotopic Data. Submittal date: 08/25/2003.

165471 LA0309EK831223.001. UTM Coordinates for Selected Amargosa Desert Wells. Submittal date: 09/05/2003.

171887 LA0309EK831231.001. SZ Flow and Transport Model, FEHM Files for Tracer Transport. Submittal date: 09/02/2003.

166546 LA0309RR831233.001. Regional Groundwater Hydrochemical Data in the Yucca Mountain Area Used as Direct Inputs for ANL-NBS-HS-000021, REV 01. Submittal date: 09/05/2003.

166548 LA0309RR831233.002. Regional Groundwater Hydrochemical Data in the Yucca Mountain Area Used as Corroborative Data for ANL-NBS-HS-000021, REV 01. Submittal date: 09/05/2003.

171889 LA0310EK831231.001. SZ Geochemical Calculations, Groundwater Travel Times for Selected Wells. Submittal date: 10/16/2003.

165995 LA0310EK831232.001. SZ Geochemical Models, PHREEQC Files for Selected Groundwater Parameters. Submittal date: 10/02/2003.

165985 LA0311EK831223.001. Well Completion Summary Information for the Nye County EWDP, Phases I and II. Submittal date: 11/04/2003.

166068 LA0311EK831232.001. Hydrochemical Data Obtained from GEOCHEM.02 Database. Submittal date: 11/06/2003.

166069 LA0311EK831232.002. Groundwater Hydrochemical Data from Nye County Early Warning Drilling Project Boreholes as Reported by Nye County. Submittal date: 11/04/2003.

171899 LA0410PR831231.001. Normalized Tracer Concentrations and Recoveries in C-Wells Tracer Tests. Submittal date: 10/04/2004.

122733 LA9909JF831222.010. Chloride, Bromide, Sulfate, and Chlorine-36 Analyses of ESF Porewaters. Submittal date: 09/29/1999.

122736 LA9909JF831222.012. Chloride, Bromide, and Sulfate Analyses of Porewater Extracted from ESF Niche 3566 (Niche #1) and ESF 3650 (Niche #2) Drillcore. Submittal date: 09/29/1999.

145401 LAJF831222AQ97.002. Chlorine-36 Analyses of Packrat Urine. Submittal date: 09/26/1997.

145402 LAJF831222AQ98.011. Chloride, Bromide, Sulfate and Chlorine-36 Analyses of Springs, Groundwater, Porewater, Perched Water and Surface Runoff. Submittal date: 09/10/1998.

163044 LB03023DSSCP9I.001. 3-D Site Scale UZ Flow Field Simulations for 9 Infiltration Scenarios. Submittal date: 02/28/2003.

148744 MO0003SZFWTEEP.000. Data Resulting from the Saturated Zone Flow and Transport Expert Elicitation Project. Submittal date: 03/06/2000.

151492 MO0007GNDWTRIS.002. Isotopic Content of Groundwater from Yucca Mountain Project Borehole, USW G-2, Extracted from ANL-NBS-HS-000021, Geochemical and Isotopic Constraints on Groundwater Flow Directions, Mixing and Recharge at Yucca Mountain, Nevada. Submittal date: 07/27/2000.

151493 MO0007GNDWTRIS.003. Isotopic Content of Groundwater from Yucca Mountain Project Boreholes UZ-14, WT-17, and WT #3, Extracted from ANL-NBS-HS-000021, Geochemical and Isotopic Constraints on Groundwater Flow Directions, Mixing and Recharge at Yucca Mountain, Nevada. Submittal date: 07/27/2000.

151494 MO0007GNDWTRIS.004. Isotopic Content of Groundwater from Borehole TW-5 Extracted from ANL-NBS-HS-000021, Geochemical and Isotopic Constraints on Groundwater Flow Directions, Mixing and Recharge at Yucca Mountain, Nevada. Submittal date: 07/27/2000.

151495 MO0007GNDWTRIS.005. Isotopic Content of Groundwater from Yucca Mountain Project Borehole JF #3, Extracted from ANL-NBS-HS-000021, Geochemical and Isotopic Constraints on Groundwater Flow Directions, Mixing and Recharge at Yucca Mountain, Nevada. Submittal date: 07/28/2000.

151496 MO0007GNDWTRIS.006. Isotopic Content of Groundwater from Selected Yucca Mountain Project WT Boreholes Extracted from ANL-NBS-HS-000021, Geochemical and Isotopic Constraints on Groundwater Flow Directions, Mixing and Recharge at Yucca Mountain, Nevada. Submittal date: 07/28/2000.

151497 MO0007GNDWTRIS.007. Isotopic Content of Groundwater from Yucca Mountain Project Boreholes WT #14, WT #15, and WT #12, Extracted from ANL-NBS-HS-000021, Geochemical and Isotopic Constraints on Groundwater Flow Directions, Mixing and Recharge at Yucca Mountain, Nevada. Submittal date: 07/28/2000.

151508 MO0007GNDWTRIS.008. Isotopic Content of Groundwater from Yucca Mountain Project Borehole UE-25 P #1 Extracted from ANL-NBS-HS-000021, Geochemical and Isotopic Constraints on Groundwater Flow Directions, Mixing and Recharge at Yucca Mountain, Nevada. Submittal date: 07/28/2000.

151509 MO0007GNDWTRIS.009. Isotopic Content of Groundwater from Selected Yucca Mountain Project Boreholes Extracted from ANL-NBS-HS-000021, Geochemical and Isotopic Constraints on Groundwater Flow Directions, Mixing and Recharge at Yucca Mountain, Nevada. Submittal date: 07/28/2000.

151500 MO0007GNDWTRIS.010. Isotopic Content of Groundwater from Selected Yucca Mountain Project Boreholes Extracted from ANL-NBS-HS-000021, Geochemical and Isotopic Constraints on Groundwater Flow Directions, Mixing and Recharge at Yucca Mountain, Nevada. Submittal date: 07/28/2000.

151501 MO0007GNDWTRIS.011. Isotopic Content of Groundwater from Selected Boreholes Not Drilled for the Yucca Mountain Project Extracted from ANL-NBS-HS-000021, Geochemical and Isotopic Constraints on Groundwater Flow Directions, Mixing and Recharge at Yucca Mountain, Nevada. Submittal date: 07/28/2000.

151504 MO0007GNDWTRIS.013. Isotopic Content of Perched Groundwater from Yucca Mountain Project Boreholes Extracted from ANL-NBS-HS-000021, Geochemical and Isotopic Constraints on Groundwater Flow Directions, Mixing and Recharge at Yucca Mountain, Nevada. Submittal date: 07/28/2000.

151507 MO0007MAJIONPH.002. Major Ion Content of Groundwater from Borehole TW-5 Extracted from ANL-NBS-HS-000021, Geochemical and Isotopic Constraints on Groundwater Flow Directions, Mixing and Recharge at Yucca Mountain, Nevada. Submittal date: 07/27/2000.

151513 MO0007MAJIONPH.003. Major Ion Content of Groundwater from Yucca Mountain Project Borehole USW G-2, Extracted from ANL-NBS-HS-000021, Geochemical and Isotopic Constraints on Groundwater Flow Directions, Mixing and Recharge at Yucca Mountain, Nevada. Submittal date: 07/27/2000.

151516 MO0007MAJIONPH.004. Major Ion Content of Groundwater from Borehole ONC #1, Extracted from ANL-NBS-HS-000021, Geochemical and Isotopic Constraints on Groundwater Flow Directions, Mixing and Recharge at Yucca Mountain, Nevada. Submittal date: 07/27/2000.

151517 MO0007MAJIONPH.005. Major Ion Content of Groundwater from Boreholes UZ-14, WT-17 and WT #3, Extracted from ANL-NBS-HS-000021, Geochemical and Isotopic Constraints on Groundwater Flow Directions, Mixing and Recharge at Yucca Mountain, Nevada. Submittal date: 07/27/2000.

151518 MO0007MAJIONPH.006. Major Ion Content of Groundwater from Selected Boreholes Not Drilled on the Yucca Mountain Project, Extracted from ANL-NBS-HS-000021, Geochemical and Isotopic Constraints on Groundwater Flow Directions, Mixing and Recharge at Yucca Mountain, Nevada. Submittal date: 07/25/2000.

151519 MO0007MAJIONPH.007. Major Ion Content of Groundwater from Yucca Mountain Project Borehole UE-25 UZ #16, Extracted from ANL-NBS-HS-000021, Geochemical and Isotopic Constraints on Groundwater Flow Directions, Mixing and Recharge at Yucca Mountain, Nevada. Submittal date: 07/27/2000.

151521 MO0007MAJIONPH.008. Major Ion Content of Groundwater from Selected YMP and Other Boreholes Extracted from ANL-NBS-HS-000021, Geochemical and Isotopic Constraints on Groundwater Flow Directions, Mixing and Recharge at Yucca Mountain, Nevada. Submittal date: 07/27/2000.

151522 MO0007MAJIONPH.009. Major Ion Content of Groundwater from Borehole NDOT Extracted from ANL-NBS-HS-000021, Geochemical and Isotopic Constraints on Groundwater Flow Directions, Mixing and Recharge at Yucca Mountain, Nevada. Submittal date: 07/27/2000.

151523 MO0007MAJIONPH.010. Major Ion Content of Groundwater from Borehole UE-25 P #1 Extracted from ANL-NBS-HS-000021, Geochemical and Isotopic Constraints on Groundwater Flow Directions, Mixing and Recharge at Yucca Mountain, Nevada. Submittal date: 07/27/2000.

151524 MO0007MAJIONPH.011. Major Ion Content of Groundwater from Selected Yucca Mountain Project Boreholes Extracted from ANL-NBS-HS-000021, Geochemical and Isotopic Constraints on Groundwater Flow Directions, Mixing and Recharge at Yucca Mountain, Nevada. Submittal date: 07/27/2000.

151529 MO0007MAJIONPH.012. Major Ion Content of Groundwater from Selected YMP and Other Boreholes Extracted from ANL-NBS-HS-000021, Geochemical and Isotopic Constraints on Groundwater Flow Directions, Mixing and Recharge at Yucca Mountain, Nevada. Submittal date: 07/27/2000.

151530 MO0007MAJIONPH.013. Major Ion Content of Groundwater from Selected YMP and Other Boreholes Extracted from ANL-NBS-HS-000021, Geochemical and Isotopic Constraints on Groundwater Flow Directions, Mixing and Recharge at Yucca Mountain, Nevada. Submittal date: 07/27/2000.

151531 MO0007MAJIONPH.014. Major Ion Content of Groundwater from Selected Boreholes Not Drilled on the Yucca Mountain Project Extracted from ANL-NBS-HS-000021, Geochemical and Isotopic Constraints on Groundwater Flow Directions, Mixing and Recharge at Yucca Mountain, Nevada. Submittal date: 07/27/2000.

151532 MO0007MAJIONPH.015. Major Ion Content of Groundwater from NC-EWDP Boreholes Extracted from ANL-NBS-HS-000021, Geochemical and Isotopic Constraints on Groundwater Flow Directions, Mixing and Recharge at Yucca Mountain, Nevada. Submittal date: 07/27/2000.

151533 MO0007MAJIONPH.016. Major Ion Content of Perched Groundwater from Selected YMP Boreholes with Perched Water Extracted from ANL-NBS-HS-000021, Geochemical and Isotopic Constraints on Groundwater Flow Directions, Mixing and Recharge at Yucca Mountain, Nevada. Submittal date: 07/28/2000.

151534 MO0008MAJIONPH.017. Major Ion Content of Groundwater from Selected WT Boreholes Drilled for the Yucca Mountain Project Extracted from ANL-NBS-HS-000021, Geochemical and Isotopic Constraints on Groundwater Flow Directions, Mixing and Recharge at Yucca Mountain, Nevada. Submittal date: 08/02/2000.

153777 MO0012MWDGFM02.002. Geologic Framework Model (GFM2000). Submittal date: 12/18/2000.

153384 MO0012URANISOT.000. Water - Selected Uranium Abundance and Isotope Ratios. Submittal date: 12/06/2000.

154733 MO0102DQRBTEMP.001. Temperature Data Collected from Boreholes Near Yucca Mountain in Early 1980's. Submittal date: 02/21/2001.

155523 MO0102DQRGWREC.001. Groundwater Recharge Rate Data for the Four Reaches of Fortymile Wash Near Yucca Mountain, Nevada. Submittal date: 02/26/2001.

179436 MO0110NYE03848.087. NC-EWDP-WASHBURN 1X Well Completion Diagram. Submittal date: 10/17/2001.

157184 MO0112DQRWLNYE.014. Well Completion Diagram for Borehole NC-EWDP-19P. Submittal date: 12/04/2001.

157187 MO0112DQRWLNYE.018. Well Completion Diagram for Borehole NC-EWDP-19D. Submittal date: 12/05/2001.

168375 MO0203GSC02034.000. As-Built Survey of Nye County Early Warning Drilling Program (EWDP) Phase III Boreholes NC-EWDP-10S, NC-EWDP-18P, and NC-EWDP-22S - Partial Phase III List. Submittal date: 03/21/2002.

168378 MO0206GSC02074.000. As-Built Survey of Nye County Early Warning Drilling Program (EWDP) Phase III Boreholes, Second Set. Submittal date: 06/03/2002.

179372 MO0206NYE04926.119. NC-EWDP-7SC Well Completion Diagram. Submittal date: 06/19/2002.

165876 MO0306NYE05259.165. Revised NC-EWDP-19IM1 Well Completion Diagram. Submittal date: 07/02/2003.

165877 MO0306NYE05260.166. Revised NC-EWDP-19IM2 Well Completion Diagram. Submittal date: 07/02/2003.

179373 MO0306NYE05261.167. Revised NC-EWDP-10S Well Completion Diagram. Submittal date: 07/03/2003.

179374 MO0306NYE05262.168. Revised NC-EWDP-10P Well Completion Diagram. Submittal date: 07/03/2003.

179375 MO0306NYE05263.169. Revised NC-EWDP-18P Well Completion Diagram. Submittal date: 07/03/2003.

179376 MO0306NYE05264.170. Revised NC-EWDP-22S Well Completion Diagram. Submittal date: 07/03/2003.

179377 MO0306NYE05265.171. Revised NC-EWDP-22PA Well Completion Diagram. Submittal date: 07/03/2003.

179378 MO0306NYE05266.172. Revised NC-EWDP-22PB Well Completion Diagram. Submittal date: 07/03/2003.

179379 MO0306NYE05267.173. Revised NC-EWDP-23P Well Completion Diagram. Submittal date: 07/03/2003.

170556 MO0307GSC03094.000. As-Built Survey of Nye County Early Warning Drilling Program Phase IV Boreholes EWDP-16P, EWDP-27P & EWDP-28P. Submittal date: 07/14/2003.

165529 MO0309THDPHRQC.000. Input Data File (PHREEQC.DAT) for Thermodynamic Data Software Code PHREEQC, Version 2.3. Submittal date: 09/22/2003.

179440 MO0310UCC008IF.003. Major Cation, Major Anion, and Trace Element Concentrations in Groundwater Collected from the October 2000 Sampling of Phase II and III Wells of the Nye County Early Warning Drilling Program (NC-EWDP). Submittal date: 10/24/2003.

179441 MO0311UCC008IF.007. Major Cation, Major Anion, and Trace Element Concentrations in Groundwaters Collected During the May 2000 Sampling of the Phase I and II Wells of the Nye County Early Warning Drilling Program (NC-EWDP). Submittal date: 11/21/2003.

174103 MO0312GSC03180.000. As-Built Survey of Nye County Early Warning Drilling Program, Phase IV Boreholes: NC-EWPD-24P & NC-EWDP-29P. Submittal date: 12/03/2003.

179380 MO0312NYE05716.204. NC-EWDP-27P Well Completion Diagram. Submittal date: 12/09/2003.

179381 MO0312NYE05718.202. NC-EWDP-28P Well Completion Diagram. Submittal date: 12/09/2003.

174102 MO0408GSC04123.000. Nye County Early Warning Drilling Program, Phase IV, As-Built Location of NC-EWDP-19PB Borehole. Submittal date: 08/12/2004.

179382 MO0409NYE06093.241. NC-EWDP-29P Well Completion Diagram. Submittal date: 09/08/2004.

179383 MO0409NYE06096.242. NC-EWDP-24P Well Completion Diagram. Submittal date: 09/08/2004.

179384 MO0409NYE06101.246. NC-EWDP-19PB Well Completion Diagram. Submittal date: 09/08/2004.

179336 MO0409SEPPSMPC.000. Potentiometric-Surface Map Showing Possible Changes After Including EWDP Phases III and IV Wells. Submittal date: 09/23/2004.

175275 MO0503GSC05025.000. As-Built Location of Nye County Early Warning Drilling Program (EWDP) Phase V Borehole Number NC-EWDP-22PC. Submittal date: 03/10/2005.

179599 MO0505NYE06464.314. NC-EWDP-22PC Well Completion Diagram. Submittal date: 05/16/2005.

177372 MO0507NYE06631.323. EWDP Manual Water Level Measurements through February 2005. Submittal date: 07/21/2005.

174523 MO0507SPAINHFM.000. Input Data for HFM - USGS-Supplied Data to Supplement Regional Hydrogeologic Framework Model. Submittal date: 07/13/2005.

177371 MO0602SPAMODAR.000. Model Archives from USGS Special Investigations Report 2004-5205, Death Valley Regional Ground-Water Flow System, Nevada and California-Hydrogeologic Framework and Transient Ground-Water Flow Model. Submittal date: 02/10/2006.

180539 MO0605SPAFABRP.004. Supporting Calculation Files for the Assessment of Bedrock Saturated Hydraulic Conductivity. Submittal date: 05/25/2006.

180020 MO0606ABLNCPVB.000. As-Built Location of Nye County Early Warning Drilling Program (EWDP) Phase V, Borehole #NC-EWDP-13P. Submittal date: 06/16/2006.

180023 MO0606NYE06949.340. NC-EWDP-24PB Well Completion Diagram. Submittal date: 06/13/2006.

180021 MO0608ABEWDPPV.000. As-Built Location of Nye County Early Warning Drilling Program (EWDP) Phase V, Boreholes #NC-EWDP-24PA, NC-EWDP-24PB, NC-EWDP-32P, and NC-EWDP-33P. Submittal date: 08/08/2006.

179352 MO0610MWDHFM06.002. Hydrogeologic Framework Model (HFM2006) Stratigraphic Horizon Grids. Submittal date: 11/01/2006.

180022 MO0611NYE06947.344. NC-EWDP-13P Well Completion Diagram. Submittal date: 11/17/2006.

179486 MO0612NYE07008.366. NC-EWDP-32P Well Completion Diagram. Submittal date: 12/04/2006.

179487 MO0612NYE07011.368. NC-EWDP-33P Well Completion Diagram. Submittal date: 12/04/2006.

179337 MO0612NYE07122.370. EWDP Manual Water Level Measurements through November 2006. Submittal date: 12/15/2006.

179443 MO0702NYE05714.375. NC-EWDP-16P Well Completion Diagram. Submittal date: 02/27/2007.

181613 MO0706SPAFEPLA.001. FY 2007 LA FEP List and Screening. Submittal date: 06/20/2007.

129714 SNT05082597001.003. TSPA-VA (Total System Performance Assessment-Viability Assessment) Saturated Zone (SZ) Base Case Modeling Analysis Results. Submittal date: 02/03/1998.

9.4 OUTPUT DATA, LISTED BY DATA TRACKING NUMBER

LA0612RR150304.001. UTM Coordinates for Selected Nye County Early Warning Drilling Program Boreholes: NC-EWDP-7SC and Phases III and IV. Submittal date: 12/18/2006.

LA0612RR150304.002. Hydrochemical Data Obtained from the Underground Test Area (UGTA) Program's Geochem05 Database. Submittal date: 12/18/2006.

LA0612RR150304.003. Geochemical and Isotopic Data for Selected NC-EWDP Wells, Phases II, III, and IV. Submittal date: 01/02/2007.

LA0612RR150304.004. Regional Groundwater Flow Pathways In The Yucca Mountain Area Inferred From Hydrochemical And Isotopic Data. Submittal date: 01/02/2007.

LA0612RR150304.005. Uranium Activity Ratios Calculated from Isotopic Ratios Reported for Nye County EWDP Boreholes and McCracken Well by Geochron Laboratories, for Samples Collected between November 1999 and June 2000. Submittal date: 12/21/2006.

LA0612TM831231.001. SZ Site-Scale Flow Model, LaGriT Files for Base-Case FEHM Grid. Submittal date: 12/21/2006.

MO0611SCALEFLW.000. Water Table for the Saturated Zone Site Scale Flow Model. Submittal date: 11/15/2006.

SN0610T0510106.001. Water Level Data, Well Location Data, and Open Well Interval Data. Submittal date: 10/02/2006.

SN0612T0510106.003. Recharge and Lateral Groundwater Flow Boundary Conditions for the Saturated Zone (SZ) Site-Scale Flow Model. Submittal date: 12/04/2006.

SN0612T0510106.004. Saturated Zone (SZ) Site-Scale Flow Model PEST and FEHM Files Using HFM2006. Submittal date: 01/17/2007.

SN0702T0510106.006. Saturated Zone (SZ) Site-Scale Flow Model with "Water Table Rise" Alternate Conceptual Model - FEHM Files Using HFM2006. Submittal date: 02/19/2007.

SN0702T0510106.007. Nye County Early Warning Drilling Program (EWDP) Well Data for Period 2/2001 through 11/2006 Used for Saturated Zone (SZ) Flow Model Potentiometric Surface, Calibration and Validation. Submittal date: 02/22/2007

SN0704T0510106.008. Flux, head and particle track output from the qualified, calibrated saturated zone (SZ) site-scale flow model. Submittal date: 05/01/2007.

SN0705T0510106.009. PEST V11.1 Predictive Uncertainty Analysis Including The Prediction Maximizer. Submittal date: 05/24/2007.

9.5 SOFTWARE CODES

155082 CORPSCON V. 5.11.08. 2001. WINDOWS NT 4.0. STN: 10547-5.11.08-00.

167994 EARTHVISION V. 5.1. 2000. IRIX 6.5. STN: 10174-5.1-00.

163072 EXT_RECH V. 1.0. 2002. Sun O.S. 5.7. STN: 10958-1.0-00.

161725 FEHM V. 2.20. 2003. SUN 9.S. 5.7 & 5.8, Windows 2000, RedHat Linux 7.1. STN: 10086-2.20-00.

179539 FEHM V. 2.24-02. 2006. WINDOWS XP. STN: 10086-2.24-02-00.

173140 LaGriT V. 1.1. 2004. Sun OS 5.7, 5.8, 5.9, IRIX64 OS 6.5. STN: 10212-1.1-00.

179480 PEST V. 11.1. 2007. Windows. STN: 611582-11.1-00.

161564 PEST V. 5.5. 2002. SUN O.S. 5.7 & 5.8, WINDOWS 2000, RedHat 7.3. STN: 10289-5.5-00.

155323 PHREEQC V. 2.3. 2001. WINDOWS 95/98/NT, Redhat 6.2. STN: 10068-2.3-00.

163070 Software Code: Extract V. 1.0. 2002. Sun UltraSPARC - SunOS 5.7. 10955-1.0-00.

163071 Software Code: Extract V. 1.1. 2002. Sun UltraSPARC - SunOS 5.7. 10955-1.1-00.

164654 Software Code: fehm2tec V. 1.0. 2003. Sun, Solaris 2.7 and 2.8. 11092-1.0-00.

164653 Software Code: maketrac V. 1.1. 2003. Sun, SunOS 5.7 and 5.8. 11078-1.1-00.

163073 Software Code: Mult_Rech V. 1.0. 2002. Sun UltraSPARC - SunOS 5.7. 10959-1.0-00.

164652 Software Code: reformat_sz V. 1.0. 2003. Sun, Solaris 2.7 and 2.8. 11079-1.0-00.

163074 Software Code: Xread_Distr_Rech V. 1.0. 2002. Sun UltraSPARC - SunOS 5.7. 10960-1.0-00.

163075 Software Code: Xread_Distr_Rech_-UZ V. 1.0. 2002. Sun UltraSPARC - SunOS 5.7. 10961-1.0-00.

163076 Software Code: Xread_Reaches V. 1.0. 2002. Sun UltraSPARC - SunOS 5.7. 10962-1.0-00.

163077 Software Code: Xwrite_Flow_New V. 1.0-125. 2002. Sun UltraSPARC - SunOS 5.7. 10963-1.0-125-00.

163078 Software Code: Zone V. 1.0. 2002. Sun UltraSPARC - SunOS 5.7. 10957-1.0-00.

180546 SPDIS.EXE V0.0. 2007. Windows XP. 611598-00-00.

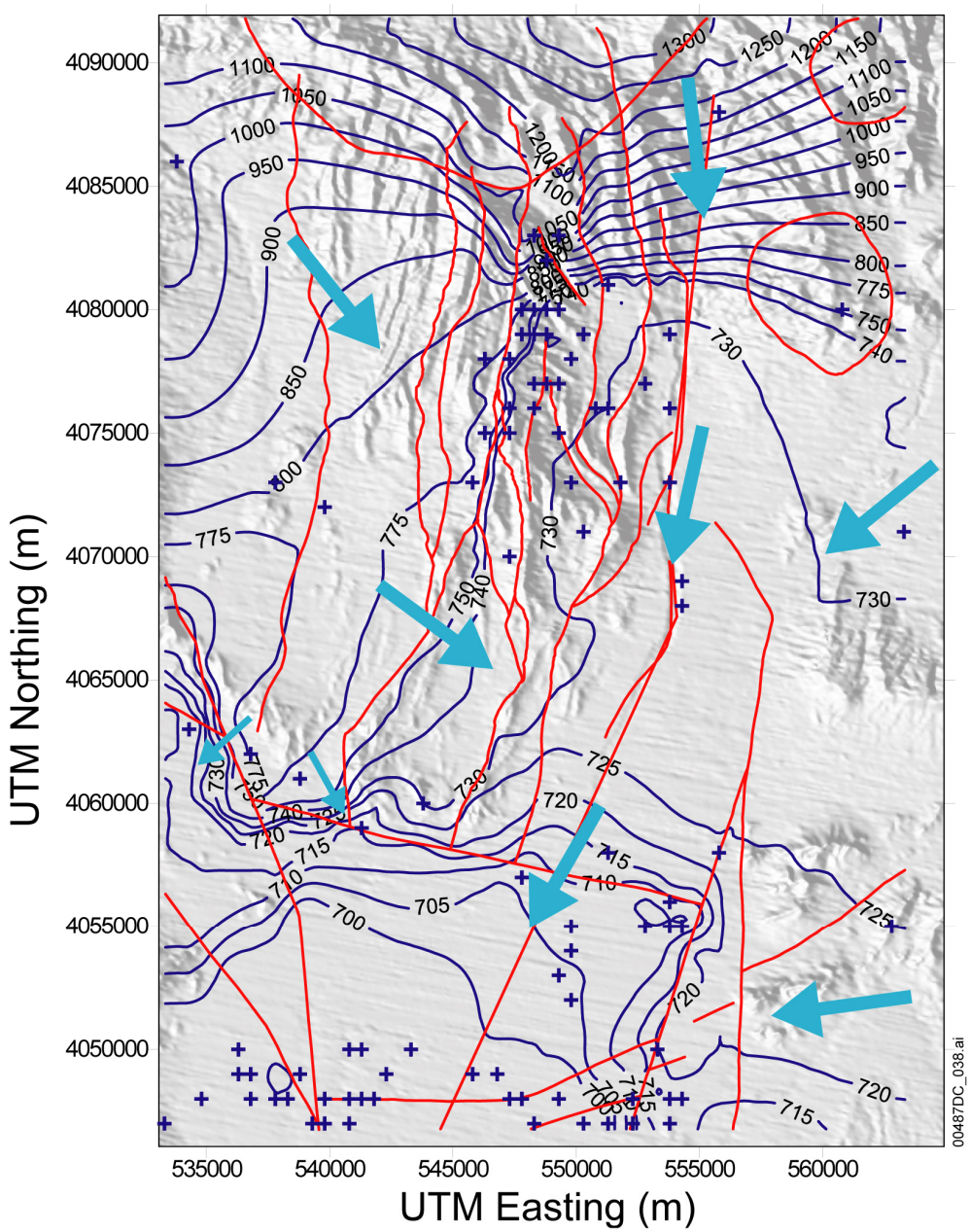

Source: USGS (2001 [DIRS 154625], Figure 1-2); DTNs: GS010908314221.001 [DIRS 145263] (Tertiary faults); GS000508312332.001 [DIRS 149947] (Water-level contours).

NOTE: The inferred groundwater flow directions are based on Assumption 1 in Table A5-1. The circular areas outlined in red near the Calico Hills in the northeast corner of the map are zones of hydrothermal alteration associated with granitic intrusions, and the semicircular area along the central northern portion of the map is the southern boundary of the Claim Canyon caldera (BSC 2004 ([DIRS 170037], Table 6-17; Zyvoloski et al. 2003 [DIRS 163341], Figure 2b). The other red lines are selected faults; blue crosses indicated the location of hydraulic head measurements. Blue lines are contours showing elevation (in meters above sea level) of the potentiometric surface; contour intervals vary. UTM=Universal Transverse Mercator. For illustrative/historical perspective purposes only.

Figure A6-3. Potentiometric Surface and Inferred Flow Directions (light blue arrows) for Yucca Mountain and Vicinity

An important conclusion derived from identification of these mixing zones is that they qualitatively illustrate the extent of transverse dispersivity along certain flow pathways. The mixing zones also illustrate that, although some flow pathways may remain intact for great distances (e.g., paths 1 and 2), even these most-persistent flow paths eventually loose their distinct character, largely through mixing. This effect is best illustrated in southern Amargosa desert where flow paths 1, 2, and 3, with contributions from 8, converge and mix. The distinct end member groundwater of the AR and FMW-S groups, representing flow paths 1 and 2, appears to be absent at the southern boundary of the study area. Whereas it is possible that these end member groundwaters have not yet been sampled, the proximity of mixed groundwater samples in the southern part of the study area (samples 141, 174, 175, 183, 184, and 185) leaves little room for unmixed (end member) groundwater to move through the area. The hydrochemical data are interpreted to indicate that groundwaters from distinct sources that merge in the Amargosa Desert eventually lose their hydrochemically distinct character and flow southward as partially mixed groundwater.

A7. SUMMARY, DATA TRACKING NUMBERS, AND UNCERTAINTIES

A7.1 SUMMARY

Hydrochemical data from the saturated zone in the Yucca Mountain region were compiled, documented, and analyzed in this appendix. The hydrochemical data are used together with physical hydraulic data to evaluate the local and regional flow system at Yucca Mountain. This report provides an independent assessment of the flow patterns (Section A6.3.11) and recharge rates (Section A6.3.6) near Yucca Mountain that can be compared with flow paths and recharge rates associated with the SZ site-scale flow model documented in *Water-Level Data Analysis for the Saturated Zone Site-Scale Flow and Transport Model* (BSC 2004 [DIRS 170009]), and for which the model input/output files are in DTN: LA0304TM831231.002 [DIRS 163788]. This report also provides an independent basis for calculating groundwater residence times (Section A6.3.9) that can be compared with particle breakthrough curves calculated using the site-scale SZ transport model. Additionally, this appendix contributes to the resolution of technical issues associated with groundwater residence times and flow path lengths in alluvium and tuff, as discussed below. The methods used in this appendix are widely accepted, the data are sufficient and the analysis appropriate for the intended use if this document.

A7.1.1 Summary of Overview Sections (Sections A6.3.1 to A6.3.5)

Areal distributions of chemical and isotopic data as well as calculated parameters show many consistent patterns throughout the study area. Groundwater that has low concentration of most solutes characterizes groundwater beneath Yucca Mountain and in Fortymile Wash. Dilute groundwaters characterize the northern part of Fortymile Wash as well as the southern part in the Amargosa Desert. Increases in most solute concentrations occur to the west of Yucca Mountain and along the southern margin of Yucca Mountain near U.S. Highway 95. Dilute groundwaters are flanked by less dilute groundwaters to the east and west in the Amargosa Desert. Hydrochemical data presented in these sections provide first-order constraints on flow pathways. Groundwater beneath Yucca Mountain and in Fortymile Wash is characterized by low concentrations of most solutes.

A7.1.4 Summary of Flow Pathways (Section A6.3.11)

Flow paths can be traced using areal plots and scatterplots of geochemical and isotopic data, inverse mixing and water/rock interaction analyses involving PHREEQC, and simulations done with the SZ flow model. Because no single chemical or isotopic species varies sufficiently to determine flow paths everywhere in the study area, multiple chemical and isotopic species were considered.

Flow Path 1 (Figure A6-62) shows groundwater moving roughly parallel to the Amargosa River from an area west of Bare Mountain toward the southwest corner of the site model area. Flow Path 2 indicates that groundwater flows parallel to Fortymile Wash to connect upgradient areas in Fortymile Canyon with downgradient areas in the Amargosa Desert. Groundwater following Flow Path 3 flows from central Jackass Flats near well J-11 through the eastern part of the Amargosa Desert. Flow Paths 4 and 5 shows groundwater moving predominantly south-southeast through Crater Flat. Mixing relations and modeling suggest that these groundwaters leak across a region with a steep hydraulic gradient to mix with more dilute groundwaters to the southeast. Flow Paths 6 and 7 show groundwater flow from the Solitario Canyon area to the south. Again, leakage to the southeast across a steep hydraulic gradient coincident with the Solitario Canyon fault is suggested by hydrochemical trends. Groundwater from northern Yucca Mountain is interpreted to flow southeast toward lower Dune Wash and then southwestward toward wells located west of Fortymile Wash near U.S. Highway 95 (Flow Path 7). The location of Flow Path 7 implies that groundwater from the repository area will flow further to the west of this path. Flow Path 8 illustrates leakage to the west across the hydrologic boundary between the carbonate aquifer to the east and the alluvial aquifer in Amargosa Desert. Flow Path 9 schematically illustrates deep underflow of groundwater from the carbonate aquifer, east of and including the GF and AF groups, beneath the Amargosa Desert and Funeral Mountains to the discharge points in Death Valley.

Regions where mixing relations are strongly suggested by hydrochemical data are also shown in Figure A6-62. An important conclusion derived from drawing these mixing zones is that they document and qualitatively illustrate the extent of transverse dispersivity along certain flow pathways. The mixing zones also illustrate that although some flow pathways may remain intact for great distances (e.g., Paths 1 and 2), even these most persistent flow paths eventually lose their distinct character largely through mixing as is demonstrated in southern Amargosa Desert along the southern border of the map area.

A7.2 DATA TRACKING NUMBERS

Several data tracking numbers (DTNs), generated in this appendix are cited elsewhere in this report where they are used as indirect input. These intermediary output DTNs are listed below in an order that coincides with the structure of the appendix. These results are not qualified and cannot be used as direct input without qualification:

- Regional groundwater hydrochemical data: DTNs: LA0309RR831233.001 [DIRS 166546] and LA0309RR831233.002 [DIRS 166548]

- Calculated hydrochemical parameters: DTN: LA0310EK831232.001 [DIRS 165995]

affect groundwater chemistry. Most sample data presented herein were collected by the United States Geological Survey (or by their contractors), who have a long and proven record of groundwater sampling using proven techniques. Furthermore, Yucca Mountain Project Quality Assurance Programs also govern many of these sampling procedures. This program is designed to assure that methods utilized are appropriate for the desired purpose. Thus, the data are accepted to be representative of in situ conditions. All analytical data presented herein have uncertainty associated with the individual values. These uncertainties reflect limits of precision of the analytical technique combined with accuracy of the measurement, which is typically determined by replicate analysis of samples (standards) with known values. The data presented herein were determined using a variety of analytical techniques by a number of laboratories, collected over a span of more than 20 years, during which time analytical techniques and associated uncertainties have changed. In some cases, uncertainties for individual analytes or groups of analytes are presented in the original data sources, however, in other data sets analytical uncertainties are neither given nor discussed. Some examples of stated uncertainties are presented below.

The National Water Quality Laboratory produced many of the data presented herein for the Yucca Mountain Program at the United States Geological Survey and uncertainties are stated in some of the DTNs. For example, accuracy for major anions, cations and strontium concentration is estimated to be better than 10% except for fluoride, which is estimated at 15% (DTN: GS000308312322.003 [DIRS 149155]). Uncertainty in concentration of major anions and cations as well as strontium concentration is quoted at less than 10% in DTN: GS011108312322.006 [DIRS 162911]. This DTN also presents uncertainties for isotopic measurements as follows (all given in per mil): deuterium 3.0, ^{18}O 0.2, ^{13}C 0.2, and ^{34}S 0.2. In some cases, strontium was determined by isotope dilution, mass spectrometry methods, for which data are more precise (e.g. 0.5%, DTN: GS970708315215.008 [DIRS 164674]). Uncertainties for ^{14}C are 0.1 pmc for data presented in DTN: GS011108312322.006 [DIRS 162911]. Uncertainties for uranium concentration are given as better than 1% (Paces et al. 2002 [DIRS 158817]). Uncertainties in uranium isotope ratios ($^{234}U/^{238}U$) are typically given with each individual analysis in the original data source. For example, uncertainties presented in Paces et al. (2002 [DIRS 158817], Table 2) range from 0.09% to 4.5% with a mean of 0.73% (with the exception of a single analysis of a rainfall sample with small U concentration for which uncertainty in the $^{234}U/^{238}U$ ratio is 9.8%). Uncertainties for strontium isotope ratios ($^{87}Sr/^{86}Sr$) are typically quoted at 0.00001 for absolute values (e.g., DTN: GS011108312322.006 [DIRS 162911] and for Nye County wells), which translates to an uncertainty of approximately 0.01 in $\delta^{87}Sr$ units.

For the purpose of this report, uncertainties assigned to analytical data are based on one or more of the following: (1) stated uncertainties in the original data set; (2) consideration that data produced by the same facility, for which no uncertainties are stated, are likely to have similar uncertainties to data with stated uncertainties; (3) typical uncertainties given in the literature; or (4) the authors' personal experience with typical uncertainties associated for various analytical techniques and analytes. Where uncertainties are not stated, the following uncertainties are assigned to the analytical data: Major anions and anions and strontium concentration: 10%; fluoride concentration: 15%; stable isotopes of hydrogen, oxygen, sulfur, and carbon (expressed as δH, δO, δS, and δC in per mil): 0.2; and ^{14}C: 0.2 pmc. Uncertainties in uranium concentration and uranium and strontium isotope ratios are given in the original data sets.

Another source of uncertainty in the calculated saturation indices of alumino-silicate minerals concerns the assumption that total dissolved Al^{3+} concentrations are in equilibrium with kaolinite. This assumption was based on an empirical fit to dissolved Al^{3+} concentrations from a subset of the Yucca Mountain area wells for which dissolved Al^{3+} data exist (see Section A6.3.5). Estimates of Al^{3+} concentrations that rely on assumed equilibrium with kaolinite underestimate measured Al^{3+} concentrations by –3.0 ±2.9 ppb. If the actual Al^{3+} concentrations were approximately 3 ppb higher than was estimated for the Yucca Mountain area, the saturation indices of all Al-bearing minerals would increase. Assuming Al^{3+} equilibrium with kaolinite, most groundwaters in the Yucca Mountain area are estimated to be saturated with smectite and Ca-clinoptilolite (Figures A6-38 and A6-39). With higher Al^{3+} concentrations, these groundwaters would be even more supersaturated with these minerals. Groundwaters in the Yucca Mountain area are presently estimated to be both undersaturated and supersaturated with K-feldspar (Figure A6-37). With higher Al^{3+} concentrations, some groundwaters that are estimated to be undersaturated with K-feldspar might be calculated to be saturated or supersaturated with K-feldspar.

A7.3.3 Calculated ^{14}C Ages

The calculations of ^{14}C ages used the downgradient increase in the DIC concentrations of selected Yucca Mountain area groundwaters, relative to the DIC concentrations of Yucca Mountain perched waters to estimate the extent of ^{14}C dilution by calcite dissolution in the saturated zone (Section A6.3.6.6.2). The selected groundwater samples were chosen because they, like the perched water samples, had high $^{234}U/^{238}U$ activity ratios relative to many Yucca Mountain area groundwaters, thus indicating the likelihood of a common origin. The estimated increases in the DIC concentrations of the groundwaters were then used to reduce the initial ^{14}C activities to below their original atmospheric values to calculate a "corrected" ^{14}C age for the groundwater. The critical assumptions in this analysis are that (1) the perched water itself required no age corrections and (2) that the measured increases in groundwater DIC relative to perched water limit the amount of ^{14}C dilution by calcite. Assumption (1) appears to be valid based on the historic variations of $^{36}Cl/Cl$ and ^{14}C activities measured on organic carbon in pack-rat middens and similar relations between $^{36}Cl/Cl$ and ^{14}C activities measured for inorganic carbon in perched water. Assumption (2) requires that no reductions in groundwater DIC concentrations take place through exsolution of CO_2 during groundwater flow or during sampling. Although CO_2 losses from groundwater to the unsaturated zone are estimated to be small because of the low diffusion of CO_2 in groundwater, exsolution of CO_2 during groundwater sampling may be a more significant effect. However, groundwater at the wells where ^{14}C age corrections were made typically had relatively low (< 7.8) pH values, indicating that the effects of degassing on DIC concentrations during sample collection were minimal.

A7.3.4 Calculations of the Fractions of "Young" Water in Yucca Mountain Groundwaters

These calculations interpret the measured ^{14}C activities of groundwater beneath Yucca Mountain to result from the mixing of groundwater that has been recharged at different times from the unsaturated zone at Yucca Mountain. Although recharge may have been added continuously over time at varying rates to Yucca Mountain groundwater, the calculations simplify the actual distribution by assuming that the measured ^{14}C activities result from the mixing of an "old"

Conceptual-model uncertainty includes the choice of mineral phases to be considered in a particular model, any constraints on the precipitation/dissolution or exchange reactions imposed on these phases, and the choice of groundwaters considered in these models as potential mixing components. The rationale behind selection of these various parameters is discussed in Section A6.3.8. It is acknowledged; however, that all possible combinations of these parameters were not exhaustively evaluated. Other combinations of end-member mixing components and reaction history could possibly be modeled to yield a particular downgradient water chemistry. Given all the potential combinations of mixing end members and reaction models, it is impossible to quantify uncertainty related to uncertainties in the conceptual model.

A7.3.6 Groundwater Velocities

The groundwater velocities calculated in Section A6.3.9 were based on the measured groundwater ^{14}C activities at wells defining a flow path segment, the linear distance between the wells, and the water-rock interactions identified by the PHREEQC models for that flow-path segment. The calculated velocities are, therefore, affected by the accuracy and representativeness of the groundwater ^{14}C measurements (see Section A7.3.1), the assumption that groundwater flows along a straight path between the wells defining the flow-path segment, and the uncertainties associated with the PHREEQC models, as described in Section A7.3.5. An indication of the quantitative uncertainty associated with transit times is provided by the standard deviations associated with transport times based on the PHREEQC models and differences between the means of these estimates and estimates made based on downgradient increases in DIC concentrations (Table A6-11). An additional uncertainty that may impact these calculations concerns the implicit assumption that no additional ^{14}C is added to the groundwater from downgradient recharge as the groundwater moves from the upgradient to downgradient wells defining a flow-path segment. Recharge at Yucca Mountain may not vary enough spatially to guarantee that upgradient and downgradient recharge could be recognized in a mixture.

A7.3.7 FEHM Groundwater Models of Nonreactive Tracer Transport in the Yucca Mountain Area

The FEHM simulations of nonreactive tracer transport described in Section A6.3.10 used the Yucca Mountain site-scale saturated zone flow model documented in *Water-Level Data Analysis for the Saturated Zone Site-Scale Flow and Transport Model* (BSC 2004 [DIRS 170009]), using the model input/output files in DTN: LA0304TM831231.002 [DIRS 163788]. Uncertainty in flow modeling arises from a number of sources including, but not limited to, the conceptual model of the processes affecting groundwater flow, water–level measurements and simplifications of the model geometry, boundary conditions, hydrogeologic unit extent and depth, and the values of permeability assigned to hydrogeologic units. Such uncertainties associated with this flow model are identified and quantified in *Saturated Zone Site-Scale Flow Model* (BSC 2004 [DIRS 170037], Section 6.8). An additional uncertainty that pertains to the tracer simulations but not the flow model itself concerns numerical dispersion associated with the advection/dispersion equation. Numerical dispersion would tend to cause greater apparent mixing and dilution than would be present solely because of hydraulic conductivity variations in the model. These effects are likely to have influenced the tracer concentration distributions shown in Section A6.3.10 and, in particular, the relatively dilute concentrations near the edges of these tracer plumes may be an artifact of this numerical dispersion.

Areal distributions of bicarbonate (as a surrogate for DIC), $\delta^{13}C$, and ^{14}C (measured on the DIC fraction) are shown in Figures B6-6, B6-9, and B6-10, respectively. These new inorganic-carbon data are generally consistent with data presented in Appendix A. Although these new data do not show consistent north to south trends, there is a general west to east increase in ^{14}C activity among the new Nye County boreholes (Figure B6-10). This shift corresponds to a decrease in bicarbonate concentration and decrease in $\delta^{13}C$ values. These data are consistent with a greater component of carbonate-derived groundwater in the west compared to the east and a greater component of more recently recharged water along Fortymile Wash.

Preliminary results of uncorrected radiocarbon ages based on ^{14}C activities measured for the total DOC fraction of several groundwaters are reported in DTN: GS031208312322.004 [DIRS 179431]. Figure B6-14 compares these uncorrected ^{14}C-TDOC ages, along with uncorrected radiocarbon ages calculated from separate analyses of the light and heavy molecular-weight DOC fractions, to uncorrected ^{14}C-DIC ages.

^{14}C ages determined from ^{14}C activities in DIC and TDOC fractions are in reasonable agreement for samples UE-29a#1, UE-29a#2, -22PA-1 (although the DOC fraction used for the -22PA-1 age estimate was not specified), -19P, and WT-3, all of which are located near Fortymile Wash. However, ^{14}C ages for these same samples determined from the low or high molecular weight fractions are in poor agreement with ages determined using ^{14}C-DIC. These data plot in fields that indicate a smaller percentage of ^{14}C activity (relative to that in modern carbon) in the DOC fraction relative to that in the DIC fraction and correspondingly older ^{14}C ages. The reason for this shift is unknown at this time. Several other samples plot in fields indicating smaller DIC percentages compared to those of TDOC, which yield older uncorrected ^{14}C ages based on DIC. Many of these samples (-1DX, -12PA, -12PC, and -9SX) are located in the CF-SW region, which hosts groundwater with a distinct carbonate signature. The age relationship noted is consistent with addition of dead carbon as inorganic carbon.

B6.6 REGIONAL FLOWPATHS INFERRED FROM HYDROCHEMICAL DATA

Hydrochemical data from the new boreholes presented above validate many of the flow pathways presented previously (Figure A6-62) and also allow minor refinements of that figure. The new boreholes are located in the region bounded between Flow Path 4 and Flow Path 3. A slightly modified version of the regional flowpath figure (Figure A6-62) is presented in Figure B6-15. The rationale underlying each modification is described below.

New hydrochemical data from -23P further validate Flow Path 3. In particular, sulfate/chloride ratios and high sulfate concentrations in -23P are similar to those from borehole J-11 (Jackass Flat grouping), strengthening the argument that water from Jackass Flat flows southwesterly to this region. Boreholes -23P and Washburn-1X constrain the position of Flow Path 3. Only minor adjustments were made to this flowpath. Based on interpretation of new data from -23P, mixing zone C was extended slightly to the north, and an additional arrow indicating westward flow of Flow Path 8 was added.

New hydrochemical data from boreholes -27P, -16P, and -28P confirm a southerly flow from the Solitario Canyon Wash (Grouping SCW) area along Flow Path 6. Slightly elevated sulfate and chloride values in two samples suggest that groundwater from regions to the northwest and/or

E1. PURPOSE

The purpose of this appendix is to describe the potentiometric surface developed for use with the SZ site-scale flow model described within this report. Also included is the process used to develop or construct the potentiometric surface. The description includes background, software used, inputs, analysis with uncertainty and limitations, and conclusions.

Previous potentiometric surfaces and analyses have been presented by *Water-Level Data Analysis for the Saturated Zone Site-Scale Flow and Transport Model* (USGS 2001 [DIRS 154625], 2004 [DIRS 168473]; BSC 2004 [DIRS 170009]). The initial version of the potentiometric surface (USGS 2001 [DIRS 154625]) was used for the calibration of the SZ site-scale flow model (BSC 2004 [DIRS 170037]).

The USGS (2004 [DIRS 168473]) used updated water-level data for selected wells through the year 2000 as the basis for estimating water-level altitudes and the potentiometric surface in the SZ site-scale flow and transport model domain based on an alternative interpretation of perched water conditions. The updated water-level data presented by the USGS (2004 [DIRS 168473]) include data obtained from NC-EWDP Phases I and II and data from USW WT-24. That revision developed computer files containing:

- Water-level data within the model area (DTN: GS010908312332.002 [DIRS 163555])
- A table of known vertical head differences (DTN: GS010908312332.003 [DIRS 168699])
- A potentiometric-surface map (DTN: GS010608312332.001 [DIRS 155307]) using an alternative concept from that presented by the USGS (2001 [DIRS 154625]) for the area north of Yucca Mountain.

The water-level data analysis (BSC 2004 [DIRS 170009]) was based on work by the USGS (2004 [DIRS 168473]) and includes an analysis of the impact of more recent water-level data and the impact of adding data from the NC-EWDP Phases III and IV wells. It also expands the discussion of uncertainty in the potentiometric-surface map.

The current potentiometric surface presented in this appendix builds on the potentiometric surface as represented by contour lines presented by the USGS (2004 [DIRS 168473], Figure 6-1) as modified by *Water-Level Data Analysis for the Saturated Zone Site-Scale Flow and Transport Model* (BSC 2004 [DIRS 170009], Figure 6-2), which includes data from two additional recently completed wells, NC-EWDP-24P and NC-EWDP-29P as found in DTN: MO0409SEPPSMPC.000 [DIRS 179336] and illustrated in Figure 6-16.

Output DTN: MO0611SCALEFLW.000 represents the current potentiometric surface and includes representations of the surface in addition to the contours as shown in Figure 6-4.

E2. USE OF SOFTWARE

The potentiometric surface was constructed primarily using EarthVision 5.1 (STN: 10174-5.1-000, [DIRS 167994],) on a Silicon Graphics Octane workstation running IRIX 6.5. EarthVision is a product of Dynamic Graphics, Inc. and is designed for the preparation of three-dimensional geologic surfaces and models. The use of EarthVision to prepare this surface is consistent with the intended use of the software. There are no limitations on the use of this potentiometric surface due to the use of EarthVision.

EarthVision 5.1 can create regularly spaced grids from irregularly spaced data points to create surfaces that represent the top of specific hydrogeological units or the saturated zone. Up to 10,000,000 data points can be used to produce a grid with dimensions up to 1,201 × 1,201 (*GS_EV_5_0.pdf*, pp. 22 and 24). The surface constructed was within the range of these limits.

Several commercially available software packages (exempt per IM-PRO-003) were also used for data handling, formatting, and data visualization in the preparation of the potentiometric surface. These software packages were Microsoft Access (97 and 2000), Microsoft Excel (97 and 2003), AutoCad (2002), EarthVision (7.5.2), and UltraEdit (11.10) by IDM Computer Solutions, Inc. Each of these software packages were used on the Windows 2000 platform. No calculations were performed by these commercial software packages and the only output was in the form of visualizations. AutoCad and EarthVision 7.5.2 were used for data visualization and are therefore exempt per IM-PRO-003. Access, Excel, and UltraEdit were used for formatting data and were also exempt per IM-PRO-003. Each of these exempt software packages is controlled by YMP Software Configuration Management.

E3. INPUTS

The inputs for the construction of the potentiometric surface consist of water level measurements and the contour lines from previous potentiometric surfaces as shown in DTN: MO0409SEPPSMPC.000 [DIRS 179336].

Water level measurements used for the construction of the latest potentiometric surface were obtained from Output DTN: SN0610T0510106.001. In some cases, more than one water-level value is given for a single well and some wells and intervals are not considered appropriate for use in construction of a potentiometric surface. Table A-2 of *Water-Level Data Analysis for the Saturated Zone Site-Scale Flow and Transport Model* (BSC 2004 [DIRS 170009]) was used to determine which wells and intervals were appropriate for use in the construction of the potentiometric surface. For wells or intervals not included in Appendix A of *Water-Level Data Analysis for the Saturated Zone Site-Scale Flow and Transport Model* (BSC 2004 [DIRS 170009]), the value for the uppermost interval found in Output DTN: SN0610T0510106.001 was used.

Contour lines from Figure 6-2 of *Water-Level Data Analysis for the Saturated Zone Site-Scale Flow and Transport Model* (BSC 2004 [DIRS 170009]) and found in DTN: MO0409SEPPSMPC.000 [DIRS 179336] were digitized and included as input data except in the immediate vicinity of the two recently completed wells, NC-EWDP-24P and NC-EWDP-29P.

E4. ANALYSIS

The potentiometric surface discussed herein is intended to be suitable for the needs of the saturated zone site-scale flow model described in this report. The area for which this potentiometric surface was constructed is identical to the area of the Hydrogeologic Framework Model HFM2006 (SNL 2007 [DIRS 174109]) and the SZ site-scale flow model of this report. The area covers about 1,350 km^2 and extends from 533,000 to 563,000 m (west to east) and 4,046,500 to 4,091,500 m (south to north), UTM (Zone 11, North American Datum 1927). The resolution, horizontal spacing, of the potentiometric surface was also established to match the Hydrogeologic Framework Model HFM2006 (SNL 2007 [DIRS 174109]) at 125 m.

The minimum tension method, generally recognized as providing geologically reasonable surfaces except where very steep surfaces are encountered (vertical distances many times greater than the horizontal data spacing), was used to construct the potentiometric surface. Control points were used to limit the tendency to overshoot in areas of very steep gradients. Some smoothing was also applied to minimize the effects of uneven data distribution.

The resulting potentiometric surface was checked at the water level measurement locations by determining the absolute value of the difference between the input value and the value indicated by the new potentiometric surface. The median difference was 0.2 m with a standard deviation of 1.9 m. This difference was determined to be suitable for use with the flow model described in this report. The potentiometric surface is intended for use with the SZ site-scale flow model and may not be suitable for other purposes. This surface does not replicate the input data exactly.

The uncertainty in the previously developed potentiometric surface map discussed in Section 6.5 of *Water-Level Data Analysis for the Saturated Zone Site-Scale Flow and Transport Model* (BSC 2004 [DIRS 170009]) is applicable to the current potentiometric surface. Uncertainty within the potentiometric surface is mostly related to the accuracy of the water-level measurements, distribution of data and relative variations of the surface. In areas of limited data and steep gradients, such as in the northwest portion of the model, uncertainty is greater than in the immediate vicinity of the repository. In general, the relatively flat portion of the potentiometric surface located just south of the repository is relatively less uncertain due to more wells located in the area. This area, from the repository extending to the south, is the most likely general direction of groundwater flow and is of more interest than the northwest portion of the model area.

The potentiometric surface intended for use with the SZ site-scale flow model is contained in Output DTN: MO0611SCALEFLW.000.

E5 CONCLUSIONS

The potentiometric surface found in Output DTN: MO0611SCALEFLW.000 has been prepared using the previous potentiometric surface (BSC 2004 [DIRS 170009]) and the most recently available water level information to create a surface suitable for use in the SZ site-scale flow model.

F1. PURPOSE

The purpose of these calculations is to convert qualified survey coordinates from Nevada State Plane (NSP) to UTM coordinates for selected NC-EWDP boreholes. Qualified borehole coordinates are required to support development of the new site-scale saturated-zone flow model.

The scope of these calculations covers NC-EWDP boreholes, through Phase IV, for which qualified UTM coordinates do not already exist in the Technical Data Management System (TDMS).

This activity is conducted under *Technical Work Plan for Saturated Zone Flow and Transport Modeling* (BSC 2006 [DIRS 177375]). It is a deviation from this TWP insofar as the conversion software used to conduct the activity is not identified in Section 9 of the TWP as software to be used for performing calculations, modeling or analyses for the work covered by the TWP. However, the software used for this activity is qualified, and the software package used to conduct the work was obtained from Software Configuration Management.

F2. QUALITY ASSURANCE

All activities in the governing TWP (BSC 2006 [DIRS 177375]) have been determined to be subject to *Quality Assurance Requirements and Description* (QARD) (DOE 2006 [DIRS 177092]), except for administrative activities. The calculations presented in this report are considered to be an analysis of data to support performance assessment and is therefore subject to the QARD (DOE 2006 [DIRS 177092]). No new data have been collected as part of this work scope. A prerequisite for this task is that all necessary qualified data are obtained from the TDMS.

In addition to the QARD (DOE 2006 [DIRS 177092]), the following procedures are used to perform this task:

- DM-PRO-001, *Document Control*
- DM-PRO-002, *Records Management*
- IM-PRO-002, *Control of the Electronic Management of Information*
- IM-PRO-003, *Software Management*
- RM-PRO-2001, *Document Control*
- SCI-PRO-004, *Managing Technical Product Inputs*
- SCI-PRO-006, *Models*
- TST-PRO-001, *Submittal and Incorporation of Data to the Technical Data Management System*.

H1. INTRODUCTION

Models are calibrated so that they make better predictions than if they were not calibrated. Unfortunately, calibrated model predictions can still be wrong. Furthermore, it is now being fully understood that a calibrated model can make even worse predictions than it did before calibration. With traditional approaches to model calibration, there is no way to find out: (1) whether a calibrated model's predictions are better than those before calibration, (2) if the predictions are better how much better they are, and (3) if their predictions are wrong how wrong they are. Traditional approaches to calibration are not able to ensure that calibrated models minimize "potential predictive wrongness" while quantifying the remaining uncertainty in the potential predictive wrongness.

The traditional approach to model calibration follows the tenet of the "principal of parsimony" espoused in many modeling texts and guidelines. First, the dimensionality of the calibration problem is reduced to facilitate a tractable model (i.e., few enough parameters are used to ensure their unique estimability) given the dataset available for calibration. The parameters values are then estimated through implicitly or explicitly maximizing some goodness-of-fit criterion. When the fit is judged to be "sufficient" (usually through minimization of an objective function), the model is deemed to be "calibrated" and therefore suitable for the making of predictions – predictions that may lay the groundwork for performance assessment calculations.

If automatic parameter estimation software is used in the calibration process, some estimates of parameter uncertainty are available. Estimates of the uncertainty of key model predictions can then be made based on the dependence of these predictions on the estimated parameters and their uncertainties.

The objective of this appendix is to show that calibrating a model and exploring the potential error of model predictions based on the theory of mathematical regularization, used in portions of this report, are better than methods based on the traditional approach to model calibration and predictive error analysis based on the principle of parsimony, which is not always effective or accurate. This same theory of mathematical regularization is regularly applied in many other branches of science where the analysis of costly and important data demands that maximum information be extracted (e.g., geophysical exploration and medical imaging). For example, a kidney is not defined prior to processing the data contained within a medical image; instead the location of the kidney "emerges" as a natural part of the data interpretation process. The same process should be used in groundwater data interpretation (which is what model calibration is) now that software that implements these methods efficiently in the groundwater modeling context are available. Public domain software that implements modern calibration and predictive uncertainty analysis based on regularized inversion is now available through the PEST package and its supporting utilities (Doherty 2003 [DIRS 178642], 2004 [DIRS 178643], 2006 [DIRS 178613]; PEST 2002 [DIRS 161564]). The groundwater industry will have to cross the same threshold that has been crossed in other industries, through application of regularized inversion as a methodology for model calibration and uncertainty analysis as a matter of course.

I1 THEORY – OVER DETERMINED CASE

This appendix is included to provide further background to the reader for the analysis conducted in Section 6.7.2, which is based on the theory presented below. Specifically, once a model is calibrated, the selected prediction made by that model can be maximized (or minimized) while maintaining a nominally calibrated model (e.g., the objective function must remain within 5% of its calibrated minimum). Changes in a model's prediction are made by varying parameters in the null space only (hence the ability of the model to remain calibrated). To the extent that the prediction depends on the null space parameters, its range can be estimated while maintaining calibration. This is a significantly more defensible way of presenting a confidence interval, because it eliminates the assumption that 95% confidence intervals are linearly dependent upon calibration parameters.

Vecchia and Cooley (1987 [DIRS 178577]) present a method for exploration of the confidence interval of a prediction made by a calibrated model, which accommodates the fact that the relationships between model outputs and parameters may not be linear. The methodology is based on a constrained optimization technique. The prediction of interest is maximized or minimized while parameters are constrained such that the model remains in a calibrated state at a certain confidence level. This confidence level is then equated to the confidence level of the prediction. Confidence is assessed in terms of the rise in the objective function that is incurred through maximizing or minimizing the prediction (and thereby incurring alterations to parameter values such that they no longer minimize that function). The relationship between objective function rise and parameter/predictive confidence interval is assessed in terms of the stochastic distribution that is assumed to pertain to measurement noise, together with a multiplier for this distribution (the so-called "reference variance") that is estimated through the calibration process.

Figure I-1 shows this process schematically. The dashed lines show contours of a prediction as a function of two parameters; let it be supposed that the value of the prediction increases to the upper right of this figure. The full line is a single contour of the objective function. The minimum of this objective function (which defines the values of parameters which calibrate the model) is within this contour. The contour itself defines the value of the objective function at which the model is no longer calibrated at a certain confidence level. The "critical points" A and B define locations in parameter space (and hence parameter values) at which the prediction of interest is minimized and maximized respectively at the same confidence level as that which applies to the contour. The difference between the corresponding model predictions defines the confidence interval of the prediction.

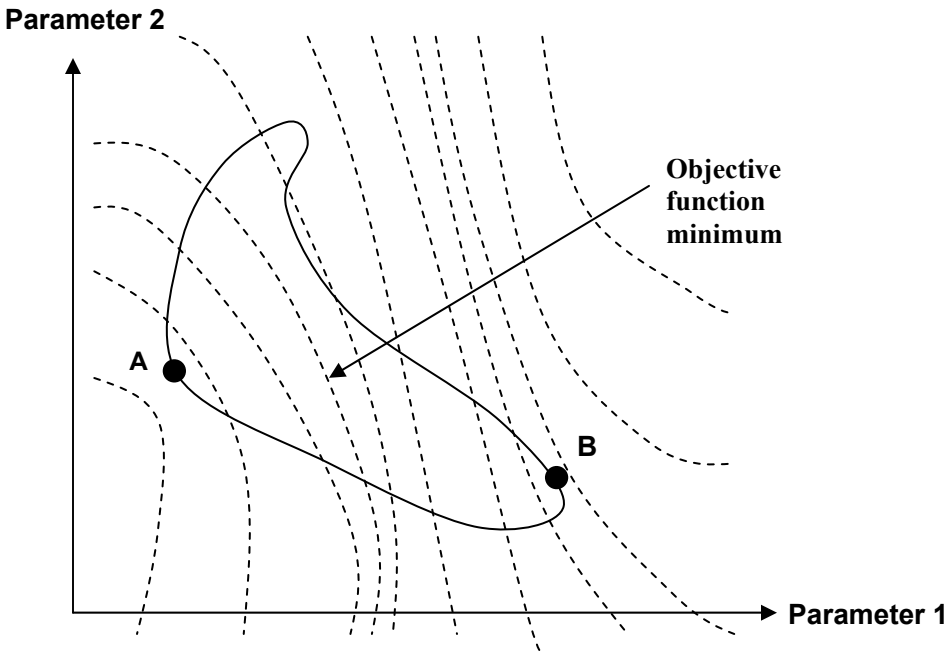

Figure I-1. Points in Parameter Space Corresponding to Maximum/Minimum Values of a Prediction at a Certain Confidence Level

Note that solution of the calibration problem through which parameters corresponding to Φ_{min} are computed, is achieved through an equation of somewhat similar form to Equation I-5, viz.:

$$\mathbf{p} = \left(\mathbf{X}^T\mathbf{Q}\mathbf{X}\right)^{-1}\mathbf{X}^T\mathbf{Q}\mathbf{h}. \quad \text{(Eq. I-31)}$$

When predictive analysis is carried out for a nonlinear model, the same equations are used. However in this case, **X** is replaced by the model Jacobian matrix, **J**, and a parameter upgrade vector is calculated instead of a solution vector. The solution process is then an iterative one in which the true solution is approached by repeated calculation of an upgrade vector based on repeated linearization of the problem through determination of a Jacobian matrix that is updated every iteration. For further details see Vecchia and Cooley (1987 [DIRS 178577]).

I2 UNDER-DETERMINED CASE

Use of the above theory assumes that the inverse problem of model calibration is unique; that is, it assumes that all contours about the minimum of the objective function are closed. Unfortunately, this is not the case for the SZ flow model, where the same objective function can be obtained using many different sets of parameters.

Fortunately, as Doherty (2006 [DIRS 178613]) and Moore (2005 [DIRS 178788]) show, the theory can be extended to the case of under-determined parameter estimation without too much difficulty.

For underdetermined parameter estimation there is no unique solution to Equation I-7. Hence, some form of regularisation must be introduced to the inverse problem. This often takes the form of a subspace method such as truncated singular value decomposition, or a Tikhonov method in which an optimal parameter set is defined as that which departs minimally from a preferred parameter condition. In either case, an optimised parameter set $\underline{\mathbf{p}}$ is computed as:

$$\underline{\mathbf{p}} = \mathbf{G}\mathbf{h}. \quad \text{(Eq. I-32)}$$

Now if the action of the model can be replaced by its linear matrix approximation, **X**, then (assuming zero offsets for simplicity):

$$\mathbf{h} = \mathbf{X}\mathbf{p} + \boldsymbol{\varepsilon}, \quad \text{(Eq. I-33)}$$

where **p** in Equation I-9 signifies the set of "real" system parameter values (can never be known), and **h** is, once again, the calibration dataset.

Thus:

$$\underline{\mathbf{p}} = \mathbf{R}\mathbf{p} + \mathbf{G}\boldsymbol{\varepsilon}, \quad \text{(Eq. I-34)}$$

where **R** is the "resolution matrix." Where noise is zero or minimal, each row of this matrix represents averaging weights through which calibrated parameter values contained in $\underline{\mathbf{p}}$ are obtained as functions of real parameter values contained in **p**. For under-determined inversion, **R** is always a rank-diminished matrix. Its null space defines the subspace of parameter space

2. The magnitude of structural noise associated with the calibration dataset (whether this be parsimonization-induced or a result of other model inadequacies) is normally assessed through the calibration process using a "reference variance" term. However, the estimation of this quantity has uncertainty associated with it. It is shown in most textbooks on parameter estimation that, even if measurement noise possesses a Gaussian distribution, parameter and predictive probabilities acquire a Student-*t* distribution for their characterization because of this. This will apply to the first term of Equation I-15, but not the second. Thus, use of the square of a normal variate for the total objective function as a means of assessing confidence will be somewhat in error.

I3 CONCLUSION

Overall, it is reiterated that the non-linear predictive error variance analysis developed in this appendix can be used to more accurately specify the range in a calibrated model prediction. That is, 95% confidence intervals are established for a model prediction while calibration is maintained and the assumption that model predictions are linearly dependent upon calibration is no longer required . While this does not ensure physical reasonableness of a prediction from a calibrated model, it demonstrates variability in a prediction based only on variation of parameters in the null space.